R-08-54

Geology Laxemar

Site descriptive modelling
SDM-Site Laxemar

Carl-Henric Wahlgren, Geological Survey of Sweden

Philip Curtis, Jan Hermanson, Ola Forssberg, Johan Öhman
Golder Associates AB

Aaron Fox, Paul La Pointe
Golder Associates Inc

Henrik Drake
Department of Earth Sciences, University of Gothenburg

Carl-Axel Triumf, Håkan Mattsson, Hans Thunehed
GeoVista AB

Christopher Juhlin
Department of Earth Sciences, Uppsala University

November 2008

Svensk Kärnbränslehantering AB
Swedish Nuclear Fuel
and Waste Management Co
Box 250, SE-101 24 Stockholm
Tel +46 8 459 84 00

ISSN 1402-3091
SKB Rapport R-08-54

Geology Laxemar

Site descriptive modelling
SDM-Site Laxemar

Carl-Henric Wahlgren, Geological Survey of Sweden

Philip Curtis, Jan Hermanson, Ola Forssberg, Johan Öhman
Golder Associates AB

Aaron Fox, Paul La Pointe
Golder Associates Inc

Henrik Drake
Department of Earth Sciences, University of Gothenburg

Carl-Axel Triumf, Håkan Mattsson, Hans Thunehed
GeoVista AB

Christopher Juhlin
Department of Earth Sciences, Uppsala University

November 2008

This report is dedicated to our dear friend and colleague Roy Stanfors, who sadly passed away in September 2008. Roy's long experience encompassed geological investigations in the Laxemar-Simpevarp area, including investigations for the construction of the nuclear power plants, Äspö Hard Rock Laboratory and Clab. Roy's engagement, inspiration, help and continuous support have been invaluable for the work presented in this report and for the Laxemar site descriptive modelling as a whole.

Preface

The Swedish Nuclear Fuel and Waste Management Company (SKB) is undertaking site characterisation at two different locations, Forsmark and Laxemar/Simpevarp, with the objective of siting a geological repository for spent nuclear fuel. The analysis and modelling of geological data from each site provide a foundation for the modelling work carried out in other disciplines (hydrogeology, thermal properties, rock mechanics, hydrogeochemistry and transport) and for the design of the potential repository. This report presents the final set of geological models for the Laxemar site, which will contribute to the design of repository layout D2 and the forthcoming safety evaluation.

The following people have contributed to the SDM-Site Laxemar geological modelling work:

Deterministic modelling of rock domains

Evaluation of primary data: Carl-Henric Wahlgren (strategy and evaluation), Ola Forssberg and Johan Öhman (histograms, stereographic projections), Johnny Andersson (tabulations), Håkan Mattsson and Carl-Axel Triumf (petrophysical data), Henrik Drake (fracture minerals).

Conceptual understanding of the site and its evolution: Carl-Henric Wahlgren.

3D modelling: Ingemar Markström with contributions by Ola Forssberg and Carl-Henric Wahlgren.

Compilation of property tables for rock domains: Carl-Henric Wahlgren with contribution by Ola Forssberg.

Deterministic modelling of deformation zones

Evaluation of primary data: Philip Curtis (strategy and evaluation), Ola Forssberg and Johan Öhman (histograms, stereographic projections), Henrik Drake (fracture minerals), Carl-Axel Triumf, Hans Thunehed and Håkan Mattsson (geophysical,topographical data and lineament interpretation), Christopher Juhlin (reflection seismic data and interpretation).

Conceptual understanding of the site (and its evolution): Philip Curtis and Carl-Henric Wahlgren with contribution by Giulio Viola.

3D modelling: Philip Curtis.

Compilation of property tables for deformation zones: Philip Curtis with contributions by Ola Forssberg and Johan Öhman.

Statistical modelling of fractures and minor deformation zones

Evaluation of primary data: Aaron Fox, Paul La Pointe (DFN modelling), Jan Hermanson, Johan Öhman, Tommy Olsson, and Roy Stanfors.

Development of DFN model: Aaron Fox and Paul La Pointe.

QA/QC: William Dershowitz, Paul La Pointe and Jan Hermanson.

Report

Chapter 1–3: Carl-Henric Wahlgren and Philip Curtis with contributions by Aaron Fox, Henrik Drake, Carl-Axel Triumf, Håkan Mattsson, Hans Thunehed, Ola Forssberg (Appendices), Johan Öhman (Appendices), Fredrik Hartz (figures), Pär Kinnbom (Wellcad diagrams) and Mats Elfström (Appendix 1).

Chapter 4: Carl-Henric Wahlgren

Chapter 5: Philip Curtis with contribution by Christopher Juhlin (Appendix 13)

Chapter 6: Aaron Fox with contribution by Paul La Pointe

Summary

Geological history and geological processes

Laxemar is located in eastern Småland within the municipality of Oskarshamn, approximately 230 km south of Stockholm. It is dominated by a geological unit referred to as the Transscandinavian Igneous Belt (TIB). The bedrock is dominated by well preserved c 1.8 Ga intrusive rocks varying in composition between granite-syenitoid-dioritoid-gabbroid. Although a non-uniformly distributed faint to weak foliation is present, the most prominent ductile structures at Laxemar are discrete, low-temperature, brittle-ductile to ductile shear zones of mesoscopic to regional character, which are related to the waning stages of the Svecokarelian orogeny. Subsequently the rock mass has been subjected to repeated phases of brittle deformation, under varying regional stress regimes, involving reactivation along earlier formed structures. There are indications that the ductile anisotropy, including both larger ductile shear zones as well as the weak to faint foliation, minor shear zones and mylonites, has had an influence on the later brittle deformation. With few exceptions, the deterministically modelled deformation zones at Laxemar are characterised by brittle deformation although virtually all the zones have their origin in an earlier ductile regime. The timing of the initiation of brittle deformation is uncertain, but it is inferred that the bedrock at Laxemar had cooled below c 300ºC prior to the intrusion of the 1.70–1.65 Ga rocks in the western part of the TIB. Brittle conditions definitely prevailed at c 1.5 Ga, which imply that the Götemar and Uthammar granites, north and south of Laxemar, respectively, intruded into a brittle crust. Later brittle reactivation related to the far-field Sveconorwegian (1.1–0.9 Ga) and Caledonian (510–400 Ma) orogenies has been documented. The brittle history of the Laxemar-Simpevarp area is complex and involves a series of reactivation events that have prevented the construction of a consistent simplistic model covering their development.

Analysis and modelling of geological data

The geological work during the SDM Site Laxemar modelling stage has involved the continued development of deterministic models for rock domains (RSM) and deformation zones (ZSM), the identification and deterministic modelling of fracture domains (FSM), and the development of statistical models for fractures and minor deformation zones (geological discrete fracture network (DFN) modelling). The geological DFN model addresses fractures/structures with a size of less than 1 km, which is the lower cut-off of structures included in the deterministic modelling of deformation zones. In order to take account of variability in data resolution, deterministic models for rock domains and deformation zones are presented in both regional and local scale model volumes, while the geological DFN model is valid only within specific fracture domains inside the Laxemar local model volume.

The geological and geophysical data that constitute the basis for the SDM-Site Laxemar modelling work comprise all data that have been acquired from Laxemar, i.e. all data that were available at the data freeze for SDM-Site Laxemar at August 31, 2007. Selected quality controlled data from the complementary cored borehole KLX27A have also been utilised in the modelling work. Data from the following investigations were acquired during the complete site investigation between the data freezes for Laxemar 1.2 and SDM-Site Laxemar as defined above:

- A revised bedrock geological map at the ground surface.
- Geological and geophysical data from 40 new cored boreholes and 14 percussion boreholes.
- Sampling and subsequent modal and geochemical analytical work of bedrock samples taken in connection with excavations in southern Laxemar.
- Detailed mapping of fractures and rock units along 10 trench excavations and 2 large surface exposures (drill sites for KLX09 and KLX11A/KLX20A).

- Special studies involving more detailed characterisation of deformation zones identified in the geological single-hole interpretation, kinematics of brittle deformation in drill cores and outcrops, as well as studies with particular focus on minor deformation zones (MDZ) in both drill cores and in the field.
- Complementary geochronological and other rock and fracture analytical data.
- High resolution airborne laser scanning (LIDAR) leading to a new digital elevation model (DEM) together with high-resolution ground magnetic and resistivity data providing the basis for further lineament interpretations.
- Further seismic refraction surveys and reprocessing and re-evaluation of seismic reflection data.

The outputs of the deterministic modelling work are geometric models in RVS format for rock domains, deformation zones and fracture domains, including detailed property tables for rock domains and deformation zones and a description of fracture domains. The outputs of the geological DFN modelling process are recommended parameters or statistical distributions that describe fracture set orientations, sizes, volumetric intensities, spatial correlations and models, and other parameters (lithology and scaling corrections, termination matrices) that are necessary for building stochastic models.

Primarily due to the establishment of additional fixed point intersections for rock domain boundaries at depth provided by drilling investigations in boreholes, adjustments have been made to earlier regional and local rock domain models. These adjustments are essentially to be regarded as minor in character. Adjustments in the local deformation zone model are more significant, based largely on results from additional boreholes. A totally revised geological DFN model is presented based on the division of the rock mass into fracture domains, as compared to the previous model based on a subdivision of rock domains. Overall it is considered that all three geological models have made significant advances in relation to earlier versions and show improved stability.

Rock domains and deformation zones in the focussed volume

Rock domain RSMD01, which is strongly dominated by equigranular quartz monzodiorite (c 89%), and RSMM01, which is dominated by finely porphyritic Ävrö quartz monzodiorite (c 75%) and a relatively large amount of diorite/gabbro (c 16%), occupy the focussed volume at Laxemar. The calculated quartz content in the quartz monzodiorite in RSMD01 and the Ävrö quartz monzodiorite in RSMM01 is 13.0±3.0% and 13.9±6.4%, respectively. A non-uniformly distributed faint to weak foliation occurs in both domains. Characteristic subordinate rock types are fine-grained granite (c 5% in both domains), fine-grained diorite-gabbro (c 2% in both domains) and pegmatite (1.5 and 0.5%, respectively). Furthermore, the occurrence of dolerite is estimated to comprise 2% of the RSMD01 domain. However, dolerite is only documented in the cored boreholes KLX14A, KLX19A and KLX20A, is spatially associated with deformation zones (DZs) and is considered not to be evenly distributed throughout the RSMD01 domain. Alteration in RSMD01 outside DZs as seen in the extended single-hole interpretation (ESHI) comprises equal amounts of oxidation (red staining) and saussuritisation (c 10% of each), while oxidation dominates in RSMM01 (c 14%).

The regional scale ductile deformation zones strike NNE-SSW and NE-SW, are subvertical and are characterised by sinistral strike-slip displacements, while E-W oriented zones, though more strongly overprinted by brittle deformation, display moderate to steep dips to the south or north. The kinematics of the latter are not resolved at Laxemar, but E-W ductile shear zones in the Simpevarp subarea show complex kinematics, including both reverse and normal dip-slip as well as sinistral and dextral strike-slip displacements. It should be noted that the regional and local major deformation zones, although the majority have a ductile precursor, are mainly brittle in character.

The focussed volume is bounded in the west by the N-S oriented, steeply dipping deformation zone ZSMNS001C, in the south by the WNW-ESE oriented, moderately south-dipping ZSMNW042A, in the north by the E-W oriented, moderately north-dipping ZSMEW007A (cf. fracture domain FSM_EW007) and in the east by the the NE-SW oriented, steeply to subvertically dipping ZSMNE005A, the latter of which corresponds to the rock domain RSMP01. All these zones, with the exception of ZSMNE005A are mainly brittle in character and ZSMNS001C in the west are occupied by a dolerite dyke. The focussed volume is transected by a series of smaller deformation zones with a variety of orientations and with dips varying from sub-vertical to sub-horizontal. Apart from a characteristic increase in fracture frequency, most of the deformation zones at Laxemar commonly contain associated fault rocks, such as different types of cataclasites, breccias and fault gouge. All available evidence indicates that multiple episodes of deformation took place within a broadly-defined brittle regime under different physical conditions.

The thickness of the deformation zones, including the transition zone and core, inside the focussed volume are up to a few tens of metres. It is judged that the presence of undetected deformation zones inside the focussed volume, which are significantly longer than 3 km, is highly unlikely.

Fracture domains and geological DFN modelling

Fracture domains provide a large-scale conceptual framework for describing spatial heterogeneity in rock fracturing. The six identified fracture domains at Laxemar (FSM_C, FSM_EW007, FSM_N, FSM_NE005, FSM_S, and FSM_W) are for the most part bounded by deformation zones, and were identified using contrasts in relative fracture frequencies between orientation sets and between open and sealed fractures. The fracture domains exist inside a volume (the 'fracture domain envelope') smaller than the local model volume within which the density of LIDAR and ground-magnetic lineaments are approximately uniform. Patterns of relative fracture intensity inside each domain appear to correspond well to the tectonic history interpreted as part of the deformation zone modelling.

Bedrock fracturing outside of deformation zones at Laxemar can be described in terms of four distinct orientation sets: A sub-vertically-dipping, N-S striking set that appears to be the oldest; an ENE-WSW striking subvertically-dipping set; a WNW-ESE striking subvertically-dipping set; and a sub-horizontally- to moderately-dipping set of fractures that generally strike N-S to NNW (SH set). Fracture sizes are described according to a power-law (Pareto) distribution of equivalent radii, with parameters dependent on which set of model assumptions were used. The majority of the fractures encountered during drilling at Laxemar are sealed; open and partly open fractures make up from 15–45% of the fracture population in most cored boreholes.

The intensity of fracturing within a given fracture domain is described in terms of the average volumetric intensity P_{32} of a given orientation set. The spatial variability of fracture intensity outside of deformation zones follows either a Gamma or a Weibull distribution at scales greater than 9 m for the N-S, SH, and WNW sets, and at scales greater than 15 m for the ENE set. Fracture set intensity was not found to be a function of depth or rock domain at a given statistically significance level, although weak to moderate correlations between specific lithologies and fracture intensity was noted. Fractures locations can be approximated using a Poisson point process, and fracture sizes appear to scale in a Euclidean fashion.

Sammanfattning

Geologisk utveckling och geologiska processer

Laxemarområdet ligger i Oskarshamns kommun i östra Småland, ca 230 km söder om Stockholm, och domineras av en geologisk enhet som kalls det transskandinaviska magmatiska bältet (TMB). Berggrunden domineras av välbevarade, även om en ställvis svagt utbildad foliation förekommer, ca 1 800 miljoner år gamla intrusiva bergarter som varierar i sammansättning mellan granit, syenitoid, dioritoid och gabbroid. De mest påtagliga plastiska strukturerna i området utgörs av låggradiga, spröd-plastiska till plastiska skjuvzoner av lokal till regional karaktär, vilka är bildade i slutfasen av den svekokarelska orogenesen. Under en efterföljande utvecklingen har berggrunden utsatts för flera faser av spröd deformation under varierande spänningsförhållanden, vilka förutom bildandet av vissa nya även innebar reaktivering av redan existerande äldre strukturer. Det finns tydliga indikationer på att den plastiska anisotropin i berggrunden, innefattande såväl större som mindre skjuvzoner, myloniter och den svaga foliationen, har haft en påverkan och varit en styrande faktor för efterföljande spröda deformationer. Med få undantag karakteriseras och domineras de deterministiskt modellerade deformationszonerna i Laxemar av spröda strukturer, även om så gott som alla en gång bildades när berggrunden fortfarande reagerade plastiskt. Det är osäkert när under den geologiska utvecklingen som berggrunden började deformeras sprött, dvs. var kallare än ca 300ºC. Det antas dock att spröda deformationsförhållanden rådde i Laxemars berggrund innan de 1 700–1 650 miljoner år gamla bergarterna i västra delen av TMB bildades. Spröda förhållanden rådde dock definitivt för ca 1 500 miljoner år sedan, vilket innebär att Götemar- och Uthammargraniten, norr respektive söder om Laxemar, intruderade i en spröd jordskorpa. Spröda reaktiveringar av sprickor och deformationszoner som kan kopplas till de svekonorvegiska och kaledoniska orogeneserna har dokumenterats. Sammanfattningsvis kan det konstateras att den spröda deformationsutvecklingen i Laxemar-Simpevarpsområdet är komplex och omfattar en serie av reaktiveringar vilket försvårar möjligheten att utröna den sprödtektoniska utvecklingen.

Analys och modellering av geologiska data

Det geologiska arbetet under modelleringssteg SDM-Site Laxemar innefattar en vidarutveckling och förfining av de deterministiska bergdomän- och deformationzonsmodellerna, identifiering och deterministisk modellering av sprickdomäner, samt utvecklingen av statistiska modeller av spricknätverket och mindre deformationszonerks (geologisk DFN-modellering). Den geologiska DFN-modelleringen behandlar strukturer som är kortare än 1 km, vilken är den lägre gränsen för strukturer som skall modelleras deterministiskt. I syfte att ta hänsyn till dataupplösningen, presenteras deterministiska modeller för bergdomäner och deformationszoner både i en regional och lokal modellvolym, medan DFN-modelleringen gäller för varje enskild sprickdomän inom den lokala modellvolymen.

Det geologiska och geofysiska dataunderlaget för arbetet i modellversion SDM-Site Laxemar omfattar alla data som genererats från Laxemar, dvs. data som var tillängliga redan vid datafrysen för version Laxemar 1.2 den 1 november 2004 men framförallt alla nya data som var tillgängliga vid datafrysen för SDM-Site Laxemar den 31 augusti 2007. Utvalda kvalitetssäkrade data från det kompletterande borrhålet KLX27A har dock också använts i modelleringsarbetet. Följande data har genererats unde det kompletta undersökningsskedet mellan datafrysarna för Laxemar 1.2 och SDM-Site Laxemar:

- En uppdaterad berggrundsgeologisk karta.
- Geologiska och geofysiska data från 40 nya kärnborrhål och 14 hammarborrhål.
- Modal och geokemisk sammansättning av bergartsprover tagna i samband med grävningar i södra Laxemar.

- Detaljerad kartering av sprickor och bergarter utmed 10 jordavrymda diken samt 2 stora jordavrymda hällar (borrplatserna för KLX09 och KLX11A/KLX20A).
- Detaljerad karakterisering av deformationszoner identifierade i den geologiska enhålstolkningen, kinematiska studier av spröd deformation i borrkärnor och hällar, samt undersökningar fokuserade på mindre deformationszoner (MDZ) i såväl borrkärnor som i fält.
- Kompletterande geokronologiska data och andra analytiska data från bergarts- och sprickmineralprover.
- En detaljerad digital terrängmodell baserad på högupplösande flygburen laserskanning (LIDAR) och magnetiska data och resistivitetsdata från högupplösande markgeofysiska mätningar har legat till grund för fortsatta arbeten med identifiering av lineament.
- Omprocessering och omutvärdering av reflektionsseismiska data, samt data från refraktionsseismiska undersökningar.

Produkterna av den deterministiska modelleringen är geometriska modeller i RVS-format för bergdomäner, deformationszoner och sprickdomäner med tillhörande detaljerade egenskapstabeller för bergdomäner och deformationszoner. Utfallet av DFN-modelleringen är rekommenderade parametrar eller statistiska fördelningar som beskriver sprickgruppernas orientering, storlek, volymetriska intensitet, rumsliga korrelationer och modeller, och andra parametrar som är nödvändiga för att utveckla stokastiska modeller.

Nya data från tillkommande borrhål har inneburit en justering av tidigare versioner av bergdomänmodellen. De nya fixpunkterna för bergdomängränserna har dock enbart medfört mindre justeringar av geometrierna. Justeringarna i den lokala deformationzonsmodellen har dock varit mer betydelsefulla baserat på nya borrhålsdata. Den geologiska DFN-modellen är totalt reviderad då den nu är baserad på sprickdomäner och inte som i tidigare versioner på indelningen i bergdomäner. Sammanfattningsvis har alla tre geologiska modellerna förbättrats avsevärt och anses vara stabila.

Bergdomäner och deformationszoner i den fokuserade volymen

Den fokuserade bergvolymen i Laxemar utgörs av bergdomän RSMD01 som domineras av jämnkornig kvartsmonzodiorit (ca 89 %), och RSMM01 som domineras av småporfyrisk Ävrökvartsmonzodiorit (ca 75 %) men med en stor andel diorit/gabbro (ca 16 %). Den beräknade kvartshalten i kvartsmonzodioriten i RSMD01 och Ävrökvartsmonzodioriten i RSMM01 är 13.0±3.0 % respektive 13.9±6.4 %. En lokalt utbildad svag foliation förekommer i bägge domänerna. Karakteristiska underordnade bergarter är finkornig granit (ca 5 % i bägge domänerna), finkornig diorit-gabbro (ca 2 % i bägge domänerna) och pegmatit (ca 1.5 % i RSMD01 och 0.5 % i RSMM01). Vidare har mängden diabas uppskattats till ca 2 % i RSMD01. Diabas har bara dokumenterats i kärnborrhålen KLX14A, KLX19A och KLX20A, samt ett antal hammarborrhål, har en rumslig koppling till deformationszoner och bedöms inte vara en allmänt förekommande bergart i den fokuserade bergvolymen i Laxemar. Omvandlingen i bergmassan i RSMD01 utanför de deformationszoner som identifierats i den geologiska enhålstolkningen omfattar lika mängder oxidation (rödfärgning) och saussuritisering (ca 10 % av varje), medan oxidation dominerar i RSMM01 (ca 14 %).

De regionala plastiska deformationszonerna i området har en NNO-SSV- och NO-SV-lig strykning, är subvertikala och karakteriseras av sinistrala (vänsterhand) horizontalrörelser. De O-V-liga zonerna, vilka är kraftigare överpräglade av spröd deformation, uppvisar medelbranta till branta såväl nordliga som sydliga stupningar. Rörelsemönstret i de senare i Laxemar är osäker, men O-V-liga plastiska zoner i delområde Simpevarp uppvisar komplex kinematik, innefattande både normalrörelser och reversa rörelser samt sinistrala och dextrala horizontalrörelser. Det skall noteras att majoriteten av de regionala och lokala större deterministiskt modellerade deformationzonerna bildades under plastiska förhållanden, men att de drabbats av flerfasig spröd reaktivering och av denna anledning idag domineras och karakteriseras av spröda strukturer.

Den fokuserade volymen i Laxemar begränsas i väster av den N-S-liga, brant stupande deformationszonen ZSMNS001C, i söder av den VNV-OSO-liga, medelbrant mot söder stupande zonen ZSMNW042A, i norr av den O-V-liga, medelbrant mot norr stupande zonen ZSMEW007A (jfr sprickdomän FSM_EW007) och i öster av den NO-SV-liga, brant till subvertikalt stupande zonen ZSMNE005A, vilken motsvarar bergdomän RSMP01. Alla zonerna förutom ZSMNE005A domineras av spröd deformation och ZSMNS001C dessutom av en diabasgång. Den fokuserade volymen i Laxemar genomsätts även av ett antal mindre deformationszoner med varierande strykning och med stupningar som varierar från subvertikala till subhorisontella. De flesta deformationszonerna i Laxemar karakteriseras, förutom av ökad sprickfrekvens, även av förekomsten av förkastningsbergarter såsom olika typer av kataklasiter, breccior och skölar. Entydiga data pekar på att flera faser av spröd deformation under olika fysikaliska förhållanden påverkat berggrunden i Laxemar.

Tjockleken på deformationszonerna, dvs. övergångszonen tillsammans med själva zonkärnan, inom den fokuserade volymen är upp till några tiotals meter. Det bedöms att förekomsten av oupptäckta deformationszoner med en längd av mer än 3 km är högst osannolik.

Sprickdomäner och geologisk DFN-modellering

Sprickdomäner utgör ett storskaligt konceptuellt ramverk för att beskriva den rumsliga heterogeniteten i uppsprickningen av bergmassan. De sex identifierade sprickdomänerna i Laxemar (FSM_C, FSM_EW007, FSM_N, FSM_NE005, FSM_S, and FSM_W) begränsas företrädesvis av deformationszoner, och baseras på observerade skillnader i relativ frekvens av sprickor med olika orienteringar (sprickgrupper), samt skillnader mellan öppna och läkta sprickor. Sprickdomänerna omfattar inte hela den lokala modellvolymen utan enbart den del inom vilken lineament förekommer som identifierats med hjälp av såväl högupplösta, detaljerade topografiska (LIDAR) som markmagnetiska data förekommer. Den relativa sprickintensiteten inom varje domän relaterar väl till den tektoniska utvecklingshistorien som framkommit som del av deformationszonsmodelleringen

Uppsprickningen i berggrunden mellan deformationszonerna i Laxemar kan beskrivas med hjälp av fyra distinkta sprickgrupper: En N-S-lig, subvertikal sprickgrupp som bedöms vara äldst; en ONO-VSV-lig, subvertikal grupp; en OSO-VNV-lig, subvertikal grupp; och en subhorisontell till medelbrant stupande sprickgrupp som huvudsakligen stryker i N-S till NNV-SSO (SH grupp). Storleken på sprickorna beskrivs med en fördelning baserad på en potensfunktion (Pareto) där sprickorna antas vara cirkulära och med parametrar som beror på vilka modellantaganden som gjorts. Majoriteten av de karterade sprickorna i borrhålen i Laxemar är läkta. Öppna och delvis öppna sprickor utgör 15–45 % av sprickpopulationen i de flesta kärnborrhål.

Sprickintensiteten hos en sprickgrupp i en given sprickdomän beskrivs som medelvärdet av den volumetriska sprickintensiteten (sprickyta/volym) P_{32}. Sprickintensitetens rumsliga variabilitetet i bergmassan mellan deformationszonerna följer antingen en Gamma- eller en Weibullfördelning för skalor större än 9 m för de N-S-liga, VNV-OSO-liga och subhorisontella sprickgrupperna, och för skalor större än 15 m för den ONO-VSV-liga sprickgruppen. Sprickgruppernas intensitet har visat sig inte vara en funktion av djup eller bergdomän på en given statistisk signifikansnivå. En svag till måttlig korrelation mellan sprickintensiteten och vissa specifika bergarter förekommer dock. Lokaliseringen av sprickorna spatiellt kan approximeras med en punktprocess (Poisson) och en euklidisk skalning har visar sig bäst lämpad för sprickstorlek.

Contents

1 Introduction

1.1 Background

The Swedish Nuclear Fuel and Waste Management Company (SKB) is undertaking site characterisation at two different locations, the Forsmark and Laxemar-Simpevarp areas, with the objective of siting a geological repository for spent nuclear fuel. The investigations are conducted in campaigns punctuated by data freezes. After each data freeze, the site data are analysed and modelling work is carried out. A site descriptive model (SDM) is an integrated model for geology, rock mechanics, thermal properties, hydrogeology, hydrogeochemistry and transport properties, along with a description of the surface system.

So far, three full versions of a site descriptive model have been completed, Simpevarp 1.1, Simpevarp 1.2 and Laxemar 1.2. Version 0 /SKB 2002/ established the state of knowledge prior to the site investigation. Simpevarp version 1.1 /SKB 2004/, which essentially was a training exercise, was completed during 2004 and Simpevarp version 1.2 during 2005 /SKB 2005a/. The latter formed the basis for a preliminary safety evaluation (PSE) of the Simpevarp subarea /SKB 2005b/ and completed the initial site investigation stage (ISI) in the Simpevarp subarea. A preliminary repository layout (D1) for the Simpevarp subarea was presented in 2006 /SKB 2006a/. Laxemar version 1.2 was also presented in 2006 /SKB 2006b/ and this preliminary site descriptive model completed the initial site investigation stage (ISI). It formed the basis for a PSE of the Laxemar subarea /SKB 2006c/, a preliminary repository layout /SKB 2006d/, and the first evaluation of the long-term safety of this layout for a KBS-3 repository in the context of the SR-Can project /SKB 2006e/.

After the completion of the initial site investigations of the Simpevarp and Laxemar subareas /SKB 2005a, 2006b/, an evaluation of the site data from the two subareas, involving results from site modelling, repository layouts and preliminary safety evaluations was carried out. Based on this evaluation, a decision was made to continue with the complete site investigation (CSI) in the central, southern and western parts of the Laxemar local model area /SKB 2007/. Three modelling stages were initially planned for the complete site investigation work. An important component of each of these planned stages was to address and continuously try to resolve uncertainties of importance for repository engineering and safety assessment. However, due to re-planning of the modelling work, neither the modelling stage 2.1 nor 2.2 included an official delivery of any updated versions of the geological models. The primary objective of the geological modelling during stage Laxemar 2.1 /SKB 2006f/, was to analyse available new data at data freeze Laxemar 2.1 (June 30, 2005) in order to provide feedback to ensure that adequate geological information was obtained during the complete site investigation stage at Laxemar. However, in order to maximise the feedback to the site investigation, a successive evaluation of data that became available in the time period between June 30, 2005 and the end of March 2006 was also included in the Laxemar 2.1 modelling work. Based on an integrated analysis of all available site data, a decision was made at the end of 2006 to expand the focussed area of the site investigation southwards to include an additional area south of the Laxemar subarea. This decision also raised an urgent need for a complementary cored borehole to minimise the uncertainty in the final geological models in the focussed area/volume. The complementary borehole was approved and the outcome of this drilling has been considered in the the geological modelling work presented here. Hence, due to lack of critical data from southern Laxemar at the time for data freeze Laxemar 2.2 (December 31, 2006), a decision was made to allow the concluding geological modelling work to also include data from the final data freeze Laxemar 2.3 (August 31, 2007). The present modelling work based on data freeze Laxemar 2.3 is referred to as modelling stage SDM-Site Laxemar.

A synthesis of the geology at Laxemar will be presented within the framework of an integrated site descriptive model (SDM-Site). The SDM-Site main report constitutes the level I report (Figure 1-1), while the SDM-Site geology report presented here forms one of the basic

background reports (level II in Figure 1-1) for the main SDM-Site report. Level III reports for SDM-Site are also shown in Figure 1-1.

Since a description and modelling of the bedrock is important for the other geodisciplines, the present report is also intended to support the down-stream users in their modelling work, e.g. the thermal, rock mechanical and hydrogeological modelling teams.

1.2 Scope and objectives

The general aim of the bedrock geological modelling work at Laxemar was to establish a detailed understanding of the geological conditions and to develop models that fulfil the needs identified by the repository engineering and safety assessment groups during the site investigation phase. The specific aims of the geological modelling stage SDM-Site Laxemar were:

- To document the geology at Laxemar as a basis for the development of an updated repository layout (layout D2).
- To provide a geological basis for the modelling work by other teams, in particular hydrogeology, thermal properties, rock mechanics and hydrogeochemistry.
- To take account of the recently completed feedback from SR-Can /SKB 2006e/ that is relevant to the geological modelling work.
- To develop an understanding of the geological conditions at Laxemar with a focus on conceptual geological models for the site.

The work has involved the development of deterministic geological models for rock domains and the larger deformation zones, along with statistical models for fractures and minor deformation zones located between the larger deformation zones, and reporting of all the analytical and modelling work. The present report does not cover the Quaternary deposits, which is presented in a separate level II report of the surface system at Laxemar (see Figure 1-1).

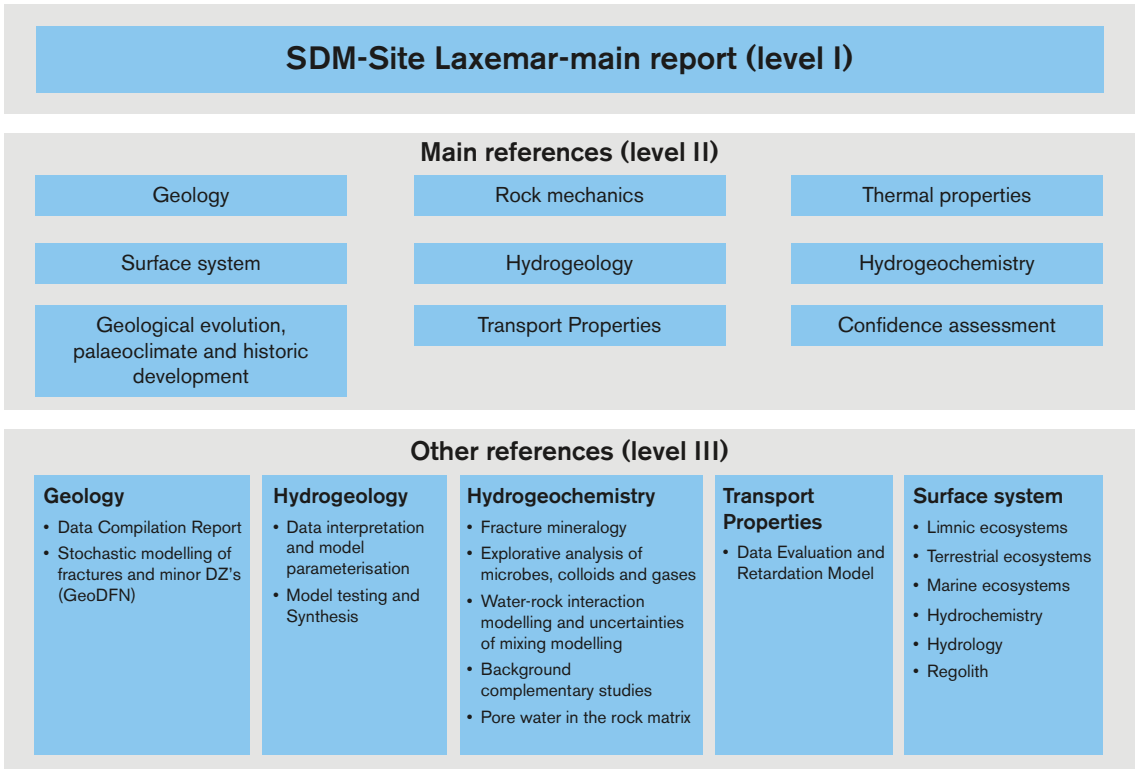

Figure 1-1. *Level I to level III reports planned during the analytical and modelling stage SDM-Site Laxemar.*

1.3 Regional geological setting

The Laxemar-Simpevarp area is located in eastern Småland within the municipality of Oskarshamn, approximately 230 km south of Stockholm. The investigation area is situated in the western part of one of planet Earth's ancient continental nuclei, referred to as the Fennoscandian Shield (Figure 1-2, /Koistinen et al. 2001/). The part of the shield where the Laxemar-Simpevarp area is situated is dominated by a geological unit referred to as the Transscandinavian Igneous

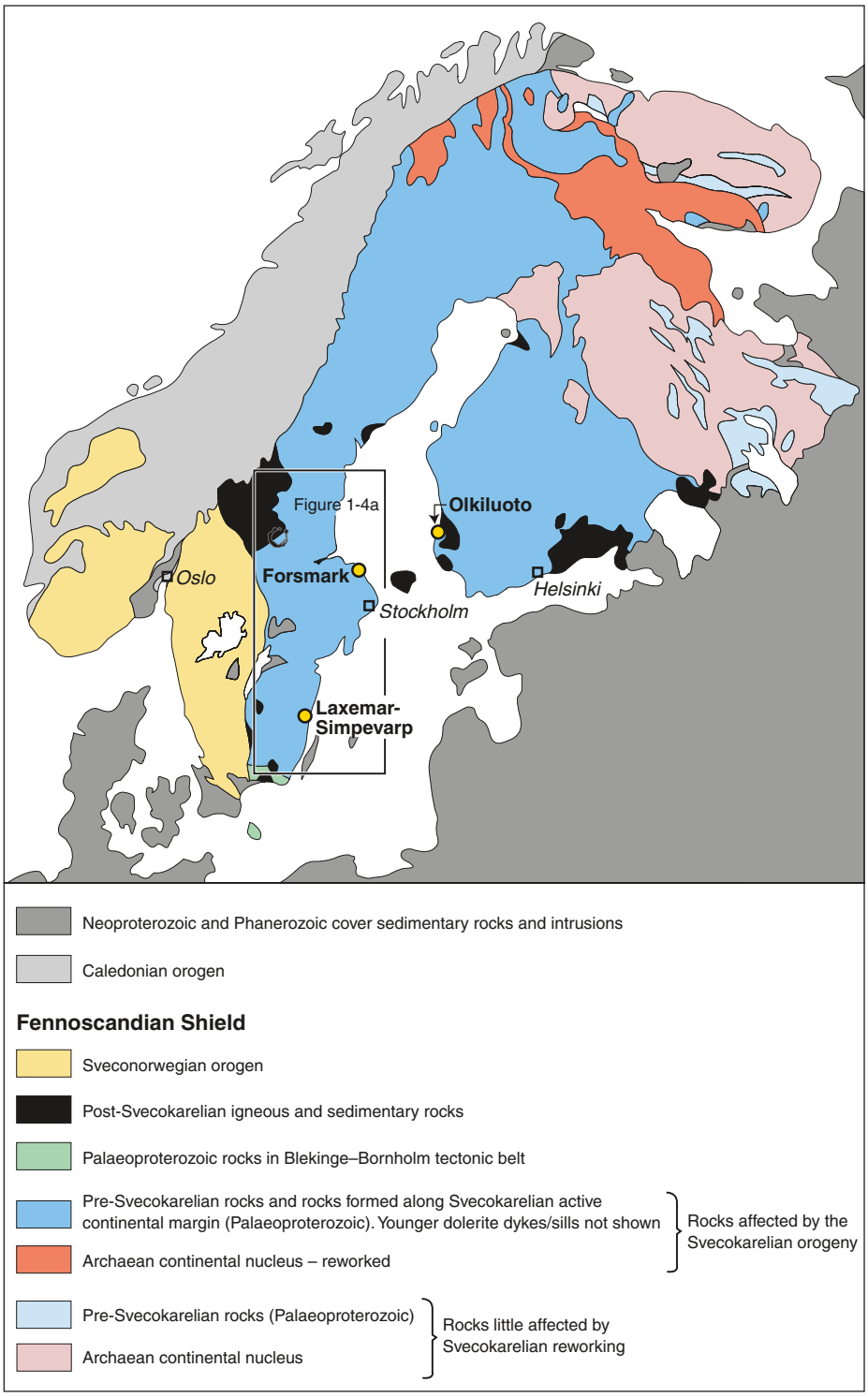

Figure 1-2. *Map showing the tectonic units in the Fennoscandian Shield (modified after /Koistinen et al. 2001/). The frame marks the geological reference area for the site investigations at Forsmark and Laxemar-Simpevarp.*

Belt (TIB; Figure 1-3). The bedrock in the latter is dominated by igneous rocks that formed in the time interval 1.86–1.65 Ga. As can be seen in Figure 1-4a, the bedrock in the geological reference area to the Forsmark and Laxemar-Simpevarp sites can be divided into 6 tectonic domains /Söderbäck 2008/. In contrast to the rocks in tectonic domains 1–4, the majority of the TIB rocks in tectonic domains 5 and 6 are more or less well preserved, except for those in domain 5 generated during the 1.86–1.84 Ga TIB event and rocks older than 1.80 Ga in domain 6. However, a non-uniformly distributed weak foliation, which is interpreted to be related to a late stage of the magmatic evolution as well as in the solid state, is commonly present in the TIB rocks in tectonic domain 5, as well as in tectonic domain 6. The most prominent ductile structures in the TIB, as well as in the Laxemar-Simpevarp area, are discrete, low-temperature, brittle-ductile to ductile shear zones of mesoscopic to regional character (Figure 1-4b). The ductile deformation in the TIB rocks in the Laxemar-Simpevarp area and the remaining part of tectonic domains 5 and 6, including the ductile shear zones, are related to the waning stages of the Svecokarelian orogeny.

As with other Precambrian shield areas, complex networks of brittle deformation zones transect the bedrock in the Laxemar-Simpevarp area. One of the challenges of the site investigation work, which presents abundant geological and geophysical data from both the surface and from depth, is to unravel the younger brittle deformational history of the Laxemar-Simpevarp area.

Laxemar is situated along the coast of the Baltic sea, in the southern part of tectonic domain 5 (Figure 1-4a, b). As mentioned above, the central, southern and western parts of the Laxemar local model area were selected as the focussed area during the complete site investigation work. As a consequence of the continuous evaluation and analysis of the new data that was generated from the ongoing site investigation, the focussed area was shifted southwards and now comprises the southern part of the Laxemar model area (Figure 1-4b).

1.4 Overview of the geological history

The bedrock in the Laxemar-Simpevarp area is dominated by 1.80 Ga intrusive rocks that formed during an intense period of igneous activity at the waning stages of the Svecokarelian orogeny. It comprises a suite of granite-syenitoid-dioritoid-gabbroid rocks that belong to the c 1.86–1.65 Ga Transscandinavian Igneous Belt. A non-uniformly distributed faint to weak foliation and discrete, low-grade, ductile to brittle-ductile shear zones are interpreted to have formed at a late stage and shortly after the emplacement and solidification of the magmas.

Around 1.76 Ga, the bedrock at Laxemar-Simpevarp cooled below c 500ºC. However, there remains a greater uncertainty concerning the cooling history after c 1.76 Ga, i.e. when did the bedrock pass through the brittle-ductile transition, i.e. the c 300ºC geotherm, in the crust and entered the realm of brittle conditions. The bedrock in Laxemar-Simpevarp is inferred to have cooled below c 300ºC prior to the intrusion of the 1.70–1.65 Ga rocks in the western part of the TIB. After a reheating event which may be related to the 1.65–1.47 Ga rapakivi magmatism, the final cooling of the bedrock below c 300ºC occurred around c 1.50 Ga. This implies that the c 1.45 Ga Götemar and Uthammar granites, north and south of Laxemar, respectively, were emplaced into a brittle crust. However, obtained $^{40}Ar/^{39}Ar$ biotite and amphibole ages in the range 1.45–1.43 Ga testifies to the local development of thermal aureoles around these granite intrusions.

The subsequent Precambrian geological evolution is dominated by deposition and erosion of sedimentary basins, local igneous activity and predominantly reactivation of existing structures in the crystalline bedrock, linked, for example, to orogenic events further to the west and south of the Laxemar-Simpevarp area. Intrusions of c 0.9 Ga dolerites /Wahlgren et al. 2007, Söderlund et al. 2008a/ as well as $^{40}Ar/^{39}Ar$ adularia /Drake et al. 2007/ and biotite /Page et al. 2007, Söderlund et al. 2008a/ ages of c 989 Ma and c 928 Ma, respectively, testify for the far-field effects of the 1.1–0.9 Ga Sveconorwegian orogeny in south-western Sweden. Furthermore, it has been inferred that this major tectonic event was associated with the development of a foreland sedimentary basin that covered central and southeastern Sweden /Larson et al. 1999/.

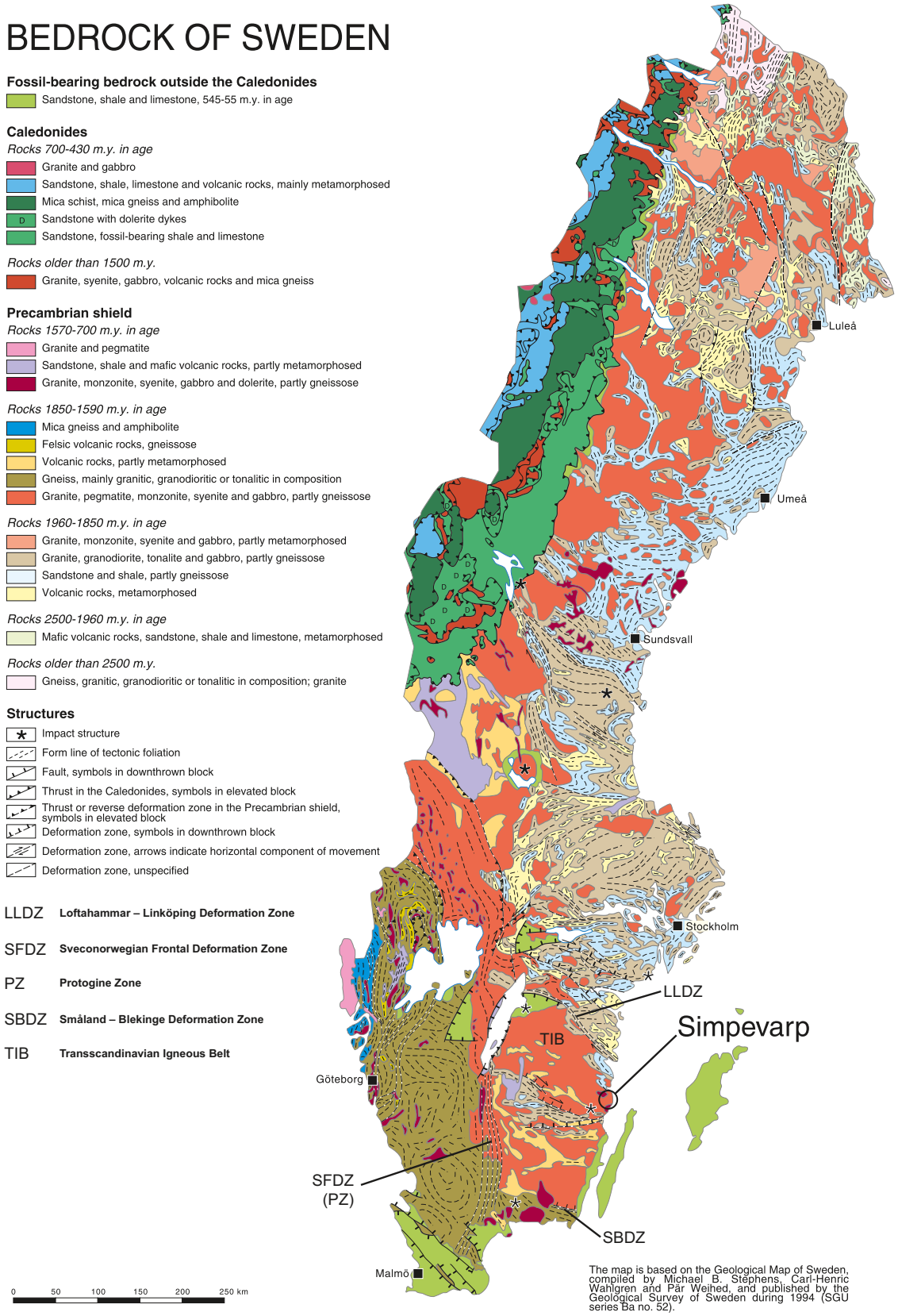

Figure 1-3. *Simplified bedrock map of Sweden. Modified after /Stephens et al. 1994/.*

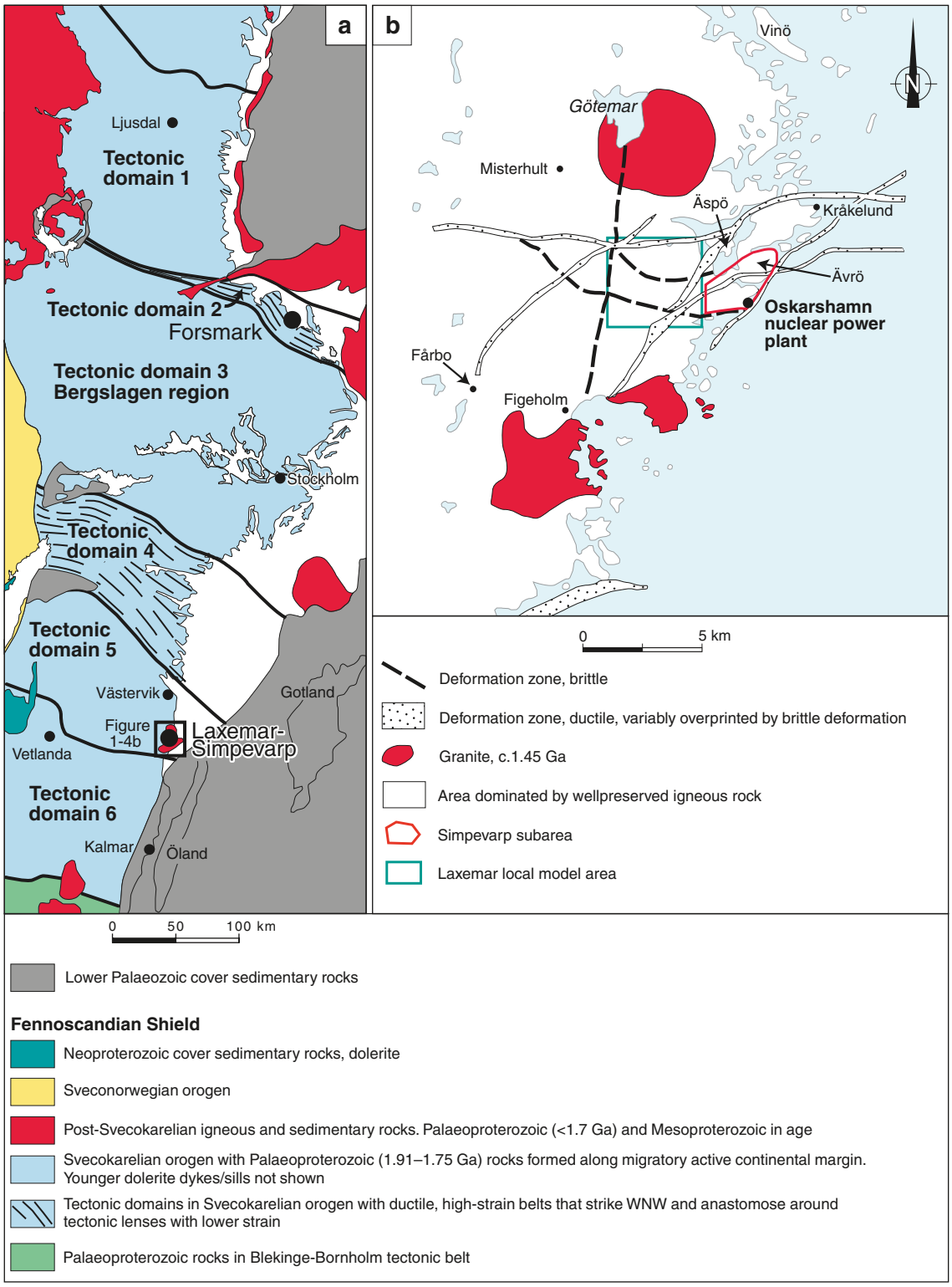

Figure 1-4. *(a) Map showing the tectonic domains in the geological reference area for the site investigations at Forsmark and Laxemar-Simpevarp. (b) Simplified map of the bedrock geology in the Laxemar-Simpevarp area and surroundings in tectonic domain 5. Only better established zones, predominantly in the area between Lake Götemar and Figeholm are shown on the map.*

Following erosion, a sub-Cambrian unconformity (peneplain) was established which has been identified over a large part of southern Sweden /Lidmar-Bergström 1996/, including the Laxemar-Simpevarp area (Figure 1-5). The latest part of the Precambrian and the early Palaeozoic in Scandinavia was characterised by the deposition of a sedimentary cover sequence which is inferred to have had a thickness of c 3 km /Söderlund et al. 2008b/. Evidence for Palaeozoic faulting in the Laxemar-Simpevarp area comprise the documentation of, 1) fractures filled with Cambrian sandstone that are overprinted by brittle deformation, 2) a fragment of Cambrian sandstone in the cored borehole KSH03A close to the hanging-wall of the NW-dipping deformation zone ZSMNE024A, and 3) $^{40}Ar/^{39}Ar$ ages in the range 448–401 Ma for adularia along fractures within and close to zone ZSMNE024A /Drake et al. 2007/.

The importance of post-Silurian faulting to the north, west and south of the tectonic domains 5 and 6 (Figure 1-4a) was emphasised by /Milnes et al. 1998/. This faulting can be exemplified by the inferred Permian faulting in the Lake Vättern area /Månsson 1996, Milnes et al.1998/. However, indications of significant displacements that are related to post-Silurian faulting is missing in south-eastern Sweden /Milnes et al. 1998/.

(U-Th)/He apatite isotopic data indicate that the exhumation rate at Laxemar slowed during the Jurassic to Cretaceous. In this context it is worth noting that the decreased exhumation rate could be related to the initiation of the marine transgression and the accompanying new loading of sedimentary material that took place in southernmost Sweden during the Cretaceous.

Alternating cold glacial and warm interglacial stages, and the associated loading and unloading cycles, have prevailed during the ongoing Quaternary period in Scandinavia /SKB 2005a/. Plate motion related to mid-Atlantic ridge push, in combination with glacial isostatic rebound following removal of the latest Weichselian ice sheet and crustal unloading, are the two geological processes that constrain current strain conditions in the crust in northern Europe /Muir Wood 1993, 1995/.

For a more comprehensive description of the geological evolution of the Laxemar-Simpevarp area, the reader is referred to /Söderbäck 2008/ and references therein.

Figure 1-5. *View of the sub-Cambrian peneplain (unconformity) in the Laxemar-Simpevarp area and the inspection of fractures that disturb this surface.*

1.5 General methodology and organisation of work

The geological analysis and modelling work conducted within the modelling stage SDM-Site Laxemar has been organised in the same general manner as for previous model versions. A core group and a GeoNet group addressed key geological issues and integrated the geological activities at both Forsmark and Laxemar-Simpevarp.

The site descriptive modelling comprises the iterative steps of identification, control and evaluation of primary data, descriptive and quantitative modelling in 3D space and an assessment of uncertainties. In the SDM-Site Laxemar modelling stage, the deterministic geological modelling of rock domains and deformation zones, the latter of which have a trace length longer than 1 km, and the statistical modelling of fractures and minor deformation zones, have made use of the guidelines given in the methodology report for geological site descriptive modelling /Munier et al. 2003/. Experience gained in previous modelling work and considerations of specific geological features in Laxemar have also played an important role. As for Forsmark, the development of a fracture domain concept and model for the site /La Pointe et al. 2008/ has formed the foundation for the statistical modelling of fractures and minor deformation zones (see Chapter 6).

In connection with the SDM-Site Laxemar geological modelling there has developed a need to carry out the following geological work which has generated separate SKB R-reports:

- Development of a data compilation report (DCR) for the site as a prerequisite for the statistical modelling of fractures and minor deformation zones. The results of this work are presented in /Hermanson et al. 2008/. It forms a level III report in the planning for SDM-Site Laxemar main report (Figure 1-1).
- Development of statistical geological DFN models for fractures and minor deformation zones in the parts of rock domains that are not affected by the more significant deterministically modelled deformation zones. The results of this work are presented in /La Pointe et al. 2008/. It also forms a level III report in the documentation for the SDM-Site Laxemar main report (Figure 1-1).
- Construction of deterministic geological models for rock domains and geologically more significant, deterministic deformation zones at the site. The results of this work form the focus of the present report. In order to provide the reader with a complete overview of the geological modelling work at the site, a summary of the fracture domain concept and model as well as the statistical modelling of fractures and minor deformation zones are also provided in this report. For the reasons outlined above, the present report forms the master geological report for modelling stage SDM-Site Laxemar and is a level II report (Figure 1-1).

In order to evaluate the possible influence of the c 1.45 Ga Götemar and Uthammar granites at Laxemar, a specific study complemented by gravity modelling and field studies of critical localities, has been carried out. The results of this study are presented in /Cruden 2008/. A synthesis of the structural evolution, with focus on the brittle structural evolution has been carried out by /Viola 2008/. Apart from the inclusion of necessary aspects for the conceptual understanding of rock domains, deformation zones and fracture domains, the geological evolutionary aspects are only briefly summarised in Section 1.3 in the current report. The geological evolution of the Laxemar-Simpevarp area is presented in detail in a separate level II report (Figure 1-1, /Söderbäck 2008/).

1.6 Structure of the report

Chapter 1 in the report includes a presentation of the scope and objectives of the SDM-Site Laxemar geological work. The first part of Chapter 2 summarises the primary geological and geophysical data that are available for model stage SDM-Site Laxemar. This chapter also presents an overview of previous geological modelling work and the context of the current work, defines the model volumes for the SDM-Site Laxemar geological modelling work, and addresses critical questions of nomenclature.

Chapter 3 presents an evaluation of the primary geological and geophysical data, with a focus on the new data that have been acquired since the Laxemar 1.2 modelling work. Geological mapping results and the recognition of rock units and possible deformation zones, especially at depth in boreholes, are addressed at the beginning of this chapter. This is followed by an evaluation of the character of rock types, ductile structures and brittle deformations and the kinematics of deformation zones. The final part of Chapter 3 addresses geophysical data, the interpretation of which is crucial for the geological modelling work. Focus here is on the geological significance of these indirect data. An evaluation of magnetic and topographical lineaments recognised with the help of the new high-resolution ground magnetic and LIDAR data, respectively, is followed by an evaluation of reflection seismic data, an analysis of refraction seismic data and an evaluation of radar reflection data from boreholes.

Chapters 4 and 5 address the modelling of rock domains and deterministic deformation zones, respectively. Relevant aspects of methodology, modelling assumptions and feedback from other disciplines, including SR-Can, are addressed in the initial parts. This is followed by a discussion of the conceptual understanding of the site, which forms an important input to the geometric modelling of both rock domains and deformation zones in the local model volume in the respective chapters. The implications for the already established regional models for rock domains and deformation zones, as well as the assessment of respective uncertainties, complete these two chapters.

Chapter 6 provides a summary of the statistical modelling of fractures and minor deformation zones inside fracture domains, which is presented in more detail in the DFN-report /La Pointe et al. 2008/. This chapter firstly summarises the concept, geometric model and broader context of fracture domains as presented in the DFN-report. This is followed by a short presentation of modelling assumptions, limitations, feedback from other disciplines, including SR-Can, and methodology. A summary of the geological DFN models in terms of the orientation, size, intensity and spatial distribution of fractures, including a presentation of parameter tables, is subsequently addressed. Finally, an evaluation of uncertainties and some recommendations to users of the geo-DFN are provided.

The main report is complemented by an extensive suite of appendices that are linked to various sections in Chapters 2 to 5. These appendices include a presentation of the available data used in modelling stage SDM-Site Laxemar and various types of data analysis and compilation that summarise the results of the modelling of rock domains and deterministic deformation zones. The reader is referred to the main report table of contents to get an overview of the content of each appendix. Appendices 10, 11 and 14 are of key importance. Appendix 10 presents a synthesis of the modelled rock domains, deformation zones and fracture domains in all cored boreholes analysed in model stage SDM-Site Laxemar. Appendices 11 and 14 present the properties of rock domains in the local model volume and descriptions and properties of the deterministic deformation zones, respectively.

2 Available data, previous geological models, model volumes and nomenclature

2.1 Overview of geological and geophysical investigations completed for model stage SDM-Site Laxemar and a summary of available data

The geological and geophysical data included in the SDM-Site Laxemar modelling work comprise all data that have been acquired from Laxemar, i.e. data that were already available at the data freeze for the modelling stage Laxemar 1.2 at November 1, 2004, but, in particular, additional new data that were available at the data freeze for SDM-Site Laxemar at August 31, 2007. However, selected quality controlled data from the complementary cored borehole KLX27A that was drilled in the autumn 2007 have also been utilised in the modelling work. Data from the following investigations were acquired during the complete site investigation between the data freezes for Laxemar 1.2 and SDM-Site Laxemar:

- Drilling of 40 new cored boreholes. The following boreholes have a borehole length varying between ca. 400 and 1,000 m: KLX07A, KLX08, KLX09, KLX10, KLX11A, KLX12A, KLX13A, KLX15A, KLX16A, KLX17A, KLX18A, KLX19A, KLX20A, KLX21B and KLX27A, while the following are shorter than ca. 200 m: KLX07B, KLX09B, KLX09C, KLX09D, KLX09E, KLX09F, KLX09G, KLX10B, KLX10C, KLX11B, KLX11C, KLX11D, KLX11E, KLX11F, KLX14A, KLX22A, KLX22B, KLX23A, KLX23B, KLX24A, KLX25A, KLX26A, KLX26B, KLX28A and KLX29A. The primary motivation for the longer boreholes was either to penetrate and characterise a modelled deformation zone or to characterise the bedrock between the deterministic deformation zones. All of the shorter boreholes except KLX07B and KLX14A were designed for either DFN analysis (KLX09B-F and KLX11B-F) or were carried out within the Minor Deformation Zone (MDZ) project (KLX22A-KLX29A), see Sections 3.12 and Chapter 6. Standard geological and geophysical data and extended single-hole interpretations (ESHI) exist for all these boreholes. Complementary analytical work (modal and geochemical analyses, petrophysical measurements, analyses of fracture mineralogy etc) has been carried out along some of the cored boreholes.
- Drilling of 14 new percussion boreholes (HLX30−HLX43). The motivation for the majority of the percussion boreholes has been to verify modelled deformation zones that are based on magnetic and topographical data, results from ground geophysical profile measurements etc.
- Sampling and subsequent modal and geochemical analytical work of bedrock samples taken in connection with excavations in southern Laxemar.
- Detailed bedrock and fracture mapping of 2 surface excavations (drill sites for KLX09 and KLX11A/KLX20A) and 10 excavated trenches.
- More detailed characterisation of deformation zones, including kinematic data that have been identified in the geological single-hole interpretation. Kinematic data have also been acquired from outcrops in both the Laxemar and Simpevarp subareas. Data exist from the cored borehole KSH03A in the Simpevarp subarea, and the cored boreholes KLX03, KLX04, KLX07A, KLX07B, KLX08, KLX09, KLX10, KLX11A, KLX12A, KLX13A, KLX15A, KLX16A, KLX17A, KLX18A, KLX19A, KLX20A and KLX21B in the Laxemar local model area.
- A special study to assess the sense of movement (kinematics) in ductile shear zones.
- Geochronological studies comprising $^{40}Ar/^{39}Ar$ and (U-Th)/He isotopic dating of minerals separated from whole-rock samples and $^{40}Ar/^{39}Ar$ data from minerals separated from fracture fillings.

- High-resolution ground magnetic measurements that cover the major part of Laxemar. Furthermore, detailed resistivity measurements have been carried out in central Laxemar and in three smaller areas in southern and western Laxemar.
- Refraction seismic measurements have been carried out along profiles that cover a large part of Laxemar.
- Low altitude aerial photographs have been acquired over Laxemar, as well as extremely detailed data for a digital elevation model (DEM) using an airborne laser scanning technique (LIDAR).
- A special study with the aim to identify and characterise minor deformation zones (MDZ). The study was based on the identified lineaments from the high resolution ground geophysical data and terrain models from the LIDAR data. The study also comprised focussed drilling of short cored boreholes (see first point above).
- Based on an evaluation of modal, geochemical and density data, supported by field observations in the outcrop database, an updated bedrock map at Laxemar has been compiled. The main difference from the bedrock map utilised in the Laxemar 1.2 modelling work is the definition of an area which is dominated by Ävrö quartz monzodiorite.
- Extended single-hole interpretation (ESHI) has been carried out for all boreholes, including boreholes in the Simpevarp subarea. The ESHI, as applied in Laxemar, mainly comprises the definition of new rock units in the boreholes where Ävrö granite has been subdivided in the two varieties, namely Ävrö quartz monzodiorite and Ävrö granodiorite to granite by use of density logs. Furthermore, an updating of the cored boreholes KLX02-KLX08 regarding existence of MDZ are also included in the ESHI.

The geological modelling work in SDM-Site Laxemar utilises the quality controlled data that is stored in the SKB databases Sicada and GIS at the time of and after the data freeze for SDM-Site Laxemar at August 31, 2007. A list of all available geological and geophysical data and a reference list of all the associated P- and R-reports are compiled in tabular format in Appendix 1. The prime purpose of these tables is to provide a reference and account of the data that were available and considered in the interpretation and modelling work. The primary data used in this work are described and evaluated in more detail in Chapter 3.

2.2 Overview of previous geological modelling work and the context of the current work

Previous geological modelling work comprises Simpevarp model versions 1.1 and 1.2 along with Laxemar versions 1.2 and 2.1. However, no geological models were constructed in connection with modelling stage Laxemar 2.1. Although the Laxemar subarea was included in the Simpevarp 1.2 model version, all available information was based on the SDM version 0. However, a crude geometry of the quartz monzodiorite dominated RSMD01 was established already in the Simpevarp 1.2 modelling stage /see also Andersson et al. 2002/.

A great step forward in the geological modelling work was achieved in modelling stage Laxemar 1.2, when a new detailed bedrock map of Laxemar and data from four new cored boreholes were available. The rock domain model presented in the modelling stage Laxemar 1.2 was considered as stabilising, and only minor modifications were expected from the outcome of the forthcoming drilling campaigns during the complete site investigation. In order to validate the Laxemar 1.2 rock domain model, it was utilised in predictions of expected intercepts of rock domain boundaries prior to drilling of new cored boreholes. In contrast to the rock domain modelling in Forsmark, no tectonic concept as a structural guidance for the modelling has been established in Laxemar-Simpevarp due to the well preserved magmatic character of the bedrock.

The modelling of rock domains was mainly based on combining the 2D rock domain boundaries at the surface with the defined rock domain boundaries at depth in the boreholes /SKB 2006b, Wahlgren et al. 2006a/. Gravity modelling based on both old and new gravity data acquired along a NNW-SSE profile across Laxemar supported the interpreted 3D geometry of rock domains as indicated from the sparse sub-surface borehole intercepts.

The deterministic modelling of deformation zones was stabilising in the Laxemar 1.2 model compared with the previous Simpevarp 1.2 model version. In particular, new surface reflection seismic, refraction seismic, magnetic, electric resistivity and electromagnetic measurements generated important data for the deformation zone model. However, considerable uncertainties still existed due to limited sub-surface data. Although targeted drilling campaigns, in combination with geophysical measurements, confirmed most of the modelled deformation zones in the Simpevarp 1.2 model, the lack of borehole intersections for most of the deformation zones at Laxemar made their characterisation and property assignment uncertain.

Considerable uncertainty remained after Laxemar model version 1.2 concerning the discrete fracture network modelling (DFN) mainly because of the relatively sparse sub-surface fracture data coverage over Laxemar and the lack of surface data in the trace length range 30–1,000 m. The uncertainties concerned the fracture size distribution, the fracture intensity and its variability, i.e. what controls small-scale fracturing at Laxemar and are these factors compatible with a 'rock domain' concept or does fracturing relate to other factors such as closeness to deformation zones? However, for the SDM-Site DFN model surface and sub-surface fracture data coverage has increased considerably and important progress has been achieved in the delineation of fracture domains that follow a large scale tectonic concept in line with the deformation zone model. A conceptual model of fracture domains at Laxemar has been developed, in a fashion similar to that at the Forsmark site during Stage 2.2 geological modelling. The fracture domain model constrains one of the primary uncertainties in the DFN models, fracture intensity, through the identification of structural domains where the primary characteristic is a relatively homogeneous intensity distribution among global orientation sets. The boundaries of the fracture domains are major deformation zones. The DFN model concept has been simplified through the introduction of a global orientation model across all identified fracture and rock domains. Analyses suggest that fracture intensity (and size, in a coupled size-intensity model) is far more important a discriminator than fracture orientation. The domain concept allows for the reduction of uncertainty in the spatial variation of fracture intensity. However, uncertainties in fracture size and local fracture intensity still remain to some degree, especially for gently dipping fractures which are difficult to assess from surface outcrops.

2.3 Model volumes

2.3.1 Regional model volume for deterministic modelling

The regional model area at the ground surface that is used for SDM-Site Laxemar modelling work is shown in Figure 2-1. This area extends downwards to an elevation of –2,100 m and up to +100 m. This volume is unchanged and identical to that used in model version 0 /SKB 2002/. The coordinates defining the regional model volume at the ground surface are (in metres):

RT90 (RAK) system; (Easting, Northing):

(1539000, 6360000)

(1539000, 6373000)

(1560000, 6373000)

(1560000, 6360000).

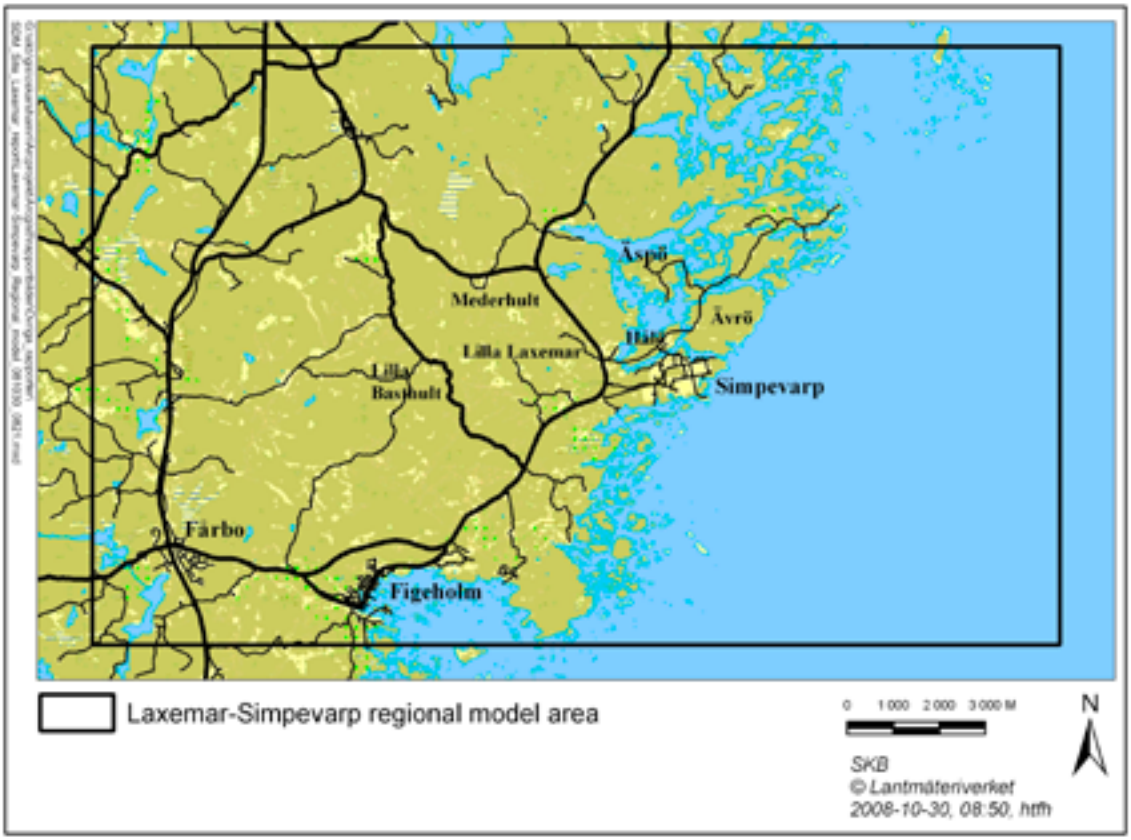

Figure 2-1. *Definition of the Laxemar-Simpevarp regional model area*

2.3.2 Local model volume for deterministic modelling

The local model volume for SDM-Site Laxemar (Figure 2-2) is focussed on the Laxemar area, and particularly on the southern and south-western parts to which the investigations were focussed during the complete site investigation. The local scale models of rock domains and deformation zones are integrated with those of the regional scale model. The model area has been extended southwards compared with version 2.1 to incorporate a greater volume of the quartz monzodiorite. The local model area extends downwards to an elevation of –1,100 m and up to +100 m. The coordinates for the local model area at the ground surface of SDM-Site Laxemar are:

1546150, 6368200 (unchanged from Laxemar model version 2.1)

1550390, 6368200 (unchanged from Laxemar model version 2.1)

1546150, 6364250 (new southern boundary)

1550390, 6364250 (new southern boundary).

2.3.3 Model volume for statistical modelling of fractures and minor deformation zones

The SDM-Site Laxemar geological DFN model utilises the same boundaries as the local model volume as a starting point, see Figure 2-2 and Section 2.3.2. However, the DFN model parameterisation is only valid for a smaller footprint named the fracture domain envelope (Figure 6-1 and Figure 6-2). The fracture domain envelope represents an area within the local model volume within which surface mapping of lineaments through high-resolution ground magnetic surveys and LIDAR topographic mapping is of approximately equal resolution. Outside of the fracture domain envelope, there are holes in the lineament map coverage. In particular, the area inside the new southward expansion of the local model volume is fairly sparse with respect to detailed lineament map coverage.

Figure 2-2. *Definition of the Laxemar local scale model area employed for SDM-Site Laxemar in relation to that used for model step L2.1 (hatched black).*

2.4 Nomenclature

Some definitions are provided here for terms that are crucial in the geological modelling work. The definitions below are based on the guidelines provided in /Munier and Hermansson 2001/ and /Munier et al. 2003/. The recognition of both rock domains for one purpose and fracture domains for another (see below) follows the guidelines presented in /Munier et al. 2003, p. 63/. In the following text, the general terms used in these reports have been more strictly defined in relation to the geological situation and the needs of other disciplines at Laxemar.

Rock unit (RU).

A rock unit is defined primarily on the basis of the composition, grain size and inferred relative age of the dominant rock type. Other geological features including the degree of bedrock homogeneity and the degree and style of ductile deformation also help define rock units. Both dominant rock type and subordinate rock types are defined for the rock units. The term rock unit is used in the bedrock mapping work at the surface (2D) and in connection with the SHI/ESHI work (essentially 1D). In the latter, rock units are referred to as RUxx, where the name of the rock unit is coupled to a single borehole. Thus, there is no unique name for the rock units at the site.

Rock domain (RD)

A rock domain refers to a rock volume in which rock units that show specifically similar composition, grain size, texture, degree of bedrock homogeneity, and degree and style of ductile deformation have been combined and distinguished from each other. The term rock domain is used in the 3D geometric modelling work and different rock domains at Laxemar are referred to as RSMxxx. The recognition of rock domains as defined here aims primarily to meet the needs of colleagues working in the disciplines of thermal modelling and rock mechanics.

Deformation zone (DZ)

Deformation zone is employed as a general notation of a structure along which there is a concentration of brittle, ductile or combined brittle and ductile deformation. In the SHI/ESHI work, deformation zones are referred to as DZxx, where the name is coupled to a single borehole.

Table 2-1 presents a terminology for brittle structures based on trace length and thickness adapted from /Andersson et al. 2000/. The estimated length of a zone takes account of the continuation of a zone outside the model volumes as well as the existence of different segments or splays of a zone.

Deformation zones that are longer than 1,000 m are modelled deterministically and are included in the deformation zone block models in RVS (Rock Visualization System). The letters NS, NE, EW and NW provide an indication of the strike of the zones. They are used as simple guidelines without any coupling to the dip direction of the zone. Deformation zones recognised in the ESHI that have an inferred thickness greater than 10 m, but have not been linked to other features such as surface lineaments or other boreholes, have been modelled as disks. The disk geometry has a standard 564 m radius based on an area equivalent to a 1,000 m × 1,000 m square and an applied inferred true thickness and orientation. This series of modelled zones has been named following the original ESHI source data, namely borehole and possible DZ number to facilitate traceability KLXxx_DZxx.

For a discussion on deformation zone thickness, see Section 5.3.2 in the present report.

Minor deformation zone (MDZ)

A hypothetical thickness-length relationship based on deterministic deformation zones suggests that a zone with a true thickness < 10 m has a length < 1,000 m (Figure 5-33). All possible deformation zones that have been identified in a single borehole (i.e. through ESHI) and have an estimated thickness ≤10 m are termed minor deformation zones (MDZ). Minor deformation zones are not modelled deterministically in RVS, but are handled stochastically in the GeoDFN modelling.

Table 2-1. Terminology and geometrical description of the brittle structures in the bedrock based on /Andersson et al. 2000/. The boundaries between the different structures are approximate.

Terminology	Length	Thickness	Geometrical description
Regional deformation zone	> 10 km	> 100 m	Deterministic
Local major deformation zone	1 km–10 km	10 m–100 m	Deterministic
Local minor deformation zone	10 m–1 km	0.1–10 m	Stochastic
Fracture	< 10 m	< 0.1 m	Stochastic

Fracture domain (FD)

A fracture domain refers to a rock volume outside major deformation zones in which rock units show similar fracture characteristics. For this modelling, we have focussed on fracture intensity as basis for domain definitions. Fracture domains at Laxemar are defined on the basis of the ESHI, i.e. modifications and extensions including identification of minor local deformation zones (MDZ), as presented in /Hermanson et al. 2008/.

The fracture data associated with deformation zones; a) those modelled deterministically in RVS, and b) possible minor local deformation zones (MDZ), i.e. all possible deformation zones which have been identified in the SHI, are excluded from the fracture domains for the purpose of initial assessment of fracture domain characteristics (eg. relative fracture intensity). In the ensuing geological DFN analysis the possible minor local deformation zones are reintroduced, but are represented by a single fracture.

The term fracture domain is used in the first instance as a basis for the discrete fracture network modelling work (geological DFN). The different fracture domains at Laxemar are referred to as FSM_XXXXX. The recognition of fracture domains as defined here is also of relevance to colleagues working in the disciplines of hydrogeology, hydrogeochemistry and rock mechanics.

Discrete fracture network (geological DFN)

A discrete fracture network model or geological DFN involves a description of the fracturing in the bedrock on the basis of a statistical model, which provides geometries, directions and spatial distributions for the fractures within defined fracture domains.

3 Evaluation of primary geological and geophysical data

3.1 Surface and borehole mapping including BIPS, radar and geophysical logs

3.1.1 Surface mapping

All data from bedrock mapping at the surface were available in connection with model version Laxemar 1.2 and an evaluation of these data was presented in /SKB 2006b, Wahlgren et al. 2006a/. Apart from surface samples and description of the bedrock that were collected in connection with excavations in southern Laxemar /Bergman et al. 2005, Sohlenius et al. 2006/, detailed fracture and bedrock mapping of excavated outcrops and trenches (see Section 3.6.1), as well as kinematic studies of selected outcrops (see Section 3.7), no new surface geological data have been produced in the time interval between the datafreezes for modelling stages Laxemar 1.2 and SDM-Site Laxemar (datafreeze Laxemar 2.3). Instead, the work has focussed entirely on generating data from the sub-surface by mapping and complementary studies of cored and percussion drilled boreholes.

3.1.2 Borehole mapping including BIPS, radar and geophysical logs

The geological mapping complemented by radar and geophysical loggings of the boreholes, generate valuable sub-surface data that are of utmost importance for geological characteristics such as rock type, rock alteration, ductile deformation (e.g. foliation, ductile shear zones) and brittle deformation (fractures). These data provide input to the geological SHI/ESHI work (see Section 3.3).

The total length of cored boreholes (including the telescope drilled part) that have been used for model version SDM-Site Laxemar is c 20 950 m. However, data are only available from c 18,155 m, since no core data exist from the uppermost telescope drilled part of the boreholes, usually the upper c 100 m. The locations of the boreholes are shown in Figure 3-1. Data from cored boreholes KLX05, KLX06, KLX07A, KLX07B, KLX08, KLX09, KLX09B, KLX09C, KLX09D, KLX09E, KLX09F, KLX09G, KLX10, KLX10B, KLX10C, KLX11A, KLX11B, KLX11C, KLX11D, KLX11E, KLX11F, KLX12A, KLX13A, KLX14A, KLX15A, KLX16A, KLX17A, KLX18A, KLX19A, KLX20A, KLX21B, KLX22A, KLX22B, KLX23A, KLX23B, KLX24A, KLX25A, KLX26A, KLX26B, KLX27A, KLX28A and KLX29A complement the data used in the Laxemar 1.2 modelling work. All boreholes, except cored boreholes KLX01, KLX02, KLX04, KLX07B, KLX09, KLX09B, KLX10, KLX11B, KLX13A and KLX18A (inclination 80–90º), were drilled with an inclination between 50º and 75º. Complementary data from the percussion drilled boreholes HLX01 through HLX43, with a total borehole length of approximately 6,400 m are also available (Figure 3-1). These boreholes are typically of length < 200 m and were drilled primarily to investigate lineaments and deformation zones. Technical information obtained in conjunction with the drilling activity, including the coordinates of the drill site (borehole collar coordinates) and the length, bearing, inclination and diameter of the borehole, have been presented in a series of reports (see Appendix 1).

The oriented image logs along each borehole obtained using the Borehole Image Processing System (BIPS) are complemented by directional borehole radar and geophysical logs. The relevant data reports for all these logs are listed in Appendix 1. A summary of the data that have been generated in the geophysical logging work can be found in /SKB 2006b, Section 5.2.8, or Wahlgren et al. 2006a, Section 2.4.4/.

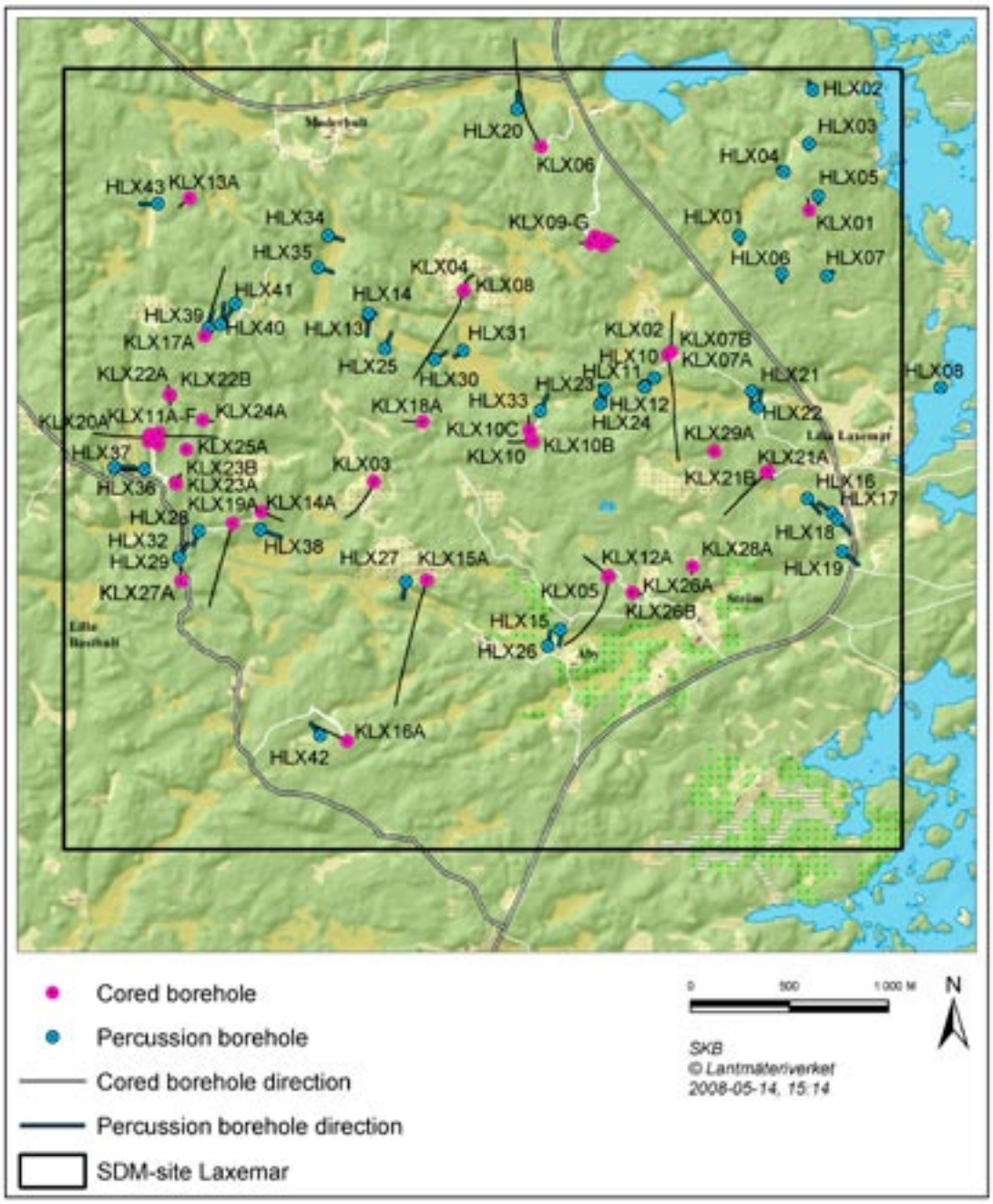

Figure 3-1. *Location of drill sites and boreholes at Laxemar from which data were available for model version SDM-Site Laxemar.*

All the cored and percussion drilled boreholes have been mapped using the Boremap methodology adopted by SKB. The mapping of the cored boreholes comprises an integrated interpretation of the drill core and the BIPS image, while the mapping of the percussion boreholes is mainly based on the BIPS image complemented by analysis of drill cuttings. The associated reports are listed in Appendix 1. In contrast to planar structures, for example, fractures, rock contacts, foliations etc, linear ductile structural data are not documented, primarily because ductile linear structures are very rare in the bedrock at Laxemar and have not been observed in the drill cores. Furthermore, no routine similar to that applied for planar structures exists to measure linear structural features in a systematic manner in the boreholes. However, shear striae along fault planes (slickensides) have been documented and measured in selected fractures with the help of fracture orientation data from Boremap and a drill core holding device, which allows the drill core to be oriented correctly in 3D space.

Due to the restricted quality of the data from the percussion boreholes, emphasis is given in the geological modelling work, as in earlier model versions, to data from the cored boreholes. Data from the percussion boreholes have primarily been used to help assist in the recognition of rock units and possible deformation zones in the SHI/ESHI (see Section 3.3) and as a support for establishing the existence of deterministically modelled deformation zones (see Chapter 5). The relevant data reports relating to the percussion boreholes are listed in Appendix 1.

3.1.3 Borehole orientation data – sources of error and uncertainty

Data derived from cored boreholes drilled across the Laxemar regional and local model areas are key elements in the site description. The cored borehole logs are used to describe the locations, orientations, morphological, chemical, and hydrologic properties of various rock mass structures (fractures, deformation zones, dykes, veins, foliation, etc). Fracture orientation data are of particular importance, as both the geological DFN and the hydrogeological DFN are based on the division of fractures by orientation set.

The question of uncertainties in borehole orientation data has been addressed extensively in previous SKB reports /Munier and Stigsson 2007/ and /Stigsson 2007/. Users of orientation data from cored borehole data are encouraged to consult both references. This section represents a summary of the salient points and conclusions from these reports.

Due to the importance of orientation data to the SDM, it is necessary to address factors that lead to uncertainty in the identification and parameterisation of the orientation of geologic structures at Laxemar. Uncertainty in the cored borehole data record can be divided into two distinct categories:

- Uncertainty in the location, orientation, and diameter of the borehole in space; and
- Uncertainty in the orientation values measured of fractures, lithologic contacts, and other geologic structures identified in the borehole.

The orientations of fractures in the cored borehole record contained within the Sicada database are affected by both categories of uncertainties.

Uncertainty in borehole location and diameter

Fracture, foliation, and lithology contact orientations in cored boreholes are derived in part from borehole (BIPS) image logs. Fractures, foliations, and lithological contacts will be displayed on the image logs as a sinusoidal curve, from which the strike and dip of the structure in space can be calculated. This calculation requires that the locations and orientations of both the borehole and the logging tool in space be known with a high level of confidence.

Fracture orientations are derived from two angles (illustrated below in Figure 3-2) measured during BHTV logging:

- α, the angle between the fracture plane or geologic structure and the core axis; and
- β, the angle between the fracture plane or geologic structure and a reference line along the core.

When fractures are mapped on the BIPS image logs, both α and β are derived from the amplitude of the sinusoid created by the intersection of a planar feature with a circular borehole. The calculation of α and β from the curve amplitude requires that the diameter of the borehole be known. To turn the relative angular deviations α and β into structure strike and dip, the orientation of the borehole and the reference line in space must also be known.

At Laxemar, several different tools have been used to measure the geometry of boreholes during site investigations. These tools rely on a combination of optical sensors, sensitive magnetometers, and accelerometers to measure the trajectory of the borehole in space /Nilsson and Nissen 2007, Stenberg and Håkanson 2007/. Small-scale angular deviations, caused by variations

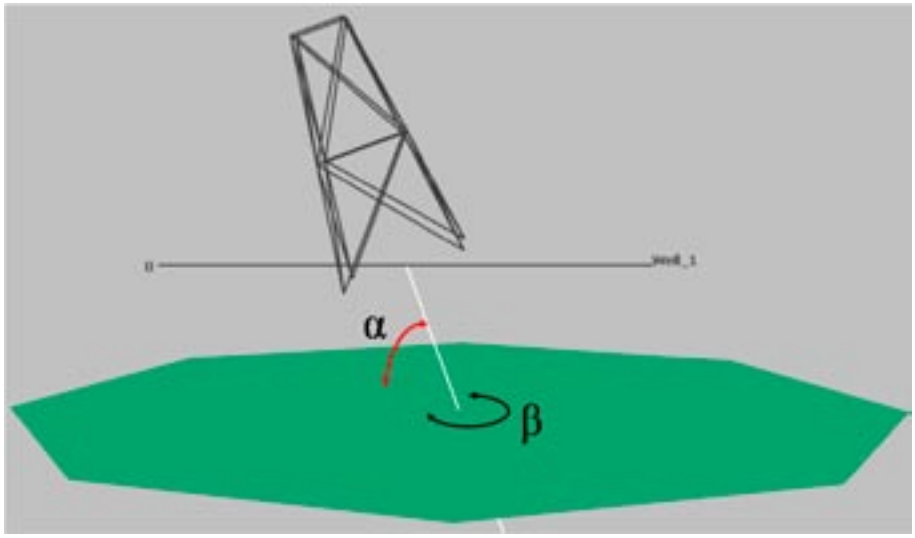

Figure 3-2. *Illustration of α and β angles measured during core drilling.*

in the local magnetic field due to magnetic rocks, variability with time in the geomagnetic field due to solar storms or induced currents from power plants or electrical cables (HVDC), and electrical interference inside the logging tool from other instruments, can all result in considerable changes in the measured borehole azimuth (particularly in steeply-dipping boreholes) /Munier and Stigsson 2007/. The uncertainty in borehole orientation is directly transferred to uncertainty in fracture and other geologic structure orientations, as they are measured as angular deviations from the orientation of the borehole or the logging tool.

Variability in the actual diameter of the borehole can also lead to uncertainty in the measured orientations of geologic structures. Most cored boreholes at Laxemar were drilled as 76 mm diameter holes. However, as with all drilling methods, variability in rock strength, drilling conditions, and repeated passes through the hole can result in sections of the borehole becoming slightly larger than 76 mm. If the borehole diameter is larger than the assumed 76 mm diameter, then the values of α and β (termed α' and β') calculated from the sinusoid amplitude will be incorrect. Figure 3-3 illustrates this issue.

Finally, the location and orientation of the BIPS logging tool must be known with confidence to be able to convert relative angular measurements α and β into strike and dip. The orientation of the BIPS image is determined by using either a magnetic compass or a clinometer built into the logging tool. BIPS tool orientations made using the two-axis magnetometer were vulnerable to local deviations caused by rock units with high magnetic susceptibility and by inertial lag of the compass needle in the instrument. BIPS tool orientations made using the original steel-ball clinometer are also susceptible to inertial lag. The steel-ball clinometer was replaced with an air-bubble level system which increased instrument accuracy /Munier and Stigsson 2007/. As both methods are dependent on the tool operator paying close attention to the magnetometer or the level, human error is also a factor /Munier and Stigsson 2007/.

Uncertainty in measured orientations of geologic structures

The identification and classification of rock types, fractures, and geologic structures in boreholes is only partly dependent on image logs. Teams of geologists, geophysicists, and geological engineers examined thousands of meters of drill core as part of single-hole interpretations (SHI) during the Oskarshamn site investigations. However, the same team members did not map every single borehole. As a result, an additional uncertainty is introduced; different scientists can potentially assign different orientations to the same fracture. This uncertainty is problematic for fractures that are visible in the physical drill core, but not in the BIPS images; there is no independent 'check' on the orientation of the fracture plane or rock contact as assigned by the geologist.

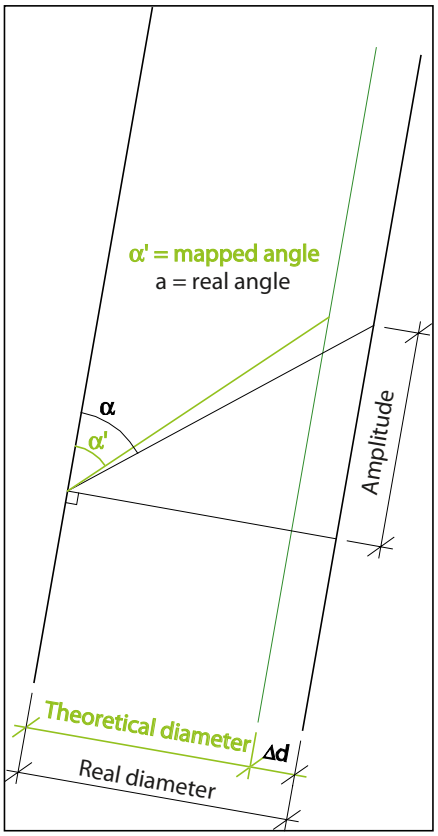

Figure 3-3. *Schematic illustration showing the mapped angle α' in relation to the real angle α (from /Munier and Stigsson 2007/).*

The potential impacts of different mapping standards for different mapping teams have been previously addressed by /Glamheden and Curtis 2006/. The authors chose two drill cores, one each from the Forsmark and Laxemar sites, and compared how two different teams mapped the same cores. Their conclusions were that, though the number of fractures and their orientations were fairly consistent between the two teams, there were important differences in how fractures not visible in BIPS were handled, as well as how fracture apertures (open, partly open, and sealed) were assigned.

The study by /Glamheden and Curtis 2006/ did not directly address orientation uncertainty; however, an algorithm developed by Nissen and Stigsson (Internal SKB document, see /Munier and Stigsson 2007/) was used to couple fractures mapped by one team to those mapped by a second team through the use of secondary fracture characteristics (mineralogy, aperture, position along the borehole). This study concluded that the uncertainty in orientation due to mapping protocol differences between teams was equal to one-half of the difference in orientations (i.e. the 'correct' orientation is approximately the average of both teams' measurements of the same feature).

Handling orientation uncertainty in data derived from cored boreholes

Orientation uncertainty in cored borehole data has been handled by the inclusion of α and β angles in the Sicada database for geological structures and contacts, and by the creation and inclusion of an average orientation uncertainty factor Ω. Ω is a composite measurement that encompasses the combination of the maximum uncertainty of α and β together /Munier and Stigsson 2007/. A maximum value for Ω of 10º, expressed as a dihedral angle from the estimated orientation of the fracture normal vector, was recommended as a cut-off for inclusion of a geologic structure in an orientation analysis /Munier and Stigsson 2007/. This recommendation was used in both the GeoDFN and HydroDFN models.

In addition, due to large uncertainties of the orientations of fractures not visible in the BIPS image logs, it was recommended that GeoDFN and HydroDFN modelling efforts not use fractures marked 'Not Visible in BIPS' in the development of fracture orientation models /Munier and Stigsson 2007/. It is important to note that visibility in BIPS is a parameter assigned only to rock fractures and not to rock contacts or ductile deformation structures, e.g. foliation.

3.2 Bedrock geological map on the ground surface

A bedrock geological map of the Laxemar-Simpevarp area at the scale 1:10,000 was compiled prior to, and was an important input to, the Laxemar 1.2 model version. A description of the bedrock geological map, including the rock type distribution and ductile structures, is presented in /Wahlgren et al. 2005, Wahlgren et al. 2006a, SKB 2006b/. However, an updated version of the combined bedrock geological map /Wahlgren et al. 2006c/ has been utilised in the SDM-Site Laxemar rock domain modelling work. The main modification compared with the older version of the bedrock geological map, is the definition of an area that is dominated by Ävrö quartz monzodiorite, i.e. a quartz poor variety of the Ävrö granite in the Laxemar local model area (Figure 3-4). The updating of the bedrock geological map was considered an important milestone for the subsequent division in rock domains and the accompanying property assignment.

The updating procedure made use of all locations where modal, geochemical and density data exist for the Ävrö granite, together with the preliminary field classification from the bedrock mapping, as stored in the outcrop database /Persson Nilsson et al. 2004/ in Sicada. In the remaining part of the Laxemar local model area it is generally not possible to divide the Ävrö granite in quartz monzodioritic (Ävrö quartz monzodiorite) from granodioritic (Ävrö granodiorite) or granitic varieties in the bedrock map due to insufficient analytical data coverage. In the remaining part of the area, the term Ävrö granite has therefore been retained, i.e. it displays a compositional variation from granite to quartz monzodiorite, including granodiorite (cf. Figure 3-9). For the division of the Ävrö granite in its different subvarieties in the boreholes, see Section 3.3.4. The updating of the bedrock geological map by defining an area dominated by Ävrö quartz monzodiorite is of utmost importance for the refinement of the rock domain model (see Section 4.3). Furthermore, the near surface recognition of dolerite in the cored borehole KLX20A and in the percussion boreholes HLX36, HLX37 and HLX43 (Figure 3-1) along the deformation zone ZSMNS001C (see Chapter 5) in the westernmost part of Laxemar, implies that the dolerite is reasonably continuous, at least along this segment of the deformation zone ZSMNS001C. Although the dolerite is not exposed due to thick glacial cover in the topographical depression along ZSMNS001C, it is anticipated that it forms the bedrock surface and, therefore, is marked on the bedrock geological map. It should be noted that a few thin dolerites have been observed in outcrops at Äspö /Wikman and Kornfält 1995/.

The major groups of rocks in the Laxemar-Simpevarp area are distinguished on the basis of their composition, grain size, texture and relative age. The nomenclature of the rock types and associated rock codes used by SKB in the Oskarshamn site investigation is presented in Appendix 2. The character of individual rock types is addressed in more detail in Section 3.4. Rock units shown on the bedrock geological map (Figure 3-4) consist of various rock types and are distinguished on the basis of the character of the dominant rock type. For example, the rock unit shown with a light pink colour on the bedrock geological map (Figure 3-4) is dominated by quartz monzodiorite but it contains different subordinate rock types as well.

The bedrock geological map also distinguishes areas which are characterised by a high frequency of low-grade ductile shear zones (dotted pattern in Figure 3-4), i.e. areas that are more strongly affected by ductile strain than the country rock in general.

In Table 3-1, the relative ages of the rock types in the Laxemar-Simpevarp area are displayed. Apart from the younger dolerite and the Götemar and Uthammar granites, the remaining rock types presented in Table 3-1 are formed more or less synchronously, though field relationships reveal their relative age.

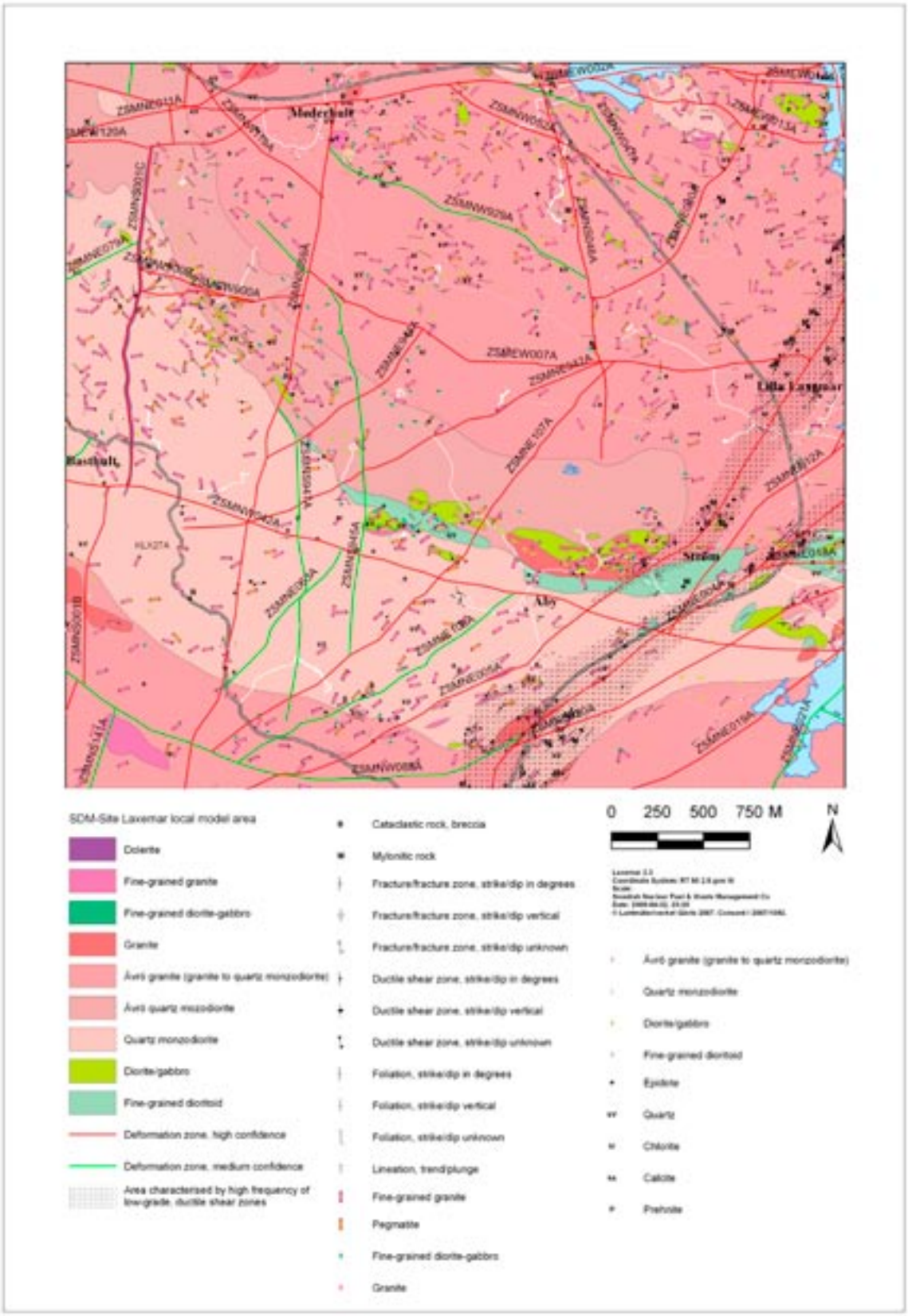

Figure 3-4. *Bedrock geological map of the Laxemar local model area.*

Table 3-1. Relative age relationships between igneous rock types in the Laxemar-Simpevarp area, based on field relationships. Obtained radiometric ages are also displayed. SKB rock codes for each rock type are shown within brackets.

Rock type	Relative age	Obtained U-Pb zircon or $^{40}Ar/^{39}Ar$[a] age
Dolerite (501027)	Youngest	c 900[a] Ma
Götemar and Uthammar granites (521058)		c 1,450 Ma
Fine-grained granite (511058) and pegmatite (501061)		c 1,800 Ma
Fine-grained diorite-gabbro (505102)		
Granite, equigranular (501058)		
Ävrö granite (501044) / Ävrö quartz monzodiorite (501046) / Ävrö granodiorite (501056)		1,800±4 Ma
Quartz monzodiorite (501036)		1,802±4 Ma
Diorite-gabbro (501033)		
Fine-grained dioritoid (501030)	Oldest	

3.2.1 Assessment of probable and possible dolerite dykes at Laxemar

Dolerite dykes may have important implications for the hydrogeological modelling since they may have considerable hydraulic significance. Although these dykes have not been observed in any outcrop at Laxemar, dolerite is encountered in a number of cored and percussion boreholes in western Laxemar, namely KLX14A and HLX38 along deformation zone ZSMNS059A; KLX20A, HLX36, HLX37 and HLX43 along deformation zone ZSMNS001C and also in KLX19A and HLX13. In order to investigate and try to predict the possible existence of dolerite dykes at Laxemar additional to those already documented in the boreholes, a special study has been carried out /Triumf 2007/. The prime aim of the activity was to try and distinguish lineaments at Laxemar, based on magnetic and topographical data, which possibly could reflect occurrences of additional dolerites. The magnetic susceptibility of the dolerites generally is lower than the average susceptibility of the country rock. Furthermore, documentation of the dolerites in the boreholes shows that they are commonly strongly fractured, which implies that the dolerites are more susceptible to erosion than normally fractured country rock. Accordingly, it is evident that the potential dolerites have the same signature in magnetic data and digital terrain models as fracture zones.

From the observed characteristics of the documented dolerite dykes in Laxemar and in the Oskarshamn region as a whole, a number of criteria, primarily strike direction, strike length and visibility in magnetic data and terrain models, were chosen for the prediction work. The application of the above mentioned criteria to the lineaments that have earlier been identified resulted in the identification of sixteen lineaments. Two of these are intersected by boreholes and are known to contain dolerite, whereas the remaining fourteen lineaments are classified as “possible” regarding the likelihood that dolerite, at least in part, may be the cause of the anomaly. Furthermore, five new short lineaments were identified adjacent to boreholes KLX19A and HLX13 due to their spatial connection to the dolerites found in these boreholes. However, the latter lineaments did not match the criteria specified. The lineaments that are predicted to possibly be associated with dolerites are displayed in Figure 3-5.

It must be noted that the uncertainty in the prediction of the possible existence of additional dolerite dykes at Laxemar is high, since fracture zones and ductile to brittle-ductile shear zones have the same character, particularly in the magnetic data set but also in the digital terrain

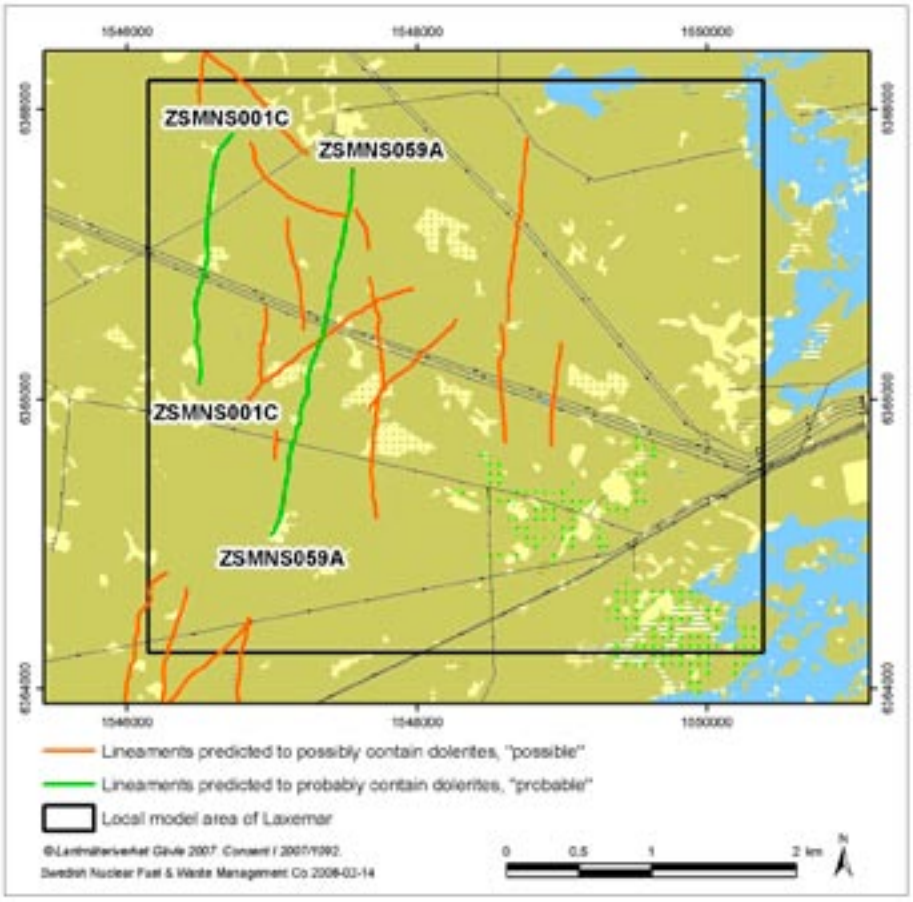

Figure 3-5. *Lineaments that are predicted to possibly contain dolerite at Laxemar.*

models, as the dolerite dykes are strongly fractured.and therefore more easily eroded. However, it is very plausible that additional dolerites do exist, since it is unreasonable that the only existing dolerites are those intersected by the boreholes. Other than the dolerite in KLX20A that is c 30 m thick, the dolerites have a thickness varying between 1 decimetre and a couple of metres. Consequently, it is inferred that any additional dolerites are thin and constitute a very subordinate rock component at Laxemar. However, due to their structural character, i.e. planar, highly fractured, close association with deformation zones, they are considered as an important rock type at Laxemar. For further information and description of the dolerites in deformation zones, see ZSMNS001C and ZSMNS059A in Appendix 14.

For a more detailed description of the assessment of additional dolerites in Laxemar, see /Triumf 2007/.

The occurrence of gently dipping thrusts in the Simpevarp region, as reported by /Nordenskjöld 1944/, has been an important issue for a long time. According to /Talbot and Ramberg 1990/, these thrusts are instead gently dipping sill-like dolerites, e.g. at Hälleberg north-west of the Götemar granite /Talbot and Ramberg 1990/. Another sill-like dolerite, which is related to a nearby dolerite dyke, was observed in the southern margin of the Uthammar granite. The possibility that any major gently dipping dolerite exist at Laxemar is considered to be unlikely, since dolerite, except for the occurrence in the inclined boreholes KLX14A, KLX19A and KLX20A (see above), has not been observed in any of the longer, sub-vertical cored boreholes. However, the possible existence of thin, gently dipping dolerites cannot be eliminated.

3.3 Rock units and deformation zones in the sub-surface – single-hole interpretation

3.3.1 Aims and approach

The single-hole interpretation (SHI) provides a synthesis of all geological and geophysical data from a borehole. It forms an important link between all the detailed borehole data that are generated and the subsequent geological modelling work. It therefore has a similar role to the bedrock map that forms an important intermediate step between the detailed outcrop data generated at the surface during the bedrock mapping and the site descriptive modelling work. The SHI aims to document rock units with a minimum length (size) of 5 m along the borehole as well as all possible deformation zones that intersect the borehole, i.e. define fixed data points at depth for the subsequent rock domain and deterministic deformation zone modelling. Note that these geological features are unique to each borehole, i.e. rock unit 1 (RU1) in one borehole may not correspond to RU1 in another borehole. In addition to the analysis of all available base data, an inspection of the drill core is also carried out in connection with the SHI work. Correlation of the geological data from the SHI and the surface information forms an important step in the 3D modelling work (see Sections 4 and 5).

The following base data have been used as input in the SHI work:

- Geological mapping data obtained using BIPS and the Boremap system.
- Directional borehole radar data and their interpretation.
- Geophysical logs and their interpretation.

The confidence in the interpretation of rock units and possible deformation zones along the borehole is addressed on the following confidence scale: 3 = high, 2 = medium, 1 = low. According to the SKB methodology applied for the SHI, the identification of possible deformation zones is based solely on geological and geophysical criteria, i.e. neither rock mechanical data nor the occurrence of groundwater-bearing fractures have played any role in the identification process. The significance of the possible zones from a rock mechanical or hydrogeological point of view needs to be addressed separately.

In Stage 1 of the SHI work, rock units and possible deformation zones in each borehole are identified and described in a series of P-reports (see Appendix 1) and the information is stored in the Sicada database. The dominant and subordinate rock types and, if appropriate and characteristic, the ductile and brittle structures, alteration of the bedrock and petrophysical characteristics, e.g. density, of the dominant rock type, are documented for each rock unit. Furthermore, the following features are addressed along each possible deformation zone:

- The geological and geophysical criteria used to identify the possible deformation zone (see Section 3.3.3).
- The orientation and aperture of fractures in the zone.
- The rock types affected by the zone.

Information from Stage 1 of the SHI is available in Sicada for all of the 45 cored boreholes and for 28 percussion boreholes included in model version SDM-Site Laxemar (Figure 3-1). Note that original SHI has been updated for all boreholes in the Laxemar-Simpevarp area (see Section 3.3.4). SHI of KLX27A was carried out in late January 2008. Although not stored in the Sicada database at the time, the outcome of the SHI of this complementary cored borehole has been evaluated in order to optimise the geological modelling work.

Stage 2 of the SHI work comprises a more detailed description of the characteristics of possible deformation zones, which have been recognised with high confidence. The following characteristics are described along many of the possible deformation zones and the kinematic data are included in the Sicada database:

- The occurrence of core intervals along each zone.
- The presence or absence of fault rocks and, if present, the character of such rocks.

- Relative time relationships between fractures with different mineralogy.
- The presence or absence of shear criteria (kinematic data).
- The sense of displacement derived from the kinematic data.

Information from Stage 2 was available in Sicada for many of the possible deformation zones in KLX03, KLX04, KLX07A, KLX07B, KLX08, KLX09, KLX10, KLX11A, KLX12A, KLX13A, KLX15A, KLX16A, KLX17A, KLX18A, KLX19A, KLX20A and KLX21B.

In order to illustrate the evolving interpretation from base data to SHI, geological and geophysical key data are presented jointly with the identified rock units and possible deformation zones in WellCad diagrams for each borehole in Appendix 3 (cf. Figure 3-6), except KLX01 that has not been re-mapped by the Boremap methodology.

More information on the methodology used to identify rock units and possible deformation zones is presented in Sections 3.3.2 (rock units) and 3.3.3 (possible deformation zones) below. The results of the Stage 2 work are evaluated separately in Section 3.7.

3.3.2 Rock units

Rock units (RU) have been defined primarily on the basis of the composition, grain size and texture of the dominant rock type. However, identification of rock units can also be based on a more or less complex mixture of rock types. These characteristics are identical to those used in the definition of rock types and rock units at the surface, in connection with the compilation of the bedrock geological map (see Figure 3-4). The identified rock units extend over the entire length in each borehole and, hence, include also the borehole intervals where possible deformation zones are identified.

Rock units are identified primarily by use of the Boremap data sets on rock type and rock occurrence. The data sets used are included in the WellCad diagrams for each cored borehole (Appendix 3) and in the example shown in Figure 3-6. In KLX08, RU1 is distinguished from RU2, although both rock units are dominated by finely porphyritic Ävrö granite, on the basis of the frequent occurrence of diorite-gabbro in the latter rock unit. RU3 is distinguished solely on the basis of rock composition and texture, i.e. the total dominance of equigranular quartz monzodiorite. The petrohysical parameters; silicate density, natural gamma radiation and magnetic susceptibility logs are also studied, as additional support for the rock classification. In all rock units where Ävrö granite constitutes an important rock type, the density log has always been studied and the variation in density is documented in the description of the rock units. Since there is a strong correlation between density and mineralogical composition of rocks, the density logs have been utilised for subdividing the Ävrö granite into its different subvarieties (see description of the extended single-hole interpretation, Section 3.3.4).

Apart from the cored boreholes KLX05, KLX06 and KLX09, rock units in the complementary cored boreholes that have been completed after the data freeze for model version Laxemar 1.2 are characterised by either dominant Ävrö granite, quartz monzodiorite or a more or less high frequency of diorite-gabbro in a dominant Ävrö granite, as exemplified in KLX08 (Figure 3-6). These conspicuous rock units in the boreholes have had great impact and form the basis for the recognition of sub-surface rock domains in the modelling work (see Section 4.3).

3.3.3 Possible deformation zones

Possible deformation zones (DZ) have been identified in the SHI of the boreholes that have been drilled during the complete site investigation and are available for model version SDM-Site Laxemar. Brittle deformation zones are dominant and have been identified primarily with the help of the geological and geophysical data sets; fracture frequency, rock alteration, occurrence of fault rocks (such as cataclasites and breccia), resistivity, single point resistivity, p-wave velocity, caliper and magnetic susceptibility. Some deformation zones are primarily characterised by low-grade ductile deformation as evidenced by occurrence of mylonitic and

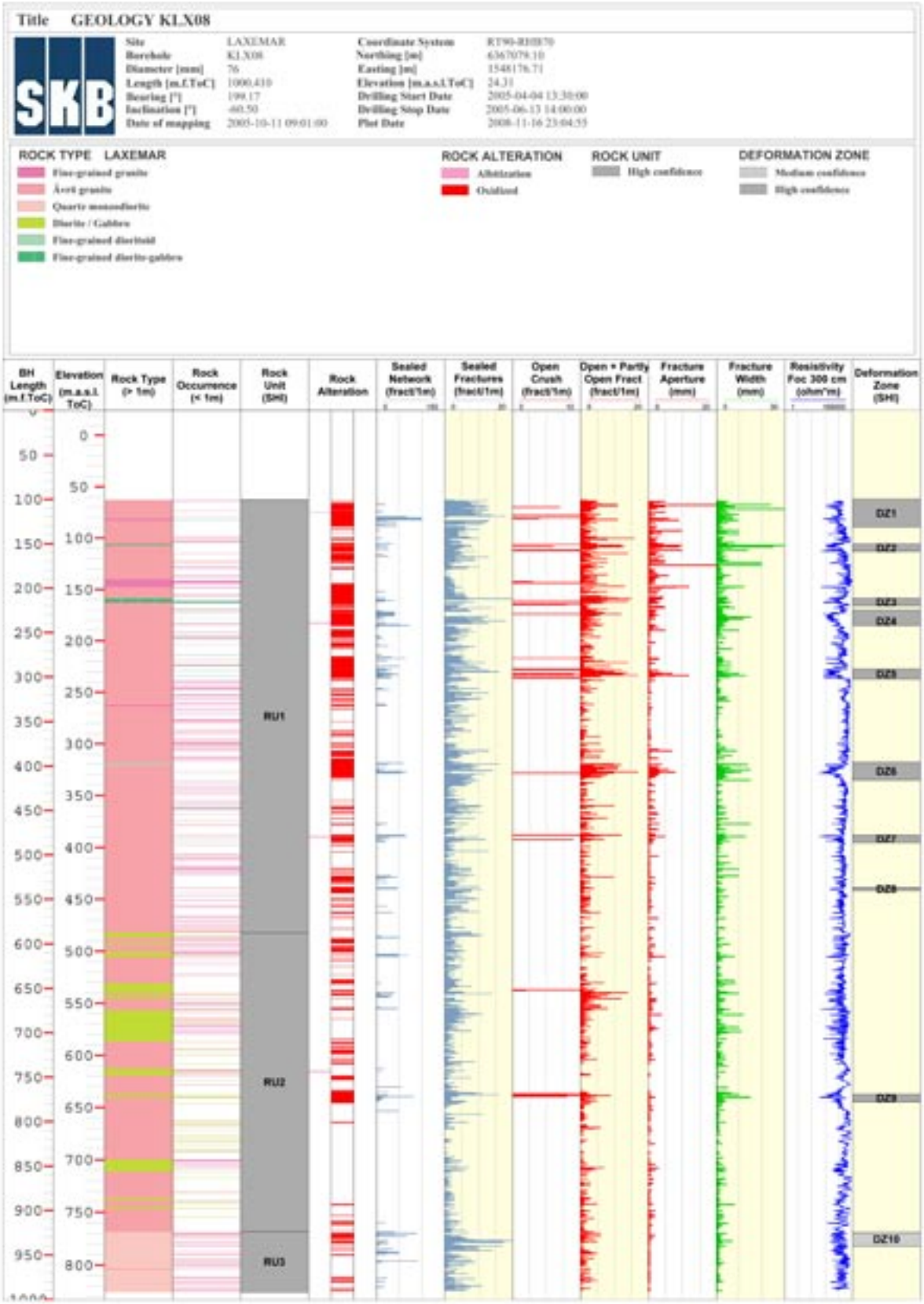

Figure 3-6. *WellCad diagram for the cored borehole KLX08, showing a selected suite of base geological and geophysical data that have been used to identify rock units and possible deformation zones in the SHI of this borehole (see text for further description).*

protomylonitc foliation. Many of the more prominent deformation zones that are dominated brittle deformation, display evidence for having been originally formed during ductile conditions, but have subsequently been reactivated by one or several phases of brittle deformation. However, deformation zones that are purely brittle in character also exist.

Sealed fractures, sealed fracture networks, open and partly open fractures, and crush zones are treated separately in the characterisation of the deformation zones. The type of alteration that is most prominent along the zones is referred to in the Sicada database as "oxidation" (see also Section 3.4.4) but is commonly referred to as "red staining". The latter is mainly caused by minute inclusions of mainly hematite, which are hosted in porous secondary K-feldspar and albite, completely replacing primary plagioclase. Accompanying this alteration is replacement of magnetite by hematite, causing a decrease in magnetic susceptibility, and of biotite by chlorite, the formation of secondary sericite, prehnite, titanite and epidote, and a general increase in porosity and decrease in density. Thus, it is emphasised that integration of geological and geophysical data form the basis in the identification of possible deformation zones during the SHI work. Furthermore, the geophysical data play a more significant role in the SHI of percussion boreholes, where the geological data are of poorer quality, primarily attributable to the lack of drill core (see Section 3.1.2).

Besides an increased frequency of sealed fractures, sealed fracture networks and commonly also an increased frequency of open fractures, many of the deformation zones at Laxemar are characterised by the occurrence of fault rocks. Cataclasites are most common but breccias and fault gouge occur as well. Fracture frequency along cored boreholes, and fracture orientation and mineralogy along possible deformation zones in the cored boreholes are addressed in more detail in Section 3.6.

The identification of possible deformation zones along the boreholes provides fixed points in the sub-surface for the modelling of deformation zones in 3D space. In contrast to rock units, all the identified possible deformation zones constitute a direct input to the modelling work (see Chapter 5).

3.3.4 Modification of the single-hole interpretation in connection with geological modelling and extended single-hole interpretation work

The methodology for SHI was revised during the Laxemar modelling work. The updated methodology (SKB MD 810.003 v. 3.0, SKB internal controlling document) comprised an increase in resolution and an optional inclusion of kinematic analyses. The modification and updating of the SHI in connection with the SDM-Site Laxemar modelling work, the so-called extended single-hole interpretation (ESHI), which replaces SHI both in terms of methodology and data, comprise the following two activities:

- Subdivision of the Ävrö granite in the two subvarieties Ävrö quartz monzodiorite and Ävrö granodiorite, i.e. in a quartz poor and quartz rich variety, respectively. This activity includes all borehole intervals in which the Ävrö granite constitute a dominant rock type.
- Identification of possible minor deformation zones (MDZ) in the cored boreholes KLX02 (200–1,000 m), KLX03, KLX04, KLX05, KLX06, KLX07A, KLX07B and KLX08 (the corresponding identification of MDZs in subsequent boreholes (after KLX08A) is included as part of the SHI).

As has been stated in all previous SDM reports, i.e. model versions Simpevarp 1.1 and 1.2 /SKB 2004, 2005a/ and Laxemar 1.2 /SKB 2006b/, including the geological background report /Wahlgren et al. 2006a/, the Ävrö granite is a complex body which shows large compositional variations. This variation made the property assignment for the rock domain RSMA01 difficult and also the effective handling of this rock domain in e.g. the thermal, rock mechanical and hydrogeological modelling work. As mentioned in Section 3.2, an area dominated by Ävrö quartz monzodiorite has been defined in the updated bedrock geological map of the Laxemar-Simpevarp area. A similar subdivision of the Ävrö granite has been carried out in all cored and percussion boreholes (including the Simpevarp subarea) in which Ävrö granite constitutes an

important rock type. In this context the density logs from the boreholes were used as the most important data set, supported by available modal and geochemical data from the drill cores. An evaluation of available geological data, supported by thermal and rock mechanical data from the Laxemar 1.2 modelling stage, indicated that a density of 2,710 kg/m^3 should be used as a threshold value for separating Ävrö quartz monzodiorite from the quartz richer Ävrö granodiorite in the boreholes. The result of this subdivision of the Ävrö granite implied that rock units that previously were characterised as dominated by Ävrö granite in general were classified as dominated by either Ävrö quartz monzodiorite or Ävrö granodiorite or separated into two or several new rock units. This subdivision constituted a great step forward and has had a fundamental impact on the refinement of the rock domain model in the Laxemar local model volume (see Chapter 4).

From KLX09 and onwards, definition of possible minor deformation zones (MDZ) was included in the SHI. Since fractures that are related to deformation zones are not included in the data sets utilised in the modelling of the discrete fracture network (DFN), there was a great need to update the SHI of earlier cored boreholes with a particular focus on the identification of minor deformation zones. The working strategy for this work is described in Section 3.12 and is in accordance with the updated instructions for SHI with a higher degree of resolution (SKB MB 810.003, version 3.0).

All updating of the SHI in boreholes according to the two activities mentioned above has been delivered to and is stored in the Sicada database as ESHI. In order to avoid confusion, even data in the boreholes where no updating work was necessary have been transferred to the ESHI database, i.e. ESHI has replaced SHI in all boreholes in the Laxemar-Simpevarp area. All analyses and evaluations that have been carried out in connection with the SDM-Site Laxemar modelling have utilised the ESHI that exists in Sicada.

The rock units and possible deformation zones from the ESHI, together with rock domains (RSM), deformation zones (ZSM) and fracture domains (FSM) are shown for the cored boreholes in Appendix 10.

Data evaluation and modelling work during model stage SDM-Site Laxemar have made use of the following deliveries of ESHI from the Sicada database: Sicada_07_326 and Sicada_07_350_2.

3.4 Rock type

3.4.1 Character of rock type based on surface and borehole data

In order to improve the characterisation of the dominant rock types in the Laxemar local model volume, in comparison to the model stage Laxemar 1.2, modal and geochemical analyses of fresh samples have been carried out on samples from KLX04, KLX06, KLX07A, KLX07B, KLX08, KLX09, KLX10, KLX11A, KLX12A, KLX14A, KLX15A, KLX16A, KLX18A, KLX19A, KLX20A and KLX21B /Wahlgren et al. 2006b, 2006c, 2007/. The sample sites for modal and analytical studies are shown in Figure 3-7.

The dominant rock types at Laxemar are the porphyritic Ävrö granite and Ävrö quartz monzodiorite, and the equigranular quartz monzodiorite. The composition of the rock types, exemplified by the quartz content in the dominant rock types in Figure 3-8, has been demonstrated to correlate strongly to the thermal conductivity and mechanical properties. This in turn has implications for canister spacing, repository design, degree of utilisation etc As can be seen, the quartz content is low for the porphyritic Ävrö quartz monzodiorite and the equigranular quartz monzodiorite which dominate the bedrock in the southern, focussed part of Laxemar. Subordinate rock types comprise diorite/gabbro, fine-grained dioritoid, granite, fine-grained granite, fine-grained diorite-gabbro and pegmatite. The fine-grained diorite-gabbro commonly constitutes composite intrusions together with veins of fine-grained granite. The fine-grained diorite-gabbro is presumed to constitute equivalents to what is commonly referred ro as uralitic dolerites /e.g. Wik et al. 2005, Nordenskjöld 1944/. The uralitic dolerites commonly constitute composite intrusions and belong to the c 1.8 Ga TIB generation /Nilsson 1992, Wik et al. 2005/.

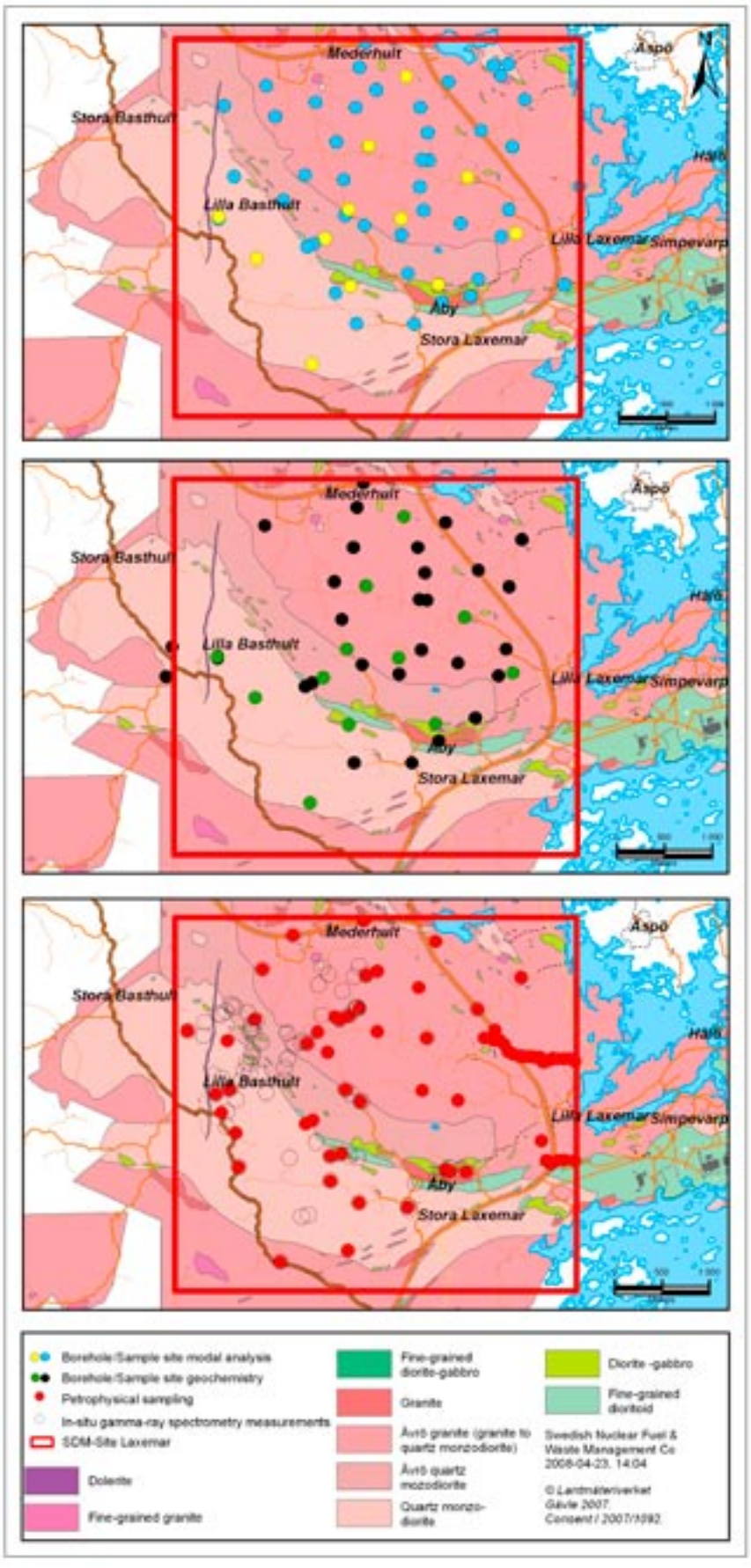

Figure 3-7. *Sample sites for modal and geochemical analytical studies and petrophysical measurements, including locations for in situ spectrometric measurements in the Laxemar local model area.*

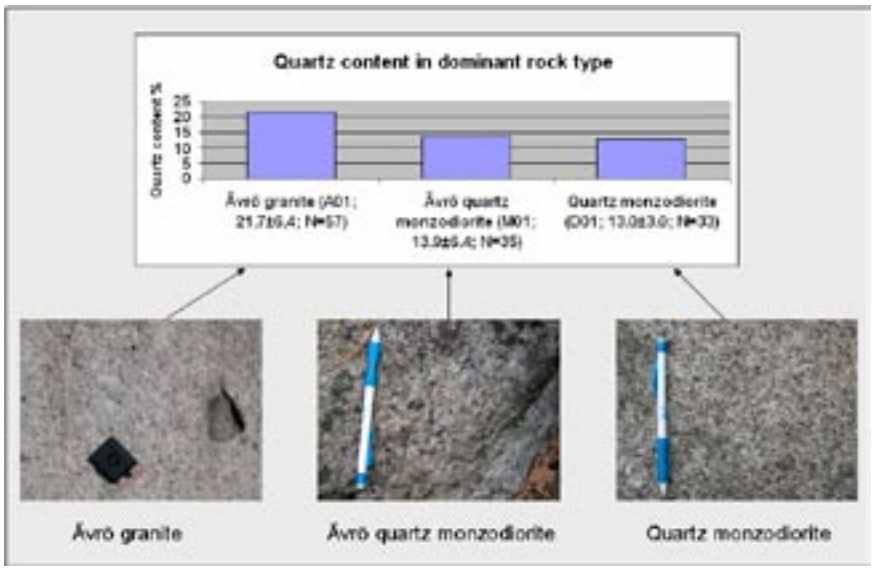

Figure 3-8. *Quartz content in the dominant rock types at Laxemar. Note the darker colour in the Ävrö quartz monzodiorite and the quartz monzodiorite compared to the quartz richer Ävrö granite. The dark inclusion to the right in the Ävrö granite is a mafic enclave.*

As mentioned above (Section 3.2), a conspicuous rock type in westernmost Laxemar is dolerite. It contains abundant olivine which is more or less strongly altered to iddingsite/serpentine /Wahlgren et al. 2006c, 2007/. The olivine content together with the steep to sub-vertical dip and N-S orientation, strongly suggest that they are equivalents to the olivine dolerites reported by /Nordenskjöld 1944/. The documented dolerite dykes, have, in general, a lower magnetic susceptibility than the country rocks and, hence, constitute low-magnetic anomalies. They are fine-grained and usually strongly fractured (shear fractures), which indicates that they have been subjected to brittle shearing after their emplacement and crystallisation.

According to the strategy for model development, the geological and petrophysical character of rock types are important for the property assignment of the rock domains /Munier et al. 2003, p. 62/. No data from the surface that bears on the character of the dominant rock types have been generated since model version Laxemar 1.2. However, the large number of new boreholes that have been drilled during the complete site investigation phase have generated new, geological data from several cored boreholes. For a more comprehensive description of the rock types at the Laxemar, the reader is referred to /SKB 2006b, Wahlgren et al. 2006a/.

The classification of surface and drill core samples from the Laxemar local model volume, based on results of the modal and geochemical analyses, are presented in Figure 3-9 and Figure 3-10, respectively.

In the Laxemar model version 1.2 SDM /SKB 2006b, Wahlgren et al. 2006a/ it was pointed out that the Ävrö granite constitutes two populations, one more granitic to granodioritic and one quartz monzodioritic. As can be seen in Figure 3-9 and Figure 3-10, this is confirmed by all new analyses from the drill cores and forms the basis for the definition of the Ävrö quartz monzodiorite. This in turn constitutes an important input for the division of the study area into rock domains (see Chapter 4).

The samples display the typical alkali-calcic trend of the Transscandinavian Igneous Belt (TIB) with variations in composition from diorite-gabbro to quartz monzodiorite to granite. As can be seen in the diagrams, the analyses of the surface and drill core samples overlap, which indicates that there is no difference between rock types sampled at the surface or at depth.

No new petrophysical data have been generated since the Laxemar model version 1.2. A compilation of all properties that characterise the dominant rock types is presented in Appendix 11.

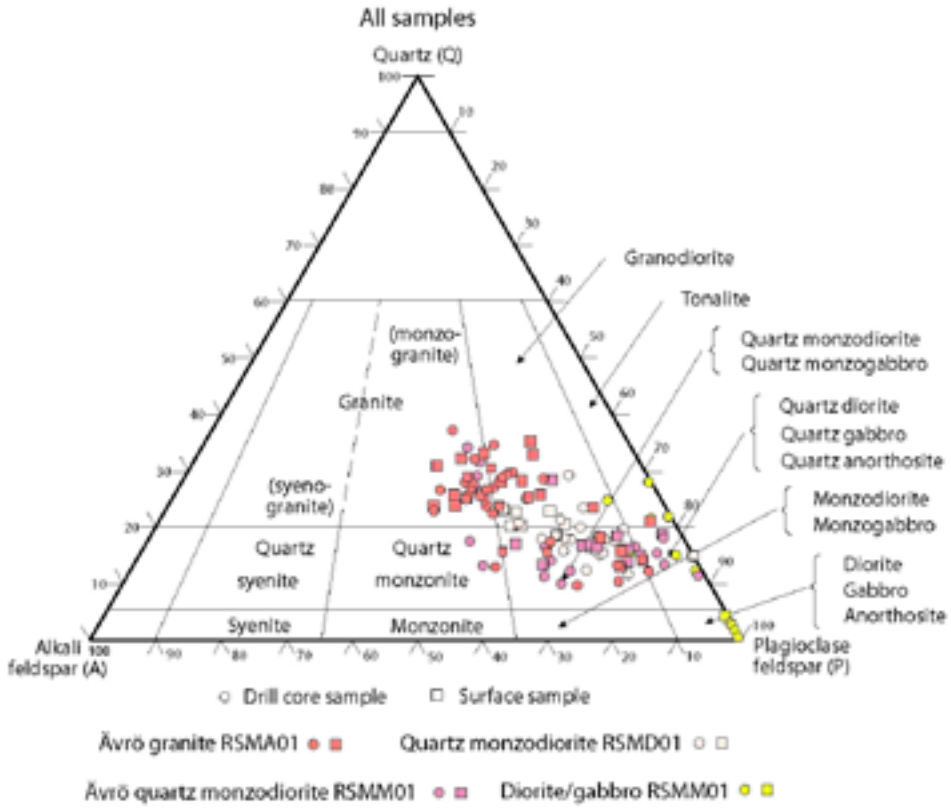

Figure 3-9. *QAP modal composition of the dominant rock types in the Laxemar local model volume according to /Streckeisen 1976/.*

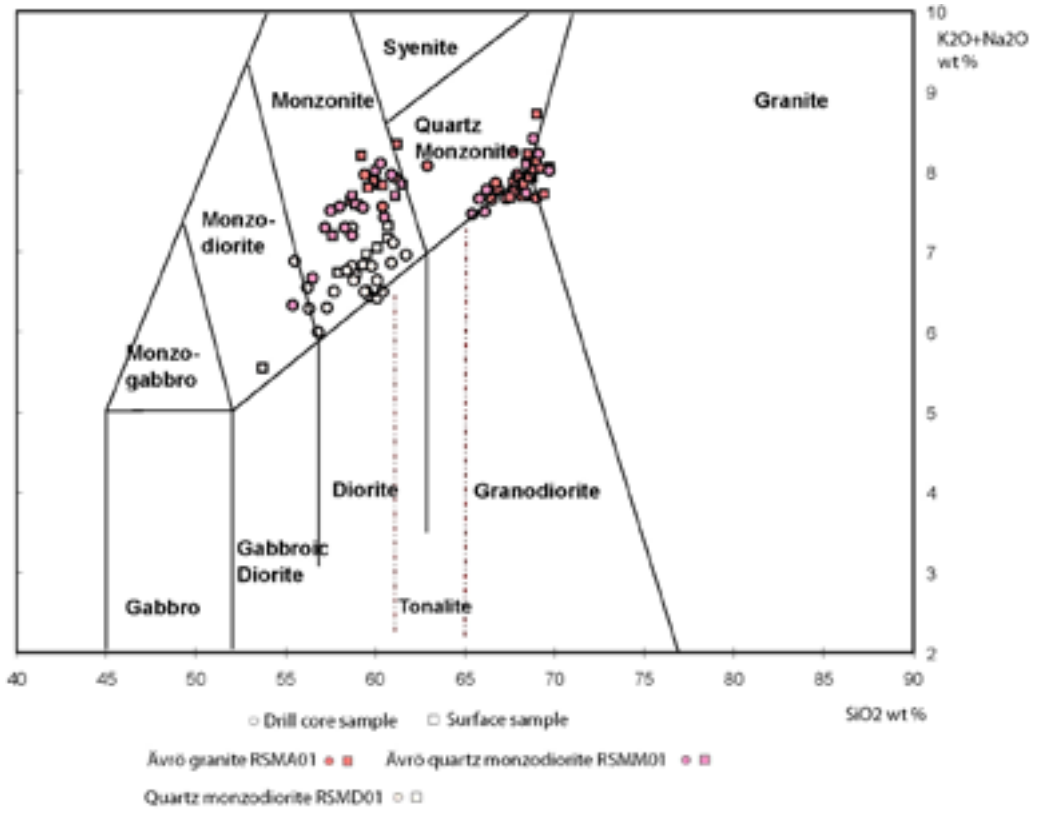

Figure 3-10. *Geochemical classification of the dominant rock types in the Laxemar local model volume according to /Middlemost 1994/.*

3.4.2 Proportions of different rocks at depth

The proportions of different rock types at depth on a borehole by borehole basis have been estimated by merging the data sets rock type (> 1 m borehole length) and rock occurrence (< 1 m borehole length) in the Sicada database. These two data sets reflect mapping at different levels of resolution. Rock types cover the whole borehole section and are greater than 1 m in length. Rock occurrences include borehole intervals less than 1 m in length and are minor segments inside rock types. For every borehole interval where there is a rock occurrence, the rock type along this interval has been removed. In a few cases, a minor rock occurrence has been defined inside another rock occurrence. In these instances, no length compensation has been carried out and, and for this reason, the mapped borehole length documented in some of the histograms is somewhat longer than the true borehole length. However, the effect of this procedure on the borehole length is considered negligible.

The results of the analysis for the cored boreholes are displayed in the form of histograms in Appendix 4, including also boreholes that are < 200 m in length and that were drilled in conjunction with the minor deformation zone (MDZ) project /Olsson et al. 2007/ (see Section 3.12). The most important data sets for the analysis of the proportion of rock types are those from the longer cored boreholes. The proportions of rock types in these boreholes are summarised in Figure 3-11, Figure 3-12 and Figure 3-13, for boreholes or parts of the boreholes that are dominated by 1) Ävrö granite, 2) Ävrö granite/Ävrö quartz monzodiorite with frequent diorite/gabbro and 3) quartz monzodiorite, respectively.

As can be seen in Figure 3-11, the proportions of rock types in the Ävrö granite dominated parts of the cored boreholes KLX04, KLX06 and KLX09 deviate from the remaining boreholes. These three boreholes are drilled in northern part of Laxemar (see Figure 3-1), and, since the southern part of Laxemar is in focus for the site investigation, these three boreholes are judged not to be representative for the Ävrö granite dominated parts of the focussed volume and, therefore, should be disregarded in the characterisation of the bedrock.

In the borehole sections that are dominated by Ävrö granite/Ävrö quartz monzodiorite with frequent occurrences of diorite/gabbro (Figure 3-12), the most obvious difference in rock proportions is the relation between Ävrö granite/Ävrö quartz monzodiorite and diorite/gabbro, i.e. when the proportion of Ävrö granite/Ävrö quartz monzodiorite decreases, the proportion of diorite/gabbro increases. However, KLX05 deviates by having an anomalously high proportion of fine-grained granite and granite, which also is to be expected from the distribution of rock types at the surface in this part of Laxemar (cf. Figure 3-4).

The boreholes that are drilled in the quartz monzodiorite in southern and southwestern Laxemar display very similar proportions of rock types. The most obvious anomalies are the elevated proportion of dolerite in KLX14A, KLX19A and KLX20A, fine-grained granite in KLX05 and Ävrö granite in KLX21B. It should be noted that the dolerites in KLX14A, KLX19A and KLX20A refer to restricted focussed occurrences and are not, like the other subordinate rock types, more or less evenly distributed along the boreholes.

3.4.3 Thickness and orientation of subordinate rock types

The most common and typical subordinate rock types in Laxemar are fine-grained granite, fine-grained diorite-gabbro and pegmatite. If local variations are disregarded, fine-grained granite constitutes approximately 4% along the boreholes which are dominated by Ävrö granite in northern to central Laxemar (Appendix 4, RSMA01), approximately 5% along the boreholes which are dominated by Ävrö granite/Ävrö quartz monzodiorite with frequent occurrence of diorite/gabbro in central Laxemar (Appendix 4, RSMM01) and approximately 5% in the quartz monzodiorite in southern Laxemar (Appendix 4, RSMD01). Corresponding values for fine-grained diorite-gabbro are 6%, 2% and 2% and for pegmatite 0.4%, 0.5% and 1.5% (Appendix 4, RSMA01, RSMM01 and RSMD01).

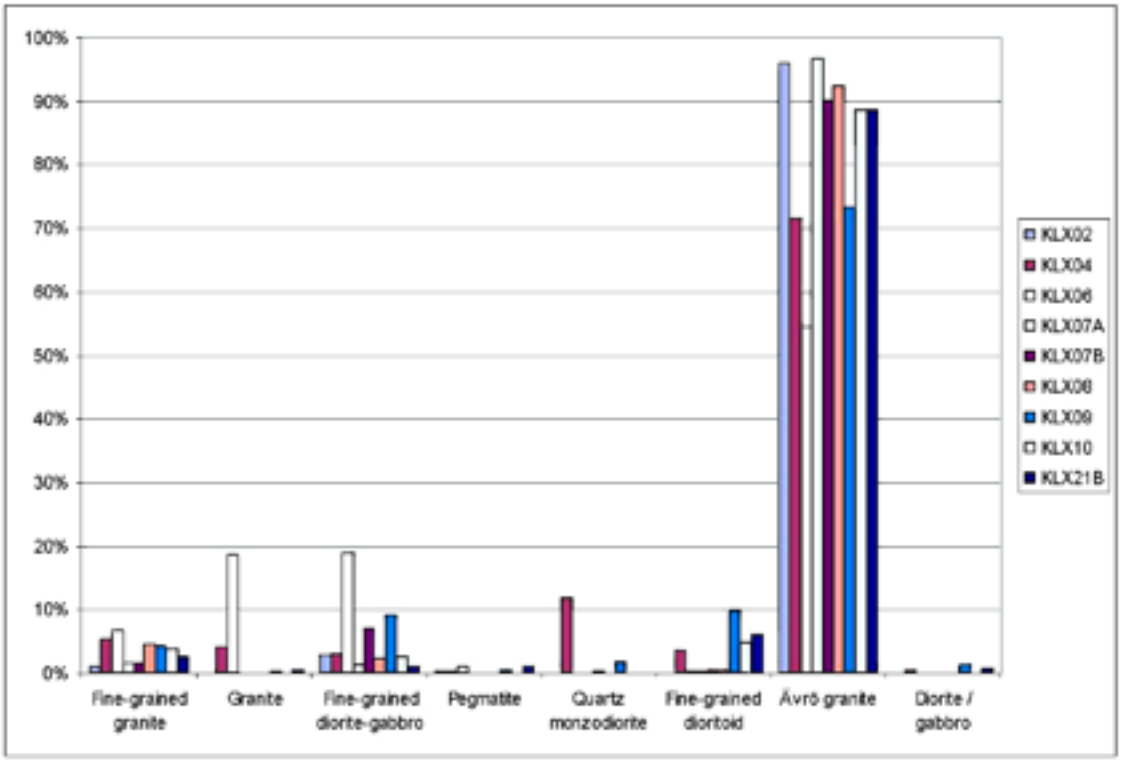

Figure 3-11. *Histogram showing the quantitative estimate (volume %) of the proportions of different rock types in cored boreholes from the Ävrö granite dominated parts of the study area in central and northern Laxemar (Figure 3-4), i.e. the RSMA01 domain (see Section 4.3).*

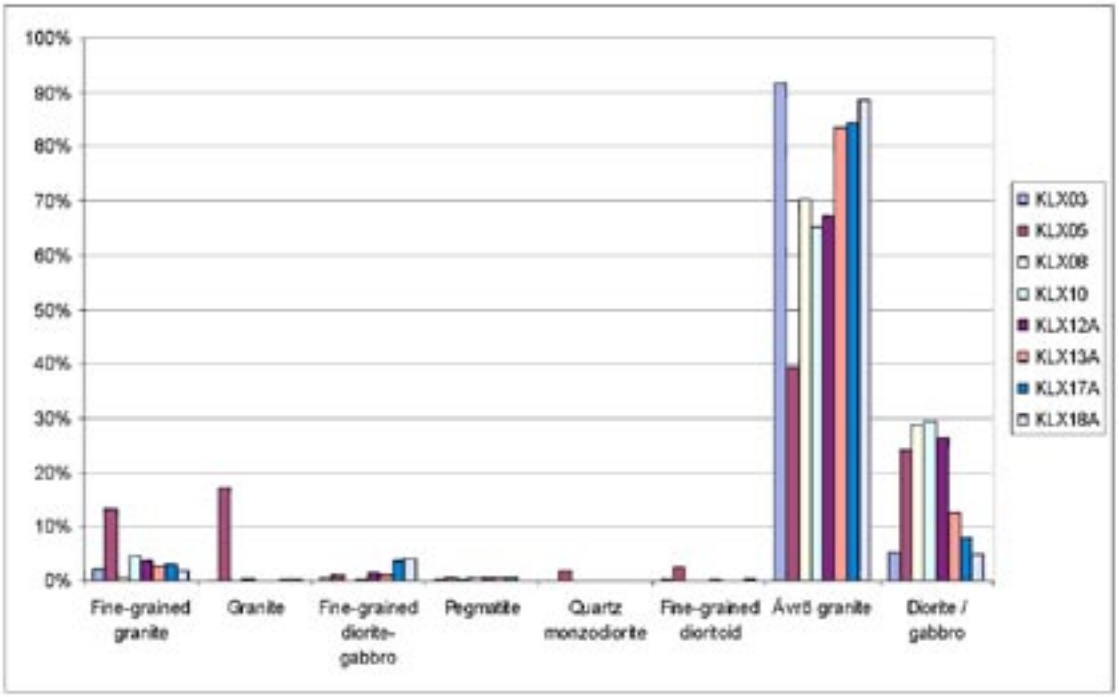

Figure 3-12. *Histogram showing the quantitative estimate (volume %) of the proportions of different rock types in cored boreholes or parts of boreholes that are dominated by Ävrö quartz monzodiorite with frequent occurrences of diorite/gabbro in central Laxemar (Figure 3-4), i.e. the RSMM01 domain (see Section 4.3).*

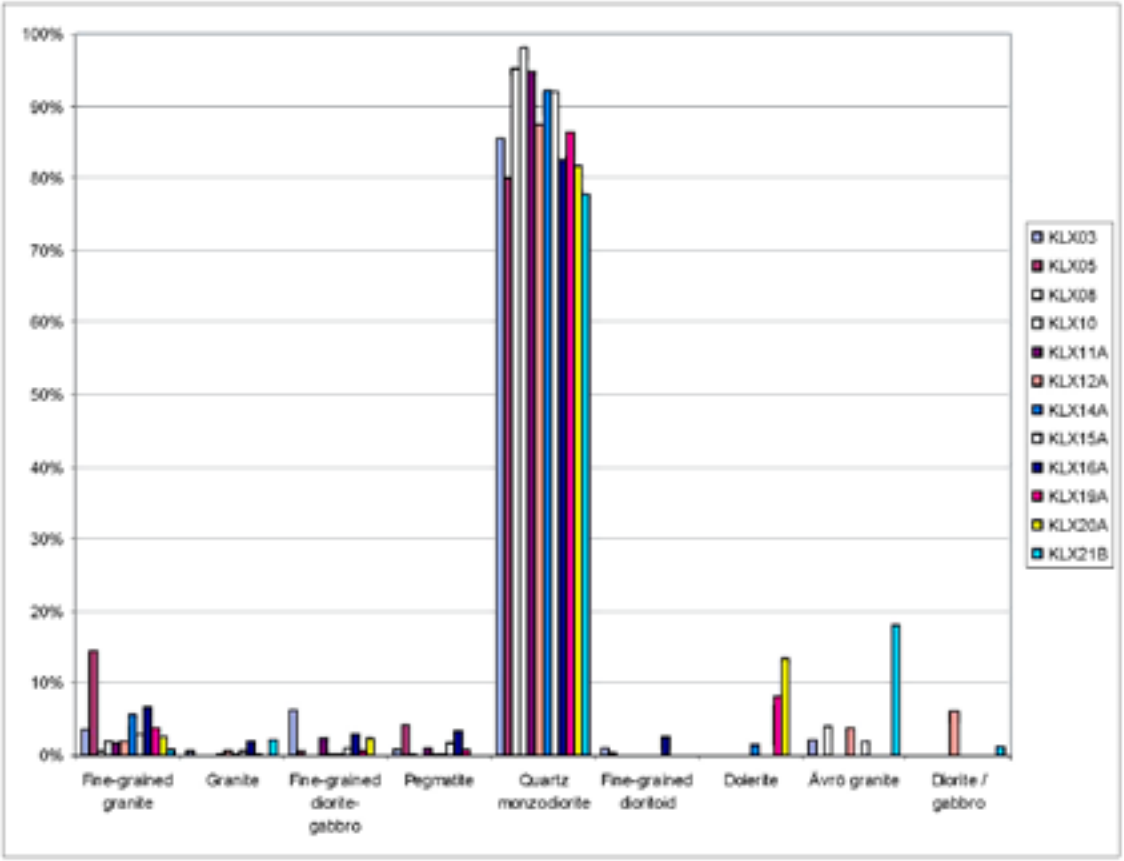

Figure 3-13. *Histogram showing the quantitative estimate (volume %) of the proportions of different rock types in cored boreholes or parts of boreholes that are dominated by quartz monzodiorite in southern Laxemar (Figure 3-4), i.e. the RSMD01 domain (see Section 4.3).*

Fine-grained granite and pegmatite are by definition quartz rich and are characterised by high thermal conductivity, while the fine-grained diorite-gabbro are poorer in quartz and are characterised by much lower thermal conductivity /see Wrafter et al. 2006/. All these three rock types usually occur as narrow, dyke-like to irregular tabular bodies. Due to the different thermal conductivities and their dyke-like appearance, i.e. a potential anisotropy factor in the thermal modelling, it was judged necessary by the thermal modelling team to assess the variation in thickness and orientation of the above-mentioned subordinate rock types. An assessment of the spatial distribution of fine-grained granite and fine-grained diorite-gabbro in Laxemar, by a stochastic simulation, is being carried out and will be reported in the SDM-Site Laxemar main report and the accompanying background report by the thermal modelling team.

Thickness

By use of the data sets rock type (> 1 m long sections along the borehole) and rock occurrence (< 1 m long sections along the borehole) in the Sicada database, the borehole length and orientation of contacts of fine-grained granite, fine-grained diorite-gabbro and pegmatite in all cored boreholes (excluding the short boreholes defined for DFN-analysis, see Section 3.6) have been documented and the true thicknesses have been estimated. In the thickness calculation (see Appendix 5), the value of the orientation of the upper contact (of the mapped occurrence) in the Sicada database has been used.

The number of occurrences and summed borehole length of different thickness classes of fine-grained granite, fine-grained diorite-gabbro and pegmatite, with a truncation threshold of 0.1 m, are presented in Appendix 5. Dolerite is also included in the estimation of true thickness

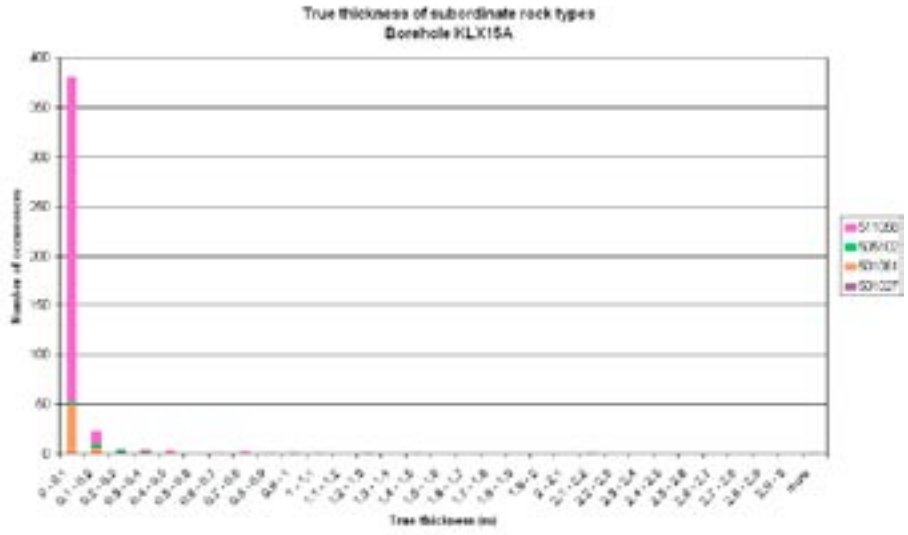

Figure 3-14. *Number of occurrences of subordinate rock types with different thickness in KLX15A using a truncation threshold of 0.1 m. The translation of rock codes to rock names is provided in Appendix 2.*

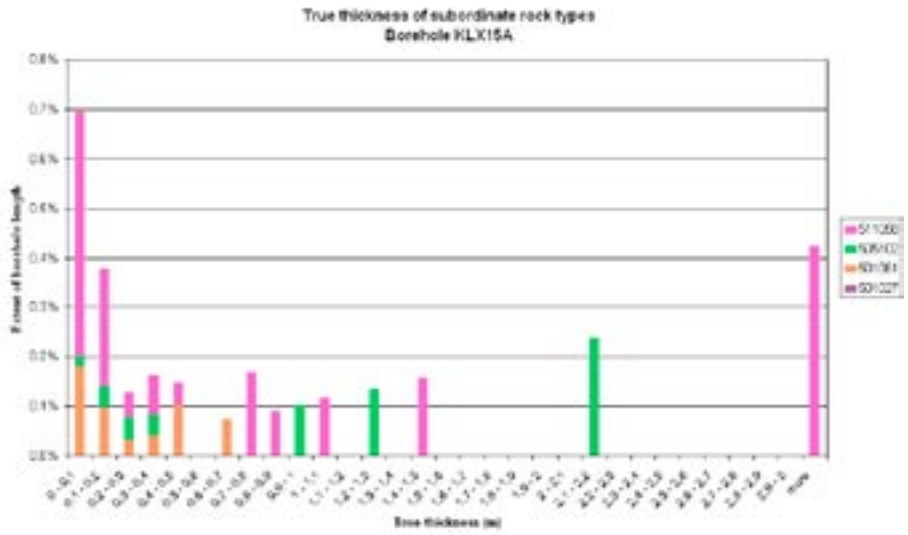

Figure 3-15. *Summed up borehole length for each thickness class in KLX15A. The translation of rock codes to rock names is provided in Appendix 2.*

for the boreholes KLX14A, KLX19A and KLX20A. Although there are a number of thicker occurrences, it is evident from the diagrams in Appendix 5 that the majority of the subordinate rock types have a thickness less than 1 m. This is exemplified by the thickness distribution of the subordinate rock types in KLX15A as shown in Figure 3-14 and Figure 3-15.

Orientation

By use of the data sets rock type (> 1 m long sections along the borehole) and rock occurrence (< 1 m long sections along the borehole) in the Sicada database, an analysis of the orientation of the subordinate rock types fine-grained granite, fine-grained diorite-gabbro and pegmatite, and, where it occurs, also dolerite, has been carried out for all cored boreholes (excluding the short boreholes defined for DFN-analysis, see Section 3.6). The orientation of the upper contact is used in the analysis. The orientation analysis is based on the assumption that the subordinate rock types can be treated as planar structures and that the orientation of the contact in the drill

Fine-grained granite

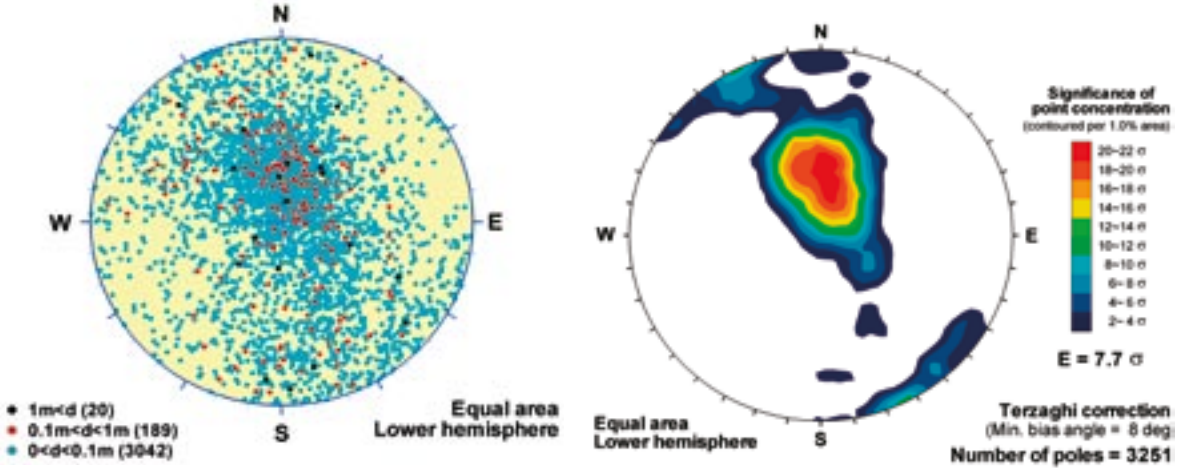

Fine-grained diorite-gabbro

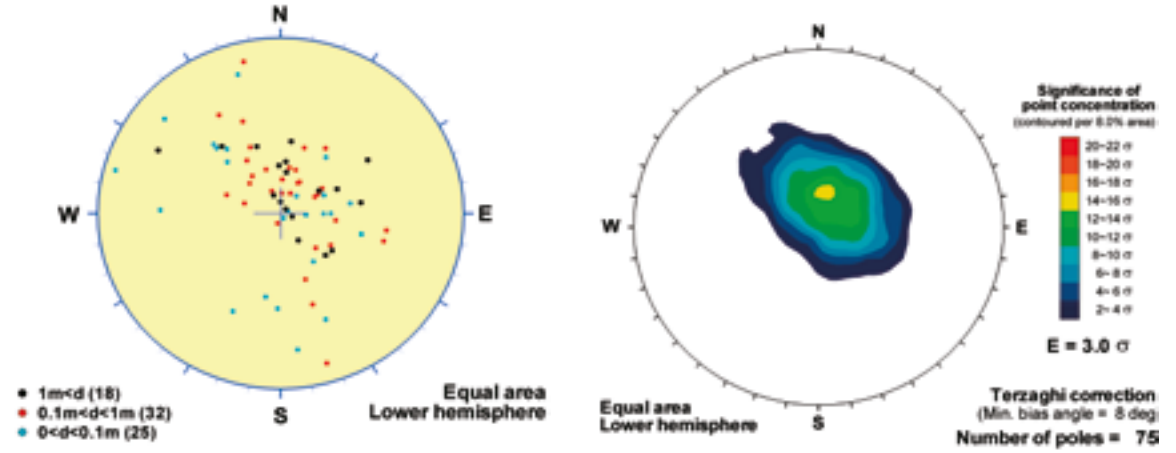

Pegmatite

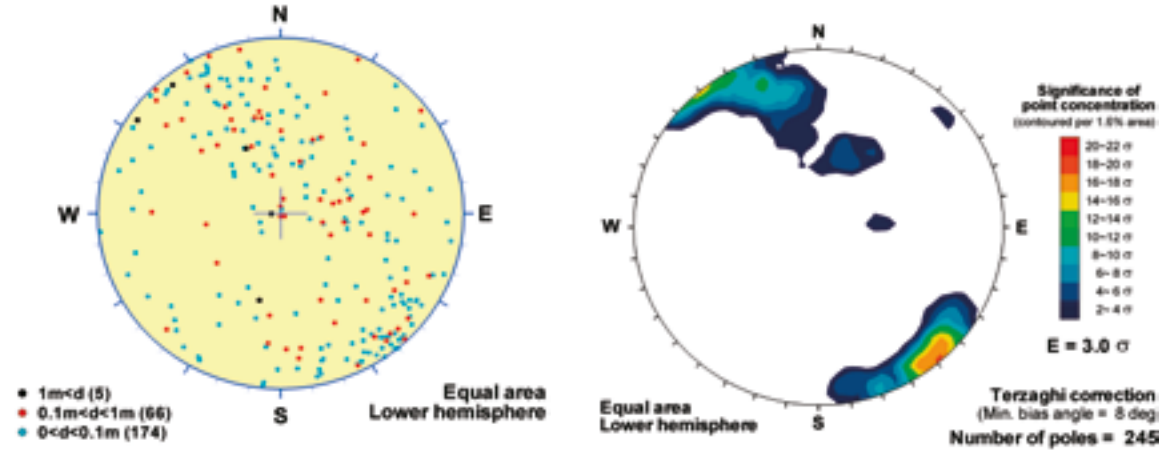

Figure 3-16. *Orientation of fine-grained granite, fine-grained diorite-gabbro and pegmatite in the quartz monzodiorite in southern Laxemar. Based on data from all cored borehole sections that have intersected the quartz monzodiorite. Note that KLX27A and the DFN-holes KLX11B-F are excluded.*

core represents the true orientation of the wall rock contact. By experience from the surface, it is known that, in particular, the fine-grained granite in many cases constitutes irregular bodies, which thus do not qualify as planar dykes. However, the immense amount of e.g. oriented fine-grained granites, (approximately 7,500 records) definitely provide a basis to establish an interpretation of the general orientation trend of subordinate rock types in Laxemar.

The results of the orientation analysis are presented in Appendix 6 as poles plotted on the lower hemisphere of an equal area stereographic projection with Fisher contouring and Kamb contouring. The data are presented on a borehole by borehole basis, on a rock domain basis in each borehole and on an overall rock domain basis.

The orientation of subordinate rock types is exemplified by fine-grained granite, fine-grained diorite-gabbro and pegmatite in the quartz monzodiorite in southern Laxemar as displayed in Figure 3-16. The absolute majority of the fine-grained granites are thin and have a thickness < 0.1 m. Furthermore, the fine-grained granites display a dominant strike in NE-SW. Sub-horizontal to moderate southerly and sub-vertical dips dominate, but fine-grained granites that dip to the north occur as well. The fine-grained diorites-gabbros display dominant sub-horizontal to gentle dips, and the pegmatites are sub-vertical and predominantly strike NE-SW, i.e. display similar orientation as the sub-vertical fine-grained granites. As can be seen in the stereographic projections on the overall rock domain basis in Appendix 6, it is strongly indicated that the majority of the occurrences of fine-grained granite and fine-grained diorite-gabbro are sub-horizontal to moderately dipping and have a dominant strike in NE-SW, although a spread between N-S and E-W occur. Southerly dips dominate in southern (RSMD01) and central (RSMM01) Laxemar, while dips both to the north and south exist in northern (RSMA01) Laxemar. The pegmatites display a similar orientation, but are dominated by steep to sub-vertical dips, although a sub-horizontal population exists, in particular in northern Laxemar (RSMA01).

3.4.4 Rock alteration – red staining and saussuritisation

An estimate of the degree of alteration has been carried out by use of the data set rock alteration in Sicada, as inferred from the Boremap mapping of the cored boreholes. It is an important factor to consider for the thermal and rock mechanical modelling, since the degree and type of alteration affects the thermal and rock mechanical properties of the bedrock. The focus has been on the degree of alteration in the rock in between interpreted deformation zones. Thus, sections identified as possible deformation zones, including also minor deformation zones, in the ESHI of the cored boreholes are excluded from the analysis.

The degree, classified as faint, weak, medium and strong in the Boremap mapping, and type of alteration is presented in Appendix 7 on a borehole by borehole basis, rock domain basis in each borehole and on an overall rock domain basis. The degree and type of alteration is exemplified in Figure 3-17 by KLX18A which is dominated by Ävrö granite and Ävrö quartz monzodiorite and in Figure 3-18 by KLX19A which is dominated by quartz monzodiorite.

As can be seen in Figure 3-17, red staining, which is referred to as oxidation in the Boremap mapping, is by far the most abundant type of alteration of the Ävrö granite and Ävrö quartz monzodiorite in KLX18A. However, in KLX19A (Figure 3-18), which is dominated by quartz monzodiorite, alteration classified as saussuritisation and epidotization are abundant in addition the oxidation. As is evident from the domain based histograms at the end of Appendix 7, it is a general phenomenon that the quartz monzodiorite (RSMD01) displays a much higher degree of saussuritisation and epidotization than the Ävrö granite (RSMA01) and Ävrö quartz monzodiorite (RSMM01). The degree of alteration in the bedrock in between the deformation zones in Laxemar is in general classified as faint to weak and, based on the analysis along the borehole length (e.g. Figure 3-17 and Figure 3-18), it is found that up to, although inhomogeneously distributed, approximately 20–25% of the bedrock is affected by alteration.

It should be noted that although the red-stained rocks appear to be oxidized, Mössbauer spectroscopy analyses have revealed that their reducing capacity have largely remained the same (cf. Section 3.6.5).

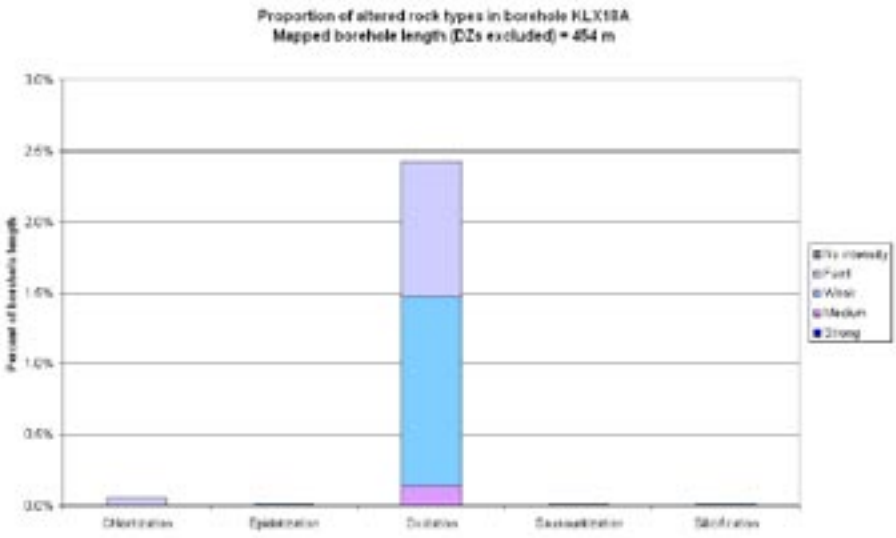

Figure 3-17. *Degree and type of alteration in KLX18A, which is dominated by Ävrö granite and Ävrö quartz monzodiorite.*

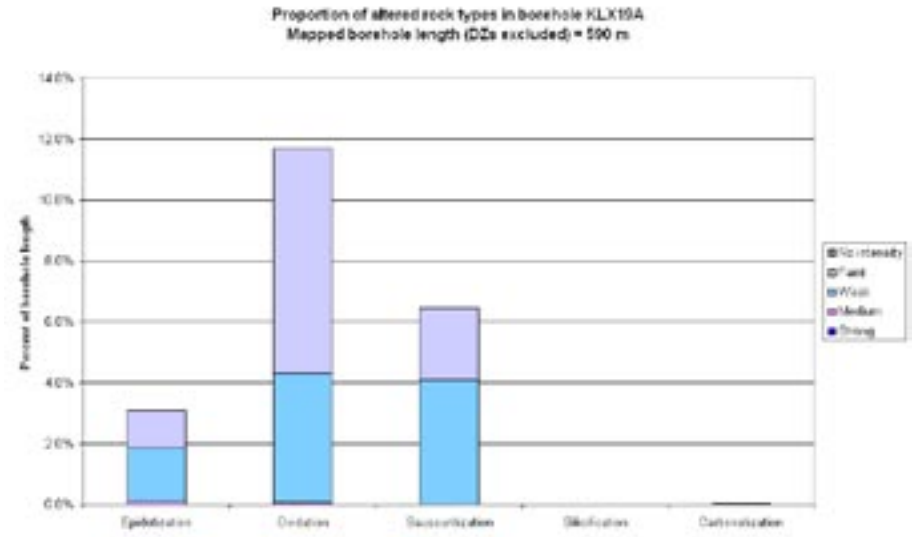

Figure 3-18. *Degree and type of alteration in KLX19A, which is dominated by quartz monzodiorite.*

3.5 Ductile deformation

From a structural point of view, the bedrock at Laxemar is dominated by well-preserved intrusive rocks. However, a faint to weak foliation, which is not uniformly distributed in the bedrock in the local model volume, is present. The percentage of the bedrock that has been documented asfoliated is presented on a borehole by borehole basis and overall rock domain basis in Table 3-2 and Table 3-3, respectively. For the definition of rock domains, see Section 4.3. In many cases it is difficult to decide whether the foliation is late-magmatic, i.e. represents a flow foliation, or whether it is a solid state foliation. It is inferred that the development of the foliation initially started at a late stage in the magmatic evolution but continued in the solid state after the crystallisation and solidification of the magmas. All rock types are affected by the foliation, in particular the dyke-like bodies of fine-grained granite and fine-grained diorite-gabbro. In particular, in the southern part of Laxemar, the foliation in these rocks formed in the solid state and is more or less strongly developed. Accordingly, this indicates that also the country rocks have suffered from a solid state deformation with the development of a foliation. In many cases, the dyke-like bodies correspond to ductile shear zones and there is a concentration of ductile strain in the youngest dyke-like intrusions.

3.5.1 Surface data

An evaluation of ductile structures from surface data was carried out in connection with the reporting of the Laxemar 1.2 model version /SKB 2006b, Wahlgren et al. 2006a/. However, the available data set from the surface measurements was limited, mainly due to problems in measuring the faintly to weakly developed foliation in the commonly flat outcrops at Laxemar. No new surface data have been generated from Laxemar during the complete site investigation stage.

The relation between the orientation of the foliation and the subordinate rock types, e.g. fine-grained granite and fine-grained diorite-gabbro, is difficult to unravel due to the faint to weak character of the foliation. However, when the foliation is more strongly developed, it displays a general concordancy to the orientation of the subordinate rock types.

As mentioned already in conjuction with the Laxemar 1.2 reporting /SKB 2006b, Wahlgren et al. 2006a/, the most spectacular and characteristic ductile, structural features in Laxemar are low-grade ductile to brittle-ductile shear zones that vary in thickness from decimetres up to tens of metres (Figure 3-19). A special study has been performed in order to unravel the kinematics in the ductile shear zones /Lundberg and Sjöström 2006/. The regional scale, most prominent, ductile shear zones strike NNE-SSW and NE-SW and are sub-vertical, while E-W oriented zones, though overprinted by brittle deformation display moderate to steep dips to the south. The study of the kinematics in the ductile shear zones /Lundberg and Sjöström 2006/ has revealed that the NNE-SSW and NE-SW oriented zones are characterised by sinistral strike-slip movement (cf. Section 3.5.4 and /Viola and Venvik Ganerød 2007a/), whereas the ENE-WSW to E-W shear zones in the Simpevarp subarea show complex kinematics. This includes both reverse and normal dip-slip as well as sinistral and dextral strike-slip displacements. It has been inferred that the ductile deformation along the various sets of zones formed in response to an approximately northward-directed shortening /Lundberg and Sjöström 2006/. Examples of structures that have been used to decipher the kinematics in the shear zones are displayed in Figure 3-20.

Figure 3-19. *Strongly deformed, protomylonitic Ävrö granite within ZSMNE004A.*

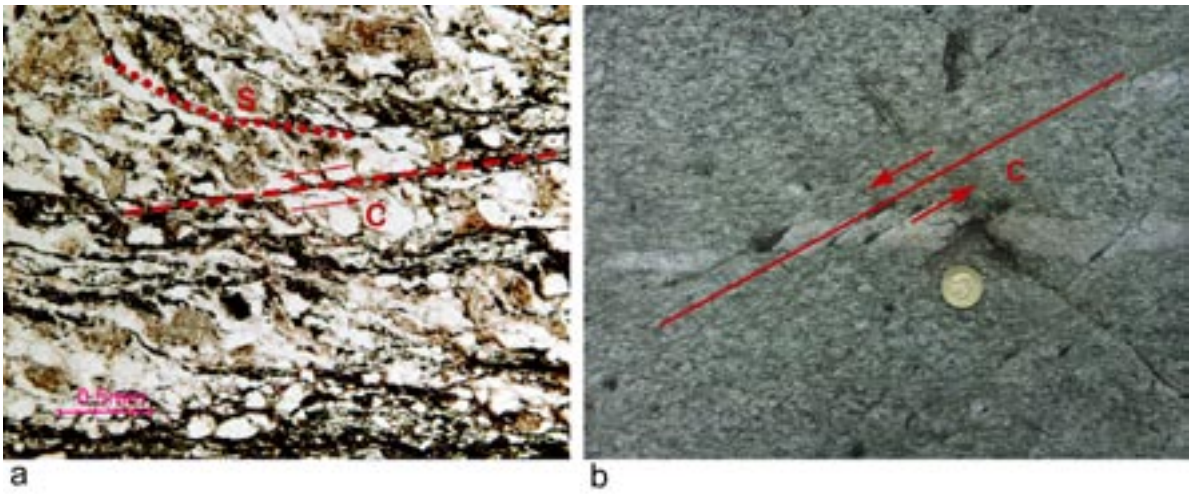

Figure 3-20. *Example of structures and fabric used to decipher the kinematics in the ductile shear zones. a) C/S fabric indicating sinistral sense of shear. b) Fine-grained granite vein displaced by a sinistral shear zone.*

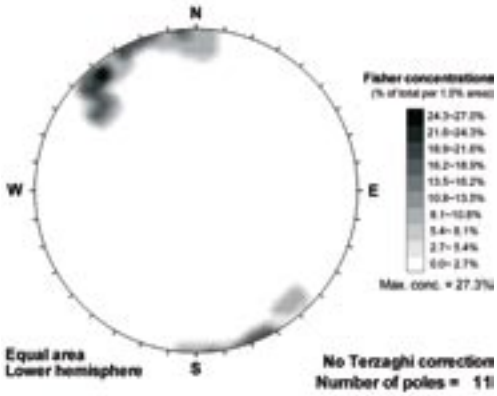

Foliation ZSMNE004A

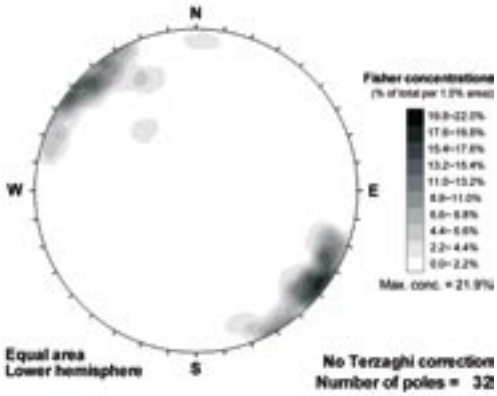

Mylonites/shear zones ZSMNE004A

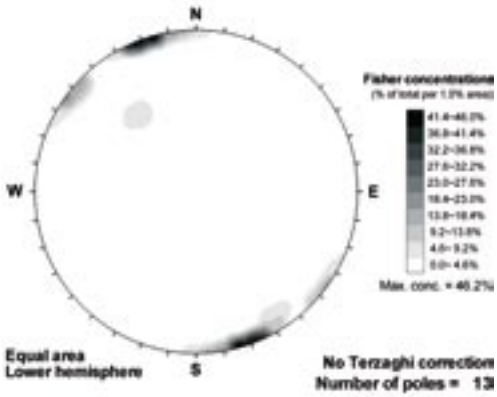

Foliation ZSMNE005A

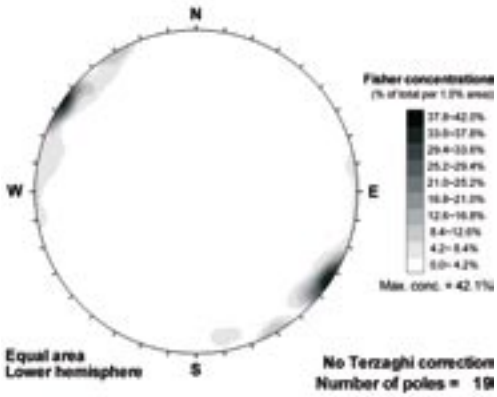

Mylonites/shear zones ZSMNE005A

Figure 3-21. *Relation between the orientation of foliation and mylonitic foliation/shear zones in the deformation zones ZSMNE004A (top) and ZSMNE005A (bottom).*

A close temporal relationship between the emplacement of the fine-grained granite and the ductile shear deformation is supported by the variable field relationships between the fine-grained granite dykes/veins and the shear deformation. Some of these dykes/veins are affected and cut by ductile shear zones, while others are unfoliated and truncate the shear zones /Lundberg and Sjöström 2006/.

As mentioned in Section 3.6.5 (see also /Drake et al. 2007/), a muscovite from a 5–10 cm thick mylonite interchanging with highly fractured rocks in the Äspö shear zone has yielded a $^{40}Ar/^{39}Ar$ age of 1,406±3 Ma. However, since obtained $^{40}Ar/^{39}Ar$ biotite ages strongly indicate that the 1.45 Ga granites intruded into a brittle crust (see Section 1.4 and /Söderbäck 2008/), the obtained muscovite age is not interpreted to date the formation or a ductile reactivation of the Äspö shear zone. Instead, a resetting of the argon system in muscovite, caused by the intrusion of the Götemar and Uthammar granites and related hydrothermal activity is favoured to explain the unexpectedly young age.

In connection with the bedrock surface mapping /Persson Nilsson et al. 2004/, structural measurements were documented within the two most prominent shear zones, or rather shear belts, in the easternmost part of Laxemar, i.e. the NE-trending parts of ZSMNE004A and ZSMNE005A which form two branches of the original extension of the Äspö shear zone (cf. Chapter 5). As can be seen in Figure 3-21, the relation between the east-northeasterly oriented foliation and the north-easterly oriented mylonitic foliation/shear zones supports the sinistral component of movement along the shear zones (Figure 3-20), as determined from the kinematic study of outcrops and thin-sections.

3.5.2 Cored borehole data

The mapping of all new cored boreholes drilled during the complete site investigation stage has generated important additional structural data from the sub-surface that complement the relatively sparse data from the surface. The procedure used for analysis of ductile structures from the cored boreholes is presented in Appendix 8, together with orientation data presented separately for foliation and shear zones on a borehole by borehole basis, on rock domain basis in each borehole and on an overall rock domain basis.

The percentage of the bedrock that has been documented as foliated is presented on borehole by borehole basis and overall rock domain basis in Table 3-2 and Table 3-3, respectively. As can be seen in Table 3-2, the percentage of the borehole length that is foliated varies considerably between the boreholes. Furthermore, this points to the non-uniform distribution of the foliation in the bedrock at Laxemar.

The percentage of the rock domains that has been documented as foliated, based on the division of the cored boreholes in rock domains, is displayed in Table 3-3. It is apparent that c 80% of the bedrock in Laxemar is massive, i.e. does not contain any ductile anisotropy.

The orientation of the non-uniformly distributed ductile foliation in the Laxemar local model volume is displayed in Figure 3-22 and Figure 3-23. Although not strictly qualifying as a girdle according to the Vollmer fabric index (see Appendix 8), there is a girdle-like distribution when all data from Laxemar are considered. By a comparison of the stereograms in Figure 3-23b, c and d, which in combination represent all data from Laxemar, it is furthermore indicated that the dip of the foliation changes from being gentle to moderate, approximately to the north in northern Laxemar to gentle approximately to the south in southern Laxemar. In the intervening area in central Laxemar, the foliation displays variable dips to the north and south. Consequently, it is inferred that the non-uniformly distributed, faint to weak foliation in Laxemar defines an irregular antiformal configuration with a sub-horizontal to gently west plunging fold axis (cf. AMS data in Section 3.5.4).

Table 3-2. Percentage of borehole length that has been documented as foliated in the Boremap mapping. Deformation zones from the ESHI are excluded. The results are presented on a borehole by borehole basis.

	Intensity of foliation	
Borehole ID	Faint to weak	Medium to strong
KLX02	44.83	0.30
KLX03	5.33	0.55
KLX04	9.77	0.00
KLX05	10.56	8.52
KLX06	47.08	1.60
KLX07A	16.41	0.00
KLX08	10.09	0.00
KLX09	13.40	0.16
KLX10	19.33	1.94
KLX11A	23.25	1.06
KLX12A	12.93	0.20
KLX13A	24.77	0.00
KLX14A	5.22	0.00
KLX15A	10.81	0.20
KLX16A	1.51	0.00
KLX17A	43.42	0.00
KLX18A	16.09	0.00
KLX19A	19.99	0.37
KLX20A	11.17	0.00
KLX21B	81.20	5.61

Table 3-3. Percentage of the rock domains that has been documented as foliated. Deformation zones from the ESHI are excluded. The results are based on data in Table 3-2.

	Intensity of foliation	
Rock domain	Faint to weak	Medium to strong
RSMA01	25.55	1.02
RSMM01	16.62	0.28
RSMD01	22.33	2.03

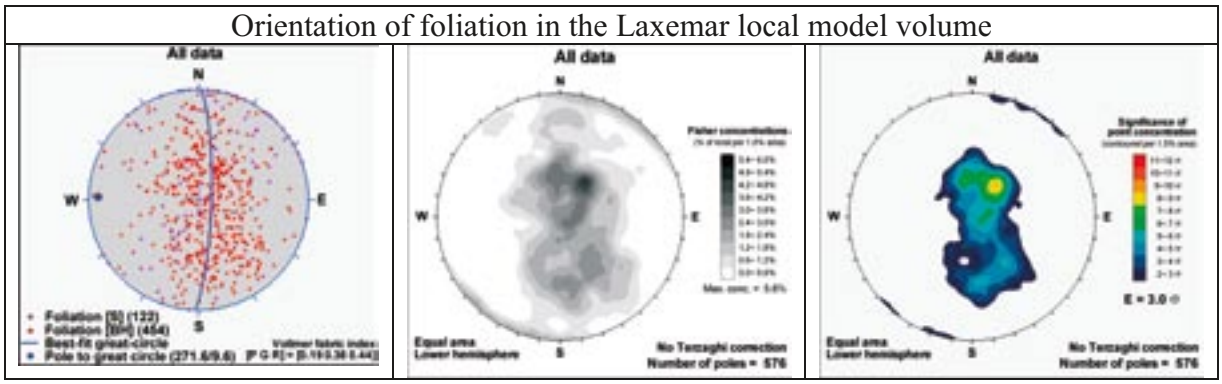

Figure 3-22. *Orientation of foliation in the Laxemar local scale model volume, based on borehole data (BH) and surface data (S).*

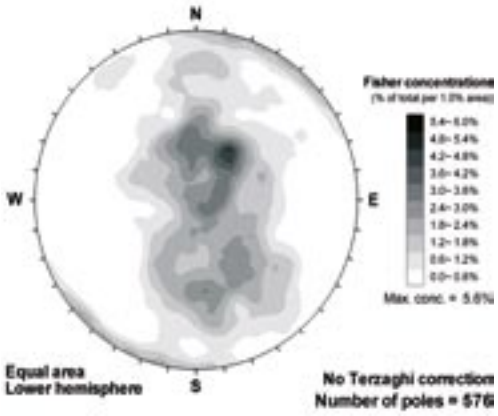

a) All data

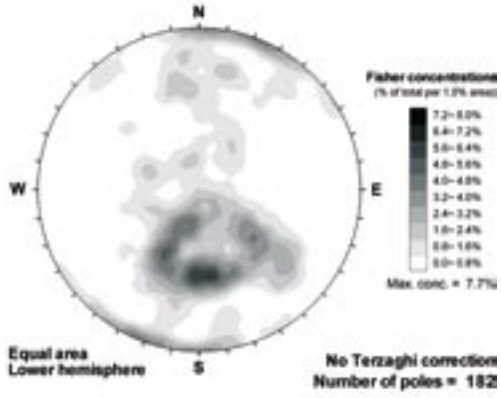

b) Foliation in the volume dominated by Ävrö granite in northern Laxemar

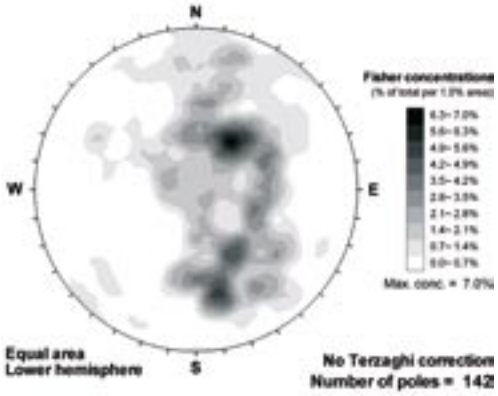

c) Foliation in the volume dominated by Ävrö quartz monzodiorite in central Laxemar

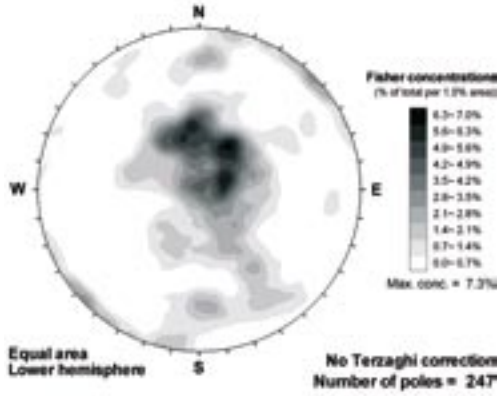

d) Foliation in the volume dominated by quartz monzodiorite in southern Laxemar

Figure 3-23. *Orientation of foliation in different parts of the Laxemar local model volume.*

Figure 3-24 shows the documented orientation of what has been classified as mylonite, ductile and brittle-ductile shear zones in the Boremap mapping of the cored boreholes in Laxemar. This includes measurements of both thicker shear zones as well as narrow mylonitic seams. As can be seen in Figure 3-24, there is a large spread in orientations, but the occurrence of sub-horizontal to gently dipping zones and NE-SW striking and sub-vertically dipping zones is clearly evident. The latter exhibit similar orientations as, and are interpreted to be small-scale equivalents to, the shear zones that define the deformation zones ZSMNE004A and ZSMNE005A (Figure 3-21).

3.5.3 Comparison of the orientation of ductile structures and subordinate rock types

A comparison of the orientation of subordinate rock types, foliation and ductile and brittle-ductile shear zones, as reported in Sections 3.4.3 and 3.5.2, respectively, is presented in stereoplots in Appendix 9 on a borehole by borehole basis and on an overall rock domain basis. When doing this comparison, it has to be remembered that the foliation is faint to weak in character and that only c 20% of the bedrock at Laxemar has been documented as foliated (Table 3-3), i.e. c 80% of the bedrock does not display any ductile structural anisotropy. This means that a large amount of the subordinate rock types occur in an undeformed (massive) host rock. Furthermore, the restricted amount of orientation data of ductile structures compared to the large amount of orientation data of the subordinate rock types, particularly fine-grained granite, also cause restrictions in the evaluation.

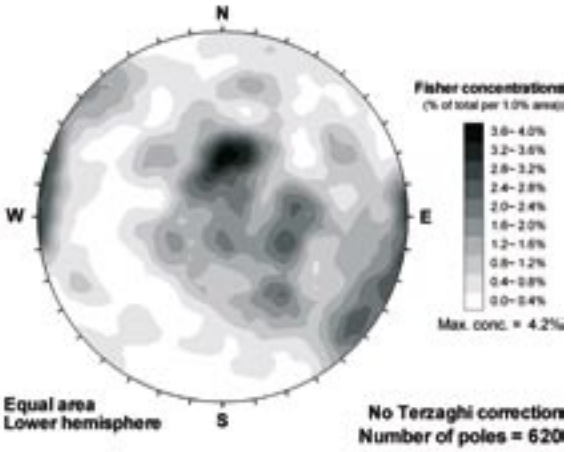

a) All data

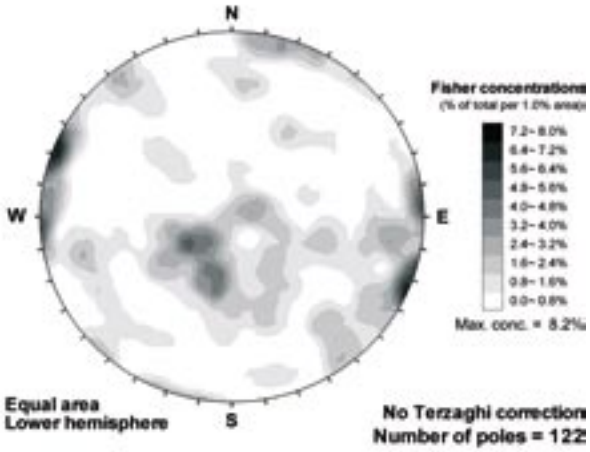

b) Shear zones in in the volume dominated by Ävrö granite in northern Laxemar

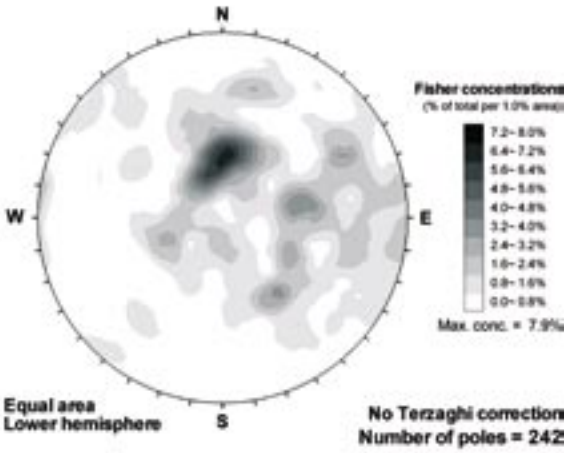

c) Shear zones in the volume dominated by Ävrö quartz monzodiorite in central Laxemar

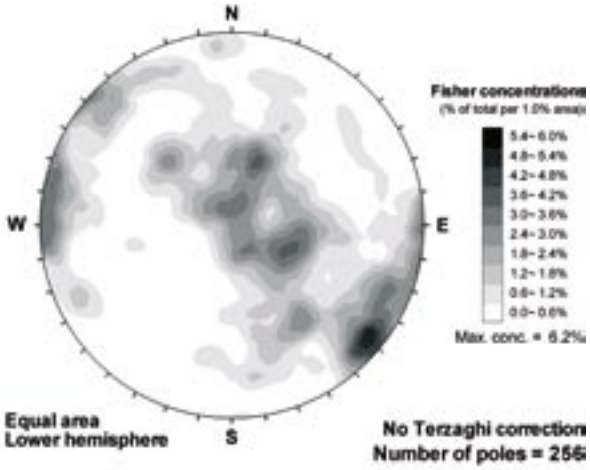

d) Shear zones in the volume dominated by quartz monzodiorite in southern Laxemar

Figure 3-24. *Orientation of ductile to brittle-ductile shear zones in the Laxemar local model volume, including surface data (S).*

As can be seen in the comparison on borehole by borehole basis in Appendix 9, there are subordinate rock types whose orientation correlates with the orientation of the foliation. However, it is also obvious that the orientations of a large amount of the subordinate rock types does not correlate at all with the orientations of the ductile structures.This is not interpreted to indicate that the subordinate rock types are discordant to the foliation, but that a large amount of the subordinate rock types occur in undeformed and well preserved host rock. Although similarities exist, the orientations of the pegmatites that are dominated by steep dips, display the largest deviations from the orientation of the ductile structures.

If a comparison is made on an overall rock domain basis (Appendix 9, Figure 3-25, Figure 3-26 and Figure 3-27), it is obvious that the best correlation between the orientation of the ductile structures and the subordinate rock types exists in the quartz monzodiorite (RSMD01) in southern Laxemar (Figure 3-25). The foliation, ductile to brittle-ductile shear zones, fine-grained granite and fine-grained diorite-gabbro display dominant sub-horizontal to moderate dips to the south. Note that mafic rocks have been suggested to be the cause of the gently south-dipping M2 and M3 seismic reflectors (cf. Appendix 13 and ZSMEW946A in Appendix 14). In contrast to the other subordinate rock types, the pegmatites are dominated by vertical to steep dips and

RSMD01 foliation

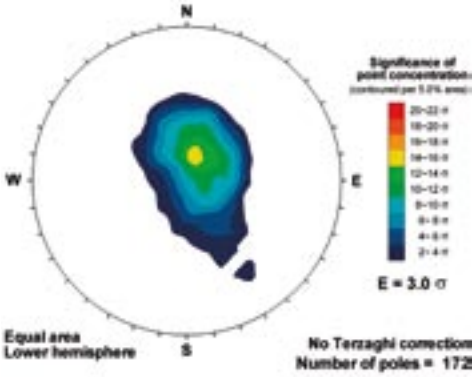

RSMD01 fine-grained granite

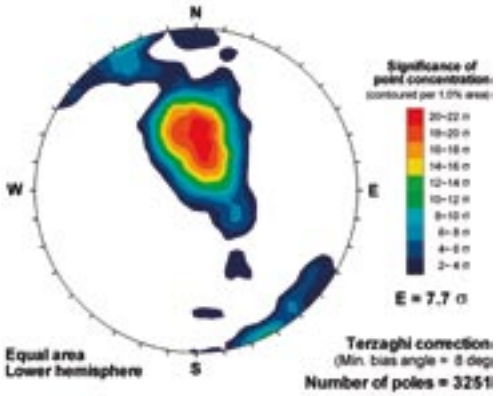

RSMD01 shear zones

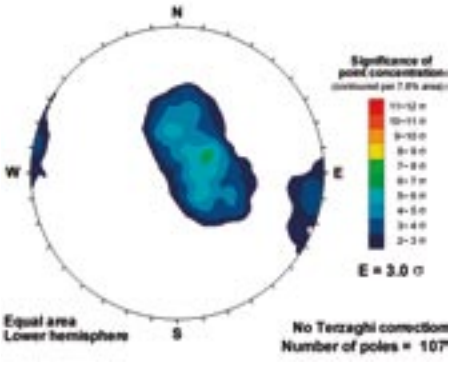

RSMD01 fine-grained diorite-gabbro

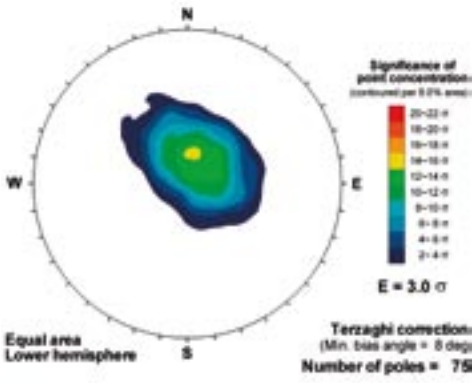

RSMD01 pegmatite

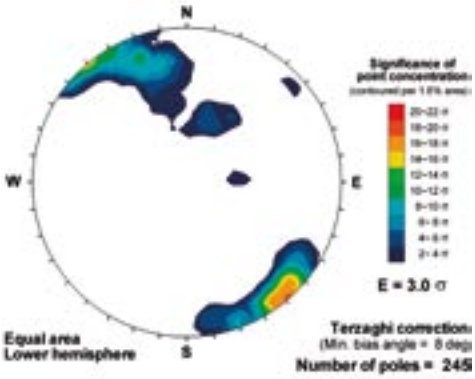

Figure 3-25. *Kamb-contoured stereoplots illustrating the comparison of the orientation of foliation, ductile and brittle-ductile shear zones and the orientation of fine-grained granite, fine-grained diorite-gabbro and pegmatite in the quartz monzodiorite (i.e. the RSMD01 domain) in southern Laxemar.*

NE-SW to ENE-WSW strike, and a set of NE-SW to ENE-WSW striking, vertically to steeply dipping fine-grained granite also occur. Apart from the sub-horizontal to gently dipping shear zones, NNE-SSW oriented steep to vertical shear zones occur as well.

Although similarities exist in the orientation of the ductile structures and the subordinate rock types in the central (RSMM01) and northern (RSMA01) part of Laxemar as well, there are obvious differences. For example, there is no corresponding orientation of subordinate rock types to the moderately north-dipping foliation in central Laxemar (Figure 3-26). In northern Laxemar (Figure 3-27), the foliation is predominantly dipping moderately to the north, while the subordinate rock types display both sub-horizontal dips, as well as dips to the north and south.

RSMM01 foliation

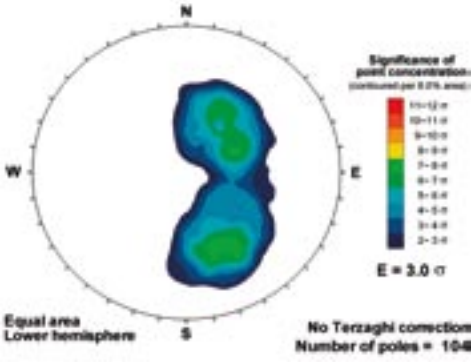

RSMM01 fine-grained granite

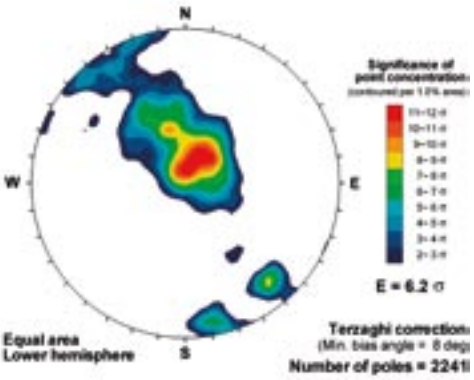

RSMM01 shear zones

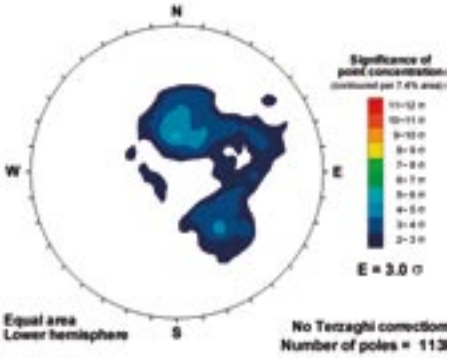

RSMM01 fine-grained diorite-gabbro

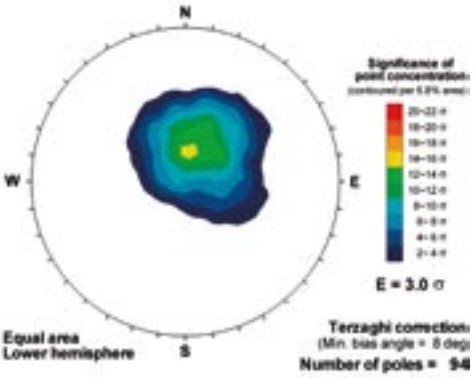

RSMM01 pegmatite

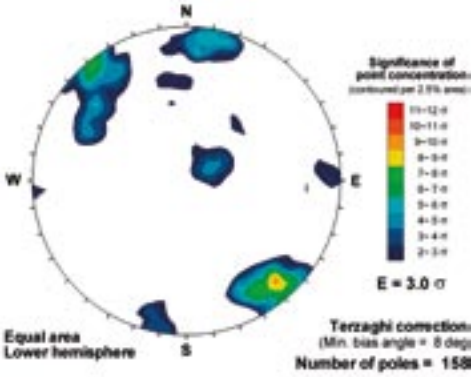

Figure 3-26. *Kamb-contoured stereoplots illustrating the comparison of the orientation of foliation, ductile and brittle-ductile shear zones and the orientation of fine-grained granite, fine-grained diorite-gabbro and pegmatite in the Ävrö quartz monzodiorite (i.e. the RSMM01 domain) in central Laxemar.*

In summary it can be said that the orientation of the ductile structures and the orientation of subordinate rock types display a similar pattern in southern Laxemar. However, this similarity decreases northwards. While the foliation displays consistent dips to the north, there is a larger spread in the orientation of the subordinate rock types. In combination, the orientation of the foliation and the subordinate rock types constitute the prime anisotropy factor in the bedrock. Due to the faint to weak nature of the foliation, its non-uniform distribution and that only c 20% of the bedrock has been classified as foliated, the subordinate rock types are considered as the most important anisotropy factor in the bedrock.

RSMA01 foliation

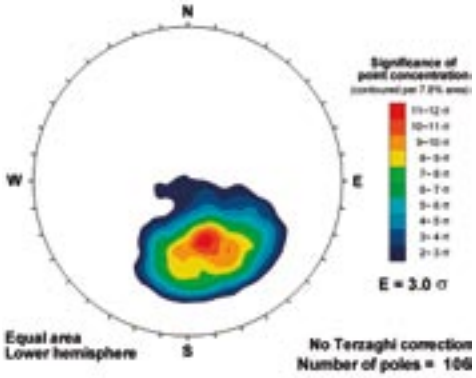

RSMA01 fine-grained granite

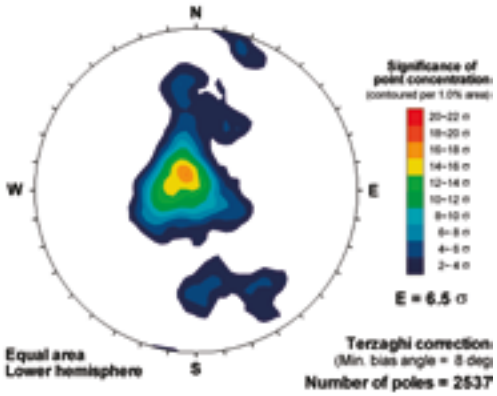

RSMA01 shear zones

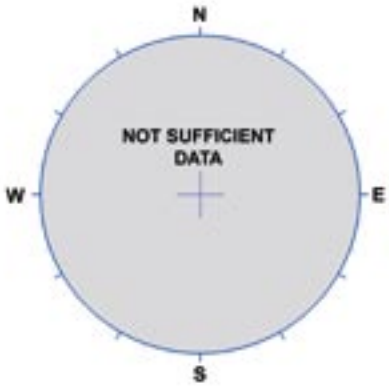

RSMA01 fine-grained diorite-gabbro

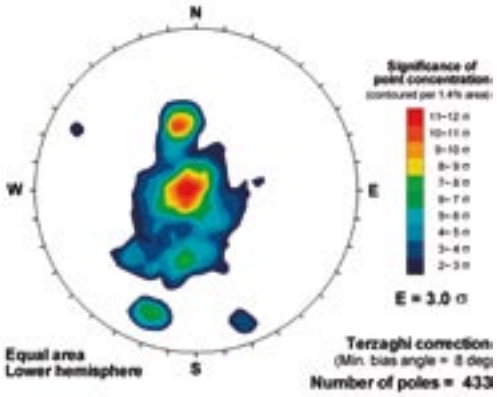

RSMA01 pegmatite

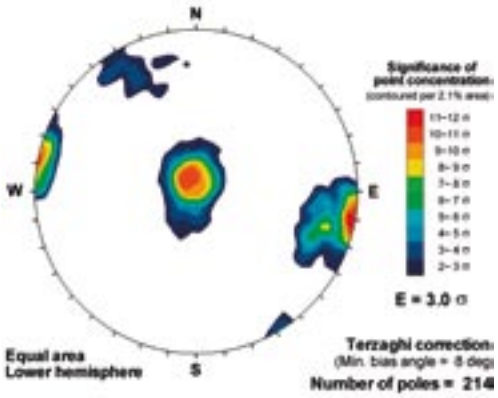

Figure 3-27. *Kamb-contoured stereoplots illustrating the comparison of the orientation of foliation, ductile and brittle-ductile shear zones and the orientation of fine-grained granite, fine-grained diorite-gabbro and pegmatite in the Ävrö quartz monzodiorite (i.e. the RSMM01 domain) in central Laxemar.*

3.5.4 Anisotropy of magnetic susceptibility (AMS)

As a complement to the structural data from the surface and the cored boreholes, studies of the anisotropy of magnetic susceptibility (AMS) have been carried out in five different projects in the Laxemar-Simpevarp area in connection with the site investigation /Mattsson et al. 2003, Mattsson et al. 2005a, Mattsson 2006a, Mattsson 2006b/. One of these projects comprised a special study of a shear zone (ZSMNE012A; denoted NE-1 in an Äspö HRL context) in the access tunnel to the Äspö Hard Rock Laboratory /Mattsson 2006b/.

Based on the determination of the magnetic susceptibility of the sampled rock types, it was concluded that magnetite is the dominant carrier of the magnetic anisotropy. This implies that the AMS is primarily governed by the grain shape and orientation of the magnetite grains. The AMS-ellipsoids show a continuous variation in shape from strongly prolate to strongly oblate. The degrees of anisotropy are below 1.4 for most unaltered rocks. This indicates that the rocks have suffered only weak ductile deformation, which is in accordance with the designated classification faint to weak in the Boremap mapping. Although there is some scatter in the data, the orientation of the magnetic foliations displays a fairly consistent pattern in Laxemar. In general, the orientation of the foliation planes is E-W to WNW-ESE, i.e. more or less concordant to the boundaries between the dominant rock types.

The stereographic plots in Figure 3-28 display the poles to the magnetic foliation planes and the magnetic lineation for unaltered rock samples from Laxemar. In Figure 3-29, which displays the complete collection of AMS data, the stereographic plots are slightly "biased" by the deformed rocks of the Äspö shear zone and the deformation zone ZSMNE012A (denoted NE-1 in an Äspö HRL context). As can be seen in Figure 3-28, it is clear that the poles to the foliations of these rocks form a girdle-like distribution, which indicates a folded geometry. The pole to the best-fit great circle is marked and, thus, corresponds to the orientation of the inferred fold axis. The majority of all foliation planes show dip directions to the north, and locations with dip directions to the south and west are concentrated close to the boundary between the quartz monzodiorite and Ävrö quartz monzodiorite.

The magnetic lineation (maximum strain) directions show consistent north-westerly to west-northwesterly orientations at Laxemar (Figure 3-29). Plunges are generally moderate to shallow. Note that the mean value for the orientation of the lineations (Figure 3-28 lower stereoplot) is very similar to the pole to the best-fit great circle (Figure 3-28 upper diagram), which indicates that the regional maximum strain is sub-parallel to the indicated fold axis. The majority of directions that deviate from the north-westerly orientation in Figure 3-29 are from locations within or close to ductile deformation zones.

The data from the northern profile of the traditional Äspö shear zone (ZSMNE005A) indicate a structural fabric that varies distinctly with distance from the deformation zone. Far west of the deformation zone the AMS fabric is identical with the fabric of Ävrö granite in Laxemar. Within a c 250 metre wide transition zone outside the deformation zone centre, there is a clearly detectable counter-clockwise rotation of the magnetic foliations, accompanied by an increase in the dip of foliation planes. Within the zone centre there is a general increase in the counter-clockwise rotation, and the dip becomes even steeper. The variation in orientation of the magnetic foliation

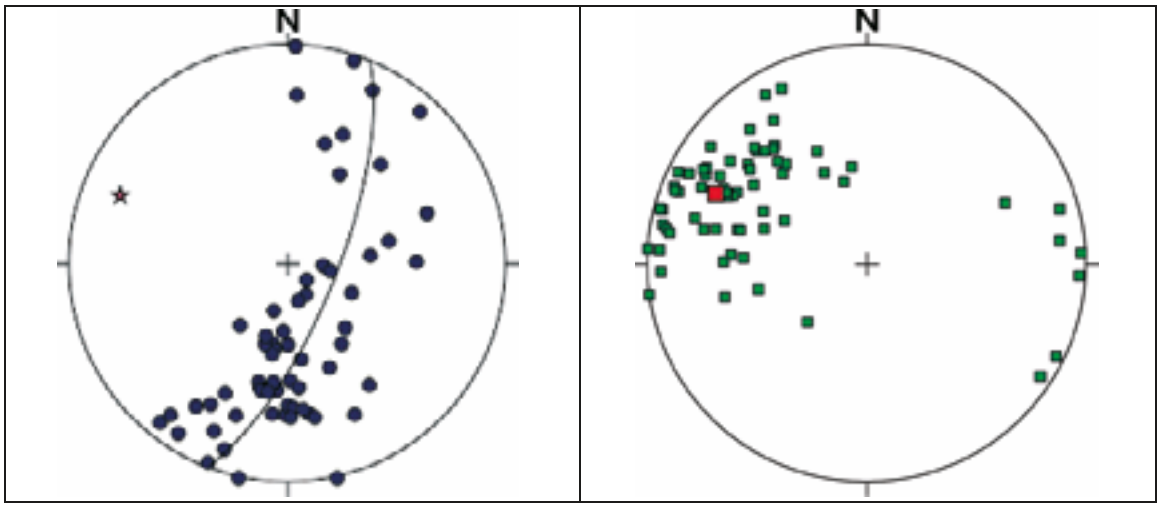

Figure 3-28. *Equal area plot (lower hemisphere) of AMS data from Laxemar showing the poles to the magnetic foliation (left) and the magnetic lineation (right). The star in the left stereoplot marks pole to great circle. The red square in the right stereoplot marks mean value of the lineations.*

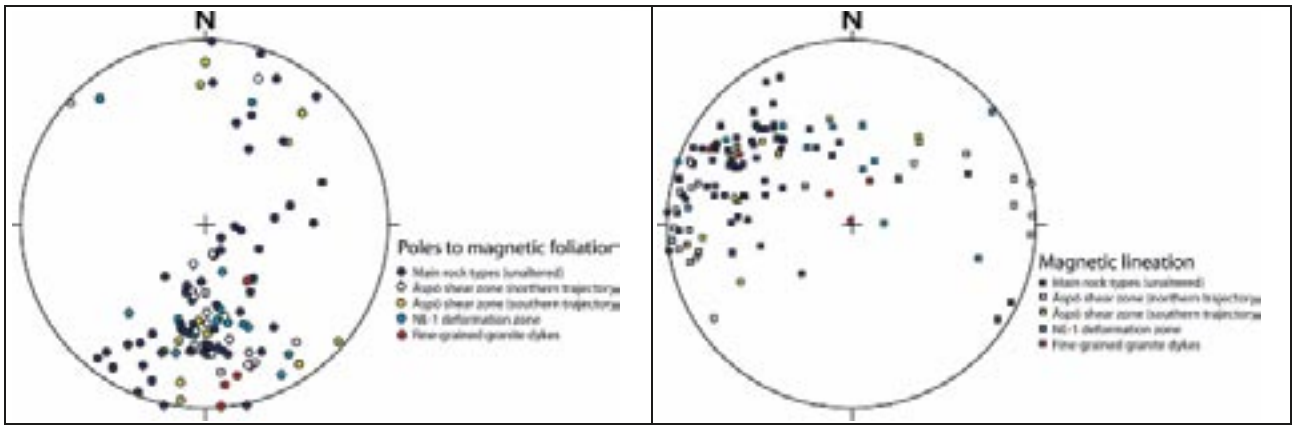

Figure 3-29. *Equal area plot (lower hemisphere) of all AMS data showing the poles to the magnetic foliation (left) and the magnetic lineation (rigth).*

across the ductile shear zone ZSMNE005A is in agreement with the sinistral sense of movement that is indicated from the kinematic data reported in Section 3.5.1. Moreover, the AMS data across the deformation zone ZSMNE012A (NE-1) in the access tunnel to the Äspö HRL is in agreement with that expected from a ductile deformation zone with a sinistral sense of movement.

For a more comprehensive description of the AMS studies, see /Mattsson et al. 2003, Mattsson et al. 2005a, Mattsson 2006a, Mattsson 2006b/.

3.6 Brittle deformation and fracture statistics

3.6.1 Data generated from detailed mapping of fractures at the surface

Data derived from the mapping of fracture traces at the ground surface are keys to understanding the size, spatial, and temporal relationships of fracturing at Laxemar. Outcrop studies are the only direct source of information regarding fracture size at scales smaller than those covered by regional geophysics or LIDAR.

Detail-mapped outcrops

A key component of the geological DFN model is the detailed fracture maps derived from outcrops in the Laxemar sub-area. These data underpin the DFN size model, and are also useful in the development of spatial models of fracturing. The four outcrops mapped represented either natural rock exposures or areas of bedrock from which overburden has been removed. They are generally rectilinear in shape, and range from 200–600 m^2 in area. Three of these bedrock surfaces were used as drill sites for percussion and cored boreholes during site investigation activities and are no longer exposed. The locations of the detail-mapped outcrops are presented below in Figure 3-30.

Mapping efforts at the outcrops were primarily focussed on describing the orientation, size, morphology, and physical properties of the exposed rock fractures; a secondary focus was bedrock lithology and rock alteration. Only fractures with a visible surface trace length longer than 0.5 m were mapped on the outcrop; however, on most outcrops, a pair of perpendicular scanlines was mapped separately. Fracture traces as small as 0.3 m were mapped along the scanlines. An example of an outcrop summary map is presented below as Figure 3-31. Summary statistics, including the number of fractures mapped and the outcrop areal fracture intensity (P_{21}), are presented in Table 3-4. Fracture traces were surveyed using a total station, with the resulting digital maps imported into the SKB GIS database SDE. Fracture properties, including orientation, aperture, termination style, lithology, mineral infillings, and morphology were recorded in Sicada.

Figure 3-30. *Locations of outcrops on which detailed fracture mapping was performed.*

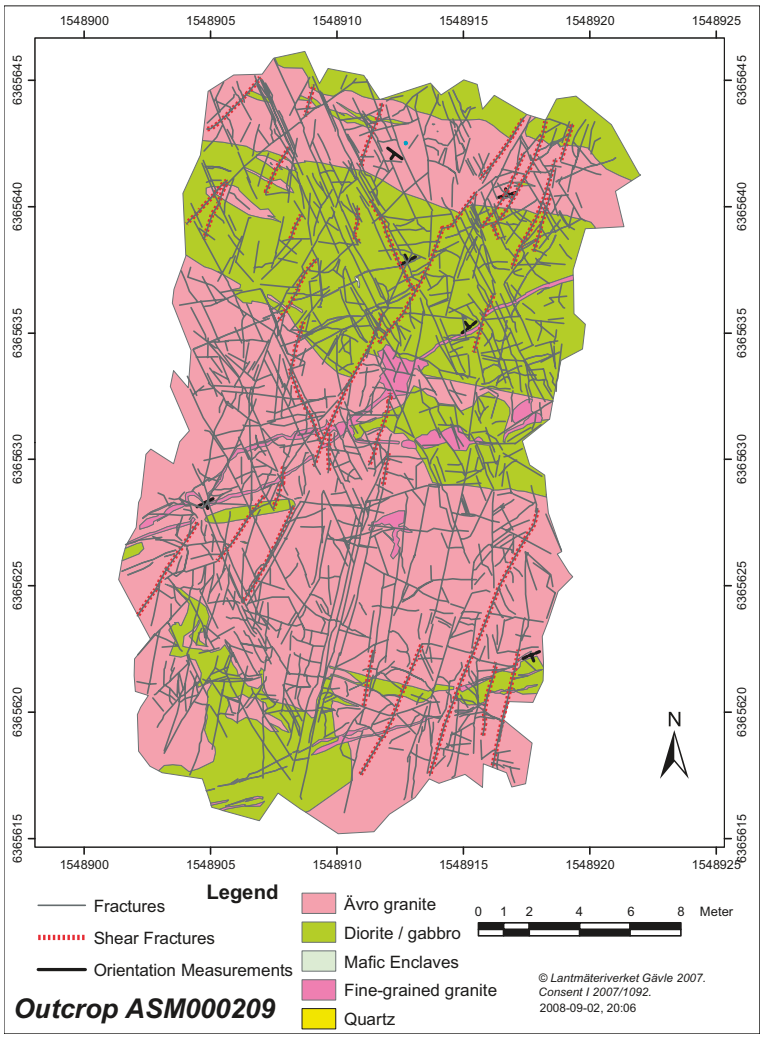

Figure 3-31. *Example of fracture map of outcrop ASM000209. This map illustrates the fracture traces and lithologies exposed on the outcrop. Shear fractures are fractures along which evidence of sinistral or dextral displacement has been observed.*

Table 3-4. Descriptive statistics of fracture traces longer than 0.5 m identified on detail-mapped outcrops.

Outcrop	# of	Tracelength of fractures				Outcrop area	P_{21}
IDCODE	Traces	Total	Mean	Median	Std. dev.	(m^2)	(1/m)
ASM000208	1,034	1,327.42	1.26	1.01	0.85	330.70	4.01
ASM000209	1,030	1,484.41	1.44	1.04	1.19	442.10	3.36
ASM100234	1,128	1,789.68	1.59	1.15	1.37	478.60	3.74
ASM100235	1,028	1,337.34	1.30	1.04	0.83	332.60	4.02

For complete details regarding the outcrop mapping process, as well as summary maps for additional outcrops, readers are encouraged to consult the SDM-Site Laxemar data compilation report /Hermanson et al. 2008/.

In general, four major fracture orientations were noted in the outcrop data; north-south striking, east-northeast striking, west-northwest striking, and, to a lesser extent, a group of fractures that strikes east-west and north-northwest which have moderate to sub-horizontal dips. Considerable variability was observed in the strike orientation of moderately- to sub-horizontally-dipping fractures. This is not surprising, however, since it is difficult to accurately measure the strike of fractures that intersect flat outcrops at very small angles. Note that the relative intensities of each pole cluster change from outcrop to outcrop. This observation is the basis for the fracture domain model at Laxemar (cf. Section 6.2.1).

Trench mapping

In 2006 and 2007, additional surface mapping was done along narrow strips of cleared land in the Laxemar local model area. The goal was to investigate the surface extent of potential minor deformation zones identified in data from regional airborne geophysics, high-resolution ground magnetic surveys, and airborne laser topographic surveys (LIDAR), as well as to provide additional data coverage for rock domain and DFN modelling efforts. The mapping results are presented in detail in the data compilation report for Laxemar by /Hermanson et al. 2008/ and by /Forssberg et al. 2007/.

The trench investigation was performed using a similar methodology as for the detailed fracture outcrops. Each trench was cleared of soil and organics, and both the fractures and the bedrock lithology were mapped in detailed. High-resolution digital photographs of each outcrop were taken, orthorectified, and merged into a continuous montage upon which mapped fracture data could be plotted. However, there were some slight differences in the fracture mapping protocol for the trenches in comparison to the outcrops described in the previous section. These differences included:

- Along each strip, fracture traces were measured within a 1 m wide corridor.
- Only traces longer than 1 m were mapped.
- Fractures with trace lengths > 1 m which had at least one end within the 1 m wide band were measured over their full length (including the section of the trace that lay outside the 1 m mapping band).

The illustration in Figure 3-34 shows orthorectified outcrop photographs, with mapped fracture traces (yellow lines) and the 1 m-swath mapping limits (dashed white line). Mapped traces extend outside as far as can be observed or to the boundary of the outcrop.

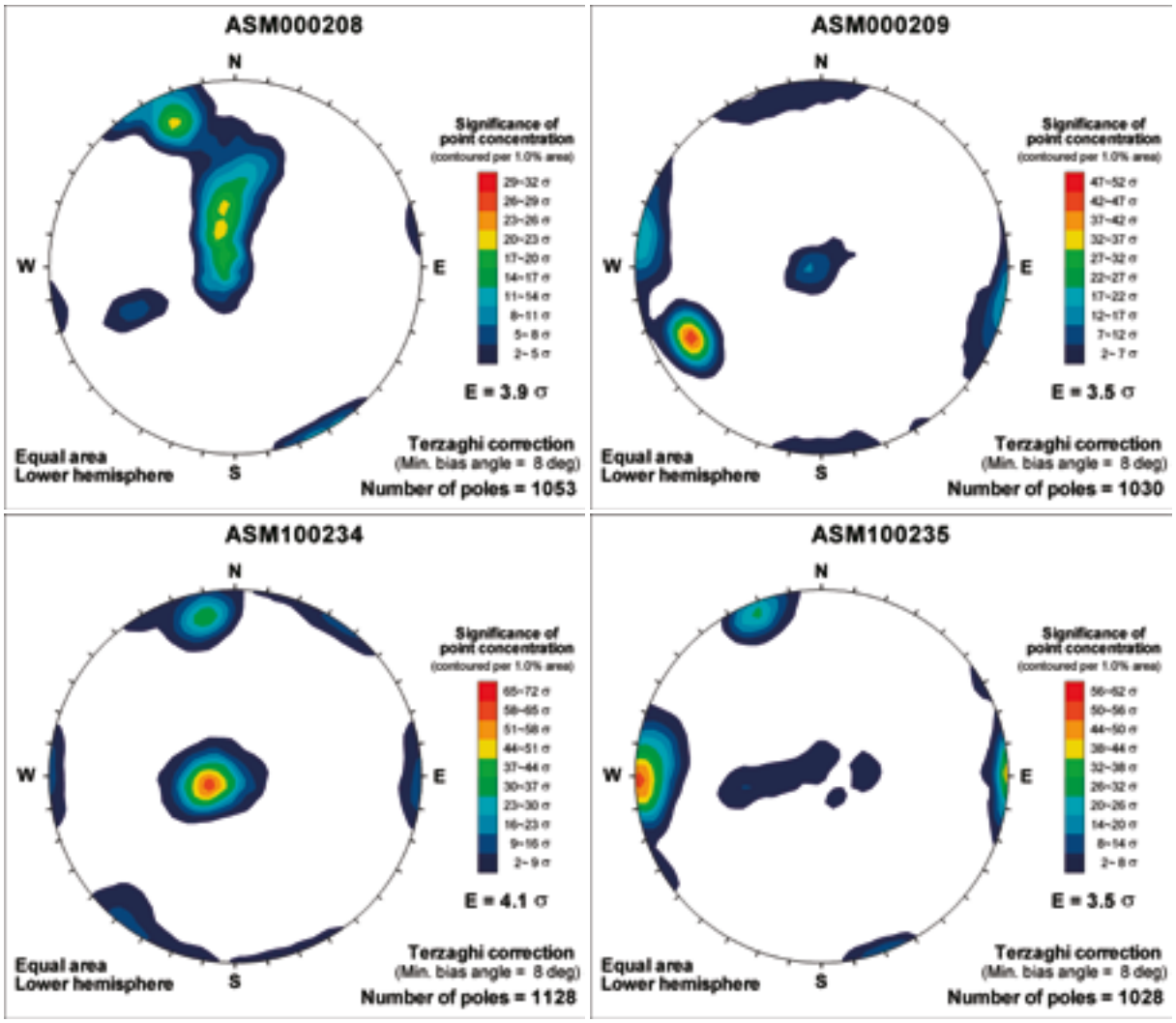

Figure 3-32. *Orientations of fracture traces exposed on detail-mapped outcrops in the Laxemar local model area. The plots represent contoured lower-hemisphere stereonets of the poles to the fracture planes derived from the fracture traces.*

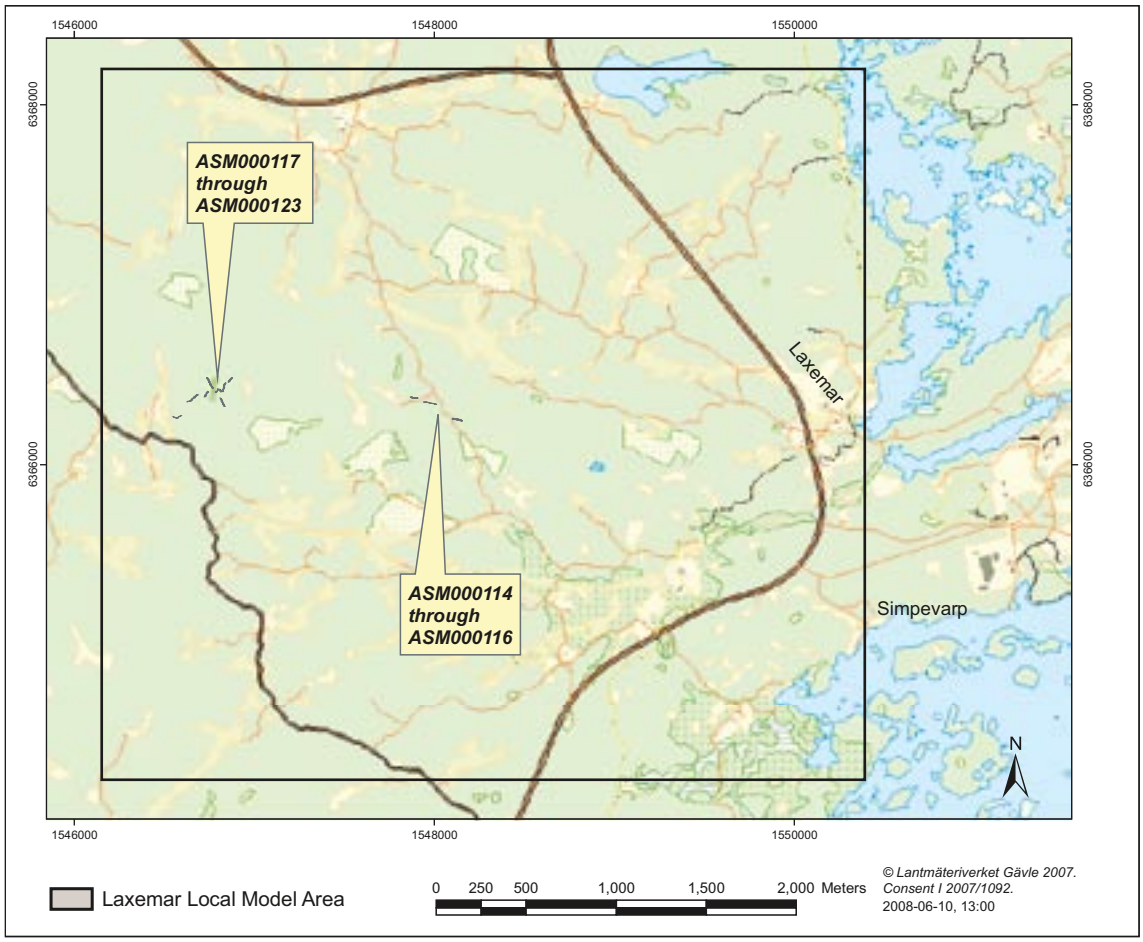

Figure 3-33. *Location of trench outcrops mapped at Laxemar in 2006 and 2007.*

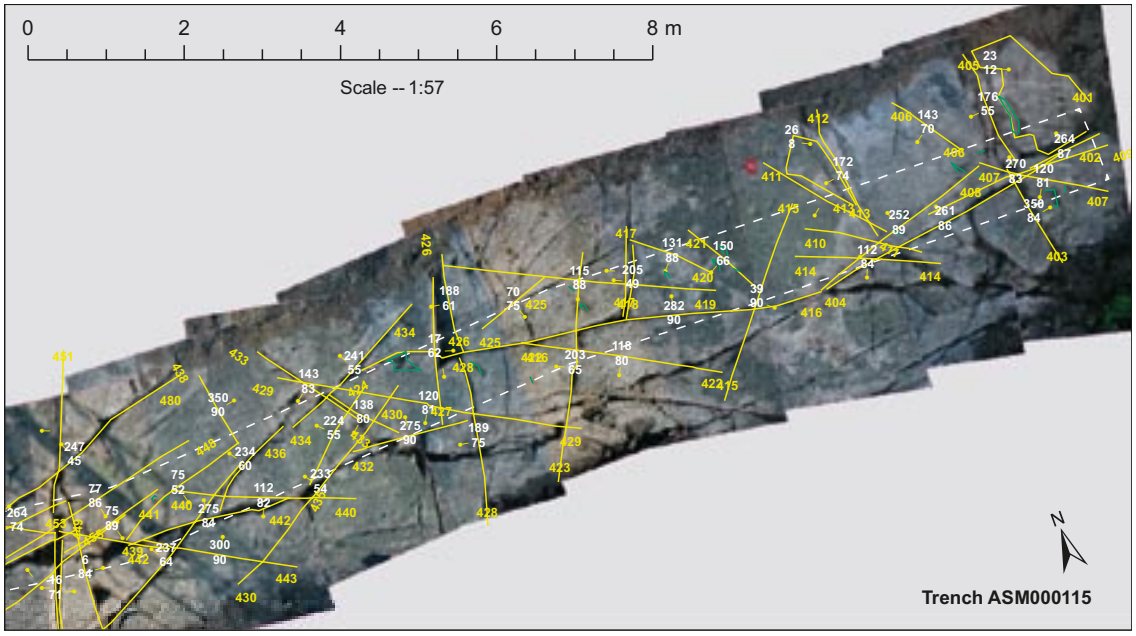

Figure 3-34. *Photographic map of trench ASM000115, illustrating bedrock fractures and extent of the 1 m mapped swath (dashed white line). Yellow text indicates fracture number, while white text indicates the strike (top) and dip (bottom) of the mapped fracture.*

The trench maps were used predominantly in the confirmation of the size, extent, and character of minor deformation zones suggested by data from regional airborne geophysics, high-resolution ground magnetic surveys, and airborne laser topographic surveys (LIDAR). The trench data set was used in the geological DFN modelling in the development of the fracture domain (Section 6.2.1) and orientation (Section 6.2.2) models.

3.6.2 Fracture orientation in cored borehole sections outside deformation zones

The orientation of fractures outside of identified deformation zones and minor deformation zones are presented below as Figure 3-35 through Figure 3-49. Fracture orientations are described as lower-hemisphere stereonet plots, with fracture pole density expressed as Kamb contours. Kamb's method /Kamb 1959/ is an alternative method of producing density contours on a stereonet that reduces the effect of sample size on the contours, as well as allowing for the direct comparison of orientation data sets with different sample sizes /Vollmer 1995/.

The fracture orientations presented in Figure 3-35 through Figure 3-49 are based on a subset of the available cored borehole fracture records from Sicada. Specifically, the figures include only fractures for which an orientation (strike and dip, expressed as a pole trend and plunge) was recorded in Sicada and has traces visible on the walls of the borehole in the BIPS image logs. Orientations of fractures logged inside identified deformation zones are presented in Section 3.6.3. The rationale behind using only fractures visible in the BIPS image logs is discussed in Section 3.1.3.

A Terzaghi correction has been applied to the contoured fracture pole data to reduce the sampling bias related to the relative orientation between the boreholes and the fractures. Fractures with orientations that are close to the orientation of the borehole will be undersampled relative to fractures with orientations roughly perpendicular to the borehole. For example, sub-vertically dipping boreholes will tend to preferentially intersect shallowly to moderately dipping fractures, resulting in a bias against sub-vertically dipping fractures. The Terzaghi correction utilises the average borehole bearing and inclination, based on the coordinates of the borehole collar and the measured end of the borehole. The drill paths of many of the cored boreholes are not straight lines; the path tends to curve with increasing depth. As a result, the Terzaghi correction will not completely correct for all effects of orientation sampling bias.

In general, five general clusters of fracture orientations are visible in the cored borehole data at Laxemar. By far the strongest cluster is made up moderately- to sub-horizontally-dipping fractures. The strike direction of these fractures is quite variable; however, a slight propensity towards north-south strike with east dip was noted. In terms of vertically- to sub-vertically-dipping fractures, clusters of north-south, east-northeast, west-northwest, and north-northwest striking fractures are noted. Data from several boreholes (KLX04, KLX07, KLX08 and the KLX09 series of boreholes; cf. Figure 3-35, Figure 3-36, Figure 3-37, and Figure 3-38) suggest that the east-northeast and west-northwest fractures may form a conjugate set.

Note that a more formal analysis of fracture orientations was conducted as part of the geological DFN model development and parameterisation. The results of this analysis are summarised in Sections 6.2.2 and 6.4.2, and are discussed in detail in the geological DFN report /La Pointe et al. 2008/. Orientation plots classified by depth and fracture domain are also presented in the Laxemar DCR report /Hermanson et al. 2008/.

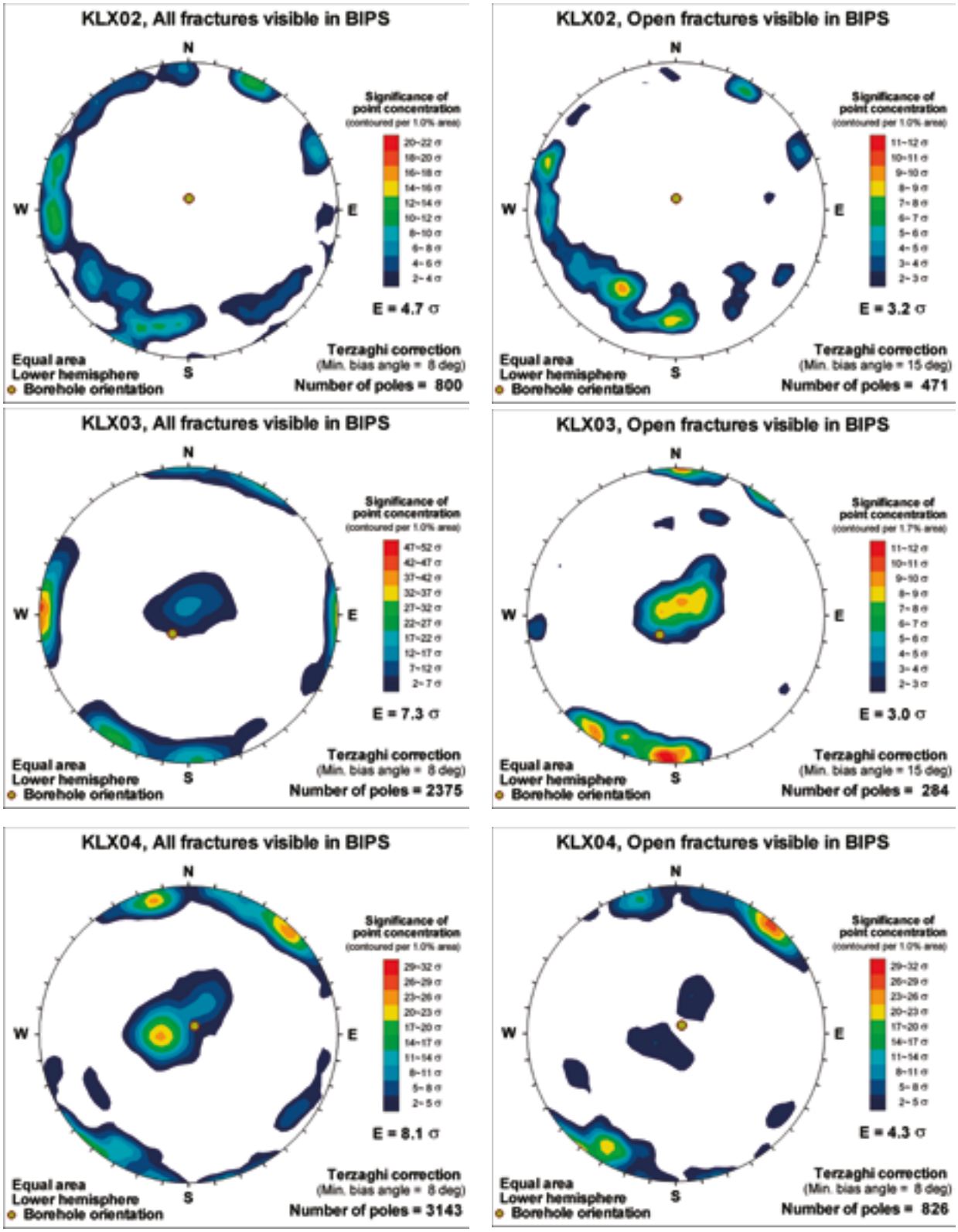

Figure 3-35. *Kamb-contoured stereoplots illustrating fracture orientations in Laxemar cored boreholes KLX02, KLX03, and KLX04.*

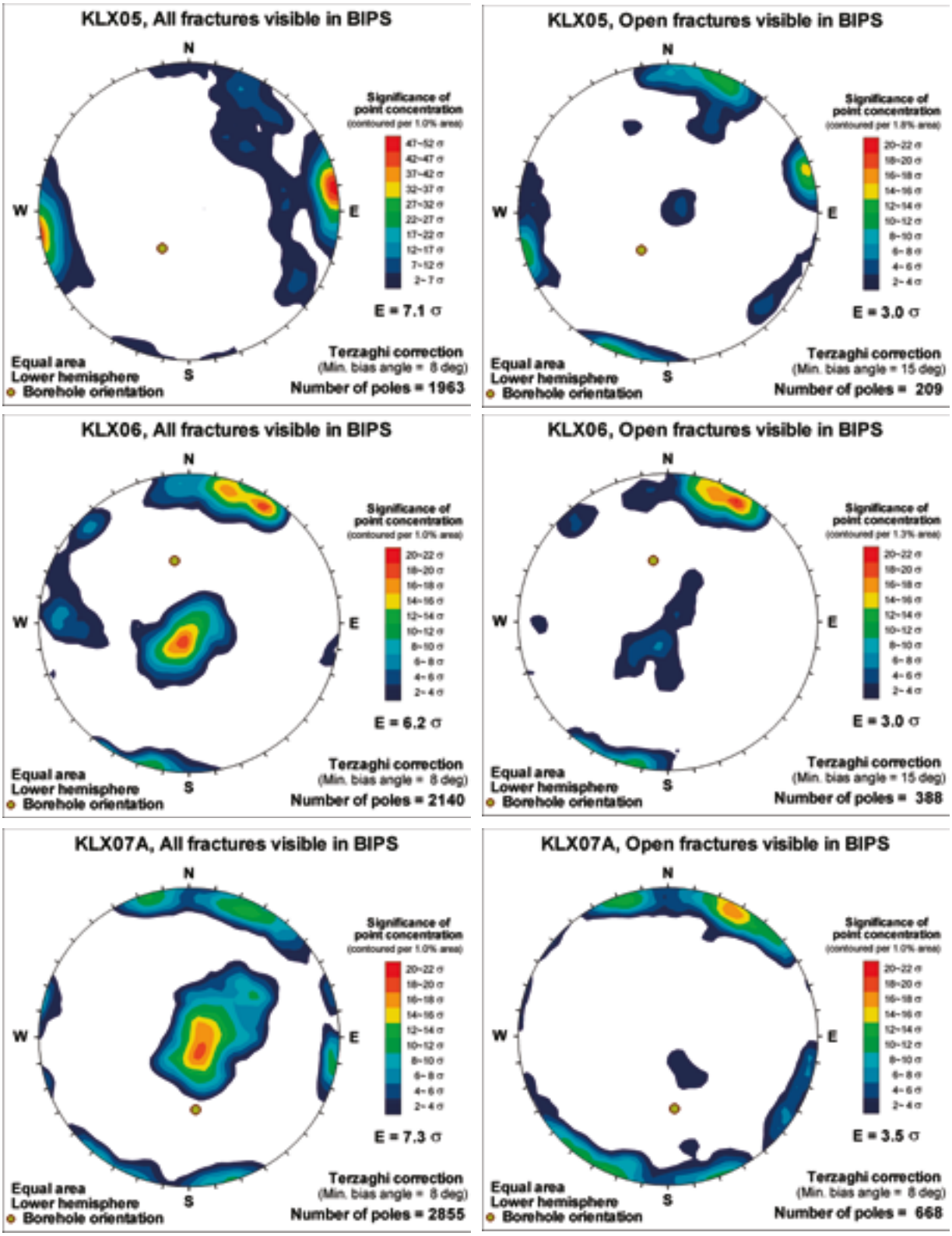

Figure 3-36. *Kamb-contoured stereoplots illustrating fracture orientations in Laxemar cored boreholes KLX05, KLX06, and KLX07A.*

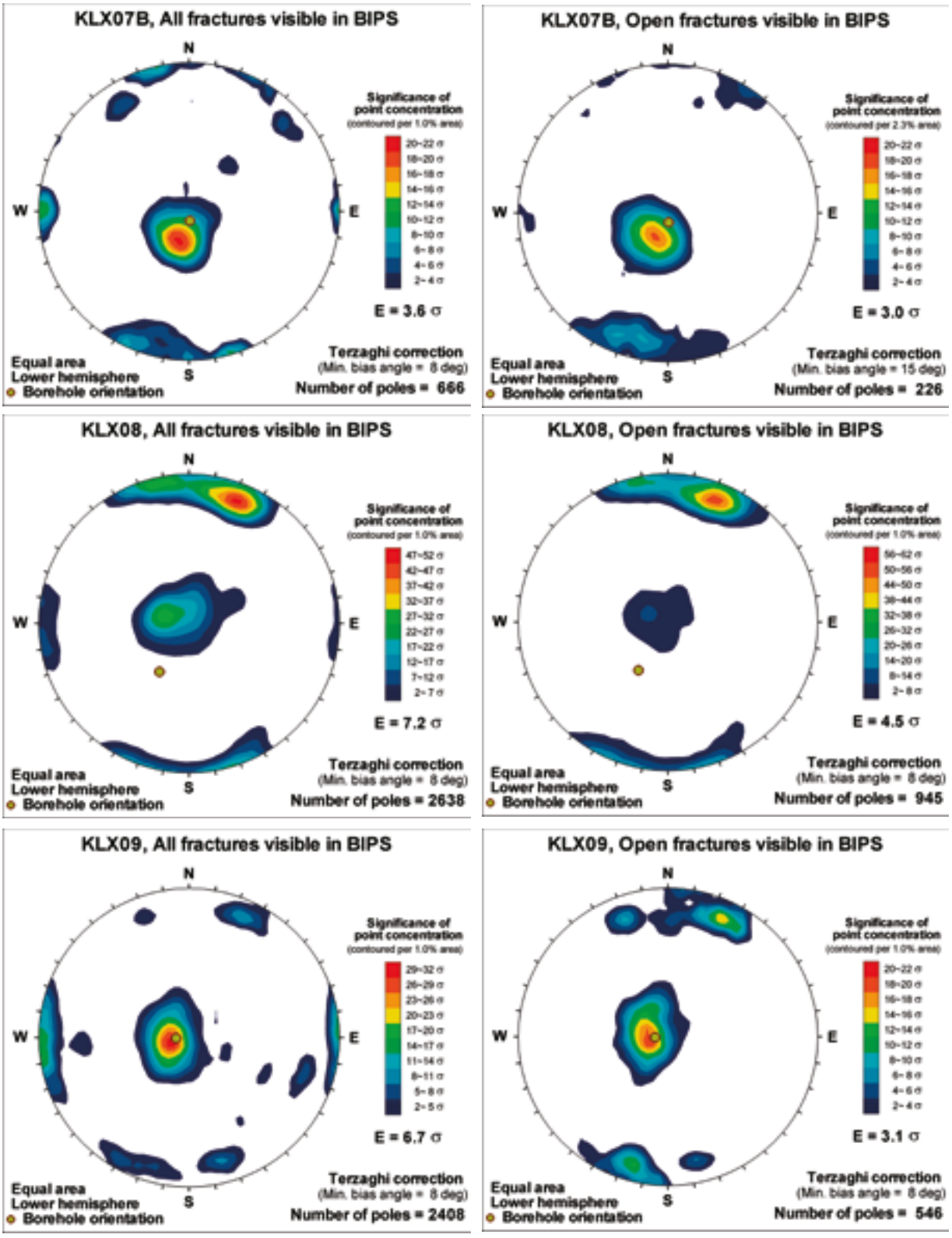

Figure 3-37. *Kamb-contoured stereoplots illustrating fracture orientations in Laxemar cored boreholes KLX07B, KLX08, and KLX09.*

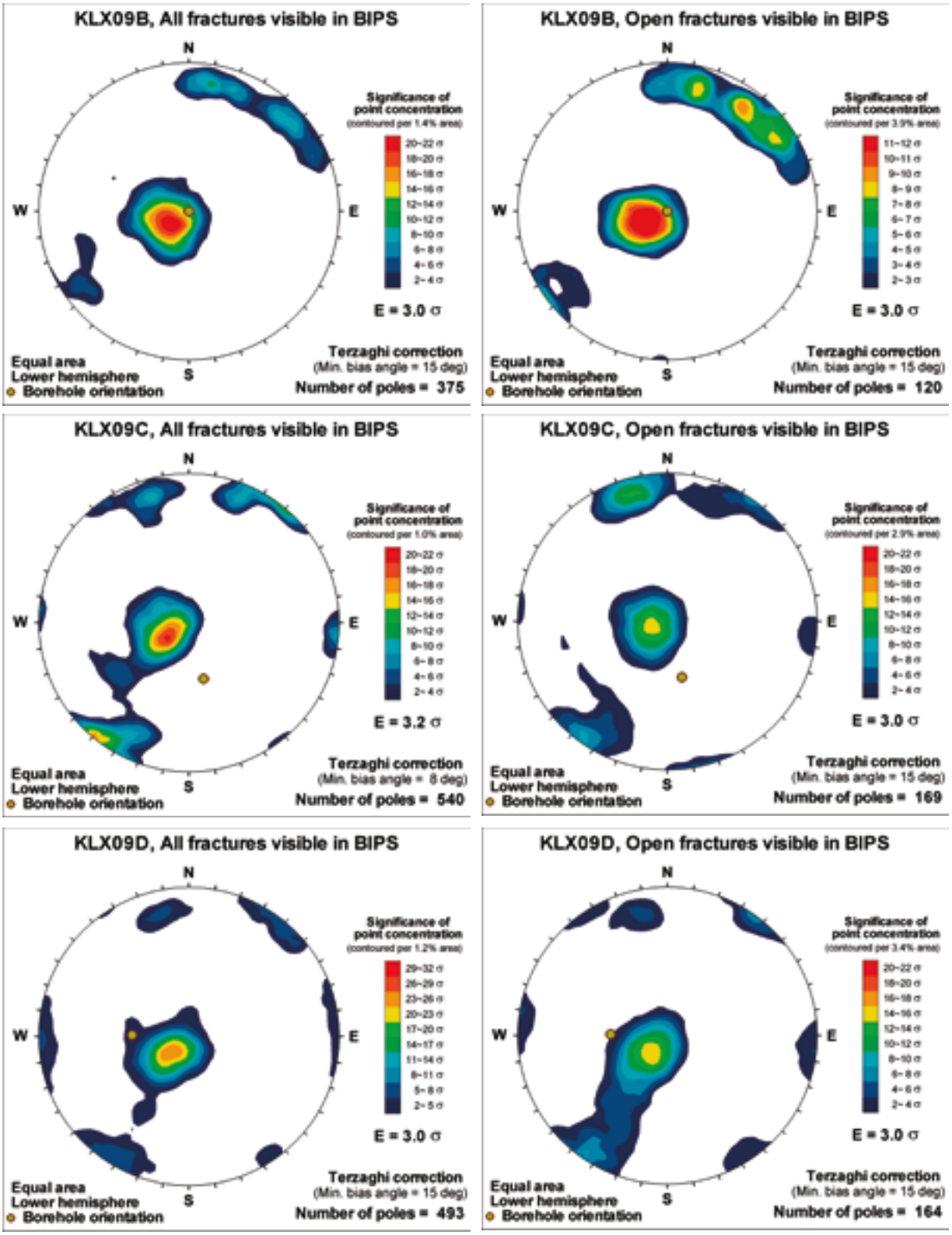

Figure 3-38. *Kamb-contoured stereoplots illustrating fracture orientations in Laxemar cored boreholes KLX09B, KLX09C, and KLX09D.*

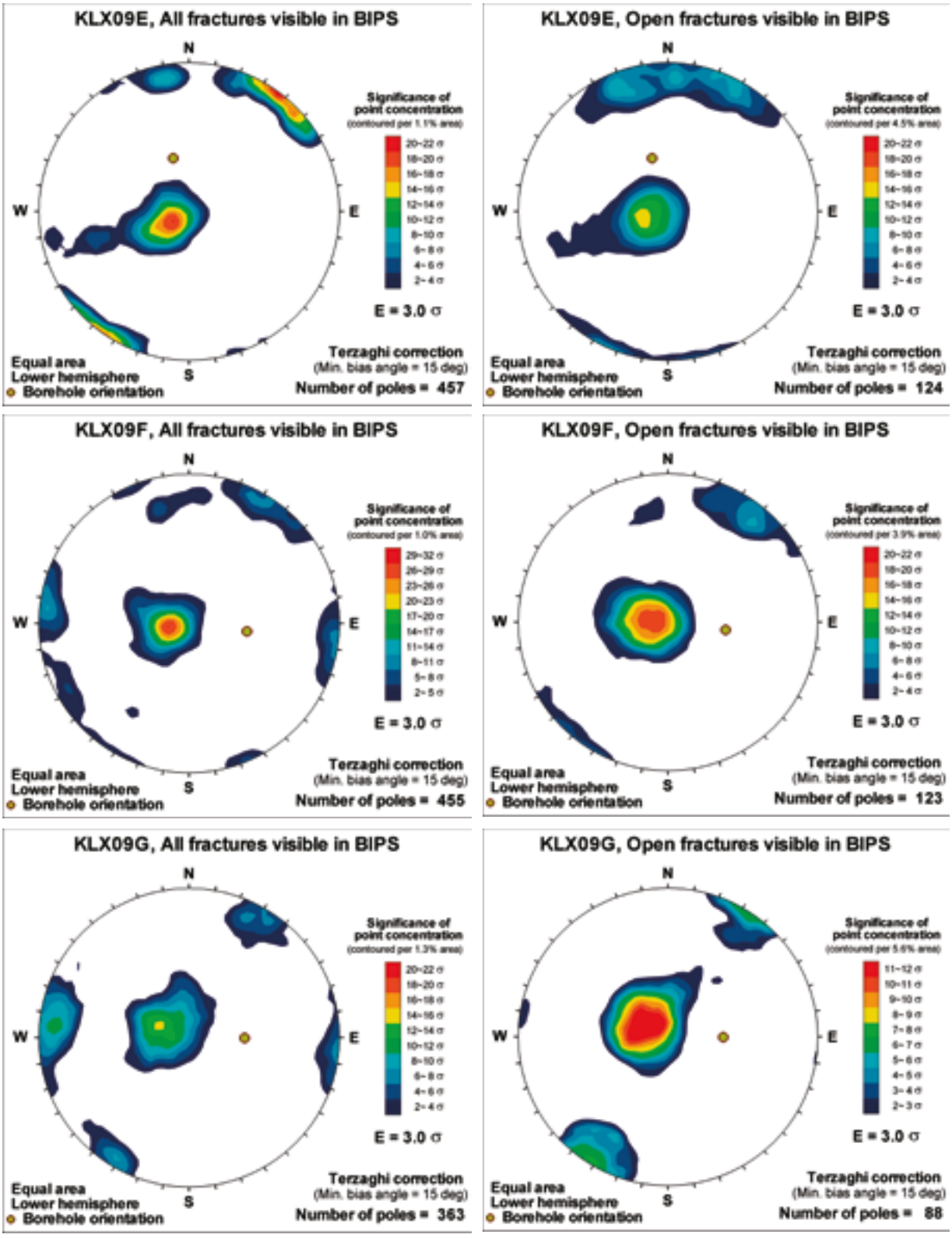

Figure 3-39. *Kamb-contoured stereoplots illustrating fracture orientations in Laxemar cored boreholes KLX09E, KLX09F, and KLX09G.*

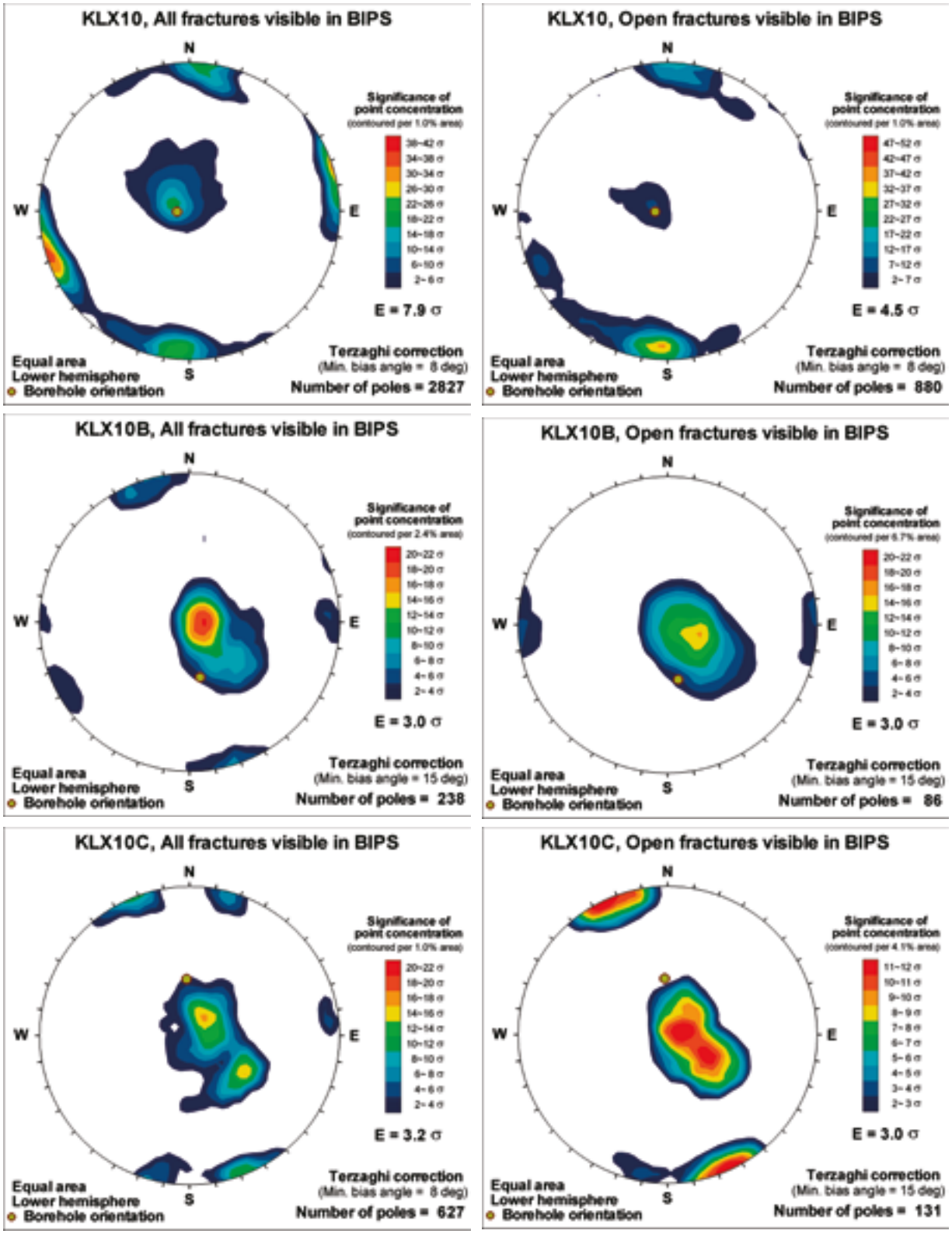

Figure 3-40. *Kamb-contoured stereoplots illustrating fracture orientations in Laxemar cored boreholes KLX10, KLX10B, and KLX10C.*

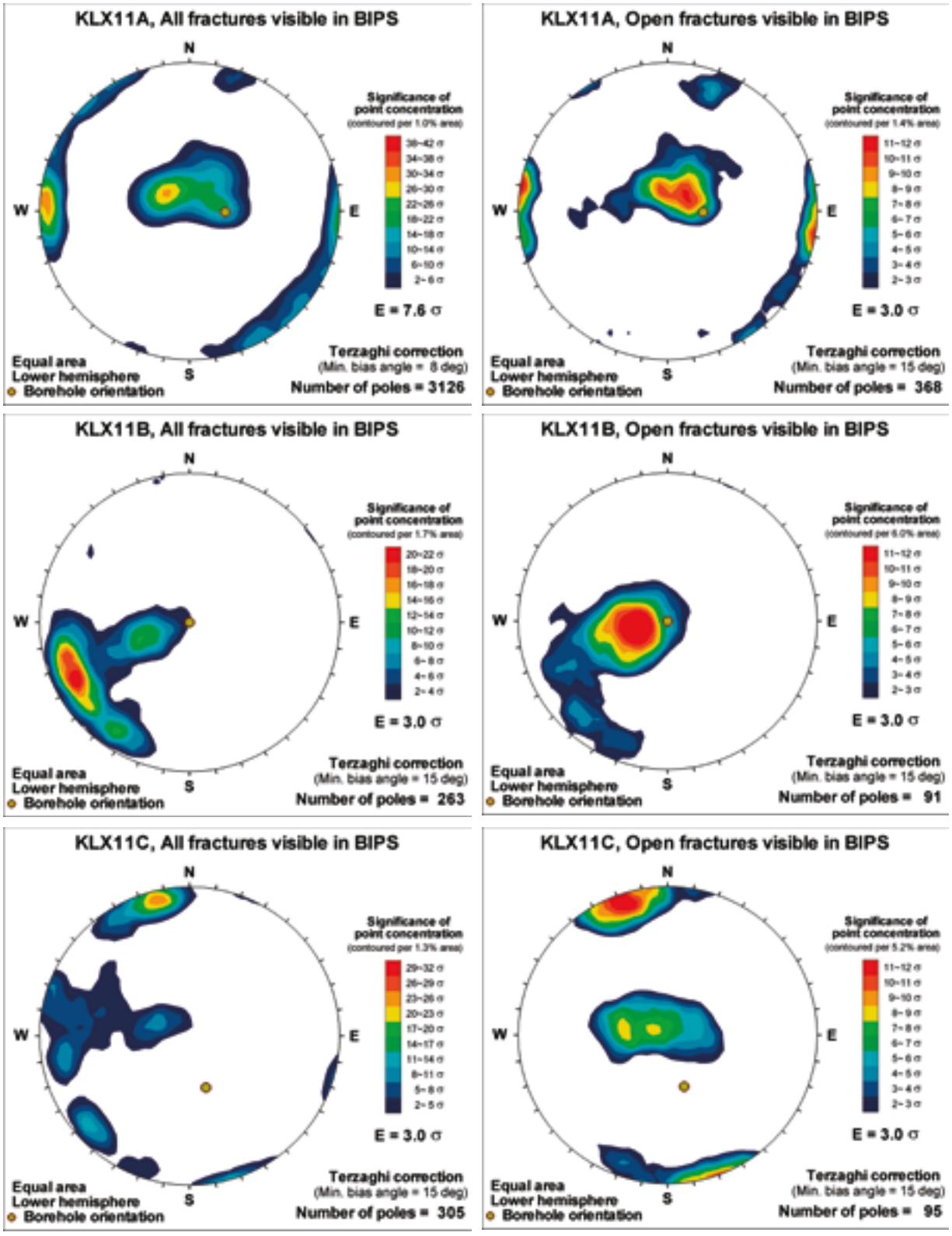

Figure 3-41. *Kamb-contoured stereoplots illustrating fracture orientations in Laxemar cored boreholes KLX11A, KLX11B, and KLX11C.*

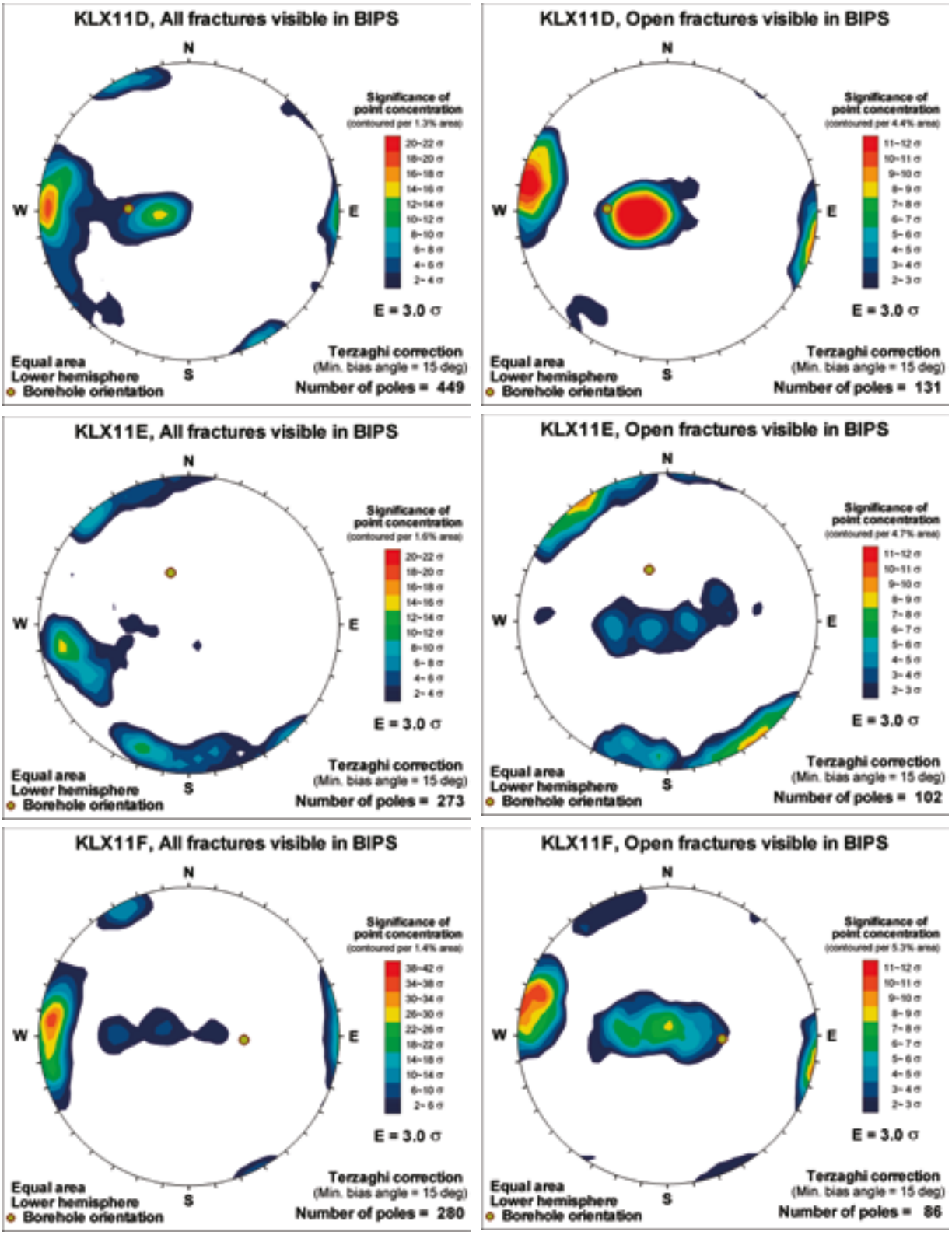

Figure 3-42. *Kamb-contoured stereoplots illustrating fracture orientations in Laxemar cored boreholes KLX11D, KLX11E, and KLX11F.*

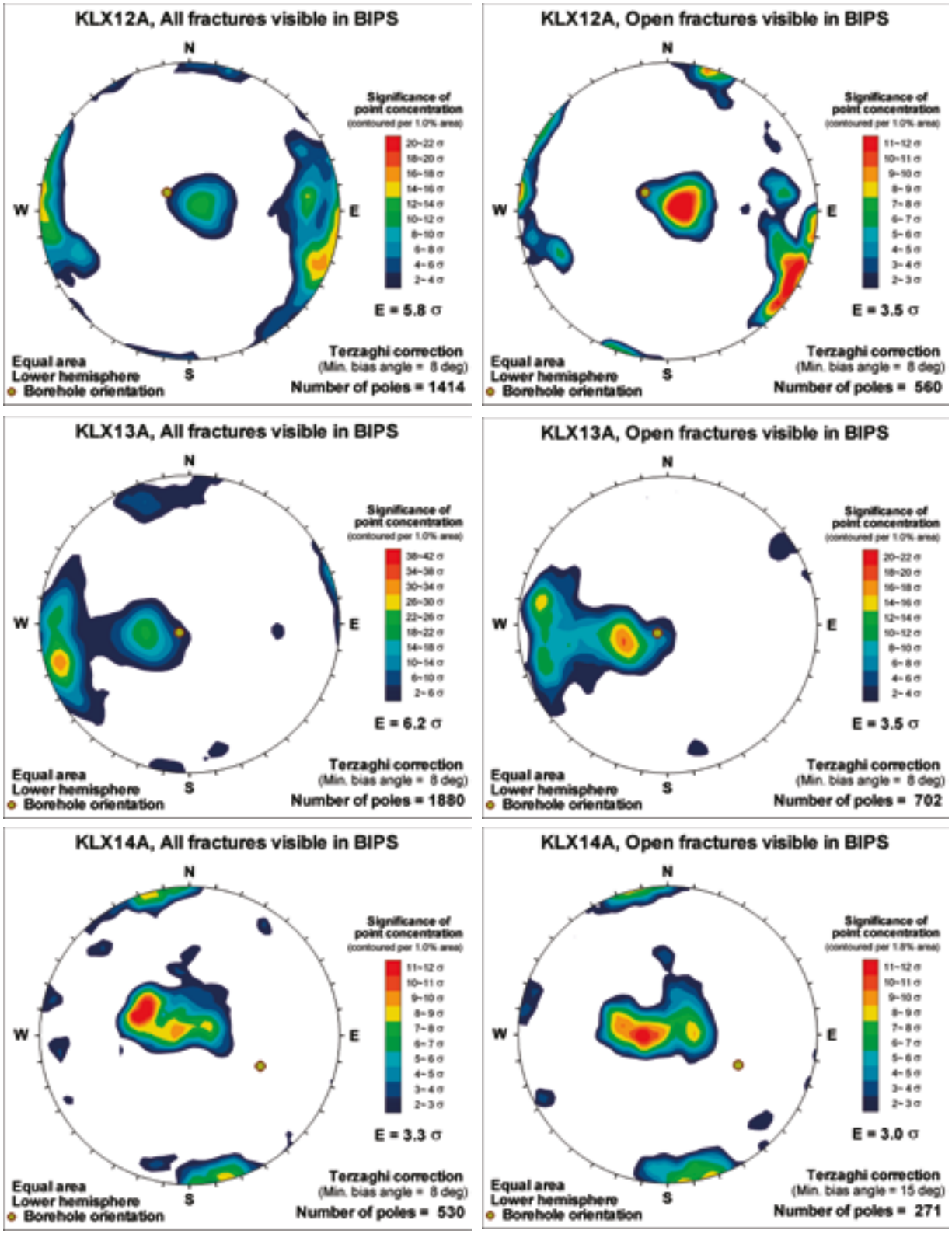

Figure 3-43. *Kamb-contoured stereoplots illustrating fracture orientations in Laxemar cored boreholes KLX12A, KLX13A, and KLX14A.*

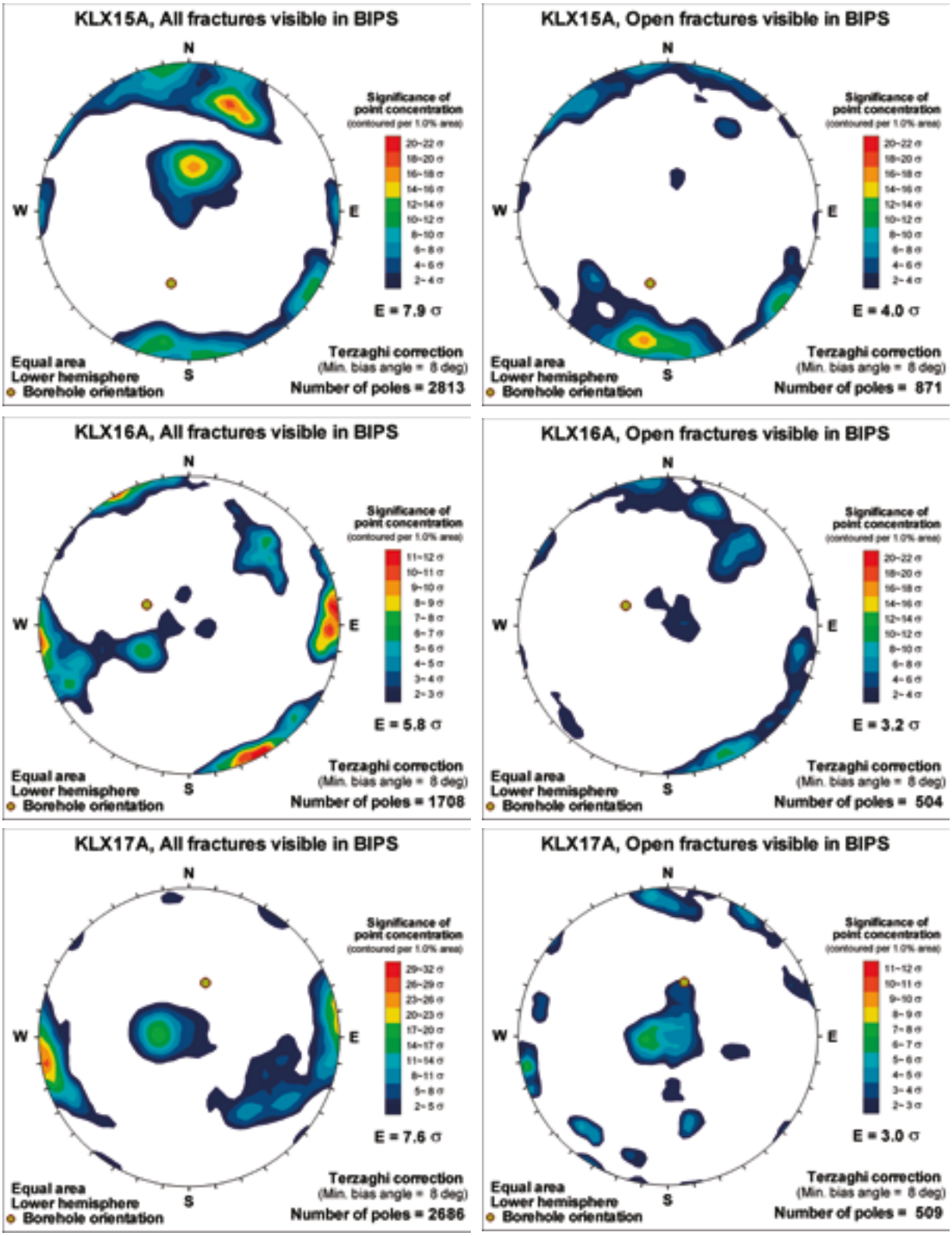

Figure 3-44. *Kamb-contoured stereoplots illustrating fracture orientations in Laxemar cored boreholes KLX15A, KLX16A, and KLX17A.*

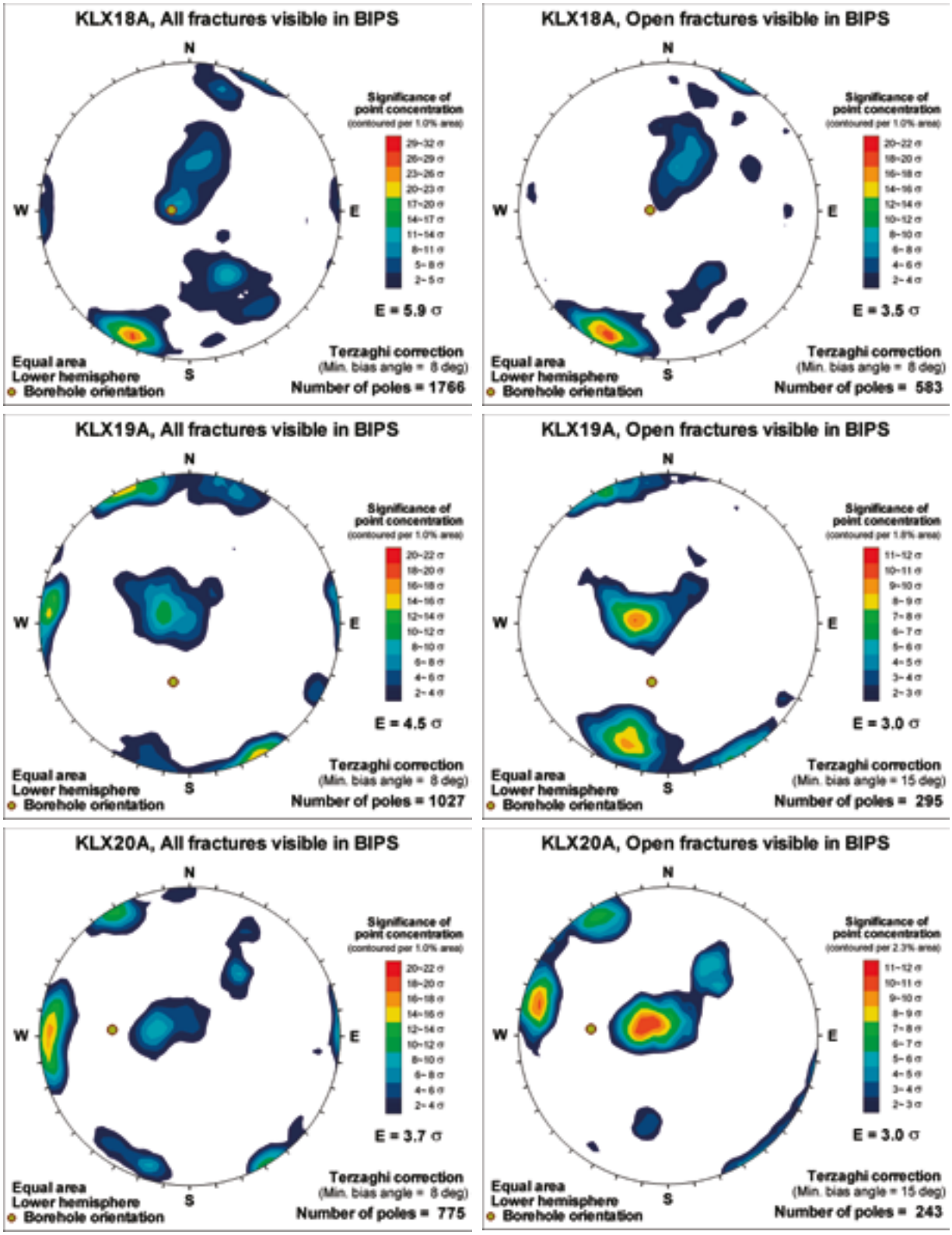

Figure 3-45. *Kamb-contoured stereoplots illustrating fracture orientations in Laxemar cored boreholes KLX18A, KLX19A, and KLX20A.*

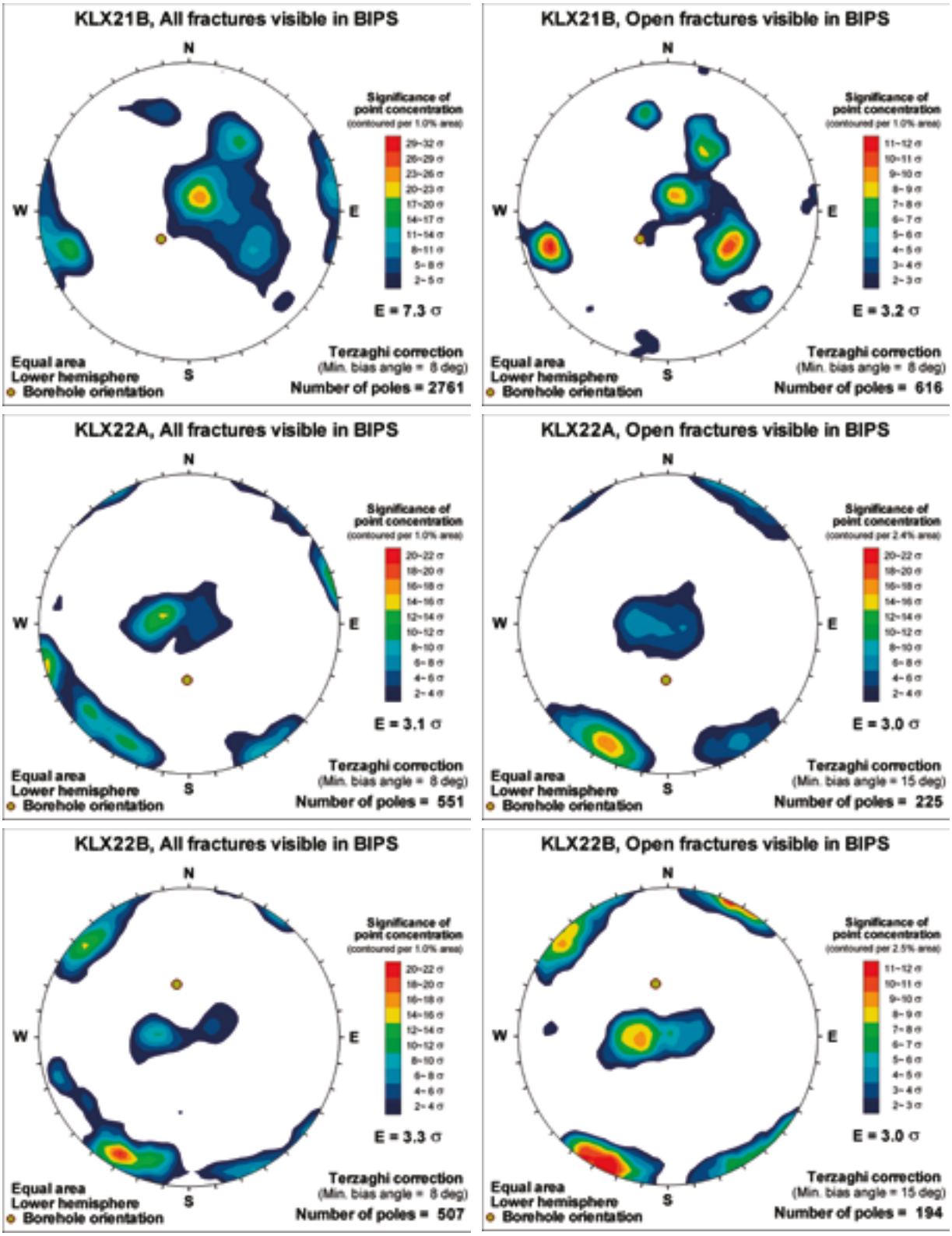

Figure 3-46. *Kamb-contoured stereoplots illustrating fracture orientations in Laxemar cored boreholes KLX21B, KLX22A, and KLX22B.*

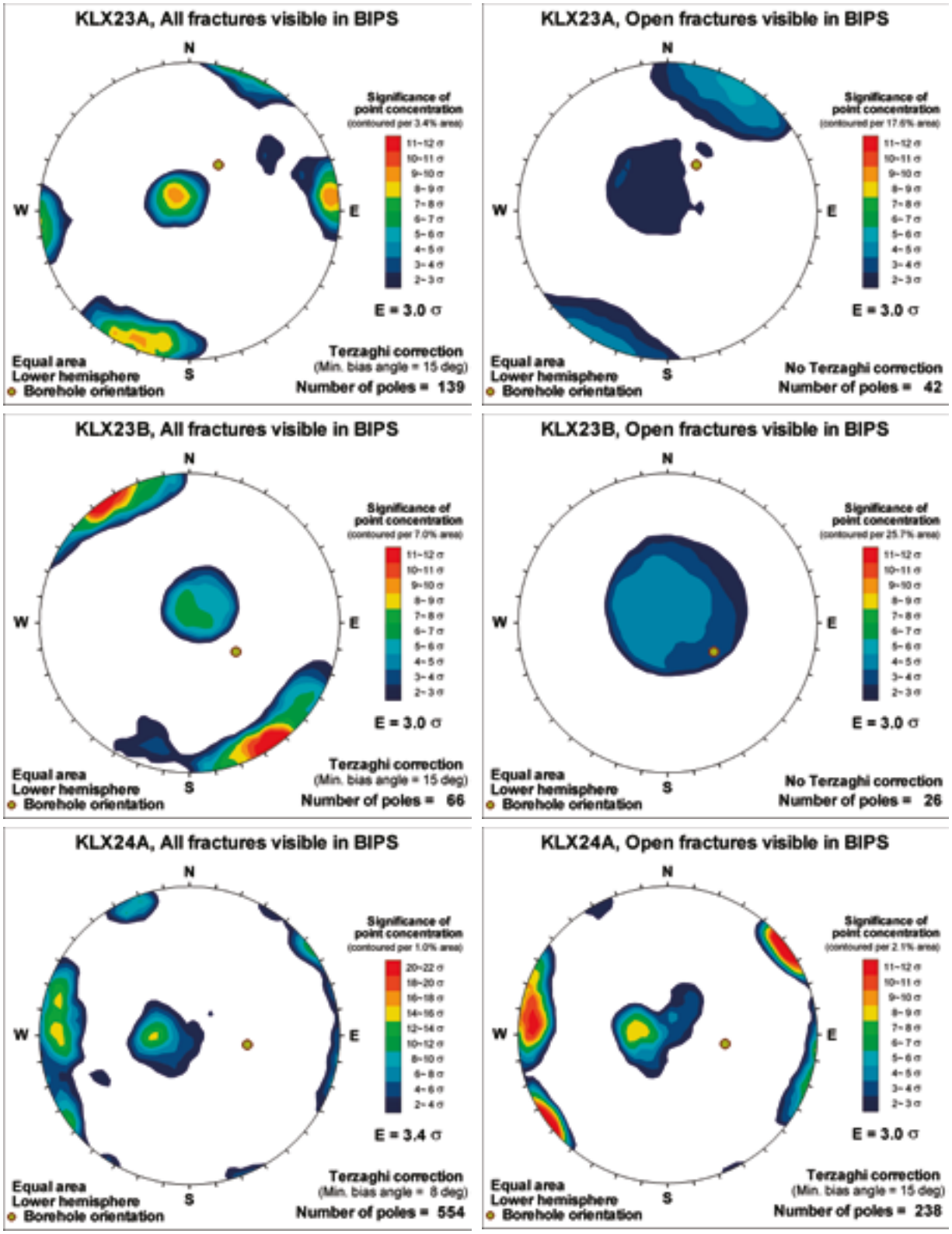

Figure 3-47. *Kamb-contoured stereoplots illustrating fracture orientations in Laxemar cored boreholes KLX23A, KLX23B, and KLX24A.*

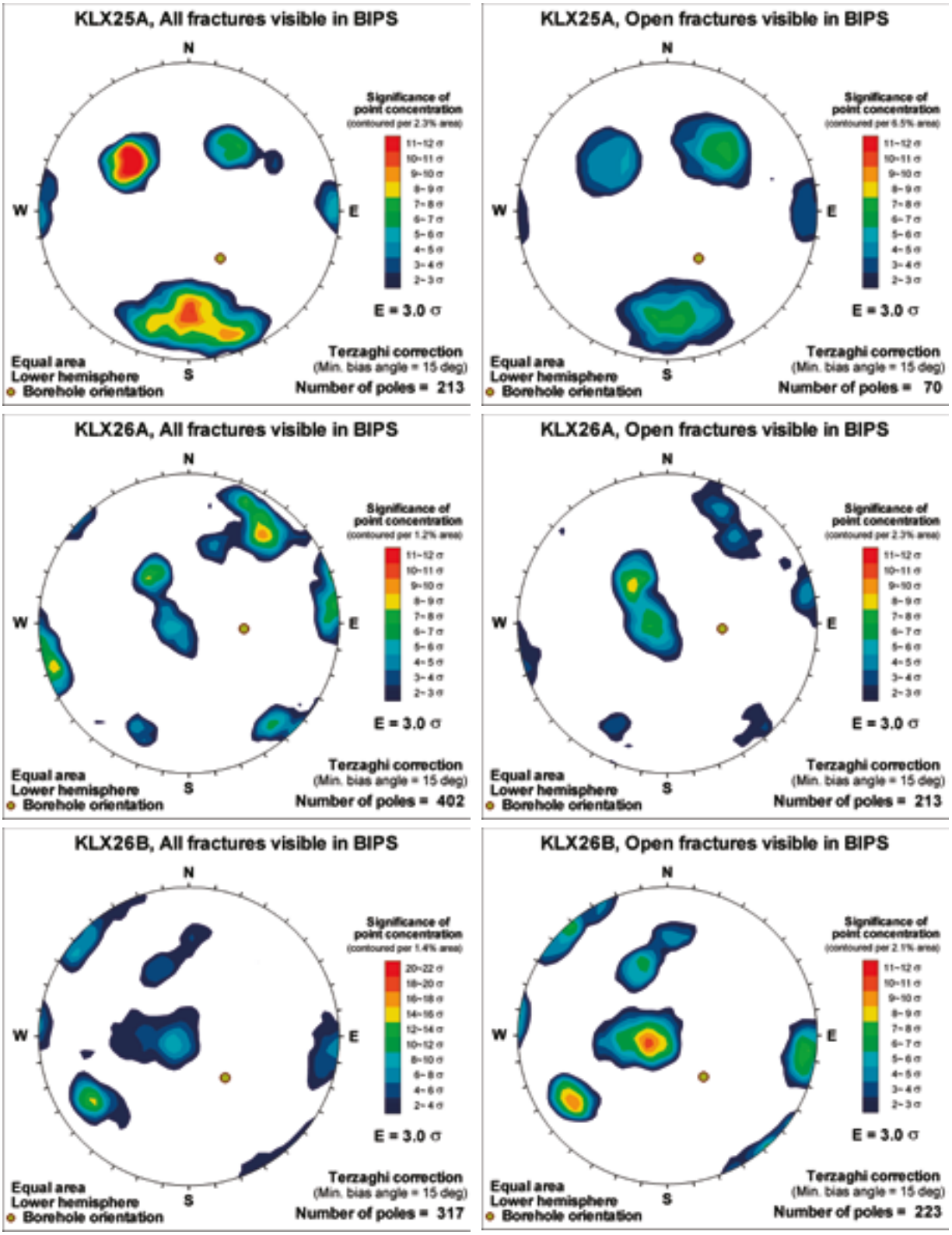

Figure 3-48. *Kamb-contoured stereoplots illustrating fracture orientations in Laxemar cored boreholes KLX25A, KLX26A, and KLX26B.*

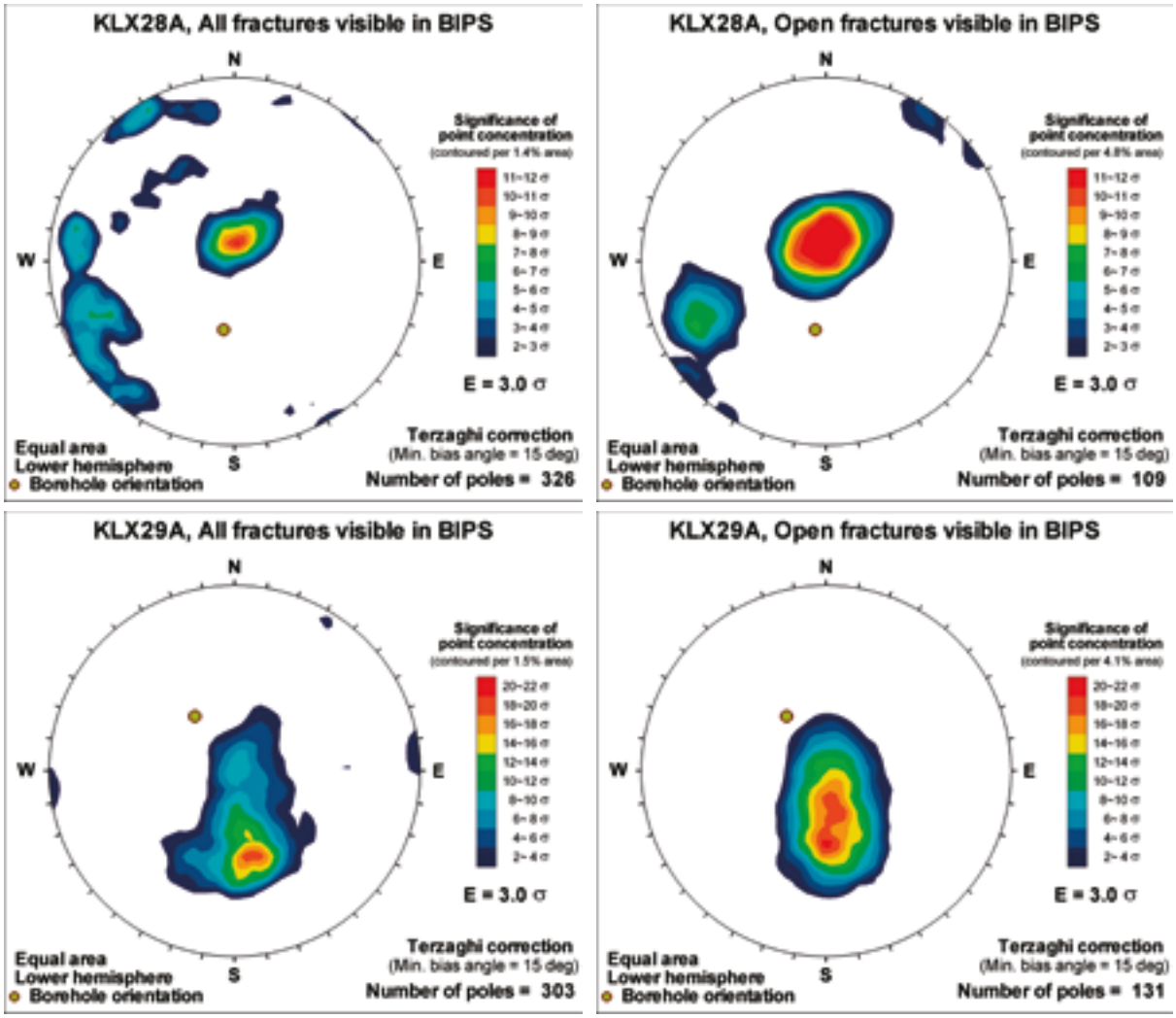

Figure 3-49. *Kamb-contoured stereoplots illustrating fracture orientations in Laxemar cored boreholes KLX25A, KLX26A, and KLX26B.*

3.6.3 Fracture orientation in cored borehole sections inside deformation zones

As previously described, only fractures outside of deformation zones are used in the parameterisation of the geological DFN. Fractures inside deformation zones, however, were used in both the hydrogeological DFN and in the deformation zone modelling efforts. The orientation of fractures, as well as the variations in the relative intensity of different fracture sets, was a key to the development of the fracture domain and deformation zone models.

For purposes of the subdivision of fracture data, ‘deformation zones’ consist of two classes:

- Regional and local major deformation zones (DZ), modelled deterministically: These features represent rock structures within the Laxemar local model area (and beyond) for which confidence in their existence, geometry, and extent is high enough that they are included in the deterministic deformation zone model (Chapter 5). DZ are defined in terms of their size; to be included in the deterministic deformation zone model, a DZ must have a surface trace length longer than 1 km.
- Minor deformation zones (MDZ): These features represent rock structures that cannot be attributed to a larger scale structure. They may exist only in a single borehole, or possess a surface trace length that is less than 1 km in length. These structures are treated stochastically by the geological DFN model (Chapter 6). However, fractures inside MDZ identified in the ESHI are also removed from the geological DFN orientation analysis.

Figure 3-50 illustrates the orientations of fractures inside identified deformation zones; no distinction is made between a deterministic DZ and a stochastic MDZ in this figure. It is important to note that the patterns of fractures inside DZ are quite similar to those outside deformation zones (cf. Section 3.6.2). This suggests that the deformation zones themselves may be the controls on fracturing in the Laxemar local model volume.

The orientations of fractures inside deformation zones are described extensively in other sections of this report. In particular, Chapter 5 presents detailed pole plots and contoured stereonets for fractures inside different classes of regional and local major deformation zones. Appendix 14, which presents a complete list of the geometries, extents, and properties of the deterministically modelled deformation zones, also contains stereoplots of the fractures mapped in each individual deformation zone.

3.6.4 Fracture frequency in cored boreholes

A key component of the geological modelling work during SDM-Site Laxemar was the analysis of the variability of fracture intensity, as recorded in logs derived from cored boreholes. Fracture intensity in boreholes is mapped as a number of fractures intersecting the centreline of the drill core over a unit-length interval (P_{10}, units of 1/m). Fracture frequency, and, in particular, the relative intensity of certain orientations of fractures, was a key input to the geological DFN. The frequency of both open and hydraulically conductive fractures was important to the hydrogeological DFN.

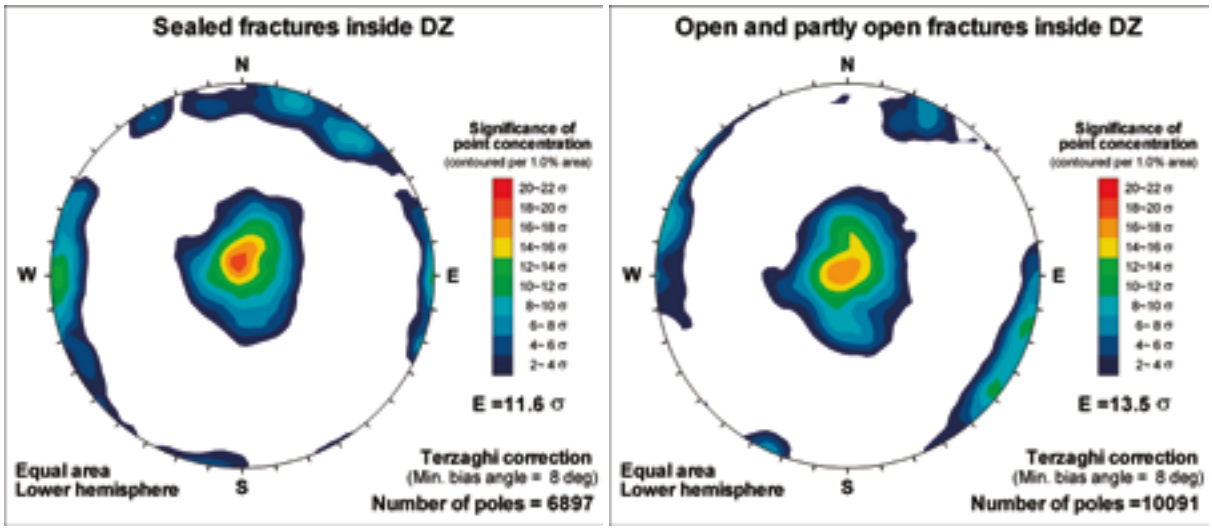

Figure 3-50. *Kamb-contoured lower-hemisphere stereonet plots of all sealed (left) and open (right) fractures inside identified deformation zones and minor deformation zones. Figures include only fractures marked as Visible in BIPS and possessing an orientation (strike, dip) in Sicada table p_fract_core_eshi.*

Table 3-5. Fracture frequency for cored boreholes at Laxemar. Numbers are based on Sicada table p_fract_core_eshi.

Cored Borehole IDCODE	Borehole Length Outside DZ (m)	Total Number of Fractures	Number of Open Fractures	Number of Partly Open Fractures	Number of Sealed Fractures	Portion of Open Fractures (%)	P_{10} Open	Total
KLX02	804.56	3,070	2,103	105	862	71.9	2.61	3.82
KLX03	896.63	4,388	679	4	3,705	15.6	0.76	4.89
KLX04	890.85	5,498	2,009	13	3,476	36.8	2.26	6.17
KLX05	886.55	3,539	319	1	3,219	9.0	0.36	3.99
KLX06	893.41	5,367	1,071	11	4,285	20.2	1.20	6.01
KLX07A	733.78	6,565	2,410	16	4,139	37.0	3.28	8.95
KLX07B	190.49	1,374	590	6	778	43.4	3.10	7.21
KLX08	891.01	5,296	1,959	19	3,318	37.3	2.20	5.94
KLX09	771.76	4,662	1,954	6	2,702	42.0	2.53	6.04
KLX09B	97.43	609	206	1	402	34.0	2.11	6.25
KLX09C	118.3	771	279	3	489	36.6	2.36	6.52
KLX09D	120.42	915	374	6	535	41.5	3.11	7.60
KLX09E	119.4	1,021	331	2	688	32.6	2.77	8.55
KLX09F	151.89	1,042	338	4	700	32.8	2.23	6.86
KLX09G	90.32	828	299	2	527	36.4	3.31	9.17
KLX10	895.62	5,601	2,340	11	3,250	42.0	2.61	6.25
KLX10B	49.94	632	346	10	276	56.3	6.93	12.66
KLX10C	145.33	1,565	421	1	1,143	27.0	2.90	10.77
KLX11A	889.29	5,358	1,077	2	4,278	20.1	1.21	6.03
KLX11B	95.5	444	160	0	284	36.0	1.68	4.65
KLX11C	115.43	446	130	0	316	29.1	1.13	3.86
KLX11D	115.2	679	204	0	475	30.0	1.77	5.89
KLX11E	116.98	655	202	0	453	30.8	1.73	5.60
KLX11F	114.83	413	120	0	293	29.1	1.05	3.60
KLX12A	499.83	3,001	1,181	3	1,817	39.5	2.36	6.00
KLX13A	490.73	3,736	2,082	3	1,651	55.8	4.24	7.61
KLX14A	171.25	1,506	730	5	771	48.8	4.26	8.79
KLX15A	922.84	5,518	1,828	9	3,681	33.3	1.98	5.98
KLX16A	432.62	3,957	1,283	5	2,669	32.5	2.97	9.15
KLX17A	634.75	4,468	1,067	6	3,394	24.0	1.68	7.04
KLX18A	510.04	3,058	1,097	7	1,954	36.1	2.15	6.00
KLX19A	695.54	2,722	1,200	2	1,520	44.2	1.73	3.91
KLX20A	356.02	2,298	920	0	1,378	40.0	2.58	6.45
KLX21B	757.95	5,900	1,663	6	4,231	28.3	2.19	7.78
KLX22A	96.37	694	266	0	428	38.3	2.76	7.20
KLX22B	95.87	669	252	0	417	37.7	2.63	6.98
KLX23A	95.93	207	72	0	135	34.8	0.75	2.16
KLX23B	45.95	115	53	0	62	46.1	1.15	2.50
KLX24A	96.13	884	361	2	521	41.1	3.76	9.20
KLX25A	46.1	347	98	0	249	28.2	2.13	7.53
KLX26A	95.94	812	433	1	378	53.4	4.51	8.46
KLX26B	46.3	346	239	1	106	69.4	5.16	7.47
KLX28A	77.15	563	215	0	348	38.2	2.79	7.30
KLX29A	58.88	463	201	1	261	43.6	3.41	7.86

Table 3-6. Fracture frequency in cored borehole sections outside identified deformation zones and minor deformation zones. Numbers are based on Sicada table p_fract_core_eshi.

Cored Borehole IDCODE	Borehole Length Outside DZ (m)	Total Number of Fractures	Number of Open Fractures	Number of Partly Open Fractures	Number of Sealed Fractures	Portion of Open Fractures (%)	P_{10} Open	P_{10} Total
KLX02	605.12	1,495	877	47	571	61.81	1.45	2.47
KLX03	794.76	3,531	418	4	3,109	11.95	0.53	4.44
KLX04	760.58	4,200	1,152	11	3,037	27.69	1.51	5.52
KLX05	875.61	3,469	294	1	3,174	8.50	0.34	3.96
KLX06	700.92	3,706	586	11	3,109	16.11	0.84	5.29
KLX07A	477.04	3,943	924	6	3,013	23.59	1.94	8.27
KLX07B	135.83	871	303	3	565	35.13	2.23	6.41
KLX08	757.4	3,691	1,265	7	2,419	34.46	1.67	4.87
KLX09	618.5	3,256	898	3	2,355	27.67	1.45	5.26
KLX09B	91.78	529	177	0	352	33.46	1.93	5.76
KLX09C	110.59	707	242	3	462	34.65	2.19	6.39
KLX09D	109.38	734	271	4	459	37.47	2.48	6.71
KLX09E	88.57	666	200	0	466	30.03	2.26	7.52
KLX09F	127.74	753	201	3	549	27.09	1.57	5.89
KLX09G	62.65	510	114	1	395	22.55	1.82	8.14
KLX10	775.62	4,310	1,399	5	2,906	32.58	1.80	5.56
KLX10B	31.2	291	124	3	164	43.64	3.97	9.33
KLX10C	86.98	744	192	1	551	25.94	2.21	8.55
KLX11A	790.43	4,263	620	0	3,642	14.54	0.78	5.39
KLX11B	91.21	389	127	0	262	32.65	1.39	4.26
KLX11C	113.29	446	130	0	316	29.15	1.15	3.94
KLX11D	99.44	525	149	0	376	28.38	1.50	5.28
KLX11E	86.66	484	139	0	345	28.72	1.60	5.59
KLX11F	112.16	390	106	0	284	27.18	0.95	3.48
KLX12A	488.42	2,880	1,105	3	1,772	38.47	2.26	5.90
KLX13A	375.16	2,559	978	3	1,578	38.34	2.61	6.82
KLX14A	115.77	917	394	0	523	42.97	3.40	7.92
KLX15A	813.34	4,439	1,335	8	3,096	30.25	1.64	5.46
KLX16A	305.06	2,411	651	5	1,755	27.21	2.13	7.90
KLX17A	558.65	3,600	678	5	2,916	18.97	1.21	6.44
KLX18A	452.77	2,510	801	4	1,705	32.07	1.77	5.54
KLX19A	589.38	1,781	467	1	1,313	26.28	0.79	3.02
KLX20A	280.56	1,504	397	0	1,107	26.40	1.42	5.36
KLX21B	604.1	3,806	830	4	2,972	21.91	1.37	6.30
KLX22A	96	686	258	0	428	37.61	2.69	7.15
KLX22B	92.81	647	233	0	414	36.01	2.51	6.97
KLX23A	92.55	176	51	0	125	28.98	0.55	1.90
KLX23B	43.85	91	37	0	54	40.66	0.84	2.08
KLX24A	88.62	793	304	2	487	38.59	3.43	8.95
KLX25A	42.34	315	87	0	228	27.62	2.05	7.44
KLX26A	77.97	639	303	1	335	47.57	3.89	8.20
KLX26B	46.06	346	239	1	106	69.36	5.19	7.51
KLX28A	56.28	392	142	0	250	36.22	2.52	6.97
KLX29A	49.35	380	155	1	224	41.05	3.14	7.70

Fracture intensity is computed from fractures mapped during the Boremap logging. The point at which the fracture intersects the centreline is recorded in a table in the Sicada database (p_fract_core), as well as other information describing the orientation, mineralogy, and morphology of the fracture. From p_fract_core, additional tables (p_freq_*m) are created in Sicada that describe the fracture intensity over intervals of a certain length (1 m, 3 m, 5 m, 10 m, and so on).

Table 3-5 presents general statistics on the frequency of fractures encountered in cored boreholes at Laxemar. Numbers in this table are based on Sicada table p_fract_core, and not on the p_freq_*m tables. It is important to note that the numbers here exclude sections of the borehole that have been mapped as 'crushed rock', and also omits the fractures that are contained in 'sealed fracture networks'. In general, sealed fracture networks have such a high frequency (on the order of 30 to 100 fractures per metre) of sealed fractures in a relatively small length of drill core that it is impossible or unfeasible to map them all.

Note that the borehole length represents the length of the borehole that was logged for fractures, and not the total length of the borehole. In some cases, the sum of open, partly open, and sealed fractures will not equal the total number of fractures recorded for the borehole. This is due to the fact that for a few cases, an aperture has not been recorded for a specific fracture in Sicada.

Fractures within the footprint of deformation zones can represent a significant percentage of the total fractures in a borehole. Locally elevated fracture intensity, in conjunction with other geologic criteria such as degree of alteration, presence of fault rocks such as cataclastite or mylonite, and geophysical indicators, is a key tool in the identification of deformation zones in the sub-surface. However, including the fractures in deformation zones can artificially bias fracture intensity statistics towards higher values. As the deformation zones are treated independently from the 'background' fractures during site modelling, it also makes sense to look at the intensity of fractures outside of the footprint of deformation zones. These values are presented in Table 3-6.

The average open fracture frequency (P_{10}) for all fractures in all boreholes combined is 2.51 1/m, compared to 1.93 1/m when fractures inside mapped deformation zones are discounted. For total fracture frequency, the average P_{10} for all fractures combined in all boreholes is 6.65 1/m, compared to 6.00 1/m when fractures inside of deformation zones are discounted. Again, readers should note that the numbers for fracture frequency specifically exclude the contribution from sealed fracture networks and from crush zones in the borehole.

Moving average and cumulative frequency plots of lineal fracture intensity (P_{10}) as functions of fracture domain, borehole, and elevation are presented in Appendix 4 of the SDM-Site Laxemar DCR /Hermanson et al. 2008/, and in Chapter 4 of the geological DFN report /La Pointe et al. 2008/.

3.6.5 Mineral coating and mineral filling along fractures in cored boreholes

Fracture minerals have been regularly determined macroscopically and mapped using the Boremap system and BIPS (Borehole Image Processing System). Many of the minerals are difficult to identify and small crystals are easily overlooked. Therefore fracture mineral analyses have been carried out for identification, mainly comprising: 1) Microscopy of fracture fillings; thin sections of open and sealed fractures and fracture surface samples of open fractures (> 200 samples) have been studied using scanning electron microscope (SEM-EDS) and 2) X-ray diffraction; especially used for identification of clay minerals and gouge material composition (45 samples). The aim of these investigations, in addition to identification of minerals, has been to distinguish different generations of fracture fillings and their chemical and morphological features and by this add to the description of the low temperature geological evolution of the site. Furthermore, the results of these investigations have provided input to the hydrochemical modelling as well as to support the sampling for transport properties analyses.

The detailed fracture mineralogical studies at Laxemar include samples from the following cored boreholes; KLX02, KLX03, KLX04, KLX06, KLX07A+B, KLX08, KLX09B-G, KLX10, KLX11B-F, KLX13A, KLX14A, KLX15A, KLX17A, KLX19A, KLX20A, KLX26A /Drake and Tullborg 2005, 2007a, b, 2008a, b, c, d, e, f /. In addition, detailed studies of fracture minerals have also been carried out on samples from the adjacent Simpevarp subarea /Drake and Tullborg, 2004, 2006a/, Äspö and Götemar /Alm and Sundblad 2002, Alm et al. 2005, Drake and Tullborg 2005, 2006b, Milodowski et al. 2005, Tullborg 2003/. Furthermore, muscovite and adularia from fracture fillings, mylonite and altered wall rock from the Simpevarp subarea, the Laxemar local model area and Äspö have been dated using $^{40}Ar/^{39}Ar$ technique /Drake et al. 2007/. Together these studies constitute the ground for the fracture filling evolution at the site. The wall rock alteration in the Laxemar and Simpevarp subareas has been studied in detail by /Drake and Tullborg 2006c, d/.

The most common fracture minerals at Laxemar are calcite and chlorite which occur in several different varieties and are present in most of the open fractures. Other common minerals are epidote, quartz, clay minerals, pyrite, prehnite, adularia (K-feldspar), hematite, zeolites (e.g. laumontite and harmotome), gypsum and fluorite. Fracture minerals that have been identified in small amounts include albite, barite, muscovite, titanite, chalcopyrite, apatite, galena, sphalerite, REE-carbonate, U-silicate and apophyllite.

Clay minerals identified using XRD (and SEM-EDS) are in addition to chlorite; corrensite (mixed layer chlorite/smectite- or chlorite/vermiculite-clay, the smectite or vermiculite layer being swelling), illite, mixed-layer illite/smectite (swelling) and a few occurrences of smectite and kaolinite. The studied drill cores are well preserved (flushing and grinding have been minimised), which has facilitated sampling of relatively undisturbed clay mineral samples, as well as other soft and brittle minerals in open fractures, such as calcite, zeolites, barite, apophyllite and gypsum.

Calcite has been analysed for stable isotope composition ($\delta^{13}C$, $\delta^{18}O$, $^{87}Sr/^{86}Sr$) and for trace elements. Fluorite has been analysed for $^{87}Sr/^{86}Sr$ and gypsum for $^{87}Sr/^{86}Sr$, $\delta^{34}S$ and trace elements. Pyrite and barite have only been analysed for $\delta^{34}S$. The information from these analyses has supported the separation of different generations of fracture fillings (relative dating of cross-cutting fractures (cf. Figure 3-51), mainly determined by microscopy) and to reveal formation conditions.

Presently water conducting fractures often exhibit non-cohesive and clayish coatings, usually of fault gouge type. The sampled water conducting fractures are mostly related to the regional or local major deformation zones, but also minor fracture zones are included. Transmissive fractures of all depths are represented. Most of the samples contain quartz, K-feldspar and albite in addition to calcite, chlorite and clay minerals. Altered wall rock fragments dominate the

Figure 3-51. *Drill core sample from KLX13A, borehole length c 300 m, showing a sealed fracture filled with epidote (1) cut by a fracture filled with calcite and laumontite (2) which is cut by an open fracture (3). Drill core diameter is 50 mm.*

gouge material and it is therefore probable that most of the quartz and feldspars belong to these rock fragments or that the samples are contaminated with wall rock material. The total clay mineral content in the open fractures is very difficult to determine appropriately and the XRD analyses should not be regarded as necessarily representative for the entire filling. Thin coatings attached to the fracture wall can consist of 90–100% chlorite and clay minerals. The amounts are relatively small as these coatings are usually thin (< 100 µm) but their active surface can be very large (Figure 3-72 and Figure 3-73). Swelling clays like corrensite and mixed-layer clays of illite/smectite type are common.

Relative sequence and absolute age determinations of fracture fillings

Several generations of fracture fillings have been identified (Table 3-7). Re-activation of older structures is commonly observed, especially in deformation zones. The formation temperatures of the different generations range from moderate (greenschist facies) to low temperature conditions (zeolite facies) grading into present conditions. This indicates that the fractures were initiated relatively early in the geological history and have been reactivated during several different periods of various physiochemical conditions. It is assumed that especially the calcite and pyrite (and also Fe-oxyhydroxide near surface) formation is ongoing processes although the amounts of possible recent precipitates are low.

A closer look at the relative sequence of events (Table 3-7) shows that it starts with greenschist facies mylonites dominated by epidote, quartz and some muscovite together with chlorite (Generation 1, Figure 3-52). The original age of the Generation 1 mylonites is interpreted to be between c 1.81 Ga and 1.77 Ga or somewhat younger, based on the crystallisation age of the rock /Wahlgren et al. 2004/, mylonite textures /Lundberg and Sjöström 2006/, and $^{40}Ar/^{39}Ar$ hornblende cooling ages of the rocks /Page et al. 2007/. Subsequent re-activation of the mylonites during semi-ductile conditions induced cataclasites dominated by epidote-quartz-chlorite (Generation 2a) and younger K-feldspar-chlorite-quartz-hematite (Generation 2b, Figure 3-53), respectively. $^{40}Ar/^{39}Ar$ dating of muscovite from a mylonite in the Äspö shear zone yielded an age of 1406±3 Ma, which was interpreted to represent resetting of the argon system caused by the intrusion of the Götemar and Uthammar granites nearby and related hydrothermal activity.

Figure 3-52. *Mylonite cut by fractures filled with calcite. KLX06, borehole length, c 373 m. Drill core diameter is 50 mm.*

Figure 3-53. *Photograph of cataclasite of Generation 2b. KLX04, borehole length c 349 m. Drill core diameter is 50 mm.*

Generation 3 consists of three different parageneses of successively lower formation temperatures: a) coarse-grained quartz, calcite, chlorite, epidote, pyrite, fluorite and K-feldspar (Figure 3-55 and Figure 3-58), b) prehnite with calcite and fluorite (Figure 3-57) and c) calcite, adularia, laumontite, chlorite and illite (Figure 3-70). Generation 3 is presumed to be formed prior to or in relation to the intrusion of the adjacent Götemar and Uthammar granites (at c 1.45–1.44 Ga). This conclusion is based on the dating of alteration features of the wall rock adjacent to Generation 3 fractures (wall rock muscovite/sericite) by /Drake et al. 2007/, who obtained a date of 1417±3 Ma using $^{40}Ar/^{39}Ar$ dating. The wall rock adjacent to Generation 3 fractures (and older shear zones) is commonly red-stained and hydrothermally altered. This alteration has caused breakdown of biotite, plagioclase and magnetite and formation of chlorite, albite, adularia and hematite (responsible for the discolouration). Although, the red-stained rock appears to be oxidized, Mössbauer spectroscopy analyses have revealed that its reducing capacity has largely remained the same. Fracture-controlled greisens (Figure 3-63) are widespread in KLX06 below ZSMEW002A (Mederhult zone, Figure 3-79b), which means close to the Götemar granite. These fractures are most probably related to the intrusion of the granite and contain coarse-grained quartz, muscovite, fluorite, pyrite and smaller amounts of calcite, topaz and chlorite. The muscovite yielded $^{40}Ar/^{39}Ar$ ages of between 1,423±3 Ma and 1,424±2 Ma /Drake et al. 2007/, which are very close to the biotite $^{40}Ar/^{39}Ar$ age of 1,421±4 Ma from the Götemar granite /Page et al. 2007/. Greisen also outcrops close to the Götemar granite contact within the TIB rocks /Kresten and Chyssler 1976/ and greisen-like fillings are found in fractures at about 900 m depth in borehole KLX10. Stable isotope signatures in calcite and pyrite from these fillings and from greisen in KLX06 are very similar to the signatures of Generation 3 fillings throughout the Laxemar and Simpevarp subareas /Drake and Tullborg 2007a/. /Lindroos 2004/ proposed that greisen close to the Götemar granite might be of economic interest (e.g. Au, Sn and W). However, detailed studies in borehole KLX06 indicate that the ore potential is insignificant /Drake and Tullborg 2007a/; the analysed samples contained a couple of minute grains of native Au (< 5µm, only visible with SEM) and Sn-bearing sulfides. It should be noted that these fillings are mainly located outside the Laxemar local model area.

Generation 4 consists of calcite, adularia, laumontite, chlorite, quartz, illite (sometimes in mixed-layer clay) and hematite (Figure 3-60). The fractures are commonly thin with a fine-grained infilling that is sometimes cataclastic and reddish brown. Based on mineralogy and appearance only, Generation 4 fillings are not easily distinguished from Generation 3. However, fluid inclusions and stable isotope analyses of Generation 4 calcite have shown that it formed under hydrothermal (inorganic) conditions at somewhat lower temperatures than Generation 3 (~ 180–220ºC, mainly above 200ºC) /Drake and Tullborg 2007b, 2008a/. These fractures are interpreted to be formed sometime after the intrusion of the Götemar granite but prior to 710±78 Ma (fission track titanite ages), when the bedrock (at ground surface) in the Laxemar local model area cooled below c 200ºC /Tullborg et al. 1996/. There are also indications from $^{87}Sr/^{86}Sr$ in calcite that it is formed at an event clearly separated from Generation 3. They might be of Sveconorwegian age as indicated by an $^{40}Ar/^{39}Ar$ age of adularia from sealed fractures in KSH03A (989±2 Ma /Drake et al. 2007/). However, the age may represent resetting of the adularia during the Sveconorwegian orogeny, as shown in biotite from the same borehole /Page et al. 2007/.

Generation 5 fillings are dominated by calcite along with e.g. adularia, Fe-chlorite, hematite, fluorite (Figure 3-66), pyrite (Figure 3-59), barite (Figure 3-65), harmotome (Figure 3-71), REE-carbonate (Figure 3-68), apophyllite (Figure 3-64), gypsum (Figure 3-69), clay minerals (illite and mixed-layer clay, e.g. corrensite, Figure 3-73), chalcopyrite, galena and laumontite. The oldest of these fillings were precipitated from saline fluids at 80–145ºC and later formed fillings of Generation 5 fractures were precipitated at gradually lower temperatures. Generation 5 is mainly of Palaeozoic age as shown by $^{40}Ar/^{39}Ar$ adularia ages of 425.8±1.7 Ma 400.9±1.1 Ma and 448.0±1.2–443.3±1.2 Ma, from drill core samples from KSH01A, KSH03A and KSH03B, respectively /Drake et al. 2007/. These ages are in accordance with less precise Sm-Nd ages of Götemar granite calcite and fluorite fracture fillings /Alm et al. 2005/, which are equivalent to Generation 5 in the Laxemar local model area /Drake and Tullborg 2006b/. Generation 5 fractures and their fillings have also been documented to cut through sandstone filled fractures of presumed Cambrian age (e.g. in boreholes KLX11D and KSH03A).

Table 3-7. Schematic fracture filling-sequence from the Laxemar local model area. Modified from /Drake and Tullborg 2007a, Drake et al. 2007/. Minerals within brackets are found in minor or trace amounts.

Generation	Age
1. Mylonite; quartz, epidote, (muscovite, chlorite, albite, calcite, K-feldspar)	> 1.45 Ga, probably older than c 1.773 Ga.
2a. Cataclasite; epidote, quartz, chlorite,	> 1.45 Ga
(K-feldspar, albite)	
2b. Cataclasite; K-feldspar, chlorite, quartz, hematite, albite, (illite)	
3a. Quartz, epidote, chlorite, calcite, pyrite, fluorite, muscovite, (K-feldspar, hornblende)	1.42 Ga or older
3b. Prehnite, calcite, (fluorite, K-feldspar)	
3c. Calcite, laumontite, adularia, chlorite, quartz, illite, hematite, (albite, fluorite)	
4. Calcite, adularia, laumontite, chlorite, quartz, illite, hematite, illite/chlorite-mixed layer clay, (albite, apatite)	1.42–0.7 Ga, possibly Sveconorwegian.
Sandstone	Cambrian
5. Calcite, adularia, chlorite, hematite, fluorite, quartz, pyrite, barite, gypsum, mixed-layer clay (e.g. corrensite), apophyllite, harmotome, REE-carbonate, (galena, illite, chalcopyrite, laumontite, sphalerite, U-silicate, apatite, albite, analcime).	The earliest and major fillings ("warm brine" precipitates) were formed at c 448–400 Ma, but fillings formed at lower temperatures might be considerably younger.
6. Calcite, pyrite, clay minerals, goethite (near surface)	Palaeozoic to recent (possibly Quaternary)

Generation 6 minerals are calcite, pyrite, clay minerals and goethite (Figure 3-67). These are the youngest fracture minerals in the area and may partly have been precipitated recently. The calcite shows stable isotope signatures and morphologies which indicate possible precipitation from saline, brackish or fresh water similar to the present groundwater at the site. The findings of small pyrite grains in the outermost layers of the fracture coatings are in agreement with the present reducing groundwater chemistry /SKB 2006g/. However, above the redox front (at c 20–40 m depth), recent oxidation is evidenced by the lack of pyrite and abundant goethite in the open fractures (cf. Figure 3-78), and further supported by positive Ce-anomalies and U-series disequilibrium in the bulk fracture coatings /Drake and Tullborg 2008b/. Based on the U-series isotopes, this corresponds to conditions prevailing during the Quaternary and partly also during the Holocene.

Orientations of different fracture filling generations

The preferred orientations of fractures filled with minerals of a certain generation can reveal information on the stress field at the time of formation and can thus help to relate the generations to specific events and also help to distinguish between different generations. However, such a linkage is not easily observed in the Laxemar-Simpevarp area because the fractures are extensively reactivated and the orientations of early formed shear zones have also influenced the orientation of the fractures /cf. Munier and Talbot 1993, Talbot and Riad 1988, Viola and Venvik Ganerød 2007a/. Because many of the minerals, e.g. calcite and chlorite are found in several generations and because reactivation of fractures may result in misleading interpretations of the fracture orientations, special care must be taken when selecting the minerals for fracture orientation interpretations. To avoid the influence on the fracture orientations by major deformation zones, borehole sections close to these zones are generally excluded. Preferred features include minerals (or a mineral paragenesis) that only exist in one generation. Fractures without wall rock alteration (e.g. if the specific mineral is of low-temperature origin), fractures including younger minerals of different formation temperatures (e.g. young zeolites together with older

epidote) should also be avoided. A selection of stereographic plots, based on these conditions is shown in Figure 3-54a–f. These indicate that greisen fractures (represented by muscovite) in KLX06 and amphibole filled fractures in KLX08 (Generation 3) are mainly sub-horizontal (Figure 3-54a, d). Epidote and prehnite-dominated fractures of Generation 3 are dominantly sub-vertical and c. N-S oriented as well as sub-horizontal (Figure 3-54b, c). Gypsum of Generation 5 is dominantly found in sub-vertical fractures trending WNW-ESE to NW-SE (Figure 3-54f).

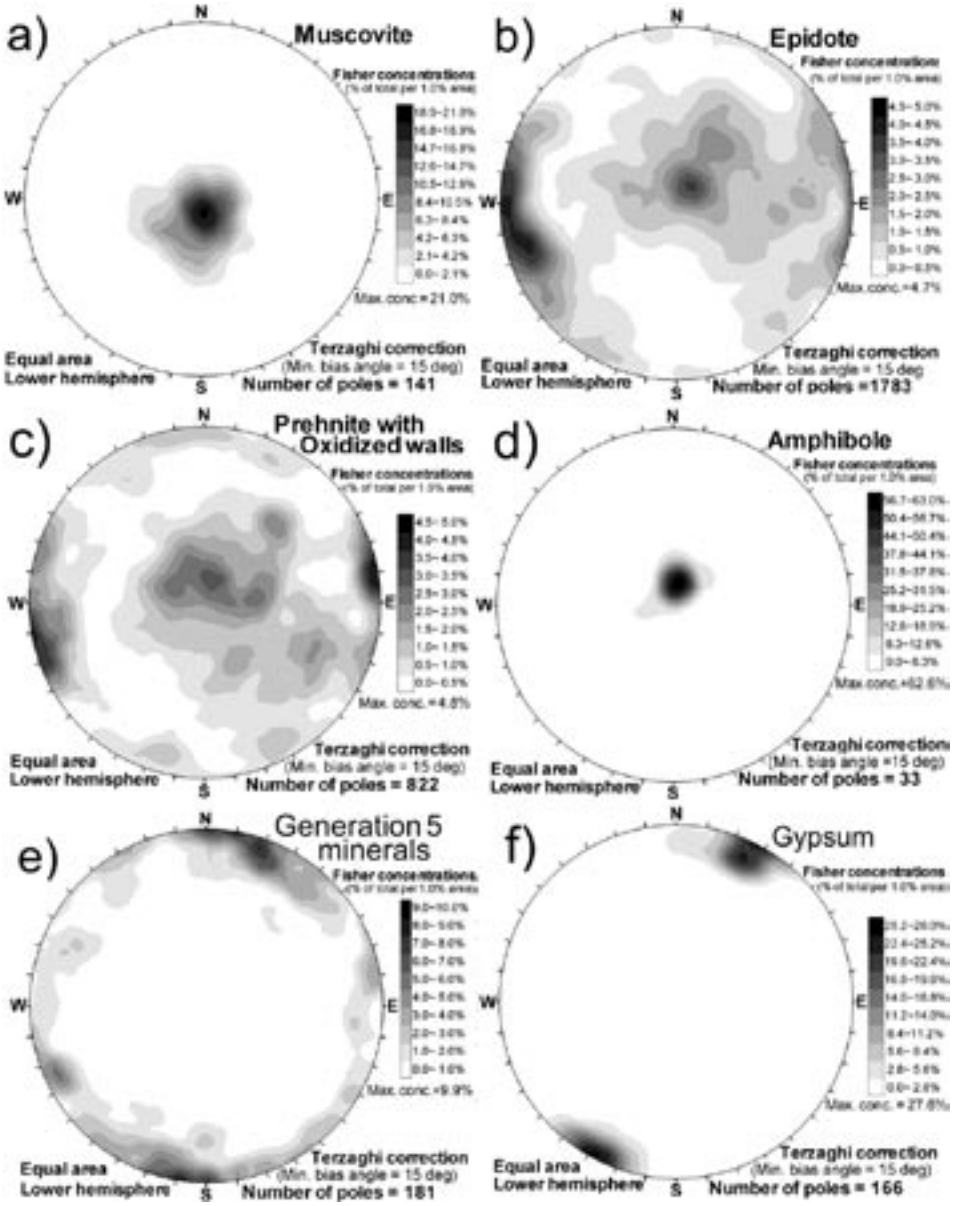

Figure 3-54. *Orientations of fractures (excluding deformation zones) containing specific minerals. a) Muscovite in greisen fractures in borehole KLX06 north of ZSMEW002A. b) Epidote-dominated (mapped as the most abundant in Boremap) sealed fractures in boreholes KLX08, 09A–B, 10, 12A, 13A, 14A, 17A, 18A, 21B, except fractures including prehnite or zeolites. c) Prehnite-dominated sealed fractures with red-stained wall rock in KLX08, 09A–B, 10, 12A, 13A, 14A, 17A, 18A, 21B, except fractures including epidote or zeolites. d) Amphibole in sealed fractures (only present in KLX08). e) Generation 5 minerals, confirmed with microscope or hand lens, in open or sealed fractures in KLX03, 04, 05, 06, 07A, 08, 09A, 09D–F, 10, 10C, 11C, 11E, 14A, 19A, 20A, 26A. Re-activated fractures containing minerals older than Generation 5 are excluded. f) Gypsum in open and sealed fractures in KLX03, 08, 10, except in fractures containing epidote, fluorite, prehnite, or feldspars or fractures with altered wall rock. Lower hemisphere of Schmidt equal area, stereographic plots. From /Drake et al. in preparation/.*

Additionally, since the Boremap data provide no information on different generations, fractures containing Generation 5 fillings exclusively were distinguished macroscopically or with microscope or SEM-EDS from cored boreholes KLX03, 04, 05, 06, 07A, 08, 09A, 09D–F, 10, 10C, 11C, 11E, 14A, 19A, 20A, 26A (Figure 3-54e). These fractures are mainly sub-vertical and trend WNW-ESE (E-W to NW-SE), but the orientations of these fractures varies more than those containing gypsum. These dominant orientations of the Palaeozoic fractures suggest a maximum compressive stress in c. WNW-ESE to NW-SE during the formation of Generation 5 fractures, or alternatively that these minerals have been preferentially dissolved in fractures of other directions. The former case is supported by a post-Ordovician fracture set at Öland /Milnes and Gee 1992/ as well as by fractures cross-cutting Cambrian sandstone dykes on the Swedish SE coast /Nordenskjöld 1944/, since both of these fracture sets are dominantly sub-vertical and NW-SE striking.

Fracture mineral characteristics

Brief descriptions of the most common fracture minerals in the Laxemar local model area are found below.

Chlorite: $(Mg,Fe^{2+},Fe^{3+},Al)_{12}[(Si,Al)_8O_{20}](OH)_{16}$

Chlorite can form at temperatures below 400ºC. Continuous solid solution extends from Mg-rich chlorite (clinochlore) to Fe-rich chlorite (chamosite). Mg- , Mg-Fe- and Fe-rich chlorites have been identified in the Laxemar local model area (Figure 3-55) and these are present in all generations. Chlorite is, next to calcite, the most common fracture mineral in the Laxemar local model area. Partial and complete chloritisation of wall rock biotite is common.

Calcite: $CaCO_3$

In the Laxemar local model area, calcite (along with chlorite) is the most common fracture mineral and it is found in several fracture mineral generations (Figures 3-55, 3-56, 3-58, 3-65, 3-70). Its formation conditions range from greenschist facies to the ambient groundwater conditions of recent times. Calcite of Palaeozoic age or younger is commonly found together with fluorite, sulfides ±sulfates.

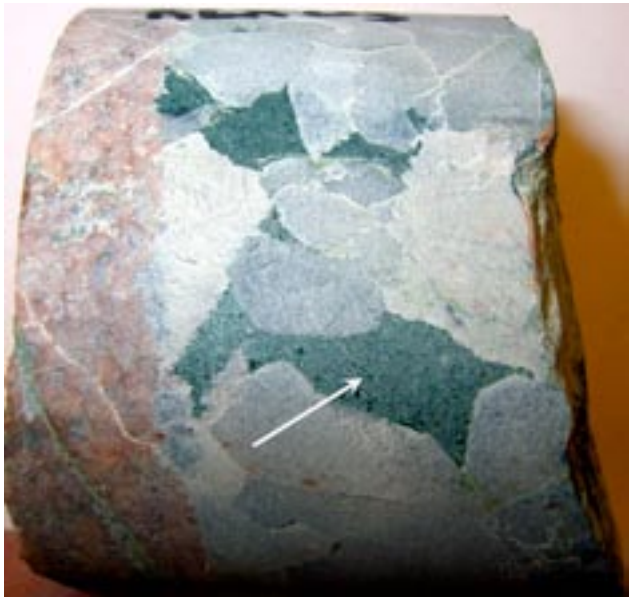

Figure 3-55. *Fracture filling with chlorite (arrow), calcite (white) and quartz (grey). KLX03, borehole length c 730 m. Drill core diameter is 50 mm.*

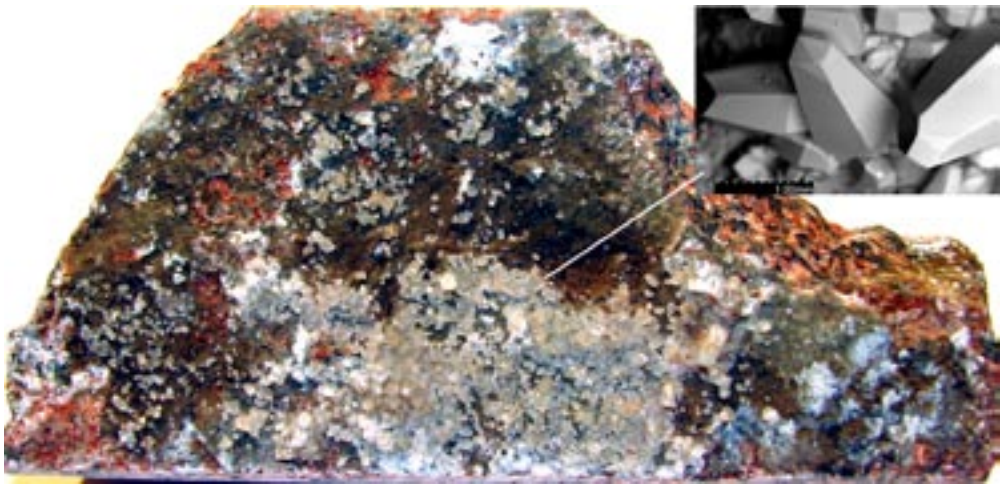

Figure 3-56. *Euhedral (scalenohedral) calcite in an open fracture (inserted close-up image is a back-scattered SEM-image) from borehole KLX15A, borehole length c 1,000 m. Drill core diameter is 50 mm (=height of image). Scale marker in the SEM-image is 1 mm.*

Quartz: SiO_2

In the Laxemar local model area quartz is found in most generations, in both sealed (Figure 3-55) and open fractures.

Prehnite: $Ca_2Al_2Si_3O_{10}(OH)_2$

Prehnite is a hydrothermal mineral often associated with calcite and fluorite. It is common in hydrothermally altered rocks. It is formed at low temperatures than epidote, commonly below 280ºC (at P < 3 ka), /Frey et al. 1991/. The low-temperature alteration of prehnite may produce zeolites (laumontite) or chlorite and clay minerals. In the Laxemar local model area it is associated with red-stained wall rock (Figure 3-57).

Epidote: $Ca_2(Fe^{3+},Al)_3(SiO_4)_3(OH)$

Epidote is characteristic in rocks of the greenschist (and epidote-amphibolite) facies, in which it is characteristically associated with chlorite, albite and quartz. Epidote also occurs as a product of the hydrothermal alteration (saussuritisation) of plagioclase and along fractures. In the Laxemar local model area it is found in mylonite, cataclasite or in sealed brittle fractures (Figure 3-58) together with quartz, fluorite and calcite.

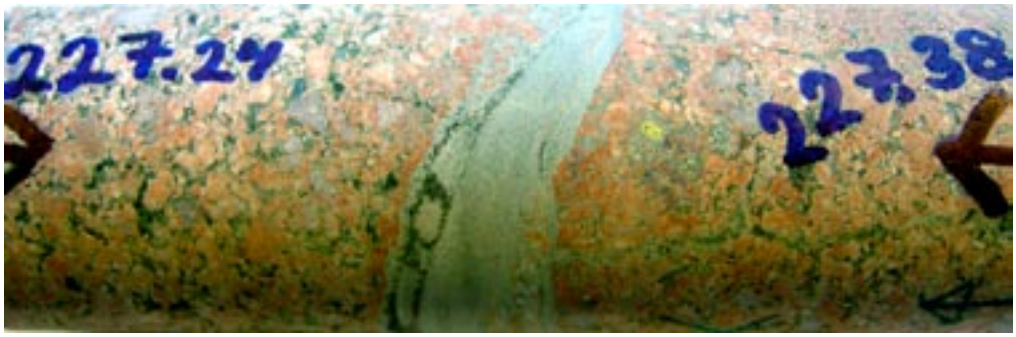

Figure 3-57. *Fracture filled with prehnite. Note the red colour of the wall rock due to hydrothermal alteration. From borehole KLX07A, borehole length c 227 m. Drill core diameter is 50 mm.*

Figure 3-58. *Sealed fracture filled by epidote, calcite and fluorite. From borehole KLX06, borehole length c. 315 m. Drill core diameter is 50 mm.*

Fluorite: CaF_2

Fluorite is a cubic, usually dark violet mineral. At Laxemar, fluorite has probably been formed as a result of fluorine (F) released during breakdown of wall rock biotite but F has also been introduced by the Götemar granite. Fluorite is mainly found both in old Generation 3 fractures (Figure 3-58) but is also found in sealed or open Generation 5 fractures, often together with calcite and pyrite.

Pyrite: FeS_2

In the Laxemar local model area pyrite is found both in hydrothermal Generation 3 fractures and in younger open fractures (Figure 3-59). Other sulfides present in the Laxemar local model area are chalcopyrite, sphalerite and galena and these mainly belong to Generation 5.

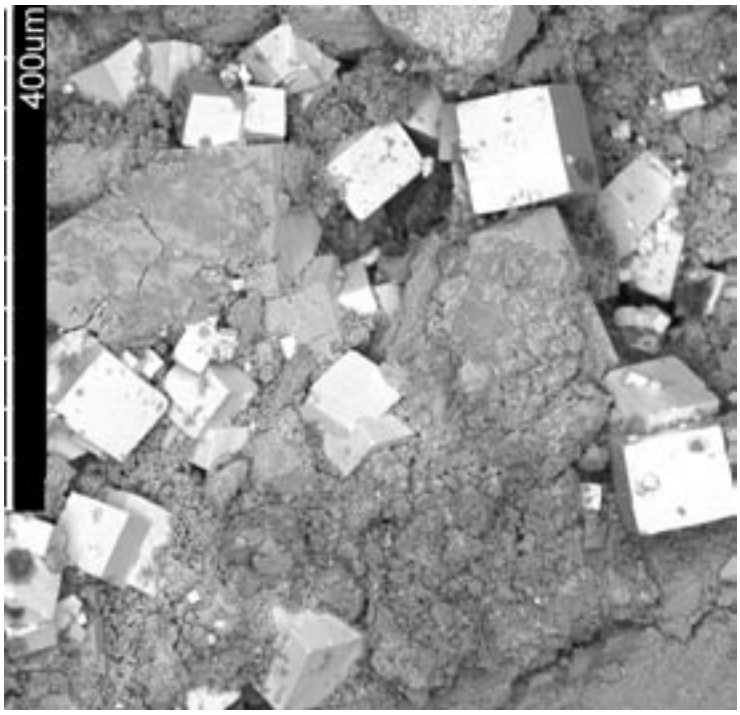

Figure 3-59. *Back-scattered SEM-image of cubic pyrite crystals coating an open fracture, borehole KLX03, borehole length c 266 m.*

Adularia: $KAlSi_3O_8$

Adularia is a low-temperature K-feldspar (Figure 3-60), identified on the basis of its habit and occurrence. In most cases adularia is crystallised under low temperature hydrothermal conditions (< roughly 450ºC). The paragenesis may include calcite, chlorite, quartz, albite, apatite, hematite and corrensite. The colour varies but is usually grey or greenish grey although red varieties are common in association with hematite.

Hematite: Fe_2O_3

Hematite is stable in the weathering environment and is commonly produced by weathering or hydrothermal alteration of iron-bearing minerals. Hematite has commonly partly replaced magnetite in hydrothermally altered wall rock. In open fractures, it is present mostly as minute grains covering other fracture minerals, giving the coating a red to brown colour (Figure 3-61). Hematite at Laxemar is a hydrothermal mineral.

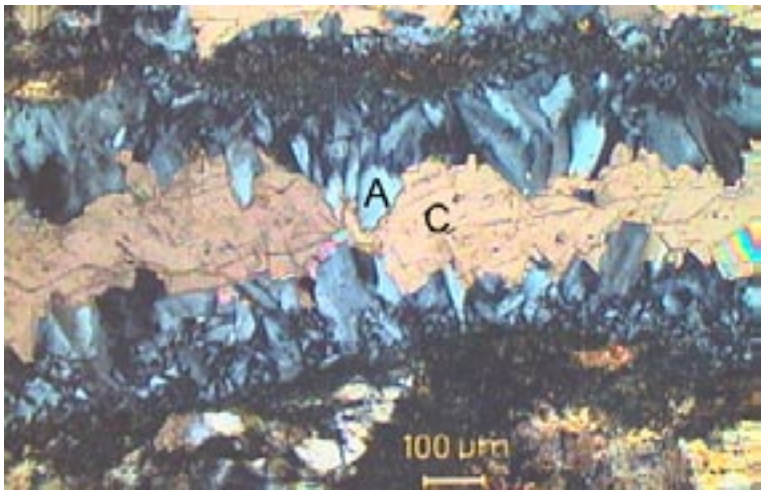

Figure 3-60. *Photomicrograph of a fracture filled with adularia (A) and calcite (C).From borehole KSH01A, borehole length c 287 m. Crossed polarised light.*

Figure 3-61. *Fracture surface covered with hematite. The white fracture filling is older calcite. From borehole KLX04, borehole length c 674 m. Drill core diameter is 50 mm.*

Albite: $NaAlSi_3O_8$

Plagioclase close to the fractures is commonly partly or completely altered (hydrothermally) to albite, K-feldspar, sericite, epidote, prehnite and calcite. Fracture fillings of albite are occasionally found in the Laxemar and Simpevarp subareas (Figure 3-62).

Muscovite: $KAl_2(Si_3Al)O_{10}(OH,F)_2$

Muscovite is found in fracture fillings (e.g. in greisen in KLX06, Figure 3-63), as sericite in hydrothermally altered rock, e.g. in red-stained rock in the Laxemar local model area.

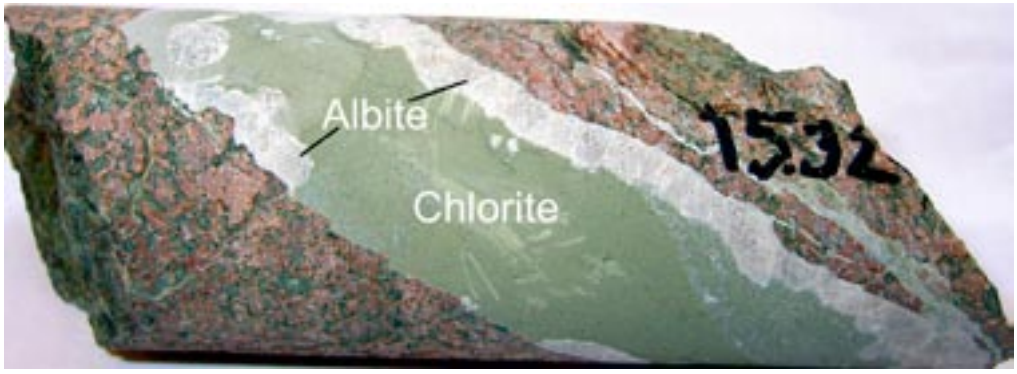

Figure 3-62. *Fracture filled with dominantly albite and chlorite (also including quartz, K-feldspar and calcite). From borehole KSH03B, borehole length c 15 m. Drill core diameter is 50 mm.*

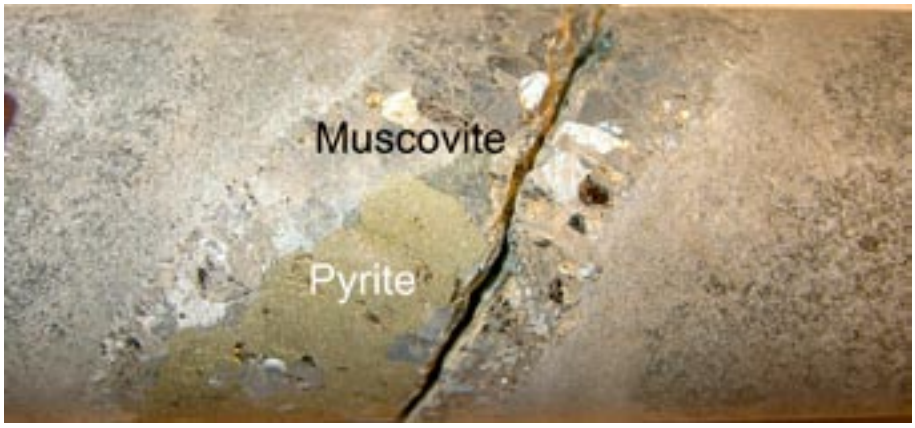

Figure 3-63. *Muscovite and pyrite in greisen fractures in borehole KLX06, borehole length c 535 m. Drill core diameter is 50 mm.*

Apophyllite: $KCa_4(Si_4O_{10})2F{\cdot}8(H_2O)$

Apophyllite is a hydrothermal sheet silicate with white to silvery surface (Figure 3-64). In the Laxemar local model area it occurs as either fluoroapophyllite or natroapophyllite, and is closely associated with gypsum.

Barite: $BaSO_4$

Barite is a sulfate mineral and it commonly occurs in Generation 5 fillings, occasionally as euhedral crystals, along with calcite (usually scalenohedral), fluorite, pyrite and zeolites (Figure 3-65).

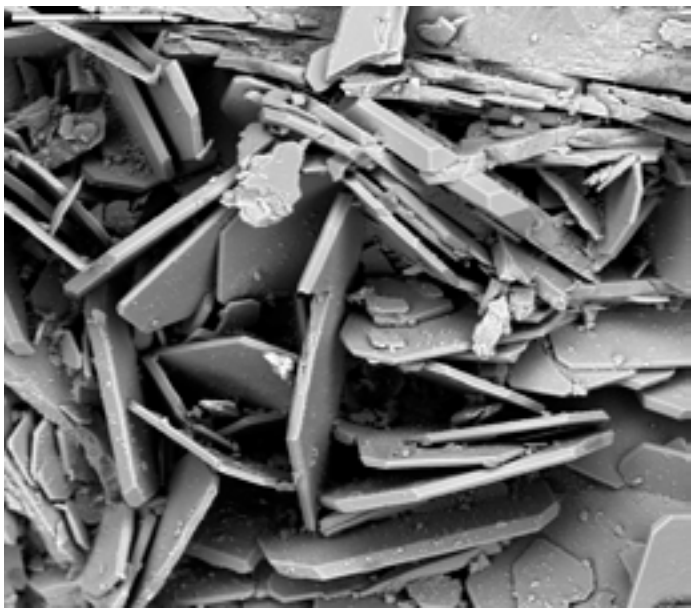

Figure 3-64. *Back-scattered SEM-image of an apophyllite fracture coating. From borehole KLX03, borehole length c 970 m. Scale bar is 200 µm.*

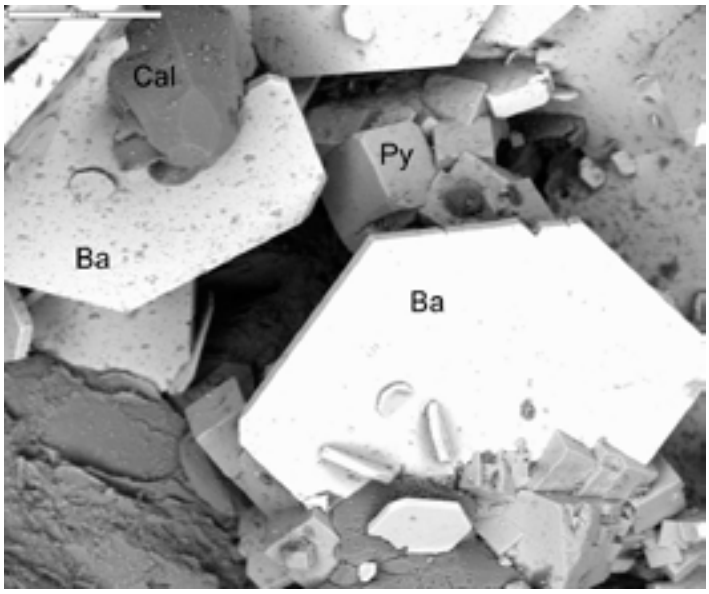

Figure 3-65. *Back-scattered SEM-image of barite (Ba), calcite (Cal) and pyrite (Py) in an open fracture. Scale bar is 200 µm. From borehole KLX03, borehole length c 457 m.*

Gypsum: $CaSO_4 \cdot 2(H_2O)$

Gypsum is easily dissolved and soft sulfate. It is e.g. formed from acidic dissolution of calcite. It is present in some fractures in the Laxemar local model area (e.g. KLX03, KLX06, KLX08, KLX10, KLX12A and KLX17A, Figure 3-66), occasionally accompanied by, calcite, pyrite, fluorite and the sulfates barite and celestine.

Goethite: $Fe^{3+}O(OH)$

Goethite commonly occurs as a weathering product (oxidation) of Fe-bearing minerals such as magnetite and pyrite. It gives the coating a yellow to brownish red colour. At Laxemar it is most common in fractures above the redox front, i.e. above c 20–40 m (Figure 3-67).

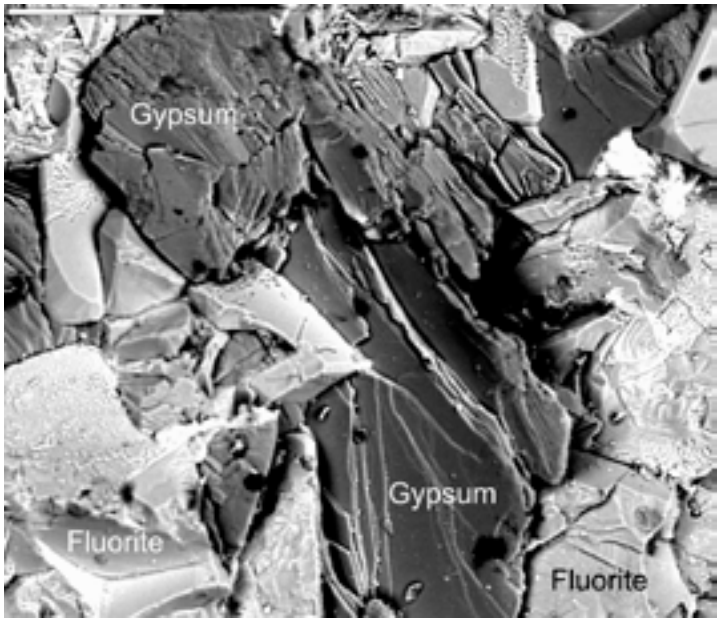

Figure 3-66. *Back-scattered SEM-image of gypsum and fluorite crystals on a fracture surface. Scale bar is 200 µm. From borehole KLX06, borehole length c 789 m.*

Figure 3-67. *Near surface fracture coated by e.g. goethite. From borehole KLX09E, borehole length c 1 m. Drill core diameter is 50 mm.*

REE-carbonate: $(Ce,La,Y)CO_3F$

In the Laxemar local model area, this mineral is found in Generation 5, together with calcite, fluorite, sulfides and sulfates (Figure 3-68). The mineral is probably bastnäsite, as indicated by X-ray diffraction analyses.

Apatite: $Ca_5(PO_4)_3(OH,F,Cl)$

Apatite is an accessory mineral in the rocks in the area, but it also occurs in hydrothermal veins together with e.g. quartz, adularia and chlorite (Figure 3-69).

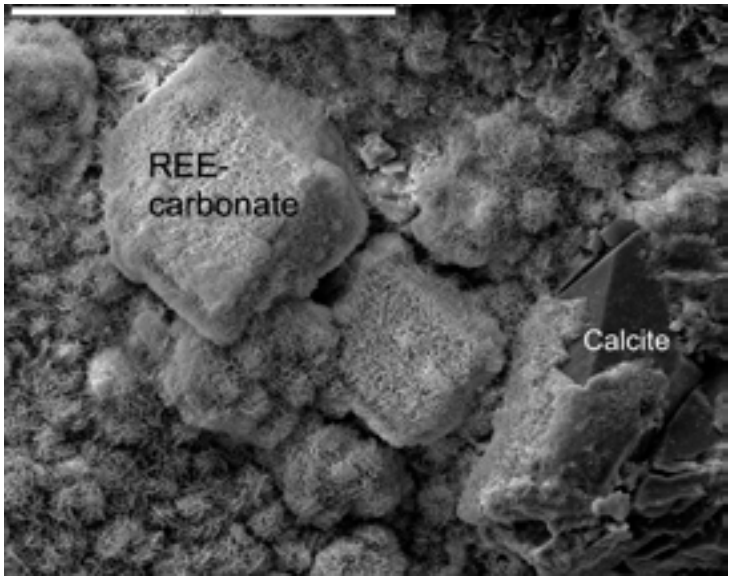

Figure 3-68. *Back-scattered SEM-image of calcite covered with REE-carbonate, from borehole KSH01A, borehole length c 289 m. Scale bar is 200 µm.*

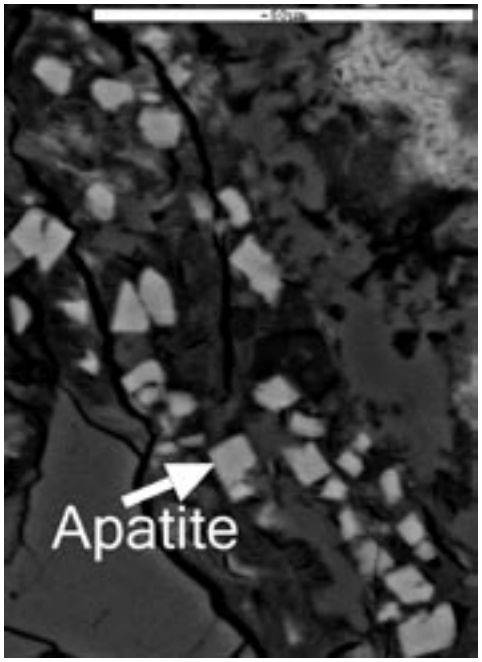

Figure 3-69. *Back-scattered SEM-image of apatite in a fracture filling. Other minerals are adularia and chlorite. From borehole KSH01A, borehole length c 208 m. Scale bar is 50 µm.*

Zeolites:
Laumontite: $CaAl_2Si_4O_{12}\cdot 4(H_2O)$
Harmotome: $Ba_2(Na,Ca_{0.5})[Al_5Si_{11}O_{32}]\cdot 12(H_2O)$
Analcime: $NaAlSi_2O_6\cdot(H_2O)$

Zeolites are chemically related to feldspars but have much more open structures and contain water. They may alter to other zeolites or clay.

Laumontite is the most common zeolite in the Laxemar local model area and is abundant in some of the deformation zones (e.g.ZSMEW002A, the Mederhult Zone, cf. Chapter 5 and Figure 3-70. It is white coloured, but may be red-stained by minute hematite crystals. The stability field of laumontite ranges from c 150–250ºC /Liou et al. 1985/. Harmotome occurs as small euhedral crystals on open fracture surfaces (Figure 3-71) and sometimes in sealed fractures. It is a low temperature zeolite with stability temperatures that are somewhat lower than that of laumontite, although the stability field of harmotome has not been as extensively studied as that of laumontite. Analcime is not as common as laumontite or harmotome in the Laxemar local model area (only found in KLX17A, Figure 3-71, but also in KSH01A, Simpevarp subarea).

Figure 3-70. *Laumontite and calcite in sealed fractures in borehole KLX06, borehole length c 400 m. Drill core diameter is 50 mm.*

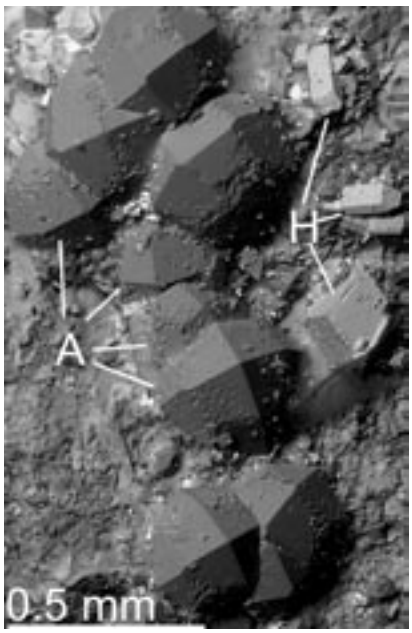

Figure 3-71. *Back-scattered SEM-image of euhedral analcime (A) and harmotome (H) on a fracture surface from borehole KLX17A, borehole length c 431 m.*

Clay minerals:
Illite: $(K,H_3O)(Al,Mg,Fe)_2(Si,Al)_4O_{10}[(OH)_2,(H_2O)]$

Illite occurs as micro- to cryptocrystalline, micaceous flakes and is often formed as an alteration product of mica or K-feldspar. Illite is together with corrensite the most frequently found clay mineral in the Laxemar local model area.

Smectite: e.g. $(Mg_3(Si_4O_{10})(OH)_2 \cdot nH_2O)$

Smectite is a swelling clay which can ’vary in composition and occur dominantly as Mg- and Fe-rich varieties.

Mixed-layer clays:

Mixed-layer clay (Figure 3-72) is the term usually applied to clays having alternating layers of e.g. illite and smectite. The ratio between the illite and smectite layers varies due to degree of re-crystallisation; and the illite component increases with increasing formation temperature. Mixed-layer illite/smectite clay is swelling.

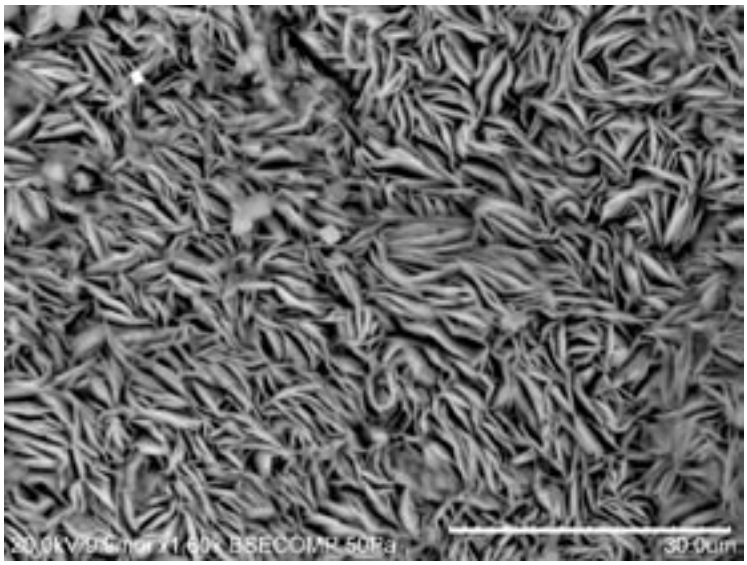

Figure 3-72. *Back-scattered SEM-image showing mixed-layer clay on a fracture surface from KLX08, borehole length c 108 m. Scale bar is 30 µm.*

Corrensite: $(Ca,Na,K)(Mg,Fe,Al)_9(Si,Al)_8O_{20}(OH)_{10}\cdot n(H_2O)$

Corrensite is a mixed-layer clay with layers of chlorite and smectite/vermiculite, usually in a ratio of 1:1. This mineral is usually swelling. Corrensite is very common in the water conducting fractures in the Laxemar local model area (Figure 3-73).

Fracture mineral frequencies

The statistical representation of the various fracture mineral frequencies is based on Boremap data from the drill core mapping (stored in Sicada). Most of the minerals have been mapped with large confidence. However, detailed microscopy and X-ray diffraction studies show that some minerals are over- or underestimated in the database. For instance, fractures mapped as only chlorite-bearing often consist of clay minerals as well and the clay mineral content may therefore be somewhat underestimated in the mapping /Drake and Tullborg 2004/. Especially hematite is overrepresented due to its ability to discolour or stain other minerals like chlorite and feldspars, i.e. hematite is identified in many fractures but the amount in every filling is generally below 1% of the coating. Calcite, in contrast is mapped with high accuracy due to the use of HCl which makes the identification certain.

The total number of open and sealed fractures in boreholes KLX02-29A is 100,728 (including fractures within deformation zones), of which 69,229 are sealed fractures (67%, including 197 partly open fractures) and 33,499 are open fractures (33%). Sealed network sections (2,348) and sections of crushed rock (477) have been left out of this statistical analysis of mineral frequencies. It should be noted that the mapping gives only the frequency of fractures carrying a specific mineral and not the amount of the mineral in the fracture. However, a mapping campaign devoted to mapping volumes of specific minerals of interest for the modelling of redox and pH buffering is ongoing.

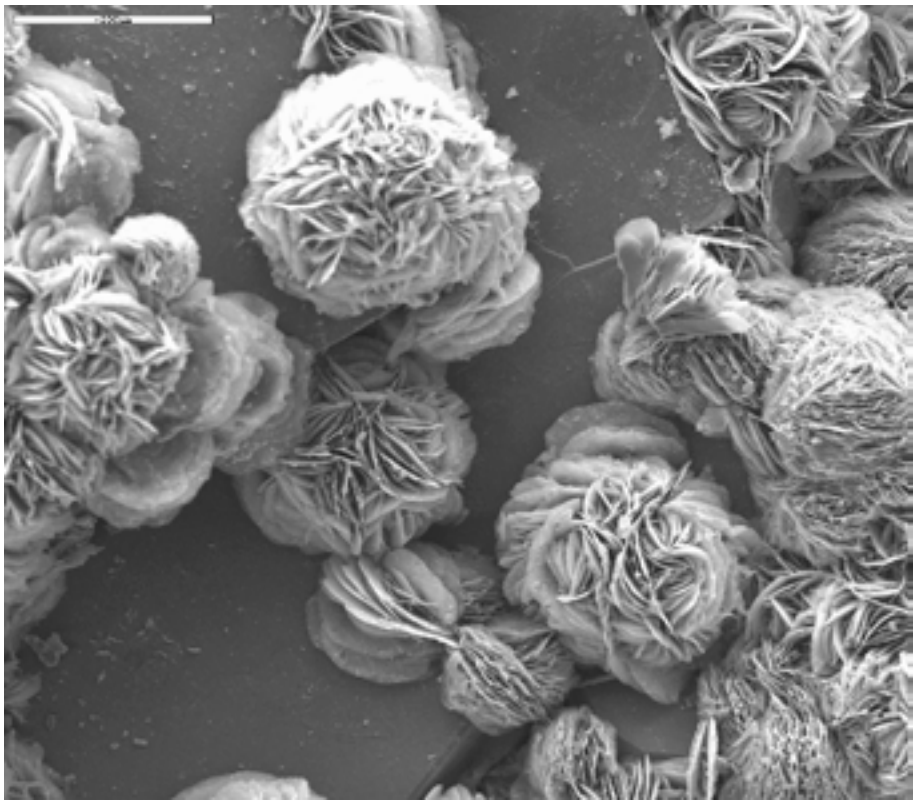

Figure 3-73. *Back-scattered SEM-image of spherulitic corrensite aggregates on a fracture surface from borehole KLX06, borehole length c 831 m. Scale bar at upper left is 200 µm.*

The most common fracture minerals at Laxemar are, as mentioned above, calcite and chlorite, which dominate in both sealed and open fractures (Figure 3-74) but are more frequently occurring in the open ones. It should be noted that Figure 3-74 gives frequencies of open as well as sealed fractures containing each mineral and not the number of fractures. For instance, calcite is found in 78% of the open fractures and in 48% of the sealed fractures, but the number of open, calcite-bearing fractures is lower (26,088) than the number of sealed, calcite-bearing fractures (31,166). Clay minerals, pyrite and hematite are also most frequently found in open fractures whereas epidote, adularia, quartz and prehnite are more frequent in sealed fractures. Additional minerals identified are zeolites (mainly laumontite and harmotome) and gypsum (mainly in open fractures). The minerals muscovite (mainly in KLX06), fluorite, goethite (mainly near surface), amphibole (mainly in KLX08), talc (mainly in KLX20A), other sulfides, barite and apophyllite are each found in less than 0.6% of the fractures (plotted as "Misc." in Figure 3-74). A large part of the sealed fractures (20%) are narrow fractures with altered wall rock and no visible filling (Figure 3-75, "No visible filling - Altered WR" in Figure 3-74.). Fractures with no visible filling and fresh wall rock are relatively rare (2.5% of the open fractures, "No visible filling -Fresh WR" in Figure 3-74). A large number of fractures have altered wall rock, usually red-stained and/or saussuritised ("Oxid. walls" and "Sauss." in Figure 3-74).

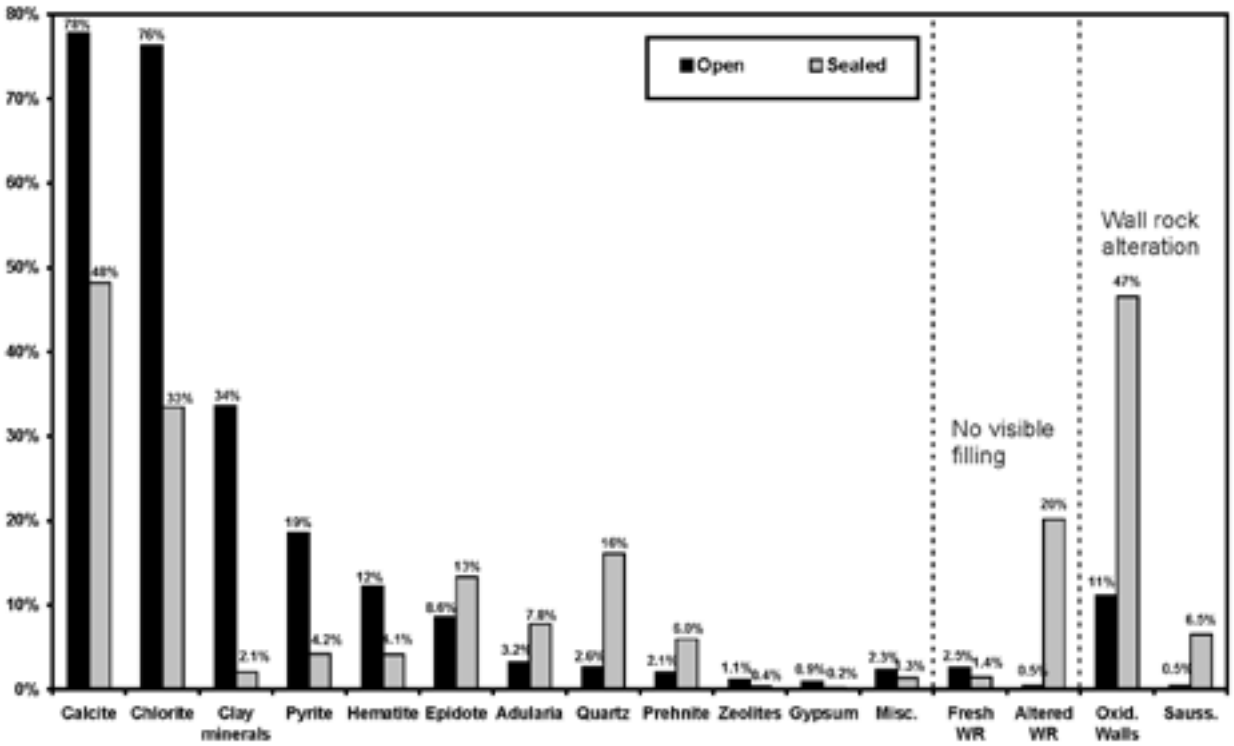

Figure 3-74. *Frequency of fractures (open as well as sealed) filled or coated with specific minerals (several minerals are usually found in the same fracture). Data are from the Boremap mapping from KLX02-KLX29A (also including minerals listed as additional minerals in the Boremap comment files). The number of sealed fractures is 69,229 and the number of open fractures is 33,499. "Adularia" includes "red feldspar" and "white feldspar". Zeolites include minerals mapped as "laumontite" and "zeolites". "Misc." includes fluorite, muscovite, sericite, talc, chalcopyrite, sphalerite, sulfides, amphibole, goethite, apophyllite, barite and biotite. "No visible filling – Fresh WR" are mapped as "Broken fractures with a fresh appearance and no mineral fill" in the Boremap mapping. "No visible filling – Altered WR" are mapped as "oxidized walls", "fractures with epidotised/saussuritised walls" or "bleached fracture walls" without any visible fracture minerals. Wall rock alteration "Oxid. Walls"and "Sauss" show frequency of fractures with oxidized (red-stained) and saussuritised wall rock, respectively.*

Figure 3-75. *Photograph of a drill core sample with a typical, hardly visible, sealed fracture with no visible fill but with altered wall rock /Drake et al. 2006/. These fractures are presented as "No visible filling - Altered WR" in Figure 3-74. Drill core diameter is 50 mm.*

The overall fracture mineralogy in the Laxemar local model area is very similar to that previously found in the Simpevarp subarea and at the Äspö HRL. The fracture frequency and abundance of different fracture minerals and generations do however vary between the different subareas (and Äspö). For instance, the frequency of cataclasites is higher in the Simpevarp subarea, whereas Generation 3a minerals are more common in the Laxemar local model area, possibly because of the proximity to the Götemar intrusion. Gypsum, apophyllite and barite are identified in a number of fractures in the Laxemar local model area (in KLX03, KLX06, KLX08, KLX10 and KLX13A) but are very rare in the Simpevarp subarea and at Äspö. Gypsum is mainly found in low permeable parts of the rock and it may have been dissolved in more permeable parts, e.g. in deformation zones, and in the more fractured Simpevarp subarea.

Variation of fracture mineralogy with depth

Analysis of variation in fracture mineralogy with depth has been carried out on a borehole by borehole basis. For each borehole, the occurrences of each specific mineral in open and sealed fractures together with the total number of fractures have been analysed. The group of open fractures also includes partly open fractures and fractures from crush zones. The group of sealed fractures includes sealed networks. Fractures in deformation zones and possible deformation zones, as interpreted in the ESHI, are also included. Calcite, chlorite, clay minerals, adularia+albite (mapped as adularia, red feldspar and white feldspar), epidote, prehnite, hematite, pyrite, goethite, quartz, gypsum, as well as fractures with no visible filling (divided into fractures with fresh or fractures with altered wall rock) have been studied. Furthermore, the variation of hydrothermal wall rock alteration features, i.e. red-staining and saussuritisation have been analysed. Additionally, for a limited number of boreholes, the occurrence of talc (mainly related to fractures in dolerite) and muscovite (mainly related to greisen fractures), has been analysed.

About 2,100 mineral distribution plots, from 46 boreholes, have been generated. These show the frequency of occurrence of a particular mineral in a particular type of fracture, as well as the overall frequency of occurrence of this fracture type, in 10 m vertical depth intervals along a borehole. However, most of the relative mineral frequencies and wall rock alteration features show no variation with depths, although exceptions exist and a number of these are discussed below together with the compilation of general features.

Except for the lack of calcite in the uppermost 10–20 meters, the most common fracture minerals chlorite and calcite show no distinctive variation with depth. This is exemplified with plots from KLX03 and KLX08 in Figure 3-76a and Figure 3-76b, respectively. The frequency of occurrence of these minerals generally follows the variation in the total fracture frequency and these minerals are common in deformation zones, e.g. in ZSMEW946A in KLX03 (vertical depth: –680 to –700 m above sea level) and in ZSMEW007A (–105 to –153 and –160 to –235 m above sea level) and ZSMEW946A (–388 to –395 m above sea level) in KLX08. The trend of decreasing calcite frequencies in the uppermost tenths of meters is exemplified by KLX09D in Figure 3-76c). This decrease is most probably due to dissolution of calcite caused by descending of diluted water unsaturated in respect of calcite /Drake and Tullborg 2008b/.

Clay minerals are found in 34% of the open fractures, which makes them the third most frequent mineral occurrence in these fractures. Their frequency of occurrence generally follows the variation in frequency of occurrence of fractures with depth, although there relative frequency is commonly higher in deformation zones, for instance in DZ10 in the ESHI (–492 to –526 m above sea level) and ZSMEW007A+ZSMNW928A (–653 to –693 m above sea level) in KLX09 (Figure 3-76d). Similarly, hematite does not vary systematically with depth, but is occasionally frequent in open fractures in deformation zones, e.g. in ZSMEW946A (–269 to –272 m above sea level) and ZSMEW007A (–284 to –359 m above sea level) in KLX04 (Figure 3-77c). The occurrence of hematite suggests oxidizing formation conditions. However, these occurrences do not necessary correspond to the current conditions since this hematite is mainly a hydrothermal mineral /Drake and Tullborg 2004, Dideriksen et al. 2007/. It should be noted that the concentration of hematite along these open fractures is very low, commonly below 1 vol.%.

Hydrothermal minerals epidote and prehnite of Generation 3 (cf. section “Relative sequence and absolute age determinations of fracture fillings“ above), show no systematic variation in occurrences with depths, as exemplified in plots from boreholes KLX11A and KLX21B in Figure 3-77a, b. Similar scattered distribution with depth is evidenced for quartz, which also dominantly belong to Generation 3.

Pyrite is a common mineral in open fractures at all depths, exemplified in borehole KLX15A in Figure 3-77d. However, near surface oxidative dissolution of pyrite and formation of goethite in the uppermost 10–20 m and partially deeper, is evidenced in shallow, cored boreholes, e.g. in KLX09B-G, KLX11B-F and in KLX26A (Figure 3-78a). The distribution of these minerals indicates the location of the recent near surface redox front, i.e. the shift from oxidizing conditions near surface, to more reducing conditions at greater depths /Drake and Tullborg 2007b/.

A couple of specific minerals only occur in limited sections in specific boreholes. Talc, for instance, is only found in open fractures within the dolerite dyke in borehole KLX20A (Figure 3-79a). The only significant occurrence of muscovite is associated to greisen fractures in KLX06, below the deformation zone ZSMEW002A (< –360 m above sea level). These fractures are mainly sub-horizontal (Figure 3-54a) and are presumably associated to the intrusion and post-magmatic circulation of the Götemar granite /Drake and Tullborg 2007a/. An interesting feature is that the gresien alteration appears to have been halted at the deformation zone ZSMEW002A and greisen alteration within the Laxemar local model area is rare.

Gypsum of Generation 5 is present in 0.9% of the open fractures and in 0.2% of the sealed fractures. It is absent in most boreholes and the largest occurrences identified are restricted to open fractures in isolated sections with low fracture frequencies and low transmissivity at depths greater than –350 m.a.s.l, e.g. in KLX03 (–490 to –620 m above sea level), KLX08 (Figure 3-79c), KLX10 (–940 to –960 m above sea level) and KLX12A (mainly –390 to –460 m above sea level) and KLX17A (–360 to –390 and –540 to –560 m above sea level). The present distribution of the gypsum occurrences is not interpreted to represent the original distribution of precipitation /Drake and Tullborg 2007a/. This distribution pattern indicates dissolution at depths above 350 m and in highly transmissive zones. The deeper groundwaters at Laxemar are relatively rich in SO_4 which is attributed to dissolution of gypsum /SKB 2006g/.

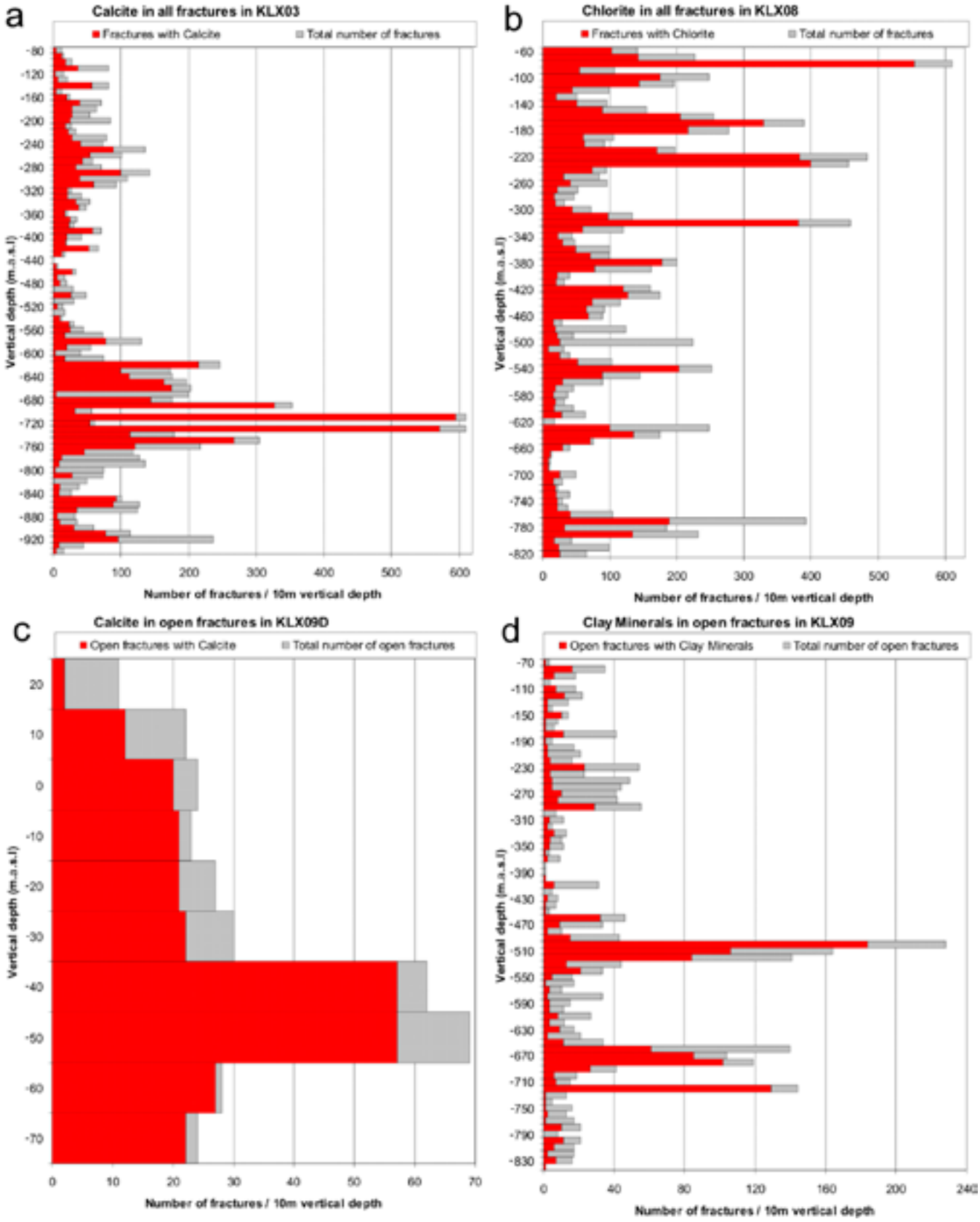

Figure 3-76. *Variation with depth of calcite (a) and chlorite (b) along all fractures in KLX03 and KLX08, respectively. Calcite (c) along open fractures versus depth in KLX09D (excluding the near surface part which lacks BIPS) and clay minerals (d) along open fractures in KLX09. The total number of fractures of the specific fracture type per 10 m borehole interval is also shown.*

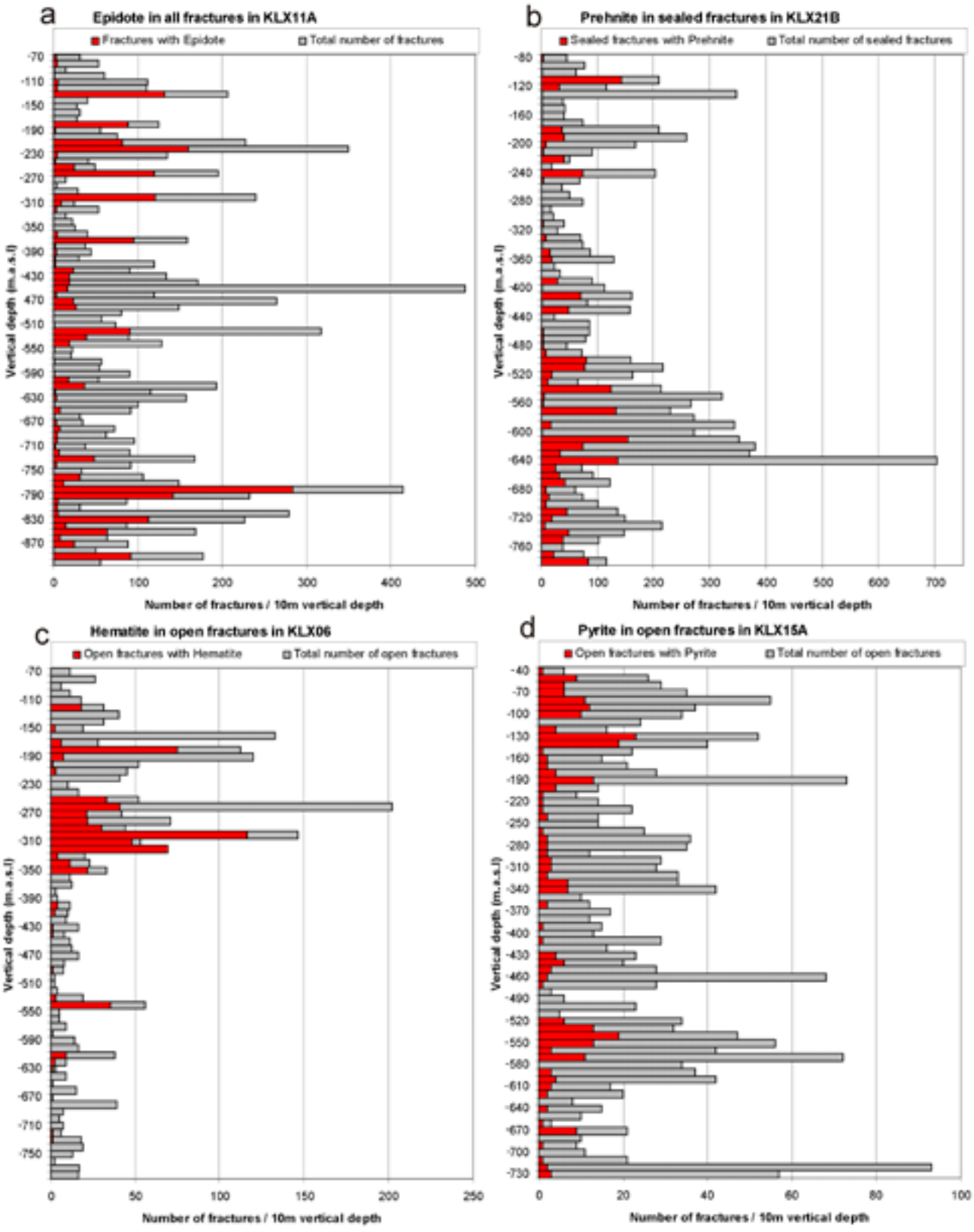

Figure 3-77. *Variation with depth of epidote (a) along all fractures in KLX11A, prehnite (b) along sealed fractures in KLX21B, hematite (c) and pyrite (d) along open fractures in KLX06 and KLX15A, respectively. The total number of fractures of the specific fracture type per 10 m borehole interval is also shown.*

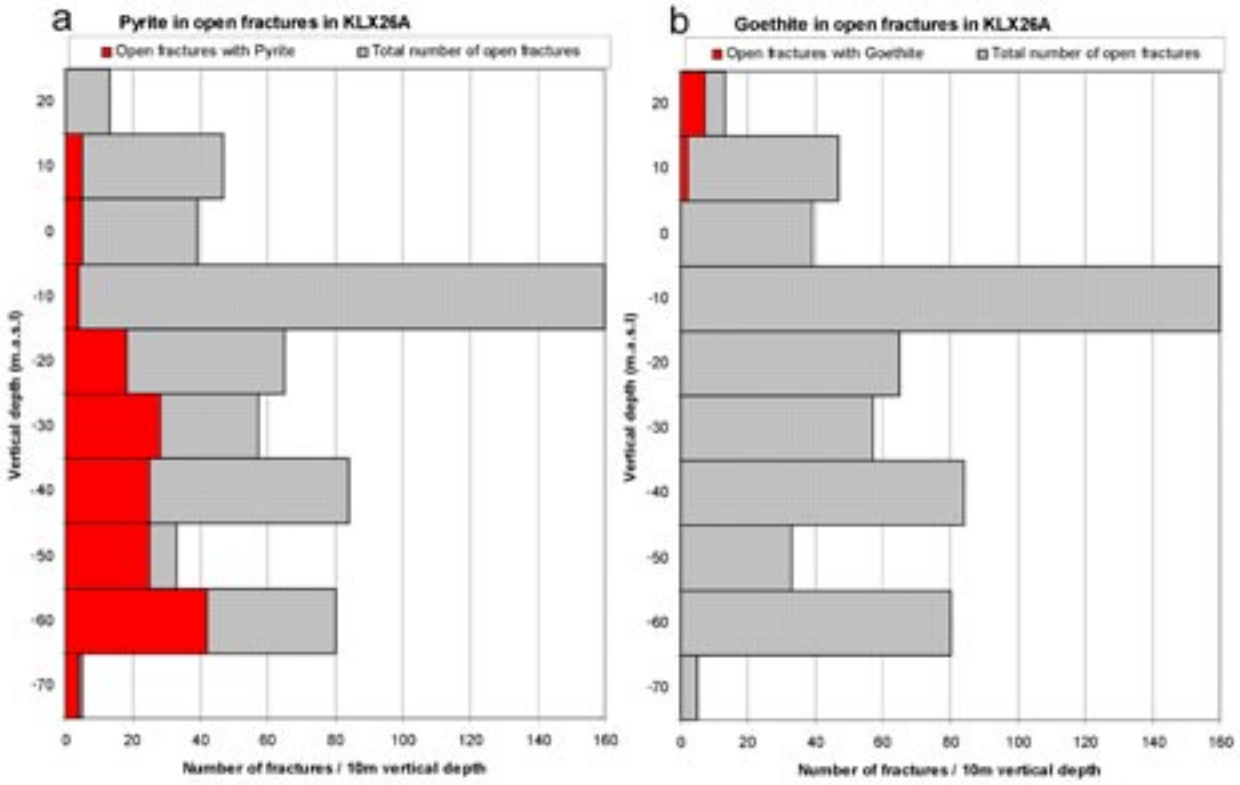

Figure 3-78. *Variation with depth of pyrite (a) and goethite (b) along open fractures in KLX26A. The total number of open fractures/10 m borehole interval is also shown.*

Open fractures that do not contain any mineral coating and have fresh wall rock are commonly low in numbers and are scattered throughout the boreholes, exemplified by the variation with depth in KLX15A in Figure 3-79d. However, some exceptions from the general pattern exist. For example, in some of the shallow boreholes, e.g. in KLX09E there is a slight increase of these fractures towards the ground surface. Furthermore, in KLX04, the relative occurrence of these fractures is elevated within deformation zones in the ESHI (DZ6B and ZSMEW007A). These fractures may potentially be recently formed and are therefore highly interesting. However, a number of uncertainties need to be addressed concerning this group of fractures. These are:

- The mineral coating or filling is so thin that it has not been possible to identify a mineral along the fracture and the occurrence has been registered as a fracture with no mineral.
- The fracture contained a mineral coating or filling, but this has been washed away in connection with the aggressive drilling activity. However, in contrast to the first few cored boreholes drilled at Forsmark, the drill core quality at Laxemar is generally good.
- The fracture may have been generated in connection with the drilling activity but was not excluded from the Sicada database.

It is therefore suggested that these fractures require further analytical work.

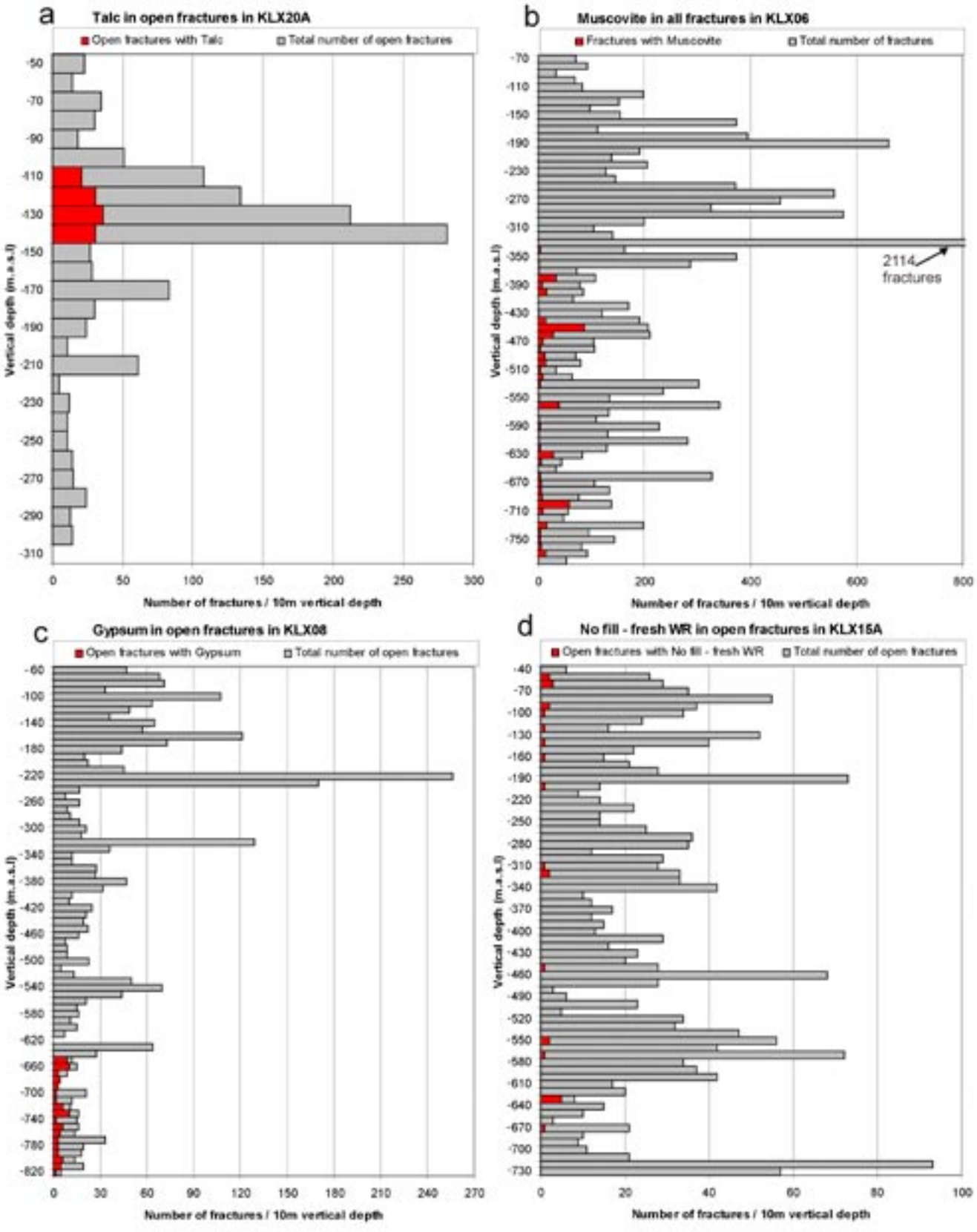

Figure 3-79. *Variation with depth of talc (a) along open fractures in KLX20A, muscovite (b, note that the x-axis has been cut) along all fractures in KLX06, gypsum (c) along open fractures in KLX08 and open fractures without any visible filling and with fresh wall rock (d) in KLX15A. The total number of fractures of the specific fracture type per 10 m borehole interval is also shown.*

3.7 Character and kinematics of brittle deformation

In order to describe the character of the brittle deformation zones and if possible to also constrain their kinematics, selected deformation zones, initially identified in the SHI, were studied in detail in a number of drill cores by /Viola and Venvik Ganerød 2007a, 2007b and 2008/. In addition, a kinematic study of selected outcrops and cleaned trenches was also carried out by the same authors. The character and kinematics of the deformation zones studied are included in Appendix 14 (an overview of the different sets of deformation zones is given in Section 5.2.2). The results presented by /Viola and Venvik Ganerød 2007a, 2007b and 2008/ are presently being compiled and interpreted with the goal of producing a coherent scheme for the brittle evolution across Laxemar and Simpevarp, including an attempt at the reconstruction of the local palaeostress evolution through time /Viola 2008/. Furthermore, the study presents a synthesis of the brittle structural evolution of the site investigation area and its relation to far-field orogenic events that might have affected the bedrock in the Laxemar-Simpavarp area during the geological evolution /Viola 2008/.

The results of the study confirm that the brittle history of the Laxemar-Simpevarp area is complex and involves series of reactivation events. Brittle structures vary from brittle-ductile shear zones with and without associated fault rocks, such as different types of cataclasites, breccias, gouge etc to late fractures and joints decorated by very low temperature and low-grade minerals, from hydrofractures to hydrobreccias. All available evidence indicates that multiple episodes of deformation took place within a broadly-defined brittle regime under different environmental and physical conditions.

A short summary of the brittle kinematic reconstruction produced by /Viola 2008/ is presented below.

Brittle kinematic data from outcrops and the drill cores were treated separately and subsequently compared and merged into a large, single dataset, considered representative of the brittle deformational evolution of the entire area. Inferences on individual, discrete compressive and extensional events were made by sorting the total fault-slip dataset on the basis of geometric and kinematic compatibility criteria and on well-constrained structural relationships. Based on this sorting procedure, individual conjugate subsets were thus extracted from both outcrop as well as drill core data. The fracture sets identified from the study of the drill cores are very similar to those identified from the outcrop measurements.

The most striking brittle features observed on outcrops of the Laxemar-Simpevarp area are systematic sets of conjugate, steep, sinistral and dextral, brittle-ductile and brittle, strike-slip faults and fractures. These are dispersed at small angle around a north-trending axis and the systematic approach mentioned above allowed their sorting into two distinct conjugate sets, conjugate set I and II, respectively. Conjugate set I contains N-S-trending steep sinistral and NNW-SSE, steep dextral fractures/faults, that were likely formed together with low-angle, top-to-the-N/NW reverse fracture/faults. Conjugate set II is only slightly misaligned with respect to set I. It is defined by N-S-trending steep dextral and NE-SW, steep sinistral fractures/faults. The common spatial overlap between sinistral and dextral fractures belonging to the two different sets, together with the fact that the angles between the conjugate structures are generally small generate significant structural complexities. A third conjugate fracture set spreads about the E-W direction. Figure 3-80 and Figure 3-81 display examples of sinistral and dextral fractures at Laxemar.

Low-angle to moderately dipping striated fracture planes were also identified in the drill cores studied and on several outcrops /Viola 2008/. These were sorted and assigned to two distinct subsets with antithetic top-to-the NE and SW and top-to-the NW and SE normal movements, respectively. Steep fracture planes /faults that bear steep striations and are characterised by transtensional movements were also recorded and are generally interpreted as being due to the extensional reactivation of pre-existing steep shear fractures.

Figure 3-80. *Sinistral N-S trending fractures belonging to set I at the cleaned outcrop for drill site KLX11A and KLX20A. Note the releasing bends and the associated dilation (shown by large white arrows). Inserted stereonet also display E/ENE-W/WSW dextral fractures at the same outcrop. View to the north. Figure from /Viola and Venvik Ganerød 2007a/.*

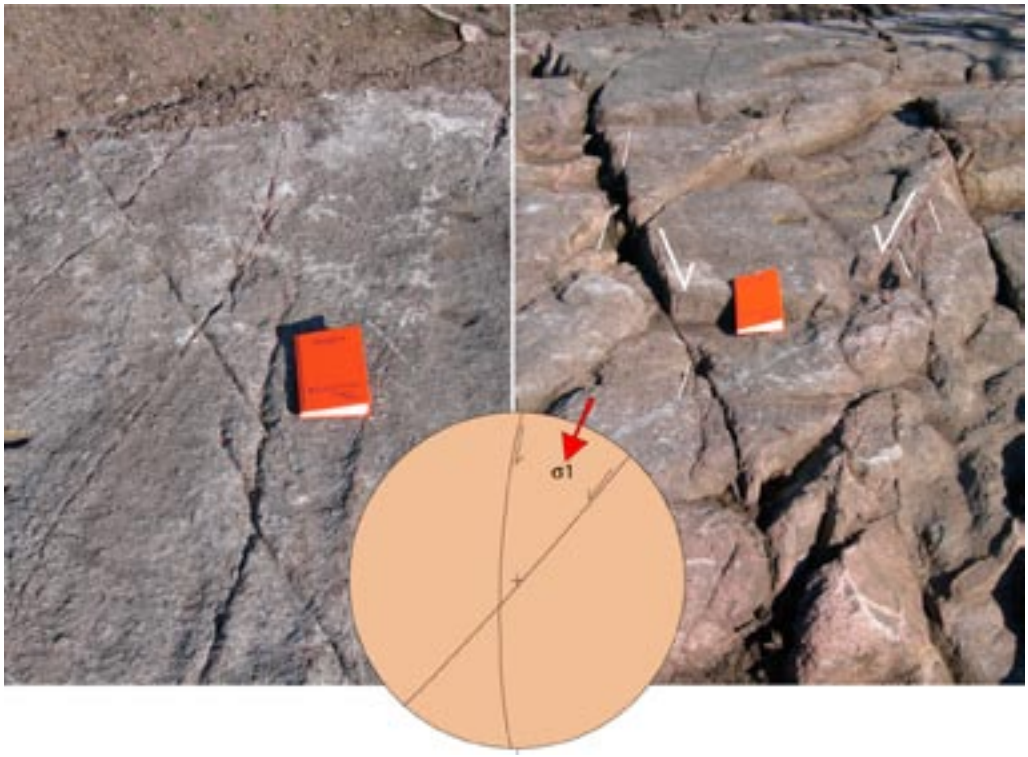

Figure 3-81. *Sinistral and dextral fractures of conjugate set II. The acute angle defined by the intersection of the conjugate pairs is bisected by σ_1. View to the northeast. Figure from /Viola and Venvik Ganerød 2007b/.*

3.8 Lineaments – data, identification, modelling and geological interpretation

The work of identifying lineaments during the early phases of SDM-Site Laxemar modelling work has followed the principal methodology adapted at earlier modelling stages. The lineament map has successively developed from a coarse version, a regional overview, to a detailed lineament map covering the Laxemar local model area. The development of the lineament maps started with the identification of lineaments from topography and large-scale geophysical surveys inside the Laxemar regional model area, followed by the use of higher- resolution data (LIDAR and detailed ground geophysical surveys) to adjust or reject former lineaments and to identify new lineaments inside the local model area /Triumf and Thunehed 2007/, /Berglund and Triumf 2007/.

In the lineament analysis, the most important data sets have been the high-resolution digital elevation model (DEM) and the high- resolution ground magnetic total field data. As the lineament mapping process evolved, the magnetic total field data had a successively stronger influence than the DEM on the final lineament model. The cause for this is found in the geological setting of Laxemar, where the magnetic total field data reflect both brittle and ductile deformation of the bedrock through a reduction in the magnetic susceptibility of the rock volume containing the zones. Furthermore, magnetic total field data are quite insensitive to variations in the overburden thickness. This means that bedrock deformation is manifested in the magnetic total field data as lineaments of magnetic lows and that the visibility of these anomalies are relatively insensitive to variations in the overburden thickness and composition typically encountered at Laxemar.

The evaluation of the lineaments began early in the site investigation process by focusing on structures of regional extent, and gradually changed focus to shorter lineaments within the local model area with lengths less than 1,000 m as the modelling stages advanced. Lineaments shorter than 1,000 m are assumed to represent the surface traces of structures analogous to minor deformation zones (MDZ) identified in cored boreholes during the extended single-hole interpretation (ESHI). The more significant minor deformation zones are characterised by brittle-ductile deformation, increased fracturing, some crush zones and mylonites, and significant hydraulic transmissivity which makes their geometry in terms of dip and continuity of importance. Forward and inverse modelling of geophysical data have revealed the near-surface geometry of some of these prominent minor deformation zones /Mattsson and Triumf 2007/.

The principal data sets in which lineaments have been identified are summarised below and the process of identification and the results is commented upon.

3.8.1 Types of data of the magnetic total field and their variable resolution

During the different phases of the site investigation, the degree of resolution of available magnetic total field data has increased and hence, the ability to identify also narrow and short lineaments has continuously improved. The characteristics for each survey type are presented in Table 3-8 and the coverage of each set of data inside the local model area is presented in Figure 3-82.

Table 3-8. Characteristics of magnetic surveys in the Laxemar local model area.

Type of survey	Contractor	Line spacing	Station spacing	Survey direction	Survey elevation	Grid resolution
Airborne, fixed-wing	SGU	200 m	17 or 40 m	EW	30 m	40×40 m
Helicopter borne	NGU	50 m	3 m	NS (tie lines EW)	Approx 40 m	5×5 m
Ground	GeoVista AB	10 m	5 m	NS	ca. 1.5 – 2 m	5×5 m

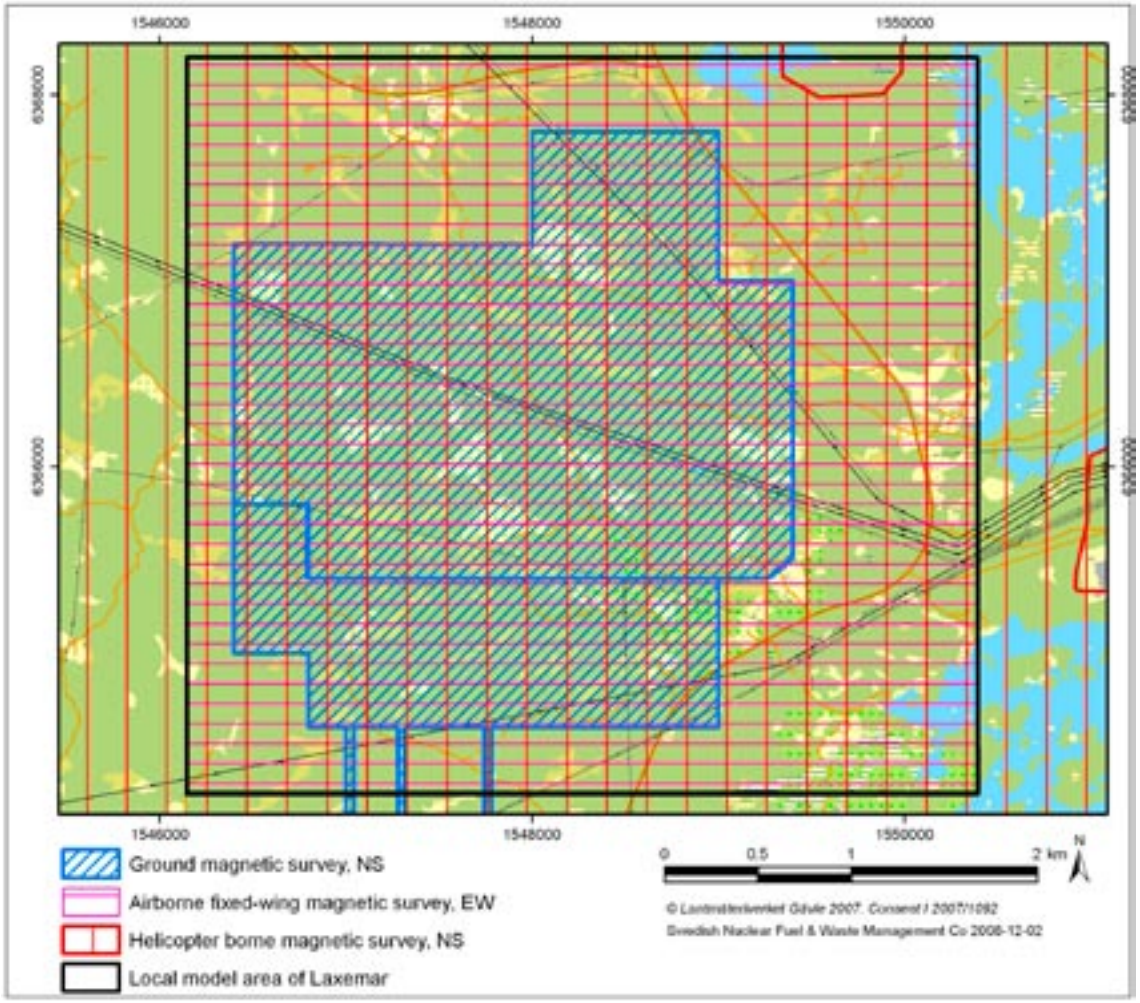

Figure 3-82. *Coverage of different survey methods of the magnetic total field according to Table 3-8.*

The entire local model area is covered by airborne geophysical data with 200 m line spacing that were acquired by the Geological Survey of Sweden (SGU), in connection with their standard mapping activities (Table 3-8). The data were available prior to the onset of the site investigation programme and were already utilised in the feasibility study work in the Oskarshamn area /Bergman et al. 1998/.

In connection with the site investigation programme during 2002, helicopter-borne geophysical measurements were performed covering the entire local model area (Figure 1-1 and /Rønning et al. 2003/). Detailed descriptions of the geophysical data and the processing and interpretation of these data can be found in /Rønning et al. 2003 and Triumf et al. 2003/.

Ground magnetic surveys of high resolution within the Laxemar local model area have been carried out, processed and interpreted in three campaigns; in spring 2005 /Thunehed and Triumf 2005/, in autumn-winter 2005–2006 /Thunehed and Triumf 2006/ and in spring 2007 /Mattsson and Triumf 2007/. The coverage is shown in Figure 3-82. Up to and including model stage SDM-Site Laxemar, an area of approximately 8 km² is covered by these data. Disturbances to the magnetic field occur close to man-made installations such as drill sites, residence areas and power lines.

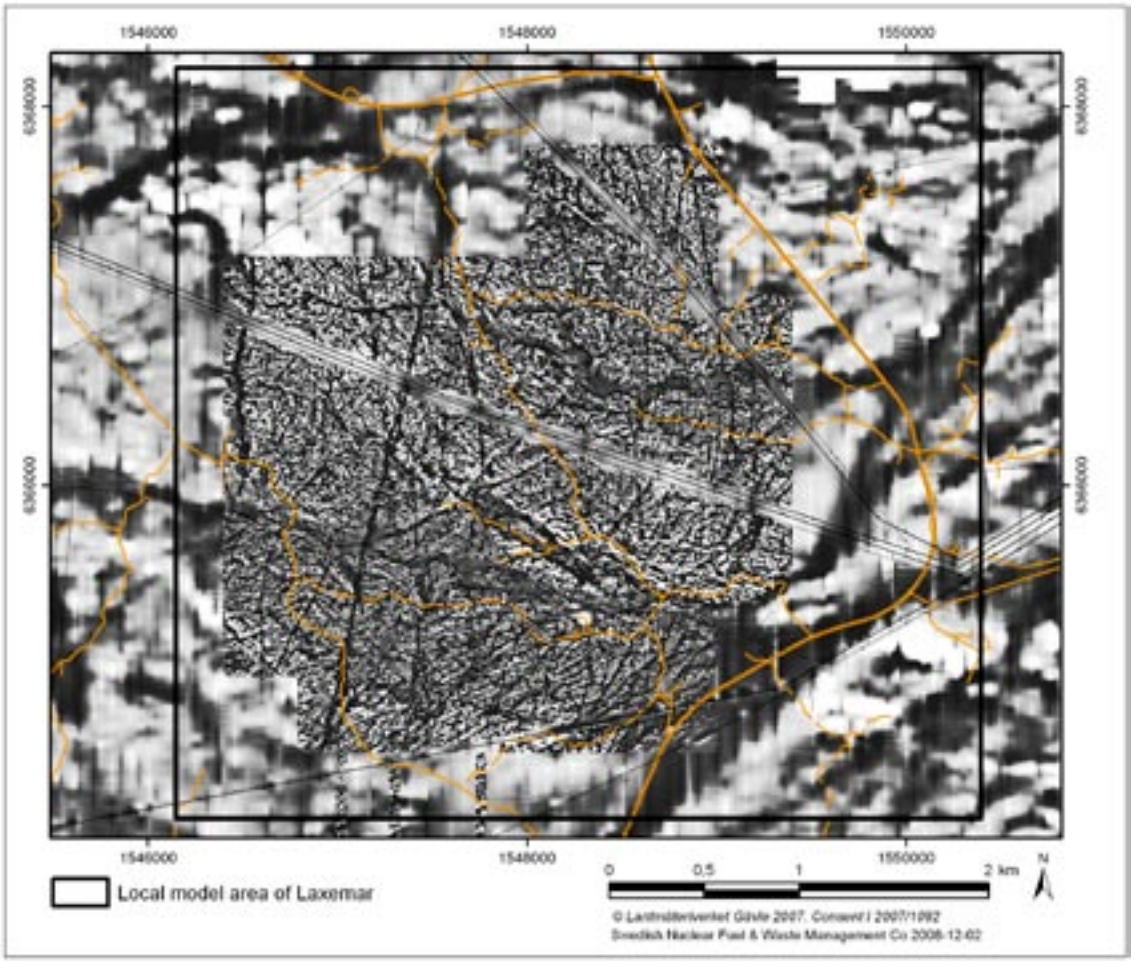

Figure 3-83. *Combined map of the 1st vertical derivative of the magnetic total field composed of the combined NS-directed helicopter and the detailed ground magnetic surveys.*

A combined map of the helicopter borne magnetic survey and the ground magnetic survey that encloses the local model area is presented in Figure 3-83. This map shows the 1st vertical derivative of the magnetic total field and enhances near-surface structural and lithological information.

3.8.2 Terrain models and their resolution

Initially during the site investigation, the entire local model area was covered by a rather coarse digital elevation model /Wiklund 2002/. In 2005, the airborne laser scanning technique (LIDAR) /Nyborg 2005/ provided a higher degree of resolution in the elevation model allowing the identification of additional narrow and short lineaments. The characteristics for each survey type are presented in Table 3-9 and the coverage of each set of data inside the local model area is presented in Figure 3-84.

Table 3-9. Data on digital elevation models (DEM) in the Laxemar local model area.

Type of survey	Contractor	Grid resolution
Airphoto 2,300 m	Metria	10×10 m
LIDAR	Swedpower AB and Blominfo AB	1×1 m

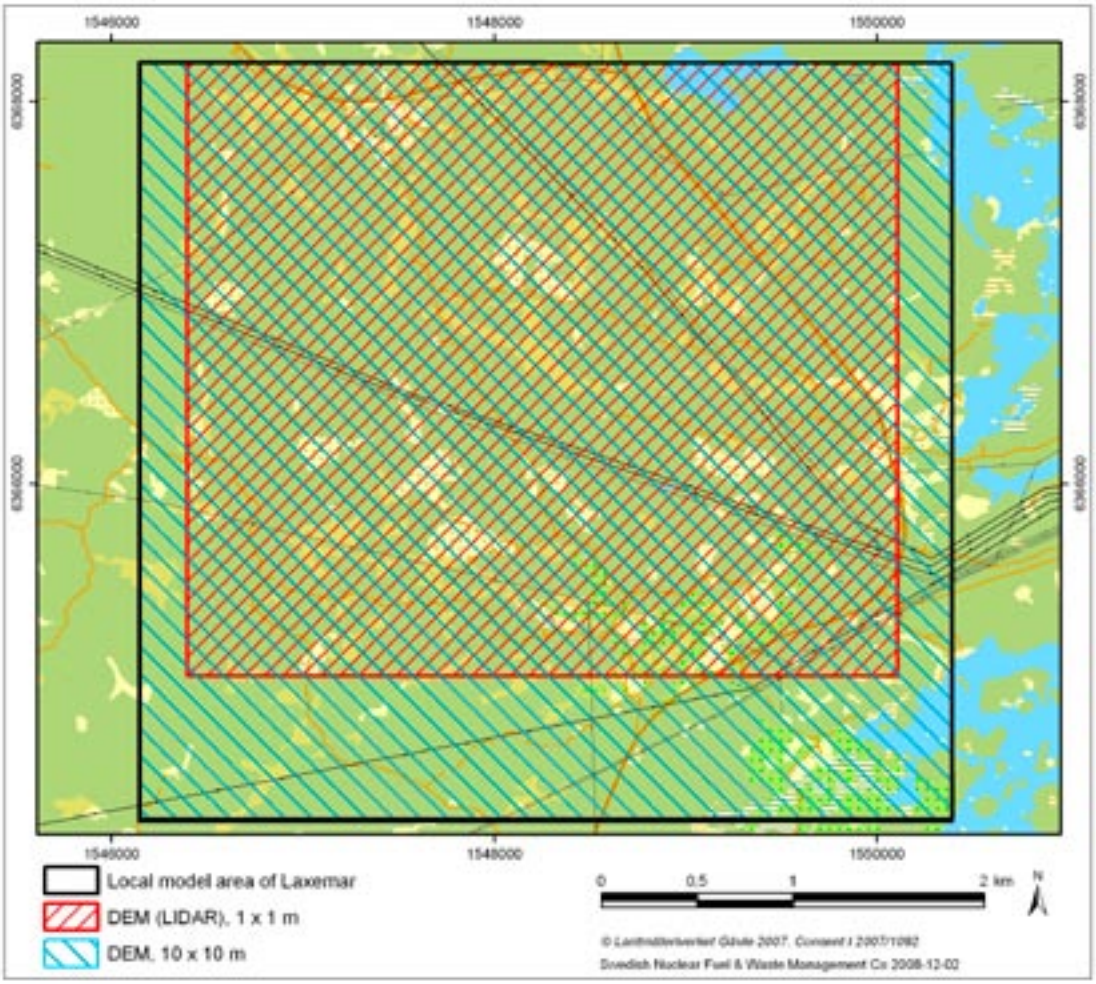

Figure 3-84. Coverage of different digital elevation models according to Table 3-9.

3.8.3 Types of electromagnetic and galvanic resistivity data and their resolution

During the initial stage of the site investigation, helicopter-borne electromagnetic data /Rønning et al. 2003/ were provided together with a re-processing and interpretation of older VLF-data from SGU /Triumf et al. 2003/. With the high resolution ground geophysical surveys that started 2005, galvanic resistivity data were also acquired, processed and interpreted /Thunehed and Triumf 2005, Thunehed and Triumf 2006/. A condensed presentation of these data sets is given in Table 3-10 and the coverage inside the local model area is shown in Figure 3-85.

Table 3-10.Characteristics of electromagnetic and galvanic resistivity surveys perfomed in the Laxemar local model area.

Type of survey	Contractor	Line spacing	Station spacing	Survey direction	Survey elevation	Grid resolution
Airborne, fixed-wing VLF	SGU	200 m	17 or 40 m	EW	30 m	50×50 m
Helicopter borne VLF and multifrequency EM	NGU	50 m	3 m	NS (tie lines EW)	40 m (60 m for VLF)	10×10 m
Ground galvanic resistivity (2005)	GeoVista AB	40 m	5 m (electrode separation)	NS and EW		
Ground galvanic resistivity (2005/2006)	GeoVista AB	10 m	5 m (electrode separation)	EW		

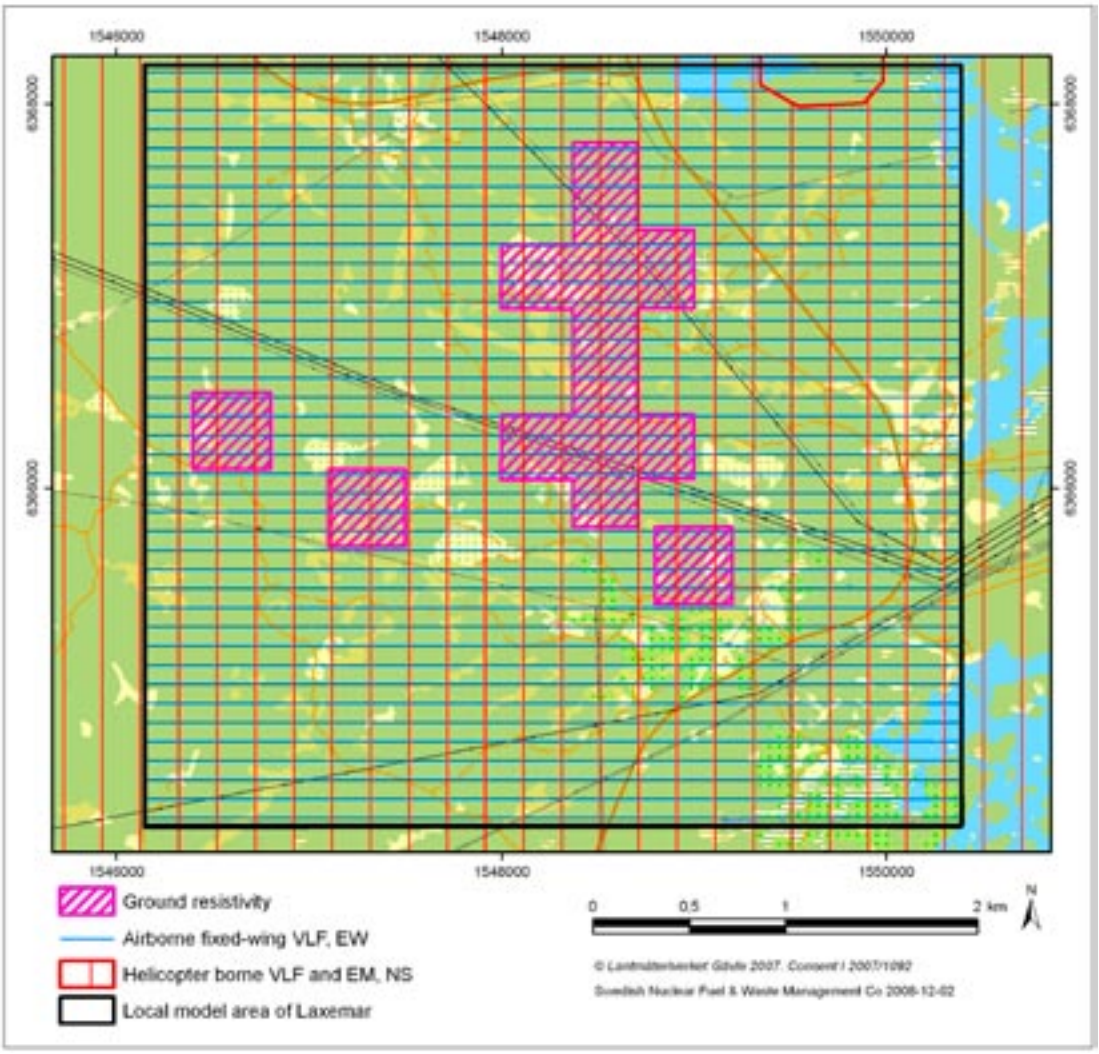

Figure 3-85. *Coverage of different electromagnetic and resistivity survey methods according to Table 3-10.*

3.8.4 Geological significance of identified lineaments and factors affecting lineament identification work

The identification of lineaments has been carried out in several steps: they include interpretations of single data sets of varying type and resolution /Triumf 2003, Triumf et al. 2003, Thunehed and Triumf 2005, 2006, Mattsson and Triumf 2007/; co-ordination /Triumf 2004a, b, Triumf and Thunehed 2007, Mattsson and Triumf 2007/ and linking, and has resulted in the final product called "linked lineaments" covering the local model area /Mattsson and Triumf 2007/. Furthermore, an alternative lineament interpretation study was performed by the Geological Survey of Finland (GTK) /Korhonen et al. 2005/, with the aim of investigating consistency and repeatability in the interpretation work. A comparison of the two independent lineament interpretation studies was carried out by /Johansson 2006/.

The process of joint interpretation of lineaments consists of the following major steps (Figure 3-86):

- Construction of "coordinated lineaments" from "method-specific lineaments".
- Parameterisation of the "coordinated lineaments".
- Construction of "linked lineaments".
- Parameterisation of "linked lineaments".

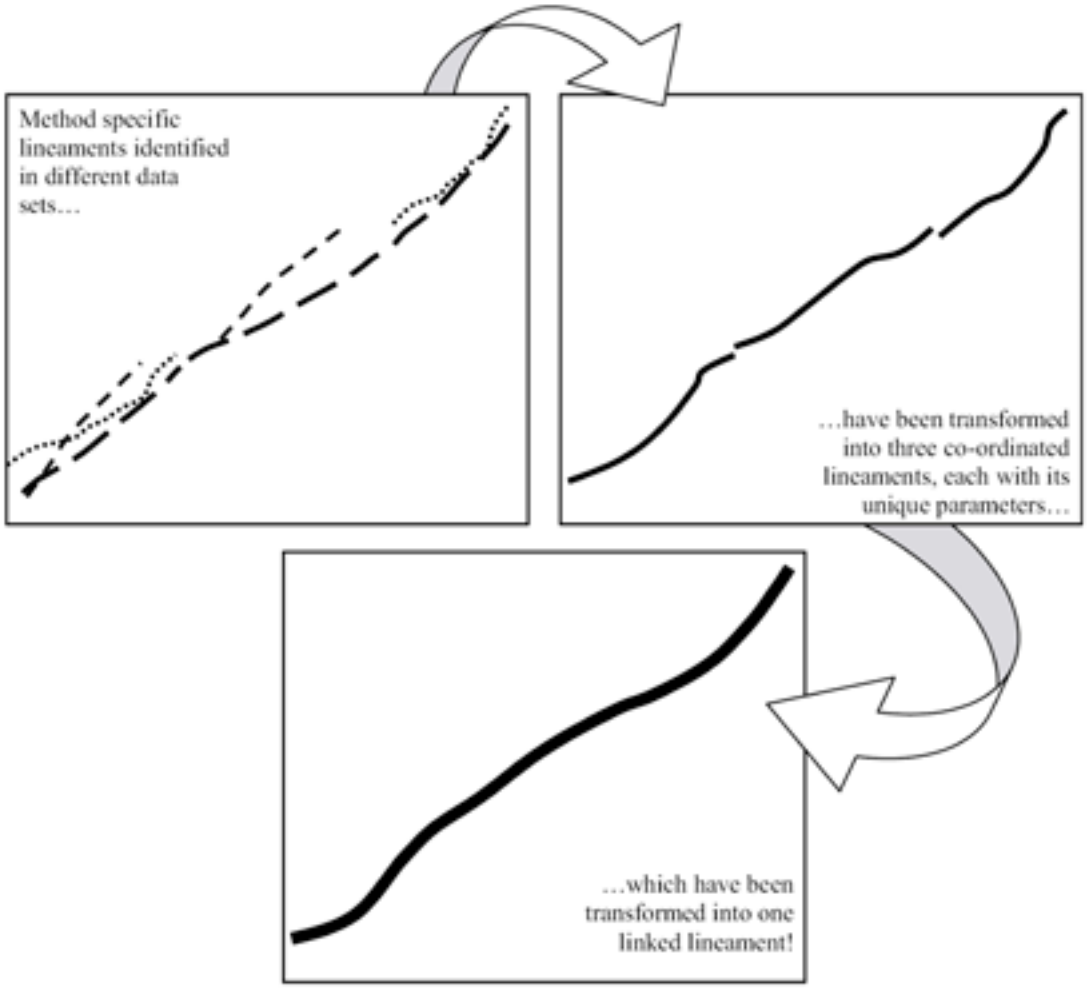

Figure 3-86. *Schematic explanation of the joint lineament interpretation process.*

The resulting lineament interpretation covers the regional model area as seen in Figure 3-87. Lineaments of low resolution that originate from model version 0 /SKB 2002/, cover the eastern part of the regional model area (sea area) and a minor rectangle in the north-west. Lineaments in the central part of the regional model area have not been changed since model version Simpevarp 1.2 /SKB 2005a/. Detailed bathymetric data along the coast line resulted in a more detailed coverage of lineaments further to the east. The linking of lineaments between the low and high resolution areas has been performed by joining together lineament ends located sufficiently close using the underlying topographical and airborne geophysical data supported by expert judgement. Note that the variable resolution of the background data imposes an artificial appearance of there being fewer lineaments at sea and in the north-west.

With the aim of investigating consistency and repeatability an alternative lineament interpretation study was performed by the Geological Survey of Finland (GTK) /Korhonen et al. 2005/. The alternative lineament interpretation showed good overall agreement with the earlier interpretation /SKB 2006f/. Where differences were noted these were investigated and the two sets were integrated in the following manner.

Only deformation zone traces and GTK lineaments with a trace length of at least 1,600 m were considered in this attempt to investigate whether the alternative lineament interpretation made by an independent team would significantly change the resulting co-interpretation of deformation zones in the RVS working-model.

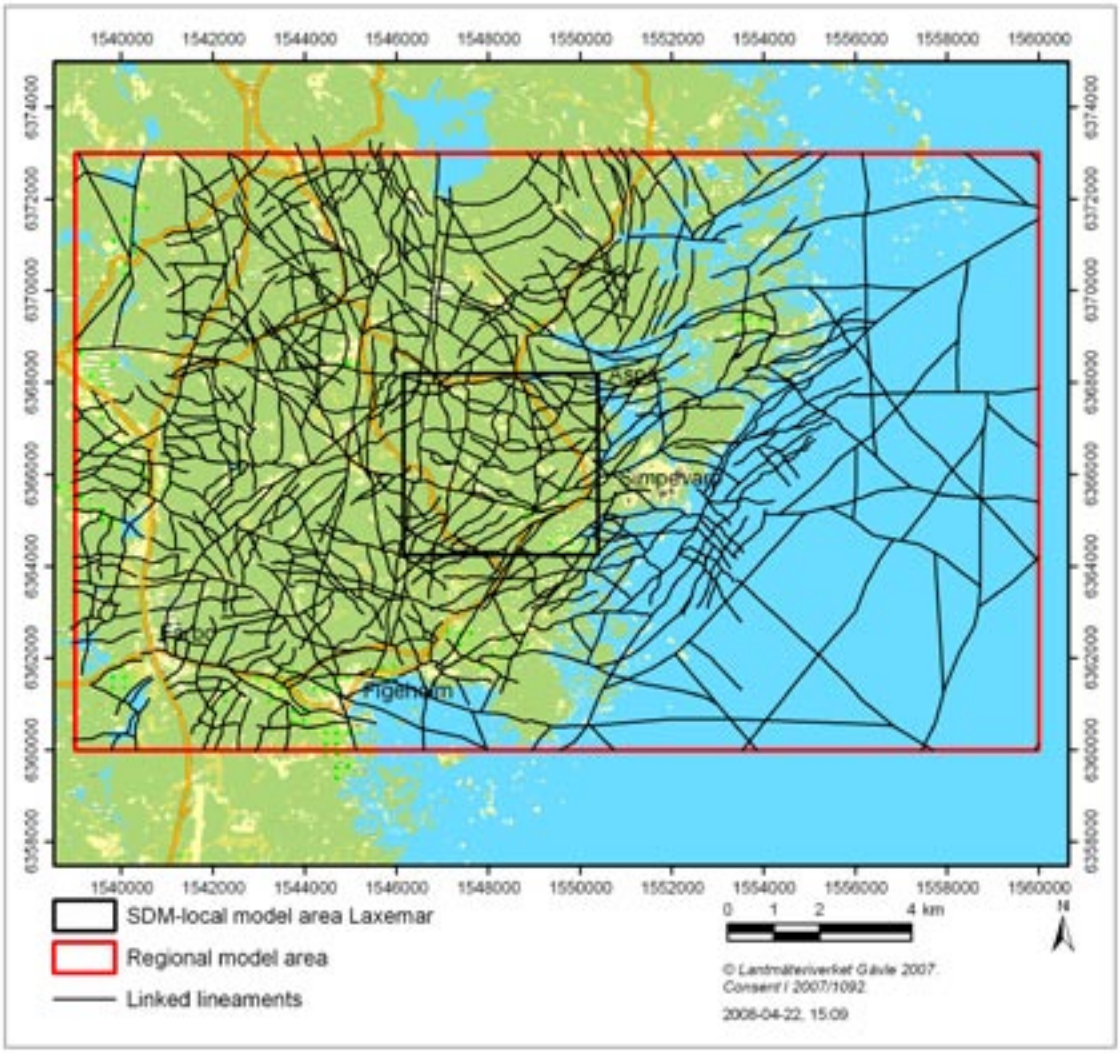

Figure 3-87. *Linked lineaments in the regional model area.*

The methodology involved comparison of both data sets over the entire regional scale domain, with special focus on the local scale model domain. Lineaments where the differences were judged to suggest significant differences for the deformation zone model were identified. This process resulted in a selected 'short list' of lineaments that were considered to justify a more detailed study of the background geophysical and topographical data.

The selection was made by taking GTKs linked lineaments; making a sub-selection of all traces > 1,600 m, corresponding to the earlier regional model scale, and selectively extracting geometries that constituted significant changes relative to the Laxemar 1.2 model. In practice this meant that traces were selected on the following basis:

- a very similar geometry to an existing trace but with a greater lateral extent resulting in a higher connectivity and possibly isolating a block that was only partially defined in the Laxemar 1.2 model,
- a similar alignment to an existing trace but with different linkages, resulting in a much more significant extent,
- a completely new geometry that simply was not identified previously, but fit in well with the current understanding of prevailing tectonic patterns.

The continued study also involved re-examination of the background data of the selected lineaments. This final review resulted in the majority of the GTK lineament alternatives being rejected based on either topographical or geophysical background data. However, a number of alternative interpretations were retained for integration in the final model /SKB 2006f/.

The focus in the ensuing text concerns the identification of lineaments within the Laxemar local model area (Figure 3-88). The last step in that process started after the ground measurements of the magnetic total field were finished in May 2007. These measurements give complementary coverage of high resolution magnetic data over the southern part of the local model area and have provided data on one of the prominent deformation zones, ZSMNW042A /Mattsson and Triumf 2007/.

An important task connected to the lineament identification during the current modelling has been to integrate the lineaments identified from the high-resolution data within the local model area, with the formerly identified lineaments. Several of the formerly identified lineaments in the regional data have been re-evaluated, which in many cases has led to re-shaping, or even rejection in the light of the high resolution data. This re-evaluation has not been possible in the parts of the local model area where high resolution data are lacking and, hence, some of the peripheral lineaments in the final lineament map may thus be considered as possibly of less significance.

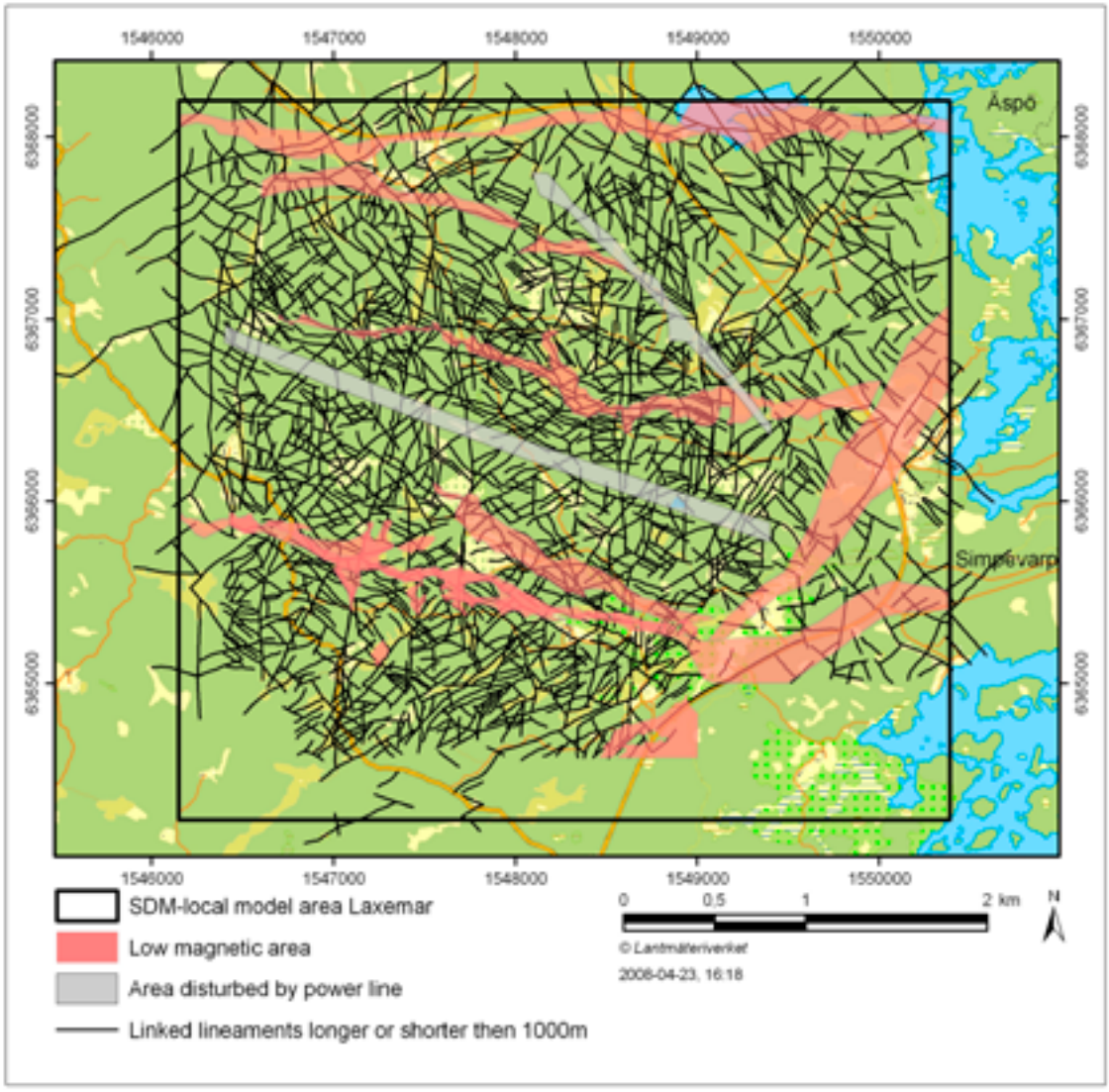

Figure 3-88. *Linked lineaments in the Laxemar local model area.*

The final lineament map over the local model area contains 1,434 linked lineaments in the length interval of 100–1,000 m, and 18 longer than 1,000 m (Figure 3-89). From the attributes of each individual lineament it is e.g. possible to observe in what data sets the lineament is detected. A majority of the linked lineaments in the local model area are visible in both magnetic and digital elevation models for more than half of their length, however, not necessarily along the same length sections of the lineaments. In areas where detailed ground magnetic total field data are missing, the density of lineaments is lower due to less resolution in the data reflecting the bedrock magnetisation; an inherent bias associated with the radically better quality and spatial resolution of the ground magnetic total field data. When studying the character of the linked lineaments it is, thus, important to relate to the data coverage.

Some prominent low-magnetic features coupled to depressions in the terrain are observed at Laxemar. Deformation zones ZSMEW007A and ZSMNW042A (Figure 5-3) are two of the most pronounced examples of the latter type. They are also visible in the helicopter-borne electromagnetics as electrically conductive features /Triumf et al. 2003/. On a regional scale these anomaly complexes may be represented by single lines drawn along the centre of the features. However, on a local scale their geometrical complexity becomes evident, and the single line representation is considered less meaningful. During the process of lineament identification these low-magnetic features were outlined and called “low magnetic belts”, the geometrical coverage of the belt reflects the extent of low magnetisation (Figure 3-88). Although the host rock within the belts appears less magnetised it is at some locations possible to follow lineaments that pass through the belt.

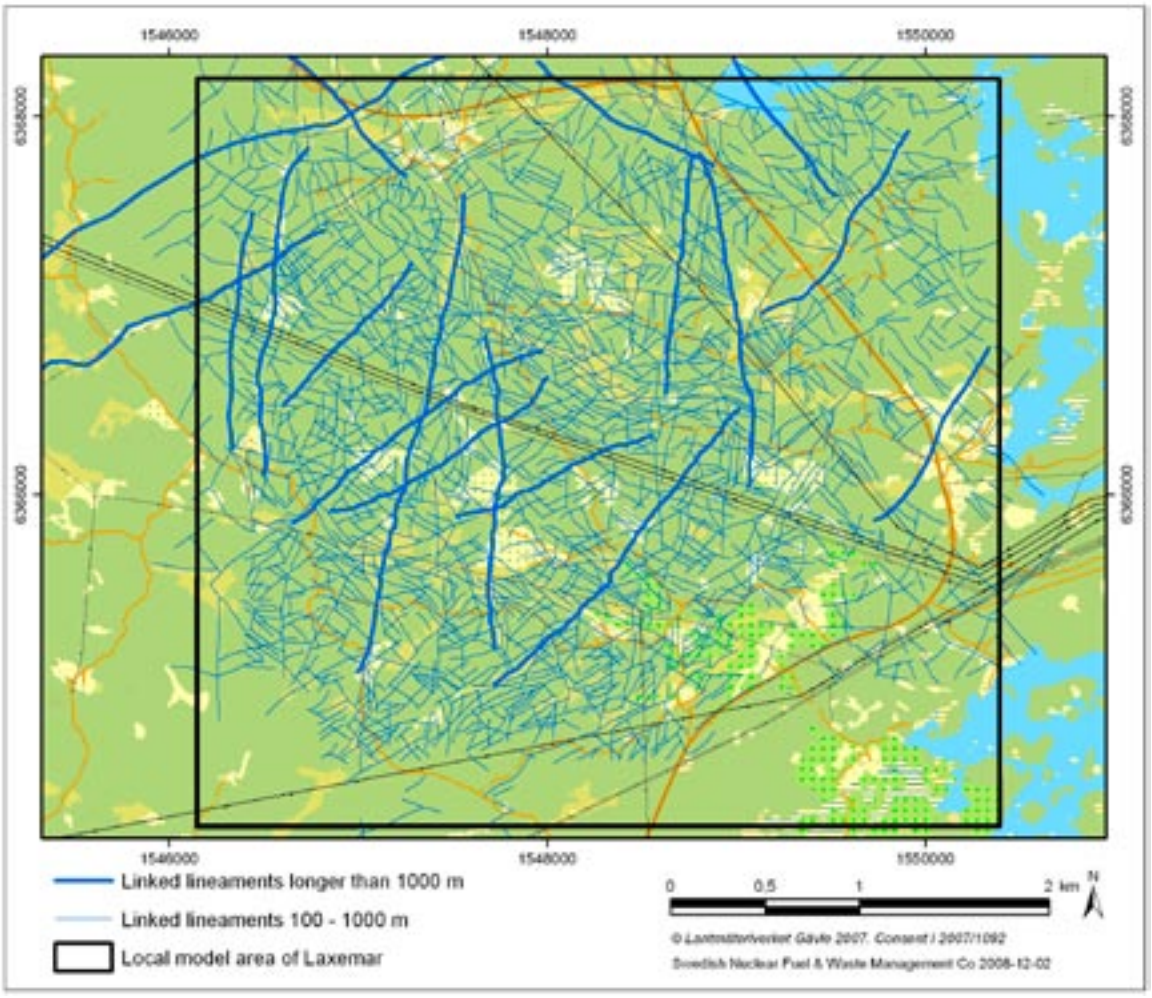

Figure 3-89. *The linked lineaments from the Laxemar local model area. Total 1,452 of which 18 are longer than 1,000 m (thicker blue).*

Dolerite has not been observed in outcrops in the Laxemar local model area, but is reported from a number of cored and percussion boreholes in western Laxemar (see Section 3.2.1). Studies of the dolerites indicate that they probably manifest themselves as lineaments with much of the same character as can be expected from lineaments representing deformation zones, i.e. as low-magnetic linear features associated with depressions of varying clarity in the digital elevation models (cf. Section 3.2.1, /Triumf 2007/). Two lineaments in the local scale model area of Laxemar are known to host dolerite as part of their anomaly source. By applying developed search criteria to all lineaments in the local model area, based on studies of the character of known dolerites at Laxemar and in the region of Oskarshamn, nineteen more lineaments have been identified that could contain dolerite (cf. Section 3.2.1 and /Triumf 2007/).

Specific aspects to investigate the geological significance of identified lineaments and low magnetic belts have been included in the site investigation programme at Oskarshamn. Field control of outcrops, geophysical profile measurements, excavation work, drilling activities and ESHI constitute the major contributions. Lineaments verified by refraction seismics appear to be more brittle in character with a higher degree of open fractures and a greater transmissivity /Olsson et al. 2007/.

Areas with low magnetisation and with low topographic relief can be related to intersections of several discordant, low magnetic lineaments or a general deformation of the bedrock. At the western part of ZSMNW042A (cf. Chapter 5), geophysical profile measurements of galvanic resistivity indicate that the topographical depression and the low-magnetic feature coincide with a resistivity low. This combination of physical properties strongly indicates the existence of deformed bedrock /Thunehed et al. 2004/. However, there are also examples where a significant low-magnetic structure is related to a topographic depression and a resistivity low, but where the magnetic features is displaced relative the other indications. One such example has been recognised by geophysical profile measurements across ZSMNS059A (cf. Chapter 5) in the northern part of Laxemar /Thunehed et al. 2004/. It is reasonable to assume that the low-magnetic feature is related primarily to ductile deformation, whereas the topographic and resistivity indications relate to brittle overprinting. Different sources for lineament identification may thus reveal information about the properties of the underlying geological structure.

Several factors affect the identification and characterisation of lineaments. One of them is the data resolution – in the local scale model area the coverage of the different data sets varies, which affects the level of significance of the lineament. In areas lacking high resolution magnetic total field data, the number of identified lineaments is lower. The geometrical significance of the lineaments found in such areas is also lower.

As the different geophysical measurements are not uniform in line and point separation a bias is introduced. In the local model area, the line direction both in the helicopter-borne magnetics and the ground magnetics is north-south. The line separation in the helicopter-borne survey is more than 10 times the point separation along the flight line. In the ground survey this relation is a factor of 2. This means that the number of lineaments striking more or less north-south is probably underestimated.

Forward modelling of the magnetic total field response has been carried out to reflect the simplified but realistic minimum dimensions of a low-magnetic zone to be detected in a survey using the survey parameters of the Laxemar measurements. The typical thin soil cover of a few metres and the typical magnetic susceptibilities of the bedrock at Laxemar have been used. The results show that in areas with a relatively low noise level in magnetisation due to rather a homogeneous distribution of magnetite in the bedrock, magnetic measurements on ground are capable of detecting vertical low-magnetic zones with thicknesses of 1–2 m. In areas with more heterogeneous magnetisation, the noisy background inhibits the detection of such thin zones. Instead it is more realistic to use a cut-off thickness of around 5 m in such areas. Noisy areas are

easily recognised on the magnetic total field map and are most pronounced between deformation zones ZSMEW007A and ZSMNW042A (cf. Chapter 5) where mafic rocks are a common lithological constituent.

Modelling of galvanic electric resistivity measurements has been performed to evaluate the lower resolution limit of deformation zones. Typical values of resisitivity known from ground, borehole and laboratory measurements have been used. The identification of a deformation zone as a resistivity lineament is to some extent dependent upon the resistivity contrast with respect to undeformed country rock. A zone of primarily ductile character and/or with sealed fractures may be difficult to detect. Of even greater importance is the thickness of the zone. It will be difficult to detect a zone with a smaller thickness than the depth of burial. The thickness of the soil cover (Quaternary overburden) in the southern parts of Laxemar is in general 5 to 8 m. This means that zones with a thickness of less than 5 to 8 m may remain undetected in a resistivity survey. A thick zone will consequently be much easier to detect, even if the resistivity contrast to undeformed country bedrock is rather subtle. Presence of a low-resistivity clayey overburden of significant thickness will also mask the appearance of minor zones.

In areas of low general magnetisation lineaments in the magnetic total field are more difficult to identify. Such areas appear as poorly constrained low-magnetic belts.

3.8.5 2D forward modelling of magnetic data – principles and uncertainty

Forward modelling of magnetic data (ground, airborne or borehole) has been performed in order to estimate geometries and magnetic properties of the sources (rock bodies) that give rise to the measured anomalies in the Earth's magnetic field /Mattsson and Triumf 2007/. The basic principle of the modelling work is to create geological bodies of certain shapes and magnetic properties, calculate the magnetic anomaly field from the model bodies (usually termed model response) and then graphically and/or statistically compare the calculated response to the measured data. The model parameters and/or geometry of the bodies are changed until a satisfactory fit of the model response to the measured data are achieved (often an expert judgement) /Mattsson and Triumf 2007/.

An example of modelling of magnetic data is shown in Figure 3-90. It should be noted that complexities are caused by the surrounding bodies with variable magnetic susceptibility, which deflect the flanks of the negative anomaly caused by the deformation zone. When the forward modelling work is based solely on susceptibility contrasts and geometry variations, without any other supportive information, the dip estimation of the inferred deformation zone should be expressed only in terms of being steeply or gently inclined.

3.9 Reflection seismic data

Reflection seismic data were acquired in 1999 /Bergman et al. 2001/ and the spring of 2004 /Juhlin et al. 2004/. In 2004, approximately 9.9 km of high resolution seismic data were acquired along three separate profiles, 3.9 km along the NNE-SSW profile 3, 1.8 km along the WNW-ESE running profile 4, and 4.2 km along the NNW-SSE running profile 5 (Figure 3-91).

Nominal source and receiver spacing was 10 m with at least 160 active channels when recording data from a dynamite source (15–75 g). The results from the seismic survey were available at the beginning of the drilling campaign in Laxemar and were used in the positioning of boreholes and other investigations as well as being used as a valuable input to the overall modelling process. A number of the interpreted reflectors were found to correlate well with later drilling results and form the basis of the interpreted geometry of some of the major deformation zones

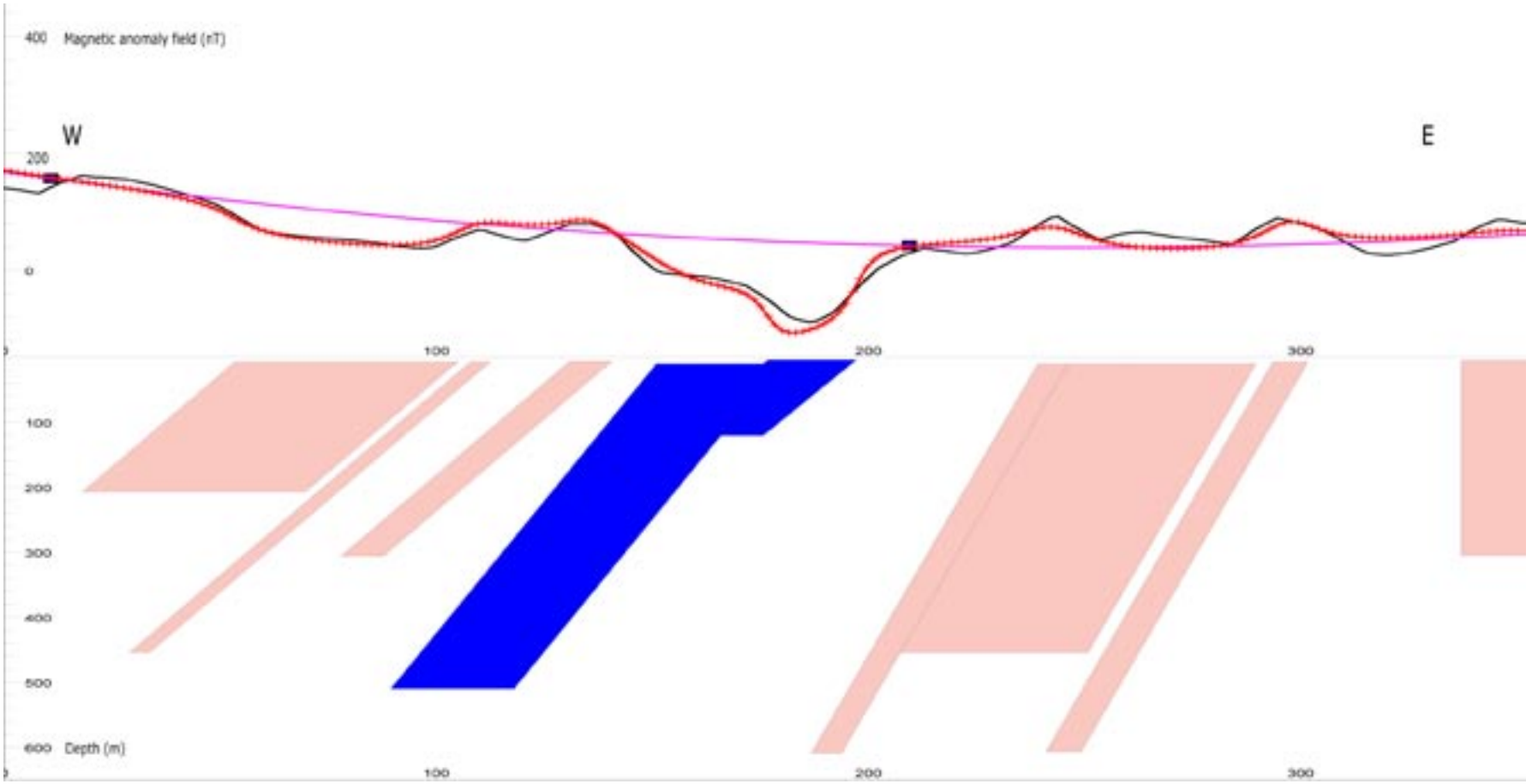

Figure 3-90. *Example of magnetic forward modelling in a vertical section perpendicular to deformation zone ZSMNS059A (interpreted to be associated with dolerite). The deformation zone is shown in dark blue colour. The black line shows measured data and the red hatched line shows the model response.*

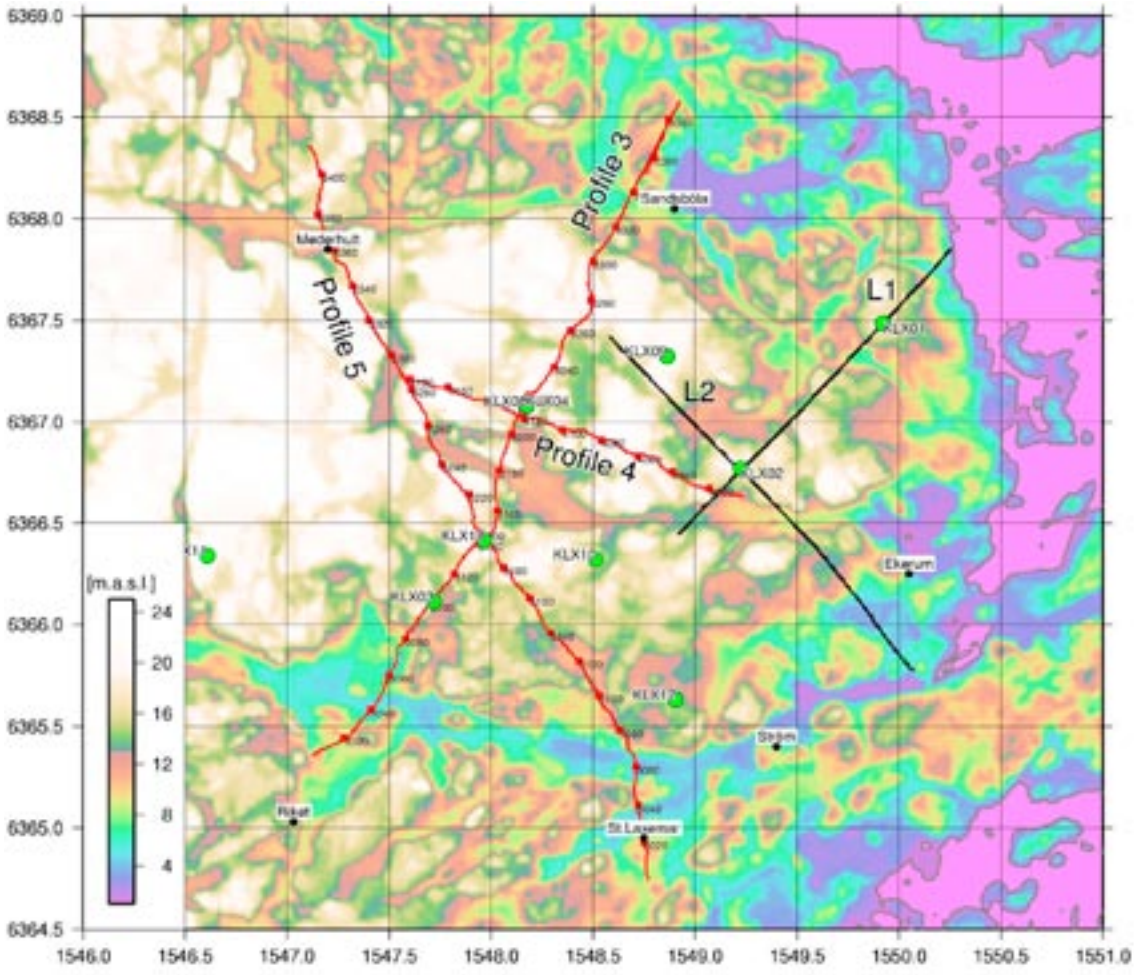

Figure 3-91. *Location of the seismic reflection profiles, profile 3, LSM000704, profile 4, LSM000705 and profile 5, LSM000706 (red lines). Reflection seismic profiles acquired in 1999 (black lines) were reported on in /Bergman et al. 2001/.*

such as ZSMEW002A and ZSMEW007A. After 2004 no further field survey work was performed, however, data from profiles 3 and 5 were reprocessed in an attempt to better image the uppermost 1,000 m of the bedrock in the vicinity of selected cored boreholes. These reprocessed results and their interpretation are presented in Apendix13 and summarised in Table 3-11 and Figure 3-92. When possible, cross-dip analysis of the data was carried out in order to constrain the geometry of the reflectors. Based on this reprocessing, the geometries of the main reflections observed on the profiles were updated. A number of the earlier 2004 geometries were modified and new reflections identified.

Focus was on the set of so called M reflections, which dip gently to the south in the upper 1.5 km of crust in the area. These reflections are generally discontinuous in nature, but are part of the general pattern of south dipping reflectivity seen in the profiles. In general, the picked reflections should not be viewed as discrete deformation zones, but rather as a group of reflections that line up along a relatively straight line. This is especially the case for the set M reflections. It was concluded that the set M reflections appear to be of a similar nature to the sub-horizontal reflections observed below KLX02 /Juhlin et al. 2002/, and they are associated both with fractured zones and mafic rock.

Table 3-11. Orientation of reflectors as determined from the surface seismic data reprocessed and reinterpreted (1999 values /Juhlin et al. 2004/ in parentheses when different, new reflectors in italics). Reflectors defined by distance to a point on the surface (better for dipping reflectors) or by depth below this point (better for sub-horizontal reflectors). Distance refers to distance from the KLX02 borehole (6,366.768 km N, 1,549.224 km W) to the closest point on the surface to which the reflector projects. Depth refers to depth below the surface at this origin. Rank indicates how sure the observation of each reflection is on the profiles that the reflection is observed on; 1- definite, 2- probable, 3- possible.

Reflector	Strike	Dip	Distance (m)	Depth (m)	Rank	Profiles observed on
A	275	43	190		1	1, 2, 4
Ba	0	3		590	1	1, 2, 4
B	0	3		760	1	1, 2, 4
Bb	0	3		930	1	1, 2, 4
C1	90	70	1,330		1	1, 2, 3, 4
C2	85	70	1,330		1	4, 5
D	253	35	840		2	1, 2, 4
G	253	35	1,170		2	1, 2, 4
K	75(30)	40(50)	–100(800)		2	4? 5
K2	60	60	470		2	3? 5
L	110	70	–300		3 (2)	3? 5
L2	110	38	–250		2	3? 5
M1	80(95)	23(20)		500(350)	1	3, 4, 5
M2	75(100)	22(25)		650(500)	1	3, 4, 5
M3	100	25		750	1	3, 4, 5
M4	100	25		950 (900)	1	3, 4, 5
N	75(120)	23(30)		1,270 (770)	2	3, 4, 5
O	200	80	–1,850		3	5
P	270	5		1,250	2	3, 4, 5
Q	75	30		540	1	5
X1	295	15		400	3	3
X2	295	15		970	3	3
X3	295	15		1,070	3	3
Y1	240(295)	35(27)		–250 (300)	3	3,4?
Y2	240(295)	23(15)		50 (350)	3	3,4?

The uppermost reflector of this series, M1, intersects the likely repository depth of –500 m above sea level and was the focus of the review. Due to its perceived importance this reflector has been included in the deterministic deformation zone model as a discrete structure ZSMEW946A. However, it can be more generally interpreted to represent the upper boundary of a thicker laterally discontinuous series of gently dipping minor deformation zones and mafic intrusions. Further description of M1 and ZSMEW946A can be found in Appendix 14.

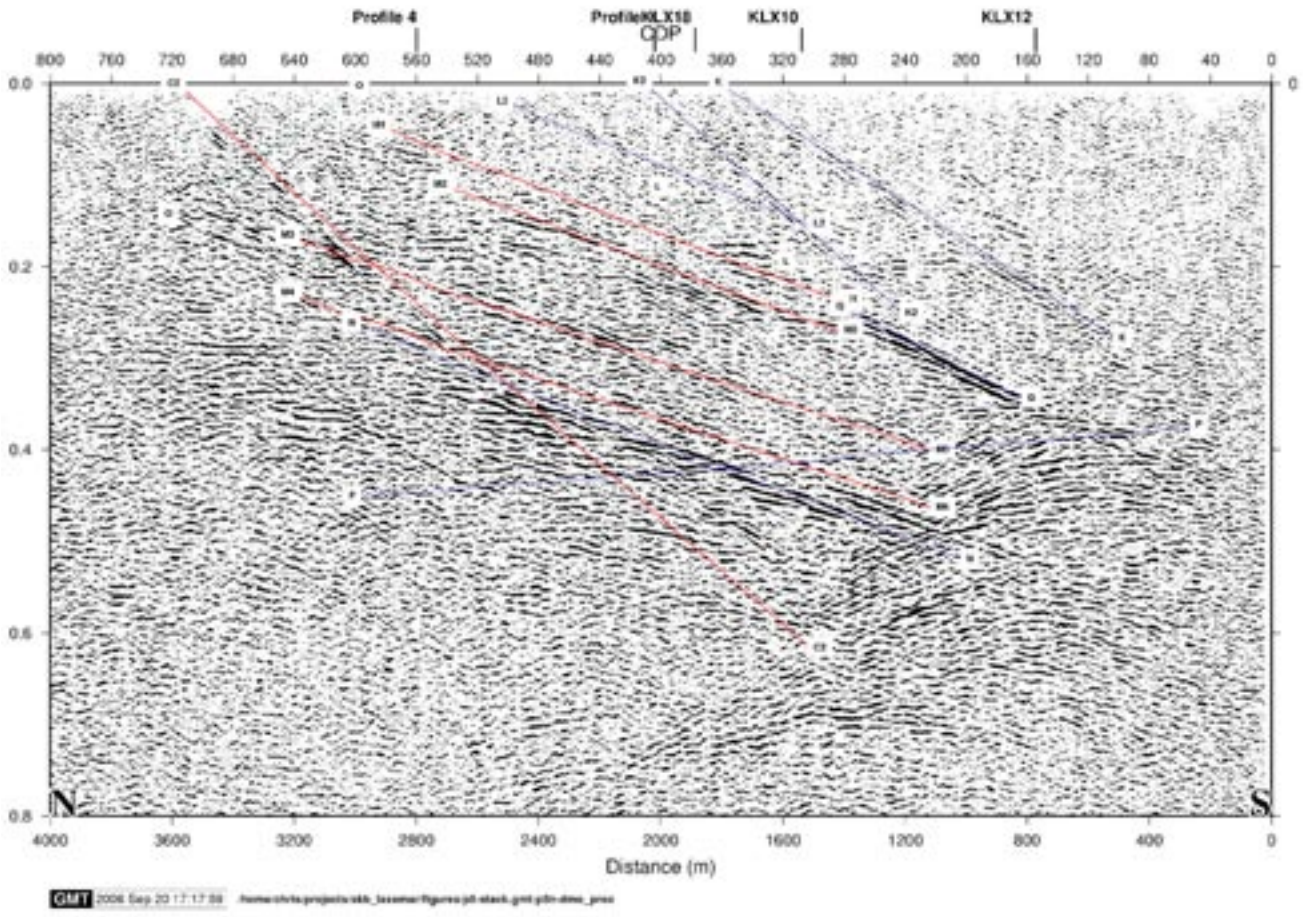

Figure 3-92. *Reprocessed stacked section of profile 5 (LSM000706) down to 0.8 seconds with picked reflections (cf. Figure 3-91). Red rank 1, blue rank 2, green rank 3. Inferred strike and dips are given in Table 3-11.*

3.10 Refraction seismic data

Laxemar and Simpevarp have been investigated by a number of seismic refraction surveys between 2004 and 2007 /Lindqvist 2004a, 2004b, 2004c, 2005, 2006, 2007/. The objective has been the focussed investigation of possible deformation zones and to investigate the soil depth. The local major (length > 1,000 m) interpreted lineaments were generally confirmed as deformation zones with lower seismic velocity, 2,500 m/s up to 4,000 m/s, while the velocity of the unaffected country rock was in the range from 5,000 m/s up to 5,900 m/s. An overview of the profile positions is presented in Figure 3-93.

3.10.1 Data evaluation

Forty-four profiles with a total length of 25,015 m were measured. The geophone spacing varied from 2.5 to 5 m depending on the survey. The interpreted apparent zone thickness varied between 2.5 and 20 m, with a majority found in the 5 to 10 m range. The lower limit must be seen as a function of the minimum geophone spacing employed. The interpreted low velocity anomalies have been interpreted to give indications of likely thicknesses and rock quality conditions associated with brittle zones. This is a coarse evaluation and the following discussion sets out to highlight this fact.

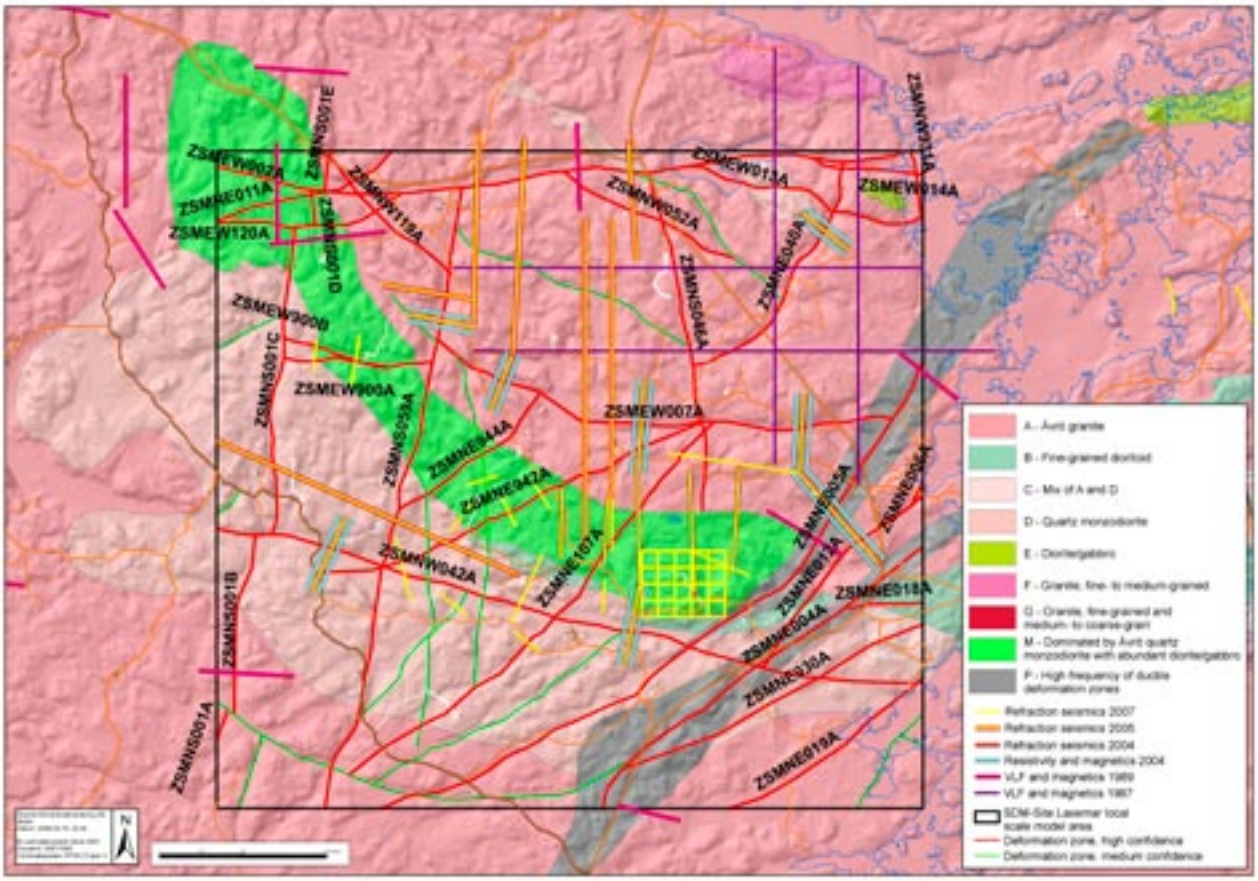

Figure 3-93. *Geophysical profiling work carried out in the Laxemar local model area. For reasons of simplicity, the prefix RSM has been excluded in the denomination of the rock domains.*

It is not possible to comment on the minimum thickness of the inferred deformation zone, apart from the fact that it is not thicker than the geophone spacing. Also, it is important to note that the estimated velocity of the deformation zone is the average velocity between two geophones. Assuming a spacing of 5 m for example, there could be a case with a 1 m thick zone core of heavily crushed rock surrounded by 1 m transition zone on each side, which in turn is surrounded by 1 m fresh rock, all three parts would fit within the 5 m geophone spacing. The estimated velocity of the zone would then be the weighted average of the velocity in fresh rock, the velocity in the transition zone and the velocity in the zone core. In order to get a good estimate of the velocity of a deformation zone, one would normally prefer coverage of at least 3 geophones, which would give three points to use for the curve fit in the time-distance graph. For a geophone spacing of 5 m, this means that a zone width of at least 10 m would be preferable in order to obtain a high accuracy identification of the average velocity of the targeted deformation zone.

When estimating the thickness of a deformation zone it is, apart from the geophone spacing discussed above, also worth noting the following two situations:

- A plan view of a geophone array making an angle with the strike of the deformation zone, shown from above, is displayed in Figure 3-94. In this case the incoming wave crosscuts the deformation zone at an angle i. According to Snell's law the wave is refracted (in the plane) due to the velocity contrast between the fresh rock (v1) and the deformed rock (v2). The actual time recorded by a geophone in position p is related to a wave having travelled the distance xs', and not along the geophone array, distance s. However, for the case with v1 = 6,000 m/s, v2 = 3,000 m/s, d = 5 m and i = 30º, the time difference between the travel paths s and xs' is = 0.08 ms, which in practice is insignificant. The actual width of the deformation zone can therefore be fairly accurately estimated at d = s cos (i).

- For the case with a dipping deformation zone (with dip angle a from the horizontal plane), a similar discussion would result in an estimated true width of the deformation zone of d = s sin (a), where s is the travel distance along the geophone array, parallel to the refractor (bedrock surface).

In practice the interpretation of refraction seismic data is further complicated by other variables and situations such as strong topographical variations of the ground surface, dipping refractors, lateral velocity contrasts and sharp variations of the bedrock surface topography. A sharp, step-wise depression in the bedrock surface, filled with soil, could for example be almost impossible to differentiate from a deformation zone related low velocity zone.

3.10.2 Relationship between low velocity (≤ 4,000 m/s) anomalies, topographical and low magnetic lineaments and deformation zones

The low velocity anomalies were interpreted as giving a general indication of the apparent thickness of a particular brittle zone core associated with a particular lineament and inferred deformation zone. The broader topographic and geophysical lineaments were interpreted as giving a general indication of the apparent thickness of the inferred deformation zone including transition zones and how this thickness was likely to vary both along a lineament at the ground surface and with depth. The presence of a low velocity anomaly was taken as supporting evidence for the presence and character of a deformation zone. However, because of scale issues, the geophone spacing (see Section 3.10.1), the lateral variability of the zones and the possible lack of an unhealed brittle component in the zone, the absence of a low velocity anomaly cannot be used to rule out the existence of a deformation zone.

3.11 Geological interpretation of oriented radar reflectors

It is considered that the directional borehole radar technique most often gives orientation estimates of discrete features. Such features may be open fractures or semi-planar rock type boundaries, if sufficient contrast in physical properties exists. Deformation zones, even minor

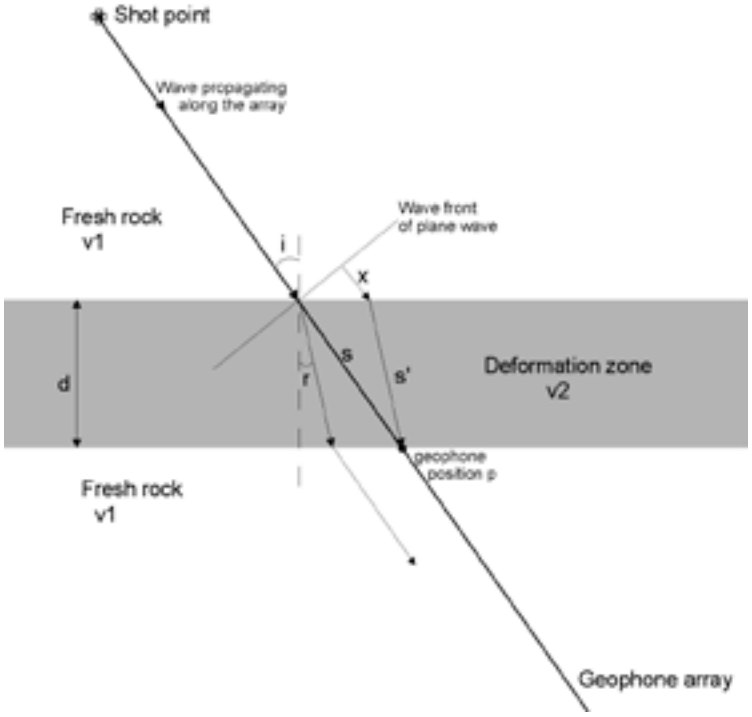

Figure 3-94. *Plan view showing theoretical wave propagation across a deformation zone which is not perpendicular to the geophone array.*

deformation zones can be seen as ‘packets’ of such features with varying, often complex, internal geometry (Figure 3-95). It is considered that even when such reflectors lie within or near a deformation zone that has been identified in the drill core, they are generally linked to discrete fracture surfaces or rock type boundaries associated with a deformation zone and are therefore considered likely to be unrepresentative of the overall geometry of the deformation zone ‘packet’ at a larger scale. Thus, radar orientations are interpreted to be secondary rather than primary supporting evidence for the interpretation of deformation zone geometry.

3.12 Minor deformation zones

Larger deterministic deformation zones (structures identified during site-descriptive modelling as regional and local major zones) are assumed to affect the overall volumes available for deposition holes and repository infrastructure. However, smaller structures, such as minor deformation zones (MDZ), are expected to affect only the locations of individual canister deposition holes.

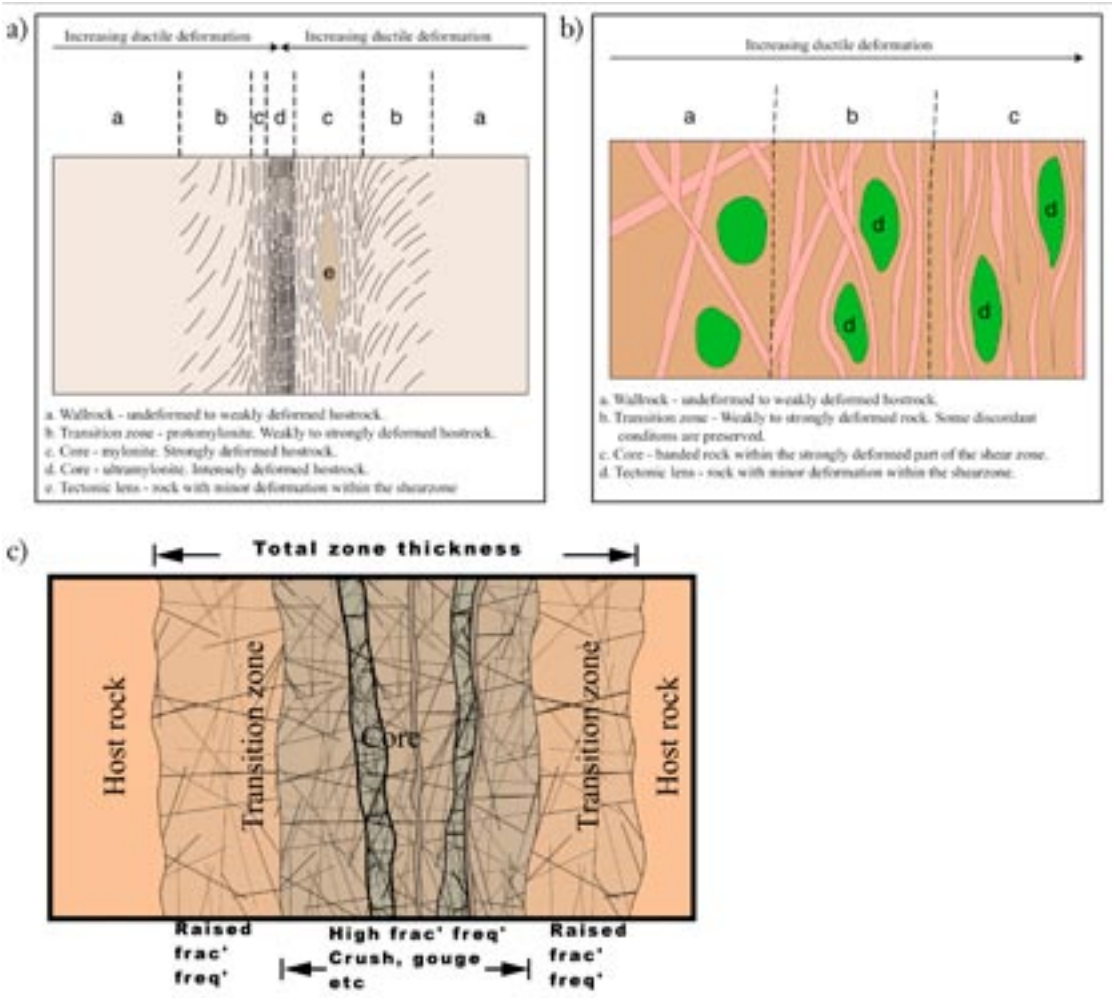

Figure 3-95. *(a) Schematic example of a ductile shear zone. Homogeneous rock which is deformed under low- to medium-grade metamorphic conditions. The increasing degree of deformation is reflected in the formation of protomylonite, mylonite and ultramylonite. The zone may contain less deformed rock volumes, often shaped as lenses. The example shows sinistral shear. (b) Schematic example of a ductile shear zone. Heterogeneous rock which is deformed under low- to high-grade metamorphic conditions. The host rock consists of e.g. tonalite (brown) intruded by an ultramafic rock (green) and a swarm of granitic dykes (pink). (c) Schematic illustration of a brittle deformation zone.*

Table 2-1 presents a terminology for deformation zones based on trace length and thickness modified after /Andersson et al. 2000/. The estimated length of a deformation zone takes account of the continuation of a deformation zone outside the model volumes. Furthermore, the total length of deformation zones, which consist of different segments or contain splays or attached branches, is accounted for in the classification according to length. As can be seen in Table 2-1, the division between minor deformation zones and local major deformation zones is set at an associated surface lineament trace length of 1,000 m. A Laxemar specific, hypothetical thickness-length relationship, based on deterministically modelled deformation zones, suggests that a deformation zone with a true thickness greater than 10 m has a length greater than 1,000 m (Figure 5-33).

All possible deformation zones that have been identified in a single borehole (i.e. that cannot be matched geometrically to a similar intercept in an adjacent borehole) and have an estimated true thickness less than or equal to 10 m are termed minor deformation zones. Minor deformation zones are assumed to be of limited spatial extent, and are therefore not modelled deterministically in RVS but are instead handled stochastically in the geological DFN modelling (Chapter 6).

3.12.1 Identification at the surface and MDZ focussed drilling investigations

A number of linear features (lineaments) with lengths less than 1,000 m have been identified inside the Laxemar local model area using high-resolution topography from airbore laser swath mapping (LIDAR) and high-resolution ground magnetic total field and resistivity survey data. Data derived from remote sensing was used in conjunction with regional geophysical survey data to develop a local-scale linked lineament map inside the Laxemar local model area (Figure 3-89). The confidence of the linked lineament interpretation is expressed in terms of the level of uncertainty applied to each linked lineament; a ranking weight is applied based on the number of properties used in lineament identification combined with the level of uncertainty /Triumf and Thunehed 2007/.

As previously mentioned (Section 3.8), linked lineaments can be assumed to be analogous to the minor deformation zones identified in cored boreholes at Laxemar. However, there is a degree of uncertainty involved in this assumption. Unlike the cored boreholes, only a small subset of the linked lineaments shorter than 1,000 m have been investigated at the ground surface or in cored boreholes. Lineaments can potentially represent minor deformation zones in the bedrock; however, they can also potentially represent other geological structures such as long single fractures, dolerite or granitic dikes, areas of pervasive ductile deformation not extensively re-activated in the brittle regieme, networks of sealed fractures, elongated zones of bedrock alteration, or topographic features not associated with bedrock deformation. It is possible that a mapped lineament, when investigated, may not exhibit the structural characteristics associated with minor deformation zones as mapped in cored borehole data, but does still represent a structure of geologic interest.

The connection between lineaments and minor deformation zones was explored through a coordinated surface mapping and core drilling program in 2006 at three sites inside the Laxemar local model area /Olsson et al. 2007/. Detailed surface mapping was performed with a focus on lineaments, over exposed rock or with shallow soil cover, with lengths in the range of 100 m to 1,000 m. Some of the more interesting lineaments were selected for excavation in order to expose their character at the bedrock surface. The exposed bedrock areas were mapped by the scan-line method and documented photographically. After the field reconnaissance, 18 of the 21 total examined lineaments were further investigated through shallow core-drilled boreholes (50–150 m in length) in order to attempt to correlate the appearance of the deformation zone between the ground surface and the borehole. The siting and orientation of the cored boreholes was based on the location and suggested orientation of the lineament based on surface mapping.

In areas with outcropping bedrock or with very thin overburden cover, the major part of identified lineaments can be explained by, or be directly related to, observations of deformed bedrock /Berglund et al. 2006/. The focused MDZ study /Olsson et al. 2007/ suggests that the most significant MDZs, indicated by lineaments < 1,000 m, are characterised by brittle-ductile deformation, increased fracturing (open and sealed fractures) and at some locations by minor crush and mylonites. The study also indicates that the most significant MDZs are characterised by a significant transmissivity ($T > 5\times10^{-7}$ m^2/s). Lineaments generating a seismic refraction low velocity anomaly appear to be more brittle in character with a higher degree of open fracturing and raised transmissivity. Some of the lineaments are connected to dykes of fine-grained granite striking north-east. They appear to be important water conduits with transmissivities (T) well over 1×10^{-6} m^2/s. The focussed surface study also suggested, that, within the limited scope of the investigation, not all investigated lineaments could be conclusively identified as MDZ 'of practical importance'. The determination of 'practical importance' is largely defined by whether the MDZ are hydraulically conductive /Olsson et al. 2007/.

When evaluating the < 1,000 m lineament interpretations it is important to recognise the difficulties involved in such work. In many cases the studies have failed to identify any obvious source of the interpreted lineaments. These lineaments are probably indications of minor ductile deformation, local rock alteration or dykes of fine-grained granite /Olsson et al. 2007/. According to the same study, it appears that correlation between a specific surface indication and deformation indications in the borehole is difficult, even at depths of only a few tens of metres. It is often not clear whether the indications represent the same zone or whether they represent two separate, possibly unrelated, minor structures. Spacing between possible MDZ indications in the 14 shallow (< 150 m) core drilled boreholes was estimated to be in the order of 50–100 m. Based on data from 5 deeper boreholes, in the 100–500 m interval, the mean spacing was estimated to be 120–200 m. /Olsson et al. 2007/.

The uncertainty in the relationship between lineaments and MDZ is explored in the geological DFN model (Chapter 6). A specific uncertainty analysis was performed to determine the effect on the fracture size-intensity parameterisation that the assumption that not all lineament traces represent minor deformation zones would have.

3.12.2 Identification in the sub-surface – extended single-hole interpretation

As a complement to the focussed MDZ study with its specific short MDZ targeted boreholes mentioned above, a review of existing drill core from other deeper boreholes across Laxemar was performed with the aim of identifying possible minor deformation zones, which earlier may have been overlooked at an earlier stage in the project when minor deformation zones were not being targeted for detailed study. This review is documented in the SDM-Site Laxemar data compilation report /Hermanson et al. 2008/.

The review was a two stage process, where the first stage comprised a desktop study of core box photographs, existing SHI, Boremap/BIPS mapping, radar data and geophysical borehole logs for the cored boreholes KLX02–KLX08 (note that the identification of MDZs was part of the SHI work from KLX09 and onwards, see Section 3.3). The aim was to address the potential existence of possible deformation zones that were too minor to be included in the original SHI. Seventy-four additional candidates of minor deformation zones were suggested in the studied boreholes KLX02 (down to borehole length 1,000 m) through KLX08 during this initial stage.

The second stage of the re-interpretation was to confirm or reject each identified candidate deformation zone by visual inspection of the core together with the same background material previously used. Out of the seventy-four suggested minor deformation zones from stage 1 (desk top study), thirty-five minor deformation zones were confirmed to exist (about 50%). These deformation zones were then described according to the established ESHI procedures.

The results from this review of earlier boreholes were combined with the results from the later boreholes resulting in a total of 211 MDZs that were mapped and described in the data compilation report /Hermanson et al. 2008/. Three types of deformation were identified, ductile, brittle and a combination of the two. Orientation and true thickness were calculated for each MDZ based on evidence in the drill core and borehole logs. Bedrock associations were also documented.

The identification of MDZ at Laxemar resulted in the following conclusions:

1. The ESHI results identify 281 deformation zones in the cored borehole array at Laxemar. This excludes borehole KLX01, for which orientation and MDZ information is not reliable, and borehole KLX27A, which was drilled and mapped after the SDM-Site Laxemar data freeze date.
2. Of these 281 DZ in the ESHI, an additional six DZ could be identified through subdivisions suggested during the development of the DZ model. If the subdivisions are used, the total number of DZ identified in the ESHI is increased to 287. The subdivisions include:
   - KLX02 DZ1 could be subdivided into two different DZ (ZSMNW928A and ZSMNE107A);
   - KLX03 DZ1 could be subdivided into three different DZ (ZSMEW946A, KLX03_dz1b, and KLX03_dz1c);
   - KLX04 DZ6 could be subdivided into three different DZ (ZSMNW928A, KLX04_dz_6b, and KLX04_dz_6c); and
   - KLX09 DZ13 could be subdivided into two different DZ (ZSMNW928A and ZSMEW007A).
3. For all MDZ analyses, the Geology team chose to lump together the aforementioned zones in KLX02, KLX03, KLX04, and KLX09. As such, for geological analysis, there are 281 identified deformation zones in the Laxemar cored borehole array.
4. Of the 281 identified DZ intercepts in the ESHI results, there are 38 which can be matched to structures described in the SDM-Site Laxemar DZ model (Chapter 5). The result is that of the 281 identified DZ intercepts, 243 of them represent minor deformation zones (MDZ).
5. Of the 243 potential MDZ identified in the ESHI and DZ model analysis, there are 32 potential MDZ for which sufficient information to assign a structure orientation (strike, dip) is not available. Without orientation data, the MDZ cannot be subdivided into fracture sets, and cannot be used in the geological DFN model parameterisation.
6. The final result is that there are 211 MDZ identified in Laxemar cored boreholes that are useable for geological DFN modelling.
7. If one chooses not to lump together the zones described in Step 2, the number of potential MDZ (Step 4) is increased to 247. However, the additional zones do not have sufficient information to determine structural orientation, so the total number of identified MDZ (Step 6) is unchanged.

More detailed discussions on the intensity of MDZ at Laxemar in the context of geological DFN modelling are presented in Section 6.4.4 of this report and Chapter 5 of the geological DFN summary report /La Pointe et al. 2008/.

3.12.3 Orientation of MDZs

Four groups of MDZ orientation sets were identified from the borehole review work; a sub-horizontal set (SH) and three near vertical sets striking approximately WSW, ESE and N-S respectively. The sub-horizontal set represents c 70% of the total amount of MDZs.

The minor deformation zone orientation sets seen in Figure 3-96 mirror the orientation sets of the local major and regional deformation zones described in Chapter 5: a N-S (NNE-SSW) set exemplified by ZSMNS059A and the ZSMNS001 series; an E-W set exemplified by ZSMEW002A and ZSMNW042A; a NE-SW set exemplified by ZSMNE005A, ZSMNE107A and ZSMNE011A; and lastly, a gently dipping set coupled to ZSMEW946A and ZSMNW928A.

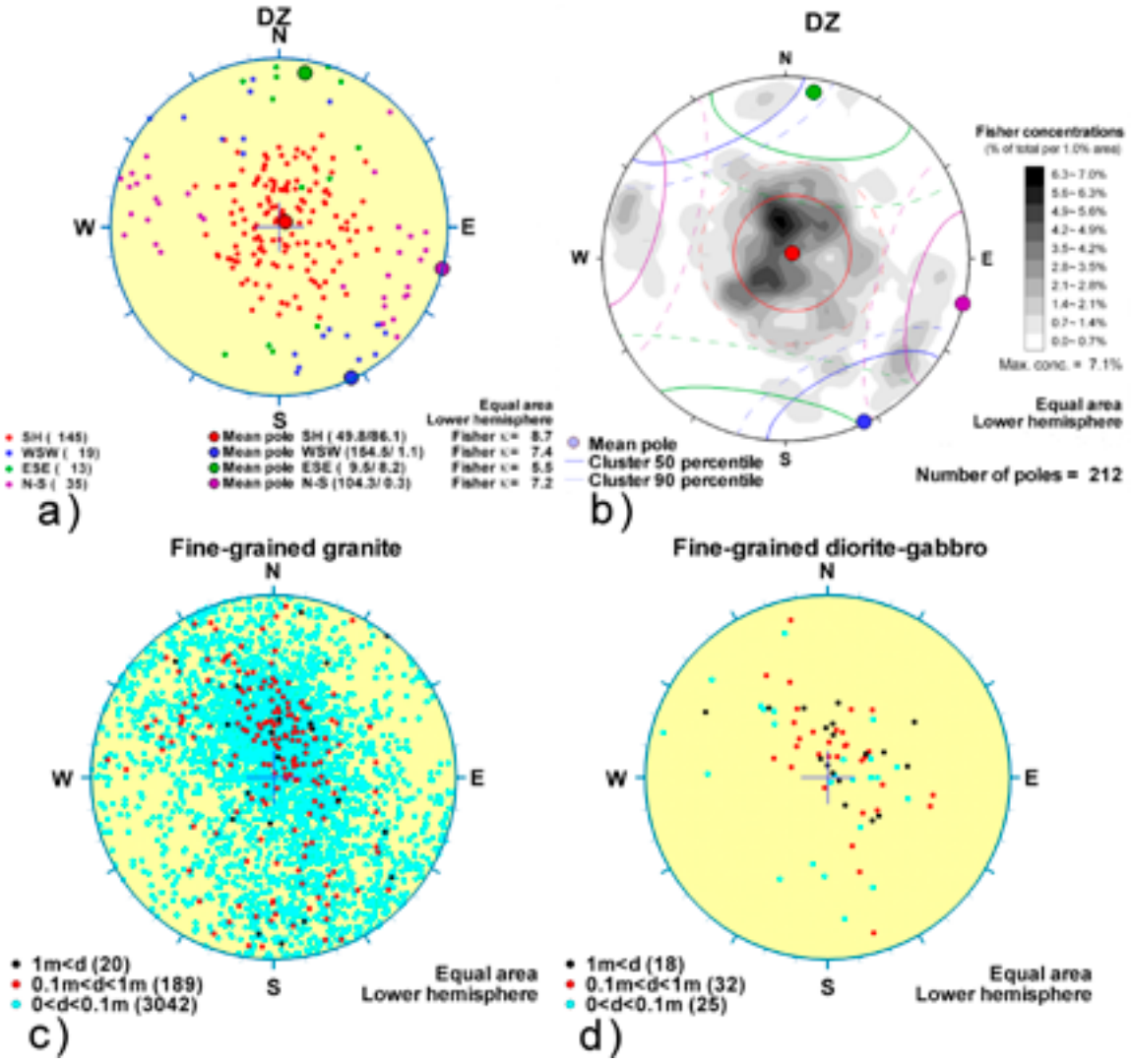

Figure 3-96. *a) and b). Orientation analysis of minor deformation zones encountered in boreholes; c) and d). Orientation of fine-grained granite (c) and fine-grained diorite-gabbro (d) in the quartz monzodiorite in southern Laxemar. Based on data from all cored borehole sections that have intersected the quartz monzodiorite. Note that KLX27A and the DFN-holes KLX11B-F are excluded*

As described in Chapters 5 and 6, this general geometrical arrangement of dominating sets appears scale consistent and is seen again in fracture sets identified in the individual fracture domains.

A high proportion (65%) of MDZs is associated with intrusions and more specifically c 45% occurs associated with fine-grained granite. The orientation of these intrusions in southern Laxemar as shown in Figure 3-96 c and d shows a similar pattern to the MDZ orientation groups seen in Figure 3-96 a and b.

If the orientations of all lineaments < 1,000 m long, identified inside the local model domain, are examined a slightly different grouping is suggested (Figure 3-97).

The lineament data have a slightly different orientation distribution compared to the MDZ borehole data. WNW is the strongest, while N-S has the weakest cluster significance. The relatve shift and dominance of the WNW group may be related to ice movement during earlier glaciations, an influence that is not present in the borehole data. A particular difficulty in using lineament data is the lack of information concerning the dip of any possibly associated deformation zone.

The spatial distributions of the MDZs identified in the Laxemar boreholes were studied and it is clear that the upper 150 m of the bedrock displays a higher density of MDZs. This concentration

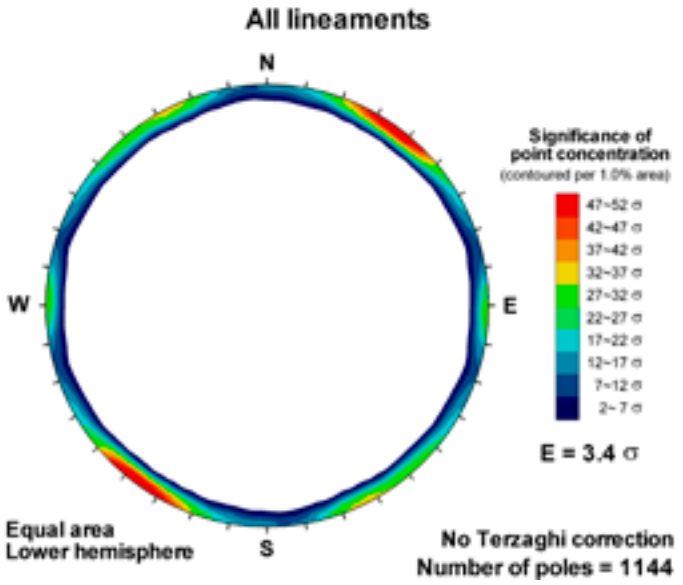

Figure 3-97. *All lineaments < 1,000 m long inside the local model domain. Note that the lineaments have no associated dip and are assumed vertical for the purposes of the plot.*

cannot be attributed the bias that is to be expected due to the dominance of shallow borehole data but may be related to the individual borehole orientations since they were generally selected to intercept particular major deformation zones and not specifically to provide an unbiased sample for MDZ analysis.

No particular pattern as regards deformation type, character or orientation could be identified that showed any depth dependency. In a similar way no pattern of changing properties could be seen in the horizontal distribution of MDZs.

50% of the MDZs in the boreholes were interpreted as brittle, 16% as ductile and 34% as brittle-ductile in character. The MDZs identified in the boreholes have a median true thickness of 1 m and the variation in true thickness is shown in Figure 3-98. Furthermore, 51% have a true thickness less than 1 m.

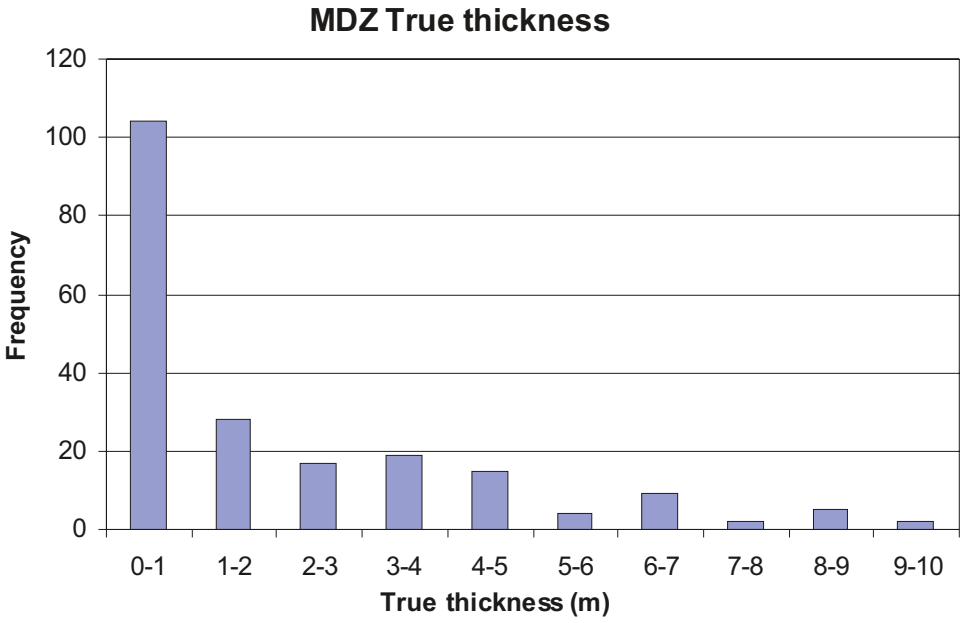

Figure 3-98. *True thickness of MDZs in cored boreholes based on ESHI. Note that MDZs in KLX27A are not included (cf. /Hermanson et al. 2008/).*

3.12.4 Fracture intensity inside MDZ

Changes in the patterns of fracture intensity, either in terms of the relative intensity of sets, the ratio of open to sealed fractures, or increases in the total fracture intensity, are key tools in the identification of deformation zones in cored boreholes. Table 3-12 presents the intensities of fractures mapped as being inside the limits of minor deformation zones in cored boreholes at Laxemar. Table 3-13 compares the mean P_{10} values for deformation zones, minor deformation zones, and fracture domains. The results in Table 3-13 suggest that the average P_{10} of both open and sealed fractures is higher inside MDZ than in the rock inside fracture domains (which represent the rock between the deterministic deformation zones).

3.12.5 Comparison with Äspö data

Data from the Äspö HRL have been re-evaluated by /Stanfors 2006/ with the aim of studying the MDZs with respect to their appearance at surface, in boreholes and in excavated openings within the Äspö HRL. Based on data from different studies the distance between MDZs mapped on surface was estimated to be in the order of 40–100 m. In the deep boreholes the equivalent distance is in the range 75–200 m but with a great variation between boreholes. These values are very similar to those obtained from Laxemar borehole data. In the tunnel the distance is approximately 75–100 m between highly conductive MDZs (often pre-grouted) and 25–35 m between less conductive structures. However, there is great variation between different sections of the tunnel.

Table 3-12. Frequency of fractures inside identified minor deformation zones (MDZ) in cored boreholes at Laxemar. Numbers are based on Sicada table p_fract_core_eshi.

Cored Borehole IDCODE	Borehole Length in MDZ (m)	Total Number of Fractures	Number of Open Fractures	Number of Partly Open Fractures	Number of Sealed Fractures	Portion of Open Fractures (%)	Average P_{10} inside MDZ	
							Open	Total
KLX02	7.73	11	0	0	11	0.00	0.00	1.42
KLX03	9.50	45	0	0	45	0.00	0.00	4.74
KLX04	21.12	36	0	2	34	5.56	0.09	1.70
KLX05	6.44	45	0	0	45	0.00	0.00	6.99
KLX06	3.77	23	0	0	23	0.00	0.00	6.10
KLX07A	14.48	256	0	2	254	0.78	0.14	17.68
KLX07B	6.37	19	0	0	19	0.00	0.00	2.98
KLX08	22.58	74	0	4	70	5.41	0.18	3.28
KLX09	77.85	139	0	1	138	0.72	0.01	1.79
KLX09B	5.26	51	0	1	50	1.96	0.19	9.70
KLX09C	7.15	27	0	0	27	0.00	0.00	3.78
KLX09D	10.97	78	0	2	76	2.56	0.18	7.11
KLX09E	1.15	6	0	1	5	16.67	0.87	5.22
KLX09F	9.65	40	19	0	21	47.50	1.97	4.15
KLX09G	No recorded MDZ							
KLX10	4.90	72	60	0	12	83.33	12.24	14.69
KLX10B	7.40	114	84	4	26	77.19	11.89	15.41
KLX10C	14.10	233	86	0	147	36.91	6.10	16.52
KLX11A	63.83	840	444	2	394	53.10	6.99	13.16
KLX11B	4.09	55	33	0	22	60.00	8.07	13.45
KLX11C	No recorded MDZ							
KLX11D	14.62	154	55	0	99	35.71	3.76	10.53
KLX11E	29.65	171	63	0	108	36.84	2.12	5.77
KLX11F	2.40	23	14	0	9	60.87	5.83	9.58
KLX12A	9.18	114	69	0	45	60.53	7.52	12.42
KLX13A	10.80	150	110	0	40	73.33	10.19	13.89
KLX14A	4.80	48	24	0	24	50.00	5.00	10.00
KLX15A	53.89	524	252	0	272	48.09	4.68	9.72
KLX16A	8.04	117	73	0	44	62.39	9.08	14.55
KLX17A	27.10	348	233	1	114	67.24	8.63	12.84
KLX18A	31.15	103	53	0	50	51.46	1.70	3.31
KLX19A	78.81	625	553	1	71	88.64	7.03	7.93
KLX20A	11.65	61	43	0	18	70.49	3.69	5.24
KLX21B	28.78	321	117	0	204	36.45	4.07	11.15
KLX22A	0.32	8	8	0	0	100.00	25.00	25.00
KLX22B	3.00	21	18	0	3	85.71	6.00	7.00
KLX23A	2.04	31	21	0	10	67.74	10.29	15.20
KLX23B	1.50	22	14	0	8	63.64	9.33	14.67
KLX24A	7.40	88	54	0	34	61.36	7.30	11.89
KLX25A	3.56	30	9	0	21	30.00	2.53	8.43
KLX26A	17.00	169	126	0	43	74.56	7.41	9.94
KLX26B	No recorded MDZ							
KLX28A	20.80	171	73	0	98	42.69	3.51	8.22
KLX29A	17.51	83	46	0	37	55.42	2.63	4.74

Table 3-13. Comparison of average P_{10} inside minor deformation zones and fracture domains.

Cored Borehole IDCODE	Average P_{10} inside MDZ		Average P_{10} inside fracture domains		Percent Difference	
	Open	Total	Open	Total	Open	Total
KLX02	0.00	1.42	1.45	2.47	–2.00	–0.54
KLX03	0.00	4.74	0.53	4.44	–2.00	0.06
KLX04	0.09	1.70	1.51	5.52	–1.76	–1.06
KLX05	0.00	6.99	0.34	3.96	–2.00	0.55
KLX06	0.00	6.10	0.84	5.29	–2.00	0.14
KLX07A	0.14	17.68	1.94	8.27	–1.73	0.73
KLX07B	0.00	2.98	2.23	6.41	–2.00	–0.73
KLX08	0.18	3.28	1.67	4.87	–1.62	–0.39
KLX09	0.01	1.79	1.45	5.26	–1.96	–0.99
KLX09B	0.19	9.70	1.93	5.76	–1.64	0.51
KLX09C	0.00	3.78	2.19	6.39	–2.00	–0.51
KLX09D	0.18	7.11	2.48	6.71	–1.73	0.06
KLX09E	0.87	5.22	2.26	7.52	–0.89	–0.36
KLX09F	1.97	4.15	1.57	5.89	0.23	–0.35
KLX09G			1.82	8.14	N/A	N/A
KLX10	12.24	14.69	1.8	5.56	1.49	0.90
KLX10B	11.89	15.41	3.97	9.33	1.00	0.49
KLX10C	6.10	16.52	2.21	8.55	0.94	0.64
KLX11A	6.99	13.16	0.78	5.39	1.60	0.84
KLX11B	8.07	13.45	1.39	4.26	1.41	1.04
KLX11C			1.15	3.94	N/A	N/A
KLX11D	3.76	10.53	1.5	5.28	0.86	0.66
KLX11E	2.12	5.77	1.6	5.59	0.28	0.03
KLX11F	5.83	9.58	0.95	3.48	1.44	0.93
KLX12A	7.52	12.42	2.26	5.9	1.08	0.71
KLX13A	10.19	13.89	2.61	6.82	1.18	0.68
KLX14A	5.00	10.00	3.4	7.92	0.38	0.23
KLX15A	4.68	9.72	1.64	5.46	0.96	0.56
KLX16A	9.08	14.55	2.13	7.9	1.24	0.59
KLX17A	8.63	12.84	1.21	6.44	1.51	0.66
KLX18A	1.70	3.31	1.77	5.54	–0.04	–0.50
KLX19A	7.03	7.93	0.79	3.02	1.60	0.90
KLX20A	3.69	5.24	1.42	5.36	0.89	–0.02
KLX21B	4.07	11.15	1.37	6.3	0.99	0.56
KLX22A	25.00	25.00	2.69	7.15	1.61	1.11
KLX22B	6.00	7.00	2.51	6.97	0.82	0.00
KLX23A	10.29	15.20	0.55	1.9	1.80	1.56
KLX23B	9.33	14.67	0.84	2.08	1.67	1.50
KLX24A	7.30	11.89	3.43	8.95	0.72	0.28
KLX25A	2.53	8.43	2.05	7.44	0.21	0.12
KLX26A	7.41	9.94	3.89	8.2	0.62	0.19
KLX26B			5.19	7.51	N/A	N/A
KLX28A	3.51	8.22	2.52	6.97	0.33	0.16
KLX29A	2.63	4.74	3.14	7.7	–0.18	–0.48

4 Rock domain model

4.1 Methodology, modelling assumptions and feedback from other disciplines

4.1.1 Methodology and modelling assumptions

The rock domains are defined on the basis of a combination of composition, grain size, texture, homogeneity and ductile structural overprinting. This follows the procedure adopted in previous model versions and is in accordance with the guidelines given in /Munier et al. 2003/. No geometric modelling of rock domains has been carried out between completion of the Laxemar 1.2 model version /SKB 2006b, Wahlgren et al. 2006a/ and the current modelling stage. The present modelling stage only comprises the Laxemar local scale model volume. Except for some very minor modifications in the immediate surroundings of the local model volume, the rock domain geometries in the surrounding regional model volume are the same as those presented inmodel version Laxemar 1.2. However, since the local and regional models are fully integrated, the regional model includes also the updated and modified rock domains included in the local model volume.

The following assumptions have been adopted in the modelling procedure:

- If no conflicting information exists, the major rock domains are presumed to extend at depth to the base of regional model volume (–2,100 m).
- One rock domain with a large extent at the surface (RSMM01) is interpreted, based on sub-surface data, to get thinner at depth and not to reach the base of the local model volume along its entire length.
- In the absence of sufficient sub-surface data, rock domains with a limited extent at the surface are not presumed to extend to the base of the local model volume (–1,100 m).

The adjustments and updating of the rock domain model in the current SDM-Site Laxemar modelling stage are primarily based on the following two new data sets:

- Updated bedrock geological map of the Laxemar-Simpevarp area.
- ESHI of all cored boreholes in Laxemar, i.e. including even boreholes that were available for model version Laxemar 1.2 and that have been reassessed.

The updated bedrock geological map primarily comprises the definition of an area that is dominated by Ävrö quartz monzodiorite, i.e. a quartz poor variety of the Ävrö granite. (cf. Section 3.2). The area that is dominated by Ävrö quartz monzodiorite is also characterised by a higher amount of diorite/gabbro occurrences than the surrounding major rock units. Thus, this has important implications for the definition of rock domains at the surface.

As described in Section 3.3.4, the ESHI includes the subdivision of the Ävrö granite into its two subvarieties Ävrö quartz monzodiorite and Ävrö granodiorite, i.e. a similar division as is presented on the bedrock map. Accordingly, the ESHI provides new important fixed points in the boreholes which, thus, help to better constrain the geometry of rock domain boundaries in the local model volume.

Properties

In the SDM-Site Laxemar model stage, the updated property assignment is restricted to rock domains in the local model volume. The properties of the rock domains outside the local model volume are identical to those presented in the Laxemar 1.2 model version /SKB 2006b, Wahlgren et al. 2006a/. All relevant surface and borehole data as defined in Table 4-1 have

Table 4-1. Properties assigned to each rock domain.

Rock domain ID (RSM***, according to the nomenclature recommended by SKB)
Property
Dominant rock type
Mineralogical composition
Grain size
Age (million years)
Structure
Texture
Density
Porosity
Magnetic susceptibility (SI units)
Electric resistivity in fresh water (ohm m)
Uranium content based on gamma ray spectrometric data (ppm)
Natural exposure rate (µR/h)
Subordinate rock types
Degree of inhomogeneity
Metamorphism/alteration (%)
Mineral fabric (type/orientation)

been evaluated and compiled for all rock domains in the local model volume. Since the definition of rock domains in Laxemar is primarily based on a dominant rock type, the properties compiled in the property table refer to the dominant rock types. However, the occurrence of subordinate rock types, degree of homogeneity, metamorphism/alteration and mineral fabric are also noted.

Confidence of existence and uncertainty in geometry

As in the Laxemar 1.2 model version /SKB 2006b, Wahlgren et al. 2006a/, judgement has been provided regarding the confidence level in the existence of the rock domains and the uncertainty relating to their geometry both at surface and at depth. The confidence in existence at the surface and at depth is coupled to the confidence in the documentation and classification of rock types during the bedrock mapping at the surface and the mapping of the drill cores. However, the uncertainty in geometry of the rock domains at the surface and at depth is also coupled to the amount of surface data available for the compilation of the bedrock geological map, and the number of available fixed points (depth intersections) for a particular rock domain boundary in the boreholes, respectively.

The confidence of existence and uncertainty in geometry of the modelled rock domains in the local model volume are presented in Appendix 11.

4.1.2 Feedback from other disciplines including the SR-CAN project

Feedback and input from the thermal and rock mechanical teams have highlighted the wide compositional range for the Ävrö granite, since this is reflected in its thermal and rock mechanical properties as well. The definition of the area dominated by Ävrö quartz monzodiorite on the surface and the corresponding working procedure in the boreholes, was initiated on a pure

geological basis, but the input and feedback from the thermal and rock mechanical modelling teams further strengthened the need for this work and the subsequent refinement of the rock domain model. Furthermore, integration work with the thermal modelling team pointed to the need for better understanding of the thicknesses and orientations of the subordinate rock types, in particular fine-grained granite and fine-grained diorite-gabbro, in the principal rock domains. This analysis is completed (Section 3.4.3) and has been utilised in the stochastic simulation of subordinate rock types which is carried out by the thermal modelling team. The results of this simulation for the different rock domains will be reported in the background report of the thermal modelling and will be incorporated in the SDM-Site Laxemar main report.

No feedback was given for the rock domain modelling from the SR-Can project /SKB 2006e/.

4.2 Conceptual understanding of rock domains at the site

As mentioned above, Laxemar is dominated by well preserved rocks although a faint to weak, non-uniformly distributed foliation is developed in the bedrock. The most prominent structural features are the sinistral, north-east trending, sub-vertically dipping, low-grade, ductile shear zones. As can be seen in Figure 4-1, Laxemar is bounded both to the west and east by the most prominent ductile shear zones in the area. Furthermore, the Simpevarp subarea to the east is much more affected by north-east trending, ductile shear zones, which is clearly indicated by the much more banded magnetic anomaly pattern compared with Laxemar (see the insert to Figure 4-1 and /Wahlgren et al. 2006a/). Even though Laxemar is not devoid of ductile shear zones and does not have a lens-like shape, it can conceptually be treated as a “tectonic lens”, i.e. as a low temperature analogue to the tectonic lens interpreted in Forsmark /Stephens et al. 2007/.

As mentioned above, a non-uniformly distributed faint to weak foliation occurs in the bedrock in Laxemar. The orientation of the foliation has been evaluated in Section 3.5, and the large-scale variation in orientation from northern to southern Laxemar is illustrated in Figure 4-2. As can be seen, the non-pervasive foliation in Laxemar constitutes an antiformal configuration,

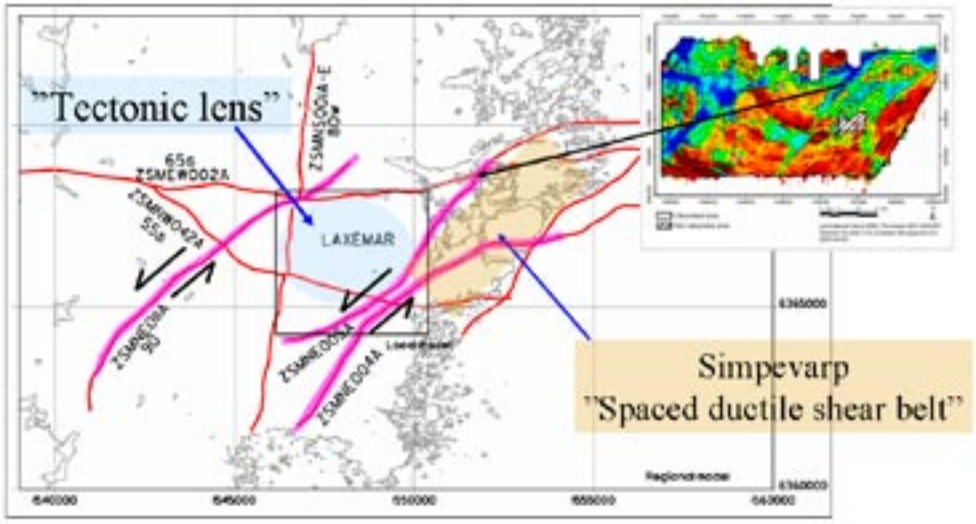

Figure 4-1. *Tectonic overview of the Laxemar-Simpevarp area showing the location of Laxemar in between the prominent north-east oriented ductile shear zones (lilac colour).*

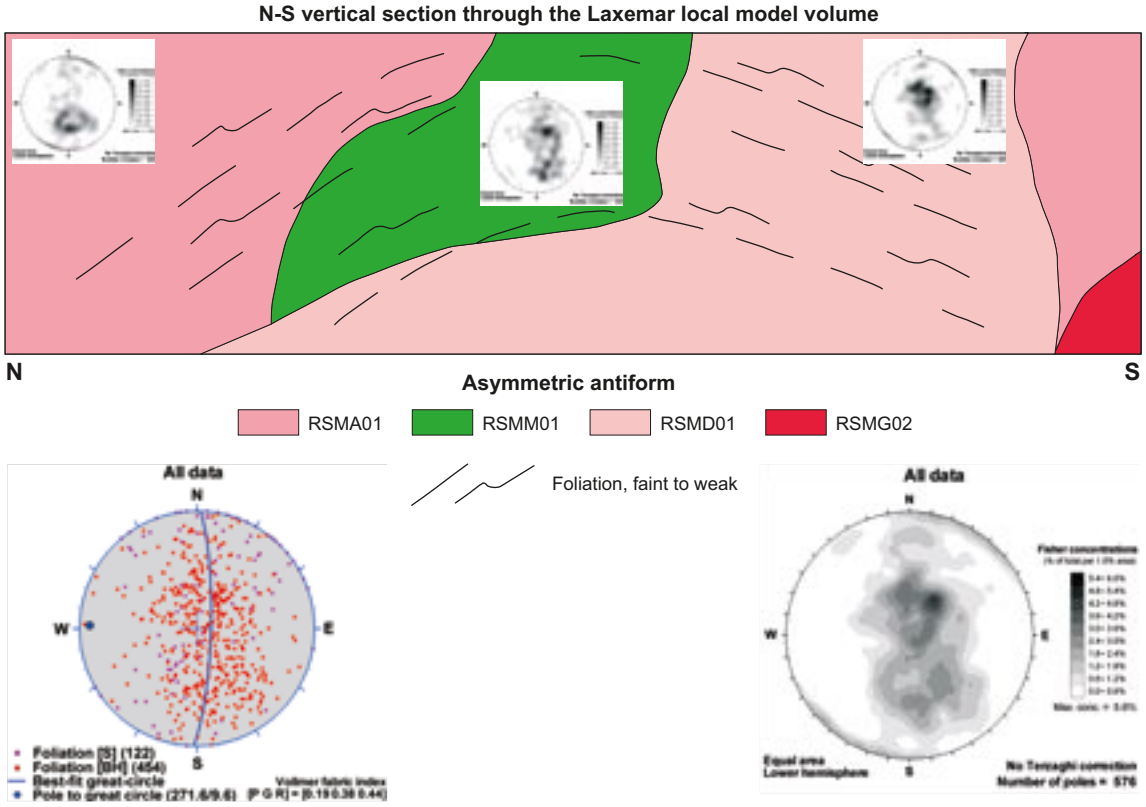

Figure 4-2. *Vertical section that illustrates the change in orientation of the faint to weak, non-pervasive foliation in the bedrock from northern to southern Laxemar. In the stereoplots in the lower left and right corners, all foliation data are plotted (cf. Figure 3-22).*

with slightly steeper dips in the northern part compared with the southern part. The pole to the best-fit great circle to the girdle-like configuration of all foliation data (Figure 4-2) from Laxemar indicates that the fold axis to the antiformal structure is east-west oriented and near horizontal (cf. AMS data Section 3.5.4). Note that the latter is in accordance with the N-S shortening as deduced from the kinematics in the ductile shear zones (cf. Section 3.5.1).As pointed out in Section 3.5.3, the subordinate rock types fine-grained granite and fine-grained diorite-gabbro display a similar orientation as the foliation in southern Laxemar, while the similarity in orientation is less clear in central and especially in northern Laxemar. The anisotropy that the foliation gives rise to is judged to be weak, which is supported by the evaluation of the AMS data (cf. Section 3.5.4). Furthermore, the foliation is discordant to the boundaries between the dominant rock types. This discordance and generally weak structural anisotropy at Laxemar is in strong contrast with the bedrock at Forsmark /Stephens et al. 2007/, where the penetrative, yet variable, ductile deformation has developed a strong anisotropy, which has guided the geometric modelling of rock domains at that site. At Laxemar, a similar structural concept for the geometrical modelling of rock domains cannot be applied due to the weak anisotropy in the generally well preserved rocks.

From the reasoning above, it is concluded with one exception, that no specified concept, e.g. structural guidance, can be applied for the sub-surface geometric modelling of the rock domains as defined at the surface at Laxemar. The exception comprises two domains which are defined on the basis of a high frequency of ductile shear zones. For these domains, the orientation of the strong foliation and the ductile shear zones that has been documented during the bedrock mapping at the surface has conceptually been applied in defining the downward geometrical projection. However, for the remaining rock domains, the geometrical shape of the rock domains at depth is determined by the defined rock domain boundaries as interpreted in the cored boreholes, supported by geophysical modelling based on gravimetric and magnetic data /Triumf 2004c/.

4.3 Division into rock domains

The division into rock domains comprised two working stages, namely:

- Definition of rock domains at the surface.
- Definition of rock domains in the cored boreholes.

The rock domains have been given different codes where domains denominated with the same capital letter are dominated by the same characteristics as displayed below.

- RSMA-domain: dominated by Ävrö granite.
- RSMB-domain: dominated by fine-grained dioritoid.
- RSMBA-domain: characterised by a mixture of Ävrö granite and fine-grained dioritoid.
- RSMC-domain: characterised by a mixture of Ävrö granite and quartz monzodiorite.
- RSMD-domain: dominated by quartz monzodiorite.
- RSME-domain: dominated by diorite/gabbro.
- RSMG-domain: dominated by the Götemar type granite.
- RSMM-domain: characterised by a high frequency of minor bodies to small enclaves of diorite/gabbro in particularly Ävrö quartz monzodiorite.
- RSMP-domain: characterised by a high frequency of low-grade ductile shear zones in the above mentioned rock types.

Rock domains of the same character that are physically separated are given different numbers, e.g. RSMP01 and RSMP02.

4.3.1 Rock domains at the surface

A primary step in the modelling procedure is the recognition and definition of rock domains at the surface by use of the bedrock geological map. This map includes rock units that are defined on the basis of:

- Composition, grain size and texture of the dominant rock type.
- Degree of bedrock homogeneity.
- Strong ductile structural overprinting (high frequency of ductile shear zones).

The rock units at the surface involve seven principal bedrock components which together with their characteristics are summarised in Table 4-2. Note that the Ävrö granite (501044) comprises both granitic and granodioritic, as well as quartz monzodioritic compositions (cf. Section 3.2). Furthermore, the Götemar type granite does not occur at the surface within the Laxemar local model area. The simplification and integration procedures relating to the surface data have yielded a rock domain map at the surface in the local model area (Figure 4-3). On this basis, 12 rock domains have been identified.

Table 4-2. Bedrock components used in the rock domain modelling procedure in the Laxemar local model area and their principal characteristics and encoding. The translation of rock codes to rock names is provided in Appendix 2. Note that the Ävrö granite (501044) comprises both granitic and granodioritic as well as quartz monzodioritic compositions.

Rock units − composition, grain size and texture of dominant rock type			
Code (SKB)	**Composition**	**Grain size**	**Texture**
501044	Granite to quartz monzodiorite	Medium-grained	Porphyritic
501046	Quartz monzonite to quartz monzodiorite	Medium-grained	Porphyritic
501036	Quartz monzodiorite	Medium-grained	Equigranular
501030	Dioritoid	Fine-grained	Unequigranular
501058	Granite	Medium-to coarse-grained	Equigranular to slightly porphyritic
511058	Granite	Fine- to medium-grained	Equigranular
501033	Diorite to gabbro	Medium-grained	Equigranular
521058	Granite (“Götemar type”)	Coarse-grained and fine- to medium-grained	Equigranular to slightly porphyritic
Independent	Independent	Protomylonitic to mylonitic foliation	

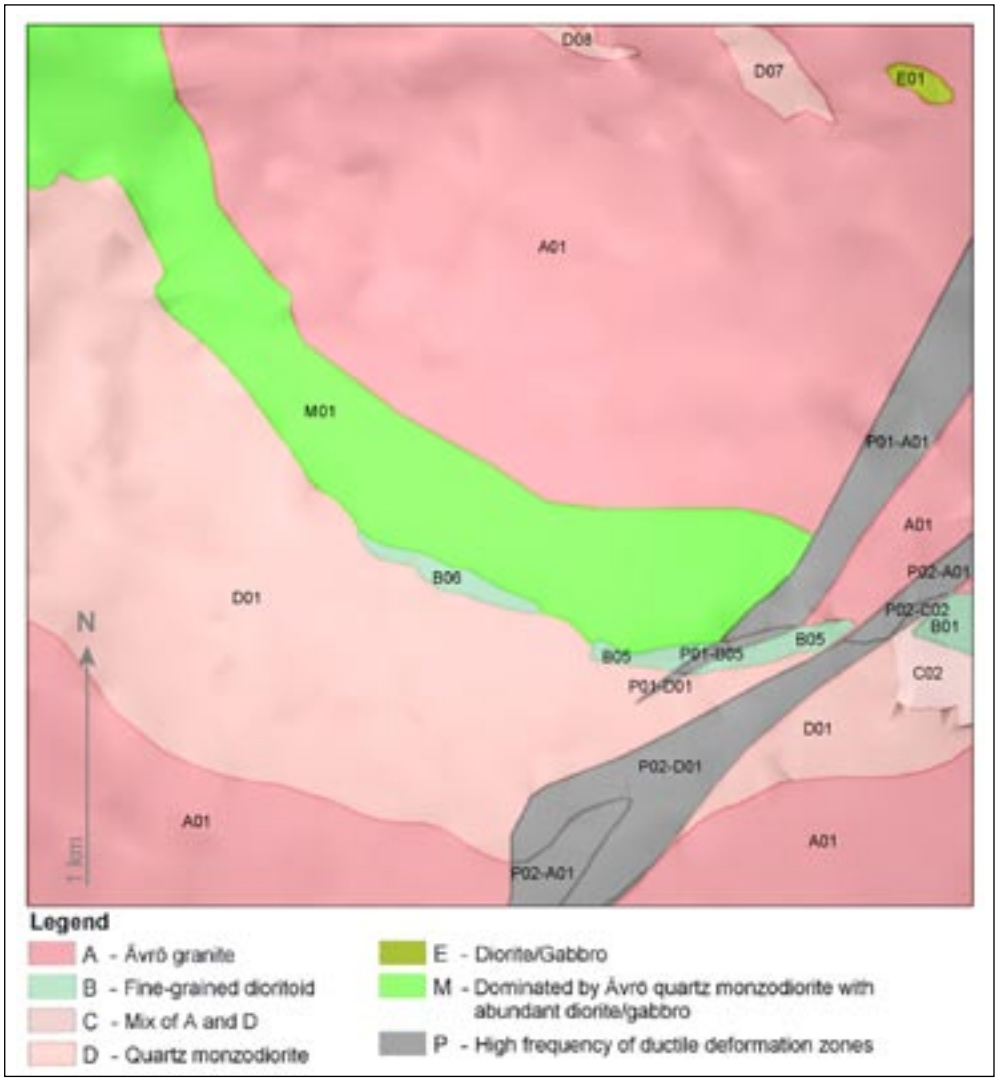

Figure 4-3. Two dimensional model at the surface for rock domains in the Laxemar local model area. For reasons of simplicity, the prefix RSM has been excluded in the denomination of the rock domains.

4.3.2 Definition of rock domains in cored boreholes

The rock units in the ESHI are mostly defined on the basis of rock composition, grain size and texture, as well as degree of mixing of different rock types, i.e. lithological inhomogeneity. Thus, the principles for defining rock units in the boreholes follow those at the surface in the bedrock geological map. The definition of rock domains in all cored boreholes in the Laxemar local model area is presented in Table 4-3. Rock domains in all cored boreholes that are utilised in the rock domain modelling are presented in Appendix 10. An example of one of these logs, which includes modelled deformation zones and defined fracture domains as well, is shown in Figure 4-4.

4.4 Local model

4.4.1 Geometric model

The rock domain model presented for SDM-Site Laxemar mainly comprises minor adjustments and refinements compared with the Laxemar 1.2 rock domain model. The most important causes for modification of the rock domain model are the definition on the bedrock geological map of the area that is dominated by Ävrö quartz monzodiorite, and the wealth of new data from the cored boreholes. Compared with the Laxemar 1.2 model, the most important modifications are listed below:

- The RSMM01 domain does not include the quartz monzodiorite, i.e. does not extend across the boundary between the quartz monzodiorite and Ävrö quartz monzodiorite (cf. bedrock geological map in Figure 3-4) which was the case in the Laxemar 1.2 model. This is based on the mapping results of cored boreholes in which the diorite/gabbro shows a strong spatial correlation with the Ävrö quartz monzodiorite and is almost absent in the quartz monzodiorite. In the present model, the extension of the RSMM01 domain at the surface is based on the area that is dominated by Ävrö quartz monzodiorite in the bedrock geological map, i.e. is not only based on a high frequency of diorite/gabbro as in the Laxemar 1.2 model version.
- The positions of the boundaries between RSMA01, RSMM01 and RSMD01 in the focussed part of the local model volume are modified and refined by use of the ESHI from all new boreholes.
- In the Laxemar 1.2 model, the minor lens-shaped domains RSMBA01 and RSMBA02 were defined on sparse and preliminary data from KLX05. These domains have been redefined as RSMB05 and RSMB06, i.e. dominated by fine-grained dioritoid, since the Boremap mapping does not confirm the anticipated mixture of fine-grained dioritoid and Ävrö granite in these domains.

The above mentioned modifications are minor in character. Thus, all new borehole data that are provided for the SDM-Site Laxemar rock domain modelling in principle verify the previously established Laxemar 1.2 model, although the latter was based on very limited sub-surface data.

Table 4-3. Definition of rock domains in cored boreholes in the Laxemar local model volume, based on rock unit boundaries in the ESHI.

Borehole	From bh-length – to bh-length (m)	Rock domain
KLX01	0.96–1,077.99	RSMA01
KLX02	200.0–540.00	RSMA01
KLX02	540.00–960.00	RSMBA03
KLX02	960.00–1,450.00	RSMA01
KLX02	1450.00–1,700.00	RSMD01
KLX03	101.48–619.87	RSMM01
KLX03	619.87–998.21	RSMD01
KLX04	101.48–991.15	RSMA01
KLX05	108.33–473.30	RSMM01
KLX05	473.30–995.22	RSMD01
KLX06	101.43–994.90	RSMA01
KLX07A	101.98–841.51	RSMA01
KLX07B	9.64–200.13	RSMA01
KLX08	100.87–587.41	RSMA01
KLX08	587.41–923.56	RSMM01
KLX08	923.56–991.87	RSMD01
KLX09	102.02–873.94	RSMA01
KLX09B	11.05–99.91	RSMA01
KLX09C	9.08–119.20	RSMA01
KLX09D	10.01–120.72	RSMA01
KLX09E	9.08–119.70	RSMA01
KLX09F	9.01–151.99	RSMA01
KLX09G	9.31–99.63	RSMA01
KLX10	101.86–857.08	RSMA01
KLX10	857.08–980.95	RSMM01
KLX10	980.95–996.49	RSMD01
KLX10B	8.00–50.24	RSMA01
KLX10C	9.00–145.34	RSMA01
KLX11A	100.87–990.15	RSMD01
KLX11B	4.00–99.50	RSMD01
KLX11C	4.00–119.43	RSMD01
KLX11D	4.00–119.20	RSMD01
KLX11E	4.02–121.00	RSMD01
KLX11F	4.00–118.83	RSMD01
KLX12A	102.01–527.90	RSMM01
KLX12A	527.90–601.05	RSMD01
KLX13A	102.01–593.32	RSMM01
KLX14A	4.00–174.33	RSMD01
KLX15A	77.59–979.60	RSMD01
KLX16A	0.93–433.55	RSMD01
KLX17A	65.85–696.69	RSMM01
KLX18A	100.81–119.25	RSMA01
KLX18A	119.25–610.91	RSMM01
KLX19A	100.42–795.97	RSMD01
KLX20A	100.93–457.01	RSMD01
KLX21B	100.83–768.11	RSMA01
KLX21B	768.11–858.41	RSMD01
KLX22A	4.00–100.37	RSMD01
KLX22B	4.00–100.07	RSMD01
KLX23A	4.00–99.96	RSMD01
KLX23B	4.00–50.25	RSMD01
KLX24A	4.00–99.81	RSMD01
KLX25A	4.00–50.10	RSMD01
KLX26A	4.00–99.93	RSMM01
KLX26B	4.00–50.30	RSMM01
KLX27A	76.13–648.69	RSMM01
KLX28A	5.24–80.00	RSMM01
KLX29A	4.00–59.18	RSMA01

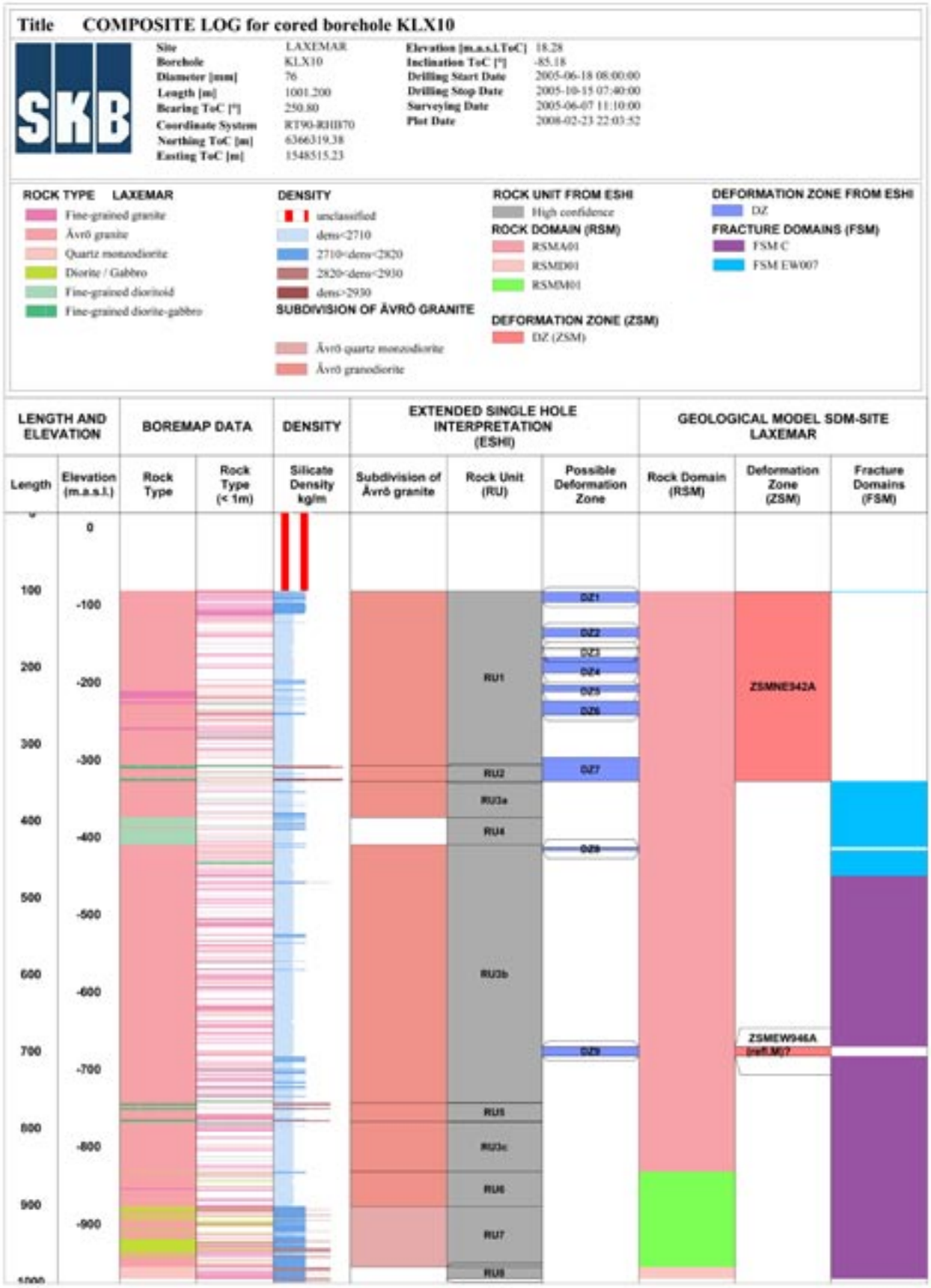

Figure 4-4. *Modelled rock domains, deformation zones and fracture domains in KLX10, and the relationship to mapped rock types, rock units and possible deformation zones in the ESHI.*

In total 13 rock domains are defined in the local model volume. As in the Laxemar 1.2 model version, RSMBA03 only occurs at depth in the lower part of the model volume. The geometry of the RSMD01 and the intersecting RSMP01 and RSMP02 domains, and a combination of RSMM01, RSMD01, RSMP01, RSMP02, RSMB05 and RSMB06 domains in the focussed volume is displayed in Figure 4-5 and Figure 4-6, respectively. As is evident from the figures, all the borehole intersections strongly indicate that the boundary surfaces between RSMD01, RSMM01 and RSMA01 (transparent in the figures) are fairly well constrained.

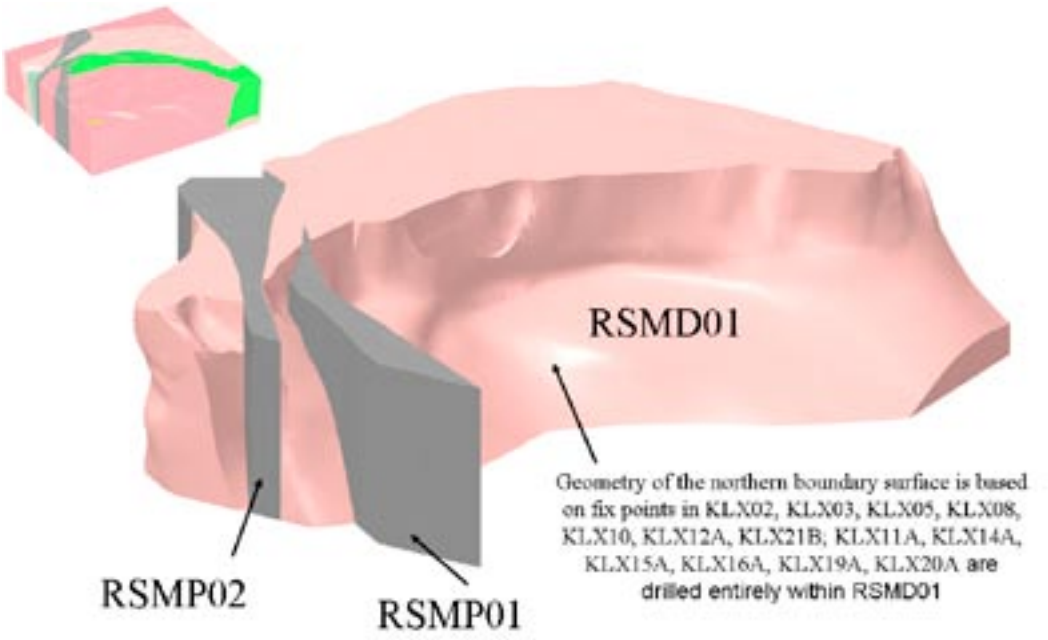

Figure 4-5. *View of the RSMD01 and intersecting RSMP01 and RSMP02 domains. View to the south-southwest.*

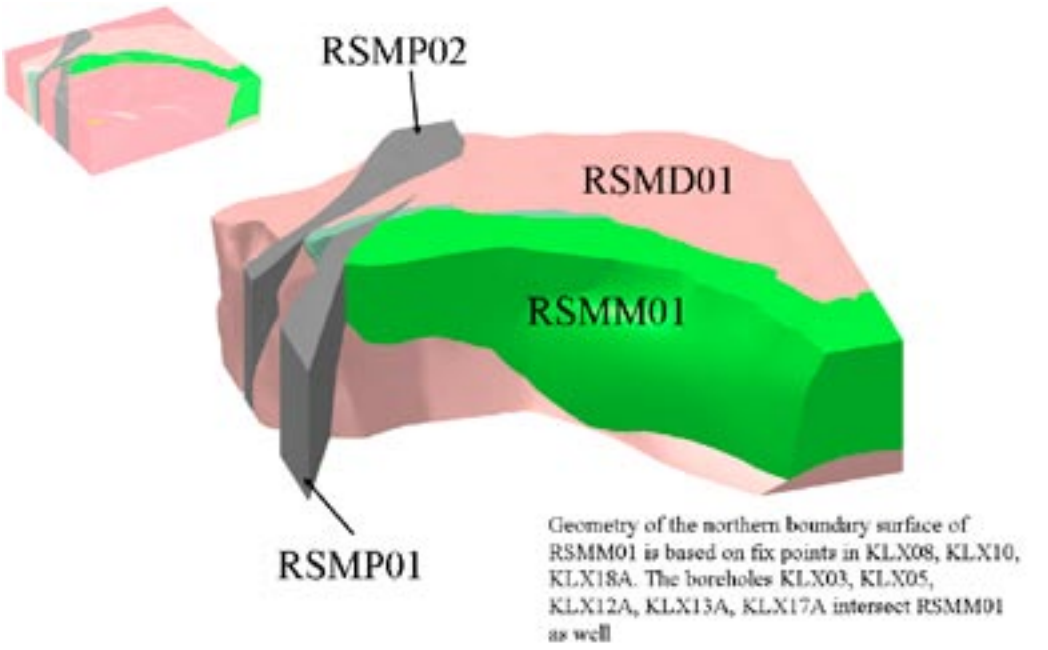

Figure 4-6. *View of the RSMM01 domain combined with RSMD01, RSMP01, RSMP02, RSMB05 and RSMB06. View to the south.*

4.4.2 Property assignment

The properties of the modelled rock domains are given in Appendix 11. A summary of the properties of the rock domains that are of importance in the southern and south-western part of the local model volume is provided below.

RSMD01

The RSMD01 domain is strongly dominated by equigranular, medium-grained quartz monzodiorite (Figure 4-7). It is compositionally relatively homogeneous with a calculated quartz content of 13.0±3.0%, and is structurally well-preserved, although a non-uniformly distributed faint to weak foliation occurs, with a dominant gentle dip to the south. The proportion of different rock types is shown in Figure 4-8. Fine-grained granite (511058), fine-grained diorite-gabbro (505102) and pegmatite (501061) are the most important subordinate rock types and occur in relatively similar amounts in all boreholes (Figure 3-13). Note that the percentage of dolerite (501027) is based only on the occurrences in KLX14A, KLX19A and KLX20A. Dolerite is not considered to be evenly distributed throughout the RSMD01 domain. As mentioned in Sections 3.5.3 and 4.2, the subordinate rock types, except the pegmatites, display similar gentle dips, dominantly to the south, as the foliation (Figure 3-25).

The estimated alteration of the RSMD01 domain (see Appendix 7), between the identified possible deformation zones from the ESHI, comprises equal proportions of faint to weak oxidation (red staining) and saussuritisation, i.e. c 10% of each. Furthermore, epidotization is observed and constitutes c 2%.

Figure 4-7. *Characteristic appearance of equigranular quartz monzodiorite.*

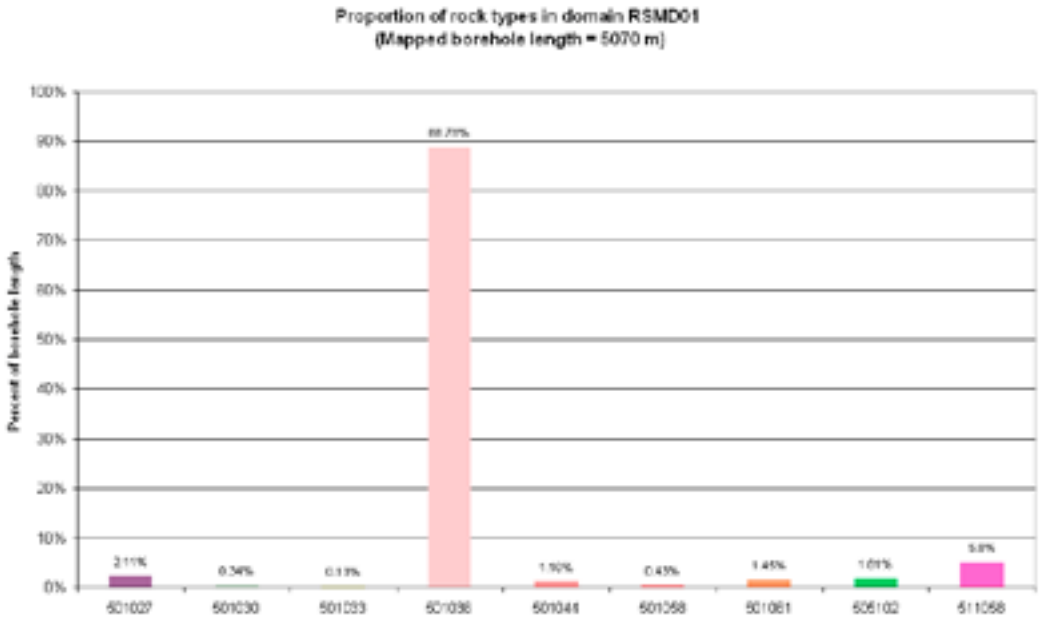

Figure 4-8. *Quantitative estimate in volume % of the proportions of different rock types in rock domain RSMD01. The translation of rock codes to rock names is provided in Appendix 2. The borehole length used in the calculation is indicated.*

RSMM01

As is shown in Figure 4-9, the RSMM01 domain is characterised by a much higher proportion of diorite/gabbro (mean value c 16%) than the other rock domains (Figure 4-10), though variably distributed both at the surface and in domain sections in boreholes (see Appendix 4). The commonly medium-grained and finely porphyritic Ävrö quartz monzodiorite which dominates and constitutes c 75% of the domain has by definition a low content of quartz. However, quartz richer varieties occur in the domain which explains the calculated quartz content of 13.9±6.4% (mean±stdv). The subordinate rock types are the same as in RSMD01 and constitute similar proportions (Figure 4-9). Furthermore medium- to coarse-grained granite (501058) occurs in minor amounts. In contrast to the RSMD01 domain, the orientation of the subordinate rock types and the faint to weak foliation do not display the same similarities in the RSMM01 domain, especially there is no corresponding orientation of the subordinate rock types to the north-dipping foliation (Sections 3.5.3 and 4.2 and Figure 3-26).

The alteration in the RSMM01 domain (see Appendix 7) between the identified deformation zones in the ESHI is dominated by oxidation (red staining). It is mostly of faint to weak character and affects c 14% of the domain, with subordinate saussuritisation (c 2%) and very sparse epidotization (< 1%). Alteration that occurs in very minor amounts comprises chloritisation and silicification.

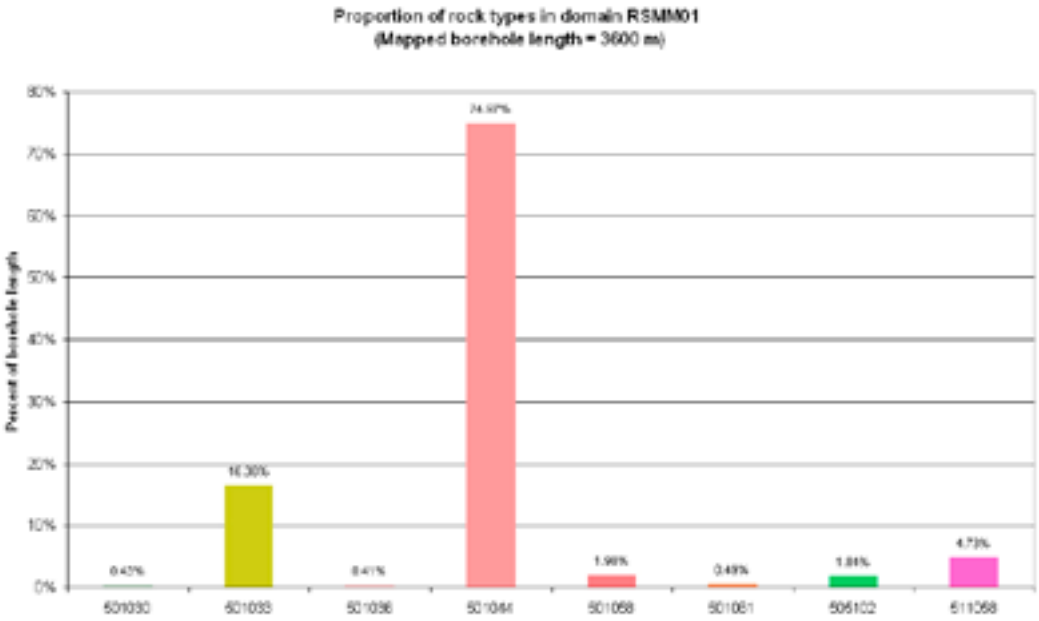

Figure 4-9. *Quantitative estimate in volume % of the proportions of different rock types in rock domain RSMM01. The translation of rock codes to rock names is provided in Appendix 2. The borehole length used in the calculation is indicated.*

Figure 4-10. *Characteristic appearance of Ävrö quartz monzodiorite (left). Inclusions of diorite/gabbro in Ävrö quartz monzodiorite which characterises the RSMM01 domain (right).*

RSMA01

The commonly medium-grained and finely porphyritic Ävrö granite is the dominant rock type in the RSMA01 domain (Figure 4-11). If all boreholes are considered, it constitutes c 82% of the volume (Figure 4-12). As can be seen in Figure 4-12, subordinate rock types which make up between c 2 and 6% of the domain volume comprise fine-grained granite (511058), fine-grained diorite-gabbro (505102), granite (501058), fine-grained dioritoid (501030) and quartz monzodiorite (501036). However, if the calculation is based only on KLX02, KLX04, KLX07A and B, KLX08, KLX10, KLX18A and KLX21B, since these boreholes are considered to be more representative for the bedrock in the central and southern part of the RSMA01 domain, the Ävrö granite constitutes c 88% (Figure 4-13). Accordingly, the subordinate rock types decrease in corresponding degree. The calculated quartz content for the Ävrö granite in RSMA01 is 21.7±6.4% (mean±stdv).The similarities between the orientation of the faint to weak foliation and orientation of the subordinate rock types are less obvious than in RSMD01 and RSMM01 domains, mainly due to a larger spread in orientation of the subordinate rock types (Sections 3.5.3 and 4.2 and Figure 3-27). This comment is in particular valid for the fine-grained granites and the pegmatites, whereas the fine-grained diorite-gabbro displays an orientation pattern that is more similar to the orientation of the foliation.

The alteration in the RSMA01 domain (see Appendix 7) between the identified deformation zones in the ESHI is dominated by oxidation (red staining). It is mostly of faint to weak character and affects c 25% of the domain. Alteration of subordinate character is saussuritisation (c 3%) and very sparse epidotization (< 1%). Alteration that occurs in very minor amounts comprises sericitisation, silification and chloritisation.

Figure 4-11. *Ävrö granite with a granodioritic composition. Note the intermediate to mafic enclave in the right part of the picture.*

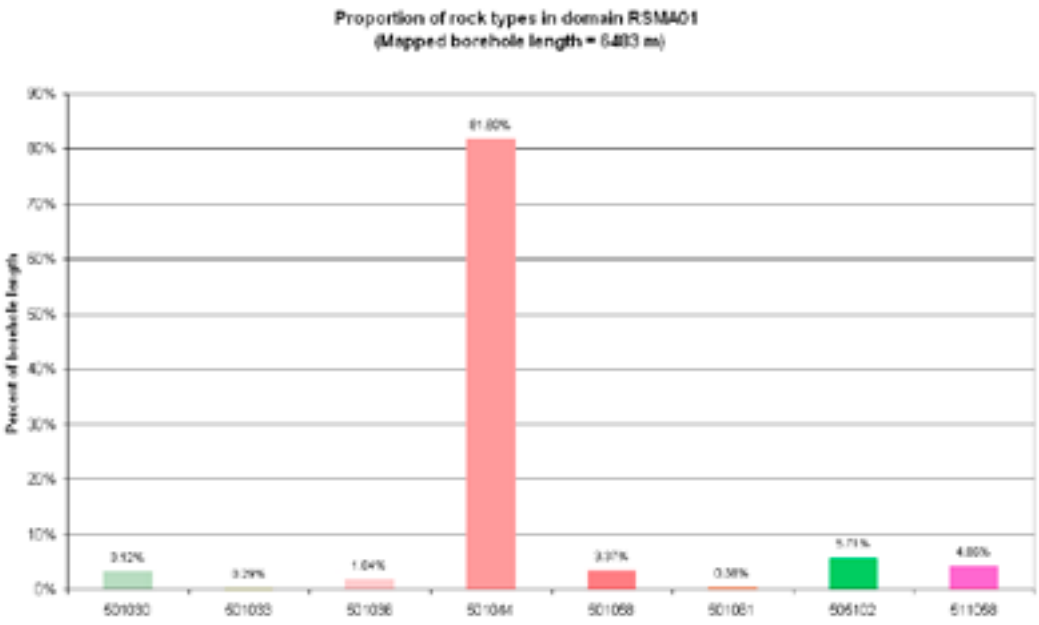

Figure 4-12. *Quantitative estimate in volume % of the proportions of different rock types in rock domain RSMA01. The translation of rock codes to rock names is provided in Appendix 2. The borehole length used in the calculation is indicated.*

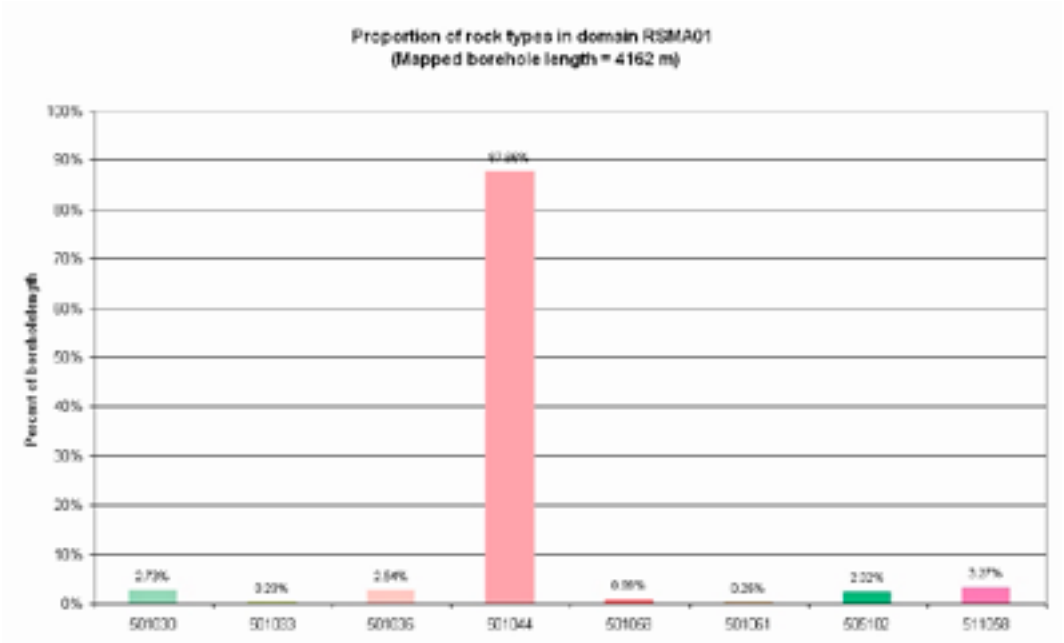

Figure 4-13. *Quantitative estimate in volume % of the proportions of different rock types in rock domain RSMA01, based only on KLX02, KLX04, KLX07A and B, KLX08, KLX10, KLX18A and KLX21B. The reason for this is that these boreholes are considered to be more representative of the bedrock in the central and southern part of the RSMA01 domain. The translation of rock codes to rock names is provided in Appendix 2. The borehole length used in the calculation is indicated.*

4.5 Implications for the established regional model

All investigations during the complete site investigations that have had implications for the rock domain model have been carried out in the local model area/volume. The results of the completed investigations have had no implications for the rock domain model in the remaining part of regional model area.

In the Laxemar 1.2 local model the RSMM01 domain was extended eastwards, but separated by the RSMP01 and RSMP02 domains. However, the eastward continuation of the RSMM01 was based on sparse data from the surface, and in order to simplify the modelling work in the present model, the RSMM01 domain is constrained not to extend east of but is delimited by the RSMP01 domain. Furthermore, the RSMP02 domain has been extended to the south-west, due to the southward shift of the southern boundary of the SDM-Site Laxemar local model area, and also extends into the regional model volume. These modifications are not based on new data, but on reinterpretation of data that existed at the data freeze for the Laxemar 1.2 modelling work. They are a consequence of the modification of the extent of the local model area applied in the SDM-Site Laxemar modelling stage. The modifications are of minor character and apart from these, the rock domain model outside the local model volume is the same as the one presented in the Laxemar 1.2 version of site descriptive modelling. The three- dimensional regional rock domain model for SDM-Site Laxemar is shown in Figure 4-14.

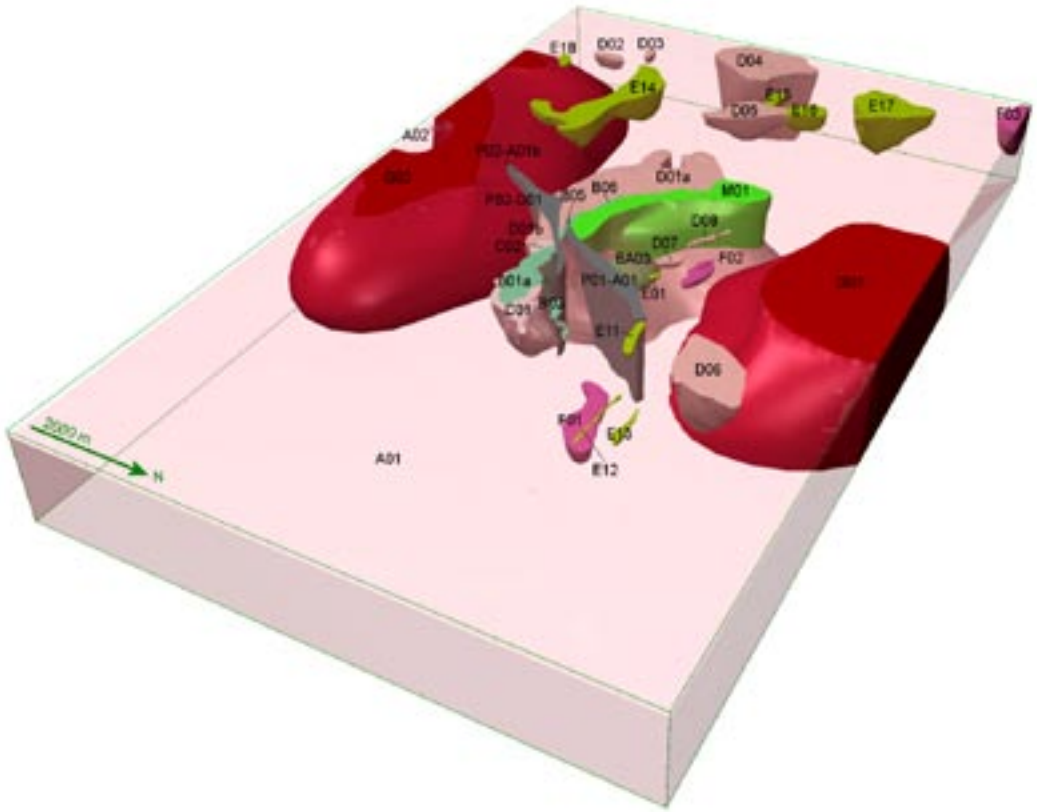

Figure 4-14. *Three dimensional model for rock domains in the regional model volume. For reasons of simplicity, the prefix RSM has been excluded in the denomination of the rock domains. View to the south-west.*

4.6 Evaluation of uncertainties

The rock domain model relies on the accuracy of the bedrock geological map and the positioning of the boreholes at depth. In turn, the accuracy of the bedrock geological map is very much dependent on the extent of available outcrops, the complexity of the bedrock and available geophysical data, especially the resolution in the magnetic data. The quality of the bedrock geological map in the local model area is judged to be high since the area is well exposed and, apart from local complexities, the dominant rock types have different characteristics. However, it should be noted that the boundary between the area dominated by Ävrö quartz monzodiorite (RSMM01) and the neighbouring Ävrö granite (RSMA01) is not as well constrained as the boundary between the Ävrö quartz monzodiorite and the equigranular quartz monzodiorite (RSMD01). The uncertainty in the former boundary depends on the similar porphyritic texture and grain size of the Ävrö quartz monzodiorite and the Ävrö granite, the main difference of which is the difference in mineralogical composition, e.g. the lower quartz content in the Ävrö quartz monzodiorite. Furthermore, the uncertainty in the boundary between the RSMM01 and RSMA01 domains also relates to the appearance of diorite/gabbro which also characterises the RSMM01 domain. Uncertainty in the geometrical boundary between RSMM01 and RSMA01 is judged to lie within ±100 m of the modelled boundary. In particular, the accuracy of the bedrock map is judged be high in the focal southern and south-western part of Laxemar. The uncertainties in the position of boreholes in three dimensions have been addressed in Section 3.1.3. However, the uncertainties in the position of boreholes at depth are judged to be minor compared to the uncertainties in the position of a boundary between two different rock types/rock units at the surface.

With the above reasoning kept in mind, an evaluation of uncertainties must consider the fact that the present rock domain modelling work primarily includes minor modifications and refinements of the rock domain model that was already established in the Laxemar 1.2 model version, despite the major increase in data from all new boreholes. For borehole KLX11A and all subsequent boreholes, a prediction was made prior to drilling that addressed lithological homogeneity, i.e. a prediction of the proportions of different rock types in the borehole. The prediction also included a verification of the Laxemar 1.2 rock domain model by making a prediction at what borehole length potential rock domain boundaries should be intersected. However, it must be noted that only the cored boreholes KLX01, KLX02, KLX03 and KLX04, and preliminary mapping of KLX05 and KLX06 were available in connection with the Laxemar 1.2 modelling stage. As is evident from Appendix 12, the prediction and outcome for the proportion of rock types in the cored boreholes that were drilled in the quartz monzodiorite in the RSMD01 domain are very similar. Bearing in mind the sparse sub-surface data that were available for the Laxemar 1.2 rock domain model, the greatest difference between prediction and outcome relates to the intersections of the rock domain boundaries between the RSMA01, RSMM01 and RSMD01. The new boreholes that intersect these boundaries have now been utilised in the modification and refinement of the model. However, it is encouraging to note that in KLX21B the difference between the predicted intercept between RSMA01 and RSMD01 and the outcome was only one metre.

For the reasons outlined above, the uncertainties in the geometrical relationships between the different rock domains in the local model volume are judged to be low, especially in the focal southern and south-western part. Furthermore, the proportion of different rock types and degree and type of alteration is also well understood, in particular for the RSMD01 domain. A question mark relates to the possible occurrence of additional dolerite dykes to the few documented in the boreholes. However, dolerite dykes are judged to constitute a very subordinate rock type at Laxemar since they have not been observed in any outcrops and only in a few boreholes.

The principal remaining uncertainties comprise the spatial distribution of subordinate rock types, not the least the distribution of diorite/gabbro and the proportion of Ävrö granodiorite in the RSMM01 domain, and the spatial distribution of alteration in the rock domains. However, these uncertainties are addressed by the thermal modelling team using a stochastic simulation process.

Based on the above discussion it is concluded that both the geometrical relationships between the rock domains and their property assignment are stable and well understood in the focal volume of southern and south-western Laxemar.

5 Model for deterministic deformation zones

5.1 Methodology, modelling assumptions and feedback from other disciplines

5.1.1 Methodology and modelling assumptions

The assumptions made in earlier modelling steps have been reassessed and where necessary revised in the light of new observations and insights. However, the set of fundamental assumptions underlying the deformation zone model remain unchanged from earlier modelling steps. It is assumed that:

- Deformation zones can be interpreted through indirect sources of data such as geophysical maps (magnetics, VLF, slingram, gravimetric), topography, seismic reflections and refractions.
- Lineaments, both topographic and geophysical, provide information about the location and extent at the surface of potential deformation zones.
- Deformation zones can further be interpreted through direct data in boreholes, tunnels and from surface field observations. The confidence in geological character and possible extent (length and thickness) of deformation zones inferred from indirect data sources is lower than for deformation zones identified from direct observations.
- Different sources of data can complement each other and increase the confidence in the interpreted deformation zone. Several types of observations, both indirect and direct, also increase the degree of detail in which the deformation zone can be described.
- Interpreted deformation zones can be interpolated between points of observation, if there are reasonable data to suggest the validity of such interpolation.
- Deformation zones are variable in their thickness and can be modelled honouring the inferred thickness (Figure 5-1) or can be modelled as surfaces without thickness if no relevant data exist.
- Within the limits of the regional or local model volumes, deformation zones interpreted at the ground surface can be extended downwards to a depth equal to the interpreted length of the mapped surface trace. This means, for example, that deformation zones longer than 1 km at the surface are extended to the bottom of the local model volume (–1,100 m above sea level).
- Each interpreted deformation zone has been ranked according to the confidence in its existence being high, medium or low. Deformation zones that have high confidence ratings have, in addition to lineament indications, also supportive information from other sources of indirect data such as geophysics and from sources of direct data, such as boreholes or tunnels.
- Deformation zones ranked with medium confidence show clear topographic, magnetic and/or surface geophysical anomalies which cannot be disregarded as being other linear structures in the landscape, such as Quaternary deposits, ditches, power lines, roads, forest fire lanes, or other man-made features.
- Interpreted deformation zones with assigned low confidence are only supported by indirect sources of information such as lineament indications of lesser strength, either from topography, magnetics or electromagnetic methods.

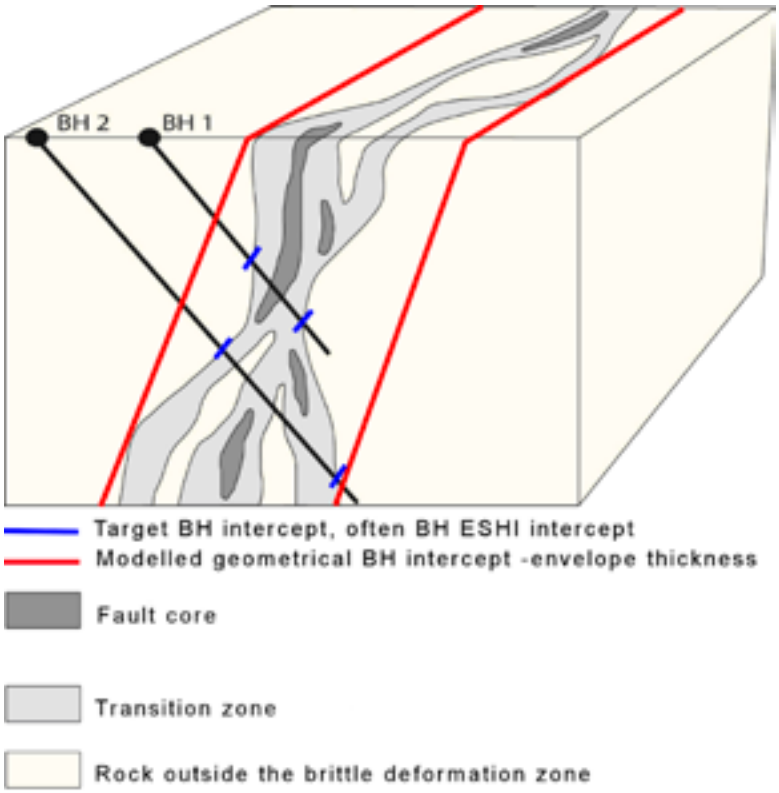

Figure 5-1. *Three-dimensional cartoon illustrating a conceptual geometric model for a brittle deformation zone at Laxemar along which shear displacement has occurred (redrawn after /Caine et al. 1996/). Note the variable character of the deformation zone along the two borehole intersections.*

The lineament map used in the Laxemar 1.2 modelling /SKB 2006b/ has been further developed and forms the basis for the surface interpretation of deformation zones (see Section 3.8). The resolution of the input data that forms the background to the lineament interpretation varies across the model area and the focus of the lineament interpretation has changed as the project has progressed from being initially focussed on local major lineament features to having a greater focus on shorter and minor features. During the deformation zone modelling work the lineaments, particularly their overall continuity, has been continually reviewed and the background data re-examined.

The current deformation zone model addresses deformation zones in the regional and local model areas on the same basis as that employed for Laxemar version 1.2 model /SKB 2006b/. The local scale model contains deformation zones that are inferred to be of length 1 km or longer, i.e. local major and regional deformation zones according to the terminology of /Andersson et al. 2000/. In addition there are deformation zones interpreted from the drilling investigations that have not been correlated with any surface lineament or neighbouring boreholes. Where such deformation zones have an inferred true thickness of 10 m or more they have also been modelled deterministically. Such deformation zones have been assigned a circular disk geometry with a surface area equivalent to a 1,000 m×1,000 m square and are included in a background model to the main local deformation zone model. In this way the resolution of the local model

remains unchanged from earlier versions. The selection of a 10 m thickness as a cut off point for the deterministic modelling is based on a conservative interpretation of the deformation zone thickness vs. deformation zone length relationship presented in Figure 5-33. The selection of 10 m is conservative in that the site specific relationships between zone thickness and zone length, at both Laxemar and Forsmark, indicate that a zone length of 1,000 m corresponds to a thickness of around 15 m. The application of a standard disk geometry with a fixed 564 m radius (an area equivalent to a 1,000×1,000 m square) does lead to the associated area being generally underestimated. However, further extrapolation of zone geometries beyond the defined disks is considered too speculative when the interpreted orientations are of low confidence.

The surface data coverage in parts of the area outside the local model domain has a lower resolution, which limits the possibilities of modelling deformation zones of 1,000 m length or more. Parts of the offshore and north-western parts of the regional model area are covered only by the lineament map from the version 0 model of relatively low resolution /SKB 2002/. In order to provide a regional model based on an even resolution of data, inferred deformation zones outside the local model area have therefore been limited to be of length 1.6 km or longer. This approach produces a model that has an increased level of resolution around the area of highest interest, i.e. the local model area.

Structures that are considered to be shorter than the modelled deformation zones in the local and regional areas are handled in a statistical way and are presented as part of the fracture statistical description in /La Pointe et al. 2008/. Hence, all lineaments shorter than 1 km are treated as part of the stochastic fracture network.

5.1.2 Feedback from other disciplines including SR-Can project

The SR-Can project /SKB 2006e/ is a preparatory stage for the SR-Site assessment, the report that will be used in support of SKB's application for a final repository. When inspecting version 1.2 of the site descriptive models, SR-Can highlighted the need for reduced levels of uncertainty, particularly concerning the deformation zones of a size of 3 km or more. It is considered that this has been addressed by the subsequent investigation plan and modelling work. As can been seen in Appendix 14, the major zones have been investigated by a suite of techniques including both direct and indirect methods. The overall confidence in the orientation and character of the basic structural framework of the major zones ZSMEW002A, ZSMEW007A, ZSMNE005A, ZSMNS001A-E, ZSMNS059A and ZSMNW042A (Figure 5-4) has been significantly increased.

During the recent modelling phase the interpreted results from in situ rock stress measurements in KLX12A in south east Laxemar appeared not to be compatible with the modelled dip of the neighbouring deformation zones (Figure 5-2). The area in question is complex as inferred from the results of aerial geophysical surveys that suggests a junction of a number of deformation zone and rock boundary geometries. This area has not been the focus of investigations and the earlier modelled deformation zone interaction relied on the 'simplest solution' based on surface inspection. In fact the zone interactions are spatially complex and even more so when considered in four dimensions. Based on the impetus from the in situ stress results, a further review of the available data from this area was undertaken at the same time as new drilling results from KLX27A, concerning the western section of ZSMNW042A, became available. The combined review and new results lead to a modification of ZSMNW042A geometry giving it a moderate dip to the south and a significant extension to the east. The increased easterly extent is based on a re-linking of lineaments. The resulting solution is considered to provide a simpler and more logical geometry from an evolutionary point of view, as well as being compatible with the nearby in situ stress results (Figure 5-2).

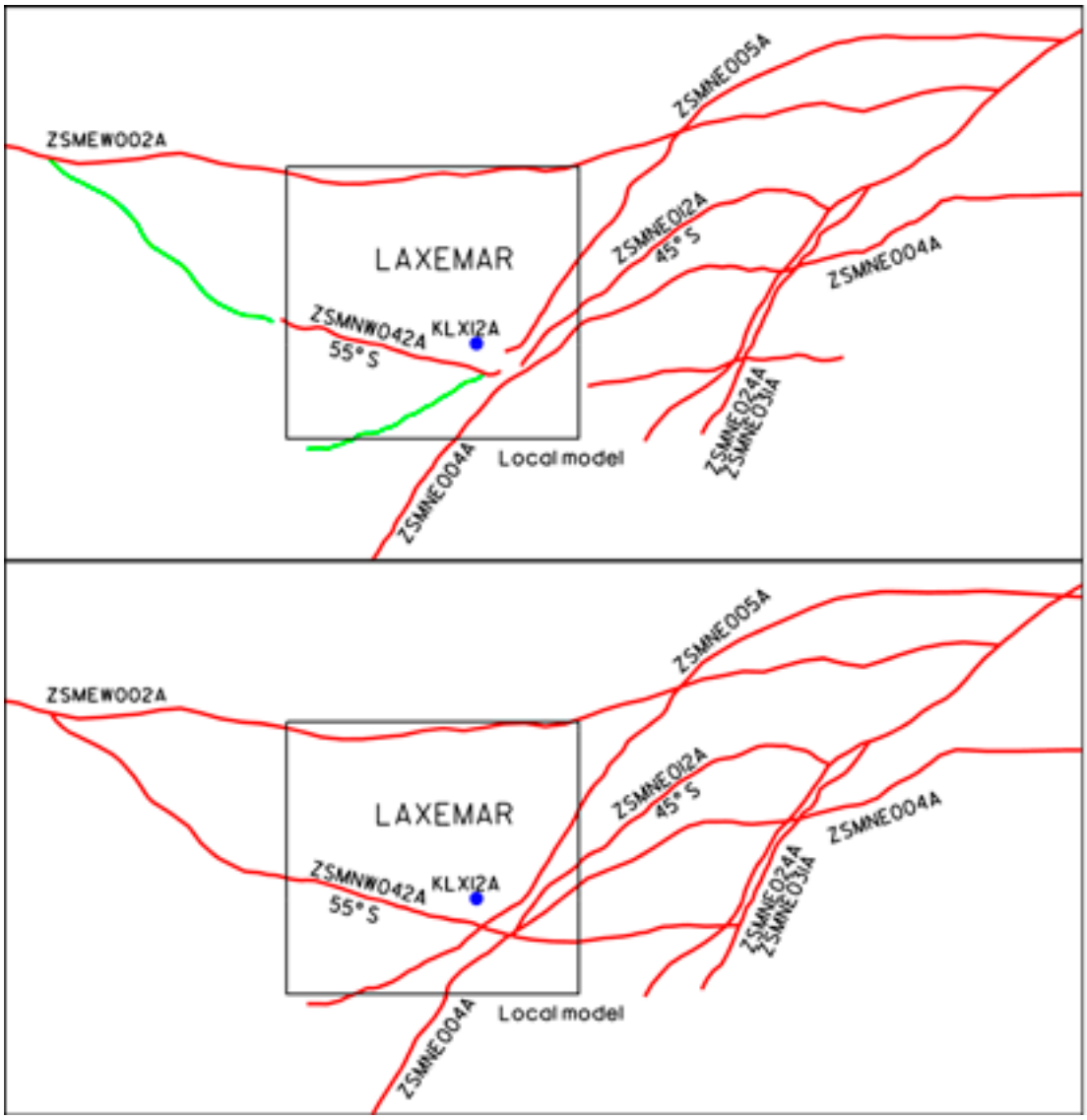

Figure 5-2. *Updating of the major deformation zones in southern Laxemar. Version 1.2 shown in the upper figure and updated in the lower figure.*

5.2 Conceptual understanding of deformation zones at the site

5.2.1 Deformation zones in 3D

In the cases where a deformation zone can be correlated with both a lineament and a borehole, the strike of the deformation zone is assumed to be the same as the trend of the matching lineament. The dip inferred from the borehole intercept is interpreted as the average dip angle of the deformation zone, along its entire extent. Deformation zones observed only at the surface, which lack information on their sub-surface extents and geometry, are assumed to be vertical.

The steeply dipping deformation zones are assumed to truncate, along their strike direction, against deformation zones as indicated by the lineament map. Gently dipping deformation zones have been detected by an integration of data from boreholes with the interpretation of seismic reflectors. In the model the gently dipping deformation zones are truncated, both along their strike and in the down-dip direction, against regional or local major, vertical and steeply dipping deformation zones. The lateral modelled extent of the gently dipping zones has been constrained based on the lateral extent of the supporting investigation evidence and then subsequent termination against the nearest steeply dipping zone beyond this evidence.

Deformation zone thickness, like deformation zone length, is often used as a general term without clear definition since it is related to the scale of interpretation. The following discussion outlines how the term and other supporting terminology have been applied in this work. The concept of a deformation zone core and transition zones for brittle deformation zones is well established and has been earlier presented (Figure 3-95) and /Munier et al. 2003/. In contrast to the original representation, the use of absolute fracture frequencies to define a transition zone or zone core boundary position is not applied. Elevated fracture frequencies in a relative sense are implied in the definition of such brittle deformation zones but the strict application of fixed threshold values is considered unwarranted. Q or RMR estimates which include fracture frequencies can be made to better describe and quantify rock quality variations across a deformation zone. It should also be noted that deformation zone geometries are often complex, discontinuous and asymmetrical.

Different borehole intercepts, topographic expressions, outcrop indications, borehole and surface geophysical surveys will all generate their respective estimates of true thickness and how this may vary along strike and dip for the same deformation zone. Generally all these values differ to a smaller or larger degree. The current modelling process aims to take all of these indications into account and make a judgement of an overall representative measure of deformation zone thickness, along with a likely span.

Two specific borehole related terms are quoted in the deformation zone descriptions and accompanying property tables, namely ‘Target borehole intercepts’ and ‘Geometrical borehole intercepts’ (Figure 5-1). These two measures underlie much of the resulting modelled 3D deformation zone geometries. Possible deformation zones, both brittle and ductile, are identified in the drill core during the SHI process (cf. Section 3.3). Any interpreted deformation zone is defined by an upper and lower borehole length which defines its apparent thickness. These deformation zone boundary estimates are made by a specialist team of geophysicists and geologists and are essentially ‘best judgement’ estimates based on all of the information available from the borehole and by a hands-on joint examination of the drill core. No reference is made to other sources of data from other studies away from the borehole. These deformation zone boundary intercepts in a borehole are referred to as ‘Target intercepts’ and are shown schematically in Figure 5-1. In general, target intercepts conform to the ESHI possible deformation zone intercepts but in certain cases adjustments have been made on the basis of other information or interpretation, related to information away from the specific borehole.

The physical location and inferred orientation of deformation zone specific target intercepts, deformation indicators from outcrop evidence, geophysical seismic reflection, refraction, magnetic and resistivity survey indications are all taken into account and an overall ‘Envelope thickness’ for a deformation zone is defined in 3D. This envelope thickness aims to contain at least the majority of a deformation zone’s core(-s), transition zones and splays. It is this envelope thickness that defines the deformation zone in the 3D RVS deterministic DZ model along with a, generally centrally located, zero thickness middle plane. The ‘Geometrical BH intercepts’ listed in the deformation zone descriptions and property tables relate to where the deformation zone envelope surfaces intercept the various boreholes.

Any estimate of deformation zone length, like thickness, is also closely related to the scale of interpretation. For the purposes of the deterministic modelling, within the local model volume, ‘deformation zone length’ generally corresponds to the length of the associated linked lineament. However, all of the associated lineaments in the local model area have been reviewed during the modelling work and adjustments have been made. This has generally resulted in the addition of links for the definition of a deformation zone. In a very few cases a linked lineament, with a length of over 1,000 m, has not been included in the model as a possible deformation zone. Whilst any associated possible deformation zone is expected to be discontinuous to some extent, in these few cases the associated possible deformation zone has been ’broken up’ on the basis that the lineament transects a number of extensive outcrops which have been visited in the field and at which no evidence of deformation has been identified. The lineament review referred to is a process performed with reference to the original background data and lineament interpreters though no absolute ‘break up’ criteria were applied. The following section of the report presents how these conceptual deformation zone representations were applied in the modelling work.

5.2.2 Characteristics of different sets of deformation zones

An overview of the location of the deterministically modelled deformation zones, along with rock domains, in the local and regional model volumes is presented in Figure 5-3 and Figure 5-4, respectively.

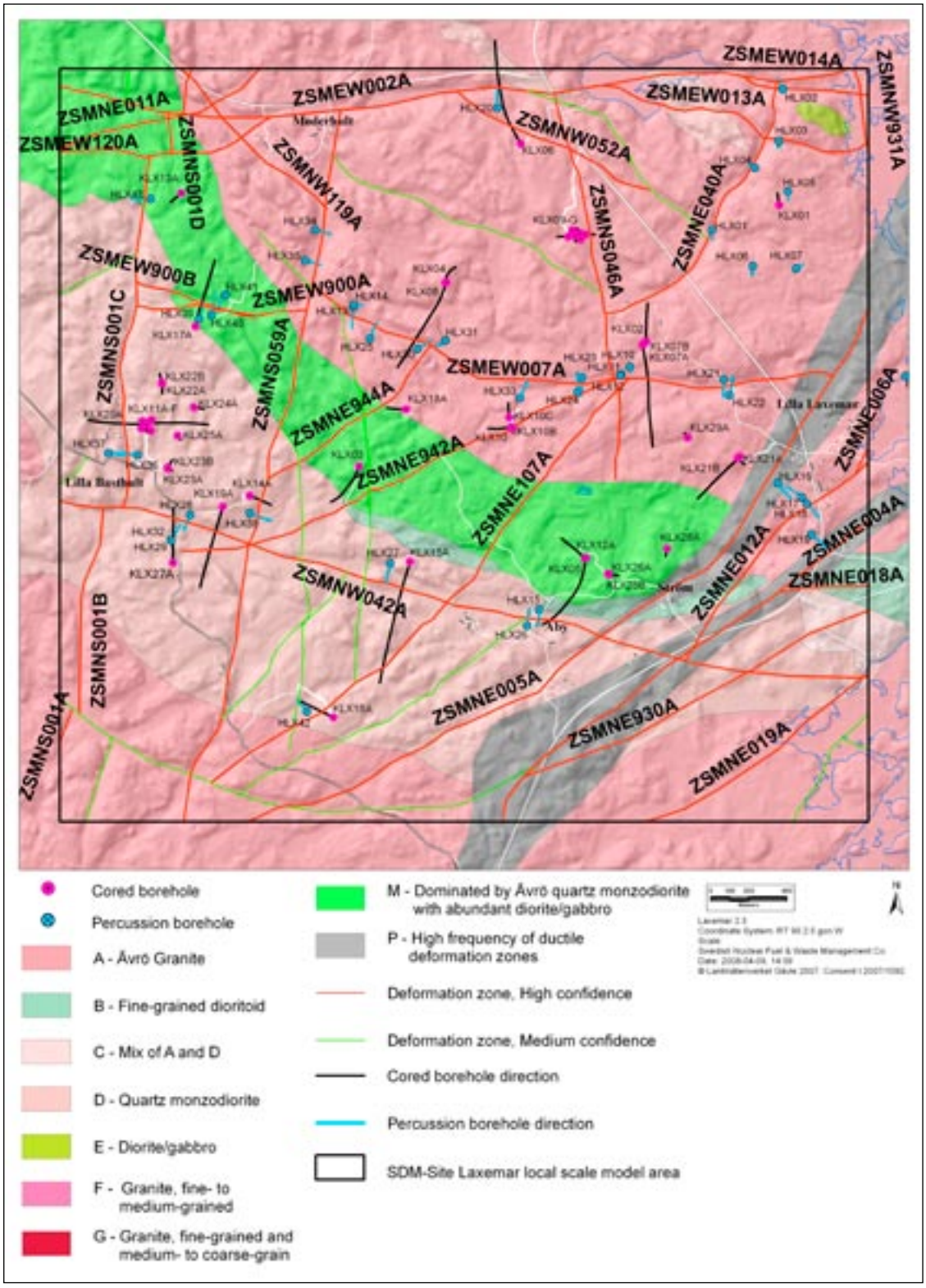

Figure 5-3. *An overview of the deformation zones and rock domains modelled deterministically in the Laxemar local model area.*

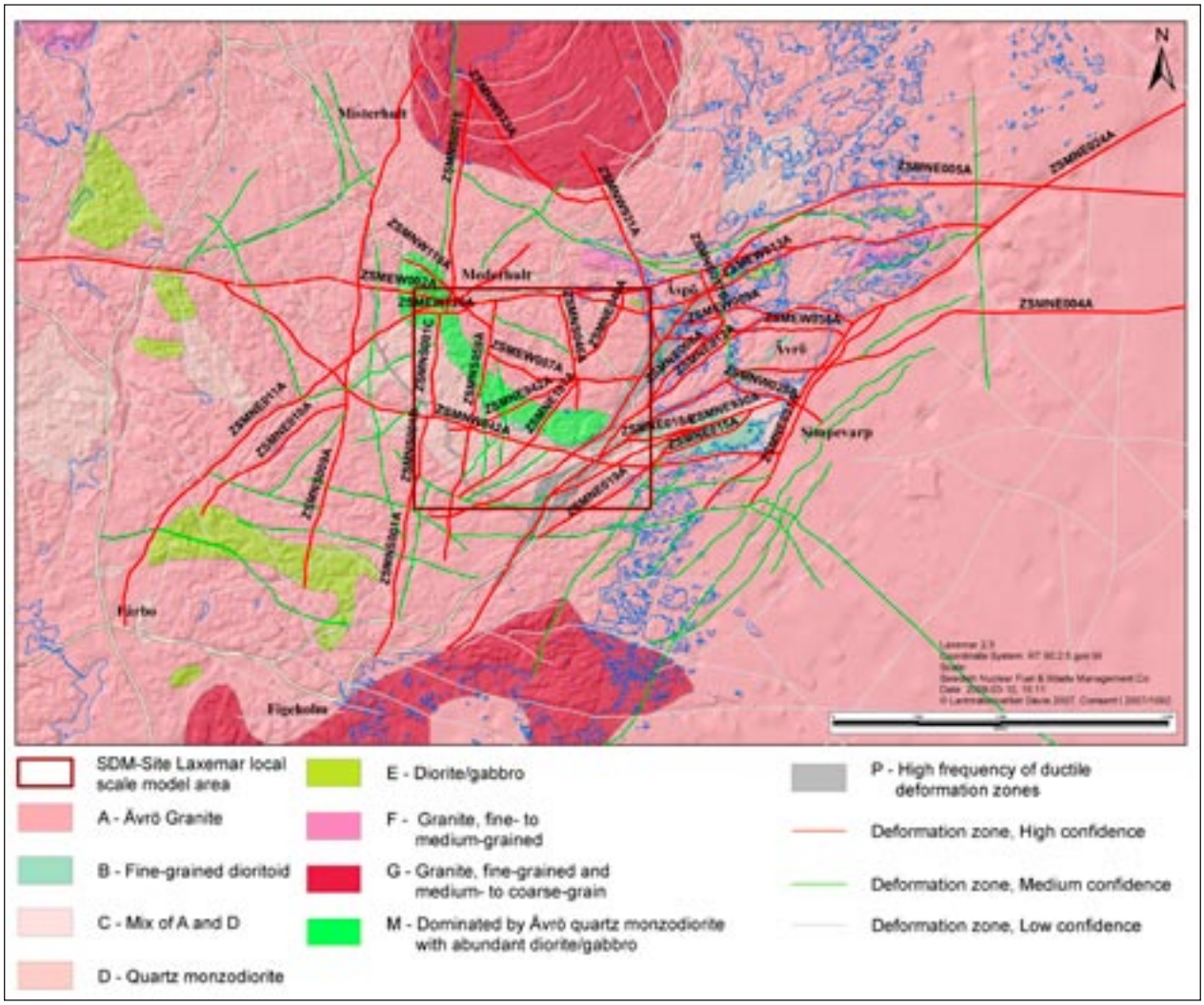

Figure 5-4. *An overview of the deformation zones and rock domains modelled deterministically in the Laxemar regional model area.*

Detailed descriptions of individual deterministically modelled deformation zones are presented in Appendix 14. In this section of the report the main deformation zones are described in a series of groups that are based on their overall orientation, origin and character. The aim of this section is to provide an overview of the modelled deformation zones and a better understanding of structural geological model. The selected groups are as follows:

- Northeast-southwest striking, moderate to steeply dipping.
- North-south striking, moderate to steeply dipping.
- East-west to northwest-southeast striking, steep to moderate dip to the south.
- East-west to northwest-southeast striking moderate dip to the north.
- Gently dipping.

Deformation zone geometries presented in red represent deformation zones which are judged to be of high confidence as to existence and are supported by both indirect evidence such as topographic and geophysical data as well as direct evidence from surface outcrop mapping or drillholes. Deformation zones presented in green are judged to be of medium confidence in existence and unlike high confidence deformation zones they lack direct evidence from outcrops or drillholes.

NE–SW striking deformation zones, moderately to steeply dipping

Three regional deformation zones, ZSMNE011A, ZSMNE005A and ZSMNE004A, volumetrically dominate this set of structures and roughly mark the outer NW and SE boundaries for the rock volume for a potential repository. All three deformation zones have a ductile origin and complex internal geometry as evidenced by the numerous mylonite fabrics identified during the outcrop mapping campaign. It is this distribution of mylonites and the results from the aerial magnetic survey taken together that define the surface expression of these deformation zones. All three deformation zones should be considered as deformation 'shear belts' composed of a large number of anastomosing sub-structures with an overall irregular thickness rather than three single structures. Field mapping results for all three deformation zones give evidence of a dominating sinistral shear.

Whilst it is possible to find small deformation zones intercepted in the drill core that show exclusively ductile deformation, on the larger scale of the local model volume, all local major and regional deformation zones that have a ductile origin can also be considered to have been subjected to multiple phases of later brittle reactivation. In practice evidence of this brittle reactivation may be seen as open fractures, crush and gouge and/or as sealed fractures and sealed networks depending on the timing of any mineralisation. This situation is true not only for the NE-SW striking set of structures but for all local major and regional deformation zones. It has become clear that the evidence from a single or couple of drill cores taken in isolation cannot be taken as providing definitive evidence of any zone's character. Ductile deformation and sealed networks found in one core intercept may vary in thickness and have an open fracture network as one moves laterally or up and down through a deformation zone. The best indication of whether a deformation zone has an overall open brittle fabric component is considered to be from hydrogeological investigations.

The three shear belts in question have not been the focus of detailed drilling activity but ZSMNE005A has been investigated by a limited number of percussion drilled holes, indirect methods such as geophysical magnetic and resistivity profiling, a very limited seismic refraction survey and marginal drilling activities associated with the Äspö HRL. Details of the investigations and interpreted results can be found in Appendix 14. A detailed characterisation of the three deformation zones is not possible, however the available information suggests that the three belts are made up of a large number of anastomosing mylonite zones and similarly the later brittle failure is distributed across the belt in a number of sub-parallel sub-structures rather than along a single major complex core zone.

As described in /SKB 2005a/ the Simpevarp peninsula, the Ävrö and Hålö islands, together with the eastern part of Äspö island are intersected by the regional NE striking shear belts. The western boundary of these belts is formed by the Äspö shear zone. This NE striking belt of regional deformation zones affects the whole of the peninsula. The NE-SW set of structures is also present across Laxemar, although their frequency and thickness are markedly reduced. The western limit of Laxemar is again defined by another broad shear belt, ZSMNE011A (Figure 5-5).

The NE-SW striking deformation zones located within Laxemar are dominated by three structures ZSMNE107A, ZSMNE942A and ZSMNE944A (Figure 5-6). Details concerning these deformation zones are presented in Appendix 14. Generally it can be said that these structures have a ductile origin, often associated with fine grained granite or composite dykes and have been subjected to multiple phases of brittle reactivation. These deformation zones are relatively narrow compared with the bounding major belts with thicknesses in the range of 10 to 35 m, zone core thicknesses of 1 to 5 m and steep dips > 75º to the NW or SE.

A summary of all the available fracture orientation data from the three central NE-SW striking deformation zones in Laxemar is presented in Figure 5-7. For comparison the orientation data from fracture domain FSM_NE005 (cf. Chapter 6) is shown in Figure 5-8.

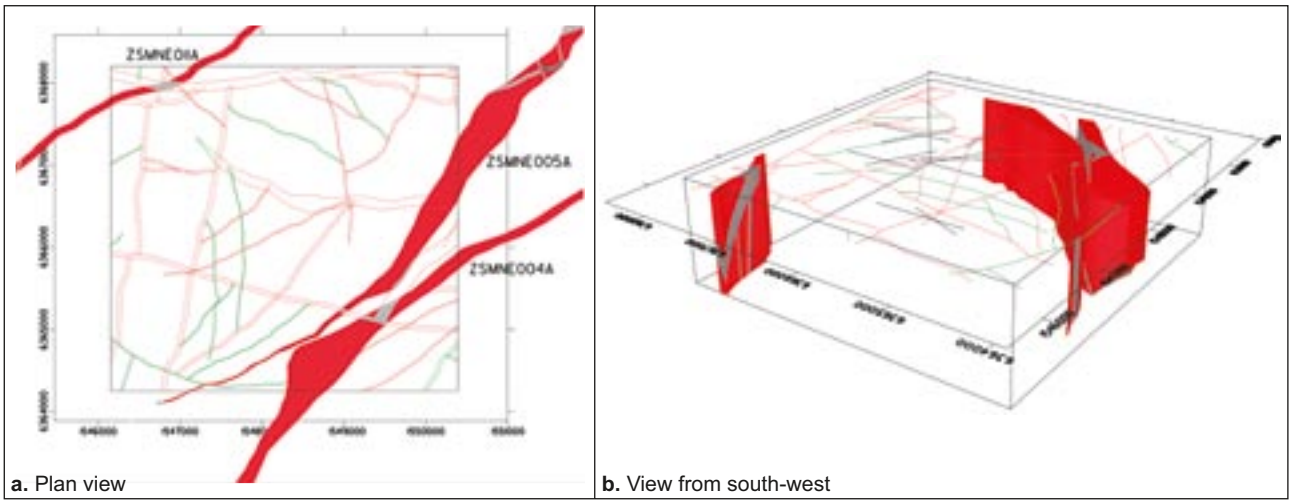

a. Plan view **b.** View from south-west

Figure 5-5. *Regional NE-SW striking deformation zones which dominate in the local model area.*

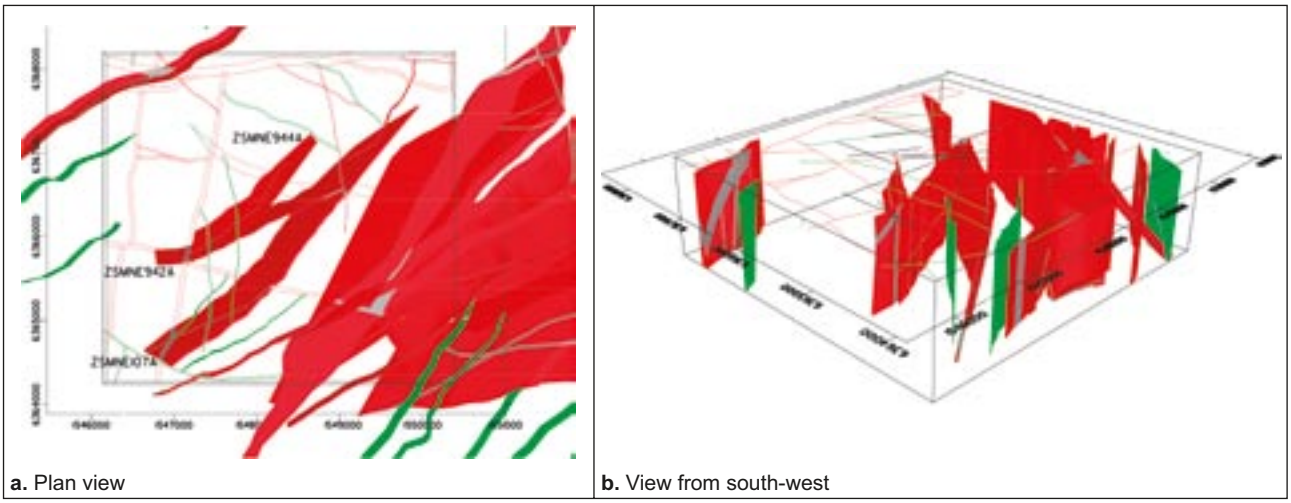

a. Plan view **b.** View from south-west

Figure 5-6. *All NE-SW striking local major and regional deformation zones which are associated with surface lineaments in the local model area*

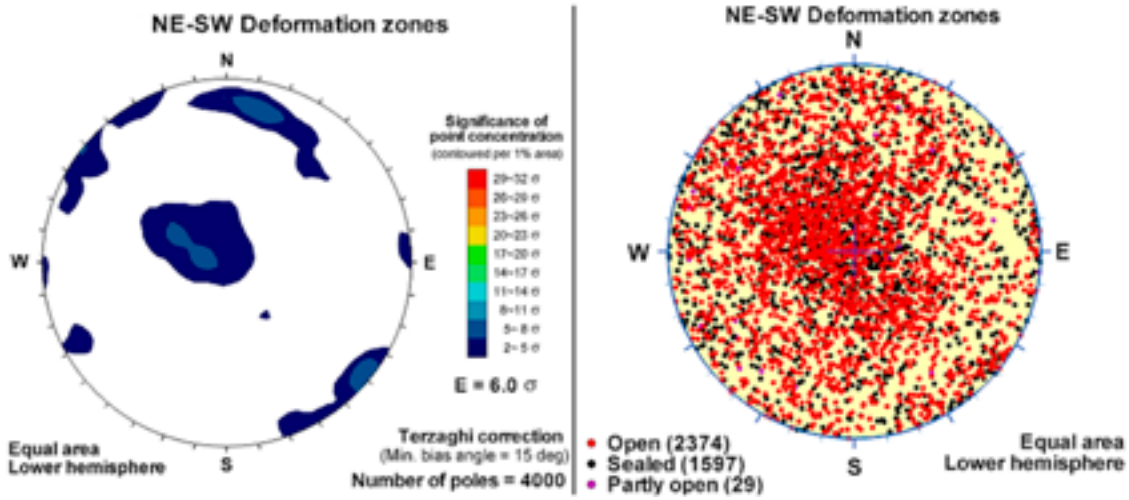

Figure 5-7. *A summary of all the available fracture orientation data (visible in BIPS) from the three central NE-SW striking deformation zones ZSMNE107A, ZSMNE942A and ZSMNE944A.*

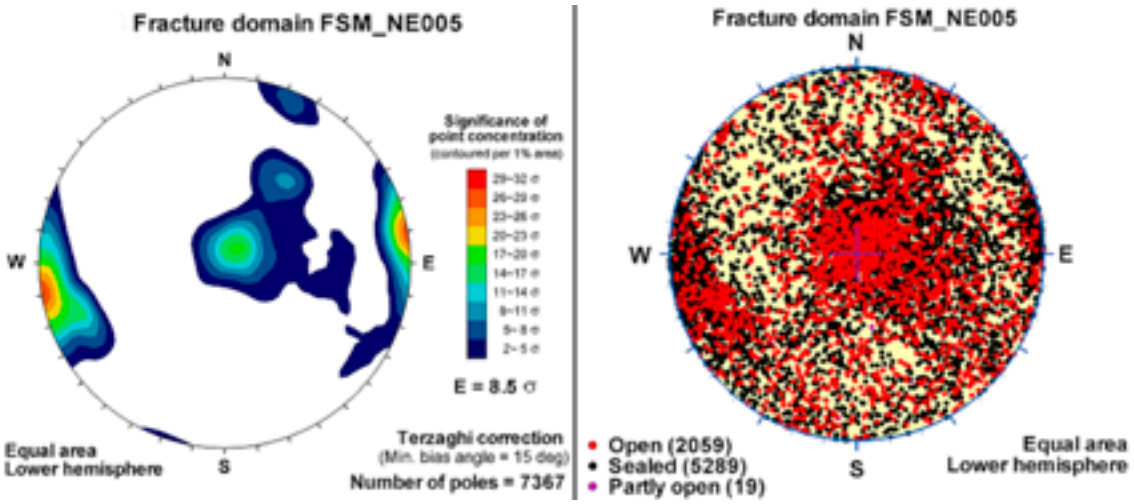

Figure 5-8. *Summary fracture orientation data from fracture domain FSM_NE005 (cf. Chapter 6).*

It can be seen from Figure 5-7 that the fractures are dominated by two sets, one corresponding to a set of vertical fractures parallel to the deformation zones (i.e.striking NE-SW) and a second sub-horizontal set . The dominant fracture orientation in the FSM_NE005 fracture domain is more N-S and may relect the reidel fracture orientation associated with the main shear belt as well as the selected domain geometry (cf. Chapter 6).

N–S striking deformation zones, moderately to steeply dipping

The north-south striking local major and regional deformation zones are dominated by ZSMNS001A-E and ZSMNS059A in the local model area (Figure 5-9). Both deformation zones have parallel strikes and dip 80–90º W. Details of these two and the other deformation zones are presented in Appendix 14. Generally speaking these two and other members of this set of so called N-S striking structures have in fact strikes varying from NNW to NNE. They are steeply dipping with a tendency to dip to the west. However, two members in this group KLX04_DZ6b and KLX04_DZ6c (Table 5-1 and Figure 5-10) are less steeply dipping though their orientation and associated thickness are judged low confidence. They are based on a subdivision of an extensive and complex deformation sequence identified in the KLX04 core during the ESHI process. Both drilling and outcrop investigations show that the deformation zones have a ductile origin and, similar to the NE-SW striking set, have been subject to multiple phases of brittle reactivation.

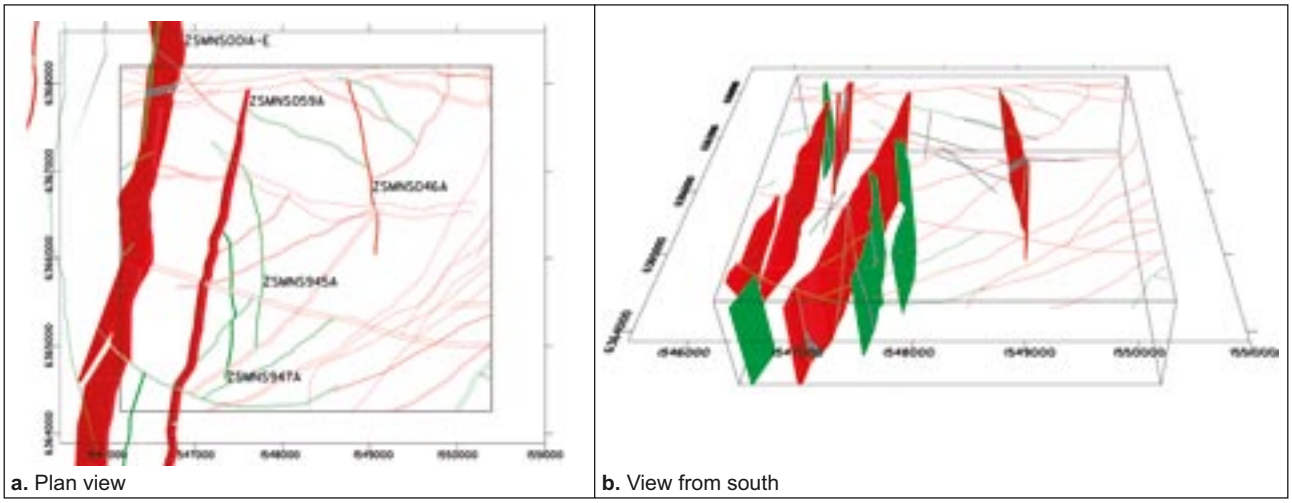

a. Plan view

b. View from south

Figure 5-9. *The main N-S striking structures encountered in the local model volume. All are sub-vertical to steeply dipping to the west.*

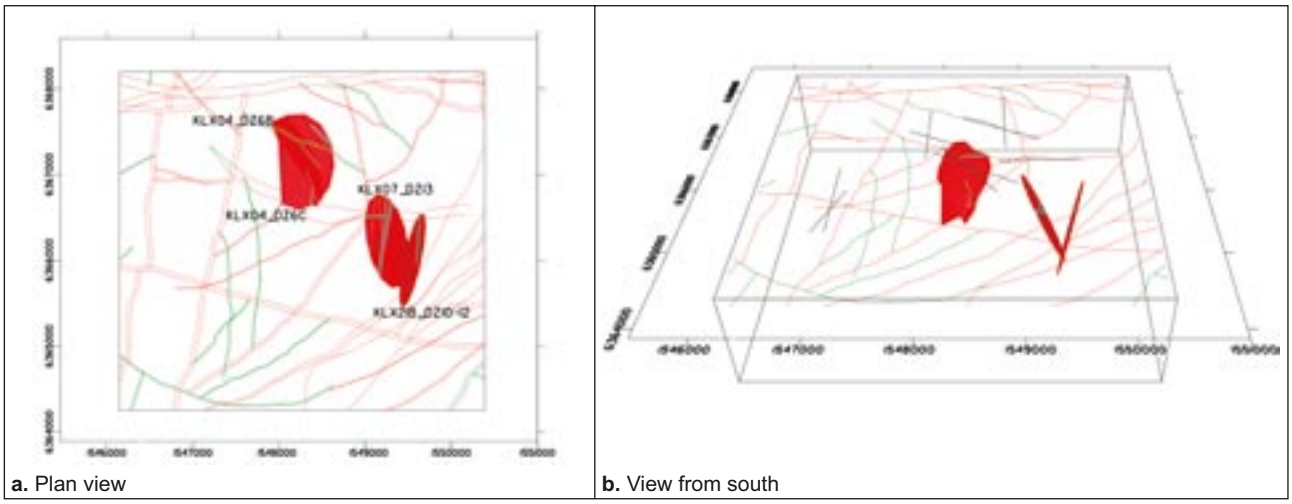

a. Plan view **b.** View from south

Figure 5-10. *N-S striking deformation zones in the local model volume without associated surface lineaments, as listed in Table 5-1.*

Table 5-1. N-S striking deformation zones in the local model volume not connected to surface lineaments, as presented in Figure 5-10.

Zone ID	Orientation (degrees)	Est. thickness (m)	Ductile	Brittle	Bh interception m.a.s.l.
KLX04_DZ6b	156/67	14		x	–874
KLX04_DZ6c	177/42	30	X	x	–935
KLX07_DZ13	348/65	10	X	x	–612
KLX21B_DZ10–12	192/80	10	X	x	–581

Kinematic studies identify strike slip, predominantly sinistral displacements, though in common with the NE-SW striking structures this sense of movement has been likely reversed at a later stage. With the exception of ZSMNS001A-E and ZSMNS059A these deformation zones are narrow with thicknesses of 10 to 20 m with multiple thin discontinuous highly fractured cores. ZSMNS001A-E and ZSMNS059A are thicker, 45 m and 50 m, respectively. Both deformation zones have associated highly fractured dolerite dykes that have been intercepted by the drillholes although they have not been identified during the surface mapping campaign. The magnetic susceptibility of the dolerites is in general lower than the average susceptibility of the country rock and the higher fracture frequency implies that the fractured dolerites are more susceptible to erosion than the normally fractured country rock. North of the investigated area, in the Götemar granite, dolerite dykes are observed with similar N-S strike directions. The other narrower deformation zones in this orientation set are also inferred to have associated dolerite dykes, but in all cases they are likely to be very thin and discontinuous /Triumf 2007/.

Immediately west of ZSMNS001A-E the detailed lineament mapping suggests the presence of a series of smaller parallel striking structures with a higher frequency than to the east of ZSMNS001A-E.

A summary of all the available fracture orientation data from the three main N-S striking deformation zones in Laxemar is presented in Figure 5-11. For comparison the orientation data from fracture domain FSM_W (cf. Chapter 6) is shown in Figure 5-12. It can be seen from Figure 5-11. that there are three pole maxima which correspond to a set of vertical fractures parallel to the deformation zones (i.e. striking NNE-SSW), a sub-vertical set at right angles to the deformation zones and a third, gently dipping to the south. It can be seen in Figure 5-12. that the fractures in the rockmass outside the three major deformation zones have a pole concentration striking more directly north-south and may represent a riedel orientation related to the strike-slip system dominated by these major zones.

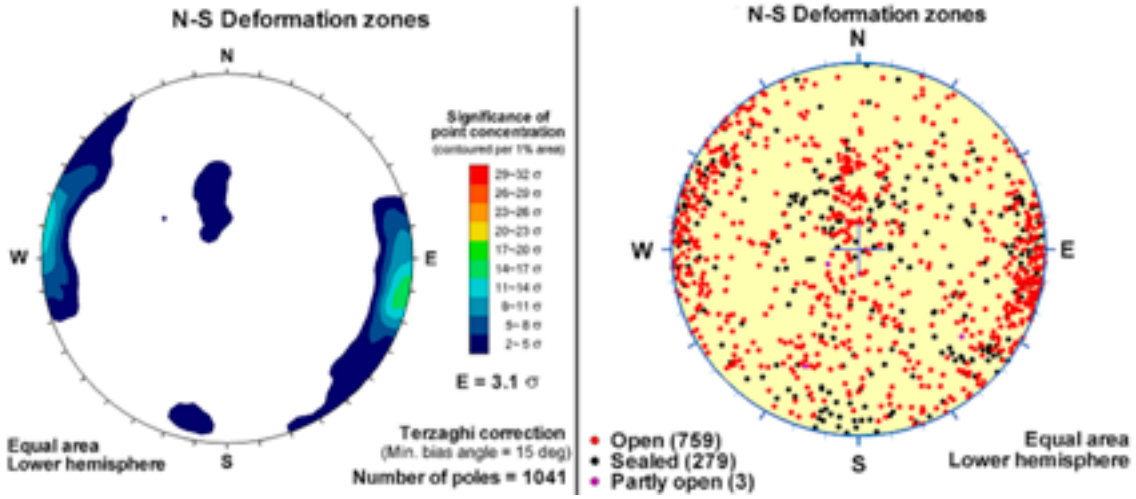

Figure 5-11. *A summary of all the available fracture orientation data (visible in BIPS) from the three main N-S striking deformation zones ZSMNS001C, ZSMNS046A and ZSMNS059A.*

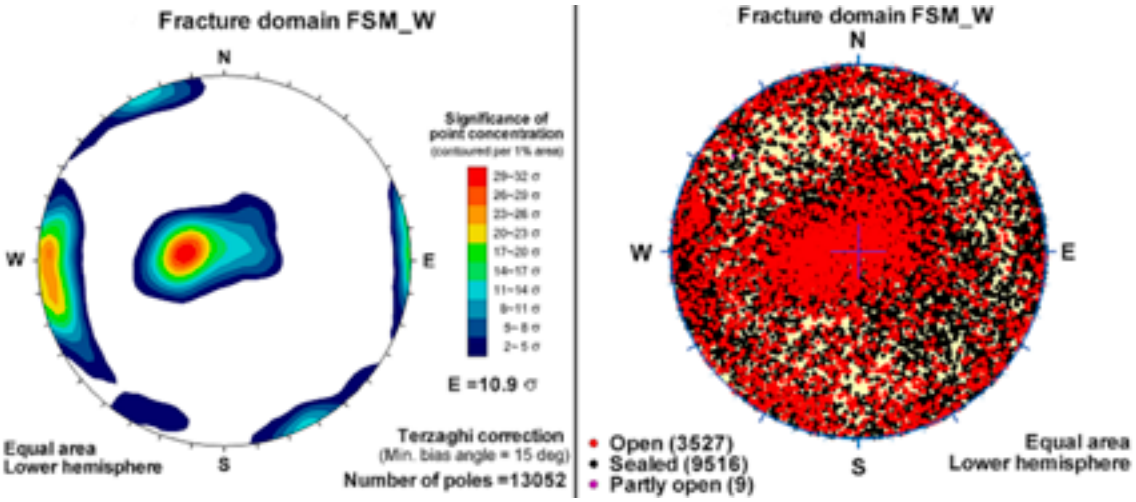

Figure 5-12. *Summary fracture orientation data from fracture domain FSM_W.*

E-W and NW-SE striking, steeply to moderately southward dipping deformation zones

This set of structures is dominated by ZSMEW002A, ZSMEW120A, ZSMEW900A-B and ZSMNW042A (Figure 5-13). ZSMNW042A is included in this group, which is otherwise dominated by the E-W structures since it has a similar character, size and inferred relationship with the regionally dominant Mederhult zone ZSMEW002A.

By far the largest deformation zone in this group is ZSMEW002A (Mederhult zone) which is more or less parallel with the northern boundary of the local model area. The deformation zone has an estimated length of up to 30 km although with a very variable thickness (20–200 m) as suggested by the regional topographic and geophysical data. The use of such surface data for zone thickness estimations is further discussed in Section 5.3.2. This irregular surface expression of the deformation zone is shared by other members of this group, particularly in the case of ZSMNW042A. All of the main deformation zones that have been investigated by drilling show an original ductile fabric that has been very heavily overprinted by brittle reactivation. Alteration, dominated by red staining, is also common in this group of deformation zones. Similarly, the main members all dip moderately to steeply (55–65º) to the south. Other smaller members of the group have not been the focus of investigations and have been modelled with a vertical dip although they are expected to have a similar dominantly brittle character.

Table 5-2. E-W, NW-SE, steep to moderately south dipping local major and regional deformation zones in the local model volume without associated surface lineaments, as presented in Figure 5-14.

Zone ID	Orientation (degrees)	Est. thickness (m)	Ductile	Brittle	Bh interception m.a.s.l.
KLX07_DZ7	267/90	30	x	x	–265
KLX18_DZ9	095/50	10	x	x	–450
KLX08_DZ6	296/89	10		x	–327

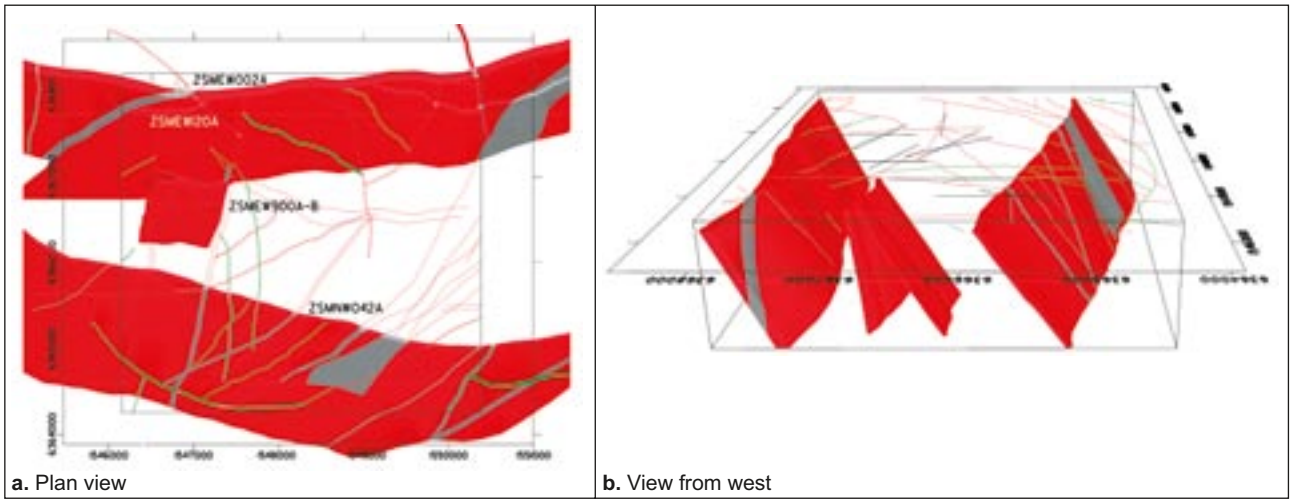

a. Plan view **b.** View from west

Figure 5-13. *The main members of the E-W and NW-SE, steep moderately southward dipping deformation zones.*

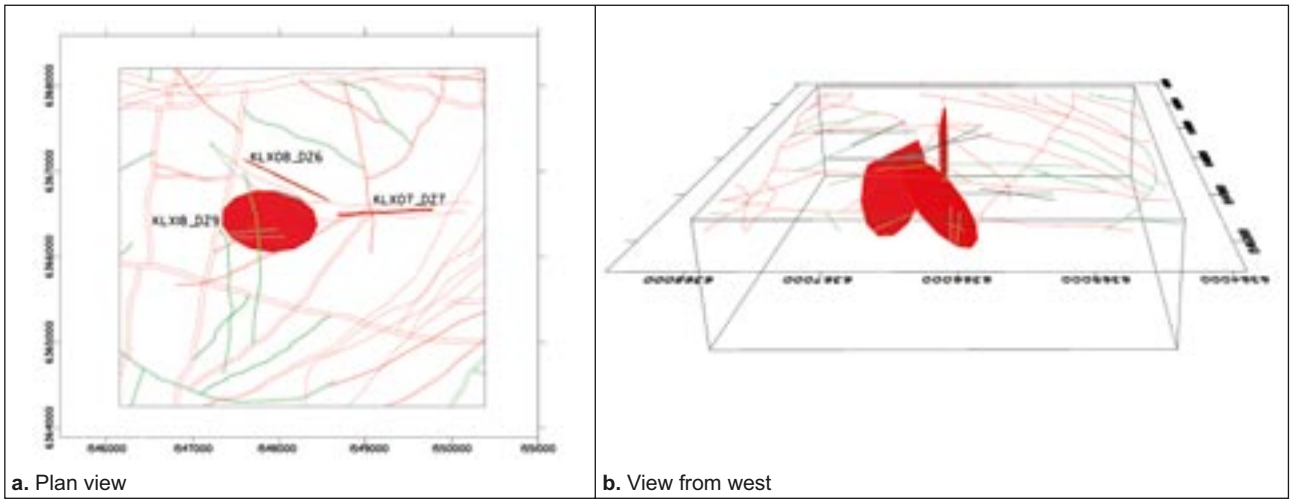

a. Plan view **b.** View from west

Figure 5-14. *E-W, NW-SE, steep to moderately south dipping local major deformation zones in the local model volume without associated surface lineaments, as listed in Table 5-2.*

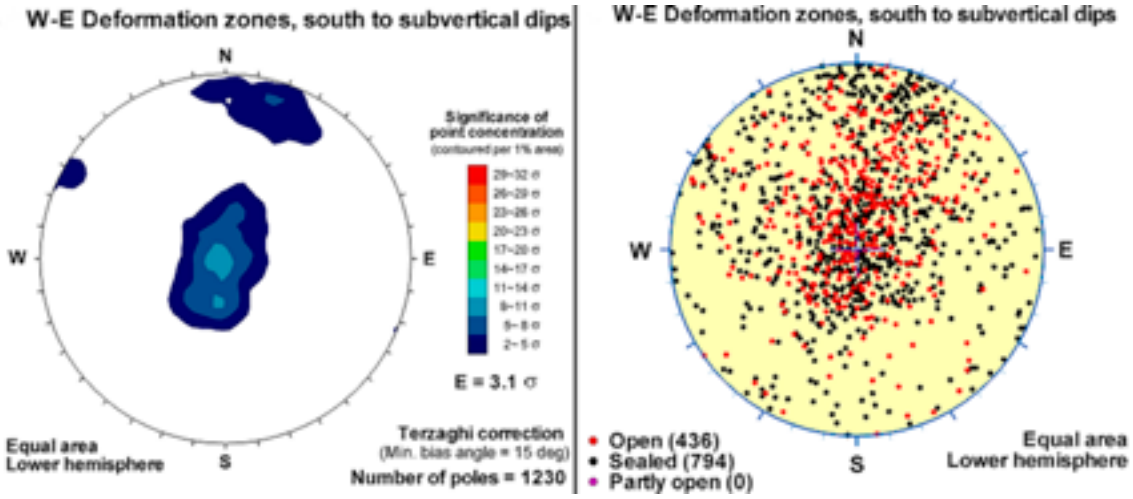

Figure 5-15. *A summary of the available fracture orientation data (visible in BIPS) from the three main E-W striking southerly to sub-vertically dipping deformation zones ZSMEW002A, ZSMEW900A/B and ZSMNW042A.*

A summary of all the available fracture orientation data from the three main E-W deformation zones with steep southerly to sub-vertical dips is presented in Figure 5-15. It can be seen from Figure 5-15 that there are three pole maxima which correspond to a set of vertical fractures sub-parallel to the deformation zones (i.e. striking WNW-ESE), a vertical set at right angles to the deformation zones and a third, sub-horizontal set.

E–W and NW-SE striking, moderately northward dipping deformation zones

For the purposes of the local model description, this group is dominated by a single member, ZSMEW007A-C, Figure 5-16, although seismic reflection surveys and drilling results give evidence of sub-parallel, thinner deformation zones with a similar character at greater depths (Figure 5-17). In common, to a certain extent, with ZSMNW042A the deformation zone has a general east- west alignment that swings and becomes more NW-SE to the west. What singles out this deformation zone from essentially all other deformation zones in the local model volume is that it has a completely brittle origin and character with well developed breccias and characteristic red-green fault gouge concentrated in a 60 cm thick clay core. As for all other deformation zones, a detailed description can be found in Appendix 14.

ZSMEW007A shares the broad irregular surface expression of the main deformation zones in the southward dipping E-W, NW-SE group. This surface expression is inferred to be linked to the dip of the zone, thickness variations (it has a mean thickness of 80 m) and complex geometric character. In common with the south dipping group, this deformation zone is strongly associated with alteration dominated by red staining, which being more susceptible to weathering may also help explain the topographic expression of the zone. In fact the distribution of red staining seen in the many borehole intercepts has been used as supporting evidence for the interpretation of the overall deformation zone dip. This red staining has been used in a similar fashion when establishing the southerly dip of ZSMNW042A.

Other deformation zones, sub-parallel with ZSMEW007A and with a similar character are listed in Table 5-3 and shown in Figure 5-17. Associations with surface lineaments have not been established for these deformation zones. Surrounding boreholes show a lack of correlation which suggests that these deformation zones, despite their thickness, have a limited lateral extent. It could be argued that other crosscutting deformation zones could generate offsets but such geometries and implied thicknesses should still be identifiable in the seismic profiling.

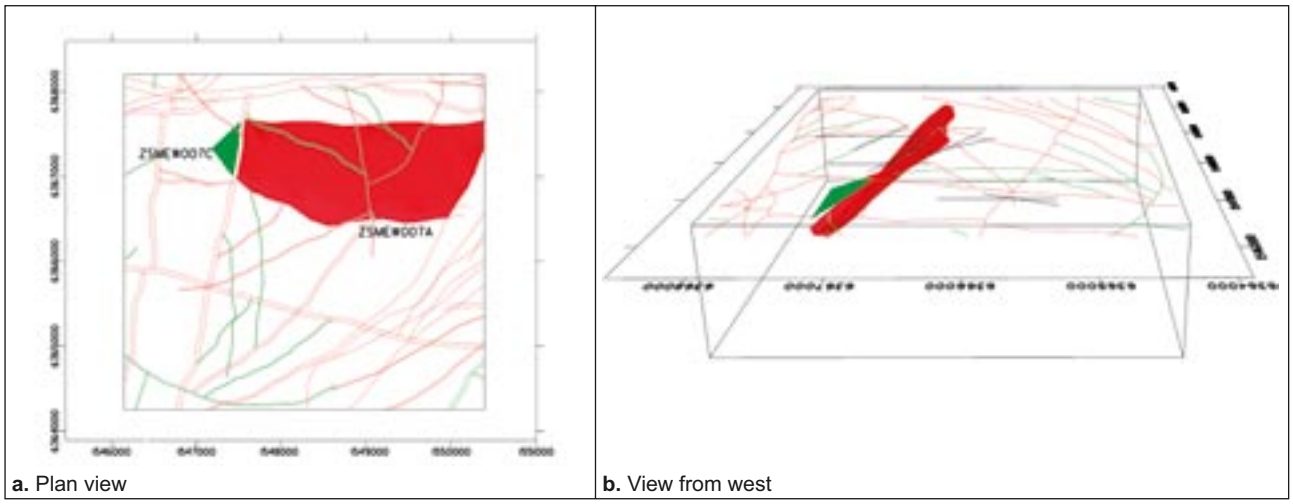

a. Plan view **b.** View from west

Figure 5-16. *ZSMEW007A-C moderately dipping 45° to the north.*

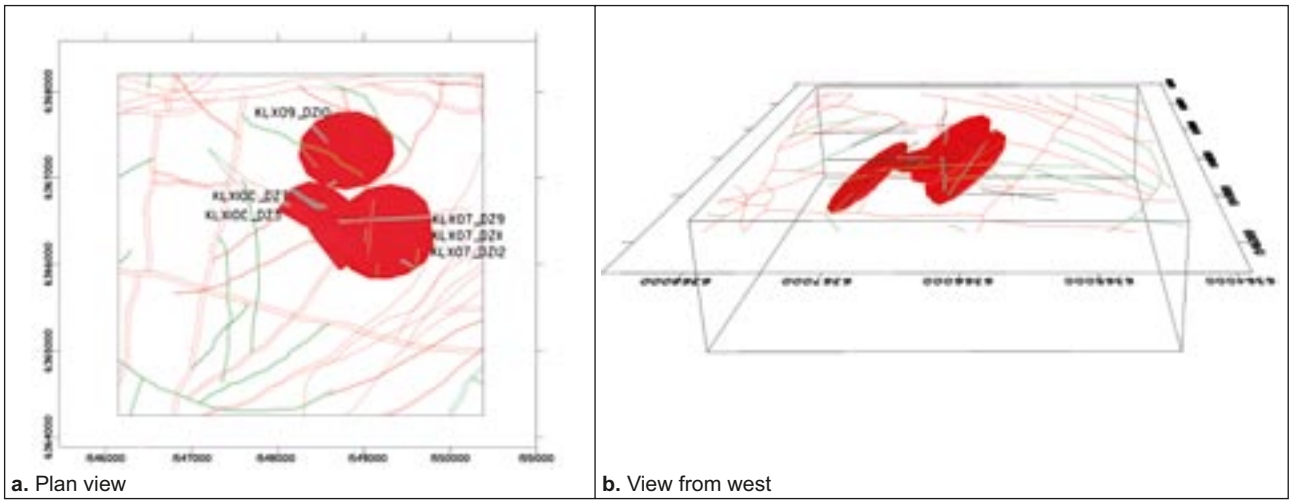

a. Plan view **b.** View from west

Figure 5-17. *E-W, NW-SE, moderately northward dipping local major deformation zones in the local model volume without associated surface lineaments, listed in Table 5-3.*

Table 5-3. E-W to NW-SE striking, moderately northward dipping deformation zones in the local model volume not associated with surface lineaments, as presented in Figure 5-17.

Zone ID	Orientation (degrees)	Est. thickness (m)	Ductile	Brittle	Bh interception m.a.s.l.
KLX07_DZ9	253/35, seismic reflector D /Juhlin et al. 2004/	10	x	x	–329
KLX07_DZ11	253/35, seismic reflector G /Juhlin et al. 2004/	30		x	–535
KLX07_DZ12	263/41	47		x	–548
KLX09_DZ10	263/37	25		x	–500
KLX10C_DZ3	300/35	10	x	x	–28
KLX10C_DZ7	323/39	10	x	x	–91

In addition /Viola and Venvik-Ganerød 2007/ investigated the drill core from parts of KLX07A and proposed significant reductions in deformation zone thicknesses. For the modelling work an overly conservative approach has possibly been taken and the interpreted intercepts from ESHI intervals have been maintained.

A summary of the available fracture orientation data from the main E-W deformation zones with moderately steep northerly dips is presented in Figure 5-18. For comparison fracture data specific to ZSMEW007A borehole intercepts and the broader fracture domain FSM_EW007 (cf. Chapter 6) are included as Figure 5-19 and Figure 5-20, respectively.

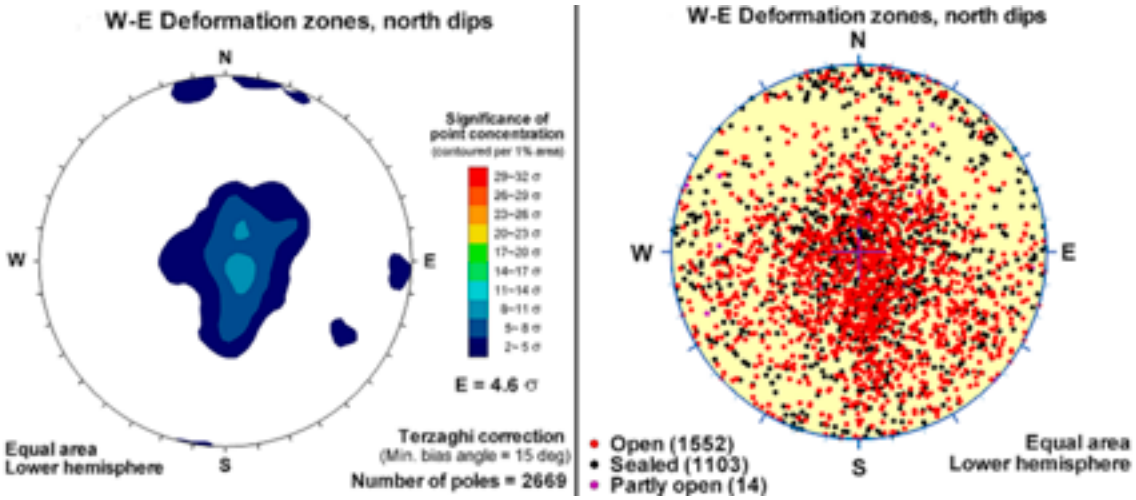

Figure 5-18. *A summary of the available fracture orientation data (visible in BIPS) from the main E-W and NW-SE striking, northerly dipping, deformation zones ZSMEW007A, KLX07A_DZ9, KLX07A_DZ11, KLX07A_DZ12 and KLX09_DZ10.*

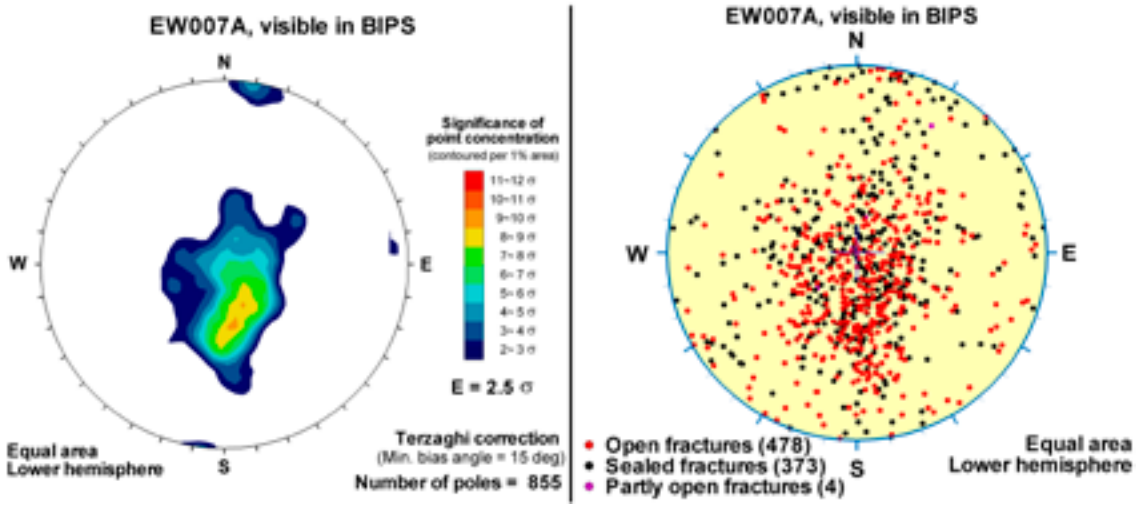

Figure 5-19. *A summary of the available fracture orientation data (visible in BIPS) from ZSMEW007A borehole intercepts.*

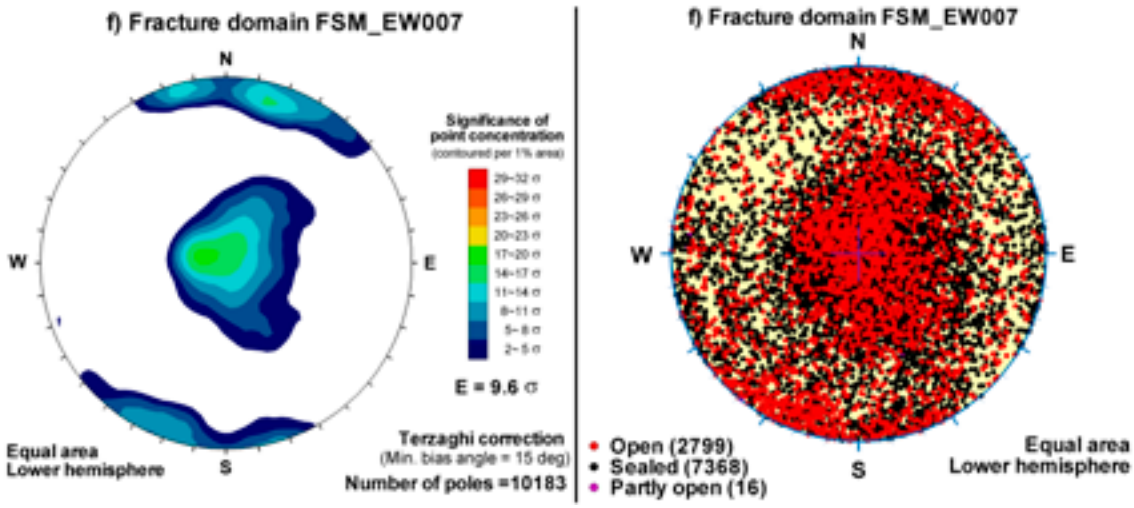

Figure 5-20. *A summary of the available fracture orientation data from fracture domain FSM_EW007.*

Gently dipping deformation zones

It is not a straightforward matter to identify the lateral extent of this type of deformation zones since often they do not have clearly identifiable intercept with the ground surface. In addition, if such deformation zones are segmented and later offset by movements along steeply dipping deformation zones, which is considered highly likely, then the interpretation and estimation of their effective extents and 'size' is extremely difficult. It is noteworthy that although the Äspö HRL, CLAB and OKG underground facilities lie to the east of the regional Äspö shear zone, in a slightly different tectonic regime, no major gently dipping deformation zone was identified throughout the entire underground works including the Äspö spiral access ramp and shafts down to c –450 m above sea level. However, such deformation zones are interpreted to occur in Laxemar but their sizes are judged to be from around the lower range of what is termed Local Major deformation zones (lower limit length of 1,000 m) to the MDZ size range (< 1,000 m). No gently dipping local major or larger deformation zones were identified as intercepting the ground surface in the local model area.

The most suitable investigation method for the identification of extensive gently dipping deformation zones is seismic reflection surveying. The two main members in this group, are largely based on the results from such seismic reflector survey work /Juhlin et al. 2004/. The two underlying reflectors and their modelled geometries should be taken to represent the upper boundaries of much thicker poorly defined and discontinuous series of smaller, gently dipping, thin, brittle deformation zones and mafic intrusions. Details of their interpretation are presented in Appendix 14 and other group members are listed in Table 5-4. Deformation zone ZSMNW928A Figure 5-21 remains rated as medium confidence even though it has interpreted BH interceptions since its overall interpreted geometry is unstable. A review of the original interpretation of the seismic survey data, along with later available borehole data, lead to a reinterpretation of the reflector geometry with an uncertain correlation with borehole data. However, both the presented interpretation and an alternative interpreted orientation result in a structure that lies significantly below the potential storage volume.

Deformation zone ZSMEW946A Figure 5-21, reflector M1, is more problematic since its modelled geometry intercepts the volume of interest at repository depth. Details of its character can be found in Appendix 14. As stated above, the presented geometry marks the upper limit of what is judged to be a thicker discontinuous series of minor deformation zones and mafic intrusions rather than an individual structure. The orientation of fine-grained diorite-gabbro in the relevant rock domain is presented in Figure 5-22. As can be seen the mapped orientations are similar in a general way to the M1 reflector orientation.

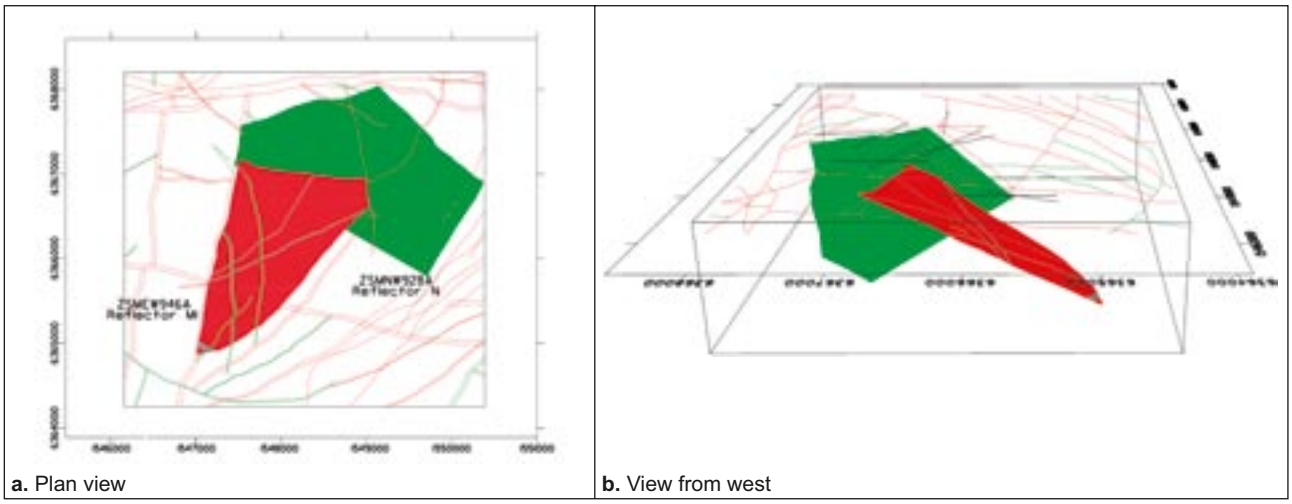

a. Plan view **b.** View from west

Figure 5-21. *Gently dipping deformation zones ZSMEW946A (080/23°) and ZSMNW928A (120/28°).*

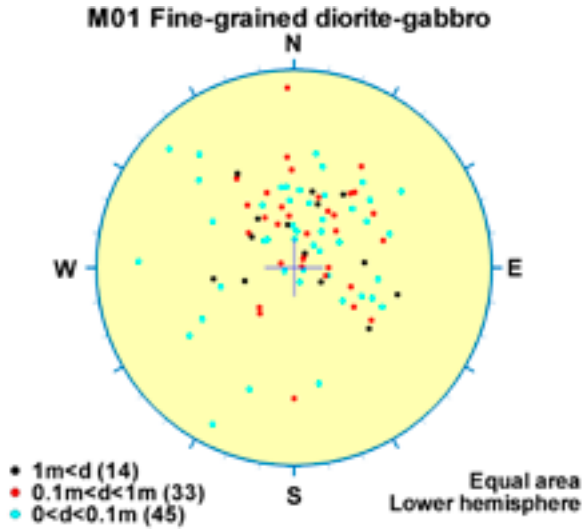

Figure 5-22. *Mapped orientations of the fine-grained diorite-gabbro boundaries as measured in all drill cores in RSMM01. The general orientation is similar to the M1 reflector series.*

Table 5-4. Gently dipping local major deformation zones without associated surface lineaments, as presented in Figure 5-23.

	Orientation (degrees)	Est. thickness (m)	Ductile	Brittle	Bh interception m.a.s.l.
KLX07_DZ10	225/28	10		x	–473
KLX08_DZ10	079/11	11		x	–770
KLX08_DZ1	000/18	27		x	–63
KLX09F_DZ1	178/19	14		x	+13
KLX03_DZ1b	121/21	10		x	–731
KLX03_DZ1c	125/13	10		x	–757
KLX09E_DZ2	295/14	22	x	x	–67
KLX11_DZ11	065/20	20		x	–439

Additional members in this group (Table 5-4) include KLX11_DZ11. This deformation zone has been modelled as a circular slab and lacks correlation with a ground surface lineament (Figure 5-23). Similar to other such deformation zones modelled in this manner it has a disk radius of 564 m, giving an area equivalent to a 1,000 m by 1,000 m square, and an applied best estimate of true thickness, in this case 20 m. The modelled geometry is centred at an elevation of –439 m above sea level. An elevation and orientation similar to the M1 reflector geometry mean that KLX11_DZ11 can be taken as a member of this series. The deformation zone is brittle with markedly open fractures.

An additional seven discrete deformation zones without associated surface lineaments, with interpreted thicknesses of 10 m or more, are modelled as circular slabs. These structures have been rated as having high confidence as to existence since they are all based on direct drill core evidence. However, essentially all their other assigned properties are generally judged to be of low confidence since the underlying individual judgement of orientation is of low confidence. This reflects the fact that dip directions in all directions have been observed, even though dips to the south and south east dominate. A summary of the available fracture orientation data from the gently dipping deformation zones listed in Table 5-4 is presented in Figure 5-24.

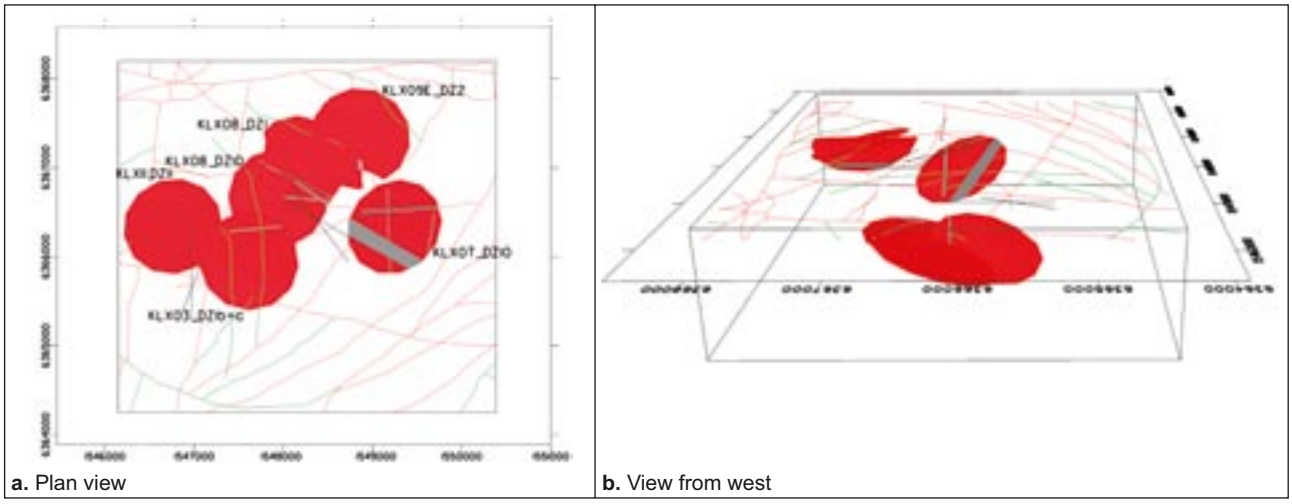

Figure 5-23. *Gently dipping local major deformation zones not linked to surface lineaments, listed in Table 5-4.*

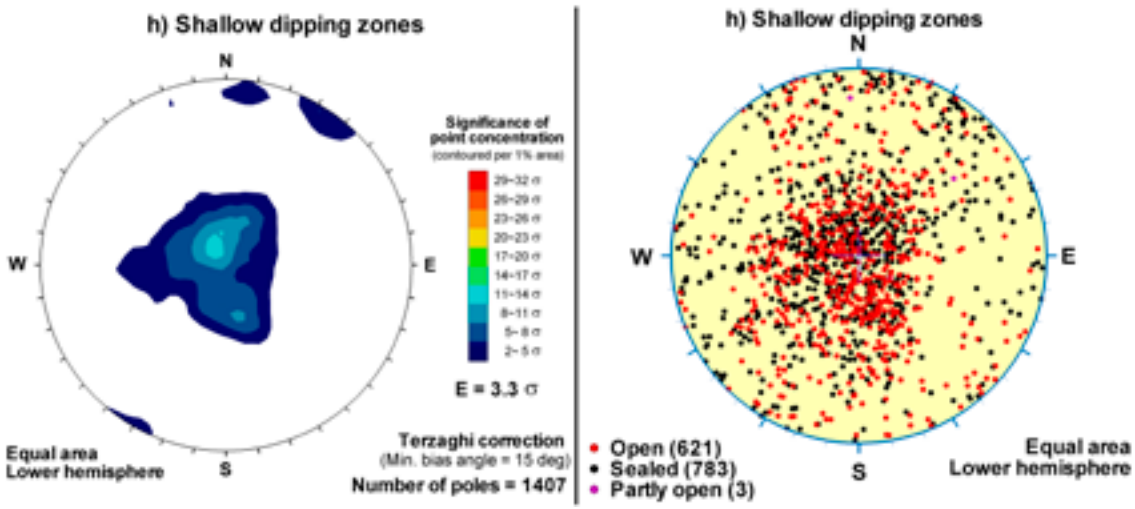

Figure 5-24. *A summary of the available fracture orientation data (visible in BIPS) from gently dipping local major deformation zones KLX03_DZ1b, KLX03_DZ1c, KLX07A_DZ10, KLX08_DZ10, KLX08_DZ01, KLX09E_DZ2, KLX09F_DZ1, KLX11_DZ11.*

5.2.3 Conceptual kinematic understanding of regional deformation zones including geological processes

Ductile framework

Laxemar is bounded to the NW and SE by a system of NE-SW striking broad ductile belts (shown in lilac in Figure 5-25). This gross structural framework was formed when the bedrock still responded to deformation in the ductile regime and discrete, low-temperature, brittle-ductile to ductile shear zones form the most prominent ductile structures in the area.

Deformation zones that were formed in the ductile regime (shown in lilac) are inferred to be related to the waning stages of the Svecokarelian orogeny (c. N-S crustal shortening). Consequently, E-W oriented deformation zones that are ductile, or exhibit a ductile component, are inferred to be characterised by predominant dip-slip components of movements in response to compression, whereas deformation zones oriented in NE-SW and NW-SE direction would be characterised by sinistral and dextral strikre-slip components of movement, respectively.

The brittle-ductile to ductile shear zones vary in size and occur all over the site investigation area. However, the area east of ZSMNE005A is more affected by ductile deformation zones (shown as grey in Figure 5-26 and Figure 5-27) relative to the Laxemar local model area. This is also indicated in the magnetic anomaly map where the eastern area is characterised by a more banded anomaly pattern (Figure 5-26).

The ductile shear zones have developed under upper greenschist facies metamorphic conditions at a temperature of c 450–500ºC. The ductile deformation is presumed to have developed in the time interval 1.81 to 1.75 Ga. A close temporal relationship between the formation of the rocks and the ductile shear deformation is seen by the variable relationships seen in the field between the fine-grained granite and the shear deformation. Some fine-grained granites are affected and cut by ductile shear zones, whereas others lack foliation and truncate the shear zones.

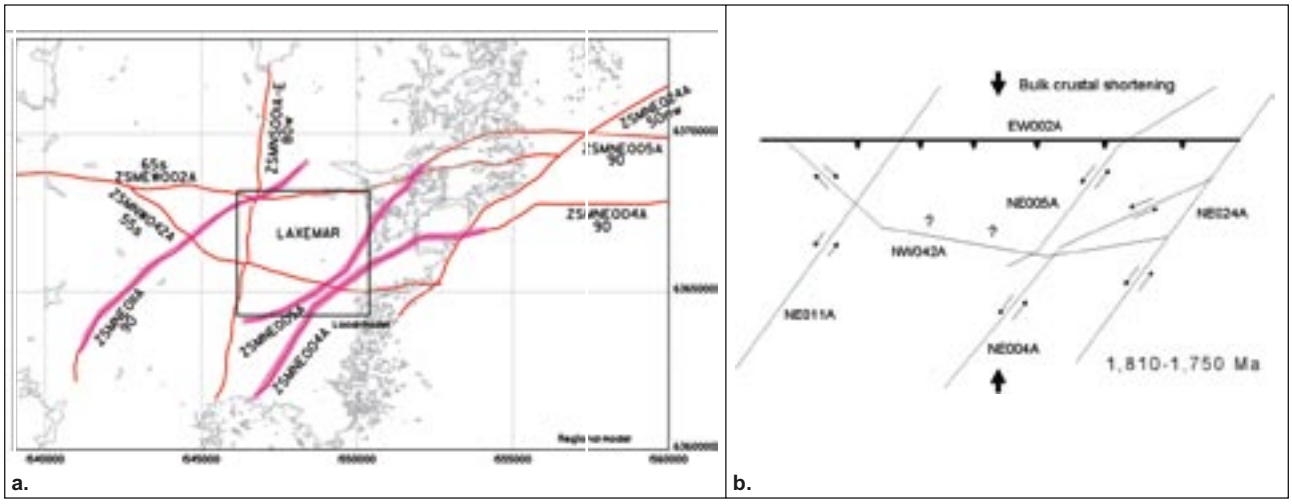

Figure 5-25. *a. Regional framework of deformation zones; three main ductile belts ZSMNE011A, ZSMNE005A and ZSMNE004A, b. A conceptual kinematic interpretation for the time period 1,810–1,750 Ma showing approximate N-S shortening direction, causing sinistral movements for NE-SW striking and dextral movements for NW-SE striking deformation zones.*

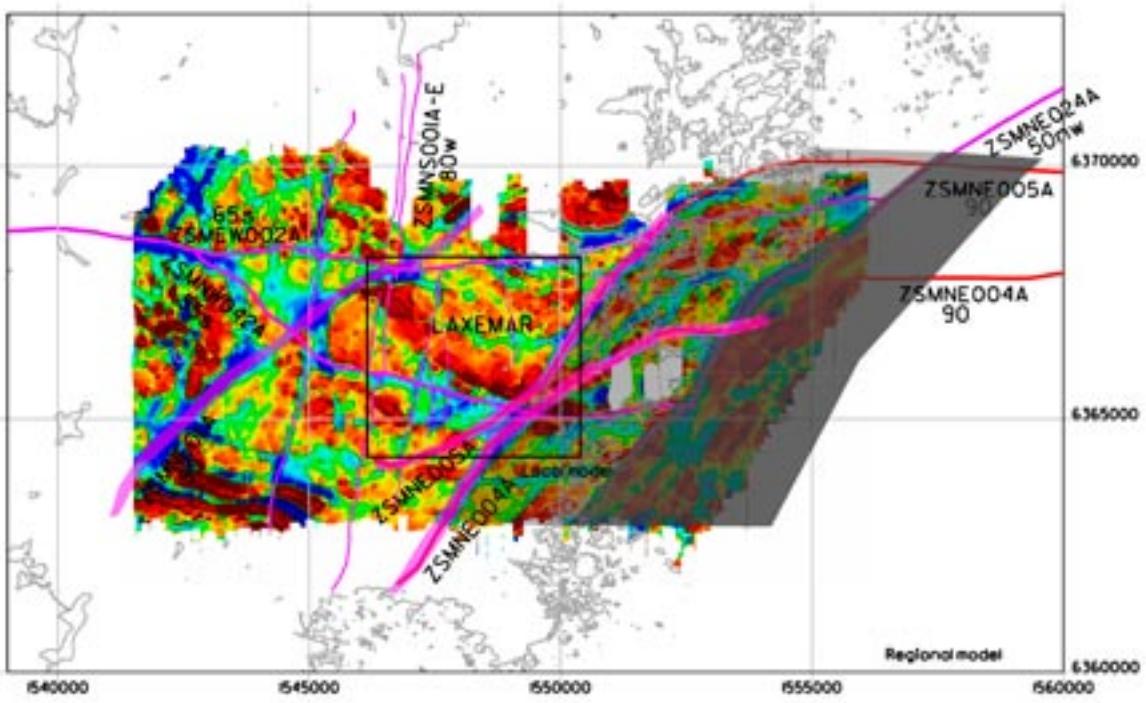

Figure 5-26. *Regional framework of ductile deformation zones displayed on the magnetic anomaly map. Progressively more frequent ductile shearing to the east is shown in grey.*

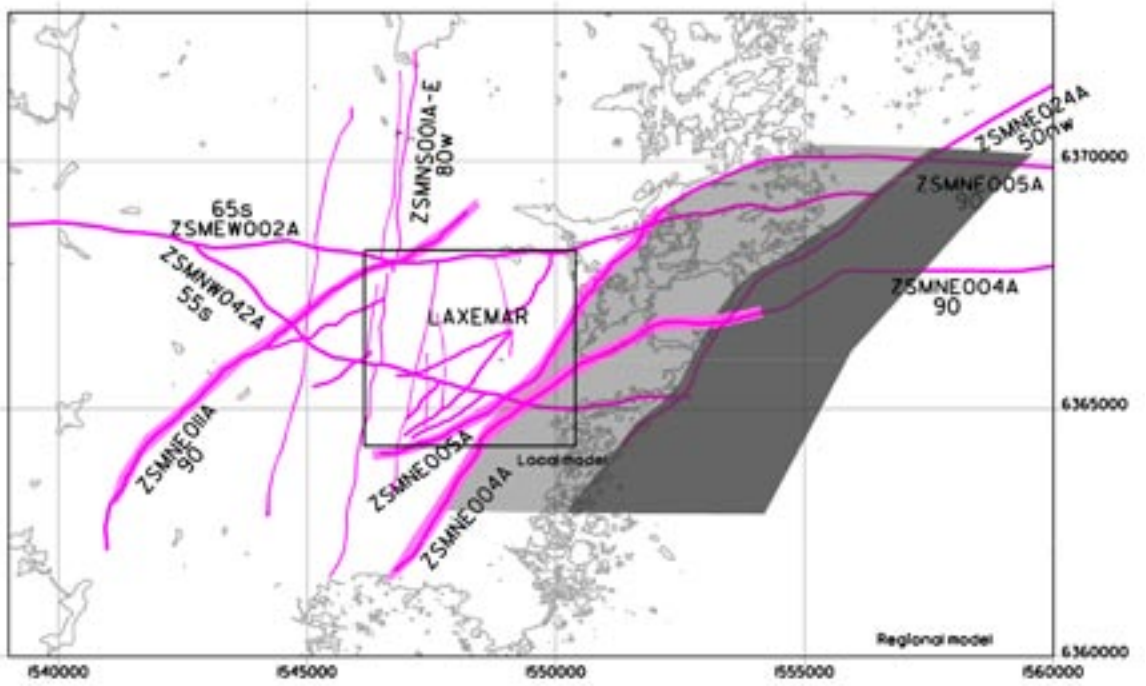

Figure 5-27. *Overall pattern of ductile deformation zones across Laxemar.*

Götemar and Uthammar granite intrusions

The Götemar and Uthammar granites to the north and south of the local model area, respectively, are c 1.45 Ga old (Figure 1-4b), i.e. they are younger than the ductile deformation in the area and the emplacement occurred above the brittle-ductile transition. The emplacements did not impose any ductile strain on their wall rocks. The apparent conformity seen in the field of ductile wall rock structures with the southern contact of the Götemar granite is not related to its emplacement, but is inherited from the 1.81–1.75 Ga ductile deformation history of the surrounding TIB rocks /Cruden 2008/. Elastic bending of the roof of the intrusion during its emplacement may have resulted in brittle reactivation of suitably oriented pre-existing fractures and shear zones in the overlying roof zone /Cruden 2008/.

Brittle framework

There remains a higher uncertainty concerning the time when the bedrock passed through the brittle-ductile transition in the crust and entered the brittle realm. Reactivation has occurred as a far-field effect of the Sveconorwegian orogeny in the southwestern part of Sweden (E-W to WNW-ESE crustal shortening /Söderbäck 2008/). This implies that the kinematics that prevailed in the NE-SW and NW-SE oriented zones during the Svecokarelian orogeny would reverse and be characterised by dextral and sinistral movements, respectively (brittle reactivation is shown in grey in Figure 5-28) during the Sveconorwegian orogeny. The N-S striking, c 0.9 Ga dolerites at Laxemar are implies that the Laxemar-Simpevarp area was subjected to extension in an E-W direction during the waning stages of the Sveconorwegian orogeny /Söderbäck 2008/. These dykes followed, at least in part, pre-existing deformation zones. Thus, the latter were reactivated in connection with the intrusion.

In conclusion, the overall extent and character of the Sveconorwegian brittle overprinting in the Laxemar-Simpevarp area is not known.

Caledonian orogeny and present day situation

The direction of the bulk crustal shortening during the Caledonian orogeny (cf. present day) was approximately WNW-ESE to NW-SE based on the shortening direction in the Scandinavian Caledonides. Thus, the NE-SW deformation zones are inferred to have been exposed to compressional forces during the Caledonian orogeny (Figure 5-29).

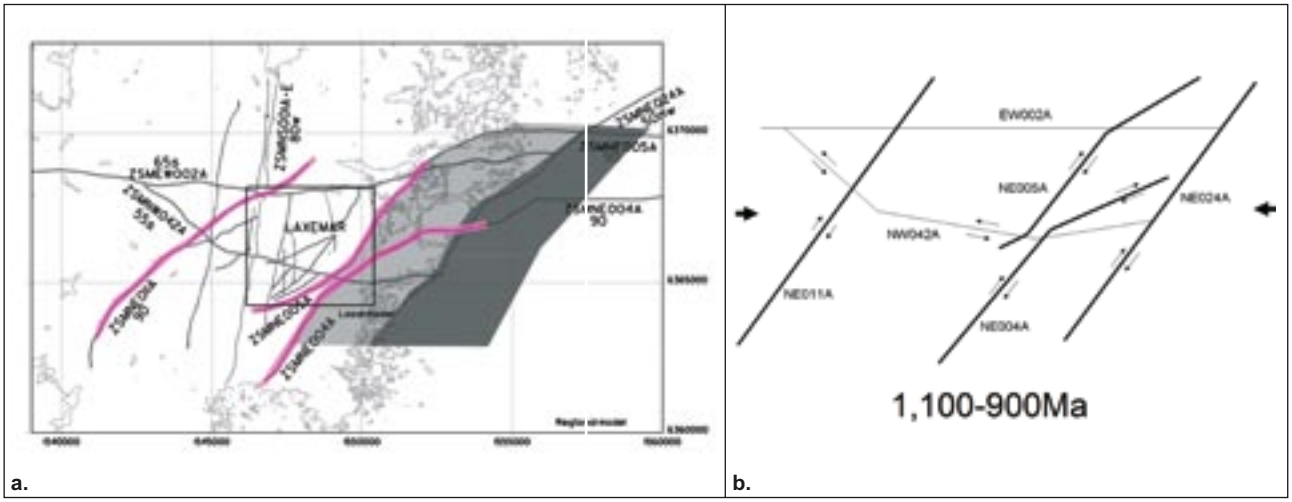

Figure 5-28. *a. Inferred brittle reactivation associated with the Sveconorwegian orogeny, shown in grey, of earlier ductile shear zones. b. A conceptual kinematic interpretation for the time period 1,100–900 Ma, showing E-W compression causing dextral reactivation for NE-SW and sinistral movements for NW-SE striking deformation zones.*

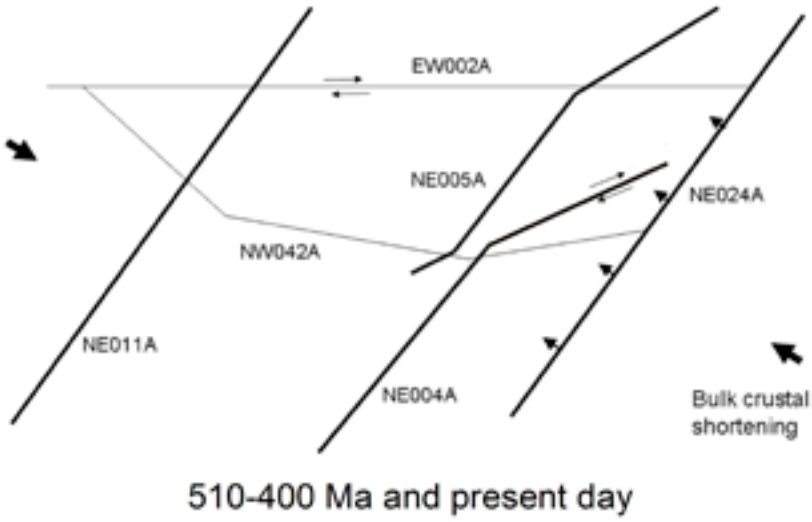

Figure 5-29. *Bulk crustal shortening and conceptual kinematic interpretation during the Caledonian orogeny (510–400 Ma) and the present day. Dextral reactivation is indicated for the E-W and ENE-WSW striking deformation zones.*

5.3 Local model for deformation zones with trace lengths longer than 1,000 m

Seventy (N=70) deformation zones have been modelled deterministically in the local model volume. Fifteen deformation zones or segments of deformation zones are classed as medium confidence in terms of existence and are largely based on the interpretation of topographic and magnetic lineaments. The remaining fifty-five (N=55) are judged to be of high confidence in existence and their interpretation is supported by direct data from boreholes, dug trenches or outcrops. All the deformation zones modelled in the local model volume are listed in Table 5-5 with their basic geometry data and borehole intercepts. Descriptions of individual deformation zones and their geological properties are presented in Appendix 14.

The majority of the deformation zones have interpretations that include an associated linked lineament at the ground surface. However, twenty-five (N=25) deformation zones lack such lineament association. Two of those deformation zones, namely ZSMEW946A and ZSMNW928A, are essentially based on seismic reflector geometries identified during surface investigations and have subsequently been coupled to borehole data. The remaining twenty-three (N=23) deterministic deformation zones, members of the KLXxx_DZxx series of deformation zones (Table 5-5), are based on the interpretation of oriented structural data from individual borehole intervals with interpreted intercept lengths in boreholes that equate to an interpreted true thickness greater than 10 m. All remaining potential deformation zones which are not included in the interpretation of the 70 deterministic deformation zones, as reviewed above, are denoted Minor deformation zones (MDZs). These deformation zones all have an interpreted thickness less than 10 m and are analysed and modelled as part of the statistical model of fractures and minor deformation zones (cf. Chapter 6). The threshold thickness of 10 m for inclusion in the deterministic model was set based on a conservative simplification of the inferred deformation zone length vs. deformation zone thickness correlation (Figure 5-33).

Table 5-5. Summary of deformation zones present in the local model volume.

High confidence in existence

Medium confidence in existence

eoh End of hole *see section 5.3.2

Def_zone	Zone thickness (m)	Zone Strike	Zone Dip	Geological length (km) *	BH	Geometrical sect' top (BH length, m)	Geometrical sect' bottom (BH length, m)	Target_sect' top (BH length, m)	Target_sect' bottom (BH length, m)
ZSMEW002A	100	90	65	30	KAS03	307	495	280	480
					KLX06	300	430	297	425
					HLX02	0	123		
					HLX20	62	184	90	170
					KAS17	238	353 (eoh)		
ZSMEW007A	80	281	44	3.3	KLX01	966	1078 (eoh)	1,000	1020
					KLX02	174	308	180	200
					KLX04	307	427	310	385
					KLX07A	96	179	105	147
					KLX07B	113	200 (eoh)	124	172
					KLX08	220	301	211	300
					KLX09	663	771	682	722
					HLX10	18	85 (eoh)		
					HLX11	0	70 (eoh)		
					HLX12	0	31 (eoh)		
					HLX13	20	103	29	103
					HLX14	44	116 (eoh)		
					HLX21	18	98	18	24
					HLX22	0	163 (eoh)	0	163
					HLX23	1	80	0	80
					HLX24	1	119	0	150
					HLX25	7	57	0	80
					HLX30	0	74	0	80
					HLX31	36	116	50	100
					HLX33	1	40	0	70
					HLX35	142	152 (eoh)		
ZSMEW007C	80	282	44	0.45					
ZSMEW013A	45	85	90	4.4	KA1755A	188	234	180	230
					KAS04	100	184	87	158
					HLX03	0	17		
					HAS01	4	100		
ZSMEW014A	10	100	90	1.2	HLX02	0	16		
ZSMEW120A	50	80	64	1.2	KLX13	480	596 (eoh)	488	596 (base)
ZSMEW316A	30	86	90	2.4					
ZSMEW900A	25	92	57	0.9	KLX17	96	124	100	114
					HLX40	30	56	50	60
					HLX39	59	85	75	85
ZSMEW900B	25	106	78	0.69	KLX17	190	228	193	227
					HLX39	117	156	-	-
					HLX40	61	96	-	-
					HLX41	145	198	-	-
ZSMEW946A	10	80	23	1.5	KLX03	727	739	727	739

Def_zone	Zone thickness (m)	Zone Strike	Zone Dip	Geological length (km) *	BH	Geometrical sect' top (BH length, m)	Geometrical sect' bottom (BH length, m)	Target_sect' top (BH length, m)	Target_sect' bottom (BH length, m)
					KLX08	471	490	478	486
					KLX10	696	707	694	706
					KLX18	575	585	575	585
KLX07_DZ7	30	267	90	>1	KLX07	343	386	347	388
					HLX21	20	71	18	110
					HLX22	76	125		
					HLX23	105	155		
					HLX24	0	26	27	40
KLX07_DZ9	10	253	35	>1	KLX07	448	459	448	459
KLX07_DZ11	30	253	35	>1	KLX07	693	723	693	724
KLX07_DZ12	47	263	41	>1	KLX07	738	785	738	785
KLX08_DZ10	11	79	11	>1	KLX08	925	940	925	940
KLX09_DZ10	25	263	37	>1	KLX09	521	553	520	554
KLX18_DZ9	10	95	50	>1	KLX18	473	488	472	489
ZSMNE004A	150	50	90	>15	HLX19	86	202 (eoh)	139	153
					TASA			302	334
ZSMNE005A	250	60	90	16	KA1755A	22	296	95	140
					KA1754A	26	160	90	115
					KA1751A	50	150 (eoh)	110	114
					KAS04	0	466	131	437
					KA3590G02	20	30 (eoh)	19	30
					KAS12	0	274	19	286
					HLX09	3	108		
					HLX16	0	119		
					HLX17	182	202		
					KAS17	85	353 (eoh)		
ZSMNE006A	130	215	65	2.1	HLX08	0	40 (eoh)		
					KA1061	94	209 (eoh)	198	209
					KA1131B	47	203 (eoh)	173	203
					KAS07	402	602 (eoh)	497	602
					KAS08	440	590	537	601
					KAS09	53	225	50	112
					KAS11	115	249 (eoh)	156	220
					KAS14	38	194	51	91
					KBH02	543	706 (eoh)	667	706
					KAS02	740	924 (eoh)	806	914
					KAS16	228	439	380	430
					TASA			1,240	1,325
ZSMNE011A	100	50	90	10.5					
ZSMNE012A	120	60	45	5.6	HAV02	90	163 (eoh)	90	150
					HAV12	18	136	51	127
					HAV13	0	121		
					HLX018	0 (Top)	181 (eoh)	16	181
					HMJ01	0 (Top)	46 (eoh)		
					KAV01	401	630	400	580
					KAV03	188	248 (eoh)	164	232
					KAV04A	756	928	840	900
					KBH02	107	245	140	194
					TASA			827	
					HLX17	1	22		

Def_zone	Zone thickness (m)	Zone Strike	Zone Dip	Geological length (km) *	BH	Geometrical sect' top (BH length, m)	Geometrical sect' bottom (BH length, m)	Target_sect' top (BH length, m)	Target_sect' bottom (BH length, m)
					HLX18	1	181(eoh)	16	181
ZSMNE018A	50	79	90	1.3					
ZSMNE019A	20	55	90	3.7					
ZSMNE021A	40	32	90	4.7					
ZSMNE024A	80	225	52	>15	OKG				
					HAV11	95	178	124	180
					KSH01A	532	660	540	631
					KSH03A	175	258	162	275
					KAV01A	674	757(eoh)	680	757
					KAV04A	928	1,004 (eoh)	940	1,004
ZSMNE040A	20	30	90	1.6	HLX01	0	31		
					HLX04	21	82		
ZSMNE063A	10	40	90	1.1					
ZSMNE065	10	057	90	1.4					
ZSMNE079A	10	72	90	2.7					
ZSMNE107A	35	225	80	3.1	HLX10	79	85 (eoh)		
					KLX02	682	1,125	770	960
					KLX15	693	762	711	744
					KLX16	221	411	228	434
ZSMNE108A	10	60	90	1.8					
ZSMNE930A	5	67	90	4.2					
ZSMNE942A	15	246	88	2.5	HLX23	124	150		
					KLX10	75	893	103	349
					KLX10B	4	21	0	20
					KLX19	436	462	437	464
ZSMNE944A	10	58	75	1.2	HLX31	129	130 (eoh)		
					KLX18	273	299	284	292
KLX07_DZ10	10	225	28	>1	KLX07	645	655	645	655
KLX11_DZ11	20	65	20	>1	KLX11	488	511	486	513
ZSMNS001A	45	191	81	10.9 (A-E)					
ZSMNS001B	45	187	81	10.9 (A-E)					
ZSMNS001C	45	187	81	10.9 (A-E)	KLX20	169	250	171	234
					HLX36	86	197	111	191
					HLX37	102	156	122	147
					HLX43	17	110	32	82
ZSMNS001D	45	173	81	10.9 (A-E)					
ZSMNS001E	45	185	81	10.9 (A-E)					
ZSMNS009A	25	328	90						
ZSMNS046A	20	170	90	2.1	KLX09G	33	73	40	68
ZSMNS057A	20	6	90	5					
ZSMNS059A	50	192	88	4.8	KLX14	53	129	75	125
					HLX34	24	114	33	113
					HLX35	59	142	116	142
					HLX38	23	99	23	67
ZSMNS141A	20	12	90	2.5					
ZSMNS945A	10	176	90	2.0					
ZSMNS947A	20	178	90	1.8	HLX42	116	153 (eoh)		
HLX28_DZ1	10	180	20	>1	HLX28	75	89	75	89
					KLX11	144	154	142	163
					HLX32	98	110	104	114

Def_zone	Zone thickness (m)	Zone Strike	Zone Dip	Geological length (km) *	BH	Geometrical sect' top (BH length, m)	Geometrical sect' bottom (BH length, m)	Target_sect' top (BH length, m)	Target_sect' bottom (BH length, m)
KLX04_DZ6b	14	156	67	>1	KLX04	886	914	887	914
KLX04_DZ6c	30	177	42	>1	KLX04	935	972	935	972
KLX07_DZ13	10	348	65	>1	KLX07	810	835	817	836
KLX08_DZ1	27	0	18	>1	KLX08	100	131	100	131
KLX09F_DZ1	14	178	19	>1	KLX09F_ DZ1	8	22	8	22
KLX21B_ DZ10-12	10	192	80	>1	KLX21B	455	764	559	707
KLX28_DZ1	13	182	33	>1	KLX28	14	33	14	33
ZSMNW042A	40	105	55	8.3	HLX26	34	81	50	80
					HLX32	91	135	20	130
					KLX15	963	1,000 (eoh)	977	1,000++
					KLX27	210	257	209	255
ZSMNW047A	25	138	90	1.3					
ZSMNW052A	15	116	90	1.1	KLX06	203	260	200	260
ZSMNW088A	20	89	90	3.2					
ZSMNW119A	10	130	90	2					
ZSMNW928A	0	120	28	1.5	KLX02	764	764	770	770
					KLX04	899	899	880	880
					KLX09	670	670	682	682
ZSMNW929A	20	114	90	1.6					
ZSMNW931A	50	165	90	3.8					
KLX03_DZ1b	10	121	20	>1	KLX03	762	774	759	777
KLX03_DZ1c	10	125	13	>1	KLX03	789	801	789	801
KLX08_DZ6	10	296	89	>1	KLX08	396	416	396	416
KLX09E_DZ2	22	295	14	>1	KLX09E	76	106	76	105
					KLX09B	63	86	75	79
					KLX09C	70	94	81	86
					KLX09D	73	98	81	90
					KLX09F	64	92	68	84
					KLX09G	79	100		
KLX10C_DZ3	10	300	35	>1	KLX10C	36	58	35	59
KLX10C_DZ7	10	323	39	>1	KLX10C	119	142	121	140

5.3.1 Geometric model

As an aid to a better understanding of the modelled deformation zone geometries, a series of sections through the deterministic deformation zone model are presented in Figure 5-30, Figure 5-31 and Figure 5-32.

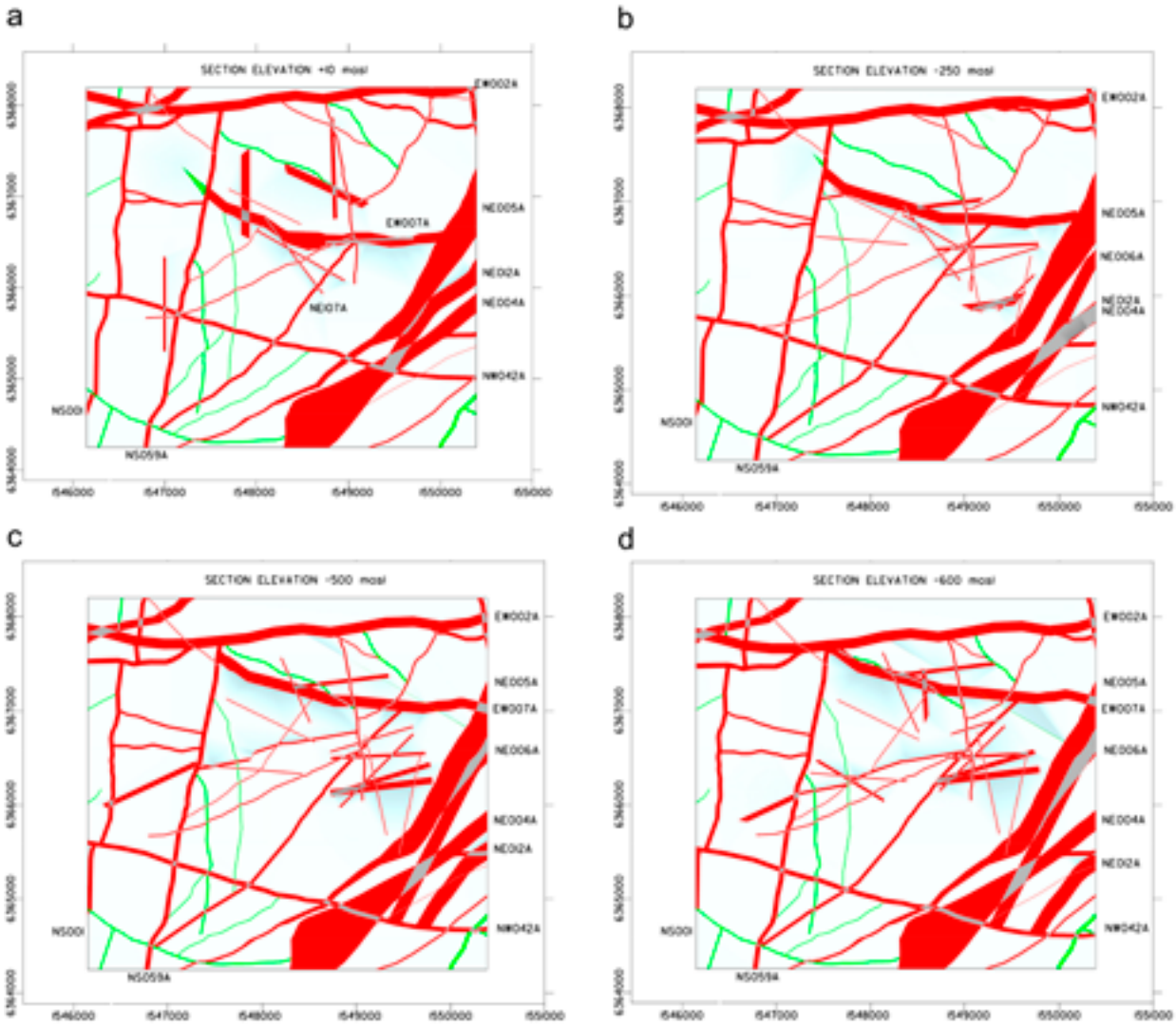

Figure 5-30. *Horizontal sections through the deformation zone model. a) Section elevation +10 m above sea level. b) Section elevation –250 m above sea level. c) Section elevation –500 m above sea level. d) Section elevation –600 m above sea level.*

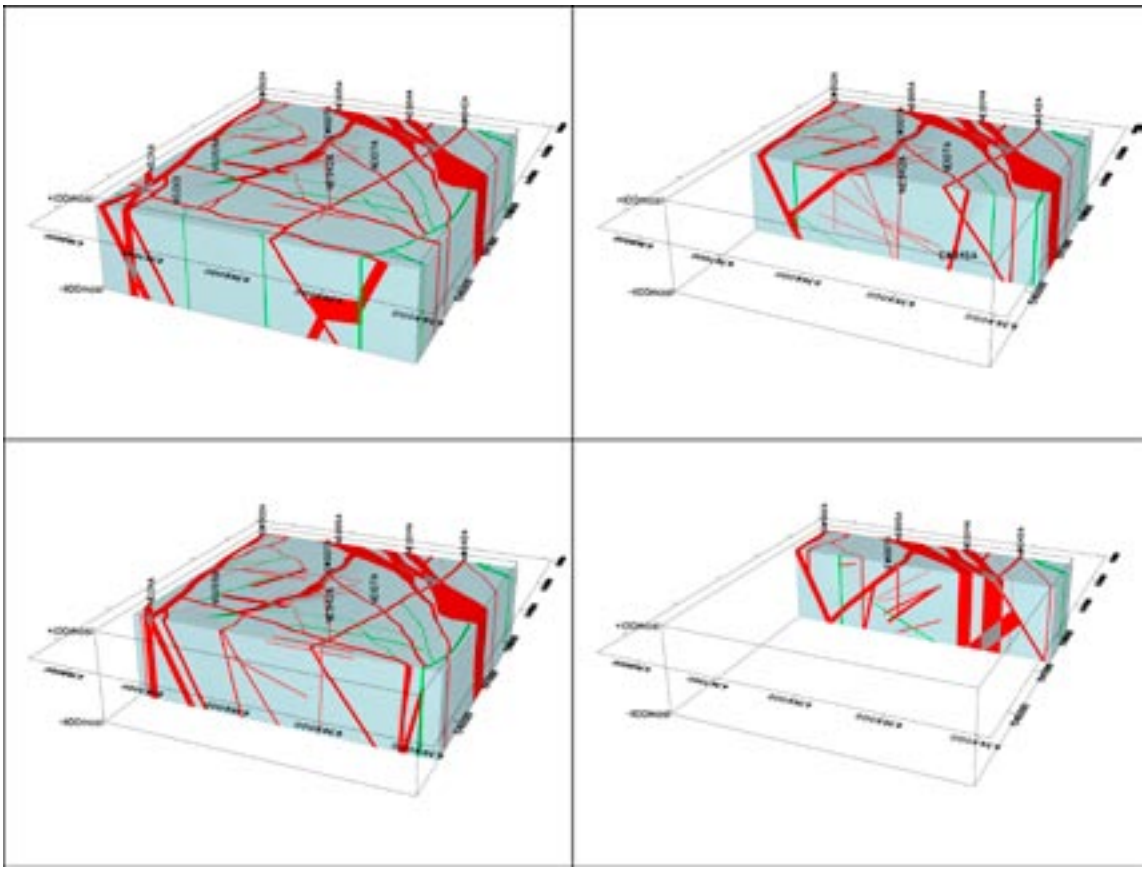

Figure 5-31. *N-S sections, progressing eastwards through the deformation zone model.*

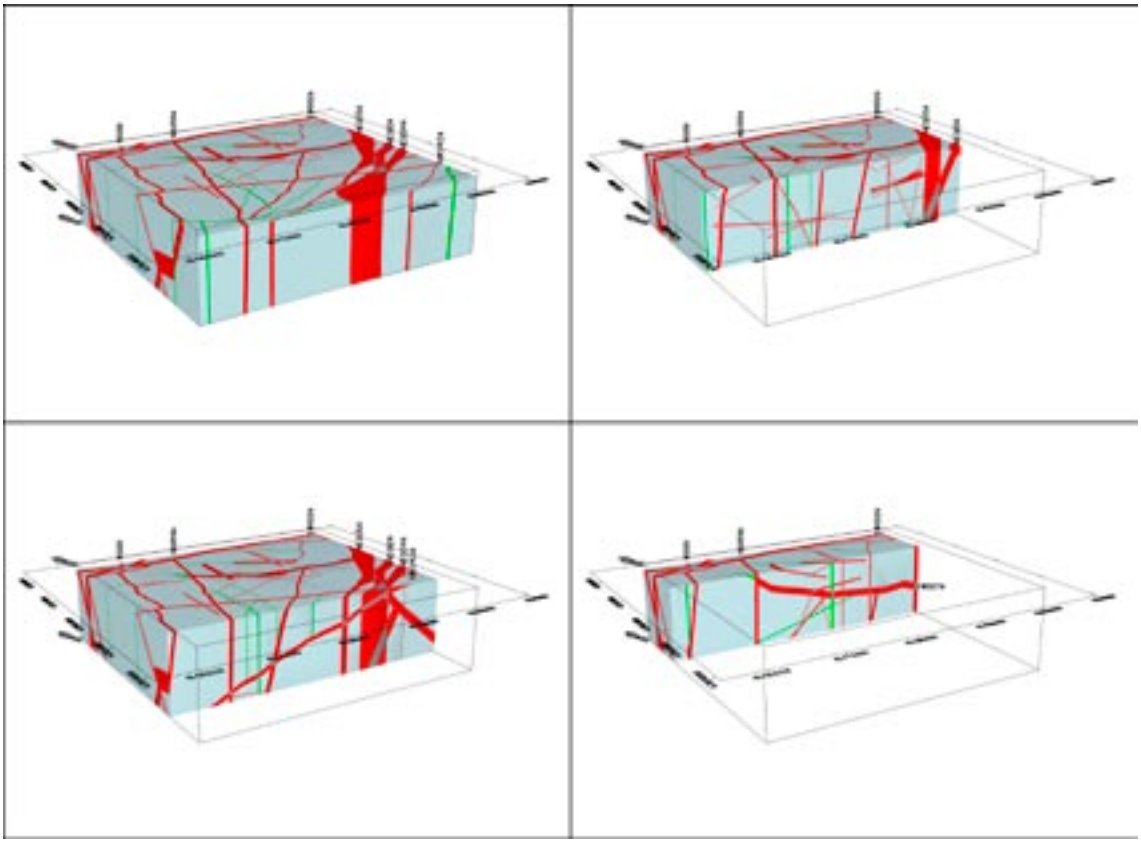

Figure 5-32. *E-W sections, progressing northwards through the deformation zone model.*

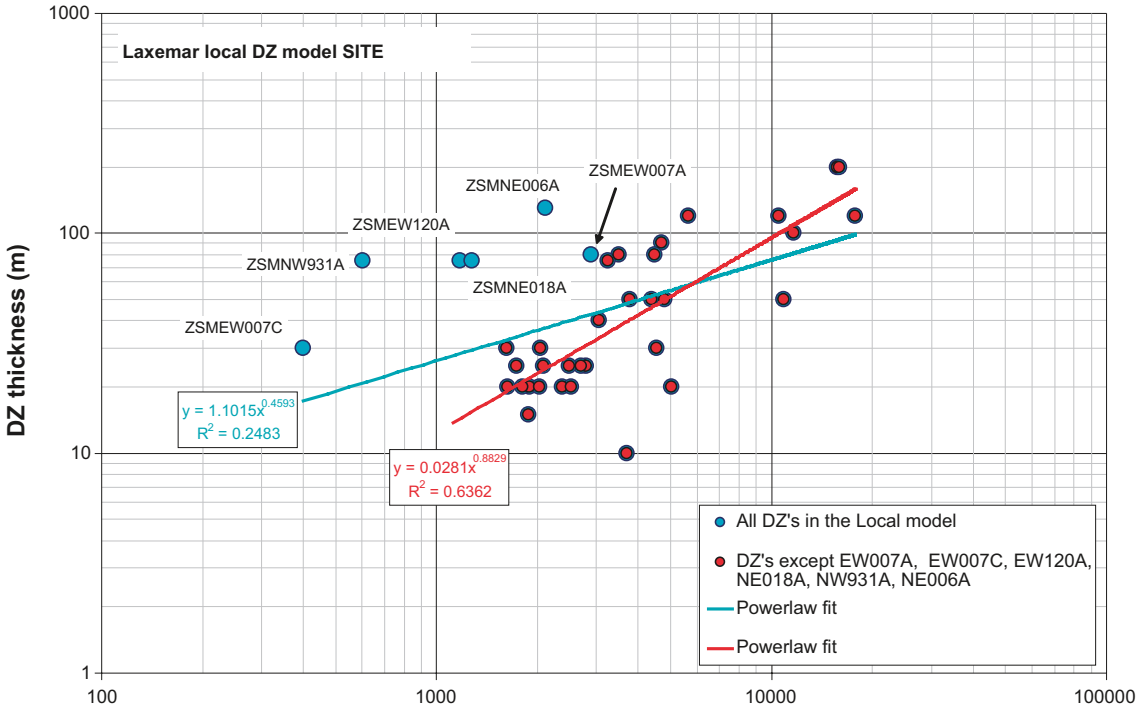

Figure 5-33. *Correlation between interpreted thickness and length for deformation zones in the Laxemar local model.*

5.3.2 Assignment of properties

Table 5-5 presents an excerpt of basic geometrical properties of each of the seventy deformation zones that are included in the local scale deformation zone model. The coupled descriptions of individual deformation zones and their geological properties are presented in Appendix 14. Some general remarks on the properties of deformation zones in the local scale model are given below.

Orientation and length (size)

The orientations, the quoted strike and dip, of the deformation zones in the zone descriptions and property tables are the average modelled values given by RVS based on the input modelling constraints. This means that these values are relevant to the scale of the modelled objects since orientation, like most other parameters, is closely linked to the scale of observation. In practice the presented strike is an average value of the trend of the associated surface lineament that has been used as input data to RVS and the dip has been constrained by the modeller, or calculated based on the resultant geometry from a series of control points, mostly borehole intercepts. The range of strikes and dips are presented to give an indication of variability.

The 'geological length' of the deterministic zones is presented in Table 5-5 and Appendix 14. This entity implies the overall traceable length of the surface expression of the interpreted deformation zone at the regional model scale. The assessment of geological lengths at this scale is not truncated by, or restricted to the local scale model boundary. It is anticipated that such length estimates only give a rough indication of deformation zone size since such values clearly vary with the elevation of measurement and the interplay with neighbouring (intersecting and truncating) deformation zones. Any estimate of deformation zone or lineament length implicitly involves a judgement of continuity related to the scale of assessment and the realisation that deformation zone geometries are not fully continuous in reality. For the local model area a minimum deformation zone trace length of 1,000 m has been applied. Lineaments with lengths greater than 1,000 m have been taken to represent Local major or Regional deformation zones

whereas lineaments shorter than 1,000 m have been assumed to represent Minor deformation zones. In a small number of cases, where a lineament crosses extensive rock outcrops without any evidence of deformation, the lineament or rather deformation zone trace has been broken up into shorter segments. This process is based on best judgement of data from a number of sources rather than on an applied absolute criterion.

The estimates of deformation zone thickness presented in Table 5-5 (and elsewhere) refer to true thickness. More specifically, the single thickness values given in the property tables in Appendix 14 refer to modelled true thickness. This means that a value has been assigned that aims to provide a representative overall thickness applicable over the entire length of the zone in the deterministic model. This modelled deformation zone thickness generates the geometrical intercepts listed in the property tables and defined in Figure 5-1. It is based on all available data, both from surface and at depth. The presented range of deformation zone thickness is generally based on an inspection of surface related data since borehole data are often limited to a single, or at best, a very small number of borehole intercepts for a specific deformation zone. It is judged that the surface geophysical surveys, namely magnetic and resistivity, along with the detailed topographic elevation models (DEM) give the best indications as to how the thickness of a deformation zone varies laterally and by inference with depth. It is accepted that this type of surface expression is in fact linked to an apparent rather than a true thickness but it is still considered to provide the best estimate with consideration made to likely lateral variations in deformation zone dip. These thickness estimates include both deformation zone cores, transition zones and, to a certain extent, local splays. As mentioned earlier the widths of the low velocity anomalies from seismic refraction surveys are taken as giving an indication of the presence and thickness of more highly fractured rock associated with brittle deformation zone cores, whereas the magnetic anomalies are interpreted as giving an indication of the thickness of both the highly fractured core and the transition zones. The modelled thickness envelope encompasses both ductile and brittle features though due to reactivation the brittle component generally gives the greater thickness value. Exceptions to this are the major complex ductile belts, ZSMNE011A, ZSMNE004A and ZSMNE005A, where the complex ductile thickness is inferred to greatly exceed the brittle component.

Deformation style

An indication as to whether an individual deformation zone has a ductile, brittle or mixed character is indicated in the property tables and deformation zone descriptions presented in Appendix 14. At the scale of local major and regional deformation zones there are no deformation zones which are solely ductile. Many deformation zones have a ductile origin but all show clear signs of brittle reactivation. Where possible an indication has been given as to whether the brittle or ductile character is dominant at the current deformation zone condition. At a smaller scale, when studying MDZs and individual borehole intercepts, it is clearly possible to identify zone or deformation indicators that are solely ductile. A single deformation zone, ZSMEW007A, which has been investigated by a number of boreholes, is the only deformation zone that is solely brittle with no evidence of an earlier ductile phase. Additional details concerning the brittle fabric are included in the descriptions of individual borehole intercepts that are included along with the property tables in Appendix 14.

Alteration

Red staining caused by a fine-grained dissemination of hematite can be found associated with a majority of the deformation zones. However, it seems to be particularly extensive and characteristic of the E-W striking deformation zones, particularly the dominant deformation zones ZSMEW002A, ZSMEW007A and ZSMNW042A. It is this red staining which contributes to the high contrast seen in the low-magnetic anomalies associated with the deformation zones. Other alteration types related to the deformation zones are also listed in the property tables.

Fracture orientation

The Terzaghi-corrected fracture pole concentrations from 'best source' borehole intercepts are presented. By best source is implied that, where possible, a borehole is selected which has the cleanest interception with the target deformation zone, rather than using information from a borehole that intercepts the deformation zone obliquely, or where interference from other structures is suspected. In some cases uncorrected measurements from ground surface /trench measurements are presented.

Fracture frequency

Terzaghi-corrected fracture frequency is presented. Open and sealed fracture frequencies are given separately in an attempt to provide at least a general indication of fracture condition and character within the deformation zone. The estimates take into account sections of the core that are mapped as sealed networks. This is done by taking the inferred number of fractures as being equal to the sealed section length / rock clast length, per sealed network section. However, the presented fracture frequencies do not take into account sections of crush which are provided separately for clarity.

Crush zone

The number and overall combined thickness of crush zones are provided. The total crush thickness has been adjusted to some degree to give a better indication of true thickness. It should be pointed out that the assessment is simplistic and it should be appreciated that any deformation zone's internal architecture is likely to be complex and crush zones need not necessarily run parallel to the overall deformation zone orientation. As for fracture orientation and fracture frequency a 'best source' borehole intercept(s) has been selected.

As described by /Drake et al. 2006/ crush zones are mapped separately during the drill core mapping and often represent zones characterised by increased hydraulic conductivity. The fracture mineralogy of these crush zones is summarised in Figure 5-34.

Fracture mineralogy of deformation zones

Fracture fillings identified in the deformation zones during Boremap logging are listed in the property tables in Appendix 14 and Figure 5-35. The fracture mineralogy concerning the rock mass in general is discussed in Section 3.6.5.

The most frequently found clay mineral, in addition to chlorite, is corrensite (mixed layer chlorite/smectite or chlorite/vermiculite clay) where the smectite or vermiculite layers are swelling. Other identified clay minerals are illite, mixed-layer illite/smectite (swelling) and a few observations of smectites. Generally it can be expected that there is a general tendency towards clay minerals being underrepresented in the core loggings, mainly due to difficulties in determining clay minerals macroscopically when mixed with other minerals but also due to possible loss of loose and soft phases during the drilling. A schematic fracture filling-sequence from Laxemar is described in Section 3.6.5.

5.4 Evaluation of uncertainties

Deterministic deformation zones interpreted with low and medium confidence are observed indirectly through lineament interpretations at the surface and are modelled with a vertical dip. Deterministic high confidence deformation zones have dip angles according to information obtained from boreholes, seismic surveys, and in some cases from tunnels. The confidence levels of all deformation zones included in the local model volume are indicated in Table 5-5. Confidence levels and a judgement of the likely spans of the individual key descriptors associated with the deformation zones, such as dip, length and thickness, are included in the deformation zone descriptions and property tables in Appendix 14.

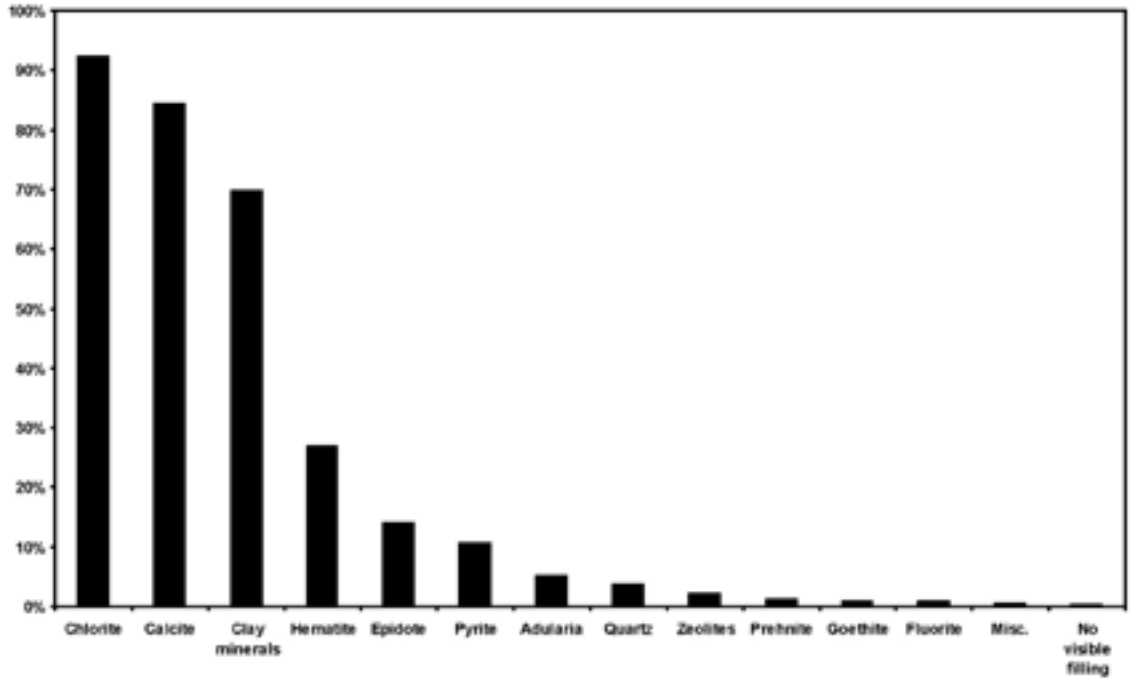

Figure 5-34. *Histogram of relative abundance of fracture minerals in crush zones as inferred from boreholes KLX02 through KLX29A as the percentage of fractures containing a given mineral. The total number of crush zones is 477 /Drake et al. 2008/.*

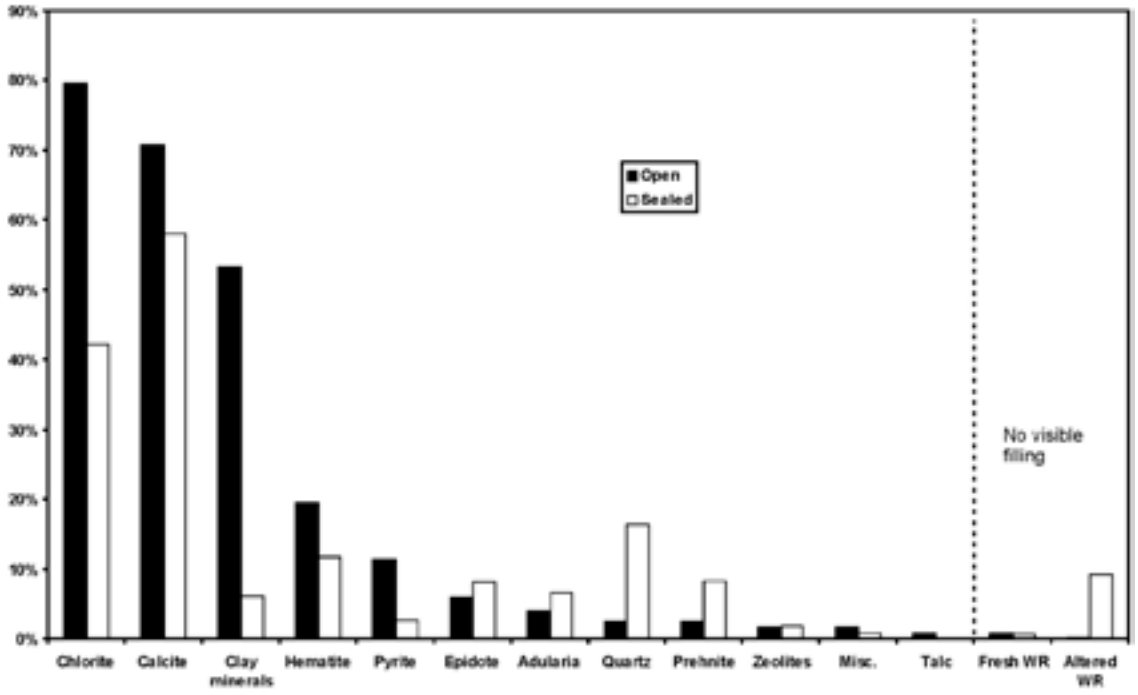

Figure 5-35. *Histogram of fracture minerals in open and sealed fractures found in ESHI interpreted deformation zones. Data from KLX02–KLX29A, number of open fractures= 10,427, number of sealed fractures = 7,869 /Drake et al. 2008/.*

A total of 70 deterministic deformation zones have been modelled in the local scale model volume. Forty-five of these deformation zones have an associated surface lineament whilst twenty-five have no such association. Of those with associated lineaments, thirty are classified as high confidence while fiftheen are classed medium confidence. Twenty-four deformation zones lacking an associated surface lineament are classed as high confidence since they are centred on a given borehole intercept. Whilst these deformation zones centred on boreholes are high confidence in terms of existence, the confidence levels of the majority of other associated descriptors are medium or low. It is important to note that these latter deformation zones are modelled deterministically based on their interpreted orientation that in turn gives inferred true thicknesses of 10 m or more (in relation to the borehole geometry). The threshold thickness of 10 m is taken as being very roughly equivalent to a deformation zone threshold length of 1,000 m, based on available site information (Figure 5-33). Even if such a deformation zone has an interpreted thickness considerably greater than 10 m, a standardised 564 m radius slab has been used to represent the deformation zone since the confidence levels associated with deformation zone orientation, thickness and extent are all considered to be low. However, it should be noted that this methodology does lead to the zones' equivalent areas being systematically underestimated.

No deformation zones with an attributed low confidence in existence occur within the local scale model volume. A total of one hundred and seventy two (N=172) deformation zones are inferred to occur in the regional model. The uncertainties in the deformation zone model outside the local model area area are largely dependent on the inherent uncertainties of the lineament map, which gives the fundamental surface information regarding the zones at this scale.

The interpretation of deformation zones outside the local model area remains largely unchanged compared with earlier model versions. Deformation zones crossing the island of Äspö and the Simpevarp peninsula are generally of high confidence, based on confirmation of their existence from earlier site investigation results. Those deformation zones that do not intercept the Äspö Hard Rock Laboratory or the Simpevarp peninsula are generally classed as medium to low confidence, since they lack direct supporting evidence from drilling or outcrop mapping. These outlying deformation zones have not been the focus of investigation and are modelled without thickness.

As there is a limited amount of sub-surface data specific to any deformation zone, there remain considerable uncertainties concerning the extension at depth of all interpreted deformation zones. It is generally assumed that deformation zones extend as deep as their interpreted surface length, although there are limited possibilities to check this assumption.

Even after the finalisation of the complete site investigation, there exists only one, or a few, borehole intersections for each interpreted deformation zone in the local scale deformation zone model. Even though deformation zones have been verified by drilling at specific depths, the detailed geometrical relationships such as zone termination and connectivity are still considered uncertain for most deformation zones.

Inspection of topographic and geophysical survey data give at least an indication as to how a deformation zone's thickness may vary laterally along its strike. A similar variation in deformation zone thickness is to be expected down dip (with increasing depth). Assessment of dip, like most other parameters, is closely related to the scale of inspection. However, whatever the considered scale, the dip of any deformation zone will vary both along the strike and down dip. An indication of likely variation in dip, at the local model scale, based on all of the information available, is included in the property tables though it must be appreciated the basis for this judgement is generally very limited.

6 Statistical model for fractures and minor deformation zones

The statistical model for fractures and minor deformation zones, hereafter referred to as the geological DFN (or GeoDFN) model, is designed to describe rock fractures and minor deformation zones with an equivalent radius less than 564.2 m (equivalent to the area created by a square fracture with a trace length of 1,000 m). This chapter is intended to serve as a brief summary of the methodology and the results of the GeoDFN modelling work. Readers are referred to /La Pointe et al. 2008/ for more details on methodology, assumptions, and limitations before using the information presented here in downstream numerical models.

6.1 Modelling prerequisites, assumptions, limitations, and feedback from other disciplines

The goal of the geological DFN model is to provide users with a quantitative basis for specifying fracture orientations, sizes, intensity, spatial variability, and correlation to geological factors at any given location within the Laxemar local model area (Figure 2-2) outside of the footprint of modelled deformation zones. Anticipated model users are expected to be hydrological and mechanical modelling, repository design and engineering planning, and to provide inputs in support of repository safety assessment.

The model is presented as a mathematical and statistical description of fracturing observed in the Laxemar local model area; it is not implemented as a specific three-dimensional object model. As such, the model parameterisation can be used in a number of different ways: as a discrete fracture network model for direct stochastic simulation, as input for an upscaled rock block continuum model (block permeability tensors, block elastic modulus tensors, porosity, fracture intensity, storage volumes, etc), or as statistical distributions for inclusion in performance-assessment or Monte Carlo-style risk analysis models. The implementation of the statistical and mathematical description is a direct function of the needs and limitations of the chosen downstream model; therefore, direct implementation of the GeoDFN model is not part of the scope of the modelling process.

6.1.1 Modelling prerequisites

The GeoDFN model is built in conjunction with other site descriptive models. In particular, the deterministic deformation zone (DZ) model (cf Chapter 5) is crucial to the geological DFN; most of the edges of fracture domain volumes (Section 2.4 and Section 6.4.1) are defined at Laxemar by the location and thickness of modelled deformation zones (DZ). This implies that if the DZ model was to change, the GeoDFN model parameterisation could change significantly.

6.1.2 Modelling assumptions and limitations

The GeoDFN model is intended only to be valid for the rock volume described by the boundaries of the target fracture domains (fracture domains are described in Sections 2.4 and 6.4.1, cf Figure 6-9). Use of this model outside of the target fracture domains is not within the intended scope of this model.

The key assumptions required to generate the GeoDFN for SDM-Site Laxemar are:

- Deterministic deformation zones constitute a distinct population of fractures different from the "background" fractures and minor deformation zones (MDZ). As such, the mathematical model for the background fractures and MDZ is a distinct model from that describing the deformation zones.
- For purposes of modelling size (in terms of surface area), fractures can be approximated as planar, circular discs of zero thickness with a radius that can be described using a probability distribution. The actual fracture shape is not required to be circular; square, rectangular, or polyhedral-shaped fractures are fully acceptable, as long as they are simulated using a one-sided surface area which is equivalent to that of a similarly-sized circular disk.
- The length of a minor deformation zone trace or a linked fracture in outcrop is an accurate and appropriate measure of a single fracture's trace length for the purpose of deriving the radius distribution of geologic structures.
- The DFN parameterisation uses a global orientation model that represents the average orientation of sets within the fracture domains. The inherent assumption, which has been tested and is described in detail in the geological DFN summary report /La Pointe et al. 2008/ is that fracture domains at Laxemar principally differ not in terms of fracture set orientations, but in terms of relative intensities of the identified orientation sets.

6.1.3 Feedback from other disciplines

The methodology and implementation for the SDM Laxemar Site geological DFN incorporates many changes and suggestions from expert reviewers of past model versions (including those related to Forsmark). This is a significant advantage of the successive and evolutionary approach to geologic modelling.

Specifically, SDM-Site DFN models incorporate the following changes, based on feedback from both expert reviewers and other modelling teams:

- The DFN implementation has been simplified where possible, so as to make the resulting model easier to understand and use. The fracture domain concept (Section 6.2.1) first used during the Forsmark Stage 2.2 geological modelling has been introduced at Laxemar to maintain consistency between the two sites and with other geological (RD, DZ) models. In addition, orientation sets were simplified so as to use the minimum number of sets to define fractures in the rock mass.
- More emphasis has been placed on quantifying spatial variability. In particular, the spatial variability of fracture intensity, both over the Laxemar local model volume and as a function of depth, has been given special attention based on feedback from expert reviewers.
- More emphasis has been placed on model verification, model uncertainty, and the ranking of alternative size, intensity, and spatial models. This was a request from expert reviewers.

6.2 Modelling methodology

The SDM-Site Laxemar DFN modelling is based on defining and delineating fracture domains in order to quantify spatially the variability of fracturing in the final GeoDFN model. The fracture domain concept, originally suggested in /Munier et al. 2003/, in line with standard practice in structural geology and applied in principle during Forsmark model version 2.2 geological model /Olofsson et al. 2007/ and DFN model /Fox et al. 2007/ modelling, is key to the understanding of the variability of fracture properties. Fracture domains are regions of geologically distinct and statistically similar rock fracturing.

The GeoDFN has four distinct sub-models, which together define the statistical behaviour of fractures and minor deformation zones at Laxemar. These sub-models are:

Fracture domain model: As described in Section 2.4, fracture domains are rock volumes outside of the bounds of modelled deformation zones in which the rocks show statistically-similar fracture characteristics. At both Forsmark and Laxemar, fracture orientation and intensity (both total intensity and the relative intensity of different sets) played a major role in the identification of fracture domains.

Fracture orientation set model: Fracture orientation set modelling consists of the identification and parameterisation of fractures into sets as a function of their orientation in space (pole trend and plunge or dip and dip direction) and possibly of other geological factors. Though orientation is the primary key for classification, other parameters, such as lithology, fracture morphology, aperture, and fracture mineralogy can also be used to divide fractures into sets if they are found to possess statistically-significant differences across the data record. The variability in orientation for each fracture set is defined using univariate Fisher hemispherical probability distributions.

Fracture size/intensity model: This sub-model describes the size of fractures, expressed as equivalent radius and the intensity, in terms of fracture area per unit volume (P_{32}), of the fractures observed in cored borehole records and on outcrops at Laxemar. Fracture size and fracture intensity, though separate properties, are mathematically related, since the value of intensity always pertains to a specified size range. Thus, it is appropriate to combine the size and intensity models into one single sub-model.

Fracture spatial model: The fracture spatial model includes a fairly wide range of analyses of the spatial properties of rock fractures at Laxemar. The spatial model describes how fractures inside fracture domains are distributed spatially, and how their intensity or location scales as a function of model scale.

In the SDM-Site Laxemar geological DFN, the spatial model consists of the following parameterisations and analyses:

- Correlation of fracture intensity to rock domains or host lithology, if possible.
- Analysis of fracture intensity scaling.
- Analysis of the spatial variability of fracture intensity, including depth-dependence
- Quantification of the termination relationships between fracture orientation sets.

6.2.1 Fracture domain model methodology

Fracture domains (abbreviated FSM throughout this chapter) provide a large-scale conceptual framework for describing spatial heterogeneity in rock fracturing. In Laxemar, the fracture orientation set definitions do not change appreciably between fracture domains. Rather, the relative intensity of fracture sets and the location of major regional structural features (DZ) are used to delineate the fracture domains. The SDM-Site Laxemar geological DFN combines statistical analysis of relative fracture set intensities with domain boundaries built atop the current understanding of the geologic and tectonic conditions at Laxemar and their evolution through time.

For the SDM-Site Laxemar modelling, fracture domains were conceptually constrained by rock domain and by regional and local deformation zones, cf Chapter 5. Fracture domains were identified and bounded using:

- The orientation and intensity of fractures by type: only sealed fractures, only open fractures, and all fractures combined.
- The orientation and intensity of regional- and local-scale lineaments derived from airborne laser swath mapping (LIDAR) and high-resolution ground geophysics, cf. Section 3.8.

Fracture domains were described only within a limited spatial footprint (Figure 6-1 and Figure 6-2) hereafter referred to as the fracture domain envelope. The boundaries of the fracture domain envelope are directly related to the amount of cored borehole data, ground geophysical survey lines, and detail-mapped surface outcrops that were available. Data do exist outside of the fracture domain envelope; however, coverage is much poorer and more variable, especially with respect to lineaments shorter than 1,000 m in ground surface trace lengths.

Only outcrop data, linked lineaments from high-resolution ground geophysics / LIDAR surveys, and data from oriented cored boreholes were used in the identification of potential fracture domains. Only fractures that were visible in the BIPS image logs were used in the analysis of preliminary domain definitions. No data from within modelled deformation zones, local minor deformation zones identified in the ESHI analysis, sealed fracture networks, or zones of crushed rock identified in the single-hole interpretations were included in the identification of fracture domains.

Other specific elements of the data analysis included:

- The distinction between ‘open’, ‘partly open’, and ‘sealed’ fractures exists only for fractures recorded in cored boreholes. Fracture aperture data recorded on surface outcrops is highly uncertain due to geomorphic effects and weathering. Therefore, when a domain definition is created based on an increase or decrease in sealed or open fracture intensity, the domain definition is based solely on borehole data.
- Data from boreholes KLX06, KLX02 inside rock domain RSMBA03, and KLX20A west of regional deformation zone ZSMNS001C were excluded. KLX06 was excluded following the recommendation against using borehole data with orientation uncertainties greater than ± 10° /Munier and Stigsson, 2007/. KLX02 inside RSMBA03 and KLX20A west of ZSMNS001C are outside the limits of the fracture domain envelope.

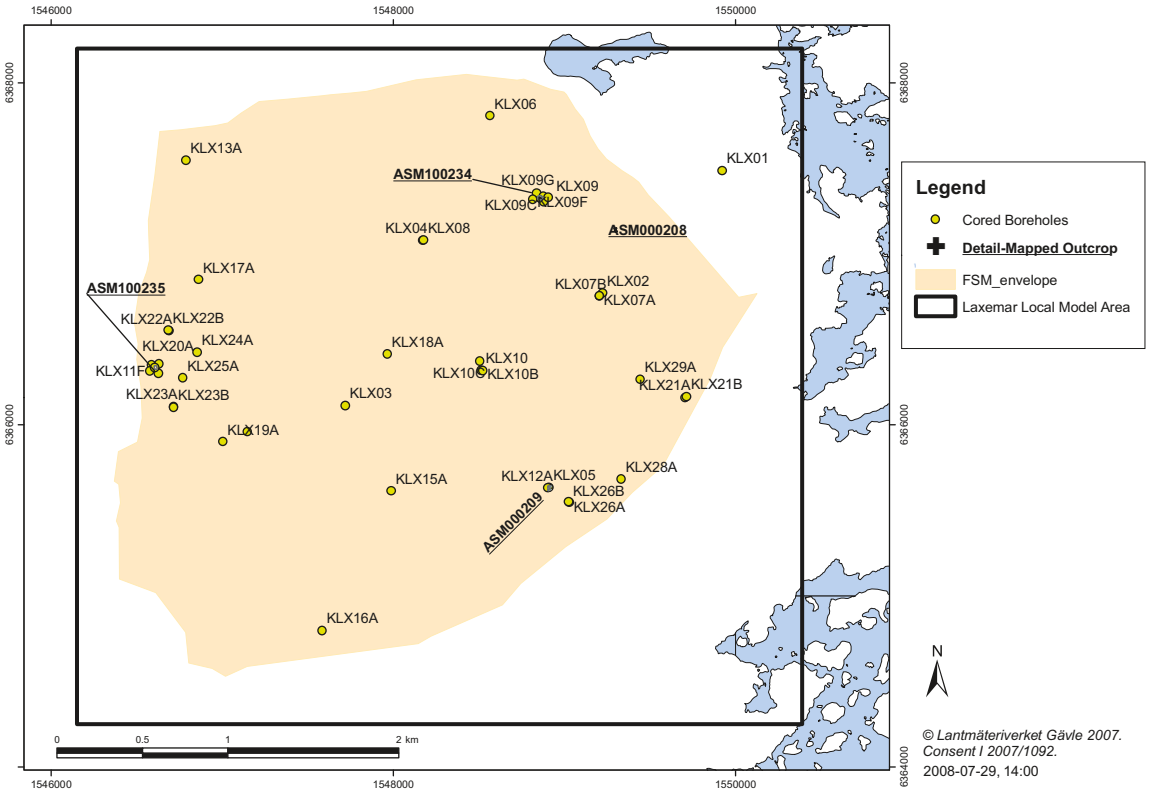

Figure 6-1. *Location of cored boreholes (green dots), detail-mapped surface outcrops, and the fracture domain model limits. Thick black border represents the limits of the SDM-Site Laxemar local model area.*

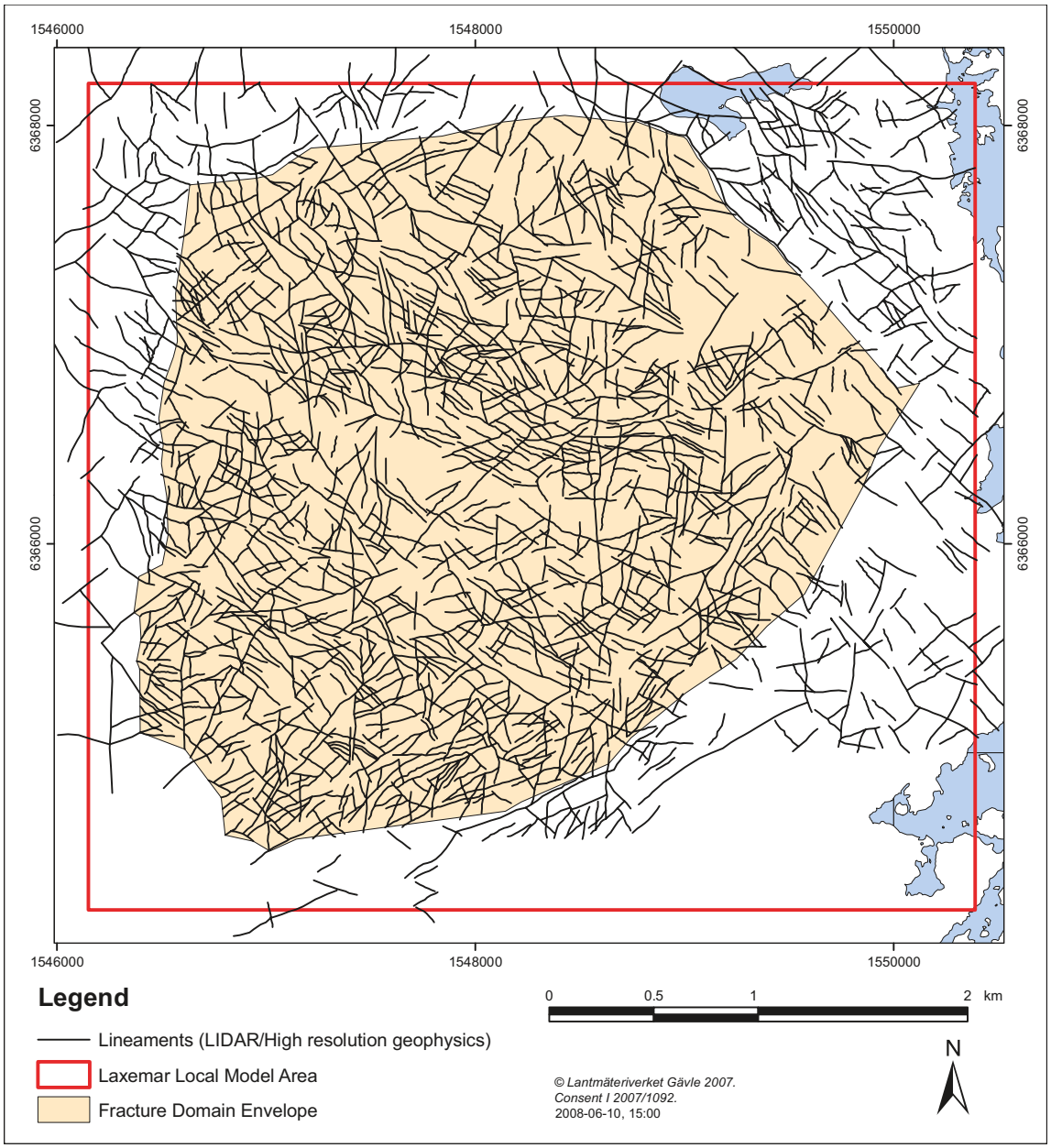

Figure 6-2. *Illustration of the limits of the SDM-Site Laxemar DFN modelling efforts. The fracture domain envelope (yellow area) is assumed to encapsulate the area where surface coverage of detailed lineaments shorter than 1,000 m is of equal resolution.*

The method used to identify and define fracture domains during the SDM-Site Laxemar DFN modelling can be summarised by the following iterative procedure:

- Individual data sets (fracture orientations from outcrops and cored boreholes, along with lineament strike orientations) were analysed. Anomalous orientations or increased fracture intensities were compared to and associated with adjacent deformation zones where possible.
- An initial geological fracture domain hypothesis was formulated by combining relative fracture intensity and the tentative orientation sets with tectonic history, deformation zone geometry, and rock domain volumes from past modelling efforts.
- The approximate boundaries of the tentative fracture domain were defined using the geometries of regional and local major deformation zones.

- Fracture data within the tentative fracture domain were combined, evaluated, and compared to the remaining data set. If the difference in the fracture pattern (in terms of orientation and relative set intensity) between the proposed fracture domain and the global population was considered small, the hypothetical domain was rejected. If the difference in the fracture pattern was relatively large, the hypothetical domain was accepted as a valid fracture domain for DFN modelling purposes. If elements of the data from the proposed fracture domain were found to deviate significantly from the domain mean as a whole, the fracture domain definitions were refined by a detailed analysis of alternative data subsets. The refinement involved adjustments of the spatial definitions of the fracture domain (given geometrical and geological constraints) in order to enhance the deviant characteristics of this fracture domain.

Once fracture domains were identified, the next step was to determine whether the identified domains were a statistically appropriate subdivision of the Laxemar local model volume. Statistical stratification of fracture data into groups will reduce the overall uncertainty of the DFN model if the groups are defined such that the variation within the groups is much less than the variation among the groups. On the other hand, if the groups share similar characteristics, then the reduction in uncertainty by adopting the grouping will be small and possibly not worth the additional effort.

It is important to note that the identification of fracture domains and the identification of fracture orientation sets occurred simultaneously through an iterative process. Tentative orientation sets based on general grouping of fracture poles to major cardinal directions (NE, NW, WNW, NS, etc) are used to identify fracture domains. The sets are further refined statistically through the orientation analysis (described below in Section 6.2.2) for use in the DFN model parameterisation.

As part of the verification of the fracture domain model, a series of statistical tests were performed on the borehole fracture data to determine whether the fracture domains were statistically different from each other, whether the fracture domains (FSM) or rock domains (RD) are statistically reasonable subdivisions for fracturing, and whether the major rock lithologies have sufficiently different fracture characteristics that there needs to be subdivision by lithology. The statistical tests that were used to address these questions consisted of:

- For nominal variables such as roughness, mineral filling, or fracture set designation, cross-tabulation, sometimes referred to as contingency table analysis, is appropriate and widely used /Pearson 1904/. Statistical significance was established using Chi-Squared goodness-of-fit tests.
- For continuous variables such as fracture width, fracture aperture, or fracture length, Linear Discriminant Analysis (LDA) /Davis 2002/ provides a way of assessing whether two groups can be differentiated based on linear combinations of the continuous variables at a prescribed level of statistical significance. Wilk's Lambda test /Shapiro and Wilk 1965/ is used to determine the strength and statistical significance of the separation of continuous variables into linear combinations.
- As fracture intensity is a parameter calculated over a region that may contain more than one fracture set, LDA and cross-tabulation is not an appropriate technique. Instead, standard 1-way ANOVA calculations /Snedecor and Cochran 1980/ were performed on P_{32} values derived for 3 m long intervals in the cored borehole records for each fracture domain. ANOVA calculations examine whether the fracture intensity variation within individual sub groups is less than the fracture intensity variation among groups. In these tests, the Null Hypothesis is that there is no difference. The Null Hypothesis is rejected if the test statistic probability is less than or equal to 0.05.

6.2.2 Fracture orientation set model methodology

The purpose of a GeoDFN orientation set model is to develop a simplified mechanism for simulating fracture orientations which reproduce the patterns of fracture strike and dips seen in outcrop and borehole data. A second constraint is to develop a parameterisation that utilises as few fracture sets as possible to produce a simple, easier-to-use model.

The orientation set model is designed to represent the general fracture orientation patterns at the repository scale. At the scale of individual data sets (i.e. outcrop-local or borehole-local), fracture orientation patterns at Laxemar exhibit complex heterogeneity. This heterogeneity is most likely due to localised geological conditions such as variations in lithology, response to local stress regimes induced by localised faulting or intrusion, or rotation and translation due to relative rock block movements over time. It should therefore be emphasised that the orientation model is not expected to reproduce the local-scale observations of clustered fracture orientations in individual data sets.

As a starting point, borehole and outcrop data were analysed in detail in order to obtain a general understanding of fracture orientation characteristics within the SDM-Site Laxemar fracture domain envelope, cf Figure 6-2 . Fracture orientation patterns were examined in all data sets (boreholes, outcrops, and lineaments); fractures without an orientation (strike, dip) assigned and fractures not visible in borehole image logs (BIPS) were excluded from the orientation analysis.

Fractures without a recorded orientation were excluded from all further analyses. It is important to note that there were relatively few fractures with no orientations; out of the 105,364 fractures in the cored borehole database used for SDM-Site Laxemar, only 164 fractures did not possess an orientation. Most of these were from cored borehole KLX01, which was not used in the model parameterisations.

Fractures not visible in BIPS were assigned to sets after the orientation set model was completed. The reasonableness of this action was evaluated through statistical analysis; borehole fracture data (aperture, morphology, host lithology, mineralogy) for fractures not visible in BIPS were compared to fracture data visible in BIPS through LDA and cross-tabulation, as described in Section 6.2.1. The analysis indicated that, in terms of all fracture properties other than orientation (which was not tested), fractures visible in BIPS and not visible in BIPS are statistically identical.

The analysis was performed on a borehole-by-borehole basis, using the fracture aperture interpretation in SICADA, the rock domain (Chapter 4), the preliminary fracture domain (Section 6.2.1), and the preliminary set divisions suggested during the fracture domain parameterisation. Data agglomeration as a function of rock domain was used as an initial starting point to evaluate whether a global orientation model (across all domains) was viable, or if a division of fracture set parameterisations by fracture domain would better reduce the spatial variability of fracture orientations.

The results of this evaluation (see Section 4.4) supported the concept of a single global orientation model across all fracture domains. Therefore, the SDM-Site Laxemar geological DFN orientation model uses global fracture orientation sets across all fracture domains. However fracture intensity and size distributions were treated as fracture-domain and fracture-set specific properties.

The global fracture sets were parameterised in terms of the location of a set mean pole. All fracture sets are parameterised using a univariate Fisher hemispherical probability distribution, described by the mean pole vector and a concentration parameter, κ, which represents the degree of clustering of pole vectors around the mean pole. Larger values of κ indicate higher clustering of fracture poles around the mean pole vector.

Fracture set assignment for the SDM-Site Laxemar GeoDFN relied on a mix of visual inspection and a quantitative non-linear clustering algorithm. As a first step, the identification of fracture sets was made by visual inspection of contoured plots of cluster significance /Kamb 1959/ and /Robin and Jowett 1986/. Initial fracture set parameters (pole vector orientation and the Fisher concentration parameter) were calculated using a hard sector search /Dershowitz et al. 1998/. In a second step, these hard sectors were transferred into a second subdivision using a univariate Fisher-distributed soft-sectoring of data /Dershowitz et al. 1998/ through a numerical algorithm (for a detailed explanation, see Section 3.4.4 of /La Pointe et al. 2008/. In the final step, fracture set parameterisation was calculated from the soft-sectored data. The reason for including the ini-

tial visual approximation of set orientation was to allow for the possibility of including subjective preferences such as the weighting of different data subset characteristics (including outcrop versus borehole data, open versus sealed fractures, rock domains, and fracture domains). These qualitative factors are difficult to include in strictly numerical approaches.

The decision to separate the orientation analysis into two steps was based on the following factors:

- A visual cluster identification based on geological judgment was preferred, as it allowed modellers to include their geological understanding and consideration of local geological conditions to the analysis.
- A soft sector division is difficult to do manually; therefore clusters are initially approximated in terms of hard sectors and then numerically adjusted using the method of soft sectoring. After soft-sectoring, the univariate Fisher distribution parameterisation can be calculated for each set. Figure 6-3 illustrates the practical differences between hard and soft-sectoring.

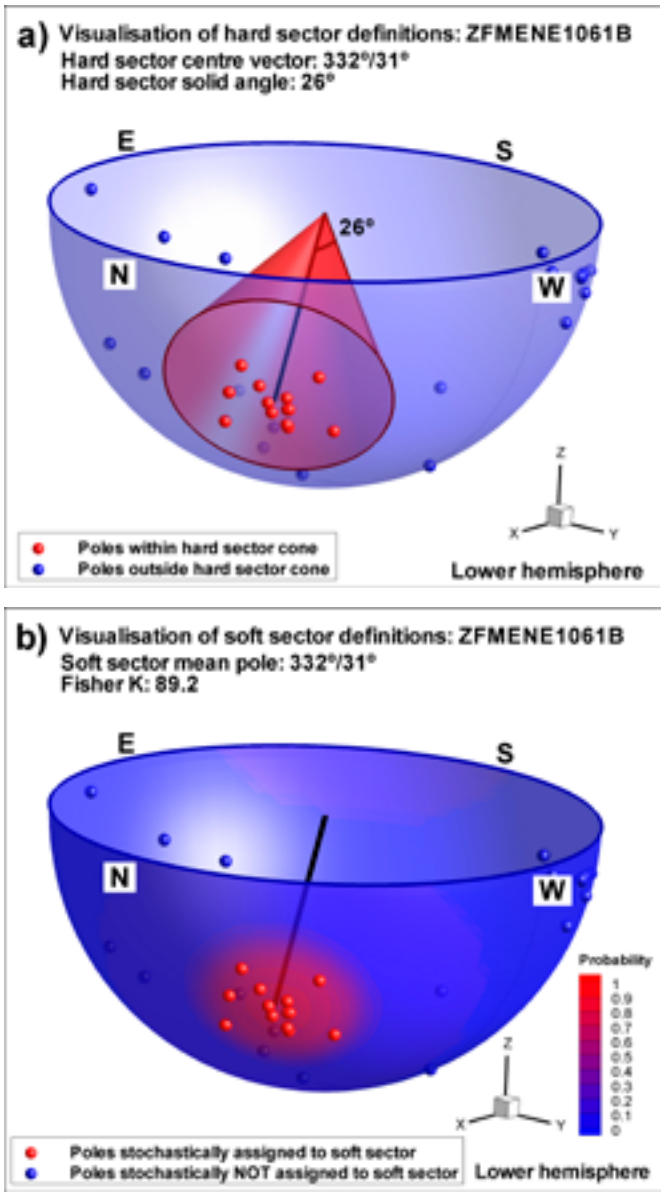

Figure 6-3. *Visualisation of pole cluster sectoring principles used; a) a manually hard-sector defined set is transformed into b) a soft sectoring probability field /taken from Stephens et al. 2007/. Note that, for example, the soft sector P=0.5 is defined by the characteristics of the fractures inside the hard sector, and does not necessarily coincide with the initial hard sector solid angle (26°).*

6.2.3 Fracture intensity model

Fracture intensity can be measured in many different ways. Common intensity measures /Dershowitz et al. 1984/ utilised in past site descriptive models include:

- P_{10}: Lineal fracture intensity, defined as the number of intersections of features (either surface traces along a scanline, or fracture intersections in a borehole log) per unit length, in units of 1/m.
- P_{21}: Fracture areal intensity, defined as the total length of all traces created by the intersection of a plane with a set of fractures, divided by the total one-sided surface area of the sampling plane, in units of m/m^2.
- P_{32}: Fracture volumetric intensity, defined as the total one-sided surface area of all features per unit volume, in units of m^2 / m^3.

For the SDM-Site Laxemar GeoDFN, coupled size-intensity modelling is based upon P_{32}, which was derived from P_{10} recorded in cored boreholes. P_{21}, as computed from the analysis of fracture traces mapped on detailed outcrops across the Laxemar local model area /Hermanson et al. 2008/, is used in conjunction with P_{32} values from boreholes to simultaneously match size and intensity to both outcrop and borehole data, so as to provide a model that is consistent at observational scales.

P_{32} is derived analytically from P_{10} values observed in boreholes using a solution derived from /Wang 2005/ stereological relationships between fracture orientation and fracture intensity. P_{32} is linearly related to P_{10} through the Wang conversion factor, C_{13}, for univariate Fisher distributions which accounts for orientation bias due to linear sampling in a fashion similar to that of the classic Terzaghi correction. P_{32} values were computed on a set-by-set basis for each fracture domain using the global set definitions presented in Section 6.4.2. The mathematical details of Wang's C_{13} are presented in /La Pointe et al. 2008, cf. Section 3.8.1/.

For coupled size-intensity modelling, the arithmetic mean P_{32} value in a given fracture domain is used to determine matches between model parameters and observed fracture intensities. Natural variability in the value of P_{32} at different scales can be accommodated stochastically using a Weibull or Gamma probability distribution, as described in the report section on spatial modelling (Section 6.2.5).

6.2.4 Coupled size-intensity model methodology

Fracture size cannot be directly measured for most fractures, since there are few techniques that reliably delineate the extent of fracture in three dimensions throughout a crystalline volume of rock unless the fracture is quite large. One of the most useful indications of fracture size is the trace pattern that the fractures produce when they intersect surfaces. These are more easily measured, and produce data sets such as lineament maps and outcrop fracture trace maps.

Computing fracture sizes from trace lengths

One way to estimate fracture size is to find a statistical description of fracture sizes that, when quantified as trace length distributions on a surface, matches a measured distribution /Dershowitz et al. 1998/. Because of the small scale of outcrop relative to fracture size, this method may be non-unique /La Pointe et al. 1993/. The non-uniqueness is a problem for data sets with limited scale ranges.

A way to avoid the scale limitations that lead to non-uniqueness is to combine data sets at different scales to extend the range of scale coverage from metres to kilometres. Thus, outcrops ranging up to scales of a few tens of metres can be combined with lineament data sets at scales of tens of kilometres. Figure 6-4 illustrates an area-normalised trace length scaling plot; on this type of plot, the size scaling relationship of fracture traces at multiple scales (outcrop fractures at 0–10 m, MDZ lineaments at 10–1,000 m scale, and local, major, and regional deformation zones at greater than 1,000 m scale) can be simultaneously evaluated.

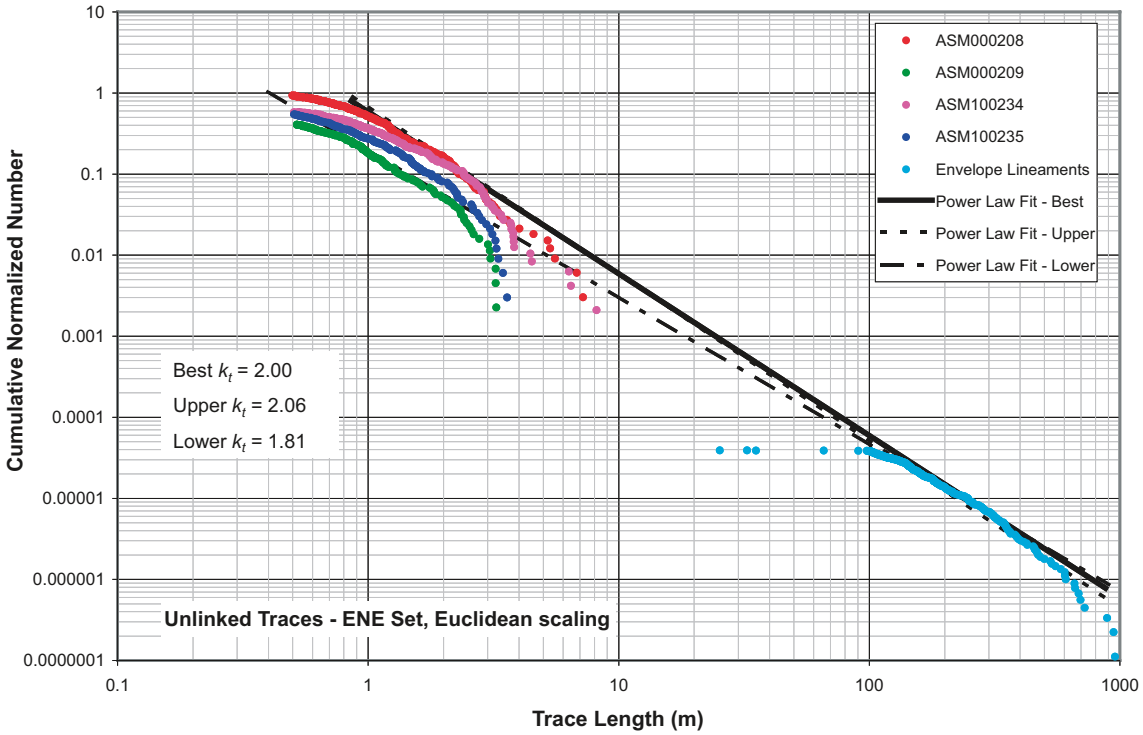

Figure 6-4. *Example area-normalised trace length complementary cumulative number frequency plot. Plots of this type allow for the estimation of fracture size models from data at several different scales (outcrop, lineament, deformation zone, regional deformation zone).*

However, it is important to note that in the SDM-Site Laxemar geological DFN, only outcrop fracture and minor deformation zone traces whose length on the ground surface was less than 1,000 m were used in the size model parameterisation. This is a change from past geological DFN models at Laxemar and Forsmark in that deformation zone traces from the DZ model were not used in the size model parameterisation. This is listed as a key assumption in Section 6.1.2.

The value on the X-axis in Figure 6-4 is trace length and the value on the Y-axis is an area-normalised cumulative number greater than or equal to the X-value. The normalisation can either be Euclidean or fractal, depending upon the appropriate intensity scaling law for the fracture set /La Pointe et al. 2008/. This type of plot is referred to as a Complementary Cumulative Number (CCN) plot. The two important features to observe on such a plot are whether the data at different scales can be approximated by a single straight line, and if so, what is the slope of that line. If the data can be represented by a straight line, then this suggests that there may be a single population of fractures that encompasses the scale range represented by the plotted data, and also that a Power Law function describes the size-intensity of the data. The slope of the line, k_t, is equal to 1.0 less than the scaling exponent, k_r, that describes the parent fracture population, or:

$$k_r = k_t + 1 \qquad \text{Equation 6-1}$$

In the example shown in Figure 6-4, the scaling exponent for the parent radius distribution would be 2.81, 3.00 or 3.06, depending on which line fit is chosen.

The probability density function (PDF) for the parent fracture set to the observed traces, if it conforms to a power-law, has the functional form:

$$P(X \geq x) = \left(\frac{x_{ot}}{x} \right)^{k_t} \qquad \text{Equation 6-2}$$

where x_{0t} is the minimum trace length,

x is any trace length greater than or equal to x_{0t},

k_t is the trace length scaling exponent, and

$P(X \geq x)$ is the probability that a radius value is greater than or equal to x.

The value r_0 corresponds to a minimum trace effective radius of the probability density function, and is not calculated from fitting a power law function to the trace length data shown in Figure 6-4, but rather through simulation.

The value of fracture intensity, size range and scaling exponent is given by Equation 6-3. This relation makes it possible to solve for r_0 through simulation.

$$P_{32}(r_{\min}, r_{\max}) = \frac{\left[r_{\min}^{2-k_r} - r_{\max}^{2-k_r}\right]}{r_0^{2-k_r}} * P_{32}(r_0, \infty) \qquad \text{Equation 6-3}$$

The simulation steps are as follows:

- For a particular set, specify a size model as a power law distribution using the exponent k_r derived from the cumulative trace number plot, and an assumed minimum size value (r_0). Also assume a value for fracture intensity (P_{32}) chosen to produce enough trace intersections for robust computation of simulation trace length statistics. For the simulations used in this report, a minimum radius of 0.5 m and a P_{32} of 0.1 m^2/m^3 were assumed.
- Assign the orientation model for the set.
- Generate the fractures in a volume. If the simulation model volume or area differs from the volume for the data set, then note the ratio of volumes for later plotting adjustment. The volume used in the simulations for 50 m beyond the outcrop limits.
- Place a surface representing the outcrop surface into the model and compute the fracture intersections with the surface.
- Export the traces and plot on a CCN plot. If the simulation volume or area differs from the volume or area of the measured data, adjust the Y-value of the simulated data by the ratio so that the volumes or areas are the same.
- Compare the simulated traces to the measured traces. The ratio of Y-values (cumulative number) for the straight-line portions of the data corresponds to the ratio by which the P_{32} should be adjusted to achieve a match.
- Make the P_{32} adjustment and re-run for verification that the results match the measured data. Everything in Equation 6-3 is known at this point except r_0 and $P_{32}(r_0, \infty)$.
- Using Equation 6-3, specify a desired value of r_0. Since all other values except $P_{32}(r_0, \infty)$ are known, calculate this value which corresponds to the desired lower limit (r_0) of model applicability.

For the SDM-Site Laxemar GeoDFN model, the size/intensity scaling is assumed to be independent of fracture domain for reasons previously discussed. However, the fracture intensity as measured in boreholes in the various fracture domains for each set is not uniform. The differences in measured borehole intensity can be accounted for by finding a value of minimum fracture radius that matches the borehole data.

The increased P_{32} observed in boreholes represents smaller fractures that were not recorded during the detailed outcrop mapping. The outcrop maps do not record any traces shorter than 0.5 m in length; for outcrop intensity matching, the minimum fracture radius ($r_{\min}$) was set at 0.5 m. Therefore, we can calculate the true distribution minimum radius (r_0) by comparing the ratios of the outcrop and borehole P_{32} values through the following steps:

The borehole P_{32} (P_{32BH}) of a given fracture set in a given fracture domain is calculated using the Wang C_{13} conversion factor and 3 m binned P_{10} values.

Given the minimum radius (r_{minOC}) and $P_{32outcrop}$ matched to outcrop data with no imposed maximum fracture sizes, and P_{32BH}, r_{minBH} is adjusted according to Equation 6-4 (which in effect is a re-statement of Equation 6-3):

$$r_{\min BH} = r_{\min OC} * \left(P_{32BH} \Big/ P_{32OC} \right)^{1/(2-k_r)} \qquad \text{Equation 6-4}$$

Alternative fracture size models

The calculation of the intensities is based on the general equation:

$$P_{32}(r_3, r_4) = \left(\frac{{r_3}^{2-k_r} - {r_4}^{2-k_r}}{{r_1}^{2-k_r} - {r_2}^{2-k_r}} \right) * P_{32}(r_1, r_2) \qquad \text{Equation 6-5}$$

Where r_i are specified minimum and maximum radius values, and the $P_{32}(r_1,r_2)$ correspond to the fracture intensity in the corresponding size range. In Equation 6-5, $r_1 = r_0$, $r_2 = \infty$, $r_3 = r_{min}$ and $r_4 = r_{max}$. This equation makes it possible to calculate the intensity for any effective radius size range from another known size range and associated fracture intensity. This equation can also be used to estimate an unknown minimum or maximum size range value if all of the other parameters are known.

The Base Model assumes that the size-intensity scaling exponent for each set does not vary by fracture domain. Under this assumption, the slope of the size-intensity and the cumulative normalised number trace length plots is constant for each set regardless of fracture domain. The differences among domains are in the minimum size, which is estimated from borehole P_{10} fracture intensities.

An alternative to the assumption behind the Base Model case is that the size model does vary between fracture domains. In this alternative model, the minimum fracture size is fixed to the borehole radius. According to the mapping protocols for Boremap, fractures smaller than the borehole radius should not have been recorded in the Sicada database. As such, the measured P_{10} in boreholes represents a minimum fixed size that is related to the borehole radius. The value of P_{10} can be converted into an equivalent P_{32} value by Wang's procedure, and the minimum size associated with that value of P_{32} taken to be the borehole radius. The maximum size is the upper size of the MDZ, or an effective radius of 564.2 m. Let these values be r_1, r_2 and $P_{32}(r_1,r_2)$ in Equation 6-5. They are specific to an individual FSM. Simulations to fit the measured trace length data have already provided values for r_3, r_3 and $P_{32}(r_3,r_4)$. This makes it possible to solve for a fracture domain-specific value of k_r, and presents and alternative to the Base Model that is FSM-specific in terms of its size-intensity scaling exponent.

In addition, there are other conceptual uncertainties that can be expounded upon to produce alternative size-intensity model parameterisations. These are discussed in detail in the geological DFN summary report /La Pointe et al. 2008/, but in summary, they include:

- Euclidean versus fractal size-intensity scaling;
- Choice of outcrop from which the trace length scaling exponent (k_t) is chosen. Three potential matches are included; the steepest slope ('Upper'), the shallowest slope ('Lower'), and the line judged to be the most consistent and appropriate for the fracture domain and fracture set being parameterised ('Best'); and
- Whether linked or unlinked traces are used in the parameterisation of the size-intensity model.

Table 6-1. Summary of alternative size-intensity models.

Model Case	Acronym	Scaling	Linkage	Scaling Exponent Fit	FSM-Specific Scaling Exponent
Base Model, Linked Traces	BM	Euclidean	Linked	Best	No
Euclidean, Upper k_r, Linked Traces	EL1	Euclidean	Linked	Upper	No
Euclidean, Lower k_r, Linked Traces	EL2	Euclidean	Linked	Lower	No
Base Model, Unlinked Traces	BMU	Euclidean	Linked	Best	No
Euclidean, Upper k_r, Unlinked Traces	EUL1	Euclidean	Unlinked	Upper	No
Euclidean, Lower k_r, Unlinked Traces	EUL2	Euclidean	Unlinked	Lower	No
Fractal, Best Fit k_r, Linked Traces	BM_F	Fractal	Linked	Best	No
Fractal, Upper Fit k_r, Linked Traces	FL1	Fractal	Linked	Upper	No
Fractal, Lower Fit k_r, Linked Traces	FL2	Fractal	Linked	Lower	No
Fractal, Best Fit, k_r, Unlinked Traces	BMUF	Fractal	Unlinked	Best	No
Fractal, Upper Fit k_r, Unlinked Traces	FUL1	Fractal	Unlinked	Upper	No
Fractal, Lower Fit k_r, Unlinked Traces	FUL2	Fractal	Unlinked	Lower	No
Euclidean, Change k_r Best Fit, Linked Traces, FSM_N	ESL1_N	Euclidean	Linked	Best	FSM_N
Euclidean, Change k_r Best Fit, Linked Traces, FSM_NE005	ESL1_NE005	Euclidean	Linked	Best	FSM_NE005
Euclidean, Change k_r Best Fit, Linked Traces, FSM_W	ESL1_W	Euclidean	Linked	Best	FSM_W
Euclidean, Change k_r Upper, Linked Traces, FSM_N	ESL2_N	Euclidean	Linked	Upper	FSM_N
Euclidean, Change k_r Upper, Linked Traces, FSM_NE005	ESL2_NE005	Euclidean	Linked	Upper	FSM_NE005
Euclidean, Change k_r Upper, Linked Traces, FSM_W	ESL2_W	Euclidean	Linked	Upper	FSM_W
Euclidean, Change k_r Lower, Linked Traces, FSM_N	ESL3_N	Euclidean	Linked	Lower	FSM_N
Euclidean, Change k_r Lower, Linked Traces, FSM_NE005	ESL3_NE005	Euclidean	Linked	Lower	FSM_NE005
Euclidean, Change k_r Lower, Linked Traces, FSM_W	ESL3_W	Euclidean	Linked	Lower	FSM_W
Fractal, Change k_r Best Fit, Linked Traces, FSM_N	FSL1_N	Fractal	Linked	Best	FSM_N
Fractal, Change k_r Best Fit, Linked Traces, FSM_NE005	FSL1_NE005	Fractal	Linked	Best	FSM_NE005
Fractal, Change k_r Best Fit, Linked Traces, FSM_W	FSL1_W	Fractal	Linked	Best	FSM_W
Fractal, Change k_r Upper, Linked Traces, FSM_N	FSL2_N	Fractal	Linked	Upper	FSM_N
Fractal, Change k_r Upper, Linked Traces, FSM_NE005	FSL2_NE005	Fractal	Linked	Upper	FSM_NE005
Fractal, Change k_r Upper, Linked Traces, FSM_W	FSL2_W	Fractal	Linked	Upper	FSM_W
Fractal, Change k_r Lower, Linked Traces, FSM_N	FSL3_N	Fractal	Linked	Lower	FSM_N
Fractal, Change k_r Lower, Linked Traces, FSM_NE005	FSL3_NE005	Fractal	Linked	Lower	FSM_NE005
Fractal, Change k_r Lower, Linked Traces, FSM_W	FSL3_W	Fractal	Linked	Lower	FSM_W

The magnitude of the impacts of these conceptual uncertainties is quantified and discussed in the DFN uncertainty analysis (Section 6.3.2), but size-intensity model alternatives are presented in the geological DFN summary report for all variants. Table 6-4 lists the various size-intensity model alternatives explored during SDM-Site Laxemar geological DFN modelling. A final size-intensity model alternative is chosen after the completion of the DFN model verification (Section 6.3.1); the verification case results are ranked to determine which size-intensity model alternative performs the best. The best-performing model is then carried through as the recommended geological DFN size-intensity model.

6.2.5 Fracture spatial model methodology

Spatial analysis quantifies how the location, size, termination, and fracture intensity of each set varies spatially. A spatial model makes it possible to extend local measurements of fracture intensity to other portions of the repository volume where there is no data. It also relates to the scaling of fracture intensity. Certain types of spatial models, such as Poissonian or fractal, imply that fracture intensity will increase, remain the same or decrease as a function of scale according to particular equations. Scaling behaviour is important to quantify as the scale at which fracture data are obtained may not be the scale at which it is used for subsequent modelling or calculations.

For the SDM-Site Laxemar geological DFN, fracture orientation has already been determined not to vary spatially; i.e. all fracture domains utilise the same orientation-based sets (see Section 6.2.2). Also, for the preferred DFN model parameterisation (BM), the fracture radius exponent (k_r) does not vary as a function of fracture domain. As such, only the fracture intensity scaling model, the location model for fracture centres, the variation of fracture intensity (including depth-dependence), and the termination relationships between fracture sets are free to vary spatially.

Fracture location and intensity scaling model

Spatial analysis quantifies how the fracture intensity of each set varies with spatial scale. A spatial intensity scaling model makes it possible to determine an appropriate mathematical model for the spatial clustering of fractures, as well as how to relate fracture intensity measured at one scale to fracture intensity at other scales of interest.

An efficient way to examine the spatial/scaling characteristics of fracture intensity is through the Mass Dimension. The Mass Dimension, D_m, describes how intensity varies with scale for fractal data sets. The Mass Dimension of a fractal data set is given by the equation:

$$N(r) = \rho r^{Dm} \qquad \text{Equation 6-6}$$

where ρ is a constant,

r is the scale,

D_m is the Mass Dimension, and

$N(r)$ is the mass, or number of things at the scale r.

The form of this equation indicates that plotting data on doubly-logarithmic axes will produce a straight line if the data conforms to this power law representation of intensity versus scale. For the situation in which the scaling exponent or mass dimension D_m equals the Euclidean dimension, the pattern is Poissonian. This means that the intensity is scale-independent. If the area or volume of rock is doubled, the fracture intensity remains constant, but the number of fractures doubles. If the data approximates a straight line but does not have a scaling exponent that equals the Euclidean dimension, then the pattern is fractal and characterised by the constant, ρ, and the scaling exponent, D_m. The scaling exponent is the slope of the line plotted on doubly-logarithmic axes.

There are two sources of data for calculating the mass dimension of fracture intensity: outcrops and boreholes. The borehole data consist of the positions of fractures along the borehole. The borehole has a Euclidean dimension of 1.0 (essentially a line). Borehole data offers the possibility to calculate the mass dimension over scales approaching the length of the borehole. A disadvantage of using borehole data is that it quantifies the scaling behaviour in a particular direction; it is possible that other directions may have a different scaling exponent or model, and unless boreholes are drilled in a very wide variety of directions, the three-dimensional scaling behaviour may not be well characterised by analyses of borehole fracture data.

Outcrops, on the other hand, provide for a two-dimensional characterisation. While this added dimension provides insight into the scaling behaviour, it is limited to the scale of the outcrops, which is something on the order of 30 m for the outcrops studied in Laxemar. Despite this scale limitation, it complements and compensates for one of the weaknesses of the borehole analyses, which is quantification of the scaling behaviour in the horizontal directions. Together, the mass dimension analyses of borehole and outcrop data provide a three-dimensional model for the variation of fracture intensity. Should the data not conform to a power law representation as given in Equation 6-6 then it is necessary to evaluate other types of spatial and scaling models. If Equation 6-6 does approximate the data, then there is no need to investigate further spatial and scaling models.

The mass dimension and the fracture intensity scaling model are interlinked; in particular, a mass dimension that indicates Euclidean scaling also implies that fracture centres have a uniform probability of being located anywhere in space (i.e. a homogeneous spatial density). This is consistent with a Poisson point-process model for fracture centres

Fractal intensity scaling implies that at some scale, the distribution of fracture centres is not random, and instead follows a different model (fractal clustering, nearest-neighbour clustering, etc). The fundamental assumption for the SDM-Site Laxemar geological DFN model is that, though fracture intensity (both total and relative set intensities) may vary between fracture domains, inside a single fracture domain and outside the footprint of deformation zones, fractures obey Euclidean intensity scaling and are (at scales useful to geological modellers) located in space following a Poisson point process.

For a detailed discussion of the mathematics behind the mass dimension calculations, as well as the implementations of the analysis of the mass dimension of borehole and outcrop fracture data, see Section 3.6.1 of /La Pointe et al. 2008/.

Depth-dependence of fracture intensity

Systematic variations of fracture intensity with depth govern how surface fracture data should be used with sub-surface borehole fracture data to infer fracture intensity at proposed repository depths. Since the variations may be functions of fracture set, fracture domain and fracture type, it is important to separate out these effects to evaluate possible systematic depth dependences. Borehole orientation effects on the fracture intensity were mitigated by using the volumetric fracture intensity P_{32}. The use of P_{32} requires that fracture intensity be calculated over a finite borehole length. A 3 m borehole length was chosen, as it provides sufficient depth resolution without producing an unduly high number of intervals with no fractures, which can make it harder to detect systematic depth trends should they exist. Only data and intervals outside of identified deformation zones were included.

The results are displayed in the geological DFN summary report /La Pointe et al. 2008/ as a histogram with a bar for each 5 m depth increment, as well as a line representing a 10-interval (50 m) moving-average.

Spatial variability of fracture intensity

It has been suggested /Dershowitz 1984/ that, in the absence of other controlling factors such as lithology or deformation zones, P_{32} for a system exhibiting Euclidean scaling behaviour with

fracture centre locations approximated by a Poisson point process, should follow a Gamma (Γ) distribution.

Alternatively, fractures can be modelled as failures following a 'weakest-link' type model /Weibull 1951/. Such a model implies that the strength of a material with flaws will decrease with specimen size, as the probability for a weak flaw increases with specimen volume. The failure rate in models of these types follows a Weibull distribution.

Spatial variability in fracture intensity was evaluated by fitting both Weibull and Gamma distributions to fracture P_{32} data derived from cored borehole logs outside of identified deformation zones and inside fracture domains. All distributions are evaluated on a set-by-set basis, by domain. In addition, the analysis is conducted at several different scales (3 m, 9 m, 15 m, 21 m, 30 m, and 51 m) so as to quantitatively evaluate the effect that simulation scale will have upon the variability of fracture intensity. Goodness-of-fit is evaluated qualitatively through the visual analysis of empirical CDF versus model CDF plots, through quartile-quartile plots, and quantitatively using the Kolmogorov-Smirnov goodness-of-fit test /NIST 2007a/.

Fracture set termination matrices

Fracture termination relationships have the potential to affect both hydrogeological and rock mechanical models, and are therefore an important part of the spatial model parameterisation.

Fracture terminations are expressed as a matrix. The columns of the matrix represent the target fracture set (the set that is being terminated against), while each row represents the orientation set being parameterised. Terminations are quantified as the percentage of traces belonging to one set that terminate against another set. A fracture trace is considered to 'terminate' against another fracture if its endpoint lies within 5 cm of another fracture trace without cutting across it, has been mapped in SICADA as terminating against another fracture in a 'T' or 'Y' intersection, and if the termination makes geological sense (i.e. if a fracture terminates against a lithological contact such as a dyke or vein, and the contact has then been fractured at a later date, the original intersection between the first fracture and the lithological contact is not termed an intersection). Matrices were computed for all fracture domains for which outcrop trace data existed.

An example of a fracture termination matrix is illustrated below as Table 6-2. In the sample termination matrix, to determine the percentage of fractures in the ENE Set (row 1) that terminate against the N-S set (column B), one reads the percentage from cell address B1 (25%). The total percentage termination can be interpreted as a proxy for the relative timing of fracturing at a given location; the higher the percentage of fracture terminations, the younger the features observed are likely to be. The percentages can also be interpreted as a probability value; for a given fracture, in a given set, on a given outcrop or in a given fracture domain, where the percentage is considered equivalent to a probability that the fracture will terminate against another fracture.

The methodology behind determining fracture termination matrices is described in detail in Section 3.6.2 of /La Pointe et al. 2008/.

Table 6-2. Example termination matrix utilizing dummy values.

		A **ENE**	B **N-S**	C **WNW**	D **SH**
1	**ENE**	0	25%	15%	5%
2	**N-S**	1%	0	3%	5%
3	**WNW**	20%	40%	0	20%
3	**SH**	10%	10%	15%	0

6.3 Model verification and evaluation of uncertainties

6.3.1 Model verification

The purpose of verification is to build confidence during model development and to establish the scientific basis and accuracy of the model within its intended scope of use. Verification is also used to evaluate the strengths and weaknesses of various alternative model cases for particular uses, and provides additional insight into the possible importance of the identified uncertainties on downstream model usage.

Verification in the SDM-Site Laxemar geological DFN modelling was conducted by building a series of small-scale DFN models using FracMan /Dershowitz et al. 1998/, conducting simulated sampling using the extent and geometries of actual outcrops, scanlines, and boreholes from the Laxemar local model volume. The verification was carried out not only for the Base Model, but also all of the identified alternative models.

The verification efforts consisted of the following test cases:

- Test OR-1: Variability of Fisher distribution mean pole vectors and concentration parameters (κ). This verification was similar to the orientation uncertainty assessments conducted as a part of the SDM Forsmark Stage 2.2 DFN modelling; 95% confidence intervals on the mean pole vector and on the Fisher κ were constructed. Then, for each set, the mean pole and actual κ simulated was recorded. These results were then plotted against the 95% confidence regions for the observed data.
- Test OR-2: The relative set intensities (percentages based on the number of fractures, Terzaghi corrected) for each fracture domain were compared to the relative set intensities (percentages based on the P_{32} for the set established for the coupled size-intensity models) to determine if the DFN model accurately reproduced the variation in relative fracture intensity between domains that is the cornerstone of the Fracture Domain model concept at Laxemar.
- Test SI-1: Fracture areal intensity (P_{21}) for simulated fracture traces versus observed outcrop traces was compared for outcrop data within the size range for which the fitted power law curve and the trace length scaling plot are collinear (as was already completed in the Draft Report).
- Test SI-2: Lineal fracture intensity (P_{10}) along simulated scan lines was compared to scan line data recorded on drill-pad outcrops; the trench data was not used for this analysis. The simulated scan lines were modelled using Monte Carlo analysis. The verification metrics are:
  - Simulated versus Actual $P_{10;}$ and
  - Length distribution of simulated versus actual traces.
- Test SI-3: Lineal fracture intensity (P_{10}) and volumetric fracture intensity (P_{32}) of simulated fractures within the minor deformation zone (MDZ) size range in boreholes were compared to the observed P_{10} of MDZ in the ESHI results. The methodology behind this method is described in Chapter 6 of the Level III DFN method-specific report, but involves calculating the minimum size required to match the observed numbers of MDZ in boreholes for different size-intensity scaling cases.
- Test SI-4: Lineal fracture intensity (P_{10}) of simulated fractures in boreholes was compared to observed P_{10} values in a number of borehole sections. The computational time requirements for this test were exceptionally long, due to the need to simulate relatively high numbers of very small fractures. Consequently, verification was completed only for fracture domain FSM_C. FSM_C is the model domain most likely to host a proposed HLW repository at Laxemar (SKB, personal communication to DFN team).
- Test SI-5: The Γ (α, β) and Weibull (κ, λ) distribution parameters for fracture P_{32} were computed at a number of different scales to determine at what scale ranges the spatial variability of fracture intensity can be described using a Gamma or Weibull probability distribution. The chosen simulation scales were: 3 m, 9 m, 15 m, 21 m, 30 m, and 51 m. Fitting a probability distribution to borehole data at scales larger than 51 m is a difficult task; at that scale, there are very few intervals in the cored borehole array that are not interrupted by a minor deformation zone or a deterministic deformation zone. As the geological DFN model explicitly

excludes fractures inside of deformation zones from the model parameterisation, the inclusion of intervals that cross DZ could dramatically skew the results of the distribution fit. As such, test SI-5 was capped at a maximum scale of 51 m. Goodness-of-fit were determined through the Kolmogorov-Smirnov test, with ECDF versus CDF and Q-Q plots included as Appendix F of /La Pointe et al. 2008/.

It should be noted that, for verification case OR-1 and OR-2, there are no 'alternative' cases; the orientation model is static across all fracture domains. In addition, verification case SI-5 also does not have any alternative model cases. The calculation of distribution fit is made based on using the cored borehole data available in each domain, and is independent of the size-intensity model. For the remaining verification cases, Table 6-3 summarizes which analyses were done on which size-intensity model alternative.

Table 6-3. Index of alternative model cases used in the verification of the SDM-Site Laxemar geological DFN.

Size-intensity model case	Case tested in verification?				
	SI-1 (> 0.5 m)	SI-1 (Fit Range)	SI-2	SI-3	SI-4
BM	Y	Y	Y	Y	FSM_C**
EL1	Y	Y	Y	Y	FSM_C**
EL2	Y	Y	Y	Y	FSM_C**
BMU	Y	Y	Y	Y	FSM_C**
EUL1	Y	Y	Y	Y	FSM_C**
EUL2	Y	Y	Y	Y	FSM_C**
BM_F	Y	Y	Y	Y	FSM_C**
FL1	Y	Y	Y	Y	FSM_C**
FL2	Y	Y	Y	Y	FSM_C**
BMUF	Y	Y	Y	Y	FSM_C**
FUL1	Y	Y	Y	Y	FSM_C**
FUL2	Y	Y	Y	Y	FSM_C**
ESL1_N	Y	N/A*	Y	Y	FSM_C**
ESL1_NE005	Y	N/A*	Y	Y	FSM_C**
ESL1_W	Y	N/A*	Y	Y	FSM_C**
ESL2_N	Y	N/A*	Y	Y	FSM_C**
ESL2_NE005	Y	N/A*	Y	Y	FSM_C**
ESL2_W	Y	N/A*	Y	Y	FSM_C**
ESL3_N	Y	N/A*	Y	Y	FSM_C**
ESL3_NE005	Y	N/A*	Y	Y	FSM_C**
ESL3_W	Y	N/A*	Y	Y	FSM_C**
FSL1_N	Y	N/A*	Y	Y	FSM_C**
FSL1_NE005	Y	N/A*	Y	Y	FSM_C**
FSL1_W	Y	N/A*	Y	Y	FSM_C**
FSL2_N	Y	N/A*	Y	Y	FSM_C**
FSL2_NE005	Y	N/A*	Y	Y	FSM_C**
FSL2_W	Y	N/A*	Y	Y	FSM_C**
FSL3_N	Y	N/A*	Y	Y	FSM_C**
FSL3_NE005	Y	N/A*	Y	Y	FSM_C**
FSL3_W	Y	N/A*	Y	Y	FSM_C**

* There is no 'fit range' for r_0-fixed models, as the radius scaling exponent (k_r) is not derived from outcrop trace data.

** Verification case SI-4 only run for domain FSM_C due to computational complexity

The results of the verification cases were ranked in terms of their percentage error, and a Kruskal-Wallis non-parametric ANOVA / Kruskal and Wallis, 1952/ used to evaluate the statistical significance of the alternative model ranking. The ranking is then used to guide the decision on a final recommended size-intensity model alternative. For additional details on the ranking and evaluation process, consult section 3.8.3 of the geological DFN summary report /La Pointe et al. 2008/.

6.3.2 Evaluation of uncertainties

The methodology for quantifying uncertainty consists of identifying the uncertainties that could have possibly significant impacts, and then quantifying those impacts using a measure that is relevant to downstream usage of the geological DFN model. There were three main conceptual uncertainties identified:

- Whether fracture size depends on fracture domain;
- Whether fracture intensity scales in a Euclidean or Fractal manner; and
- Whether linked or unlinked traces are the most appropriate model for assessing fracture sizes from detail-mapped outcrops.

In addition to the conceptual uncertainties, three important parameter uncertainties were identified:

- The uncertainty of the size-intensity scaling exponent (k_r) due to the assumption that not all lineaments represent fractures or minor deformation zones; and
- The uncertainty of the size-intensity scaling exponent (k_r) due to differences among outcrop fracture intensity;
- The uncertainty arising from basing the parameterizations on only the open fracture intensity or upon both the open and sealed fracture intensity in the borehole data.

The primary impacts of the uncertainties listed above on the GeoDFN model are in two areas. The first impact is on the number of large fractures that are likely to be intersected by canisters. The intensity of fracturing for larger fractures in the size range 75 m to 564.2 m represents the component of fracturing that is of the greatest interest for canister safety calculations. In this size range, factures are large enough to potentially have secondary slip induced during earthquakes that might impact safety, yet are small enough that they may be difficult to detect with 100% reliability during site reconnaissance and construction. Uncertainty in the number of fractures in this size range may also be of concern for site hydrology and repository design. The second impact concerns the deposition hole acceptance criteria, which takes into account fractures of approximately 2.7–3 m in radius up to 564.2 m.

These two size ranges (2.7 m–564.2 m and 75 m–564.2 m) are of interest for downstream uses of the GeoDFN model, and as a result, the uncertainty of the GeoDFN model is evaluated for each of these size ranges. The impact of each uncertainty was quantified by comparing the uncertainty in the value of P_{32} in this size range relative to the P_{32} of the base case model. This ratio provides a measure of how much of an impact the uncertainty might have, and whether it would lead to an increased or decreased estimate of P_{32}.

6.4 Derivation of the statistical geological DFN base model

6.4.1 Identification of fracture domains

The fracture domain model used in the SDM-Site Laxemar geological DFN modelling is based on the tectonic concept that three deformation zones (ZSMEW002A, ZSMNE005A and ZSMEW007A) constitute the primary control on fracturing within the Laxemar local model area. In addition, several other local major deformation zones (ZSMNW0042A, ZSMNS059A,

ZSMNW928A, ZSMNE107A and ZSMNS001C serve as boundaries to the fracture domains. These additional local major deformation zones represent block boundaries inside the regional tectonic framework defined by the NE-SW striking ductile zones. The controlling deformation zones used in the establishment of the fracture domains at Laxemar are illustrated below in Figure 6-5.

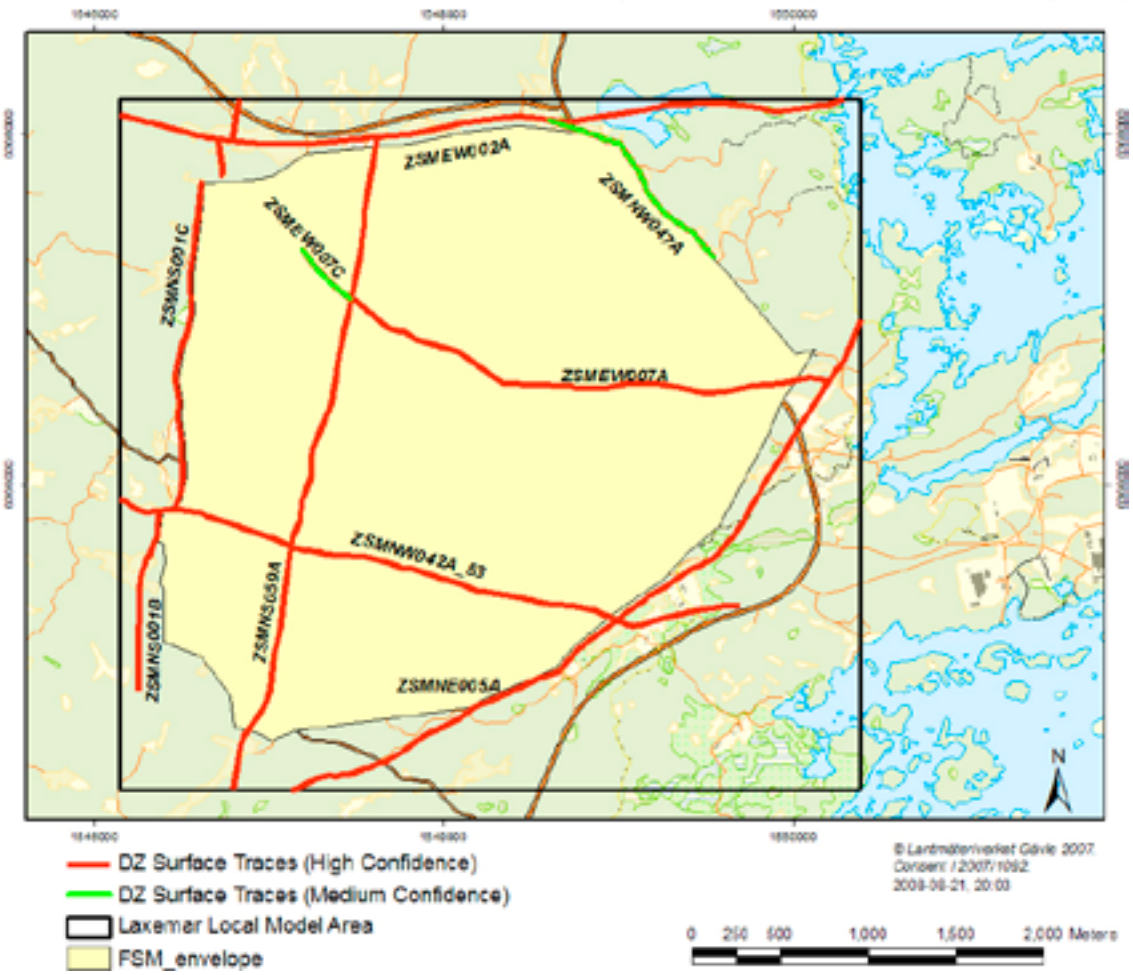

Figure 6-5. *Illustration of major deformation zones ZSMEW007A, ZSMEW002A, ZSMNW042A, ZSMNE005A, ZSMNS059A and ZSMNS001C, in the context of the fracture domain envelope used for SDM-Site DFN modelling. These deterministic deformation zones appear to influence the fracture pattern inside the fracture domain envelope (yellow). All northings and eastings coordinates are in the Swedish RT90(25 gon W) coordinate system.*

The analysis of fracture orientations, relative set intensities and tectonic histories suggest that there are six distinct fracture domains within the Laxemar model sub-region. The domains are illustrated below in Figure 6-9 through Figure 6-12. These six domains are:

- Domain FSM_EW007: This domain represents a volume of rock, approximately 250 m thick on the south side and 100 m thick on the north side of ZSMEW007A, in which distinct fracture patterns were observed in cored borehole records. This domain features a reduced intensity of both N-S striking fractures and open sub-horizontally-dipping fractures (Figure 6-6). In this domain, most open fractures appear to belong to the WNW-striking set. Both fracture intensity and orientation have been interpreted as being affected by E-W striking deformation zone ZSMEW007A. FSM_EW007 terminates against deformation zone ZSMNE005 in the east, and is assumed to terminate against ZSMNS059A in the west. The western termination is based on the increase in N-S striking fractures west of ZSMNS059A, as well as the die-out of structure ZSMEW007A into a shorter structure of lower-confidence (ZSMEW007C, cf Figure 6-5).
- Domain FSM_NE005: This domain represents a volume of rock west of regional deformation zone ZSMNE005. This deformation zone represents one of several major belts of NE-SW trending ductile deformation belts that appear to have resulted from major crustal shortening in the Oskarshamn region during the waning stages of the Svecokarelian orogeny (cf. Section 5.2.3). These ductile belts form the tectonic backbone of the Laxemar-Simpevarp region. Domain FSM_NE005 is characterised by a significant increase in the relative intensity of N-S striking sealed fractures, relative to the rest of the Laxemar local model area (Figure 6-6). It is possible that the increased intensity of N-S striking fractures represents brittle reactivation of smaller Riedel conjugate shears originally created in the ductile regime during N-S crustal shortening. FSM_NE005 is terminated against ZSMNE005 on the east, against ZSMNE107A in the west, (based on the patterns of fractures observed in boreholes on the west side of ZSMNE107A), and against ZSMNW042A in the south. The southern termination of FSM_NE005 is the most uncertain, due primarily to a paucity of data south of ZSMNW042A. The current geometry of FSM_NE005 is that it makes up the footwall of ZSMNW042A.
- Domain FSM_W: This domain represents a volume of rock between zones ZSMNS001C, ZSMNS059A, ZSMNW042A, and south of ZSMEW002A. Borehole data west of ZSMNS059A suggests dominant north-south fracture strikes. This north-south strike dominance is noted in both sub-vertically- and sub-horizontally-dipping fracture sets (Figure 6-7). The third set of fractures, which strike ENE and roughly parallel the NE-SW striking sinistral shear zones that make up the tectonic fabric of the Laxemar-Simpevarp region, are relatively subdued in intensity when compared to the rest of the Laxemar local model area. This finding (largely from borehole data) is in agreement with surface kinematic investigation results /Viola and Venvik Ganerød G 2007a/ described in Section 3.7. This domain is interpreted to terminate against ZSMNW042A in the south, ZSMNS059A in the east, ZSMNS001C in the west, and ZSMNEW002A in the north. Again, this domain fundamentally represents a crustal block isolated by the major ENE and N-S sinestral tectonic structures (cf. Section 5.2.3).
- Domain FSM_C: This domain represents a volume of rock south of FSM_EW007, north of ZSMNW042A, and bounded by ZSMNS059A on its western edge and FSM_NE005 on its eastern edge. This fracture domain is dominated by sealed N-S striking fractures in a fashion similar to FSM_W, and open WNW striking fractures (Figure 6-8). It is likely that the open WNW-striking fractures represent either primary fracturing (tension gashes) or brittle reactivation of older fractures in extension due to inferred NW-SE compression during the Caledonian orogeny and the present day (Figure 5-29). This may also explain the prevalence of N-S striking sealed fractures (in compression since ~ 400 Ma).

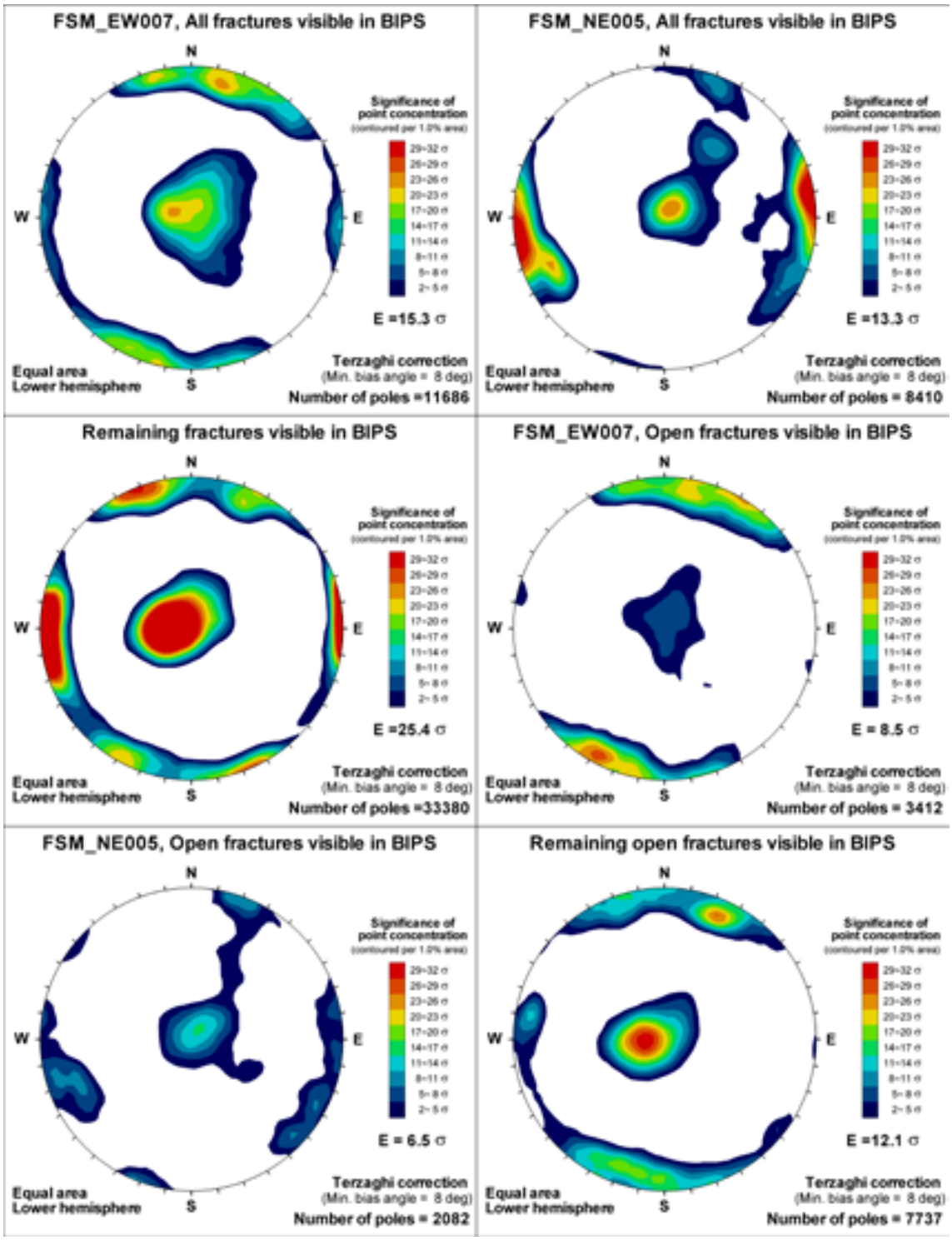

Figure 6-6. *Kamb-contoured polar stereoplots illustrating fracture set orientations from cored boreholes in fracture domains FSM_EW007 and FSM_NE005, relative to fracture orientation from cored boreholes in the remainder of the Laxemar local model area.*

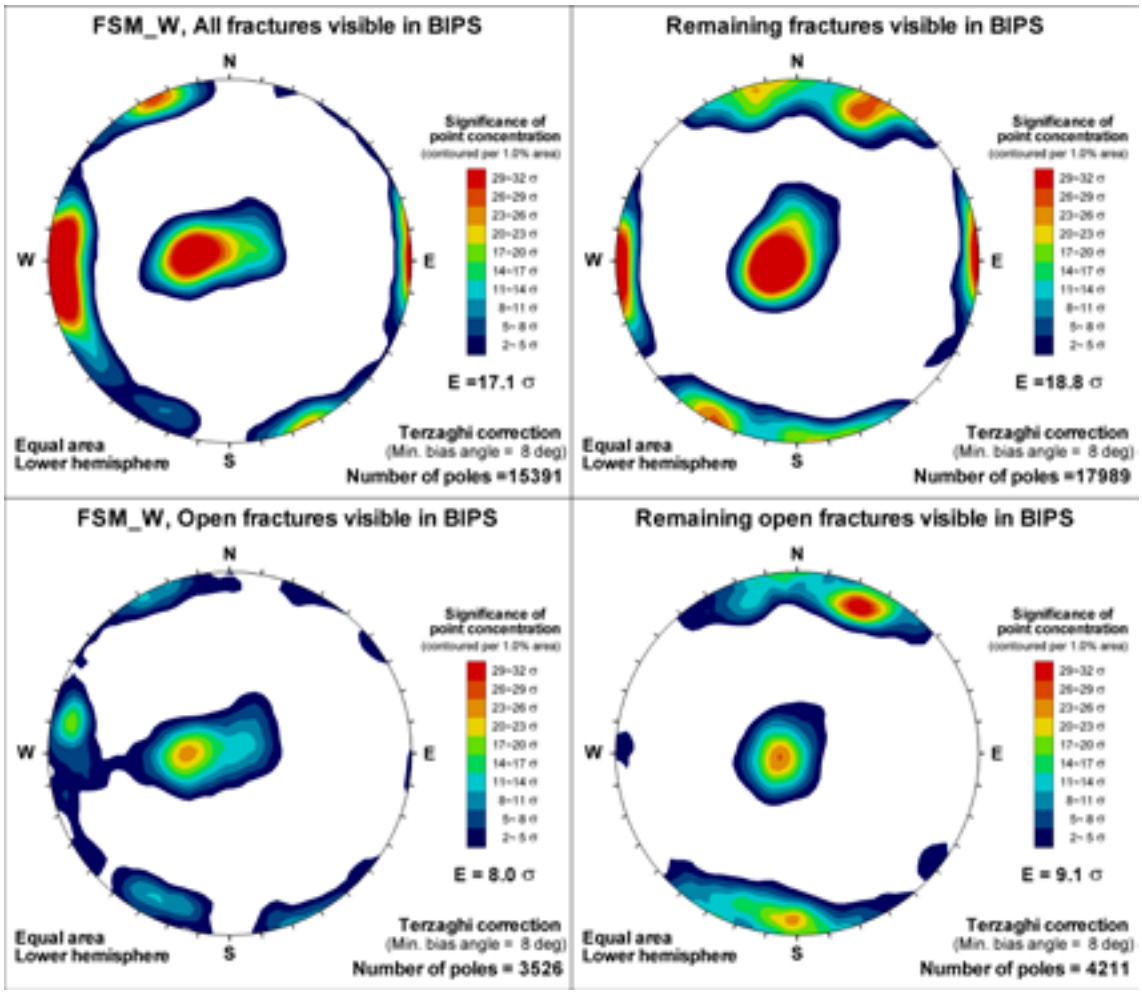

Figure 6-7. *Kamb-contoured polar stereoplots illustrating fracture set orientations from cored boreholes in fracture domain FSM_W, relative to fracture orientations from cored boreholes in the remainder of the Laxemar local model area (FSM_EW007 and FSM_NE005 excluded).*

As the fracture domains are largely defined based on differences in the relative intensity of fracture orientation sets, the most logical way to illustrate the differences between domains is through the use of polar stereoplots, with fracture pole densities contoured using the Kamb method /Kamb, 1959/. In Kamb contouring, each contour interval represents a certain number of standard deviations (σ) away from the fracture pole density expected for a random sample drawn from a uniform distribution. This standardization allows for the direct comparison of data sets with different sample sizes /Vollmer 1995/. The contoured stereonet plots in Figure 6-5 through Figure 6-7 have also been adjusted for one-dimensional orientation bias through the use of Terzaghi compensation /Terzaghi 1965/; a minimum bias angle is used to limit the correction so that the relative intensity of fractures subparallel to the borehole are not over-estimated.

- Domain FSM_N: This domain represents a volume of rock north of domain FSM_EW007 and east of ZSMNS059A. This fracture domain is dominated by sub-horizontally-dipping fractures, but lacks the dominating open WNW fracture set that is observed in FSM_C (Figure 6-8). The domain is bounded on the north by ZSMEW002A and ZSMNW047A.
- Domain FSM_S: This domain represents the rock volume south of ZSMNW042A (i.e. the hanging wall). The definition of this rock volume as a separate fracture domain is highly uncertain due to the lack of data from this area; cored borehole KLX16A represents the only fracture data south of ZSMNW042A. In addition, the data from KLX16A is believed to have been strongly influenced by the adjacent structure ZSMNE107A. This zone is characterised

by a relative lack of sub-horizontally-dipping fractures. In this domain, the ENE and N-S fracture sets dominate (Figure 6-8). If one views structure ZSMNS059A (and the associated rock block representing FSM_W) as a restraint on the western edge of this domain, then the fracture pattern could be explained as conjugate Riedel R shears (N-S set) combined with the brittle re-activation along NE-SW striking shear bands (ENE set) parallel to the dominant regional tectonic fabric.

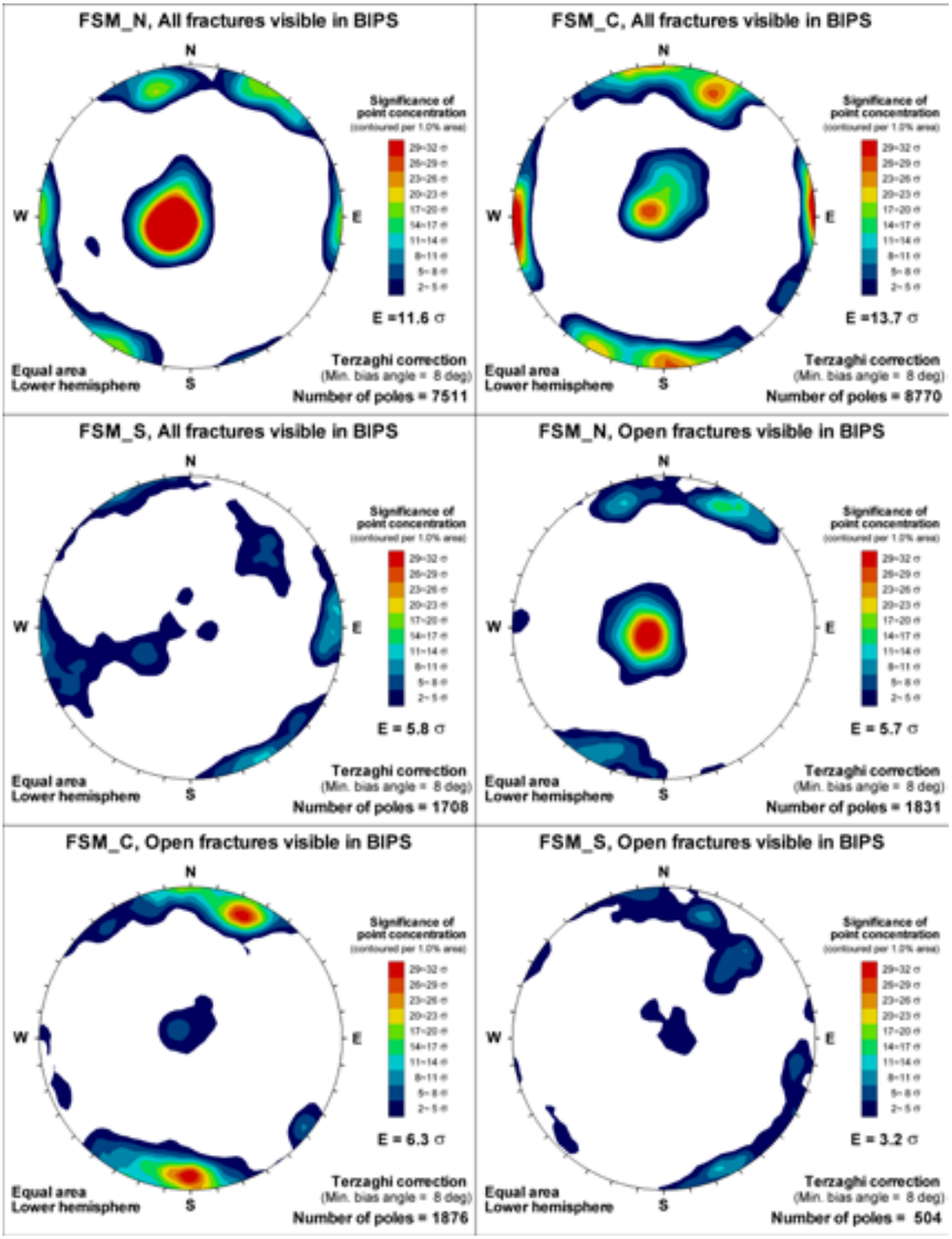

Figure 6-8. *Kamb-contoured polar stereoplots illustrating fracture set orientations from cored boreholes in fracture domains FSM_N, FSM_C, and FSM_C.*

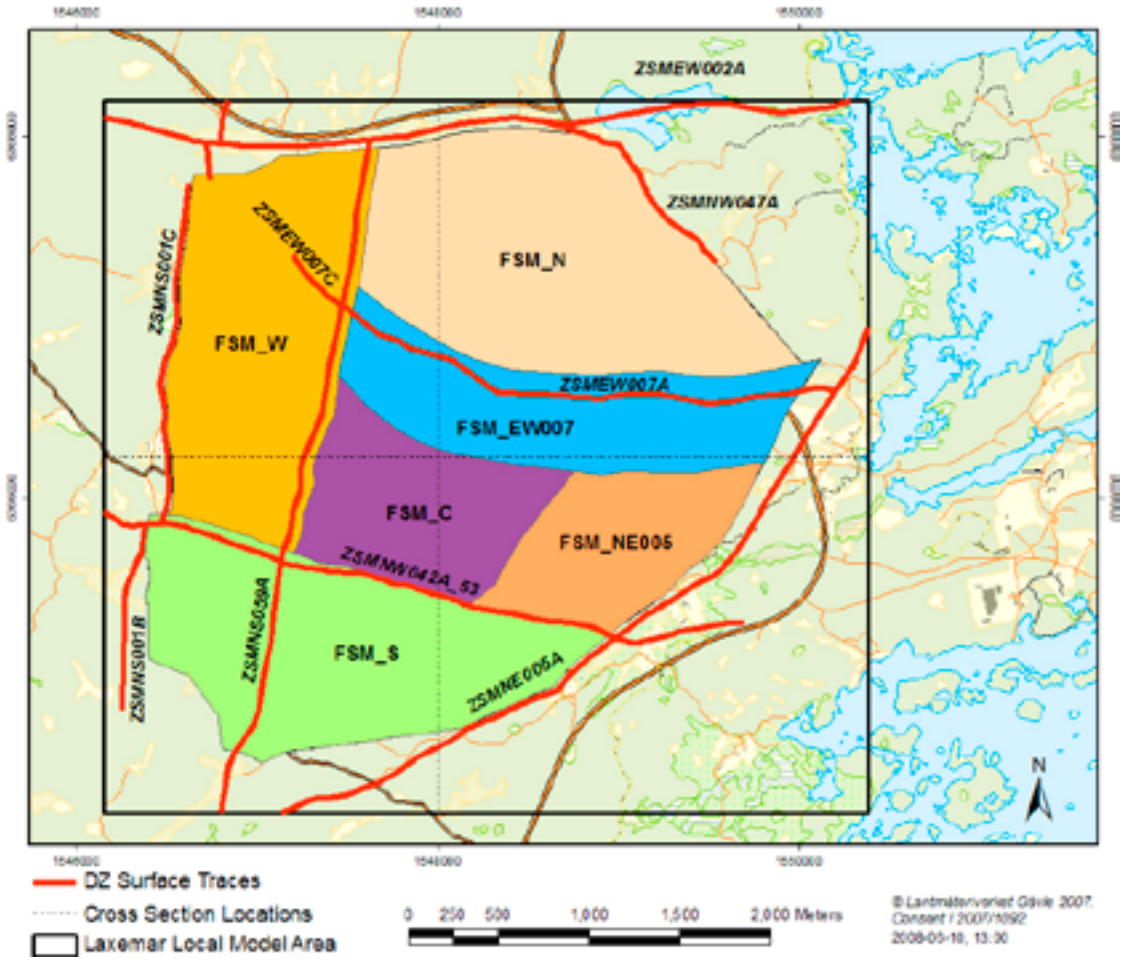

Figure 6-9. *Illustration of the SDM-Site Laxemar Fracture Domain Model. All northings and eastings coordinates are in the Swedish RT90(25 gon W) coordinate system.*

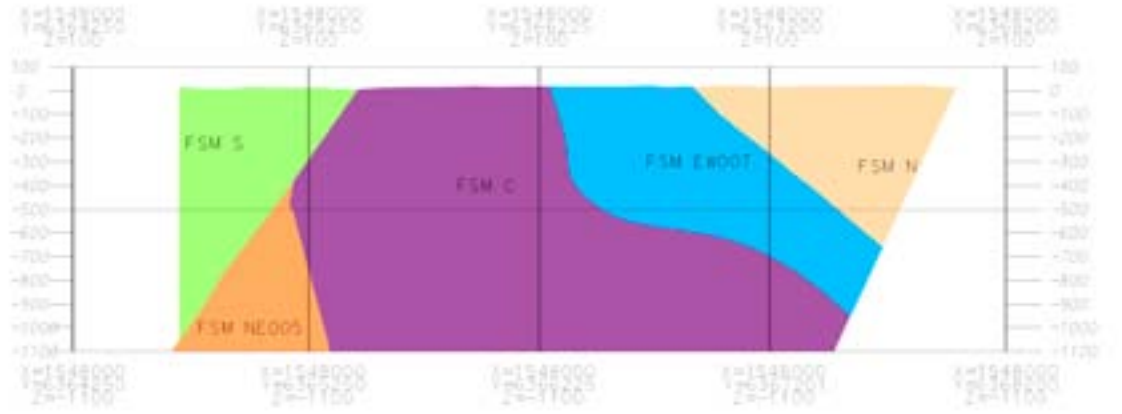

Figure 6-10. *Cross section in the RVS model of identified fracture domains, oriented north-south through the middle of the Laxemar local model volume. All northings and eastings coordinates are in the Swedish RT90(25 gon W) coordinate system.*

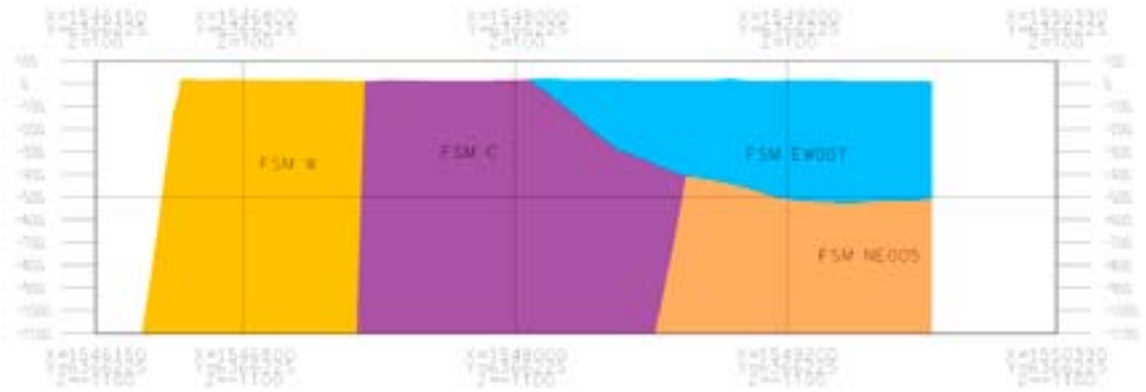

Figure 6-11. *Cross section in the RVS model of identified fracture domains, oriented east-west through the middle of the Laxemar local model volume. All northings and eastings coordinates are in the Swedish RT90(25 gon W) coordinate system.*

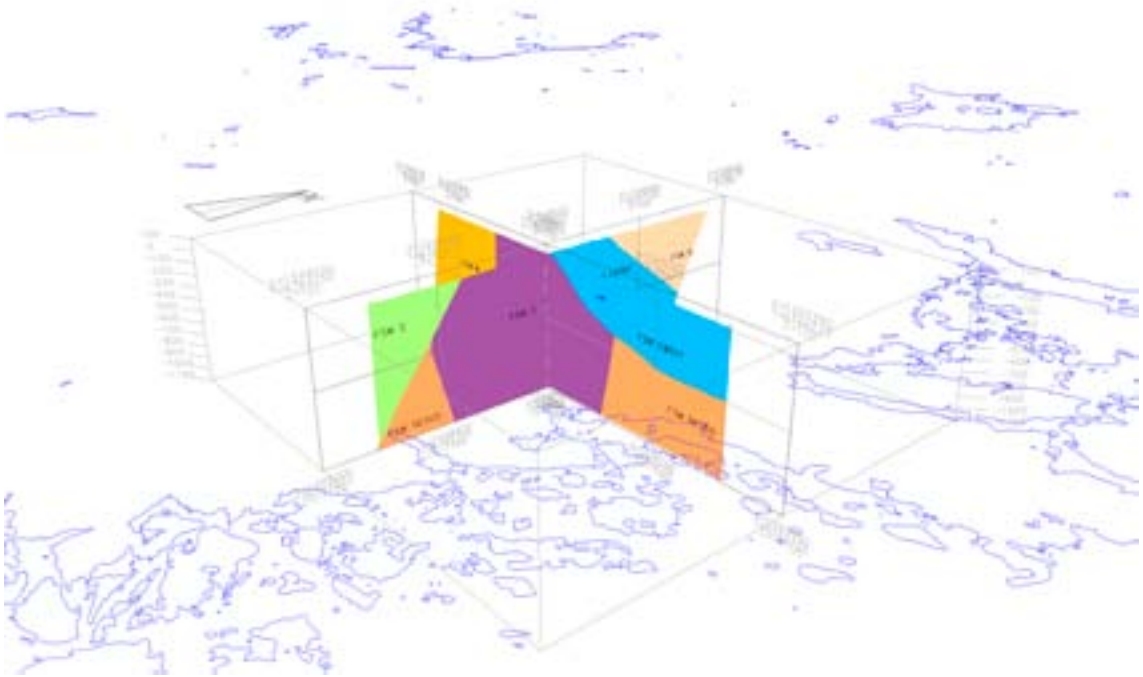

Figure 6-12. *Isometric view, looking NW, of locations of RVS cross sections relative to Laxemar local model volume and the Baltic coastline. All northings and eastings coordinates are in the Swedish RT90(25 gon W) coordinate system.*

6.4.2 Fracture set orientation distribution

On the scale of the Laxemar local model area, four orientation sets are present in cored borehole data and outcrop fracture records. The orientation set distributions are summarised in Table 6-3.

The strongest fracture set (SH), in terms of relative fracture set intensity, consists of sub-horizontally dipping fractures that generally strikes north-south to north-northwest (260°–280°), and dip predominantly to the east. However, the strike orientation of the mean pole vector for sub-horizontal set can vary significantly between fracture domains, and, in some cases, between boreholes in the same fracture domain. In addition, there can be significant uncertainty in the strike orientation of a subhorizontally-dipping fracture derived from a vertically-dipping well.

The next strongest sub-vertically dipping set is the N-S set, (Figure 6-13) which strikes roughly north-south with a mean fracture pole trend of 265°. The relative intensity of this fracture set was an important criterion in fracture domain identification.

The third and fourth fracture sets consist of east-northeast striking (mean pole of 335°–340°) and west-northwest striking (mean pole trend of 25°) fractures, respectively. Dips are predominantly south for the ENE set; in the WNW set, dips are split between north and south. In general, these fracture sets are less intense than the N-S and SH sets. However, the intensity of the WNW set, specifically in terms of the open-sealed aperture ratio, was also important for the identification of fracture domains.

Orientation sets are parameterised in term of univariate Fisher hemispherical probability distributions. The distribution fits are presented below in Table 6-4.

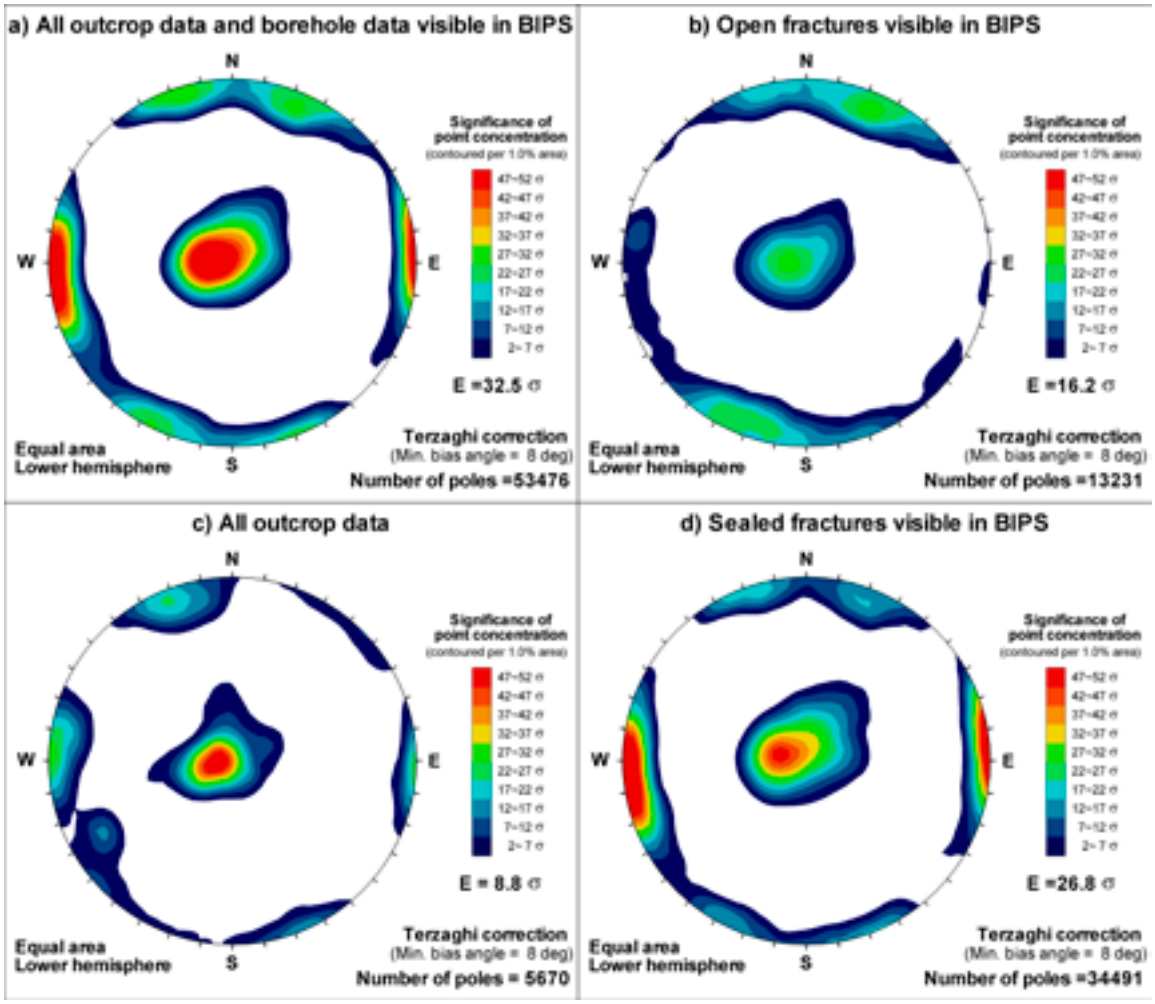

Figure 6-13. *The four data sets used in the parameterisation of the orientation model. Note that open and sealed fractures only relate to borehole data. As discussed in brief in the orientation model methodology section (and in detail in /La Pointe et al. 2008/), data from some boreholes have been omitted from this analysis.*

Table 6-4. Summary of global fracture set parameterisation.

Initial hard sector definitions
(initial input based on visual inspection and judgment)

	Mean Pole		Distribution
Set	Trend [º]	Plunge [º]	Solid angle [º]
SH	339	87	28
ENE	345	3	24
WNW	23	4	28
N-S	86	0	28

Underlying parameterisation of probability fields (DFN Orientation Model)
(numerically iterated from the initial hard sector definitions)

	Mean Pole		Distribution
Set	Trend [º]	Plunge [º]	Fisher κ
SH	335.1	87.1	7.2
ENE	340.3	0.5	9.9
WNW	24.1	3.1	7.5
N-S	269.1	1.7	7.3

Overall statistics of all set-divided data
(all outcrops and borehole data, including non-visible in BIPS)

	Mean Pole		Distribution	Fractures used in DFN model Parameterisation	
Set	Trend [º]	Plunge [º]	Fisher κ	Number of fractures	Terzaghi weight sum
SH	341.6	87	6.9	36,730	49,916.0
ENE	340.2	0.5	9.8	8,655	22,050.2
WNW	24	2.7	7.4	12,540	31,800.6
N-S	269.4	1.4	7.0	16,056	42,829.6

6.4.3 Fracture set size/intensity distribution parameters

As mentioned in brief in Section 6.2.4 and Section 6.3.2, there are conceptual uncertainties related to the parameterisation of the coupled size-intensity model. All alternative variants of the size/intensity model were parameterised and carried through to verification and uncertainty assessment. The alternative models considered are listed in Table 6-4.

The model judged most geologically consistent is referred to as the unlinked Base Model (BMU). Conceptually, this model assumes:

- Fracture coupled size-intensity follow a power-law and can be described through a Pareto distribution.
- The fracture radius scaling exponent (k_r) does not vary as a function of fracture domain; it is conceptually acceptable to model the radius exponent as a function of fracture orientation set and not of lithology or fracture domain.
- For all fracture sets, the "Best Fit" radius exponent was used. Full parameterisations for bounding cases (Upper and Lower radius exponents in Figure 6-15 through Figure 6-18) are presented in /La Pointe et al. 2008/.
- Fracture domains differ principally in terms of the observed mean volumetric fracture intensity (P_{32}) and the minimum radius (r_0); i.e. the size of the smallest fractures expected. This hypothesis complements the fracture domain model, where volumes are identified primarily through variations of fracture intensity by set.

- Fracture intensity obeys Euclidean scaling.
- Unlinked fracture traces (Appendix A, /La Pointe et al. 2008/) used to estimate radius scaling exponent (k_r).

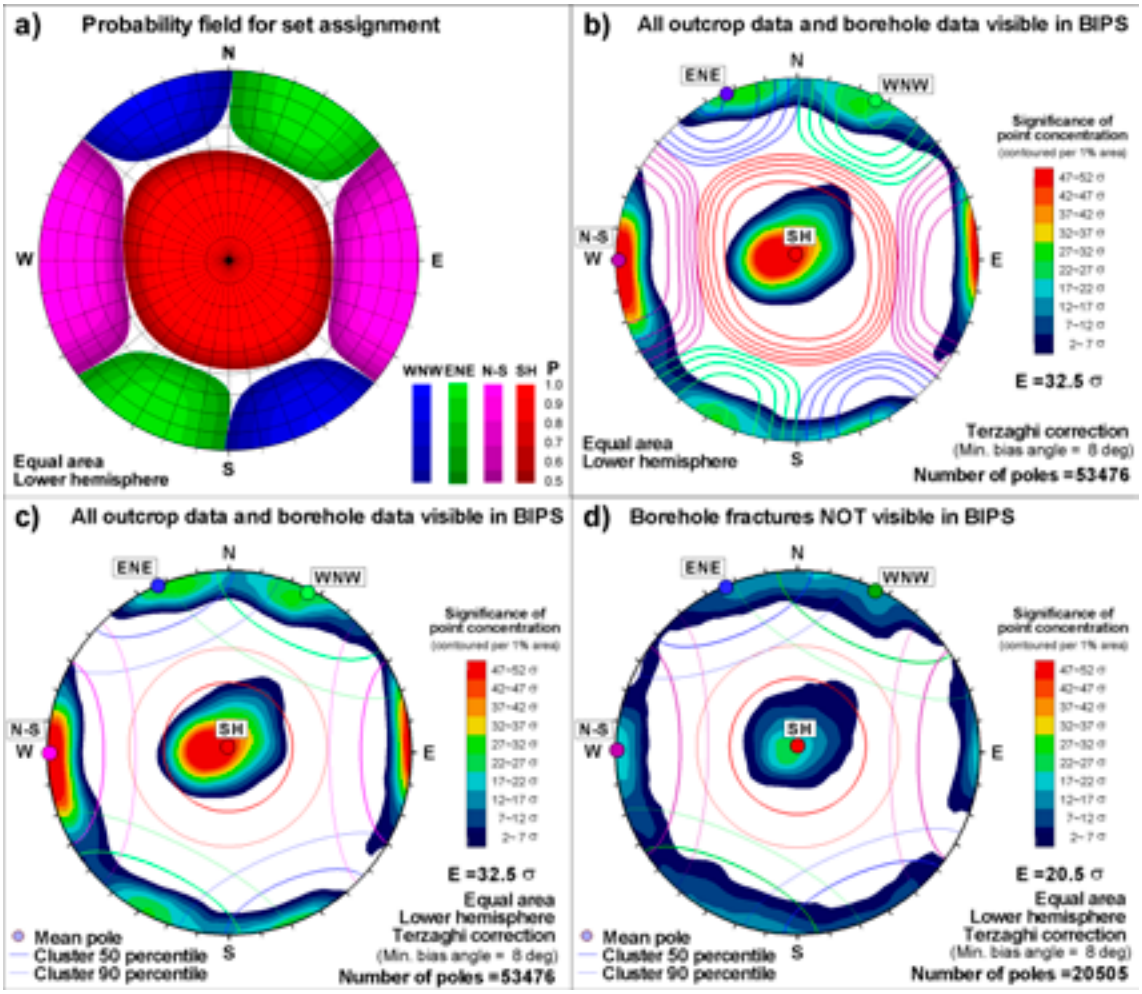

Figure 6-14. *Set assignment of fracture data. Visualization of the probability field for set assignment: a) contours shown for P > 0.5, and b) probability levels P = 0.5, 0.6, 0.7, 0.8, and 0.9 related to fracture orientation clusters. Resulting mean poles and cluster Fisher percentiles visualized for set divided data, c) for outcrops and borehole data visible in BIPS and d) for borehole data not visible in BIPS. KLX02 (RSMBA03), KLX06, and KLX20A west of ZSMNS001 are excluded.*

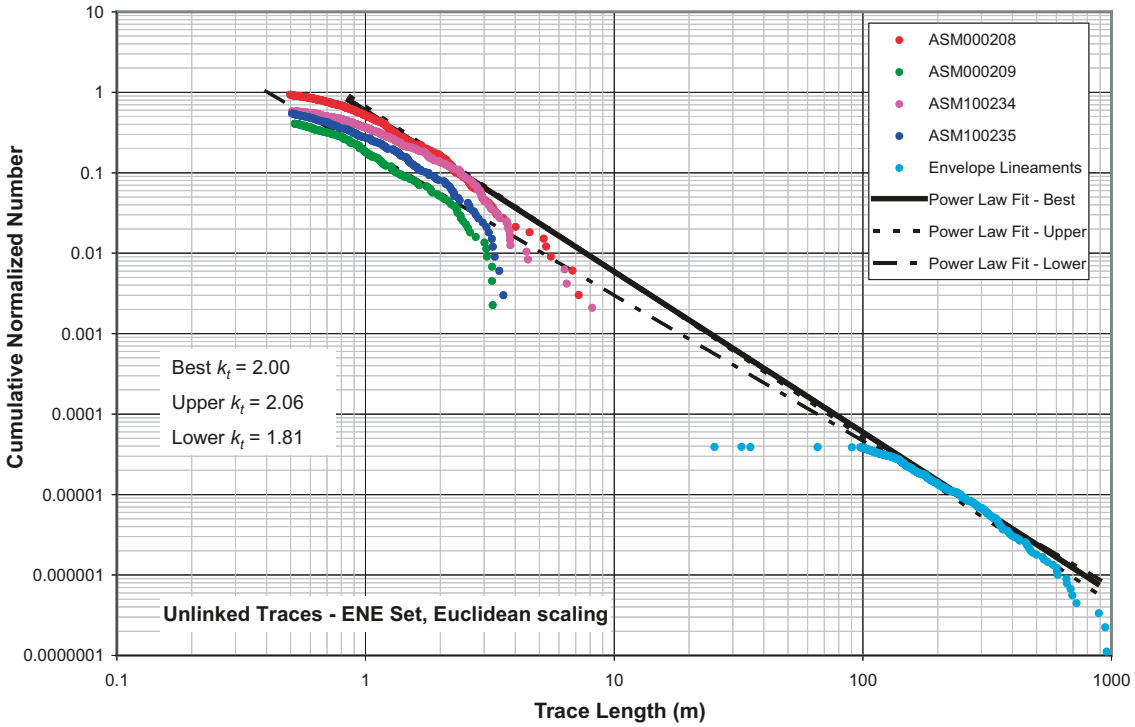

Figure 6-15. *Area-normalised complementary cumulative number (CCN) plot for the ENE fracture set, unlinked Base Model (BMU). Note that the coupled size-intensity model presented in uses the 'Best Fit' trace length scaling exponent.*

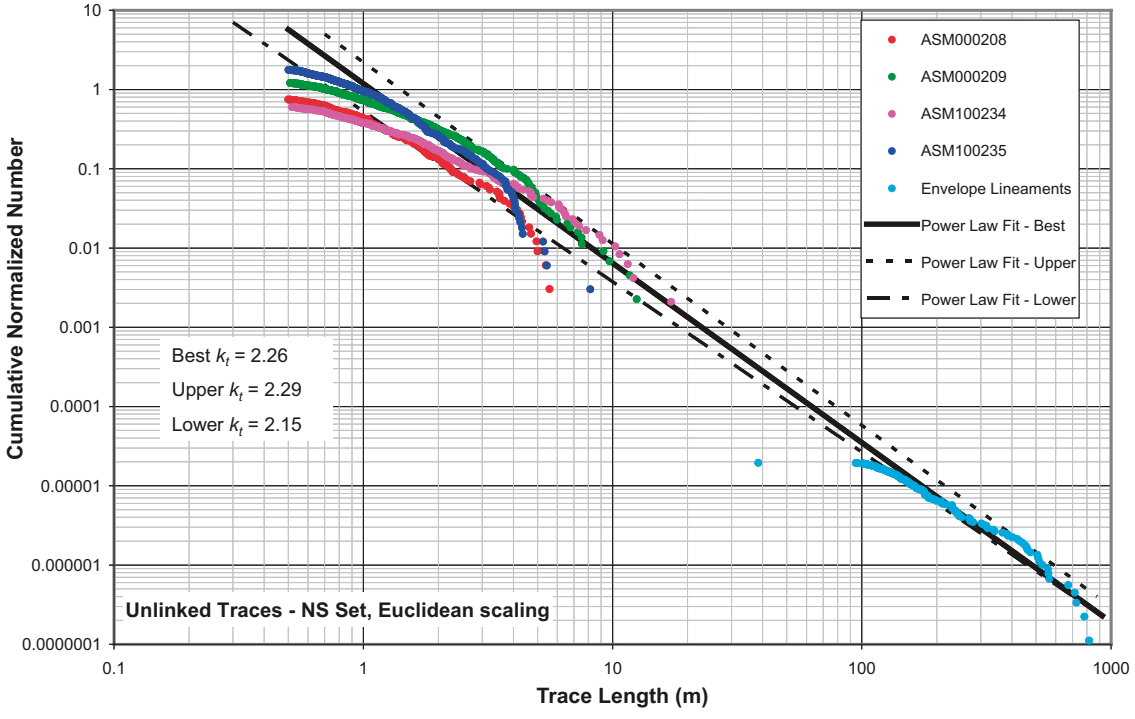

Figure 6-16. *Area-normalised complementary cumulative number (CCN) plot for the N-S fracture set, unlinked Base Model (BMU). Note that the coupled size-intensity model presented in uses the 'Best Fit' trace length scaling exponent.*

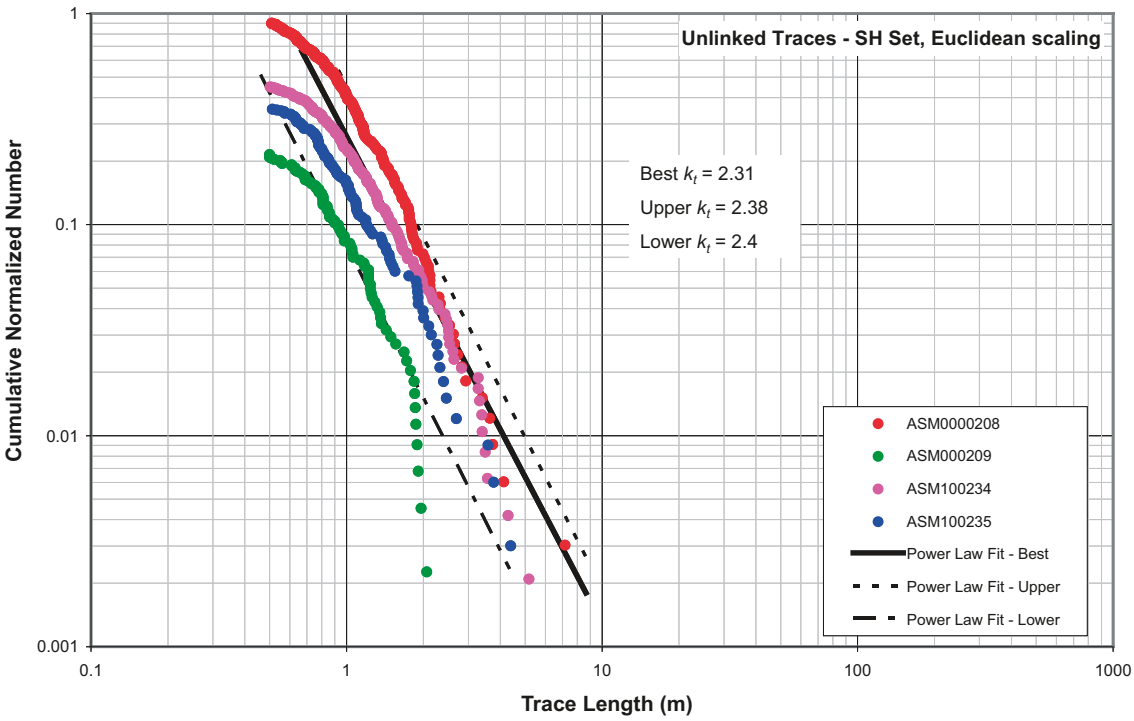

Figure 6-17. *Area-normalised complementary cumulative number (CCN) plot for the SH fracture set, unlinked Base Model (BMU). Note that the coupled size-intensity model presented in uses the 'Best Fit' trace length scaling exponent.*

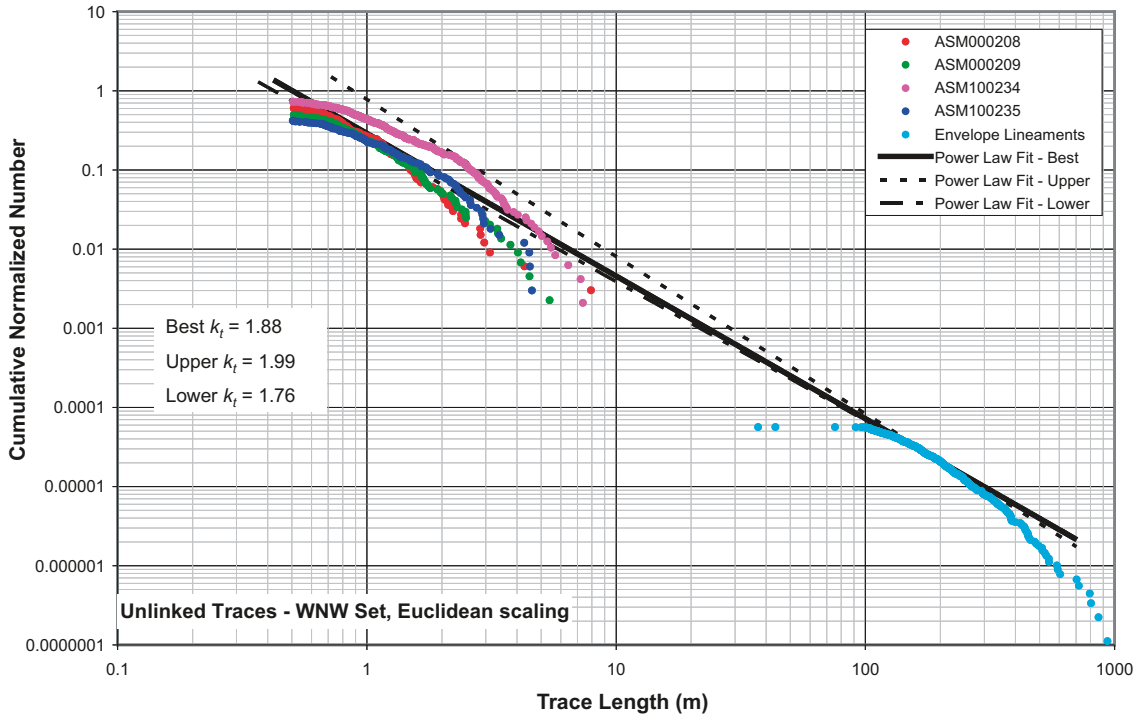

Figure 6-18. *Area-normalised complementary cumulative number (CCN) plot for the WNW fracture set, unlinked Base Model (BMU). Note that the coupled size-intensity model presented in uses the 'Best Fit' trace length scaling exponent.*

Parameters for the BMU model are presented below in Table 6-5. Figure 6-15 through Figure 6-18 show the CCN plots for the unlinked Euclidean-scaling cases in which the scaling exponent is not a function of fracture domain. The solid black line in each figure represents the BMU case, i.e. the identified 'best-fit' trace length scaling slope. Note that, for each fracture set, there are trace data from four different outcrops. A different trace length scaling exponent can be calculated depending on which outcrop's trace data are used to fit the line. The dashed lines in each, which are labelled 'Upper' and 'Lower', represent the upper and lower bounding estimates of the trace length scaling exponent. They are included in the alternative model parameterisations to address uncertainty.

6.4.4 DFN spatial model

As discussed in Section 6.2.5, the SDM-Site Laxemar GeoDFN spatial model describes several different aspects of the spatial patterning of fractures. Each spatial property is supported by statistical analysis; the analysis and model parameterisations are summarised in the report sections that follow.

Borehole mass dimension calculations

Figure 6-19 through Figure 6-22 show the mass dimension calculations for each of the four sets for all of the borehole data. The individual values for each borehole are plotted in blue, while the mean values of all of the data are shown as red circles. The black dashed line is for reference; it has a slope of 1.0, which represents Euclidean scaling.

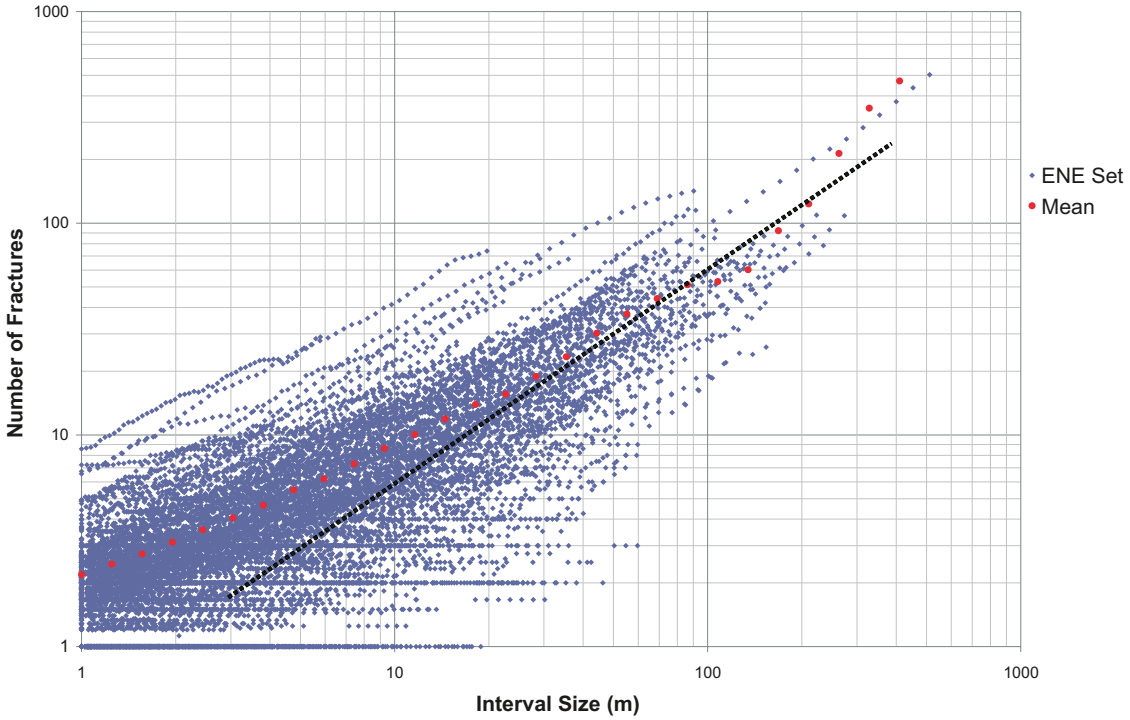

Figure 6-19. *Mass dimension analysis for ENE set from all fracture data outside of mapped deformation zones. Red circles are the mean values; the dashed line has a slope of 1.0, and corresponds to a mass dimension of 2.0.*

Table 6-5. Coupled size-intensity parameters for the unlinked Base Model (BMU) alternative.

Envelope Set	Fit Type	k_r	r_{max}	FSM_C Total r_{min}	FSM_C P_{32} Total	FSM_C Open r_{min}	FSM_C P_{32} Open	FSM_EW007 Total r_{min}	FSM_EW007 P_{32} Total	FSM_EW007 Open r_{min}	FSM_EW007 P_{32} Open	FSM_N Total r_{min}	FSM_N P_{32} Total	FSM_N Open r_{min}	FSM_N P_{32} Open
ENE	Best	3.00	564.2	0.37	1.72	1.28	0.50	0.32	1.98	1.01	0.64	0.46	1.38	1.34	0.48
NS	Best	3.26	564.2	0.59	2.33	2.16	0.45	0.49	2.96	1.35	0.82	0.53	2.63	1.83	0.56
SH	Best	3.31	564.2	0.33	2.66	1.18	0.51	0.23	4.42	0.63	1.16	0.22	4.62	0.52	1.50
WNW	Best	2.80	564.2	0.08	2.53	0.36	0.77	0.07	2.90	0.23	1.11	0.08	2.67	0.33	0.84

Envelope Set	Fit Type	k_r	r_{max}	FSM_NE005 Total r_{min}	FSM_NE005 P_{32} Total	FSM_NE005 Open r_{min}	FSM_NE005 P_{32} Open	FSM_S Total r_{min}	FSM_S P_{32} Total	FSM_S Open r_{min}	FSM_S P_{32} Open	FSM_W Total r_{min}	FSM_W P_{32} Total	FSM_W Open r_{min}	FSM_W P_{32} Open
ENE	Best	3.00	564.2	0.40	1.60	1.42	0.45	0.15	4.28	0.50	1.30	0.40	1.60	1.75	0.37
NS	Best	3.26	564.2	0.36	4.30	1.41	0.78	0.27	6.09	0.85	1.45	0.42	3.60	1.38	0.79
SH	Best	3.31	564.2	0.29	3.17	0.73	0.96	0.23	4.22	0.52	1.50	0.28	3.40	0.75	0.93
WNW	Best	2.80	564.2	0.09	2.37	0.49	0.61	0.03	5.39	0.18	1.38	0.11	1.97	0.56	0.55

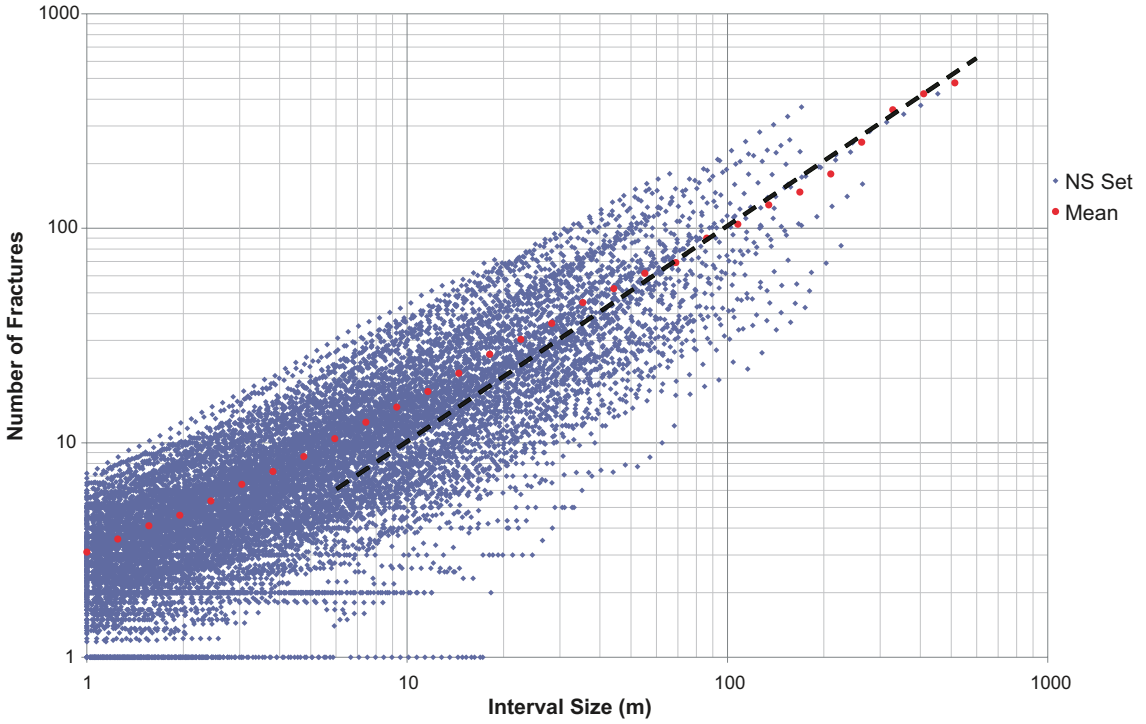

Figure 6-20. *Mass dimension analysis for NS set from all fracture data outside of mapped deformation zones. Red circles are the mean values; the dashed line has a slope of 1.0.*

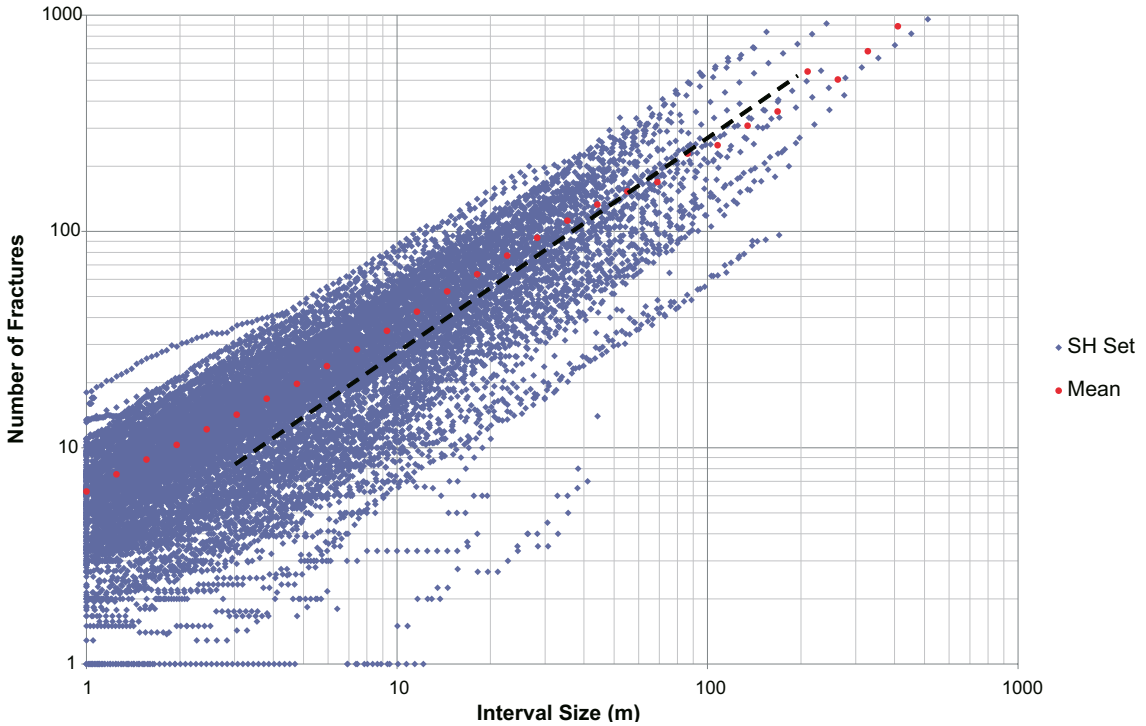

Figure 6-21. *Mass dimension analysis for WNW set from all fracture data outside of mapped deformation zones. Red circles are the mean values; the dashed line has a slope of 1.0.*

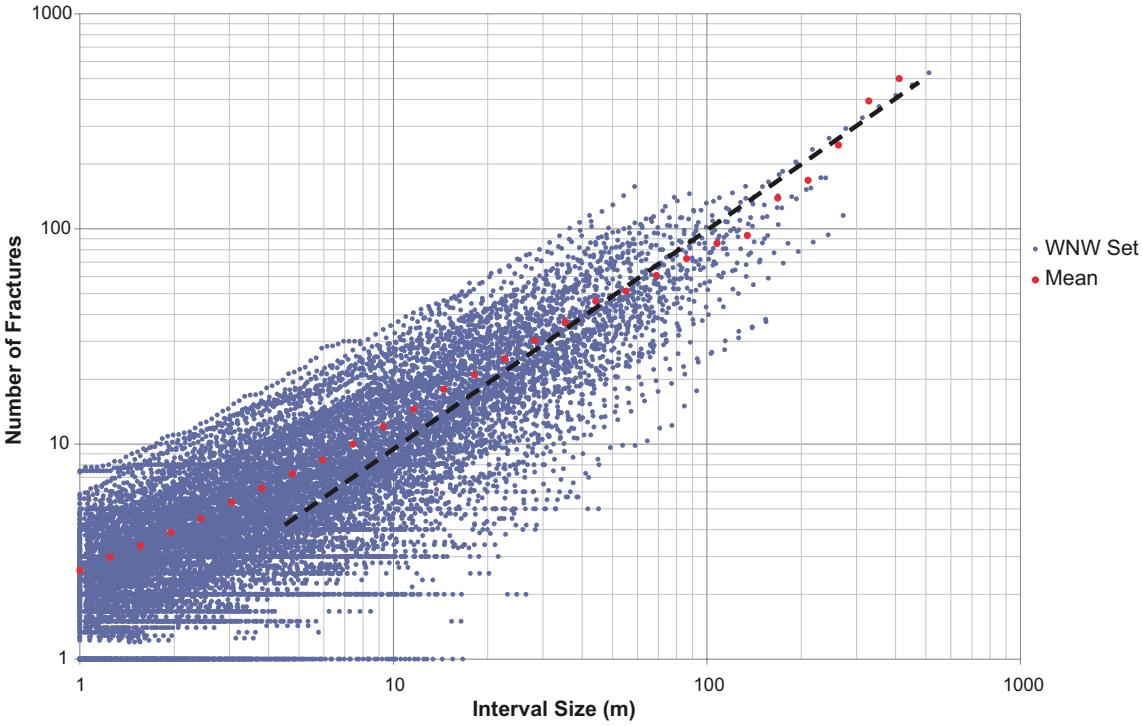

Figure 6-22. *Mass dimension analysis for SH set from all fracture data outside of mapped deformation zones. Red circles are the mean values; the dashed line has a slope of 1.0. The orange line is an alternative fit to the SH data.*

Outcrop mass dimension calculations

The mass dimensions for each set and outcrop were calculated. The mass dimension plots for the detailed fracture outcrop maps are contained in Appendix D in /La Pointe et al. 2008/. Table 6-6 summarises the calculations for each set at each of the four Laxemar outcrops. A value of $D_m = 2.0$ indicates Euclidean scaling. This table shows that many of the sets scale very close to Euclidean scaling. For example, with the exception of ASM000209, the sub-horizontal set has mass dimensions of 2.00, 2.02 and 1.99. The parameters SSQ (Sums of Squares) and SE (Standard Error) quantify how well the Power Law model with the given ρ and D_m fit the data.

Overall, the mass dimension values for the outcrop data suggests Euclidean or mildly fractal scaling over the scale ranges that were possible to evaluate. Scales larger than the outcrops could not be investigated, so the results shown in the table are relevant to scales no larger than a few tens of metres at the most. However, the fact that the mass dimension results are Euclidean or nearly so in this scale range is consistent with the results from the borehole data which covers data over much larger scale ranges. This suggests that Euclidean scaling and Poissonian spatial intensity are adequate models for characterising the fracture intensity data at scales greater than 10–30 m.

Fracture intensity as a function of depth

As described in Section 6.2.5, fracture intensity as a function of depth was analysed by looking at P_{32} from cored borehole data in 5 m bins, using a 10-period moving average (50 m depth window). There is evidence of some changes in fracture intensity as a function of depth. For example, in fracture domain FSM_C , open fracture intensity appears to not be a systematic function of depth for the ENE (Figure 6-23) set and possible the NS set, but does appear to systematically decrease with increasing depth for the SH (Figure 6-24) and WNW sets. Total fracture intensity, however, shows not obvious decrease with depth for FSM_C.

Table 6-6. Summary of mass dimension calculations for outcrops at Laxemar. SSQ = sum of squares; SE = standard error.

Outcrop	Set	ρ	D_m	SSQ	SE
ASM000208	ENE	9.37	1.93	1.372E+04	44.28
ASM000208	NS	7.90	1.91	3.389E+04	69.59
ASM000208	SH	8.80	2.00	2.160E+04	65.73
ASM000208	WNW	6.10	1.92	1.030E+06	22.55
ASM000209	ENE	8.61	1.76	6.259E+04	6.12
ASM000209	NS	17.20	1.97	7.149E+05	19.90
ASM000209	SH	3.50	1.78	4.246E+04	5.07
ASM000209	WNW	8.44	1.77	4.037E+05	16.00
ASM100234	ENE	12.10	1.95	7.430E+06	60.82
ASM100234	NS	17.89	1.85	6.700E+06	57.02
ASM100234	SH	7.40	2.02	2.058E+07	100.16
ASM100234	WNW	14.47	1.89	1.044E+07	71.19
ASM100235	ENE	13.80	1.91	7.550E+06	62.80
ASM100235	NS	30.12	1.98	4.167E+07	145.62
ASM100235	SH	4.70	1.99	1.710E+06	29.76
ASM100235	WNW	7.02	2.23	1.930E+07	97.94

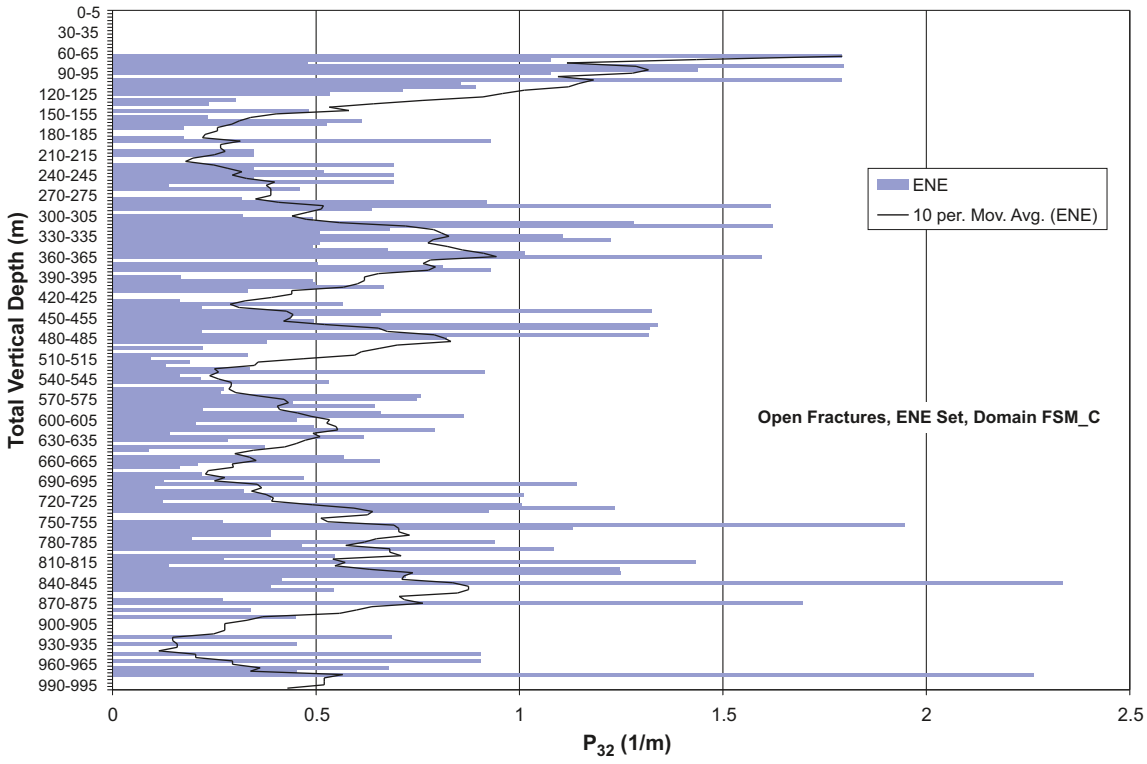

Figure 6-23. *Fracture domain FSM_C, open fractures, ENE set, as a function of vertical depth below ground surface.*

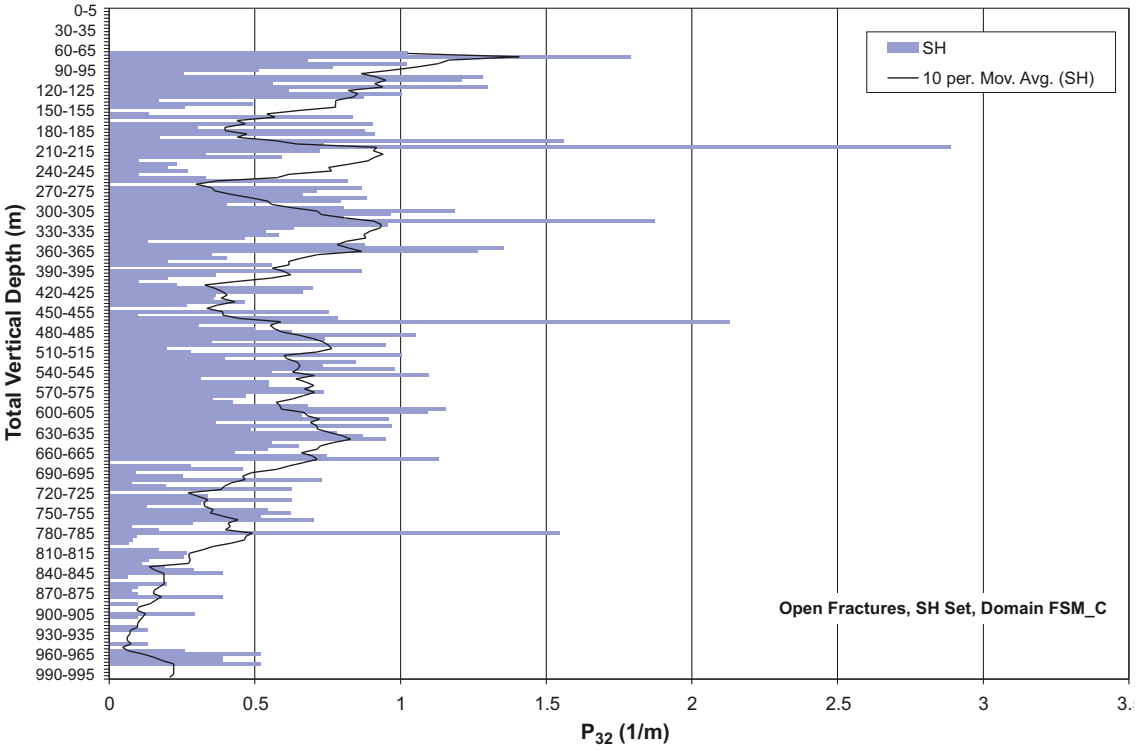

Figure 6-24. *Fracture domain FSM_C, open fractures, SH set, as a function of vertical depth below ground surface.*

Open fracture intensity for the SH set shows a decrease in intensity with depth for some domains, for example FSM_C and FSM_N, but no obvious decrease for other domains, such as FSM_W. However, total fracture intensity sometimes shows different patterns than open fracture intensity. Overall, total fracture intensity shows many fewer instances of possible depth dependence, regardless of fracture set or fracture domain. About the only cases where there appears to be a decrease in total fracture intensity with depth is in fracture domain FSM_N (Figure 6-25). In this domain, total fracture intensity appears to decrease below a depth of 300 m below ground surface. However, there is some uncertainty in this trend, as there is only one well in domain FSM_N (KLX09) that is drilled deeper than ~300 m depth.

In conclusion, while there is certainly variability in intensity as a function of fracture set, fracture domain, there do not appear to be any significant systematic site-wide decreases in total or open fracture intensity as a function of depth at Laxemar. Depth versus intensity plots of all orientation sets and all fracture domains are contained in Appendix E in /La Pointe et al. 2008/.

Intensity of minor deformation zones (MDZ) at Laxemar

The freqeuncy of MDZ at Laxemar is quantified by their P_{10}: calculated as the number of MDZ intersecting a borehole, divided by the length of the borehole. A list of the minor deformation zones in the cored borehole array is presented as Appendix 3 of the SDM-Site Laxemar DCR /Hermanson et al. 2008/; in this appendix, the orientation and locations of MDZ quantified during the ESHI analysis are summarised. The length of the borehole used in the P_{10} calculation is the total length (MD) of the borehole, minus the length of sections of boreholes inside mapped deformation zones (DZ).

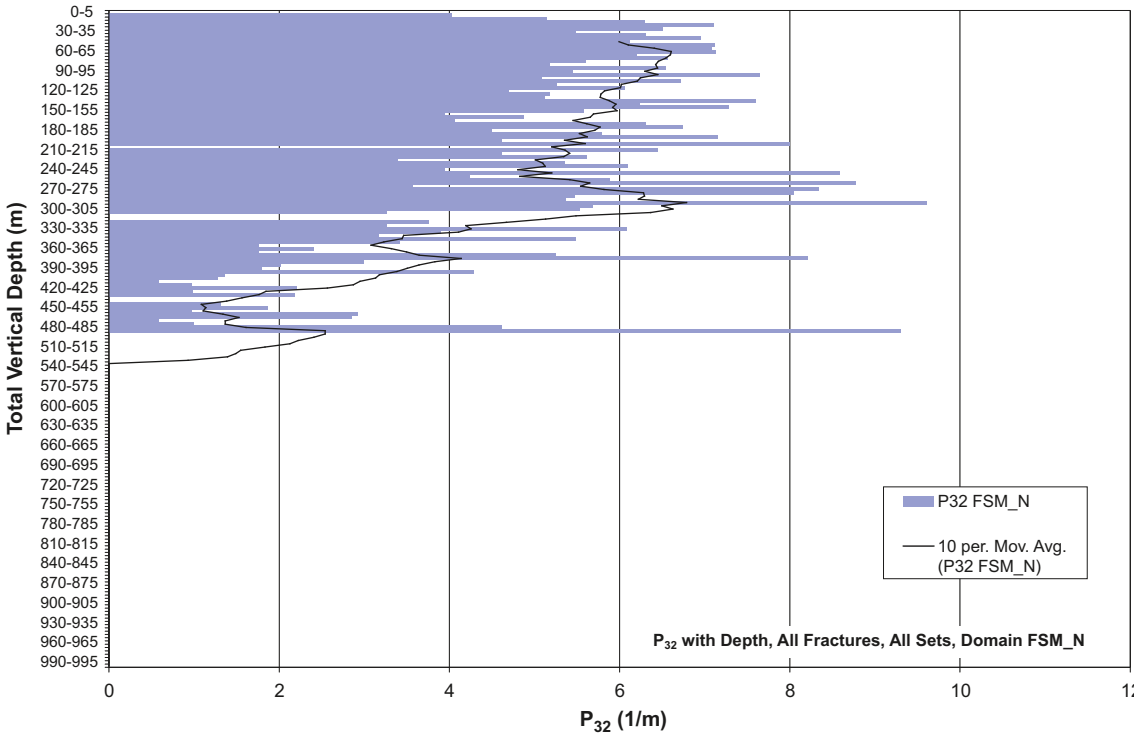

Figure 6-25. *Fracture domain FSM_N, all fractures in all orientation sets, as a function of vertical depth below ground surface.*

Geological DFN modelling, however, relies on P_{32} as the measure of fracture intensity. Therefore, for borehole MDZ intercept data to be useful in geological modelling, it is necessary to transform MDZ P_{10} to MDZ P_{32}. This is accomplished using the Wang approximation (Section 6.2.2). The MDZ intercepts contained in Appendix 3 of the SDM Site Laxemar data compilation report /Hermanson et al. 2008/ were assigned to the fracture orientation sets developed for the SDM-Site Laxemar geological DFN. For the purposes of geological DFN modelling, each borehole used the average C_{13} value over 3 m long intervals for each fracture set. The P_{32} of MDZ at Laxemar are presented below, organised by orientation set and fracture domain, in Table 6-7. FSM_S is not included in Table 6-7, as this domain has generally been excluded from analyses due to a distinct lack of available data (only a single borehole). The P_{32} values presented for a single fracture set in a single fracture domain represent the arithmetic average of the P_{32} values calculated for that set for each individual borehole inside the fracture domain.

A basic assumption concerning MDZ is that they represent larger structures than most of the fractures exposed in the cored boreholes. The SDM-Site Laxemar geological DFN model considers that all structures (fractures and MDZ) with a equivalent radius less than or equal to 564.2 m are treated stochastically in the geological DFN. However, the true size of the MDZ exposed in the cored borehole record at Laxemar is not known; as none of the MDZ can be traced to intercepts with other boreholes or identified uniquely at the ground surface by geophysics, their true size distribution is unknown. In particular, there are no data on the minimum size of MDZ.

An issue is that the power-law size-intensity scaling models used by the geological DFN model do not discriminate between MDZ and large fractures; the size-intensity model only gives the P_{32} of all structures in a certain size range. Therefore, the radius scaling exponent (k_r), which is derived from outcrop fracture maps and lineament traces, is used to describe both MDZ and large single fractures.

There are two possible alternatives to deal with the lack of information on the minimum size of MDZ-sized features without collecting additional data:

- Method 1: The P_{32} of MDZ can be used in conjunction with the various size-intensity alternative models to analytically determine a minimum size (r_{min}) of MDZ. This value will vary as a function of the radius scaling exponent (k_r) and the fitted mean P_{32} chosen for the specific size-intensity model alternative. The result of this implies that all structures between the fitted r_{min} value and the maximum size allowed for structures in the stochastic DFN model are MDZ. Data from the surface are only used to establish the radius scaling exponent, and not to determine the intensity of MDZ-sized structures; or
- Method 2: One can assume that every surface lineament recorded by the detailed ground magnetic and LIDAR surveys represents an MDZ. The minimum size (r_{min}) of the structures that created the surface lineaments can be estimated using the trace length 'rollover effect' on the area-normalised complementary cumulative number plots; the method is described below. As it is not possible to assign the lineaments to individual fracture domains without incurring substantial truncation effects, Method 2 produces r_{min} values that are global in scope. This method is described in detail in Section 5.5 of the geological DFN summary report /La Pointe et al. 2008/.

The P_{32} values presented below in Table 6-7 are based solely on the P_{10} values observed during the ESHI and DZ modelling activities, and do not represent a fixed value for the minimum size (r_{min}) of MDZ. It is suggested that a functional definition of 75 m (equivalent radius) be used as the minimum size of MDZ at Laxemar. 75 m is the radius at which a fracture intersecting a deposition hole is considered large enough to undergo significant slip during an earthquake and potentially compromise canister integrity / Munier and Hökmark 2004/. However, readers are strongly encouraged to consult Section 5.5 of the geological DFN /La Pointe et al. 2008/; the choice of a minimum size for MDZ can have significant consequences in downstream models.

Table 6-7. Number and intensity (P_{10}, P_{32}) of minor deformation zones (MDZ) at Laxemar as a function of fracture set and fracture domain.

Fracture Domain	Fracture Set	Number of MDZ	Total borehole length (m)	P_{10} (1/m)	Average P_{32} (m^2/m^3)
FSM_C	ENE	5	2,691.81	0.0019	0.0031
FSM_EW007	ENE	5	2,669.93	0.0019	0.0053
FSM_N	ENE	0	1,327.04	0.0000	0.0000
FSM_NE005	ENE	4	2,225.28	0.0018	0.0168
FSM_W	ENE	5	3,458.56	0.0014	0.0056
FSM_C	N-S	4	2,691.81	0.0015	0.0040
FSM_EW007	N-S	5	2,669.93	0.0019	0.0154
FSM_N	N-S	1	1,327.04	0.0008	0.0037
FSM_NE005	N-S	7	2,225.28	0.0031	0.0189
FSM_W	N-S	13	3,458.56	0.0038	0.0118
FSM_C	SH	15	2,691.81	0.0056	0.0096
FSM_EW007	SH	33	2,669.93	0.0124	0.0213
FSM_N	SH	26	1,327.04	0.0196	0.0234
FSM_NE005	SH	18	2,225.28	0.0081	0.0129
FSM_W	SH	41	3,458.56	0.0119	0.0219
FSM_C	WNW	4	2,691.81	0.0015	0.0048
FSM_EW007	WNW	2	2,669.93	0.0007	0.0019
FSM_N	WNW	3	1,327.04	0.0023	0.0078
FSM_NE005	WNW	1	2,225.28	0.0004	0.0069
FSM_W	WNW	5	3,458.56	0.0014	0.0038

Spatial variation of fracture intensity

In the absence of other controlling factors such as lithology, depth, or rock alteration, the spatial variability of fracture intensity (P_{32}) for a given fracture set in a single fracture domain can be quantified through a probability distribution. As discussed in Section 6.2.5, for a Poisson point pattern of fractures in 3D space, the mean fracture intensity variation should follow a Gamma (Γ) or Weibull distribution. The analysis of fracture data during the parameterisation of the SDM-Site Laxemar DFN modelling suggests that, at scales between 10 and 30 metres and larger, the assumption of Euclidean size-intensity scaling and a Poisson fracture location model is appropriate and may well be appropriate for even smaller scales (< 10 m).

The assumption of a Gamma or Weibull distribution implies that, at scales relevant to repository design and simulation, there are no other significant spatial controls on fracture intensity other than fracture domain. The analysis described in the previous section indicated no systematic depth relationship for fracture intensity. Statistical analysis of borehole data in the geological DFN summary report /La Pointe et al. 2008/ suggests that there no statistically significant correlation of rock alteration to fracture intensity, but that there is a weak correlation between fracture intensity and lithology for more mafic rocks (amphibolite and fine-grained mafic dykes). The geological DFN model assumes (but does not test or evaluate), that at scales larger than 10 m, it is adequate to ignore the weak correlation of intensity to lithology and to treat fracture intensity within a single fracture domain as a stationary process.

Both the Gamma and Weibull distributions can be described in terms of a shape parameter (α) and a location parameter (β). Essentially, for a constant value of α, changing β shifts the PDF curve left or right on the graph. For a constant value of β, changing α results in a change in the shape of the probability density. Figure 6-26 illustrates the effects of changing the shape factor on both distributions.

The results of the analysis are presented below in Table 6-8; only domain FSM_C is presented as an example table. Please consult /La Pointe et al. 2008/ for full parameterisations. The notation “fail to reject” and “reject” in these tables relates to the decision on the Null Hypothesis for the K-S test, which is that the two distributions are the same. “Fail to reject” implies that there was insufficient evidence in the data to reject the Null Hypothesis, and hence it is concluded that the measured intensities are Gamma- or Weibull-distributed. “Reject” implies that the measured intensities do not appear to be Gamma-distributed.

A full suite of plots of the simulated CDF versus the ECDF and Q-Q plots are presented in an Appendix F in /La Pointe et al. 2008/; they are not reprinted here for brevity. Note that there are two values for in Table 6-7; α is the shape parameter of the Gamma distribution, while α_{crit} represents the significance level for a one-sided Kolmogorov-Smirnov goodness-of-fit test.

The analysis of the spatial variation of fracture intensity suggests that for the N-S, SH, and WNW fracture sets, both the Gamma and the Weibull distributions can be used to accurately model P_{32} intensity at scales between 9 and 51 metres in all domains. The ENE fracture set, however, does not appear to be well-represented by either distribution at scales smaller than 15 m.

Table 6-8. Fracture intensity as a Γ (Gamma) distribution, FSM_C (example).

Fracture-Set	Section-Length	Test-Statistic	Critical-Value	Test Result $\alpha_{crit} = 0.05$	Distribution Parameters	
					α	β
ENE	3 m	0.377	0.046	Reject	2.491	1.083
ENE	9 m	0.125	0.084	Reject	2.118	0.856
ENE	15 m	0.068	0.112	Fail to Reject	2.214	0.754
ENE	21 m	0.081	0.137	Fail to Reject	2.667	0.618
ENE	30 m	0.081	0.168	Fail to Reject	3.520	0.468
ENE	51 m	0.061	0.218	Fail to Reject	4.769	0.359
N-S	3 m	0.356	0.046	Reject	2.014	1.672
N-S	9 m	0.081	0.084	Fail to Reject	1.195	1.917
N-S	15 m	0.050	0.112	Fail to Reject	1.574	1.434
N-S	21 m	0.065	0.137	Fail to Reject	1.980	1.112
N-S	30 m	0.051	0.168	Fail to Reject	1.935	1.140
N-S	51 m	0.111	0.218	Fail to Reject	2.349	0.961
SH	3 m	0.151	0.046	Reject	1.433	2.100
SH	9 m	0.031	0.084	Fail to Reject	1.482	1.771
SH	15 m	0.040	0.112	Fail to Reject	1.852	1.382
SH	21 m	0.054	0.137	Fail to Reject	1.838	1.355
SH	30 m	0.061	0.168	Fail to Reject	2.608	0.937
SH	51 m	0.105	0.218	Fail to Reject	2.933	0.882
WNW	3 m	0.256	0.046	Reject	2.187	1.453
WNW	9 m	0.047	0.084	Fail to Reject	1.872	1.303
WNW	15 m	0.046	0.112	Fail to Reject	2.365	1.036
WNW	21 m	0.050	0.137	Fail to Reject	2.846	0.852
WNW	30 m	0.081	0.168	Fail to Reject	3.574	0.676
WNW	51 m	0.086	0.218	Fail to Reject	4.269	0.557
All Fracs	3 m	0.039	0.046	Fail to Reject	2.025	4.642
All Fracs	9 m	0.062	0.084	Fail to Reject	3.557	2.526
All Fracs	15 m	0.052	0.112	Fail to Reject	4.592	1.946
All Fracs	21 m	0.076	0.137	Fail to Reject	5.510	1.591
All Fracs	30 m	0.068	0.168	Fail to Reject	6.336	1.375
All Fracs	51 m	0.089	0.218	Fail to Reject	6.747	1.324

Fracture termination matrices

The results of the fracture termination studies, described in Section 6.2.5 are presented below in Table 6-9 through Table 6-12. The recommended usage is to assume the global average values for any regional-scale studies. In general, the fracture termination results suggest that, depending on outcrop, either the N-S or ENE fracture set is the oldest set, followed by a younger WNW fracture set. At outcrop ASM000208 and ASM100235, the ENE set shows distinct banding against an older N-S set. At ASM000209 and ASM100234, the timing is less-apparent; N-S and ENE set fracturing may have been nearly contemporaneous at ASM100234. The timing of the SH set is almost impossible to determine from surface data alone. Further details regarding the terminations of fractures are available in section 5.2 of the SDM Site Laxemar data compilation report (DCR) /Hermanson et al. 2008/.

Table 6-9. Termination matrices for fracture domain FSM_N.

ASM000208

	Terminates Against				
Target Set	**ENE**	**N-S**	**WNW**	**SH**	**Total Percentage of terminations**
ENE	0	15.42%	8.12%	9.74%	**33.28%**
N-S	20.24%	0	13.16%	10.32%	**43.72%**
WNW	19.25%	20.00%	0	10.50%	**49.75%**
SH	16.95%	15.94%	9.06%	0	**41.95%**

ASM100234

	Terminates Against				
Target Set	**ENE**	**N-S**	**WNW**	**SH**	**Total Percentage of terminations**
ENE	0	20.32%	17.09%	5.40%	**42.81%**
N-S	12.02%	0	13.94%	3.83%	**29.79%**
WNW	13.65%	20.55%	0	5.89%	**40.09%**
SH	12.09%	16.05%	18.60%	0	**46.74%**

Table 6-10. Termination matrix for fracture domain FSM_W.

ASM100235

	Terminates Against				
Target Set	**ENE**	**N-S**	**WNW**	**SH**	**Total Percentage of terminations**
ENE	0	34.62%	15.38%	5.77%	**55.77%**
N-S	10.61%	0	10.02%	3.74%	**24.36%**
WNW	19.29%	32.14%	0	3.57%	**55.00%**
SH	10.68%	32.48%	8.97%	0	**52.14%**

Table 6-11. Termination matrix for fracture domain FSM_NE005.

ASM000208

Target Set	Terminates Against ENE	N-S	WNW	SH	Total Percentage of terminations
ENE	0	41.94%	8.61%	3.33%	**53.89%**
N-S	8.97%	0	11.21%	2.99%	**23.18%**
WNW	7.05%	39.32%	0	3.18%	**49.55%**
SH	7.89%	31.05%	10.53%	0	**49.47%**

Table 6-12. Global average termination matrix (all domains).

Global Average

Target Set	Terminates Against ENE	N-S	WNW	SH	Total Percentage of terminations
ENE	0	25.53%	12.24%	6.54%	**44.30%**
N-S	11.82%	0	11.58%	4.46%	**27.86%**
WNW	14.10%	26.87%	0	5.95%	**46.92%**
SH	13.22%	20.66%	12.12%	0	**46.01%**

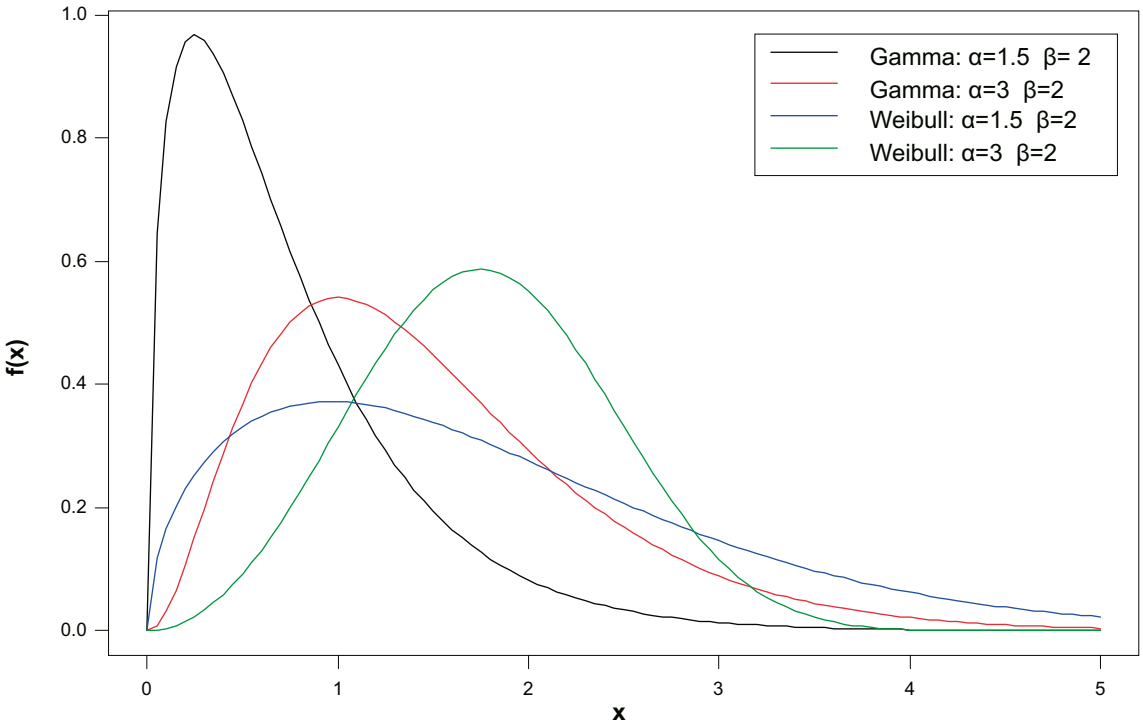

Figure 6-26. *Comparison of Gamma and Weibull distributions for two different values of α and β.*

6.5 Uncertainty analysis, verification and partial validation

6.5.1 Verification

The most notable results out of the SDM-Site Laxemar geological DFN verification efforts are the Gamma and Weibull distribution results from case SI-5, and the results of the alternative model ranking (AMR) process of cases SI-1, SI-2, SI-3, and SI-4. The verification cases, including results of all simulations and AMR calculations, are described in detail in Chapter 6 of /La Pointe et al. 2008/.

Alternative model rankings (AMRs)

There are several possible ways to calculate a final rank for each alternative model across verification cases SI-1, SI-2, SI-3, and SI-4 of the SDM-Site Laxemar GeoDFN. These possibilities occur because it was not possible to carry out all verification cases for all alternative models. For example, Case SI-1 consisted of two sub-analyses: one in which simulated P_{21} values were compared to measured trace data for all fracture traces longer than 0.5 m, and a second case in which only traces within the match range (an example is shown in Figure 6-26) were compared. Since detailed fracture maps do not exist for all possible fracture domains, the fracture domain-specific alternative models could not be all tested.

The first ranking case (AMR-1) consists of only the three verification cases in which domain-specific alternative models could compared to measured data. Moreover, since there are artefacts outside the match ranges that cause the measured traces on an outcrop to depart from a perfect power law model, comparison of model predictions to measurements of trace length intensity for all traces greater than 0.5 m may not be as useful a verification case as comparing traces within the match range. This consideration leads to ranking AMR-2 and AMR-3. AMR-2 consists of all alternative models for which the parameterisation is independent of fracture domain for all possible verification cases. AMR-3 is similar to AMR-2, except that the comparison of the P_{21} of fracture traces longer than 0.5 m (SI-1, which is outside the match ranges, is not included.

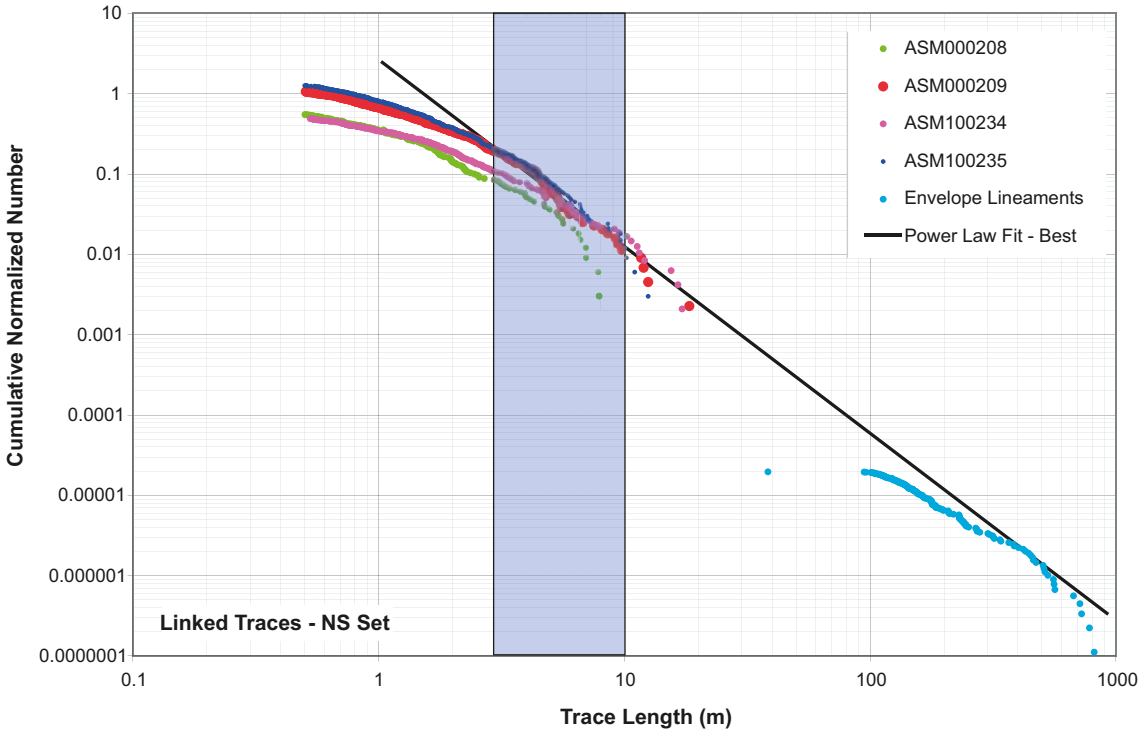

Figure 6-27. *Trace length match interval for the NS Set, with the trace length scaling exponent matched to traces from Outcrop ASM100234. The blue bar represents the limits of the trace length interval used in the verification.*

Another alternative to consider in the overall ranking is how to weight verification case SI-2. Verification case SI-2 compares the fracture intensity of simulated scanline data to scanline data recorded on each of the detail-fracture mapped outcrops. There are several impacts on the average value of P_{10} for the measured data due to scanline sampling that make the mean value potentially more uncertain than other measures of fracture intensity (discussed in detail in Chapter 7 of /La Pointe et al. 2008/). This leads to the final ranking option AMR-4. It is identical to AMR-3, except that verification case SI-2 is not included in the ranking.

The rankings for the alternative models and verification cases are shown in Table 6-13 and Table 6-15. The ANOVA results are presented in Table 6-14 and Table 6-16.

For all of the verification cases where the model parameterisation is fracture domain-dependent, alternative model BMU is the highest ranked. Alternative model BMU is the original BM, with the size model parameterised using unlinked traces from detail-fracture mapped outcrops. Although the BMU case is never the top ranked model for any individual verification case, it is consistently the second or third best model. Other alternative models that are the highest-ranked in an individual verification case have much poorer rankings in the two other verification cases. Using ranking method AMR-1, the BMU model is the highest ranked and the most consistently highly ranked of all alternative models.

Table 6-13. Ranking of alternative models for case AMR-1.

Model	SI-1 (> 0.5 m)	SI-2	SI-3	Sum of Ranks	Rank of Sum
BM	28	25	3	56	22
BMF	11	26	10	47	12
BMU	3	2	2	7	1
BMUF	1	10	11	22	4
EL1	8	30	7	45	11
EL2	5	4	15	24	5
ESL1_N	17	5	5	27	6
ESL1_NE005	21	8	19	48	14
ESL1_W	22	17	15	54	18.5
ESL2_N	30	11.5	13	54.5	20
ESL2_NE005	14	11.5	25	50.5	17
ESL2_W	24.5	23	24	71.5	28
ESL3_N	26	22	27	75	30
ESL3_NE005	13	15	29	57	23.5
ESL3_W	19	21	30	70	27
EUL1	9	28	17	54	18.5
EUL2	2	7	22	31	7
FL1	10	29	9	48	14
FL2	4	1	12	17	2.5
FSL1_N	27	9	4	40	10
FSL1_NE005	12	6	18	36	9
FSL1_W	18	16	14	48	14
FSL2_N	29	14	20	63	26
FSL2_NE005	16	13	28	57	23.5
FSL2_W	23	24	26	73	29
FSL3_N	24.5	18	6	48.5	16
FSL3_NE005	15	20	20	55	21
FSL3_W	20	19	23	62	25
FUL1	7	27	1	35	8
FUL2	6	3	8	17	2.5

Table 6-14. Kruskal-Wallis ANOVA results for AMR-1.

Model Comparison	K Statistic	Probability
BM vs. BMF	0.05	0.83
BM vs. BMU	3.23	0.07
BM vs. BMUF	1.19	0.28
BM vs. EL1	0.05	0.83
BM vs. EL2	0.43	0.51
BM vs. ESL1_N	0.44	0.51
BM vs. ESL1_NE005	0.43	0.51
BM vs. ESL1_W	0.43	0.51
BM vs. ESL2_N	0.05	0.83
BM vs. ESL2_NE005	0.20	0.66
BM vs. ESL2_W	0.43	0.51
BM vs. ESL3_N	0.05	0.83
BM vs. ESL3_NE005	0.05	0.83
BM vs. ESL3_W	0.05	0.83
BM vs. EUL1	0.00	1.00
BM vs. EUL2	1.19	0.28
BM vs. FL1	0.05	0.83
BM vs. FL2	1.19	0.28
BM vs. FSL1_N	0.05	0.83
BM vs. FSL1_NE005	0.43	0.51
BM vs. FSL1_W	0.43	0.51
BM vs. FSL2_N	0.05	0.83
BM vs. FSL2_NE005	0.00	1.00
BM vs. FSL2_W	0.05	0.83
BM vs. FSL3_N	0.43	0.51
BM vs. FSL3_NE005	0.44	0.51
BM vs. FSL3_W	0.43	0.51
BM vs. FUL1	0.43	0.51
BM vs. FUL2	0.78	0.38

The Kruskal-Wallis ANOVA analysis of the various alternative model cases show which models are statistically similar in pair-wise comparisons (Table 6-14). The results in Table 6-14 show that the Base Model (BM) does not significantly differ in its ranking results from the other models; i.e. there is little difference between the alternative cases and the base models in terms of rankings. It should be noted that the power for the test for all ranking cases is fairly low due to the small number of verification cases, so that the conclusion that there is not a significant difference may be an artefact of low statistical power.

The results for rankings AMR-2, AMR-3, and AMR-4 are shown in Table 6-15. The corresponding pair-wise comparisons are shown in Table 6-16. The results show that when the verification case for SI-1 in which all traces longer than 0.5 m are included is deleted from the rankings (AMR-3), the BM is ranked third overall. For all three ranking cases, the pair-wise ANOVA results show that there is no statistically significant difference at the 0.05 probability level between the BM performance and the performance of the other models considered.

Table 6-15. Ranking of alternative models for cases AMR-2 through AMR-4.

Model Alternative	SI-1 (> 0.5 m)	SI-1 (match range)	SI-2	SI-3	SI-4	Ranking AMR-2	Ranking AMR-3	Ranking AMR-4
BM	28	2	25	3	10	6	3.5	2
BMF	11	5	26	10	9	9	8.5	8
BMU	3	9.5	2	2	6	1	2	3
BMUF	1	7	10	11	5	4	6	6.5
EL1	8	8	30	7	12	11	11	10
EL2	5	4	4	15	8	7	7	10
EUL1	9	6	28	17	4	10	10	10
EUL2	2	12	7	22	7	12	12	12
FL1	10	1	29	9	1.5	5	5	1
FL2	4	3	1	12	3	2	1	4
FUL1	7	11	27	1	11	8	8.5	6.5
FUL2	6	9.5	3	8	1.5	3	3.5	5

Table 6-16. Kruskal-Wallis ANOVA results for AMR cases II-IV.

Model Comparison	AMR-2		AMR-3		AMR-4	
	K Statistic	Probability	K Statistic	Probability	K Statistic	Probability
BM vs. BMF	0.40	0.53	1.03	0.31	0.78	0.38
BM vs. BMU	1.13	0.29	0.35	0.55	0.00	1.00
BM vs. BMUF	0.18	0.68	0.53	0.47	1.19	0.28
BM vs. EL1	1.13	0.29	2.58	0.11	1.19	0.28
BM vs. EL2	0.10	0.75	0.76	0.38	1.19	0.28
BM vs. EUL1	0.40	0.53	1.03	0.31	1.19	0.28
BM vs. EUL2	0.18	0.67	1.71	0.19	2.33	0.13
BM vs. FL1	0.18	0.68	0.08	0.77	1.19	0.28
BM vs. FL2	0.41	0.52	0.09	0.77	0.48	0.49
BM vs. FUL1	0.04	0.83	0.76	0.38	0.44	0.51
BM vs. FUL2	0.40	0.53	0.02	0.88	0.05	0.83

Considering all three of the ranking cases, alternative model BMU (the unlinked version of the BM) has the most consistently low rank values. This implies that the BMU alternative model probably is the best overall model for predicting the verification cases. Nonetheless, the BM is also an adequate model for DFN model parameterisation, as the rankings performance does not differ significantly from the BMU, especially for cases AMR-3 and AMR-4. Even considering the lack of power in the ANOVA tests, the similarity in rankings between BM and BMU for Ranking Cases AMR-3 and AMR-4 indicates very little difference.

Results of verification case SI-5

Verification case SI-5 consisted of fitting Gamma and Weibull probability distributions to fracture P_{32} calculated from cored borehole data over intervals of certain scales. P_{32} was calculated using the borehole P_{10} (number of fractures per meters), the Wang C_{13} conversion factor /Wang 2005/, and the global orientation set definitions defined in Section 6.4.2. Distributions were fit at the 3 m, 9 m, 15 m, 21 m, 30 m, and 51 m scales.

Table 6-17 below summarises the verification results. For all fracture orientation sets except the ENE set, in all fracture domains, both the Gamma and Weibull distributions can be used to describe the spatial variability at scales equal to or greater than 9 m. The ENE set can be described using either a Gamma or Weibull distribution at scales greater than 15 m. At scales smaller than 9 m (or 15 m for the ENE set), both distributions fail to reproduce the number of intervals with no recorded fractures.

In all domains except FSM_EW007 and FSM_W, the total fracture intensity (all fracture orientation sets combined, including both open and sealed fractures), can be described using a Gamma or a Weibull distribution down to a scale of 3 m. It is possible that even smaller scales may be valid; however, none were tested during the SDM-Site Laxemar geological DFN verification. In domains FSM_EW007 and FSM_W, total fracture intensity can be described using a Gamma or Weibull distribution at scales of 9 m or larger.

6.5.2 Uncertainty analysis

Table 6-18 summarises the impact of the key uncertainties described in Section 6.3.2. This table lists the type of uncertainty, the range of its impact on P_{32} relative to the base model, including its impact on the sub-horizontal set which is of most concern for estimating earthquake effects on fractures intersecting vertical canister holes, and some general comments about how the uncertainty relates to factors like fracture domain and fracture set. The uncertainty analysis results, along with complete tables for each calculated uncertainty (parameter or conceptual), are described in Chapter 5 in /La Pointe et al. 2008/.

Table 6-17. Summary of Gamma and Weibull distribution analysis results.

Fracture Domain	Orientation Set	Valid scales (tested)	
		Gamma	Weibull
FSM_C	ENE	15 m–51 m	15 m–51 m
FSM_C	N-S	9 m–51 m	9 m–51 m
FSM_C	SH	9 m–51 m	9 m–51 m
FSM_C	WNW	9 m–51 m	9 m–51 m
FSM_EW007	ENE	15 m–51 m	15 m–51 m
FSM_EW008	N-S	9 m–51 m	9 m–51 m
FSM_EW009	SH	9 m–51 m	9 m–51 m
FSM_EW010	WNW	9 m–51 m	9 m–51 m
FSM_N	ENE	9 m–30 m*	9 m–30 m*
FSM_N	N-S	9 m–30 m*	9 m–30 m*
FSM_N	SH	9 m–30 m*	9 m–30 m*
FSM_N	WNW	9 m–30 m*	9 m–30 m*
FSM_NE005	ENE	15 m–51 m	15 m–51 m
FSM_NE006	N-S	9 m–51 m	9 m–51 m
FSM_NE007	SH	9 m–51 m	9 m–51 m
FSM_NE008	WNW	9 m–51 m	9 m–51 m
FSM_W	ENE	15 m–51 m	15 m–51 m
FSM_W	N-S	9 m–51 m	9 m–51 m
FSM_W	SH	9 m–51 m	9 m–51 m
FSM_W	WNW	9 m–51 m	9 m–51 m

* Insufficient number of data points to test at 51 m scale.

Table 6-18. Summary of key uncertainties and their expected impacts on downstream modelling.

Uncertainty	Range of the Ratio of Alternative Model Intensity to Base Model Intensity	Comments
Scaling Exponent Dependence on Fracture Domain Conceptual Uncertainty	0.1 to 1.5; generally 0.13 for sub-horizontal sets	Greatest variability is by set, not fracture domain.
Euclidean vs. Fractal Scaling Conceptual Uncertainty	0.8 to 1.2; 0.84 for sub-horizontal sets	Varies by set
Linked vs. Unlinked Traces Conceptual Uncertainty	0.63 to 1.03; 1.03 for sub-horizontal sets	Fairly minor impact, especially on sub-horizontal fractures
Number of lineaments used in size-intensity model parameterisation	0.44 to 1.11; unable to test subhorizontal sets	Smaller than uncertainty in scaling exponent parameter fit
Scaling Exponent Parameter Uncertainty	0.3–0.5; 0.36 for sub-horizontal sets	Not highly variable among different sets
Open vs. Closed Parameter Uncertainty	0.05 to 0.10 for outcrops; 0.20 to 0.30 for boreholes; generally around 30% for sub-horizontal set (borehole data)	Varies by set and domain

The results shown in Table 6-17 suggest that the best measures to reduce uncertainty in downstream models are to:

- Model each fracture domain separately;
- Model each fracture set within each fracture domain separately; and
- Minimise the scale difference between the scale over which fracture data are collected and the scale to which it is applied. Extrapolating outcrop data to 100 m simulation grid cells produces less uncertainty than extrapolating to 500 m grid cells.

The uncertainties listed in Table 6-17 represent scenarios, with the possible exception of the variation of the scaling exponent parameter, which could also be treated as a continuous variable rather than as a set of bounding values. For scenarios, a useful way to propagate or take into account the uncertainty is to assign a probability that the scenario may occur. If the scenario occurs, then the model would have the parameter values related to the scenario; if not, then the parameter values related to the Base model would be used. In this way, the uncertainties identified and quantified for the fracture model could be propagated into downstream models or calculations with minimal computational effort.

6.5.3 Validation of geological DFN using borehole KLX27A

The validation of the SDM-Site Laxemar geological DFN parameterisation involved the comparison of predicted fracture intensities in borehole KLX27A (fracture domain FSM_W) to observed borehole data, using the top five ranked model alternative cases from the verification results (Section 6.5.1). The validation is described in detail in Appendix G of the SDM-Site Laxemar geological DFN summary report /La Pointe et al. 2008/. Borehole KLX27A was drilled from the southwest corner of fracture domain FSM_S through deformation zone ZSMNW042A and into fracture domain FSM_W at depth. KLX27 is approximately 649 m long, of which 209 m is inside domain FSM_W. The borehole plunges approximately 65 degrees and trends directly north.

The validation utilized stochastic Monte-Carlo simulation of fractures within the full size-intensity range and within the hypothesized MDZ size range (~ 65–125 m, up to 564.2 m).

The minimum size for the MDZ-range simulations was calculated using the trace rollover method described in Section 5.5 of the geological DFN summary report /La Pointe et al. 2008/. 8 to 25 model iterations were completed and sampled with boreholes with geometries identical to that of KLX27A. The validation metric was simulated versus observed mean P_{10} for the full-intensity simulations, and the number of MDZ intersecting the borehole for the MDZ size-range case.

The validation simulations indicated that all five of the top-ranked model alternatives did a good job of predicting total mean fracture intensities in domain FSM_W, but over-predicted fracture intensity in KLX27A. All five size-intensity model alternatives were able to correctly predict the number of MDZ-sized structures intersecting KLX27A. Further analysis indicated that borehole KLX27A (and its neighbour KLX19A) sample a volume of rock that is noticeably different than the rest of domain FSM_W; the total P_{10} value in KLX27A is roughly half that of the average value for FSM_W, and the fractures exhibit a different pattern of relative set intensities than the fracture domain FSM_W as a whole. It is hypothesized that the rock in the footwall of ZSMNW042A where KLX19A and KLX27A may be anomalous with respect to the rest of fracture domain FSM_W; it is significantly less-fractured than the rest of FSM_W. It is possible that the rock in the footwall of ZSMNW042A might best be parameterised as a different fracture domain; however, with only two boreholes and no surface outcrops, it may be difficult to identify the spatial limits of such a domain without further study.

6.6 Discussion and recommendations for DFN usage

1. The division of the Laxemar site into fracture domains has reduced the overall uncertainty of the model, primarily because the fracture intensity varies more between fracture domains than within fracture domains.
2. The difference among fracture domains is not due to changes in the fracture orientations, but to changes in the intensity of individual sets.
3. Given the above conclusion, scaling exponents should be a function of fracture orientation set, but not of fracture domain, and the size/intensity parameterisation should mainly reflect differences in individual set intensity in each domain, not scaling exponent.
4. Fracture termination relationships suggest that the N-S set appears to have formed earliest, while the three remaining sets formed later. The relative chronology of the SH, ENE and WNW sets cannot be distinguished from the termination relations.
5. Analysis of scaling behaviour indicates that intensity scaling is well-modelled by Euclidean scaling at scales greater than a few tens of metres; evidence exists for fractal scaling at smaller scales, although this is not universal and may be due as well to data limitations.
6. We recommend that, where possible, spatial variability in fracture intensity be modelled as a Gamma distribution. A Weibull distribution may also be used if desired; parameters for both cases are presented in /La Pointe et al. 2008/. Both the Gamma and the Weibull distributions were good fit to binned intensity data from Laxemar cored boreholes. Analysis results indicate that at scales of 9–15 m, this is an accurate characterisation of fracture intensity patterns.
7. A Base Model (BM) was defined. It had the following properties.
   - Euclidean scaling.
   - Scaling exponent independent of fracture domain.
   - Based on linked traces.
   - Based on all fractures, not just open.
   - Based on average outcrop intensity values, rather than extremal values.

8. Several alternative models were identified. Relative to the Base Model, these include:
   - Fractal scaling.
   - Scaling exponent dependent on fracture domain.
   - Based on unlinked traces.
   - Based on open fracture intensity.
   - Based on extremal (bounding) outcrop intensity values.
9. Uncertainty analyses were carried out on the alternative models. Uncertainty was quantified as the ratio in fracture intensity by set for each alternative case relative to the Base Case. The Alternative models tends to produce lower fracture intensities, with maximum reductions to about 10% for the case where the model is based on open fracture intensity rather than total fracture intensity. The impact of each uncertainty typically varies by fracture set and fracture domain, in the cases where the latter consideration is relevant to the model parameterisation.
10. Verification efforts built confidence in the SDM Laxemar Site geological DFN for its intended purposes. The verification analysis, which consisted of comparisons of observed fracture intensity and size data to simulation results, suggests that:
11. The BMU (the Base Model parameterisation built using unlinked fracture traces on outcrop instead of linked traces) was generally the highest-ranked model. This model was chosen as the recommended size-intensity model alternative for the SDM-Site Laxemar geological DFN.
12. The alternative model ranking process also suggested that, among the top five alternative models, there was very little difference in the fracture size and intensity produced through simulation.

7 References

Alm E, Sundblad K, 2002. Fluorite-calcite-galena-bearing fractures in the counties of Kalmar and Blekinge, Sweden. SKB R-02-42, Svensk Kärnbränslehantering AB.

Alm E, Sundblad K, Huhma H, 2005. Sm-Nd isotope determinations of low-temperature fluorite-calcite-galena mineralization in the margins of the Fennoscandian Shield. SKB R-05-66, Svensk Kärnbränslehantering AB.

Andersson J, Ström A, Svemar C, Almén K-A, Ericsson L-O, 2000. What requirements does the KBS-3 repository make on the host rock? Geoscientific suitability indicators and criteria for siting and site evaluation. SKB TR-00-12, Svensk Kärnbränslehantering AB.

Andersson J, Berglund J, Follin S, Hakami E, Halvarson J, Hermanson J, Laaksoharju M, Rhén I, Wahlgren C-H, 2002. Testing the methodology for site descriptive modelling. Application for the Laxemar area. SKB TR-02-19, Svensk Kärnbränslehantering AB.

Berglund J, Nyborg M, Triumf C-A, 2006. Oskarshamn site investigation. Lineaments longer than 10 m in two sub areas of Laxemar. Identification of short lineaments from LIDAR and magnetic total field data. SKB P-06-295, Svensk Kärnbränslehantering AB.

Bergman T, Isaksson H, Johansson R, Lindén A H, Lindgren J, Lindroos H, Rudmark L, Wahlgren C-H, 1998. Förstudie Oskarshamn. Jordarter, bergarter och deformationszoner. SKB R-98-56, Svensk Kärnbränslehantering AB.

Bergman B, Juhlin C, Palm H, 2001. Reflektionsseismiska studier inom Laxemarområdet. SKB R-01-07, Svensk Kärnbränslehantering AB.

Bergman T, Malmberg Persson K, Persson M, Albrecht J, 2005. Oskarshamn site investigation. Characterisation of bedrock and Quaternary deposits from excavations in the southern part of Laxemar subarea. SKB P-05-47, Svensk Kärnbränslehantering AB.

Caine J S, Evans J P, Forster C B, 1996. Fault zone architecture and permeability structure. Geology 24 (11), 1025–1028.

Cruden A, 2008. Emplacement mechanisms and structural influences of a younger granite intrusion into older wall rocks – a principal study with application to the Götemar and Uthammar granites. SKB R-08-138, Svensk Kärnbränslehantering AB.

Davis J, 2002. Statistics and Data Analysis in Geology, Third Edition. John Wiley and Sons, New York, New York, USA.

Dershowitz W, 1984. Rock Joint Systems, Doctoral dissertation, Massachusetts Institute of Technology, Cambridge, MA, USA.

Dershowitz W, Lee G, Geier J, Foxford T, La Pointe P, Thomas A, 1998. FRACMAN, Interactive discrete feature data analysis, geometric modelling and exploration simulation. User documentation, version 2.6. Golder Associates, Inc. Redmond, Washington, USA.

Dideriksen K, Christiansen B C, Baker J A, Frandsen C, Balic-Zunic T, Tullborg E-L, Mørup S, Stipp S L S, 2007. Fe-oxide fracture-fillings as a palæo-temperature and -redox indicator: Structure, crystal form, REE content and Fe isotope composition. Chemical Geology 244, 330–343.

Drake H, Tullborg E-L, 2004. Oskarshamn site investigation. Fracture mineralogy and wall rock alteration, results from drill core KSH01A+B. SKB P-04-250, Svensk Kärnbränslehantering AB.

Drake H, Tullborg E-L, 2005. Oskarshamn site investigation. Fracture mineralogy and wall rock alteration, results from drill cores KAS04, KA1755A and KLX02. SKB P-05-174, Svensk Kärnbränslehantering AB.

Drake H, Tullborg E-L, 2006a. Oskarshamn site investigation. Fracture mineralogy. Results from drill core KSH03A+B. SKB P-06-03, Svensk Kärnbränslehantering AB.

Drake H, Tullborg E-L, 2006b. Oskarshamn site investigation. Fracture mineralogy of the Götemar granite. Results from drill cores KKR01, KKR02 and KKR03. SKB P-06-04, Svensk Kärnbränslehantering AB.

Drake H, Tullborg E-L, 2006c. Oskarshamn site investigation. Mineralogical, chemical and redox features of red-staining adjacent to fractures. Results from drill cores KSH01A+B and KSH03A+B. SKB P-06-01, Svensk Kärnbränslehantering AB.

Drake H, Tullborg E-L, 2006d. Oskarshamn site investigation. Mineralogical, chemical and redox features of red-staining adjacent to fractures. Results from drill core KLX04. SKB P-06-02, Svensk Kärnbränslehantering AB.

Drake H, Sandström B, Tullborg E-L, 2006. Mineralogy and geochemistry of rocks and fracture fillings from Forsmark and Oskarshamn. Compilation of data for SR-Can. SKB R-06-109, Svensk Kärnbränslehantering AB.

Drake H, Tullborg E-L, 2007a. Oskarshamn site investigation. Fracture mineralogy, Results from drill cores KLX03, KLX04, KLX06, KLX07A, KLX08 and KLX10A. SKB P-07-74, Svensk Kärnbränslehantering AB.

Drake H, Tullborg E-L, 2007b. Paleohydrogeology of the Simpevarp area, southeastern Sweden, as evidenced by stable isotopes in fracture minerals. In Bullen, T D, and Wang, Y, eds. Water-rock Interaction: Proceedings of the 12th International Symposium on Water-Rock Interaction, Kunming, China, 31 July–5 August 2007, v. 1: London, UK, Taylor & Francis, p. 723–726.

Drake H, Page L, Tullborg E-L, 2007. Oskarshamn site investigation. $^{40}Ar/^{39}Ar$ dating of fracture minerals. SKB P-07-27, Svensk Kärnbränslehantering AB.

Drake H, Tullborg E-L, 2008a. Paleohydrogeological evidences from stable isotopes, fluid inclusions and trace elements in fracture minerals in crystalline rock, Simpevarp area, south-eastern Sweden. Abstract Volume of the 28th Nordic Geological Winter Meeting, Aalborg, Denmark, January 7–10, 2008, Department of Civil Engineering, Aalborg University, Aalborg, Denmark, p. 105.

Drake H, Tullborg E-L, 2008b. Oskarshamn site investigation. Detecting the near surface redox front in crystalline rock. Results from drill cores KLX09B-G and KLX11B-F. SKB P-08-44, Svensk Kärnbränslehantering AB.

Drake H, Tullborg E-L, 2008c. Oskarshamn site investigation. Fracture mineralogy. Results from drill core KLX15A. SKB P-08-11, in press, Svensk Kärnbränslehantering AB.

Drake H, Tullborg E-L, 2008d. Oskarshamn site investigation. Mineralogy in water conducting zones. Results from drill cores KLX13A and KLX17A with additional fracture mineralogical data from drill cores KLX14A, KLX19A, KLX20A and KLX26A. SKB P-08-12, in press, Svensk Kärnbränslehantering AB.

Drake H, Tullborg E-L, 2008e. Oskarshamn site investigation. Mineralogy in water conducting zones. Results from boreholes KLX03, KLX04, KLX06, KSH01A+B, KSH02 and KSH03A. SKB P-08-41, in press, Svensk Kärnbränslehantering AB.

Drake H, Tullborg E-L, 2008f. Oskarshamn site investigation. Mineralogy in water conducting zones. Results from boreholes KLX07A+B and KLX08. SKB P-08-42, in press, Svensk Kärnbränslehantering AB.

Drake H, Tullborg E-L, Smellie J, in preparation. Fracture mineralogy of the Laxemar site. Final report. SKB R-08-XX, Svensk Kärnbränslehantering AB.

Forssberg O, Cronquist T, Vestgård J, Bergkvist L, Hermanson J, Öhman J, Pettersson A, Koyi S, Bergman T, 2007. Oskarshamn site investigation. Detailed outcrop mapping in trenches. SKB P-07-29, Svensk Kärnbränslehantering AB.

Fox A, La Pointe P, Öhman J, Hermanson J, 2007. Forsmark modelling stage 2.2. Statistical geological discrete fracture network model for the Forsmark site, stage 2.2. SKB R-07-46, Svensk Kärnbränslehantering AB.

Frey M, de, C C, Liou J G, 1991. A new petrogenetic grid for low-grade metabasites. Sixth meeting of the European Union of Geosciences, v. 3; 1: Oxford, International, Blackwell Scientific Publications, p. 106.

Glamheden R, Curtis P, 2006. Comparative evaluation of core mapping results for KFM06C and KLX07B. SKB R-06-55, Svensk Kärnbränslehantering AB.

Hermanson J, Fox A, Öhman J, Rhén I, 2008. Site Descriptive Modelling SDM-Site Laxemar. Compilation of data used for the analysis of the geological and hydrogeological DFN models. SKB P-08-56, Svensk Kärnbränslehantering AB.

Johansson R, 2006. A comparison of two independent interpretations of lineaments from geophysical and topographic data from the Simpevarp area. SKB R-06-53, Svensk Kärnbränslehantering AB.

Juhlin C, Bergman B, Cosma C, Keskinen J, Enescu N, 2002. Vertical seismic profiling and integration with reflection seismic studies at Laxemar, 2000. SKB TR-02-04, Svensk Kärnbränslehantering AB.

Juhlin C, Bergman B, Palm H, 2004. Oskarshamn site investigation. Reflection seismic studies performed in the Laxemar area during 2004. SKB P-04-215, Svensk Kärnbränslehantering AB.

Kamb W B, 1959. Ice petrofabric observations from Blue Glacier, Washington, in relation to theory and experiments, J. Geophys. Res. 64, 1891–1909.

Koistinen T, Stephens M B, Bogatchev V, Nordgulen O, Wennerström M, Korhonen J, 2001. Geological map of the Fennoscandian Shield, scale 1:2 000 000. Geological Surveys of Finland, Norway and Sweden and the North-West Department of Natural Resources of Russia.

Korhonen K, Kuivamäki A, Ruotoistenmäki T, Paananen M, 2005. Interpretation of lineaments from airborne geophysical and topographic data. An alternative model within version Laxemar 1.2 of the Oskarshamn modelling project. SKB P-05-247, Svensk Kärnbränslehantering AB.

Kresten P, Chyssler J, 1976. The Götemar Massif in south-eastern Sweden; a reconnaissance survey. Geologiska Föreningen i Stockholm Förhandlingar 98, 155–161.

La Pointe P, Wallmann P, Dershowitz W, 1993. Stochastic estimation of fracture size from simulated sampling. Int. Jour. Rock Mech. Min. Sci. & Geomech. Abstr. v. 30, 1611–1617.

La Pointe P, Fox A, Hermanson J, Öhman J, 2008. Site Descriptive Modelling. SDM-Site Laxemar. Geological discrete fracture network model for the Laxemar site SKB R-08-55, Svensk Kärnbränslehantering AB.

Larson S Å, Tullborg E-L, Cederbom C, Stiberg J-A, 1999. Sveconorwegian and Caledonian foreland basins in the Baltic Shield revealed by fission-track thermochronology. Terra Nova 11, 210–215.

Lidmar-Bergström K, 1996. Long term morphotectonic evolution in Sweden. Geomorphology 16, 33–59.

Lindqvist G, 2004a. Oskarshamn site investigation. Refraction seismic measurements in the water outside Simpevarp and Ävrö and on land on Ävrö. SKB P-04-201, Svensk Kärnbränslehantering AB.

Lindqvist G, 2004b. Oskarshamn site investigation. Refraction seismic measurements in Laxemar. SKB P-04-134, Svensk Kärnbränslehantering AB.

Lindqvist G, 2004c. Oskarshamn site investigation.Refraction seismic measurements in Laxemar autumn 2004. SKB P-04-298, Svensk Kärnbränslehantering AB.

Lindqvist G, 2005. Oskarshamn site investigation.Refraction seismic measurements in Laxemar spring 2005. SKB P-05-155, Svensk Kärnbränslehantering AB.

Lindqvist G, 2006. Oskarshamn site investigation.Refraction seismic measurements in Laxemar spring 2006. SKB P-06-49, Svensk Kärnbränslehantering AB.

Lindqvist G, 2007. Oskarshamn site investigation.Refraction seismic measurements in Laxemar spring 2007. SKB P-07-131, Svensk Kärnbränslehantering AB.

Lindroos H, 2004. The potential for ore, industrial minerals and commercial stones in the Simpevarp area. SKB R-04-72, Svensk Kärnbränslehantering AB.

Liou J G, Maruyama S, Cho M, 1985. Phase equilibria and mixed parageneses of metabasites in low-grade metamorphism, Diagenesis and low-temperature metamorphism. v. 49, Part 3; 352: London, United Kingdom, Mineralogical Society, p. 321–333.

Lundberg E, Sjöström H, 2006. Oskarshamn site investigation. Kinematic analysis of ductile and brittle/ductile shear zones in Simpevarp and Laxemar subarea. SKB P-06-118, Svensk Kärnbränlehantering AB.

Mattsson H, Thunehed H, Triumf C-A, 2003. Oskarshamn site investigation. Compilation of petrophysical data from rock samples and in situ gamma-ray spectrometry measurements. SKB P-03-97, Svensk Kärnbränslehantering AB.

Mattsson H, Thunehed H, Triumf C-A, 2005a. Oskarshamn site investigation. Compilation of petrophysical data from rock samples and in situ gamma-ray spectrometry measurements, Stage 2 – 2004 (including 2002). SKB P-04-294, Svensk Kärnbränslehantering AB.

Mattsson H, 2006a. Oskarshamn site investigation. The magnetic anisotropy of rocks across two major deformation zones in the Laxemar and Simpevarp area. SKB P-06-100, Svensk Kärnbränslehantering AB.

Mattsson H, 2006b. The magnetic anisotropy of rocks across the deformation zone NE-1 at the Äspö HRL. SKB IPR-06-32, Svensk Kärnbränslehantering AB.

Mattsson H, Triumf C-A, 2007. Oskarshamn site investigation. Detailed ground geophysics at Laxemar, spring 2007. Magnetic total field. SKB P-07-168, Svensk Kärnbränslehantering AB.

Middlemost E A K, 1994. Naming materials in the magma/igneous rock system. Earth-Science Reviews 37, 215–224.

Milnes A G, Gee D G, 1992. Bedrock stability in southeastern Sweden. Evidence from fracturing in the Ordovician limestones of northern Öland. SKB TR-92-23, Svensk Kärnbränslehantering AB.

Milnes A G, Gee D D, Lund C-E, 1998. Crustal structure and regional tectonics of SE Sweden and the Baltic Sea. SKB TR-98-21, Svensk Kärnbränslehantering AB.

Milodowski A E, Tullborg E-L, Buil B, Gomez P, Turrero M-J, Haszeldine S, England G, Gillespie M R, Torres T, Ortiz J E, Zacharias J, Silar J, Chvatal M, Strnad L, Sebek O, Bouch J E, Chenery S R, Chenery C, Shepherd T J, McKervey J A, 2005. Application of Mineralogical, Petrological and Geochemical tools for Evaluating the Palaeohydrogeological Evolution of the PADAMOT Study Sites. PADAMOT Project Technical Report WP2.

Muir Wood R, 1993. A review of the seismotectonics of Sweden. SKB TR-93-13, Svensk Kärnbränslehantering AB.

Muir Wood R, 1995. Reconstructing the tectonic history of Fennoscandia from its margins: The past 100 million years. SKB TR-95-36, Svensk Kärnbränslehantering AB.

Munier R, Talbot C J, 1993. Segmentation, fragmentation and jostling of cratonic basement in and near Aspo, Southeast Sweden. Tectonics, v. 12, p. 713–727.

Munier R, Hermanson J, 2001. Metodik för geometrisk modellering. Presentation och administration av platsbeskrivande modeller. SKB R-01-15, Svensk Kärnbränslehantering AB.

Munier R, Stenberg L, Stanfors R, Milnes A G, Hermanson J, Triumf C-A, 2003. Geological Site Descriptive Model. A strategy for the development during site investigations. SKB R-03-07, Svensk Kärnbränslehantering AB.

Munier R, Stigsson M, 2007. Implementation of uncertainties in borehole geometries and geological orientation data in SICADA. SKB R-07-19, Svensk Kärnbränslehantering AB.

Månsson A G M, 1996. Brittle reactivation of ductile basement structures; a tectonic model for the Lake Vättern basin, southern Sweden. GFF 118, A19 (extended abstract).

Nilsson M, 1992. Geochemistry of Middle Proterozoic mafic and composite mafic-felsic dykes in southeastern Sweden. Geologiska Föreningens i Stockholm Förhandlingar 114, 113–130.

Nilsson G, Nissen J, 2007. Revision of borehole deviation measurements in Forsmark, SKB P-07-28, Svensk Kärnbränslehantering AB.

NIST, 2007a. Kolomogorov-Smirnov Goodness-of-Fit Test, Chapter 1.3.5.16, NIST/ SEMATECH e-Handbook of Statistical Methods, National Institute of Standards and Technology, United States Department of Commerce, Washington D.C. USA. Last accessed 20070903. http://www.itl.nist.gov/div898/handbook/eda/section3/eda35g.htm.

Nordenskjöld C E, 1944. Morphologiska studier inom övergångsområdet mellan Kalmarslätten och Tjust. Meddelanden Lunds Universitets Geografiska institution, Avhandlingar VIII.

Nyborg M, 2005. Oskarshamn site investigation. Aerial photography and airborne laser scanning Laxemar – Simpevarp. The 2005 campaign. SKB P-05-223, Svensk Kärnbränslehantering AB.

Olofsson I, Simeonov A, Stephens M B, Follin S, Nilsson A-C, Röshoff K, Lindberg U, Lanaro F, Fredriksson A, Persson L, 2007. Site descriptive modelling Forsmark. stage 2.2. A fracture domain concept as a basis for the statistical modelling of fractures and minor deformation zones, and interdisciplinary coordination. SKB R-07-15, Svensk Kärnbränslehantering AB.

Olsson T, Stanfors R, Sigurdsson O, Erlström M, 2007. Oskarshamn site investigation. Identification and characterisation of minor deformation zones based on lineament interpretation. SKB P-06-282, Svensk Kärnbränslehantering AB.

Page L, Söderlund P, Wahlgren C-H, 2007. Oskarshamn site investigation. $^{40}Ar/^{39}Ar$ and (U-Th)/He Geochronology of samples from the cored boreholes KSH03A, KSH03B, KLX01, KLX02 and the access tunnel to the Äspö Hard Rock Laboratory. SKB P-07-160, Svensk Kärnbränslehantering AB.

Pearson K, 1904. Mathematical Contributions to the Theory of Evolution XIII: On the theory of contingency and its relation to association and normal correlation. Draper's Company Research Memoirs, Biometric Series, No. 1. Dulau & Company, London, U.K.

Persson Nilsson K, Bergman T, Eliasson T, 2004. Oskarshamn site investigation. Bedrock mapping 2004 – Laxemar subarea and regional model area. Outcrop data and description of rock types. SKB P-04-221, Svensk Kärnbränslehantering AB.

Robin P-Y F, Jowett C, 1986. Computerized density contouring and statistical evaluation of oriented data using counting circles and continuous weighing functions, Tectonophysics, 121, pp. 207–223.

Rønning H J S, Kihle O, Mogaard J O, 2003. Simpevarp site investigation. Helicopter borne geophysics at Simpevarp, Oskarshamn, Sweden. SKB P-03-25, Svensk Kärnbränslehantering AB.

Shapiro S S, Wilk M B, 1965. An analysis of variance test for normality (complete samples), Biometrika 52, 591–611.

SKB, 2002. Simpevarp – site descriptive model version 0. SKB R-02-35, Svensk Kärnbränslehantering AB.

SKB, 2004. Preliminary site description. Simpevarp area – version 1.1. SKB R-04-25, Svensk Kärnbränslehantering AB.

SKB, 2005a. Preliminary site description. Simpevarp subarea – version 1.2. SKB R-05-08, Svensk Kärnbränslehantering AB.

SKB, 2005b. Preliminary safety evaluation for the Simpevarp subarea – Based on data and site descriptions after the initial site investigation stage. SKB R-05-12, Svensk Kärnbränslehantering AB.

SKB, 2006a. Final repository for spent nuclear fuel. Underground design for Simpevarp, Layout D1. SKB R-06-35, Svensk Kärnbränslehantering AB.

SKB, 2006b. Preliminary site description, Laxemar subarea – version 1.2. SKB R-06-10, Svensk Kärnbränslehantering AB.

SKB, 2006c. Preliminary safety evaluation for the Laxemar subarea – Based on data and site descriptions after the initial site investigation satge. SKB R-06-06, Svensk Kärnbränslehantering AB.

SKB, 2006d. Final repository for spent nuclear fuel. Underground design Laxemar, Layout D1. SKB R-06-36, Svensk Kärnbränslehantering AB.

SKB, 2006e. Long-term safety for KBS-3 repositories at Forsmark and Laxemar – a first evaluation. Main report of the SR-Can project. SKB TR-06-09, Svensk Kärnbränslehantering AB.

SKB, 2006f. Preliminary site description Laxemar stage 2.1. Feedback for the completion of the site investigation including input from safety assessment and repository engineering. SKB R-06-110, Svensk Kärnbränslehantering AB.

SKB, 2006g. Hydrogeochemical evaluation. Preliminary site description Laxemar subarea – version 1.2. SKB R-06-12, Svensk Kärnbränlehantering AB.

SKB, 2007. Prioritering av platsen för ett slutförvar i Oskarshamn. SKB R-07-21, Svensk Kärnbränslehantering AB.

Snedecor G W, Cochran W G, 1980. Statistical methods, 7th edition, Iowa State University Press, Ames, Iowa, USA.

Sohlenius G, Bergman T, Snäll S, Lundin L, Lode E, Stendahl J, Riise A, Nilsson J, Johansson T, Göransson M, 2006. Oskarshamn site investigation. Soils, Quaternary deposits and bedrock in topographic lineaments situated in the Laxemar subarea. SKB P-06-121, Svensk Kärnbränlehantering AB.

Stanfors R, 2006. Review of existing information from the Äspö HRL area, with focus on hydraulically important minor structures. SKB P-06-117, Svensk Kärnbränslehantering AB.

Stenberg L, Håkanson N, 2007. Oskarshamn site investigation. Revision of borehole deviation measurements in Oskarshamn. SKB P-07-55, Svensk Kärnbränslehantering AB.

Stephens M B, Wahlgren C-H, Weihed P, 1994. Geological Map of Sweden, scale 1:3 000 000. SGU series Ba 52, Sveriges Geologiska Undersökning.

Stephens M B, Fox A, La Pointe P, Simeonov A, Isaksson H, Hermanson J, Öhman J, 2007. Geology Forsmark. Site descriptive modelling Forsmark stage 2.2. SKB R-07-45, Svensk Kärnbränslehantering AB.

Stigsson M, 2007. Analysis of uncertainty and changes in orientation of fractures coupled to PFL anomalies. Forsmark site investigation. SKB P-07-178, Svensk Kärnbränslehantering AB.

Streckeisen A, 1976. To each plutonic rock its proper name. Earth Science Reviews 12, 1–33.

Söderbäck B (edit.), 2008. Geological evolution, palaeoclimate and historical development of the Forsmark and Laxemar-Simpevarp areas. SKB R-08-19, Svensk Kärnbränslehantering AB.

Söderlund P, Page L, Söderlund U, 2008a. $^{40}Ar/^{39}Ar$ biotite and hornblende geochronology from the Oskarshamn area, SE Sweden: Discerning multiple Proterozoic tectonothermal events. Geological Magazine 145, 790–799.

Söderlund P, Juez-Larré J, Page L M, Stuart F M, Andriessen P M, 2008b. Assessment of discrepant (U-Th)/He and apatite fission-track ages in slowly cooled Precambrian terrains: a case study from SE Sweden. In Söderlund P, ^{40}Ar-^{39}Ar, AFT and (U-Th)/He thermochronologic implications for the low-temperature geological evolution in SE Sweden. PhD thesis volume, University of Lund, Sweden.

Talbot C, Riad L, 1988. Natural fractures in the Simpevarp area. SKB PR-25-87-03, Svensk Kärnbränlehantering AB.

Talbot C, Ramberg H, 1990. Some clarification of the tectonics of Äspö and its surroundings. SKB PR 25-90-15, Svensk Kärnbränlehantering AB.

Thunehed H, Triumf C-A, Pitkänen T, 2004. Oskarshamn site investigation. Geophysical profile measurements over interpreted lineaments in the Laxemar area. SKB P-04-211, Svensk Kärnbränslehantering AB.

Thunehed H, Triumf C-A, 2005. Oskarshamn site investigation. Detailed ground geophysical survey at Laxemar. Magnetic total field and resistivity. SKB P-05-188, Svensk Kärnbränslehantering AB.

Thunehed H, Triumf C-A, 2006. Oskarshamn site investigation. Detailed ground geophysics at Laxemar, autumn/winter 2005/2006. Magnetic total field and resistivity. SKB P-06-137, Svensk Kärnbränslehantering AB.

Triumf C-A, 2003. Oskarshamn site investigation. Identification of lineaments in the Simpevarp area by the interpretation of topographical data. SKB P-03-99, Svensk Kärnbränslehantering AB.

Triumf C-A, Thunehed H, Kero L, Persson L, 2003. Oskarshamn site investigation. Interpretation of airborne geophysical survey data. Helicopter borne survey data of gamma ray spectrometry, magnetics and EM from 2002 and fixed wing airborne survey data of the VLF-field from 1986. SKB P-03-100, Svensk Kärnbränslehantering AB.

Triumf C-A, 2004a. Joint interpretation of lineaments in the eastern part of the site descriptive model area. Oskarshamn site investigation. SKB P-04-37, Svensk Kärnbränslehantering AB.

Triumf C-A, 2004b. Oskarshamn site investigation. Joint interpretation of lineaments. SKB P-04-49, Svensk Kärnbränslehantering AB.

Triumf C-A, 2004c. Oskarshamn site investigation. Gravity measurements in the Laxemar model area with surroundings. SKB P-04-128, Svensk Kärnbränslehantering AB.

Triumf C-A, 2007. Oskarshamn site investigation. Assessment of probable and possible dolerite dykes in the Laxemar sub-area from magnetic total field data and digital elevation models. SKB P-07-223, Svensk Kärnbränslehantering AB.

Triumf C-A, Thunehed H, 2007. Oskarshamn site investigation. Co-ordinated lineaments longer than 100 m at Laxemar. Identification of lineaments from LIDAR data and co-ordination with lineaments in other topographical and geophysical data. SKB P-06-262, Svensk Kärnbränslehantering AB.

Tullborg E-L, Larson S Å, Stiberg J P, 1996. Subsidence and uplift of the present land surface in the southeastern part of the Fennoscandian Shield. GFF 118, 126–128.

Tullborg E-L, 2003. Palaeohydrogeological evidences from fracture filling minerals – Results from the Äspö/Laxemar area. Mat. Res.Soc. Symp. 807, 873–878.

Viola G, Venvik Ganerød G, 2007a. Oskarshamn site investigation. Structural analysis of britle deformation zones in the Simpevarp-Laxemar area, Oskarshamn, southeast Sweden. SKB P-07-41, Svensk Kärnbränslehantering AB.

Viola G, Venvik Ganerød G, 2007b. Oskarshamn site investigation. Structural characterisation of deformation zones (faults and ductile shear zones) from selected drill cores and outcrops from the Laxemar area – results from Phase 2. SKB P-07-227, Svensk Kärnbränslehantering AB.

Viola G, 2008. Ductile and brittle structural evolution of the Laxemar-Simpevarp area: an independent analysis based on local and regional constraints. SKB R-08-124, Svensk Kärnbränslehantering AB.

Viola G, Venvik Ganerød G, 2008. Oskarshamn site investigation. Structural characterisation of deformation zones (faults and ductile shear zones) from selected drill cores from the Laxemar area. SKB P-08-07, Svensk Kärnbränslehantering AB.

Vollmer F, 1995. C program for automatic contouring of spherical orientation data using a modified Kamb method, Computers and Geosciences 21, 31–49.

Wahlgren C-H, Ahl M, Sandahl K-A, Berglund J, Petersson J, Ekström M, Persson P-O, 2004. Oskarshamn site investigation. Bedrock mapping 2003 – Simpevarp subarea. Outcrop data, fracture data, modal and geochemical classification of rock types, bedrock map, radiometric dating. SKB P-04-102, Svensk Kärnbränlehantering AB.

Wahlgren C-H, Bergman T, Persson Nilsson K, Eliasson T, Ahl M, Ekström M, 2005. Oskarshamn site investigation. Bedrock map of the Laxemar subarea and surroundings. Description of rock types, modal and geochemical analyses, including the cored boreholes KLX03, KSH03 and KAV01. SKB P-05-180, Svensk Kärnbränslehantering AB.

Wahlgren C-H, Hermanson J, Curtis P, Triumf C-A, Drake H, Tullborg E-L, 2006a. Geological description of rock domains and deformation zones in the Simpevarp and Laxemar

subareas. Preliminary site description Laxemar subarea – version 1.2. SKB R-05-69, Svensk Kärnbränslehantering AB.

Wahlgren C-H, Bergman T, Ahl M, Ekström M, 2006b. Oskarshamn site investigation. Modal and geochemical analyses of drill core samples 2005. Classification of rock types in KLX03, KLX04, KLX06, KLX07A, KLX07B, KLX08 and KLX10. SKB P-06-07, Svensk Kärnbränslehantering AB.

Wahlgren C-H, Bergman T, Ahl M, Ekström M, 2006c. Oskarshamn site investigation. Modal and geochemical analyses of drill core samples 2006 and updated bedrock map of the Laxemar subarea. Classification of rock types in KLX08, KLX10, KLX11A, KLX12A, KLX18A and KLX20A. SKB P-06-279, Svensk Kärnbränslehantering AB.

Wahlgren C-H, Bergman T, Ahl M, Ekström M, Page L, Söderlund U, 2007. Oskarshamn site investigation. Modal and geochemical analyses of drill core samples 2007 and $^{40}Ar/^{39}Ar$ dating of a dolerite. Classification of rock types in KLX15A, KLX16A, KLX19A, KLX20A and KLX21B. SKB P-07-191, Svensk Kärnbränslehantering AB.

Wang X, 2005. Stereological Interpretation of Rock Fracture Traces on Borehole Walls and Other Cylindrical Surfaces, Virginia Polytechnic Institute and State University, doctoral dissertation.

Weibull W, 1951. A statistical distribution function of wide applicability. Journal of Applied Mechanics 18, pp. 293–305.

Wik N-G, Bergström U, Bruun Å, Claeson D, Jelinek C, Juhojontti N, Kero L, Lundqvist L, Stephens M B, Sukotjo S, Wikman H, 2005. Beskrivning till regional berggrundskarta över Kalmar län. Sveriges geologiska undersökning Ba 66.

Wiklund S, 2002. Digitala ortofoton och höjdmodeller. Redovisning av metodik för platsundersökningsområdena Oskarshamn och Forsmark samt förstudieområdet Tierp Norra. SKB P-02-02, Svensk Kärnbränslehantering AB.

Wikman H, Kornfält K-A, 1995. Updating of a lithological model of the bedrock of the Äspö area. SKB PR 25-95-04, Svensk Kärnbränslehantering AB.

Wrafter J, Sundberg J, Ländell M, Back P-E, 2006. Thermal modelling, Laxemar subarea – version 2.1. SKB R-06-84, Svensk Kärnbränslehantering AB.

Appendix 1

Specification of available data

A specification of quality-assured, geological and geophysical data that were available for use in the geological modelling work in the SDM-Site Laxemar stage is presented in Table A1-1. A summary of the actual application of these data in the analytical and modelling work is also included in this table. The reference list to all the P- and R-reports is provided in Table A1-2. Furthermore, references to supporting R-, PR,- TR- and IPR-reports are also included in Table A1-2.

Table A1-1. Available bedrock geological and geophysical data and their treatment in SDM-Site Laxemar model stage. Data reports in italics show older data already available at data freeze Laxemar 2.1.

Data specification	Reference to data report	Reference in Sicada/GIS	Usage in analysis/ modelling
Data from core-drilled boreholes			
Technical data in connection with drilling (KSH01A, KSH01B, KSH02, KSH03A, KSH03B, KAV01, KAV04A, KAV04B, KLX03, KLX04, KLX05, KLX06, KLX07A, KLX07B, KLX08, KLX09, KLX09B-F, KLX09G, KLX10, KLX10B, KLX10C, KLX11A, KLX11B-F, KLX12A, KLX13A, KLX14A, KLX15A, KLX16A, KLX17A, KLX18A, KLX19A, KLX20A, KLX21B, KLX22A, KLX22B, KLX23A, KLX23B, KLX24A, KLX25A, KLX26A, KLX26B, KLX27A, KLX28A, KLX29A)	P-03-113 P-04-151 P-04-233 P-05-25 P-05-167 P-05-111 P-05-233 P-05-234 P-06-14 P-06-222 P-06-265 P-06-297 P-06-116 P-06-306 P-06-283 P-06-305 P-07-195 P-08-21 P-07-221 P-07-98 P-07-202 P-07-134 P-08-24	AP PS 400-02-004 AP PS 400-02-019 AP PS 400-02-021 AP PS 400-03-042 AP PS 400-03-050 AP PS 400-03-050 tillägg 1 AP PS 400-03-050 tillägg 2 AP PS 400-04-008 AP PS 400-04-008 tillägg AP PS 400-04-008 tillägg 2 AP PS 400-04-007 AP PS 400-04-056 AP PS 400-04-056 tillägg AP PS 400-04-055 AP PS 400-04-055 tillägg AP PS 400-04-096 AP PS 400-04-096 tillägg AP PS 400-04-096 tillägg 2 AP PS 400-04-096 tillägg 3 AP PS 400-04-096 tillägg 4 AP PS 400-04-096 tillägg 5 AP PS 400-04-115 AP PS 400-04-115 tillägg 1 AP PS 400-05-020 AP PS 400-05-075 AP PS 400-05-075 tillägg AP PS 400-05-100 AP PS 400-05-021 AP PS 400-05-021 tillägg AP PS 400-05-102 AP PS 400-05-065 AP PS 400-05-065 tillägg AP PS 400-06-020 AP PS 400-05-070 AP PS 400-06-010 AP PS 400-06-010 tillägg AP PS 400-06-010 tillägg AP PS 400-06-091 AP PS 400-06-101 AP PS 400-06-101 tillägg 1 AP PS 400-06-101 tillägg 2 AP PS 400-06-133 AP PS 400-06-073 AP PS 400-06-073 tillägg	Siting and orientation of boreholes in modelling work.

Data specification	Reference to data report	Reference in Sicada/GIS	Usage in analysis/ modelling
		AP PS 400-06-073 tillägg 2 AP PS 400-06-011 AP PS 400-06-011 tillägg 1 AP PS 400-06-011 tillägg 2 AP PS 400-06-054 AP PS 400-06-026 AP PS 400-06-108 AP PS 400-06-108 tillägg 1 AP PS 400-06-108 tillägg 2 AP PS 400-06-055 AP PS 400-06-055 tillägg 1 AP PS 400-06-055 tillägg 2 AP PS 400-06-055 tillägg 3 AP PS 400-07-058 AP PS 400-07-058 tillägg 1	
Radar and BIPS-logging, and interpretation of radar logs (KSH01A, KSH01B, KSH02, KSH03A, KSH03B, KAV01, KAV04A, KAV04B, KLX03, KLX04, KLX05, KLX06, KLX07A, KLX07B, KLX08, KLX09, KLX09B-F, KLX09G, KLX10, KLX10B, KLX10C, KLX11A, KLX11B-F, KLX12A, KLX13A, KLX14A, KLX15A, KLX16A, KLX17A, KLX18A, KLX19A, KLX20A, KLX21B, KLX22A, KLX22B, KLX23A, KLX23B, KLX24, KLX25, KLX26A, KLX26B, KLX27A, KLX28A, KLX29A)	*P-03-109* *P-03-120* *P-03-73* *P-04-195* *P-04-218* *P-04-239* *P-04-275* *P-04-48* *P-04-66* P-05-231 P-05-240 *P-05-30* *P-05-82* P-05-161 P-06-156 P-06-159 P-06-167 P-06-260 P-06-48 P-06-50 P-06-99 P-07-117 P-07-12 P-07-13 P-07-57 P-07-58 P-08-30	AP PS 400-03-002 AP PS 400-03-032 AP PS 400-03-055 AP PS 400-03-081 AP PS 400-03-097 AP PS 400-04-046 AP PS 400-04-060 AP PS 400-04-080 AP PS 400-04-120 AP PS 400-05-004 AP PS 400-05-004 tillägg AP PS 400-05-050 AP PS 400-05-058 AP PS 400-05-089 AP PS 400-05-093 AP PS 400-06-016 AP PS 400-06-032 AP PS 400-06-033 AP PS 400-06-033 tillägg nr 1 AP PS 400-06-058 AP PS 400-06-058 tillägg nr 1 AP PS 400-06-058 tillägg nr 2 AP PS 400-06-083 AP PS 400-06-083 tillägg nr 1 AP PS 400-06-083 tillägg nr 2 AP PS 400-06-083 tillägg nr 3 AP PS 400-06-117 AP PS 400-06-136 AP PS 400-06-156 AP PS 400-06-156 tillägg nr 1 AP PS 400-07-004 AP PS 400-07-037 AP PS 400-07-064	Data used in borehole mapping (BIPS) and in single-hole interpretation (radar logging) with focus on the identification of brittle deformation zones. Input for both rock domain and DZ modelling.
Geophysical logging (KAV01, KAV01, KAV04A, KAV04B, KLX03, KLX04, KLX05, KLX06, KLX07A, KLX07B, KLX08, KLX09, KLX09B, KLX09D, KLX09F, KLX09G, KLX10 , KLX10B, KLX10C, KLX11A, KLX11B, KLX12A, KLX13A, KLX14A, KLX15A, KLX16A, KLX18A, KLX19, KLX20, KLX21B, KLX22A, KLX22B, KLX23A, KLX23B, KLX24, KLX25, KLX26A, KLX26B, KLX27A, KLX28, KLX29A, KSH01A, KSH01B, KSH02, KSH03A, KSH03B)	*P-03-16* *P-03-111* *P-04-232* *P-04-50* *P-04-202* *P-04-306* *P-04-280* *P-05-31* P-05-144 P-05-228 P-05-270 P-06-20 P-06-154 P-06-197 P-06-198 P-06-290 P-06-307 P-06-314 P-06-315	AP PS 400-03-001 AP PS 400-03-031 AP PS 400-03-031 AP PS 400-03-082 AP PS 400-04-047 AP PS 400-04-061 AP PS 400-04-081 AP PS 400-04-119 AP PS 400-05-005 AP PS 400-05-005 tillägg AP PS 400-05-051 AP PS 400-05-059 AP PS 400-05-088 AP PS 400-05-092 AP PS 400-06-030 AP PS 400-06-031 AP PS 400-06-031 tillägg nr 1 AP PS 400-06-061 AP PS 400-06-082	Data used in borehole mapping and in single-hole interpretation. Input for both rock domain and DZ modelling.

Data specification	Reference to data report	Reference in Sicada/GIS	Usage in analysis/ modelling
		AP PS 400-06-082 tillägg nr 1	
	P-07-15	AP PS 400-06-116	
	P-07-56	AP PS 400-06-154	
	P-07-152	AP PS 400-07-003	
	P-08-03	AP PS 400-07-036	
		AP PS 400-07-065	
Interpretation of geophysical logs (KAV01, KAV04A, KAV04B, KLX01, KLX02, KLX03, KLX04, KLX05, KLX06, KLX07A, KLX07B, KLX08, KLX09A, KLX09B, KLX09D, KLX09F, KLX09G, KLX10 , KLX10B, KLX10C, KLX11A , KLX11B, KLX12A , KLX13A, KLX14A, KLX15A, KLX16A, KLX17A, KLX18A, KLX19A, KLX20A, KLX21B, KLX22A, KLX22B, KLX23A, KLX23B, KLX24A, KLX25A, KLX26A, KLX26B, KLX27A, KLX28A, KLX29A, KSH01A, KSH01B, KSH02, KSH03A, KSH03B)	*P-04-214* *P-04-217* *P-04-27* *P-04-28* *P-04-77* *P-05-34* P-05-189 P-05-259 *P-05-44* P-06-124 P-06-157 P-06-162 P-06-253 P-06-264 P-06-292 P-06-317 P-06-65 P-07-114 P-07-21 P-07-25 P-07-75 P-07-97 P-08-04	AP PS 400-03-008 AP PS 400-03-019 AP PS 400-03-060 AP PS 400-04-003 AP PS 400-04-051 AP PS 400-04-094 AP PS 400-05-002 AP PS 400-05-006 AP PS 400-05-054 AP PS 400-05-060 AP PS 400-05-094 AP PS 400-05-094 tillägg nr 1 AP PS 400-05-095 AP PS 400-06-049 AP PS 400-06-050 AP PS 400-06-052 AP PS 400-06-074 AP PS 400-06-096 AP PS 400-06-096 tillägg nr 1 AP PS 400-06-116 AP PS 400-06-118 AP PS 400-06-135 AP PS 400-06-137 AP PS 400-06-157 AP PS 400-07-010 AP PS 400-07-040 AP PS 400-07-066	Used in single-hole interpretation. Input for both rock domain and DZ modelling.
Boremap mapping (KAV01, KAV04, KLX02, KLX03, KLX04, KLX05, KLX06, KLX07A, KLX07B, KLX08, KLX09, KLX09B, KLX09C, KLX09D, KLX09E, KLX09F, KLX09G, KLX10, KLX10B, KLX10C, KLX11A, KLX11B, KLX11C, KLX11D, KLX11E, KLX11F, KLX12A, KLX13A, KLX14A, KLX15A, KLX16A, KLX17A, KLX18A, KLX19A, KLX20A, KLX21B, KLX22A, KLX22B, KLX23A, KLX23B, KLX24A, KLX25A, KLX26A, KLX26B, KLX27A, KLX28A, KLX29A, KSH01A, KSH01B, KSH02, KSH03A, KSH03B)	*P-04-01* *P-04-02* *P-04-129* *P-04-130* *P-04-131* *P-04-132* P-05-185 *P-05-22* P-05-224 *P-05-23* *P-05-24* P-05-263 P-06-236 P-06-237 P-06-238 P-06-240 P-06-241 P-06-242 P-06-243 P-06-244 P-06-255 P-06-256 P-06-257 P-06-42 P-06-51 P-06-82 P-07-71 P-07-157 P-07-158 P-07-159 P-07-210 P-07-211 P-07-218 P-08-39	AP PS 400-03-005 AP PS 400-03-037 AP PS 400-03-057 AP PS 400-03-078 AP PS 400-03-088 AP PS 400-04-044 AP PS 400-04-070 AP PS 400-04-103 AP PS 400-04-125 AP PS 400-05-018 AP PS 400-05-057 AP PS 400-05-080 AP PS 400-05-084 AP PS 400-05-099 AP PS 400-06-017 AP PS 400-06-019 AP PS 400-06-041 AP PS 400-06-042 AP PS 400-06-046 AP PS 400-06-068 AP PS 400-06-069 AP PS 400-06-088 AP PS 400-06-089 AP PS 400-06-103 AP PS 400-06-104 AP PS 400-06-123 AP PS 400-06-126 AP PS 400-06-139 AP PS 400-06-140 AP PS 400-06-148 AP PS 400-07-015 AP PS 400-07-021 AP PS 400-07-023 AP PS 400-07-046 AP PS 400-07-070	Rock type, ductile deformation in the bedrock, fracture statistics. Data used in identification of rock units and brittle deformation zones in single-hole interpretation. Input for rock domain, DZ and DFN modelling.

Data specification	Reference to data report	Reference in Sicada/GIS	Usage in analysis/ modelling
Mineralogical and geochemical analyses of rock types and fracture fillings (KLX03, KLX04, KLX06, KLX07A, KLX07B, KLX08, KLX09, KLX10, KLX11A, KLX12A, KLX13A, KLX15A, KLX16A, KLX18A, KLX19A, KLX20A,KLX21B, KLX26A, KLX26A, KSH01, KSH02, KSH03, KAV01)	P-04-102 P-04-250 P-05-174 P-05-180 P-06-01 P-06-02 P-06-03 P-06-04 P-06-07 P-06-279 P-07-03 P-07-74 P-07-191 P-08-11 P-08-12 P-08-41 P-08-42 P-08-44	AP PS 400-03-056 AP PS 400-03-045 AP PS 400-03-045 AP PS 400-04-020 AP PS 400-04-018 AP PS 400-04-018 AP PS 400-04-018 AP PS 400-04-018 AP PS 400-04-020 AP PS 400-05-022 AP PS 400-06-015 AP PS 400-06-040 AP PS 400-05-053 AP PS 400-05-074 AP PS 400-06-015 AP PS 400-07-022 AP PS 400-06-132 AP PS 400-06-132 AP PS 400-05-052 AP PS 400-05-053 AP PS 400-03-045 AP PS 400-05-074 AP PS 400-06-059	Mineralogical and geochemical properties of rock types and fracture fillings. Input for rock domain, DZ and DFN modelling.
Characterisation of brittle deformation zones. KSH03A, KLX03, KLX04, KLX06, KLX07A, KLX07B, KLX08, KLX09, KLX10, KLX11A, KLX12A, KLX13A, KLX15A, KLX16A, KLX17A, KLX18A, KLX19A, KLX20A, KLX21B.	P-07-41 P-07-227 P-08-07 R-08-124	AP PS 400-05-086 AP PS 400-06-098 AP PS 400-07-016 AP PS 400-07-016 addition no 1	Input for DZ modelling and geological evolution.
Single-hole interpretation (KAV01, KAV04A, KAV04B, KLX01, KLX02, KLX03, KLX04, KLX05, KLX06, KLX07A, KLX07B, KLX08 , KLX09, KLX09B, KLX09C, KLX09D, KLX09E, KLX09F, KLX09G, KLX10, KLX10B, KLX10C , KLX11A , KLX11B, KLX11C, KLX11D, KLX11E, KLX11F, KLX12A, KLX13A, KLX14A, KLX15A, KLX16A, KLX17A, KLX18A, KLX19A, KLX20A, KLX21B, KLX22A, KLX22B, KLX23A, KLX23B, KLX24A, KLX25A, KLX26A, KLX26B, KLX27A, KLX28A, KLX29A, KSH01A, KSH01B, KSH02, KSH03A, KSH03B)	*P-04-133* *P-04-231* *P-04-308* *P-04-309* *P-04-32* *P-05-38* P-06-128 P-06-129 P-06-174 P-06-175 P-06-176 P-07-153 P-07-155 P-07-156 P-07-161 P-07-208 P-07-209 P-07-66 P-07-67 P-07-68 P-07-69 P-07-70 P-08-05 P-08-06 P-08-48	AP PS 400-03-038 AP PS 400-04-037 AP PS 400-04-071 AP PS 400-04-091 AP PS 400-04-101 AP PS 400-04-108 AP PS 400-05-017 AP PS 400-05-046 AP PS 400-05-046 tillägg nr 1 AP PS 400-05-068 AP PS 400-05-098 AP PS 400-06-018 AP PS 400-06-047 AP PS 400-06-056 AP PS 400-06-065 AP PS 400-06-081 AP PS 400-06-127 AP PS 400-06-128 AP PS 400-06-146 AP PS 400-06-152 AP PS 400-06-153 AP PS 400-07-011 AP PS 400-07-042 AP PS 400-07-043 AP PS 400-07-049 AP PS 400-07-060 AP PS 400-08-004	Interpretation used in rock domain, DZ and DFN modelling.
Calculation of Fracture zone index KSH01	P-03-93	AP PS 400-03-048	Input for DZ modelling.

Data specification	Reference to data report	Reference in Sicada/GIS	Usage in analysis/ modelling
Data from percussion-drilled boreholes			
Radar and BIPS-logging, and interpretation of radar logs (HSH01, HSH02, HSH03, HAV09, HAV10 , HAV11, HAV12, HAV13, HLX10, HLX13, HLX15, HLX17, HLX18, HLX19, HLX20, HLX21, HLX22, HLX23, HLX24, HLX25, HLX26, HLX27, HLX28, HLX30, HLX31, HLX32, HLX33, HLX34, HLX35, HLX36, HLX37, HLX38, HLX39, HLX40, HLX41, HLX42, HLX43)	P-03-15 P-04-195 P-04-275 P-04-279 P-04-297 P-04-48 P-05-231 P-05-240 P-06-159 P-06-260 P-07-12 P-07-58	AP PS 400-02-010 AP PS 400-04-046 AP PS 400-04-047 AP PS 400-04-080 AP PS 400-04-081 AP PS 400-04-069 AP PS 400-04-099 AP PS 400-03-081 AP PS 400-05-050 AP PS 400-05-058 AP PS 400-06-083 AP PS 400-06-083 tillägg nr 1 AP PS 400-06-083 tillägg nr 2 AP PS 400-06-083 tillägg nr 3 AP PS 400-05-093 AP PS 400-06-136 AP PS 400-07-004 AP PS 400-06-058 tillägg nr 1 AP PS 400-06-058 tillägg nr 2	Data used in borehole mapping (BIPS) and in single-hole interpretation (radar logging) with focus of identification of brittle deformation zones. Input for both rock domain and DZ modelling.
Geophysical logging (HAV09, HAV10, HLX13, HLX15, HLX17, HLX18, HLX19, HLX20, HLX21, HLX22, HLX23, HLX24, HLX25, HLX26, HLX27 HLX28, HLX30, HLX31, HLX32, HLX33, HLX34, HLX35, HLX36, HLX37, HLX38, HLX39, HLX40, HLX41, HLX43, HSH01, HSH02, HSH03)	P-03-15 P-04-202 P-04-240 P-04-280 P-04-306 *P-04-50* P-05-228 P-05-270 P-06-197 P-06-290 P-06-315	AP PS 400-02-010 AP PS 400-03-082 AP PS 400-04-047 AP PS 400-04-067 AP PS 400-04-081 AP PS 400-04-097 AP PS 400-05-051 AP PS 400-05-059 AP PS 400-06-030 AP PS 400-06-061 AP PS 400-06-135	Data used in borehole mapping and in single-hole interpretation. Input for both rock domain and DZ modelling.
Interpretation of geophysical logs (HSH01, HSH02, HSH03, HAV09, HAV10, HLX13, HLX15, HLX17, HLX18, HLX19, HLX20, HLX21, HLX22, HLX23, HLX24, HLX25, HLX26, HLX27, HLX28, HLX30, HLX31, HLX32, HLX33, HLX34, HLX35, HLX36, HLX37, HLX38, HLX39, HLX40, HLX41, HLX43, Percussion drilled part of KSH01A)	P-04-28 P-04-214 P-04-217 P-04-27 P-04-284 P-05-34 P-05-259 P-06-264 P-06-292 P-06-65 P-07-25	AP-PS 400-03-019 AP PS 400-03-008 AP PS 400-04-003 AP PS 400-04-051 AP PS 400-04-068 AP PS 400-04-094 AP PS 400-04-100 AP PS 400-05-054 AP PS 400-05-060 AP PS 400-06-052 AP PS 400-06-074 AP PS 400-06-137	Used in single-hole interpretation. Input for both rock domain and DZ modelling.
Boremap mapping (HLX13, HLX15, HLX17, HLX18, HLX19, HLX20, HLX21, HLX22, HLX23, HLX24, HLX25, HLX26, HLX27, HLX27, HLX28, HLX30, HLX31, HLX32, HLX33, HLX34, HLX35, HLX36, HLX37, HLX38, HLX39, HLX40, HLX41, HLX42, HLX43, HSH01, HSH02, HSH03, HAV09, HAV10, HAV11, HAV12, HAV13)	*P-04-02* *P-05-104* P-05-163 *P-05-83* P-05-164 P-05-279 P-05-162	AP PS 400-03-005 AP PS 400-04-053 AP PS 400-04-124 AP PS 400-04-124 tillägg AP PS 400-06-013 AP PS 400-06-134 AP PS 400-04-030	Data mainly used for identification of rock units and DZ in single-hole interpretation. Input for rock domain and DZ modelling. Problem with recognition of rock types and mineral coatings along fractures. Also underestimation of the amount of fractures inferred solely on the basis of BIPS images.

Data specification	Reference to data report	Reference in Sicada/GIS	Usage in analysis/ modelling
Single-hole interpretation (HAV09, HAV10, HLX13, HLX15, HLX17, HLX18, HLX19, HLX20, HLX21, HLX22, HLX23, HLX24, HLX25, HLX26, HLX27, HLX28, HLX30, HLX31, HLX32, HLX33, HLX34, HLX35, HLX36, HLX37, HLX38, HLX39, HLX40, HLX41, HLX42, HLX43, HSH01, HSH02, HSH03)	*P-04-231* *P-04-309* *P-04-32* P-06-128 P-06-129 P-06-174 P-06-175 P-07-153 P-07-155 P-07-156 P-07-161 P-07-209 P-07-67 P-08-05 P-08-06	AP PS 400-03-038 AP PS 400-04-071 AP PS 400-04-101 AP PS 400-05-017 AP PS 400-05-046 AP PS 400-05-046 tillägg nr 1 AP PS 400-05-068 AP PS 400-06-018 AP PS 400-06-047 AP PS 400-06-127 AP PS 400-06-146 AP PS 400-06-152 AP PS 400-06-153 AP PS 400-07-011 AP PS 400-07-042 AP PS 400-07-049	Interpretation used in rock domain and DZ modelling.
Calculation of Fracture zone index HSH01	P-04-26	AP PS 400-03-094	
Surface-based data			
Bedrock mapping – outcrop data.	P-03-06 P-04-102 P-04-221 P-05-47 P-06-121	AP-PS-400-02-025 AP PS 400-03-056 AP PS 400-04-001 AP PS 400-04-093 AP PS 400-05-048	Rock type, rock type distribution, ductile deformation in the bedrock, fracture statistics, and identification of deformation zones at surface. Input for rock domain, DZ and DFN modelling.
Bedrock geological map	P-04-102 P-05-180 P-06-279	AP PS 400-03-056 AP PS 400-04-020 AP PS 400-06-015	Input for rock domain modelling.
Mineralogical and geochemical analyses of rock types	P-04-102 P-05-47 P-05-180	AP PS 400-03-056 AP PS 400-04-093 AP PS 400-04-020	Mineralogical and geochemical properties of rock types. Input for rock domain modelling.
Petrophysical and in-situ gamma-ray spectrometric data of rock types	P-03-97 P-04-294 P-06-100 IPR-06-32	AP PS 400-02-015 AP PS 400-04-002 AP PS 400-95-067	Input for rock domain modelling.
U-Pb, $^{40}Ar/^{39}Ar$, (U-Th)/He geochronological data of bedrock and fracture minerals (including samples from drill cores)	P-04-102 P-07-27 P-07-160 P-07-191 R-01-60 PR 25-95-04	AP PS 400-03-056 AP PS 400-06-158 AP PS 400-05-033 AP PS 400-06-015	Input for conceptual understanding of the geological modelling work.
Characterization of deformation zones	P-05-181 P-06-118 P-06-282 P-07-41 P-07-227	AP PS 400-05-036 AP PS 400-05-062 AP PS 400-05-096 AP PS 400-06-053 AP PS 400-05-086 AP PS 400-06-098	Focused lineament investigations, MDZ studies and outcrop structural investigations. Input for DZ modelling.
Detailed bedrock mapping	P-04-102 P-04-274 P-04-35 P-05-260 P-06-06 P-07-29 P-04-244	AP PS 400-03-056 AP PS 400-03-020 AP PS 400-04-045 AP PS 400-05-049 AP PS 400-05-078 AP PS 400-06-099 AP PS 400-04-059	Fracture statistics (orientation, length) and identification of brittle and ductile features at surface. Input for rock domain, DZ and DFN modelling.
Digital orthorectified aerial photographs and digital terrain model	P-02-02		Input for lineament identification and subsequent DZ modelling.

Data specification	Reference to data report	Reference in Sicada/GIS	Usage in analysis/ modelling
Methodology for construction of digital terrain models	P-04-03		
Aerial orthophotos and laser scanning (LIDAR)	P-05-223	AP 400-05-035	Detailed elevation model and orthophotos. Input for lineament identification and subsequent DZ modelling.
Marine geological survey	P-05-35	AP PS 400-02-017	Input for lineament interpretation and subsequent DZ modelling.
Helicopterborna geophysical data (magnetic, VLF, EM and gamma-ray spectrometry)	P-03-25	AP PS 400-02-006	Base data for identification of lineaments and subsequent DZ modelling.
Electric soundings	P-06-21 P-07-88	AP PS 400-05-066	
High-resolution seismic reflection data	P-03-71 P-03-72 P-04-52 P-04-204 P-04-215 R-01-07 TR-02-04	AP PS 400-02-005 AP PS 400-03-068 AP PS 400-04-024	Identification of seismic reflectors in the bedrock that may correspond to deformation zones or boundaries between different types of bedrock. Input for DZ modelling.
Seismic refraction data	*P-04-134* *P-04-201* *P-04-298* P-05-155 P-05-179 P-06-49 P-07-131	AP PS 400-03-070 AP PS 400-04-038 AP PS 400-04-092 AP PS 400-05-015 AP PS 400-05-032 AP PS 400-06-043 AP PS 400-07-022	Identification of low velocity anomalies in the bedrock that may correspond to deformation zones. Input for DZ modelling.
Ground geophysical data (magnetic and EM data)	P-03-06 P-03-66 P-04-211 P-05-188 P-06-137 P-07-168	AP PS 400-02-021 AP PS 400-03-027 AP PS 400-04-040 AP PS 400-05-014 AP PS 400-05-079 AP PS 400-07-018	Input for DZ modelling Assessment of possible dolerite dykes.
Gravity data (profiles)	P-04-128	AP PS 400-04-002	Geophysical modelling. Input for rock domain modelling.
Interpretation of topographic, bathymetric and helicopterborne geophysical data including alternative lineament interpretation	P-03-99 P-04-37 P-04-49 P-05-188 P-05-247 R-06-53 P-07-223	AP PS 400-03-009 AP PS 400-03-076 AP PS 400-04-004 AP PS 400-05-038	Identification of lineaments. Input for DZ modelling. Assessment of dolerite dykes – input to rock domain modelling.
Previous models			
RVS-modelling Ävrö	R-01-06		DZ modelling.
Laxemar	TR-02-19		Methodology test.
Simpevarp site descriptive model versions 0, 1.1, 1.2	R-02-35 R-04-25 R-05-08	The approved models are stored in the SKB model database	Comparison and updating of models.
Laxemar site descriptive model versions 1.2, 2.1	R-06-10 R-06-110 R-05-45 R-05-69	The approved models are stored in the SKB model database	Comparison and updating of models.
Äspö Hard rock Laboratory	IPR-03-34		DZ modelling.

Table A1-2. Available reported bedrock geological and geophysical data in SDM-Site Laxemar model stage.

P-02-02	Wiklund S, 2002. Digitala ortofoton och höjdmodeller. Redovisning av metodik för platsundersökningsområdena Oskarshamn och Forsmark samt förstudieområdet Tierp Norra.
P-02-05	Mattsson H, Triumf C-A, Wahlgren C-H, 2002. Prediktering av förekomst av finkorniga granitgångar i Simpevarpsområdet.
P-03-06	Wahlgren C-H, Persson L, Danielsson P, Berglund J, Triumf C-A, Mattsson H, Thunehed H, 2003. Oskarshamn site investigation. Geologiskt underlag för val av prioriterad plats inom området väster om Simpevarp.
P-03-07	Curtis P, Elfström M, Stanfors R, 2003. Oskarshamn site investigation. Compilation of structural geological data covering the Simpevarp peninsula, Ävrö and Hålö.
P-03-15	Nilsson P, Gustafsson C, 2003. Simpevarp site investigation. Geophysical, radar and BIPS logging in borehole KSH01A, HSH01, HSH02 and HSH03.
P-03-16	Nielsen U T, Ringgaard J, 2003. Simpevarp site investigation. Geophysical borehole logging in borehole KSH01A, KSH01B and part of KSH02.
P-03-25	Rønning H J S, Kihle O, Mogaard J O, 2003. Simpevarp site investigation. Helicopter borne geophysics at Simpevarp, Oskarshamn, Sweden.
P-03-36	Curtis P, Elfström M, Stanfors R, 2003. Oskarshamn site investigation. Visualization of structural geological data covering the Simpevarp peninsula, Ävrö and Hålö.
P-03-66	Triumf C-A, 2003. Oskarshamn site investigation. Geophysical measurements for the siting of a deep borehole at Ävrö and for investigations west of CLAB.
P-03-71	Vangkilde-Pedersen T, 2003. Oskarshamn site investigation. Reflection seismic surveys on Simpevarpshalvön 2003 using the vibroseismic method.
P-03-72	Juhlin C, 2003. Oskarshamn site investigation. Evaluation of RAMBØLL reflection seismic surveys on Simpevarpshalvön 2003 using the vibroseismic.
P-03-73	Aaltonen J, Gustafsson C, Nilsson P, 2003. Oskarshamn site investigation. RAMAC and BIPS logging and deviation measurements in boreholes KSH01A, KSH01B and the upper part o KSH02.
P-03-93	Lindqvist L, Thunehed H, 2003. Oskarshamn site investigation. Calculation of Fracture Zone Index (FZI) for KSH01A.
P-03-97	Mattsson H, Thunehed H, Triumf C-A, 2003. Oskarshamn site investigation. Compilation of petrophysical data from rock samples and in situ gamma-ray spectrometry measurements.
P-03-99	Triumf C-A, 2003. Oskarshamn site investigation. Identification of lineaments in the Simpevarp area by the interpretation of topographical data.
P-03-100	Triumf C-A, Thunehed H, Kero L, Persson L, 2003. Oskarshamn site investigation. Interpretation of airborne geophysical survey data. Helicopter borne survey data of gamma ray spectrometry, magnetics and EM from 2002 and fixed wing airborne survey data of the VLF-field from 1986.
P-03-109	Aaltonen J, Gustafsson C, 2003. Oskarshamn site investigation. RAMAC and BIPS logging in borehole KSH02.
P-03-111	Nielsen T, Ringgaard J, Horn F, 2003. Oskarshamn site investigation. Geophysical borehole logging in boreholes KSH02 and KLX02.
P-03-113	Ask H, Morosini M, Samuelsson L-E, Stridsman H, 2004. Oskarshamn site investigation. Drilling of cored borehole KSH01.
P-03-120	Aaltonen J, Gustafsson C, 2003. Oskarshamn site investigation. RAMAC logging in boreholes KAV01 and KLX02.
P-04-01	Ehrenborg J, Stejskal V, 2004. Oskarshamn site investigation. Boremap mapping of core drilled boreholes KSH01A and KSH01B.
P-04-02	Nordman C, 2004. Oskarshamn site investigation. Boremap mapping of percussion boreholes HSH01–03.
P-04-03	Brydsten, L, 2004. A method for construction of digital elevation models for site investigation program at Forsmark and Simpevarp.
P-04-26	Lindqvist L, Thunehed H, 2004. Oskarshamn site investigation. Calculation of Fracture Zone Index (FZI) for HSH01.
P-04-27	Mattsson H, 2004. Oskarshamn site investigation. Interpretation of borehole geophysical data from the percussion drilled part of the borehole KSH01A.
P-04-28	Mattsson H, Thunehed H, 2004. Oskarshamn site investigation. Interpretation of geophysical borehole data from KSH01A, KSH01B, KSH02 (0–100 m), HSH01, HSH02 and HSH03, and compilation of petrophysical data from KSH01A and KSH01B.
P-04-32	Mattsson H, Stanfors R, Wahlgren C-H, Carlsten S, Hultgren P, 2004. Oskarsham site investigation. Geological single-hole interpretation of KSH01A, KSH01B, HSH01, HSH02 and HSH03.

P-04-35 Hermanson J, Hansen L, Wikholm M, Cronquist T, Leiner P, Vestgård J, Sandah K-A, 2004. Oskarshamn site investigation. Detailed fracture mapping of four outgrops at the Simpevarp peninsula and Ävrö.

P-04-37 Triumf C-A, 2004. Oskarshamn site investigation. Joint interpretation of lineaments in the eastern part of the site descriptive model area.

P-04-48 Gustafsson J, Gustafsson C, 2004. Oskarshamn site investigation. RAMAC and BIPS logging in boreholes KSH03A, KSH03B, HAV09, HAV10 and BIPS in KAV01. Revised April 2006.

P-04-49 Triumf C-A, 2004. Oskarshamn site investigation. Joint interpretation of lineaments.

P-04-50 Nielsen T, Ringgaard J, 2004. Oskarshamn site investigation. Geophysical borehole logging in borehole KSH03A, KSH03B, HAV09 and HAV10.

P-04-52 Juhlin C, Bergman B, Palm H, Tryggvason A, 2004. Oskarshamn site investigation. Reflection seismic studies on Ävrö and Simpevarpshalvön, 2003.

P-04-66 Gustafsson J, Gustafsson C, 2004. Oskarshamn site investigation. RAMAC logging with directional radar antenna in boreholes KSH01A, KSH01B and KSH02. Revised April 2006.

P-04-77 Mattsson H, Thunehed H, 2004. Oskarshamn site investigation. Interpretation of geophysical borehole data and compilation of petrophysical data from KSH02 (80–1,000 m) and KAV01.

P-04-102 Wahlgren C-H, Ahl M, Sandahl K-A, Berglund J, Petersson J, Ekström M, Persson P-O, 2004. Oskarshamn site investigation. Bedrock mapping 2003 – Simpevarp subarea. Outcrop data, fracture data, modal and geochemical classification of rock types, bedrock map, radiometric dating.

P-04-128 Triumf C-A, 2004. Oskarshamn site investigation. Gravity measurements in the Laxemar model area with surroundings.

P-04-129 Ehrenborg J, Stejskal V, 2004. Oskarshamn site investigation. Boremap mapping of core drilled borehole KLX02.

P-04-130 Ehrenborg J, Stejskal V, 2004. Oskarshamn site investigation. Boremap mapping of core drilled borehole KAV01.

P-04-131 Ehrenborg J, Stejskal V, 2004. Oskarshamn site investigation. Boremap mapping of core drilled borehole KSH02.

P-04-132 Ehrenborg J, Stejskal V, 2004. Oskarshamn site investigation. Boremap mapping of core drilled boreholes KSH03A and KSH03B.

P-04-133 Mattsson H, Stanfors R, Wahlgren C-H, Carlsten S, Hultgren P, 2004. Oskarsham site investigation. Geological single-hole interpretation of KSH02 and KAV01.

P-04-134 Lindqvist G, 2004. Oskarshamn site investigation. Refraction seismic measurements in Laxemar.

P-04-151 Ask H, Morosini M, Samuelsson L-E, Ekström L, 2004. Oskarshamn site investigation. Drilling of cored borehole KSH02.

P-04-195 Gustafsson J, Gustafsson C, 2004. Oskarshamn site investigation. RAMAC and BIPS logging in boreholes KAV04A, KAV04B, HLX13 and HLX15.

P-04-201 Lindqvist G, 2004. Oskarshamn site investigation. Refraction seismic measurements in the water outside Simpevarp and Ävrö and on land on Ävrö.

P-04-202 Nielsen U T, Ringgaard J, 2004. Oskarshamn site investigation. Geophysical borehole logging in borehole KAV04A, KAV04B, HLX13 and HLX15.

P-04-204 Schmelzbach C, Juhlin C, 2004. Oskarshamn site investigation. 3D processing of reflection seismic data acquired within and near the array close to KAV04A on Ävrö, 2003.

P-04-211 Thunehed H, Triumf C-A, Pitkänen T, 2004. Oskarshamn site investigation. Geophysical profile measurements over interpreted lineaments in the Laxemar area.

P-04-214 Mattsson H, 2004. Oskarshamn site investigation. Interpretation of geophysical borehole data and compilation of petrophysical data from KSH03A (100–1,000 m), KSH03B, HAV09, HAV10 and KLX02 (200–1,000 m).

P-04-215 Juhlin C, Bergman B, Palm H, 2004. Oskarshamn site investigation. Reflection seismic studies performed in the Laxemar area during 2004.

P-04-217 Mattsson H, 2004. Oskarshamn site investigation. Interpretation of geophysical borehole data and compilation of petrophysical data from KAV04A (100–1,000 m), KAV04B, HLX13 and HLX15.

P-04-218 Carlsten S, 2004. Oskarshamn site investigation. Geological interpretation of borehole radar reflectors in KSH01, HSH01–03, KAV01 and KSH02. Revised June 2006.

P-04-221 Persson Nilsson K, Bergman T, Eliasson T, 2004. Oskarshamn site investigation. Bedrock mapping 2004 – Laxemar subarea and regional model area. Outcrop data and description of rock types.

P-04-231 Hultgren P, Stanfors R, Wahlgren C-H, Carlsten S, Mattsson H, 2004. Oskarshamn site investigation. Geological single-hole interpretation of KSH03A, KSH03B, KLX02, HAV09 and HAV10.

P-04-232 Nielsen T, Ringgaard J, Horn F, 2004. Oskarshamn site investigation. Geophysical borehole logging in borehole KAV01.

P-04-233 Ask H, Morosini M, Samuelsson L-E, Ekström L, Håkansson N, 2004. Oskarshamn site investigation. Drilling of cored borehole KSH03.

P-04-235 Ask H, Samuelsson L-E, Zetterlund M, 2005. Oskarshamn site investigation. Percussion drilling of boreholes HLX15, HLX26, HLX27, HLX28, HLX29 and HLX32 for investigation of lineament NW042.

P-04-239 Gustafsson J, Gustafsson C, 2004. Oskarshamn site investigation. RAMAC and BIPS logging in borehole KLX04.

P-04-240 Nielsen U T, Vangkilde-Pedersen T, Ringgaard J, 2004. Oskarshamn site investigation. Geophysical borehole logging in borehole HLX17, HLX18 and HLX19.

P-04-244 Berglund J, 2004. Oskarshamn site investigation. Scan line fracture mapping. Subarea Laxemar and passage for tunnel.

P-04-250 Drake H, Tullborg E-L, 2004. Oskarshamn site investigation. Fracture mineralogy and wall rock alteration, results from drill core KSH01A+B.

P-04-274 Cronquist T, Forssberg O, Hansen L, Jonsson A, Koyi S, Leiner P, Sävås J, Vestgård J, 2004. Oskarshamn site investigation. Detailed fracture mapping of two outcrops at Laxemar.

P-04-275 Gustafsson J, Gustafsson C, 2004. Oskarshamn site investigation. RAMAC and BIPS logging in boreholes KLX03, HAV11 to HAV13 and HLX21 to HLX25. Revised April 2006.

P-04-279 Gustafsson J, Gustafsson C, 2004. Oskarshamn site investigation. RAMAC and BIPS logging in boreholes HLX17, HLX18 and HLX19.

P-04-280 Nielsen U T, Horn F, 2004. Oskarshamn site investigation. Geophysical borehole logging in borehole KLX03, HLX21, HLX22, HLX23, HLX24 and HLX25.

P-04-284 Mattsson H, Keisu M, 2004. Oskarshamn site investigation. Interpretation of geophysical borehole data from HLX17, HLX18 and HLX19.

P-04-294 Mattsson H, Thunehed H, Triumf C-A, 2005. Oskarshamn site investigation. Compilation of petrophysical data from rock samples and in situ gamma-ray spectrometry measurements, Stage 2 – 2004 (including 2002).

P-04-297 Gustafsson J, Gustafsson C, 2004. Oskarshamn site investigation. RAMAC and BIPS logging in boreholes HLX10, HLX26, HLX27 and HLX28.

P-04-298 Lindqvist G, 2004. Oskarshamn site investigation. Refraction seismic measurements in Laxemar autumn 2004.

P-04-306 Nielsen U T, Ringgaard J, Horn F, 2004. Oskarshamn site investigation. Geophysical borehole logging in boreholes KLX04, HLX26, HLX27 and HLX28.

P-04-308 Carlsten, S, Hultgren P, Mattsson H, Stanfors R, Wahlgren C-H, 2006. Oskarshamn site investigation. Geological single-hole interpretation of KAV04A, KAV04B, KLX01 and HLX15.

P-04-309 Carlsten, S, Hultgren P, Mattsson H, Stanfors R, Wahlgren C-H, 2006. Oskarshamn site investigation. Geological single-hole interpretation of KLX04, HLX21, HLX22, HLX23, HLX24 and HLX25.

P-05-22 Ehrenborg J, Stejskal V, 2005. Oskarshamn site investigation.
Boremap mapping of core drilled boreholes KAV04A and KAV04B.

P-05-23 Ehrenborg J, Dahlin P, 2005. Oskarshamn site investigation.
Boremap mapping of core drilled borehole KLX04.

P-05-24 Ehrenborg J, Dahlin P, 2005. Oskarshamn site investigation.
Boremap mapping of core drilled borehole KLX03.

P-05-25 Ask H, Morosini M, Samuelsson L-E, Ekström L, Håkansson N, 2005. Oskarshamn site investigation. Drilling of cored borehole KAV04.

P-05-30 Gustafsson J, Gustafsson C, 2004. Oskarshamn site investigation. RAMAC and BIPS logging in borehole KLX06. Revised April 2006.

P-05-31 Nielsen U T, Ringgaard J, Horn F, 2005. Oskarshamn site investigation. Geophysical borehole logging in borehole KLX06.

P-05-34 Mattsson H, Thunehed H, Keisu, M, 2005. Oskarshamn site investigation. Interpretation of geophysical borehole measurements and compilation of petrophysical data from KLX01, KLX03, KLX04, HLX21, HLX22, HLX23, HLX24, HLX25, HLX26, HLX27 and HLX28.

P-05-35 Elhammer A, Sandkvist Å, 2005. Oskarshamn site investigation. Detailed marine geological survey of the sea bottom outside Simpevarp.

P-05-38 Carlsten, S, Hultgren P, Mattsson H, Stanfors R, Wahlgren C-H, 2006. Oskarshamn site investigation. Geological single-hole interpretation of KLX03, HLX26 and HLX27.

P-05-44 Mattsson H, 2005. Oskarshamn site investigation. Interpretation of geophysical borehole measurements from KLX06.

P-05-47 Bergman T, Malmberg Persson K, Persson M, Albrecht J, 2005. Oskarshamn site investigation. Characterisation of bedrock and quaternary deposits from excavations in the southern part of laxemar subarea.

P-05-82 Gustafsson J, Gustafsson C, 2004. Oskarshamn site investigation. RAMAC and BIPS logging in boreholes KLX05 and HLX32.

P-05-83 Sigurdsson O, 2005. Oskarshamn site investigation. Simplified Boremap mapping of percussion boreholes HLX15, HLX26, HLX27, HLX28 and HLX32 on lineament NW042.

P-05-104 Sigurdsson O, 2005. Oskarshamn site investigation. Simplified Boremap mapping of percussion boreholes HLX17, HLX18 and HLX19.

P-05-111 Ask H, Morosini M, Samuelsson L-E, Ekström L, Håkansson N, 2005. Oskarshamn site investigation. Drilling of cored borehole KLX04.

P-05-144 Nielsen U T, Ringgaard J, Dahl J F, 2005. Oskarshamn site investigation. Geophysical borehole logging in boreholes KLX05 and HLX32.

P-05-155 Lindqvist G, 2005. Oskarshamn site investigation. Refraction seismic measurements in Laxemar spring 2005.

P-05-161 Gustafsson J, Gustafsson C, 2004. Oskarshamn site investigation. RAMAC directional logging in borehole KLX05 and RAMAC and BIPS logging in borehole HLX20. Revised April 2006.

P-05-162 Sigurdsson O, 2005. Oskarshamn site investigation. Simplified Boremap mapping of percussion boreholes HAV11, HAV12 and HAV13.

P-05-163 Sigurdsson O, 2005. Oskarshamn site investigation. Simplified Boremap mapping of percussion borehole HLX20 on lineament EW002.

P-05-164 Sigurdsson O, 2005. Oskarshamn site investigation. Simplified Boremap mapping of percussion boreholes HLX13, HLX21, HLX22, HLX23, HLX24, HLX25, HLX30, HLX31 and HLX33 on lineament EW007.

P-05-167 Ask H, Morosini M, Samuelsson L-E, Ekström L, Håkansson N, 2005. Oskarshamn site investigation. Drilling of cored borehole KLX03.

P-05-174 Drake H, Tullborg E-L, 2005. Oskarshamn site investigation. Fracture mineralogy and wall rock alteration, results from drill cores KAS04, KA1755A and KLX02.

P-05-179 Mattsson H, Triumf C-A, Lindqvist G, 2005. Oskarshamn site investigation. Re-interpretation of the refraction seismic profiles 277, 280 and 506 by use of Wavepath Eikonal Traveltime Tomography. A comparison with the traditional interpretation technique.

P-05-180 Wahlgren C-H, Bergman T, Persson Nilsson K, Eliasson T, Ahl M, Ekström M, 2005. Oskarshamn site investigation. Bedrock map of the Laxemar subarea and surroundings. Description of rock types, modal and geochemical analyses, including the cored boreholes KLX03, KSH03 and KAV01.

P-05-181 Braathen A, Nordgulen Ö, 2005. Oskarshamn site investigation. Structural investigations of deformation zones (ductile shear zones and faults) around Oskarshamn – a pilot study.

P-05-185 Ehrenborg J, Dahlin P, 2005. Oskarshamn site investigation. Boremap mapping of core drilled borehole KLX06.

P-05-188 Thunehed H, Triumf C-A, 2005. Oskarshamn site investigation. Detailed ground geophysical survey at Laxemar. Magnetic total field and resistivity.

P-05-189 Mattsson H, Keisu M, 2005. Oskarshamn site investigation. Interpretation of geophysical borehole measurements from KLX05.

P-05-223 Nyborg M, 2005. Oskarshamn site investigation. Aerial photography and airborne laser scanning Laxemar-Simpevarp. The 2005 campaign.

P-05-224 Ehrenborg J , Dahlin P, 2005. Oskarshamn site investigation. Boremap mapping of core drilled boreholes KLX05.

P-05-228 Nielsen U, Ringgaard J, Fris Dahl J, 2005. Oskarshamn site investigation. Geophysical borehole logging in boreholes KLX07A, KLX07B, HLX20, HLX34 and HLX35.

P-05-231 Gustafsson J, Gustafsson C, 2005. Oskarshamn site investigation. RAMAC and BIPS logging in boreholes KLX07A, KLX07B, HLX34 and HLX35 and deviation logging in boreholes KLX07B, HLX34 and HLX35. Revised April 2006.

P-05-233 Ask H, Morosini M, Samuelsson L-E, Ekström L, Håkansson N, 2005. Oskarshamn site investigation. Drilling of cored borehole KLX05.

P-05-234 Ask H, Morosini M, Samuelsson L-E, Ekström L, Håkansson N, 2005. Oskarshamn site investigation. Drilling of cored borehole KLX06.

P-05-240 Gustafsson J, Gustafsson C, 2005. Oskarshamn site investigation. RAMAC, BIPS and deviation logging in boreholes KLX08, HLX30 and HLX33.

P-05-247 Korhonen K, Kuivamäki A, Ruotoistenmäki T, Paananen M, 2005. Interpretation of lineaments from airborne geophysical and topographic data. An alternative model within version Laxemar 1.2 of the Oskarshamn modelling project.

P-05-259 Mattsson, H, Keisu, M, 2005. Oskarshamn site investigation. Interpretation of geophysical borehole measurements from KLX07A, KLX07B, HLX20, HLX32, HLX34 and HLX35.

P-05-260 Forssberg O, Cronquist T, Hansen, L, Vestgård J, 2005. Oskarshamn site investigation. Detailed outcrop mapping at the drill site of KLX09 in Laxemar.

P-05-263 Ehrenborg J , Dahlin P, 2005. Oskarshamn site investigation.
Boremap mapping of core drilled boreholes KLX07A and KLX07B.

P-05-270 Nielsen U T, Ringgaard J, 2005. Oskarshamn site investigation. Geophysical borehole logging in boreholes KLX08, HLX30, HLX31 and HLX33.

P-05-279 Sigurdsson O, 2005. Oskarshamn site investigation. Simplified Boremap mapping of percussion boreholes HLX34 and HLX35 on lineament NS059 and of percussion boreholes HLX36 and HLX37 on lineament NS001.

P-05-279 Sigurdsson O, 2006. Oskarshamn site investigation. Simplified Boremap mapping of percussion boreholes HLX34 and HLX35 on lineament NS059 and of percussion boreholes HLX36 and HLX37 on lineament NS001. Revised March 2008.

P-06-01 Drake H, Tullborg E-L, 2006. Oskarshamn site investigation. Mineralogical, chemical and redox features of red-staining adjacent to fractures. Results from drill cores KSH01A+B and KSH03A+B.

P-06-02 Drake H, Tullborg E-L, 2006. Oskarshamn site investigation. Mineralogical, chemical and redox features of red-staining adjacent to fractures. Results from drill core KLX04.

P-06-03 Drake H, Tullborg, E-L, 2006. Oskarshamn site investigation. Fracture mineralogy. Results from drill core KSH03A+B.

P-06-04 Drake H, Tullborg E-L, 2006. Oskarshamn site investigation. Fracture mineralogy of the Götemar granite. Results from drill cores KKR01, KKR02 and KKR03.

P-06-06 Cronquist T, Forssberg O, Hansen L, Koyi S, Vestgård J, Wikholm M, 2006. Oskarshamn site investigation. Detailed outcrop mapping on drillsite KLX11.

P-06-07 Wahlgren C-H, Bergman T, Ahl M, Ekström M, 2006. Oskarshamn site investigation. Modal and geochemical analyses of drill core samples 2005. Classification of rock types in KLX03, KLX04, KLX06, KLX07A, KLX07B, KLX08 and KLX10.

P-06-14 Ask H, Morosini M, Samuelsson L-E, Ekström L, Håkansson N, 2006. Oskarshamn site investigation. Drilling of cored boreholes KLX07A and KLX07B.

P-06-20 Nielsen U T, Ringgaard J, Fris Dahl J, 2006. Oskarshamn site investigation. Geophysical borehole logging in borehole KLX10.

P-06-21 Thunehed H, Pitkänen T, 2006. Oskarshamn site investigation. Transient electromagnetic soundings at Laxemar and the regional surroundings. Estimations of depth to saline groundwater.

P-06-42 Dahlin, P, Ehrenborg J, 2006. Oskarshamn site investigation.
Boremap mapping of core drilled borehole KLX08.

P-06-48 Dahlin, P, Ehrenborg J, 2006. Oskarshamn site investigation.
Boremap mapping of core drilled borehole KLX08.

P-06-49 Lindqvist, G, 2006. Oskarshamn site investigation.
Refraction seismic measurements in Laxemar spring 2006.

P-06-50 Gustafsson J, Gustafsson C, 2006. Oskarshamn site investigation. RAMAC and BIPS logging in boreholes KLX10 and HLX31.

P-06-51 Dahlin P, Mattsson K, Ehrenborg J, 2007. Oskarshamn site investigation. Boremap mapping of telescopic drilled borehole KLX10.

P-06-65 Mattsson H, Keisu M, 2006. Oskarshamn site investigation. Interpretation of geophysical borehole measurements from KLX08, HLX30, HLX31 and HLX33.

P-06-82 Petersson J, Skogsmo G, Berglund J, Stråhle A, 2006. Oskarshamn site investigation. Comparative geological logging with the Boremap system: 9.6–132.2 m of borehole KLX07B.

P-06-99 Gustafsson J, Gustafsson C, 2006. Oskarshamn site investigation. RAMAC, BIPS and deviation logging in boreholes KLX09B, KLX09C, KLX09D, KLX09E, KLX09F and KLX09G.

P-06-100 Mattsson H, 2006. Oskarshamn site investigation. The magnetic anisotropy of rocks across two major deformation zones in the Laxemar and Simpevarp area.

P-06-116 Ask H, Morosini M, Samuelsson L-E, Ekström L, Håkansson N, 2006. Oskarshamn site investigation. Drilling of cored borehole KLX10.

P-06-117 Stanfors R, 2006. Review of existing information from the Äspö HRL area, with focus on hydraulically important minor structures.

P-06-118 Lundberg E, Sjöström H, 2006. Oskarshamn site investigation. Kinematic analysis of ductile and brittle/ductile shear zones in Simpevarp and Laxemar subarea.

P-06-121 Sohlenius G, Bergman T, Snäll S, Lundin L, Lode E, Stendahl J, Riise A, Nilsson J, Johansson T, Göransson M, 2006. Oskarshamn site investigation. Soils, Quaternary deposits and bedrock in topographic lineaments situated in the Laxemar subarea.

P-06-124 Mattsson H, Keisu M, 2006. Oskarshamn site investigation. Interpretation of geophysical borehole measurements from KLX09.

P-06-128 Carlsten S, Hultgren P, Mattsson H, Stanfors R, Wahlgren C-H, 2006. Oskarshamn site investigation. Geological single-hole interpretation of KLX05, HLX15, HLX18, HLX19 and HLX32.

P-06-129 Carlsten S, Hultgren P, Mattsson H, Stanfors R, Wahlgren C-H, 2007. Oskarshamn site investigation. Geological single-hole interpretation of KLX06, HLX13, HLX17 and HLX28.

P-06-137 Thunehed H, Triumf C-A, 2006. Oskarshamn site investigation. Detailed ground geophysics at Laxemar, autumn/winter 2005/2006. Magnetic total field and resistivity.

P-06-154 Nielsen U, Ringgaard J, Fris D, 2006. Oskarshamn site investigation. Geophysical borehole logging in borehole KLX09.

P-06-156 Gustafsson J, Gustafsson C, 2006. Oskarshamn site investigation. RAMAC and BIPS logging in borehole KLX11A.

P-06-157 Mattsson H, 2006. Oskarshamn site investigation. Interpretation of geophysical borehole measurements from KLX11A. Revised September 2006.

P-06-159 Gustafsson J, Gustafsson C, 2006. Oskarshamn site investigation. RAMAC, BIPS and deviation logging in boreholes KLX11B, KLX11C, KLX11D, KLX11E, KLX11F, KLX18A, KLX20A, HLX38 and HLX40 and BIPS and deviation logging in KLX19A.

P-06-162 Mattsson H, 2006. Oskarshamn site investigation. Interpretation of geophysical borehole measurements and petrophysical data from KLX10.

P-06-167 Gustafsson J, Gustafsson C, Friborg J, 2006. Oskarshamn site investigation. RAMAC and BIPPS logging in boreholes KLX10B, KLX10C and KLX12A.

P-06-174 Carlsten S, Hultgren P, Mattsson H, Stanfors R, Wahlgren C-H, 2007. Oskarshamn site investigation. Geological single-hole interpretation of KLX10, HLX20 and HLX36.

P-06-175 Carlsten S, Hultgren P, Mattsson H, Stanfors R, Wahlgren C-H, 2007. Oskarshamn site investigation. Geological single-hole interpretation of KLX07A, KLX07B, HLX34 and HLX35.

P-06-176 Carlsten S, Stråhle A, Hultgren P, Mattsson H, Stanfors R, Wahlgren C-H, 2007. Oskarshamn site investigation. Geological single-hole interpretation of KLX08.

P-06-197 Nielsen U, Ringgaard J, 2006. Oskarshamn site investigation. Geophysical borehole logging in boreholes KLX11A, HLX36 and HLX37.

P-06-198 Nielsen U, Ringgaard J, 2006. Oskarshamn site investigation. Geophysical borehole logging in boreholes KLX12A, KLX09G, KLX10B and KLX10C.

P-06-222 Ask H, Morosini M, Samuelsson L-E, Ekström L, Håkansson N, 2006. Oskarshamn site investigation. Drilling of cored borehole KLX08.

P-06-236 Mattsson K-J, Eklund S, 2007. Oskarshamn site investigation. Boremap mapping of core drilled MDZ boreholes KLX09G, KLX10B and KLX10C.

P-06-237 Rauséus G, Mattsson K-J, Eklund S, Ehrenborg J, 2007. Oskarshamn site investigation. Boremap mapping of core drilled borehole KLX11A.

P-06-238 Mattsson K-J, Eklund S, 2007. Oskarshamn site investigation. Boremap mapping of core drilled borehole KLX18A.

P-06-240 Rauséus G, Mattsson K-J, Ehrenborg J, 2007. Oskarshamn site investigation. Boremap mapping of core drilled borehole KLX09.

P-06-241 Rauséus G, Ehrenborg J, 2007. Oskarshamn site investigation. Boremap mapping of core drilled borehole KLX20A.

P-06-242 Rauséus G, Ehrenborg J, 2007. Oskarshamn site investigation. Boremap mapping of core drilled borehole KLX12A.

P-06-243 Mattsson K-J, Eklund S, Ehrenborg J, 2007. Oskarshamn site investigation. Boremap mapping of core drilled MDZ boreholes KLX22A, KLX22B, KLX23A and KLX23B.

P-06-244 Mattsson K-J, Rauséus G, Eklund S, Ehrenborg J, 2007. Oskarshamn site investigation. Boremap mapping of core drilled DFN boreholes KLX11B–KLX11F.

P-06-253 Mattsson H, 2006. Oskarshamn site investigation. Interpretation of geophysical borehole measurements from KLX12A. Revised January 2008.

P-06-255 Rauséus G, Mattsson K-J, Ehrenborg J, 2007. Oskarshamn site investigation. Boremap mapping of telescopic drilled borehole KLX13A.

P-06-256 Mattsson K-J, Rauséus G, Ehrenborg J, 2007. Oskarshamn site investigation. Boremap mapping of core drilled MDZ boreholes KLX26A and KLX26B.

P-06-257 Mattsson K-J, Rauséus G, Ehrenborg J, 2007. Oskarshamn site investigation. Boremap mapping of core drilled MDZ boreholes KLX24A and KLX25A.

P-06-260 Gustafsson J, Gustafsson C, 2006. Oskarshamn site investigation. RAMAC, BIPS and deviation logging in boreholes KLX13A, KLX14A, KLX22A, KLX22B, KLX23A, KLX23B, KLX24A, KLX25A, KLX26A, KLX26B, HLX39 and HLX41.

P-06-262 Triumf C-A, Thunehed H, 2007. Oskarshamn site investigation. Co-ordinated lineaments longer than 100 m at Laxemar. Identification of lineaments from LIDAR data and co-ordination with lineaments in other topographical and geophysical data.

P-06-264 Mattsson H, Keisu M, 2006. Oskarshamn site investigation. Interpretation of geophysical borehole measurements from KLX09G, KLX10B, KLX10C, HLX36 and HLX37.

P-06-265 Ask H, 2007. Oskarshamn site investigation. Core drilling of short boreholes KLX09B, KLX09C, KLX09D, KLX09E and KLX09F for discrete fracture network investigation (DFN).

P-06-279 Wahlgren C-H, Bergman T, Ahl M, Ekström M, 2006. Oskarshamn site investigation. Modal and geochemical analyses of drill core samples 2006 and updated bedrock map of the Laxemar subarea. Classification of rock types in KLX08, KLX10, KLX11A, KLX12A, KLX18A and KLX20A.

P-06-282 Olsson T, Stanfors R, Sigurdsson O, Erlström M, 2007. Oskarshamn site investigation. Identification and characterization of minor deformation zones based on lineament interpretation.

P-06-283 Ask H, 2006. Oskarshamn site investigation. Core drilling of short boreholes KLX11B, KLX11C, KLX11D, KLX11E and KLX11F for discrete fracture network investigation (DFN).

P-06-290 Nielsen U, Ringgaard J, 2006. Oskarshamn site investigation. Geophysical borehole logging in boreholes KLX20A, KLX18A, KLX11B, KLX09B, KLX09D, KLX09F, HLX38, HLX39, HLX40 and HLX41.

P-06-292 Mattsson H, Keisu M, 2006. Oskarshamn site investigation. Interpretation of geophysical borehole measurements from KLX18A, KLX20A, KLX09B, KLX09D, KLX09F, KLX11B, HLX38, HLX39, HLX40, HLX41 and interpretation of petrophysical data from KLX20A.

P-06-295 Berglund J, Nyborg M, Triumf C-A, 2007. Oskarshamn site investigation. Lineaments longer than 10 m in two sub areas of Laxemar. Identification of short lineaments from LIDAR and magnetic total field data.

P-06-297 Ask H, 2007. Oskarshamn site investigation. Core drilling of 13 short boreholes (KLX09G, KLX10B, KLX10C, KLX22A, KLX22B, KLX23A, KLX23B, KLX24A, KLX25A, KLX26A, KLX26B, KLX28A and KLX29A) for investigation of minor deformation zones (MDZ).

P-06-305 Ask H, Morosini M, Samuelsson L-E, Ekström L, Håkansson N, 2007. Oskarshamn site investigation. Drilling of cored borehole KLX12A.

P-06-306 Ask H, Morosini M, Samuelsson L-E, Ekström L, Håkansson N, 2007. Oskarshamn site investigation. Drilling of cored borehole KLX11A.

P-06-307 Nielsen U T, Ringgaard J, 2006. Oskarshamn site investigation. Geophysical borehole logging in boreholes KLX13A, KLX14A, KLX22A, KLX22B, KLX23A, KLX23B, KLX24A, KLX25A, KLX26A and KLX26B.

P-06-314 Nielsen U, Ringgaard J, 2006. Oskarshamn site investigation. Geophysical borehole logging in boreholes KLX19A, KLX28A and KLX29A.

P-06-315 Nielsen U, Ringgaard J, 2006. Oskarshamn site investigation. Geophysical borehole logging in boreholes KLX17A and HLX43.

P-06-317 Mattsson H, Keisu M, Thunehed H, 2006. Oskarshamn site investigation. Interpretation of geophyscial borehole measurements from KLX13A, KLX14A, KLX22A, KLX22B, KLX23A, KLX23B, KLX24A, KLX25A, KLX26A and KLX26B.

P-07-03 Janson T, Ljunggren B, Bergman T, 2007. Oskarshamn site investigation. Modal analyses on rock mechanical specimens. Specimens from borehole KLX03, KLX04, KQ0064G, KQ0065G, KF0066A and KF0069A.

P-07-12 Gustafsson J, Gustafsson C, 2007. Oskarshamn site investigation. RAMAC, BIPS and deviation logging in boreholes KLX17A and HLX43.

P-07-13 Gustafsson J, Gustafsson C, 2007. Oskarshamn site investigation. RAMAC, BIPS and deviation logging in boreholes KLX19A, KLX28A and KLX29A.

P-07-15 Nielsen U, Ringgaard J, 2007. Oskarshamn site investigation. Geophysical borehole logging in borehole KLX21B.

P-07-21 Mattsson H, Keisu M, 2007. Oskarshamn site investigation. Interpretation of geophysical borehole measurements from KLX19A, KLX28A and KLX29A.

P-07-25 Mattsson H, Keisu M, 2007. Oskarshamn site investigation. Interpretation of geophysical borehole measurements from KLX17A and HLX43.

P-07-27 Drake H, Page L, Tullborg E-L, 2007. Oskarshamn site investigation. $^{40}Ar/^{39}Ar$ dating of fracture minerals.

P-07-29 Forssberg O, Cronquist T, Vestgård J, Bergkvist L, Hermanson J, Öhman J, Pettersson A, Koyi S, Bergman T, 2007. Oskarshamn site investigation. Detailed outcrop mapping in trenches.

P-07-41 Viola G, Venvik Ganerod G, 2007. Oskarshamn site investigation. Structural analysis of brittle deformation zones in the Simpevarp-Laxemar area, Oskarshamn, southeast Sweden.

P-07-55 Stenberg L, Håkanson N, 2007. Oskarshamn site investigation. Revision of borehole deviation measurements in Oskarshamn. SKB P-07-55, Svensk Kärnbränslehantering AB.

P-07-56 Nielsen U, Ringgaard J, 2007. Oskarshamn site investigation. Geophysical borehole logging in borehole KLX16A.

P-07-57 Gustafsson J, Gustafsson C, 2007. Oskarshamn site investigation. RAMAC, BIPS and deviation logging in boreholes KLX21A and KLX21B.

P-07-58 Gustafsson J, Gustafsson C, 2007. Oskarshamn site investigation. RAMAC, BIPS and deviation logging in boreholes KLX16A and HLX42.

P-07-66 Carlsten S, Mattsson K-J, Curtis P, Hultgren P, Stanfors R, Thunehed H, Wahlgren C-H,2007. Oskarshamn site investigation. Geological single-hole interpretation of KLX22A-B, KLX23A-B, KLX24A, KLX25A and KLX26A-B.

P-07-67 Carlsten S, Stråhle A, Hultgren P, Thunehed H, Stanfors R, Wahlgren C-H, 2007. Oskarshamn site investigation. Geological single-hole interpretation of KLX09 and HLX37.

P-07-68 Carlsten S, Stråhle A, Hultgren P, Mattsson H, Wahlgren C-H,2007. Oskarshamn site investigation. Geological single-hole interpretation of KLX12A, KLX09G, KLX10B and KLX10C.

P-07-69 Carlsten S, Stråhle A, Hultgren P, Keisu, M, Wahlgren C-H, 2007. Oskarshamn site investigation. Geological single-hole interpretation of KLX11A.

P-07-70 Carlsten S, Stråhle A, Hultgren P, Mattsson H, Wahlgren C-H, 2007. Oskarshamn site investigation. Geological single-hole interpretation of KLX18A and KLX20A.

P-07-71 Sigurdsson O, 2007. Oskarshamn site investigation. Simplified Boremap mapping of percussion drilled telescope boreholes KLX08, KLX09, KLX10, KLX11A, KLX19A and KLX21B.

P-07-74 Drake H, Tullborg E-L, 2007. Oskarshamn site investigation. Fracture mineralogy. Results from drill cores KLX03, KLX04, KLX06, KLX07A, KLX08 and KLX10A.

P-07-75 Mattsson H, Keisu M, 2007. Oskarshamn site investigation. Interpretation of geophysical borehole measurements from KLX21B.

P-07-88 Thunehed H, 2007. Oskarshamn site investigation. Comparison between measurements of Total Dissolved Solids and Transient Electromagnetic Soundings in the regional model area.

P-07-97 Mattsson H, Keisu M, 2007. Oskarshamn site investigation. Interpretation of geophysical borehole measurements from KLX16A.

P-07-98 Ask H, Morosini M, Samuelsson L-E, Ekström L, Håkansson N, 2007. Oskarshamn site investigation. Drilling of cored borehole KLX18A.

P-07-114 Mattsson H, Keisu M, 2007. Oskarshamn site investigation. Interpretation of geophysical borehole measurements from KLX15A.

P-07-117 Gustafsson J, Gustafsson C, 2007. Oskarshamn site investigation. RAMAC, BIPS and deviation logging in borehole KLX15A.

P-07-131 Lindqvist G, 2007. Oskarshamn site investigation. Refraction seismic measurements in Laxemar spring 2007.

P-07-134 Ask H, Morosini M, Samuelsson L-E, Ekström L, Håkansson N, 2007. Oskarshamn site investigation. Drilling of cored borehole KLX20A.

P-07-152 Nielsen U, Ringgaard, J, 2007. Oskarshamn site investigation. Geophysical borehole logging in borehole KLX15A.

P-07-153 Carlsten S, Mattsson K-J; Stråhle A, Curtis P, Hultgren P, Mattsson H, Stanfors R, Wahlgren, C-H, 2007. Oskarshamn site investigation. Geological single-hole interpretation of KLX28A and KLX29A.

P-07-155 Carlsten S, Mattsson K-J; Stråhle A, Curtis P, Hultgren P, Mattsson H, Stanfors R, Wahlgren, C-H, 2007. Oskarshamn site investigation. Geological single-hole interpretation of KLX14A and HLX43.

P-07-156 Carlsten S, Stråhle A, Hultgren P, Mattsson H, Stanfors R, Wahlgren C-H, 2007. Oskarshamn site investigation. Geological single-hole interpretation of KLX13A, HLX39 and HLX41.

P-07-157 Mattsson K-J, Dahlin P, 2007. Oskarshamn site investigation. Boremap mapping of telescopic drilled borehole KLX15A.

P-07-158 Mattsson K-J, Dahlin P, 2007. Oskarshamn site investigation. Boremap mapping of telescopic drilled borehole KLX17A.

P-07-159 Mattsson K-J, Dahlin P, 2007. Oskarshamn site investigation. Boremap mapping of core drilled MDZ boreholes KLX28A and KLX29A.

P-07-160 Page L, Söderlund P, Wahlgren C-H, 2007. Oskarshamn site investigation. $^{40}Ar/^{39}Ar$ and (U-Th)/He geochronology of samples from the cored boreholes KSH03A, KSH03B, KLX01, KLX02 and the access tunnel to the Äspö Hard Rock Laboratory.

P-07-161 Carlsten S, Mattsson K-J, Stråhle A, Hultgren P, Mattsson H, Wahlgren C-H, 2007. Oskarshamn site investigation. Geological single-hole interpretation of KLX19A and HLX38.

P-07-168 Mattsson H, Triumf C-A, 2007. Oskarshamn site investigation. Detailed ground geophysics at Laxemar, spring 2007. Magnetic total field.

P-07-191 Wahlgren C-H, Bergman T, Ahl M, Ekström M, Page L, Söderlund U, 2007. Oskarshamn site investigation. Modal and geochemical analyses of drill core samples 2007 and $^{40}Ar/^{39}Ar$ dating of a dolerite. Classification of rock types in KLX15A, KLX16A, KLX19A, KLX20A and KLX21B

P-07-195 Ask H, Morosini M, Samuelsson L-E, Tiberg L, 2007. Oskarshamn site investigation. Drilling of cored borehole KLX13A.

P-07-202 Ask H, Morosini M, Samuelsson L-E, Tiberg L, 2007. Oskarshamn site investigation. Drilling of cored borehole KLX19A.

P-07-208 Carlsten S, Mattsson K-J, Stråhle A, Curtis P, Hultgren P, Mattsson H, Wahlgren C-H, 2007. Oskarshamn site investigation. Geological single-hole interpretation of KLX16A.

P-07-209 Carlsten S, Mattsson K-J, Stråhle A, Hultgren P, Mattsson H, Wahlgren C-H, 2007. Oskarshamn site investigation. Geological single-hole interpretation of KLX17A and HLX42.

P-07-210 Mattsson K-J, Dahlin P, Ehrenborg J, 2007. Oskarshamn site investigation. Boremap mapping of telescopic drilled borehole KLX19A.

P-07-211 Mattsson K-J, Dahlin P, Lundberg E, 2007. Oskarshamn site investigation. Boremap mapping of core drilled borehole KLX16A.

P-07-218 Mattsson K-J, Dahlin P, Lundberg E, 2007. Oskarshamn site investigation. Boremap mapping of telescopic drilled borehole KLX21B.

P-07-221 Ask H, Morosini M, Tiberg L, 2008. Oskarshamn site investigation. Drilling of cored borehole KLX17A.

P-07-223 Triumf C-A, 2007. Oskarshamn site investigation. Assessment of possible dolerite dykes in the Laxemar subarea from magnetic total field data and digital elevation models.

P-07-227 Viola G, Venvik Ganerod G, 2007. Oskarshamn site investigation. Structural characterisation of deformation zones (faults and ductile shear zones) from selected drill cores and outcrops from the Laxemar area – Results from Phase 2.

P-08-03 Nielsen U T, Ringgaard J, 2008. Oskarshamn site investigation. Geophysical borehole logging in borehole KLX27A.

P-08-04 Mattsson H, 2008. Oskarshamn site investigation. Interpretation of geophysical borehole measurements from KLX27A.

P-08-05 Carlsten S, Mattsson K-J, Stråhle A, Hultgren P, Mattsson H, Wahlgren C-H, 2008. Oskarshamn site investigation. Geological single-hole interpretation of KLX15A and HLX30, HLX31 and HLX33.

P-08-06 Carlsten S, Mattsson K-J, Stråhle A, Curtis P, Thunehed H, Wahlgren C-H, 2008. Oskarshamn site investigation. Geological single-hole interpretation of KLX21B and HLX40.

P-08-07 Viola G, Venvik Ganerod G, 2008. Oskarshamn site investigation. Structural characterization deformation zones (faults and ductile shear zones) from selected drill cores from Laxemar area, Oskarshamn, southeast Sweden.

P-08-11 Drake H, Tullborg E-L, 2008. Oskarshamn site investigation. Fracture mineralogy. Results from drill core KLX15A.

P-08-12 Drake H, Tullborg E-L, 2008. Oskarshamn site investigation. Mineralogy in water conducting zones. Results from drill cores KLX13A and KLX17A with additional fracture mineralogical data from drill cores KLX14A, KLX19A, KLX20A and KLX26A.

P-08-21 Ask H, 2008. Oskarshamn site investigation. Core drilling of short borehole KLX14A.

P-08-24 Ask H, Morosini M, Tiberg L, 2008. Oskarshamn site investigation. Drilling of boreholes KLX21A and KLX21B.

P-08-30 Gustafsson J, Gustafsson G, 2008. Oskarshamn site investigation. RAMAC, BIPS and deviation logging in borehole KLX27A.

P-08-39 Mattsson K-J, Eklund S, 2008. Oskarshamn site investigation.
Boremap mapping of telescopic drilled borehole KLX27A.

P-08-41 Drake H, Tullborg E-L, 2008. Oskarshamn site investigation. Mineralogy in water conducting zones. Results from boreholes KLX03, KLX04, KLX06, KSH01A+B, KSH02 and KSH03A.

P-08-42 Drake H, Tullborg E-L, 2008. Oskarshamn site investigation. Mineralogy in water conducting zones. Results from boreholes KLX07A+B and KLX08.

P-08-44 Drake H, Tullborg E-L, 2007. Oskarshamn site investigation. Detecting the near surface redox front in crystalline rock. Results from drill cores KLX09B-G and KLX11B-F.

P-08-48 Carlsten S, Mattsson K-J, Stråhle A, Mattsson H, Wahlgren C-H, 2008. Oskarshamn site investigation. Geological single-hole interpretation of KLX27A.

R-98-56 Bergman T, Isaksson H, Johansson R, Lindén A H, Lindgren J, Lindroos H, Rudmark L, Wahlgren C-H, 1998. Förstudie Oskarshamn. Jordarter, bergarter och deformationszoner.

R-99-04 Bergman T, Follin S, Isaksson H, Johansson R, Lindén A H, Lindroos H, Rudmark L, Stanfors R, Wahlgren C-H, 1999. Förstudie Oskarshamn. Erfarenheter från geovetenskapliga undersökningar i nordöstra delen av kommunen.

R-00-45 Bergman T, Rudmark L, Wahlgren C-H, Johansson R, Isaksson H, 2000. Förstudie Oskarshamn. Kompletterande geologiska studier.

R-01-06 Markström I, Stanfors R, Juhlin C, 2001. Äspölaboratoriet. RVS-modellering, Ävrö. Slutrapport.

R-01-07 Bergman B, Juhlin C, Palm H, 2001. Reflektionsseismiska studier inom Laxemarområdet.

R-01-15 Munier R, Hermanson J, 2001. Metodik för geometrisk modellering. Presentation och administration av platsbeskrivande modeller.

R-01-37 Landström O, Tullborg E-L, Eriksson G, Sandell Y, 2001. Effects of glacial/post-glacial weathering compared with hydrothermal alteration – implications for matrix diffusion.

R-01-60 Åhäll K-I, 2001. Åldersbestämning av svårdaterade bergarter i sydöstra Sverige.

R-02-35 SKB, 2002. Simpevarp – site descriptive model version 0.

R-02-37 Röshoff K, Cosgrove J, 2002. Sedimentary dykes in the Oskarshamn-Västervik area – A study of the mechanism of formation.

R-02-42 Alm E, and Sundblad K, 2002. Fluorite-calcite-galena-bearing fractures in the counties of Kalmar and Blekinge, Sweden.

R-03-07 Munier R, Stenberg L, Stanfors R, Milnes A G, Hermanson J, Triumf C-A, 2003. Geological Site Descriptive Model. A strategy for the development during site investigations.

R-04-09 Smellie J, 2004. Recent geoscientific information relating to deep crustal studies.

R-04-25 SKB, 2004. Preliminary site description. Simpevarp area – version 1.1.

R-04-66 Munier R, 2004. Statistical analysis of fracture data, adapted for modelling Discrete Fracture Networks – version 2.

R-04-72 Lindroos H, 2004. The potential for ore, industrial minerals and commercial stones in the Simpevarp area.

R-05-08 SKB, 2005. Preliminary site description. Simpevarp subarea – version 1.2.

R-05-12 SKB, 2005. Preliminary safety evaluation for the Simpevarp subarea – Based on data and site descriptions after the initial site investigation stage.

R-05-45 Hermanson J, Forsberg O, Fox A, La Pointe P, 2005. Statistical model of fractures and deformation zones. Preliminary site description, Laxemar subarea, version 1.2.

R-05-69 Wahlgren C-H, Hermanson J, Curtis P, Triumph C-A, Drake H, Tullborg E-L, 2006. Geological description of rock domains and deformation zones in the Simpevarp and Laxemar subareas. Preliminary site description Laxemar subarea – version 1.2.

R-06-06 SKB, 2006. Preliminary safety evaluation for the Laxemar subarea – Based on data and site descriptions after the initial site investigation stage.

R-06-10 SKB, 2006. Preliminary site description, Laxemar subarea – version 1.2.

R-06-35 SKB, 2006. Final repository for spent nuclear fuel. Underground design for Simpevarp, Layout D1.

R-06-36 SKB, 2006. Final repository for spent nuclear fuel. Underground design Laxemar, Layout D1.

R-06-53 Johansson R, 2006. A comparison of two independent interpretations of lineaments from geophysical and topographic data from the Simpevarp area.

R-06-109 Drake H, Sandström B, Tullborg E-L, 2006. Mineralogy and geochemistry of rocks and fracture fillings from Forsmark and Oskarshamn. Compilation of data for SR-Can.

R-06-110 SKB, 2006. Preliminary site description Laxemar stage 2.1. Feedback for the completion of the site investigation including input from safety assessment and repository engineering.

R-08-124 Viola G, 2008. Ductile and brittle structural evolution of the Laxemar-Simpevarp area: an independent analysis based on local and regional constraints.

PR-25-87-03 Talbot C, Riad L, 1988. Natural fractures in the Simpevarp area.

PR 25-87-04 Nisca D, 1987. Aerogeophysical interpretation. Bedrock and tectonic analysis.

PR-25-88-12 Kornfält K-A, Wikman H, 1988. The rocks of the Äspö island. Description to the detailed maps of solid rocks including maps of 3 uncovered trenches.

PR 25-89-13 Stenberg L, Sehlstedt S, 1989. Geophysical profile measurements on interpreted regional aeromagnetic lineaments in the Simpevarp area.

PR 25-89-15 Munier R, 1989. Brittle tectonics on Äspö, SE Sweden.

PR 25-89-23 Rydström H, Gereben L, 1989. Regional geological study. Seismic refraction survey.

PR 25-94-39 Stanfors R, Rhén I, Forsmark T, Wikberg P, 1994. Evaluation of the fracture zone EW-1, based on the cored boreholes KA1755A, KA1751, KA1754A and KAS04.

PR 25-95-04 Wikman H, Kornfält K-A, 1995. Updating of a lithological model of the bedrock of the Äspö area.

PR-95-21 Munier R, 1995. Studies of the geological structures at Äspö. Comprehensive summary of results.

TR-93-06 Eliasson T, 1993. Mineralogy, geochemistry and petrophysics of red coloured granite adjacent to fractures.

TR 95-13 Landström O, Tullborg E-L, 1995. Interactions of trace elements with fracture filling minerals from the Äspö Hars Rock laboratory.

TR 97-06 Rhén I, Gustafson G, Stanfors R, Wikberg P, 1997. Äspö HRL – Geoscientific evaluation 1997/5. Models based on site characterization 1986–1995.

TR-00-12 Andersson J, Ström A, Svemar C, Almén K-A, Ericsson L-O, 2000. What requirements does the KBS-3 repository make on the host rock? Geoscientific suitability indicators and criteria for siting and site evaluation.

TR-02-04 Juhlin C, Bergman B, Cosma C, Keskinen J, Enescu , 2002. Vertical seismic profiling and integration with reflection seismic studies at Laxemar, 2000.

TR-02-19 Andersson J, Berglund J, Follin S, Hakami E, Halvarson J, Hermanson J, Laaksoharju M, Rhén I, Wahlgren C-H, 2002. Testing the methodology for site descriptive modelling. Application for the Laxemar area.

TR-06-09 SKB, 2006e. Long-term safety for KBS-3 repositories at Forsmark and Laxemar – a first evaluation. Main report of the SR-Can project.

TR-97-03 Rhén, I (ed.), Bäckblom G (ed.), Gustafson G, Stanfors R, Wikberg P, 1997. Äspö HRL – Geoscientific evaluation 1997/2. Results from pre-investigations and detailed site characterization. Summary report.

TR-97-06 Rhén I (ed.) 1), Gustafson G, Stanfors R, Wikberg P, 1997. Äspö HRL – Geoscientific evaluation 1997/5. Models based on site characterization 1986–1995.

IPR-03-34 Berglund J, Curtis P, Eliasson T, Ohlsson T, Starzec P, Tullborg E-L, 2003. Äspö Hard Rock Laboratory – Update of the geological model 2002.

IPR-06-32 Mattsson H, 2006.The magnetic anisotropy of rocks across the deformation zone NE-1 at the Äspö HRL.

Appendix 2

Nomenclature of rock types

Nomenclature of rock types (in English and Swedish), including rock codes and colour codes applied in the site investigation in Oskarshamn.

Rock code	Rock nomenclature (names within parenthesis refer to nomenclature used in the the Äspö Hard Rock Laboratory and related studies)	Descriptive nomenclature of rock type	R	G	B
501027	Dolerite Diabas	Dolerite Diabas	152	83	161
531058	Fine-grained Götemar granite Finkornig Götemargranit	Granite, fine- to medium-grained, (”Götemar granite”) Granit, fin- till medelkornig, (”Götemargranit”)	255	0	0
521058	Coarse-grained Götemar granite Grovkornig Götemargranit	Granite, coarse-grained, (”Götemar granite”) Granit, grovkornig, (”Götemargranit”)	200	24	56
511058	Fine-grained granite Finkornig granit	Granite, fine- to medium-grained Granit, fin- till medelkornig	235	122	179
501061	Pegmatite Pegmatit	Pegmatite Pegmatit	241	157	86
501058	Granite Granit	Granite, medium- to coarse-grained Granit, medel- till grovkornig	237	113	116
501044	Ävrö granite (Småland-Ävrö granite) Ävrögranit (Småland-Ävrögranit)	Granite to quartz monzodiorite, generally porphyritic Granit till kvartsmonzodiorit, vanligtvis porfyrisk	246	162	168
501056	Ävrö granodiorite Ävrögranodiorit	Granite to granodiorite, generally porphyritic Granit till granodiorit, vanligtvis porfyrisk	239	146	136
501046	Ävrö quartz monzodiorite Ävrökvartsmonzodiorit	Quartz monzonite to quartz monzodiorite, generally porphyritic Kvartsmonzonit till kvartsmonzodiorit, vanligtvis porfyrisk	229	170	170
501036	Quartz monzodiorite (Äspö diorite, tonalite) Kvartsmonzodiorit (Äspödiorit, tonalit)	Quartz monzonite to monzodiorite, equigranular to weakly porphyritic Kvartsmonzonit till monzodiorit, jämnkornig till glest porfyrisk	250	199	193
501033	Diorite/gabbro Diorit/Gabbro	Diorite to gabbro Diorit till gabbro	193	221	53
501030	Fine-grained dioritoid (Metavolcanite, volcanite) Finkornig dioritoid (Metavulkanit, vulkanit)	Intermediate magmatic rock* Intermediär magmatisk bergart	168	216	183
505102	Fine-grained diorite-gabbro (Greenstone) Finkornig diorit-gabbro (Grönsten)	Mafic rock, fine-grained Mafisk bergart, finkornig	69	185	124
506007	Sandstone Sandsten	Sandstone Sandsten	217	192	106

Appendix 3

Primary geological and geophysical borehole data and the single hole interpretation of cored boreholes

The identification and description of rock units and possible deformation zones in the single-hole interpretation (SHI) is a very important component in the geological modelling work. In order to illustrate the working procedure from primary geological and geophysical data to the identification of rock units and possible deformation zones, WellCAD diagrams for all cored boreholes, which show selected primary geological and geophysical data as well as the result of the single-hole interpretation work, are presented in Appendix 3. Elevation values (metres above sea level) are those provided in the Sicada database after the correction procedures carried out (see section 3.1.3). All the WellCad diagrams can be viewed on the CD-Rom attached to this report. For further discussion of these geological and geophysical data, the reader is referred to section 3.3 in this report.

Title GEOLOGY KLX02

Site	LAXEMAR	Coordinate System	RT90-RHB70
Borehole	KLX02	Northing [m]	6366768.99
Diameter [mm]	76	Easting [m]	1549224.09
Length [m.f.ToC]	1700.500	Elevation [m.a.s.l.ToC]	18.40
Bearing [°]	357.30	Drilling Start Date	1992-08-15 00:00:00
Inclination [°]	-84.99	Drilling Stop Date	1992-09-05 00:00:00
Date of mapping	2003-11-20 00:00:00	Plot Date	2008-11-17 23:05:26

ROCK TYPE LAXEMAR
- Fine-grained granite
- Ävrö granite
- Fine-grained dioritoid
- Fine-grained diorite-gabbro

ROCK ALTERATION
- Oxidized

ROCK UNIT
- High confidence

DEFORMATION ZONE
- High confidence

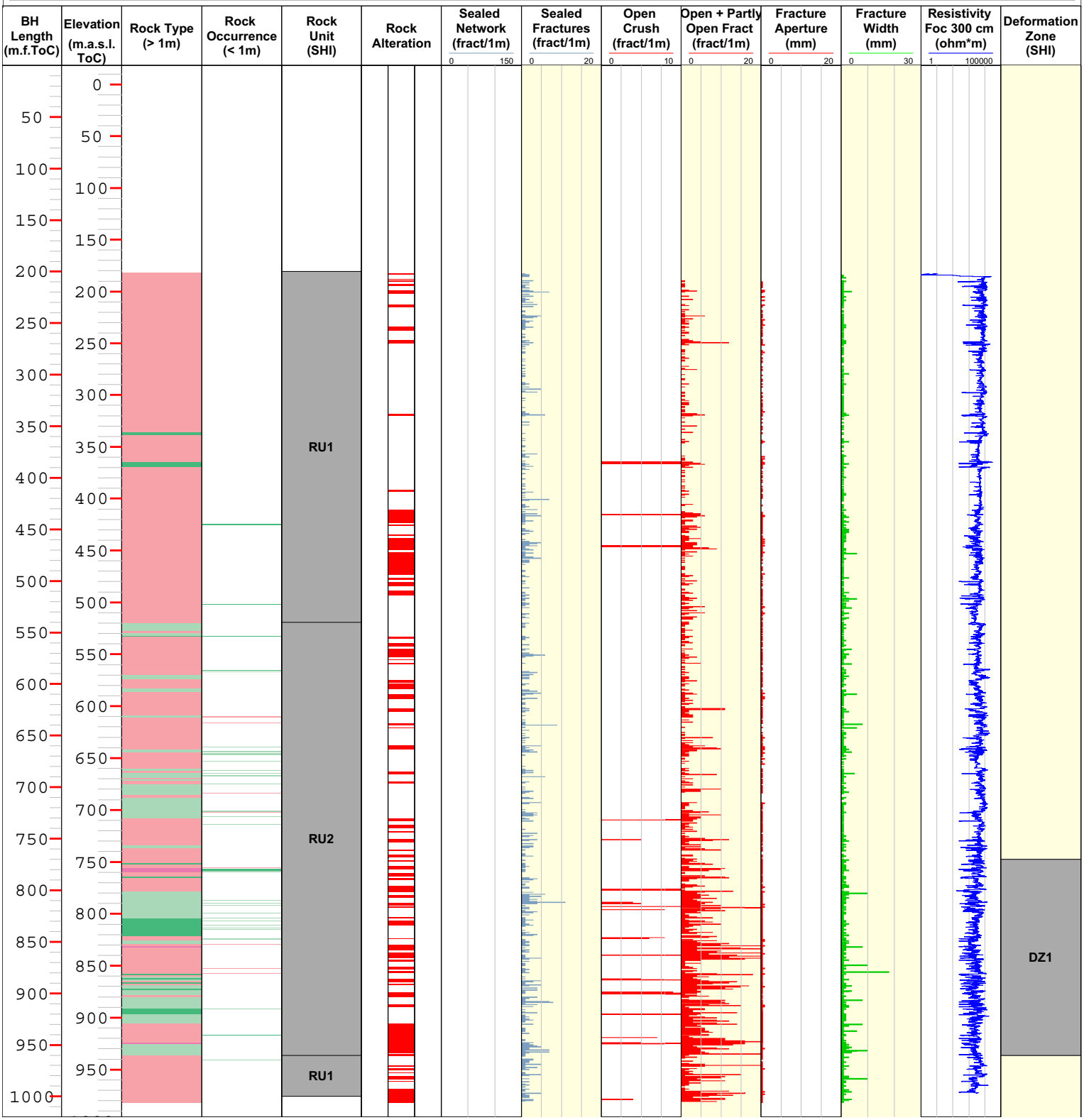

Title GEOLOGY KLX03

Site	LAXEMAR	Coordinate System	RT90-RHB70
Borehole	KLX03	Northing [m]	6366112.59
Diameter [mm]	76	Easting [m]	1547718.93
Length [m]	1000.420	Elevation [m.a.s.l.ToC]	18.49
Bearing [°]	199.04	Drilling Start Date	2004-05-28 18:00:00
Inclination [°]	-74.92	Drilling Stop Date	2004-09-07 09:00:00
Date of mapping	2004-10-27 00:00:00	Plot Date	2008-11-16 23:04:55

ROCK TYPE LAXEMAR
- Fine-grained granite
- Ävrö granite
- Quartz monzodiorite
- Diorite / Gabbro
- Fine-grained dioritoid
- Fine-grained diorite-gabbro

ROCK ALTERATION
- Quartz dissolution
- Oxidized

ROCK UNIT
- High confidence

DEFORMATION ZONE
- High confidence

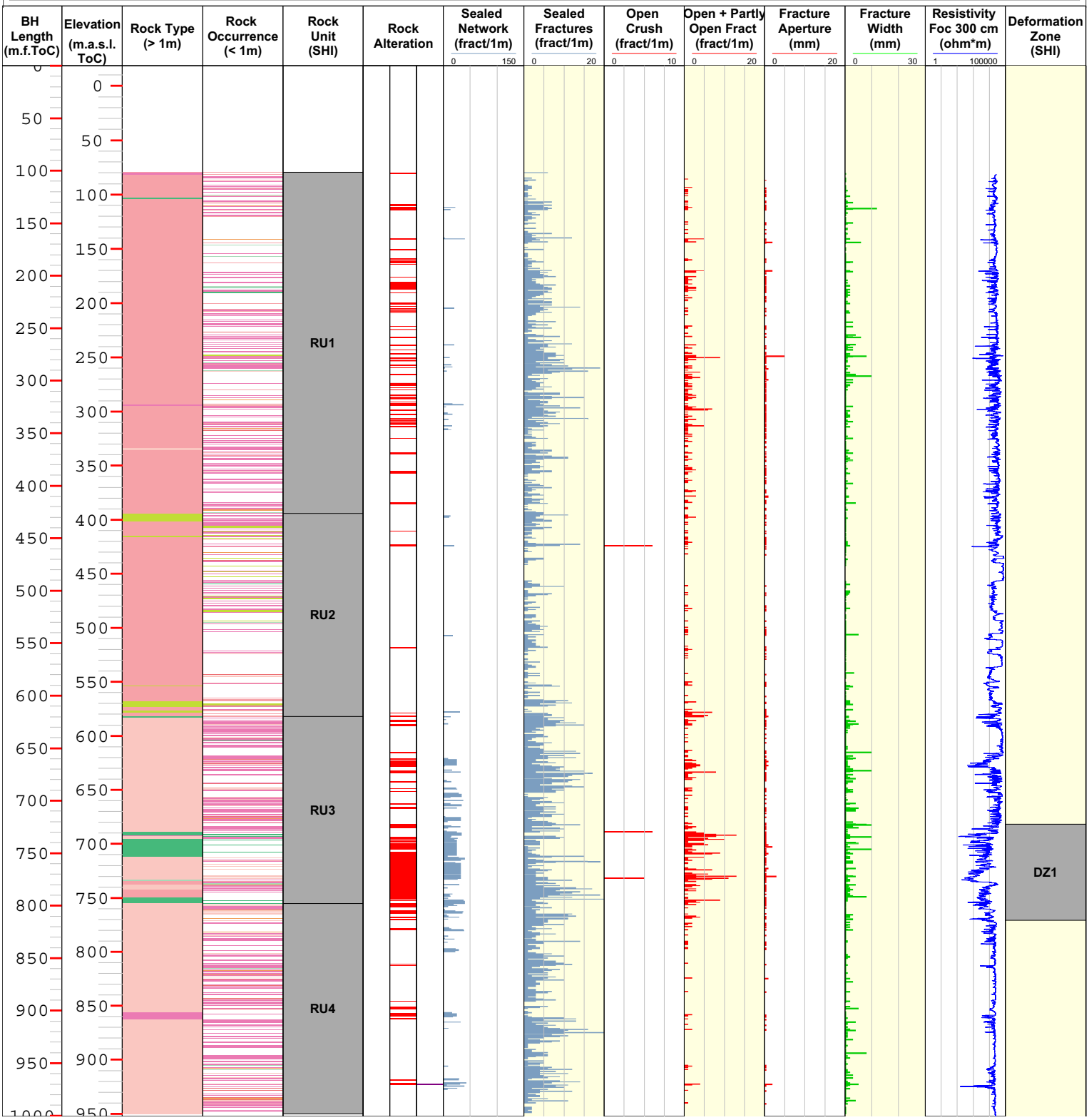

Title GEOLOGY KLX04

Site	LAXEMAR	Coordinate System	RT90-RHB70
Borehole	KLX04	Northing [m]	6367077.19
Diameter [mm]	76	Easting [m]	1548171.94
Length [m.f.ToC]	993.490	Elevation [m.a.s.l.ToC]	24.09
Bearing [°]	0.93	Drilling Start Date	2004-03-13 11:00:00
Inclination [°]	-84.75	Drilling Stop Date	2004-06-28 10:12:00
Date of mapping	2004-07-22 00:00:00	Plot Date	2008-11-16 23:04:55

ROCK TYPE LAXEMAR
- Fine-grained granite
- Granite
- Ävrö granite
- Quartz monzodiorite
- Diorite / Gabbro
- Fine-grained dioritoid
- Fine-grained diorite-gabbro

ROCK ALTERATION
- Quartz dissolution
- Oxidized

ROCK UNIT
- High confidence

DEFORMATION ZONE
- High confidence

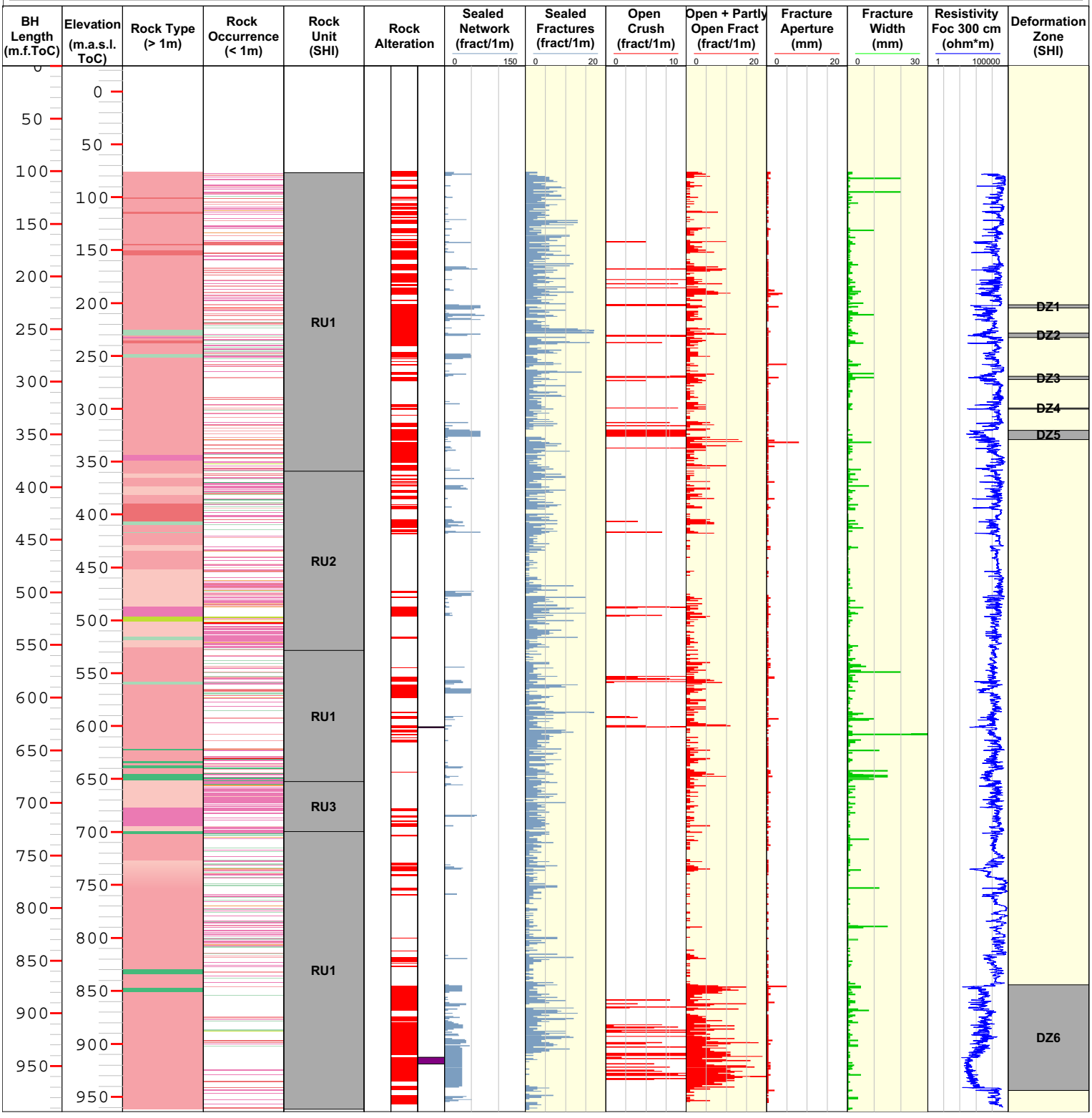

Title GEOLOGY KLX05

Site	LAXEMAR	Coordinate System	RT90-RHB70
Borehole	KLX05	Northing [m]	6365633.34
Diameter [mm]	76	Easting [m]	1548909.41
Length [m.f.ToC]	1000.160	Elevation [m.a.s.l.ToC]	17.63
Bearing [°]	190.19	Drilling Start Date	2004-10-01 14:00:00
Inclination [°]	-65.21	Drilling Stop Date	2005-01-22 13:45:00
Date of mapping	2005-03-14 16:38:00	Plot Date	2008-11-16 23:04:55

ROCK TYPE LAXEMAR

- Fine-grained granite
- Pegmatite
- Granite
- Ävrö granite
- Quartz monzodiorite
- Diorite / Gabbro
- Fine-grained dioritoid
- Fine-grained diorite-gabbro

ROCK ALTERATION

- Oxidized

ROCK UNIT

- High confidence

DEFORMATION ZONE

- Low confidence
- High confidence

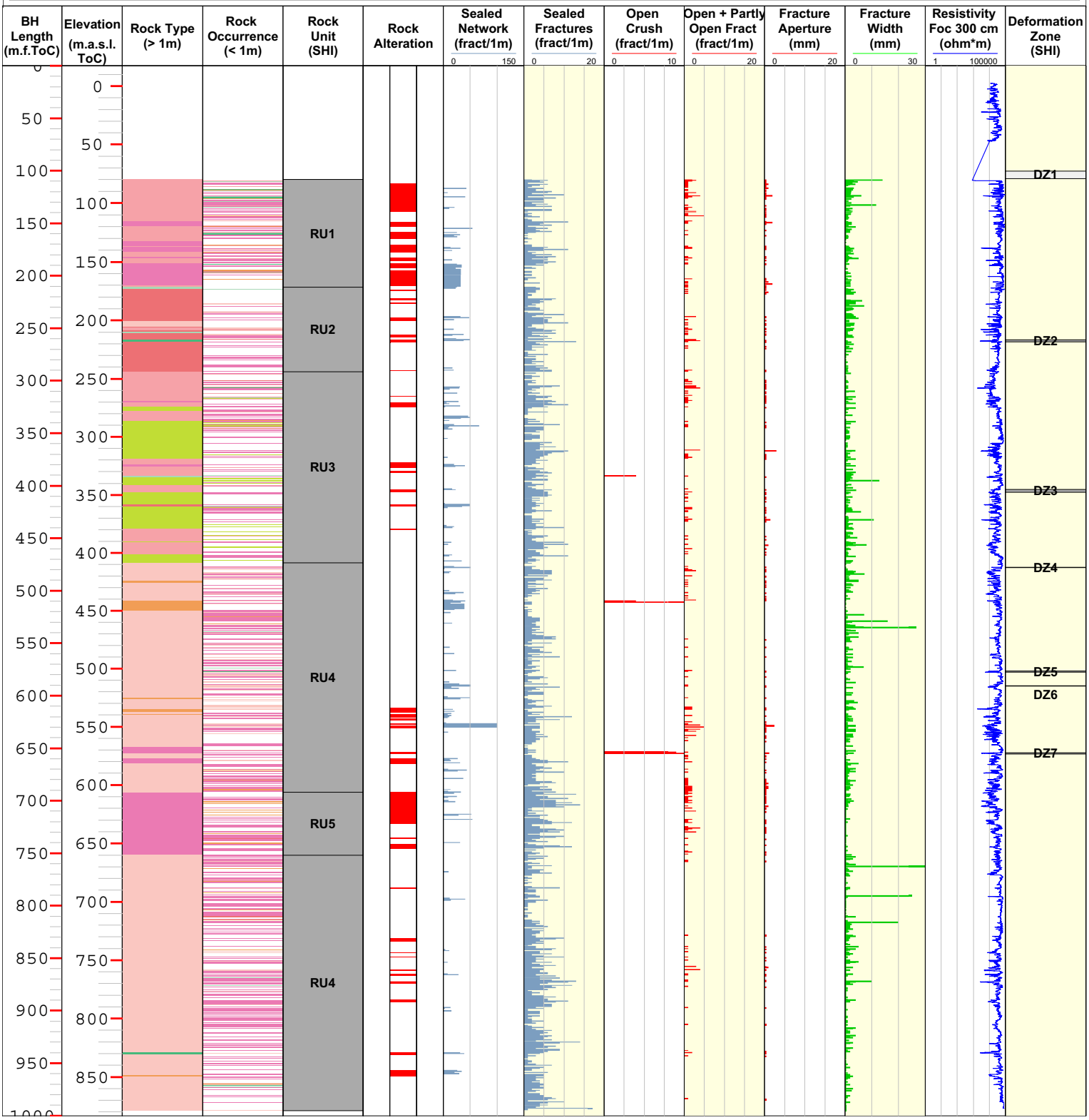

Title GEOLOGY KLX06

Site	LAXEMAR	Coordinate System	RT90-RHB70
Borehole	KLX06	Northing [m]	6367806.64
Diameter [mm]	76	Easting [m]	1548566.88
Length [m.f.ToC]	994.940	Elevation [m.a.s.l.ToC]	17.68
Bearing [°]	329.65	Drilling Start Date	2004-08-25 17:00:00
Inclination [°]	-65.19	Drilling Stop Date	2004-11-25 11:30:00
Date of mapping	2005-01-11 11:53:00	Plot Date	2008-11-16 23:04:55

ROCK TYPE LAXEMAR
- Fine-grained granite
- Granite
- Ävrö granite
- Fine-grained dioritoid
- Fine-grained diorite-gabbro

ROCK ALTERATION
- Quartz dissolution
- Oxidized

ROCK UNIT
- Medium confidence
- High confidence

DEFORMATION ZONE
- High confidence

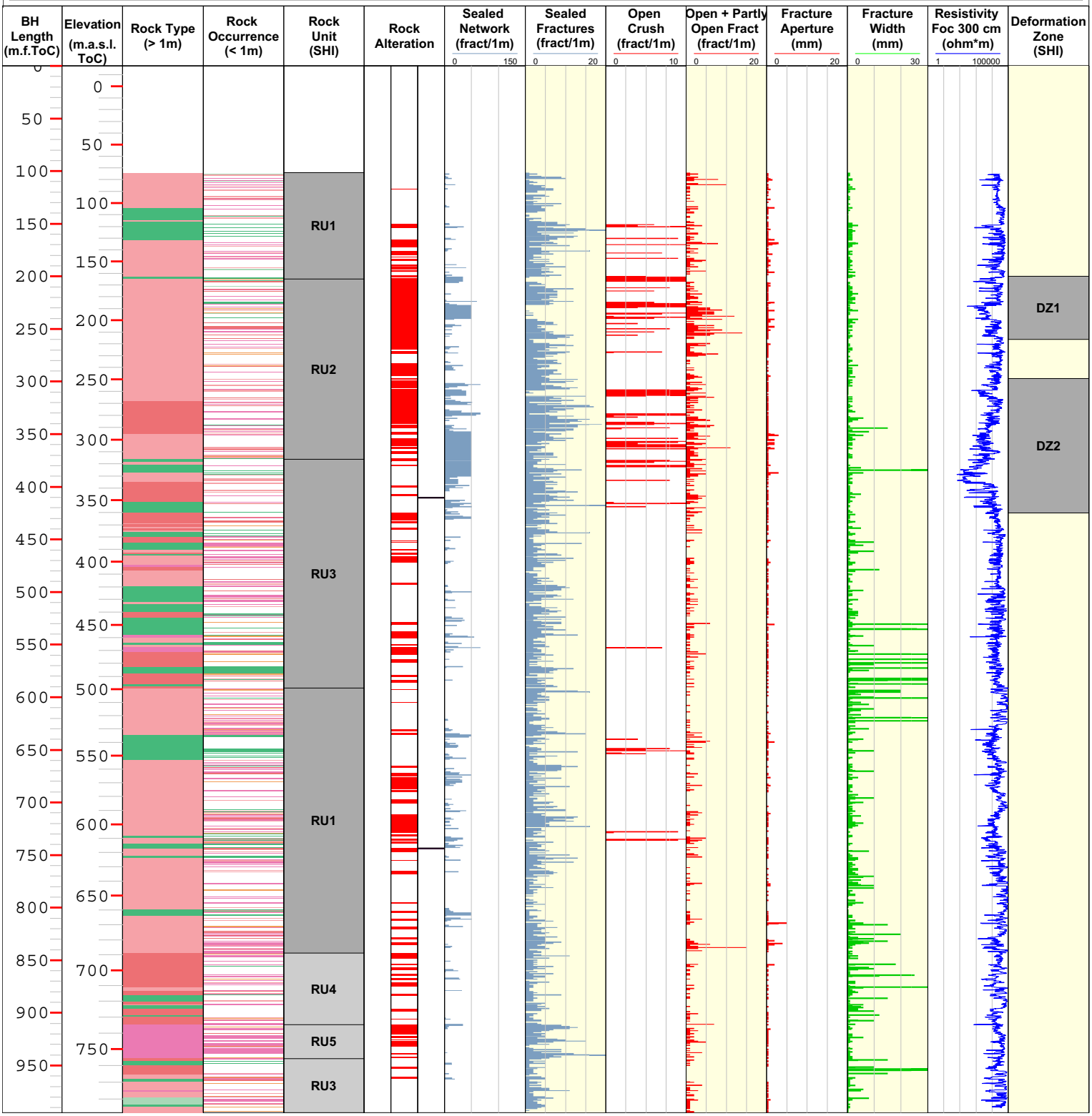

Title GEOLOGY KLX07A

Site	LAXEMAR	Coordinate System	RT90-RHB70
Borehole	KLX07A	Northing [m]	6366752.09
Diameter [mm]	76	Easting [m]	1549206.86
Length [m.f.ToC]	844.730	Elevation [m.a.s.l.ToC]	18.47
Bearing [°]	174.18	Drilling Start Date	2005-01-06 14:00:00
Inclination [°]	-60.03	Drilling Stop Date	2005-05-04 10:00:00
Date of mapping	2005-07-07 15:06:00	Plot Date	2008-11-16 23:04:55

ROCK TYPE LAXEMAR
- Fine-grained granite
- Ävrö granite
- Fine-grained diorite-gabbro

ROCK ALTERATION
- Albitization
- Quartz dissolution
- Oxidized

ROCK UNIT
- High confidence

DEFORMATION ZONE
- Medium confidence
- High confidence

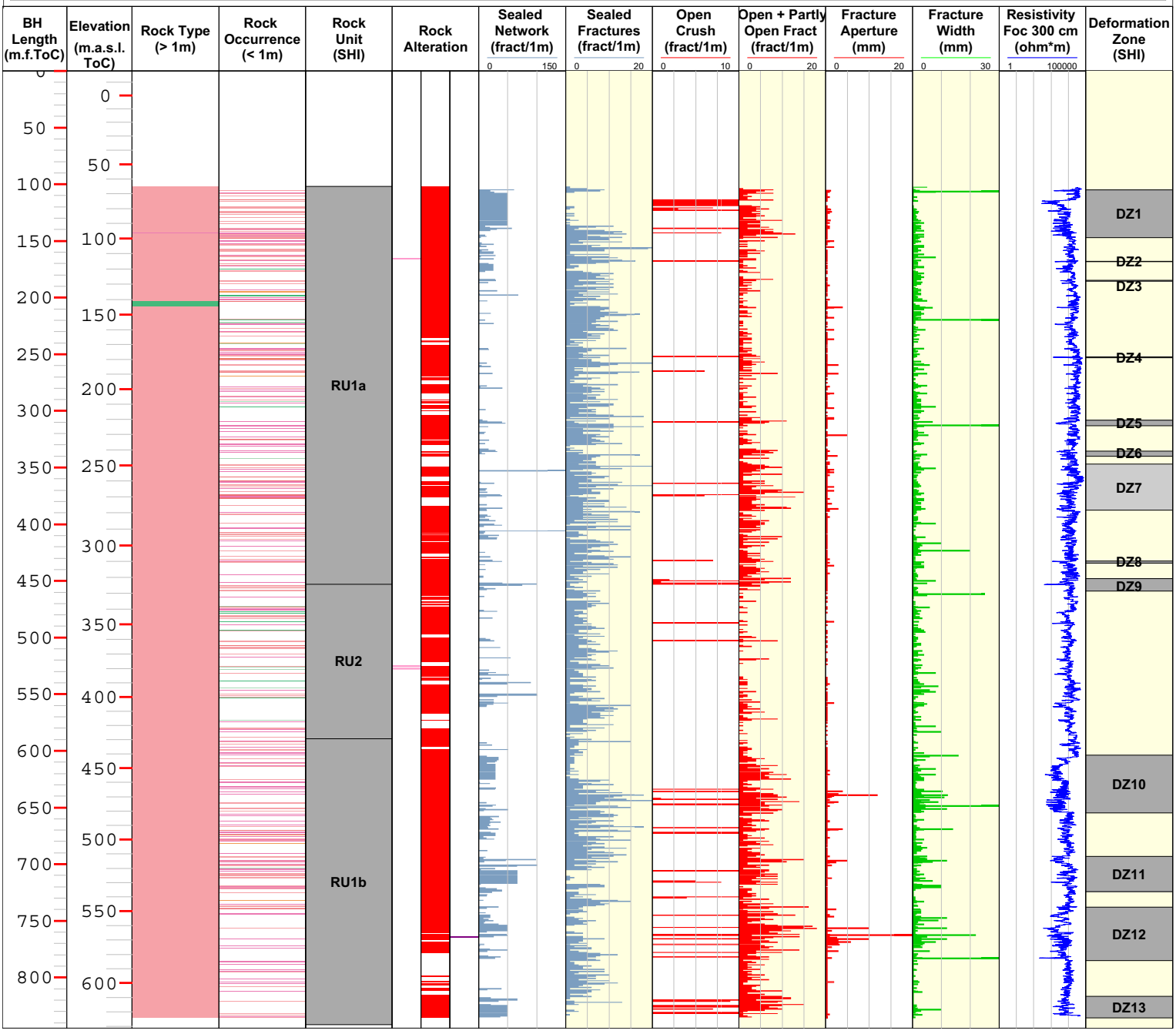

Title GEOLOGY KLX07B

Site	LAXEMAR	**Coordinate System**	RT90-RHB70
Borehole	KLX07B	**Northing [m]**	6366753.14
Diameter [mm]	76	**Easting [m]**	1549206.76
Length [m.f.ToC]	200.130	**Elevation [m.a.s.l.ToC]**	18.38
Bearing [°]	174.33	**Drilling Start Date**	2005-05-23 18:00:00
Inclination [°]	-85.14	**Drilling Stop Date**	2005-06-03 08:00:00
Date of mapping	2005-09-13 08:00:00	**Plot Date**	2008-11-16 23:04:55

ROCK TYPE LAXEMAR
- Ävrö granite
- Fine-grained diorite-gabbro

ROCK ALTERATION
- Albitization
- Oxidized

ROCK UNIT
- High confidence

DEFORMATION ZONE
- High confidence

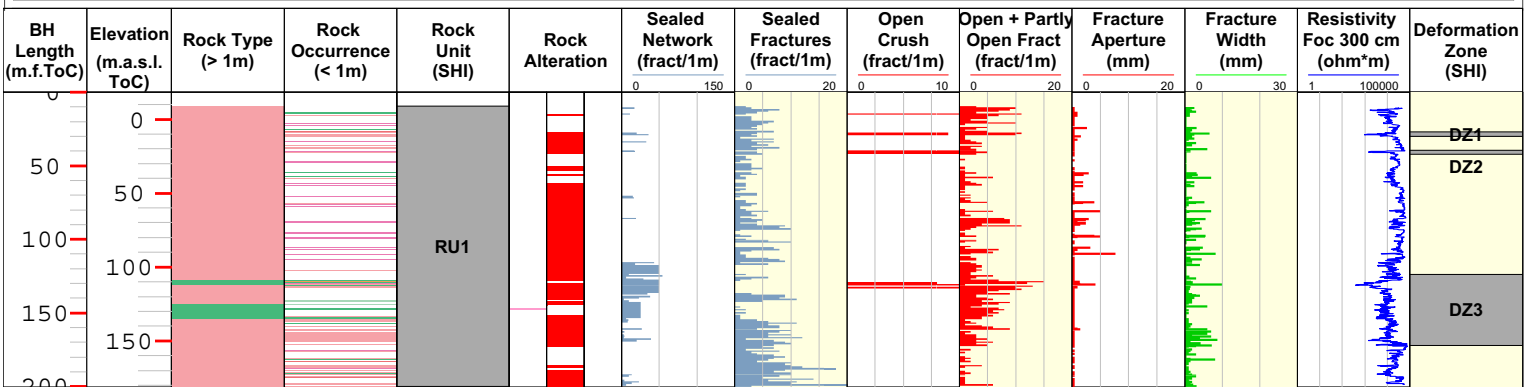

Title GEOLOGY KLX08

Site	LAXEMAR	Coordinate System	RT90-RHB70
Borehole	KLX08	Northing [m]	6367079.10
Diameter [mm]	76	Easting [m]	1548176.71
Length [m.f.ToC]	1000.410	Elevation [m.a.s.l.ToC]	24.31
Bearing [°]	199.17	Drilling Start Date	2005-04-04 13:30:00
Inclination [°]	-60.50	Drilling Stop Date	2005-06-13 14:00:00
Date of mapping	2005-10-11 09:01:00	Plot Date	2008-11-16 23:04:55

ROCK TYPE LAXEMAR
- Fine-grained granite
- Ävrö granite
- Quartz monzodiorite
- Diorite / Gabbro
- Fine-grained dioritoid
- Fine-grained diorite-gabbro

ROCK ALTERATION
- Albitization
- Oxidized

ROCK UNIT
- High confidence

DEFORMATION ZONE
- Medium confidence
- High confidence

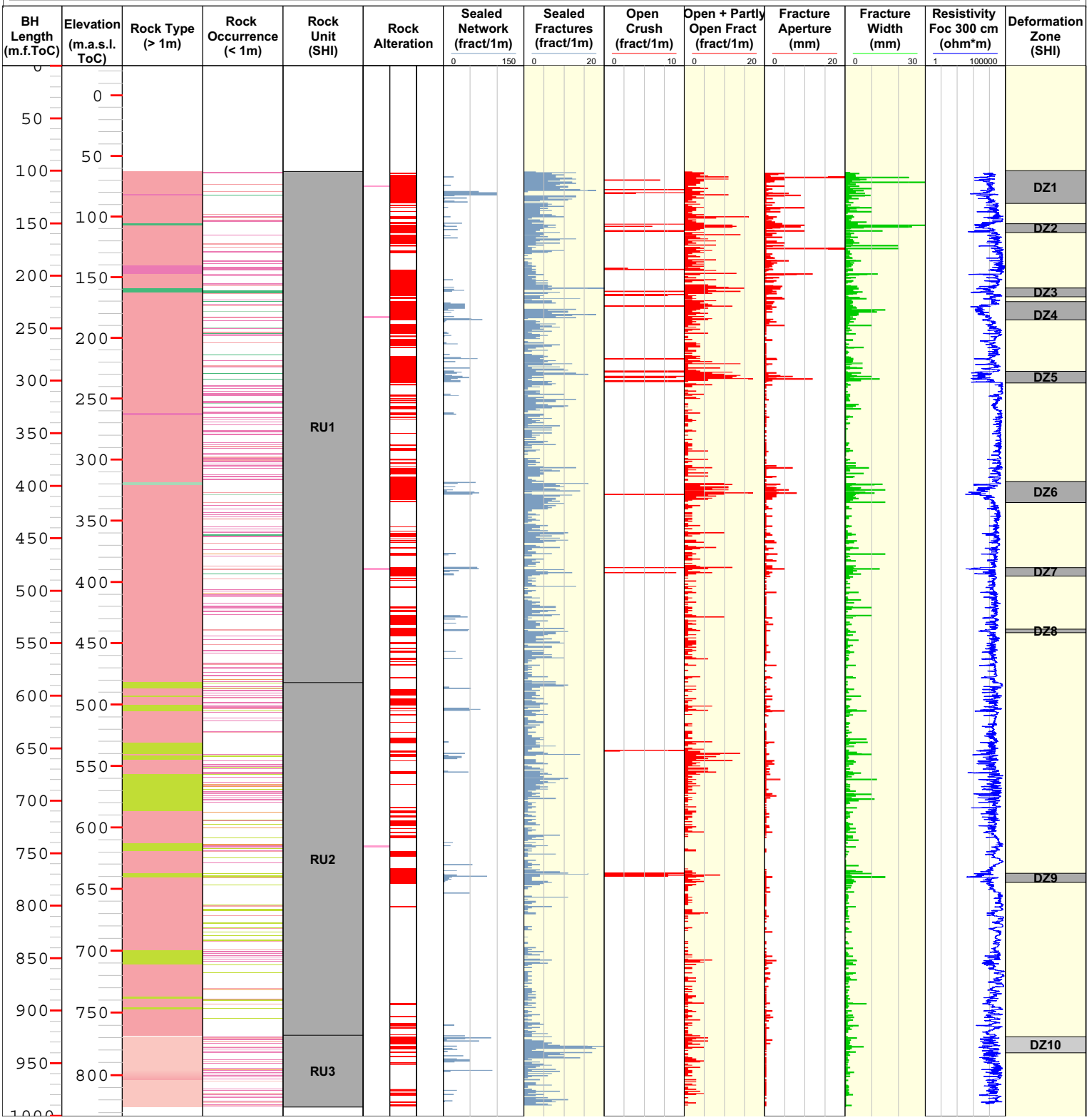

Title GEOLOGY KLX09

Site	LAXEMAR	Coordinate System	RT90-RHB70
Borehole	KLX09	Northing [m]	6367323.45
Diameter [mm]	76	Easting [m]	1548863.18
Length [m.f.ToC]	880.380	Elevation [m.a.s.l.ToC]	23.45
Bearing [°]	267.41	Drilling Start Date	2005-08-26 09:30:00
Inclination [°]	-84.93	Drilling Stop Date	2005-10-15 12:00:00
Date of mapping	2006-02-02 14:40:00	Plot Date	2008-11-16 23:04:55

ROCK TYPE LAXEMAR
- Fine-grained granite
- Ävrö granite
- Quartz monzodiorite
- Diorite / Gabbro
- Fine-grained dioritoid
- Fine-grained diorite-gabbro

ROCK ALTERATION
- Quartz dissolution
- Oxidized

ROCK UNIT
- High confidence

DEFORMATION ZONE
- High confidence

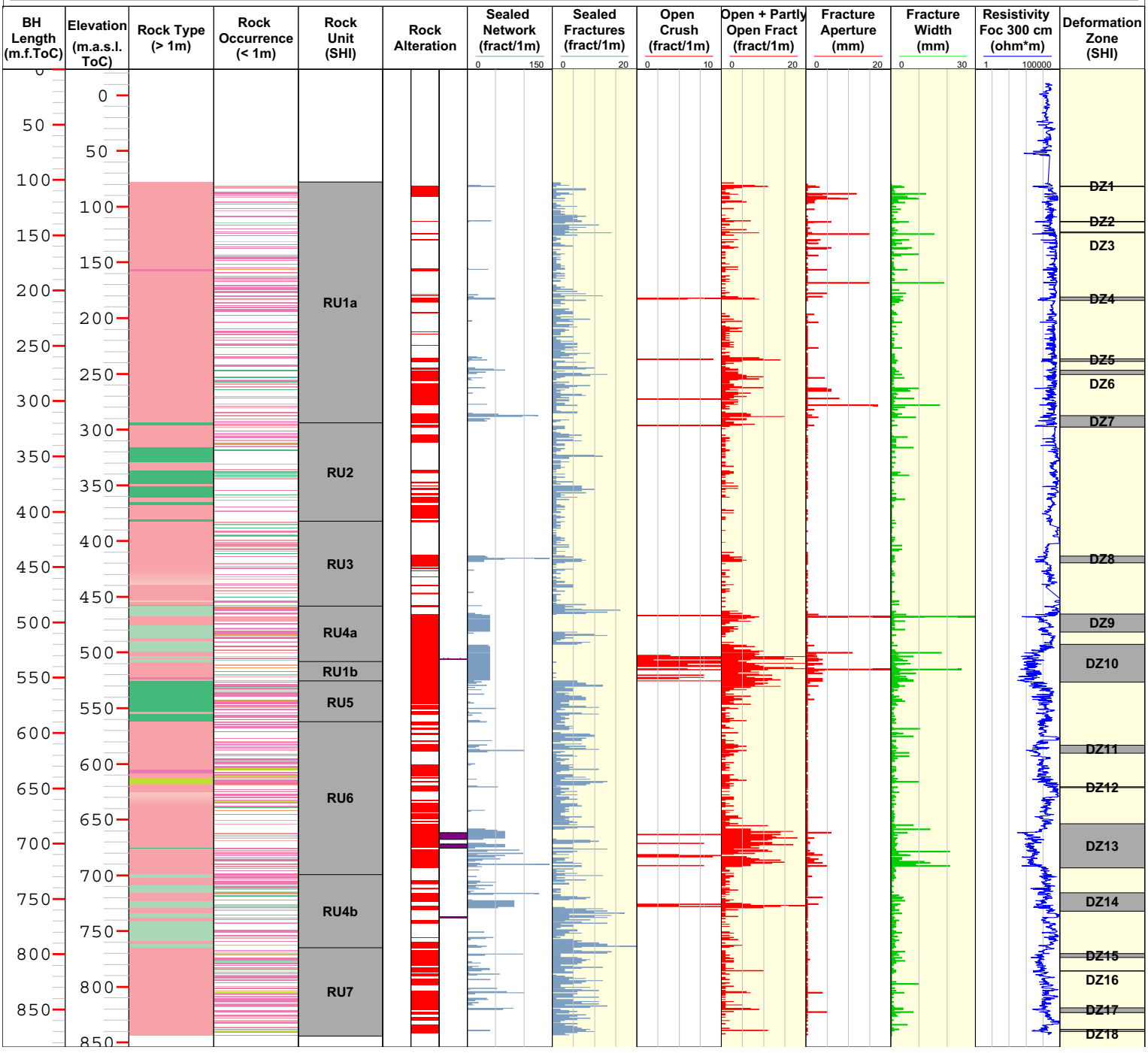

Title GEOLOGY KLX09B

Site	LAXEMAR	**Coordinate System**	RT90-RHB70
Borehole	KLX09B	**Northing [m]**	6367329.07
Diameter [mm]	76	**Easting [m]**	1548859.01
Length [m.f.ToC]	100.220	**Elevation [m.a.s.l.ToC]**	23.62
Bearing [°]	21.25	**Drilling Start Date**	2006-01-16 14:00:00
Inclination [°]	-89.82	**Drilling Stop Date**	2006-01-26 12:00:00
Date of mapping	2006-02-16 09:19:00	**Plot Date**	2008-11-16 23:04:55

ROCK TYPE LAXEMAR
- Fine-grained granite
- Ävrö granite
- Fine-grained diorite-gabbro

ROCK ALTERATION
- Oxidized

ROCK UNIT
- High confidence

DEFORMATION ZONE
- High confidence

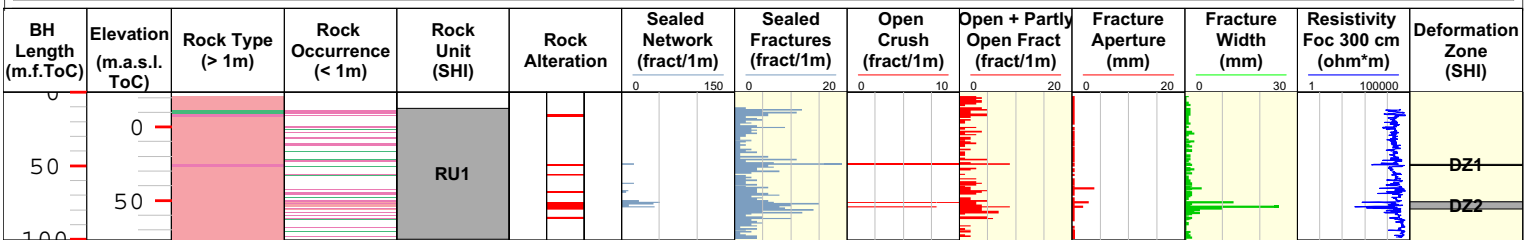

Title GEOLOGY KLX09C

Site	LAXEMAR	**Coordinate System**	RT90-RHB70
Borehole	KLX09C	**Northing [m]**	6367353.43
Diameter [mm]	76	**Easting [m]**	1548838.82
Length [m.f.ToC]	120.050	**Elevation [m.a.s.l.ToC]**	23.75
Bearing [°]	160.39	**Drilling Start Date**	2006-01-07 11:00:00
Inclination [°]	-59.51	**Drilling Stop Date**	2006-01-15 12:00:00
Date of mapping	2006-02-16 09:31:00	**Plot Date**	2008-11-16 23:04:55

ROCK TYPE LAXEMAR

- Fine-grained granite
- Ävrö granite
- Fine-grained diorite-gabbro

ROCK ALTERATION

- Oxidized

ROCK UNIT

- High confidence

DEFORMATION ZONE

- High confidence

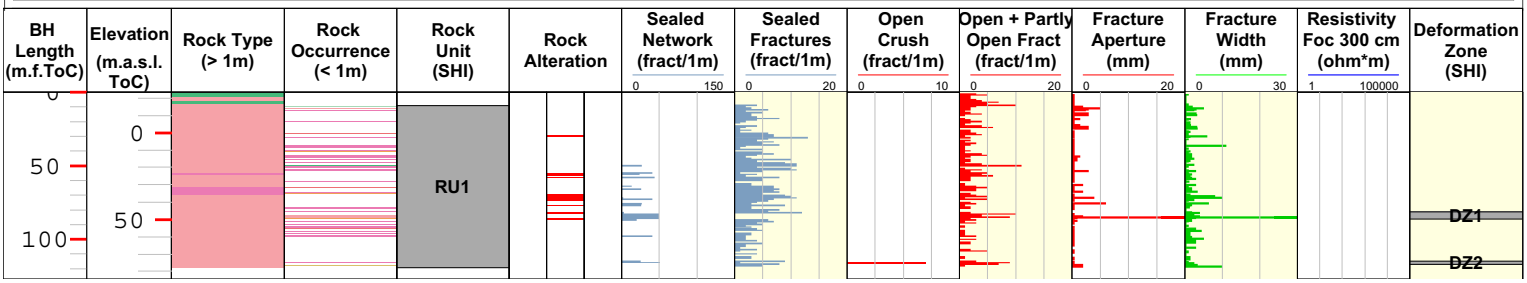

Title GEOLOGY KLX09D

Site	LAXEMAR	**Coordinate System**	RT90-RHB70
Borehole	KLX09D	**Northing [m]**	6367336.99
Diameter [mm]	76	**Easting [m]**	1548878.22
Length [m.f.ToC]	121.020	**Elevation [m.a.s.l.ToC]**	23.10
Bearing [°]	270.15	**Drilling Start Date**	2005-11-05 06:00:00
Inclination [°]	-60.24	**Drilling Stop Date**	2005-11-17 14:00:00
Date of mapping	2006-02-16 09:32:00	**Plot Date**	2008-11-16 23:04:55

ROCK TYPE LAXEMAR
- Fine-grained granite
- Ävrö granite
- Fine-grained diorite-gabbro

ROCK ALTERATION
- Oxidized

ROCK UNIT
- High confidence

DEFORMATION ZONE
- High confidence

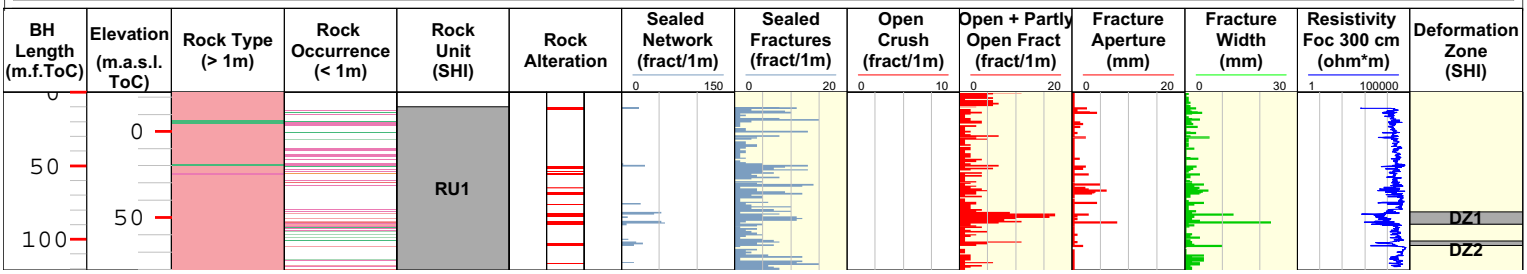

Title GEOLOGY KLX09E

Site	LAXEMAR	**Coordinate System**	RT90-RHB70
Borehole	KLX09E	**Northing [m]**	6367304.45
Diameter [mm]	76	**Easting [m]**	1548880.37
Length [m.f.ToC]	120.000	**Elevation [m.a.s.l.ToC]**	22.16
Bearing [°]	338.90	**Drilling Start Date**	2005-11-23 08:25:00
Inclination [°]	-59.95	**Drilling Stop Date**	2005-12-05 07:00:00
Date of mapping	2006-02-16 09:33:00	**Plot Date**	2008-11-16 23:04:55

ROCK TYPE LAXEMAR
- Fine-grained granite
- Ävrö granite
- Fine-grained diorite-gabbro

ROCK ALTERATION
- Oxidized

ROCK UNIT
- High confidence

DEFORMATION ZONE
- High confidence

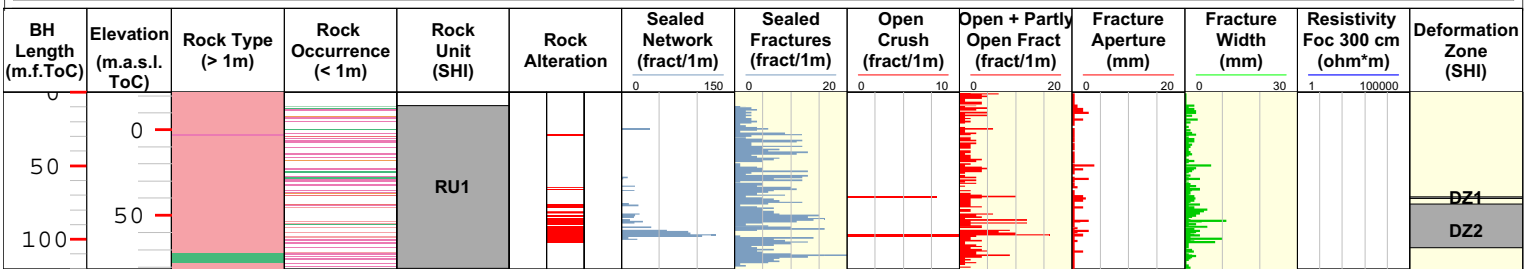

Title GEOLOGY KLX09F

Site	LAXEMAR	**Coordinate System**	RT90-RHB70
Borehole	KLX09F	**Northing [m]**	6367318.02
Diameter [mm]	76	**Easting [m]**	1548817.27
Length [m.f.ToC]	152.300	**Elevation [m.a.s.l.ToC]**	19.57
Bearing [°]	90.67	**Drilling Start Date**	2005-12-06 09:00:00
Inclination [°]	-59.73	**Drilling Stop Date**	2006-01-06 13:00:00
Date of mapping	2006-02-14 11:07:00	**Plot Date**	2008-11-16 23:04:55

ROCK TYPE LAXEMAR
- Fine-grained granite
- Granite
- Ävrö granite
- Fine-grained diorite-gabbro

ROCK ALTERATION
- Oxidized

ROCK UNIT
- High confidence

DEFORMATION ZONE
- High confidence

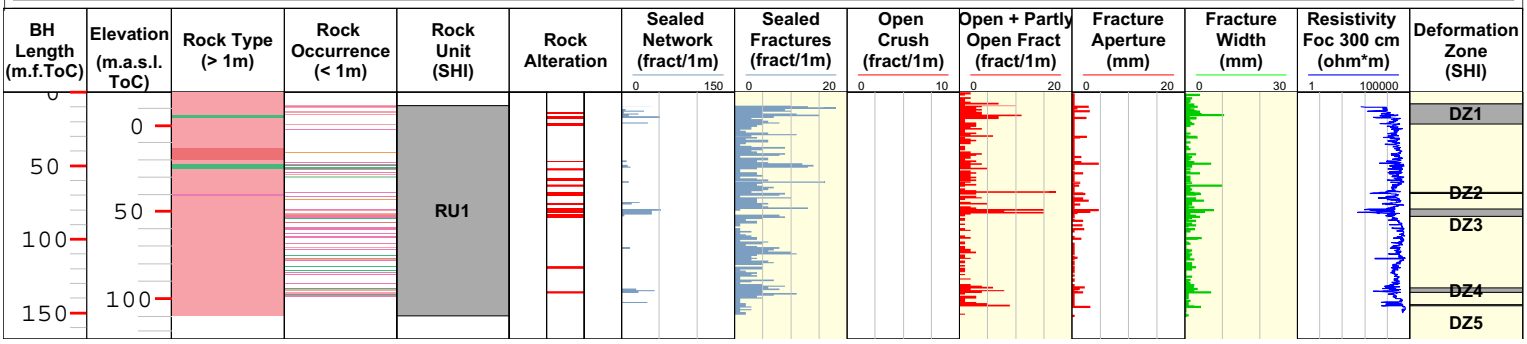

Title GEOLOGY KLX09G

Site	LAXEMAR	**Coordinate System**	RT90-RHB70
Borehole	KLX09G	**Northing [m]**	6367330.09
Diameter [mm]	76	**Easting [m]**	1548905.77
Length [m.f.ToC]	100.100	**Elevation [m.a.s.l.ToC]**	19.63
Bearing [°]	85.41	**Drilling Start Date**	2006-01-27 16:00:00
Inclination [°]	-61.07	**Drilling Stop Date**	2006-02-03 12:00:00
Date of mapping	2006-04-24 08:56:00	**Plot Date**	2008-11-16 23:04:55

ROCK TYPE LAXEMAR
- Fine-grained granite
- Ävrö granite
- Fine-grained diorite-gabbro

ROCK ALTERATION
- Oxidized

ROCK UNIT
- High confidence

DEFORMATION ZONE
- High confidence

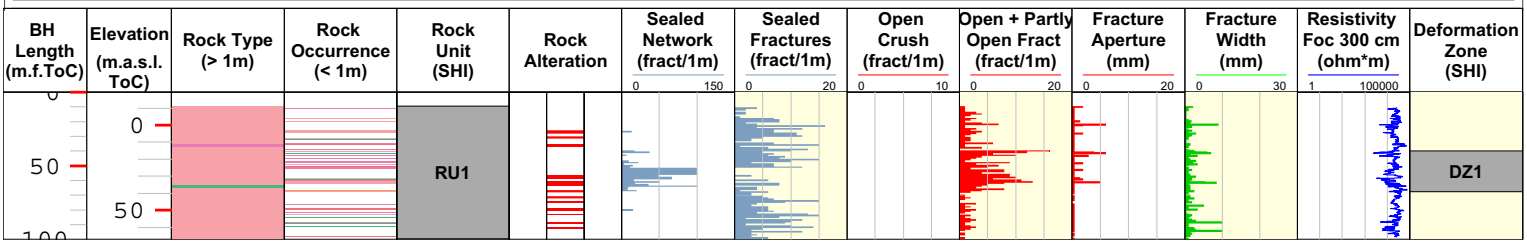

Title GEOLOGY KLX10

Site	LAXEMAR	Coordinate System	RT90-RHB70
Borehole	KLX10	Northing [m]	6366319.38
Diameter [mm]	76	Easting [m]	1548515.23
Length [m.f.ToC]	1001.200	Elevation [m.a.s.l.ToC]	18.28
Bearing [°]	250.80	Drilling Start Date	2005-06-18 08:00:00
Inclination [°]	-85.18	Drilling Stop Date	2005-10-15 07:40:00
Date of mapping	2005-11-29 09:18:00	Plot Date	2008-11-16 23:04:55

ROCK TYPE LAXEMAR
- Fine-grained granite
- Ävrö granite
- Quartz monzodiorite
- Diorite / Gabbro
- Fine-grained dioritoid
- Fine-grained diorite-gabbro

ROCK ALTERATION
- Quartz dissolution
- Albitization
- Oxidized

ROCK UNIT
- High confidence

DEFORMATION ZONE
- Medium confidence
- High confidence

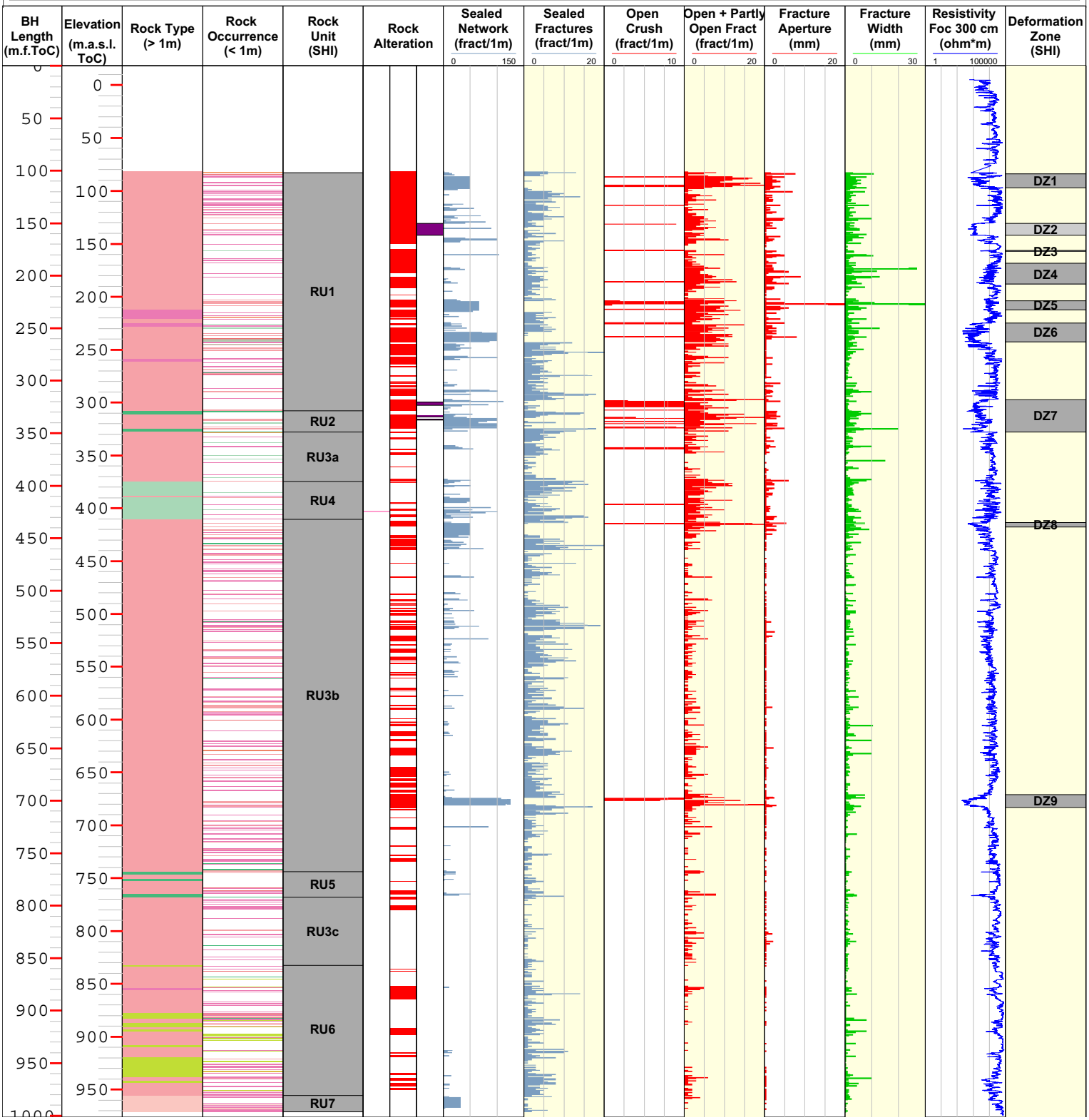

Title GEOLOGY KLX10B

Site	LAXEMAR	**Coordinate System**	RT90-RHB70
Borehole	KLX10B	**Northing [m]**	6366316.49
Diameter [mm]	76	**Easting [m]**	1548525.15
Length [m.f.ToC]	50.250	**Elevation [m.a.s.l.ToC]**	18.15
Bearing [°]	170.33	**Drilling Start Date**	2006-02-08 16:35:00
Inclination [°]	-59.96	**Drilling Stop Date**	2006-02-14 06:55:00
Date of mapping	2006-04-12 17:24:00	**Plot Date**	2008-11-16 23:04:55

ROCK TYPE LAXEMAR
- Fine-grained granite
- Ävrö granite

ROCK ALTERATION
- Oxidized

ROCK UNIT
- High confidence

DEFORMATION ZONE
- High confidence

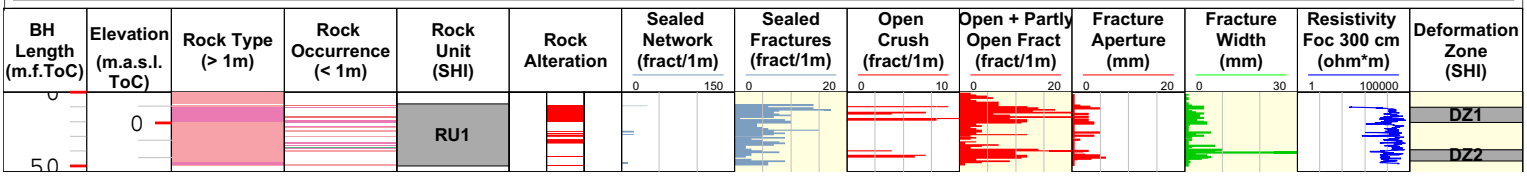

Title GEOLOGY KLX10C

Site	LAXEMAR	**Coordinate System**	RT90-RHB70
Borehole	KLX10C	**Northing [m]**	6366372.07
Diameter [mm]	76	**Easting [m]**	1548506.94
Length [m.f.ToC]	146.250	**Elevation [m.a.s.l.ToC]**	16.94
Bearing [°]	352.43	**Drilling Start Date**	2006-02-15 14:38:00
Inclination [°]	-60.02	**Drilling Stop Date**	2006-02-28 07:22:00
Date of mapping	2006-04-03 13:38:00	**Plot Date**	2008-11-16 23:04:55

ROCK TYPE LAXEMAR
- Ävrö granite
- Fine-grained dioritoid
- Fine-grained diorite-gabbro

ROCK ALTERATION
- Oxidized

ROCK UNIT
- Medium confidence

DEFORMATION ZONE
- Medium confidence
- High confidence

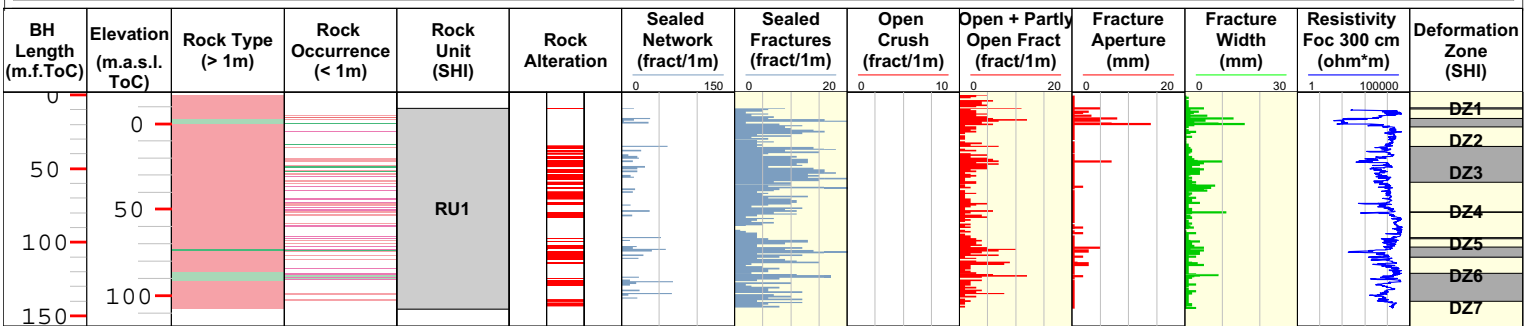

Title GEOLOGY KLX11A

Site	LAXEMAR	**Coordinate System**	RT90-RHB70
Borehole	KLX11A	**Northing [m]**	6366339.72
Diameter [mm]	76	**Easting [m]**	1546608.49
Length [m.f.ToC]	992.290	**Elevation [m.a.s.l.ToC]**	27.14
Bearing [°]	89.84	**Drilling Start Date**	2005-11-24 06:00:00
Inclination [°]	-76.76	**Drilling Stop Date**	2006-03-02 11:00:00
Date of mapping	2006-05-04 10:49:00	**Plot Date**	2008-11-16 23:04:55

ROCK TYPE LAXEMAR

- Fine-grained granite
- Pegmatite
- Quartz monzodiorite
- Fine-grained diorite-gabbro

ROCK ALTERATION

- Oxidized

ROCK UNIT

- High confidence

DEFORMATION ZONE

- High confidence

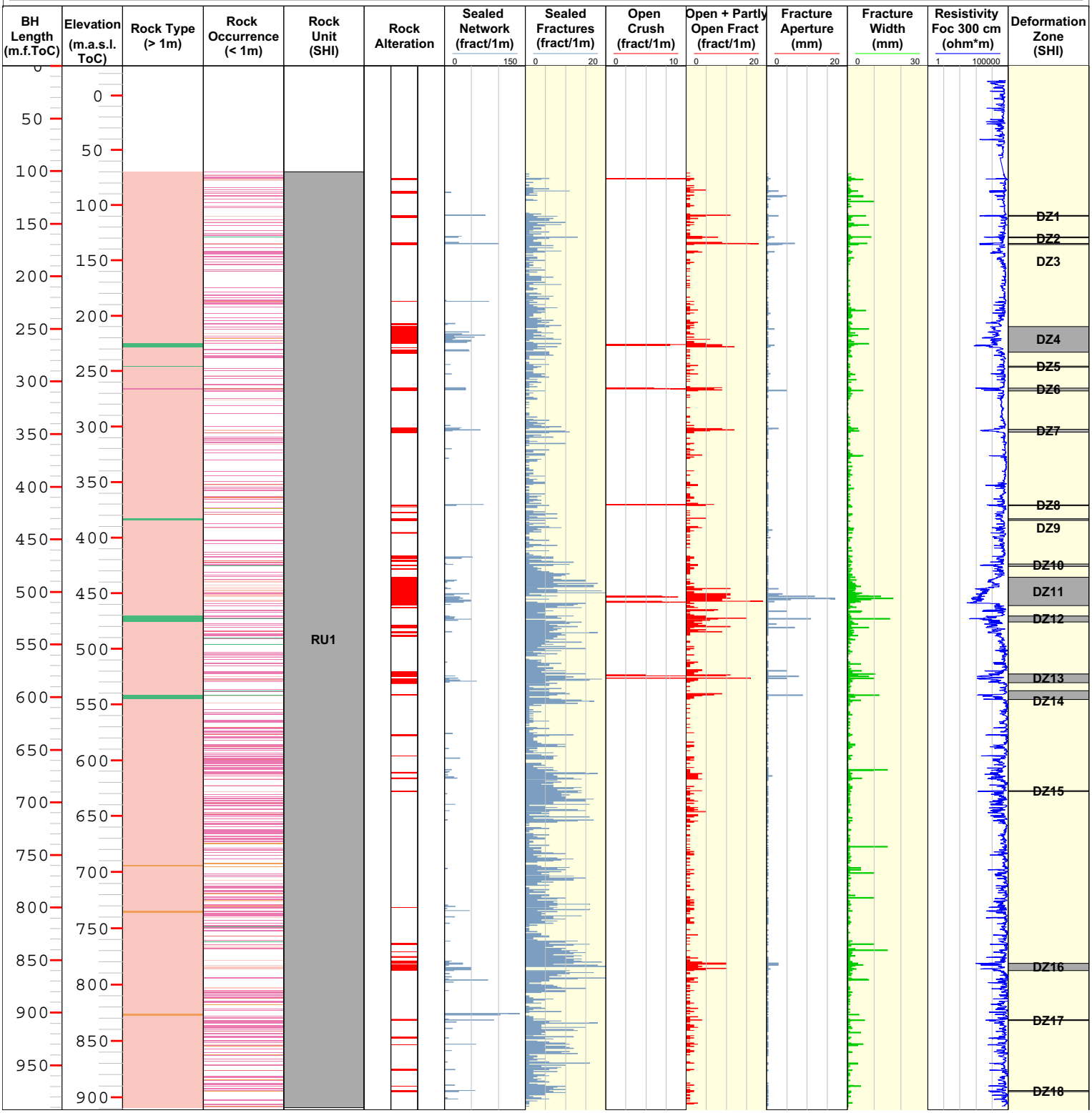

Title GEOLOGY KLX11B

Site	LAXEMAR	**Coordinate System**	RT90-RHB70
Borehole	KLX11B	**Northing [m]**	6366339.51
Diameter [mm]	76	**Easting [m]**	1546604.89
Length [m.f.ToC]	100.200	**Elevation [m.a.s.l.ToC]**	27.27
Bearing [°]	136.16	**Drilling Start Date**	2006-04-22 16:00:00
Inclination [°]	-89.92	**Drilling Stop Date**	2006-04-28 08:50:00
Date of mapping	2006-06-29 16:56:00	**Plot Date**	2008-11-16 23:04:55

ROCK TYPE LAXEMAR
- Fine-grained granite
- Quartz monzodiorite

ROCK ALTERATION
- Oxidized

ROCK UNIT
- High confidence

DEFORMATION ZONE
- High confidence

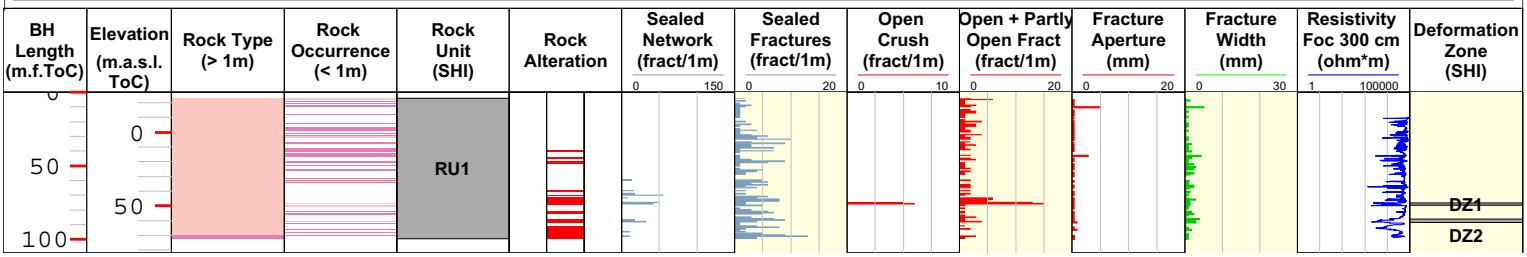

Title GEOLOGY KLX11C

Site	LAXEMAR	**Coordinate System**	RT90-RHB70
Borehole	KLX11C	**Northing [m]**	6366350.26
Diameter [mm]	76	**Easting [m]**	1546586.89
Length [m.f.ToC]	120.150	**Elevation [m.a.s.l.ToC]**	27.19
Bearing [°]	159.34	**Drilling Start Date**	2006-03-30 06:00:00
Inclination [°]	-60.72	**Drilling Stop Date**	2006-04-05 14:30:00
Date of mapping	2006-06-29 16:57:00	**Plot Date**	2008-11-16 23:04:55

ROCK TYPE LAXEMAR
Quartz monzodiorite

ROCK ALTERATION
Oxidized

ROCK UNIT
High confidence

DEFORMATION ZONE

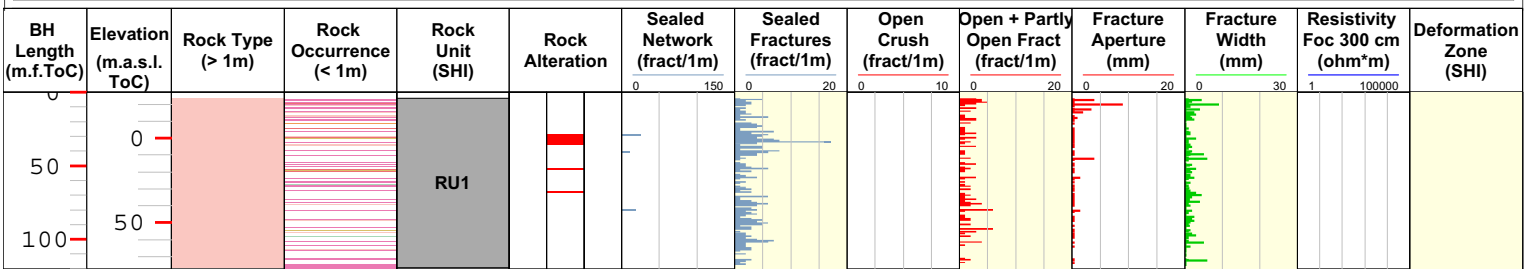

Title GEOLOGY KLX11D

Site	LAXEMAR	**Coordinate System**	RT90-RHB70
Borehole	KLX11D	**Northing [m]**	6366357.37
Diameter [mm]	76	**Easting [m]**	1546631.42
Length [m.f.ToC]	120.350	**Elevation [m.a.s.l.ToC]**	25.57
Bearing [°]	268.70	**Drilling Start Date**	2006-04-06 06:00:00
Inclination [°]	-58.99	**Drilling Stop Date**	2006-04-13 08:00:00
Date of mapping	2006-06-29 16:57:00	**Plot Date**	2008-11-16 23:04:55

ROCK TYPE LAXEMAR
- Fine-grained granite
- Quartz monzodiorite

ROCK ALTERATION
- Quartz dissolution
- Albitization
- Oxidized

ROCK UNIT
- High confidence

DEFORMATION ZONE
- High confidence

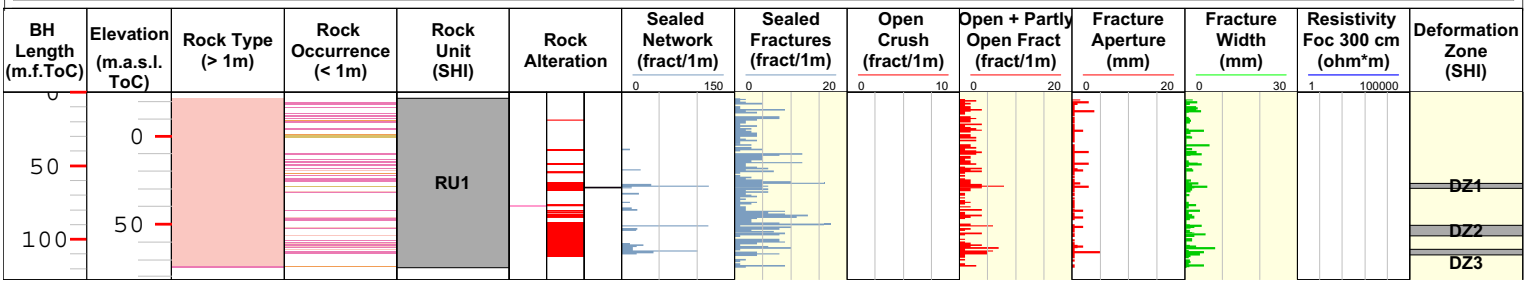

Title GEOLOGY KLX11E

Site	LAXEMAR	**Coordinate System**	RT90-RHB70
Borehole	KLX11E	**Northing [m]**	6366300.39
Diameter [mm]	76	**Easting [m]**	1546627.23
Length [m.f.ToC]	121.300	**Elevation [m.a.s.l.ToC]**	22.65
Bearing [°]	336.17	**Drilling Start Date**	2006-04-13 08:00:00
Inclination [°]	-60.91	**Drilling Stop Date**	2006-04-21 14:08:00
Date of mapping	2006-06-29 16:58:00	**Plot Date**	2008-11-16 23:04:55

ROCK TYPE LAXEMAR
- Quartz monzodiorite

ROCK ALTERATION
- Quartz dissolution
- Oxidized

ROCK UNIT
- High confidence

DEFORMATION ZONE
- High confidence

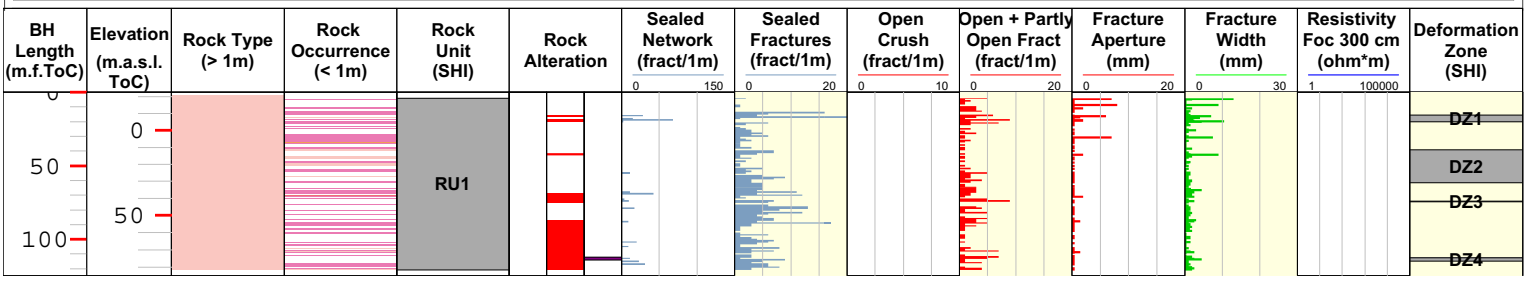

Title GEOLOGY KLX11F

Site	LAXEMAR	**Coordinate System**	RT90-RHB70
Borehole	KLX11F	**Northing [m]**	6366314.09
Diameter [mm]	76	**Easting [m]**	1546577.96
Length [m.f.ToC]	120.050	**Elevation [m.a.s.l.ToC]**	24.47
Bearing [°]	88.61	**Drilling Start Date**	2006-03-14 06:00:00
Inclination [°]	-61.13	**Drilling Stop Date**	2006-03-17 18:00:00
Date of mapping	2006-06-29 16:59:00	**Plot Date**	2008-11-16 23:04:55

ROCK TYPE LAXEMAR
- Fine-grained granite
- Quartz monzodiorite

ROCK ALTERATION
- Oxidized

ROCK UNIT
- High confidence

DEFORMATION ZONE
- High confidence

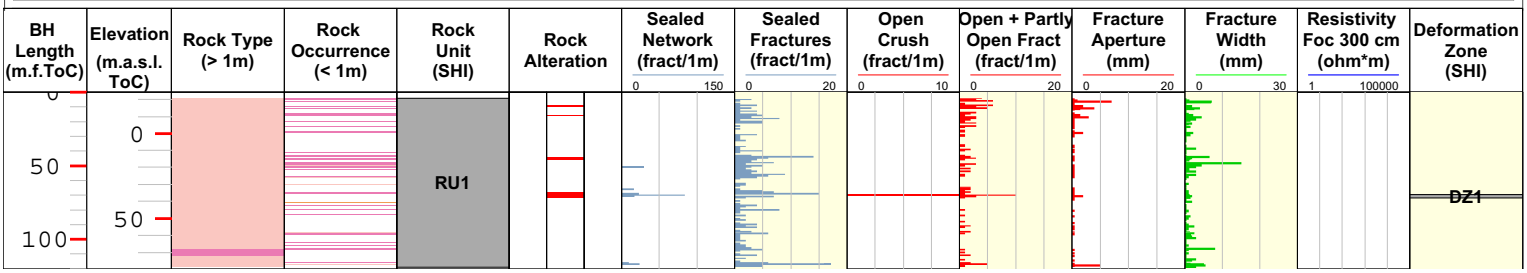

Title GEOLOGY KLX12A

Site	LAXEMAR	**Coordinate System**	RT90-RHB70
Borehole	KLX12A	**Northing [m]**	6365630.78
Diameter [mm]	76	**Easting [m]**	1548904.44
Length [m.f.ToC]	602.290	**Elevation [m.a.s.l.ToC]**	17.74
Bearing [°]	315.92	**Drilling Start Date**	2005-11-10 09:30:00
Inclination [°]	-75.30	**Drilling Stop Date**	2006-03-04 14:48:00
Date of mapping	2006-04-03 10:15:00	**Plot Date**	2008-11-16 23:04:55

ROCK TYPE LAXEMAR

- Fine-grained granite
- Ävrö granite
- Quartz monzodiorite
- Diorite / Gabbro
- Fine-grained dioritoid
- Fine-grained diorite-gabbro

ROCK ALTERATION

- Oxidized

ROCK UNIT

- High confidence

DEFORMATION ZONE

- High confidence

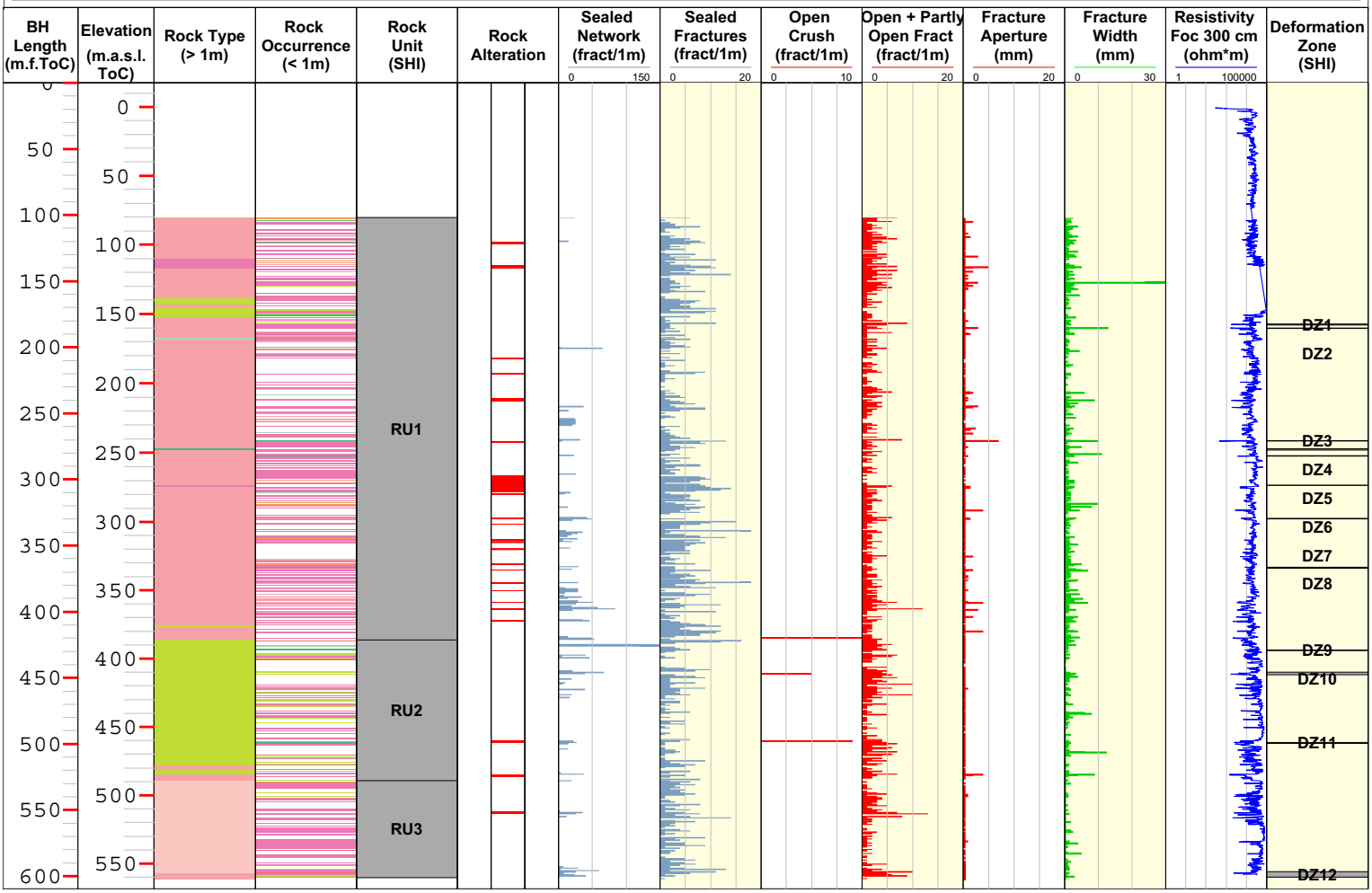

Title GEOLOGY KLX13A

Site	LAXEMAR	**Coordinate System**	RT90-RHB70
Borehole	KLX13A	**Northing [m]**	6367547.14
Diameter [mm]	76	**Easting [m]**	1546787.36
Length [m.f.ToC]	595.850	**Elevation [m.a.s.l.ToC]**	24.15
Bearing [°]	224.48	**Drilling Start Date**	2006-05-19 14:02:00
Inclination [°]	-82.23	**Drilling Stop Date**	2006-08-16 09:02:00
Date of mapping	2006-09-06 11:38:00	**Plot Date**	2008-11-16 23:04:55

ROCK TYPE LAXEMAR
- Fine-grained granite
- Ävrö granite
- Diorite / Gabbro
- Fine-grained diorite-gabbro

ROCK ALTERATION
- Oxidized

ROCK UNIT
- High confidence

DEFORMATION ZONE
- Medium confidence
- High confidence

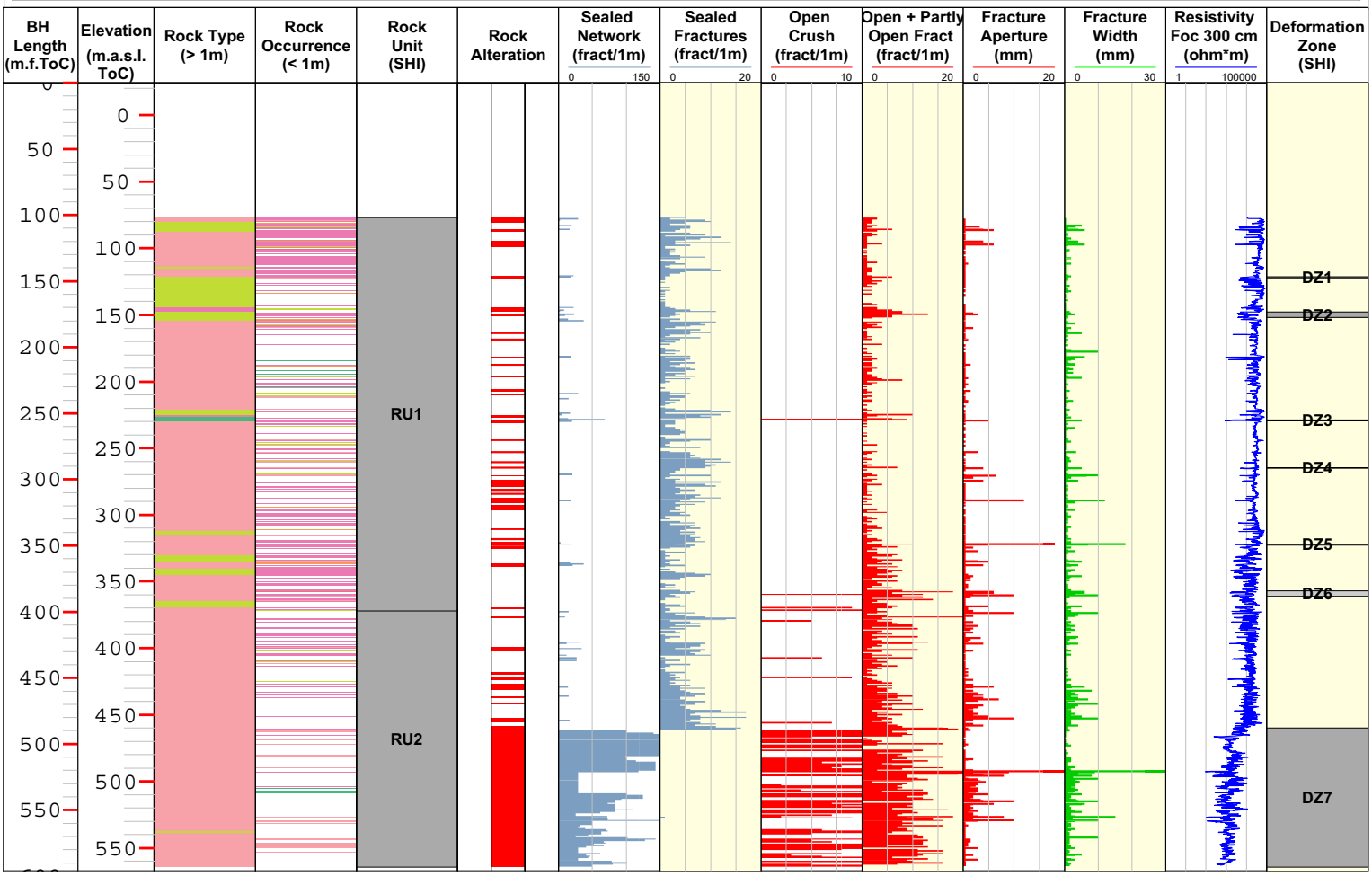

Title GEOLOGY KLX14A

Site	LAXEMAR	**Coordinate System**	RT90-RHB70
Borehole	KLX14A	**Northing [m]**	6365959.69
Diameter [mm]	76	**Easting [m]**	1547146.87
Length [m.f.ToC]	176.270	**Elevation [m.a.s.l.ToC]**	16.35
Bearing [°]	111.95	**Drilling Start Date**	2006-08-19 08:00:00
Inclination [°]	-49.95	**Drilling Stop Date**	2006-09-04 15:22:00
Date of mapping	2006-11-22 18:29:00	**Plot Date**	2008-11-16 23:04:55

ROCK TYPE LAXEMAR
- Dolerite
- Fine-grained granite
- Quartz monzodiorite

ROCK ALTERATION
- Quartz dissolution
- Oxidized

ROCK UNIT
- High confidence

DEFORMATION ZONE
- High confidence

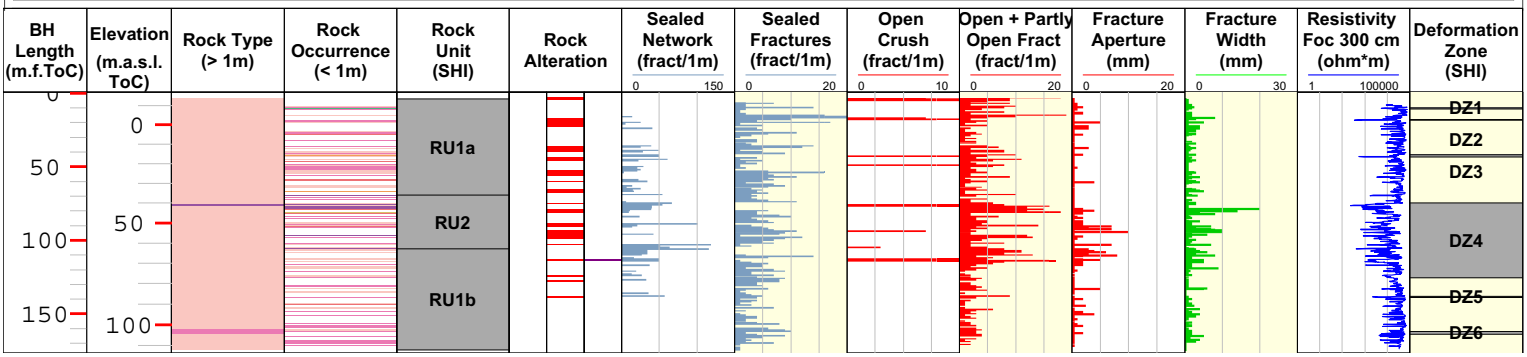

Title GEOLOGY KLX15A

Site	LAXEMAR	Coordinate System	RT90-RHB70
Borehole	KLX15A	Northing [m]	6365614.17
Diameter [mm]	76	Easting [m]	1547987.47
Length [m.f.ToC]	1000.430	Elevation [m.a.s.l.ToC]	14.59
Bearing [°]	198.83	Drilling Start Date	2007-01-17 10:30:00
Inclination [°]	-54.41	Drilling Stop Date	2007-02-25 20:00:00
Date of mapping	2007-04-04 16:08:00	Plot Date	2008-11-16 23:04:55

ROCK TYPE LAXEMAR

- Fine-grained granite
- Pegmatite
- Granite
- Ävrö granite
- Quartz monzodiorite
- Fine-grained diorite-gabbro

ROCK ALTERATION

- Oxidized

ROCK UNIT

- High confidence

DEFORMATION ZONE

- High confidence

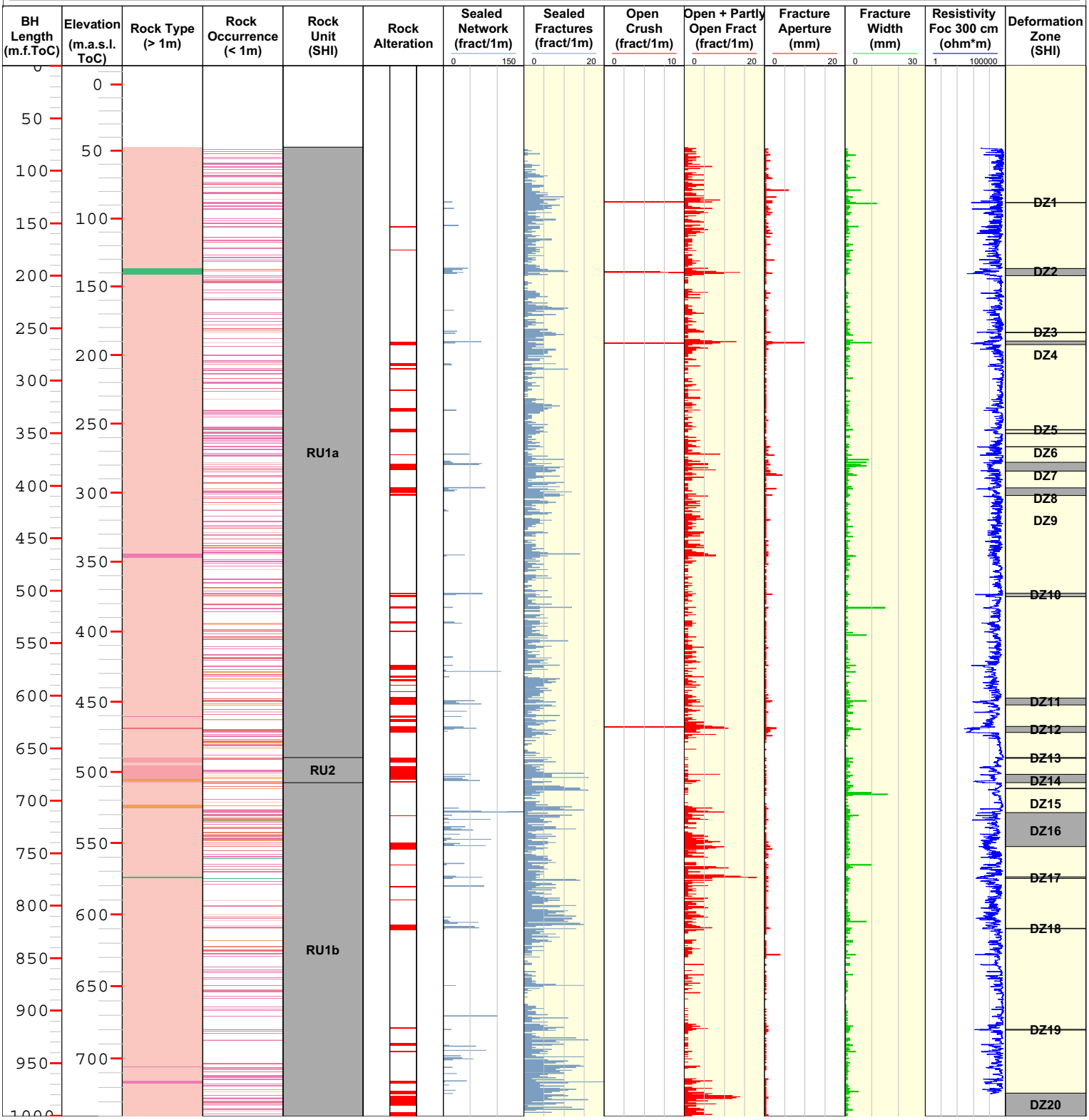

Title GEOLOGY KLX16A

Site	LAXEMAR	**Coordinate System**	RT90-RHB70
Borehole	KLX16A	**Northing [m]**	6364797.69
Diameter [mm]	76	**Easting [m]**	1547584.06
Length [m.f.ToC]	433.550	**Elevation [m.a.s.l.ToC]**	18.85
Bearing [°]	294.37	**Drilling Start Date**	2006-11-28 13:00:00
Inclination [°]	-64.97	**Drilling Stop Date**	2007-01-09 13:00:00
Date of mapping	2007-03-01 09:13:00	**Plot Date**	2008-11-16 23:04:55

ROCK TYPE LAXEMAR

- Fine-grained granite
- Pegmatite
- Granite
- Quartz monzodiorite
- Fine-grained dioritoid
- Fine-grained diorite-gabbro

ROCK ALTERATION

- Albitization
- Oxidized

ROCK UNIT

- High confidence

DEFORMATION ZONE

- High confidence

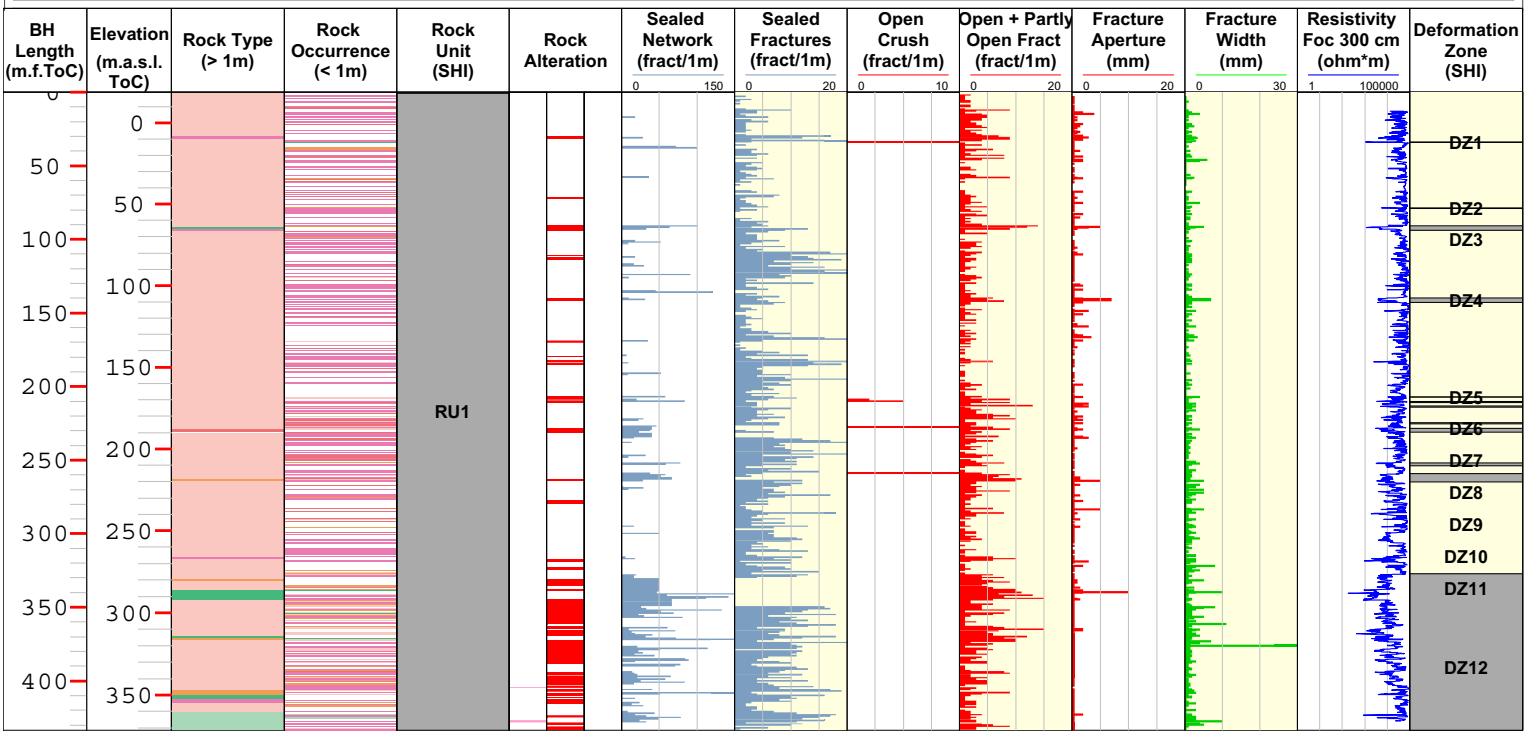

Title GEOLOGY KLX17A

Site	LAXEMAR	**Coordinate System**	RT90-RHB70
Borehole	KLX17A	**Northing [m]**	6366848.75
Diameter [mm]	76	**Easting [m]**	1546862.09
Length [m.f.ToC]	701.080	**Elevation [m.a.s.l.ToC]**	27.63
Bearing [°]	11.21	**Drilling Start Date**	2006-09-13 06:00:00
Inclination [°]	-61.33	**Drilling Stop Date**	2006-10-23 09:30:00
Date of mapping	2006-12-06 11:49:00	**Plot Date**	2008-11-16 23:04:55

ROCK TYPE LAXEMAR
- Fine-grained granite
- Ävrö granite
- Diorite / Gabbro
- Fine-grained diorite-gabbro

ROCK ALTERATION
- Oxidized

ROCK UNIT
- High confidence

DEFORMATION ZONE
- High confidence

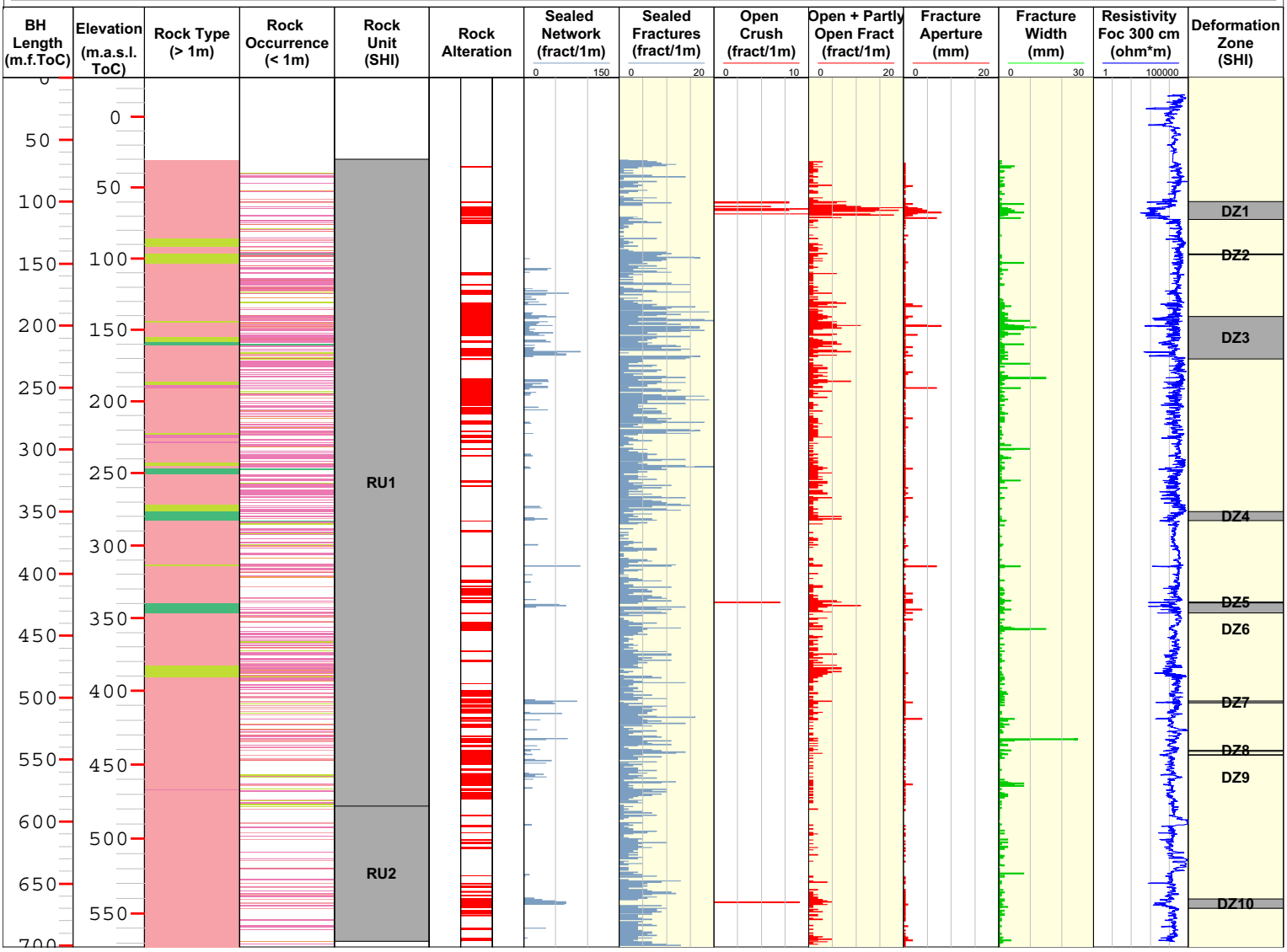

Title GEOLOGY KLX18A

Site	LAXEMAR	Coordinate System	RT90-RHB70
Borehole	KLX18A	Northing [m]	6366413.39
Diameter [mm]	76	Easting [m]	1547966.35
Length [m.f.ToC]	611.280	Elevation [m.a.s.l.ToC]	21.01
Bearing [°]	271.40	Drilling Start Date	2006-03-29 10:00:00
Inclination [°]	-82.10	Drilling Stop Date	2006-05-02 12:22:00
Date of mapping	2006-05-22 08:46:00	Plot Date	2008-11-16 23:04:55

ROCK TYPE LAXEMAR
- Fine-grained granite
- Ävrö granite
- Diorite / Gabbro
- Fine-grained diorite-gabbro

ROCK ALTERATION
- Oxidized

ROCK UNIT
- High confidence

DEFORMATION ZONE
- Medium confidence
- High confidence

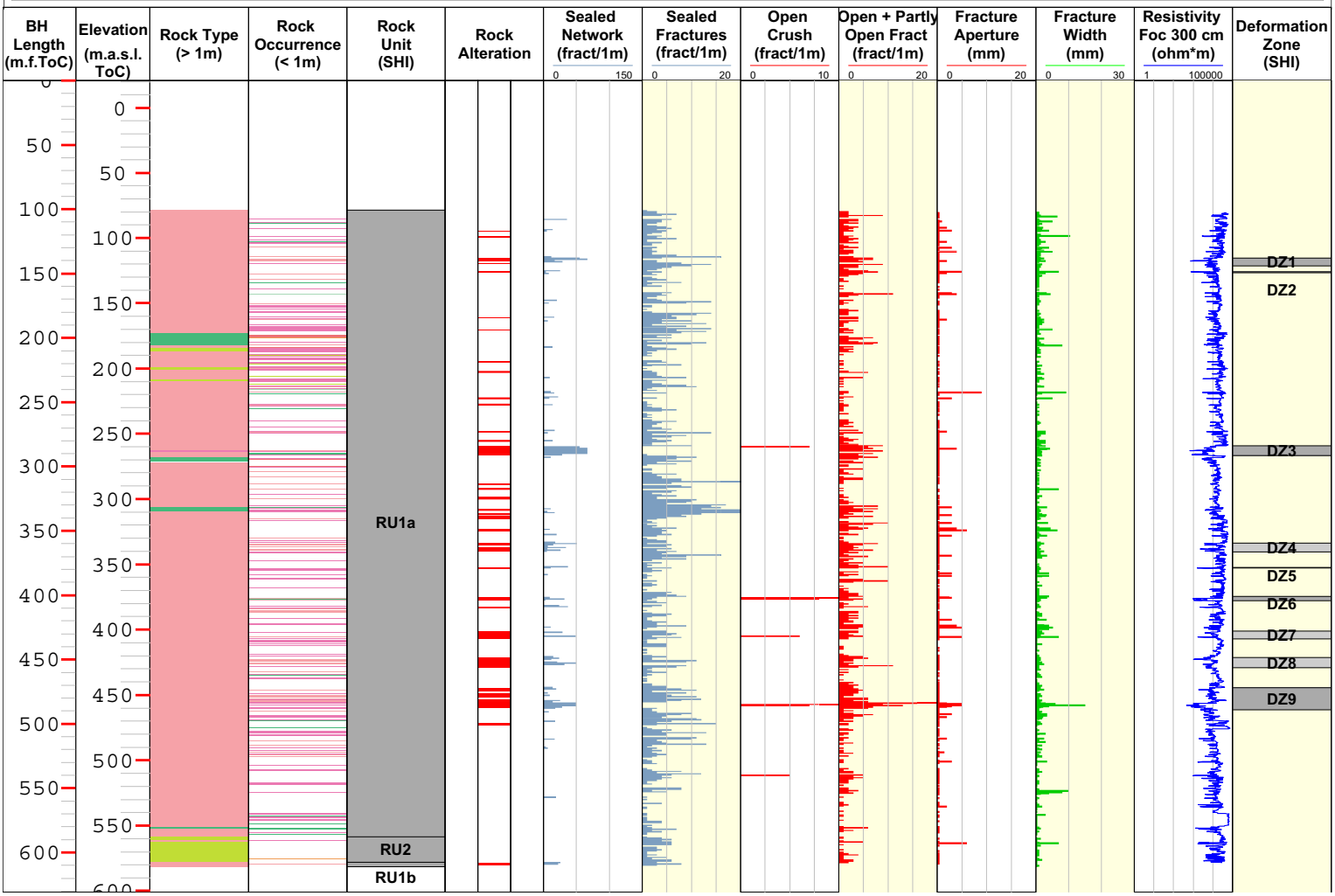

Title GEOLOGY KLX19A

Site	LAXEMAR	Coordinate System	RT90-RHB70
Borehole	KLX19A	Northing [m]	6365901.42
Diameter [mm]	76	Easting [m]	1547004.62
Length [m.f.ToC]	800.070	Elevation [m.a.s.l.ToC]	16.87
Bearing [°]	197.13	Drilling Start Date	2006-06-03 11:00:00
Inclination [°]	-57.54	Drilling Stop Date	2006-09-20 17:27:00
Date of mapping	2006-10-16 08:57:00	Plot Date	2008-11-17 23:05:26

ROCK TYPE LAXEMAR
- Dolerite
- Fine-grained granite
- Pegmatite
- Quartz monzodiorite
- Fine-grained diorite-gabbro

ROCK ALTERATION
- Oxidized

ROCK UNIT
- High confidence

DEFORMATION ZONE
- High confidence

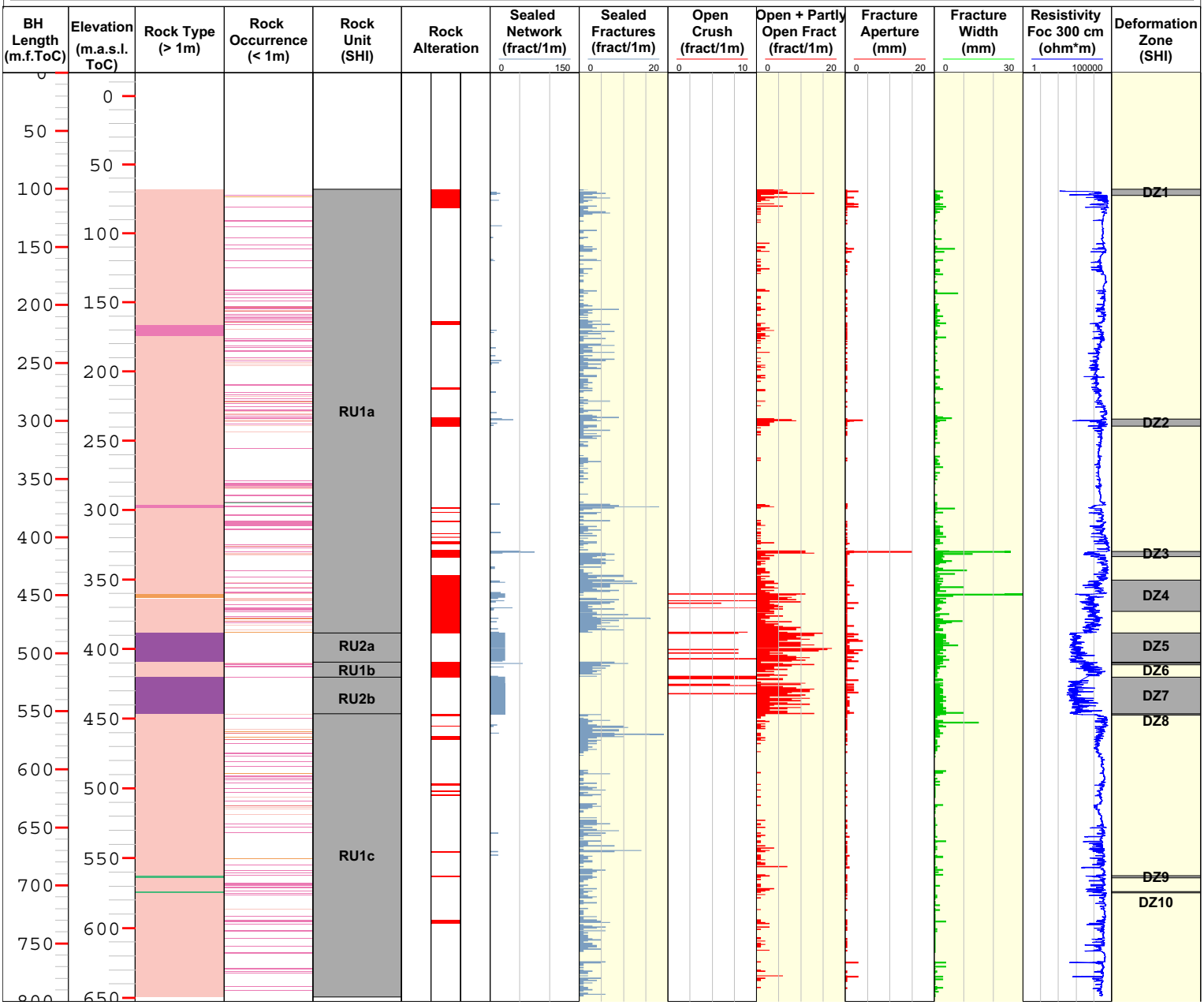

Title GEOLOGY KLX20A

Site	LAXEMAR	**Coordinate System**	RT90-RHB70
Borehole	KLX20A	**Northing [m]**	6366334.57
Diameter [mm]	76	**Easting [m]**	1546604.89
Length [m.f.ToC]	457.920	**Elevation [m.a.s.l.ToC]**	27.24
Bearing [°]	270.60	**Drilling Start Date**	2006-03-25 06:00:00
Inclination [°]	-50.02	**Drilling Stop Date**	2006-04-24 13:20:00
Date of mapping	2006-05-29 08:59:00	**Plot Date**	2008-11-17 23:05:26

ROCK TYPE LAXEMAR
- Dolerite
- Fine-grained granite
- Quartz monzodiorite
- Fine-grained diorite-gabbro

ROCK ALTERATION
- Quartz dissolution
- Albitization
- Oxidized

ROCK UNIT
- High confidence

DEFORMATION ZONE
- Medium confidence
- High confidence

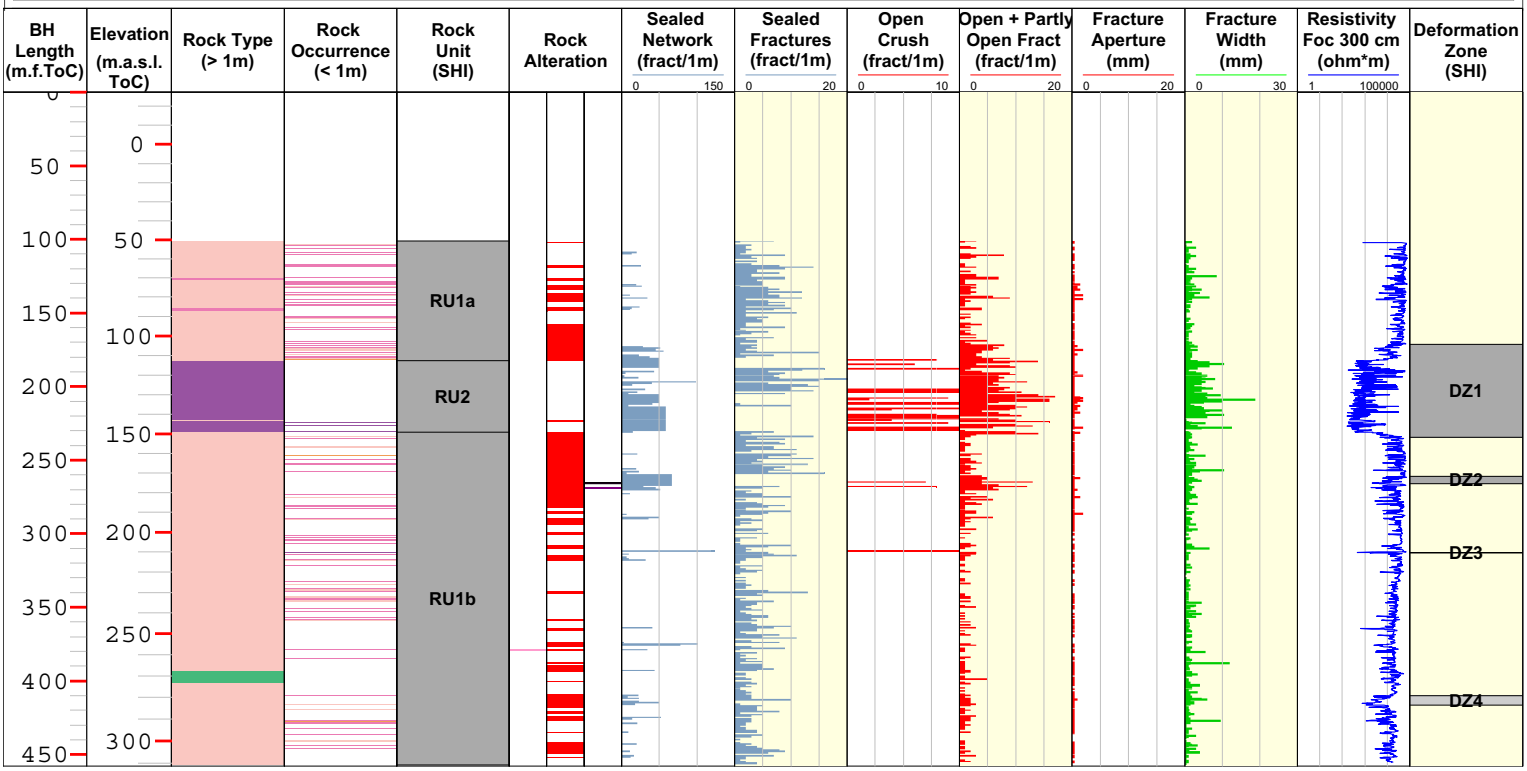

Title GEOLOGY KLX21B

Site	LAXEMAR	Coordinate System	RT90-RHB70
Borehole	KLX21B	Northing [m]	6366164.00
Diameter [mm]	76	Easting [m]	1549715.10
Length [m.f.ToC]	858.780	Elevation [m.a.s.l.ToC]	10.68
Bearing [°]	225.05	Drilling Start Date	2006-10-12 08:00:00
Inclination [°]	-70.85	Drilling Stop Date	2006-11-29 10:30:00
Date of mapping	2007-01-30 15:06:00	Plot Date	2008-11-17 23:05:26

ROCK TYPE LAXEMAR
- Fine-grained granite
- Ävrö granite
- Quartz monzodiorite
- Diorite / Gabbro
- Fine-grained dioritoid
- Fine-grained diorite-gabbro

ROCK ALTERATION
- Albitization
- Oxidized

ROCK UNIT
- High confidence

DEFORMATION ZONE
- High confidence

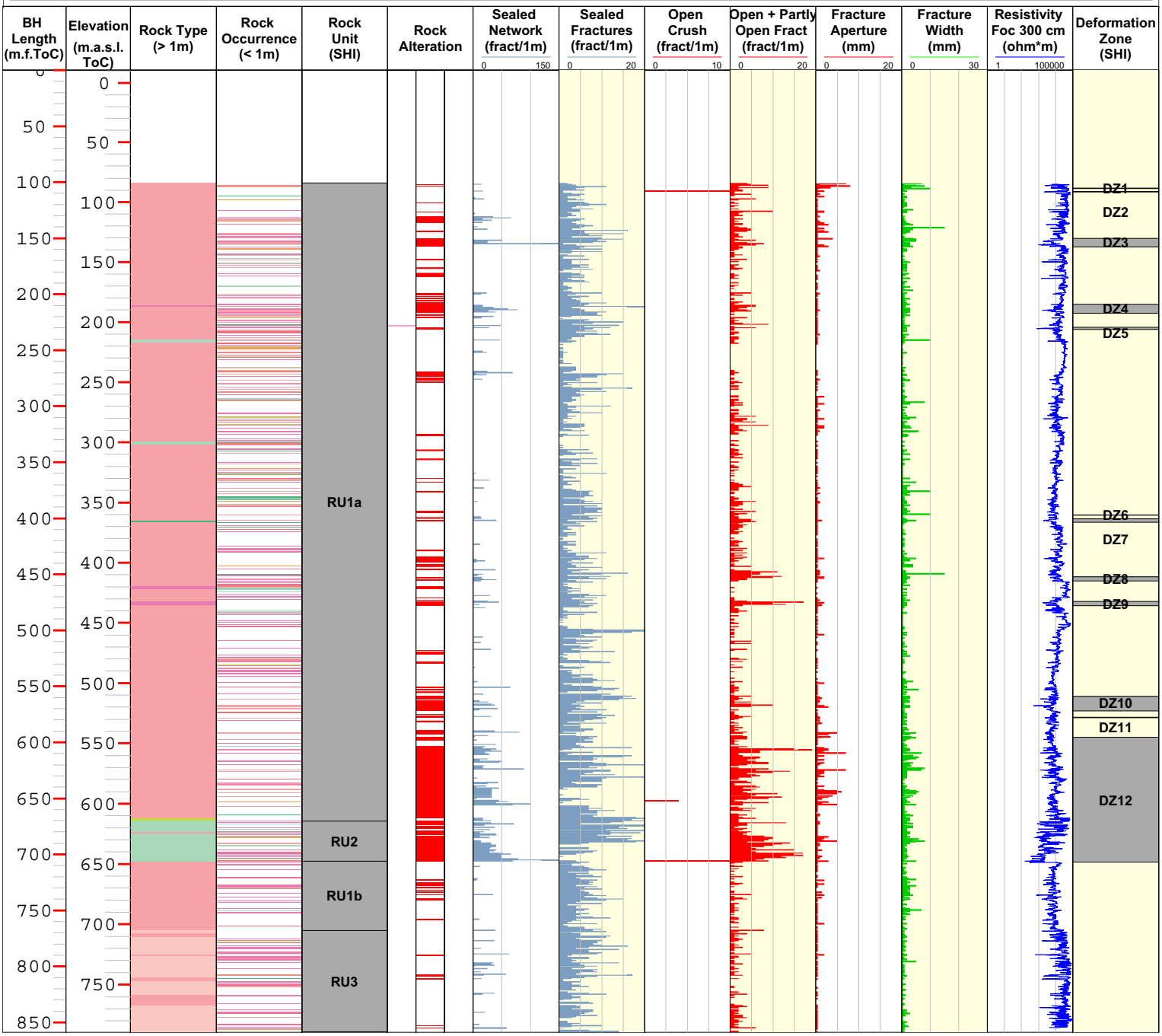

Title GEOLOGY KLX22A

Site	LAXEMAR	**Coordinate System**	RT90-RHB70
Borehole	KLX22A	**Northing [m]**	6366548.35
Diameter [mm]	76	**Easting [m]**	1546688.60
Length [m.f.ToC]	100.450	**Elevation [m.a.s.l.ToC]**	21.97
Bearing [°]	179.19	**Drilling Start Date**	2006-05-05 12:00:00
Inclination [°]	-60.33	**Drilling Stop Date**	2006-05-12 13:40:00
Date of mapping	2006-06-29 16:54:00	**Plot Date**	2008-11-17 23:05:26

ROCK TYPE LAXEMAR
- Fine-grained granite
- Quartz monzodiorite
- Fine-grained diorite-gabbro

ROCK ALTERATION
- Oxidized

ROCK UNIT
- High confidence

DEFORMATION ZONE
- High confidence

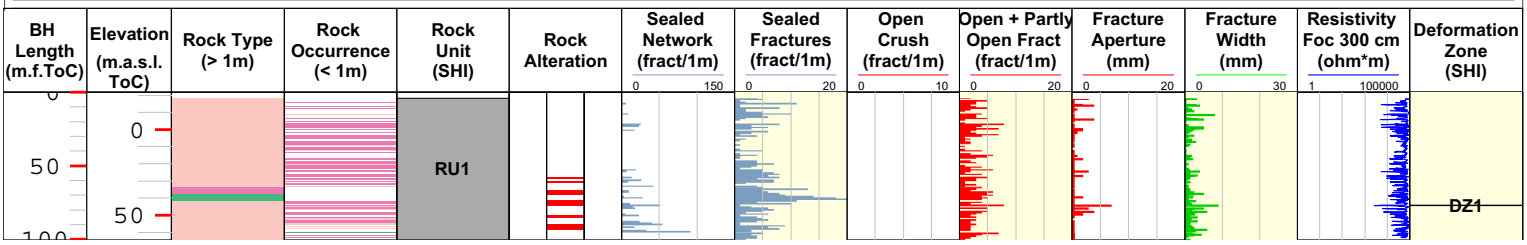

Title GEOLOGY KLX22B

Site	LAXEMAR	**Coordinate System**	RT90-RHB70
Borehole	KLX22B	**Northing [m]**	6366553.13
Diameter [mm]	76	**Easting [m]**	1546685.41
Length [m.f.ToC]	100.250	**Elevation [m.a.s.l.ToC]**	21.58
Bearing [°]	343.97	**Drilling Start Date**	2006-05-13 09:13:00
Inclination [°]	-61.24	**Drilling Stop Date**	2006-05-18 13:03:00
Date of mapping	2006-06-29 16:55:00	**Plot Date**	2008-11-17 23:05:26

ROCK TYPE LAXEMAR
- Fine-grained granite
- Quartz monzodiorite
- Fine-grained diorite-gabbro

ROCK ALTERATION
- Oxidized

ROCK UNIT
- High confidence

DEFORMATION ZONE
- High confidence

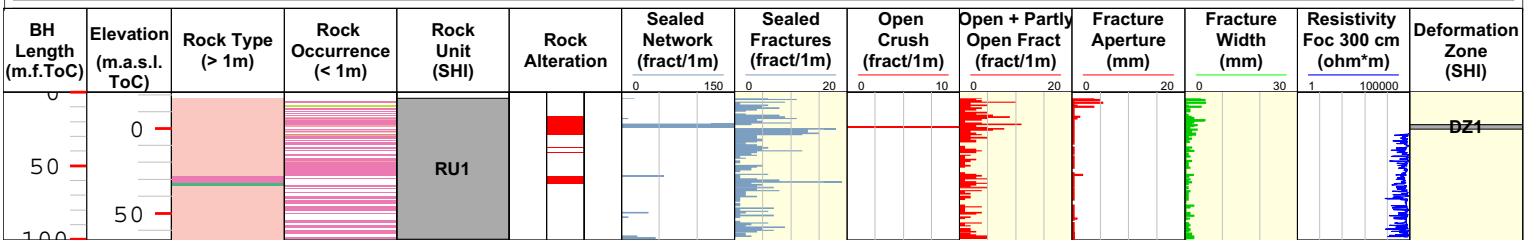

Title GEOLOGY KLX23A

Site	LAXEMAR	**Coordinate System**	RT90-RHB70
Borehole	KLX23A	**Northing [m]**	6366106.89
Diameter [mm]	76	**Easting [m]**	1546715.74
Length [m.f.ToC]	100.150	**Elevation [m.a.s.l.ToC]**	22.26
Bearing [°]	28.73	**Drilling Start Date**	2006-05-21 10:27:00
Inclination [°]	-61.35	**Drilling Stop Date**	2006-05-27 07:45:00
Date of mapping	2006-07-25 07:14:00	**Plot Date**	2008-11-17 23:05:26

ROCK TYPE LAXEMAR
Quartz monzodiorite

ROCK ALTERATION
Oxidized

ROCK UNIT
High confidence

DEFORMATION ZONE
High confidence

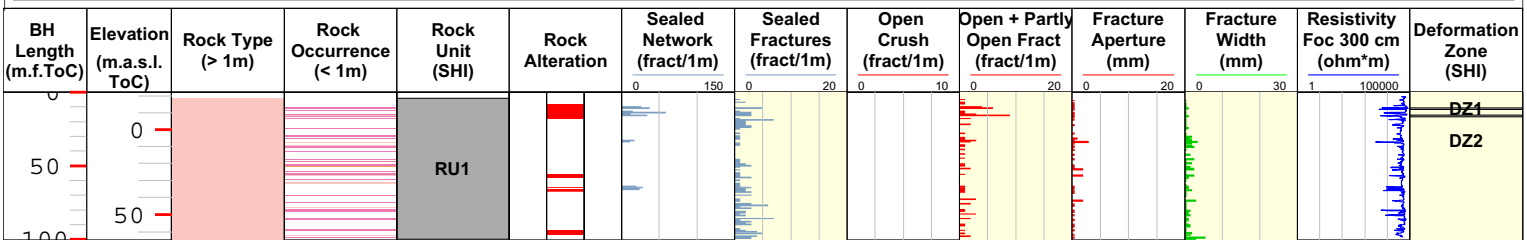

Title GEOLOGY KLX23B

Site	LAXEMAR	**Coordinate System**	RT90-RHB70
Borehole	KLX23B	**Northing [m]**	6366101.90
Diameter [mm]	76	**Easting [m]**	1546717.33
Length [m.f.ToC]	50.270	**Elevation [m.a.s.l.ToC]**	22.32
Bearing [°]	121.36	**Drilling Start Date**	2006-05-28 13:55:00
Inclination [°]	-60.84	**Drilling Stop Date**	2006-05-31 11:15:00
Date of mapping	2006-07-24 08:47:00	**Plot Date**	2008-11-17 23:05:26

ROCK TYPE LAXEMAR
Quartz monzodiorite

ROCK ALTERATION
Oxidized

ROCK UNIT
High confidence

DEFORMATION ZONE
High confidence

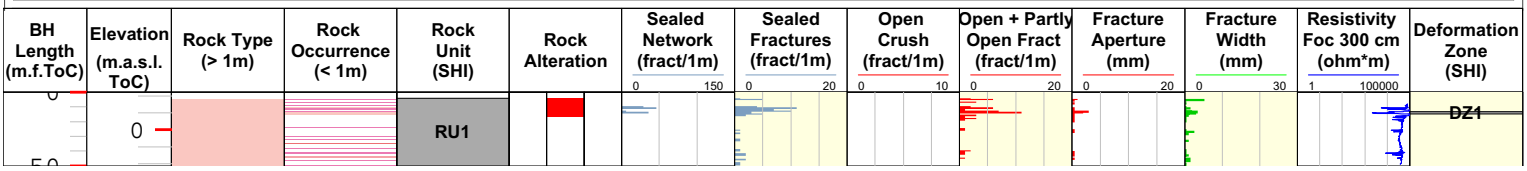

Title GEOLOGY KLX24A

Site	LAXEMAR	**Coordinate System**	RT90-RHB70
Borehole	KLX24A	**Northing [m]**	6366423.35
Diameter [mm]	76	**Easting [m]**	1546853.80
Length [m.f.ToC]	100.170	**Elevation [m.a.s.l.ToC]**	21.29
Bearing [°]	98.41	**Drilling Start Date**	2006-06-14 11:00:00
Inclination [°]	-59.14	**Drilling Stop Date**	2006-06-29 08:45:00
Date of mapping	2006-08-14 12:13:00	**Plot Date**	2008-11-17 23:05:26

ROCK TYPE LAXEMAR
- Fine-grained granite
- Quartz monzodiorite

ROCK ALTERATION
- Oxidized

ROCK UNIT
- High confidence

DEFORMATION ZONE
- High confidence

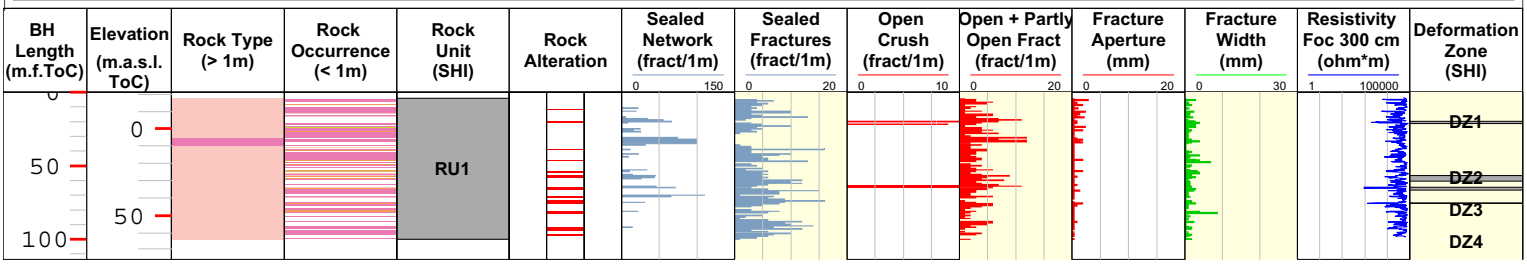

Title GEOLOGY KLX25A

Site	LAXEMAR	**Coordinate System**	RT90-RHB70
Borehole	KLX25A	**Northing [m]**	6366274.74
Diameter [mm]	76	**Easting [m]**	1546769.66
Length [m.f.ToC]	50.240	**Elevation [m.a.s.l.ToC]**	22.84
Bearing [°]	145.73	**Drilling Start Date**	2006-07-01 14:00:00
Inclination [°]	-59.45	**Drilling Stop Date**	2006-07-04 14:00:00
Date of mapping	2006-08-14 13:30:00	**Plot Date**	2008-11-17 23:05:26

ROCK TYPE LAXEMAR
Quartz monzodiorite

ROCK ALTERATION
Oxidized

ROCK UNIT
High confidence

DEFORMATION ZONE
High confidence

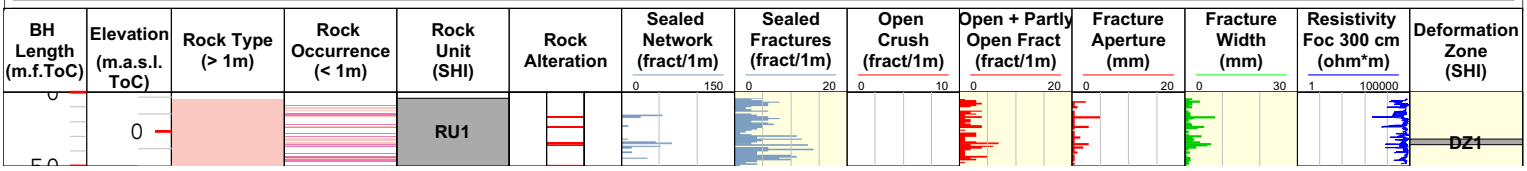

Title GEOLOGY KLX26A

Site	LAXEMAR	**Coordinate System**	RT90-RHB70
Borehole	KLX26A	**Northing [m]**	6365546.49
Diameter [mm]	76	**Easting [m]**	1549029.90
Length [m.f.ToC]	101.140	**Elevation [m.a.s.l.ToC]**	15.63
Bearing [°]	93.47	**Drilling Start Date**	2006-08-03 06:00:00
Inclination [°]	-60.44	**Drilling Stop Date**	2006-08-11 11:00:00
Date of mapping	2006-09-05 18:33:00	**Plot Date**	2008-11-17 23:05:26

ROCK TYPE LAXEMAR

- Fine-grained granite
- Ävrö granite
- Quartz monzodiorite
- Diorite / Gabbro
- Fine-grained diorite-gabbro

ROCK ALTERATION

- Oxidized

ROCK UNIT

- High confidence

DEFORMATION ZONE

- High confidence

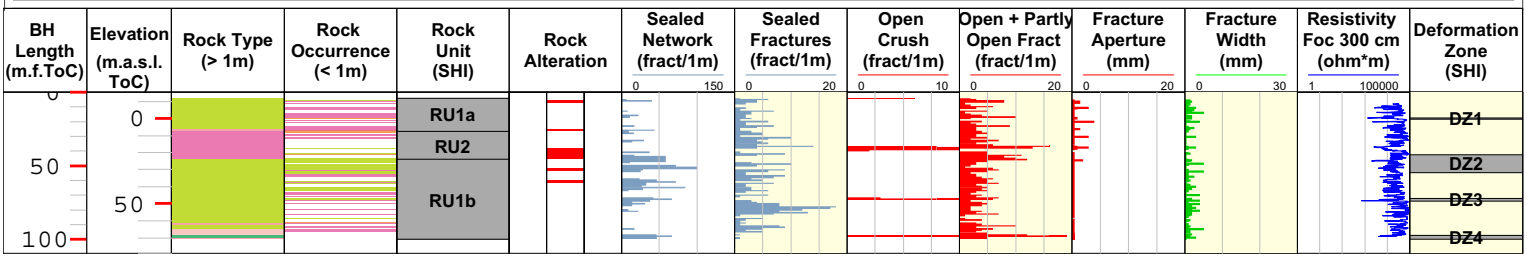

Title GEOLOGY KLX26B

Site	LAXEMAR	**Coordinate System**	RT90-RHB70
Borehole	KLX26B	**Northing [m]**	6365550.66
Diameter [mm]	76	**Easting [m]**	1549025.61
Length [m.f.ToC]	50.370	**Elevation [m.a.s.l.ToC]**	15.82
Bearing [°]	137.42	**Drilling Start Date**	2006-08-12 09:00:00
Inclination [°]	-60.00	**Drilling Stop Date**	2006-08-17 07:15:00
Date of mapping	2006-09-13 09:19:00	**Plot Date**	2008-11-17 23:05:26

ROCK TYPE LAXEMAR

- Fine-grained granite
- Diorite / Gabbro

ROCK ALTERATION

ROCK UNIT

- High confidence

DEFORMATION ZONE

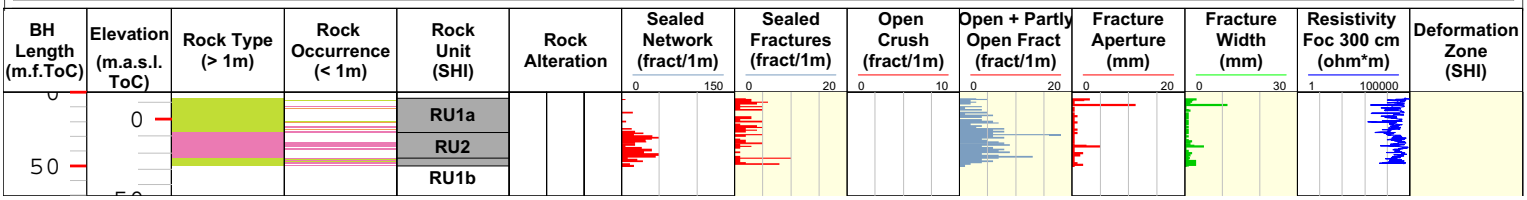

Title GEOLOGY KLX27A

Site	LAXEMAR	Coordinate System	RT90-RHB70
Borehole	KLX27A	Northing [m]	6365608.29
Diameter [mm]	76	Easting [m]	1546742.63
Length [m.f.ToC]	650.560	Elevation [m.a.s.l.ToC]	16.98
Bearing [°]	0.73	Drilling Start Date	2007-10-08 14:00:00
Inclination [°]	-65.36	Drilling Stop Date	2007-11-21 11:30:00
Date of mapping	2007-12-12 09:03:00	Plot Date	2008-11-17 23:05:26

ROCK TYPE LAXEMAR
- Fine-grained granite
- Quartz monzodiorite
- Fine-grained diorite-gabbro

ROCK ALTERATION
- Oxidized

ROCK UNIT
- High confidence

DEFORMATION ZONE
- Medium confidence
- High confidence

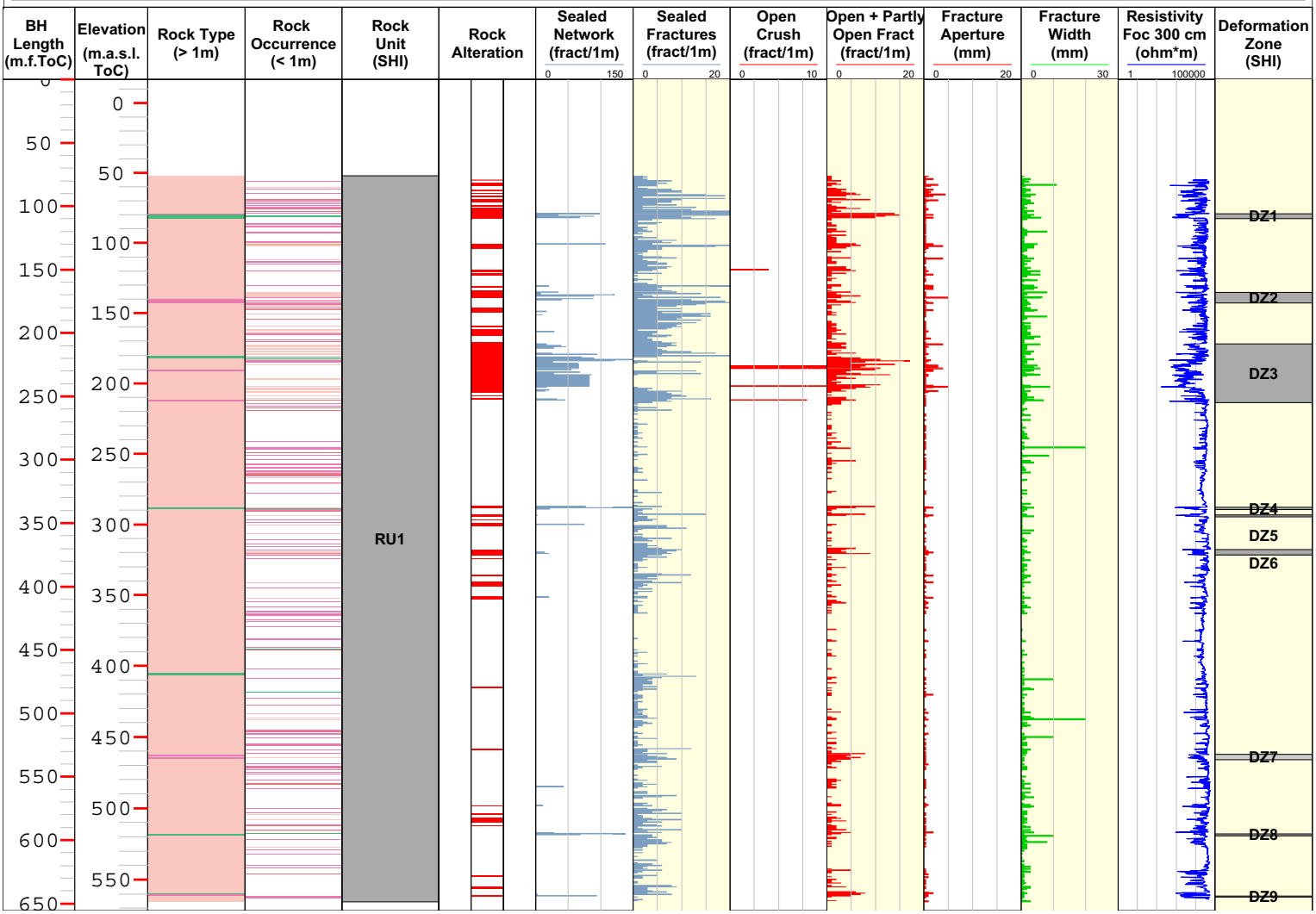

Title GEOLOGY KLX28A

Site	LAXEMAR	**Coordinate System**	RT90-RHB70
Borehole	KLX28A	**Northing [m]**	6365682.22
Diameter [mm]	76	**Easting [m]**	1549333.71
Length [m.f.ToC]	80.230	**Elevation [m.a.s.l.ToC]**	10.05
Bearing [°]	189.70	**Drilling Start Date**	2006-09-14 16:00:00
Inclination [°]	-60.05	**Drilling Stop Date**	2006-09-20 08:55:00
Date of mapping	2006-11-14 08:32:00	**Plot Date**	2008-11-17 23:05:26

ROCK TYPE LAXEMAR
- Fine-grained granite
- Ävrö granite
- Fine-grained diorite-gabbro

ROCK ALTERATION
- Oxidized

ROCK UNIT
- High confidence

DEFORMATION ZONE
- High confidence

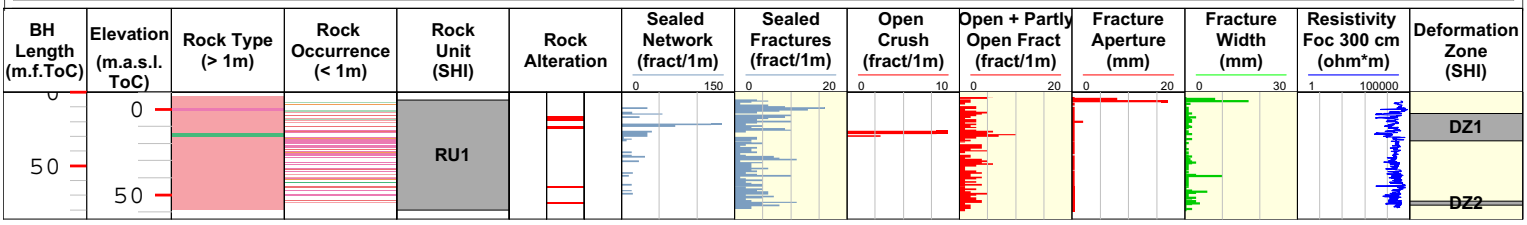

Title GEOLOGY KLX29A

Site	LAXEMAR	**Coordinate System**	RT90-RHB70
Borehole	KLX29A	**Northing [m]**	6366264.54
Diameter [mm]	76	**Easting [m]**	1549443.99
Length [m.f.ToC]	60.250	**Elevation [m.a.s.l.ToC]**	13.63
Bearing [°]	321.21	**Drilling Start Date**	2006-09-09 10:00:00
Inclination [°]	-60.90	**Drilling Stop Date**	2006-09-13 11:40:00
Date of mapping	2006-11-16 15:34:00	**Plot Date**	2008-11-17 23:05:26

ROCK TYPE LAXEMAR

- Ävrö granite
- Fine-grained diorite-gabbro

ROCK ALTERATION

- Oxidized

ROCK UNIT

- High confidence

DEFORMATION ZONE

- High confidence

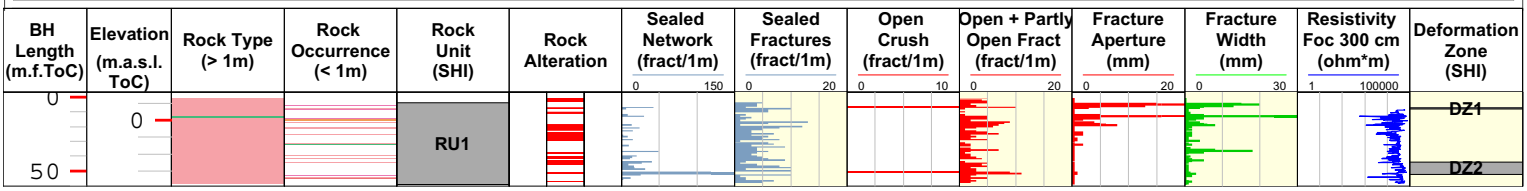

Appendix 4

Quantitative estimates (volume %) of the proportions of different rock types on a borehole by borehole basis, on a rock domain basis in each borehole and on an overall rock domain basis

Data from Sicada: p_rock_occur.xls and p_rock.xls in Sicada_07_134 and Sicada_07_283

Procedure: An integrated file has been created with rock type intervals from p_rock.xls and p_rock_occur.xls. This procedure implies that rock occurrences (< 1.0 m in the drill core) are merged together with rock type (>1.0 m in the drill core) and, in order to preserve the correct borehole length, compensation is carried out by removing an equal portion of the original rock type interval. However, in those cases where one rock occurrence is defined inside another rock occurrence, this compensation is omitted since the effect on the total borehole length is negligible.

The diagrams that present the proportions of different rock types in each borehole, in each rock domain in each borehole and in the overall rock domains can be viewed on the CD-Rom attached to this report. The translation from rock codes to rock names is provided in Appendix 2, and the results of this analysis are addressed in section 3.4.2 in this report.

Proportions of different rock types on a borehole by borehole basis

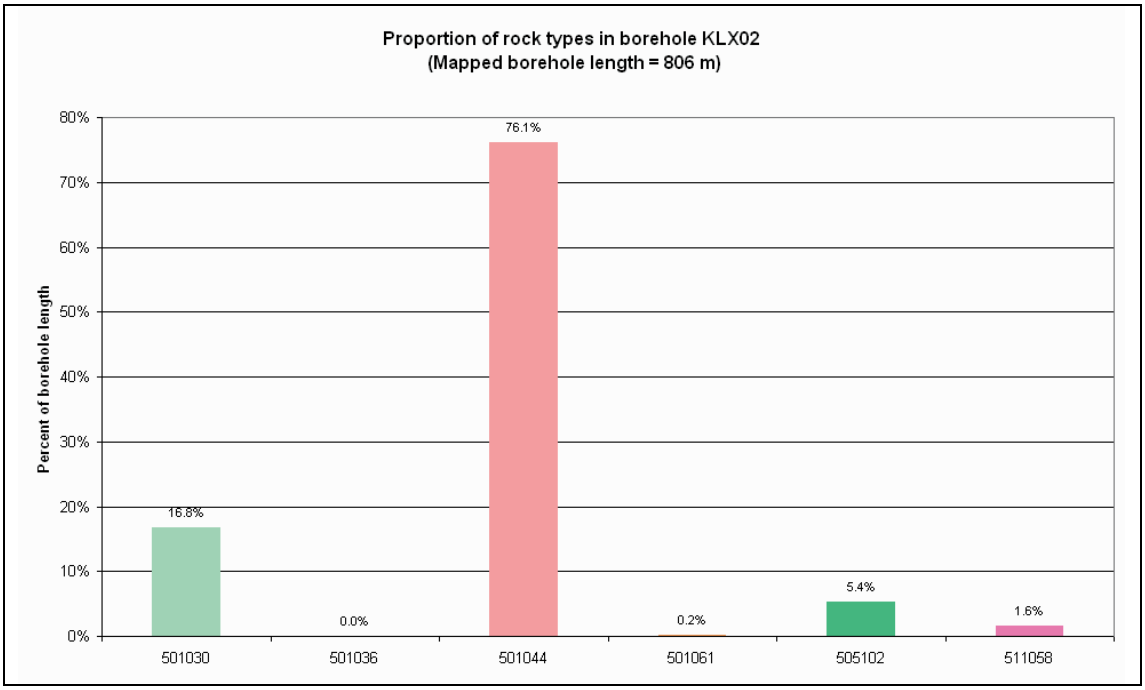

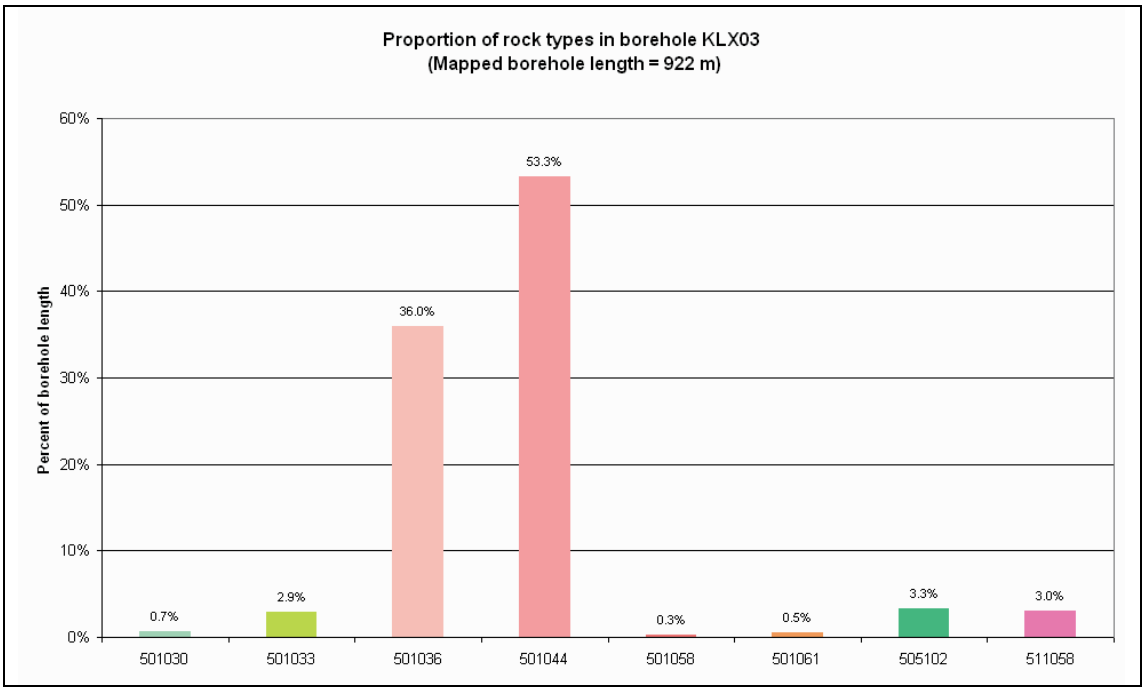
Proportion of rock types in borehole KLX03
(Mapped borehole length = 922 m)
Percent of borehole length
60%
50%
40%
30%
20%
10%
0%
0.7%
2.9%
36.0%
53.3%
0.3%
0.5%
3.3%
3.0%
501030
501033
501036
501044
501058
501061
505102
511058

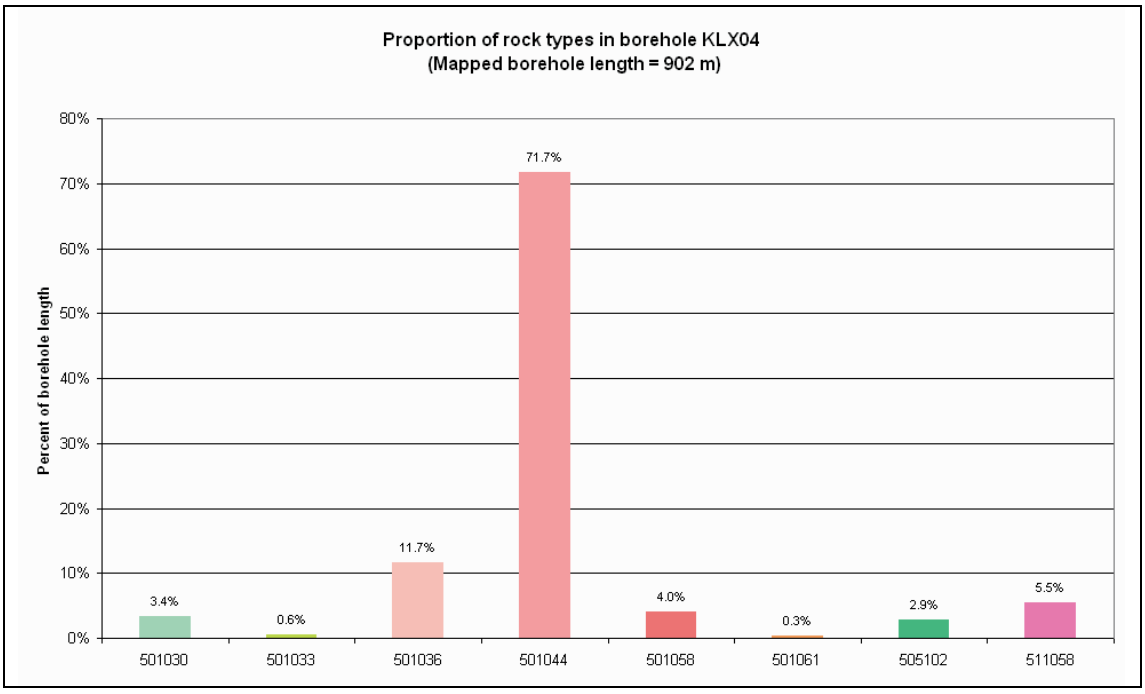
Proportion of rock types in borehole KLX04
(Mapped borehole length = 902 m)
Percent of borehole length
80%
70%
60%
50%
40%
30%
20%
10%
0%
3.4%
0.6%
11.7%
71.7%
4.0%
0.3%
2.9%
5.5%
501030
501033
501036
501044
501058
501061
505102
511058

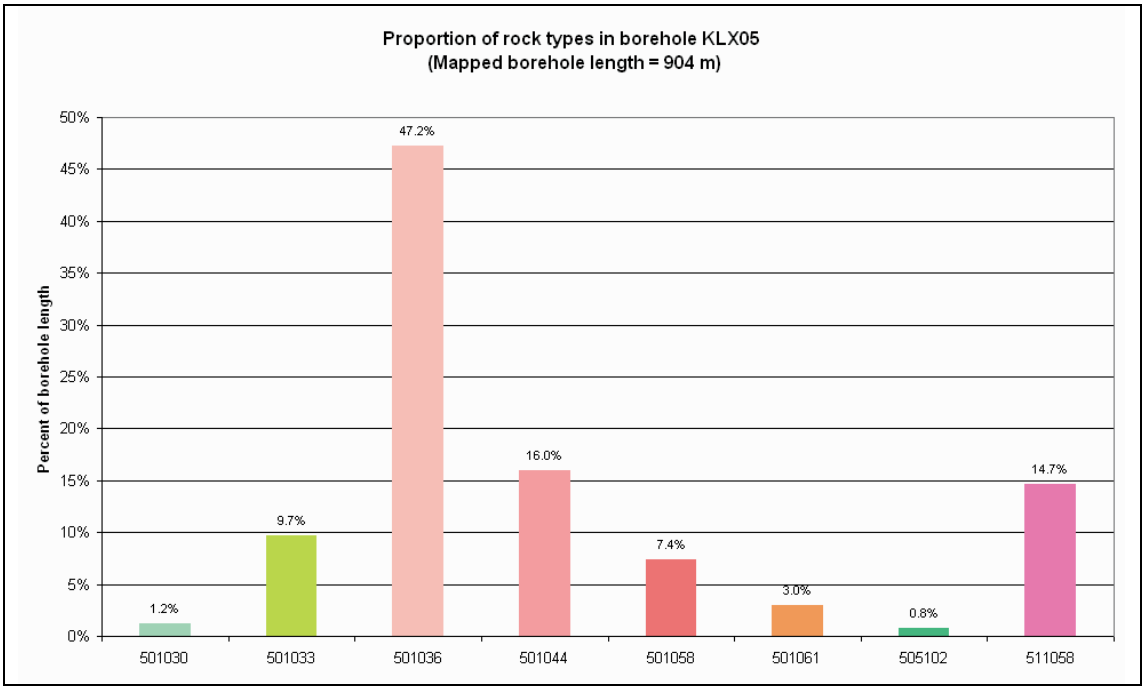
Proportion of rock types in borehole KLX05
(Mapped borehole length = 904 m)
Percent of borehole length
50%
45%
40%
35%
30%
25%
20%
15%
10%
5%
0%
1.2%
9.7%
47.2%
16.0%
7.4%
3.0%
0.8%
14.7%
501030
501033
501036
501044
501058
501061
505102
511058

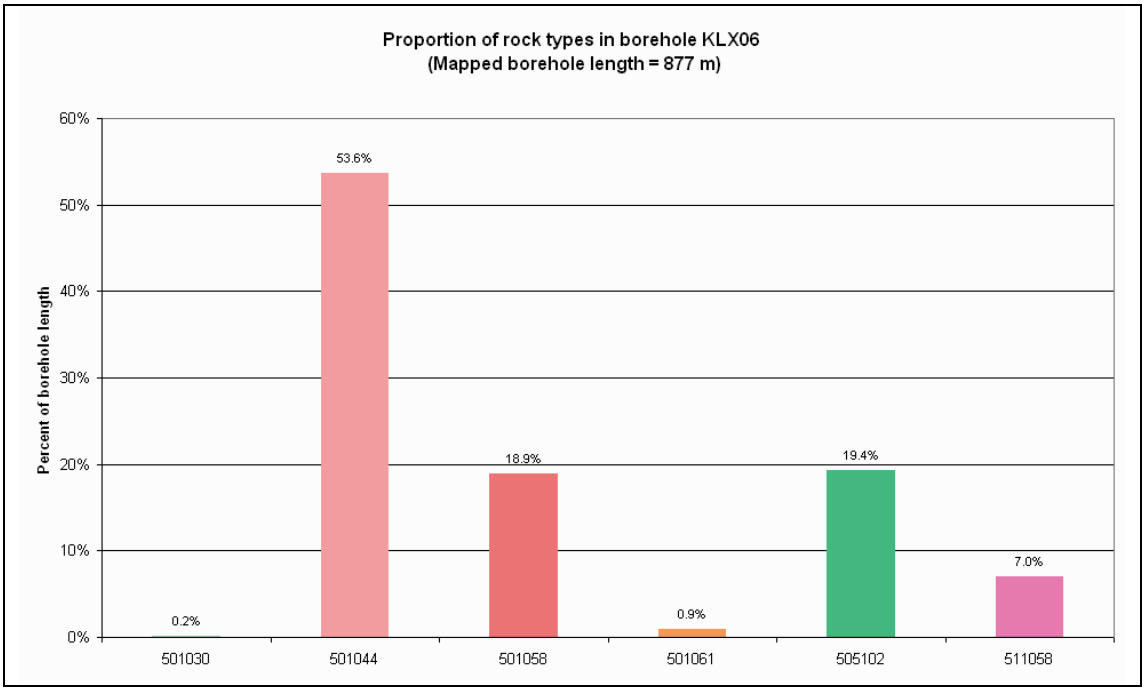
Proportion of rock types in borehole KLX06
(Mapped borehole length = 877 m)
Percent of borehole length
60%
50%
40%
30%
20%
10%
0%
0.2%
53.6%
18.9%
0.9%
19.4%
7.0%
501030
501044
501058
501061
505102
511058

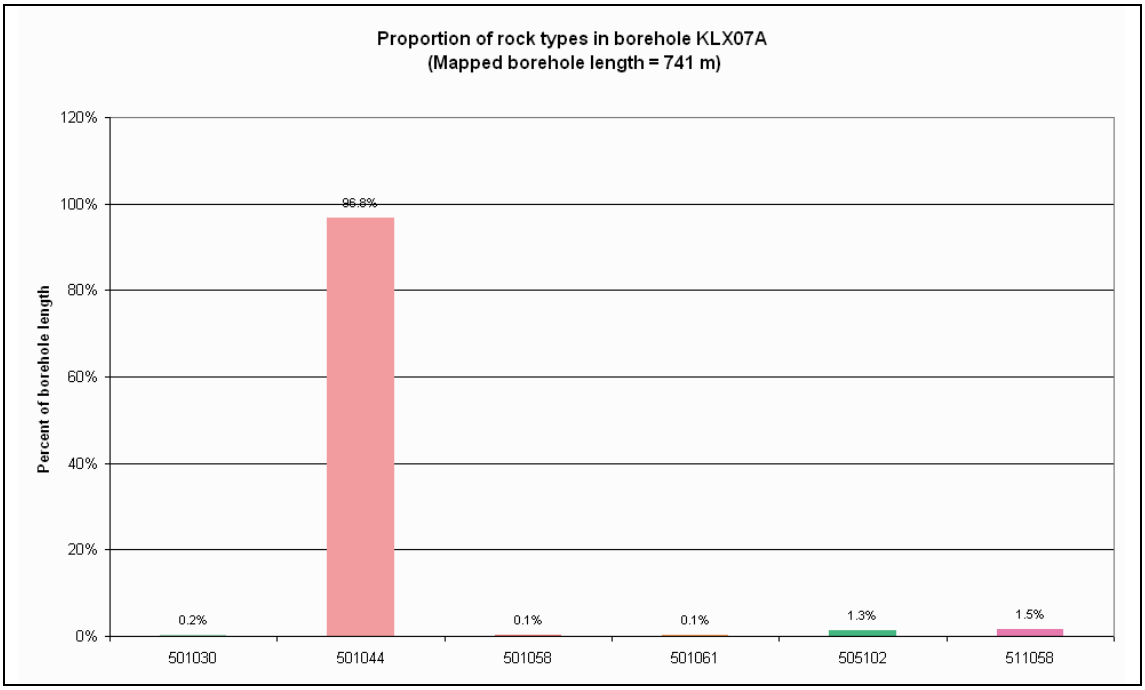
Proportion of rock types in borehole KLX07A
(Mapped borehole length = 741 m)
Percent of borehole length
120%
100%
80%
60%
40%
20%
0%
96.8%
0.2%
0.1%
0.1%
1.3%
1.5%
501030
501044
501058
501061
505102
511058

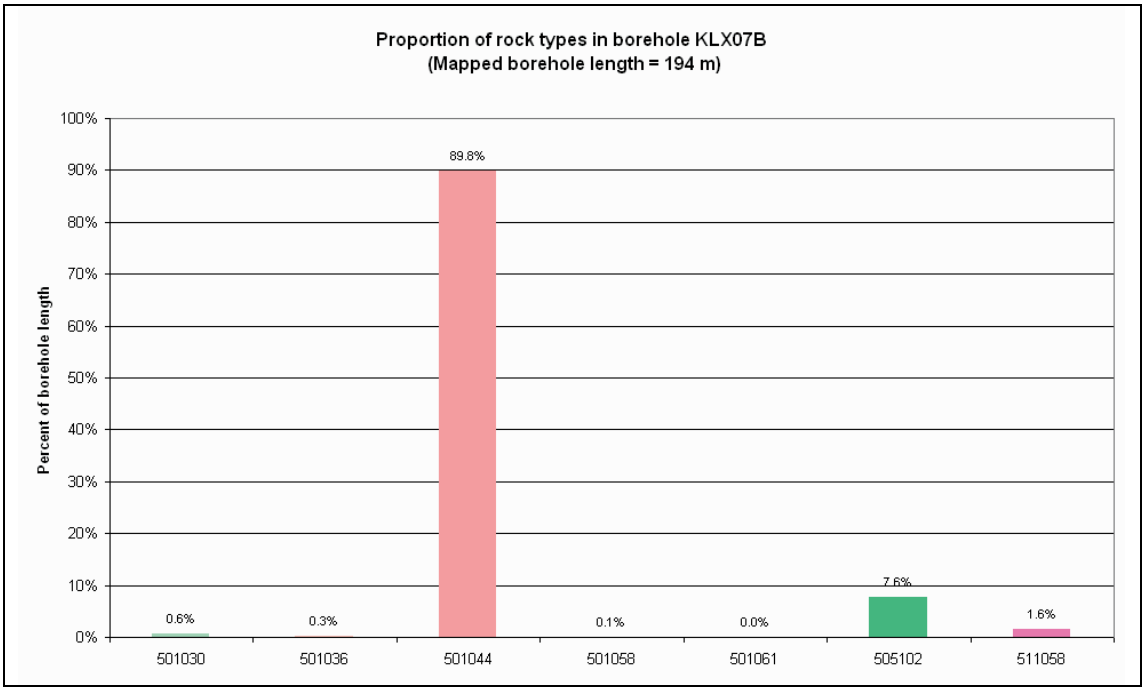
Proportion of rock types in borehole KLX07B
(Mapped borehole length = 194 m)
Percent of borehole length
100%
90%
80%
70%
60%
50%
40%
30%
20%
10%
0%
89.8%
0.6%
0.3%
0.1%
0.0%
7.6%
1.6%
501030
501036
501044
501058
501061
505102
511058

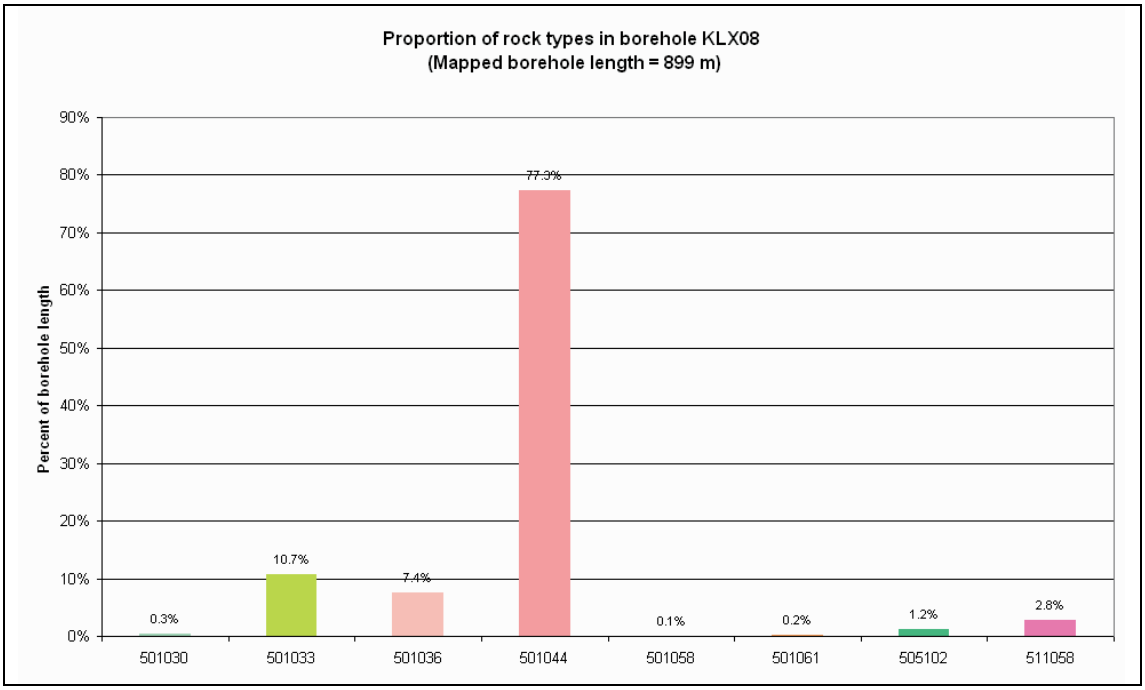
Proportion of rock types in borehole KLX08
(Mapped borehole length = 899 m)
Percent of borehole length
90%
80%
70%
60%
50%
40%
30%
20%
10%
0%
0.3%
10.7%
7.4%
77.3%
0.1%
0.2%
1.2%
2.8%
501030
501033
501036
501044
501058
501061
505102
511058

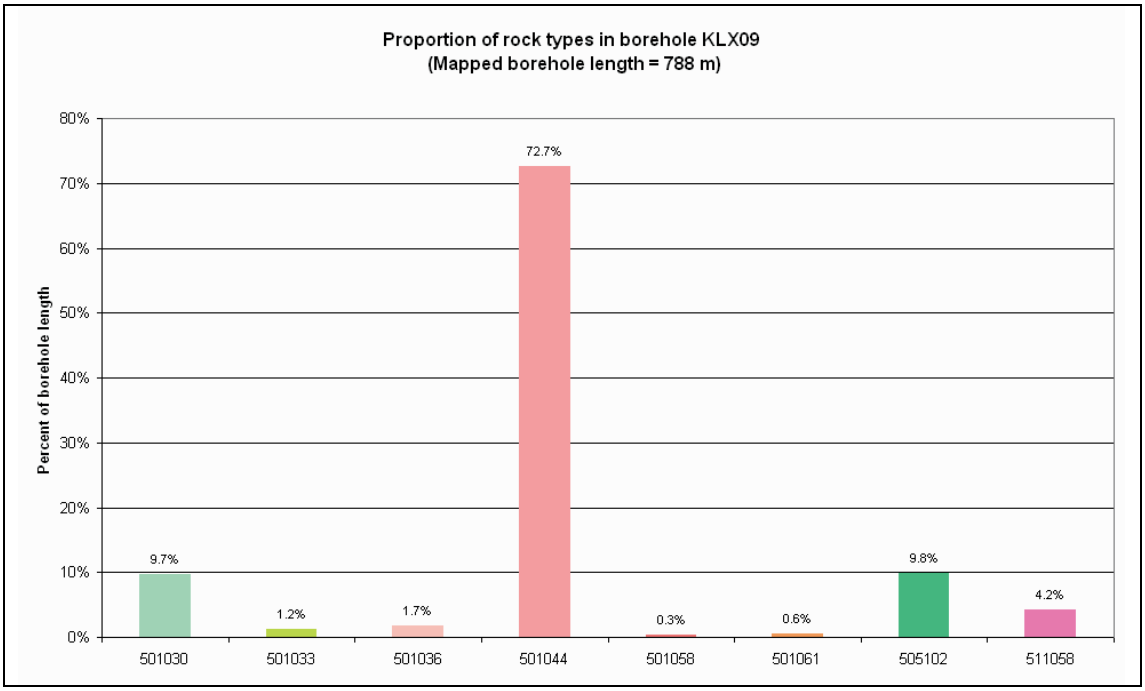
Proportion of rock types in borehole KLX09
(Mapped borehole length = 788 m)
Percent of borehole length
80%
70%
60%
50%
40%
30%
20%
10%
0%
9.7%
1.2%
1.7%
72.7%
0.3%
0.6%
9.8%
4.2%
501030
501033
501036
501044
501058
501061
505102
511058

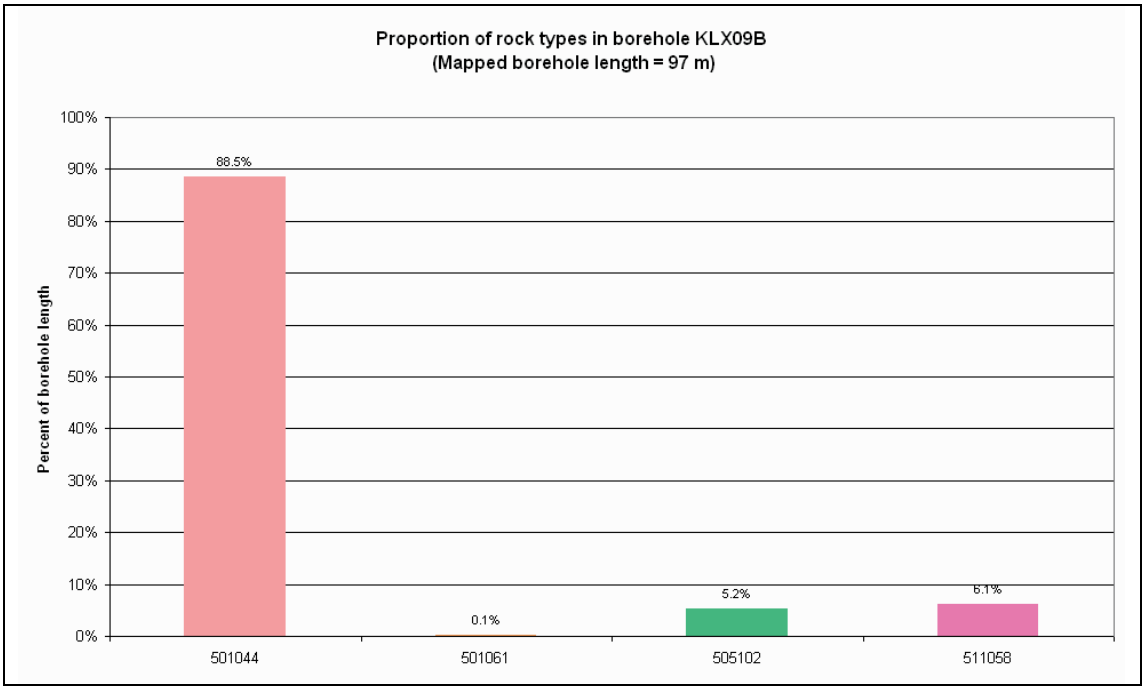
Proportion of rock types in borehole KLX09B
(Mapped borehole length = 97 m)
Percent of borehole length
100%
90%
80%
70%
60%
50%
40%
30%
20%
10%
0%
88.5%
0.1%
5.2%
6.1%
501044
501061
505102
511058

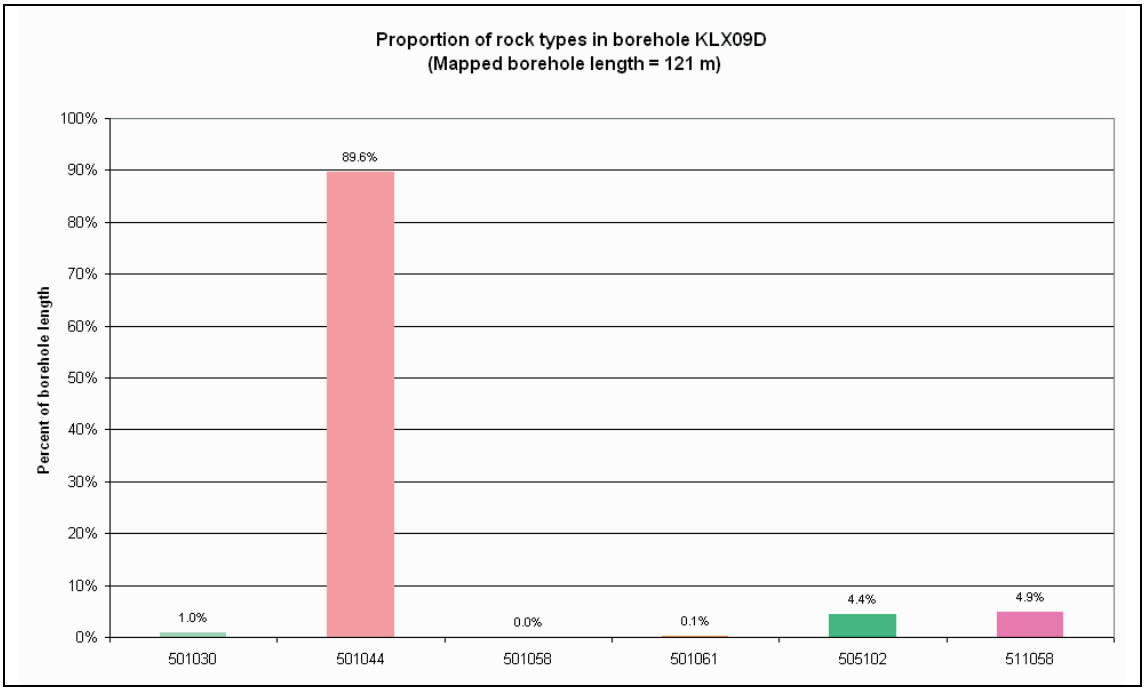
Proportion of rock types in borehole KLX09D
(Mapped borehole length = 121 m)
Percent of borehole length
100%
90%
80%
70%
60%
50%
40%
30%
20%
10%
0%
1.0%
89.6%
0.0%
0.1%
4.4%
4.9%
501030
501044
501058
501061
505102
511058

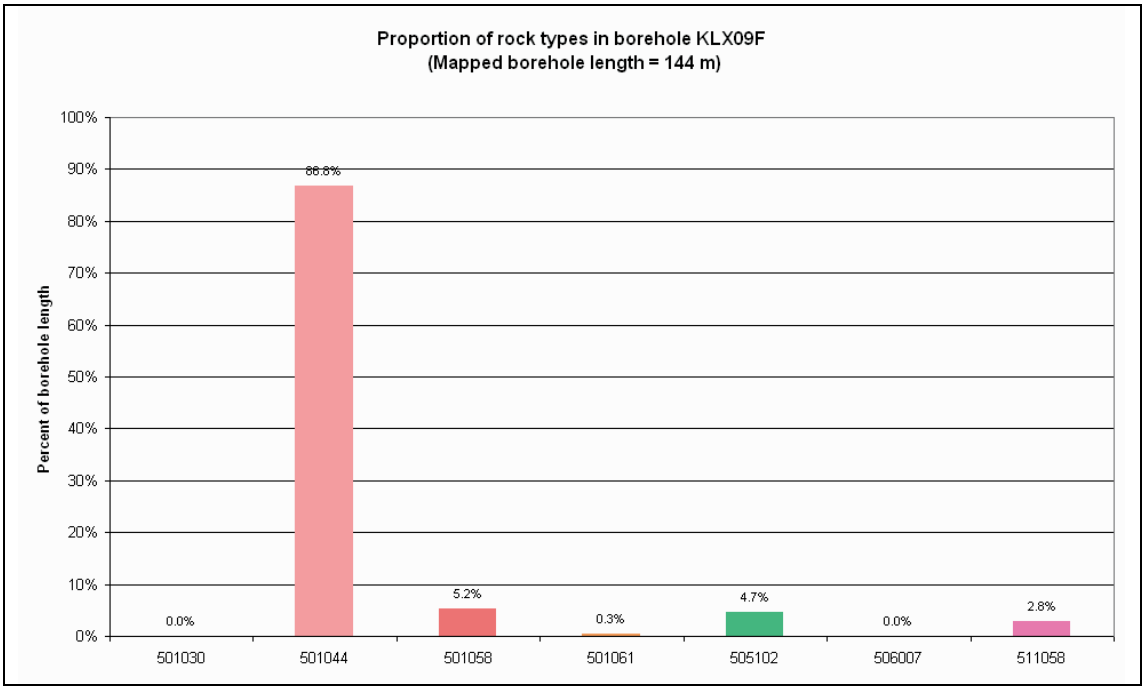
Proportion of rock types in borehole KLX09F
(Mapped borehole length = 144 m)
Percent of borehole length
100%
90%
80%
70%
60%
50%
40%
30%
20%
10%
0%
0.0%
86.8%
5.2%
0.3%
4.7%
0.0%
2.8%
501030
501044
501058
501061
505102
506007
511058

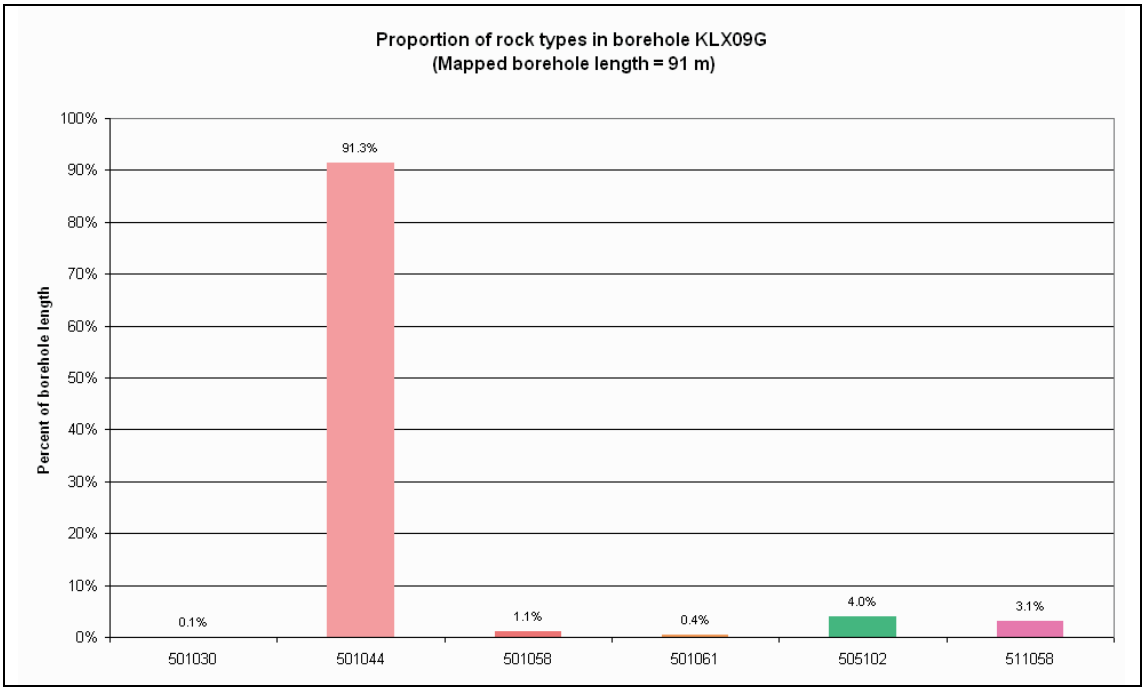
Proportion of rock types in borehole KLX09G
(Mapped borehole length = 91 m)
Percent of borehole length
100%
90%
80%
70%
60%
50%
40%
30%
20%
10%
0%
0.1%
91.3%
1.1%
0.4%
4.0%
3.1%
501030
501044
501058
501061
505102
511058

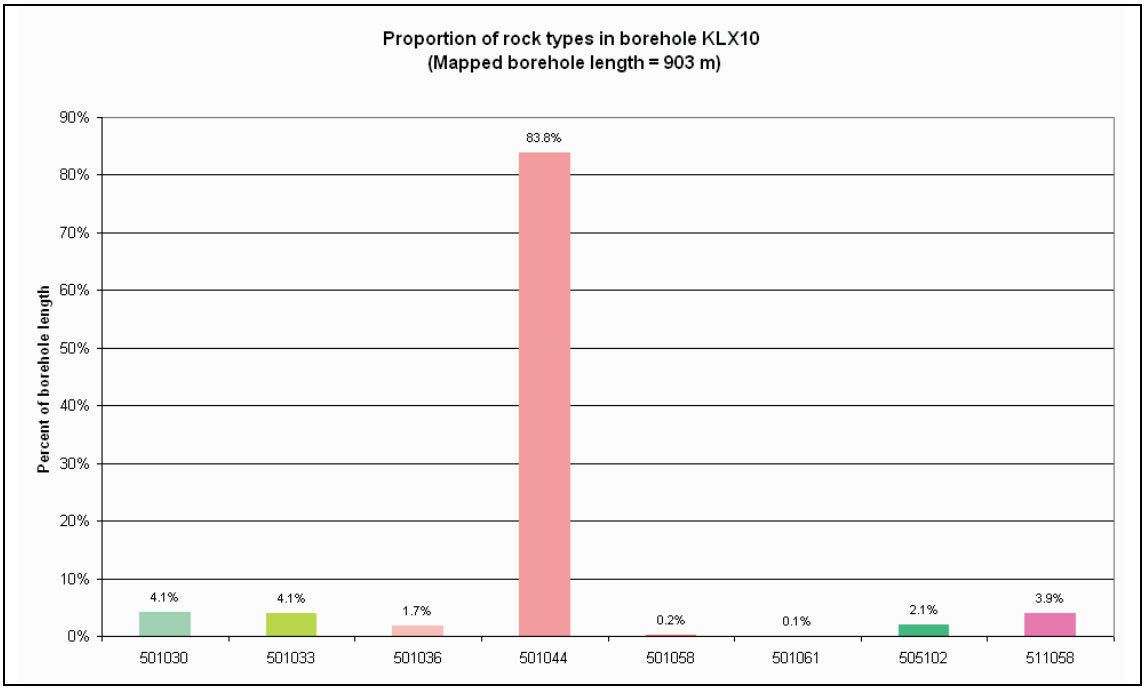
Proportion of rock types in borehole KLX10
(Mapped borehole length = 903 m)
Percent of borehole length
90%
80%
70%
60%
50%
40%
30%
20%
10%
0%
4.1%
4.1%
1.7%
83.8%
0.2%
0.1%
2.1%
3.9%
501030
501033
501036
501044
501058
501061
505102
511058

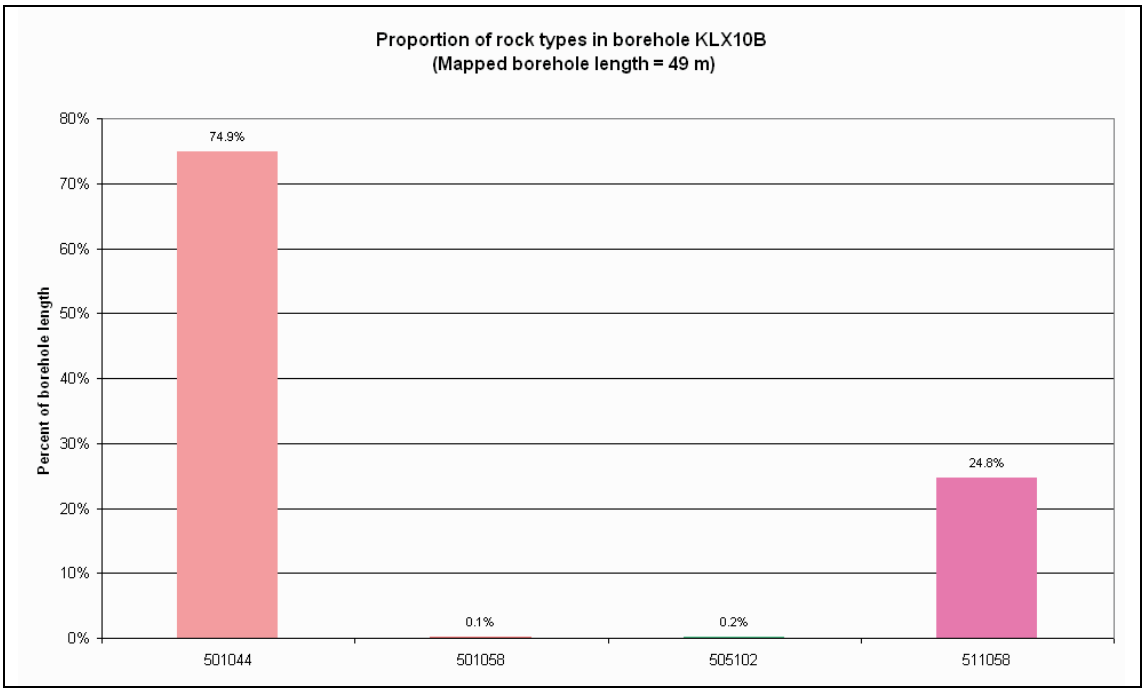
Proportion of rock types in borehole KLX10B
(Mapped borehole length = 49 m)
Percent of borehole length
80%
70%
60%
50%
40%
30%
20%
10%
0%
74.9%
0.1%
0.2%
24.8%
501044
501058
505102
511058

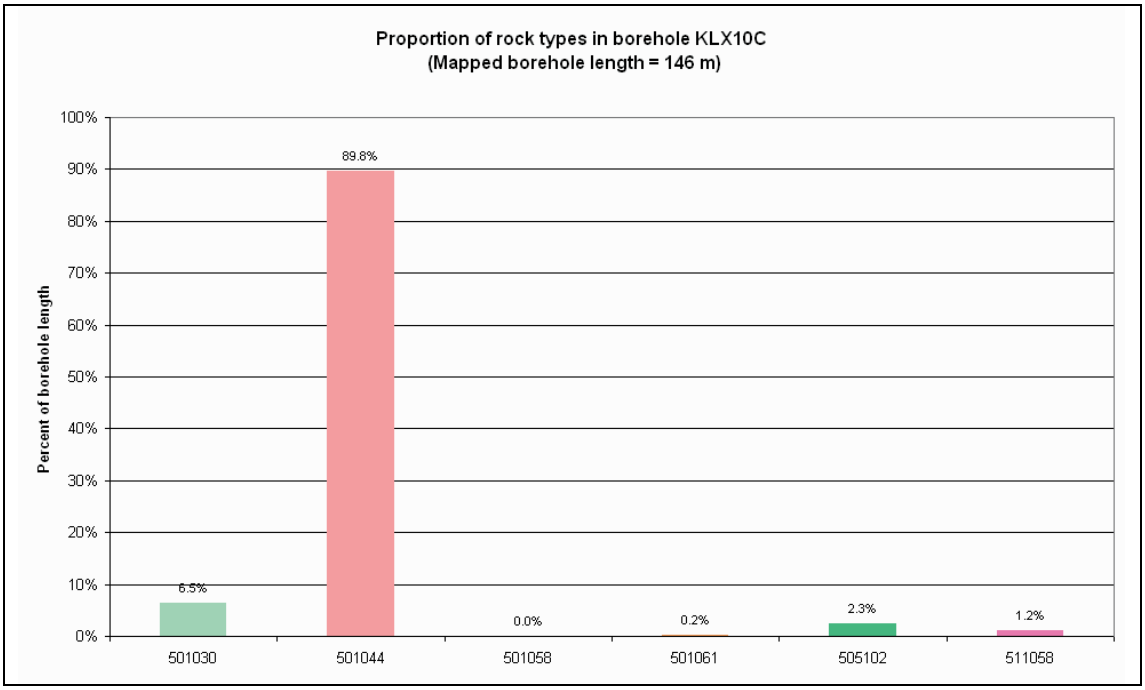
Proportion of rock types in borehole KLX10C
(Mapped borehole length = 146 m)
Percent of borehole length
100%
90%
80%
70%
60%
50%
40%
30%
20%
10%
0%
6.5%
89.8%
0.0%
0.2%
2.3%
1.2%
501030
501044
501058
501061
505102
511058

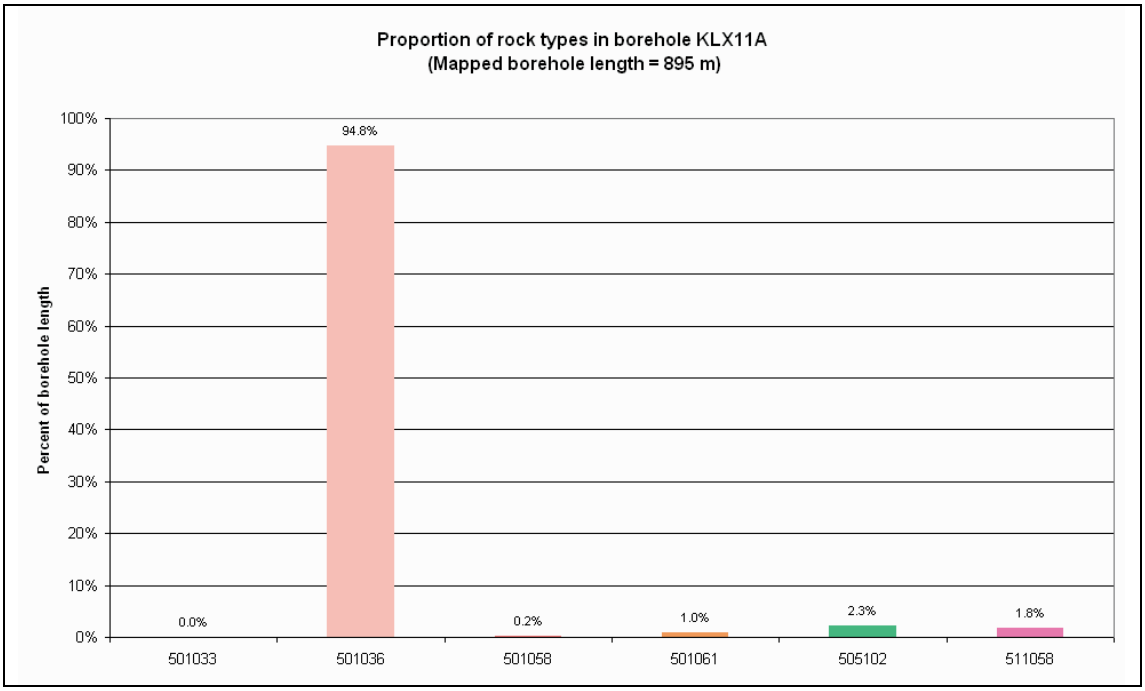
Proportion of rock types in borehole KLX11A
(Mapped borehole length = 895 m)
Percent of borehole length
100%
90%
80%
70%
60%
50%
40%
30%
20%
10%
0%
0.0%
94.8%
0.2%
1.0%
2.3%
1.8%
501033
501036
501058
501061
505102
511058

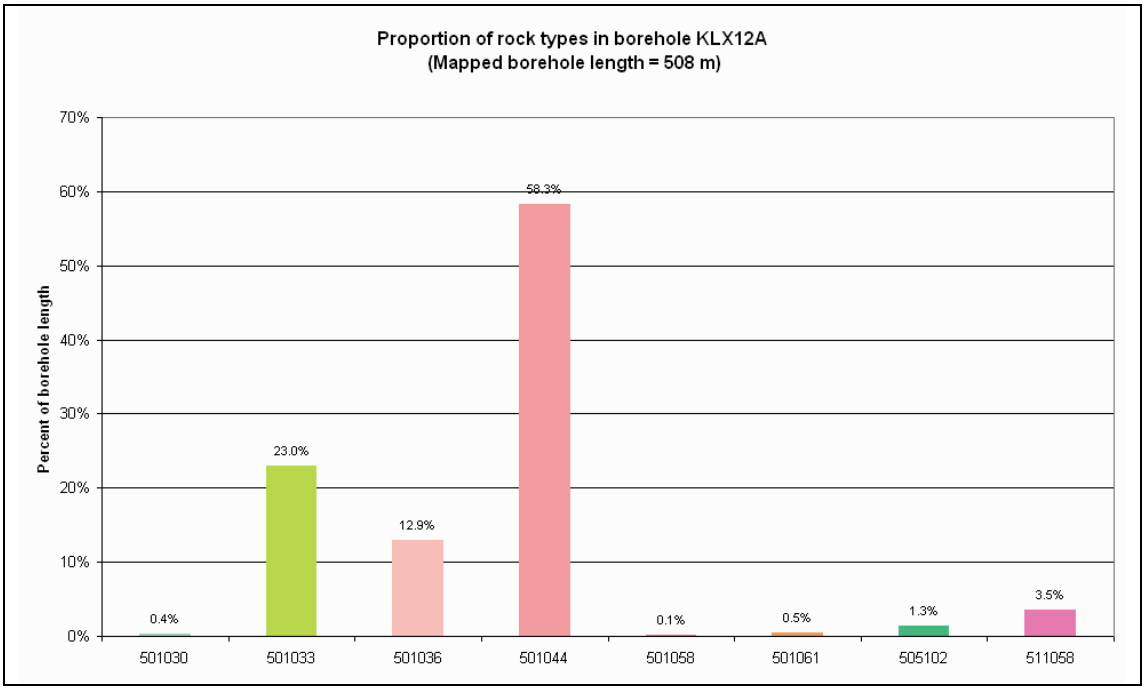
Proportion of rock types in borehole KLX12A
(Mapped borehole length = 508 m)
Percent of borehole length
70%
60%
50%
40%
30%
20%
10%
0%
0.4%
23.0%
12.9%
58.3%
0.1%
0.5%
1.3%
3.5%
501030
501033
501036
501044
501058
501061
505102
511058

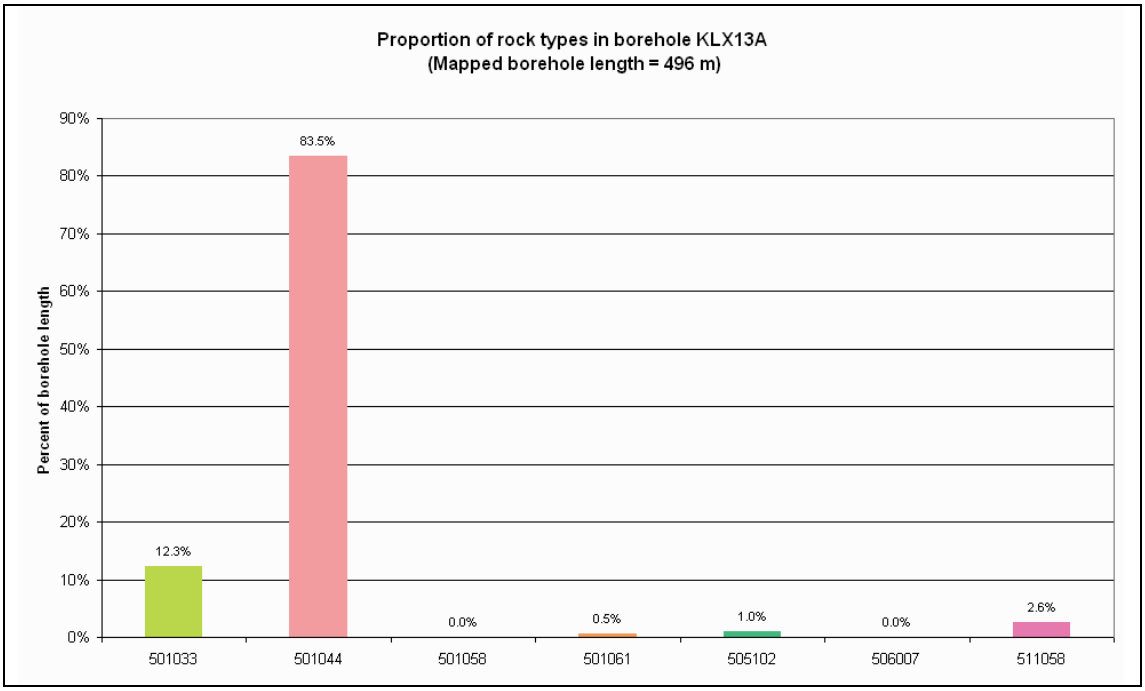
Proportion of rock types in borehole KLX13A
(Mapped borehole length = 496 m)
Percent of borehole length
90%
80%
70%
60%
50%
40%
30%
20%
10%
0%
12.3%
83.5%
0.0%
0.5%
1.0%
0.0%
2.6%
501033
501044
501058
501061
505102
506007
511058

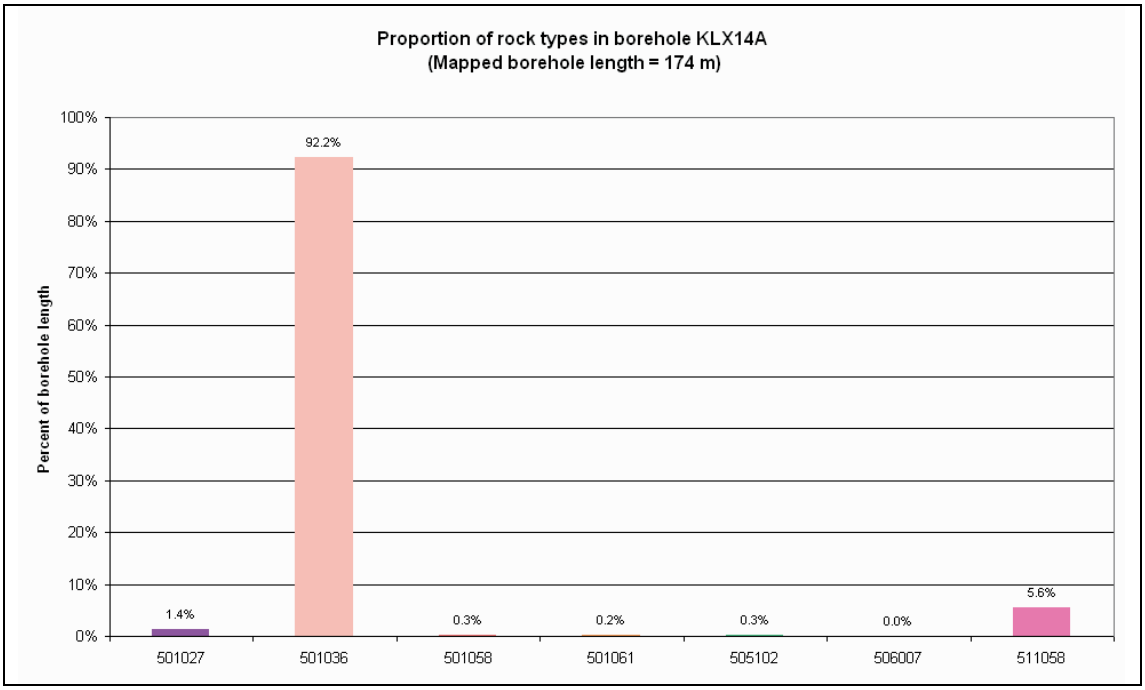
Proportion of rock types in borehole KLX14A
(Mapped borehole length = 174 m)
Percent of borehole length
100%
90%
80%
70%
60%
50%
40%
30%
20%
10%
0%
92.2%
1.4%
0.3%
0.2%
0.3%
0.0%
5.6%
501027
501036
501058
501061
505102
506007
511058

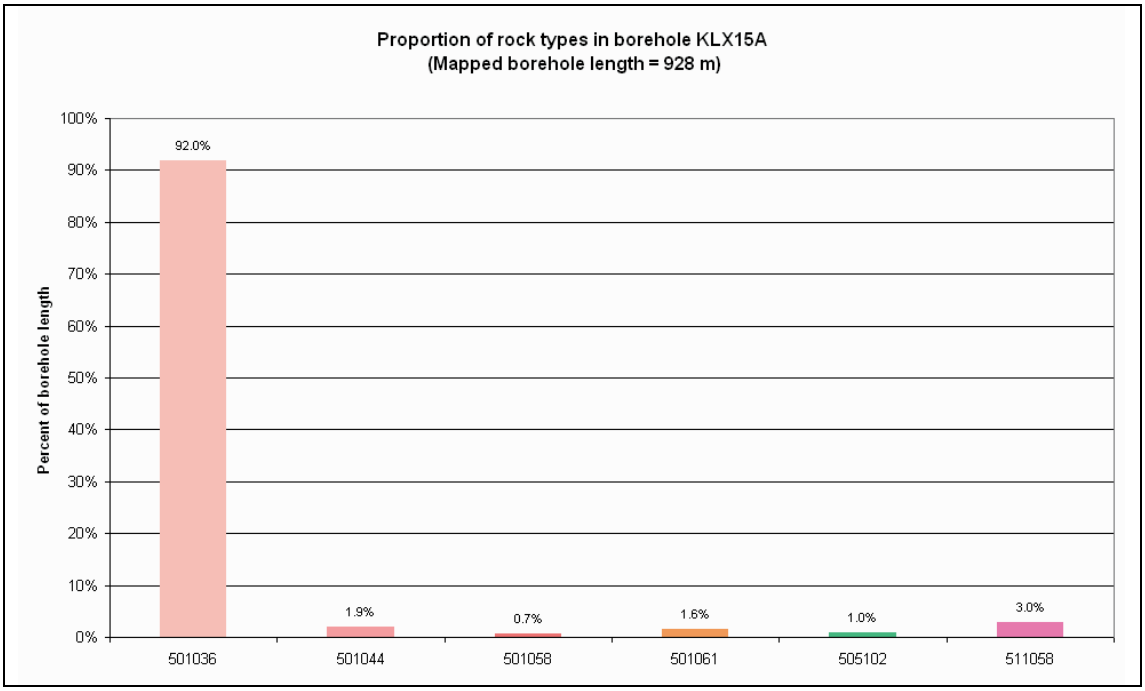
Proportion of rock types in borehole KLX15A
(Mapped borehole length = 928 m)
Percent of borehole length
100%
90%
80%
70%
60%
50%
40%
30%
20%
10%
0%
92.0%
1.9%
0.7%
1.6%
1.0%
3.0%
501036
501044
501058
501061
505102
511058

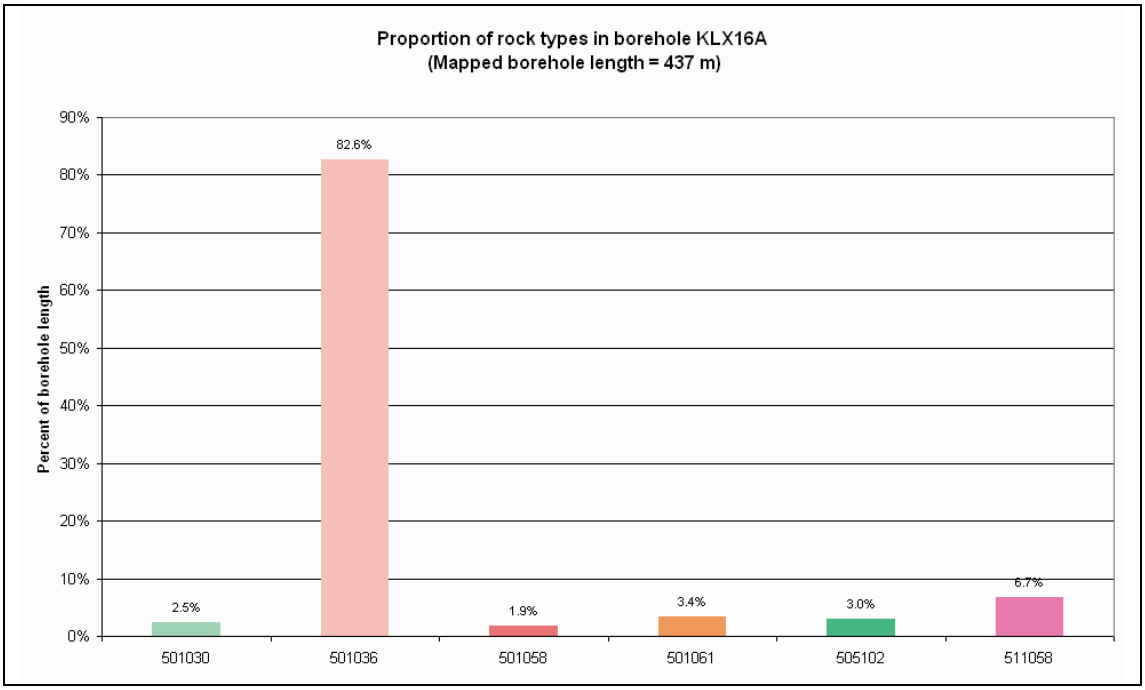
Proportion of rock types in borehole KLX16A
(Mapped borehole length = 437 m)
Percent of borehole length
90%
80%
70%
60%
50%
40%
30%
20%
10%
0%
2.5%
82.6%
1.9%
3.4%
3.0%
6.7%
501030
501036
501058
501061
505102
511058

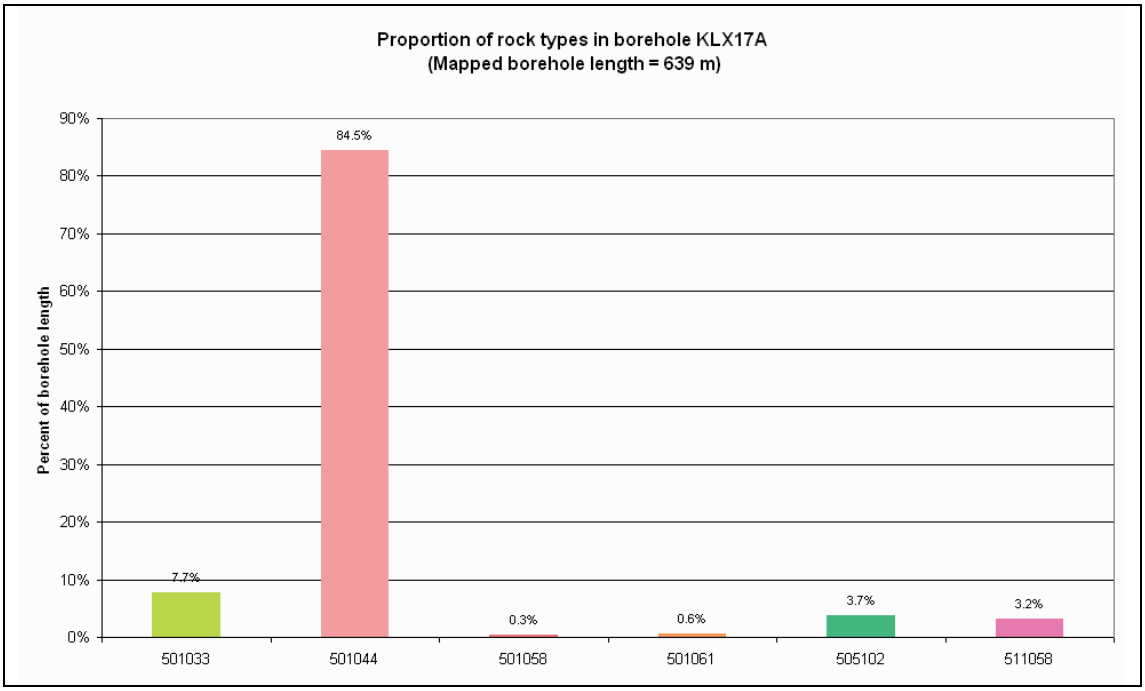
Proportion of rock types in borehole KLX17A
(Mapped borehole length = 639 m)
Percent of borehole length
90%
80%
70%
60%
50%
40%
30%
20%
10%
0%
7.7%
84.5%
0.3%
0.6%
3.7%
3.2%
501033
501044
501058
501061
505102
511058

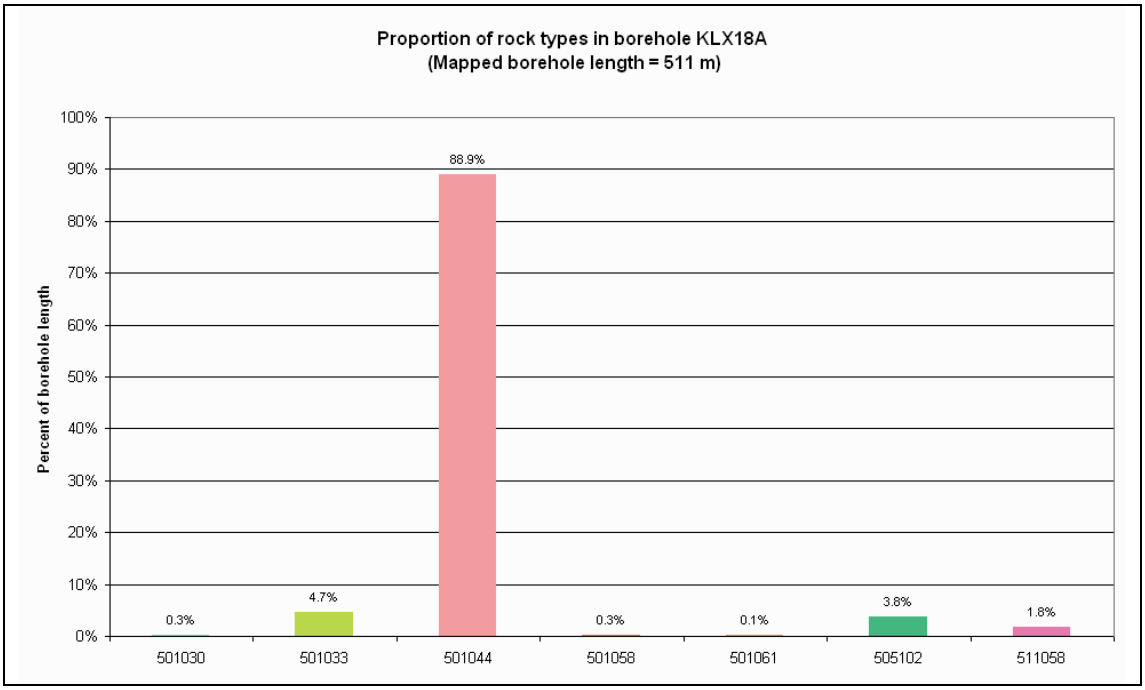
Proportion of rock types in borehole KLX18A
(Mapped borehole length = 511 m)
Percent of borehole length
100%
90%
80%
70%
60%
50%
40%
30%
20%
10%
0%
0.3%
4.7%
88.9%
0.3%
0.1%
3.8%
1.8%
501030
501033
501044
501058
501061
505102
511058

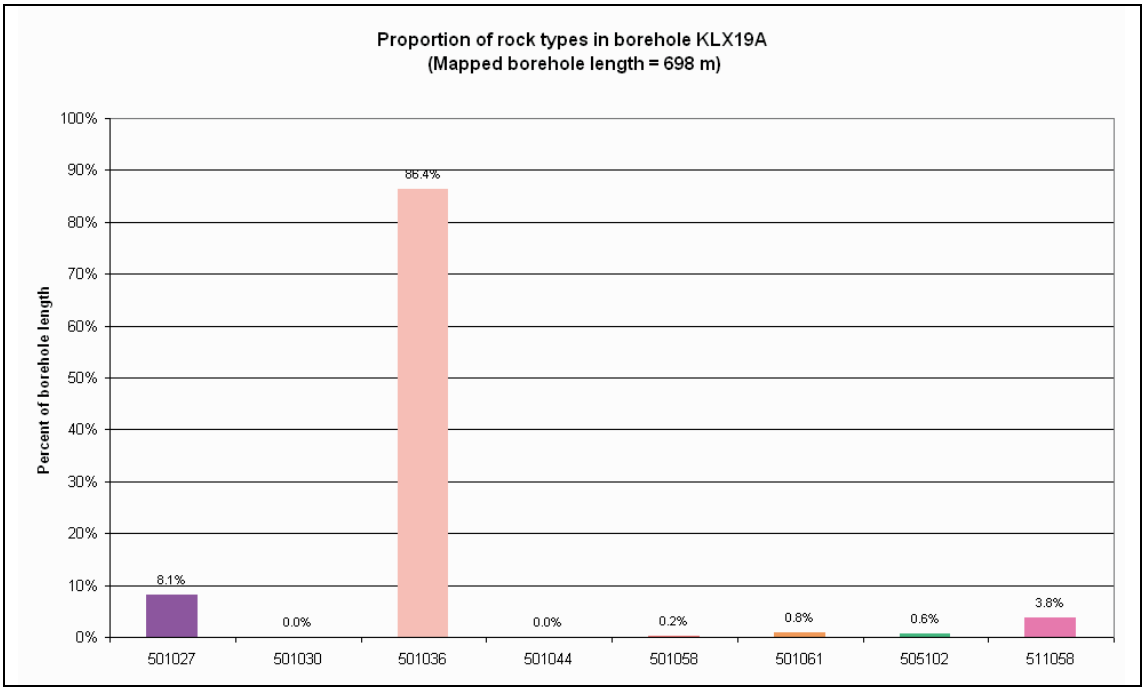
Proportion of rock types in borehole KLX19A
(Mapped borehole length = 698 m)
Percent of borehole length
100%
90%
80%
70%
60%
50%
40%
30%
20%
10%
0%
8.1%
0.0%
86.4%
0.0%
0.2%
0.8%
0.6%
3.8%
501027
501030
501036
501044
501058
501061
505102
511058

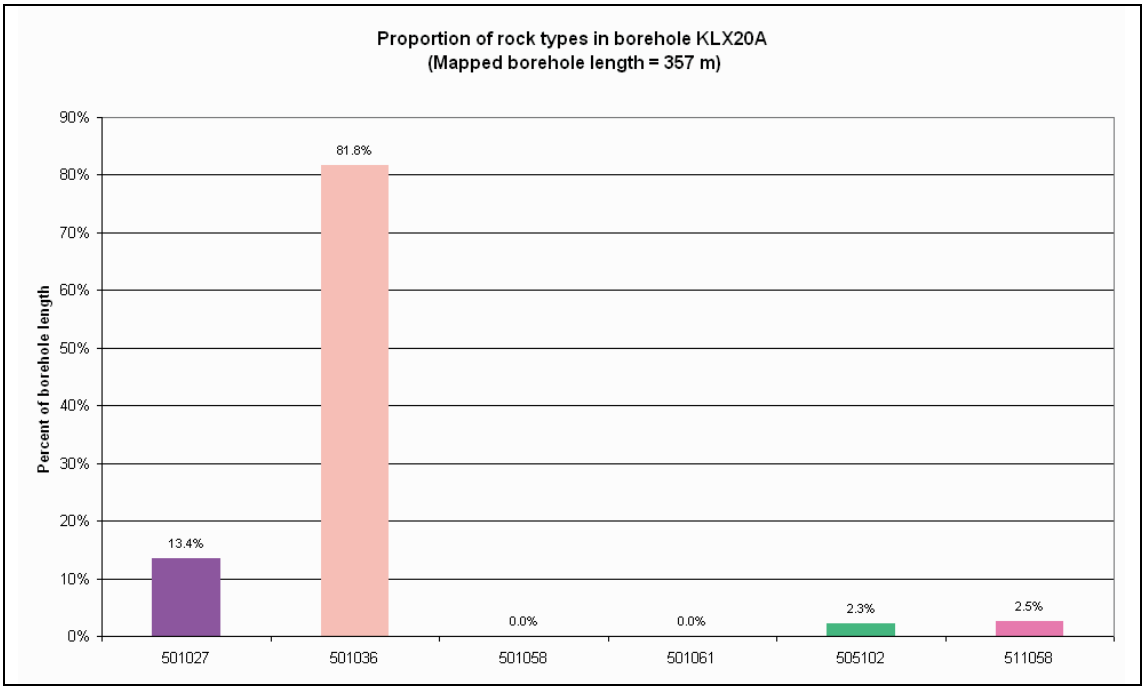
Proportion of rock types in borehole KLX20A
(Mapped borehole length = 357 m)
Percent of borehole length
90%
80%
70%
60%
50%
40%
30%
20%
10%
0%
13.4%
81.8%
0.0%
0.0%
2.3%
2.5%
501027
501036
501058
501061
505102
511058

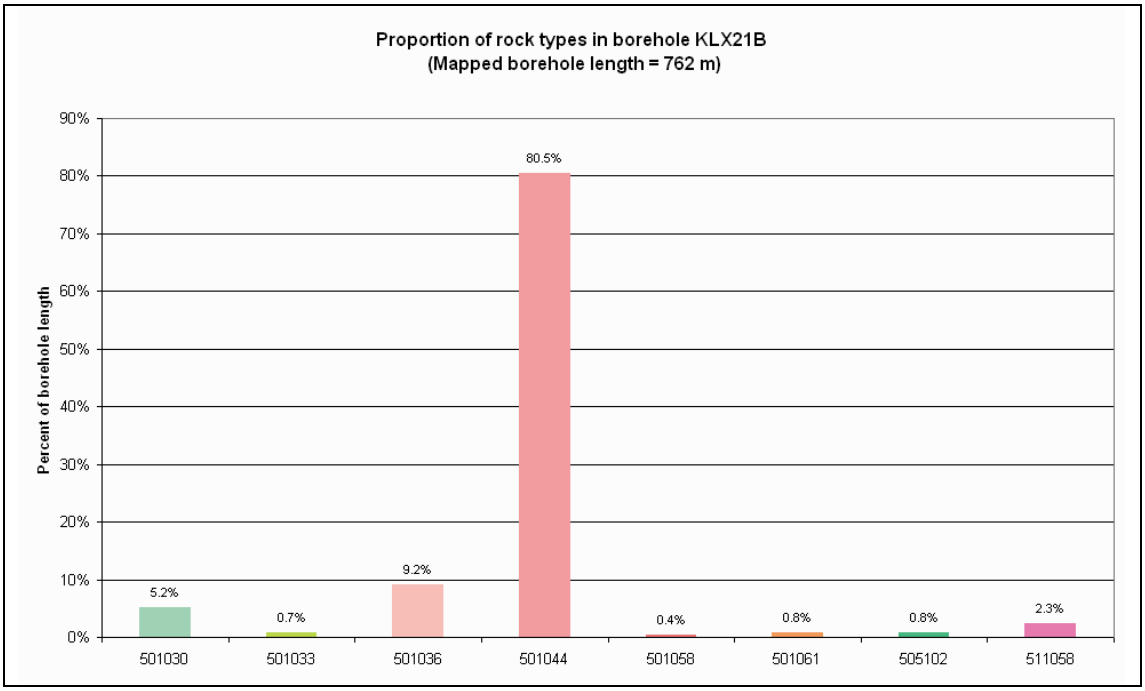
Proportion of rock types in borehole KLX21B
(Mapped borehole length = 762 m)
Percent of borehole length
90%
80%
70%
60%
50%
40%
30%
20%
10%
0%
5.2%
0.7%
9.2%
80.5%
0.4%
0.8%
0.8%
2.3%
501030
501033
501036
501044
501058
501061
505102
511058

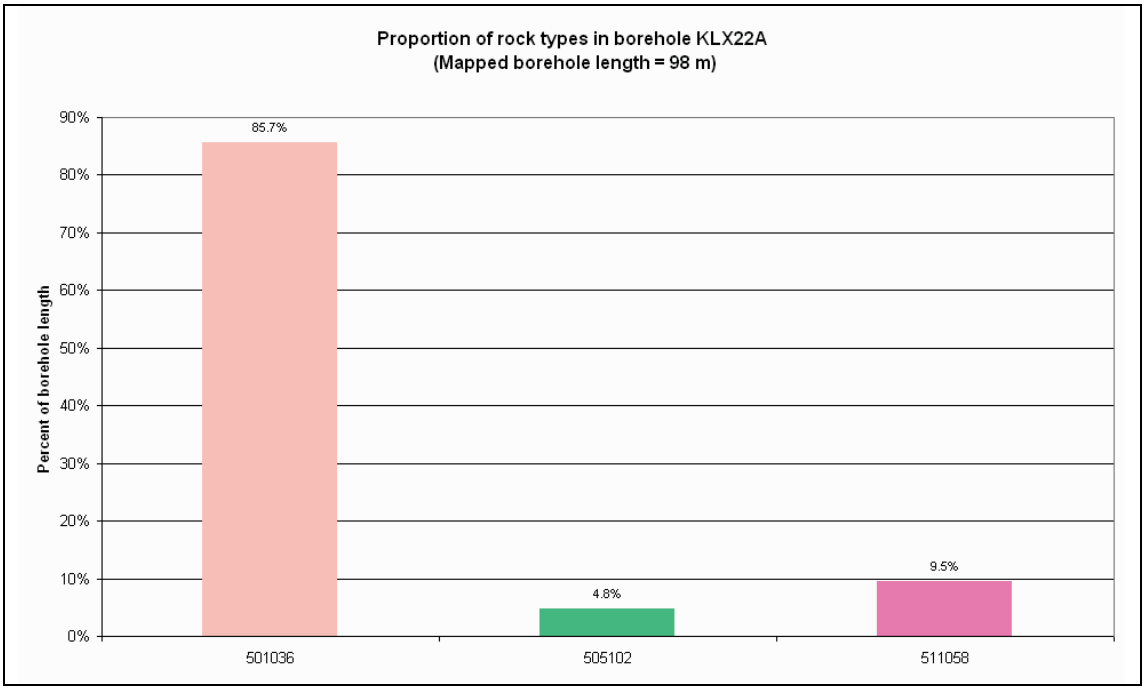
Proportion of rock types in borehole KLX22A
(Mapped borehole length = 98 m)
Percent of borehole length
90%
80%
70%
60%
50%
40%
30%
20%
10%
0%
85.7%
4.8%
9.5%
501036
505102
511058

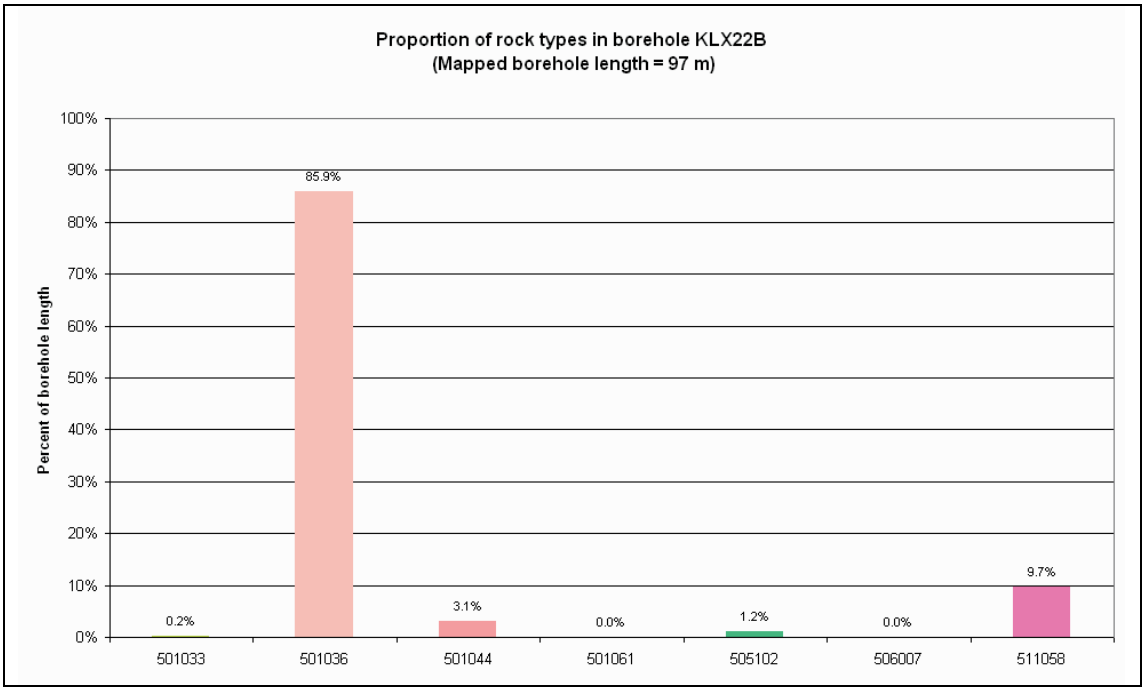
Proportion of rock types in borehole KLX22B
(Mapped borehole length = 97 m)
Percent of borehole length
100%
90%
80%
70%
60%
50%
40%
30%
20%
10%
0%
0.2%
85.9%
3.1%
0.0%
1.2%
0.0%
9.7%
501033
501036
501044
501061
505102
506007
511058

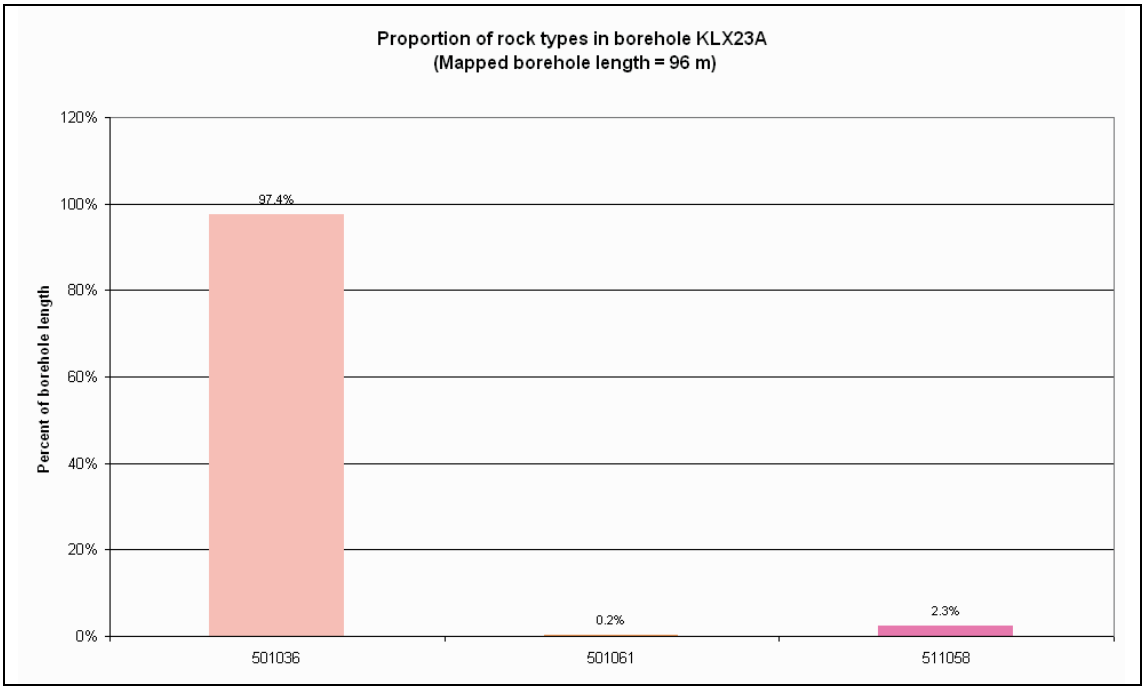
Proportion of rock types in borehole KLX23A
(Mapped borehole length = 96 m)
Percent of borehole length
120%
100%
80%
60%
40%
20%
0%
97.4%
0.2%
2.3%
501036
501061
511058

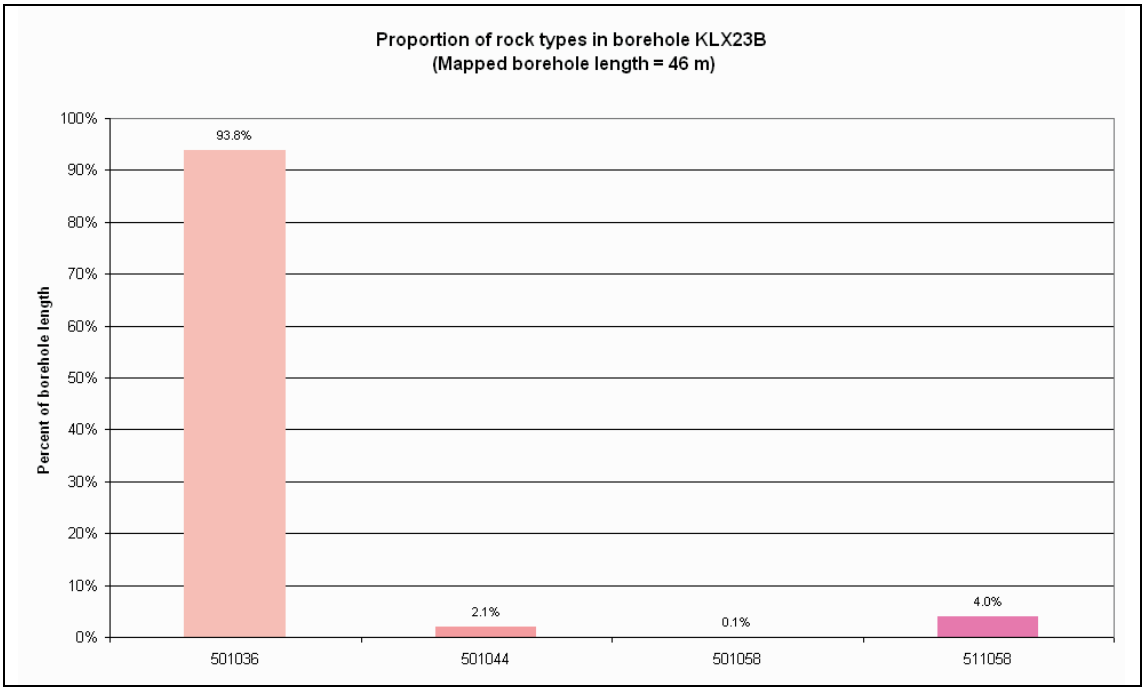
Proportion of rock types in borehole KLX23B
(Mapped borehole length = 46 m)
Percent of borehole length
100%
90%
80%
70%
60%
50%
40%
30%
20%
10%
0%
93.8%
2.1%
0.1%
4.0%
501036
501044
501058
511058

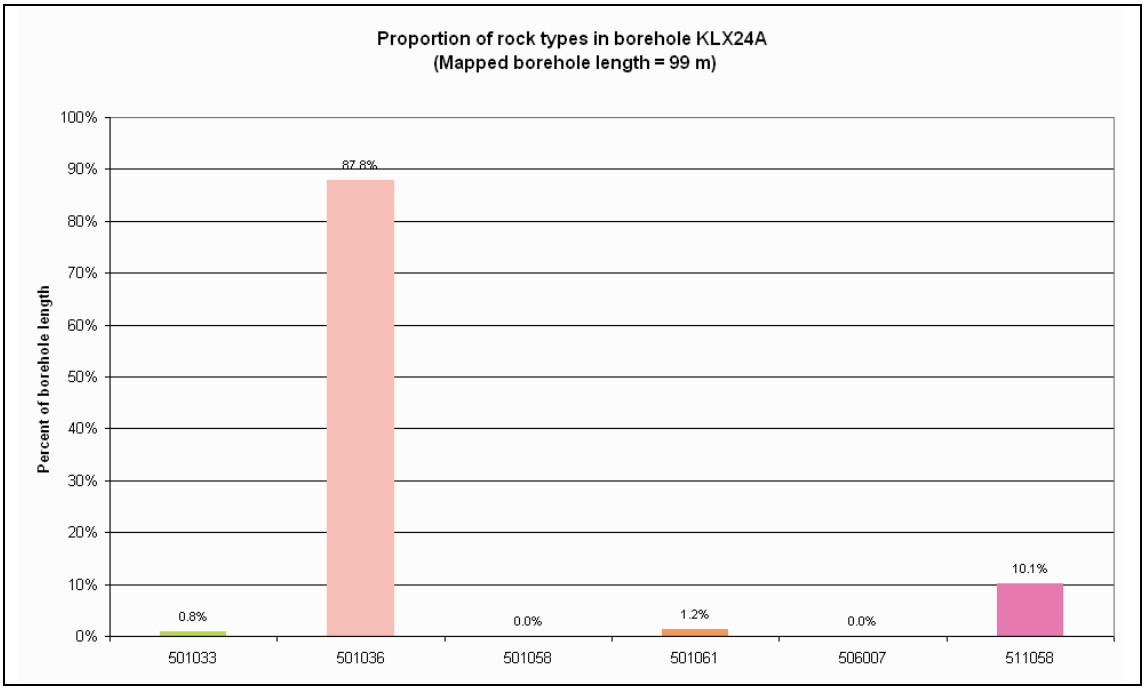
Proportion of rock types in borehole KLX24A
(Mapped borehole length = 99 m)
Percent of borehole length
100%
90%
80%
70%
60%
50%
40%
30%
20%
10%
0%
87.8%
0.8%
0.0%
1.2%
0.0%
10.1%
501033
501036
501058
501061
506007
511058

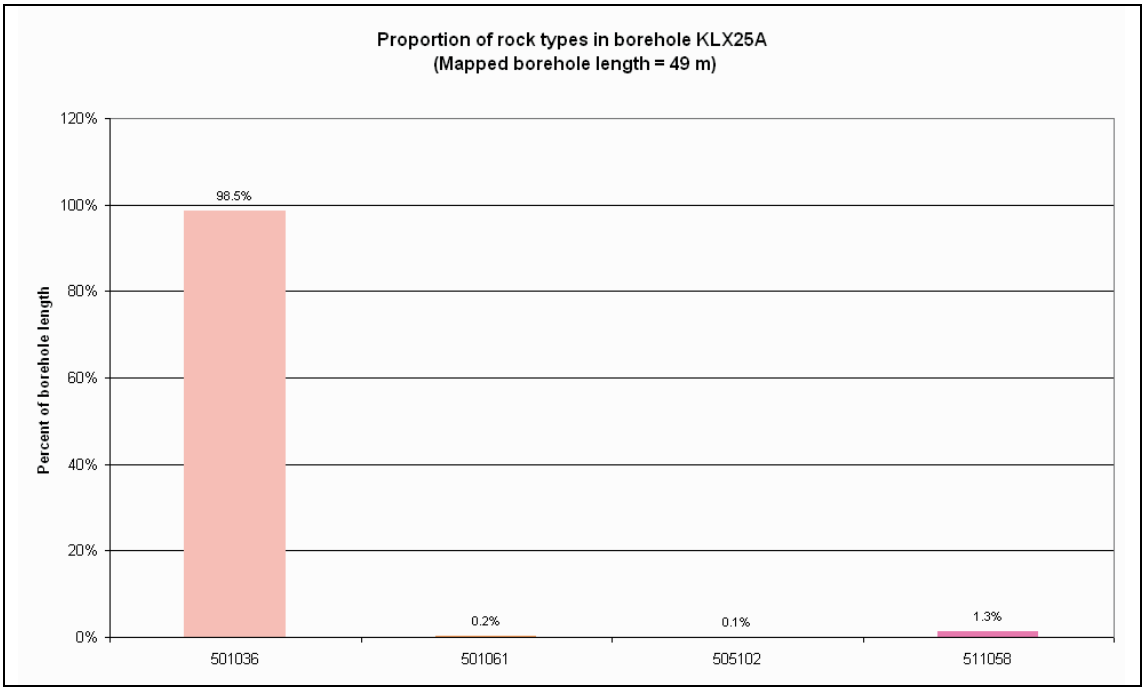
Proportion of rock types in borehole KLX25A
(Mapped borehole length = 49 m)
Percent of borehole length
120%
100%
80%
60%
40%
20%
0%
98.5%
0.2%
0.1%
1.3%
501036
501061
505102
511058

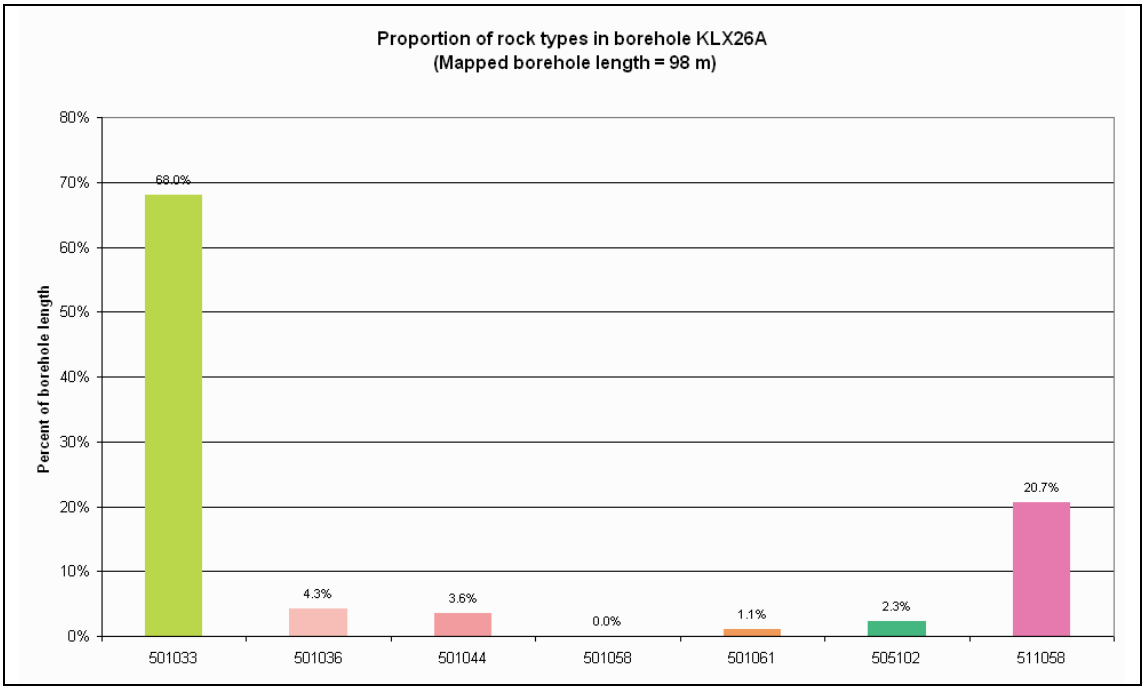
Proportion of rock types in borehole KLX26A
(Mapped borehole length = 98 m)
Percent of borehole length
80%
70%
60%
50%
40%
30%
20%
10%
0%
68.0%
4.3%
3.6%
0.0%
1.1%
2.3%
20.7%
501033
501036
501044
501058
501061
505102
511058

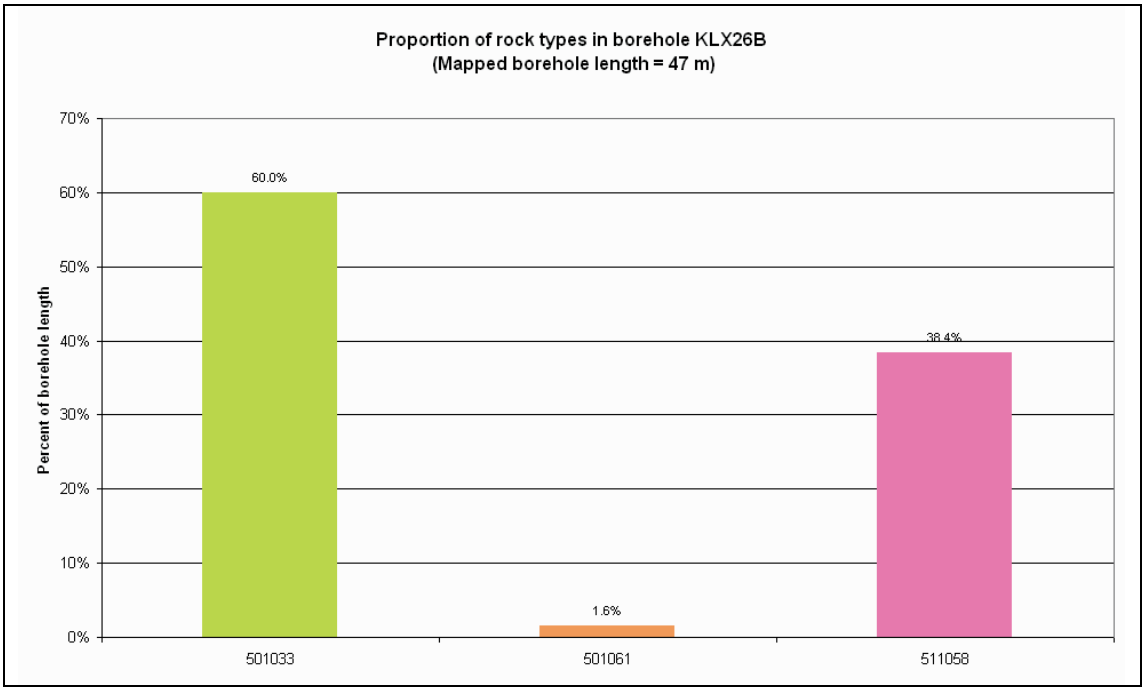
Proportion of rock types in borehole KLX26B
(Mapped borehole length = 47 m)
Percent of borehole length
70%
60%
50%
40%
30%
20%
10%
0%
60.0%
1.6%
38.4%
501033
501061
511058

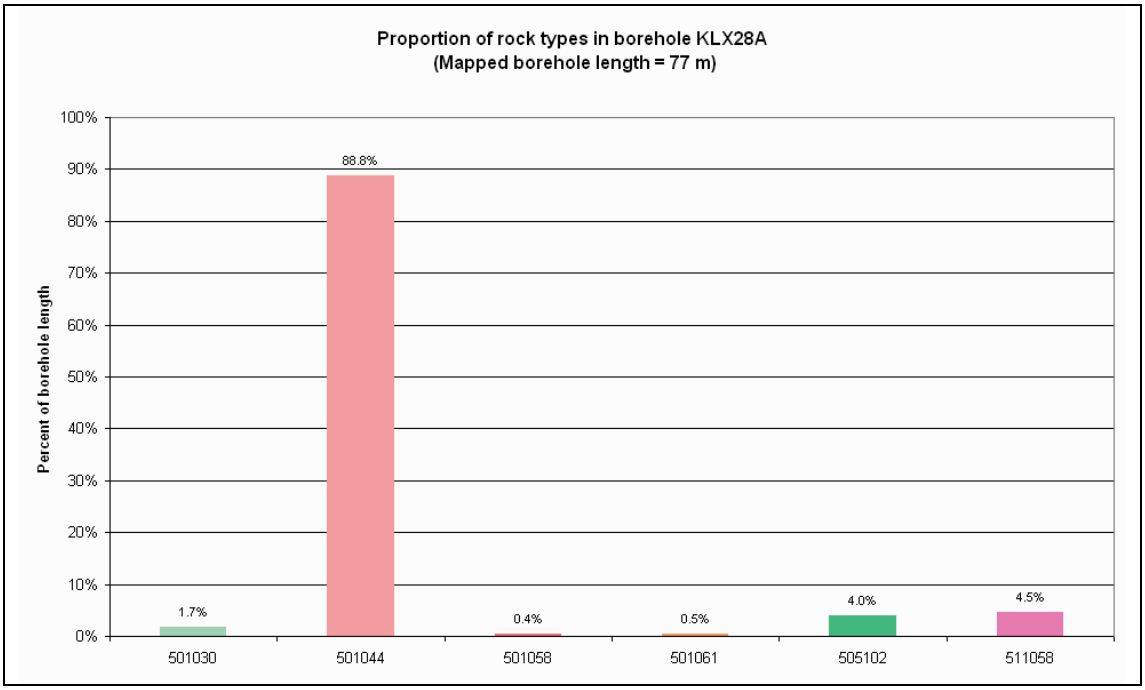
Proportion of rock types in borehole KLX28A
(Mapped borehole length = 77 m)
Percent of borehole length
100%
90%
80%
70%
60%
50%
40%
30%
20%
10%
0%
88.8%
1.7%
0.4%
0.5%
4.0%
4.5%
501030
501044
501058
501061
505102
511058

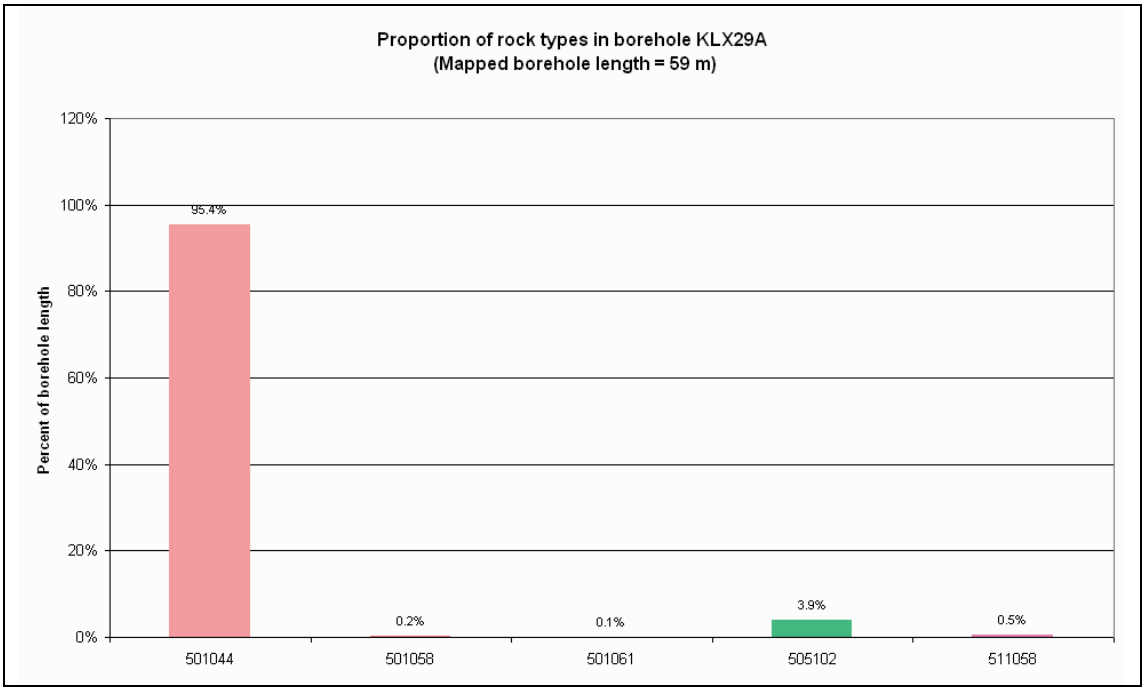
Proportion of rock types in borehole KLX29A
(Mapped borehole length = 59 m)
Percent of borehole length
120%
100%
80%
60%
40%
20%
0%
95.4%
0.2%
0.1%
3.9%
0.5%
501044
501058
501061
505102
511058

Proportions of different rock types on a rock domain basis in each borehole

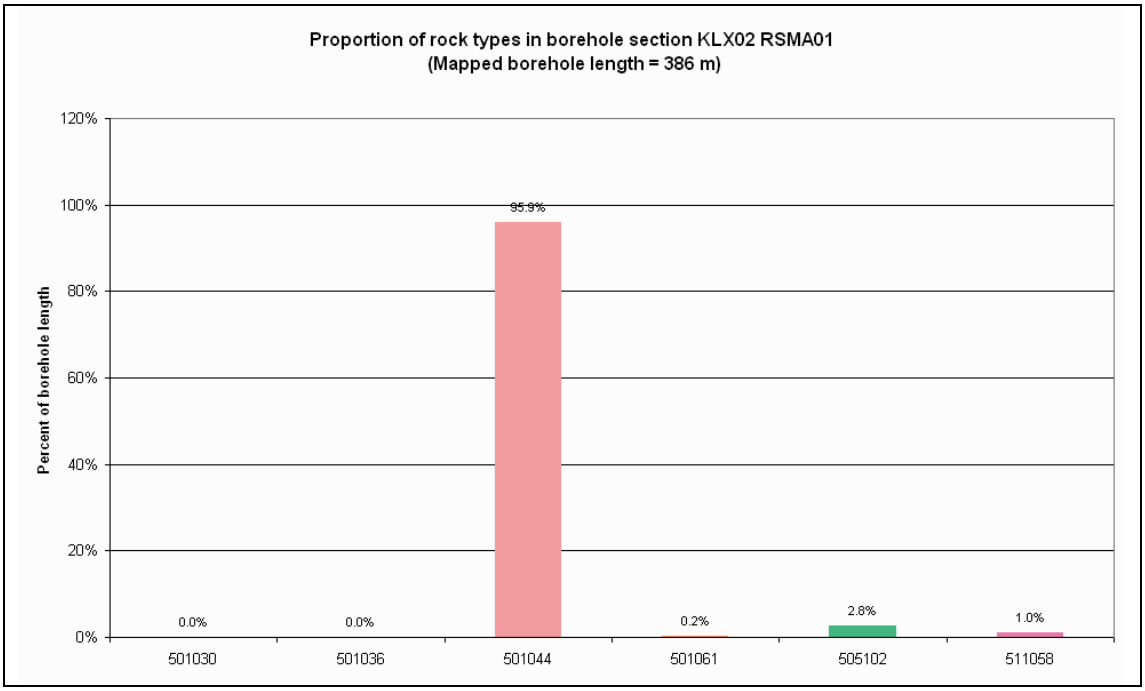

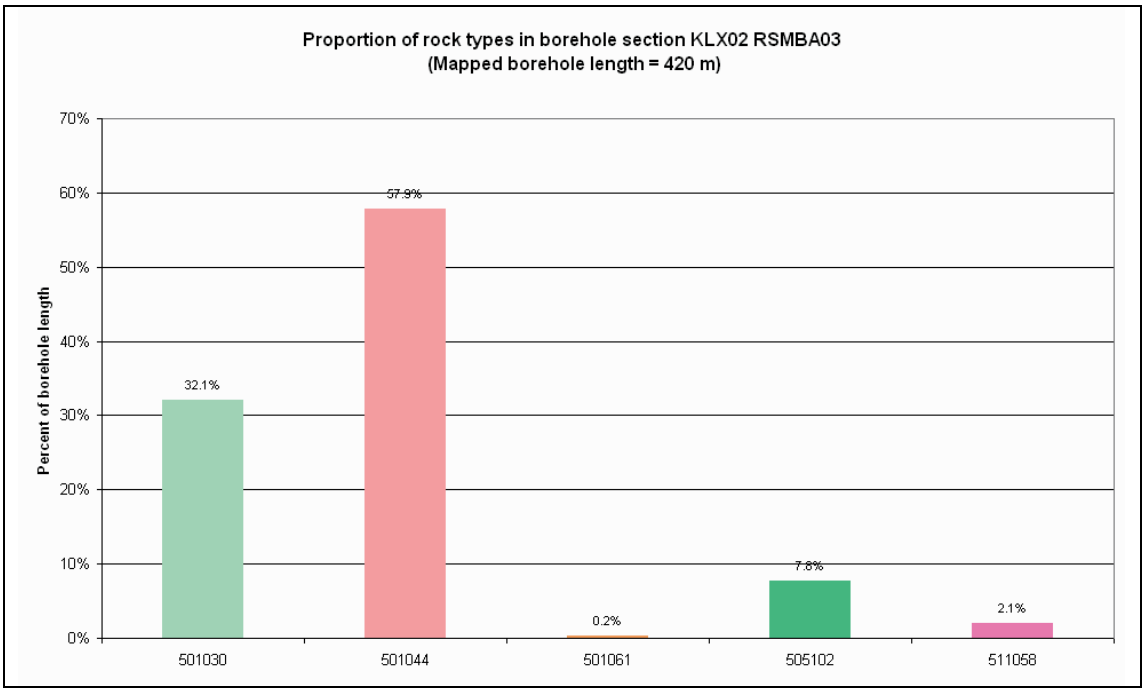

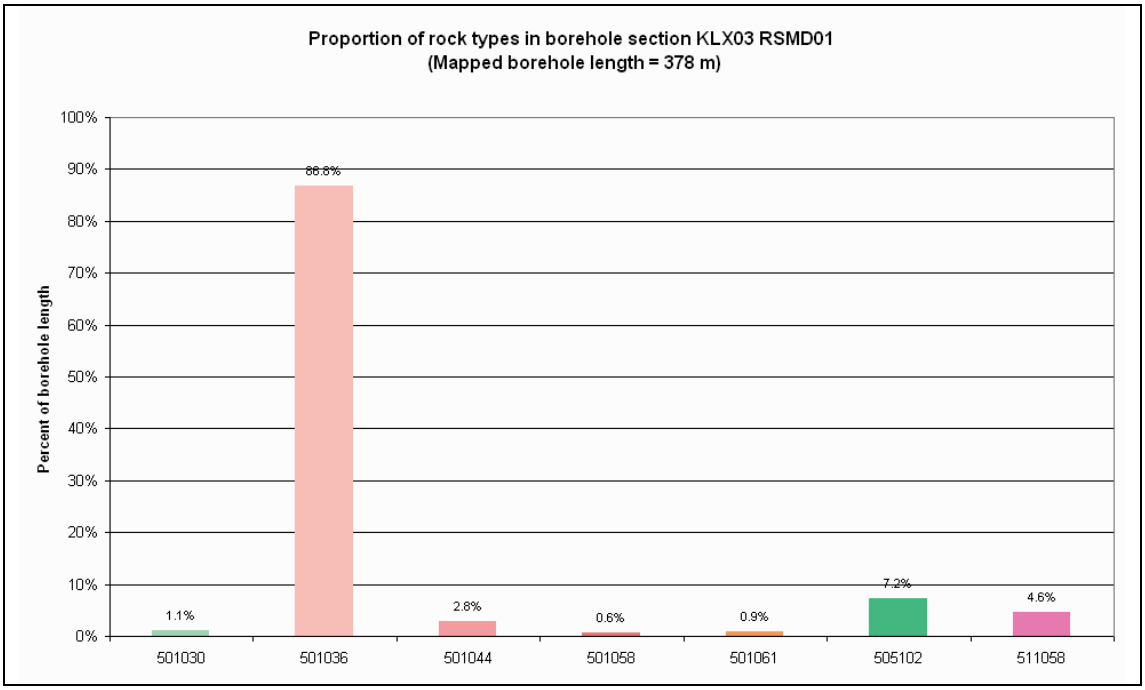
Proportion of rock types in borehole section KLX03 RSMD01
(Mapped borehole length = 378 m)
Percent of borehole length
100%
90%
80%
70%
60%
50%
40%
30%
20%
10%
0%
1.1%
86.8%
2.8%
0.6%
0.9%
7.2%
4.6%
501030
501036
501044
501058
501061
505102
511058

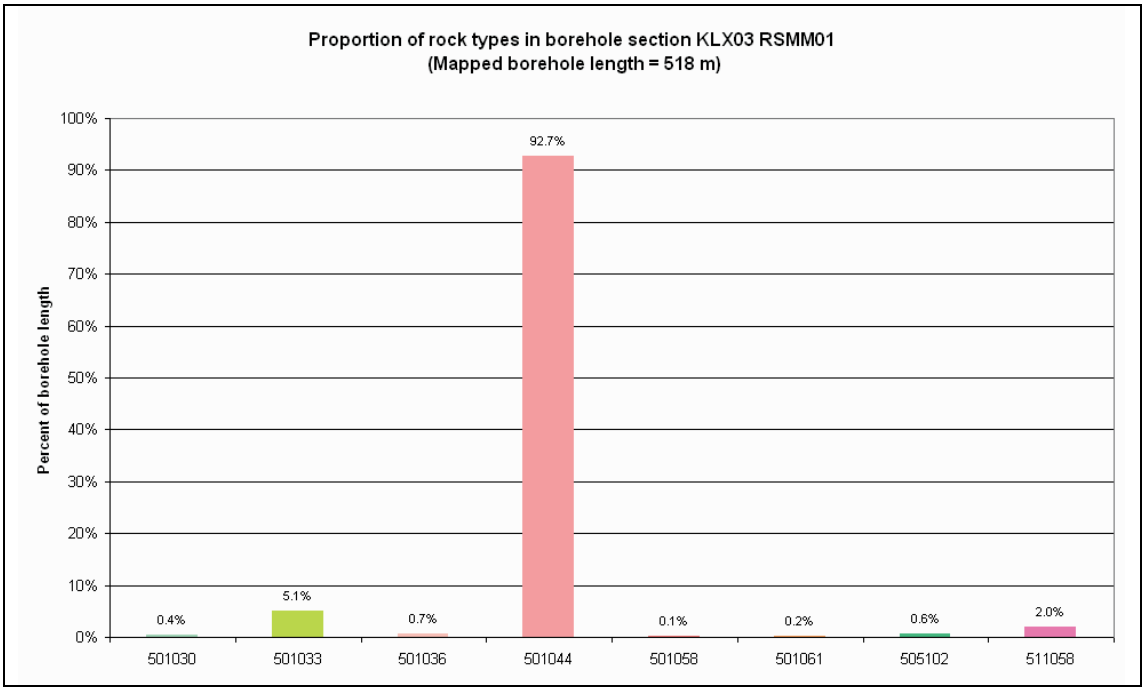
Proportion of rock types in borehole section KLX03 RSMM01
(Mapped borehole length = 518 m)
Percent of borehole length
100%
90%
80%
70%
60%
50%
40%
30%
20%
10%
0%
0.4%
5.1%
0.7%
92.7%
0.1%
0.2%
0.6%
2.0%
501030
501033
501036
501044
501058
501061
505102
511058

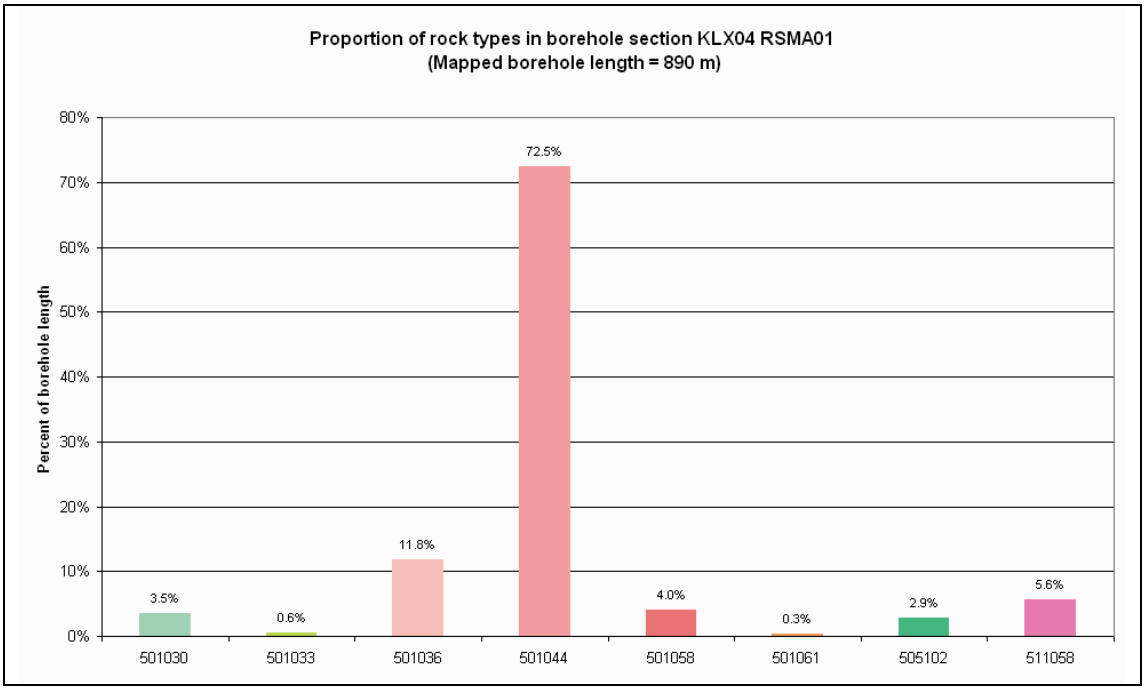
Proportion of rock types in borehole section KLX04 RSMA01
(Mapped borehole length = 890 m)
Percent of borehole length
80%
70%
60%
50%
40%
30%
20%
10%
0%
3.5%
0.6%
11.8%
72.5%
4.0%
0.3%
2.9%
5.6%
501030
501033
501036
501044
501058
501061
505102
511058

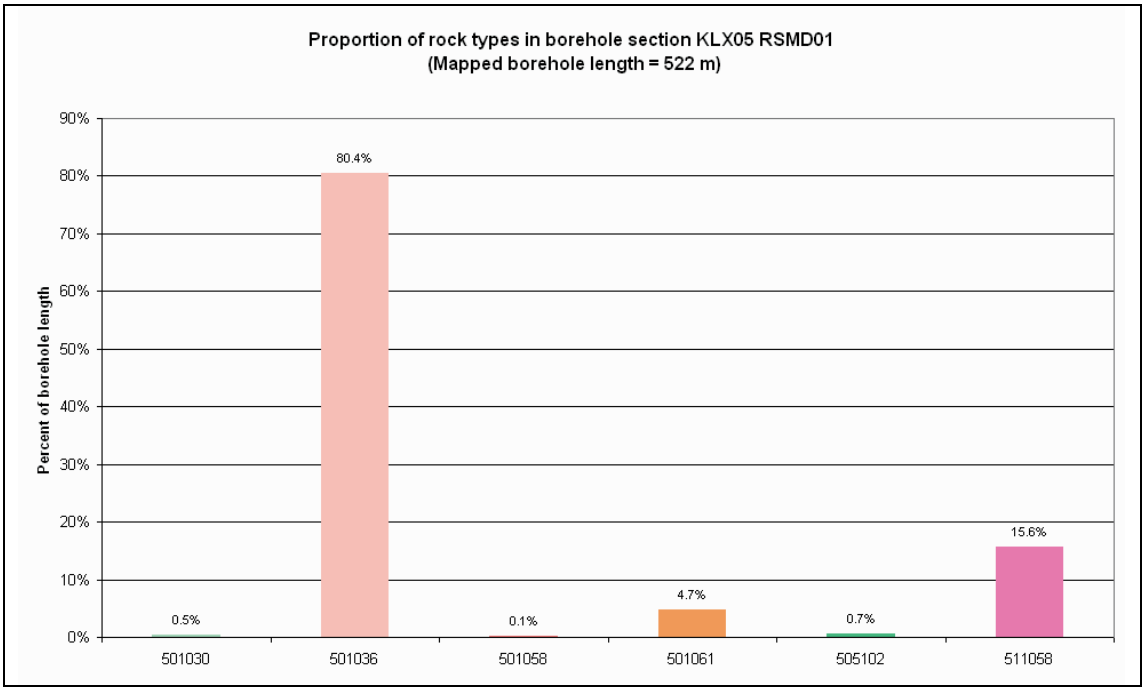
Proportion of rock types in borehole section KLX05 RSMD01
(Mapped borehole length = 522 m)
Percent of borehole length
90%
80%
70%
60%
50%
40%
30%
20%
10%
0%
0.5%
80.4%
0.1%
4.7%
0.7%
15.6%
501030
501036
501058
501061
505102
511058

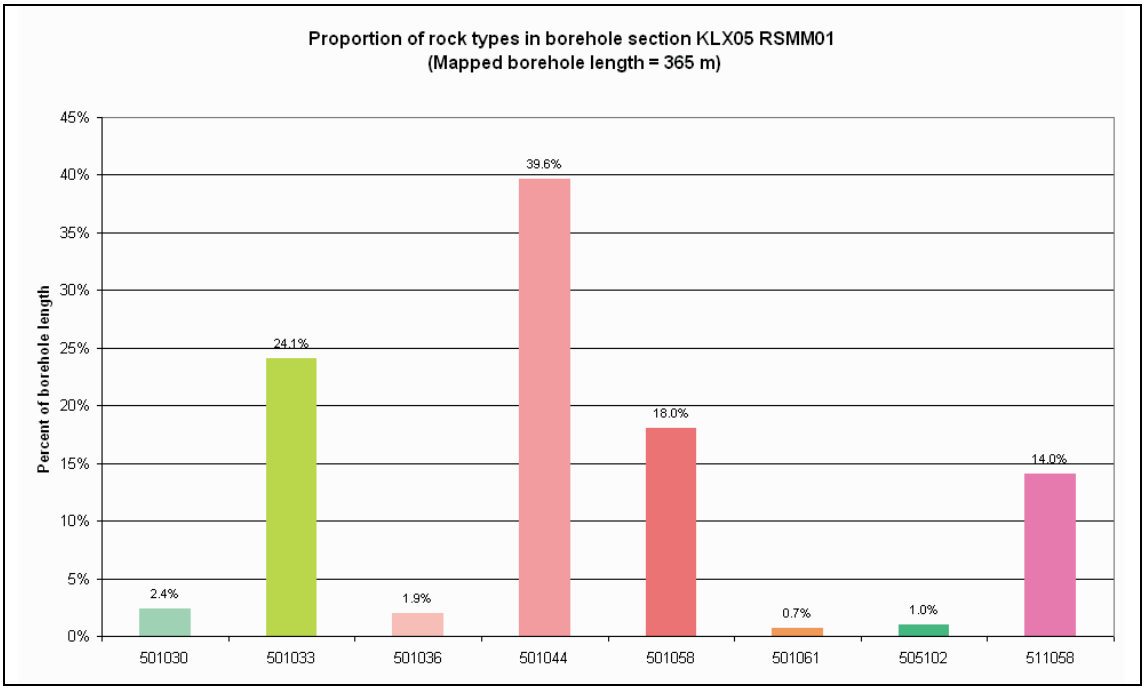
Proportion of rock types in borehole section KLX05 RSMM01
(Mapped borehole length = 365 m)
Percent of borehole length
45%
40%
35%
30%
25%
20%
15%
10%
5%
0%
2.4%
24.1%
1.9%
39.6%
18.0%
0.7%
1.0%
14.0%
501030
501033
501036
501044
501058
501061
505102
511058

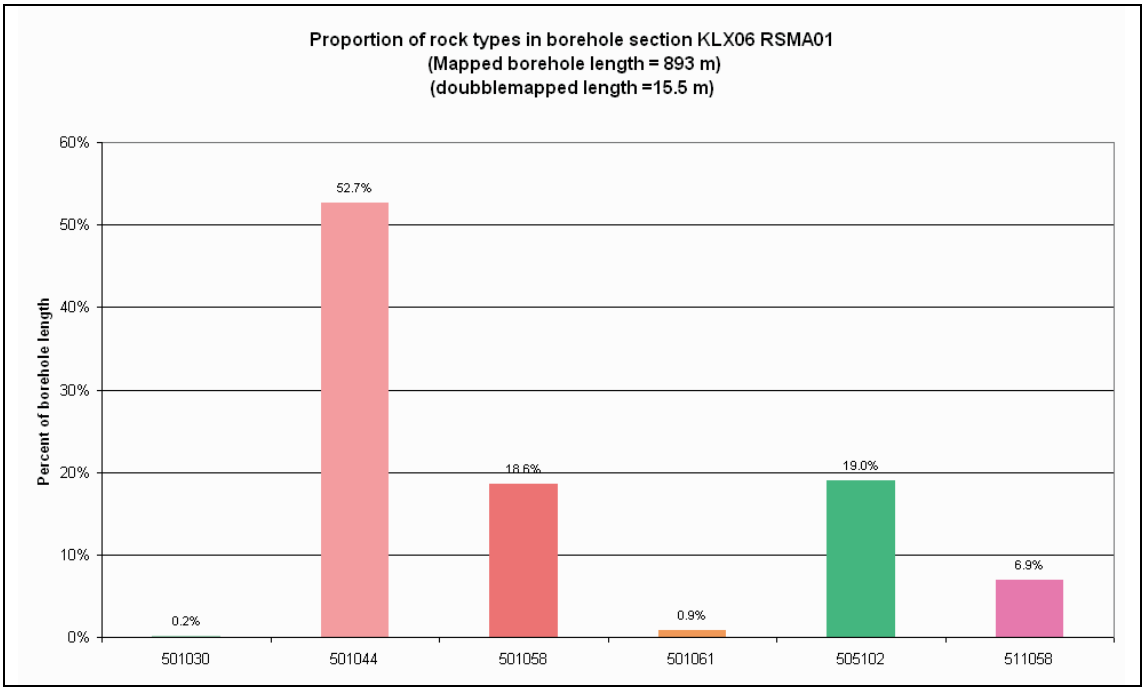
Proportion of rock types in borehole section KLX06 RSMA01
(Mapped borehole length = 893 m)
(doubblemapped length =15.5 m)
Percent of borehole length
60%
50%
40%
30%
20%
10%
0%
0.2%
52.7%
18.6%
0.9%
19.0%
6.9%
501030
501044
501058
501061
505102
511058

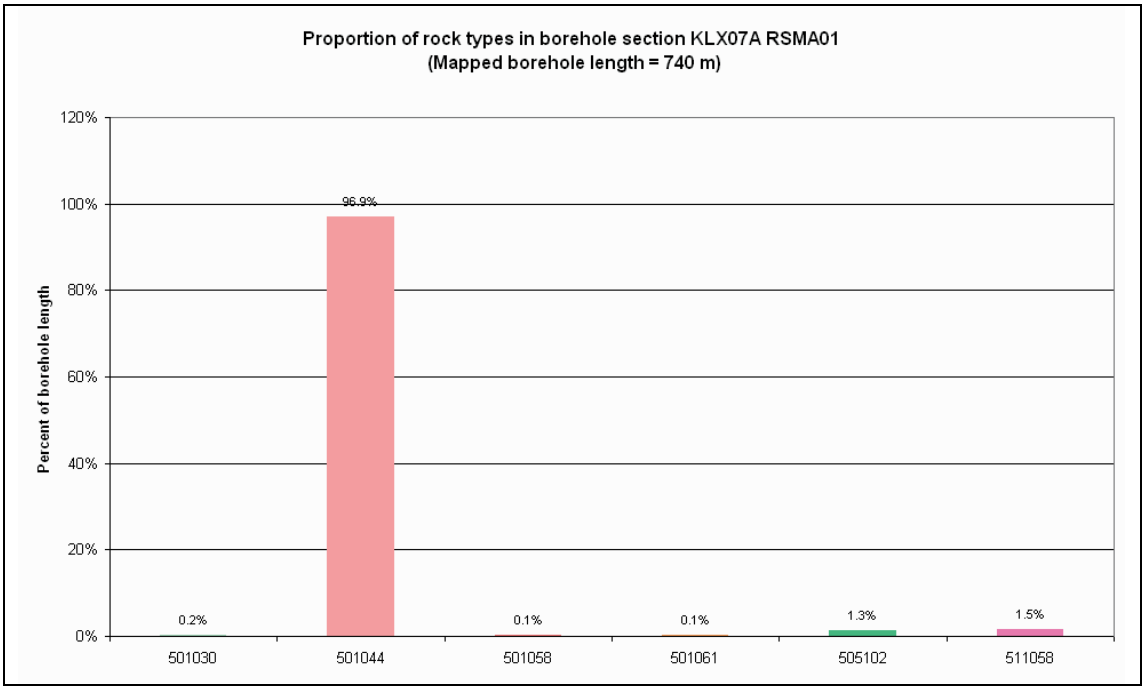
Proportion of rock types in borehole section KLX07A RSMA01
(Mapped borehole length = 740 m)
Percent of borehole length
120%
100%
80%
60%
40%
20%
0%
96.9%
0.2%
0.1%
0.1%
1.3%
1.5%
501030
501044
501058
501061
505102
511058

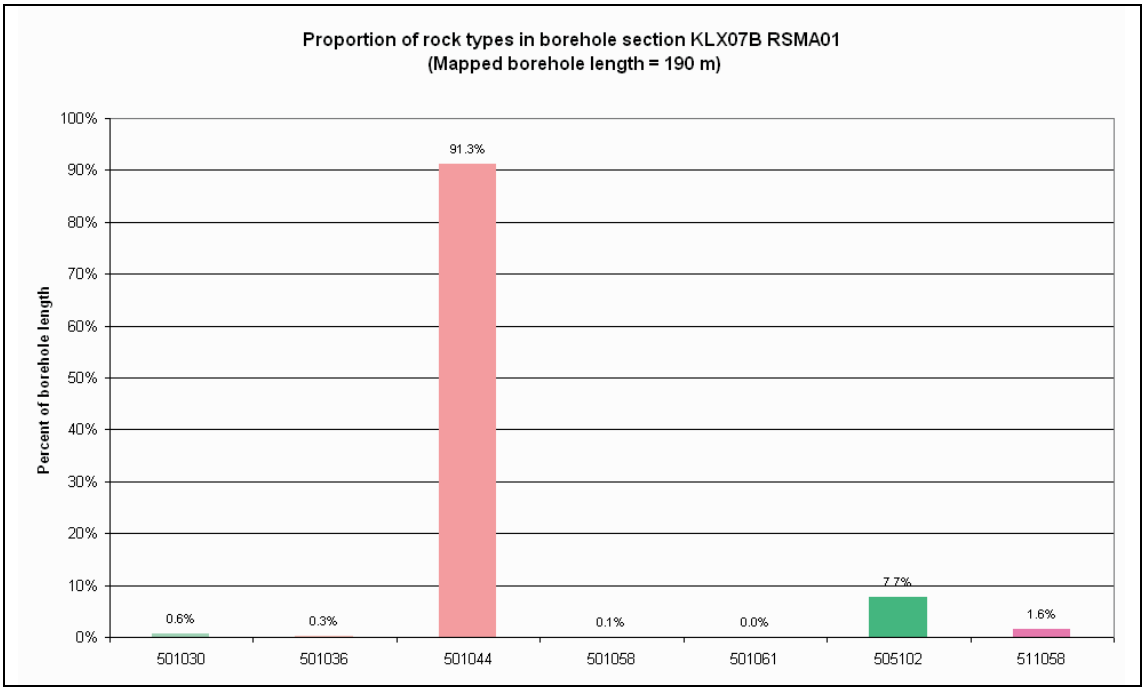
Proportion of rock types in borehole section KLX07B RSMA01
(Mapped borehole length = 190 m)
Percent of borehole length
100%
90%
80%
70%
60%
50%
40%
30%
20%
10%
0%
91.3%
0.6%
0.3%
0.1%
0.0%
7.7%
1.6%
501030
501036
501044
501058
501061
505102
511058

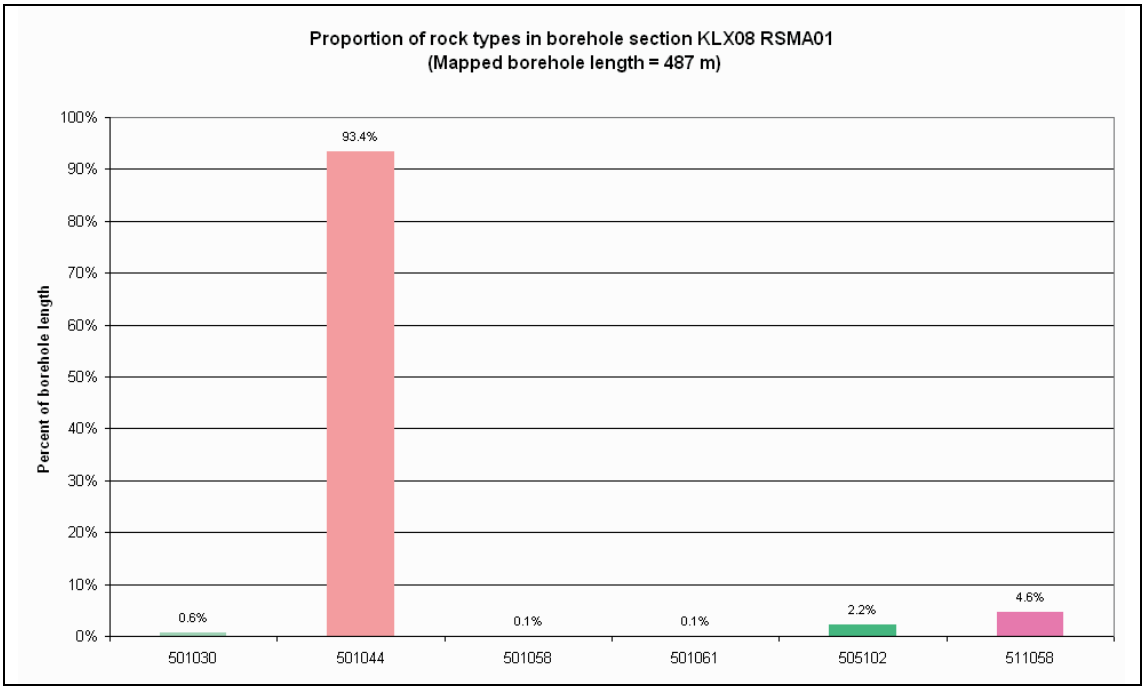
Proportion of rock types in borehole section KLX08 RSMA01
(Mapped borehole length = 487 m)
Percent of borehole length
100%
90%
80%
70%
60%
50%
40%
30%
20%
10%
0%
93.4%
0.6%
0.1%
0.1%
2.2%
4.6%
501030
501044
501058
501061
505102
511058

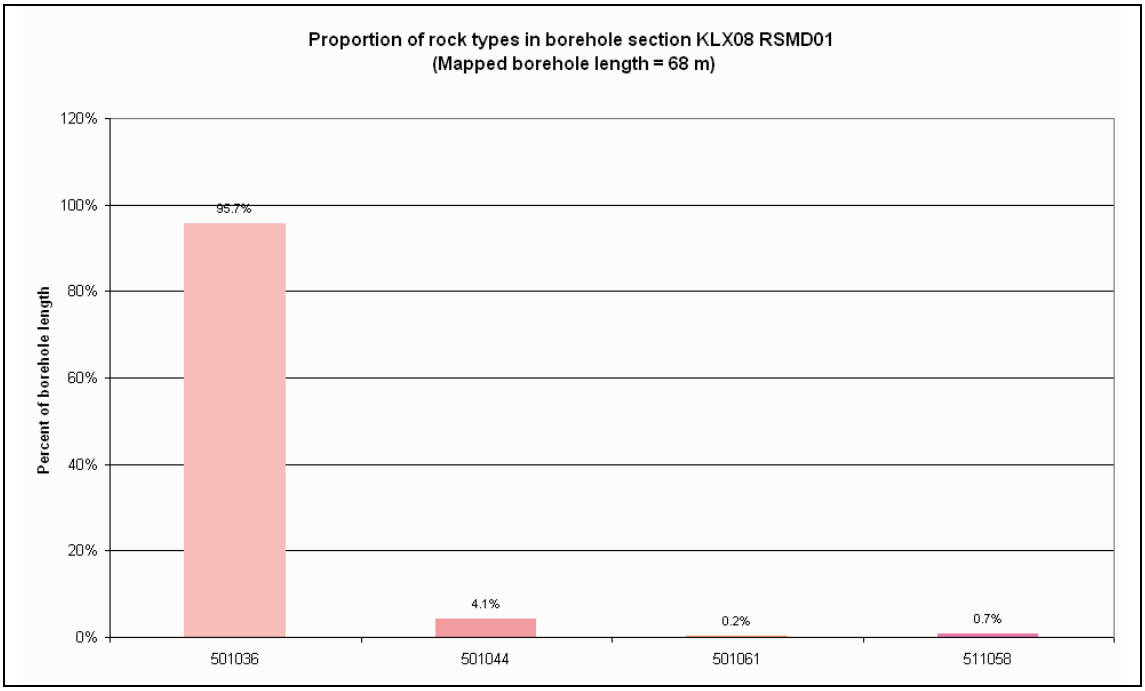
Proportion of rock types in borehole section KLX08 RSMD01
(Mapped borehole length = 68 m)
Percent of borehole length
120%
100%
80%
60%
40%
20%
0%
95.7%
4.1%
0.2%
0.7%
501036
501044
501061
511058

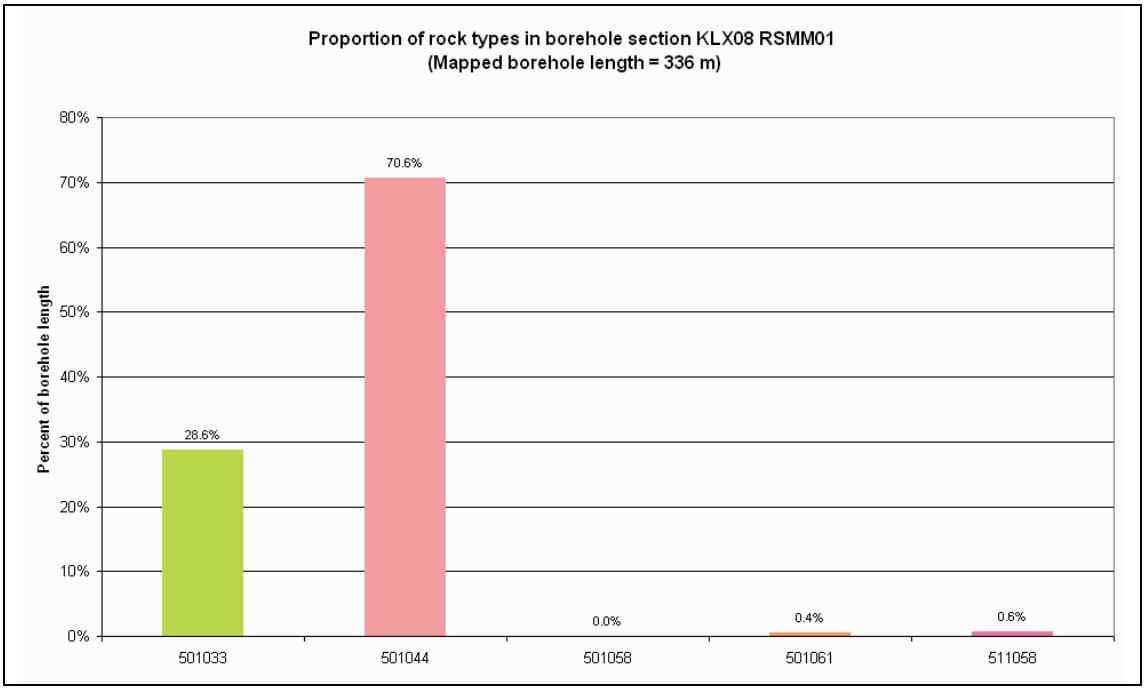
Proportion of rock types in borehole section KLX08 RSMM01
(Mapped borehole length = 336 m)
Percent of borehole length
80%
70%
60%
50%
40%
30%
20%
10%
0%
28.6%
70.6%
0.0%
0.4%
0.6%
501033
501044
501058
501061
511058

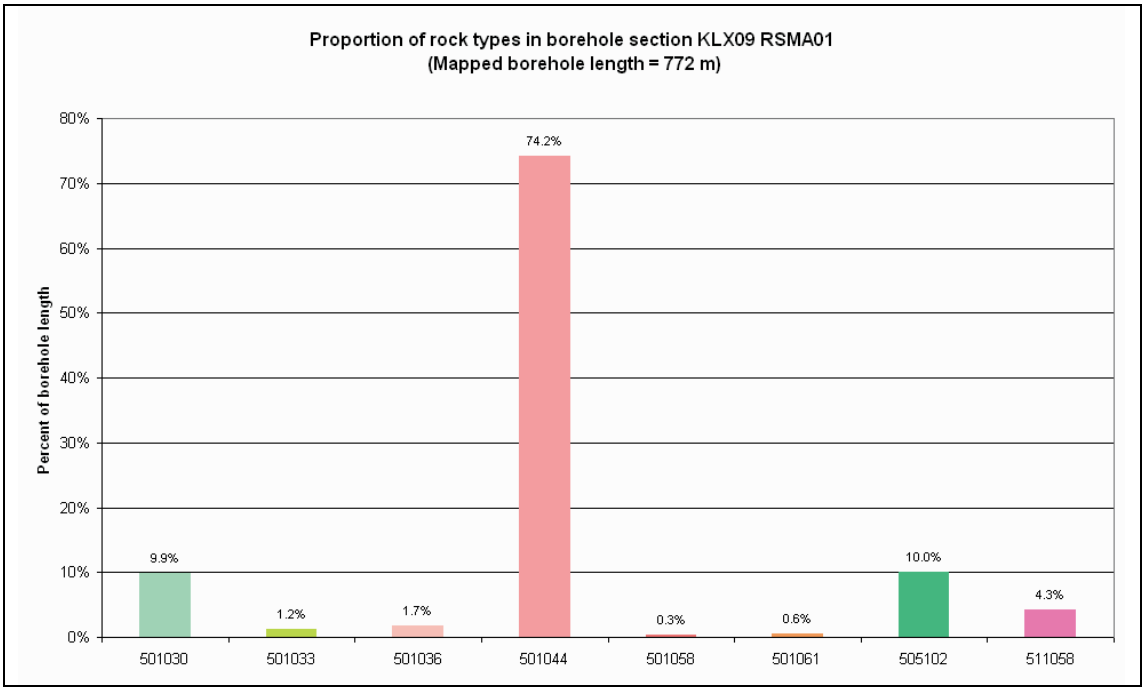
Proportion of rock types in borehole section KLX09 RSMA01
(Mapped borehole length = 772 m)
Percent of borehole length
80%
70%
60%
50%
40%
30%
20%
10%
0%
9.9%
1.2%
1.7%
74.2%
0.3%
0.6%
10.0%
4.3%
501030
501033
501036
501044
501058
501061
505102
511058

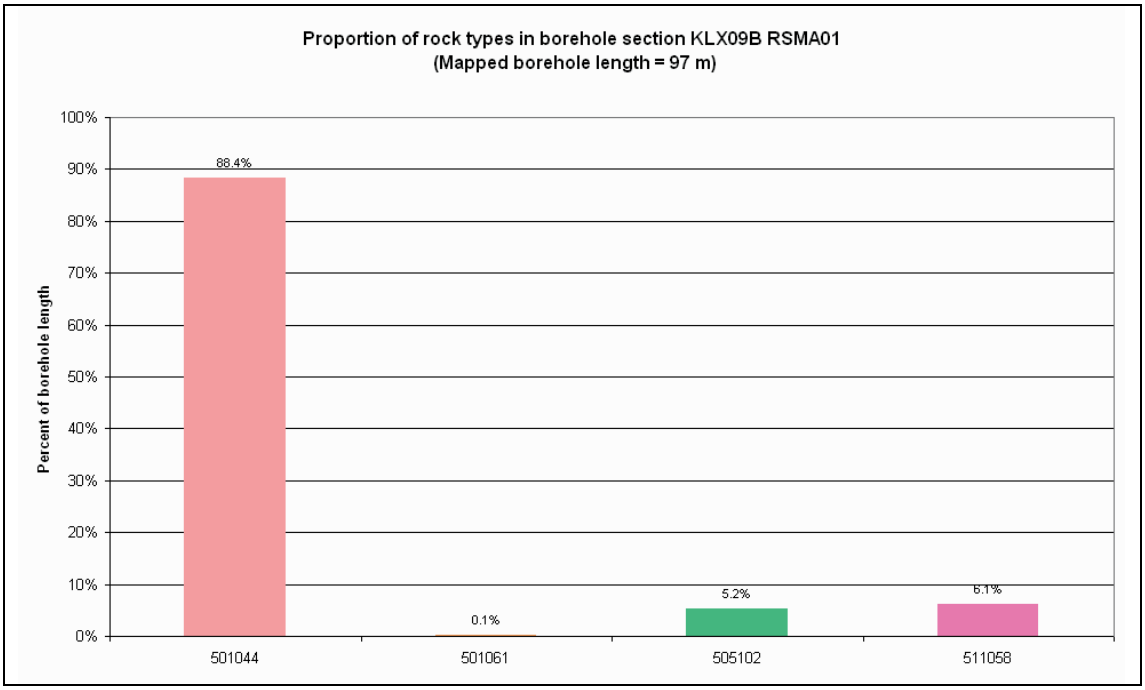
Proportion of rock types in borehole section KLX09B RSMA01
(Mapped borehole length = 97 m)
Percent of borehole length
100%
90%
80%
70%
60%
50%
40%
30%
20%
10%
0%
88.4%
0.1%
5.2%
6.1%
501044
501061
505102
511058

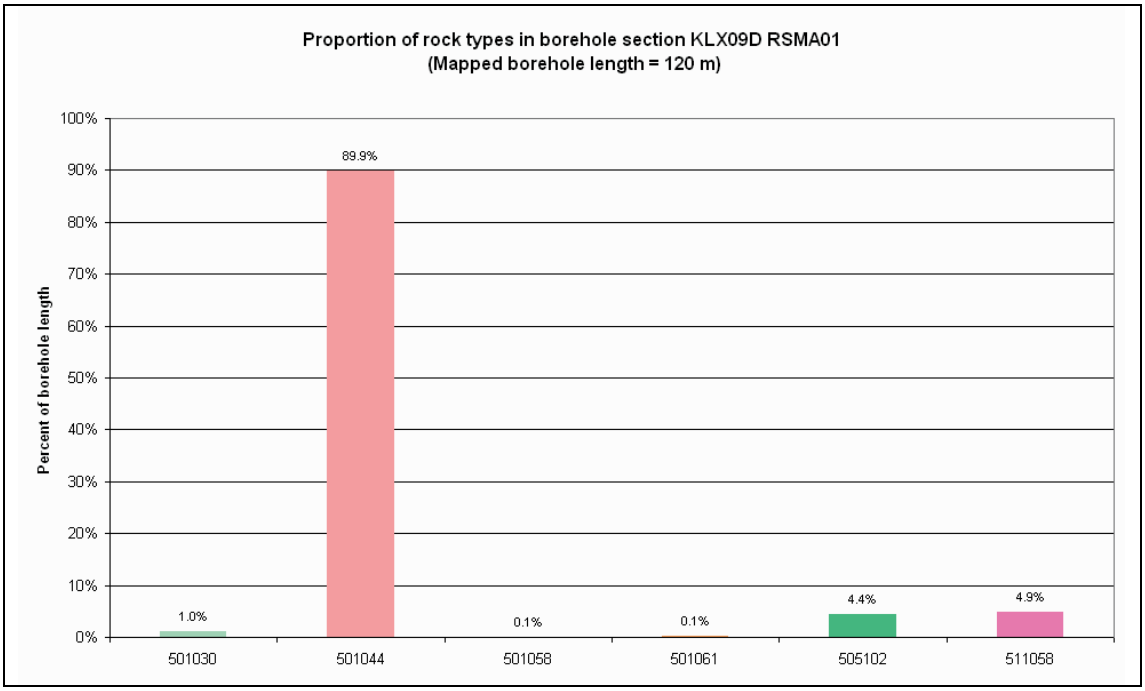
Proportion of rock types in borehole section KLX09D RSMA01
(Mapped borehole length = 120 m)
Percent of borehole length
100%
90%
80%
70%
60%
50%
40%
30%
20%
10%
0%
1.0%
89.9%
0.1%
0.1%
4.4%
4.9%
501030
501044
501058
501061
505102
511058

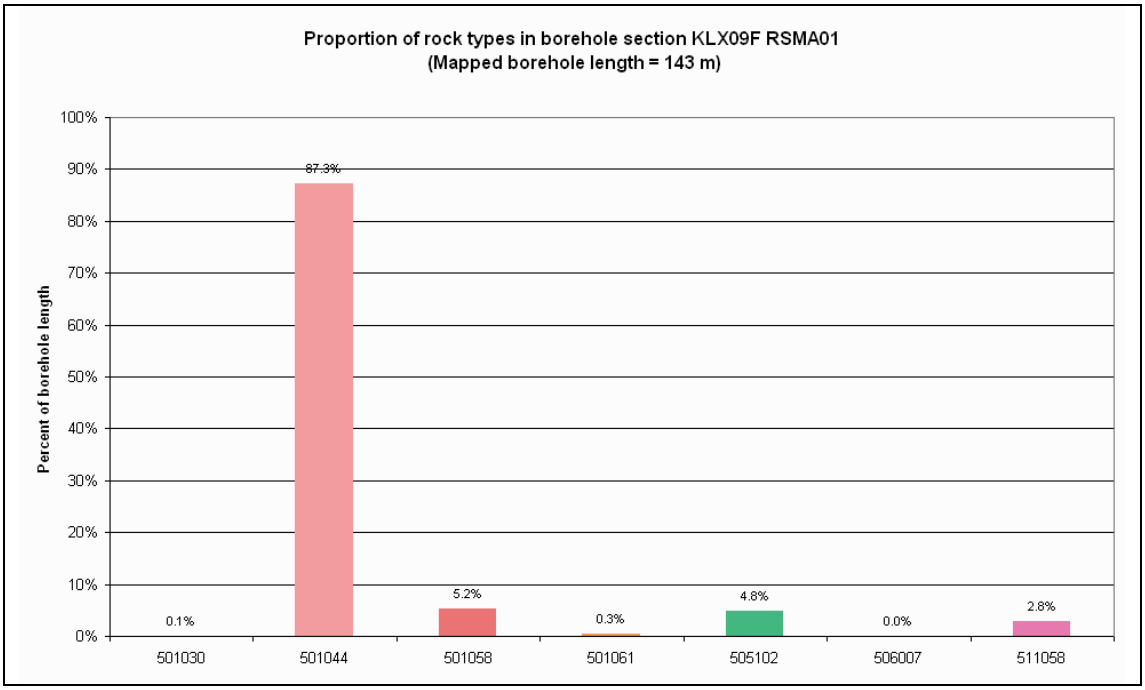
Proportion of rock types in borehole section KLX09F RSMA01
(Mapped borehole length = 143 m)
Percent of borehole length
100%
90%
80%
70%
60%
50%
40%
30%
20%
10%
0%
87.3%
0.1%
5.2%
0.3%
4.8%
0.0%
2.8%
501030
501044
501058
501061
505102
506007
511058

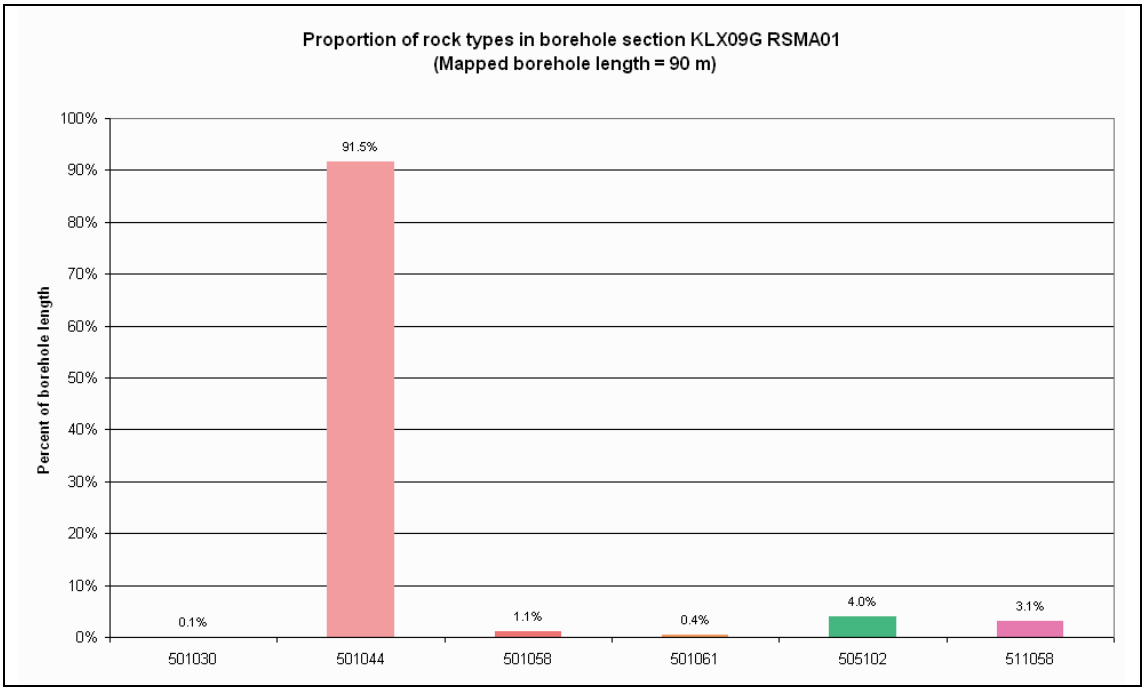
Proportion of rock types in borehole section KLX09G RSMA01
(Mapped borehole length = 90 m)
Percent of borehole length
100%
90%
80%
70%
60%
50%
40%
30%
20%
10%
0%
91.5%
0.1%
1.1%
0.4%
4.0%
3.1%
501030
501044
501058
501061
505102
511058

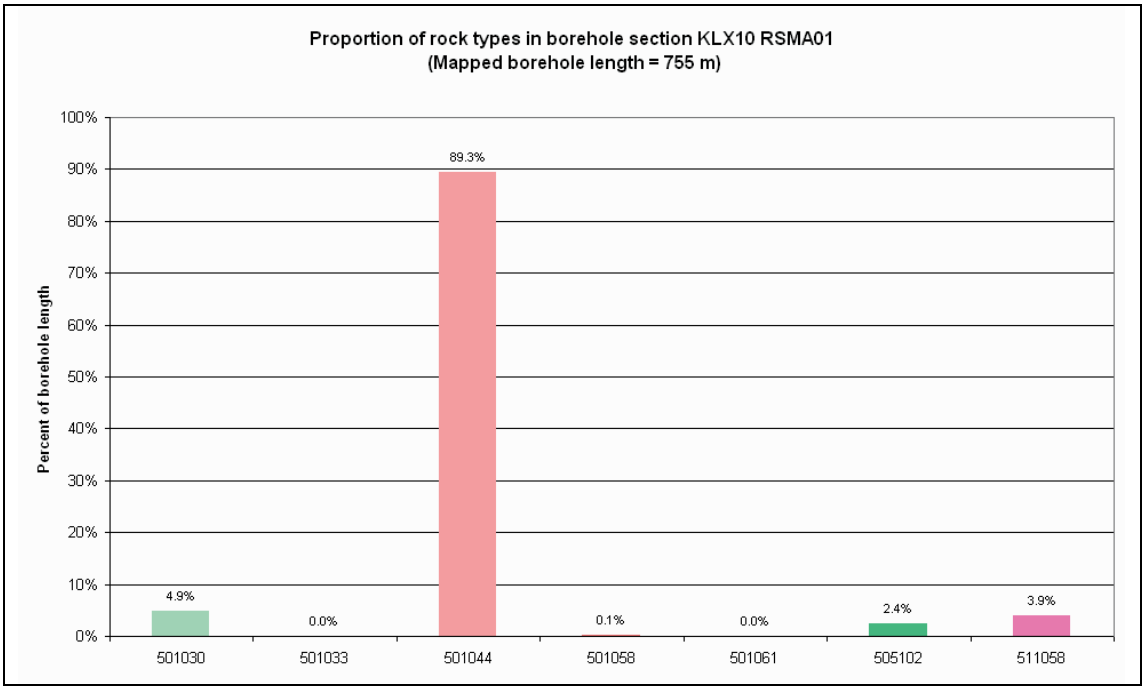
Proportion of rock types in borehole section KLX10 RSMA01
(Mapped borehole length = 755 m)
Percent of borehole length
100%
90%
80%
70%
60%
50%
40%
30%
20%
10%
0%
89.3%
4.9%
0.0%
0.1%
0.0%
2.4%
3.9%
501030
501033
501044
501058
501061
505102
511058

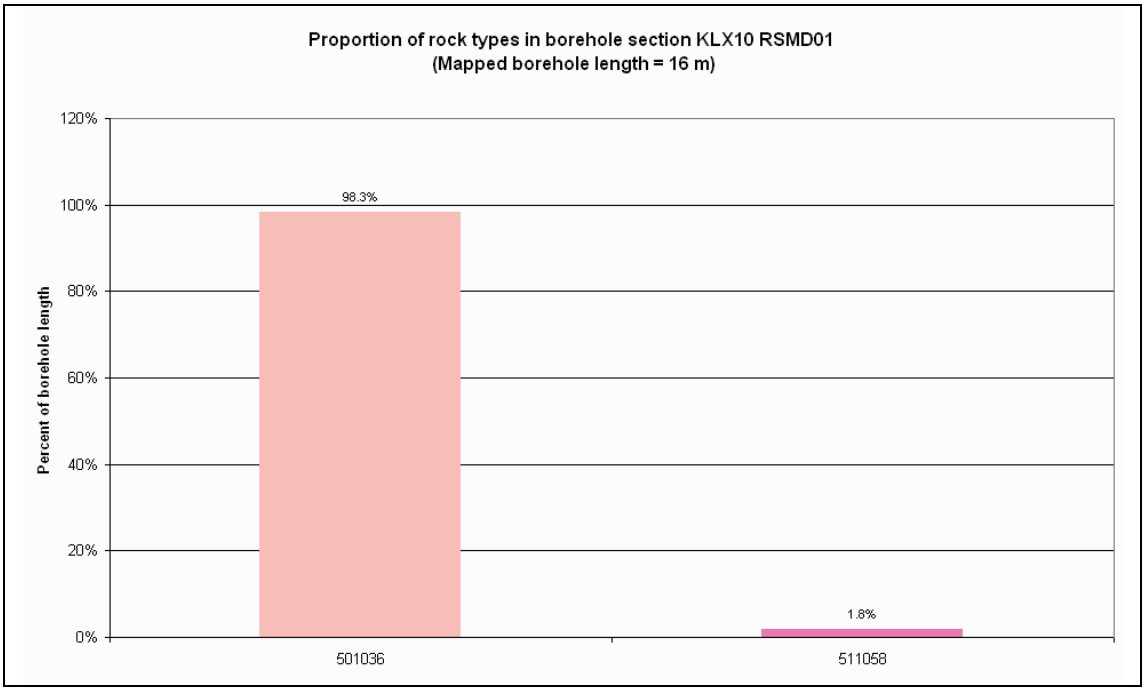
Proportion of rock types in borehole section KLX10 RSMD01
(Mapped borehole length = 16 m)
Percent of borehole length
120%
100%
80%
60%
40%
20%
0%
98.3%
1.8%
501036
511058

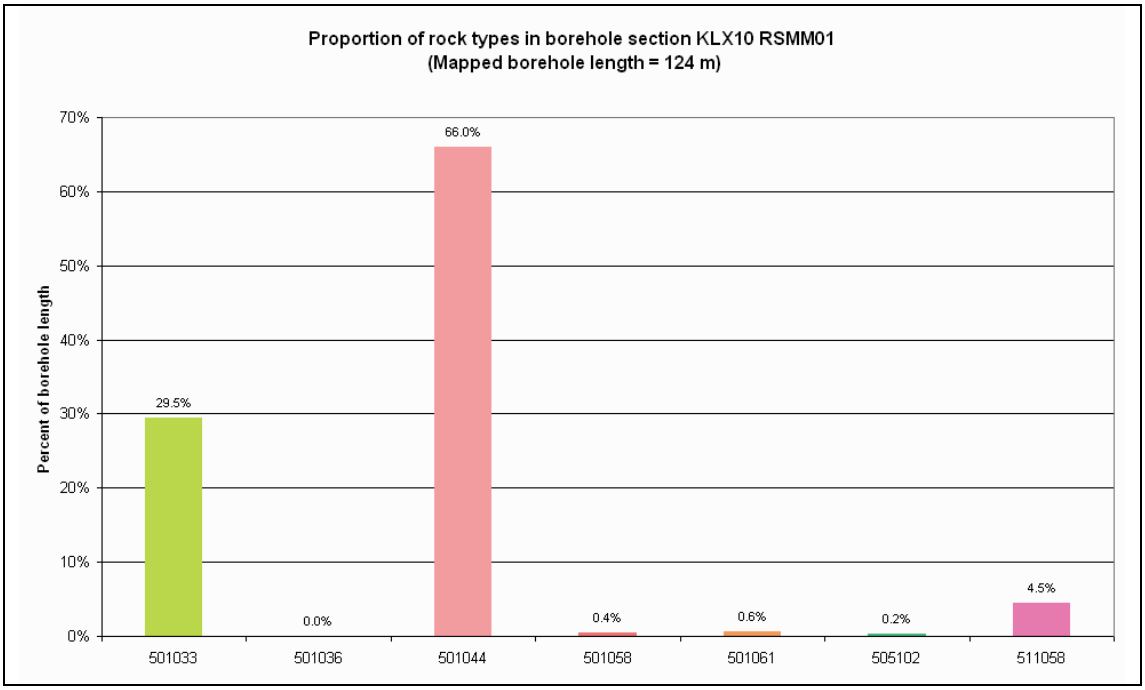
Proportion of rock types in borehole section KLX10 RSMM01
(Mapped borehole length = 124 m)
Percent of borehole length
70%
60%
50%
40%
30%
20%
10%
0%
29.5%
0.0%
66.0%
0.4%
0.6%
0.2%
4.5%
501033
501036
501044
501058
501061
505102
511058

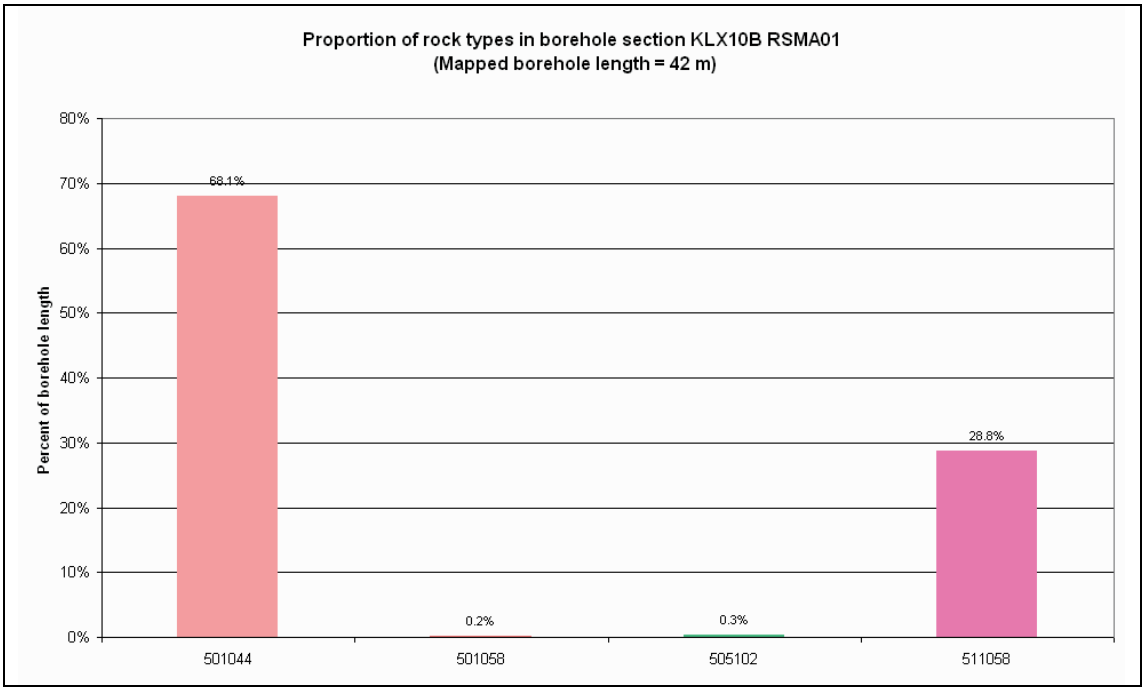
Proportion of rock types in borehole section KLX10B RSMA01
(Mapped borehole length = 42 m)
Percent of borehole length
80%
70%
60%
50%
40%
30%
20%
10%
0%
68.1%
0.2%
0.3%
28.8%
501044
501058
505102
511058

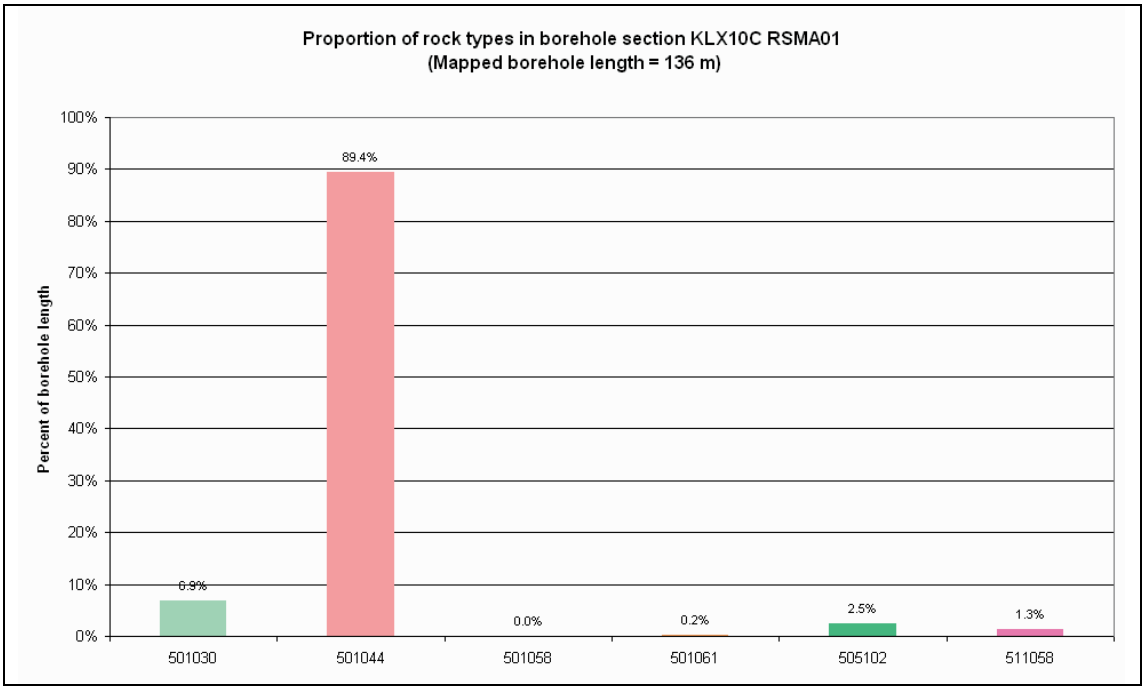
Proportion of rock types in borehole section KLX10C RSMA01
(Mapped borehole length = 136 m)
Percent of borehole length
100%
90%
80%
70%
60%
50%
40%
30%
20%
10%
0%
6.9%
89.4%
0.0%
0.2%
2.5%
1.3%
501030
501044
501058
501061
505102
511058

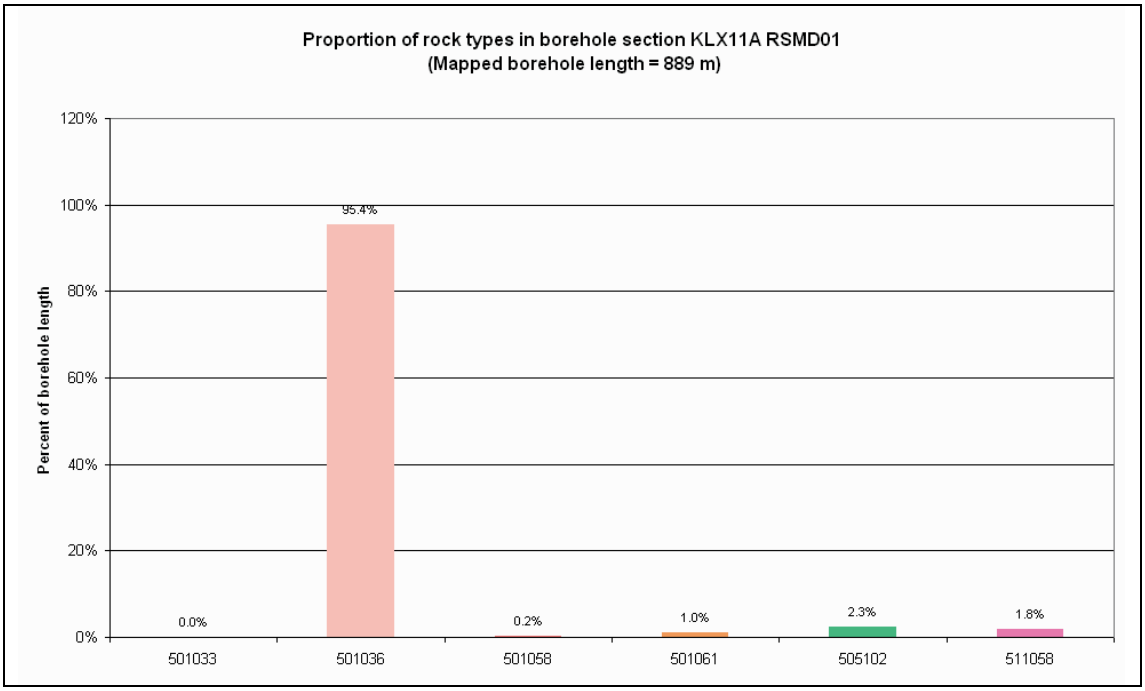
Proportion of rock types in borehole section KLX11A RSMD01
(Mapped borehole length = 889 m)
Percent of borehole length
120%
100%
80%
60%
40%
20%
0%
0.0%
95.4%
0.2%
1.0%
2.3%
1.8%
501033
501036
501058
501061
505102
511058

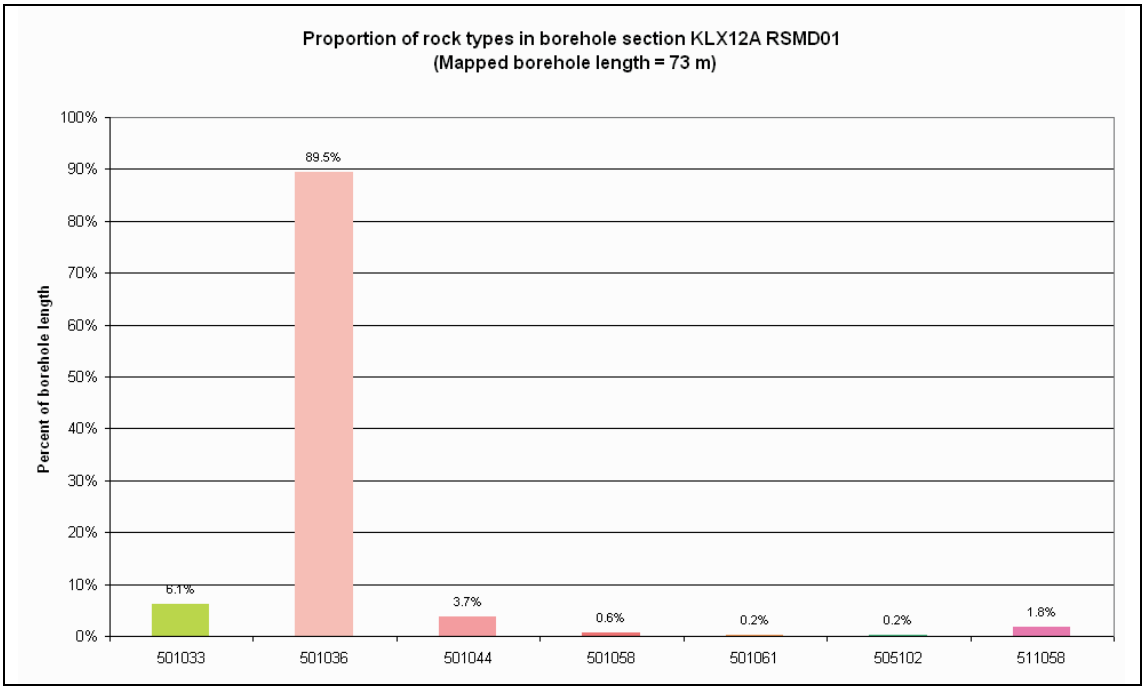
Proportion of rock types in borehole section KLX12A RSMD01
(Mapped borehole length = 73 m)
Percent of borehole length
100%
90%
80%
70%
60%
50%
40%
30%
20%
10%
0%
6.1%
89.5%
3.7%
0.6%
0.2%
0.2%
1.8%
501033
501036
501044
501058
501061
505102
511058

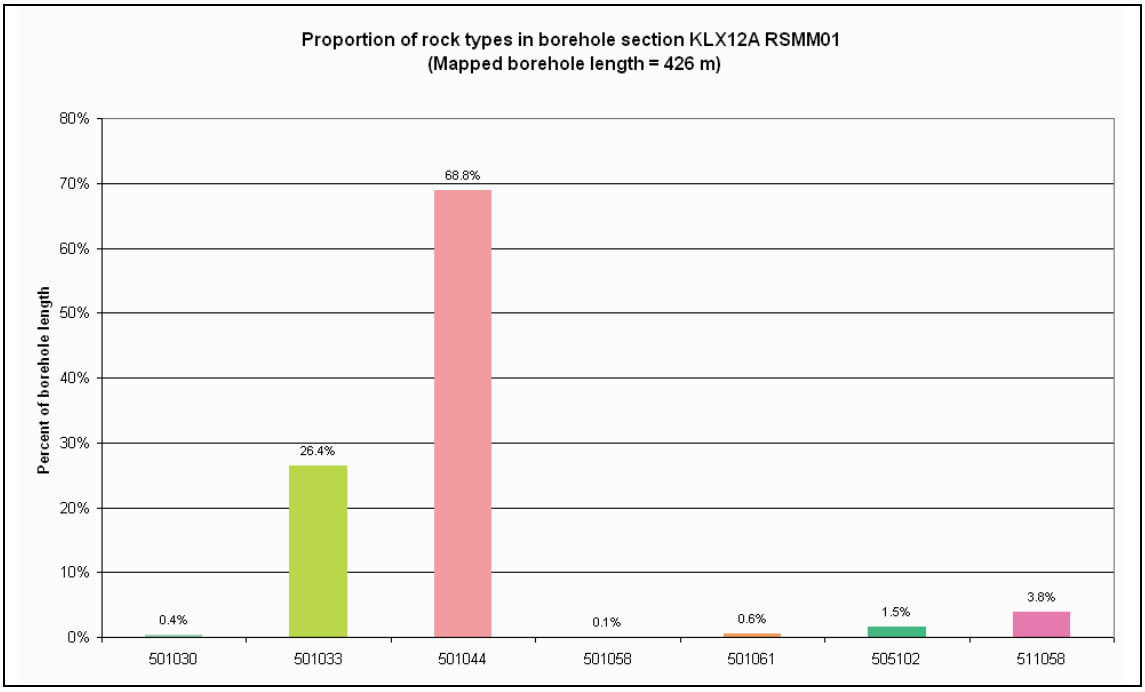
Proportion of rock types in borehole section KLX12A RSMM01
(Mapped borehole length = 426 m)
Percent of borehole length
80%
70%
60%
50%
40%
30%
20%
10%
0%
0.4%
26.4%
68.8%
0.1%
0.6%
1.5%
3.8%
501030
501033
501044
501058
501061
505102
511058

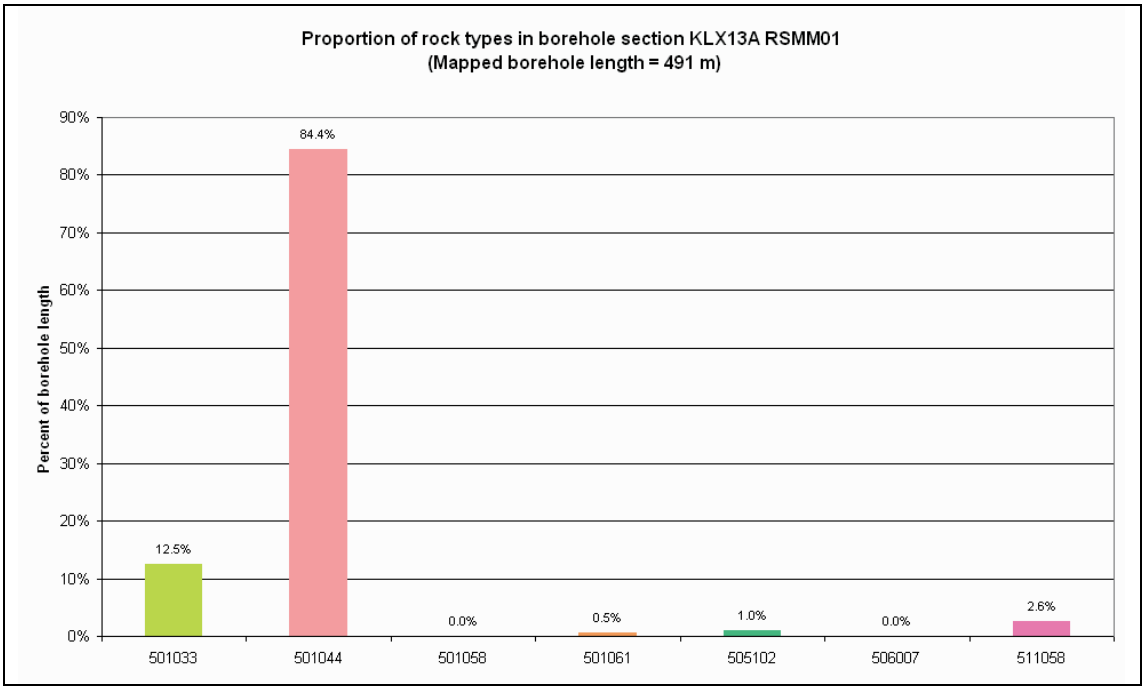
Proportion of rock types in borehole section KLX13A RSMM01
(Mapped borehole length = 491 m)
Percent of borehole length
90%
80%
70%
60%
50%
40%
30%
20%
10%
0%
84.4%
12.5%
0.0%
0.5%
1.0%
0.0%
2.6%
501033
501044
501058
501061
505102
506007
511058

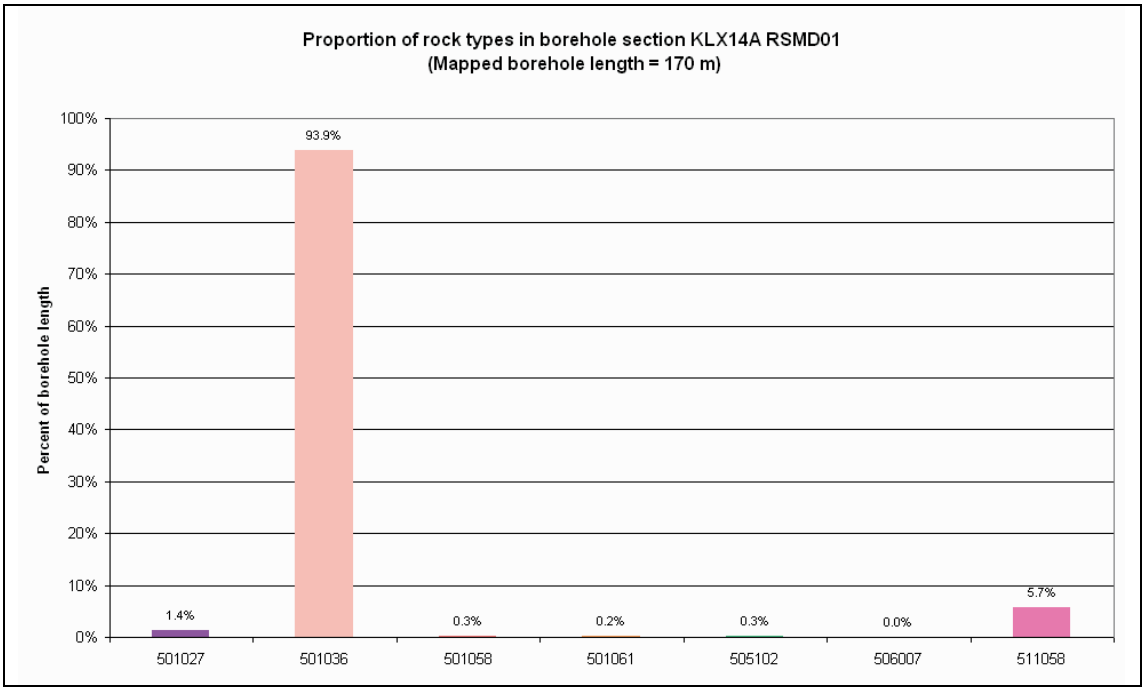
Proportion of rock types in borehole section KLX14A RSMD01
(Mapped borehole length = 170 m)
Percent of borehole length
100%
90%
80%
70%
60%
50%
40%
30%
20%
10%
0%
93.9%
1.4%
0.3%
0.2%
0.3%
0.0%
5.7%
501027
501036
501058
501061
505102
506007
511058

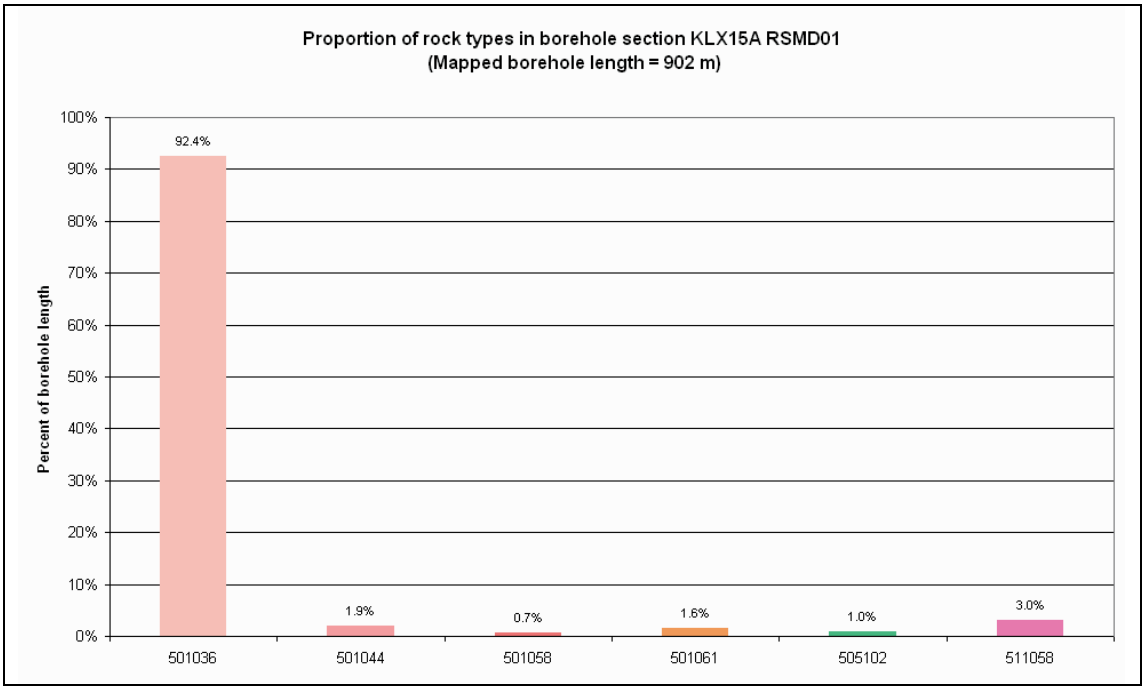
Proportion of rock types in borehole section KLX15A RSMD01
(Mapped borehole length = 902 m)
Percent of borehole length
100%
90%
80%
70%
60%
50%
40%
30%
20%
10%
0%
92.4%
1.9%
0.7%
1.6%
1.0%
3.0%
501036
501044
501058
501061
505102
511058

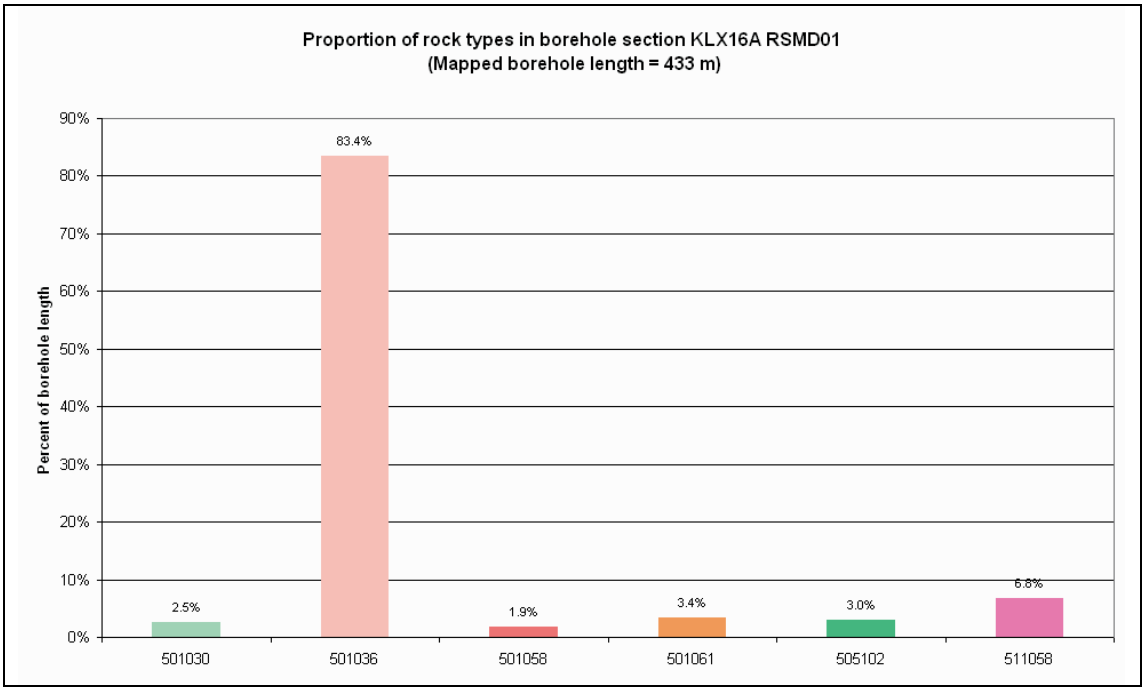
Proportion of rock types in borehole section KLX16A RSMD01
(Mapped borehole length = 433 m)
Percent of borehole length
90%
80%
70%
60%
50%
40%
30%
20%
10%
0%
2.5%
83.4%
1.9%
3.4%
3.0%
6.8%
501030
501036
501058
501061
505102
511058

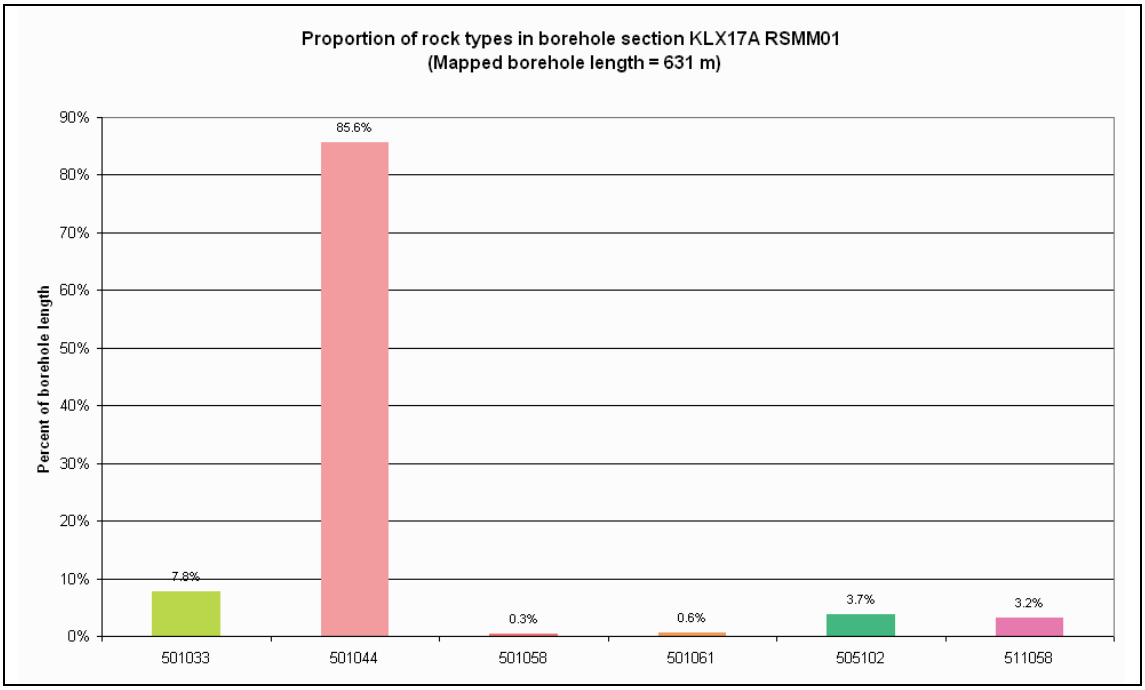
Proportion of rock types in borehole section KLX17A RSMM01
(Mapped borehole length = 631 m)
Percent of borehole length
90%
80%
70%
60%
50%
40%
30%
20%
10%
0%
7.8%
85.6%
0.3%
0.6%
3.7%
3.2%
501033
501044
501058
501061
505102
511058

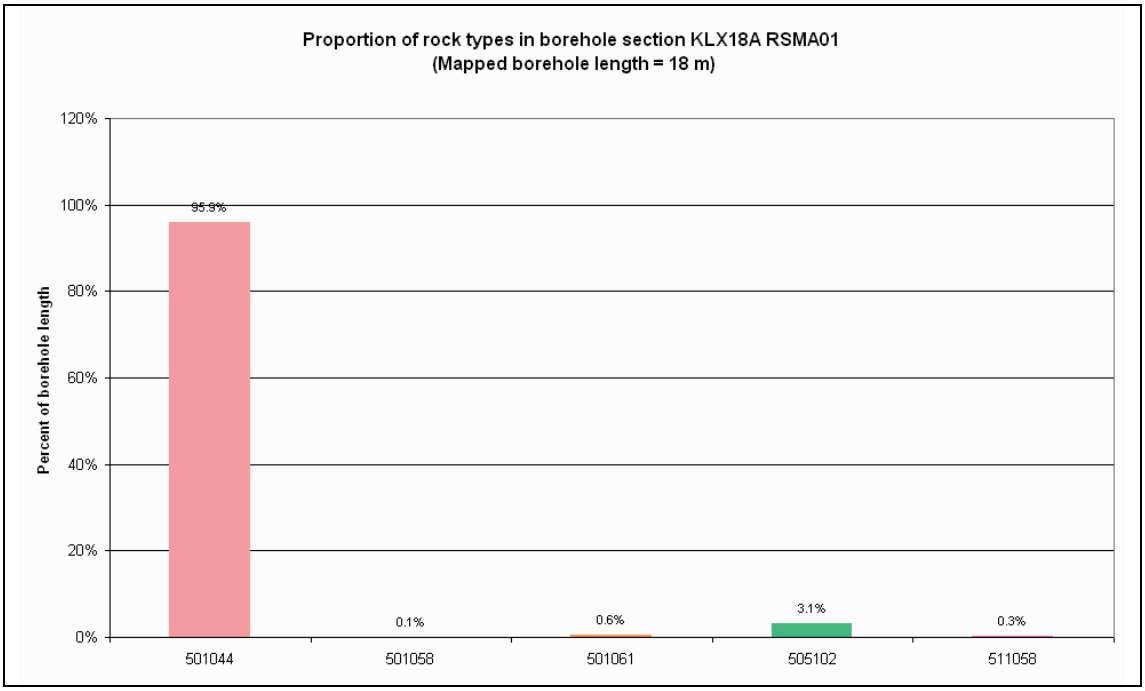
Proportion of rock types in borehole section KLX18A RSMA01
(Mapped borehole length = 18 m)
Percent of borehole length
120%
100%
80%
60%
40%
20%
0%
95.9%
0.1%
0.6%
3.1%
0.3%
501044
501058
501061
505102
511058

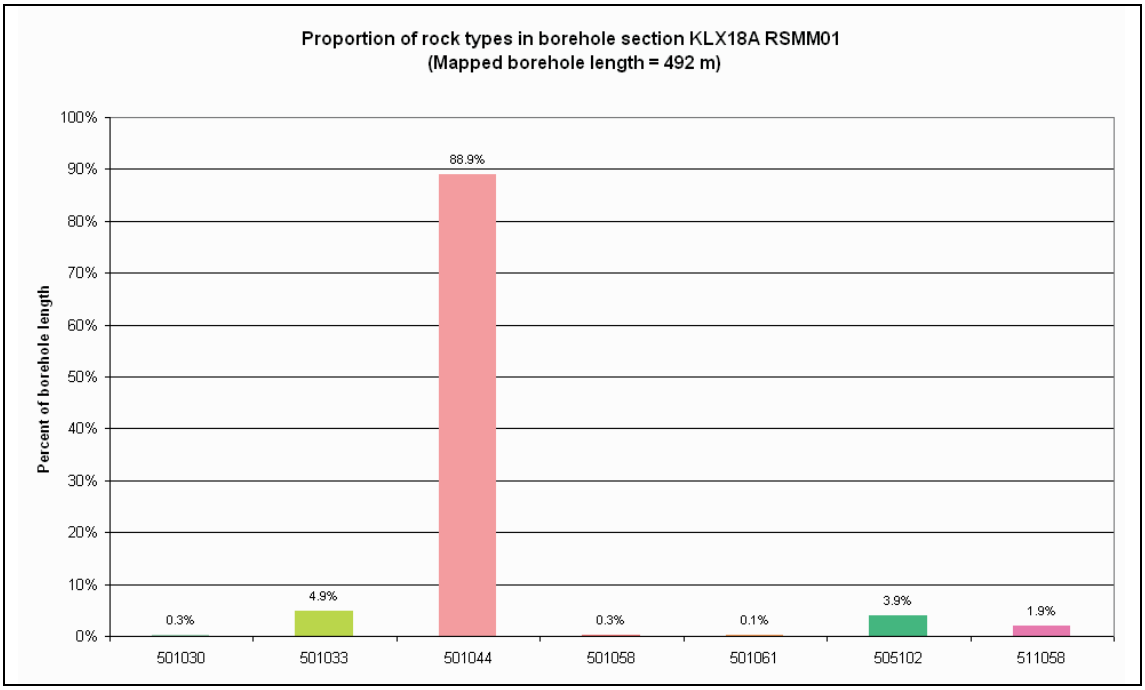
Proportion of rock types in borehole section KLX18A RSMM01
(Mapped borehole length = 492 m)
Percent of borehole length
100%
90%
80%
70%
60%
50%
40%
30%
20%
10%
0%
0.3%
4.9%
88.9%
0.3%
0.1%
3.9%
1.9%
501030
501033
501044
501058
501061
505102
511058

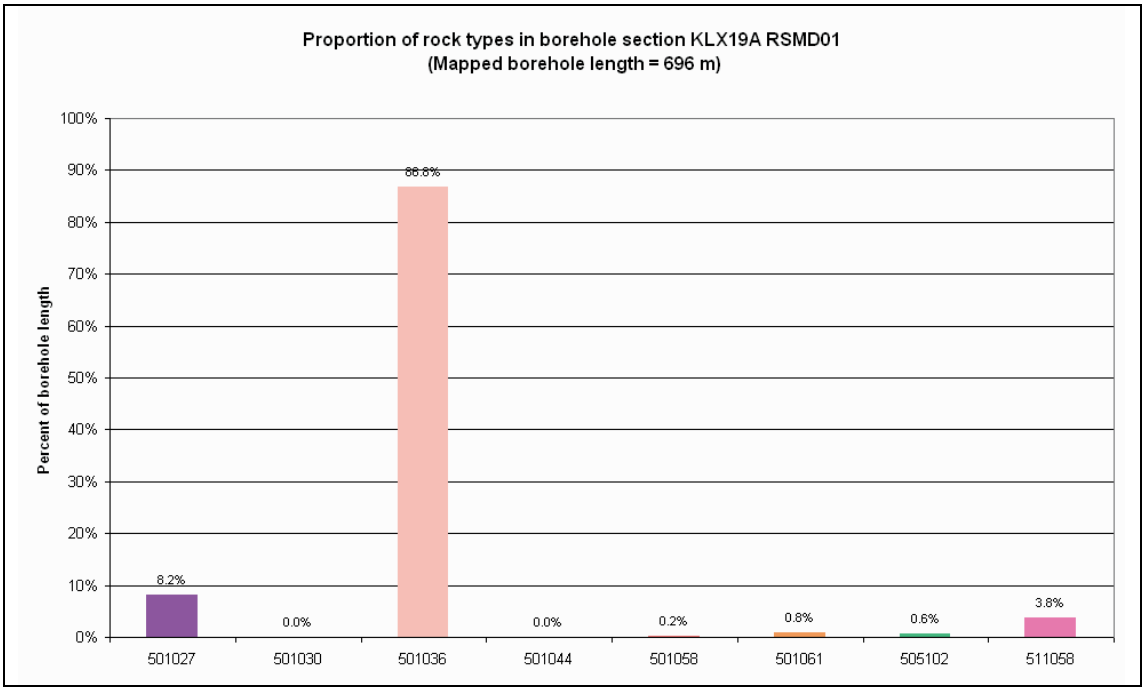
Proportion of rock types in borehole section KLX19A RSMD01
(Mapped borehole length = 696 m)
Percent of borehole length
100%
90%
80%
70%
60%
50%
40%
30%
20%
10%
0%
8.2%
0.0%
86.8%
0.0%
0.2%
0.8%
0.6%
3.8%
501027
501030
501036
501044
501058
501061
505102
511058

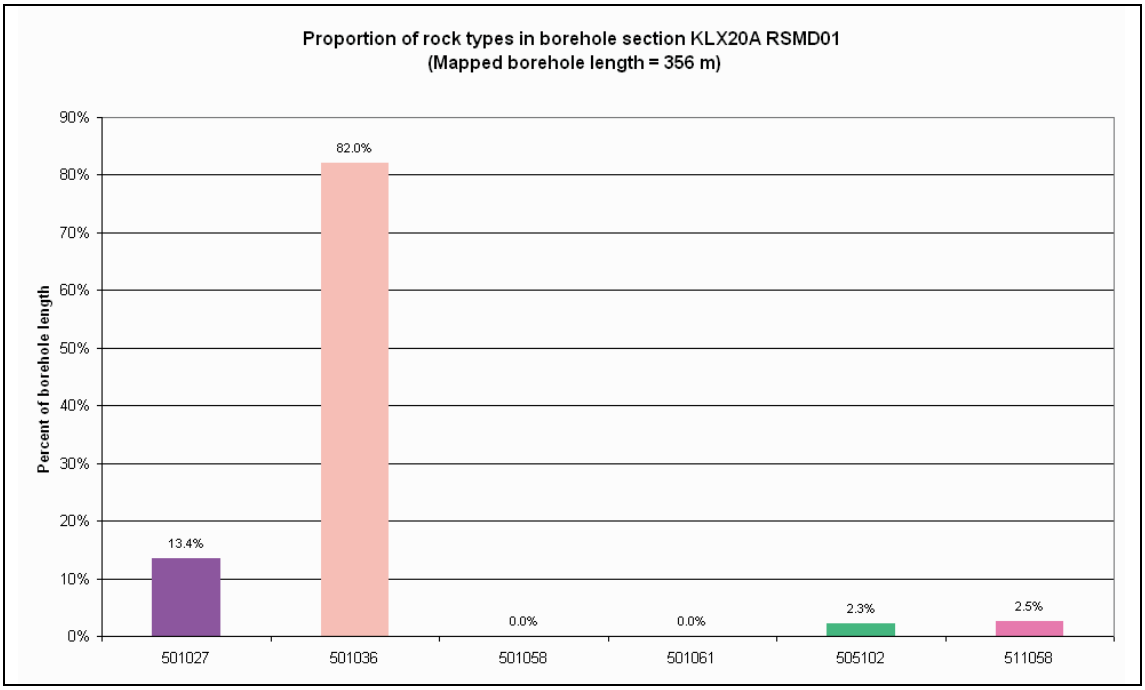
Proportion of rock types in borehole section KLX20A RSMD01
(Mapped borehole length = 356 m)
Percent of borehole length
90%
80%
70%
60%
50%
40%
30%
20%
10%
0%
13.4%
82.0%
0.0%
0.0%
2.3%
2.5%
501027
501036
501058
501061
505102
511058

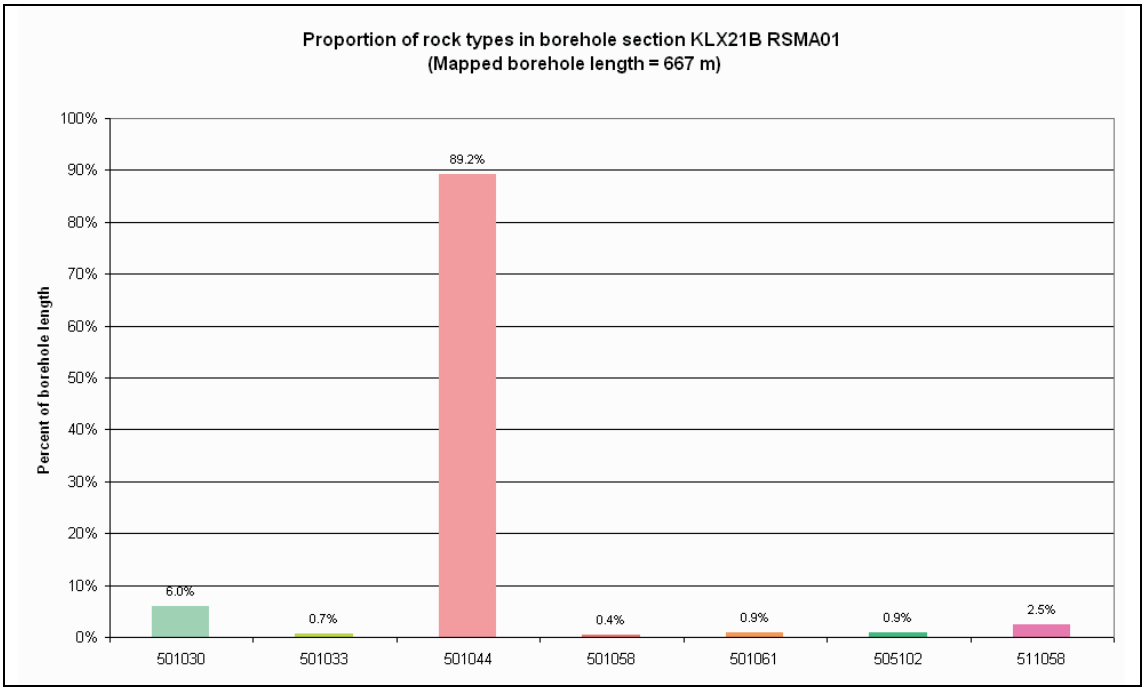
Proportion of rock types in borehole section KLX21B RSMA01
(Mapped borehole length = 667 m)
Percent of borehole length
100%
90%
80%
70%
60%
50%
40%
30%
20%
10%
0%
6.0%
0.7%
89.2%
0.4%
0.9%
0.9%
2.5%
501030
501033
501044
501058
501061
505102
511058

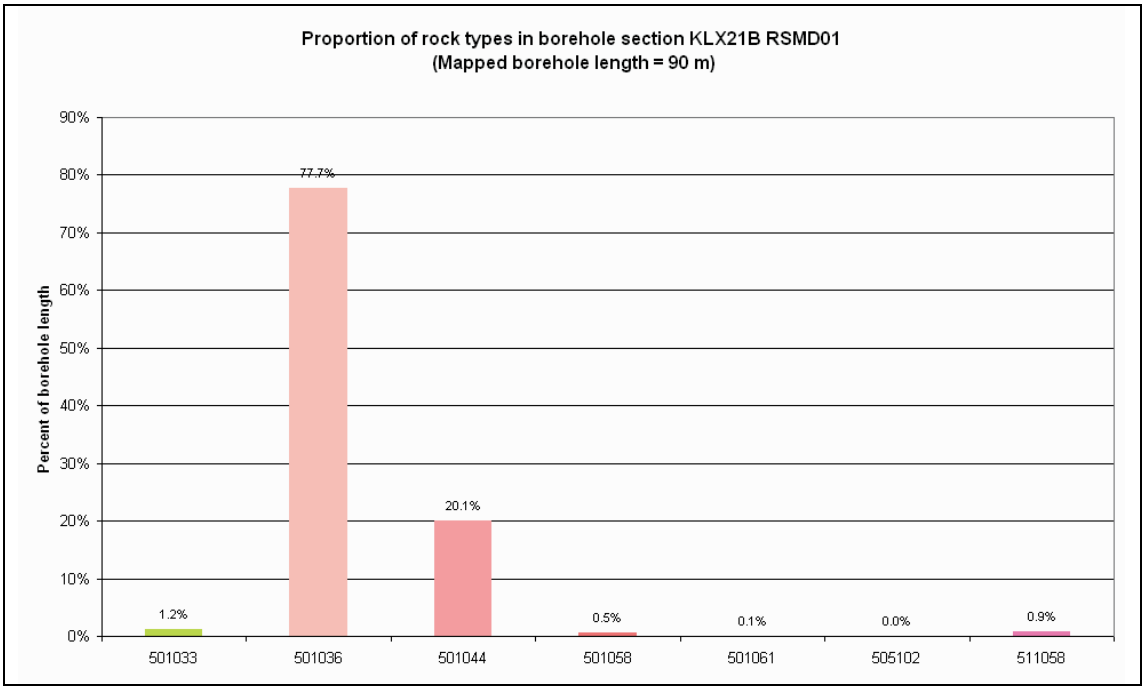
Proportion of rock types in borehole section KLX21B RSMD01
(Mapped borehole length = 90 m)
Percent of borehole length
90%
80%
70%
60%
50%
40%
30%
20%
10%
0%
77.7%
20.1%
1.2%
0.5%
0.1%
0.0%
0.9%
501033
501036
501044
501058
501061
505102
511058

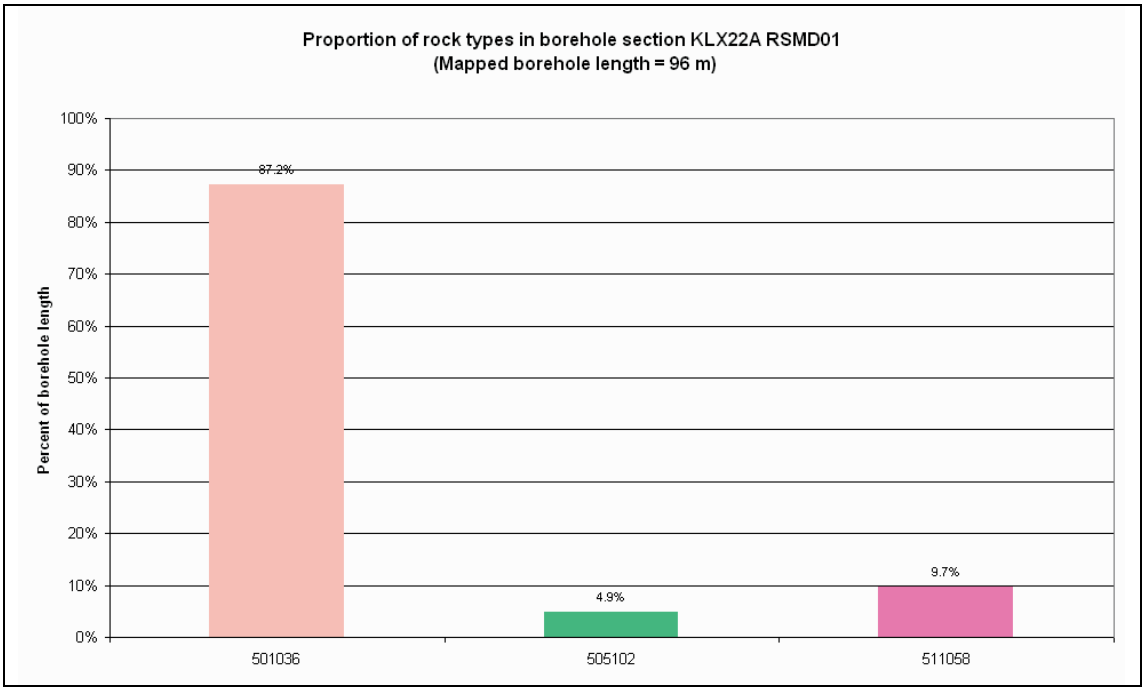
Proportion of rock types in borehole section KLX22A RSMD01
(Mapped borehole length = 96 m)
Percent of borehole length
100%
90%
80%
70%
60%
50%
40%
30%
20%
10%
0%
87.2%
4.9%
9.7%
501036
505102
511058

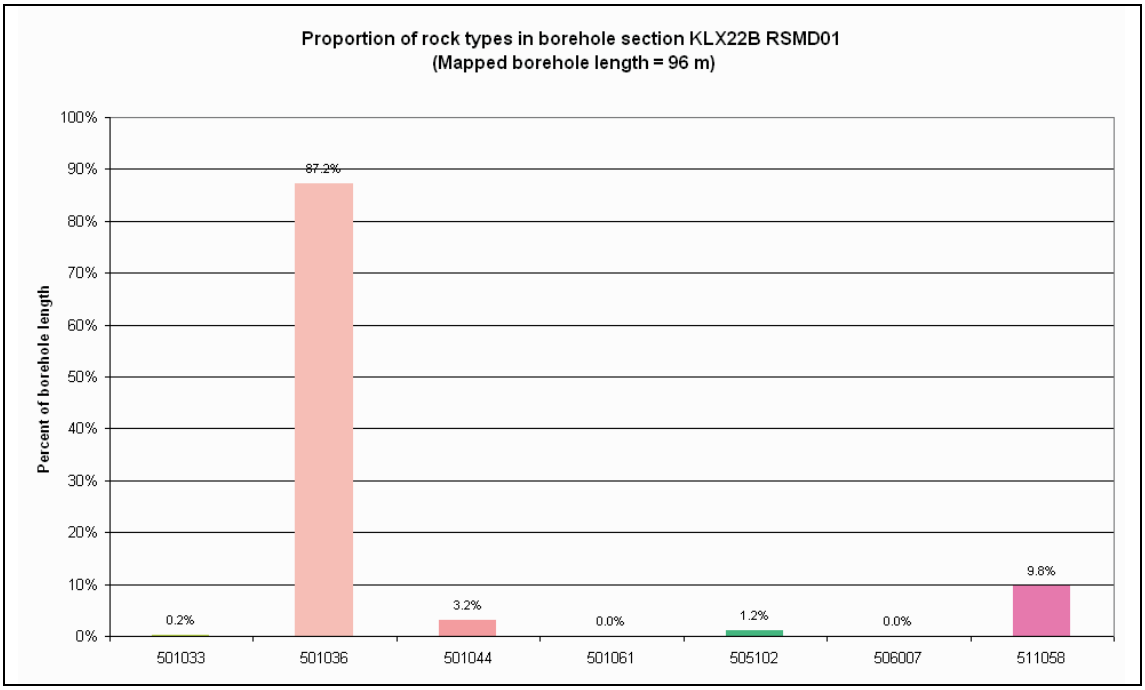
Proportion of rock types in borehole section KLX22B RSMD01
(Mapped borehole length = 96 m)
Percent of borehole length
100%
90%
80%
70%
60%
50%
40%
30%
20%
10%
0%
0.2%
87.2%
3.2%
0.0%
1.2%
0.0%
9.8%
501033
501036
501044
501061
505102
506007
511058

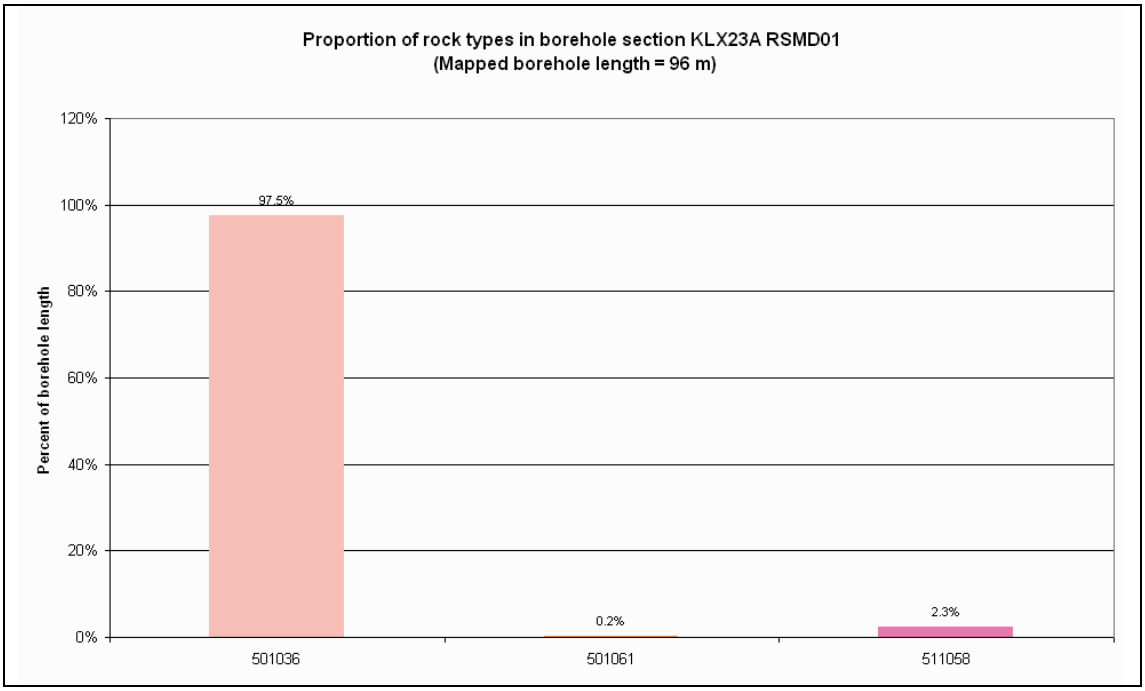
Proportion of rock types in borehole section KLX23A RSMD01
(Mapped borehole length = 96 m)
Percent of borehole length
120%
100%
80%
60%
40%
20%
0%
97.5%
0.2%
2.3%
501036
501061
511058

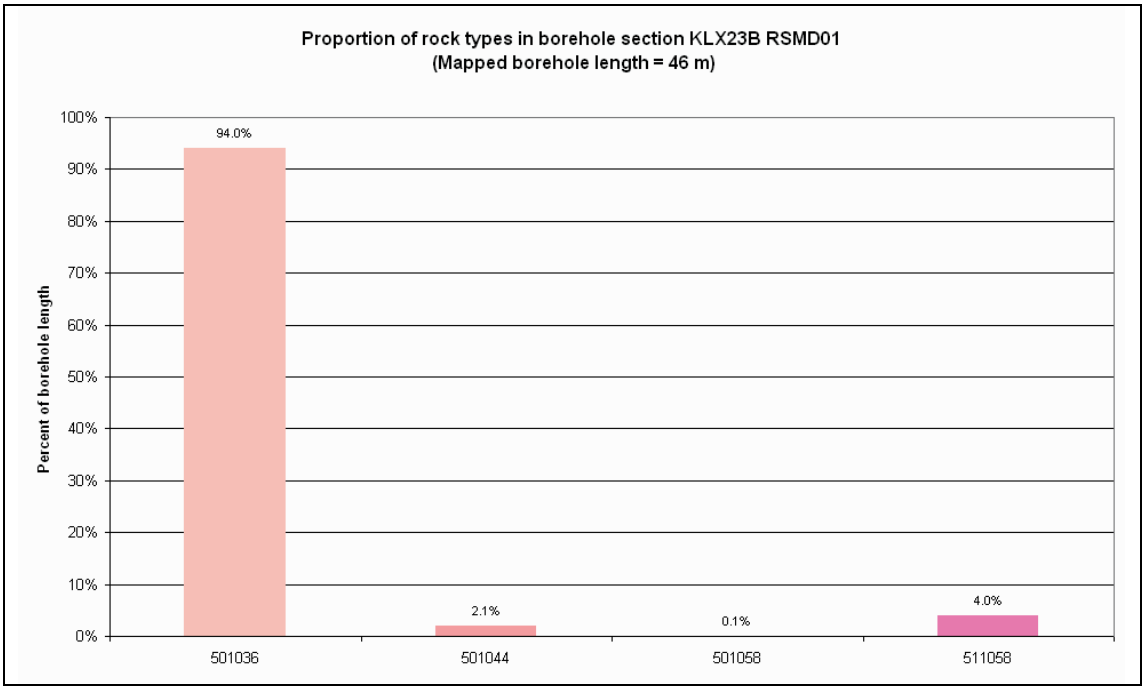
Proportion of rock types in borehole section KLX23B RSMD01
(Mapped borehole length = 46 m)
Percent of borehole length
100%
90%
80%
70%
60%
50%
40%
30%
20%
10%
0%
94.0%
2.1%
0.1%
4.0%
501036
501044
501058
511058

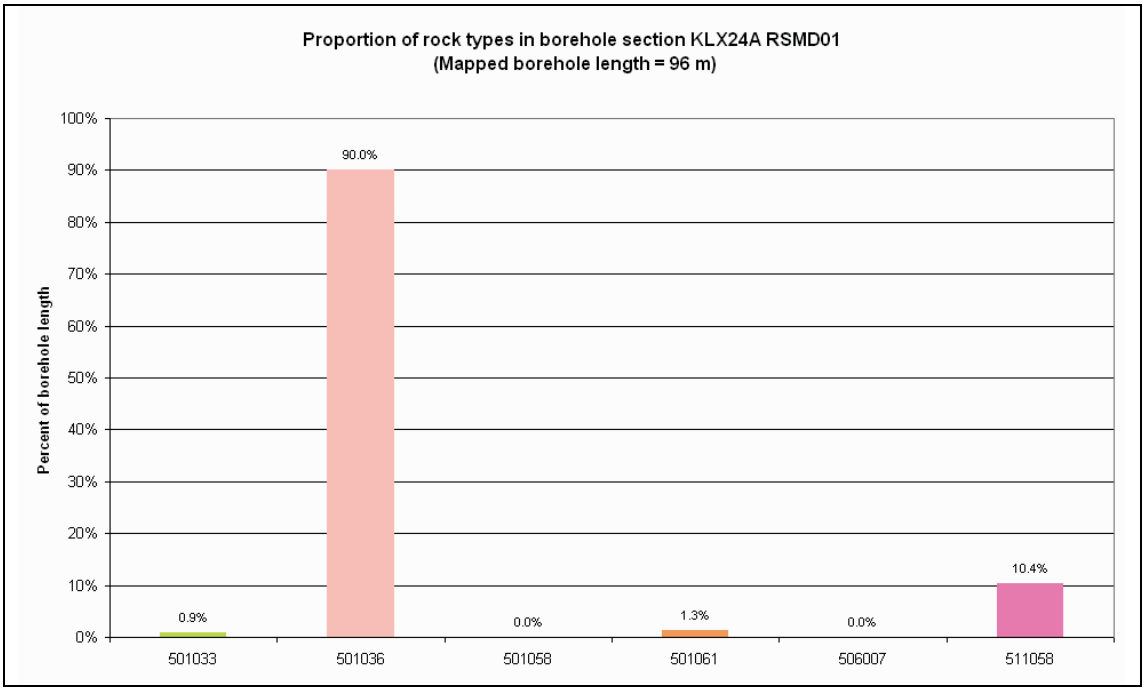
Proportion of rock types in borehole section KLX24A RSMD01
(Mapped borehole length = 96 m)
Percent of borehole length
100%
90%
80%
70%
60%
50%
40%
30%
20%
10%
0%
0.9%
90.0%
0.0%
1.3%
0.0%
10.4%
501033
501036
501058
501061
506007
511058

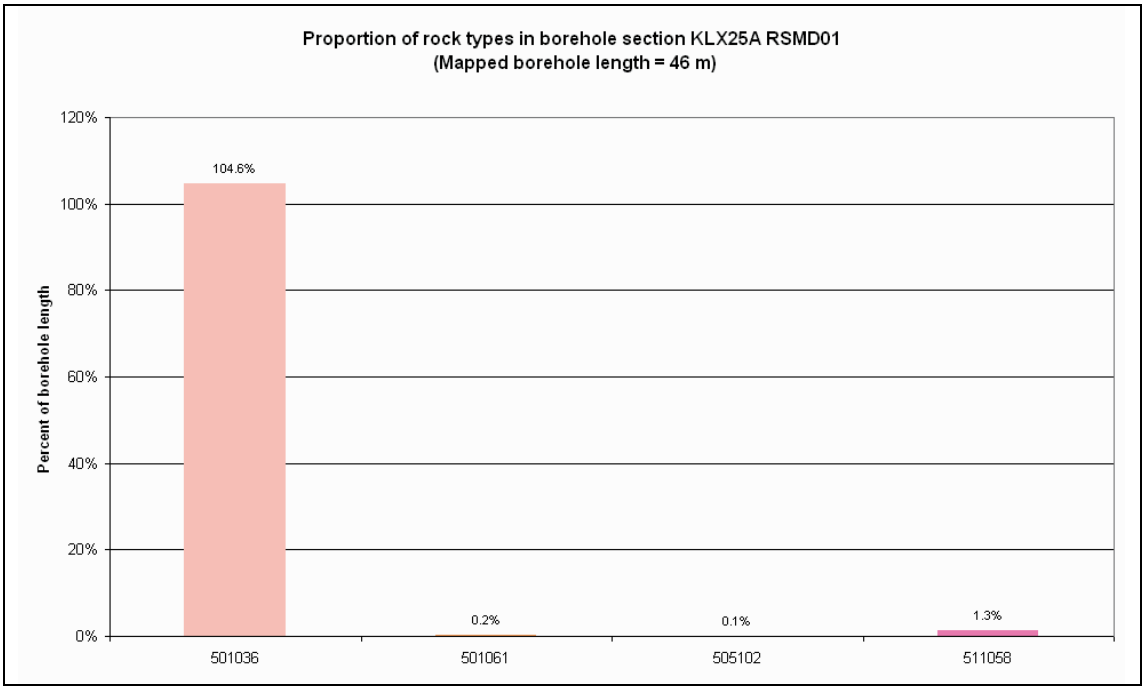
Proportion of rock types in borehole section KLX25A RSMD01
(Mapped borehole length = 46 m)
Percent of borehole length
120%
100%
80%
60%
40%
20%
0%
104.6%
0.2%
0.1%
1.3%
501036
501061
505102
511058

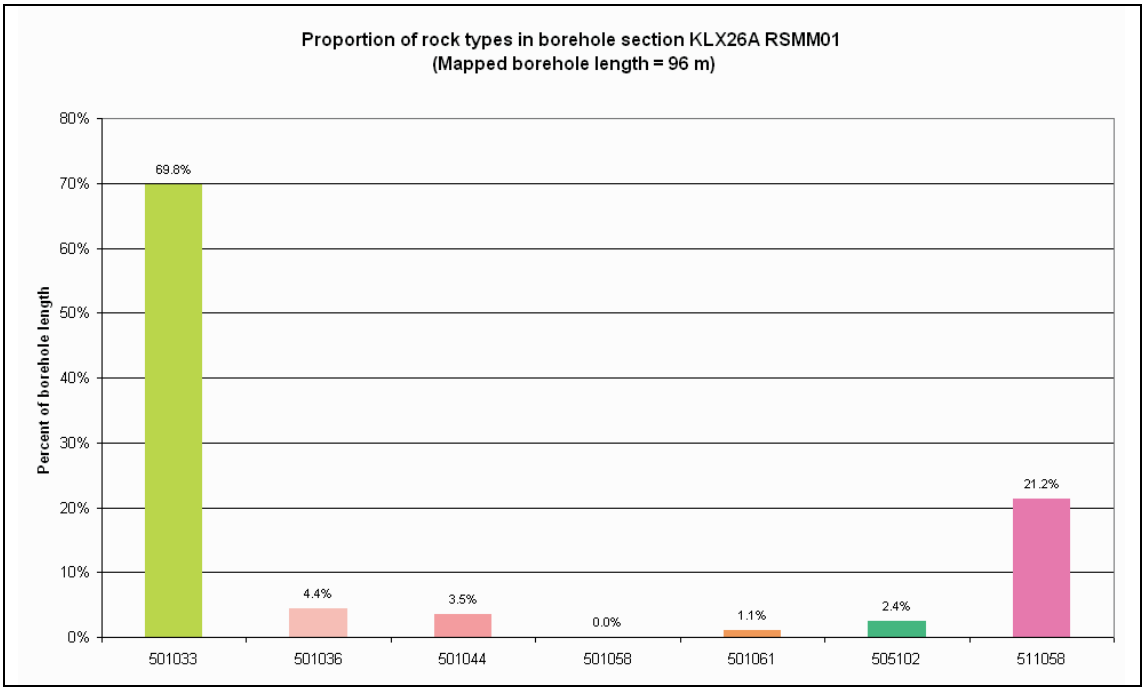
Proportion of rock types in borehole section KLX26A RSMM01
(Mapped borehole length = 96 m)
Percent of borehole length
80%
70%
60%
50%
40%
30%
20%
10%
0%
69.8%
4.4%
3.5%
0.0%
1.1%
2.4%
21.2%
501033
501036
501044
501058
501061
505102
511058

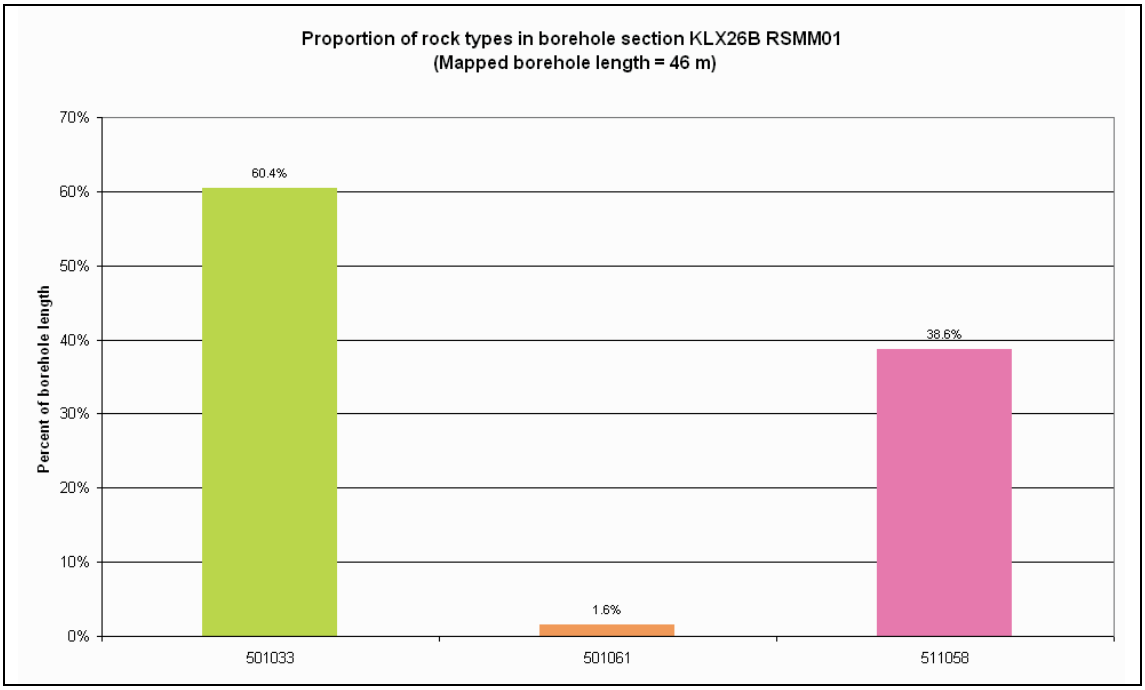
Proportion of rock types in borehole section KLX26B RSMM01
(Mapped borehole length = 46 m)
Percent of borehole length
70%
60%
50%
40%
30%
20%
10%
0%
60.4%
1.6%
38.6%
501033
501061
511058

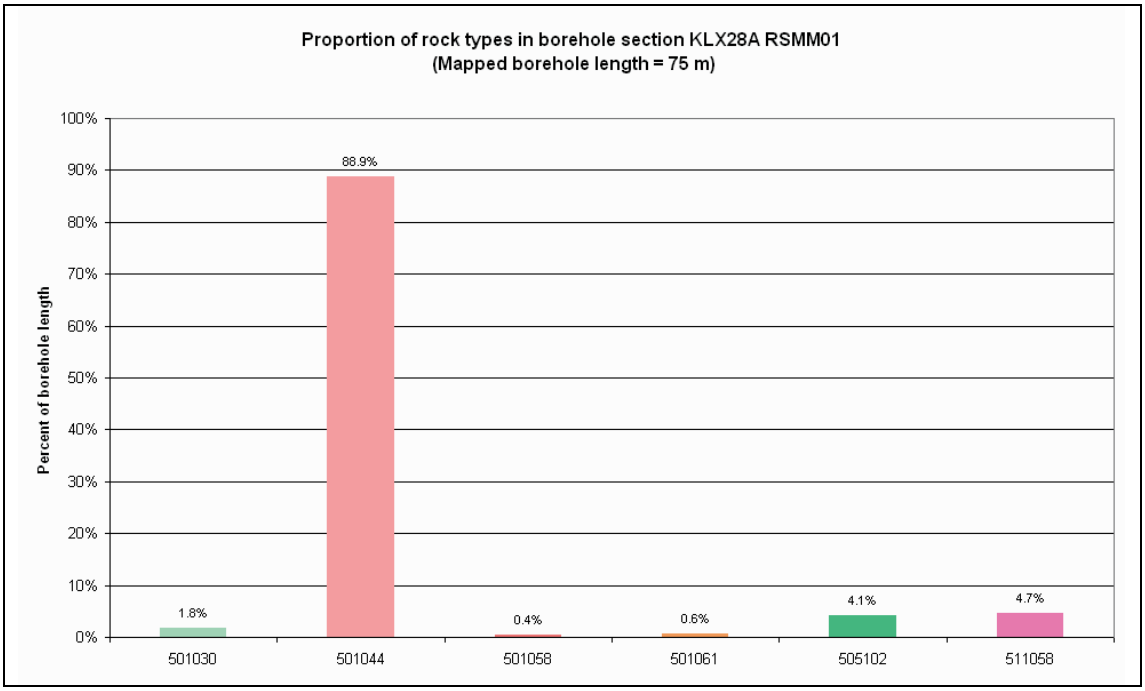
Proportion of rock types in borehole section KLX28A RSMM01
(Mapped borehole length = 75 m)
Percent of borehole length
100%
90%
80%
70%
60%
50%
40%
30%
20%
10%
0%
1.8%
88.9%
0.4%
0.6%
4.1%
4.7%
501030
501044
501058
501061
505102
511058

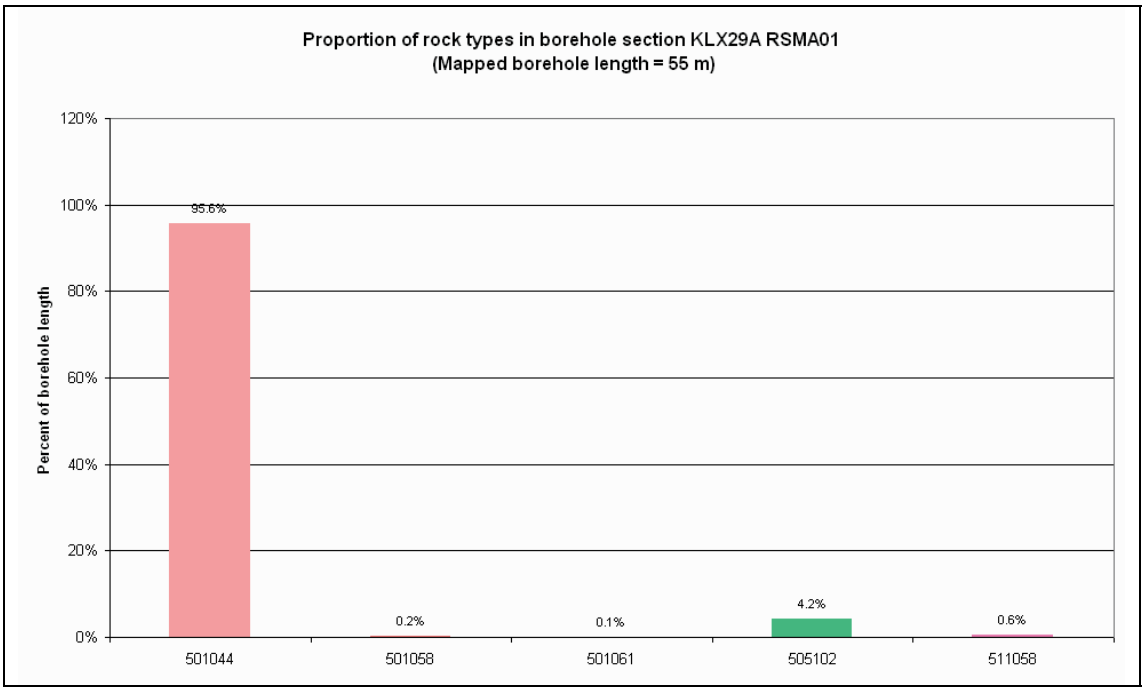

Proportions of different rock types on an overall rock domain basis

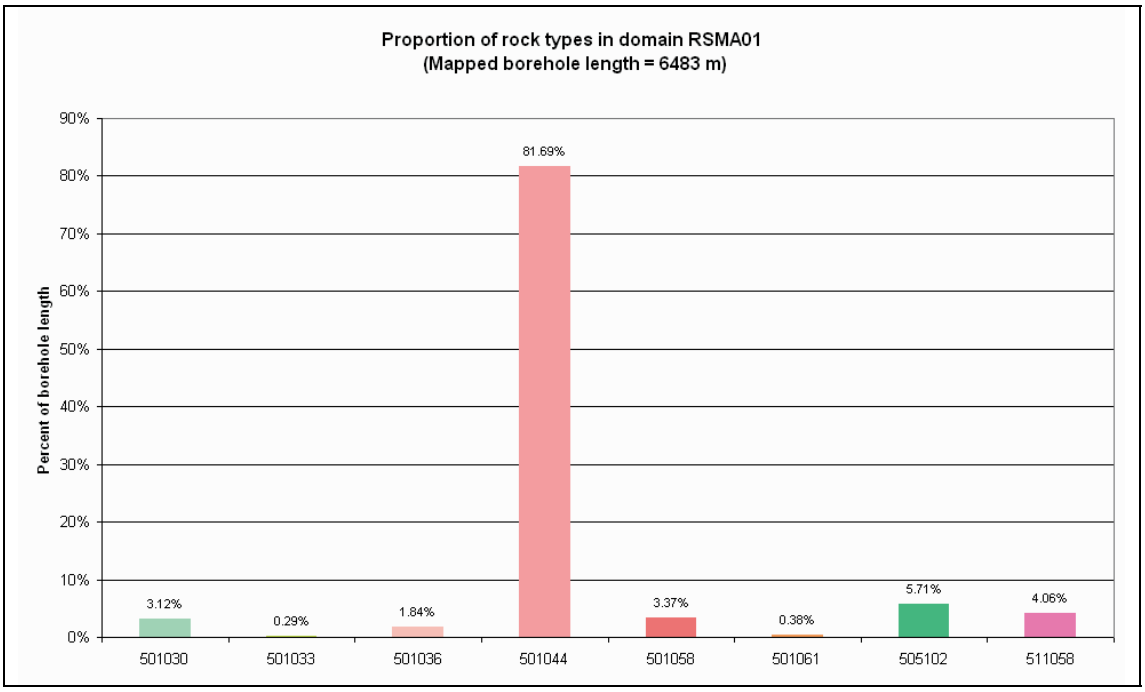

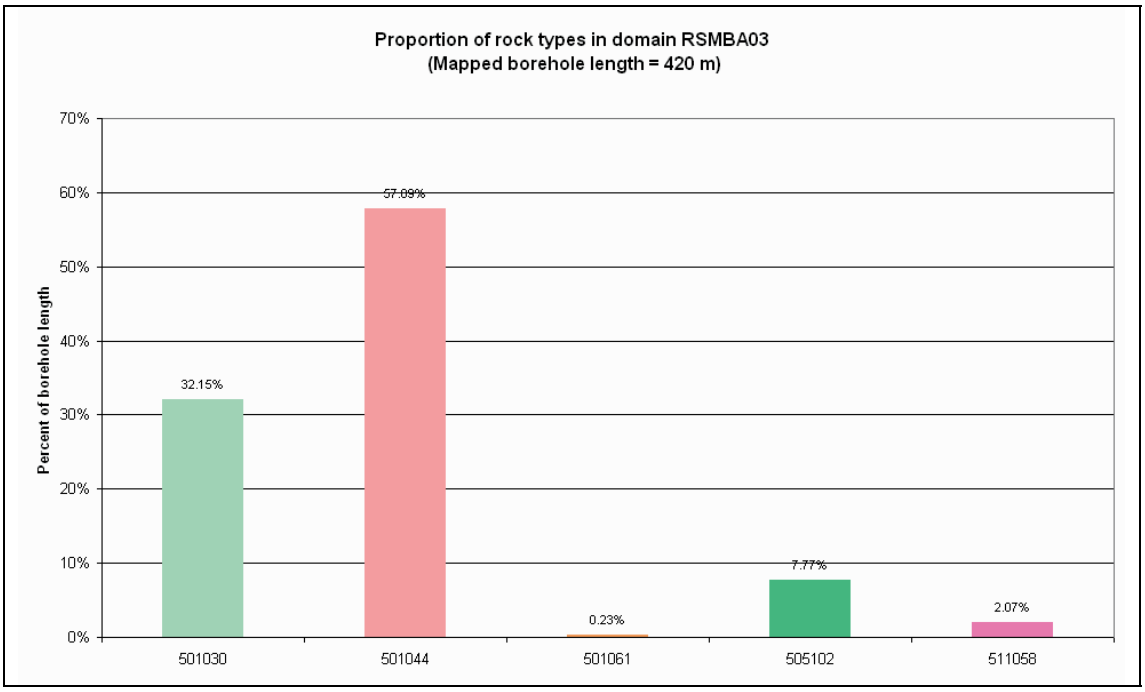
Proportion of rock types in domain RSMBA03
(Mapped borehole length = 420 m)
Percent of borehole length
70%
60%
50%
40%
30%
20%
10%
0%
32.15%
57.69%
0.23%
7.77%
2.07%
501030
501044
501061
505102
511058

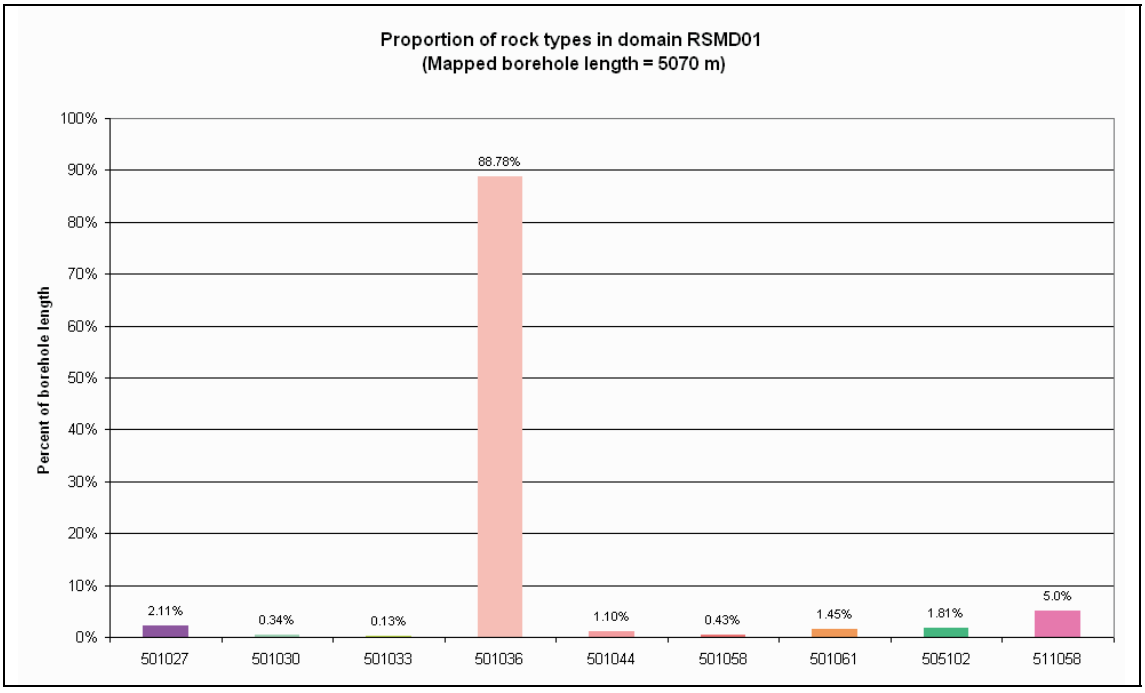
Proportion of rock types in domain RSMD01
(Mapped borehole length = 5070 m)
Percent of borehole length
100%
90%
80%
70%
60%
50%
40%
30%
20%
10%
0%
2.11%
0.34%
0.13%
88.78%
1.10%
0.43%
1.45%
1.81%
5.0%
501027
501030
501033
501036
501044
501058
501061
505102
511058

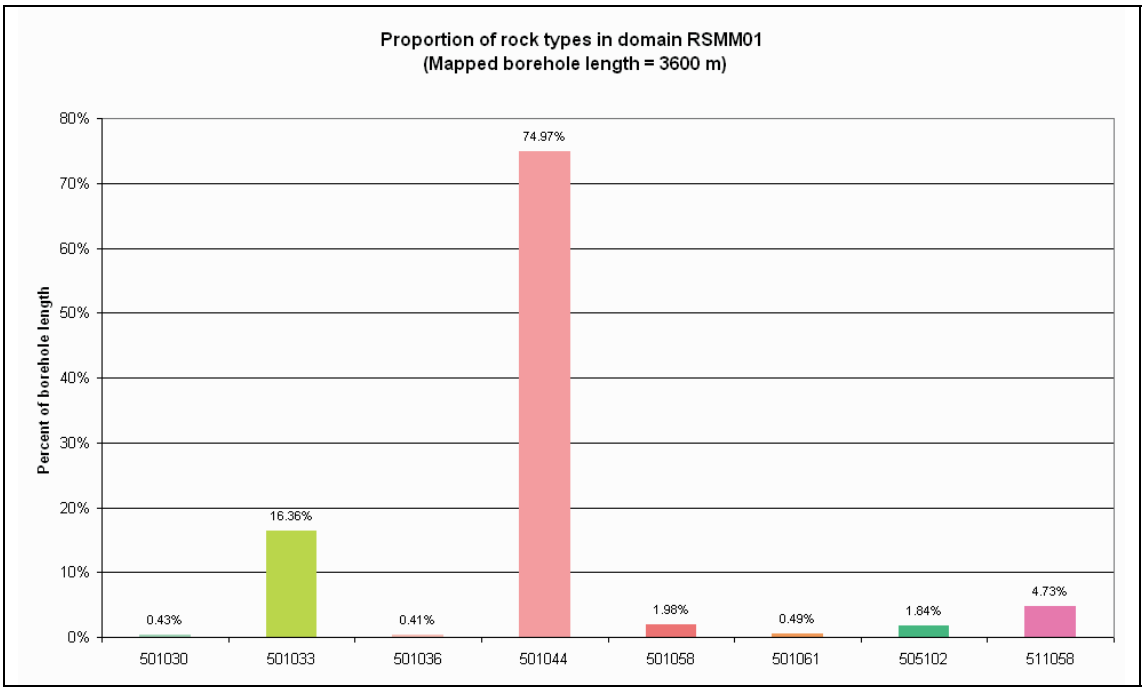
Proportion of rock types in domain RSMM01
(Mapped borehole length = 3600 m)
Percent of borehole length
80%
70%
60%
50%
40%
30%
20%
10%
0%
0.43%
16.36%
0.41%
74.97%
1.98%
0.49%
1.84%
4.73%
501030
501033
501036
501044
501058
501061
505102
511058

Appendix 5

Thickness distribution of subordinate rock types on a borehole by borehole basis, on a rock domain basis in each borehole and on an overall rock domain basis

Data from Sicada: p_rock.xls and p_rock_occur.xls in Sicada_07_134 and Sicada_07_283. Fine-grained granite, pegmatite, fine-grained diorite-gabbro and dolerite are included in the analysis.

Procedure: The following steps have been carried out:

Data files p_rock.xls and p_rock_occur.xls have been combined according to the procedure described in Appendix 4.

The true thickness has been calculated for the subordinate rock types fine-grained granite (511058), pegmatite (501061), fine-grained diorite-gabbro (505102) and dolerite (501027), and the apparent thickness has been calculated for other rock types (see explanation below).

Thickness distribution histograms are plotted for each borehole, for each rock domain in each borehole and for each rock domain.

Calculation of true thickness (d)

The apparent thickness, Δs, can be calculated from adjusted secup and seclow. In 2-D, the true thickness, d, can be calculated by $d = \Delta s \sin \alpha$ if α is the angle between the borehole axis and the rock contact. Alternatively, if s is a vector, the thickness d can be calculated by the dot product $d = s \cdot p$, where d is the projection of s to p, provided p is a unit-length vector and normal to the structure, i.e. its pole.

In 3-D, the dot product of vectors is preferable, as it does not require α to be known beforehand. The vector s can be calculated from the borehole coordinates [E, N, z] of adjusted secup and seclow, and the pole of the structure, p, is taken as the mean pole of the upper and lower contacts along the borehole, the resultant vector method being used. For rock occurrences, only the upper contact is used to define its orientation. Furthermore, all d calculated less than 0.001 m was assigned a value of 0.001 m.

The histograms that show the true thickness of the subordinate rock types can be viewed on the CD-Rom attached to this report. The results of the analysis of true thickness are discussed in Section 3.4.3 in this report.

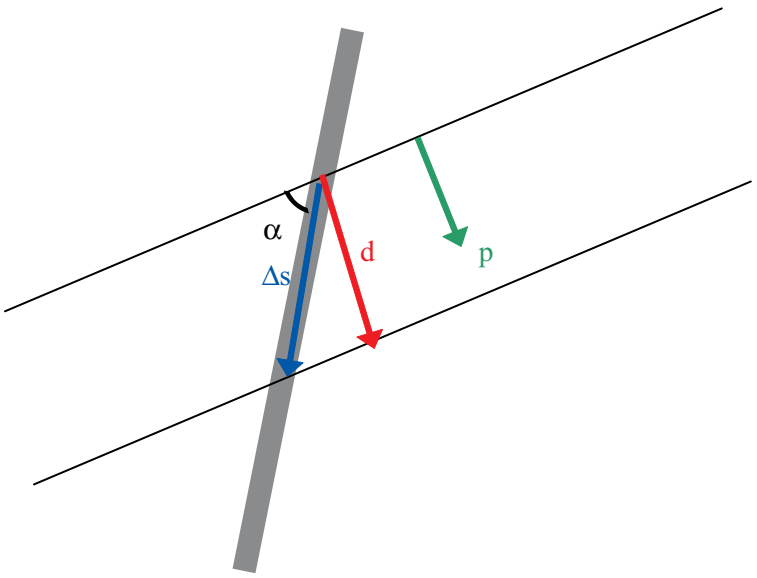

Figure A5-1. *Definition of parameters used in the calculation of true thickness of subordinate rock types. A borehole is shown in dark grey and a subordinate rock type by the two parallel black lines.*

Appendix 6

Orientation of contacts of subordinate rock types on a borehole by borehole basis, on a rock domain basis in each borehole and on an overall rock domain basis

Data from Sicada: p_rock.xls and p_rock_occur.xls in Sicada_07_134 and Sicada_07_283.

Procedure: The orientation of the upper contact along the borehole of fine-grained granite (511058), pegmatite (501061), fine-grained diorite-gabbro (505102) and dolerite (501027), were extracted from Sicada. The orientation of the contacts is plotted as poles in an equal area stereographic projection on a borehole by borehole basis, on a rock domain basis in each borehole and on an overall rock domain basis.

Stereoplots of contoured cluster significance are also displayed. The methods by /Kamb 1959/ and /Robin and Jowett 1986/ are useful to evaluate clustering in directional data of large data sets. This method uses the null-hypothesis that in absence of clustering, all poles are uniformly distributed over the hemisphere, such that for a hemispherical cap of 1 % binning area the expected value is 1 % of the total population. Thus, cluster significance can be visualized in terms of the difference between observed and expected values, expressed in standard deviations.

In the original method /Kamb 1959/, the binning area was dependent on sample size (such that $E=3\sigma$) in order to reduce exaggeration of cluster significance in small data sets. On the other hand, a sample-size dependent binning area becomes unfeasible for larger data sets, say on the order $n > 1000$. Therefore, the minimum binning area was set to 1% for large data sets /Robin and Jowett 1986/. For small data sets ($n < 50$), Kamb contouring is not appropriate and the pole plots and Fisher contouring should be used for evaluation and interpretation.

The stereographic projections can be viewed on the CD-Rom attached to this report. The results of the orientation analysis are discussed in section 3.4.3.

Note that the concentration of horizontal to sub-horizontal orientations in the stereoplots with Fisher and Kamb contouring of data from KLX02 is based on a large amount of data with the same orientation, i.e. one pole in the stereoplot represents several orientations.

References

Kamb W B, 1959. Ice petrofabric observations from Blue Glacier, Washington, in relation to theory and experiment, Journal of Geophysical Research 64, 1891–1909.

Robin P Y F, Jowett E C, 1986. Computerized density contouring and statistical evaluation of orientation data using counting circles and continuous weighting functions. Tectonophysics 121, 207–223.

Orientation of contacts of subordinate rock types on a borehole by borehole basis

KLX02

Fine-grained granite

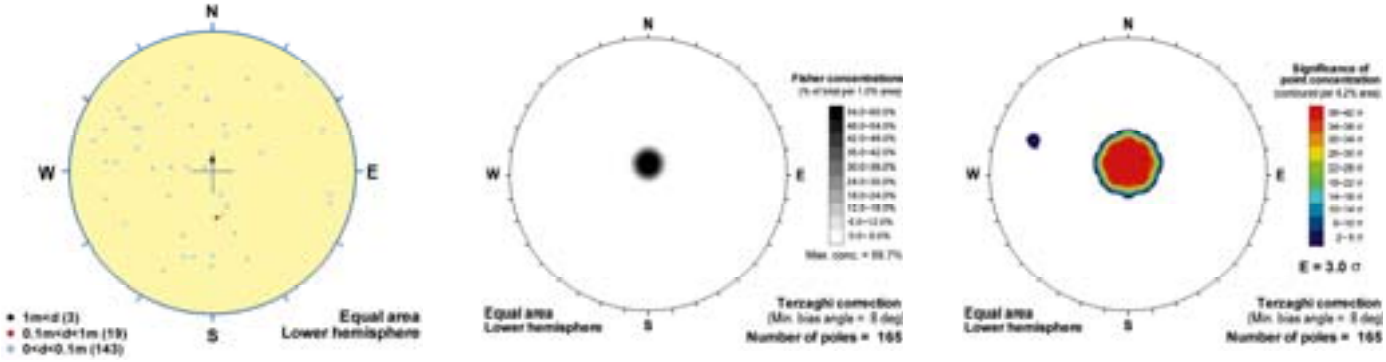

Fine-grained diorite-gabbro

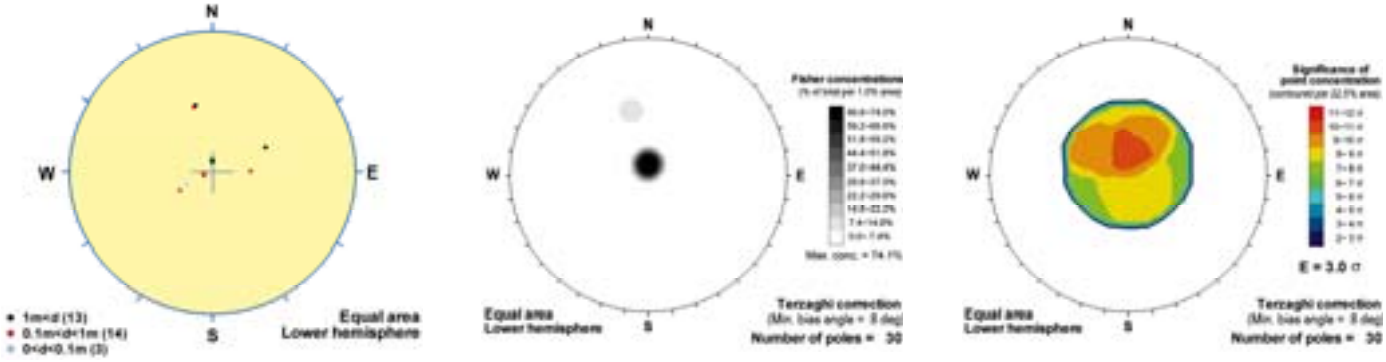

Pegmatite

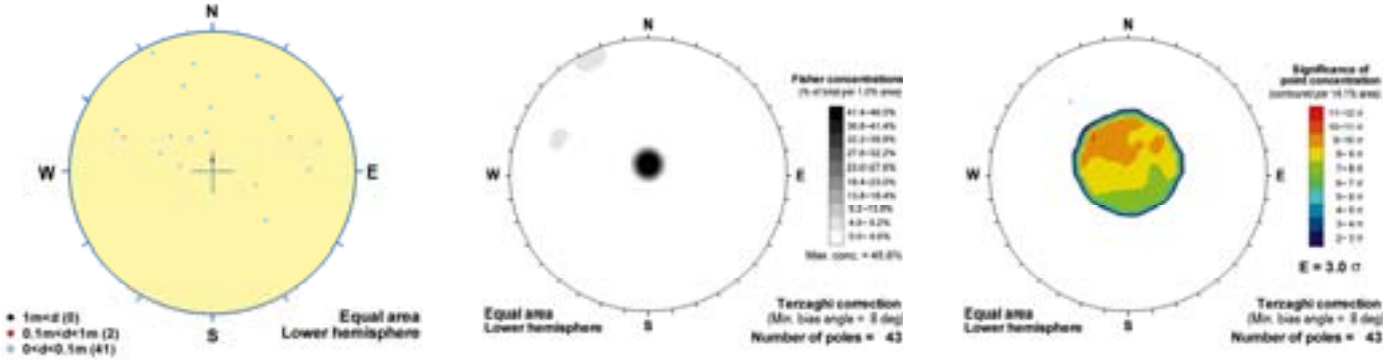

KLX03

Fine-grained granite

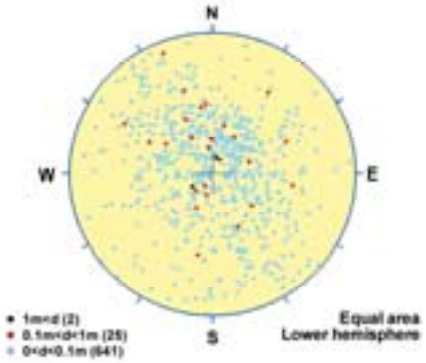

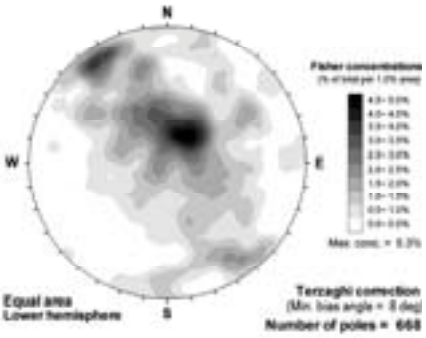

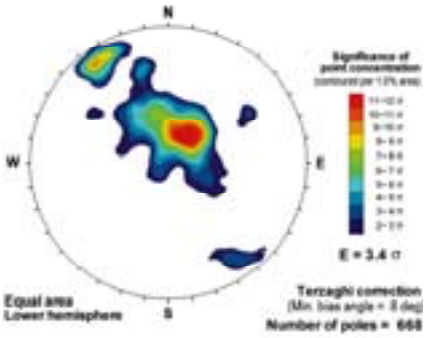

Fine-grained diorite-gabbro

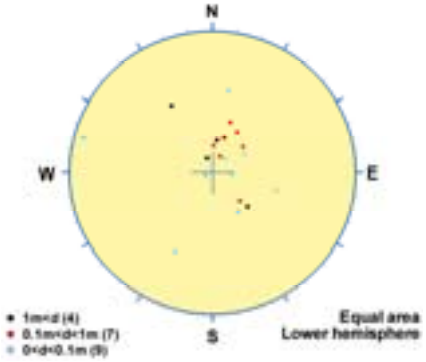

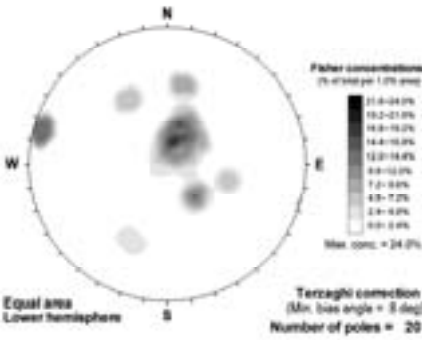

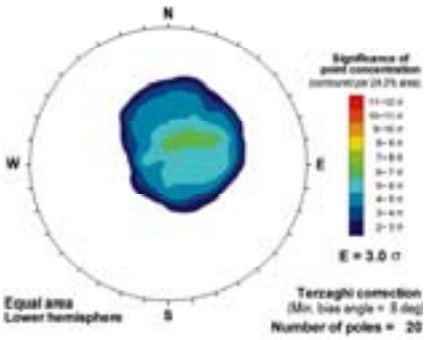

Pegmatite

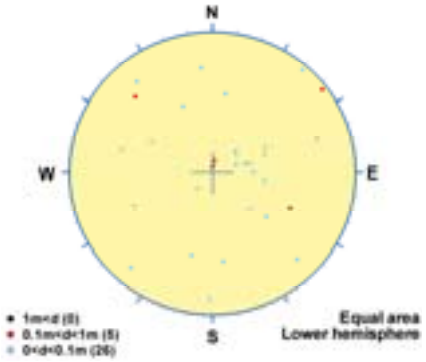

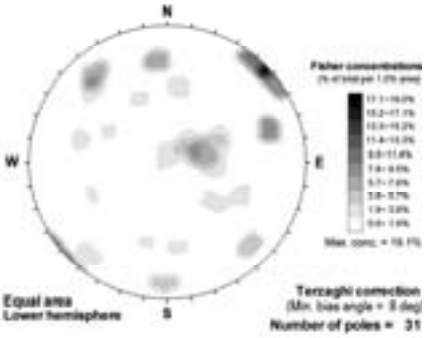

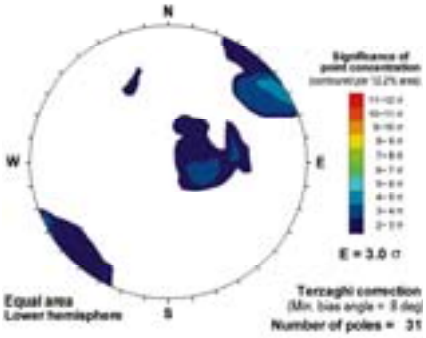

KLX04

Fine-grained granite

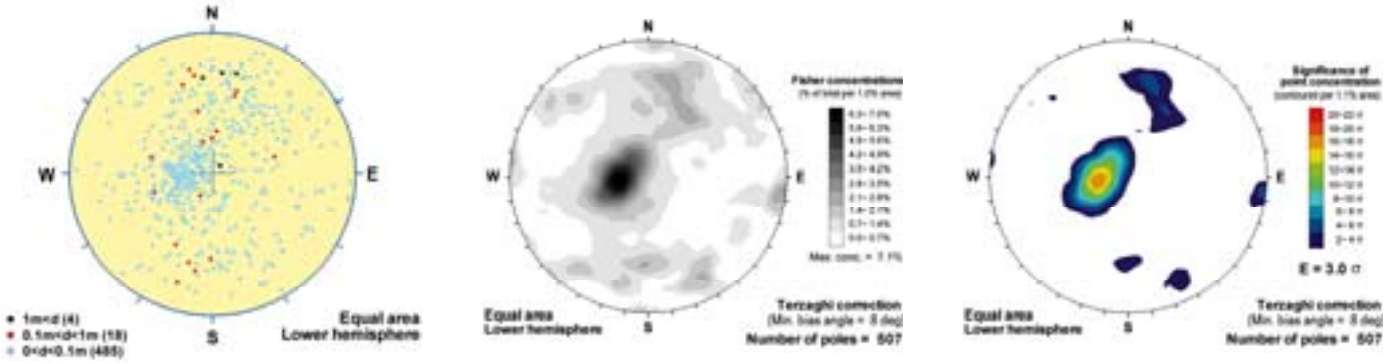

Fine-grained diorite-gabbro

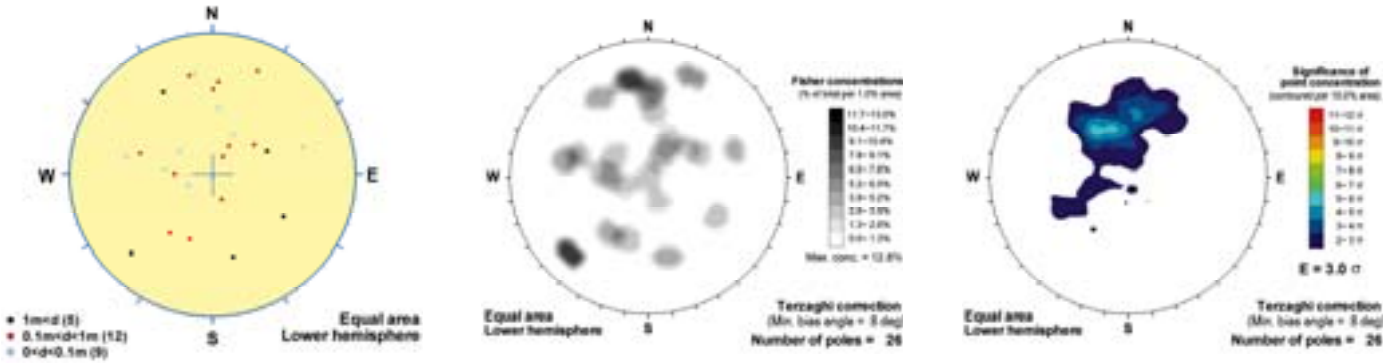

Pegmatite

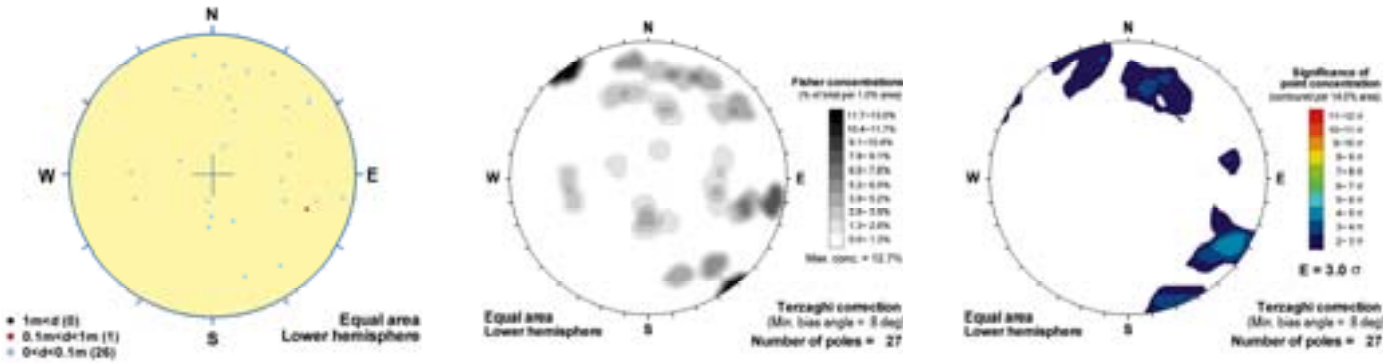

KLX05

Fine-grained granite

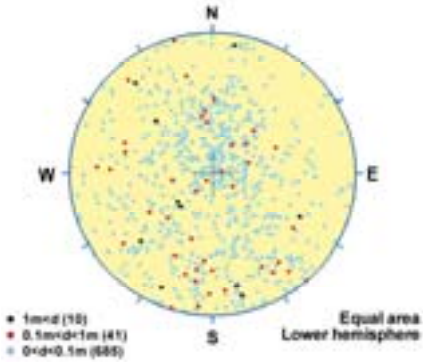

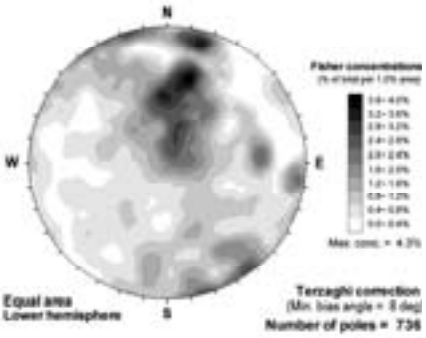

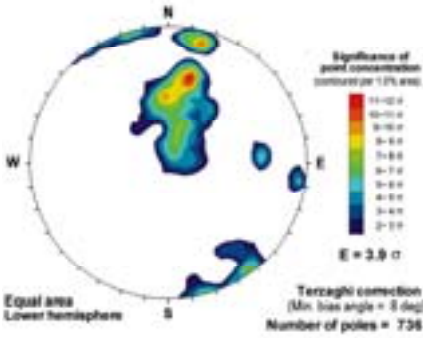

Fine-grained diorite-gabbro

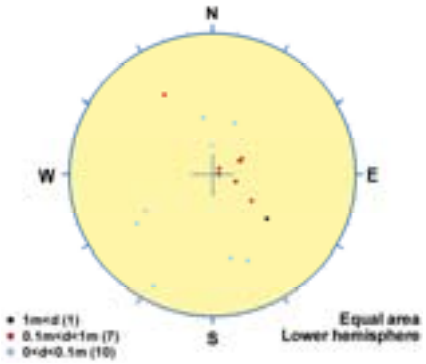

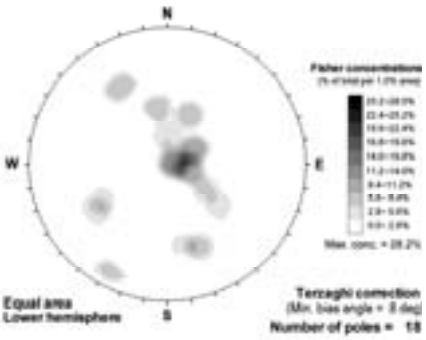

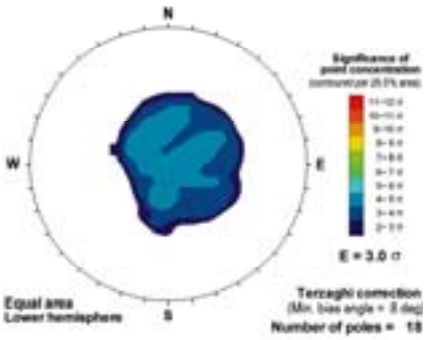

Pegmatite

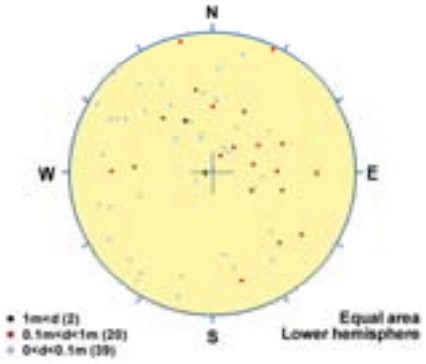

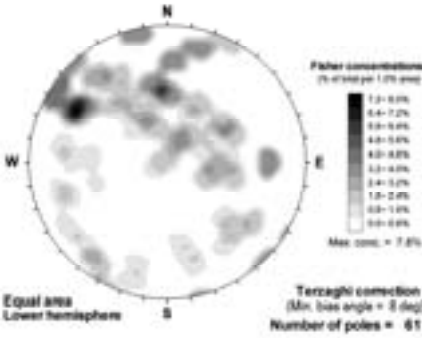

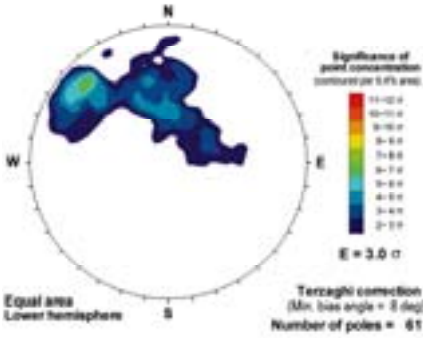

KLX06

Fine-grained granite

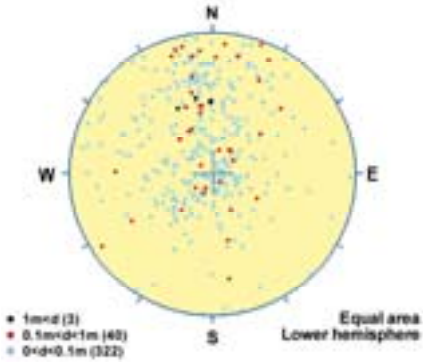

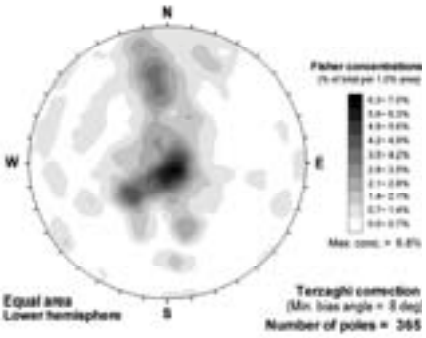

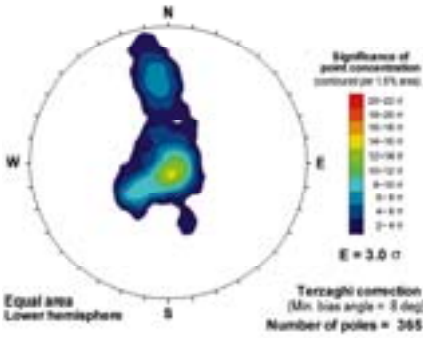

Fine-grained diorite-gabbro

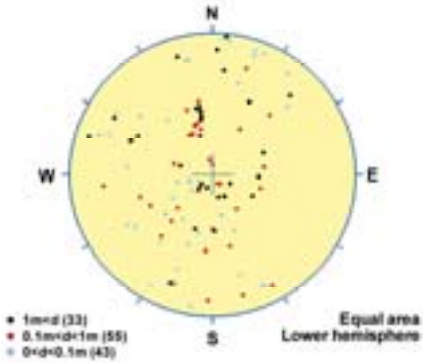

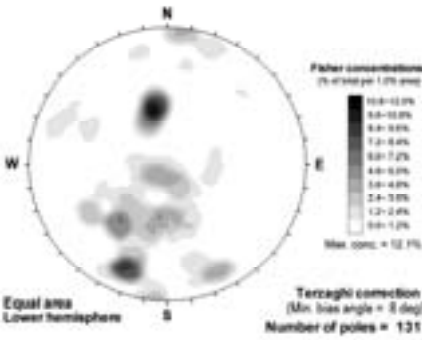

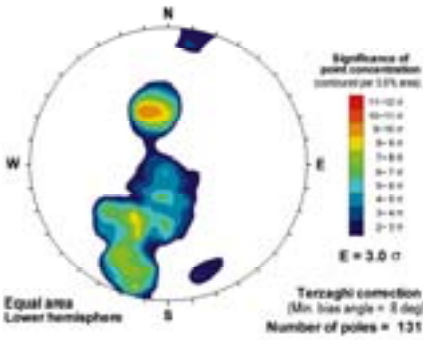

Pegmatite

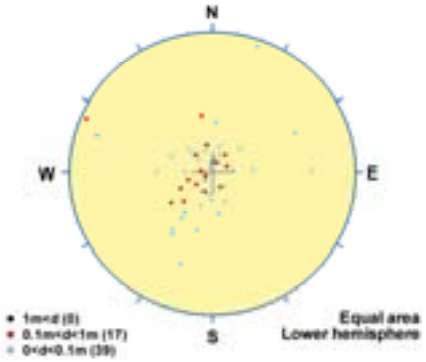

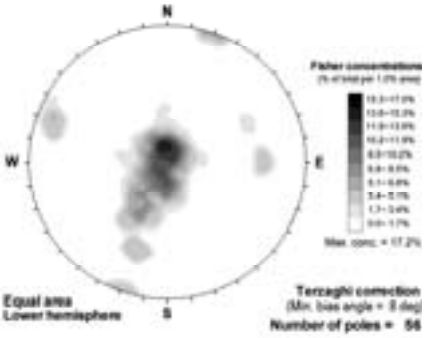

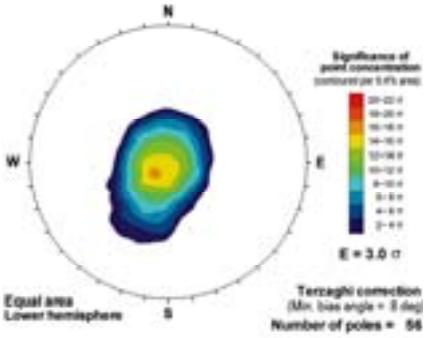

KLX07A

Fine-grained granite

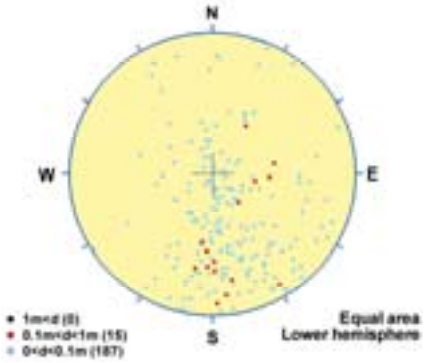

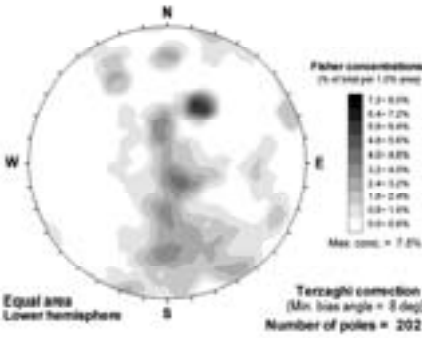

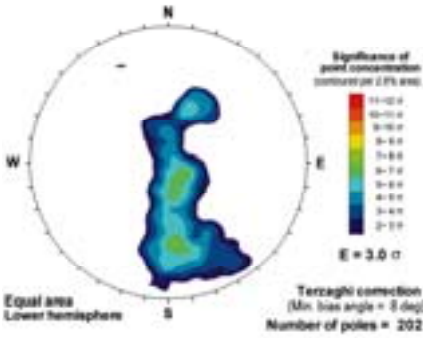

Fine-grained diorite-gabbro

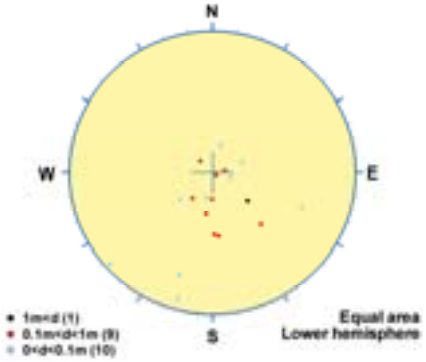

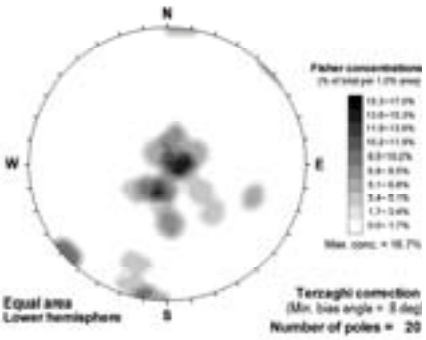

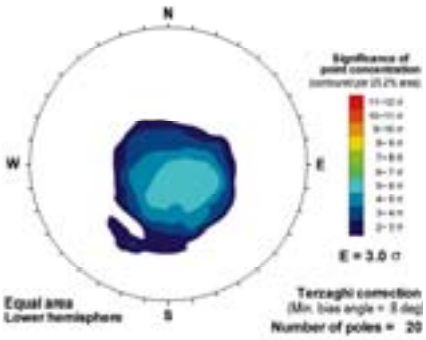

Pegmatite

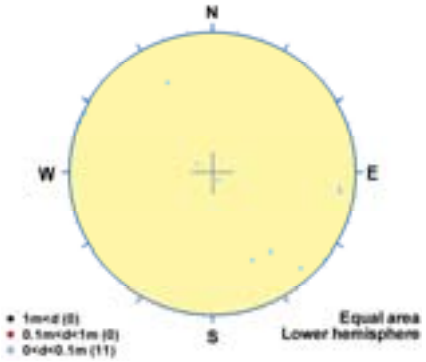

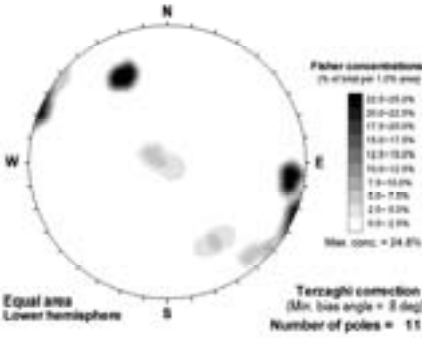

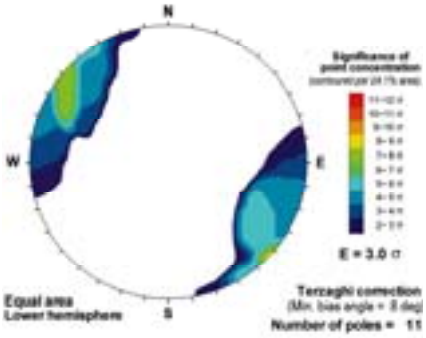

KLX07B

Fine-grained granite

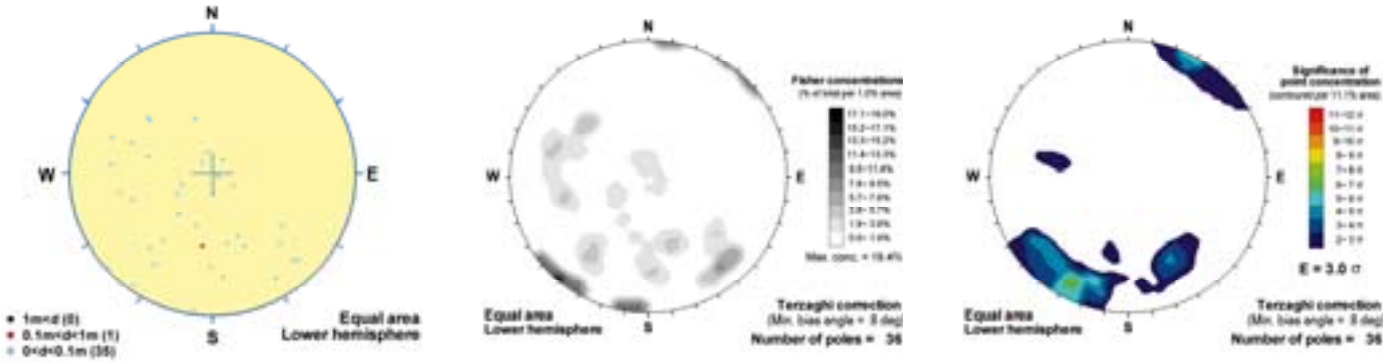

Fine-grained diorite-gabbro

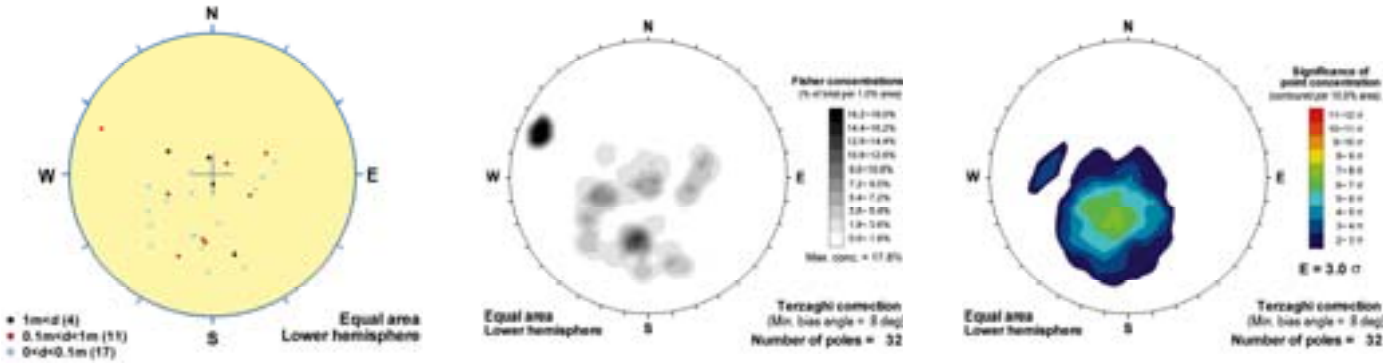

Pegmatite

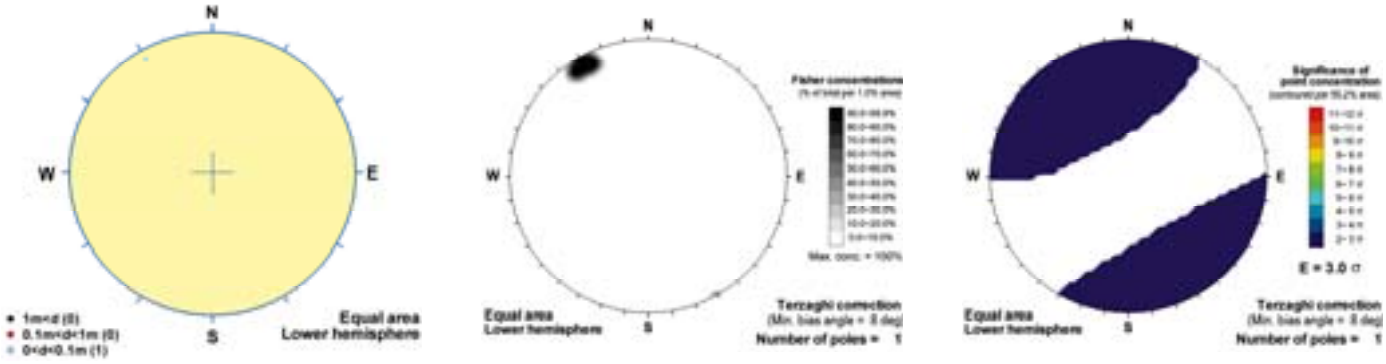

KLX08

Fine-grained granite

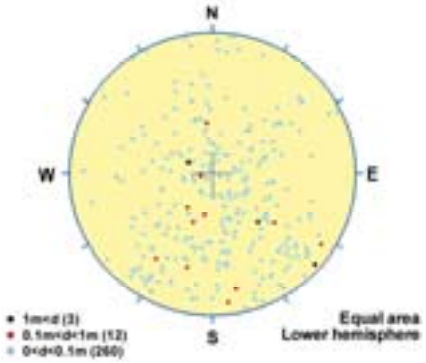

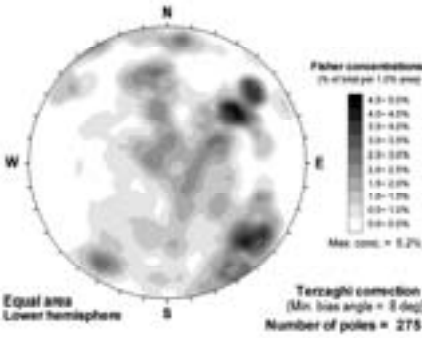

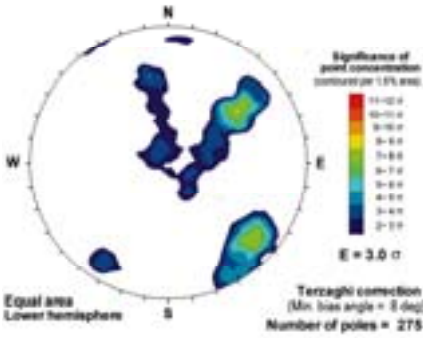

Fine-grained diorite-gabbro

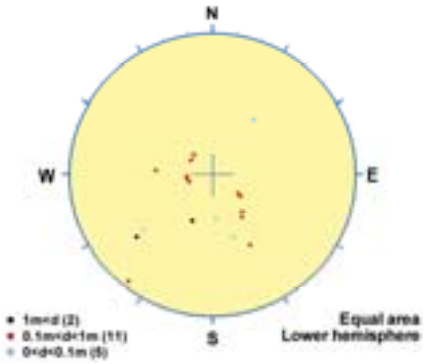

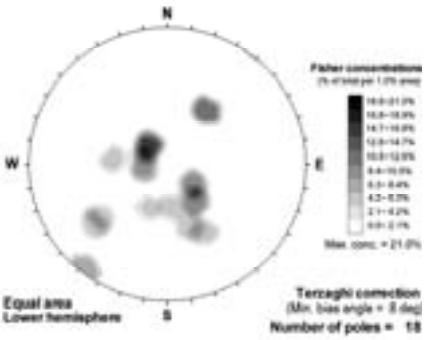

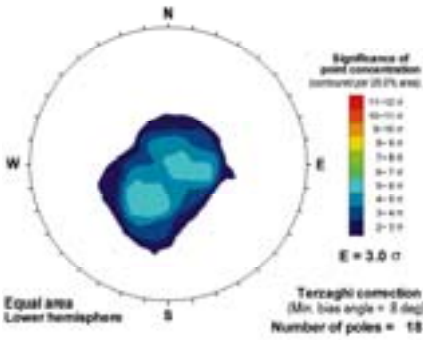

Pegmatite

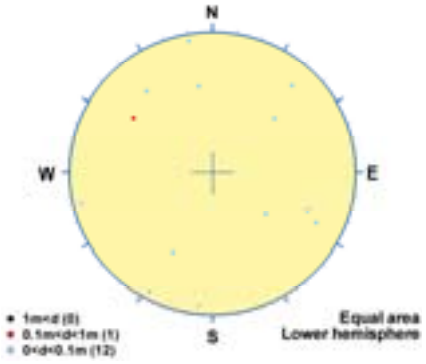

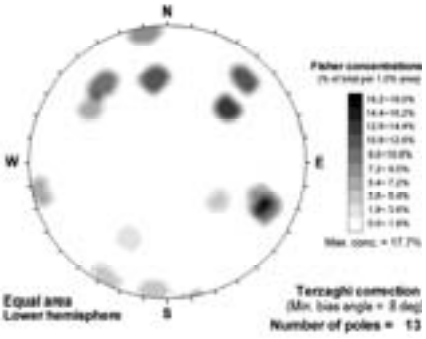

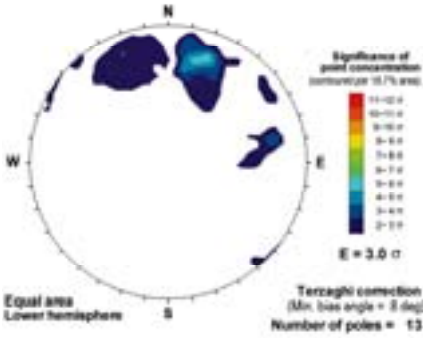

KLX09

Fine-grained granite

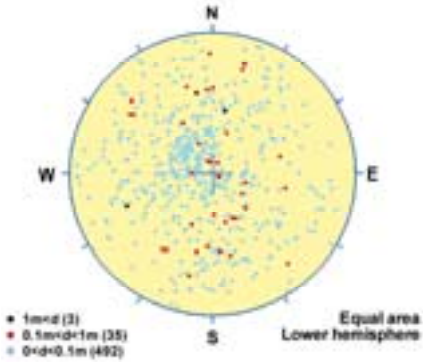

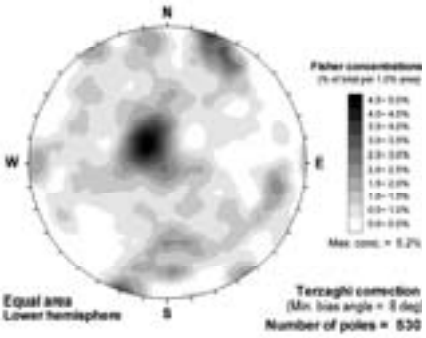

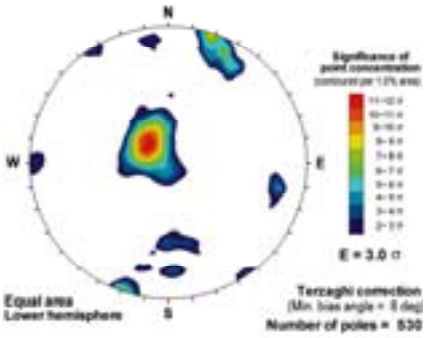

Fine-grained diorite-gabbro

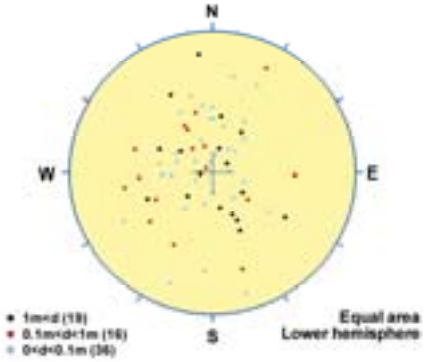

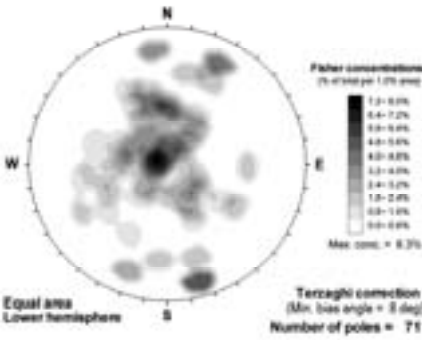

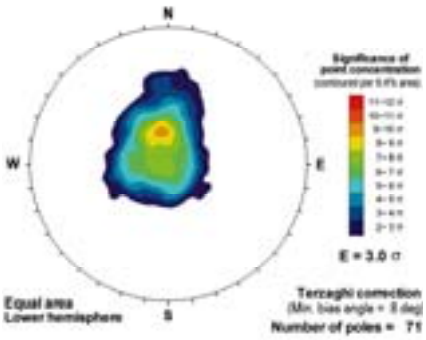

Pegmatite

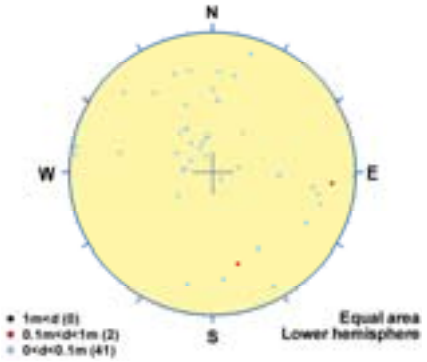

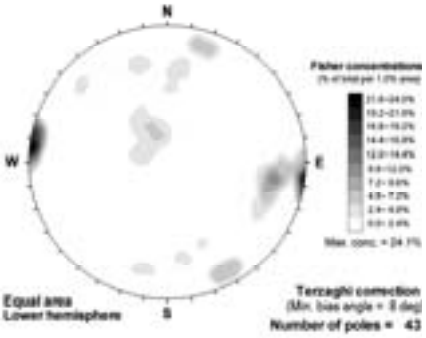

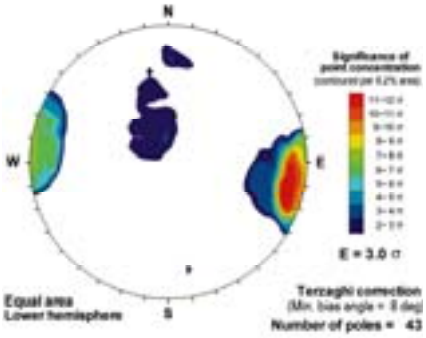

KLX09B

Fine-grained granite

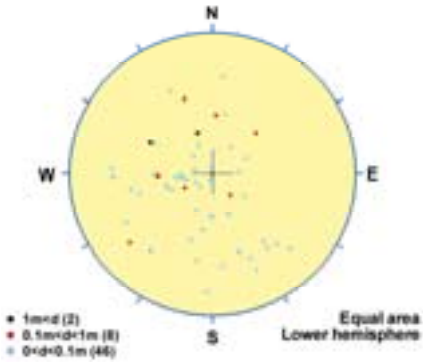

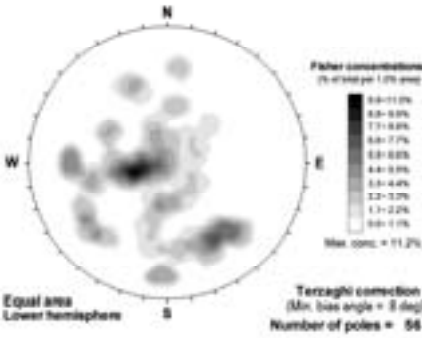

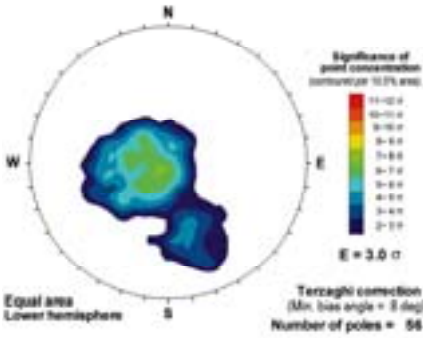

Fine-grained diorite-gabbro

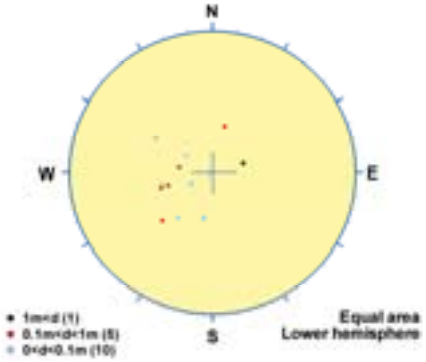

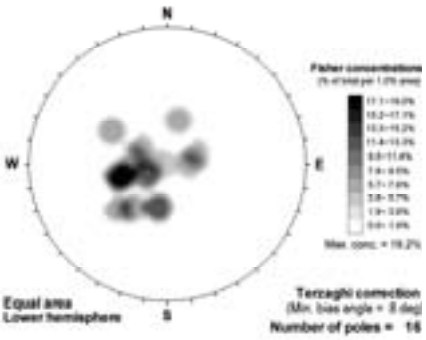

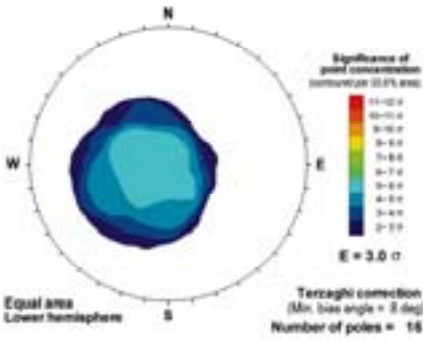

Pegmatite

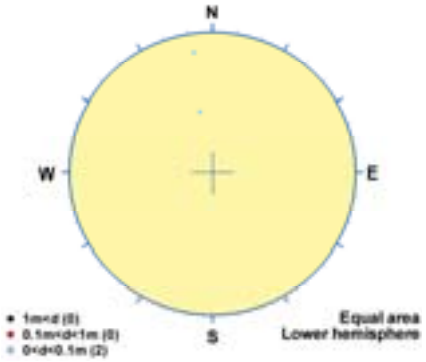

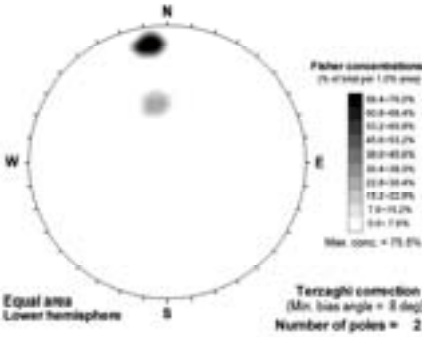

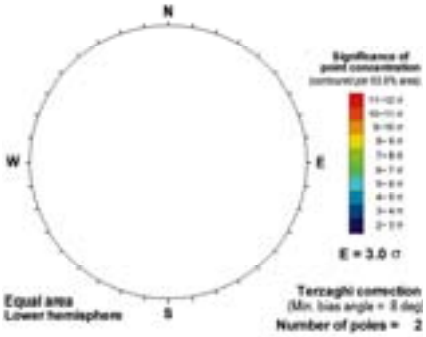

KLX09D

Fine-grained granite

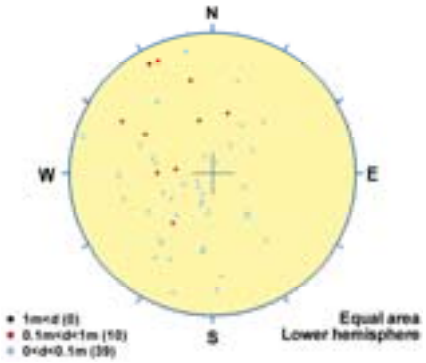

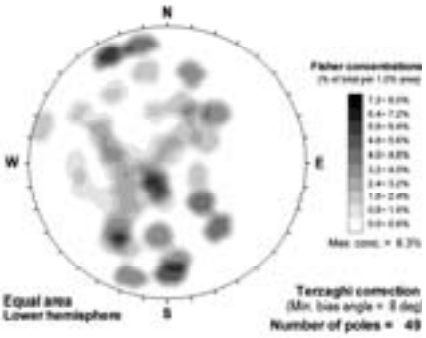

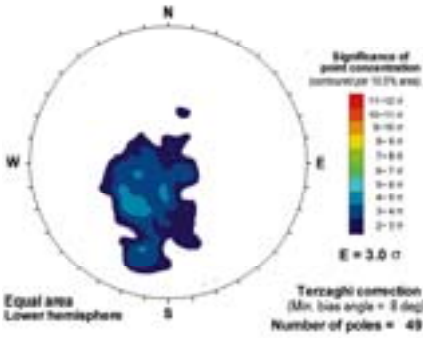

Fine-grained diorite-gabbro

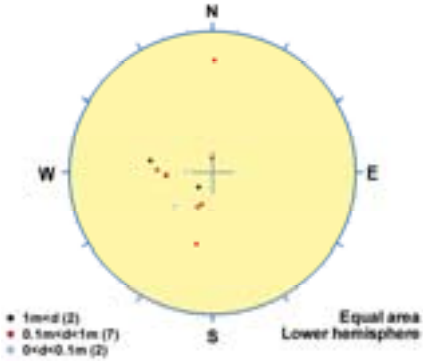

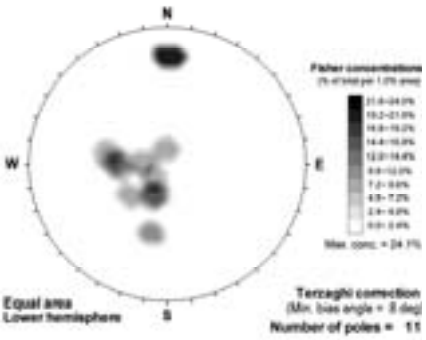

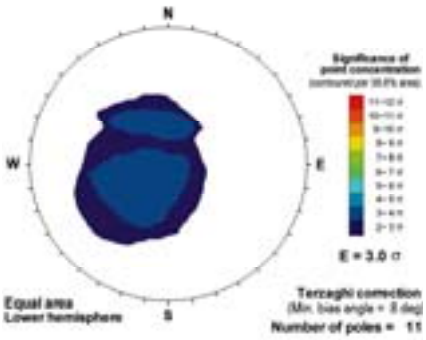

Pegmatite

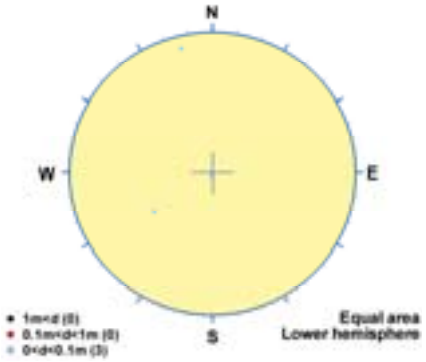

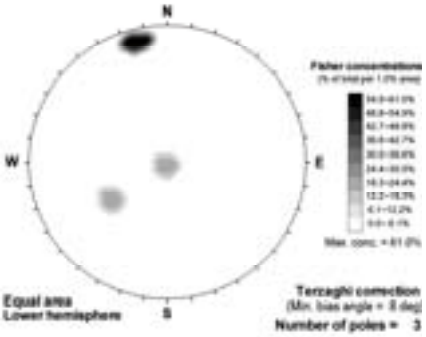

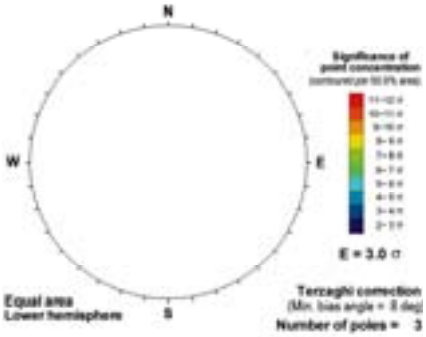

KLX09F

Fine-grained granite

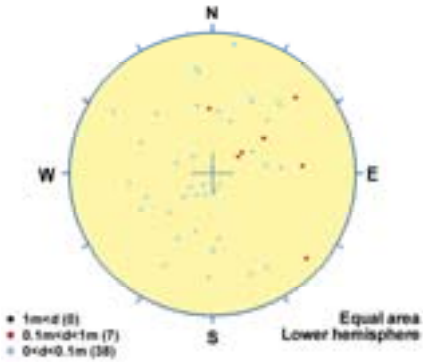

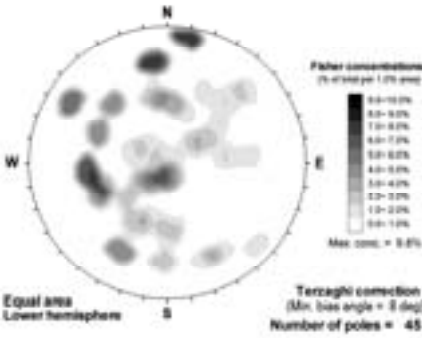

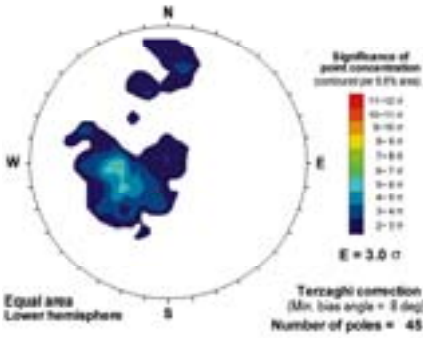

Fine-grained diorite-gabbro

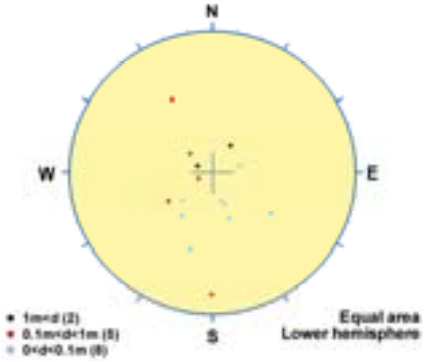

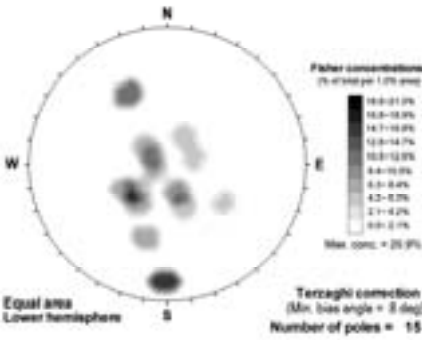

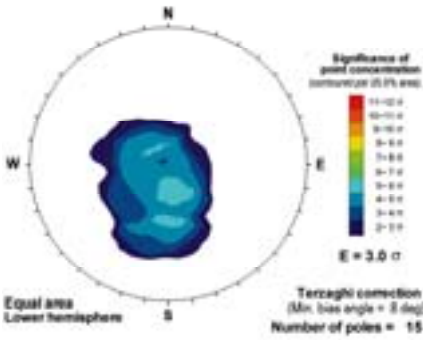

Pegmatite

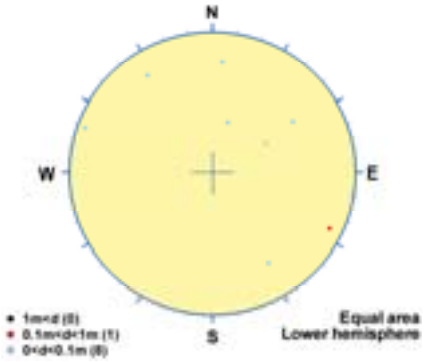

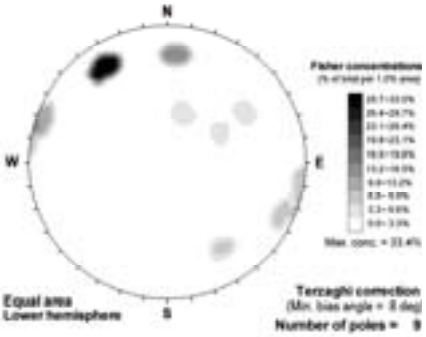

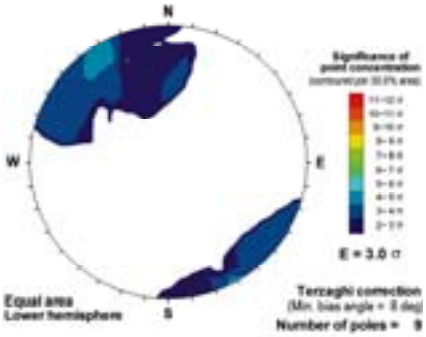

KLX09G

Fine-grained granite

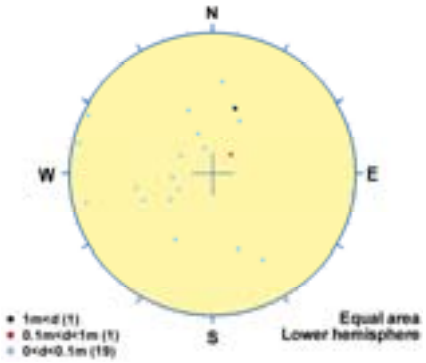

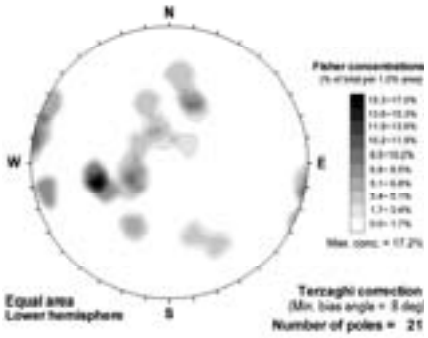

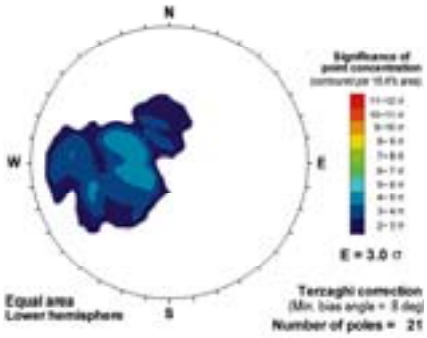

Fine-grained diorite-gabbro

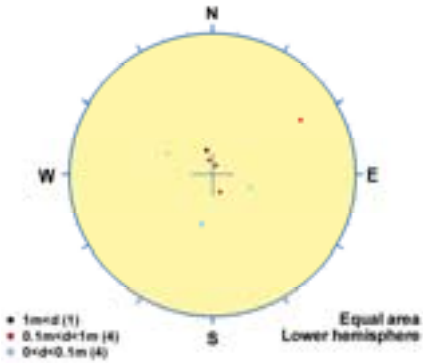

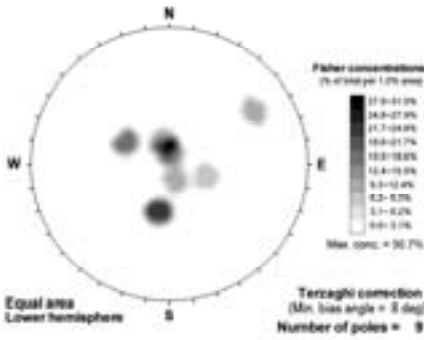

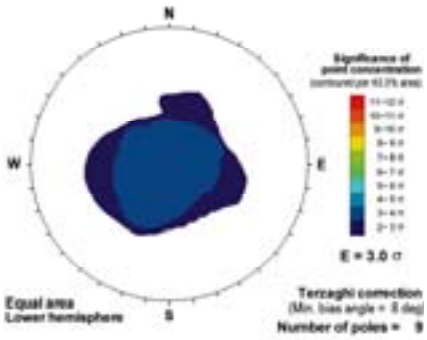

Pegmatite

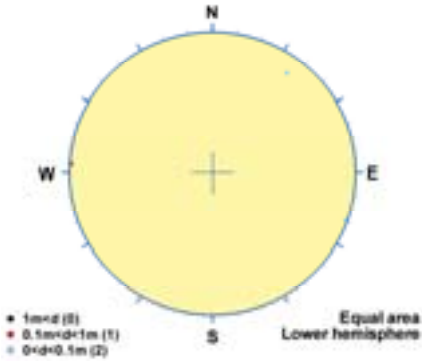

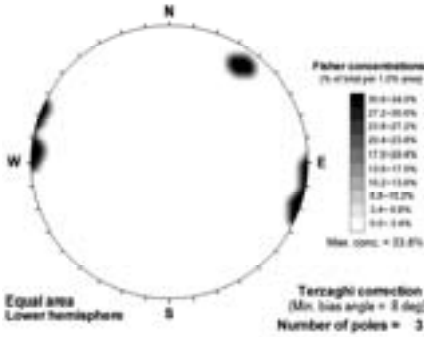

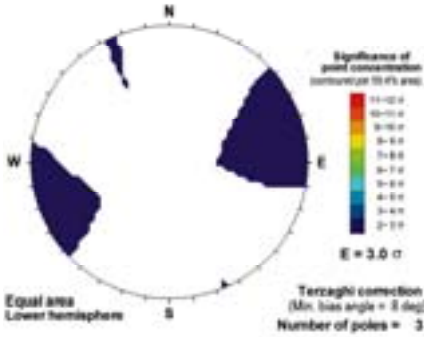

KLX10

Fine-grained granite

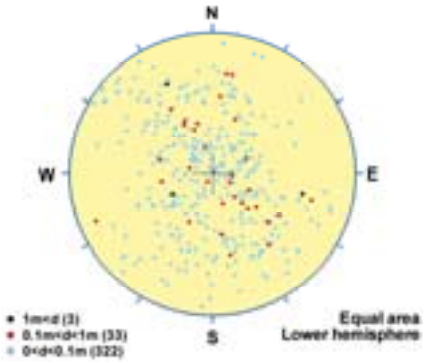

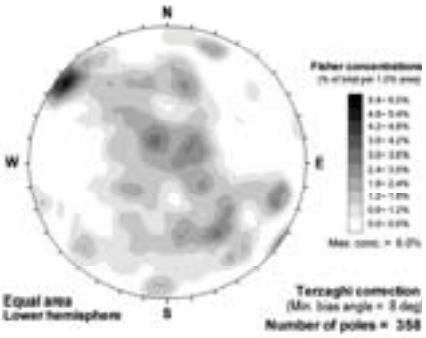

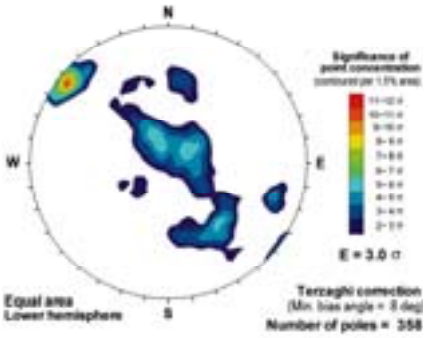

Fine-grained diorite-gabbro

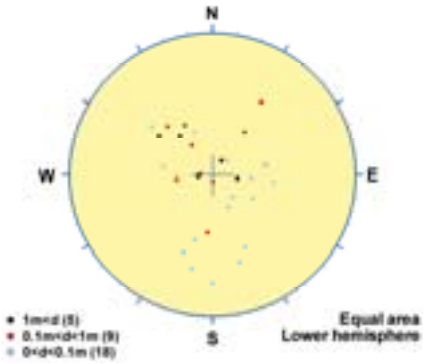

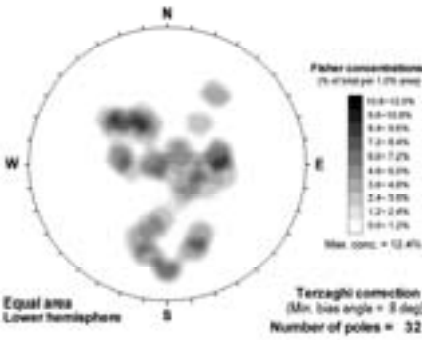

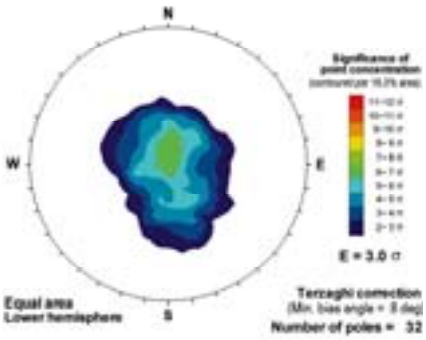

Pegmatite

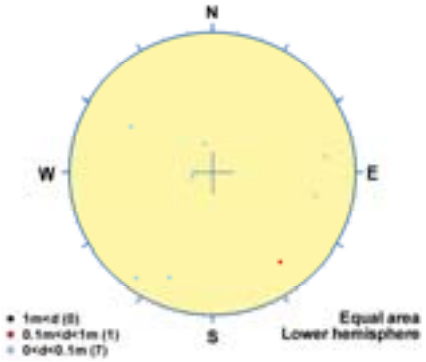

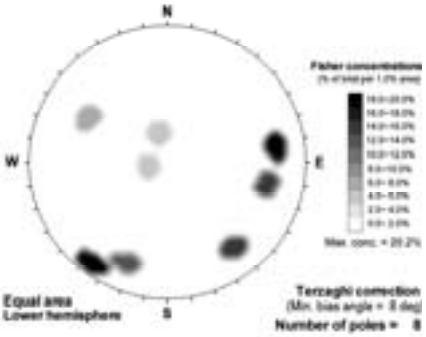

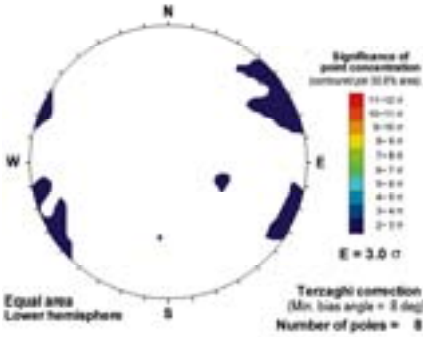

KLX10B

Fine-grained granite

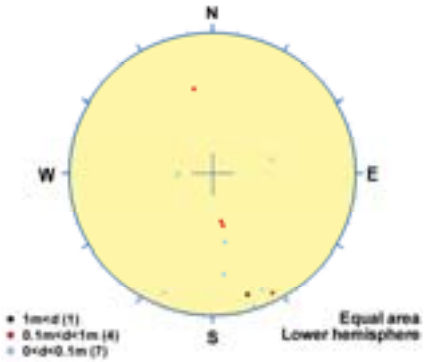

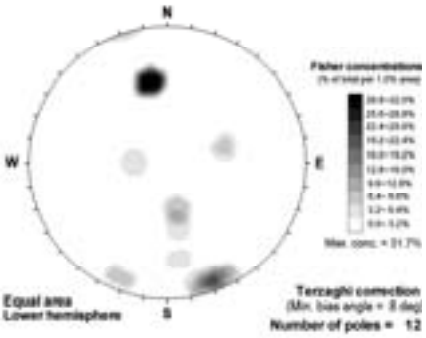

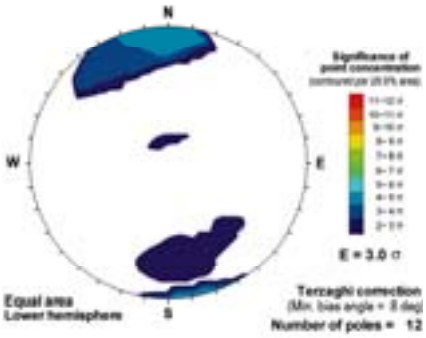

Fine-grained diorite-gabbro

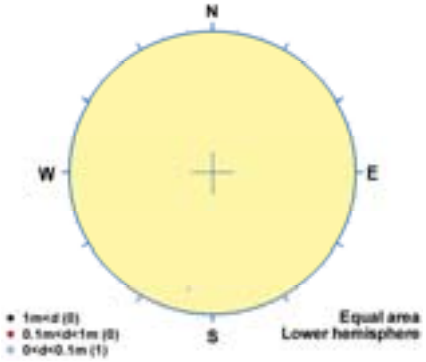

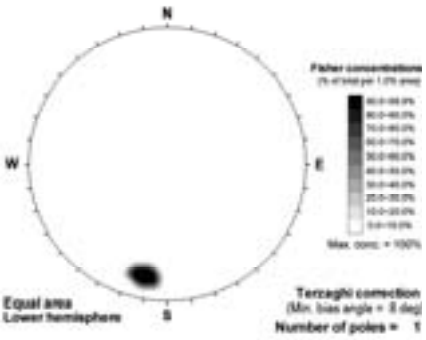

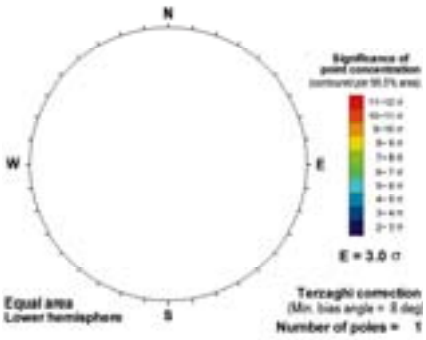

Pegmatite

KLX10C

Fine-grained granite

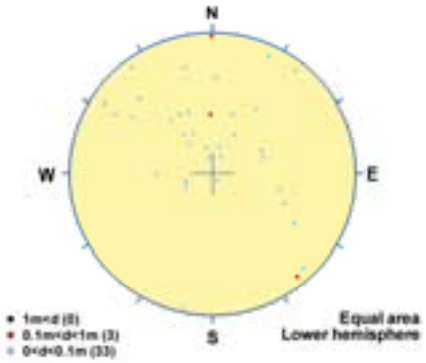

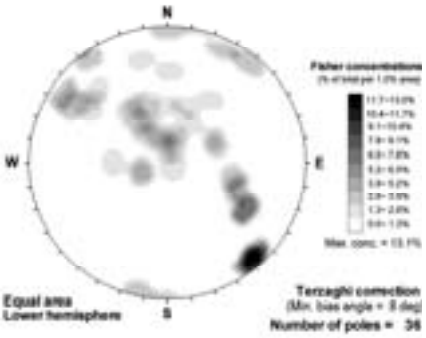

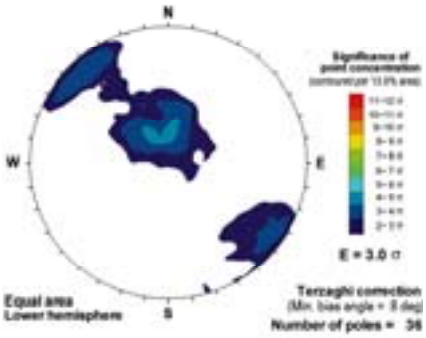

Fine-grained diorite-gabbro

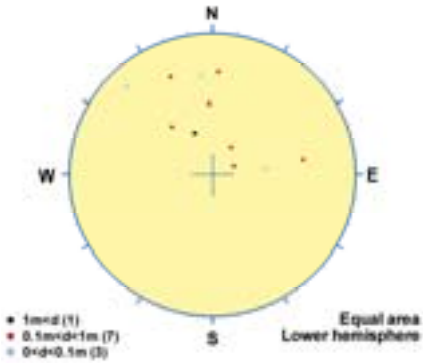

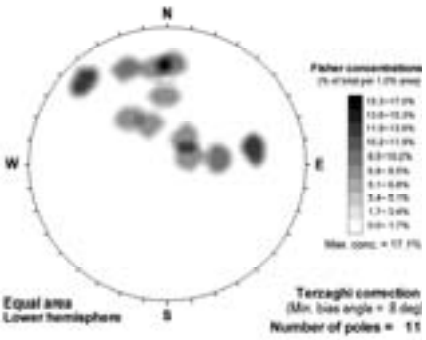

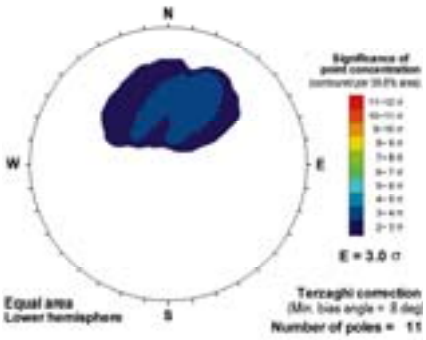

Pegmatite

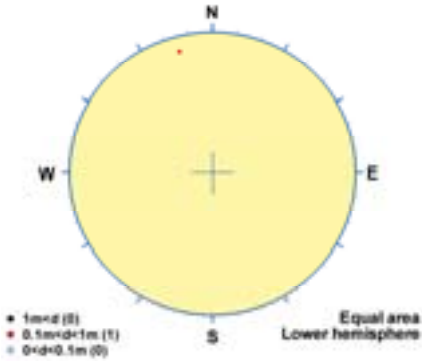

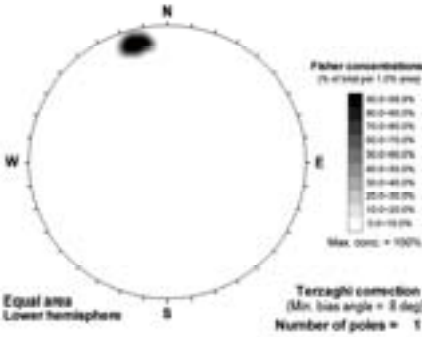

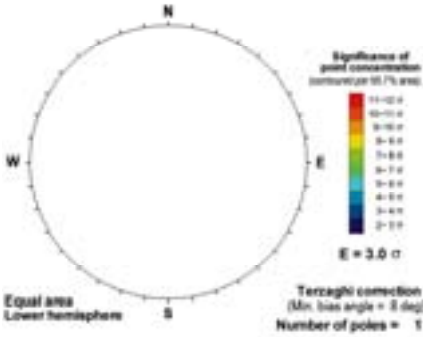

KLX11A

Fine-grained granite

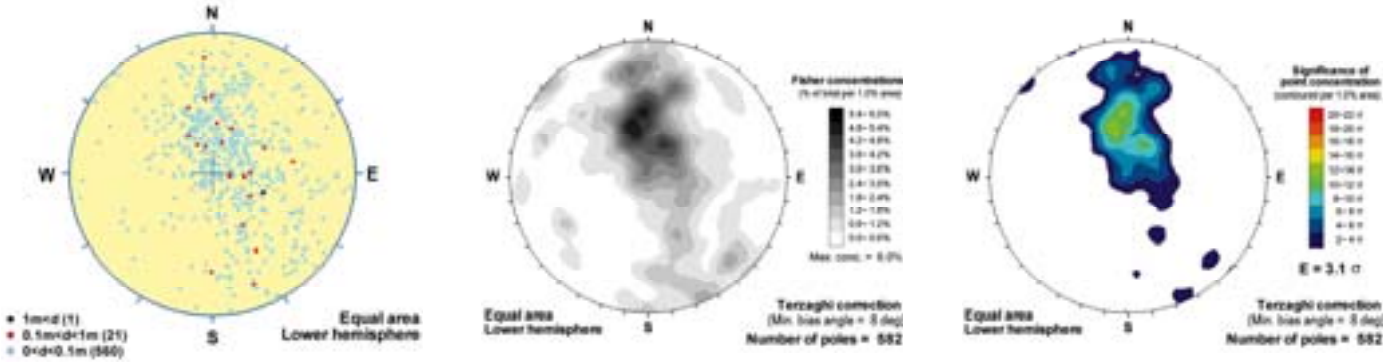

Fine-grained diorite-gabbro

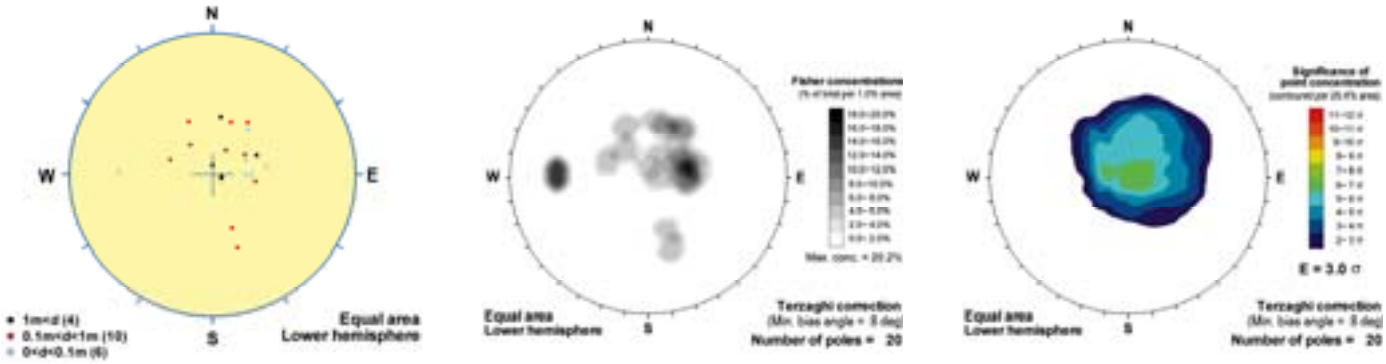

Pegmatite

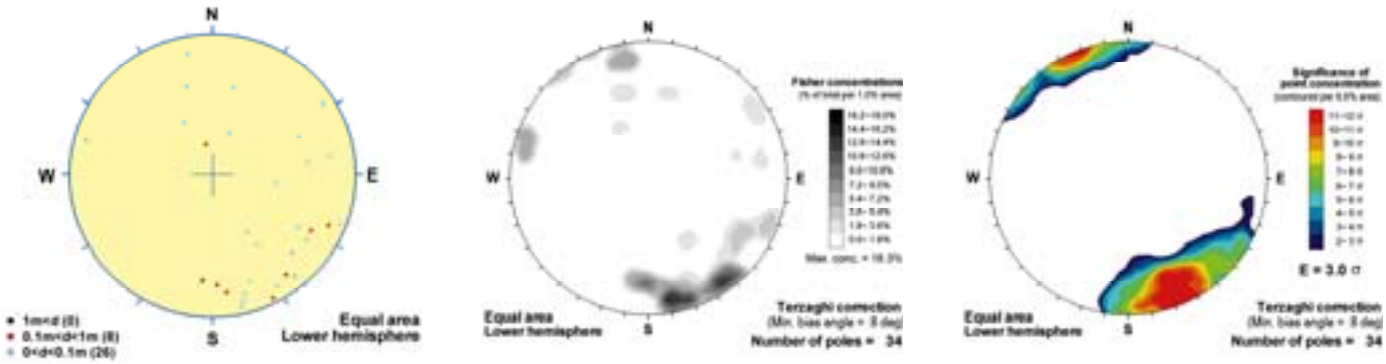

KLX12A

Fine-grained granite

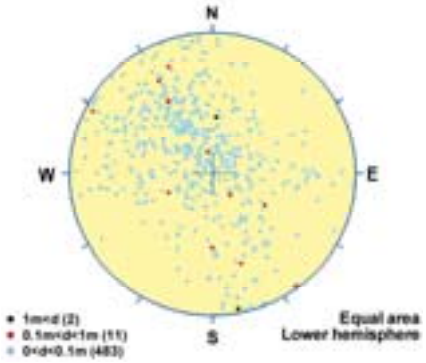

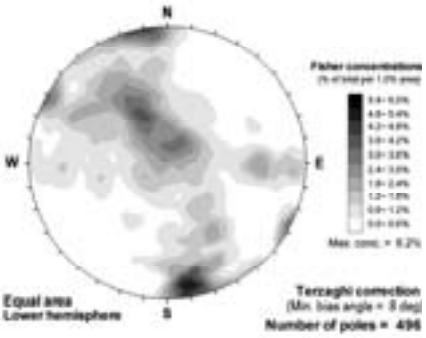

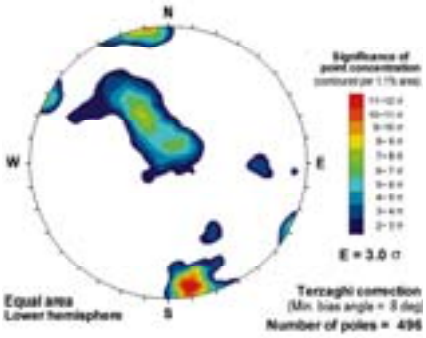

Fine-grained diorite-gabbro

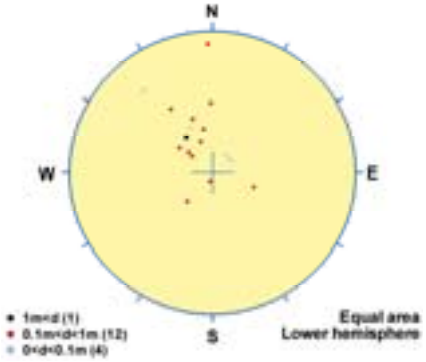

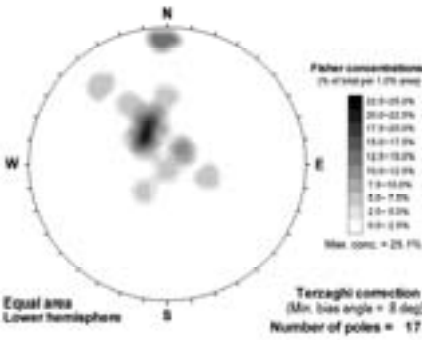

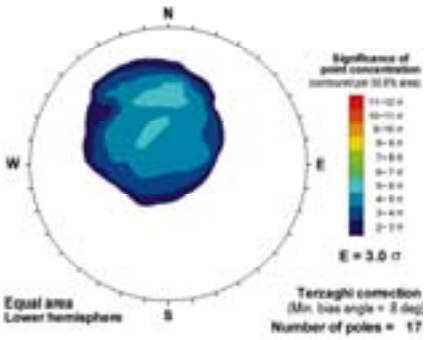

Pegmatite

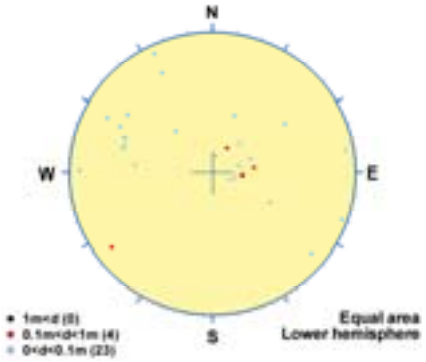

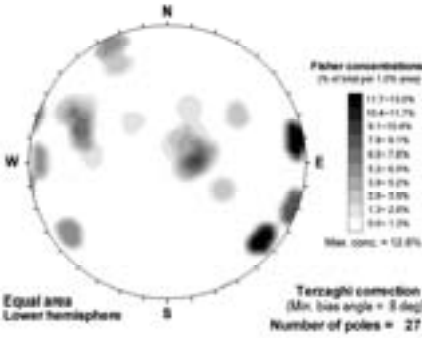

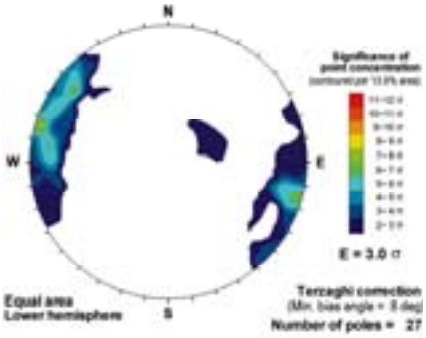

KLX13A

Fine-grained granite

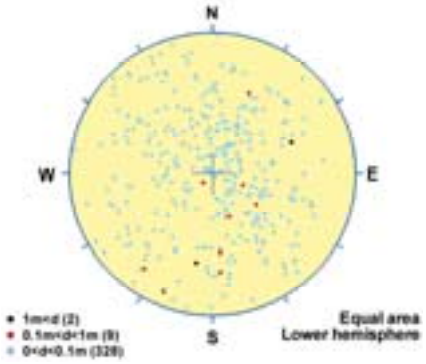

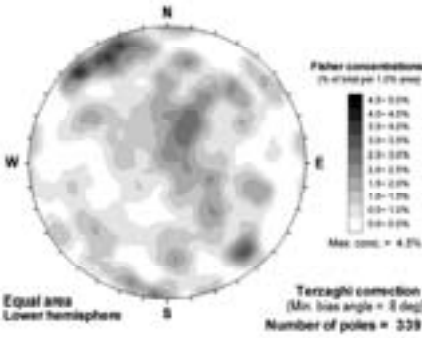

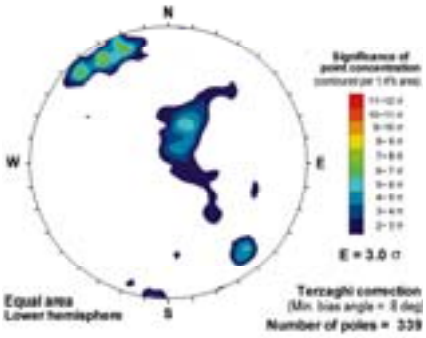

Fine-grained diorite-gabbro

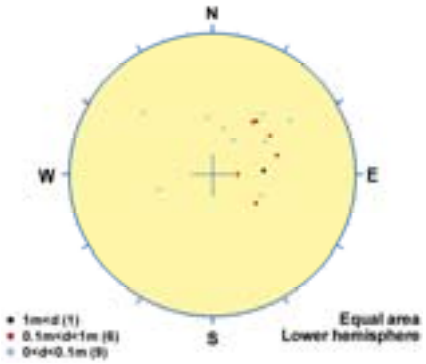

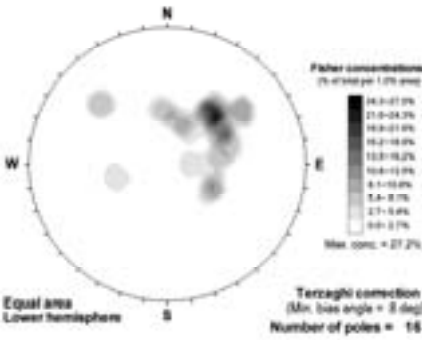

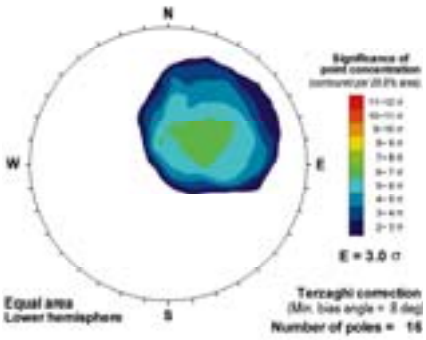

Pegmatite

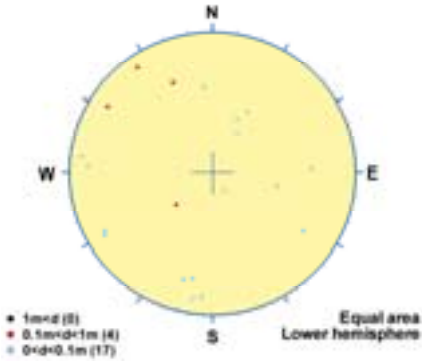

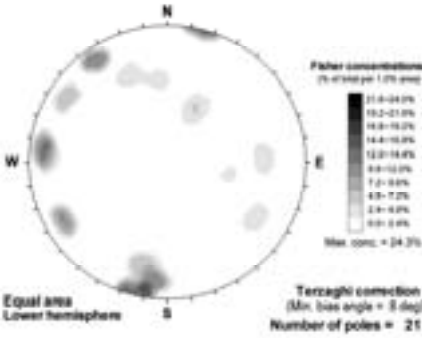

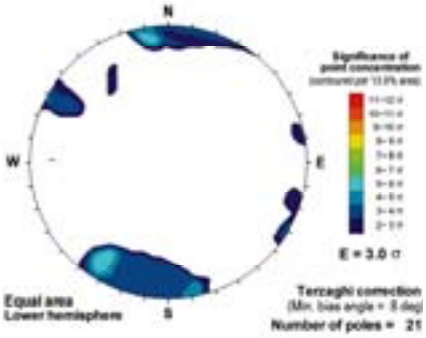

KLX14A

Fine-grained granite

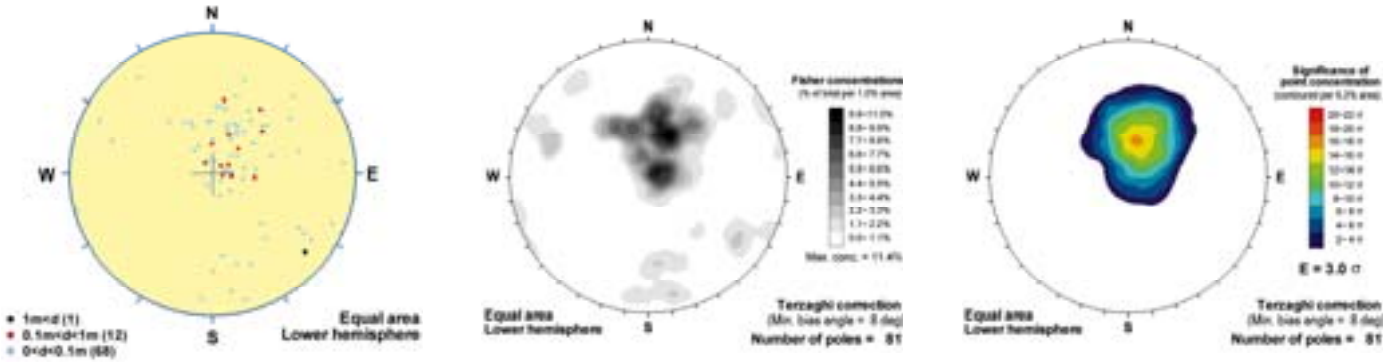

Fine-grained diorite-gabbro

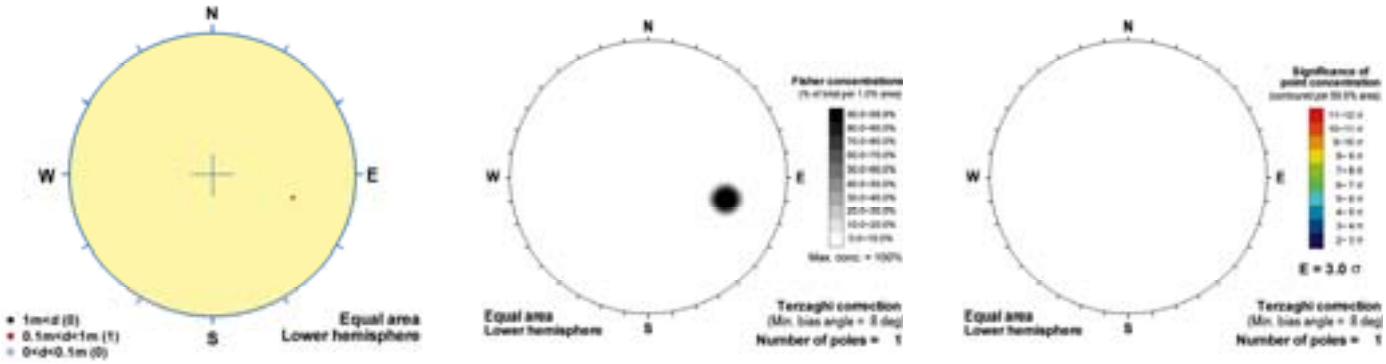

Pegmatite

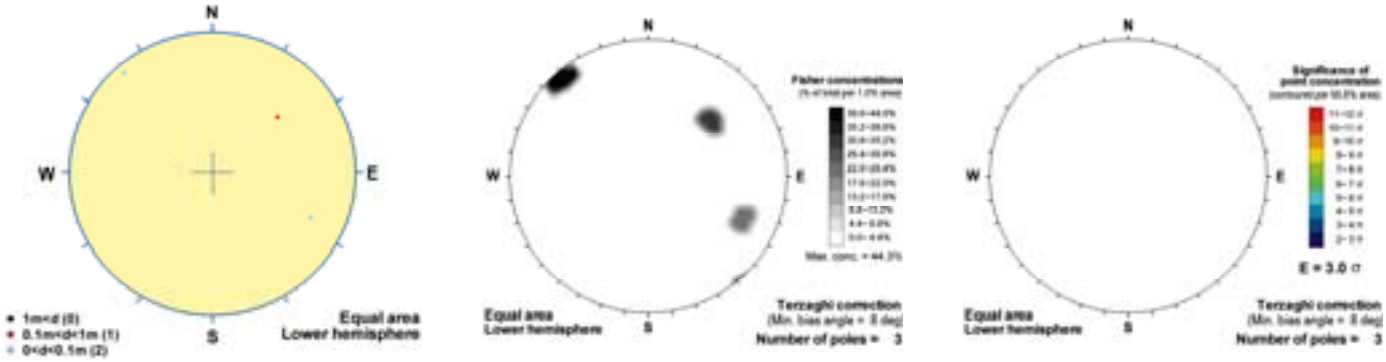

KLX15A

Fine-grained granite

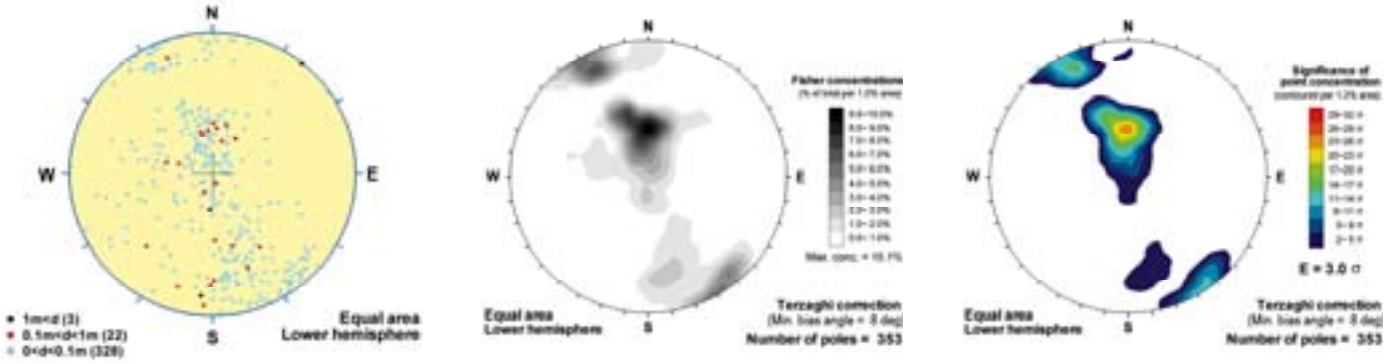

Fine-grained diorite-gabbro

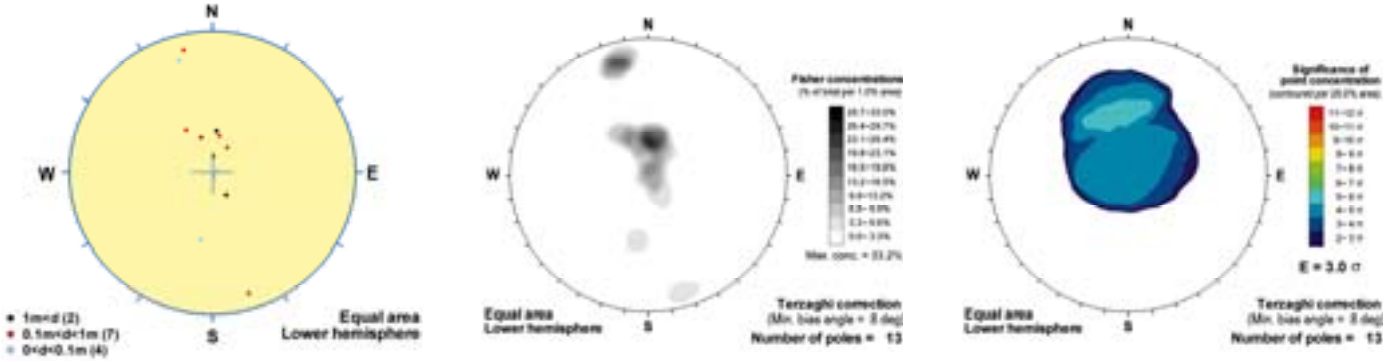

Pegmatite

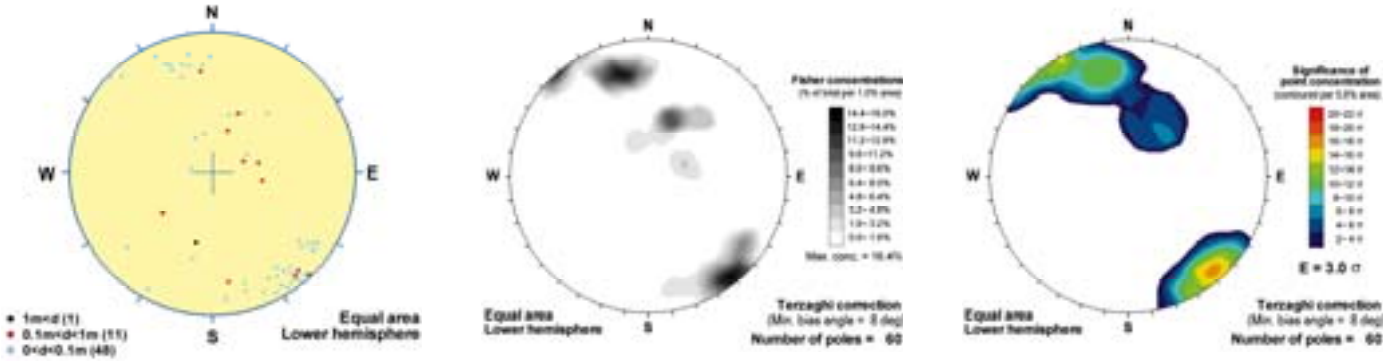

KLX16A

Fine-grained granite

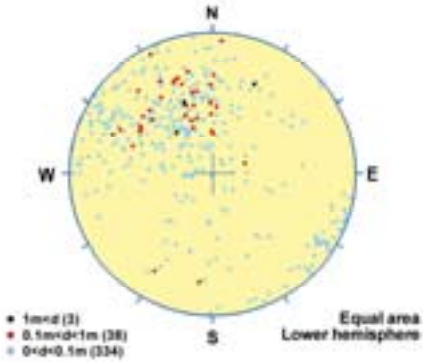

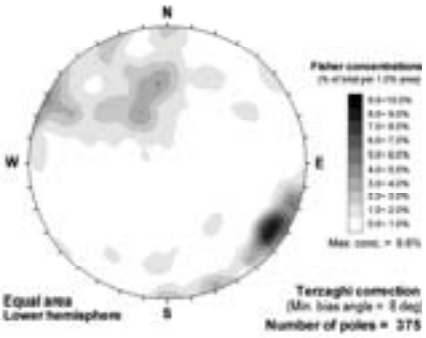

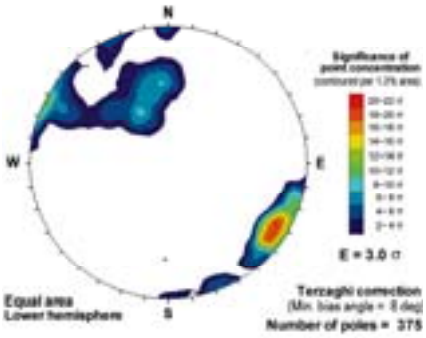

Fine-grained diorite-gabbro

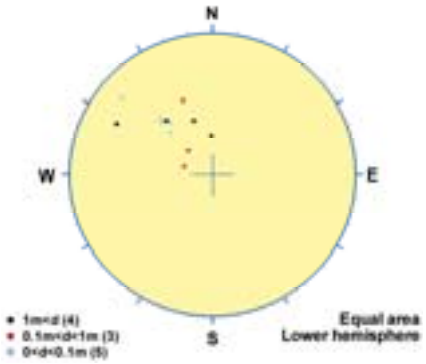

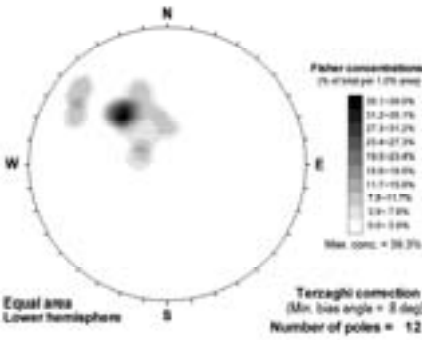

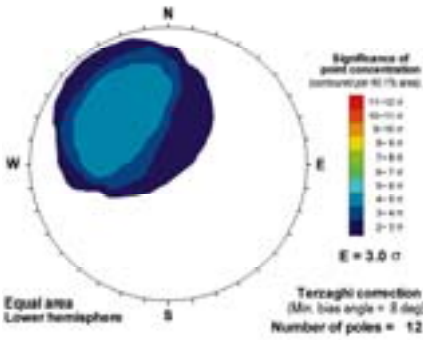

Pegmatite

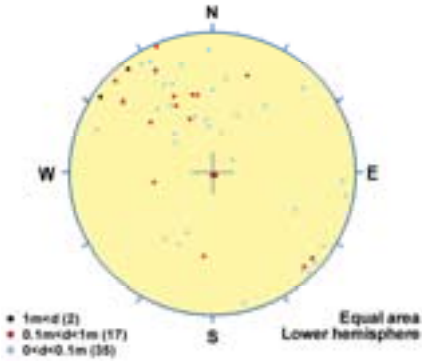

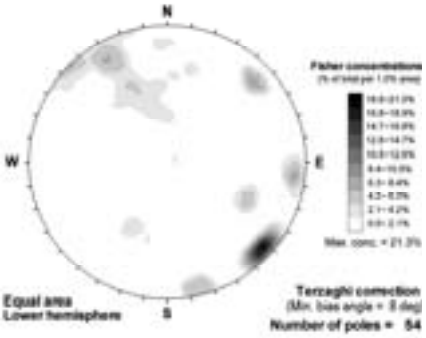

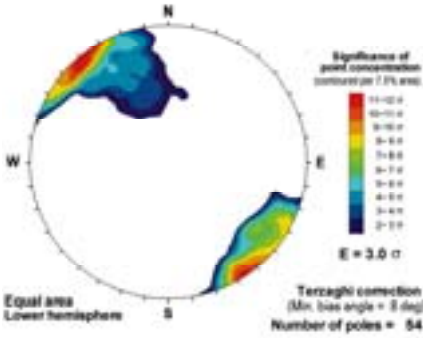

KLX17A

Fine-grained granite

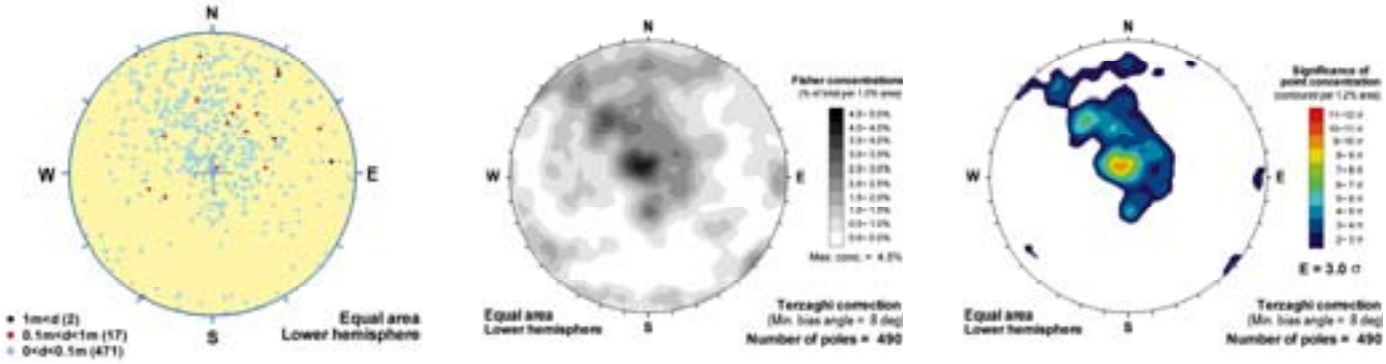

Fine-grained diorite-gabbro

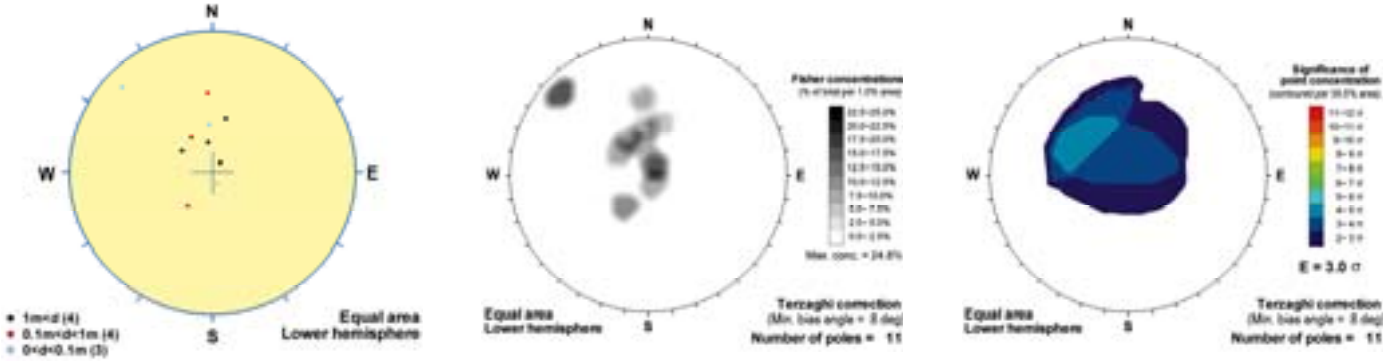

Pegmatite

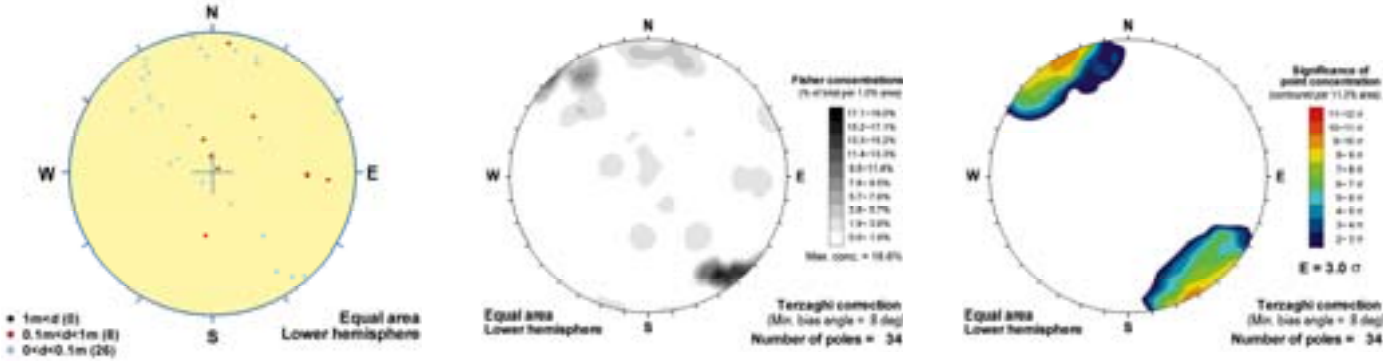

KLX18A

Fine-grained granite

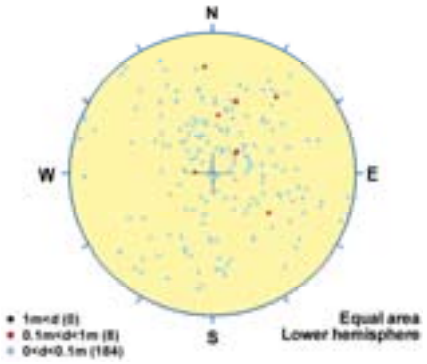

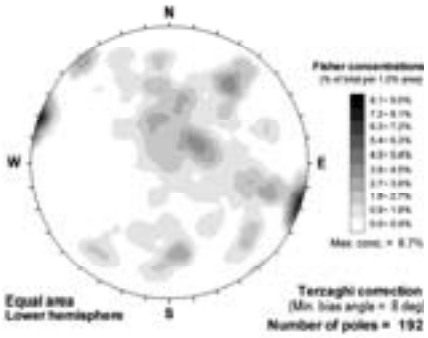

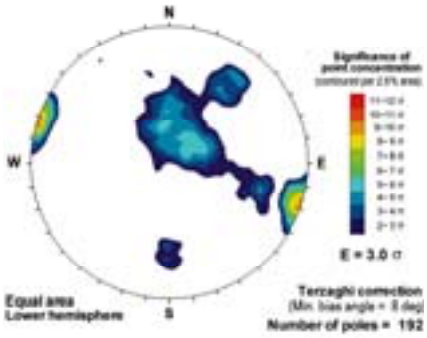

Fine-grained diorite-gabbro

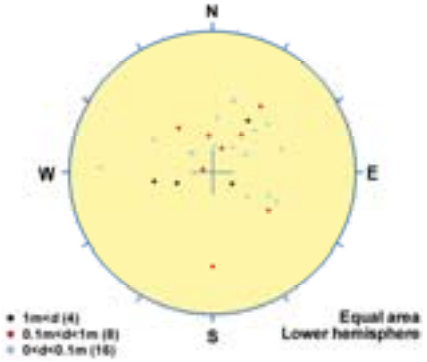

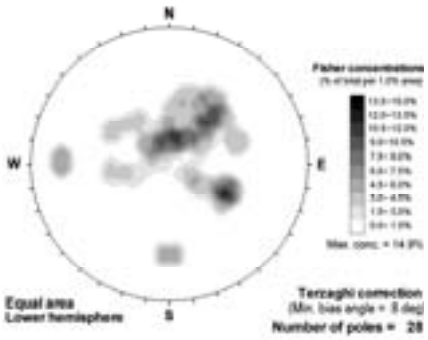

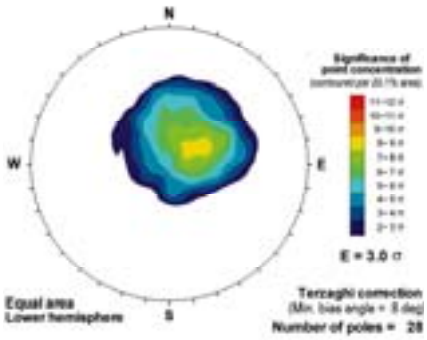

Pegmatite

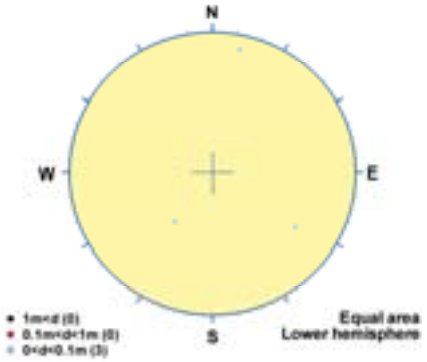

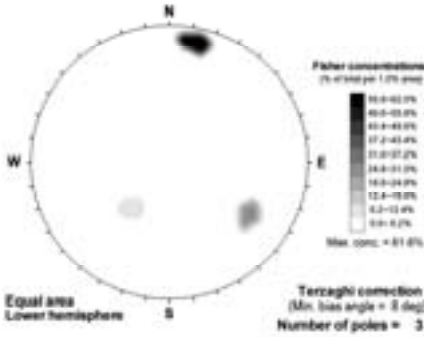

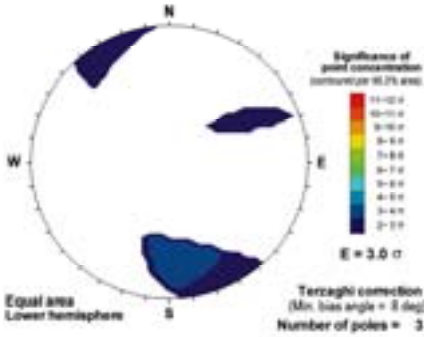

KLX19A

Fine-grained granite

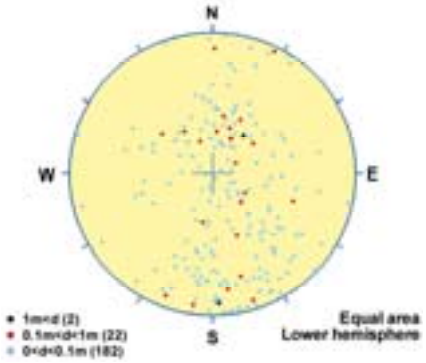

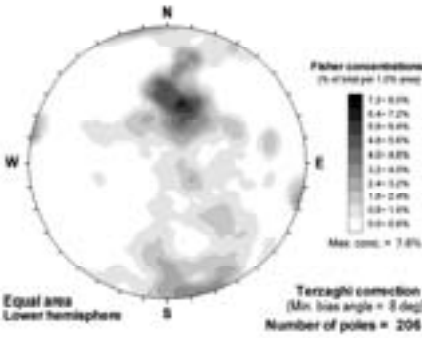

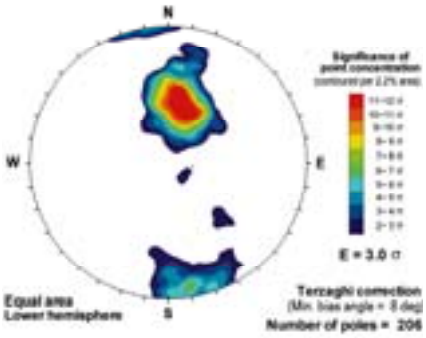

Fine-grained diorite-gabbro

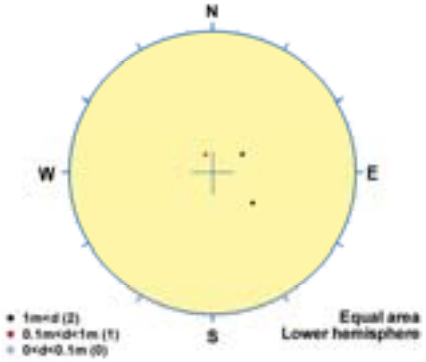

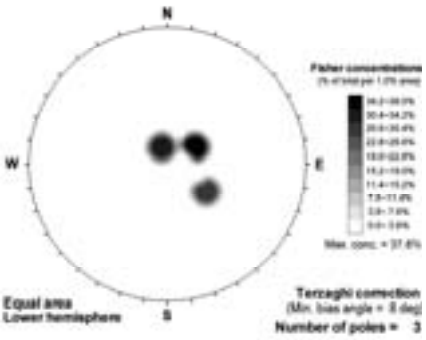

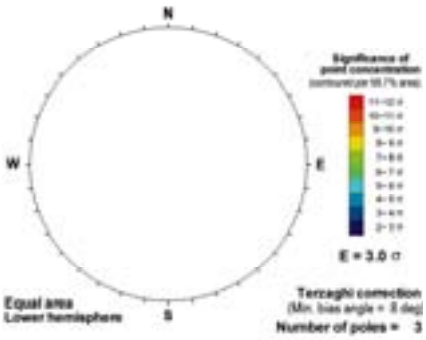

Pegmatite

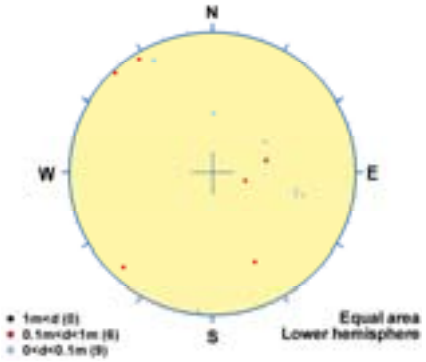

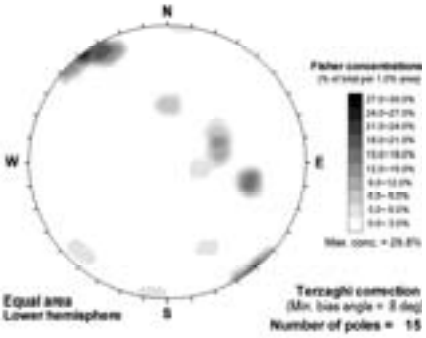

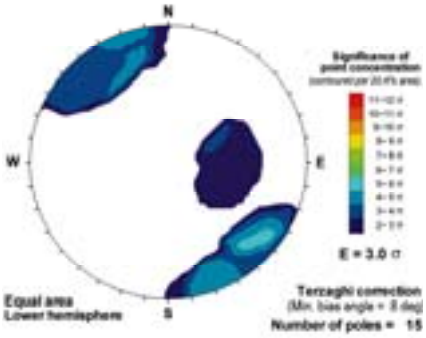

KLX20A

Fine-grained granite

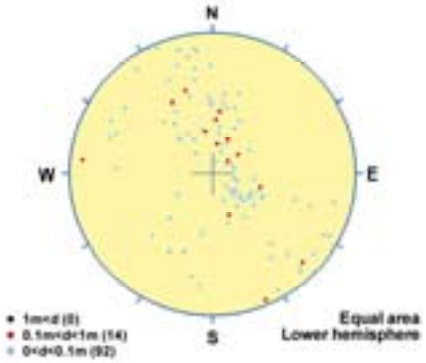

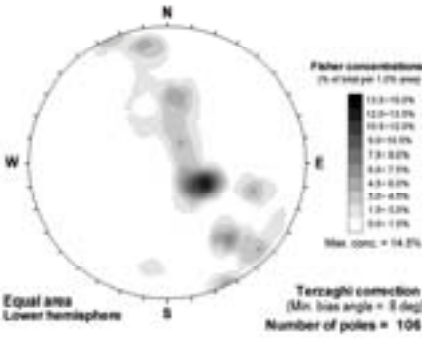

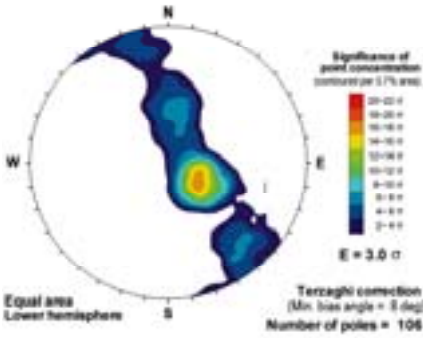

Fine-grained diorite-gabbro

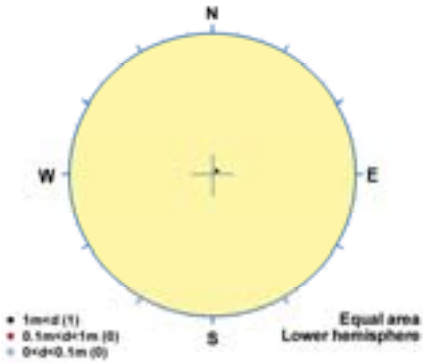

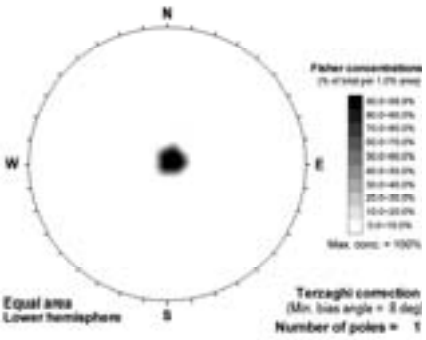

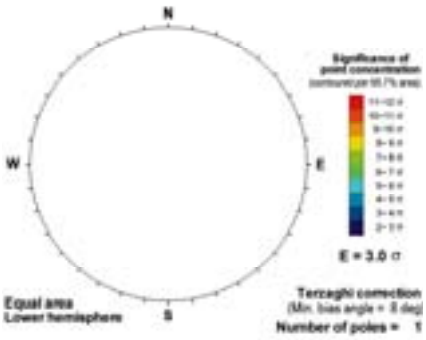

Pegmatite

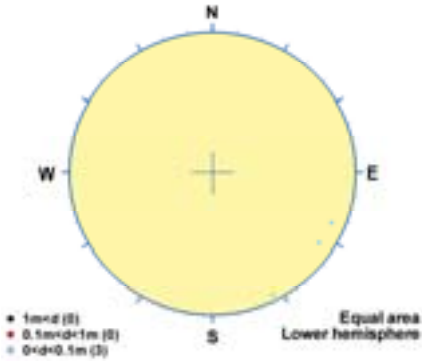

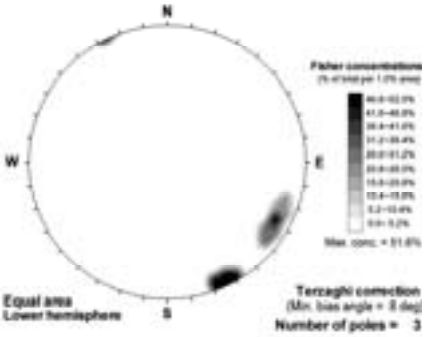

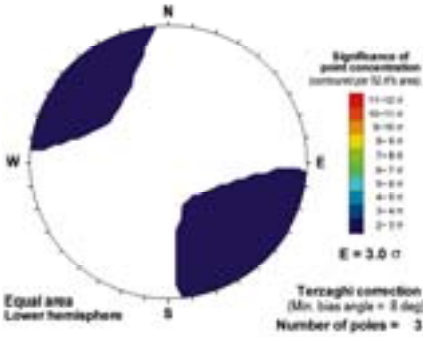

KLX21B

Fine-grained granite

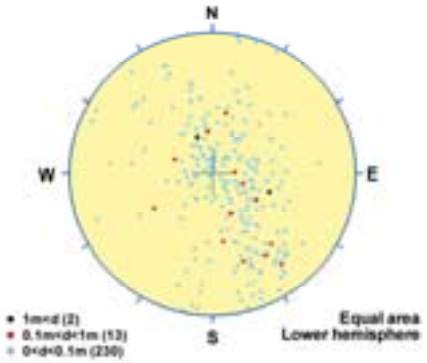

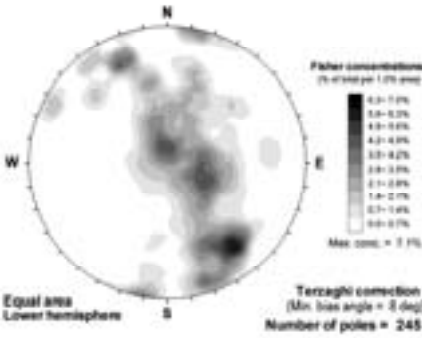

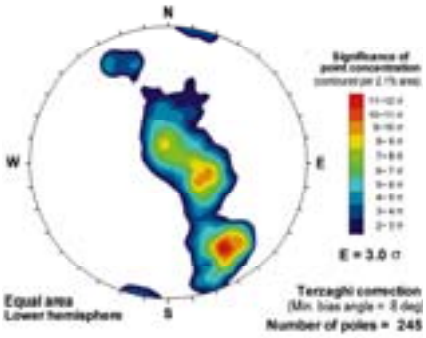

Fine-grained diorite-gabbro

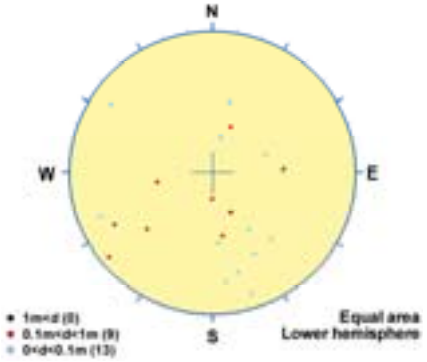

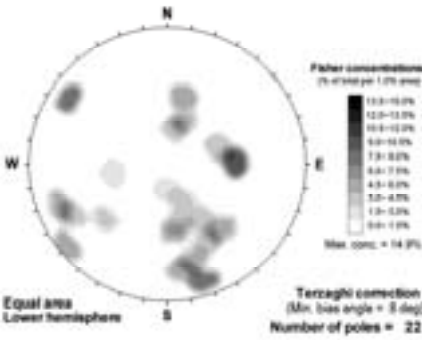

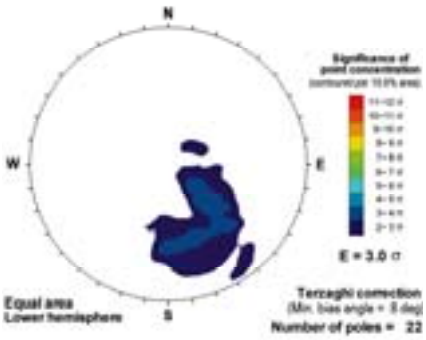

Pegmatite

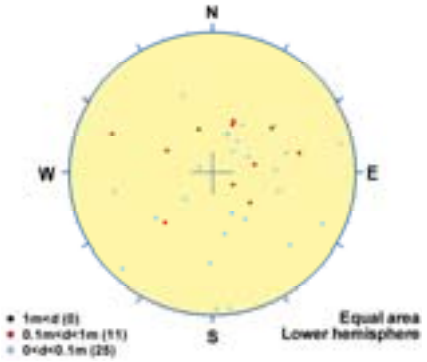

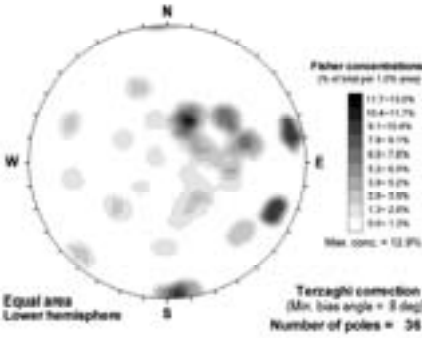

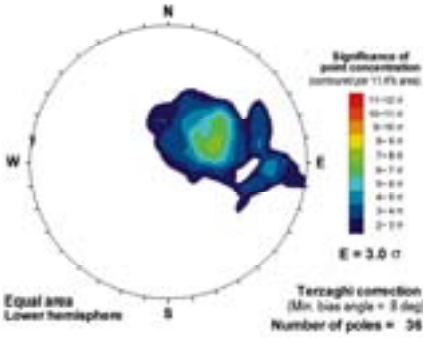

KLX22A

Fine-grained granite

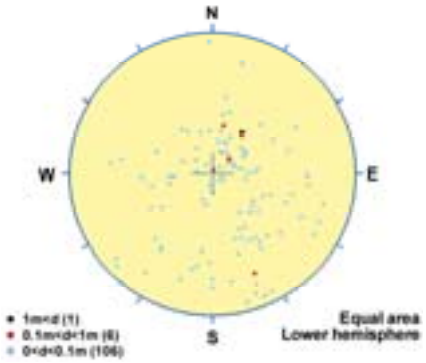

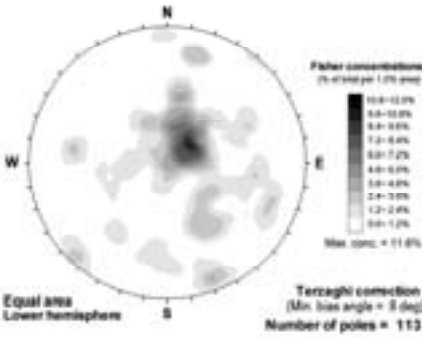

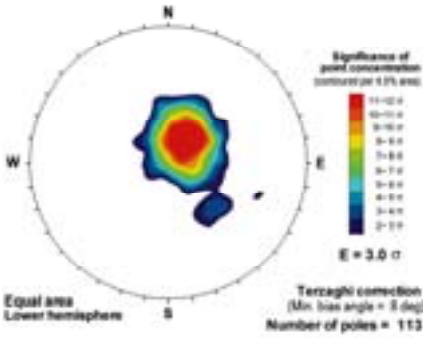

Fine-grained diorite-gabbro

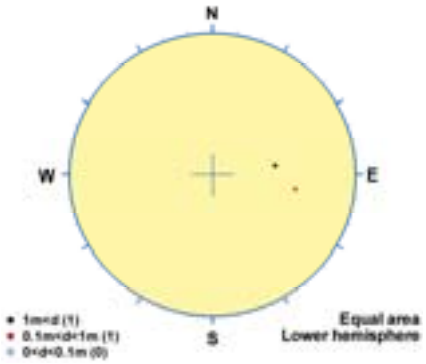

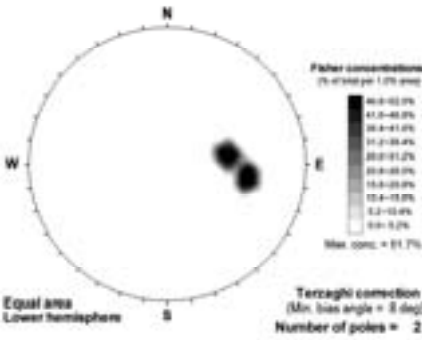

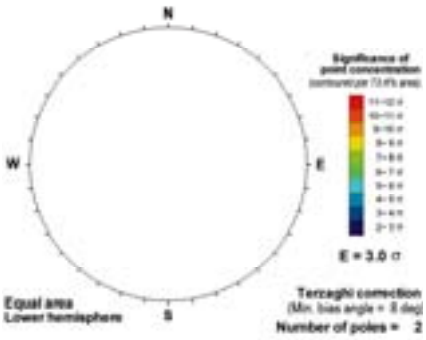

Pegmatite

KLX22B

Fine-grained granite

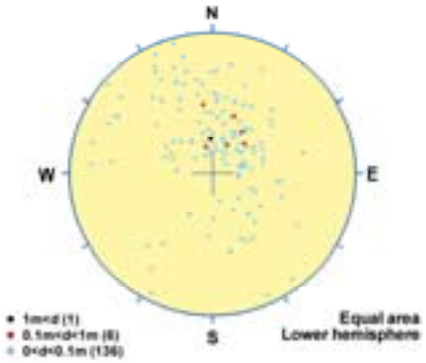

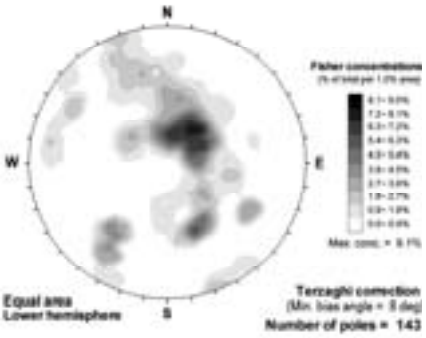

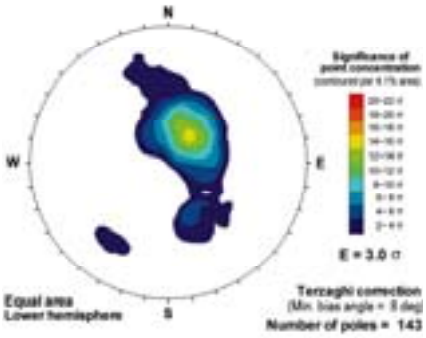

Fine-grained diorite-gabbro

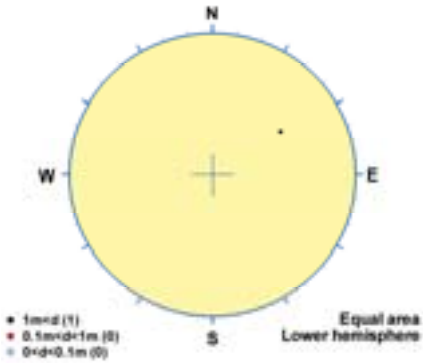

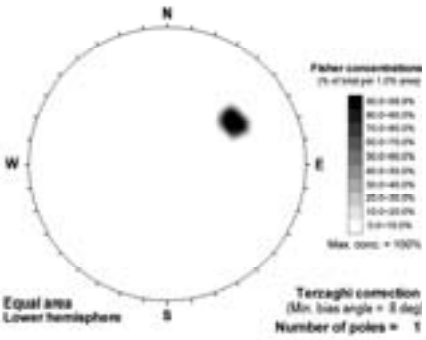

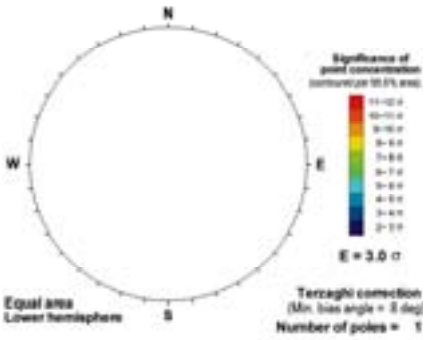

Pegmatite

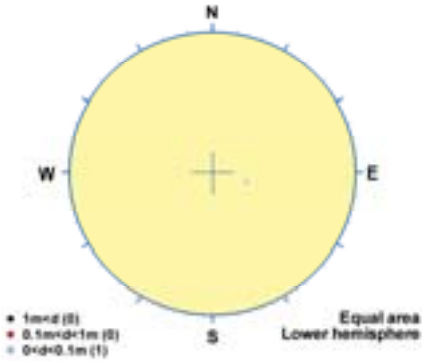

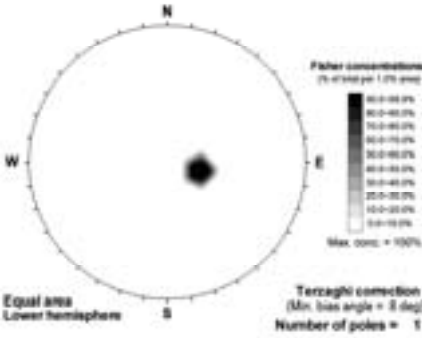

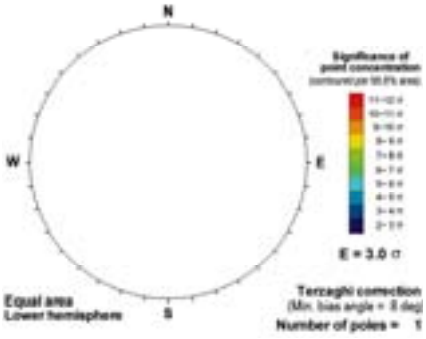

KLX23A

Fine-grained granite

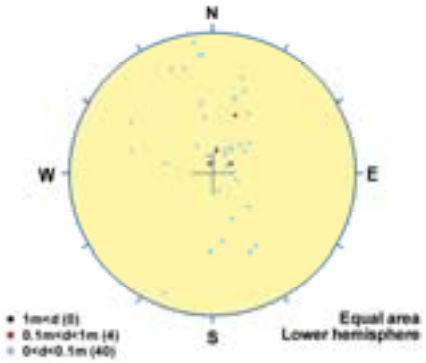

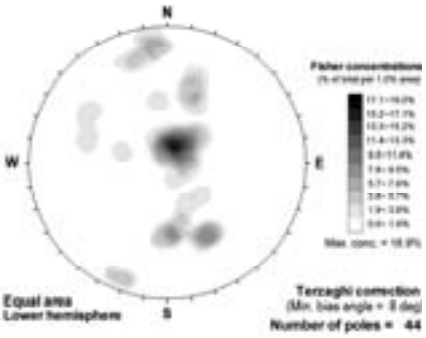

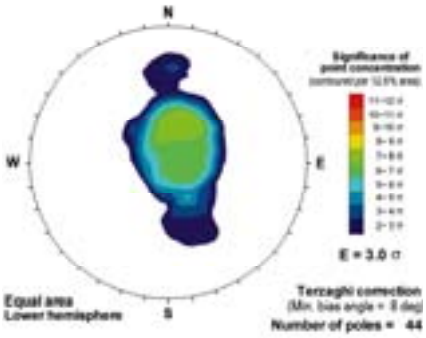

Fine-grained diorite-gabbro

Pegmatite

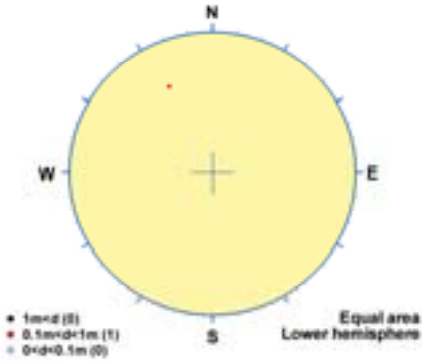

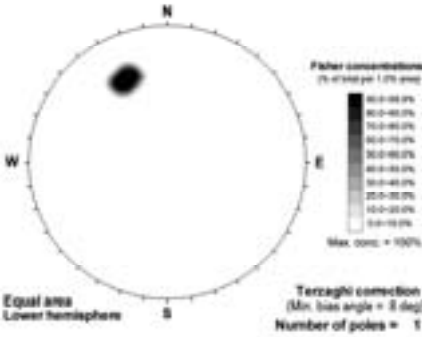

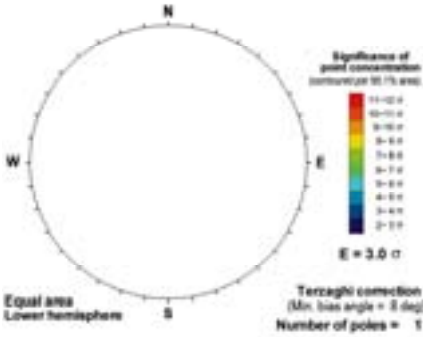

KLX23B

Fine-grained granite

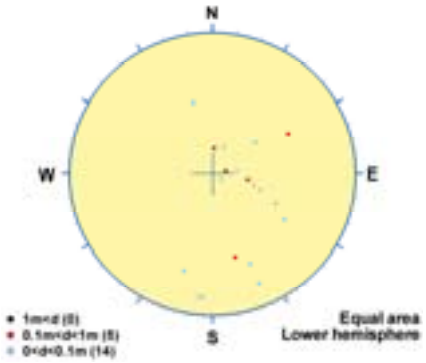

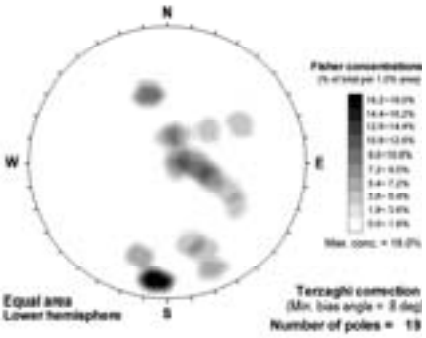

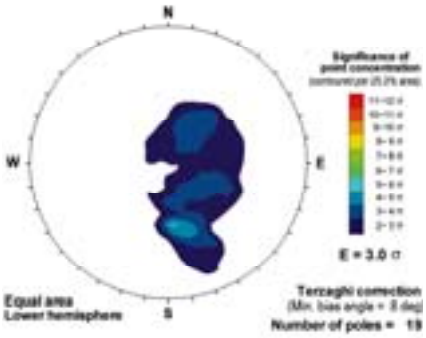

Fine-grained diorite-gabbro

Pegmatite

KLX24A

Fine-grained granite

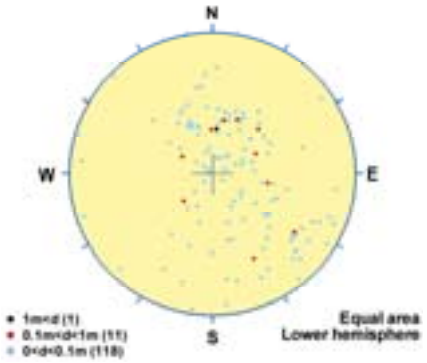

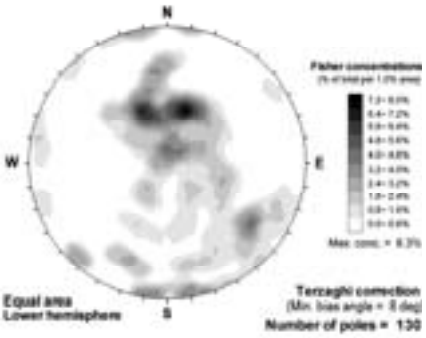

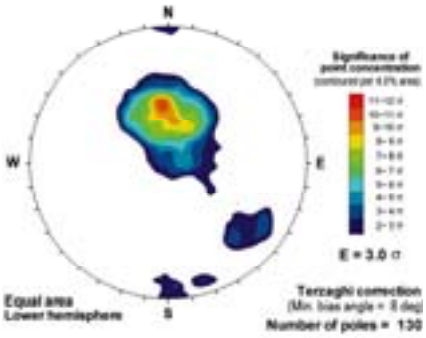

Fine-grained diorite-gabbro

Pegmatite

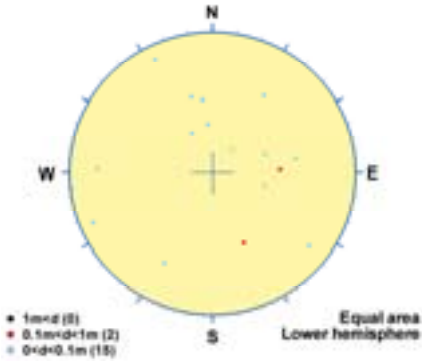

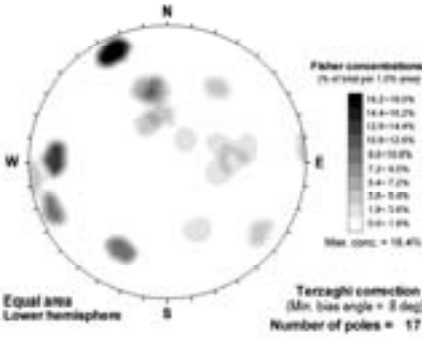

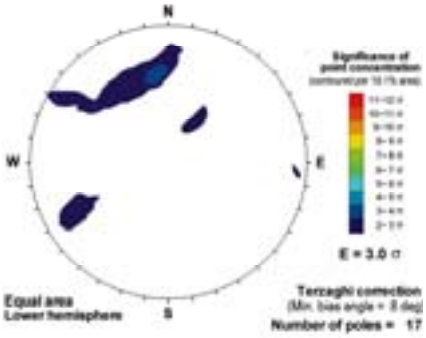

KLX25A

Fine-grained granite

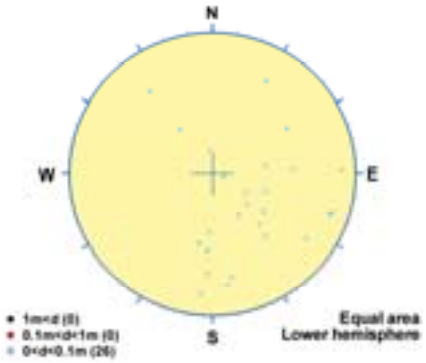

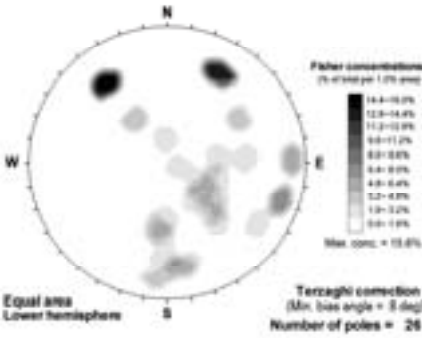

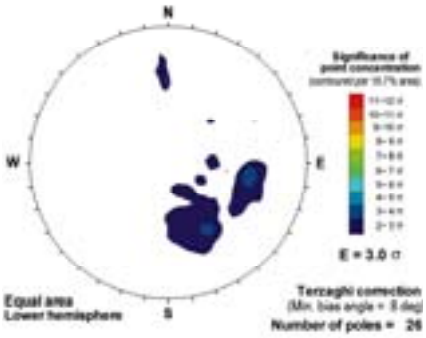

Fine-grained diorite-gabbro

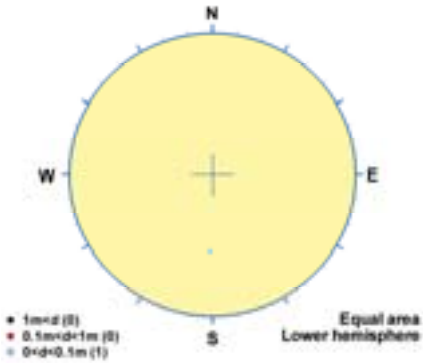

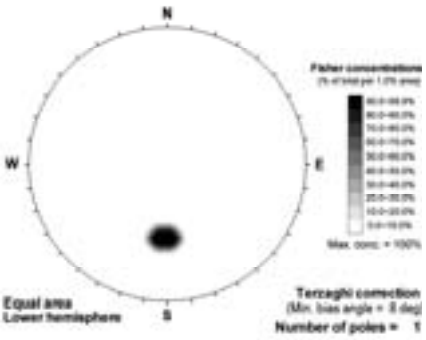

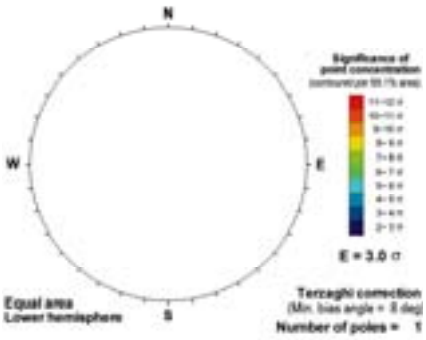

Pegmatite

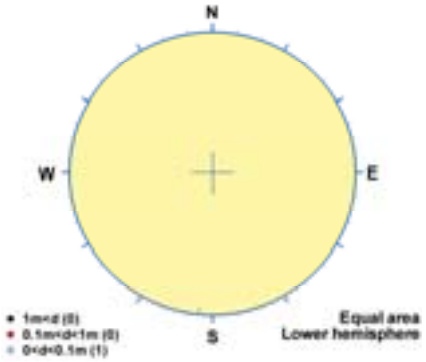

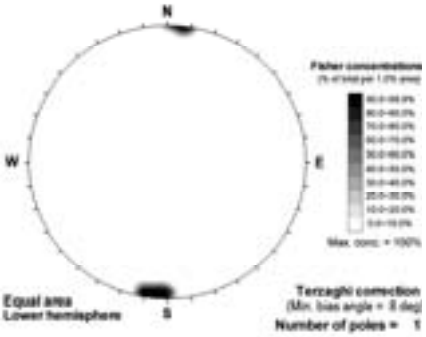

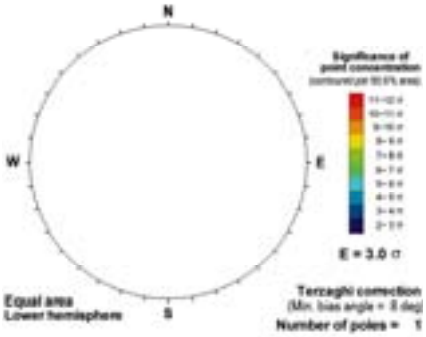

KLX26A

Fine-grained granite

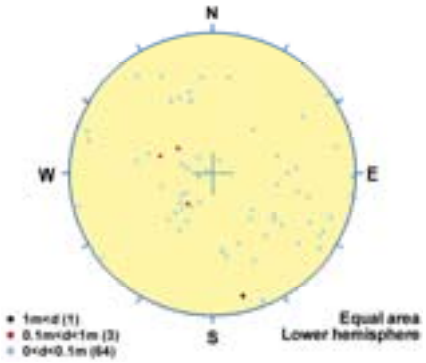

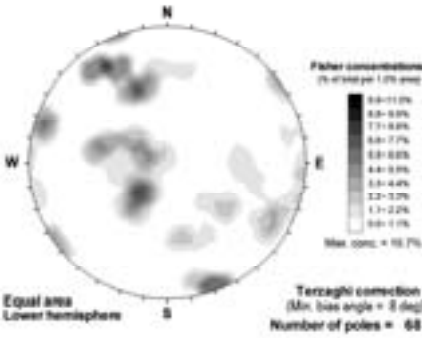

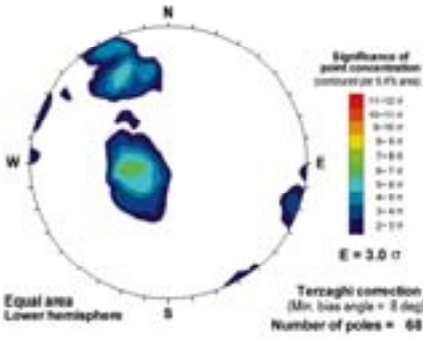

Fine-grained diorite-gabbro

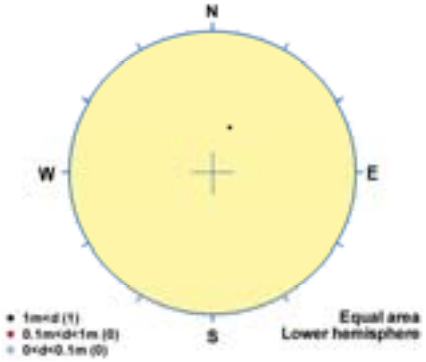

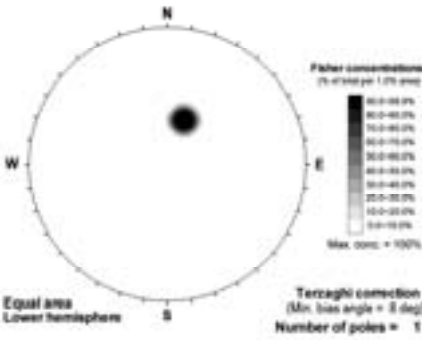

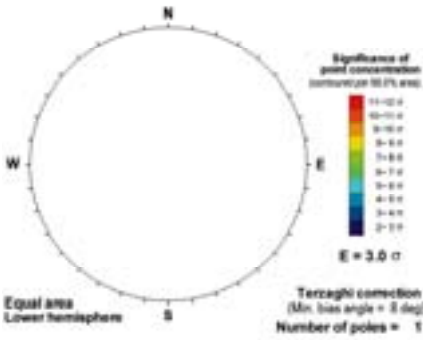

Pegmatite

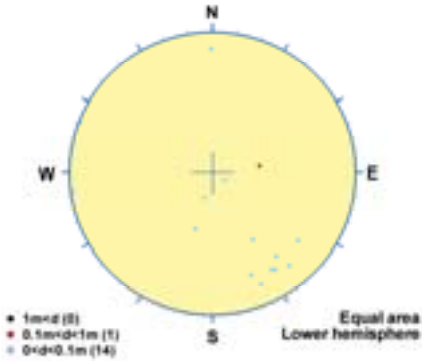

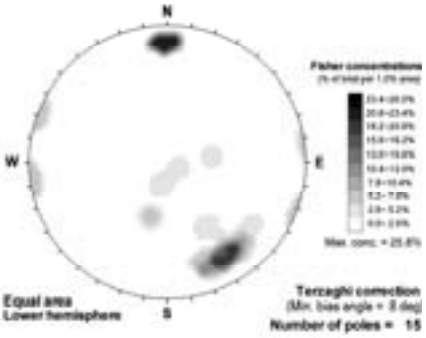

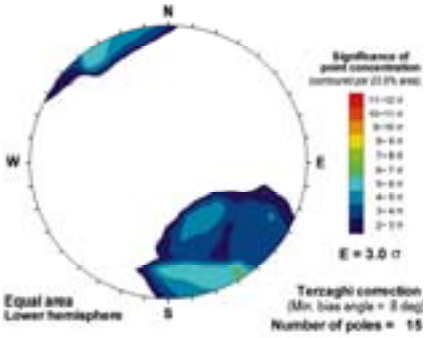

KLX26B

Fine-grained granite

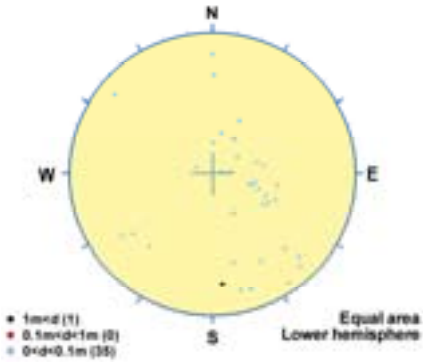

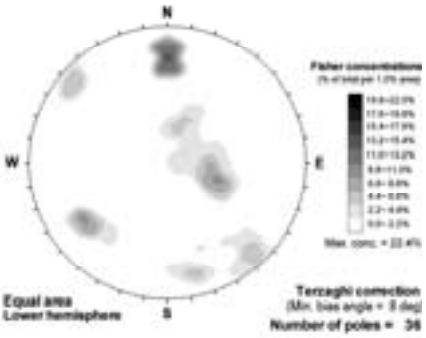

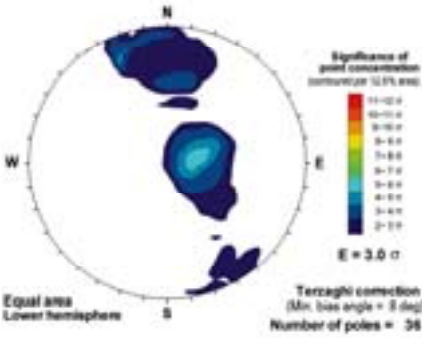

Fine-grained diorite-gabbro

Pegmatite

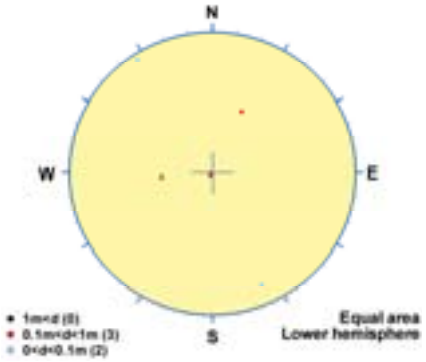

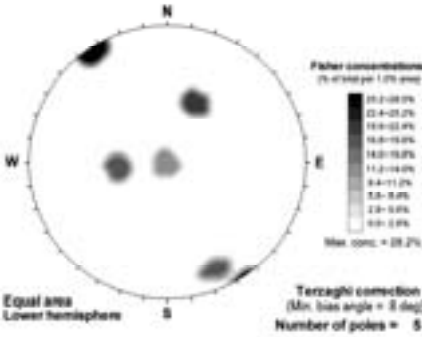

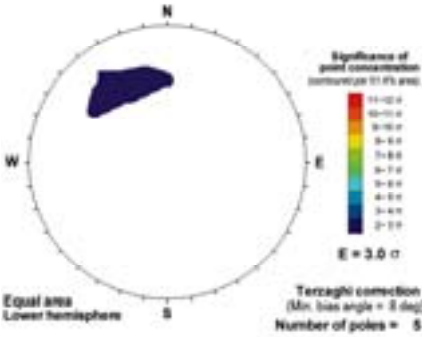

KLX28A

Fine-grained granite

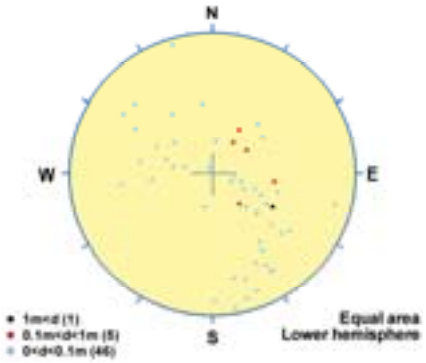

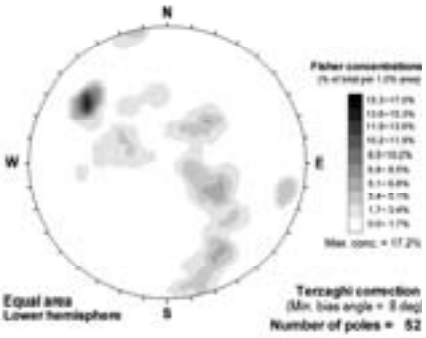

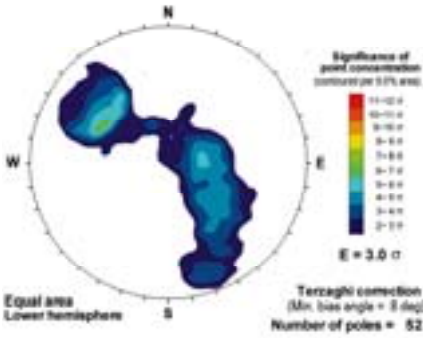

Fine-grained diorite-gabbro

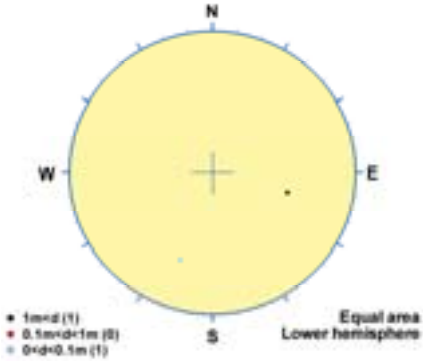

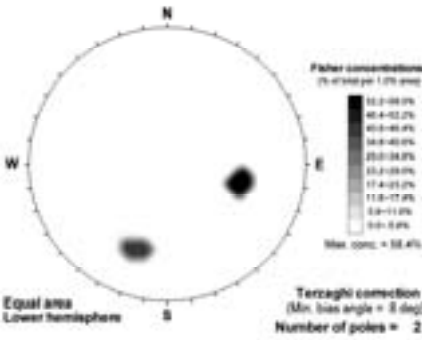

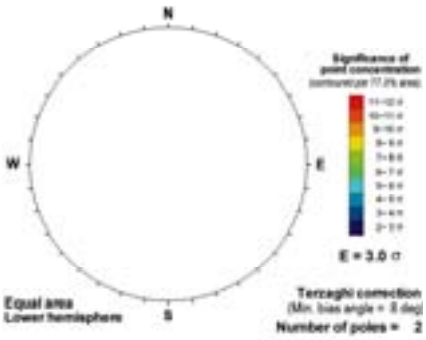

Pegmatite

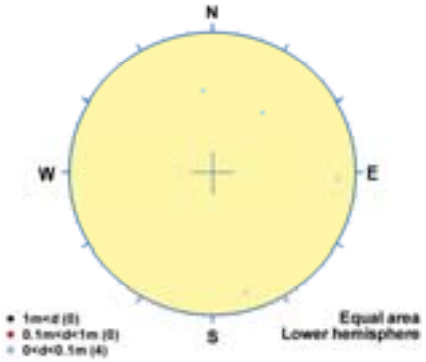

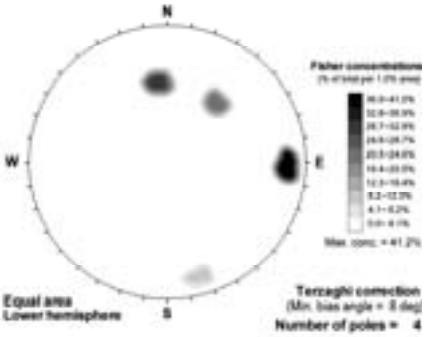

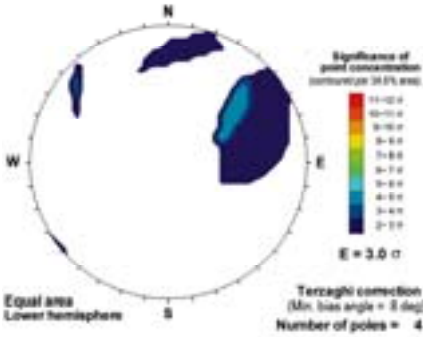

KLX29A

Fine-grained granite

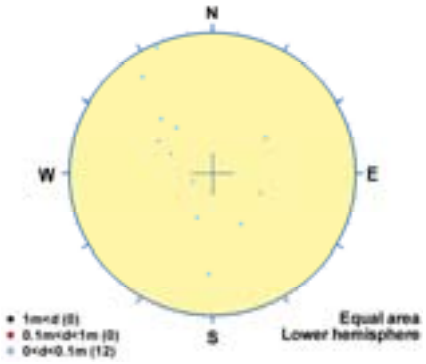

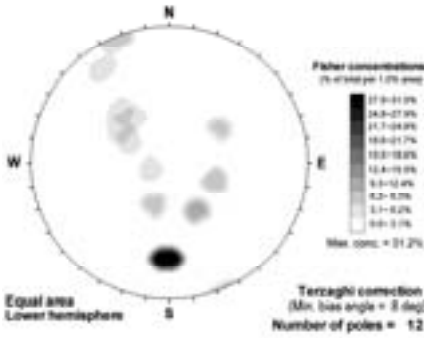

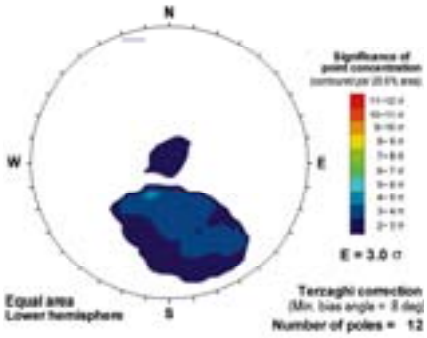

Fine-grained diorite-gabbro

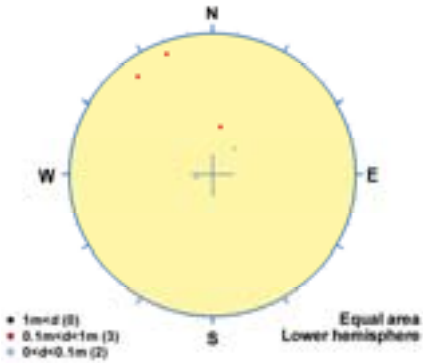

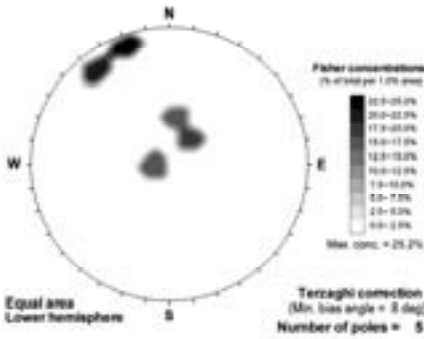

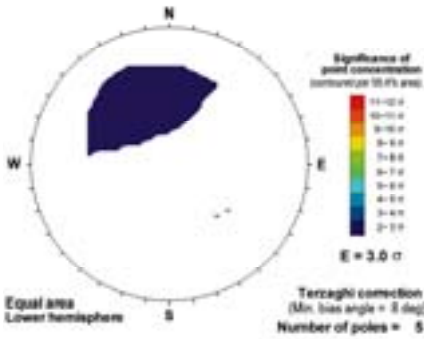

Pegmatite

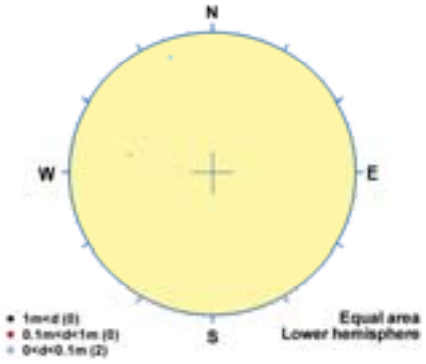

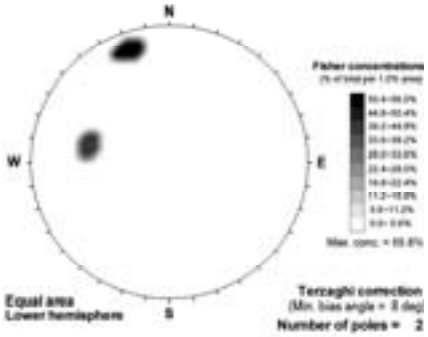

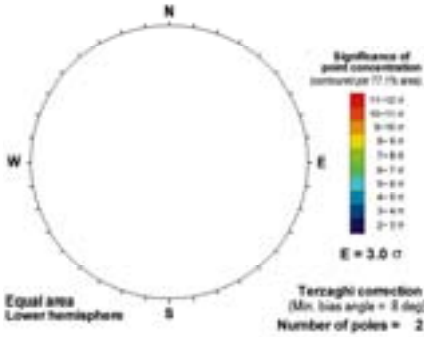

Orientation of contacts of subordinate rock types on a rock domain basis in each borehole

KLX02_RSMA01

Fine-grained granite

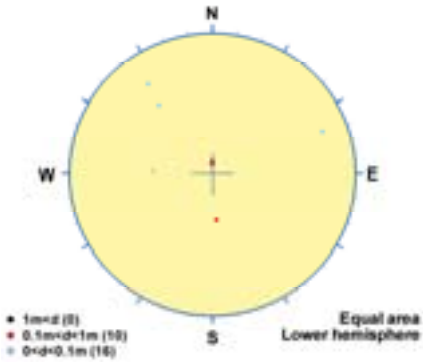

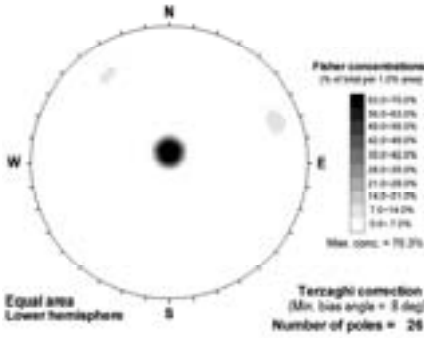

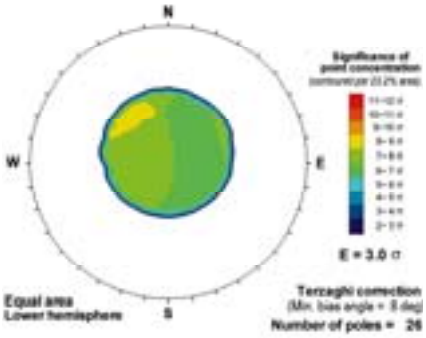

Fine-grained diorite-gabbro

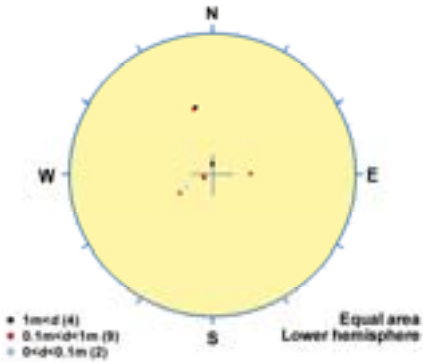

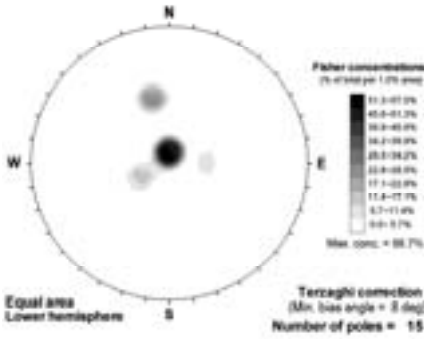

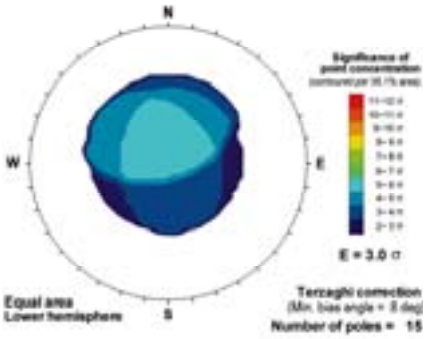

Pegmatite

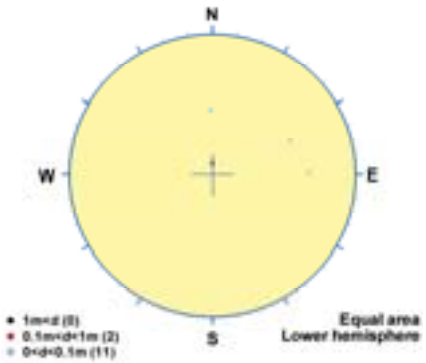

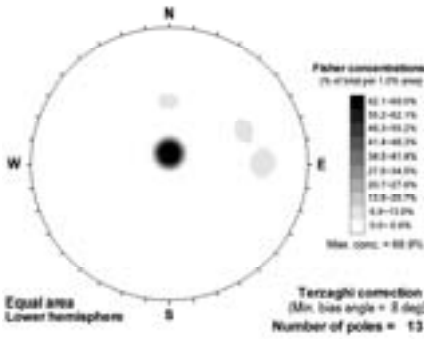

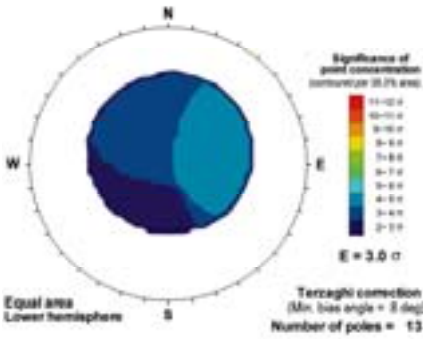

KLX02_RSMBA03

Fine-grained granite

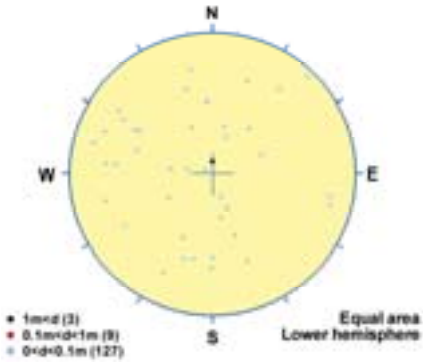

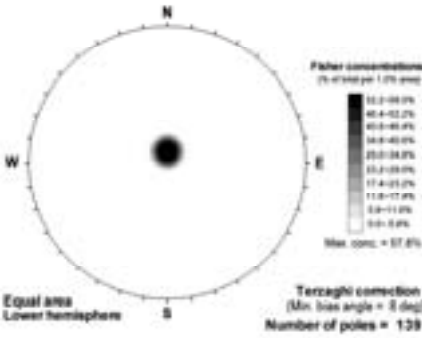

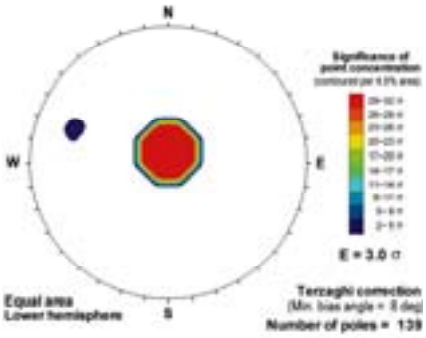

Fine-grained diorite-gabbro

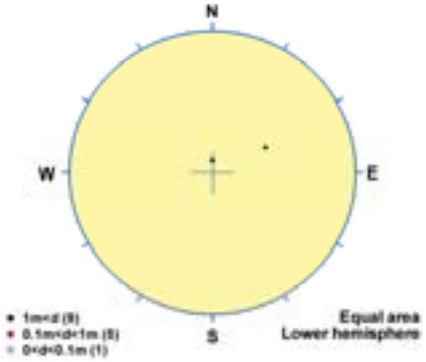

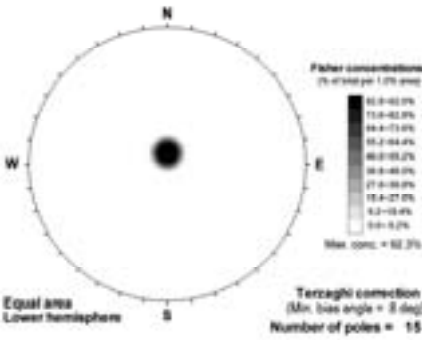

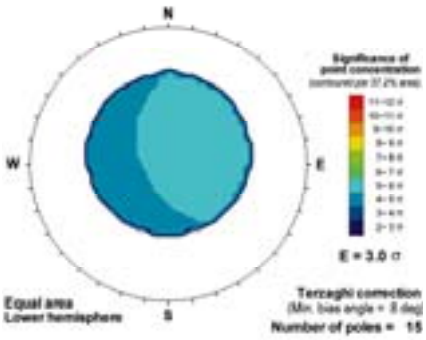

Pegmatite

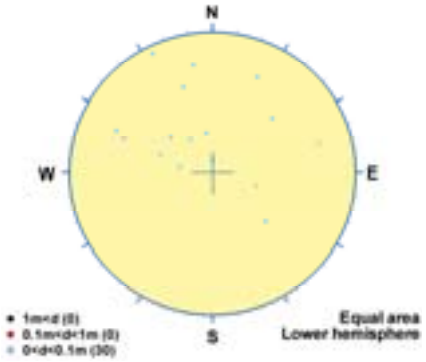

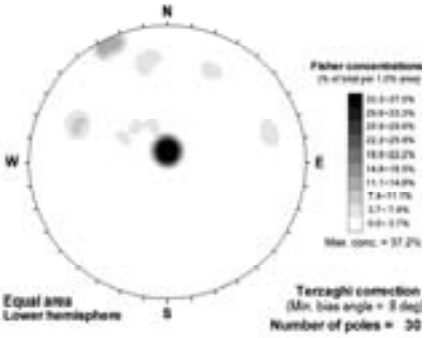

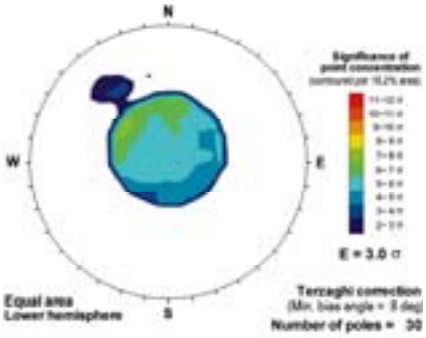

KLX03_RSMD01

Fine-grained granite

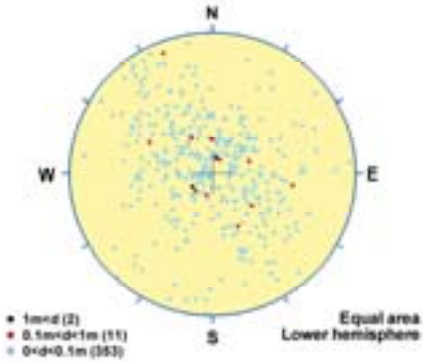

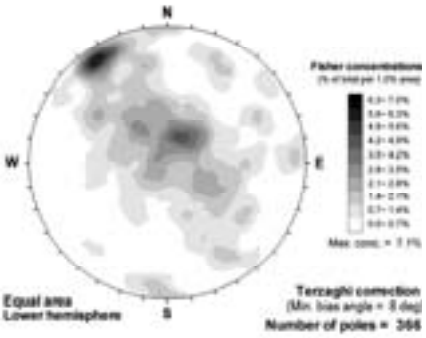

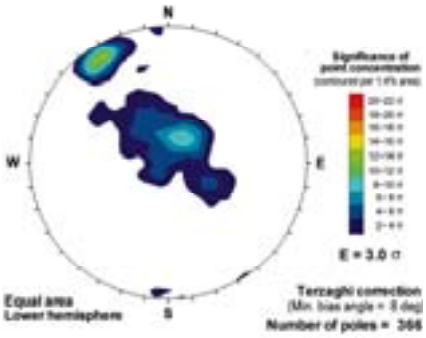

Fine-grained diorite-gabbro

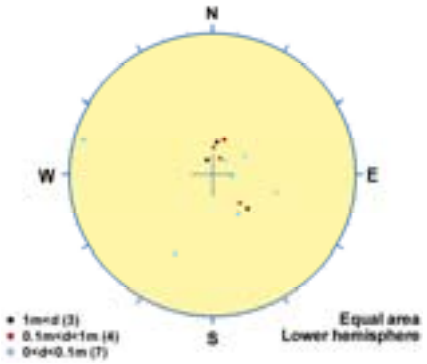

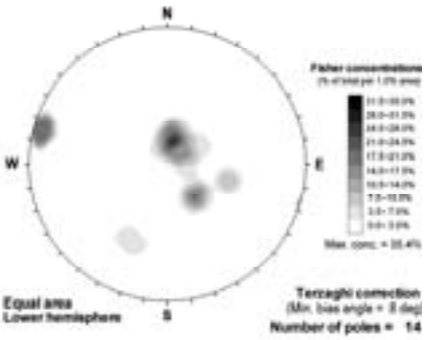

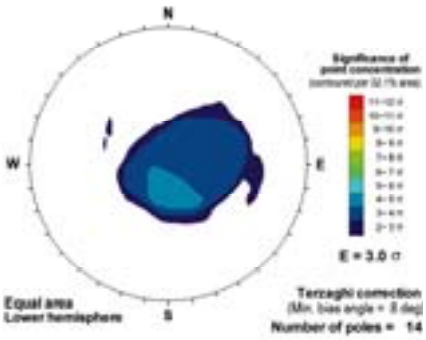

Pegmatite

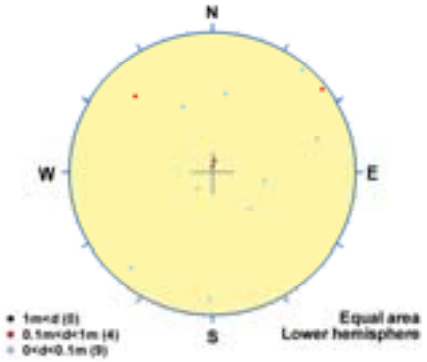

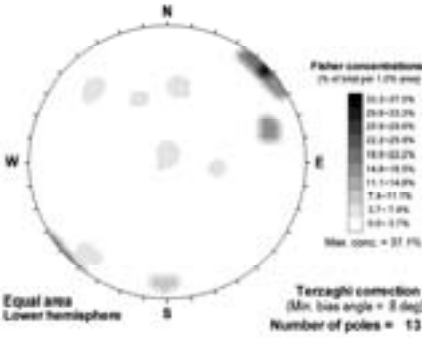

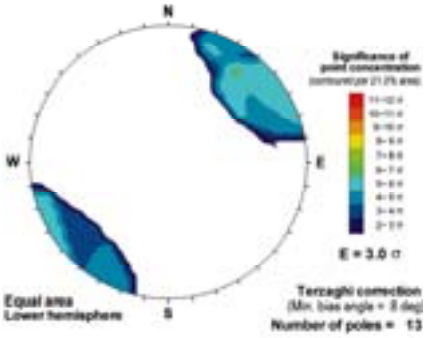

KLX03_RSMM01

Fine-grained granite

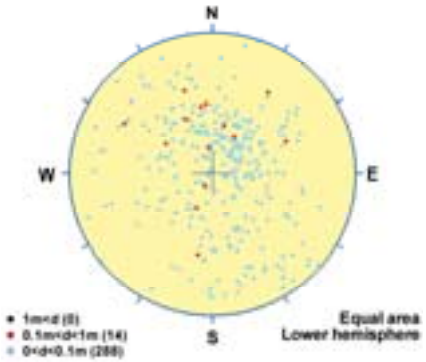

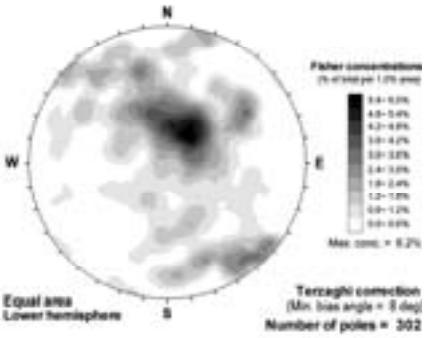

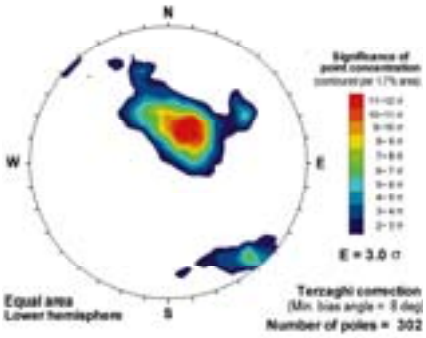

Fine-grained diorite-gabbro

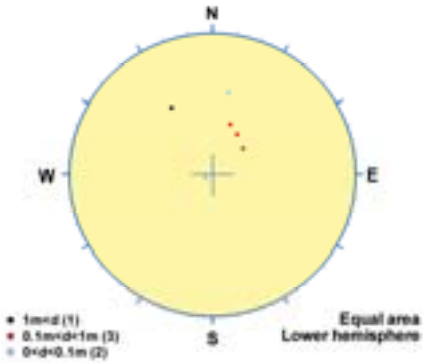

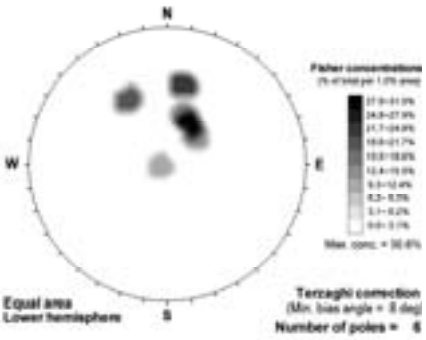

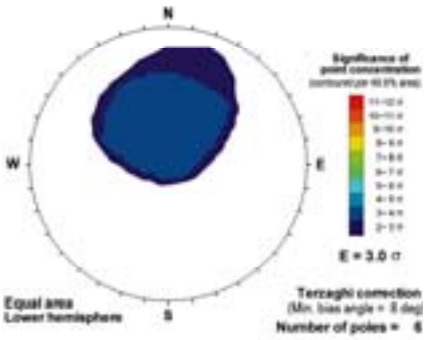

Pegmatite

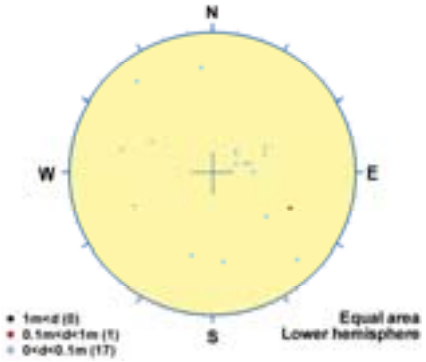

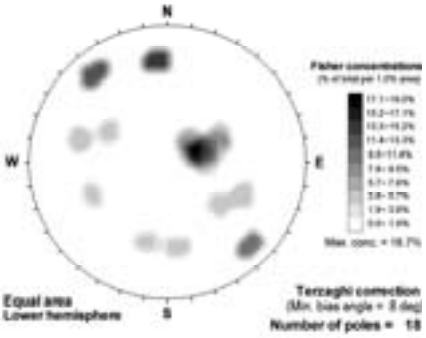

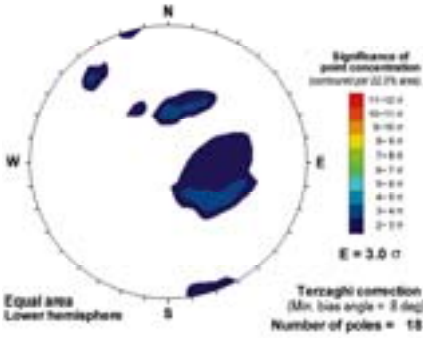

KLX04_RSMA01

Fine-grained granite

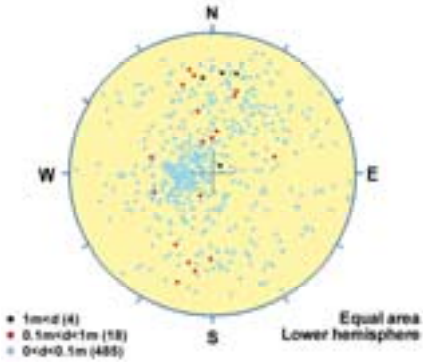

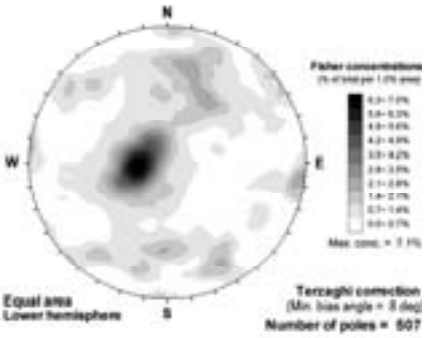

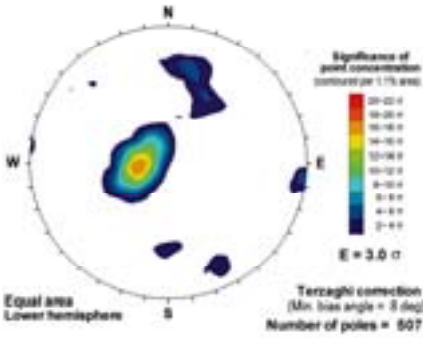

Fine-grained diorite-gabbro

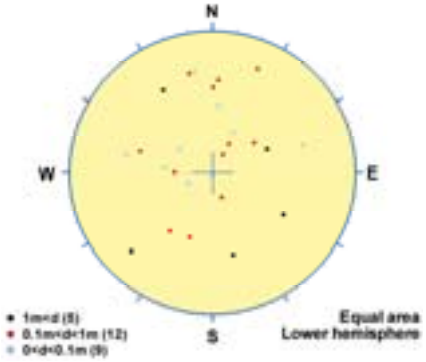

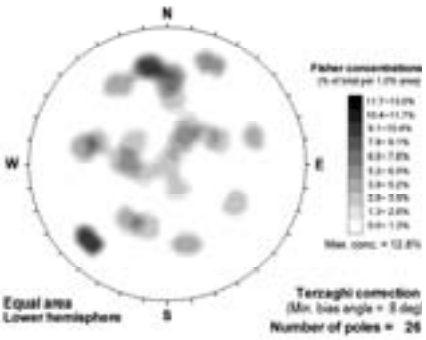

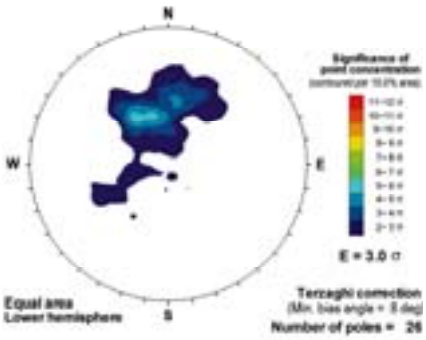

Pegmatite

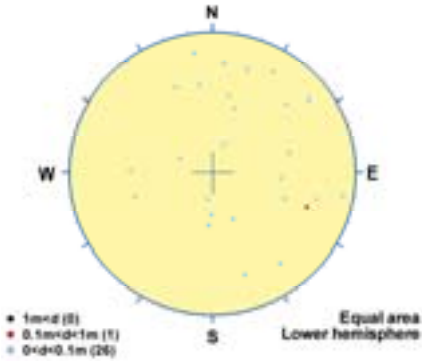

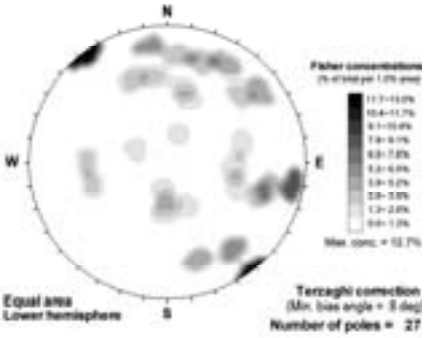

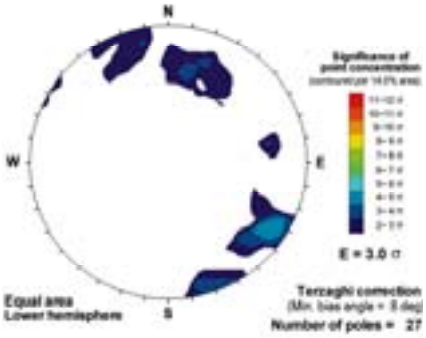

KLX05_RSMD01

Fine-grained granite

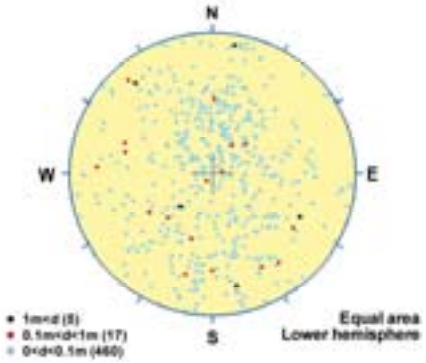

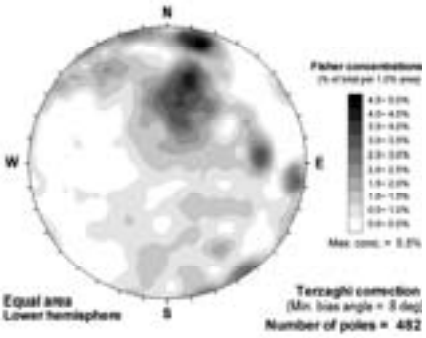

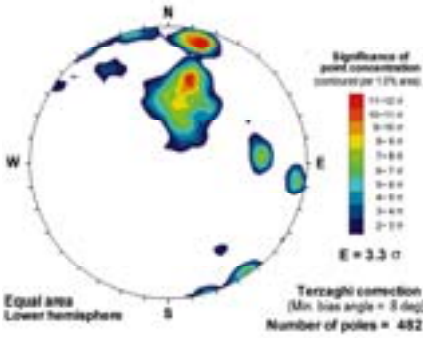

Fine-grained diorite-gabbro

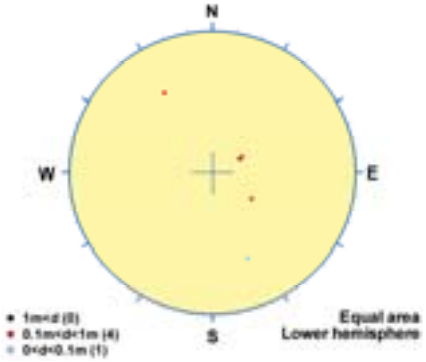

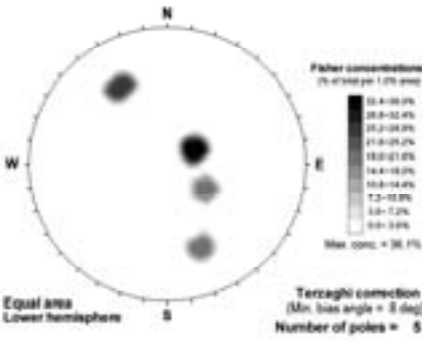

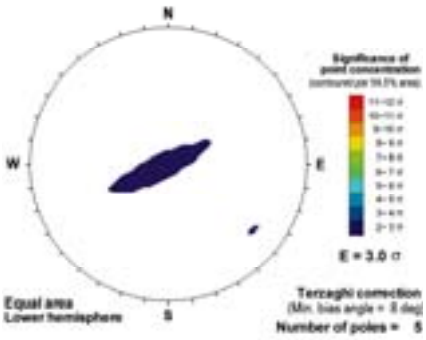

Pegmatite

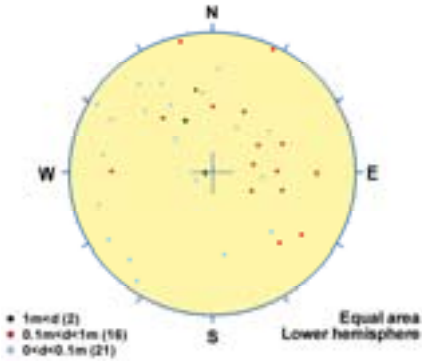

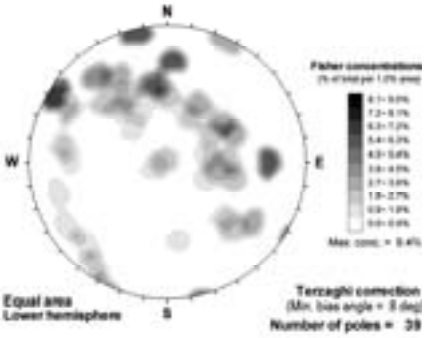

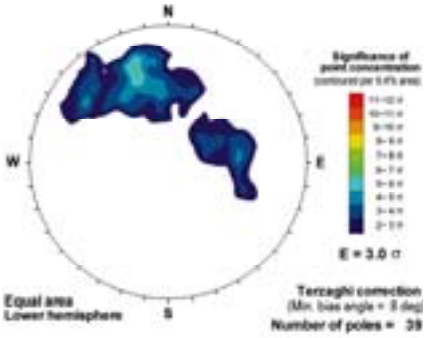

KLX05_RSMM01

Fine-grained granite

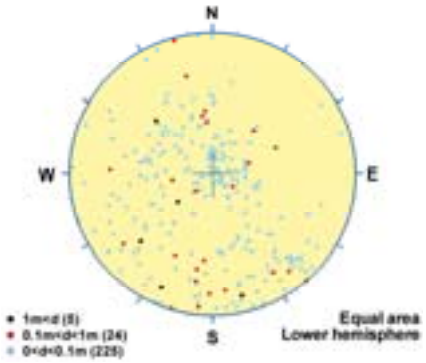

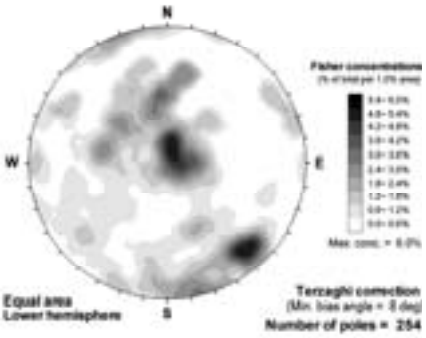

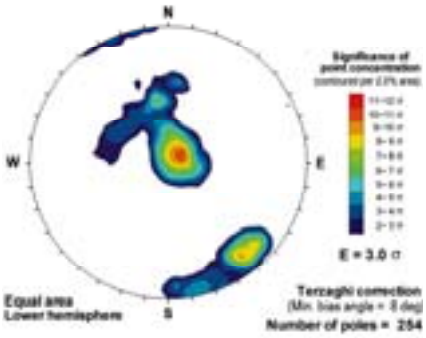

Fine-grained diorite-gabbro

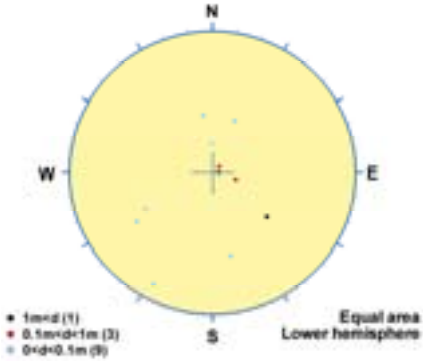

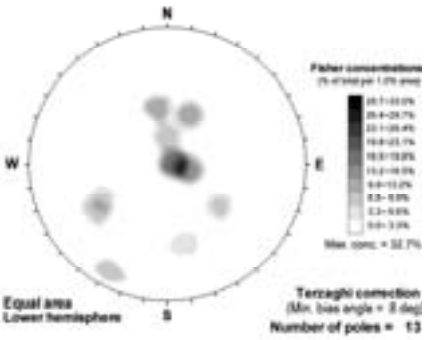

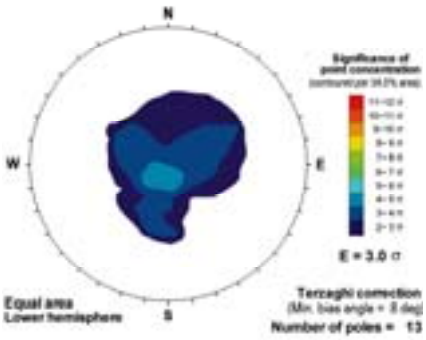

Pegmatite

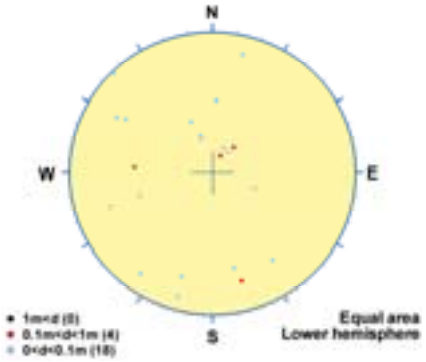

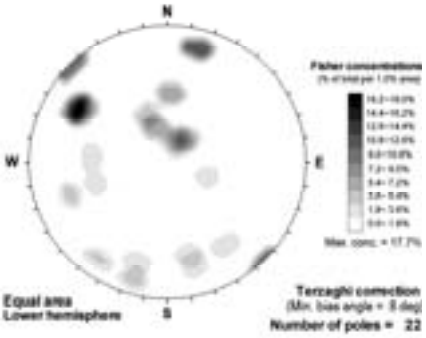

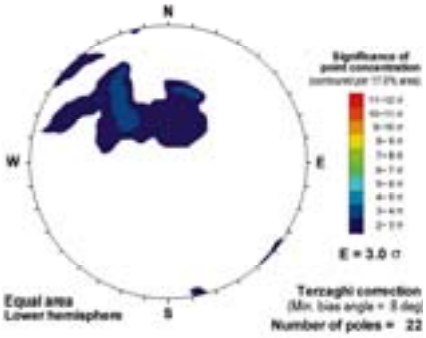

KLX06_RSMA01

Fine-grained granite

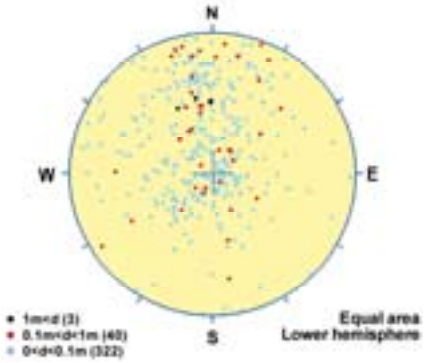

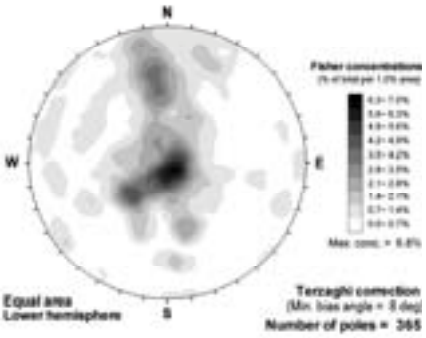

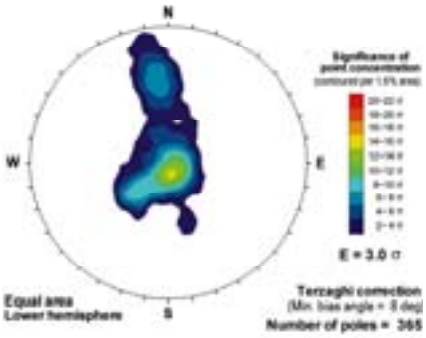

Fine-grained diorite-gabbro

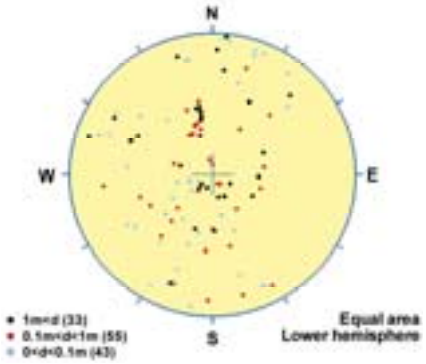

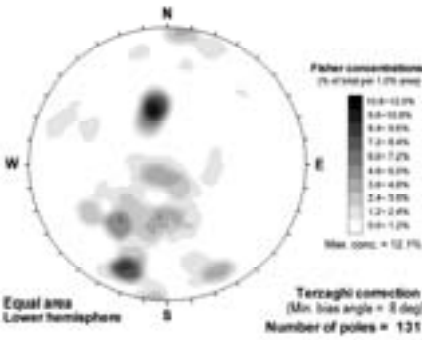

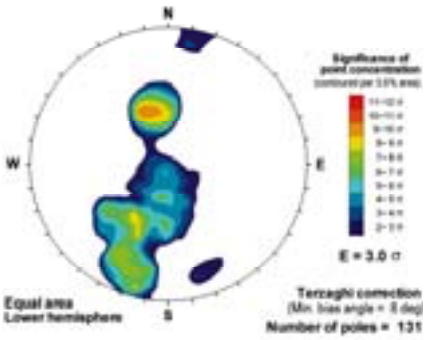

Pegmatite

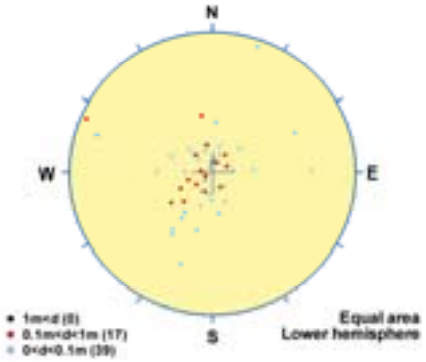

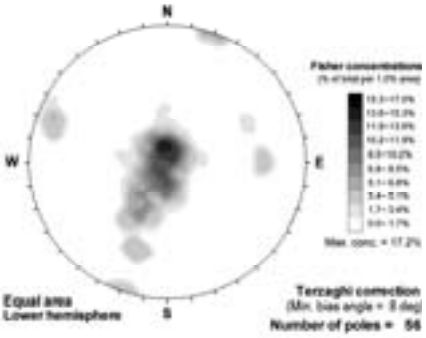

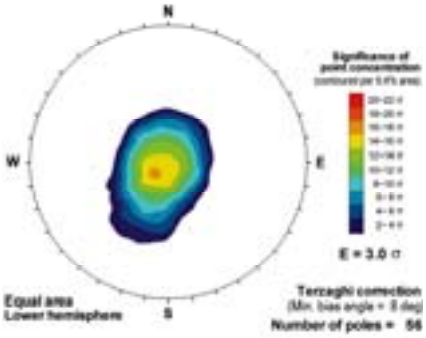

KLX07A_RSMA01

Fine-grained granite

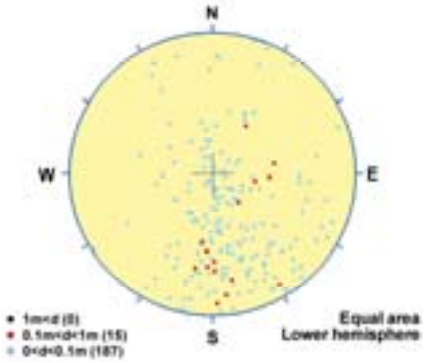

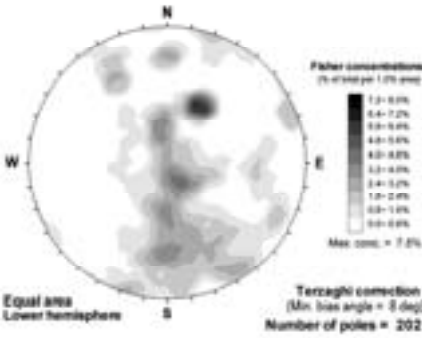

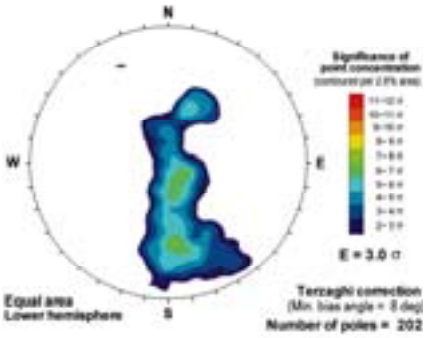

Fine-grained diorite-gabbro

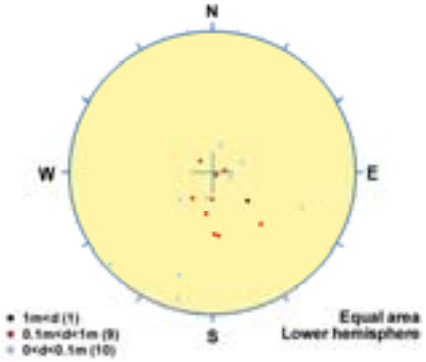

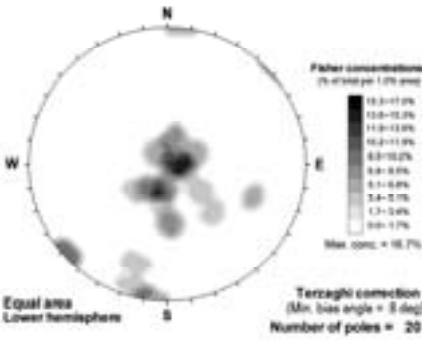

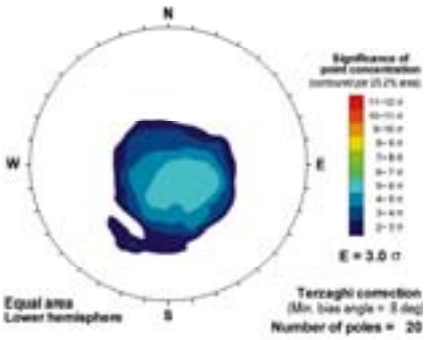

Pegmatite

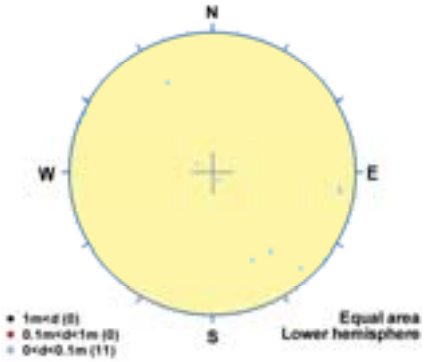

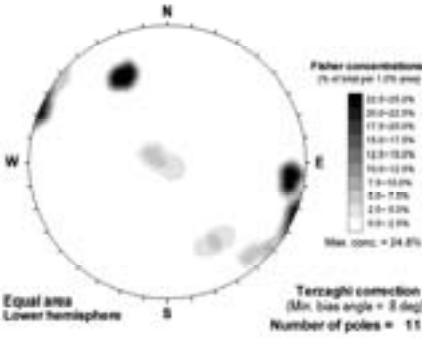

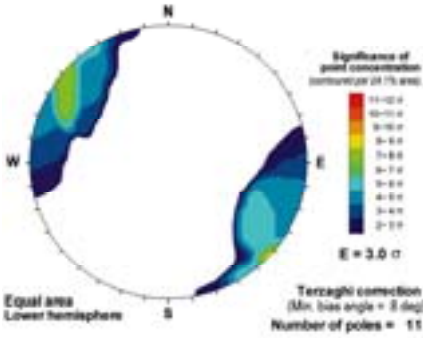

KLX07B_RSMA01

Fine-grained granite

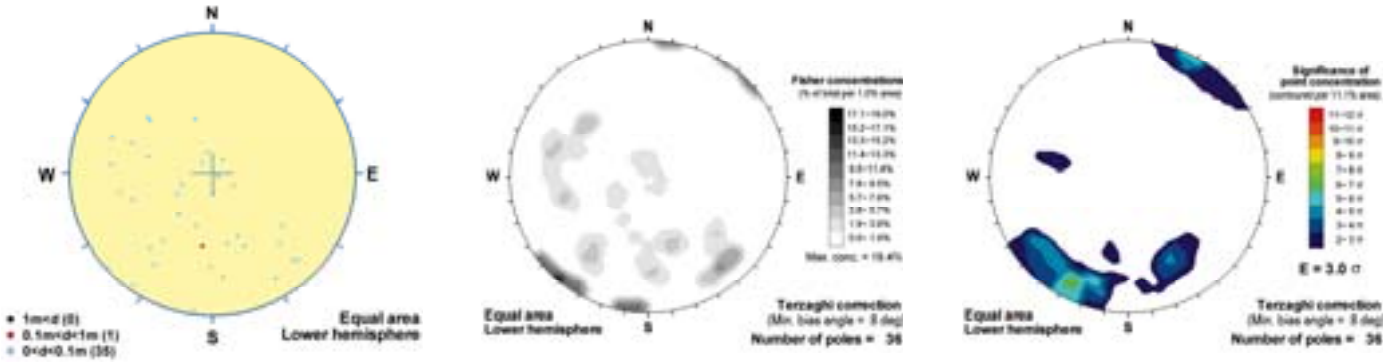

Fine-grained diorite-gabbro

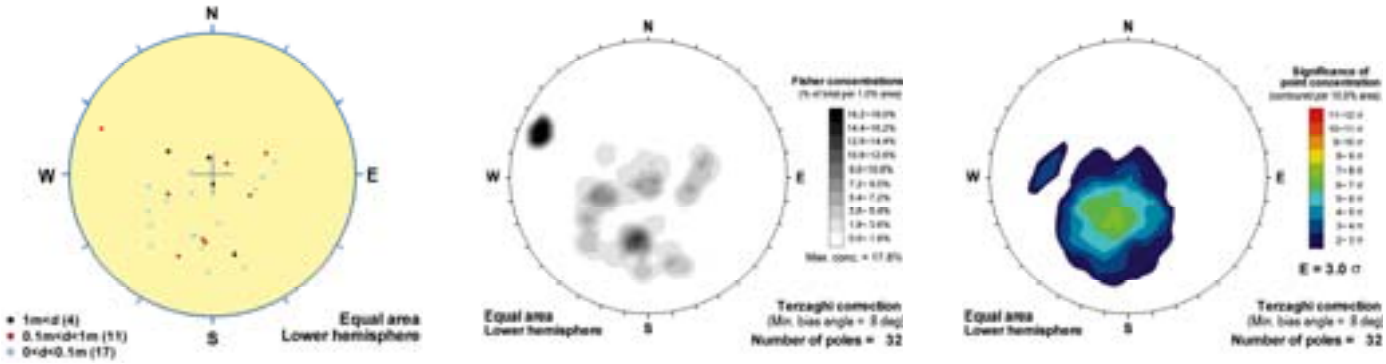

Pegmatite

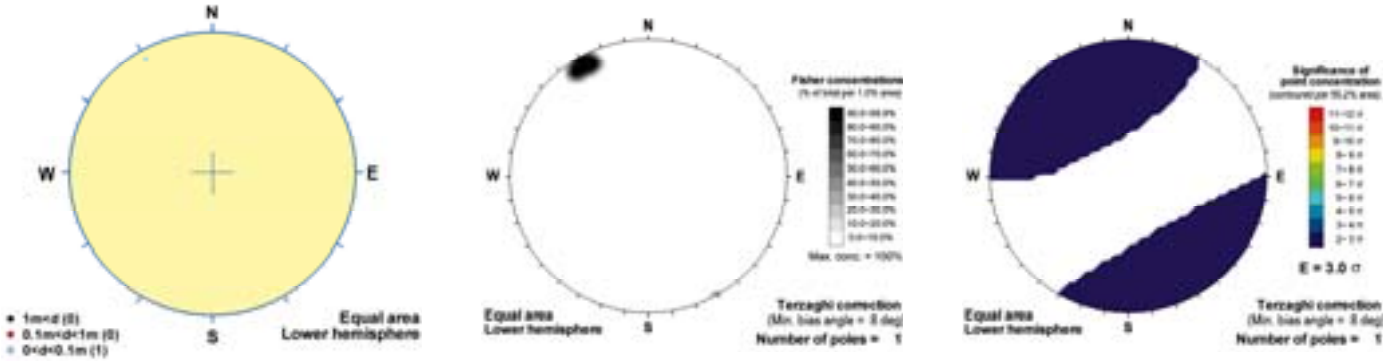

KLX08_RSMA01

Fine-grained granite

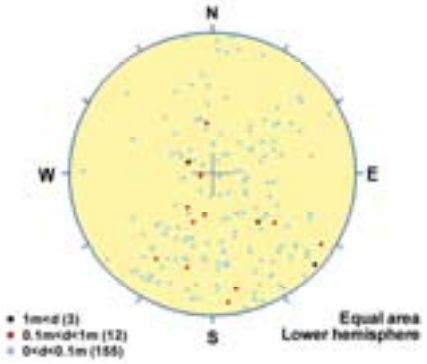

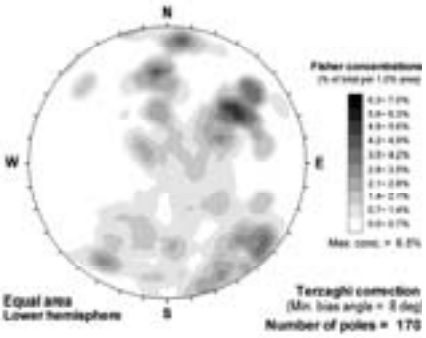

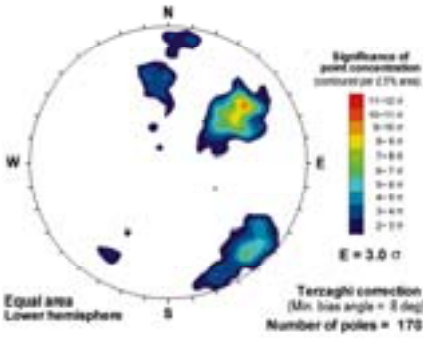

Fine-grained diorite-gabbro

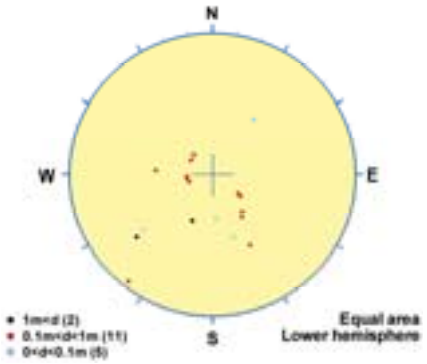

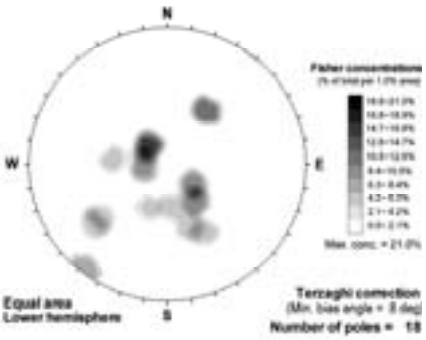

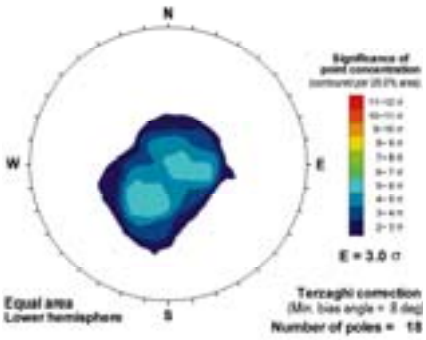

Pegmatite

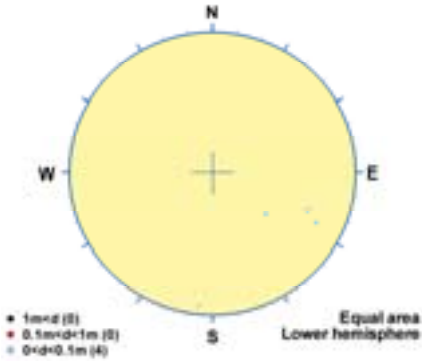

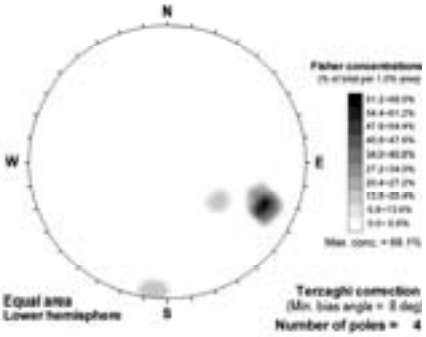

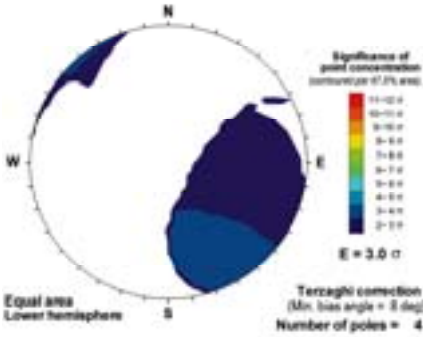

KLX08_RSMD01

Fine-grained granite

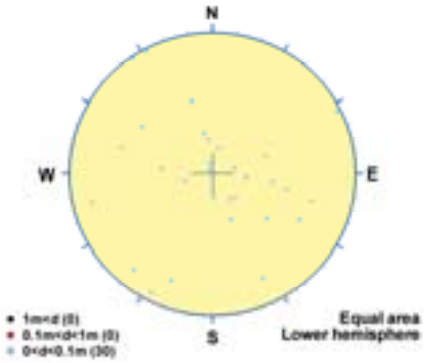

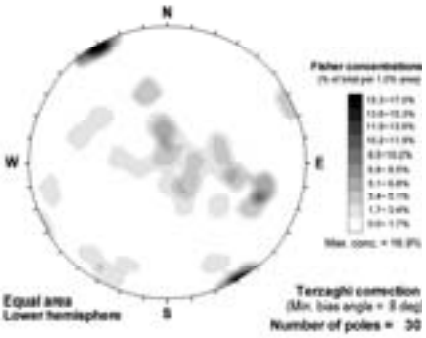

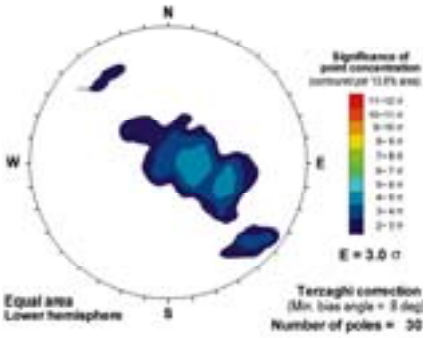

Fine-grained diorite-gabbro

Pegmatite

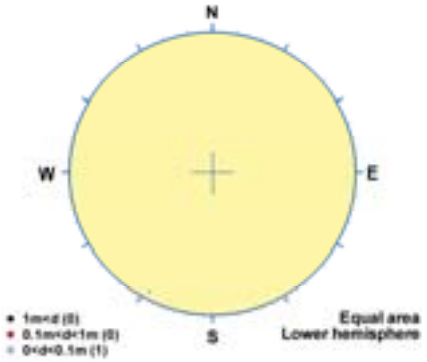

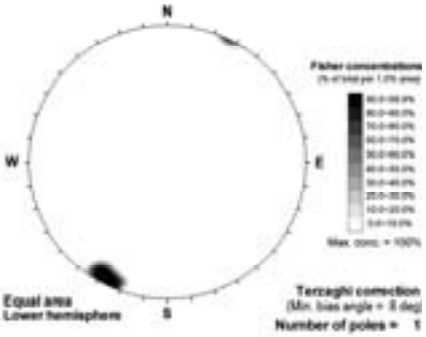

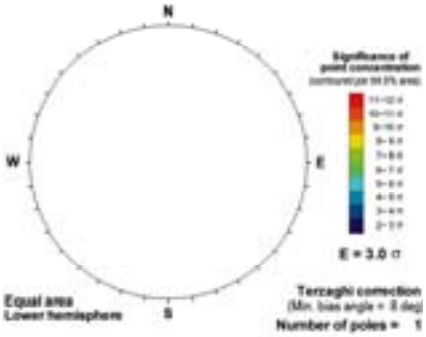

KLX08_RSMM01

Fine-grained granite

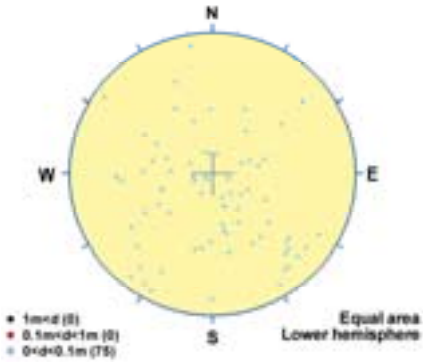

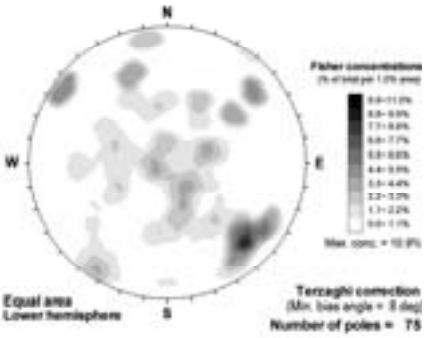

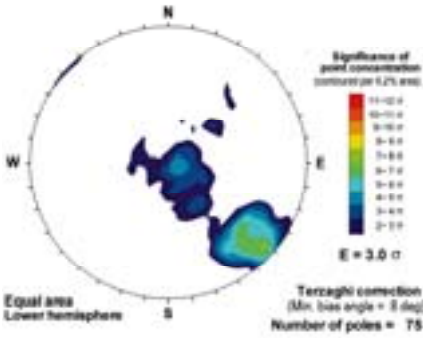

Fine-grained diorite-gabbro

Pegmatite

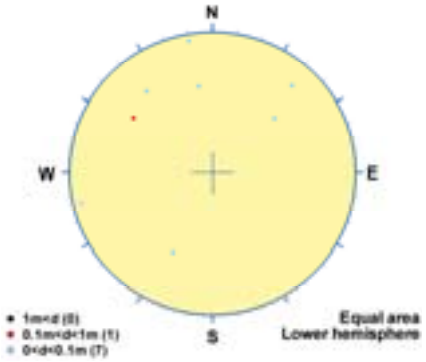

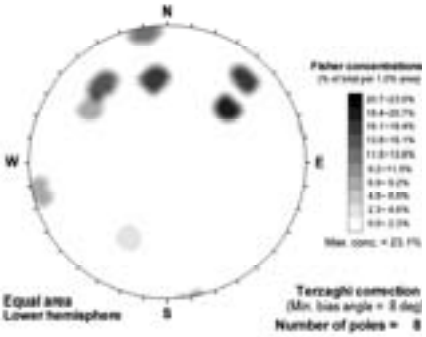

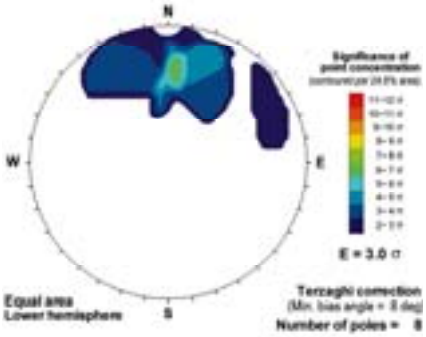

KLX09_RSMA01

Fine-grained granite

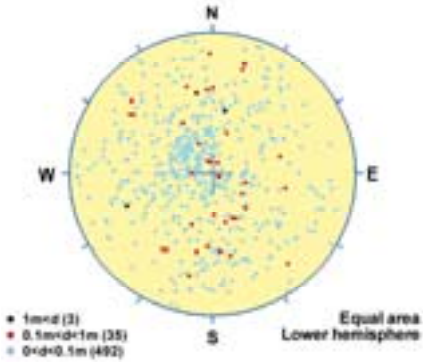

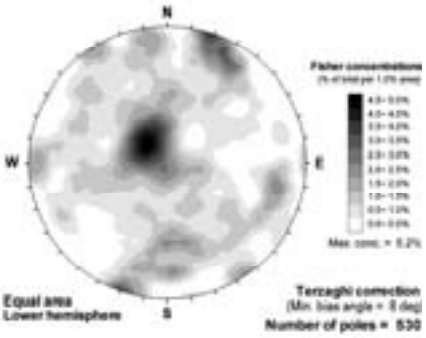

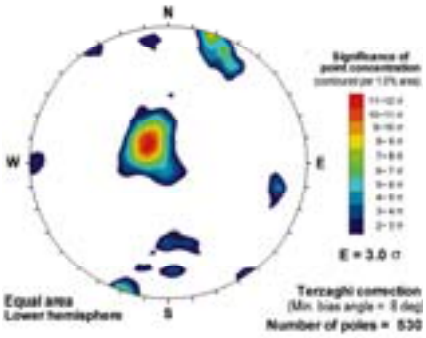

Fine-grained diorite-gabbro

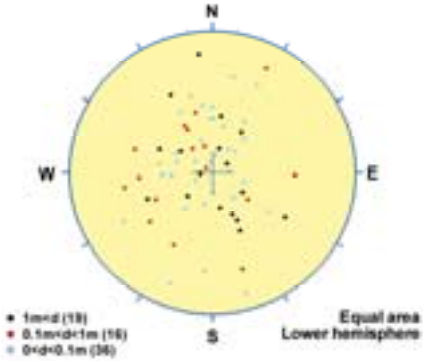

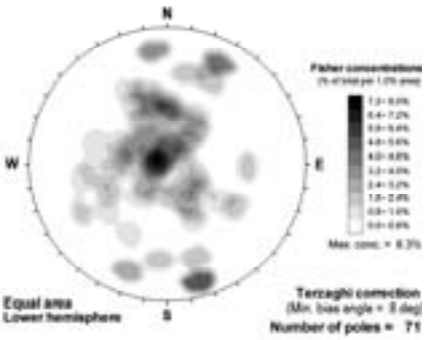

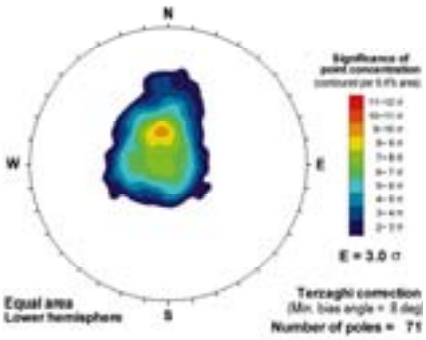

Pegmatite

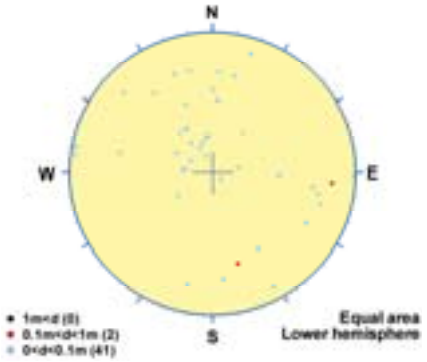

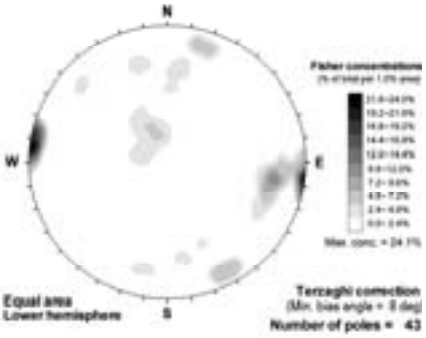

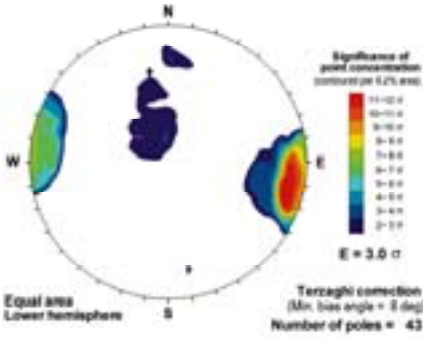

KLX09B_RSMA01

Fine-grained granite

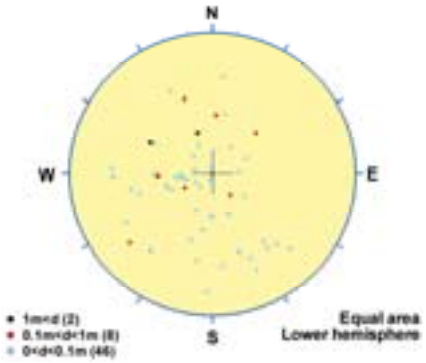

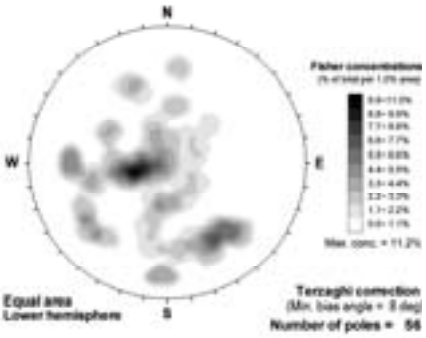

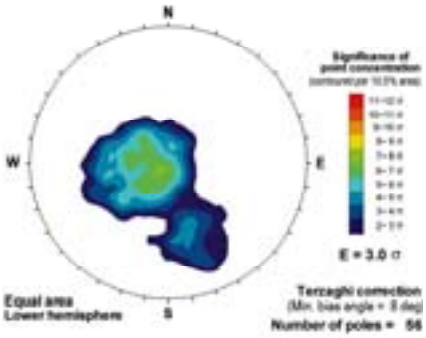

Fine-grained diorite-gabbro

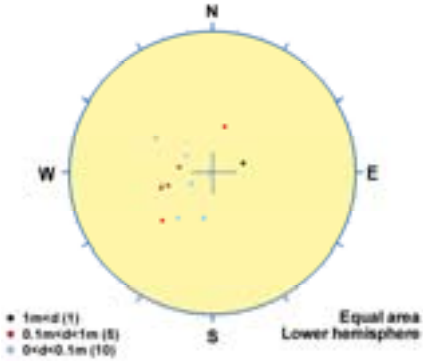

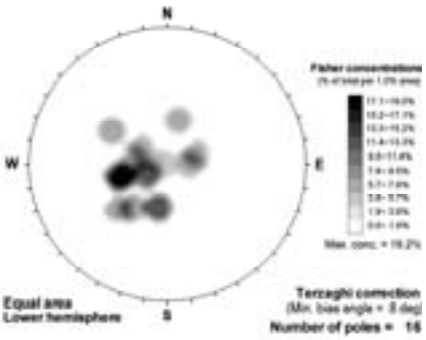

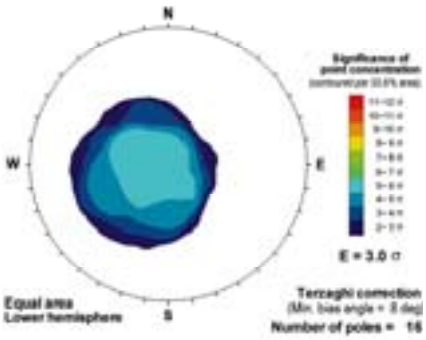

Pegmatite

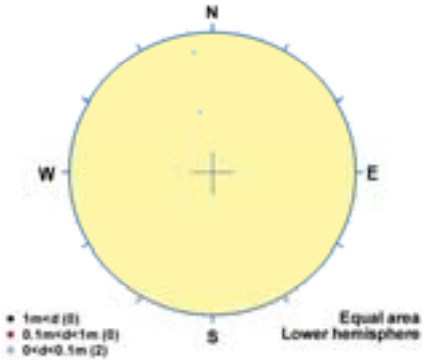

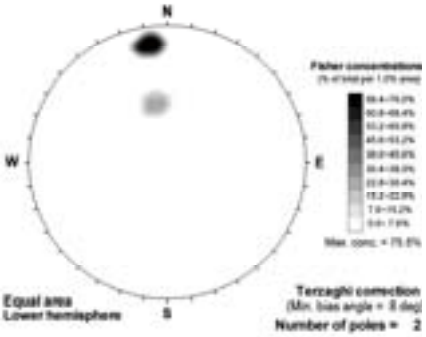

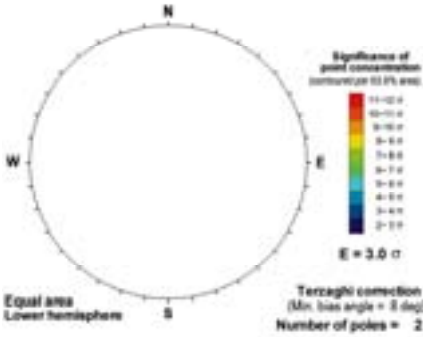

KLX09D_RSMA01

Fine-grained granite

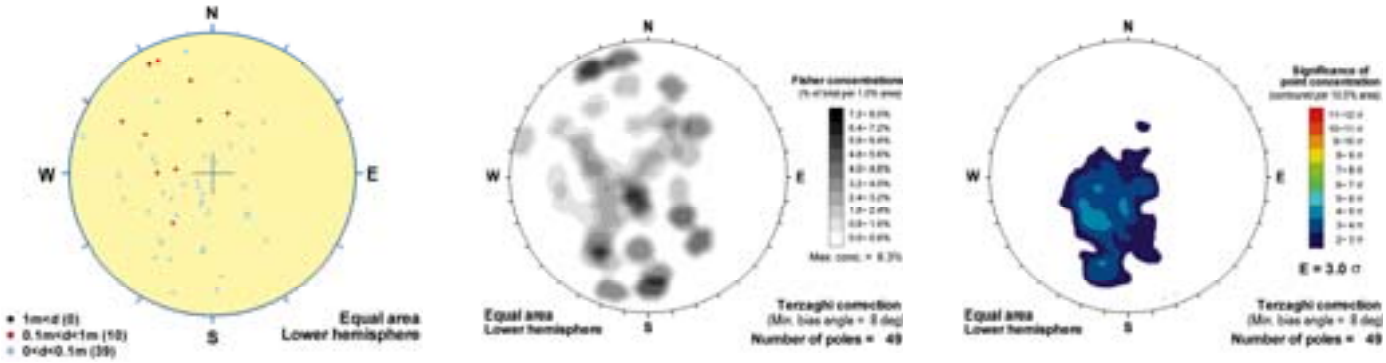

Fine-grained diorite-gabbro

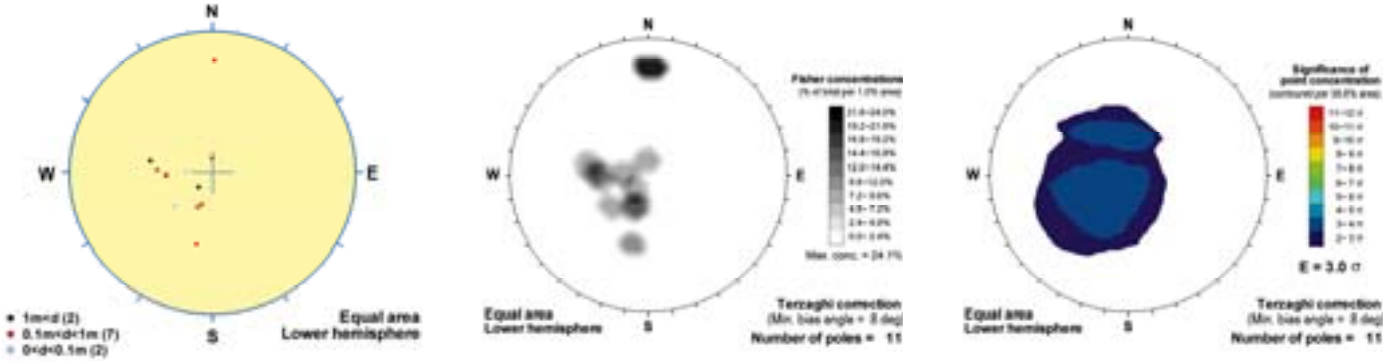

Pegmatite

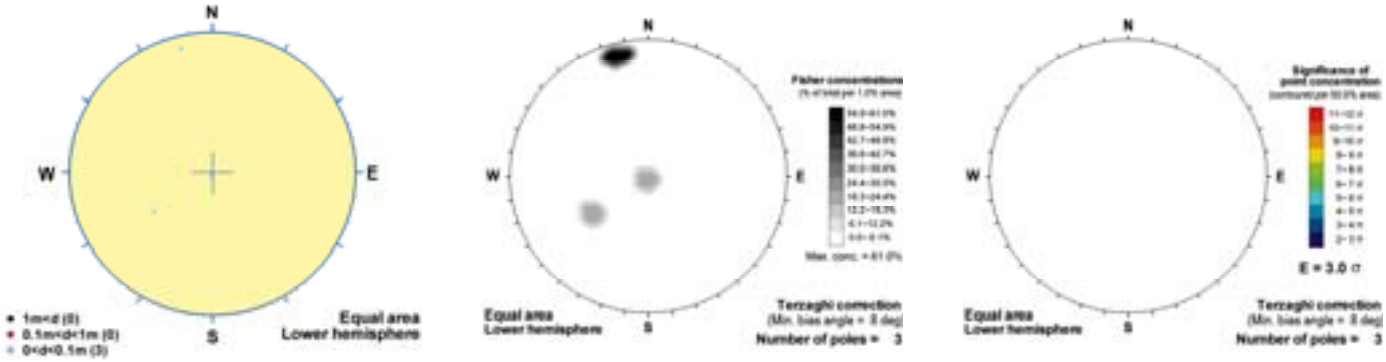

KLX09F_RSMA01

Fine-grained granite

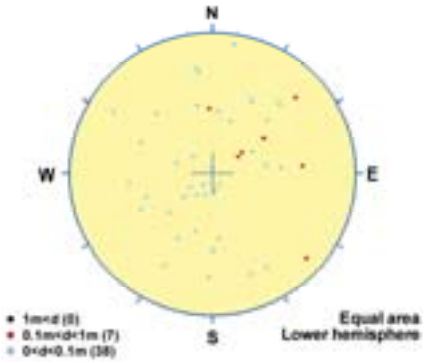

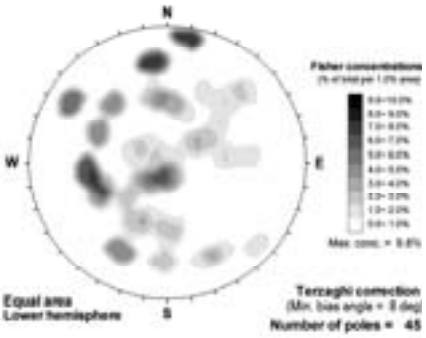

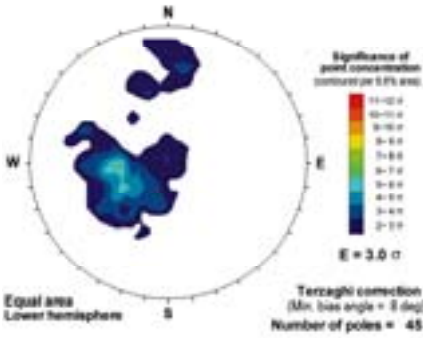

Fine-grained diorite-gabbro

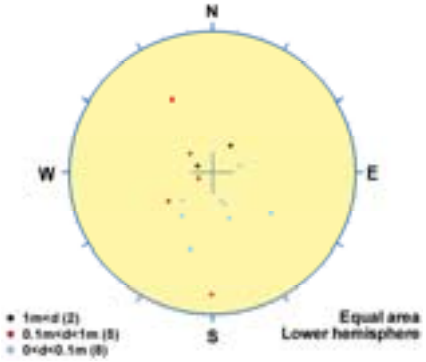

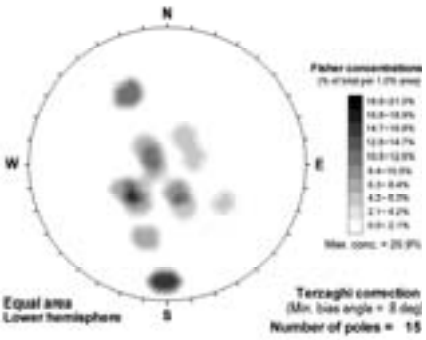

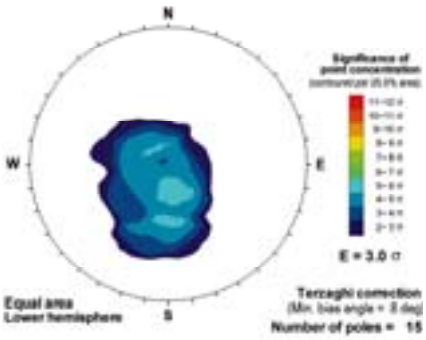

Pegmatite

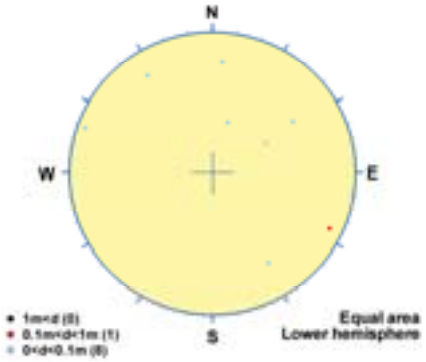

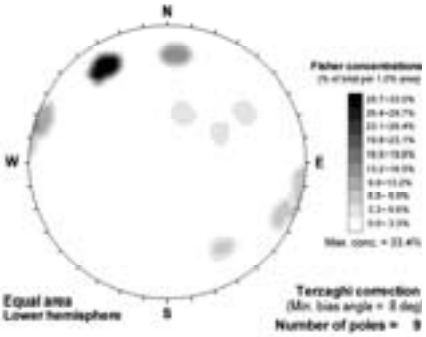

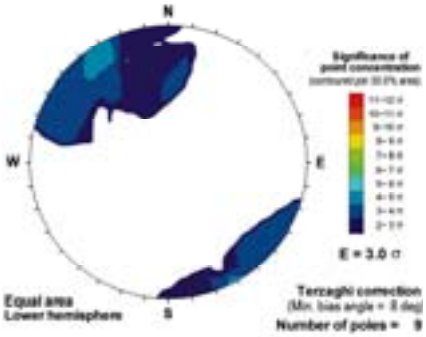

KLX09G_RSMA01

Fine-grained granite

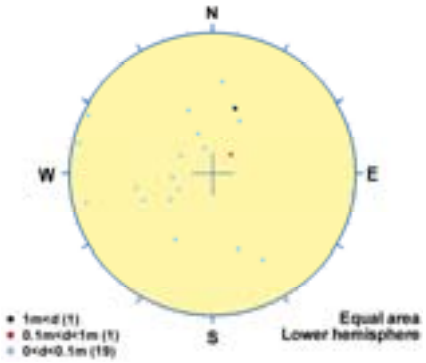

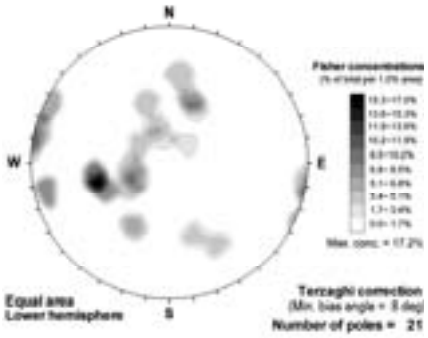

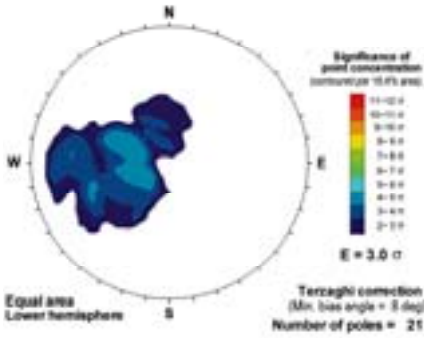

Fine-grained diorite-gabbro

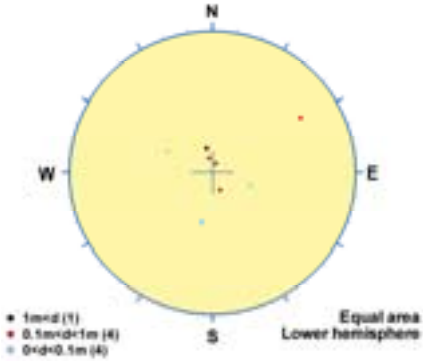

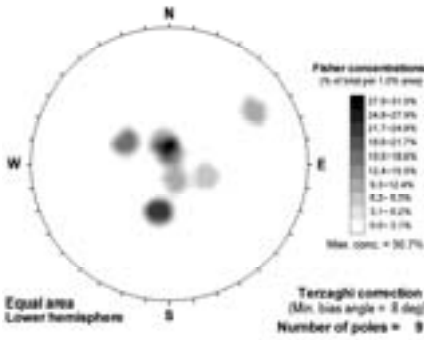

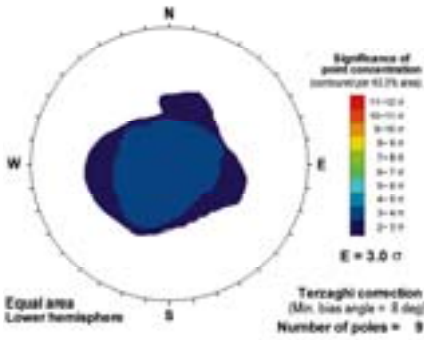

Pegmatite

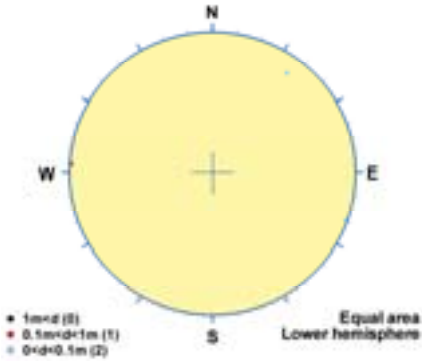

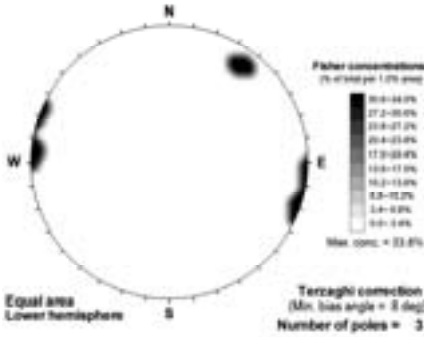

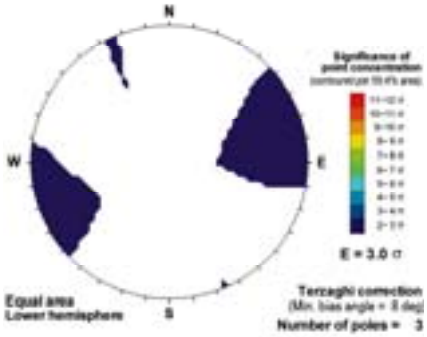

KLX10_RSMA01

Fine-grained granite

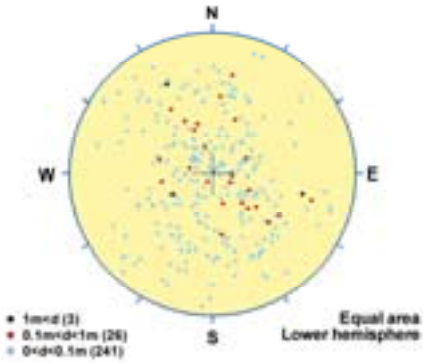

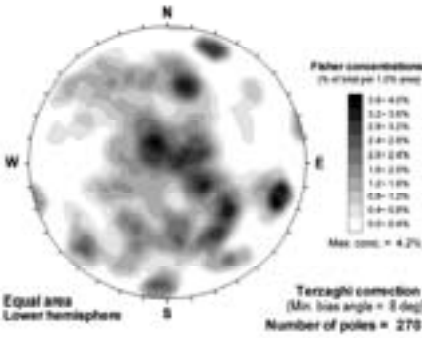

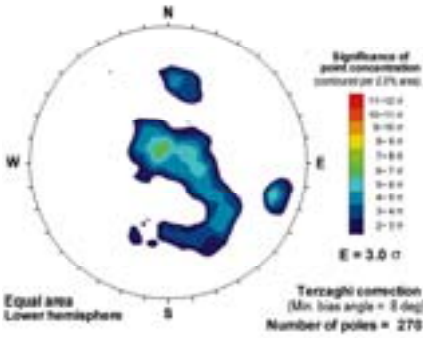

Fine-grained diorite-gabbro

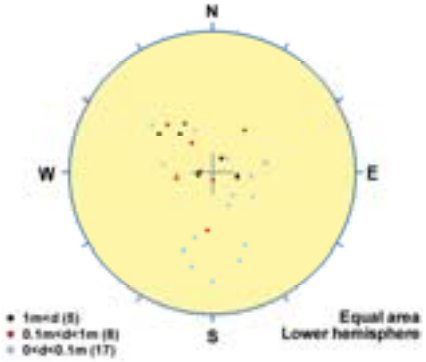

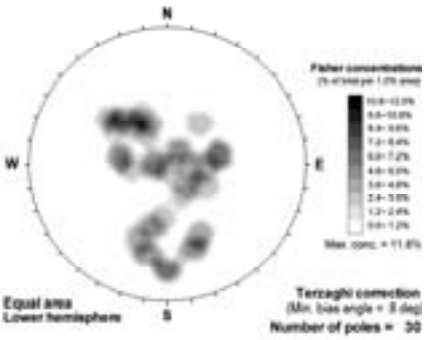

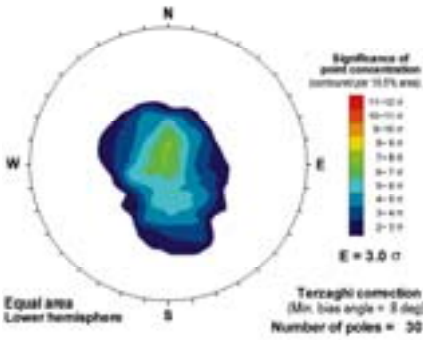

Pegmatite

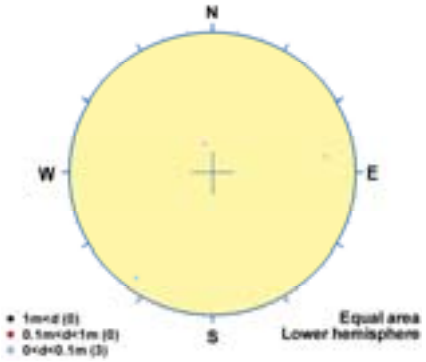

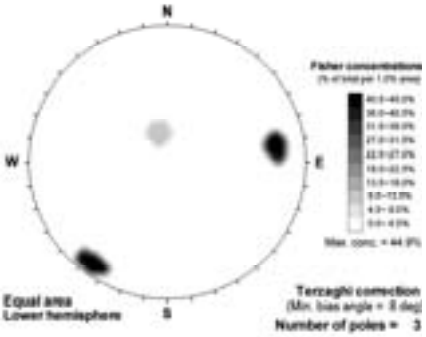

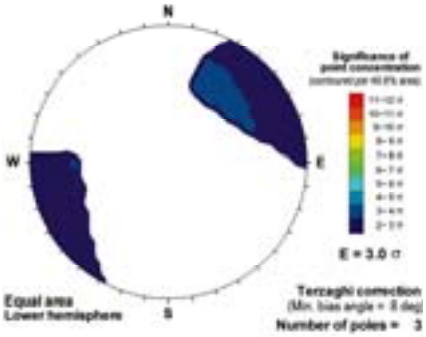

KLX10_RSMD01

Fine-grained granite

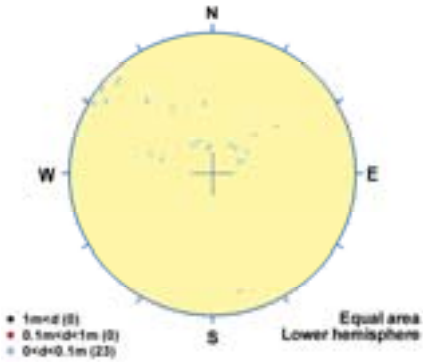

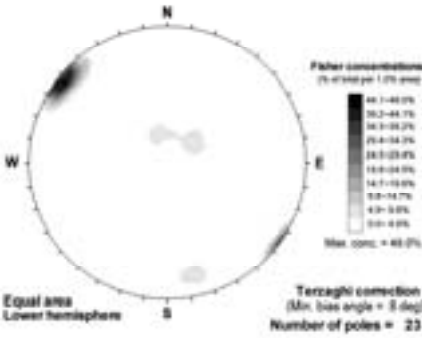

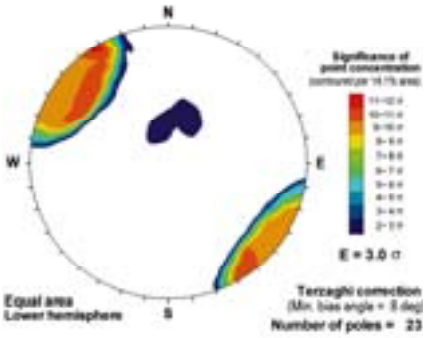

Fine-grained diorite-gabbro

Pegmatite

KLX10_RSMM01

Fine-grained granite

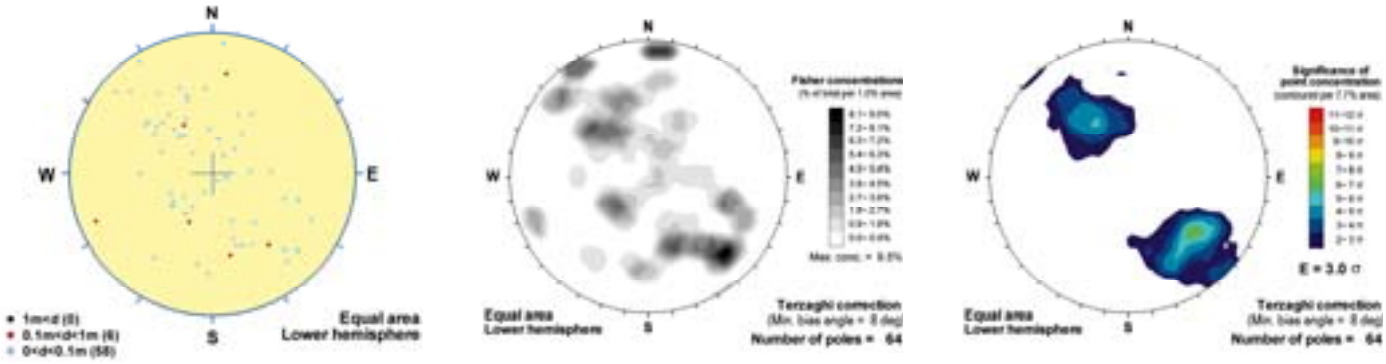

Fine-grained diorite-gabbro

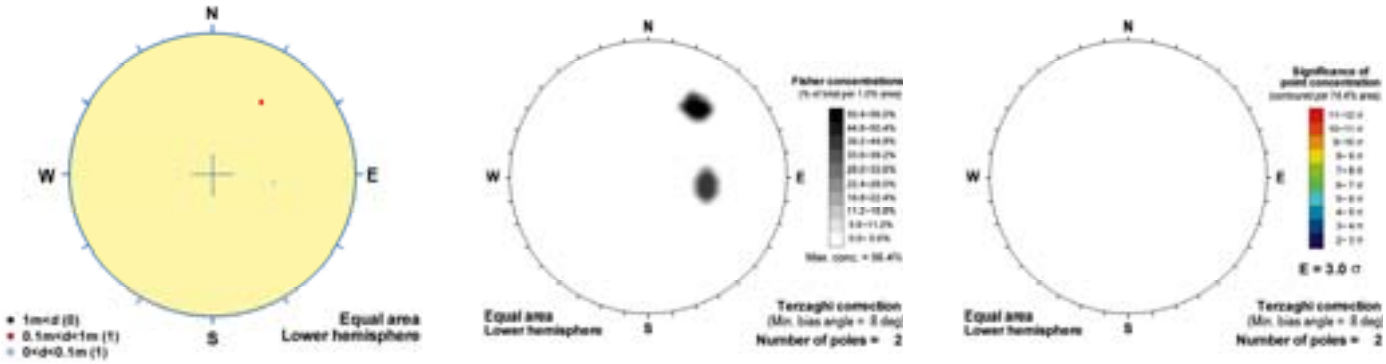

Pegmatite

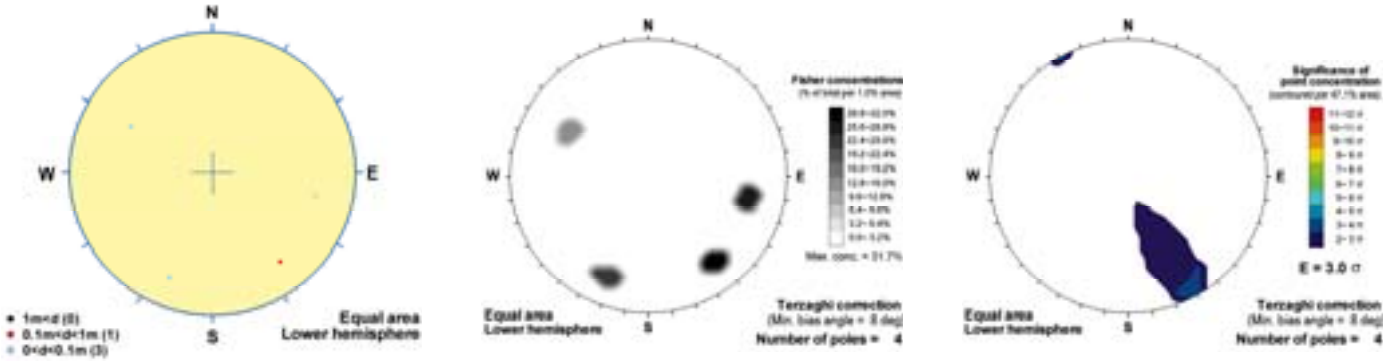

KLX10B_RSMA01

Fine-grained granite

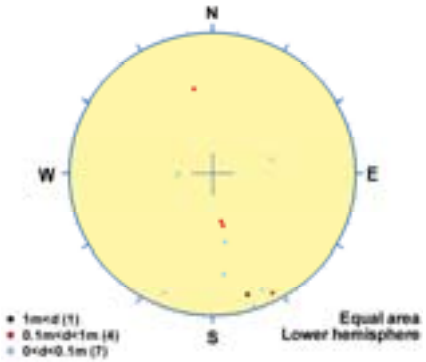

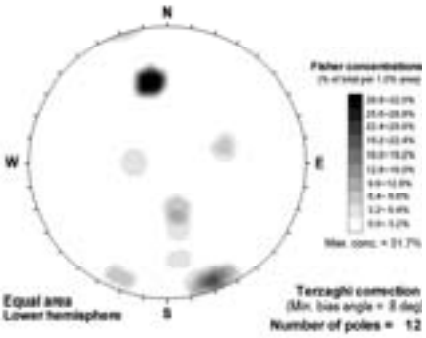

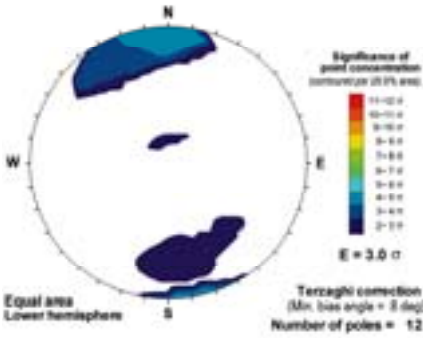

Fine-grained diorite-gabbro

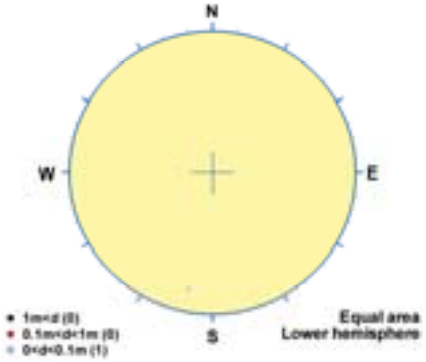

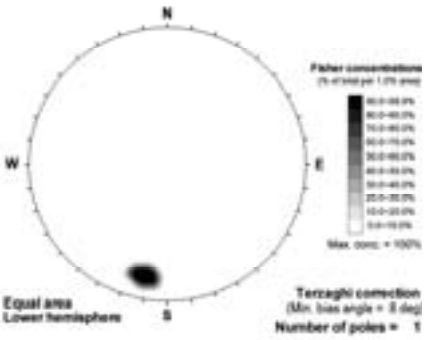

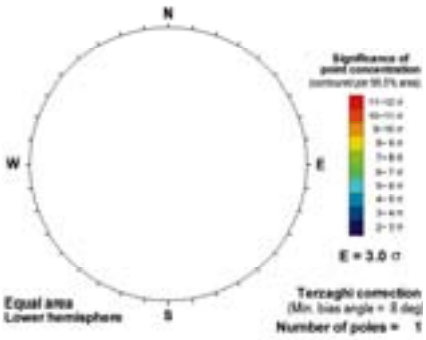

Pegmatite

KLX10C_RSMA01

Fine-grained granite

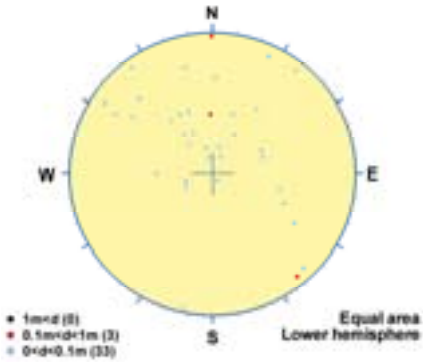

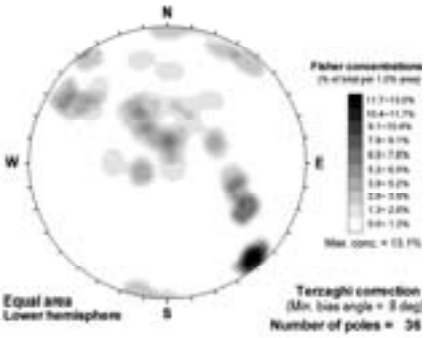

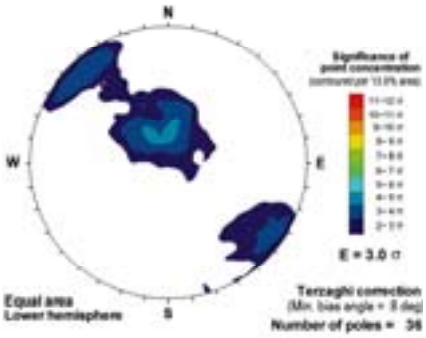

Fine-grained diorite-gabbro

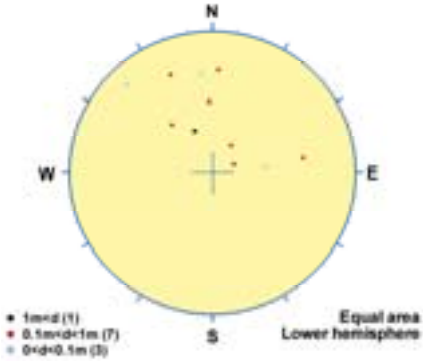

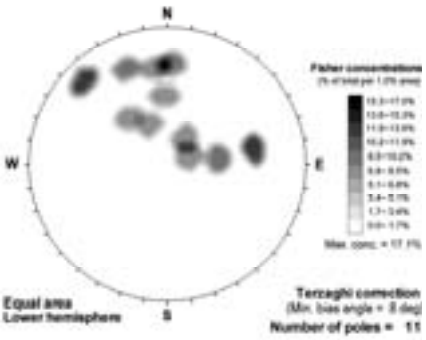

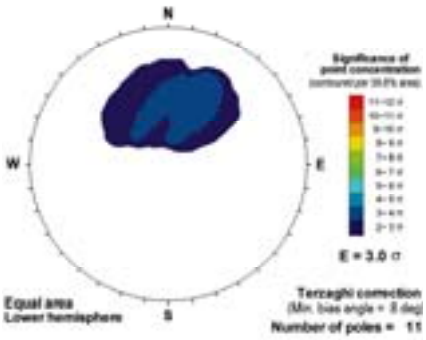

Pegmatite

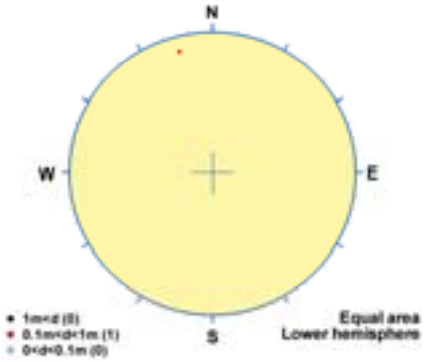

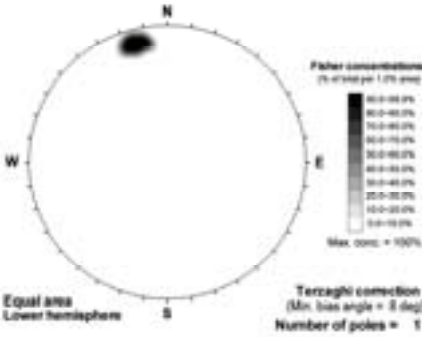

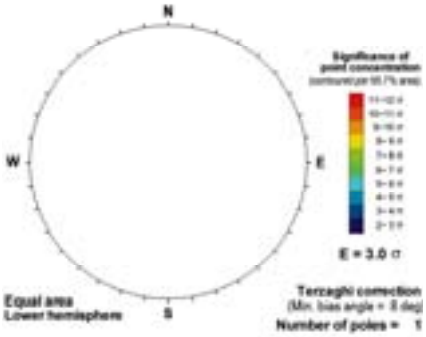

KLX11A_RSMD01

Fine-grained granite

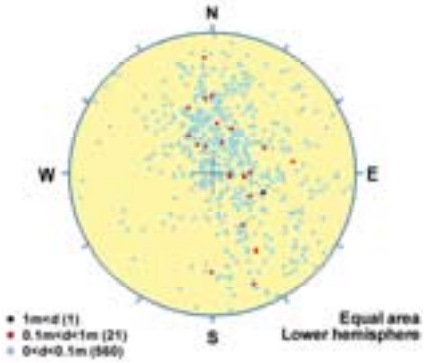

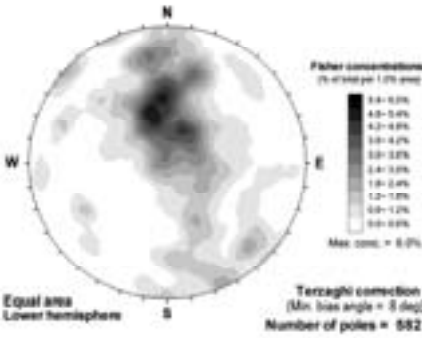

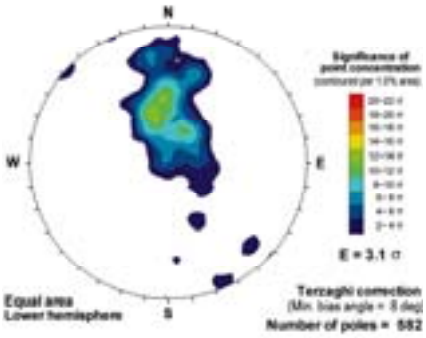

Fine-grained diorite-gabbro

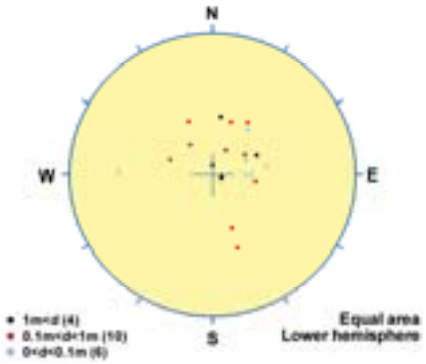

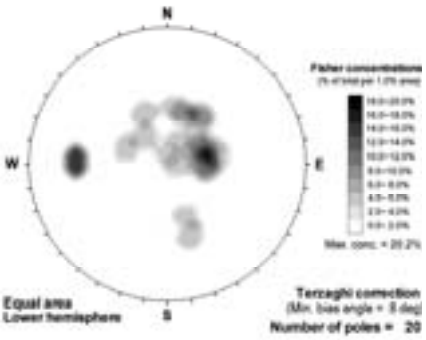

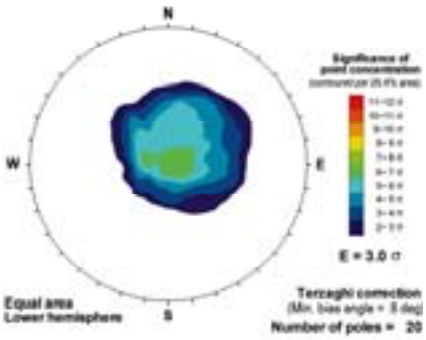

Pegmatite

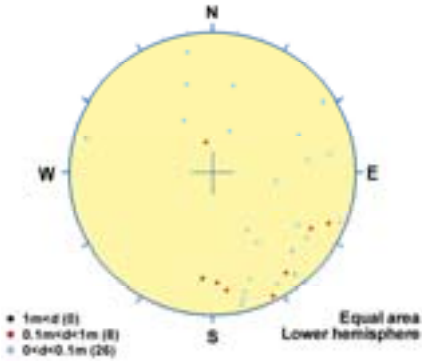

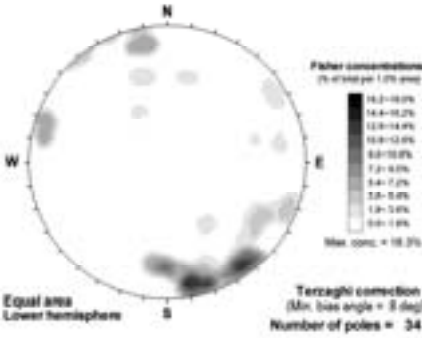

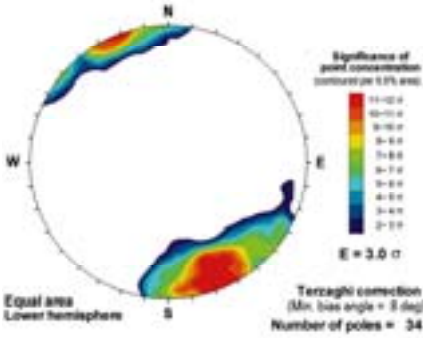

KLX12A_RSMD01

Fine-grained granite

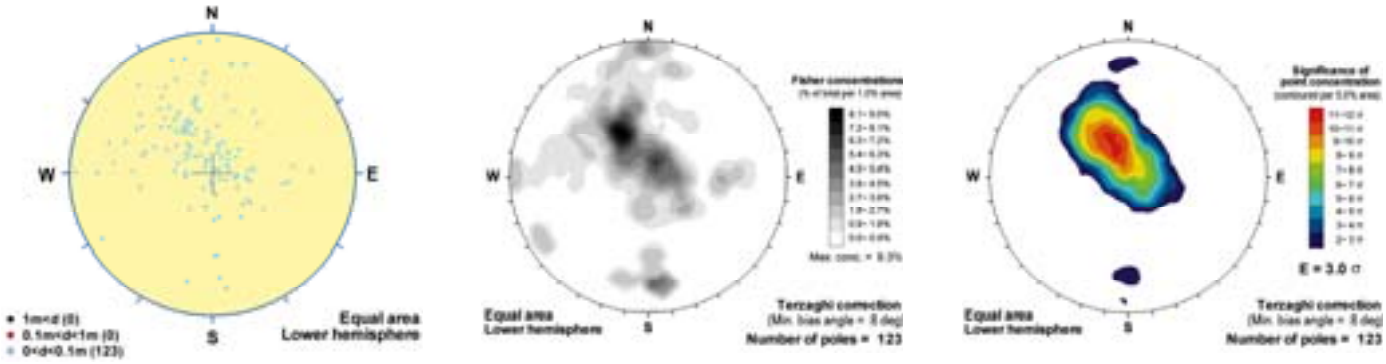

Fine-grained diorite-gabbro

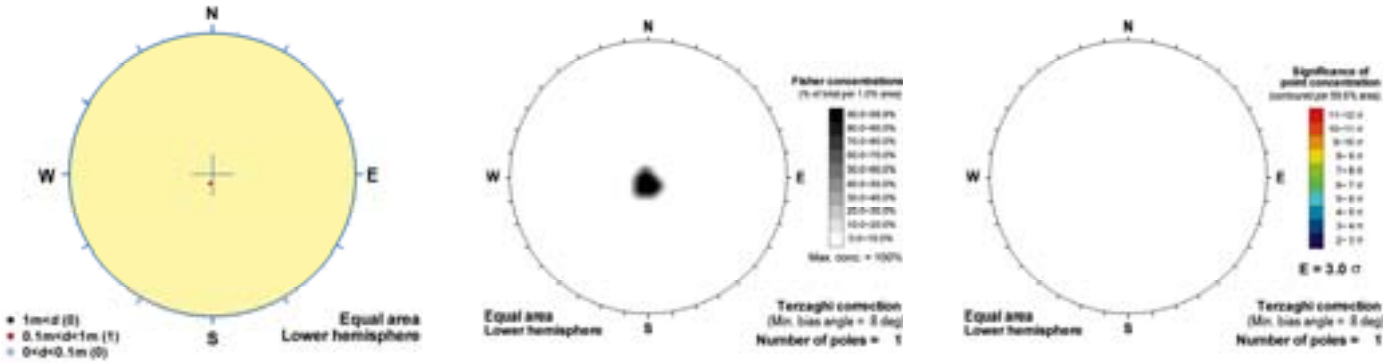

Pegmatite

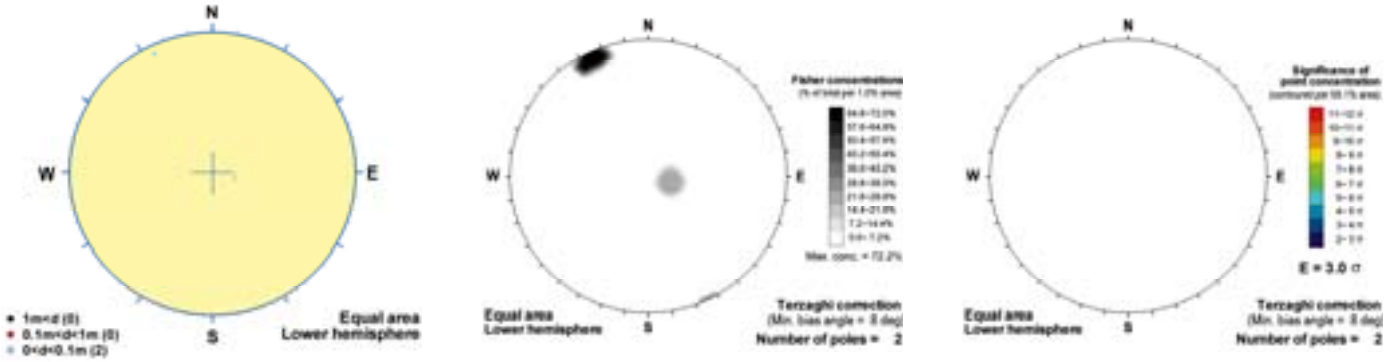

KLX12A_RSMM01

Fine-grained granite

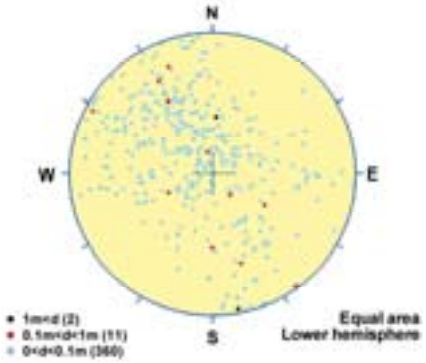

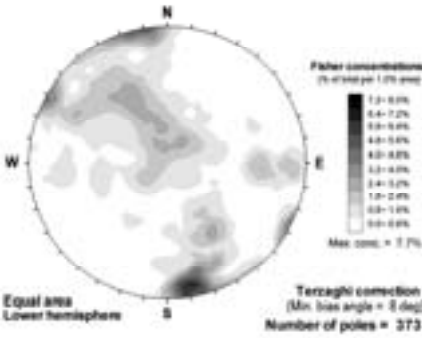

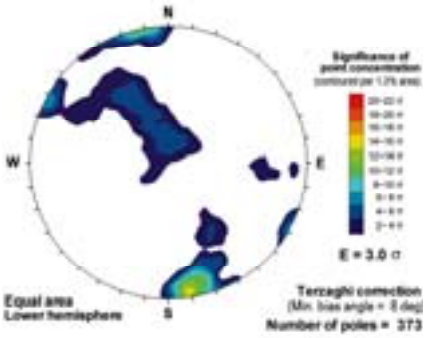

Fine-grained diorite-gabbro

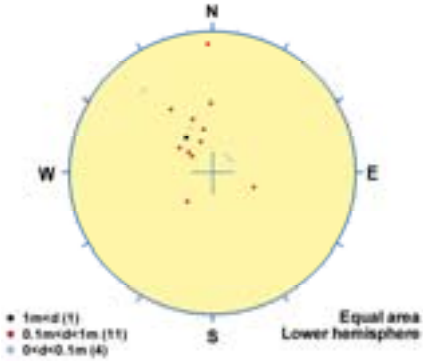

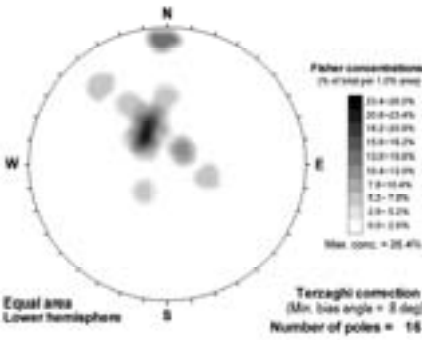

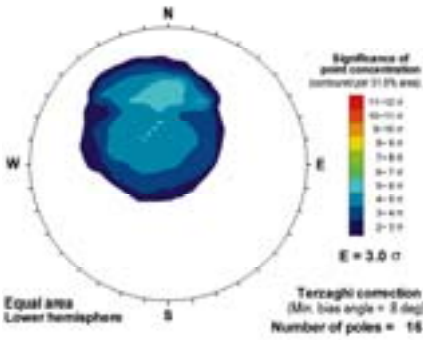

Pegmatite

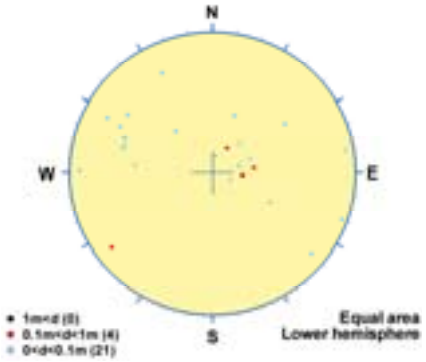

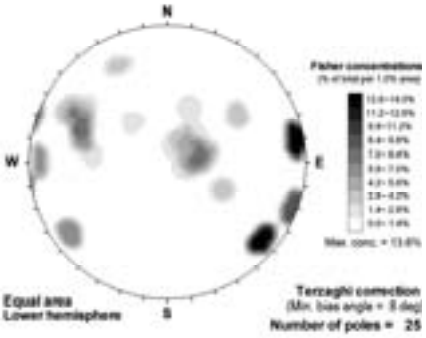

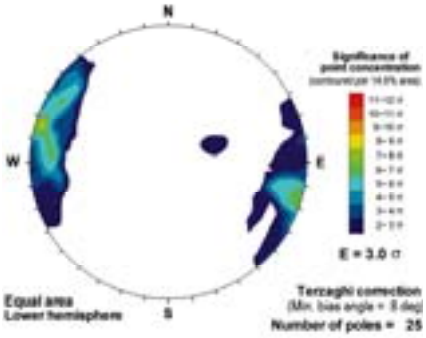

KLX13A_RSMM01

Fine-grained granite

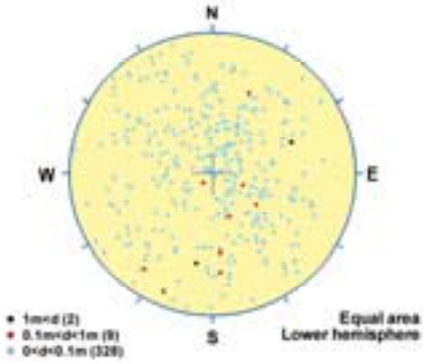

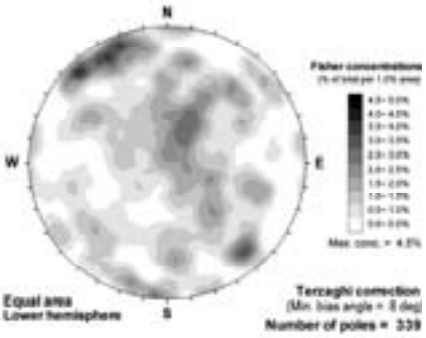

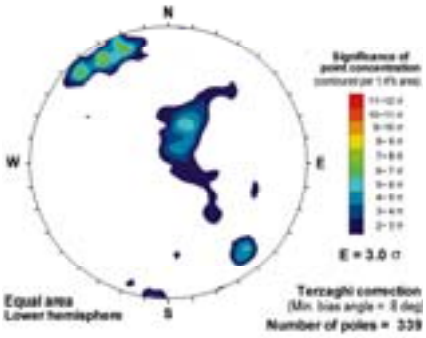

Fine-grained diorite-gabbro

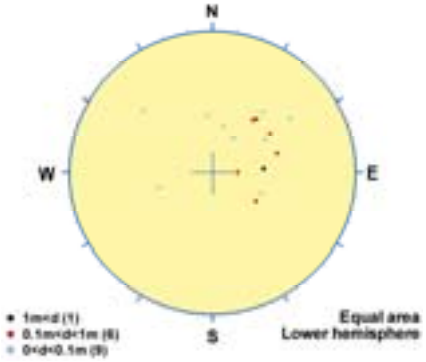

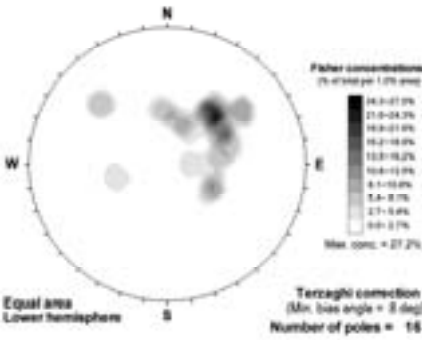

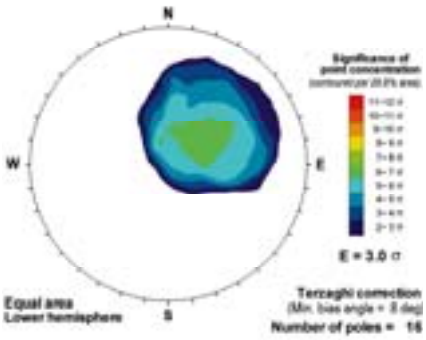

Pegmatite

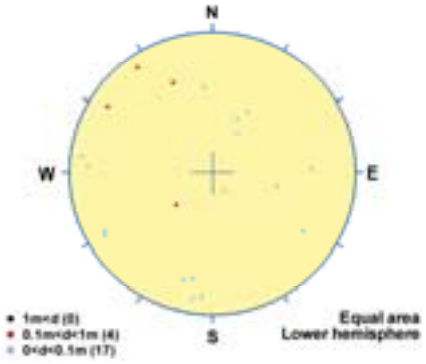

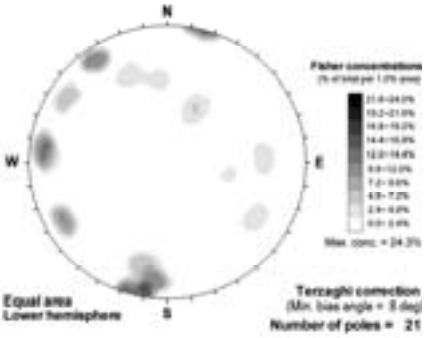

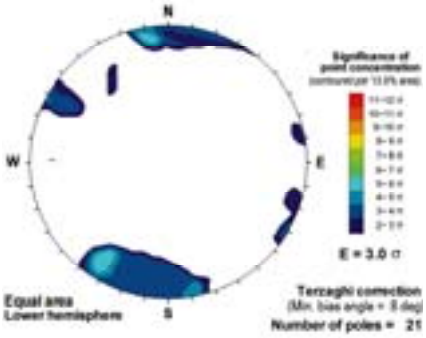

KLX14A_RSMD01

Fine-grained granite

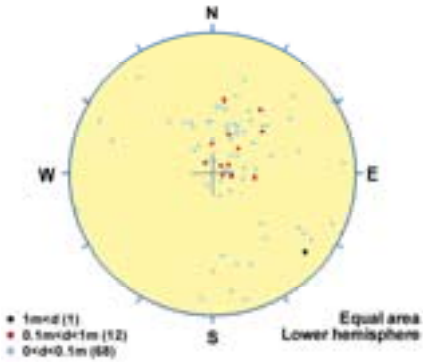

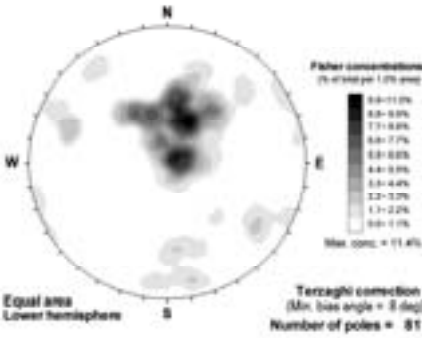

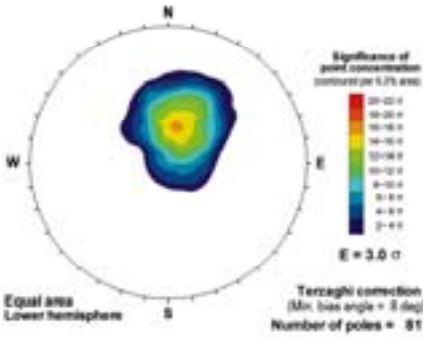

Fine-grained diorite-gabbro

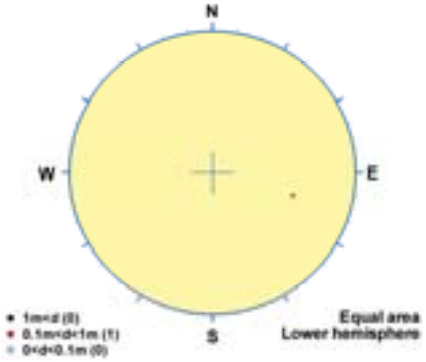

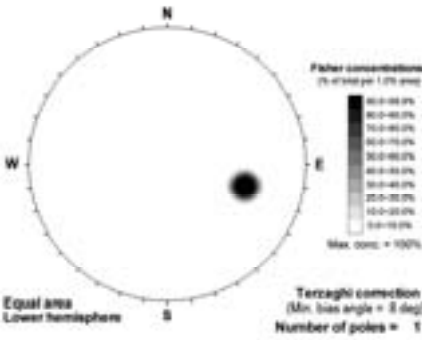

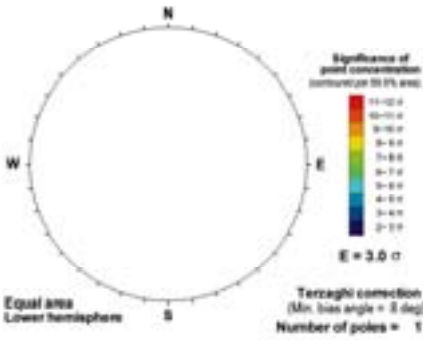

Pegmatite

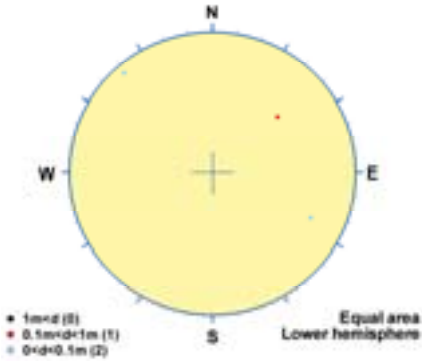

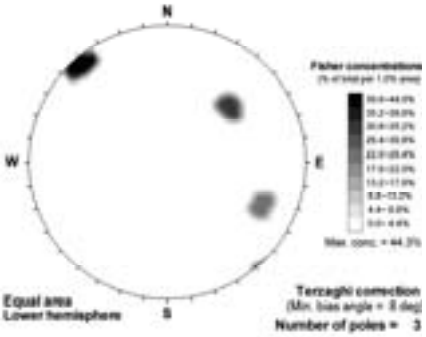

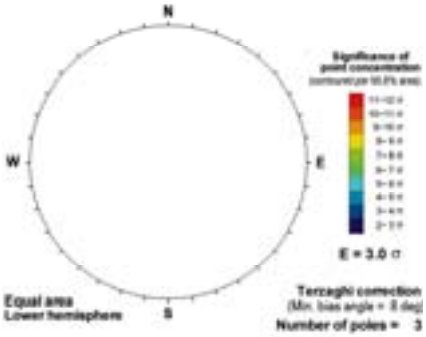

KLX15A_RSMD01

Fine-grained granite

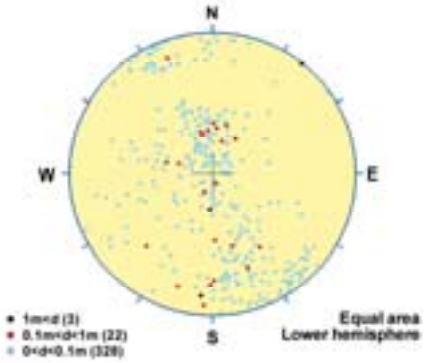

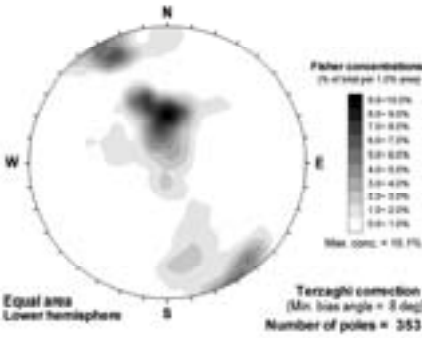

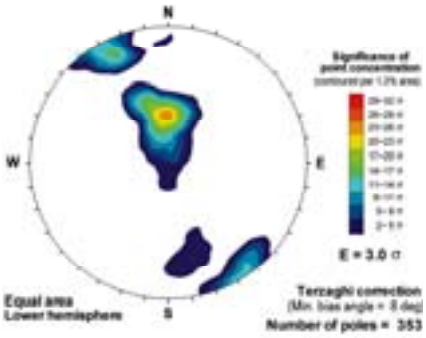

Fine-grained diorite-gabbro

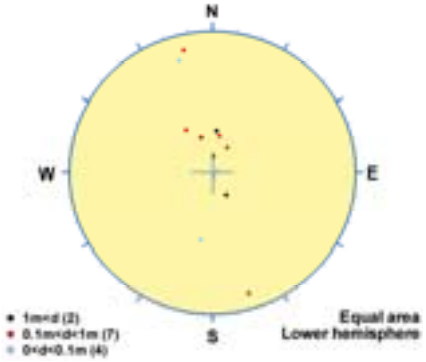

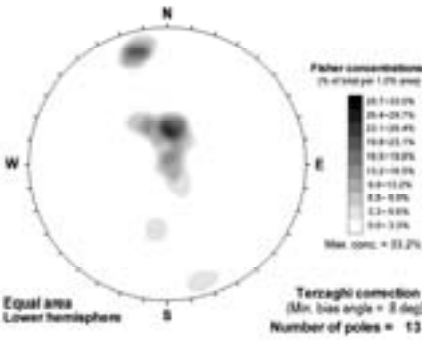

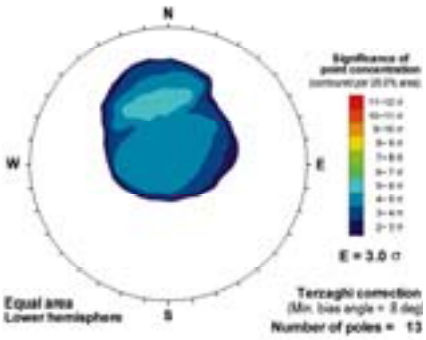

Pegmatite

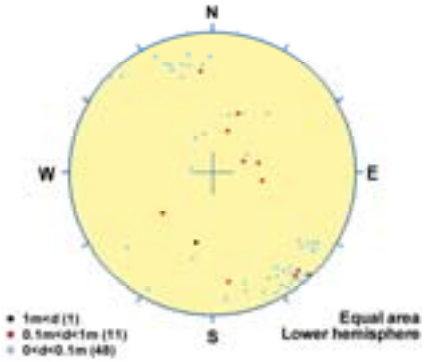

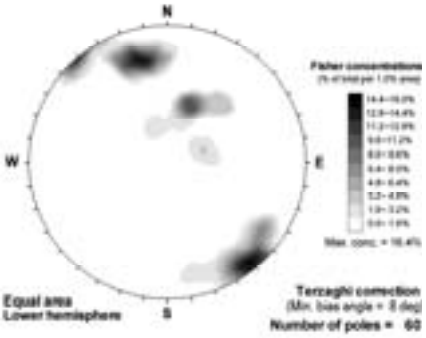

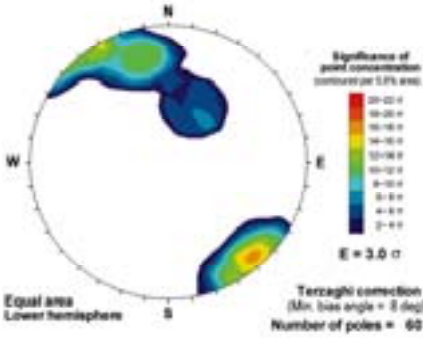

KLX16A_RSMD01

Fine-grained granite

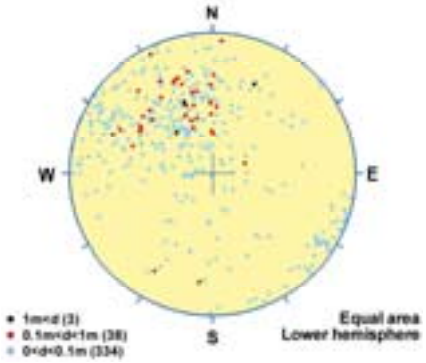

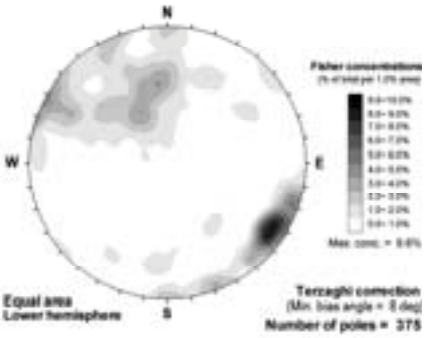

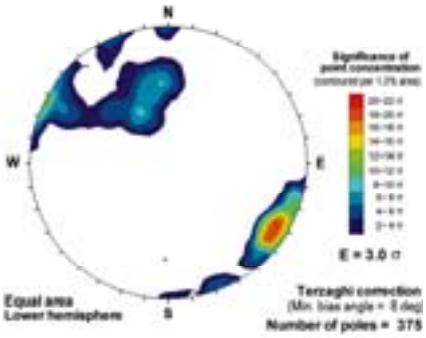

Fine-grained diorite-gabbro

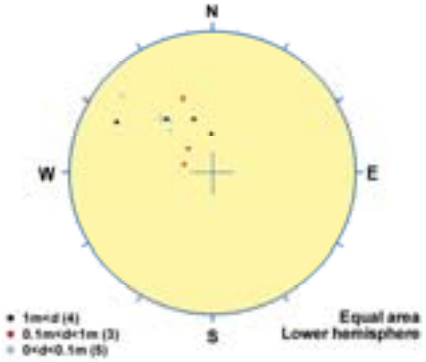

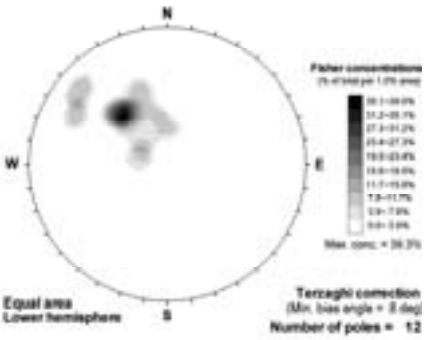

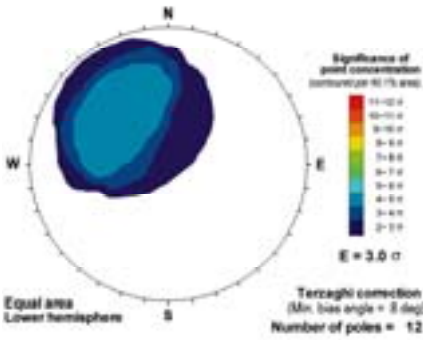

Pegmatite

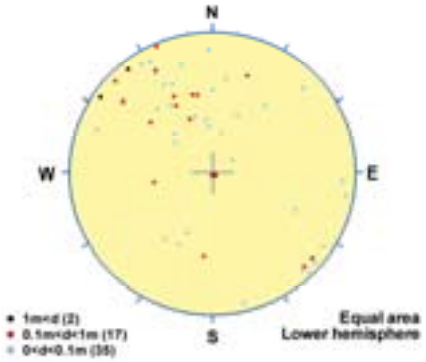

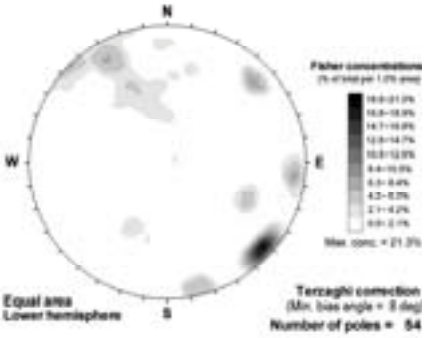

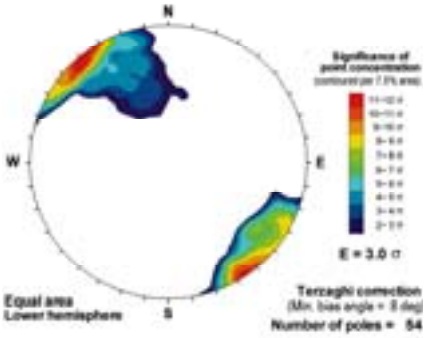

KLX17A_RSMM01

Fine-grained granite

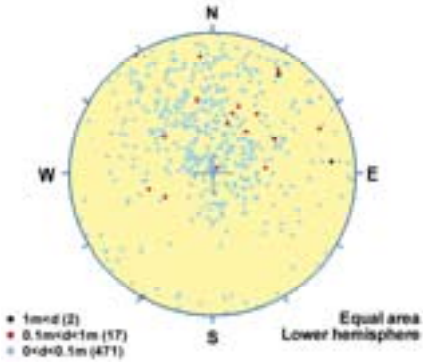

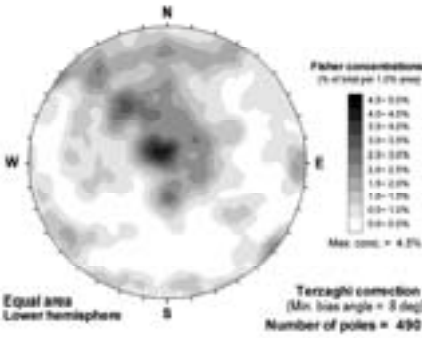

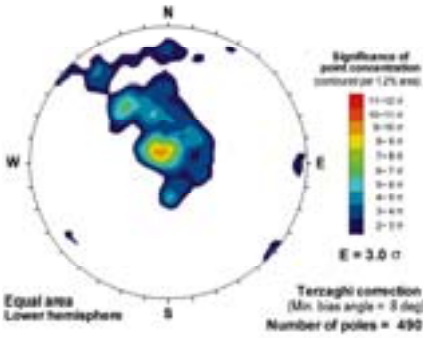

Fine-grained diorite-gabbro

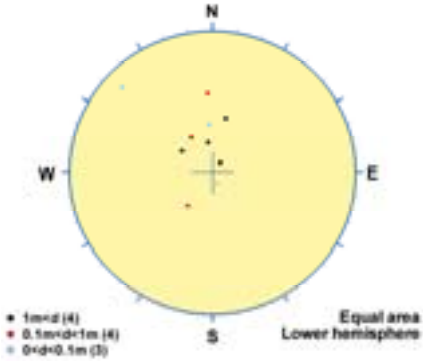

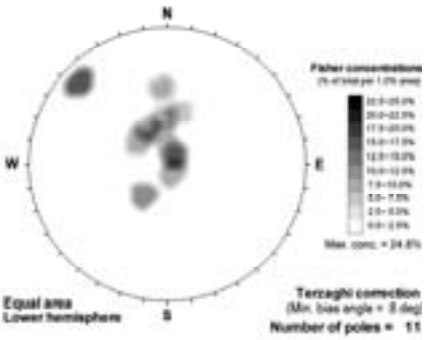

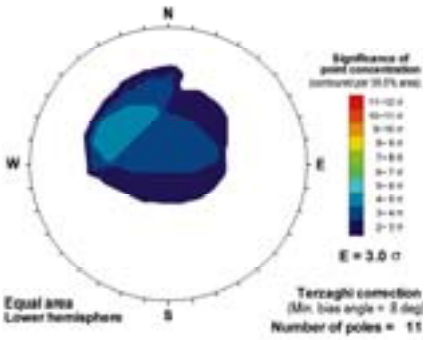

Pegmatite

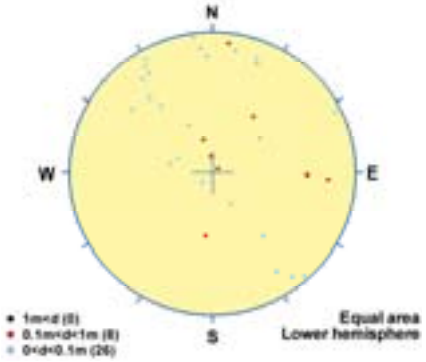

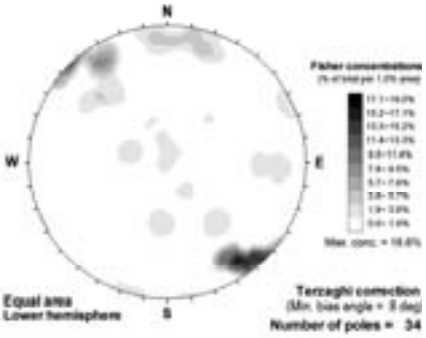

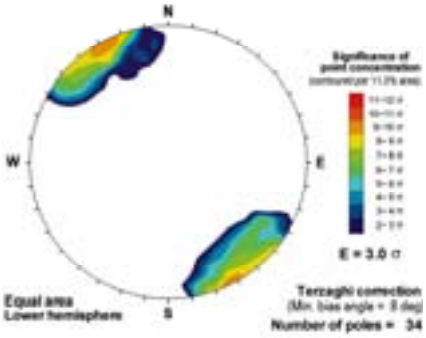

KLX18A_RSMA01

Fine-grained granite

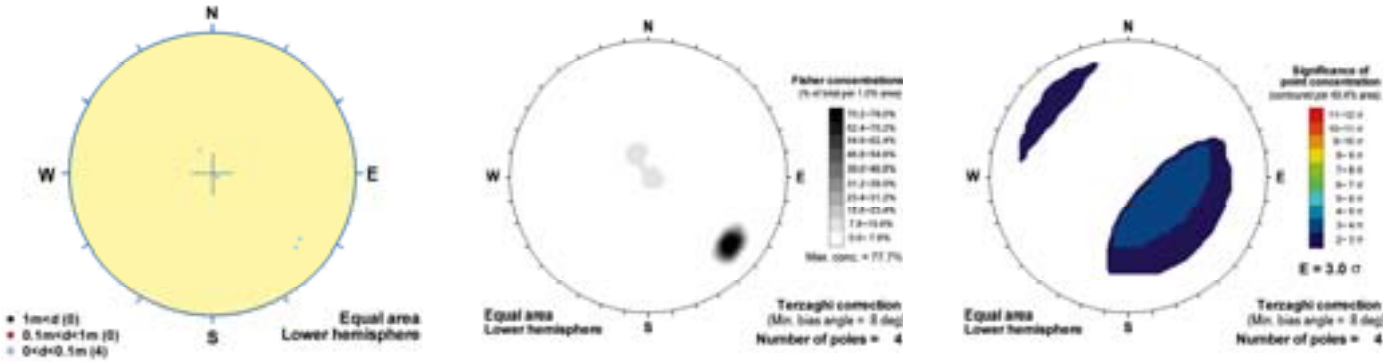

Fine-grained diorite-gabbro

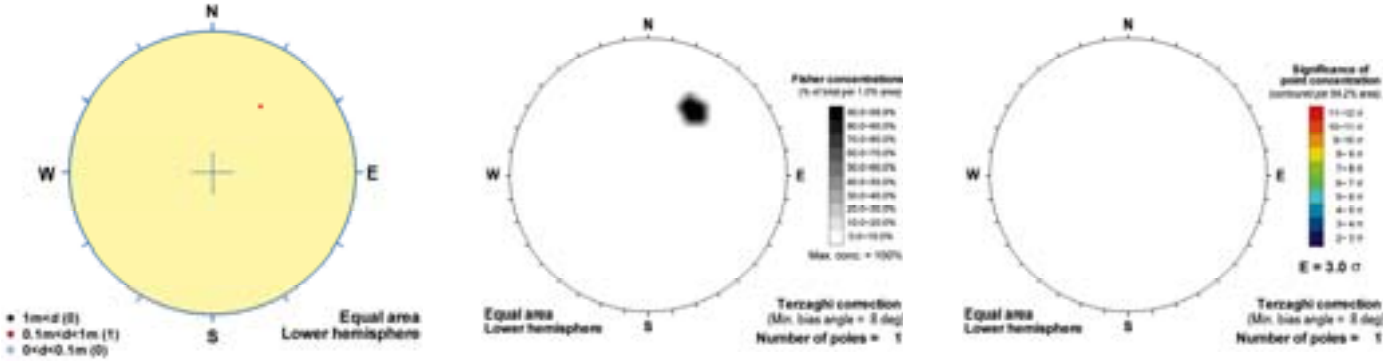

Pegmatite

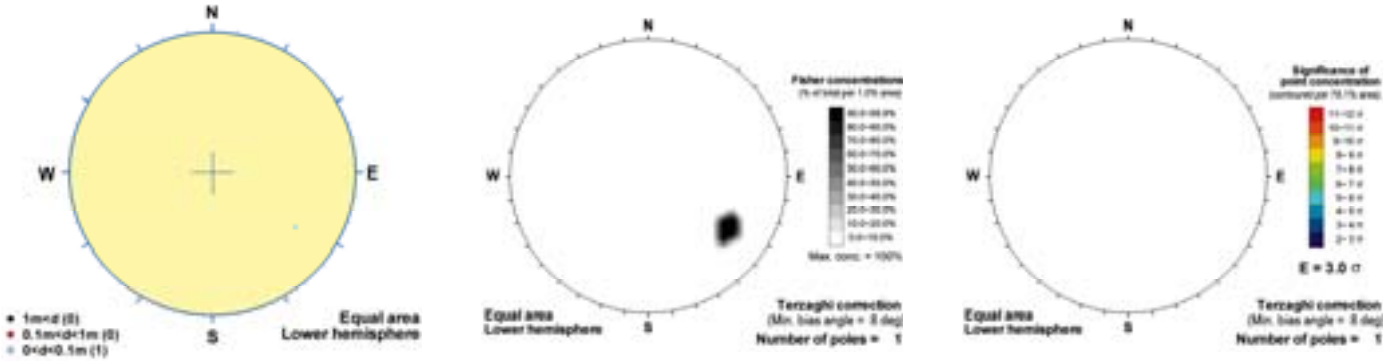

KLX18A_RSMM01

Fine-grained granite

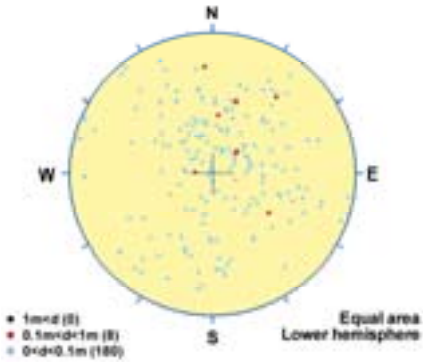

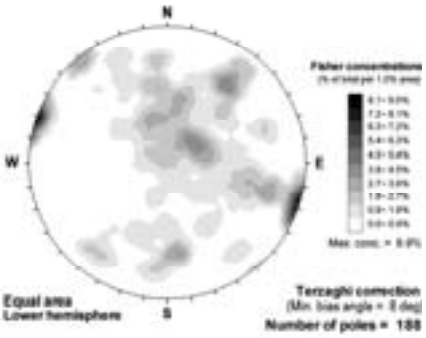

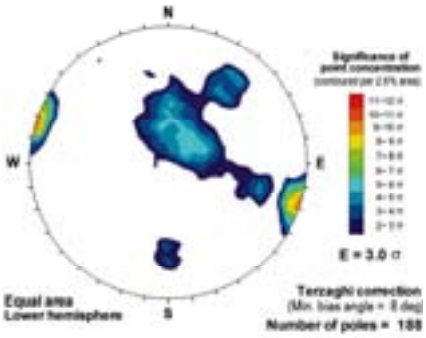

Fine-grained diorite-gabbro

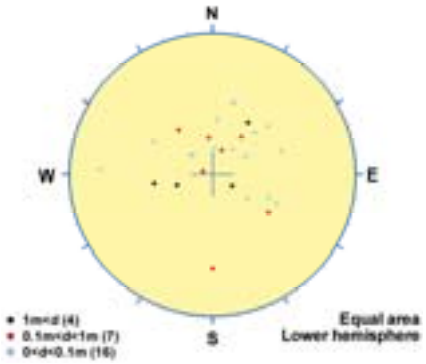

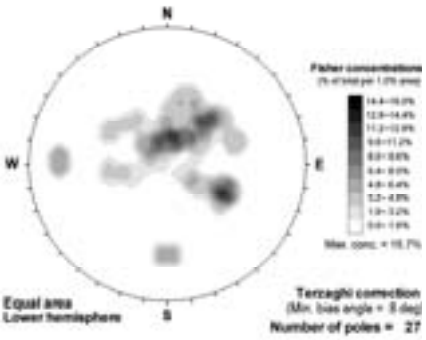

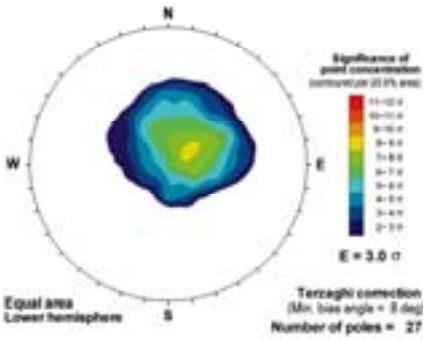

Pegmatite

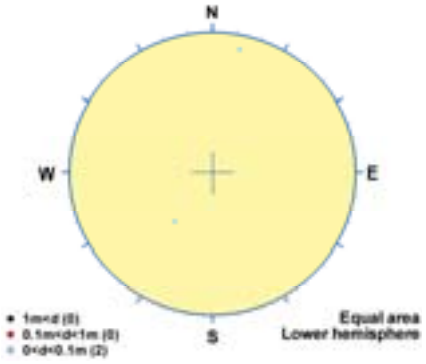

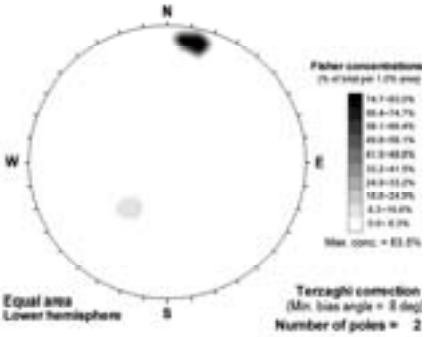

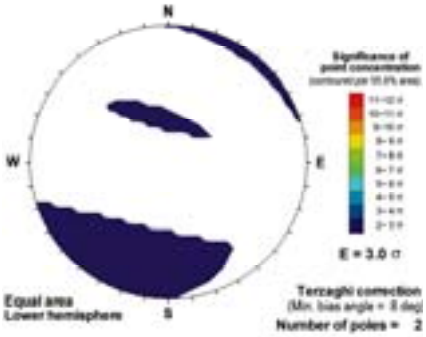

KLX19A_RSMD01

Fine-grained granite

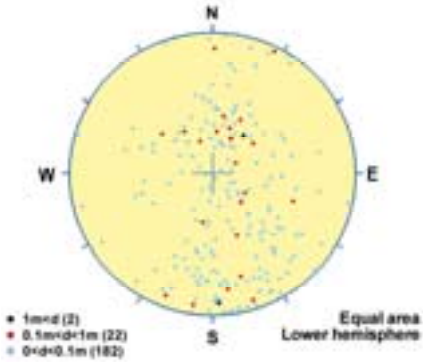

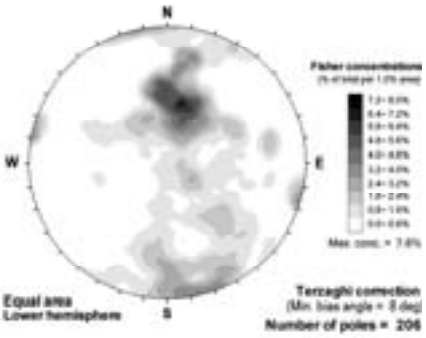

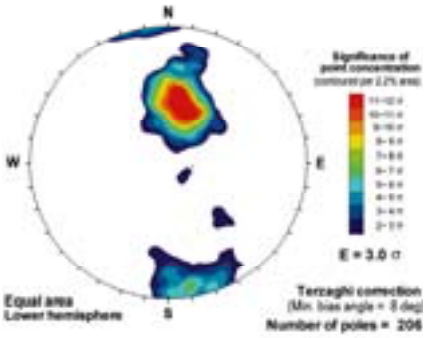

Fine-grained diorite-gabbro

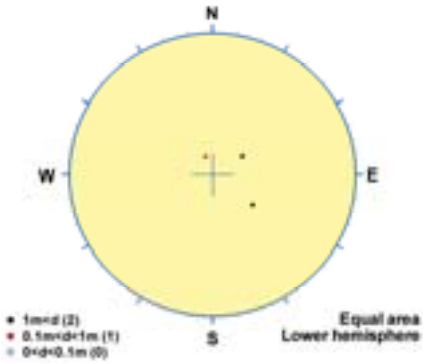

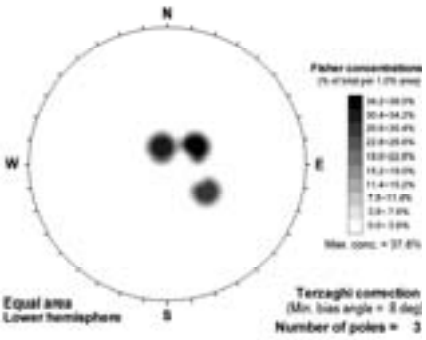

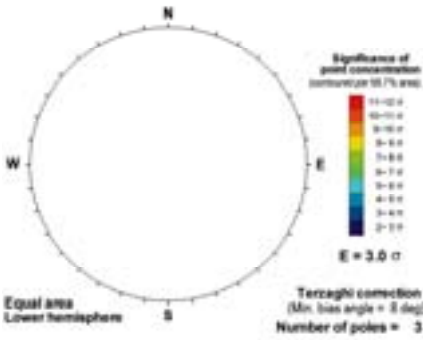

Pegmatite

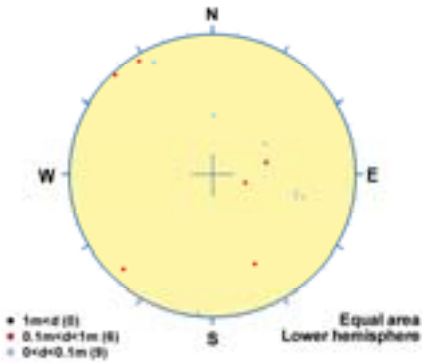

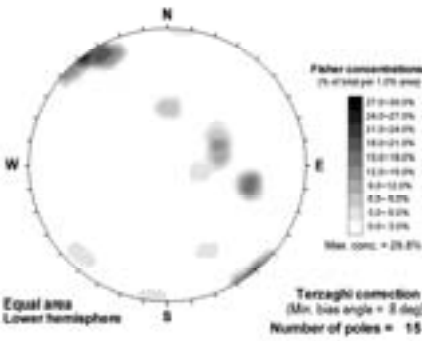

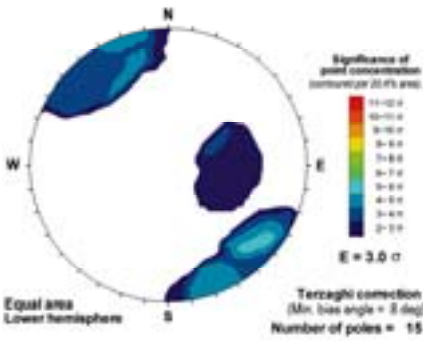

KLX20A_RSMD01

Fine-grained granite

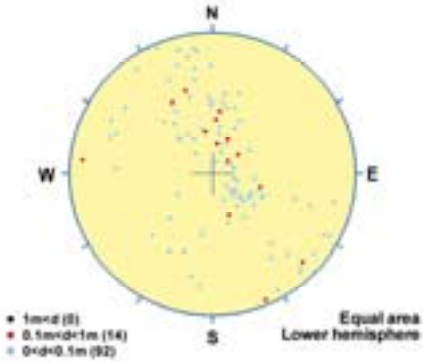

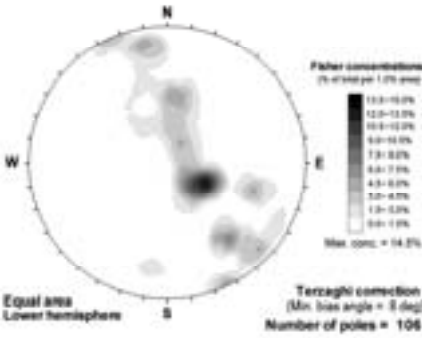

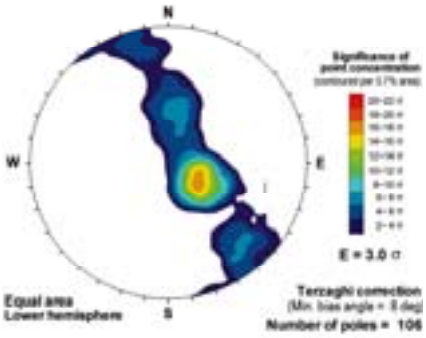

Fine-grained diorite-gabbro

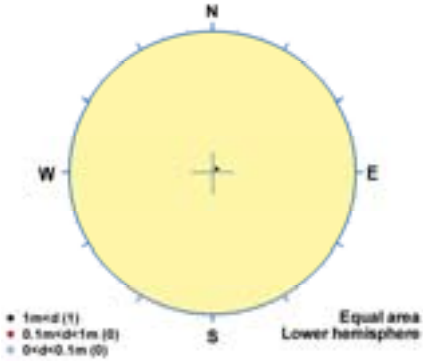

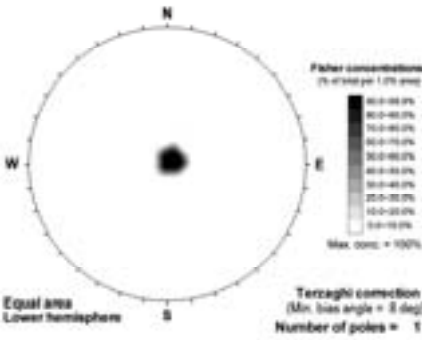

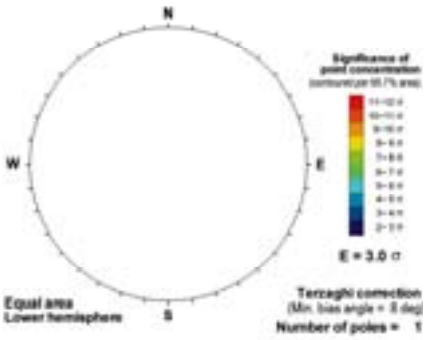

Pegmatite

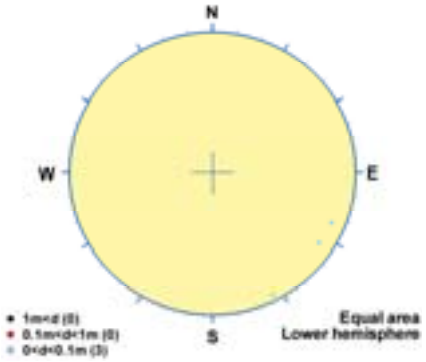

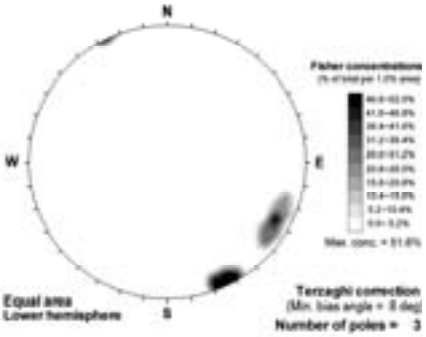

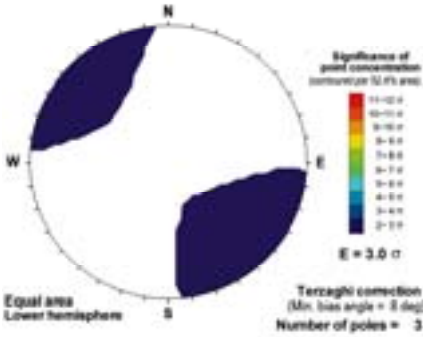

KLX21B_RSMA01

Fine-grained granite

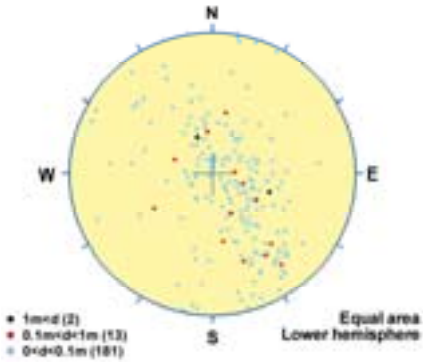

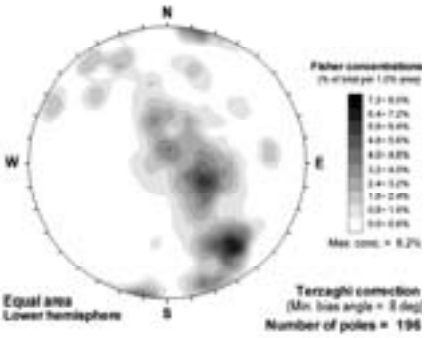

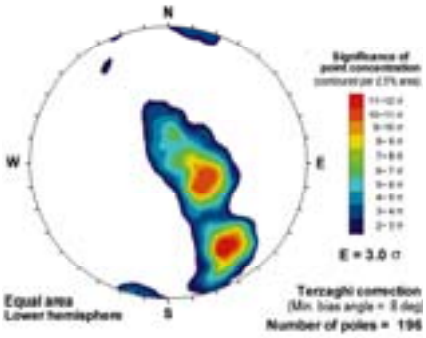

Fine-grained diorite-gabbro

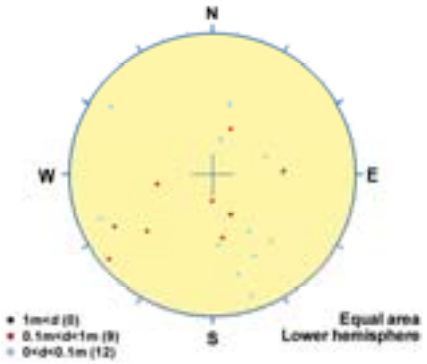

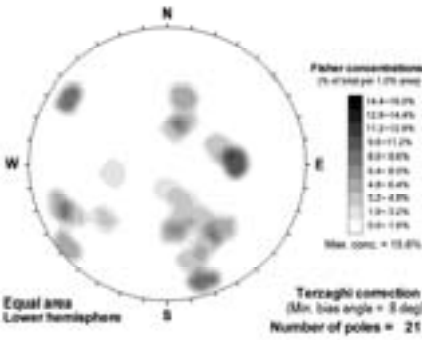

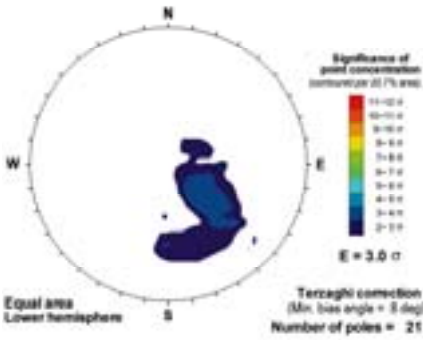

Pegmatite

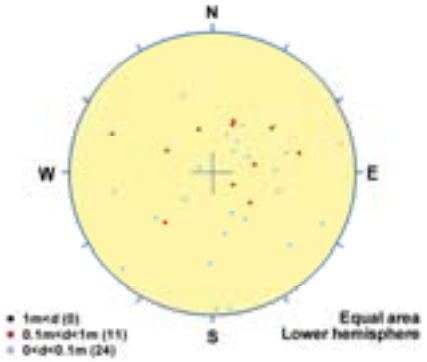

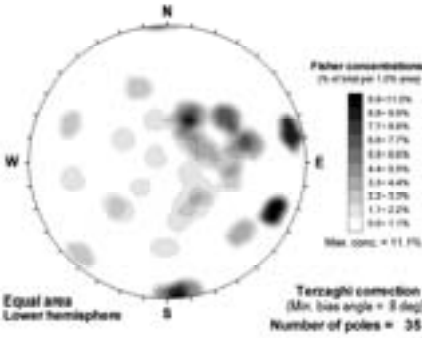

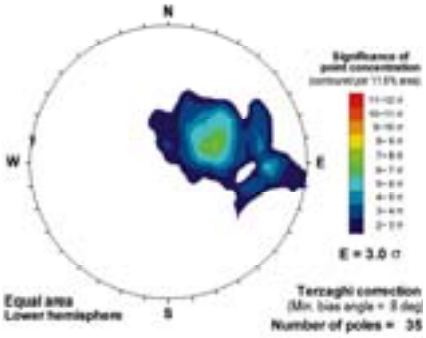

KLX21B_RSMD01

Fine-grained granite

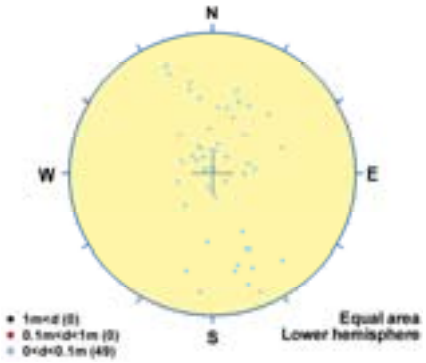

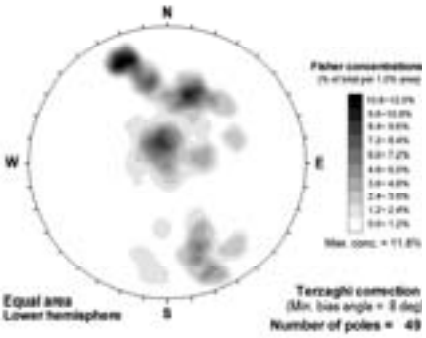

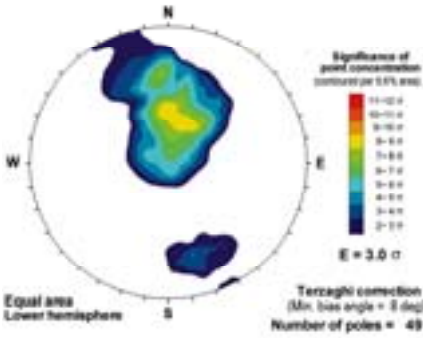

Fine-grained diorite-gabbro

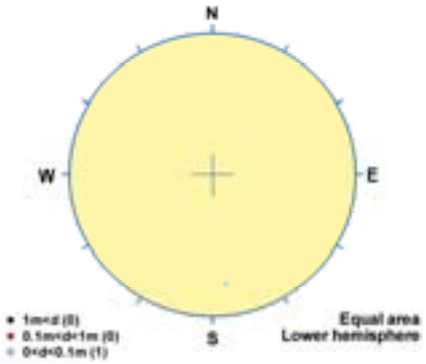

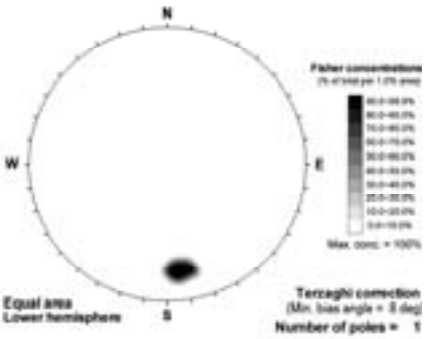

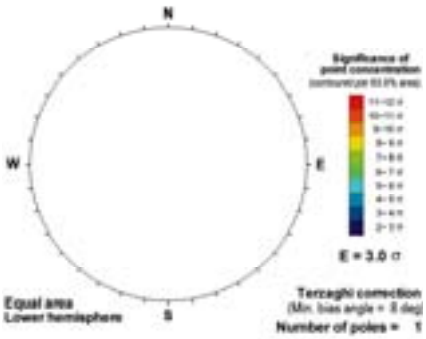

Pegmatite

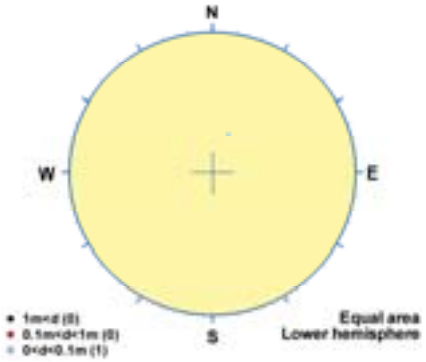

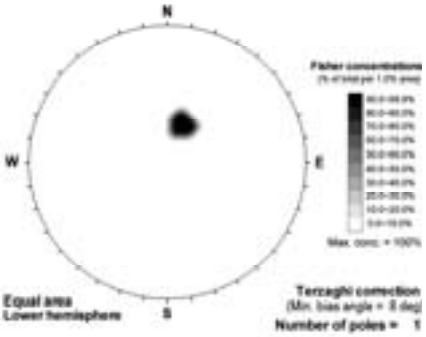

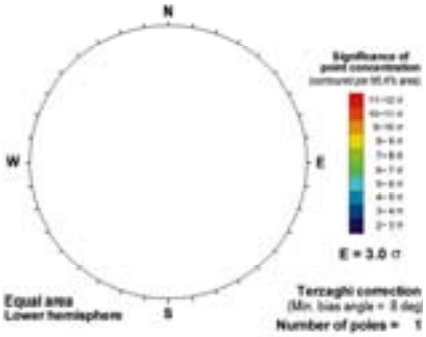

KLX22A_RSMD01

Fine-grained granite

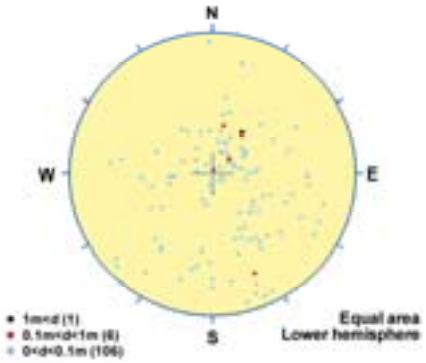

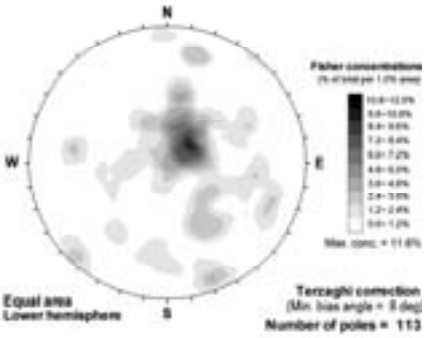

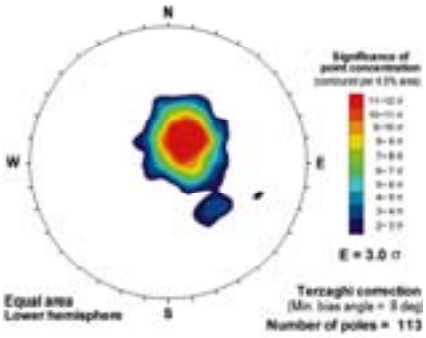

Fine-grained diorite-gabbro

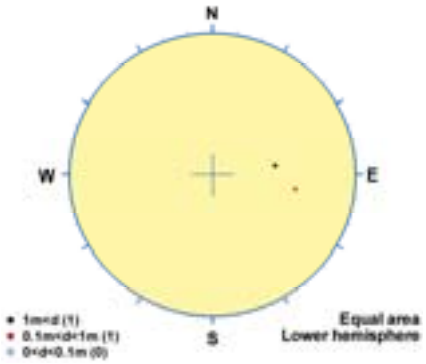

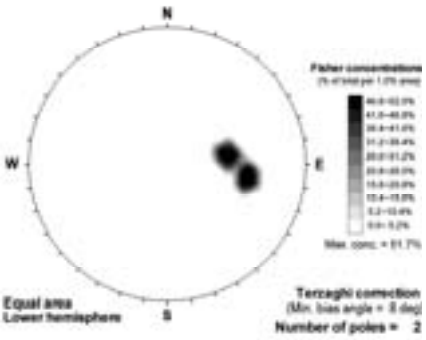

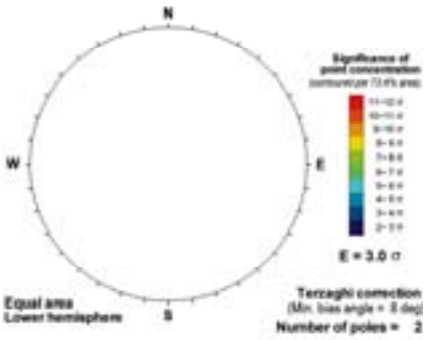

Pegmatite

KLX22B_RSMD01

Fine-grained granite

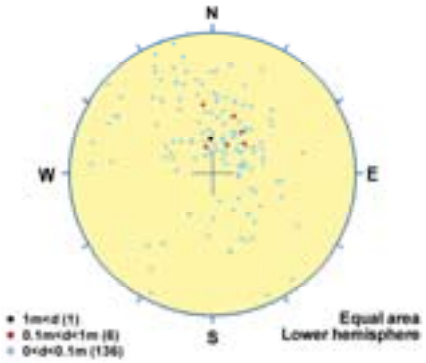

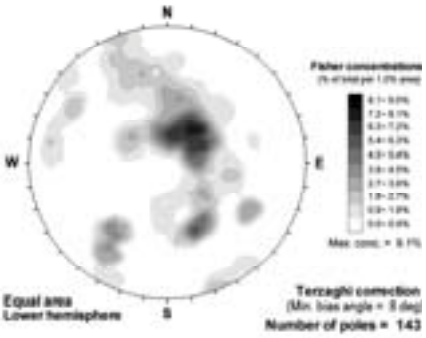

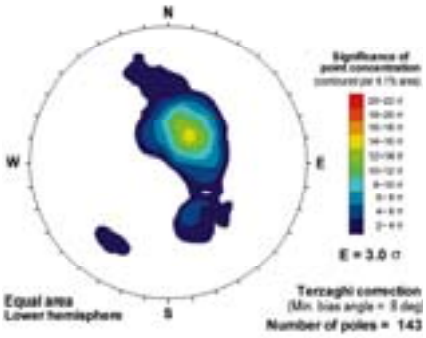

Fine-grained diorite-gabbro

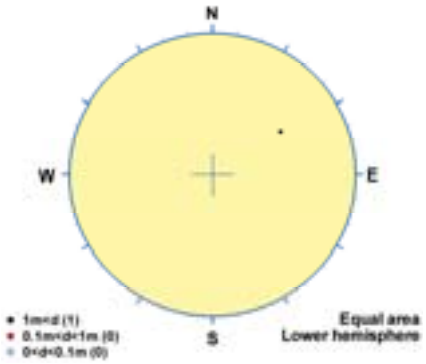

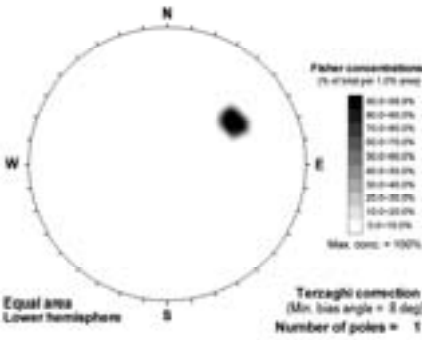

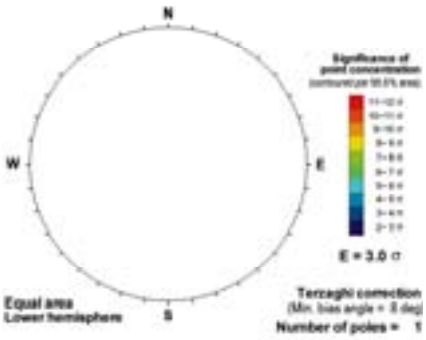

Pegmatite

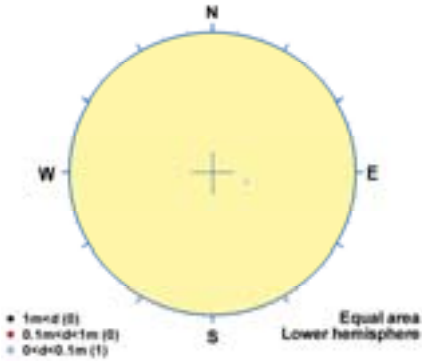

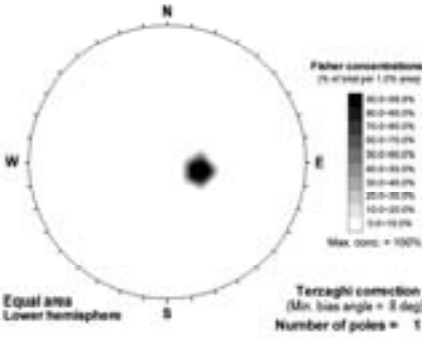

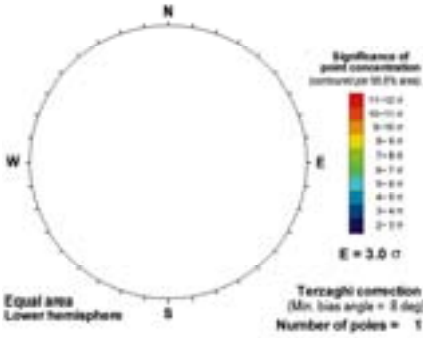

KLX23A_RSMD01

Fine-grained granite

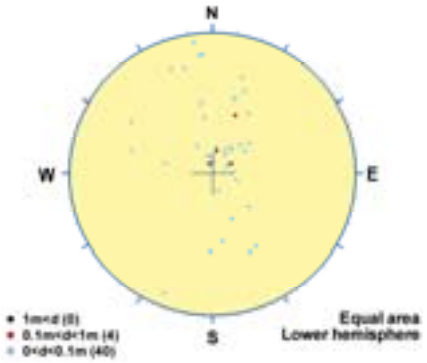

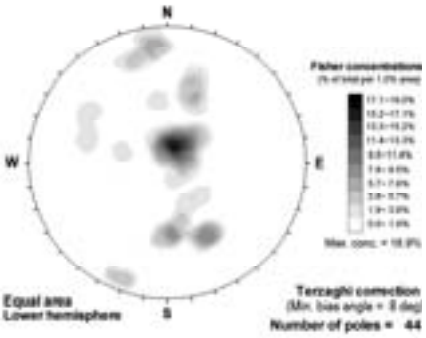

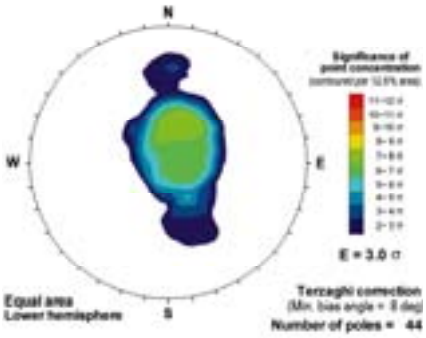

Fine-grained diorite-gabbro

Pegmatite

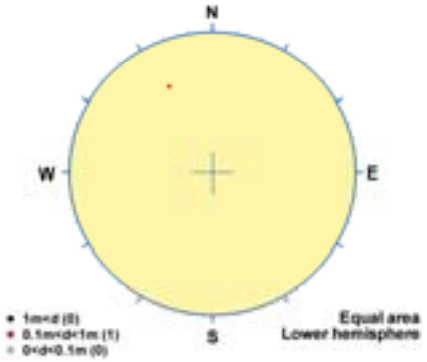

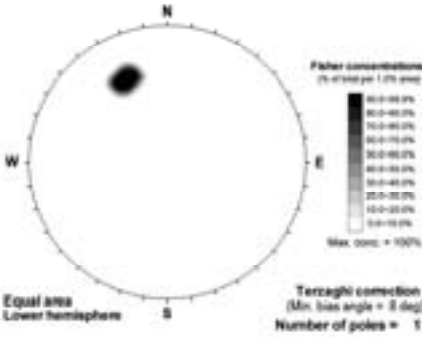

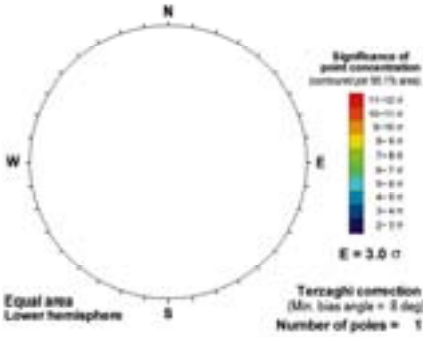

KLX23B_RSMD01

Fine-grained granite

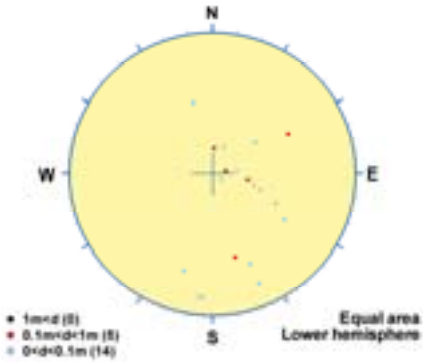

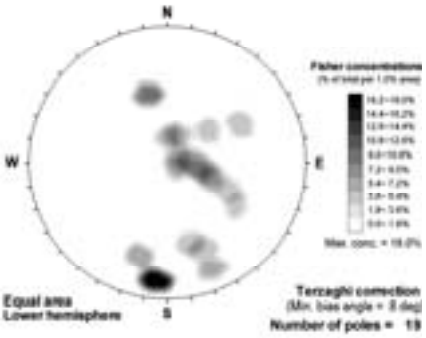

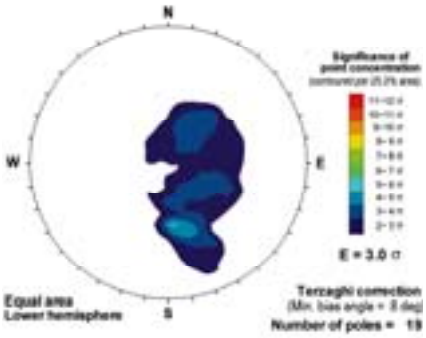

Fine-grained diorite-gabbro

Pegmatite

KLX24A_RSMD01

Fine-grained granite

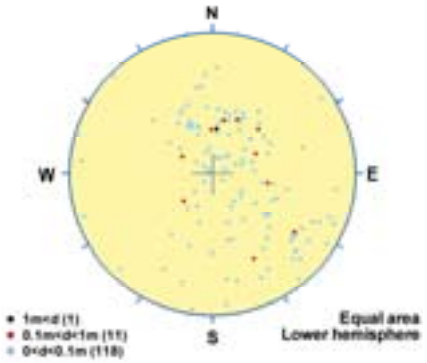

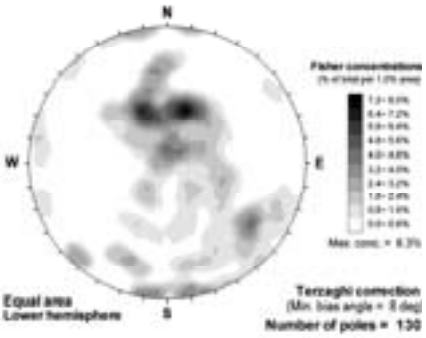

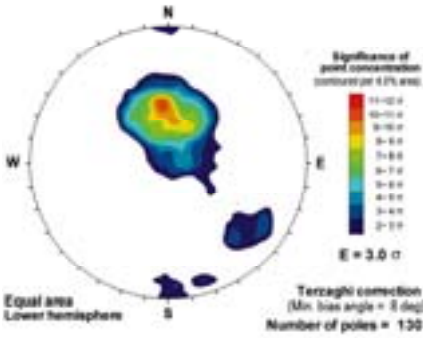

Fine-grained diorite-gabbro

Pegmatite

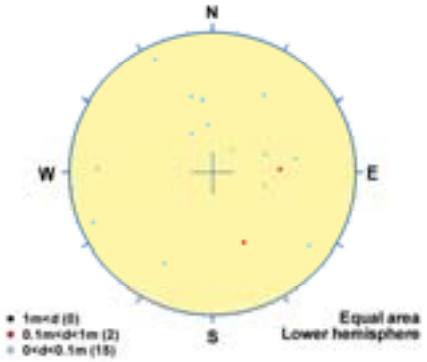

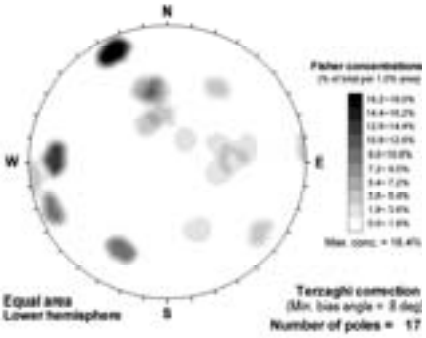

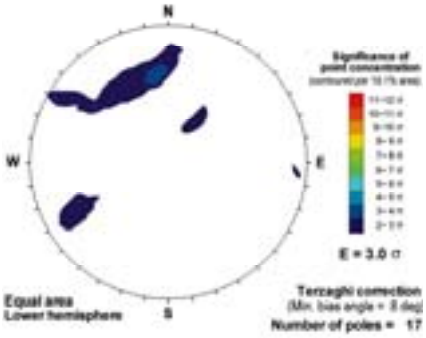

KLX25A_RSMD01

Fine-grained granite

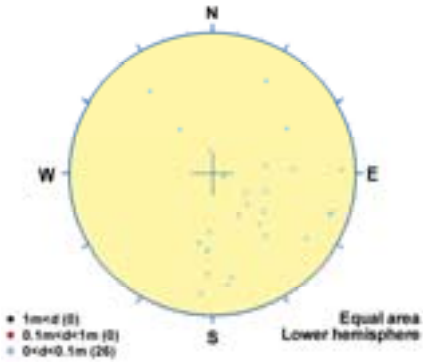

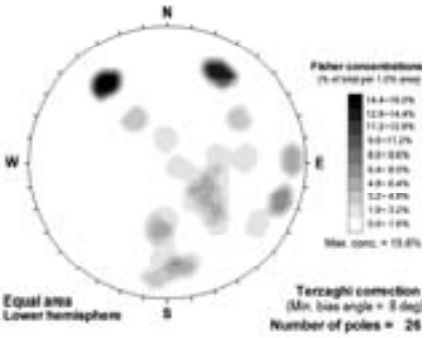

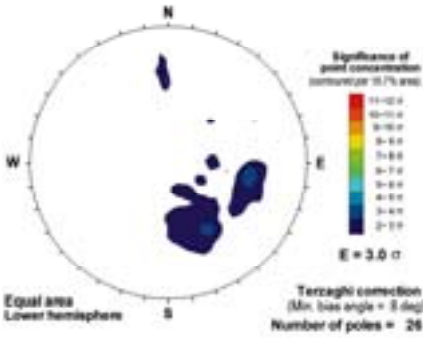

Fine-grained diorite-gabbro

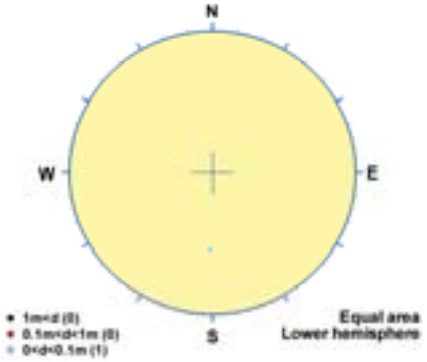

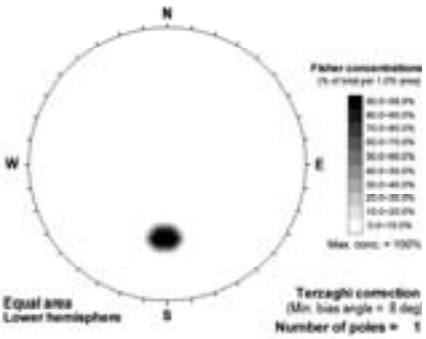

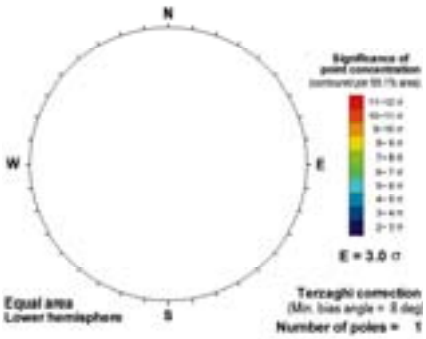

Pegmatite

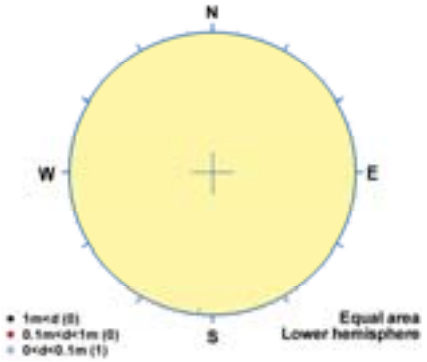

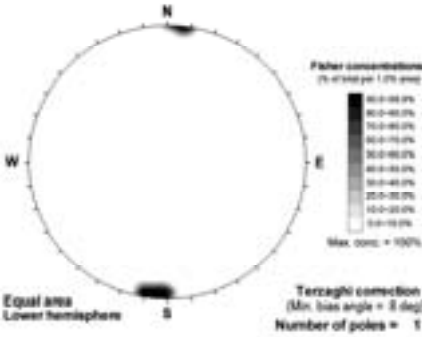

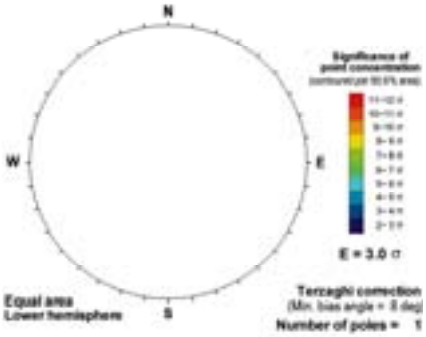

KLX26A_RSMM01

Fine-grained granite

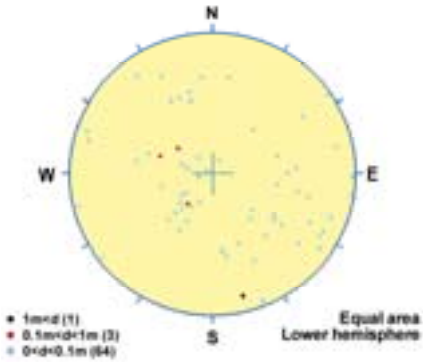

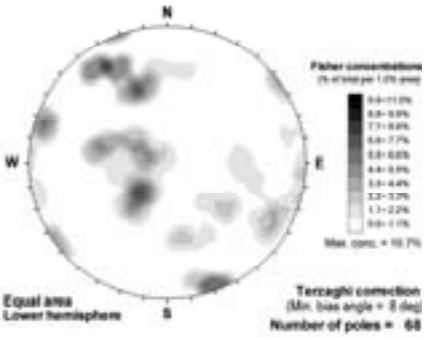

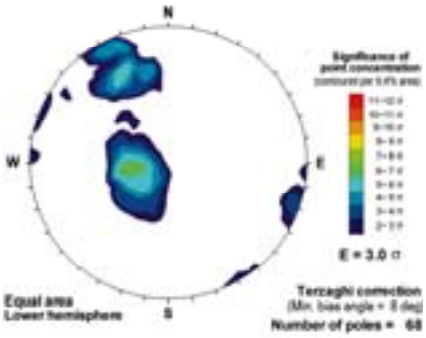

Fine-grained diorite-gabbro

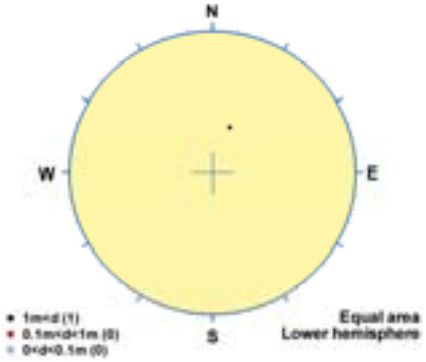

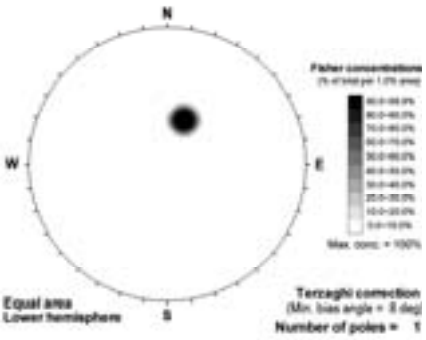

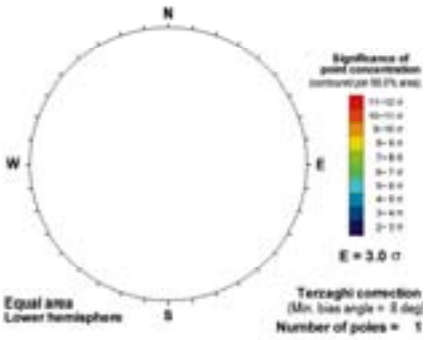

Pegmatite

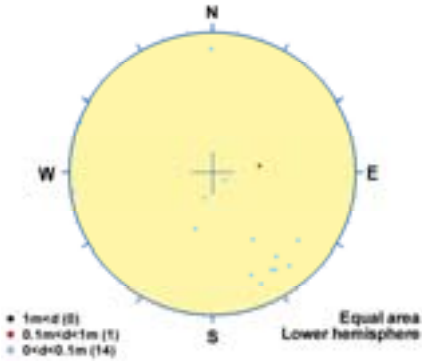

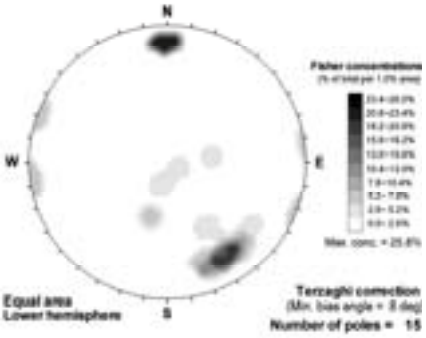

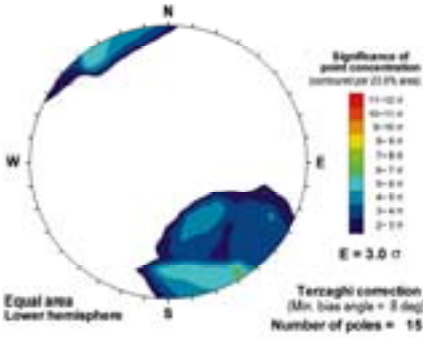

KLX26B_RSMM01

Fine-grained granite

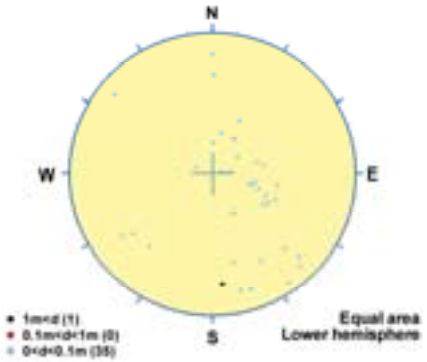

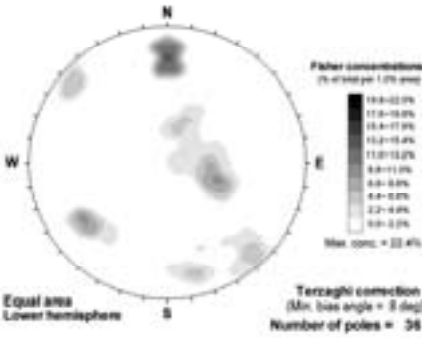

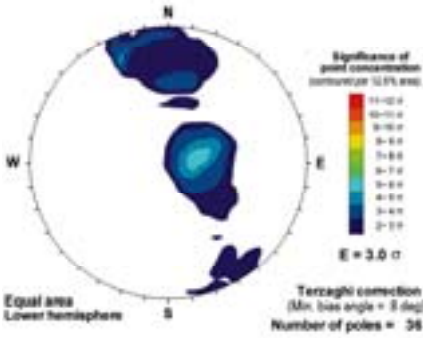

Fine-grained diorite-gabbro

Pegmatite

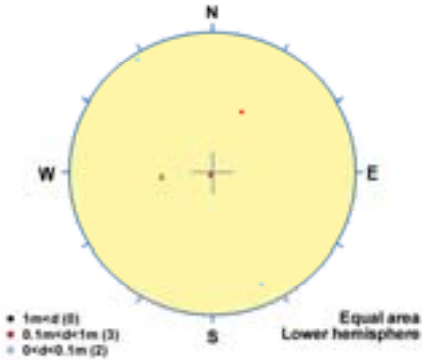

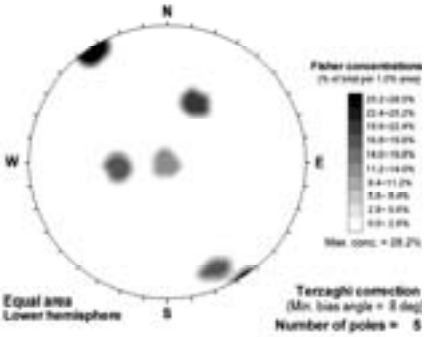

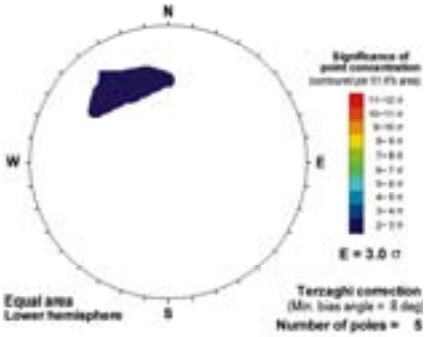

KLX28A_RSMM01

Fine-grained granite

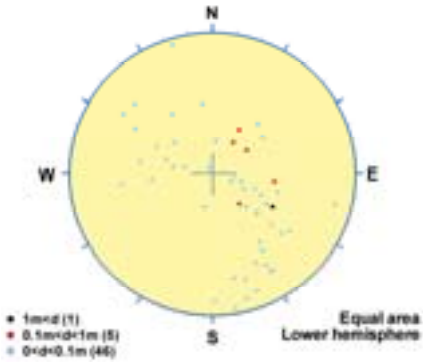

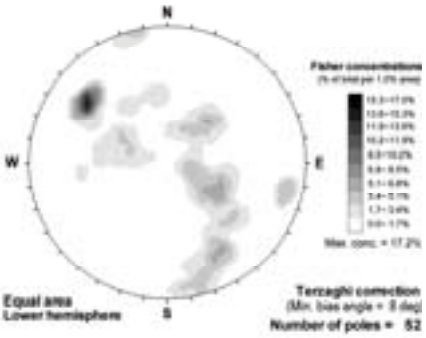

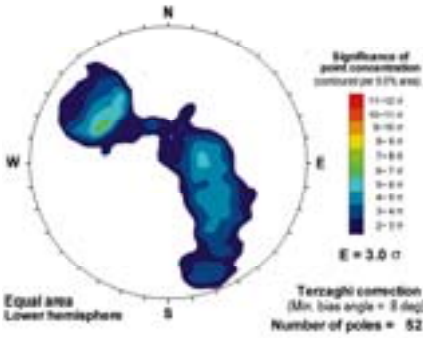

Fine-grained diorite-gabbro

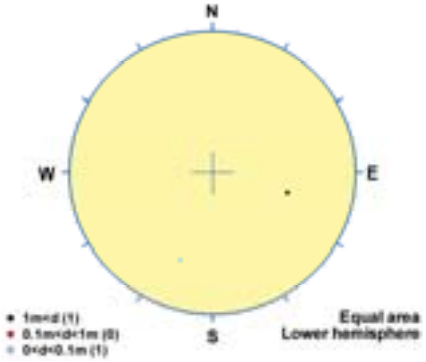

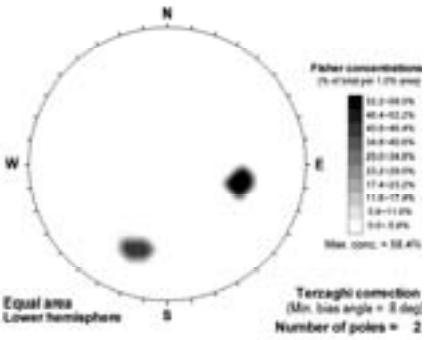

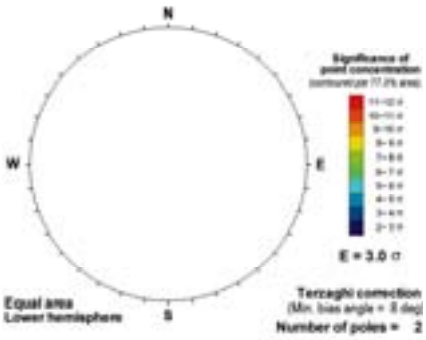

Pegmatite

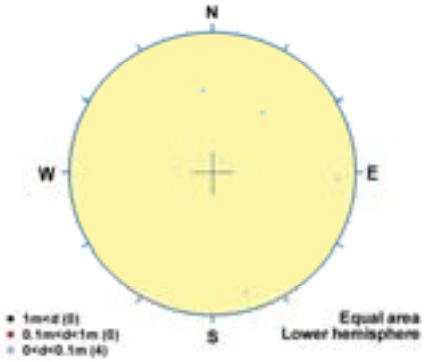

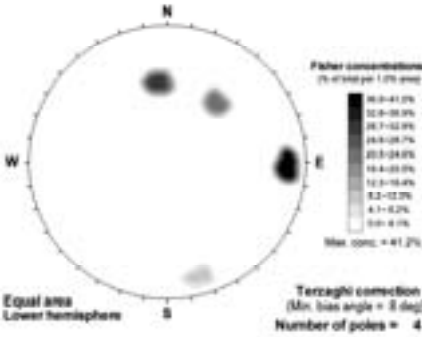

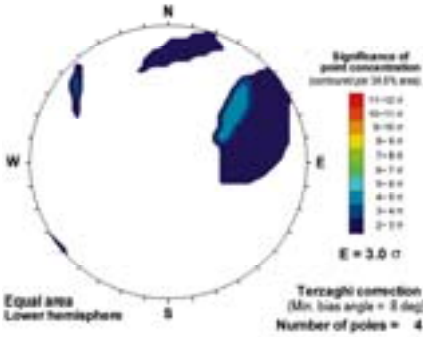

KLX29A_RSMA01

Fine-grained granite

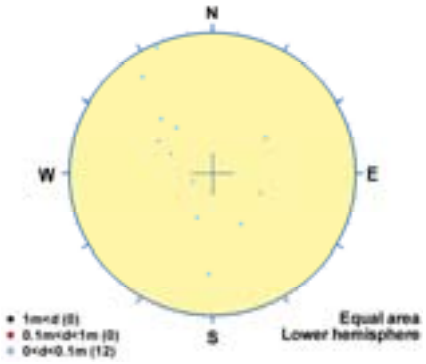

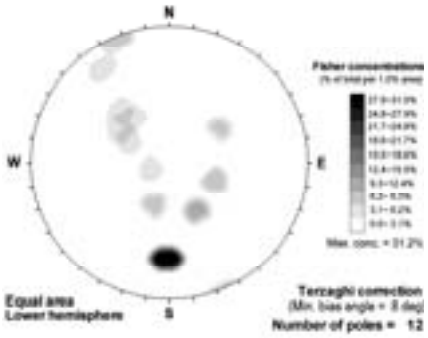

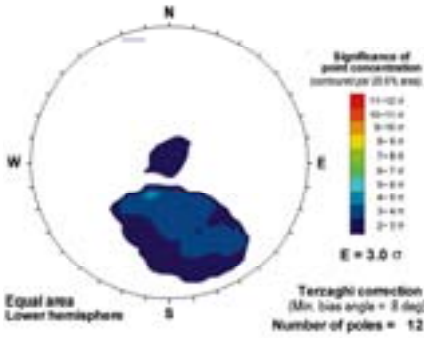

Fine-grained diorite-gabbro

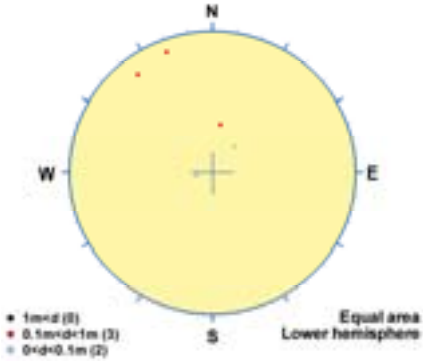

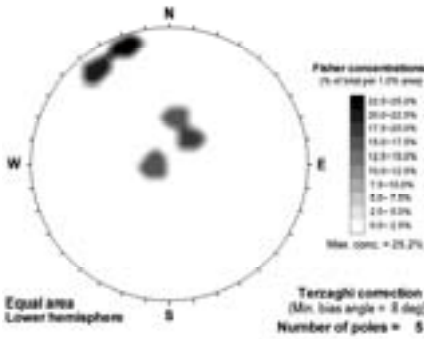

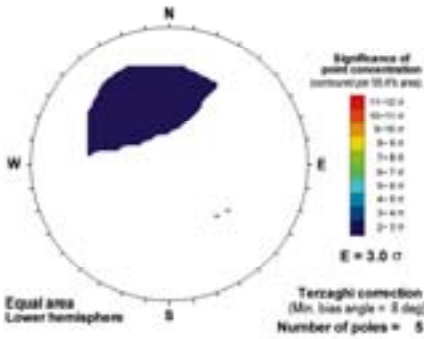

Pegmatite

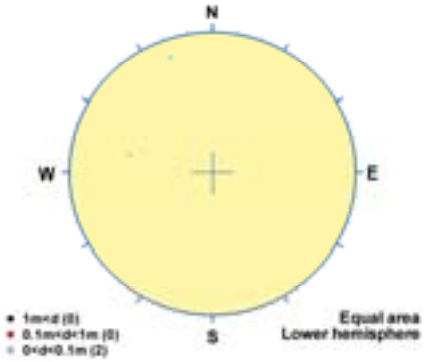

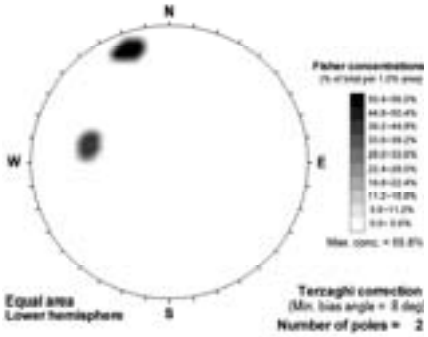

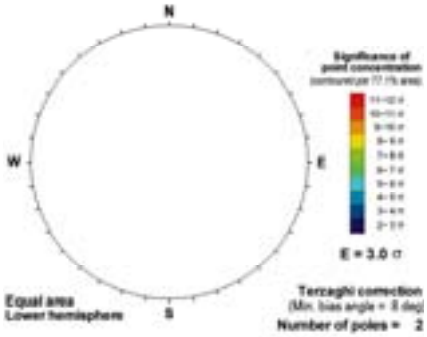

Orientation of contacts of subordinate rock types on an overall rock domain basis

RSMA01

Fine-grained granite

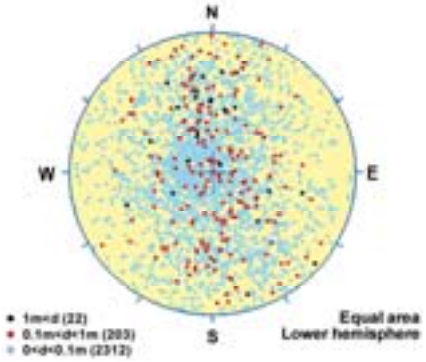

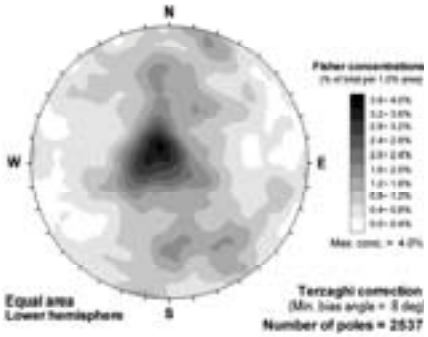

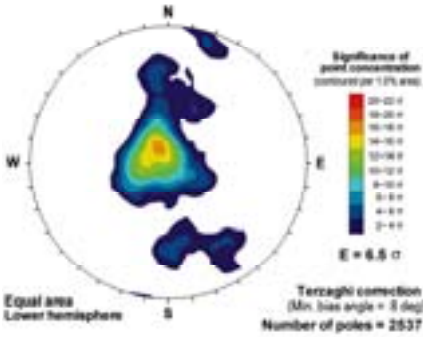

Fine-grained diorite-gabbro

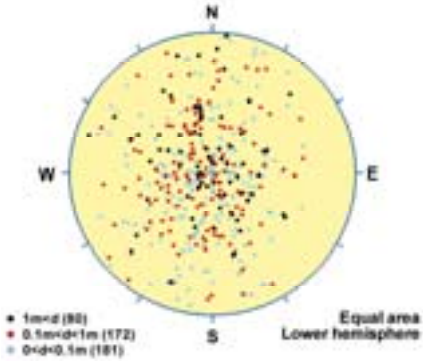

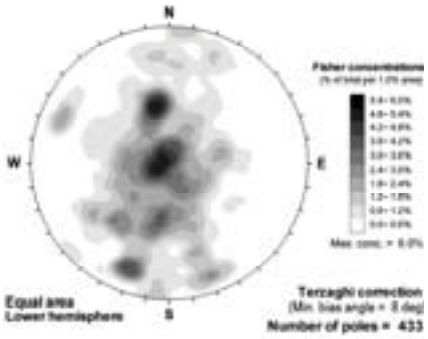

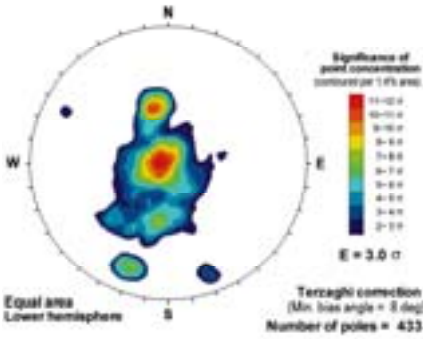

Pegmatite

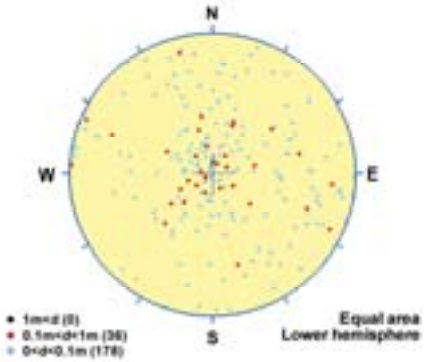

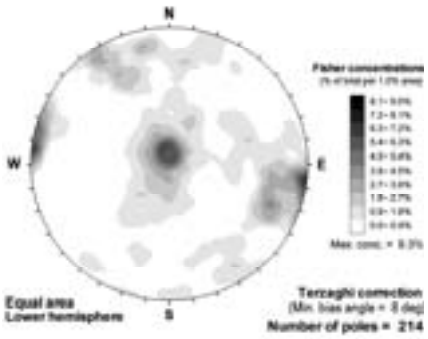

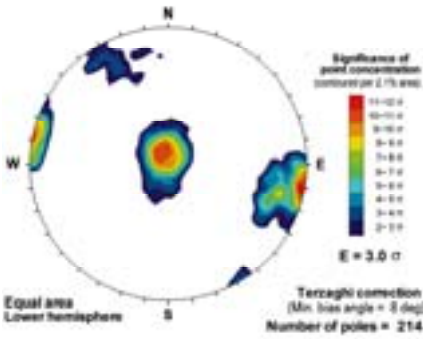

RSMD01

Fine-grained granite

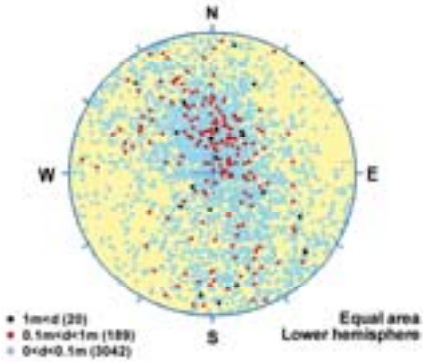

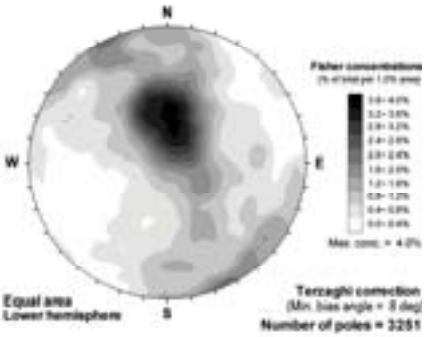

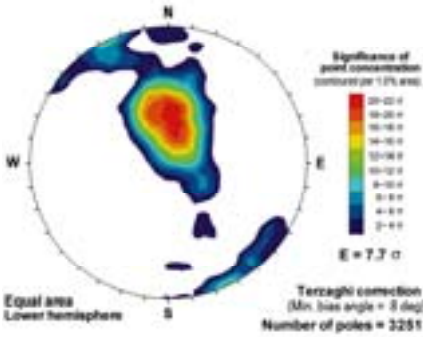

Fine-grained diorite-gabbro

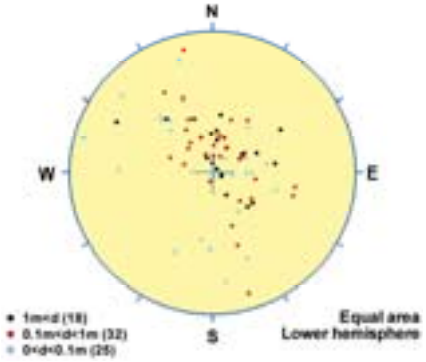

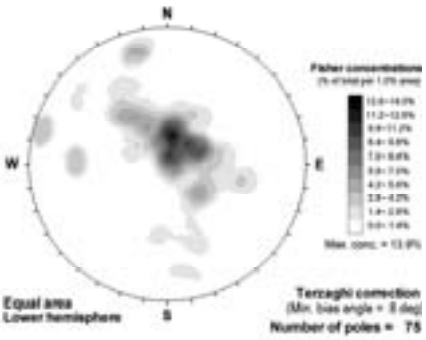

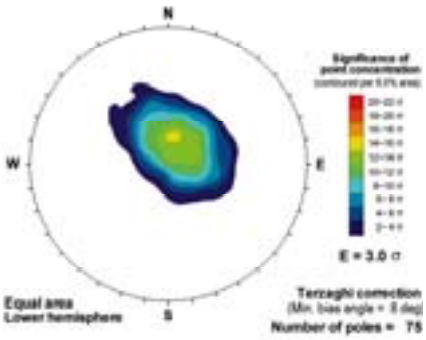

Pegmatite

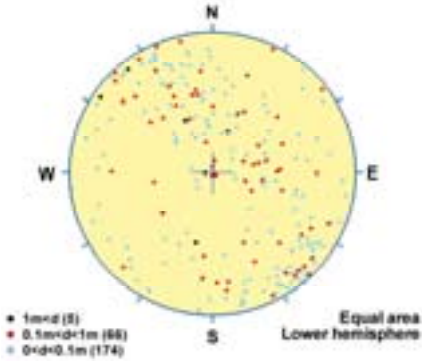

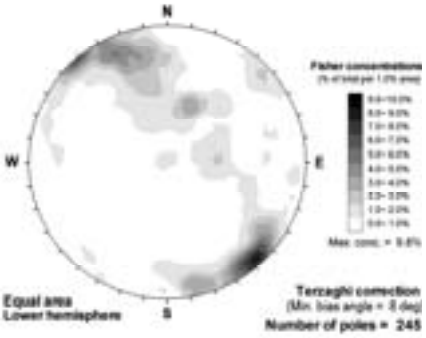

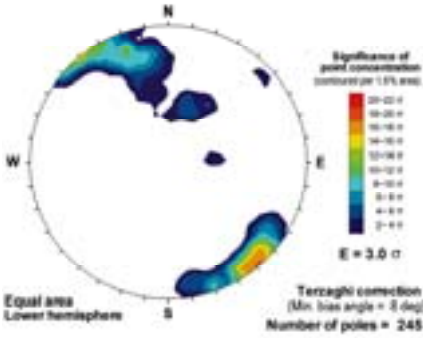

RSMM01

Fine-grained granite

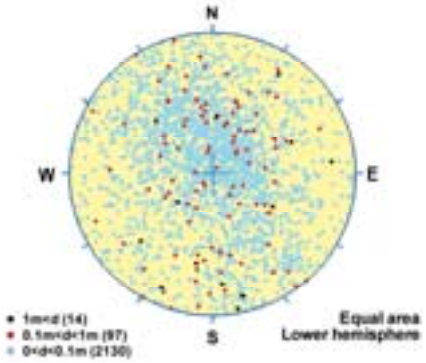

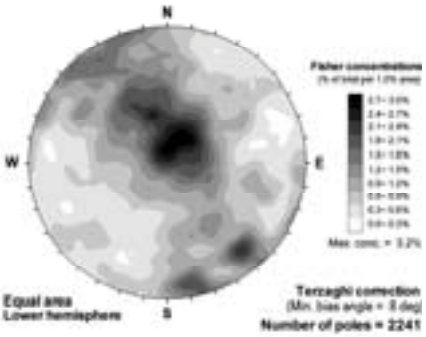

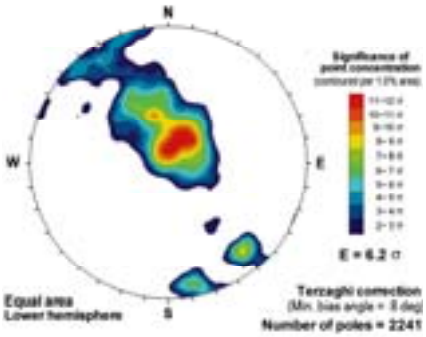

Fine-grained diorite-gabbro

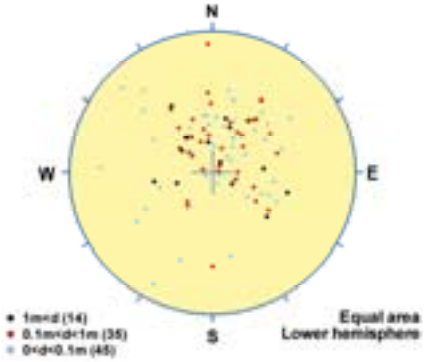

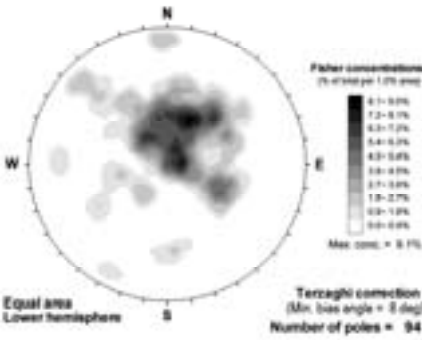

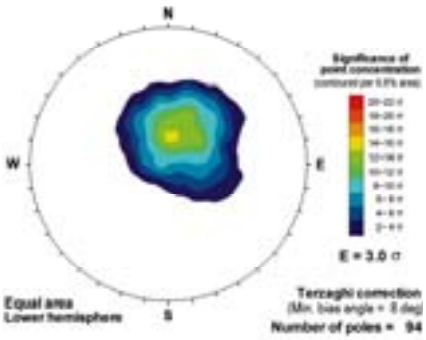

Pegmatite

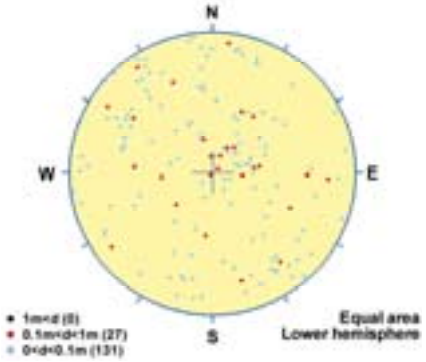

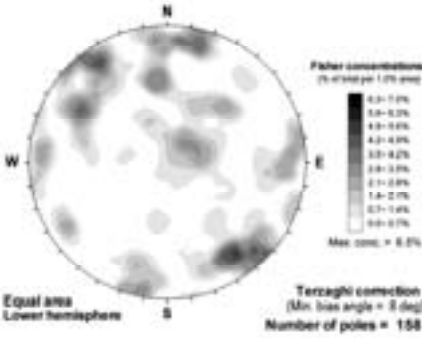

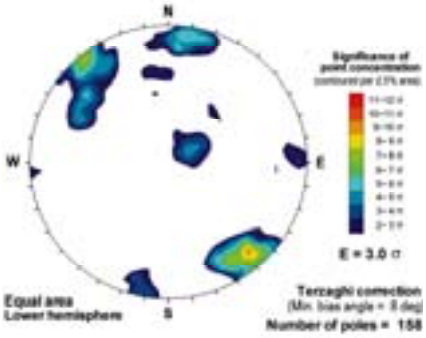

Appendix 7

Type and degree of alteration outside deformation zones on a borehole by borehole basis, on a rock domain basis in each borehole and on an overall rock domain basis

Data from Sicada: p_rock_alter.xls and p_eshi_dz.xls in Sicada_07_323 and Sicada_07_350_2

Procedure: For each borehole, rock domain in each borehole and the overall rock domain, the proportions of the bedrock affected by the alteration referred to primarily as oxidation and saussuritisation, but also other types of alteration, outside deformation zones, have been estimated. The degree of alteration recorded in the Sicada database, classified as faint, weak, medium and strong, is also addressed. The results are presented in a series of histograms.

The various histograms can be viewed on the CD-Rom attached to this report. Further discussion of the results of this analysis is presented in section 3.4.4 in this report.

Type and degree of alteration outside deformation zones on a borehole by borehole basis

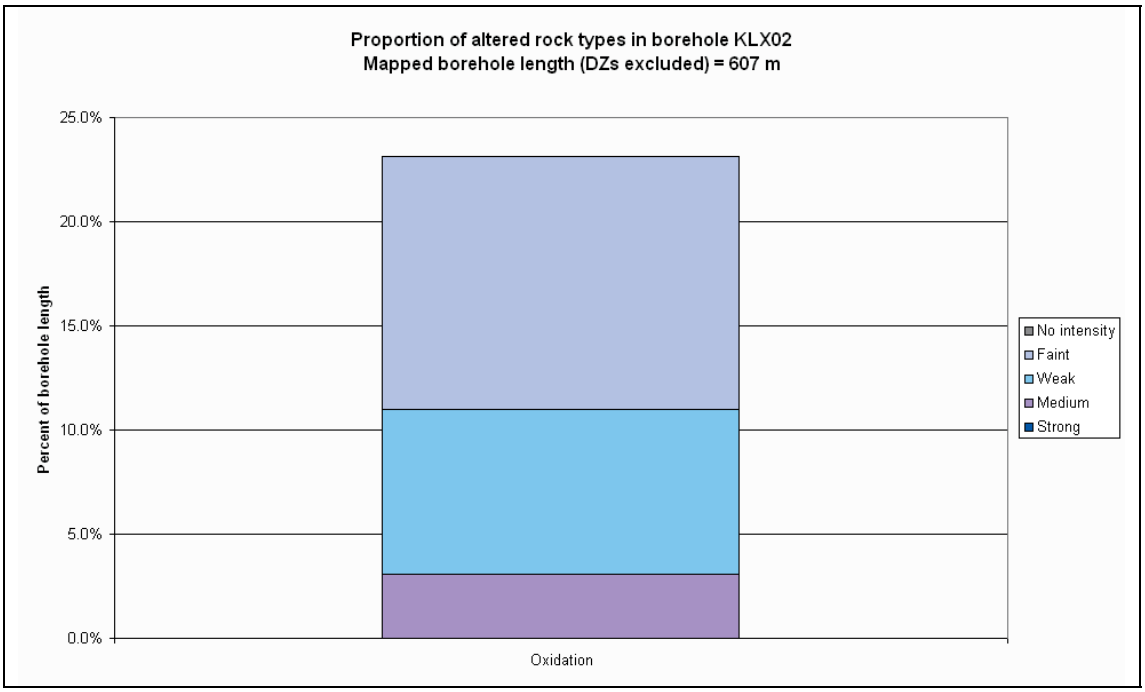

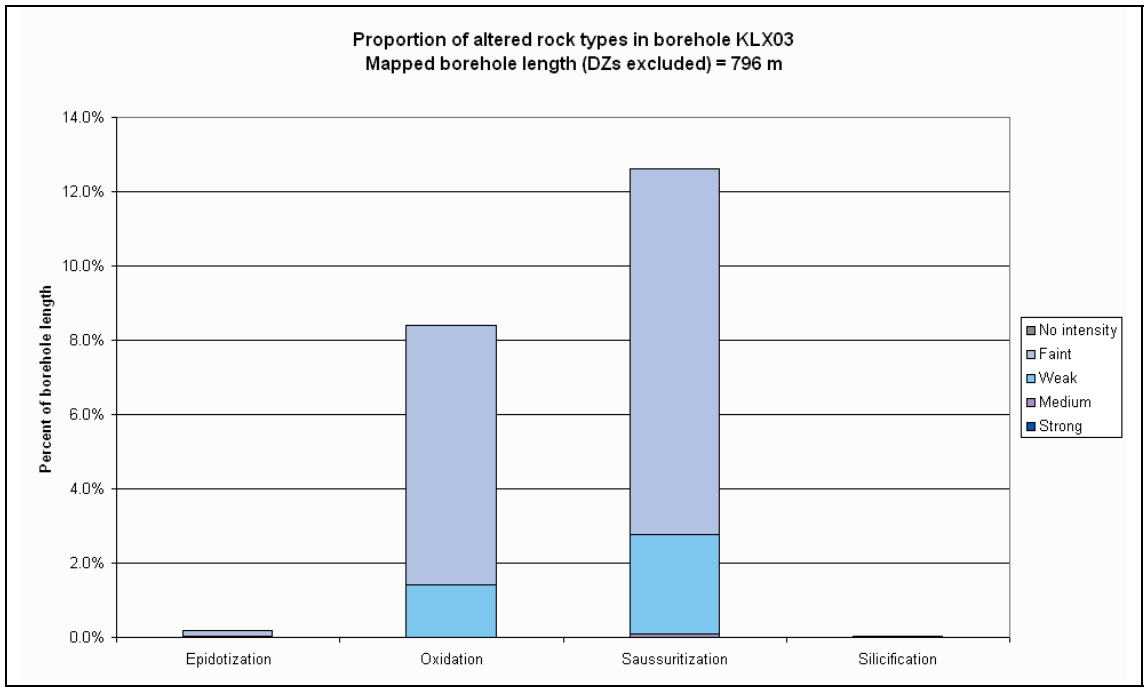
Proportion of altered rock types in borehole KLX03
Mapped borehole length (DZs excluded) = 796 m
Percent of borehole length
14.0%
12.0%
10.0%
8.0%
6.0%
4.0%
2.0%
0.0%
Epidotization
Oxidation
Saussuritization
Silicification
No intensity
Faint
Weak
Medium
Strong

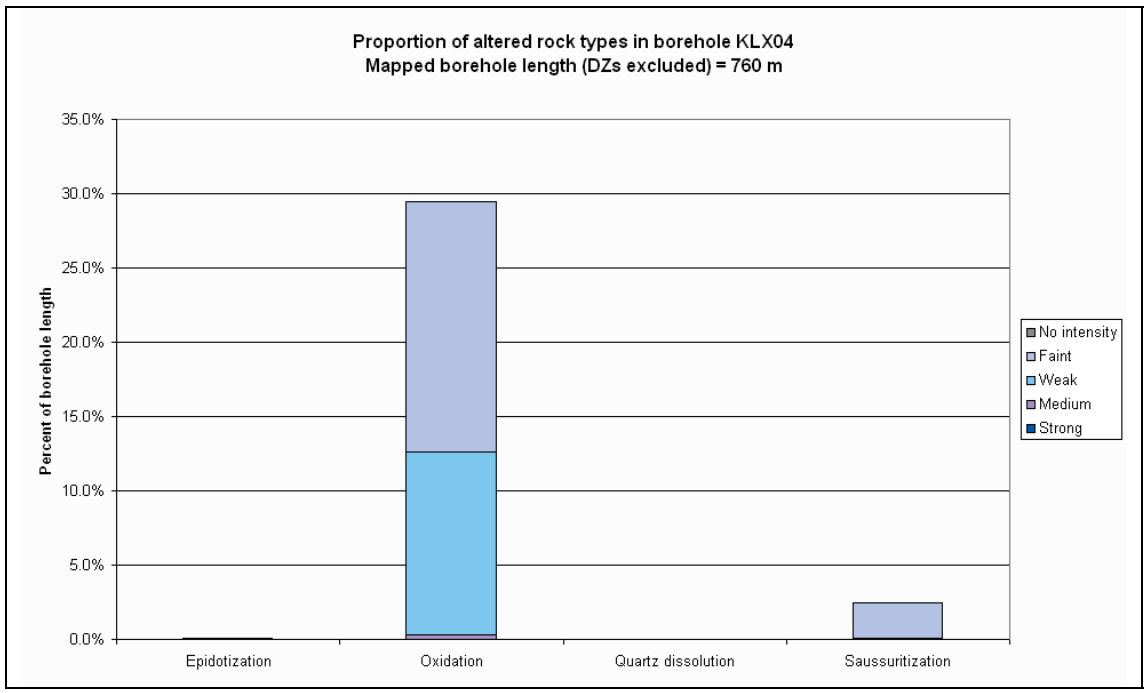
Proportion of altered rock types in borehole KLX04
Mapped borehole length (DZs excluded) = 760 m
Percent of borehole length
35.0%
30.0%
25.0%
20.0%
15.0%
10.0%
5.0%
0.0%
Epidotization
Oxidation
Quartz dissolution
Saussuritization
No intensity
Faint
Weak
Medium
Strong

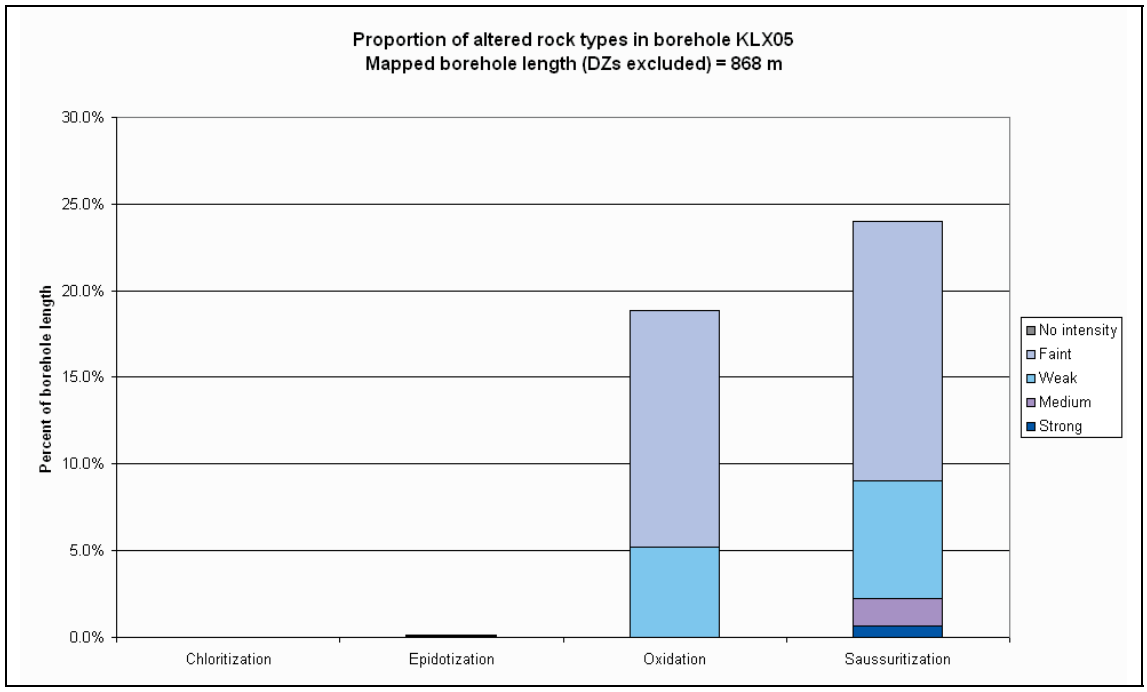
Proportion of altered rock types in borehole KLX05
Mapped borehole length (DZs excluded) = 868 m
Percent of borehole length
30.0%
25.0%
20.0%
15.0%
10.0%
5.0%
0.0%
Chloritization
Epidotization
Oxidation
Saussuritization
No intensity
Faint
Weak
Medium
Strong

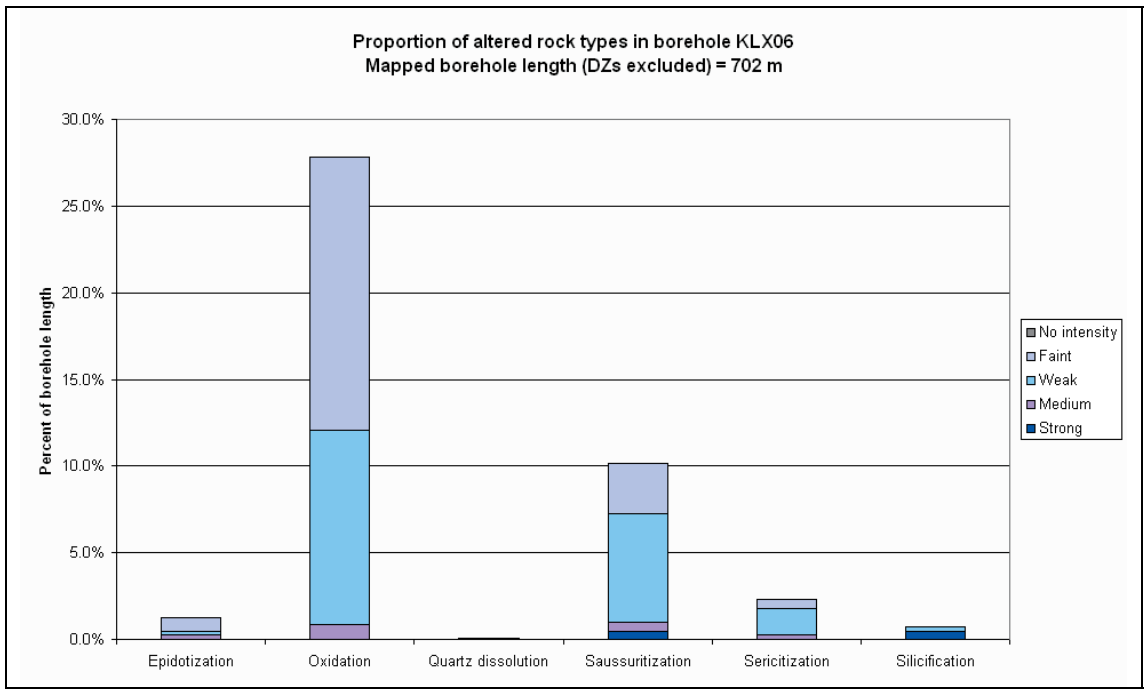
Proportion of altered rock types in borehole KLX06
Mapped borehole length (DZs excluded) = 702 m
Percent of borehole length
30.0%
25.0%
20.0%
15.0%
10.0%
5.0%
0.0%
Epidotization
Oxidation
Quartz dissolution
Saussuritization
Sericitization
Silicification
No intensity
Faint
Weak
Medium
Strong

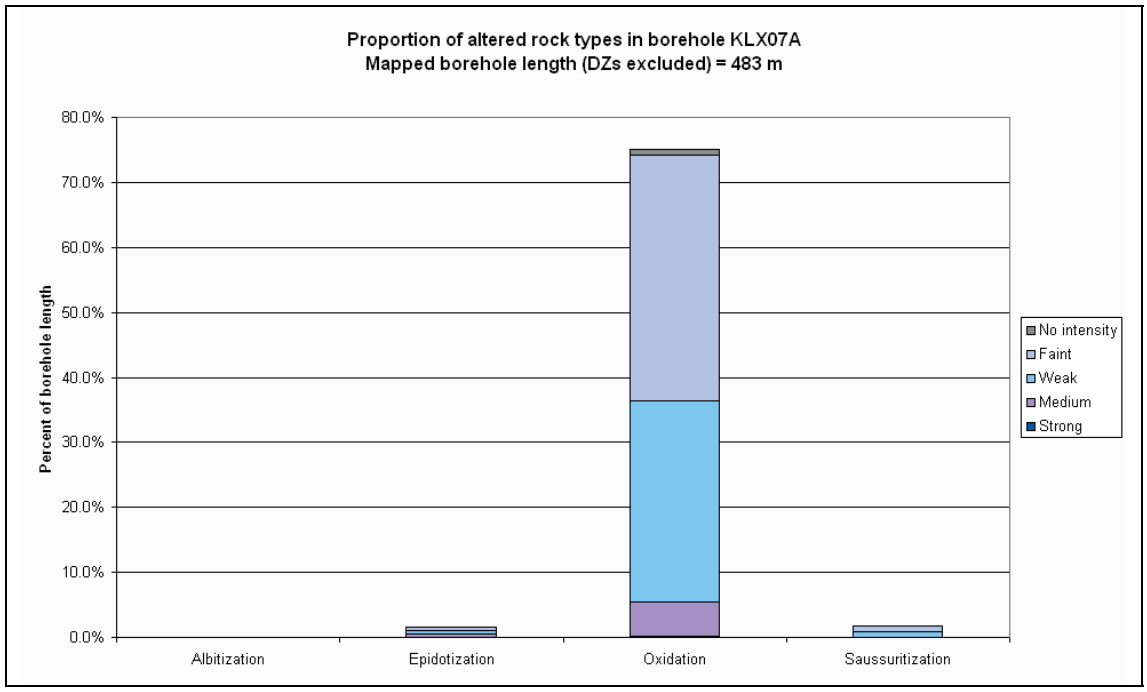
Proportion of altered rock types in borehole KLX07A
Mapped borehole length (DZs excluded) = 483 m
Percent of borehole length
80.0%
70.0%
60.0%
50.0%
40.0%
30.0%
20.0%
10.0%
0.0%
Albitization
Epidotization
Oxidation
Saussuritization
No intensity
Faint
Weak
Medium
Strong

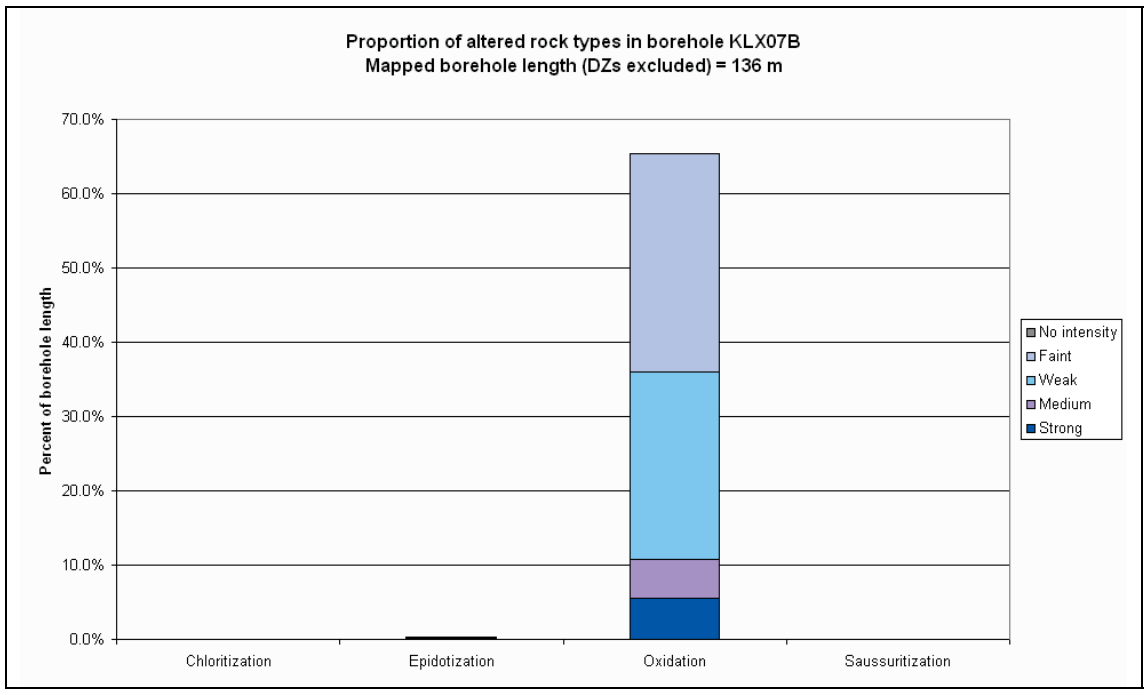
Proportion of altered rock types in borehole KLX07B
Mapped borehole length (DZs excluded) = 136 m
Percent of borehole length
70.0%
60.0%
50.0%
40.0%
30.0%
20.0%
10.0%
0.0%
Chloritization
Epidotization
Oxidation
Saussuritization
No intensity
Faint
Weak
Medium
Strong

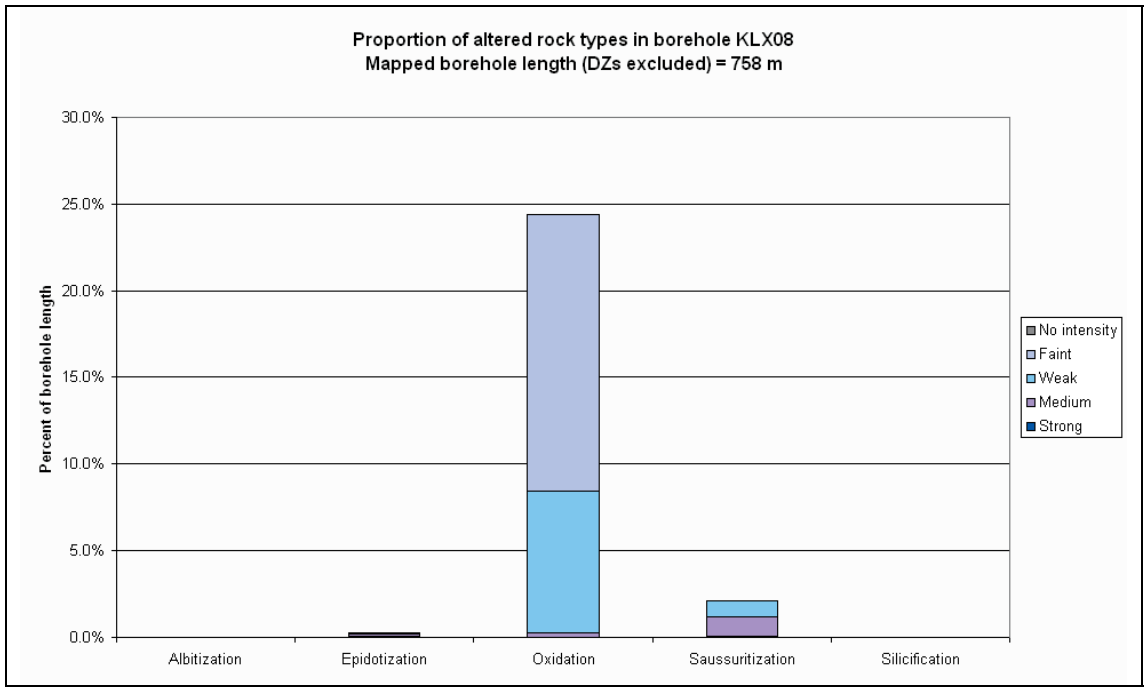
Proportion of altered rock types in borehole KLX08
Mapped borehole length (DZs excluded) = 758 m
Percent of borehole length
30.0%
25.0%
20.0%
15.0%
10.0%
5.0%
0.0%
Albitization
Epidotization
Oxidation
Saussuritization
Silicification
No intensity
Faint
Weak
Medium
Strong

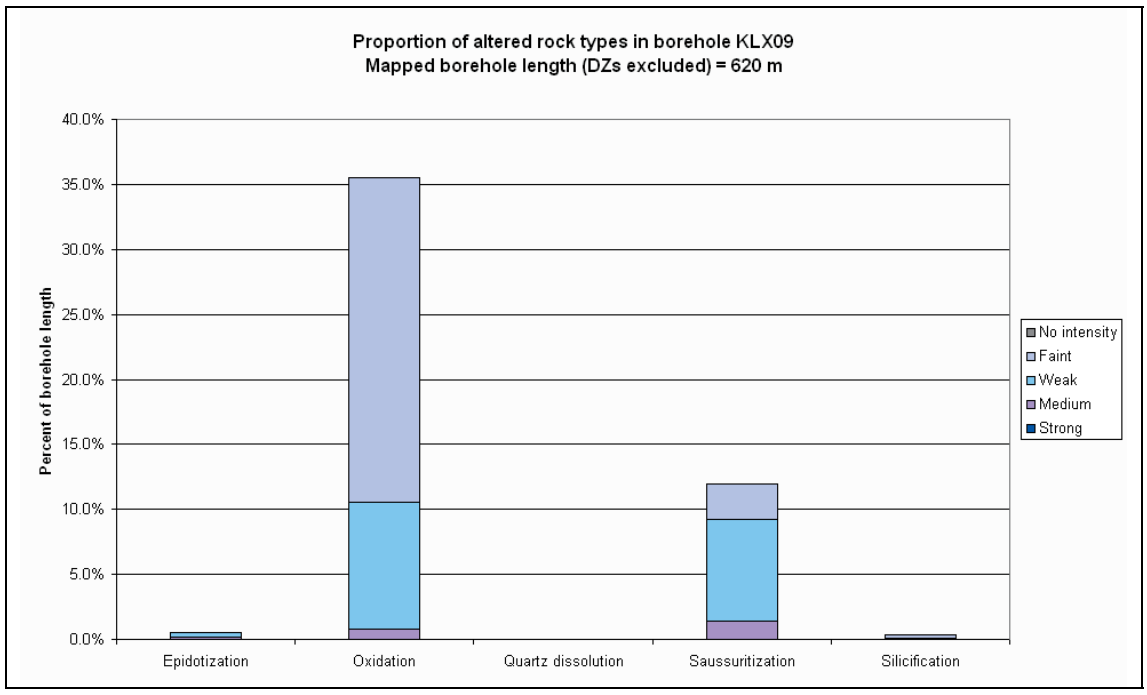
Proportion of altered rock types in borehole KLX09
Mapped borehole length (DZs excluded) = 620 m
Percent of borehole length
40.0%
35.0%
30.0%
25.0%
20.0%
15.0%
10.0%
5.0%
0.0%
Epidotization
Oxidation
Quartz dissolution
Saussuritization
Silicification
No intensity
Faint
Weak
Medium
Strong

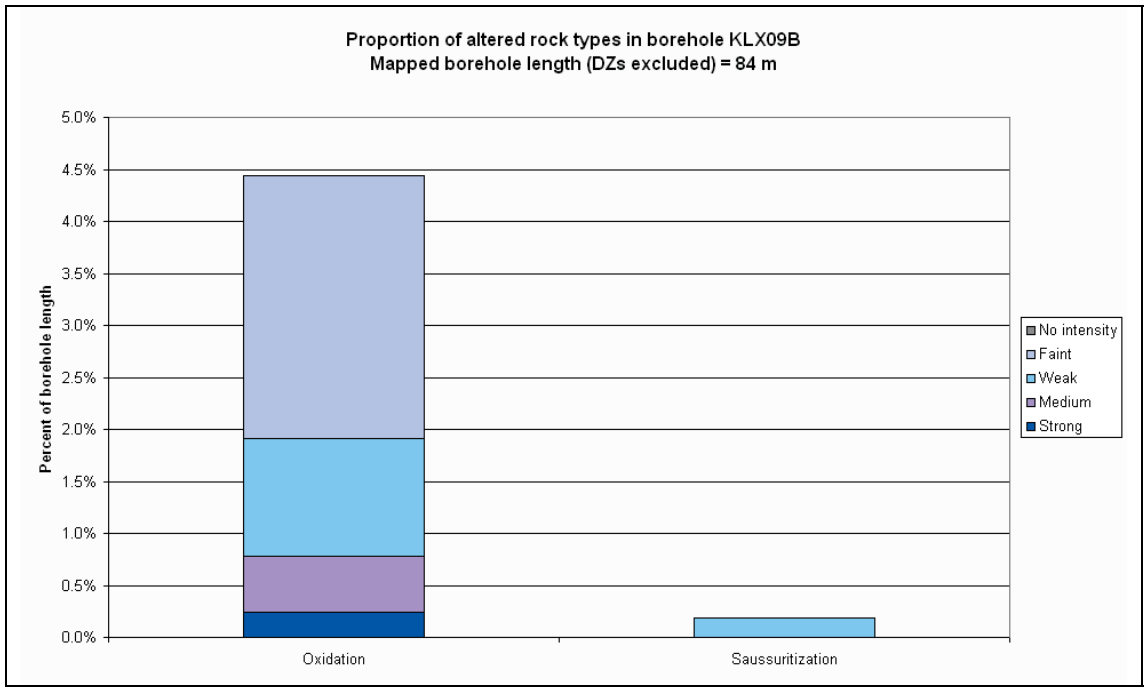
Proportion of altered rock types in borehole KLX09B
Mapped borehole length (DZs excluded) = 84 m
Percent of borehole length
5.0%
4.5%
4.0%
3.5%
3.0%
2.5%
2.0%
1.5%
1.0%
0.5%
0.0%
Oxidation
Saussuritization
No intensity
Faint
Weak
Medium
Strong

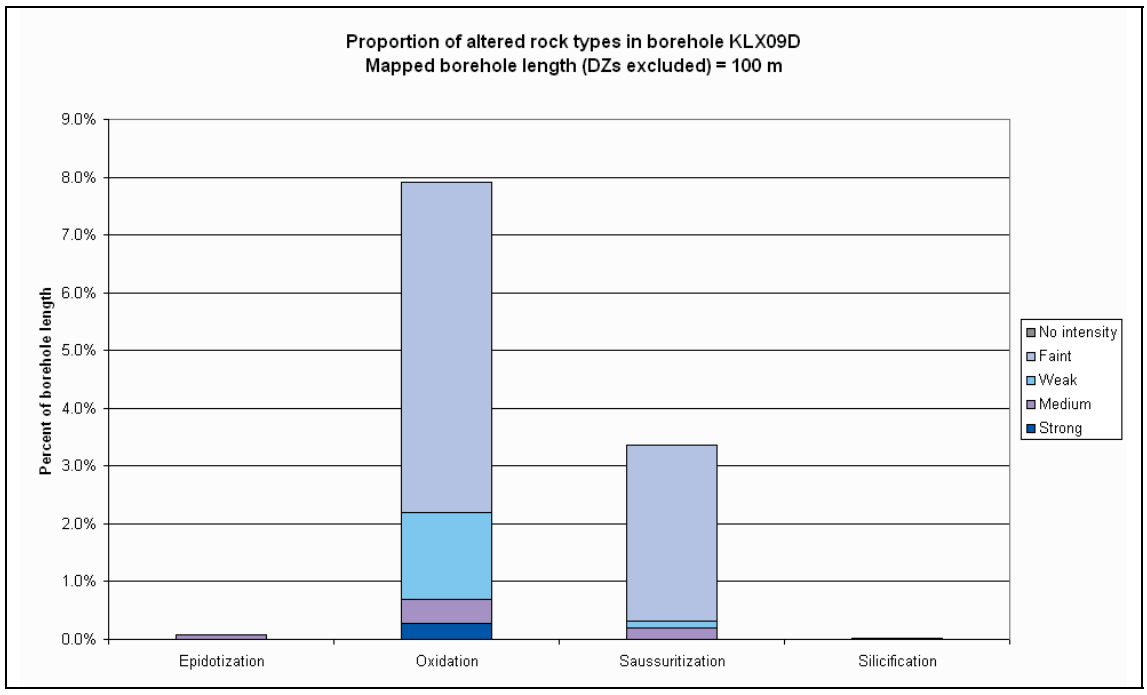
Proportion of altered rock types in borehole KLX09D
Mapped borehole length (DZs excluded) = 100 m
Percent of borehole length
9.0%
8.0%
7.0%
6.0%
5.0%
4.0%
3.0%
2.0%
1.0%
0.0%
Epidotization
Oxidation
Saussuritization
Silicification
No intensity
Faint
Weak
Medium
Strong

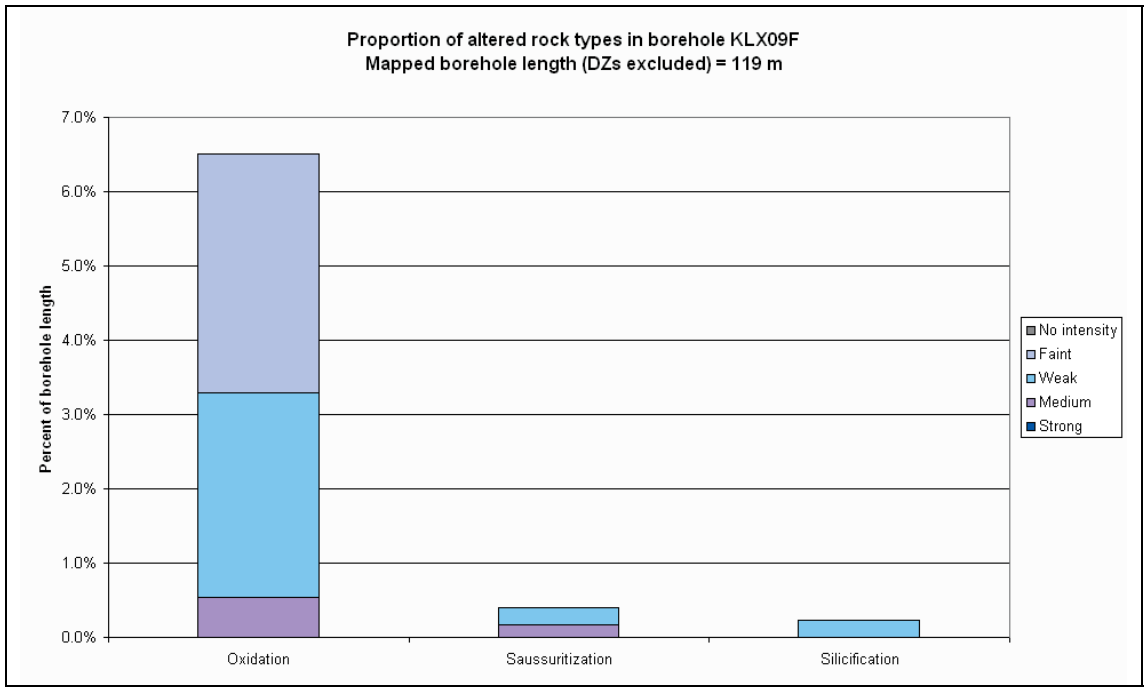
Proportion of altered rock types in borehole KLX09F
Mapped borehole length (DZs excluded) = 119 m
Percent of borehole length
7.0%
6.0%
5.0%
4.0%
3.0%
2.0%
1.0%
0.0%
Oxidation
Saussuritization
Silicification
No intensity
Faint
Weak
Medium
Strong

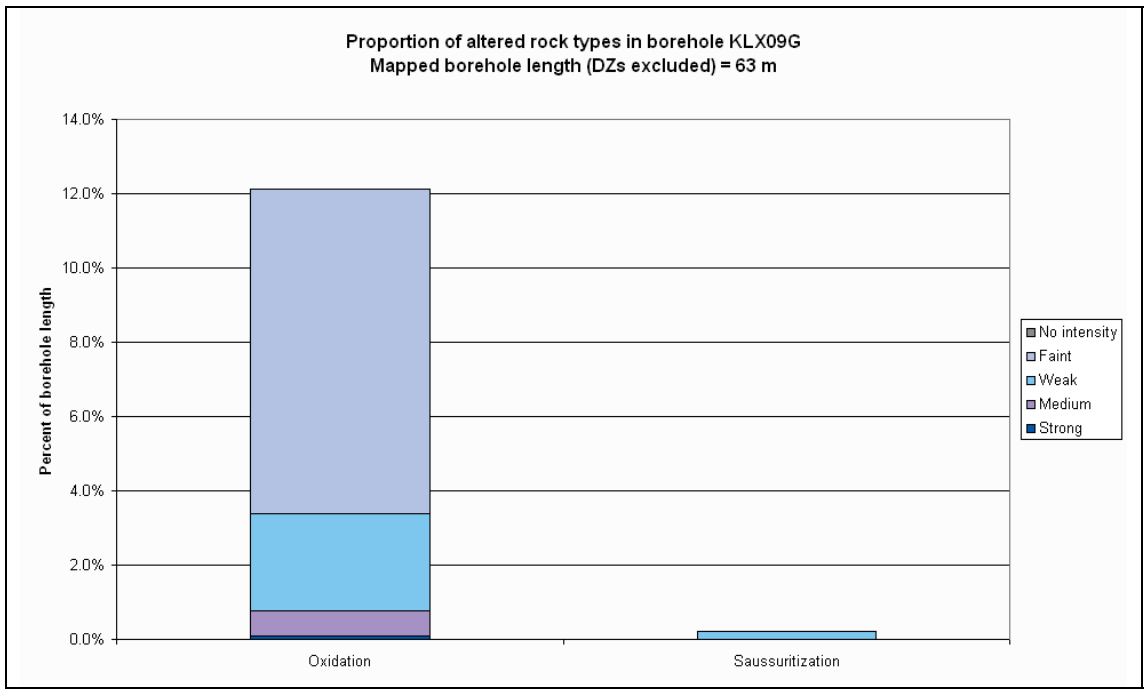
Proportion of altered rock types in borehole KLX09G
Mapped borehole length (DZs excluded) = 63 m
Percent of borehole length
14.0%
12.0%
10.0%
8.0%
6.0%
4.0%
2.0%
0.0%
Oxidation
Saussuritization
No intensity
Faint
Weak
Medium
Strong

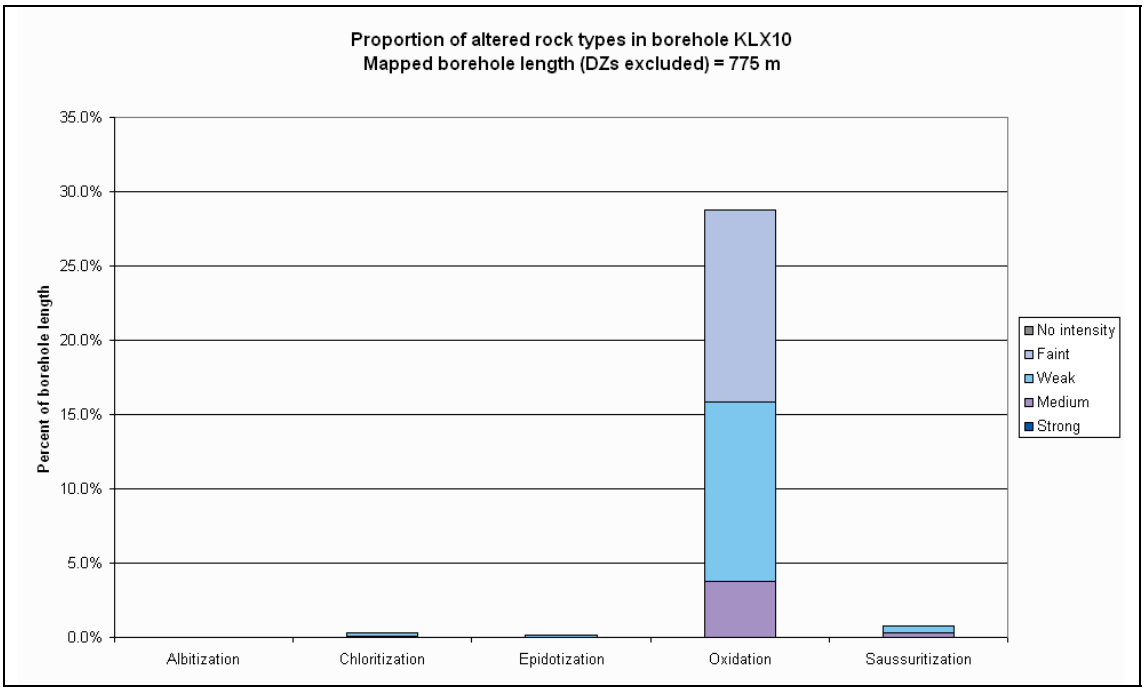
Proportion of altered rock types in borehole KLX10
Mapped borehole length (DZs excluded) = 775 m
Percent of borehole length
35.0%
30.0%
25.0%
20.0%
15.0%
10.0%
5.0%
0.0%
Albitization
Chloritization
Epidotization
Oxidation
Saussuritization
No intensity
Faint
Weak
Medium
Strong

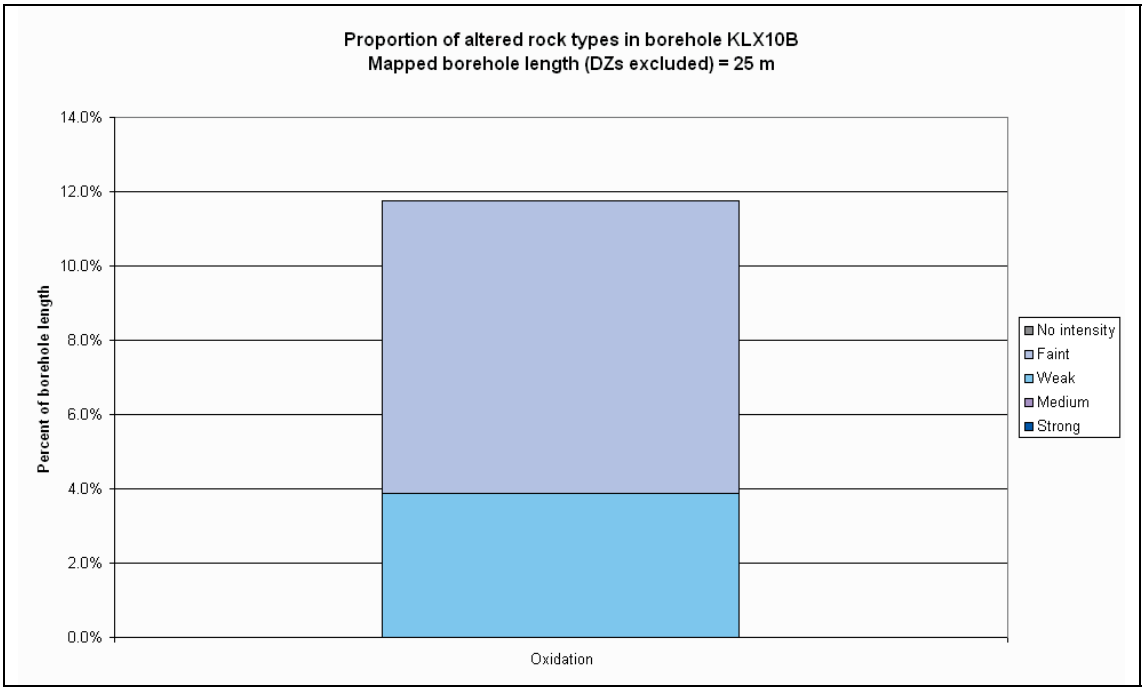
Proportion of altered rock types in borehole KLX10B
Mapped borehole length (DZs excluded) = 25 m
Percent of borehole length
14.0%
12.0%
10.0%
8.0%
6.0%
4.0%
2.0%
0.0%
Oxidation
No intensity
Faint
Weak
Medium
Strong

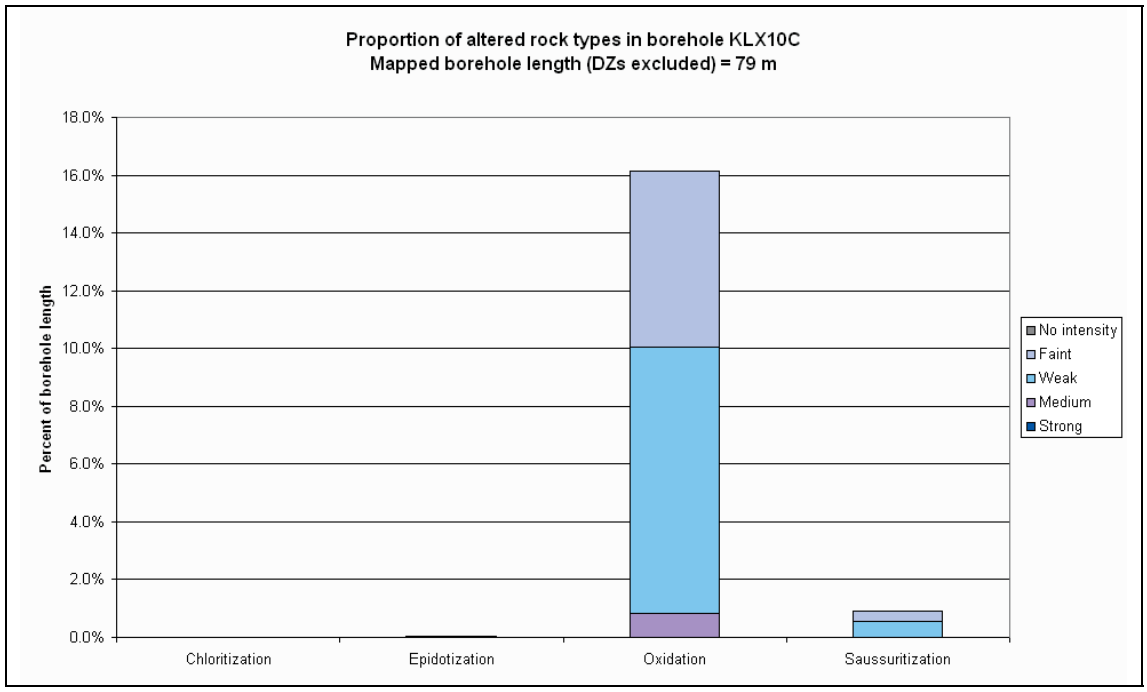
Proportion of altered rock types in borehole KLX10C
Mapped borehole length (DZs excluded) = 79 m
Percent of borehole length
18.0%
16.0%
14.0%
12.0%
10.0%
8.0%
6.0%
4.0%
2.0%
0.0%
Chloritization
Epidotization
Oxidation
Saussuritization
No intensity
Faint
Weak
Medium
Strong

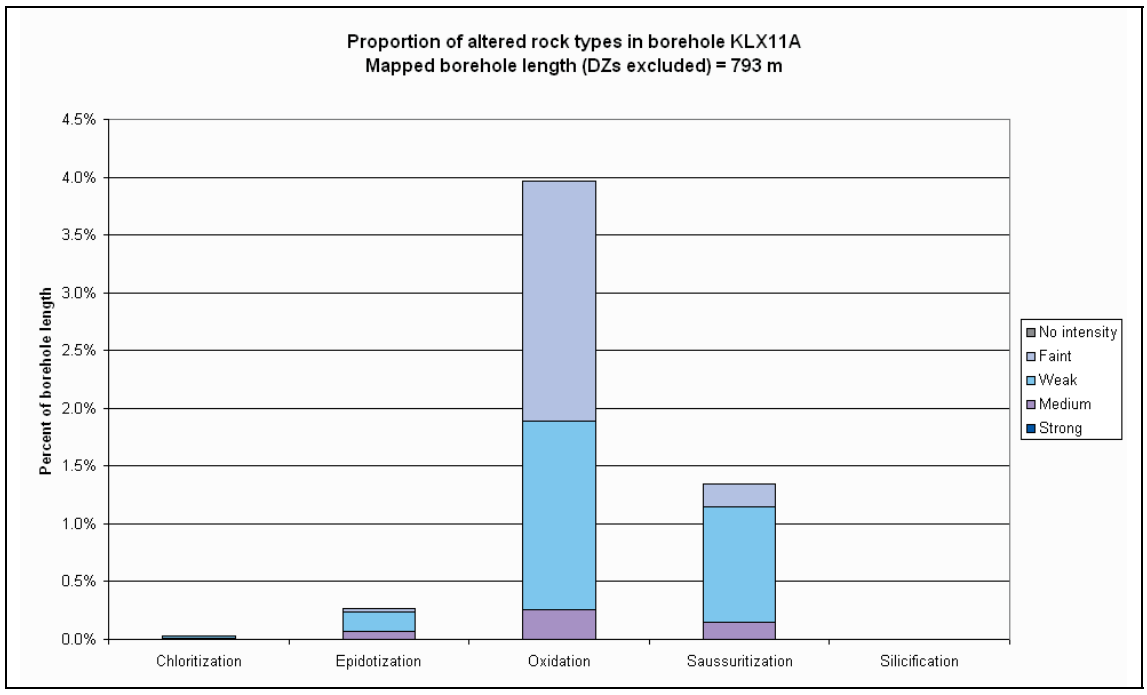
Proportion of altered rock types in borehole KLX11A
Mapped borehole length (DZs excluded) = 793 m
Percent of borehole length
4.5%
4.0%
3.5%
3.0%
2.5%
2.0%
1.5%
1.0%
0.5%
0.0%
Chloritization
Epidotization
Oxidation
Saussuritization
Silicification
No intensity
Faint
Weak
Medium
Strong

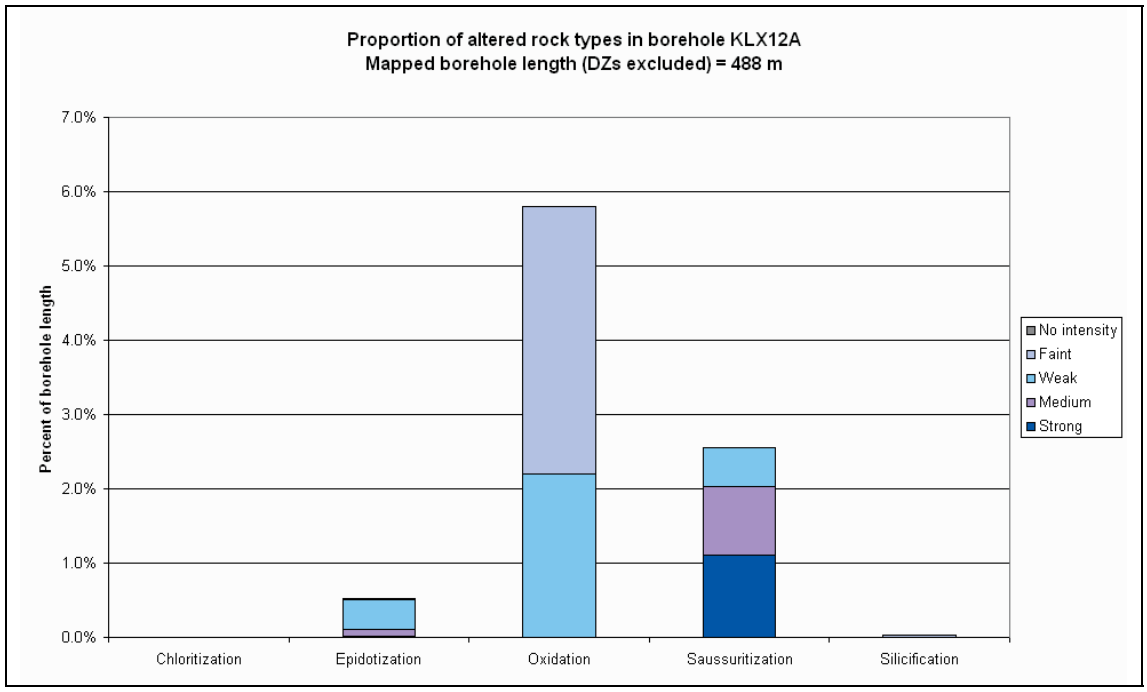
Proportion of altered rock types in borehole KLX12A
Mapped borehole length (DZs excluded) = 488 m
Percent of borehole length
7.0%
6.0%
5.0%
4.0%
3.0%
2.0%
1.0%
0.0%
Chloritization
Epidotization
Oxidation
Saussuritization
Silicification
No intensity
Faint
Weak
Medium
Strong

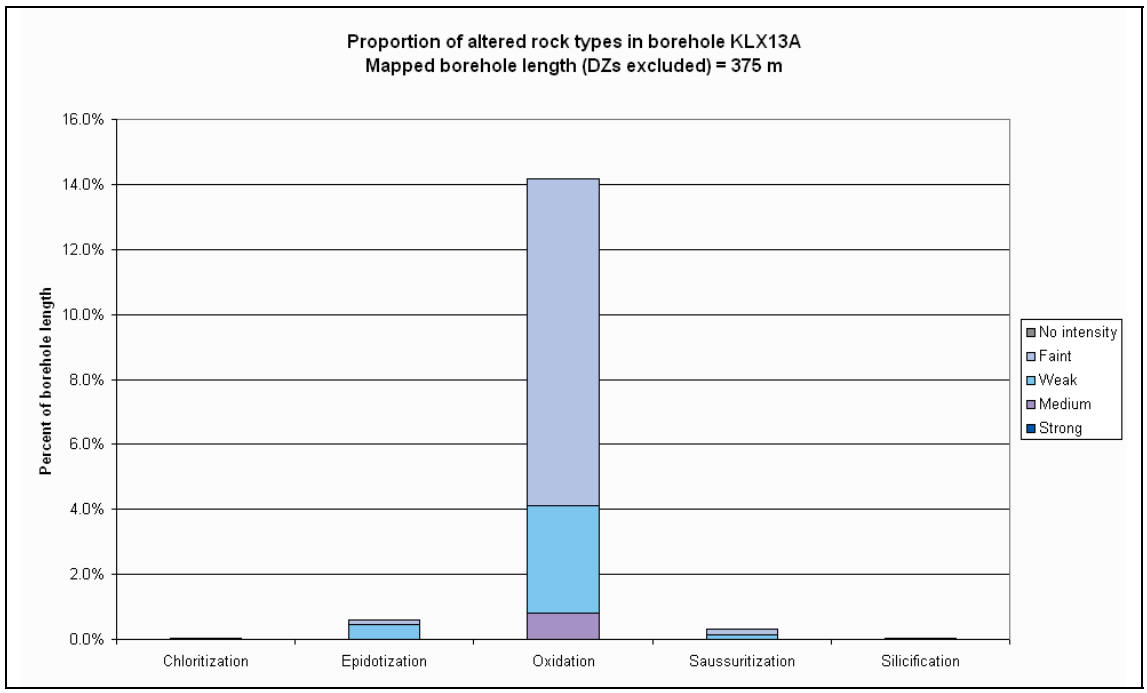
Proportion of altered rock types in borehole KLX13A
Mapped borehole length (DZs excluded) = 375 m
Percent of borehole length
16.0%
14.0%
12.0%
10.0%
8.0%
6.0%
4.0%
2.0%
0.0%
Chloritization
Epidotization
Oxidation
Saussuritization
Silicification
No intensity
Faint
Weak
Medium
Strong

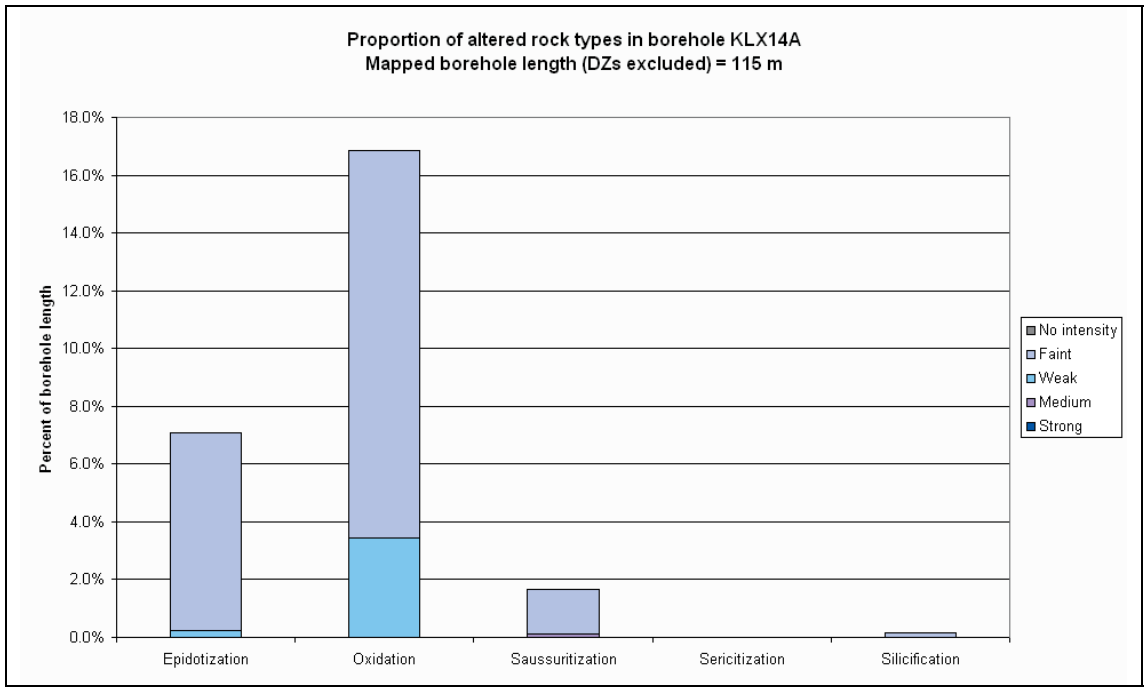
Proportion of altered rock types in borehole KLX14A
Mapped borehole length (DZs excluded) = 115 m
Percent of borehole length
18.0%
16.0%
14.0%
12.0%
10.0%
8.0%
6.0%
4.0%
2.0%
0.0%
Epidotization
Oxidation
Saussuritization
Sericitization
Silicification
No intensity
Faint
Weak
Medium
Strong

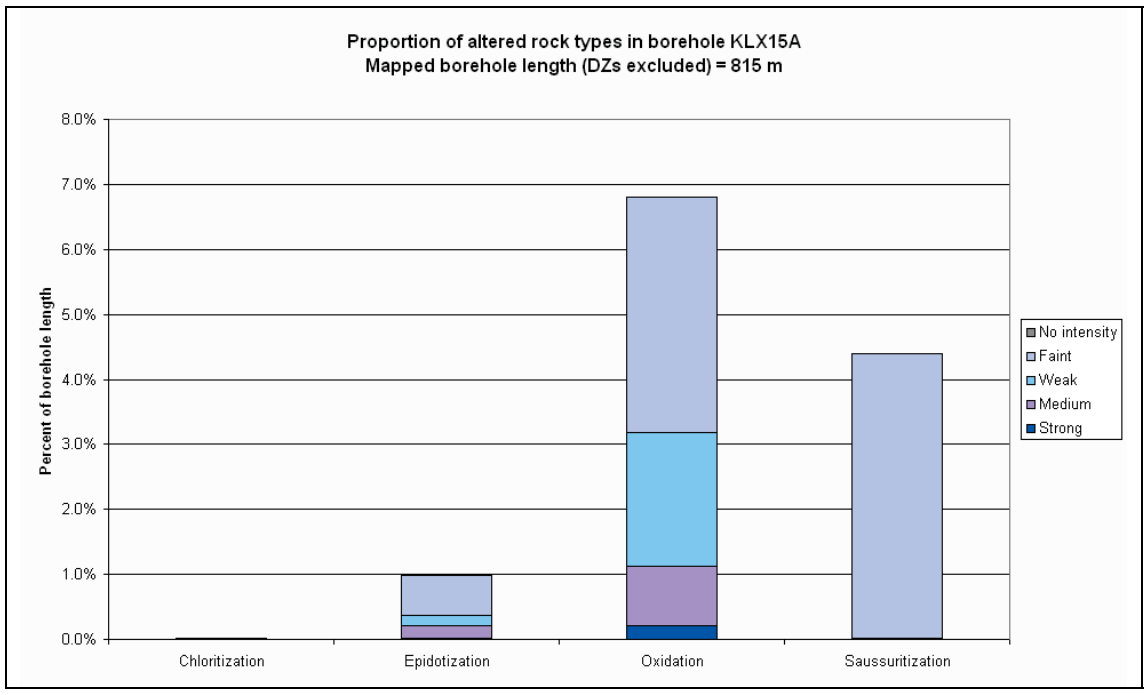
Proportion of altered rock types in borehole KLX15A
Mapped borehole length (DZs excluded) = 815 m
Percent of borehole length
8.0%
7.0%
6.0%
5.0%
4.0%
3.0%
2.0%
1.0%
0.0%
Chloritization
Epidotization
Oxidation
Saussuritization
No intensity
Faint
Weak
Medium
Strong

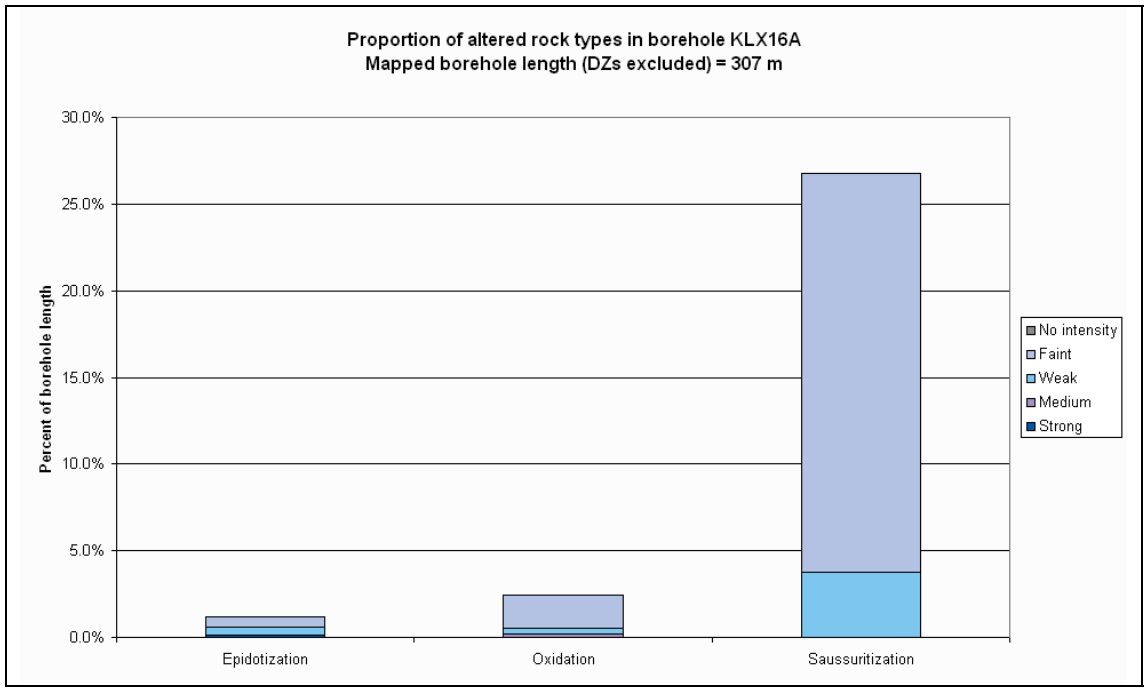
Proportion of altered rock types in borehole KLX16A
Mapped borehole length (DZs excluded) = 307 m
Percent of borehole length
30.0%
25.0%
20.0%
15.0%
10.0%
5.0%
0.0%
Epidotization
Oxidation
Saussuritization
No intensity
Faint
Weak
Medium
Strong

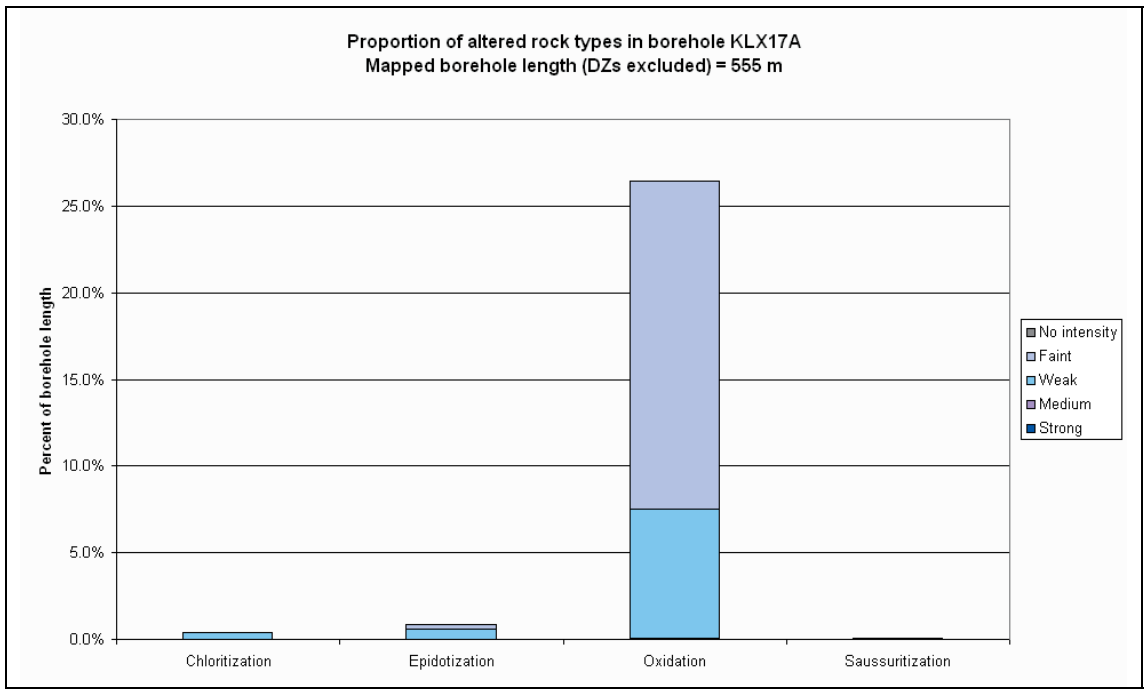
Proportion of altered rock types in borehole KLX17A
Mapped borehole length (DZs excluded) = 555 m
Percent of borehole length
30.0%
25.0%
20.0%
15.0%
10.0%
5.0%
0.0%
Chloritization
Epidotization
Oxidation
Saussuritization
No intensity
Faint
Weak
Medium
Strong

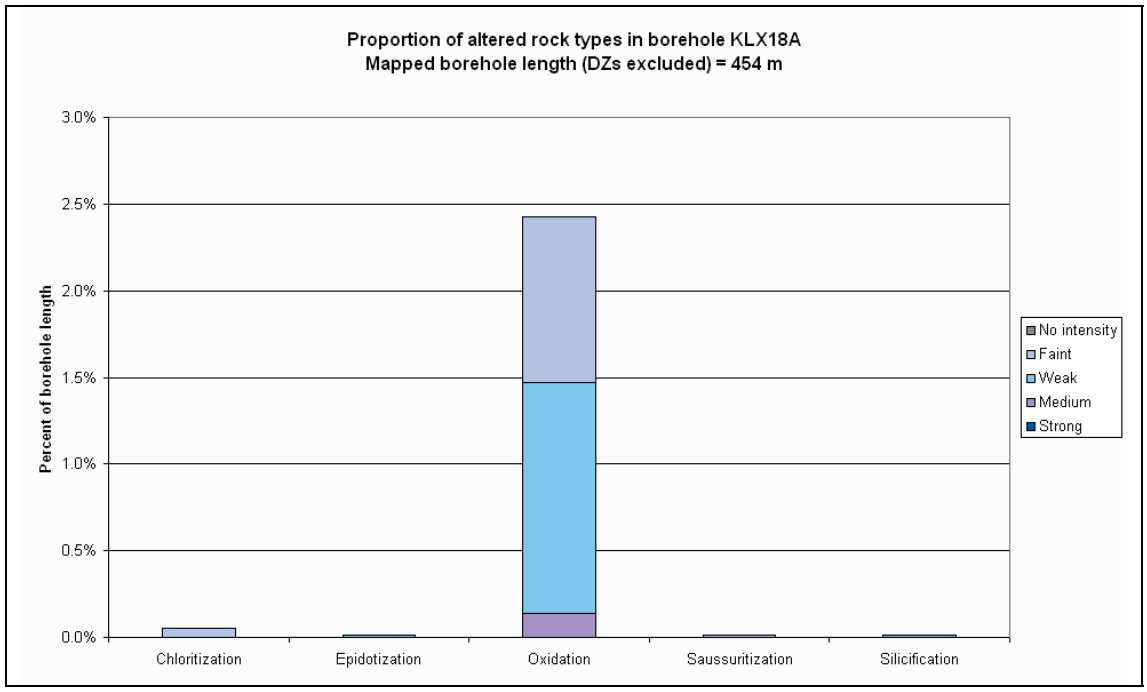
Proportion of altered rock types in borehole KLX18A
Mapped borehole length (DZs excluded) = 454 m
Percent of borehole length
3.0%
2.5%
2.0%
1.5%
1.0%
0.5%
0.0%
Chloritization
Epidotization
Oxidation
Saussuritization
Silicification
No intensity
Faint
Weak
Medium
Strong

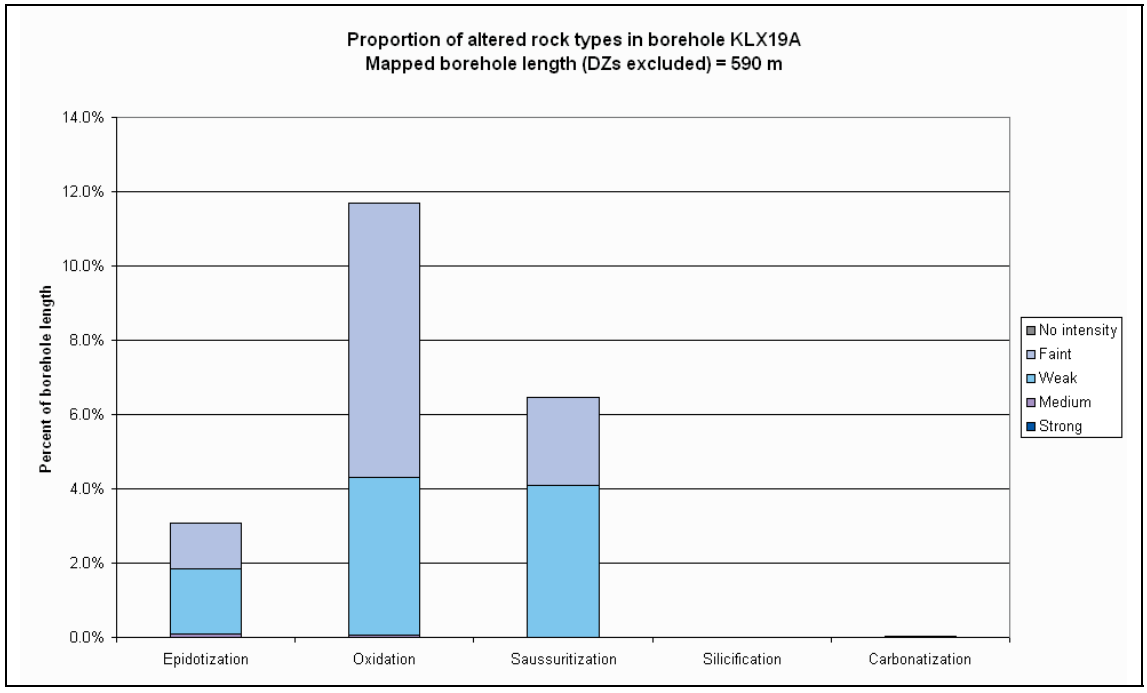
Proportion of altered rock types in borehole KLX19A
Mapped borehole length (DZs excluded) = 590 m
Percent of borehole length
14.0%
12.0%
10.0%
8.0%
6.0%
4.0%
2.0%
0.0%
Epidotization
Oxidation
Saussuritization
Silicification
Carbonatization
No intensity
Faint
Weak
Medium
Strong

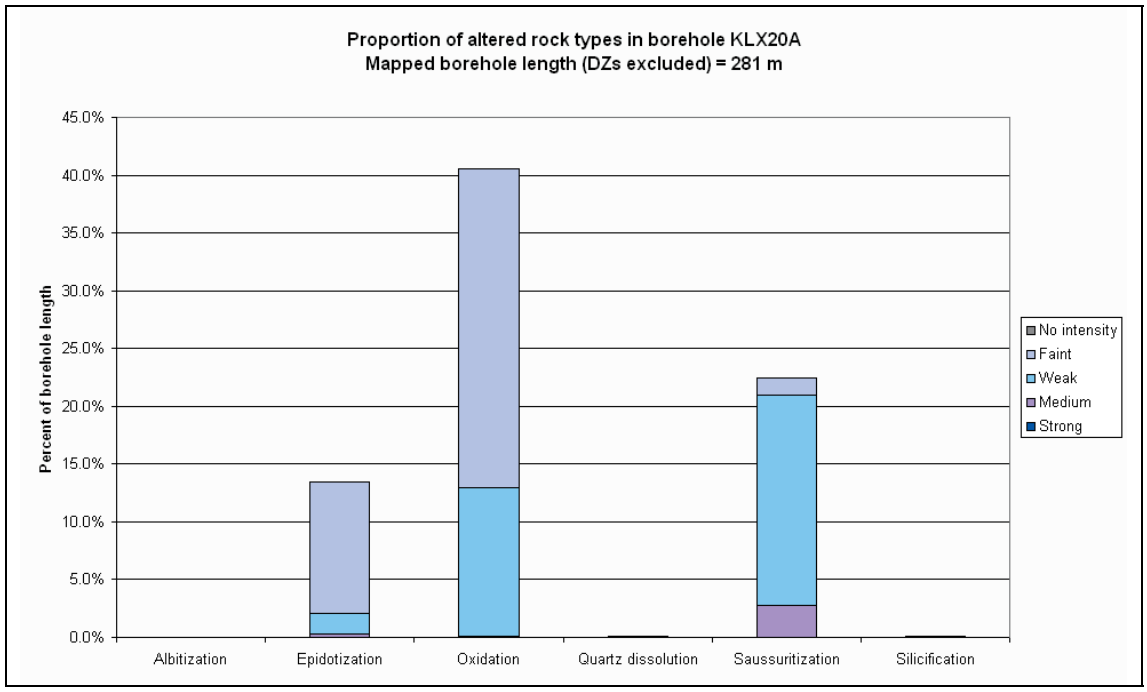
Proportion of altered rock types in borehole KLX20A
Mapped borehole length (DZs excluded) = 281 m
Percent of borehole length
45.0%
40.0%
35.0%
30.0%
25.0%
20.0%
15.0%
10.0%
5.0%
0.0%
Albitization
Epidotization
Oxidation
Quartz dissolution
Saussuritization
Silicification
No intensity
Faint
Weak
Medium
Strong

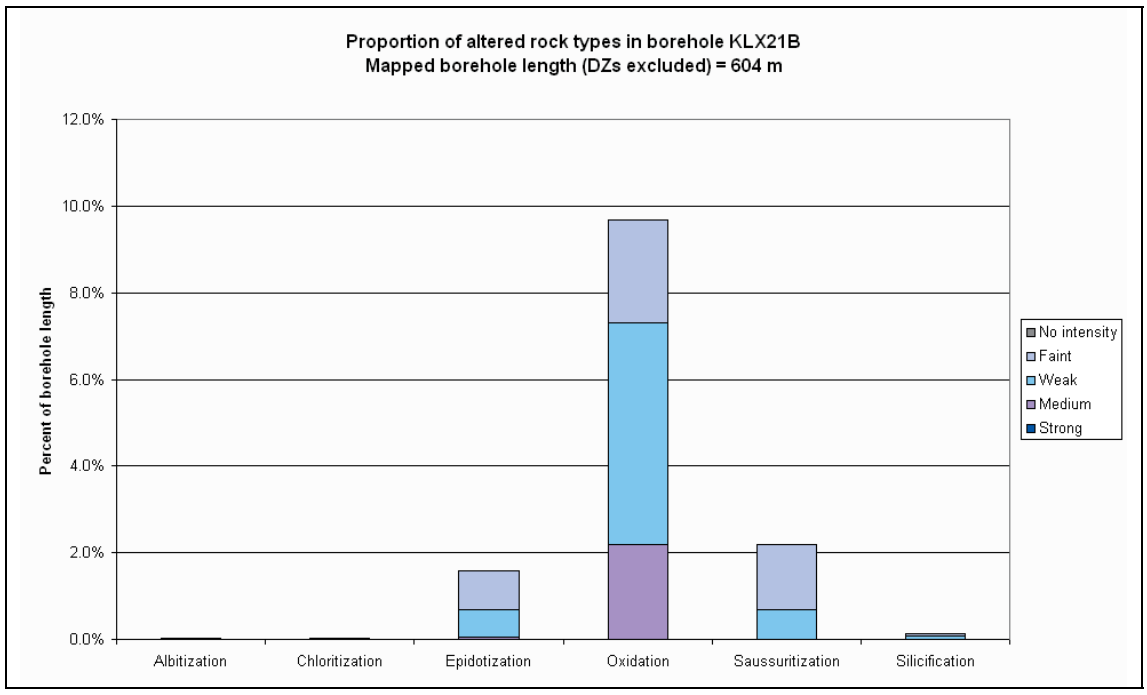
Proportion of altered rock types in borehole KLX21B
Mapped borehole length (DZs excluded) = 604 m
Percent of borehole length
12.0%
10.0%
8.0%
6.0%
4.0%
2.0%
0.0%
Albitization
Chloritization
Epidotization
Oxidation
Saussuritization
Silicification
No intensity
Faint
Weak
Medium
Strong

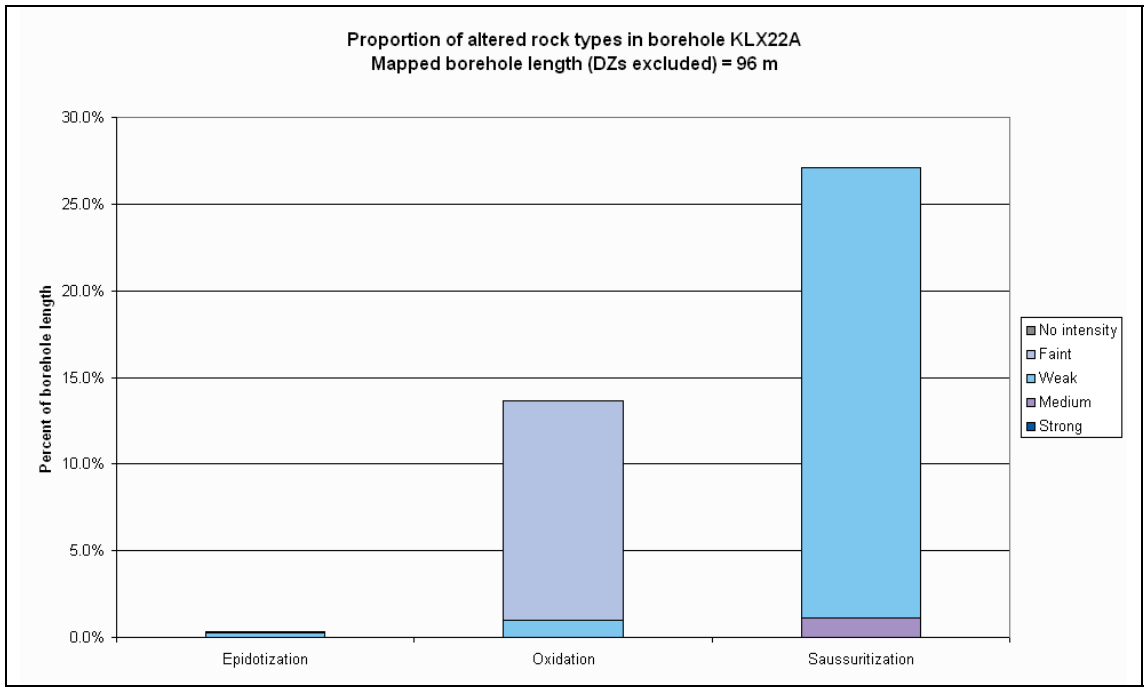
Proportion of altered rock types in borehole KLX22A
Mapped borehole length (DZs excluded) = 96 m
Percent of borehole length
30.0%
25.0%
20.0%
15.0%
10.0%
5.0%
0.0%
Epidotization
Oxidation
Saussuritization
No intensity
Faint
Weak
Medium
Strong

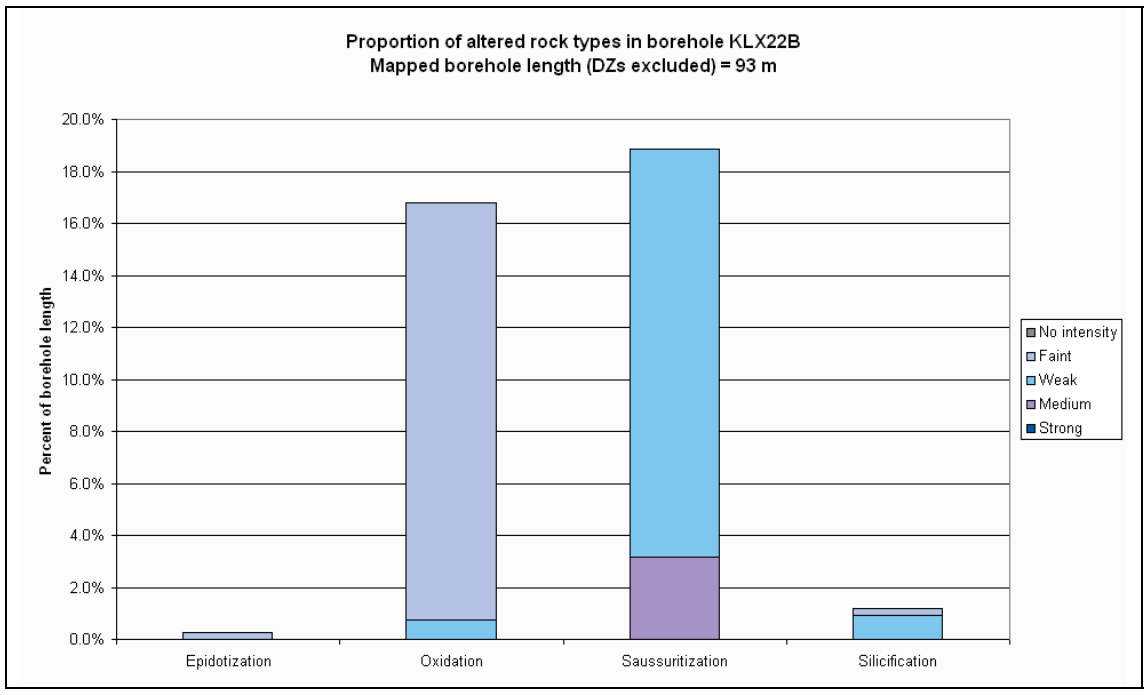
Proportion of altered rock types in borehole KLX22B
Mapped borehole length (DZs excluded) = 93 m
Percent of borehole length
20.0%
18.0%
16.0%
14.0%
12.0%
10.0%
8.0%
6.0%
4.0%
2.0%
0.0%
Epidotization
Oxidation
Saussuritization
Silicification
No intensity
Faint
Weak
Medium
Strong

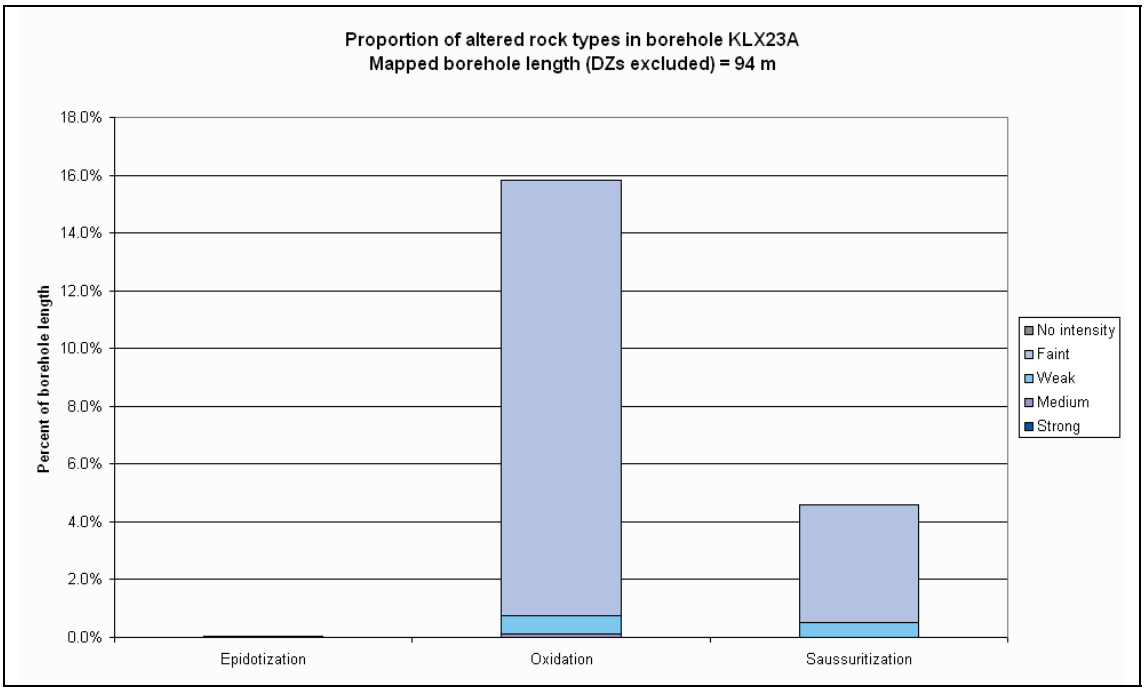
Proportion of altered rock types in borehole KLX23A
Mapped borehole length (DZs excluded) = 94 m
Percent of borehole length
18.0%
16.0%
14.0%
12.0%
10.0%
8.0%
6.0%
4.0%
2.0%
0.0%
Epidotization
Oxidation
Saussuritization
No intensity
Faint
Weak
Medium
Strong

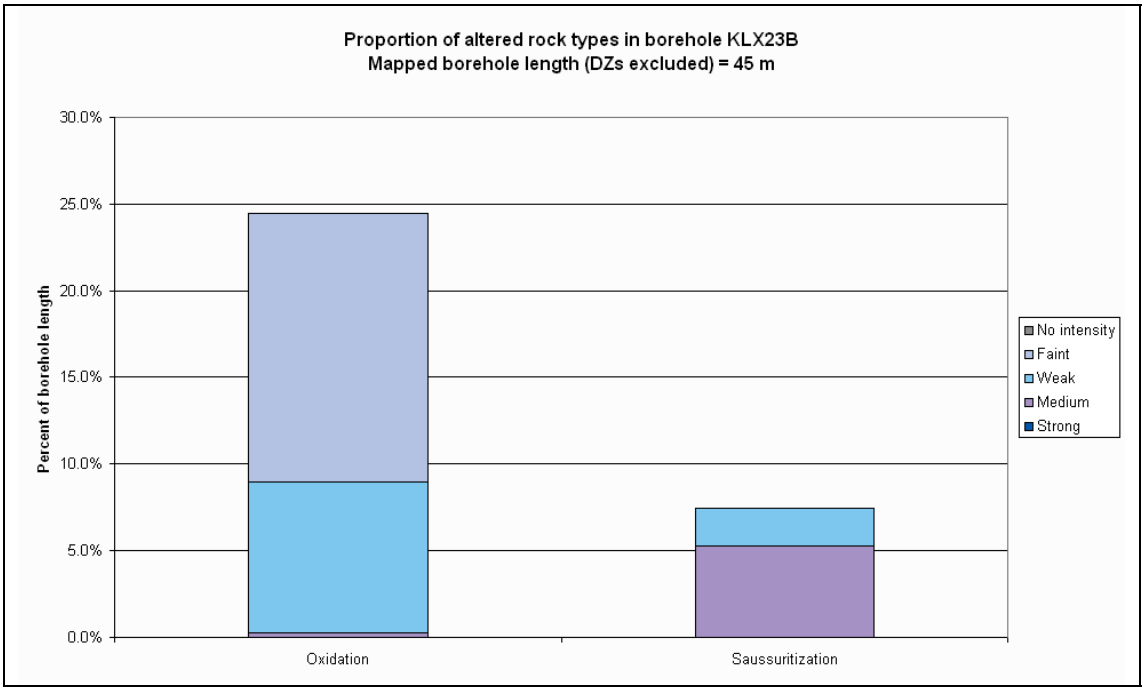
Proportion of altered rock types in borehole KLX23B
Mapped borehole length (DZs excluded) = 45 m
Percent of borehole length
30.0%
25.0%
20.0%
15.0%
10.0%
5.0%
0.0%
Oxidation
Saussuritization
No intensity
Faint
Weak
Medium
Strong

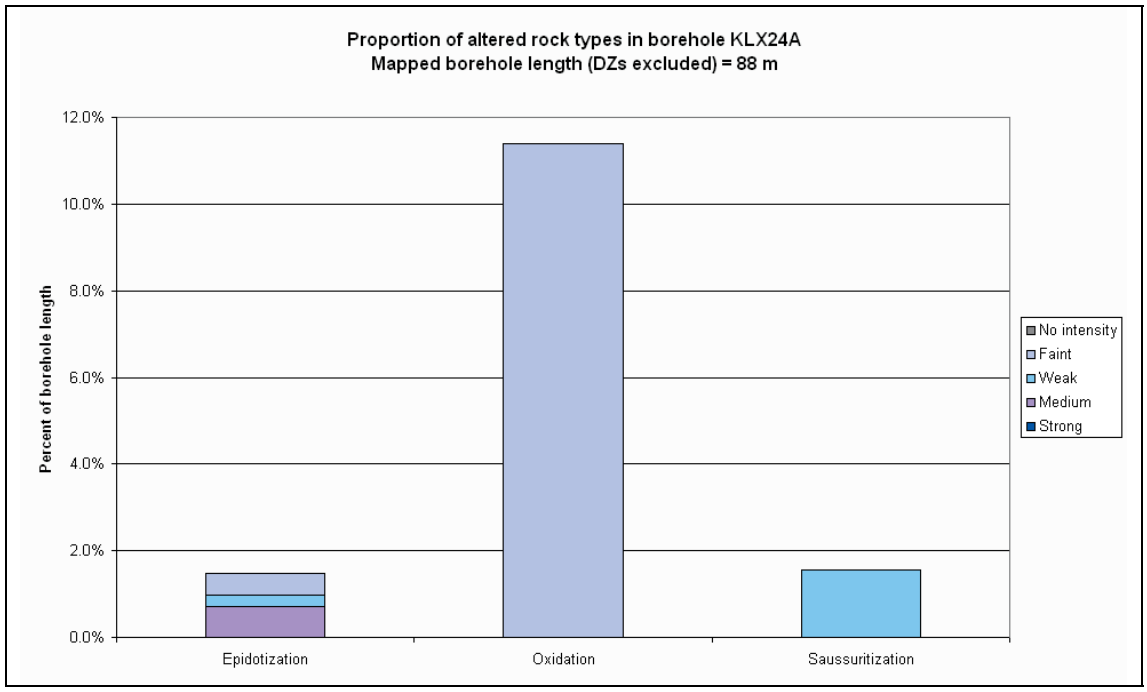
Proportion of altered rock types in borehole KLX24A
Mapped borehole length (DZs excluded) = 88 m
Percent of borehole length
12.0%
10.0%
8.0%
6.0%
4.0%
2.0%
0.0%
Epidotization
Oxidation
Saussuritization
No intensity
Faint
Weak
Medium
Strong

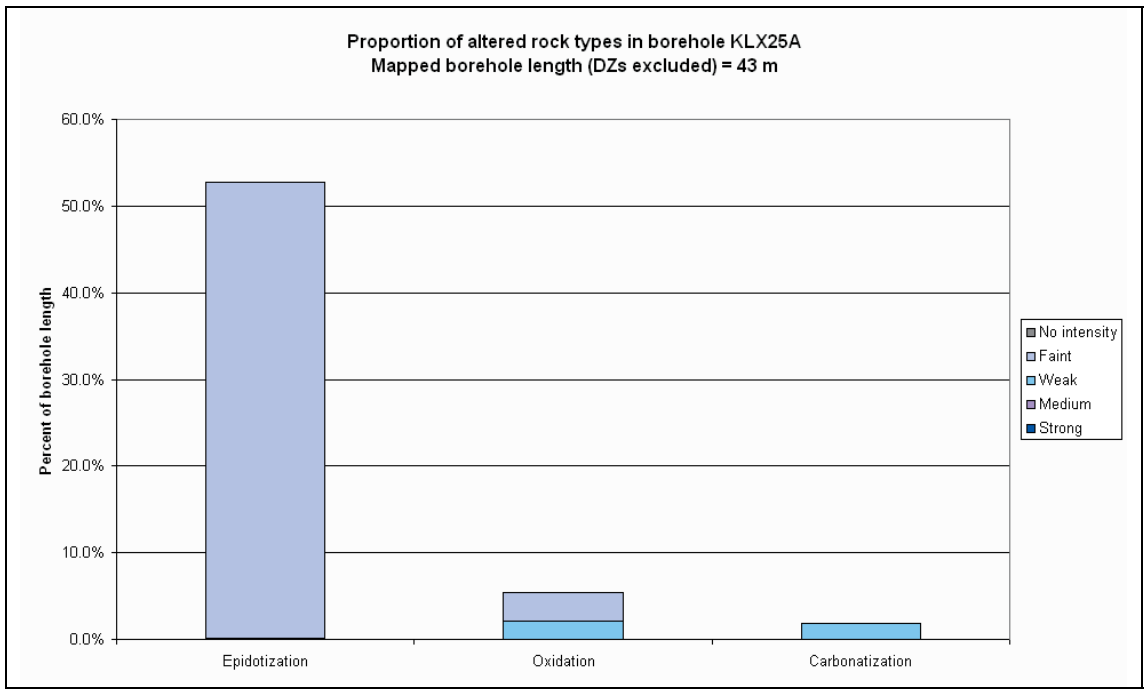
Proportion of altered rock types in borehole KLX25A
Mapped borehole length (DZs excluded) = 43 m
Percent of borehole length
60.0%
50.0%
40.0%
30.0%
20.0%
10.0%
0.0%
Epidotization
Oxidation
Carbonatization
No intensity
Faint
Weak
Medium
Strong

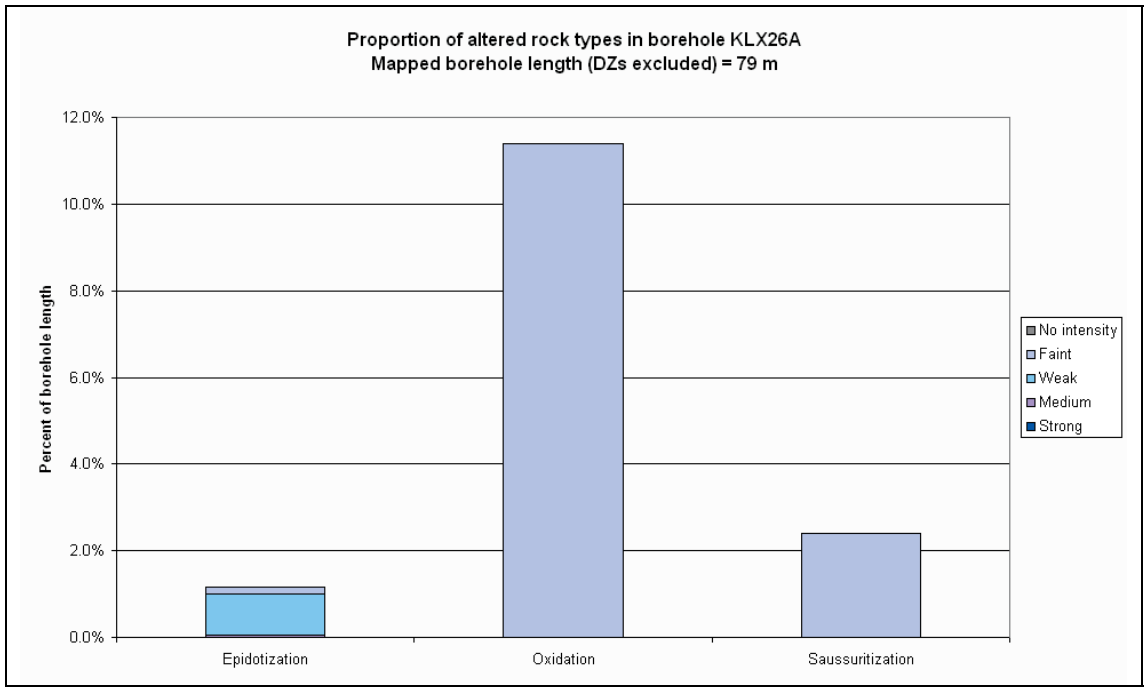
Proportion of altered rock types in borehole KLX26A
Mapped borehole length (DZs excluded) = 79 m
Percent of borehole length
12.0%
10.0%
8.0%
6.0%
4.0%
2.0%
0.0%
Epidotization
Oxidation
Saussuritization
No intensity
Faint
Weak
Medium
Strong

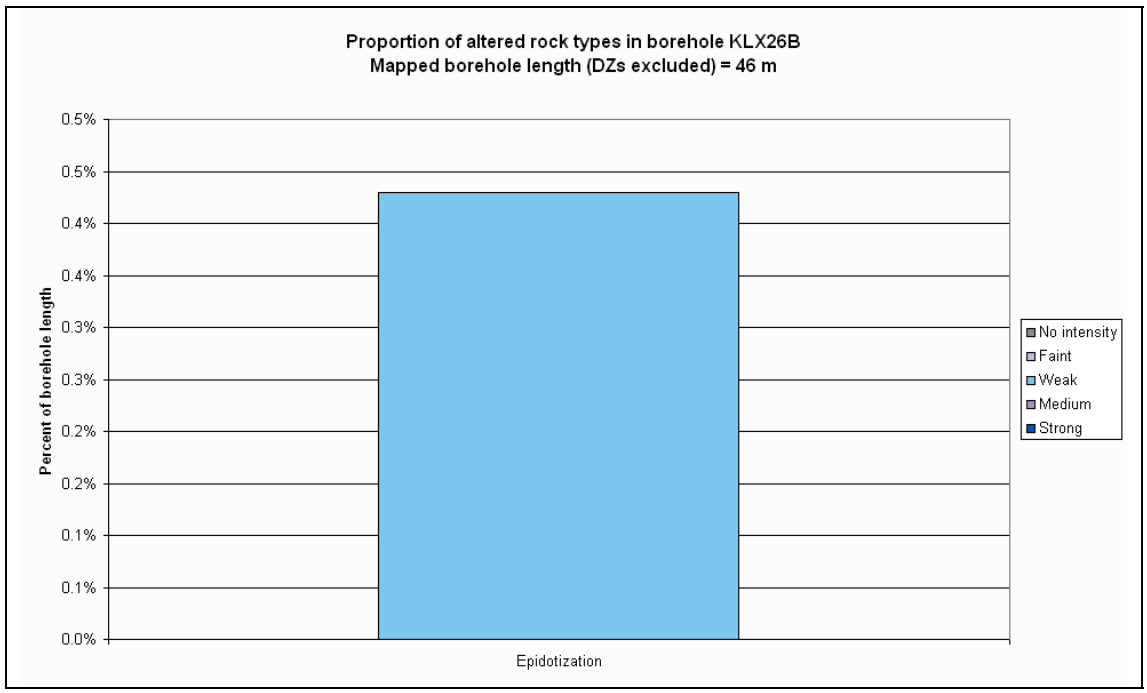
Proportion of altered rock types in borehole KLX26B
Mapped borehole length (DZs excluded) = 46 m
Percent of borehole length
0.5%
0.5%
0.4%
0.4%
0.3%
0.3%
0.2%
0.2%
0.1%
0.1%
0.0%
Epidotization
No intensity
Faint
Weak
Medium
Strong

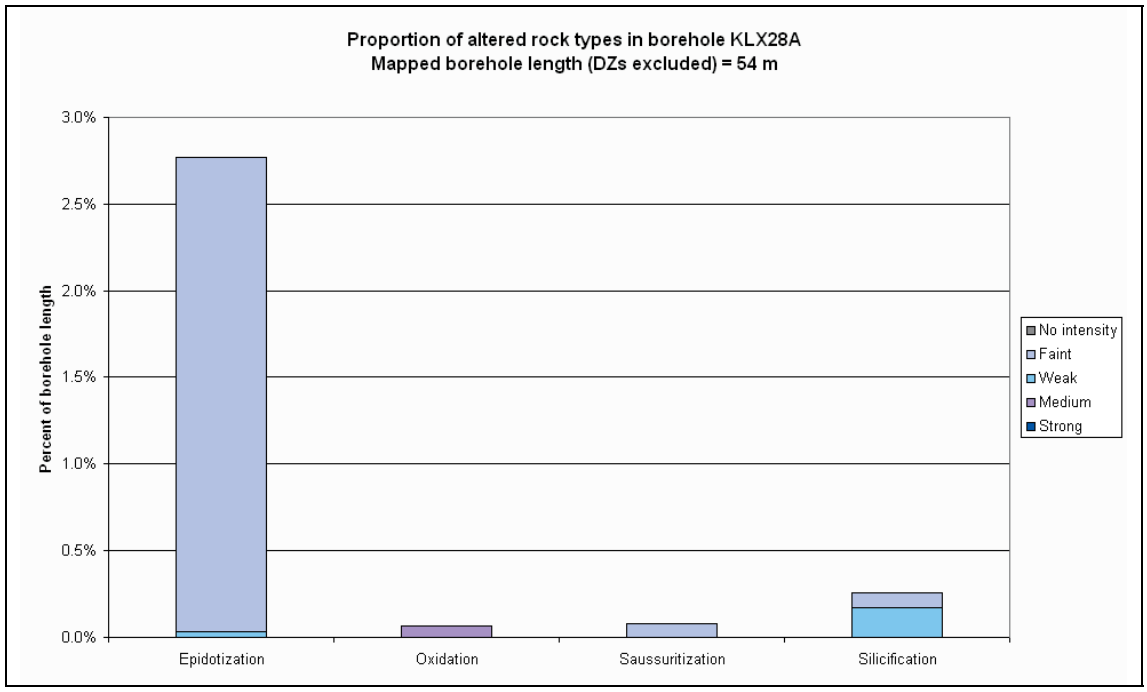
Proportion of altered rock types in borehole KLX28A
Mapped borehole length (DZs excluded) = 54 m
Percent of borehole length
3.0%
2.5%
2.0%
1.5%
1.0%
0.5%
0.0%
Epidotization
Oxidation
Saussuritization
Silicification
No intensity
Faint
Weak
Medium
Strong

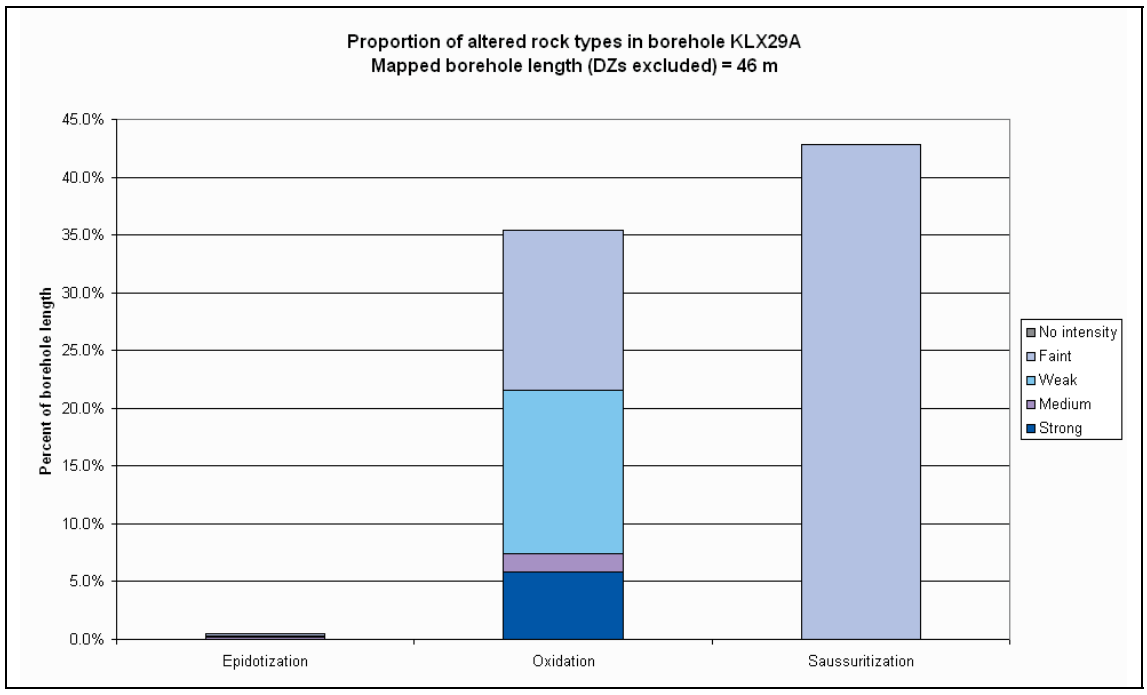
Proportion of altered rock types in borehole KLX29A
Mapped borehole length (DZs excluded) = 46 m
Percent of borehole length
45.0%
40.0%
35.0%
30.0%
25.0%
20.0%
15.0%
10.0%
5.0%
0.0%
Epidotization
Oxidation
Saussuritization
No intensity
Faint
Weak
Medium
Strong

Type and degree of alteration outside deformation zones on a rock domain basis in each borehole

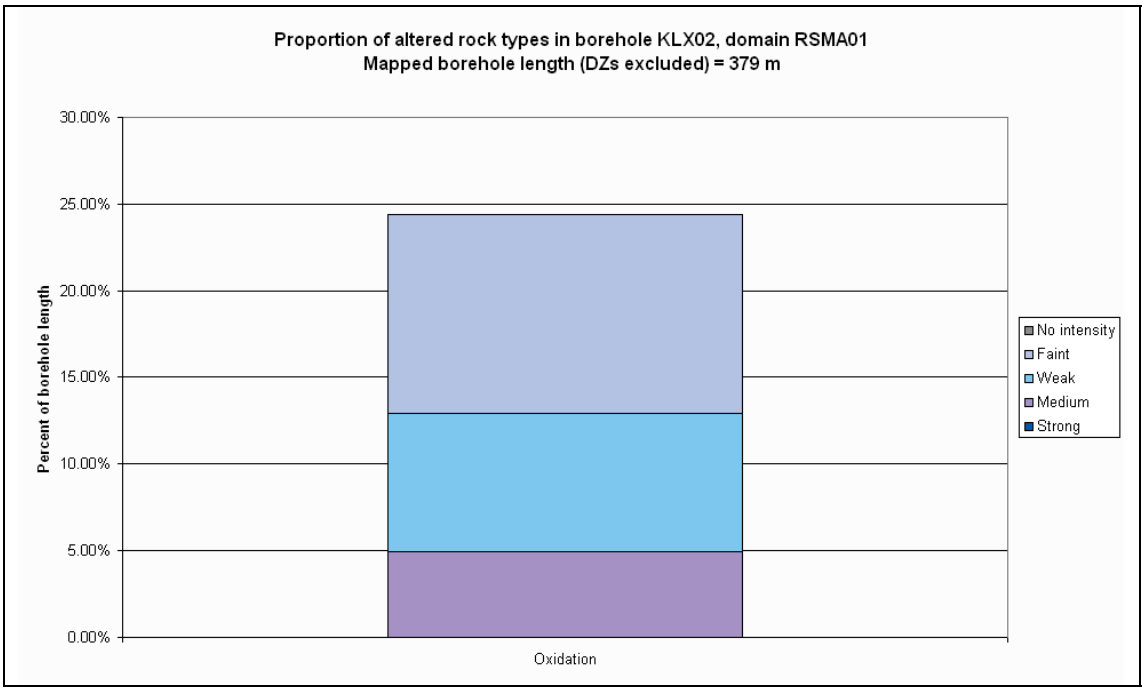

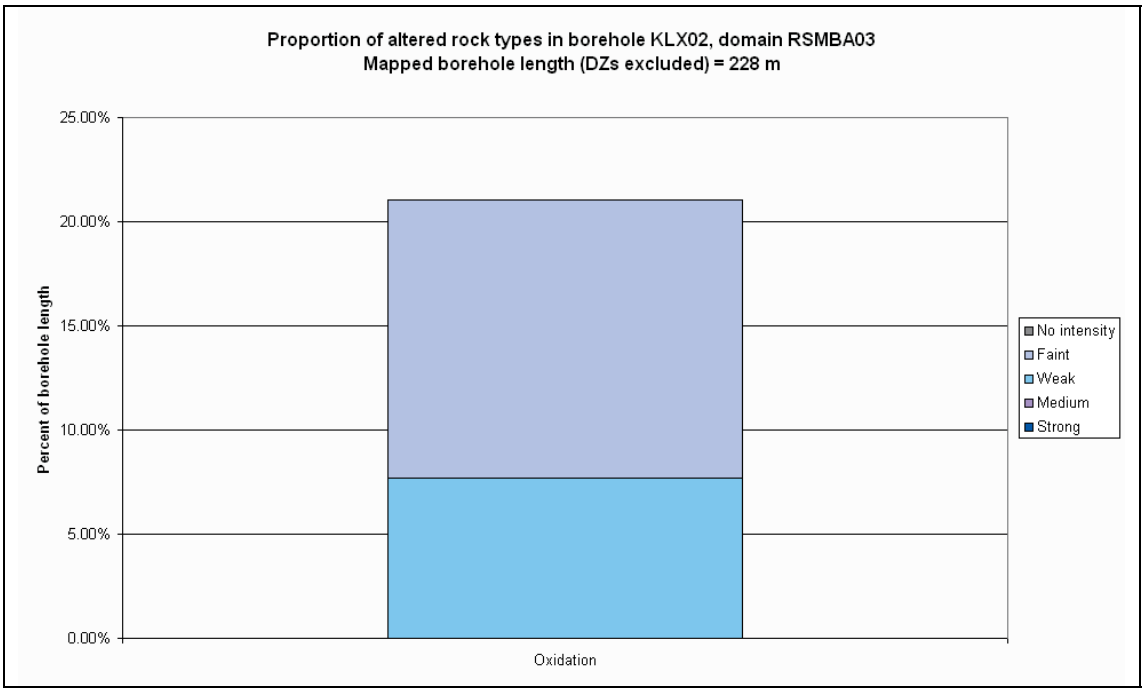

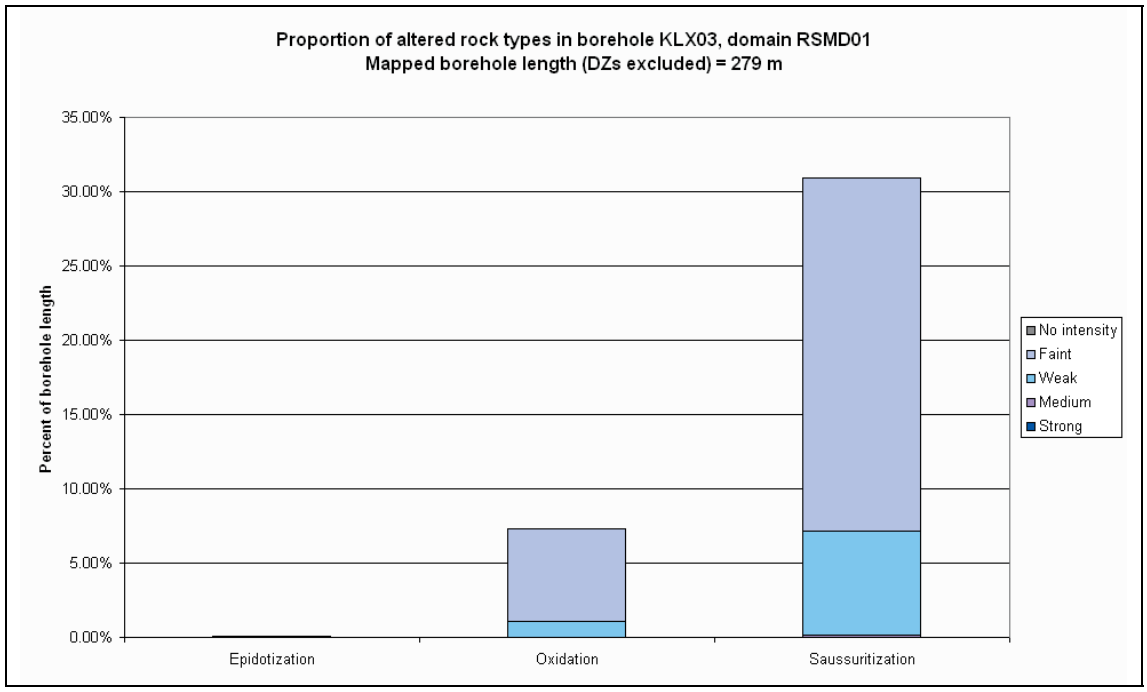
Proportion of altered rock types in borehole KLX03, domain RSMD01
Mapped borehole length (DZs excluded) = 279 m
Percent of borehole length
35.00%
30.00%
25.00%
20.00%
15.00%
10.00%
5.00%
0.00%
Epidotization
Oxidation
Saussuritization
No intensity
Faint
Weak
Medium
Strong

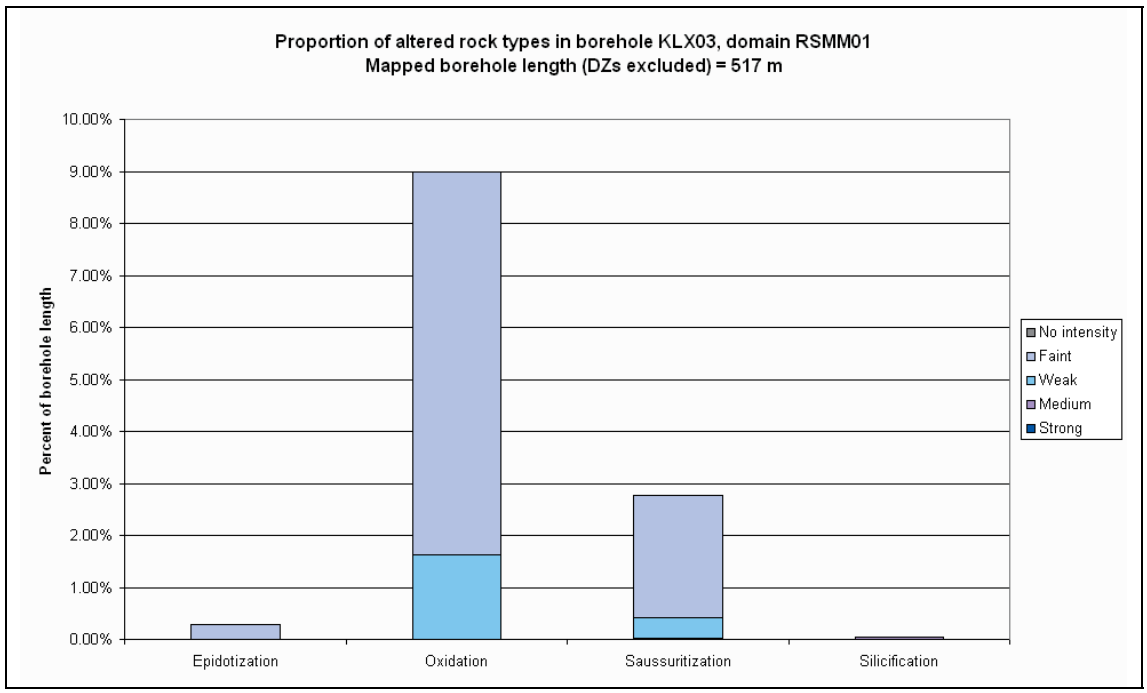
Proportion of altered rock types in borehole KLX03, domain RSMM01
Mapped borehole length (DZs excluded) = 517 m
Percent of borehole length
10.00%
9.00%
8.00%
7.00%
6.00%
5.00%
4.00%
3.00%
2.00%
1.00%
0.00%
Epidotization
Oxidation
Saussuritization
Silicification
No intensity
Faint
Weak
Medium
Strong

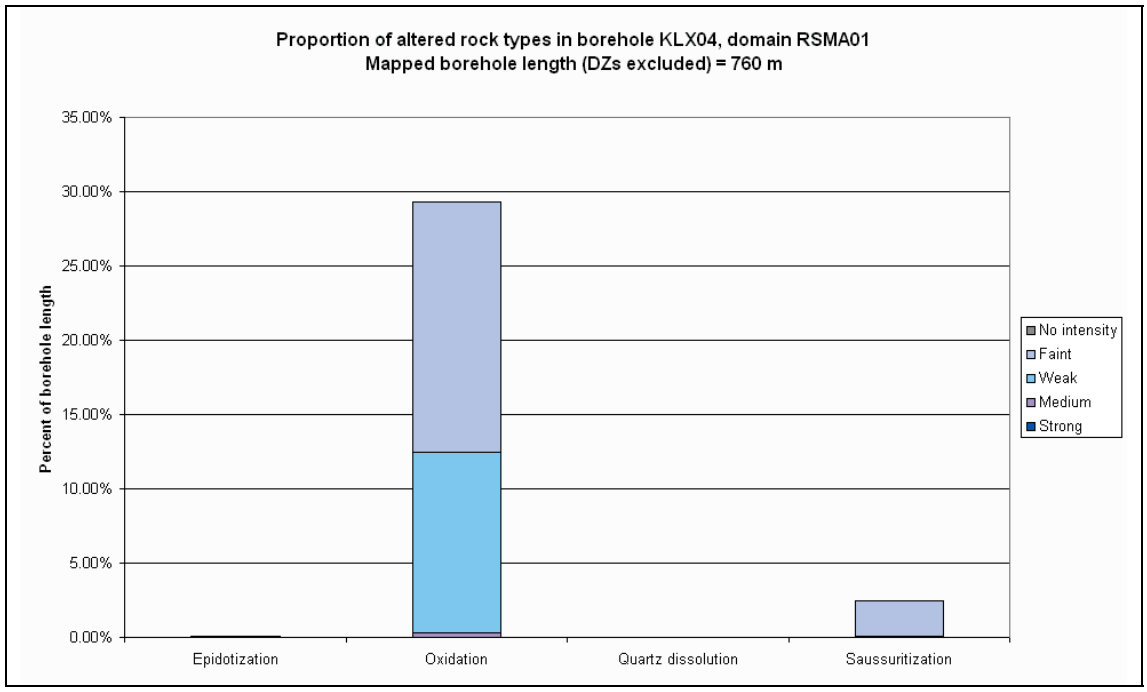
Proportion of altered rock types in borehole KLX04, domain RSMA01
Mapped borehole length (DZs excluded) = 760 m
Percent of borehole length
35.00%
30.00%
25.00%
20.00%
15.00%
10.00%
5.00%
0.00%
Epidotization
Oxidation
Quartz dissolution
Saussuritization
No intensity
Faint
Weak
Medium
Strong

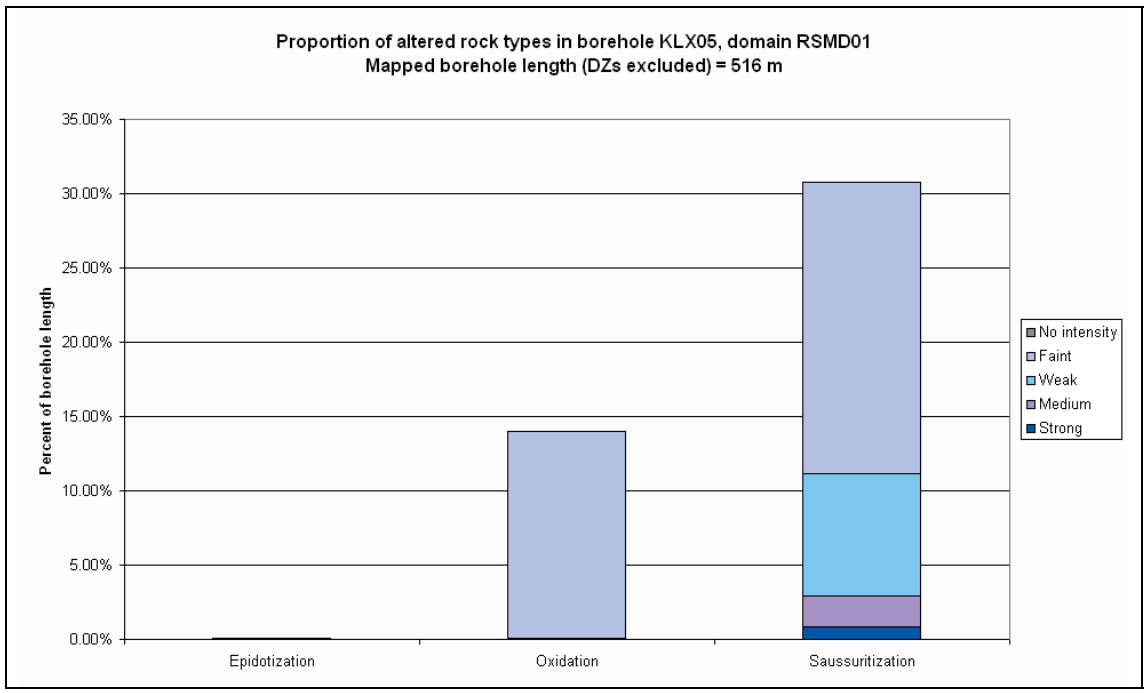
Proportion of altered rock types in borehole KLX05, domain RSMD01
Mapped borehole length (DZs excluded) = 516 m
Percent of borehole length
35.00%
30.00%
25.00%
20.00%
15.00%
10.00%
5.00%
0.00%
Epidotization
Oxidation
Saussuritization
No intensity
Faint
Weak
Medium
Strong

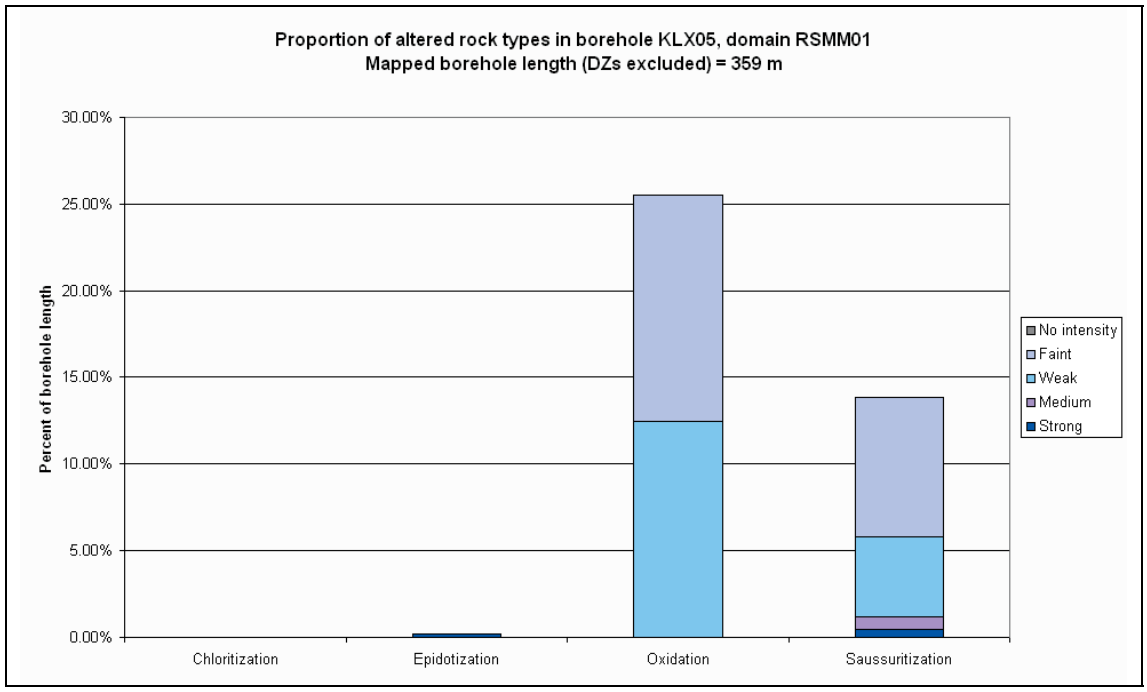
Proportion of altered rock types in borehole KLX05, domain RSMM01
Mapped borehole length (DZs excluded) = 359 m
Percent of borehole length
30.00%
25.00%
20.00%
15.00%
10.00%
5.00%
0.00%
Chloritization
Epidotization
Oxidation
Saussuritization
No intensity
Faint
Weak
Medium
Strong

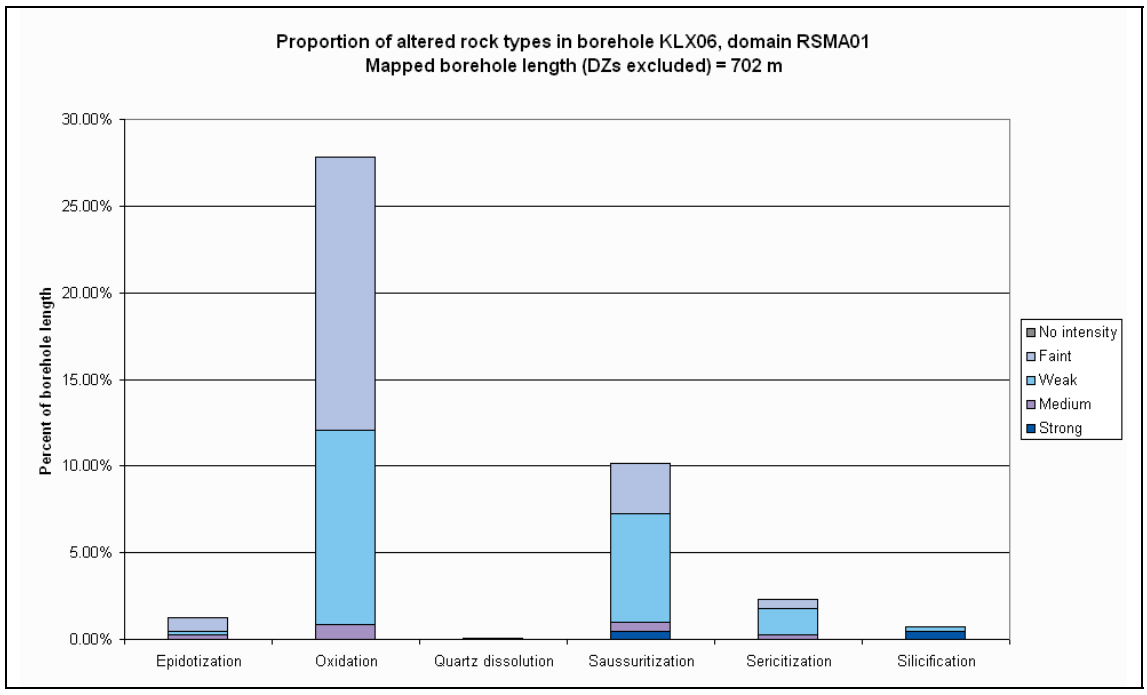
Proportion of altered rock types in borehole KLX06, domain RSMA01
Mapped borehole length (DZs excluded) = 702 m
Percent of borehole length
30.00%
25.00%
20.00%
15.00%
10.00%
5.00%
0.00%
Epidotization
Oxidation
Quartz dissolution
Saussuritization
Sericitization
Silicification
No intensity
Faint
Weak
Medium
Strong

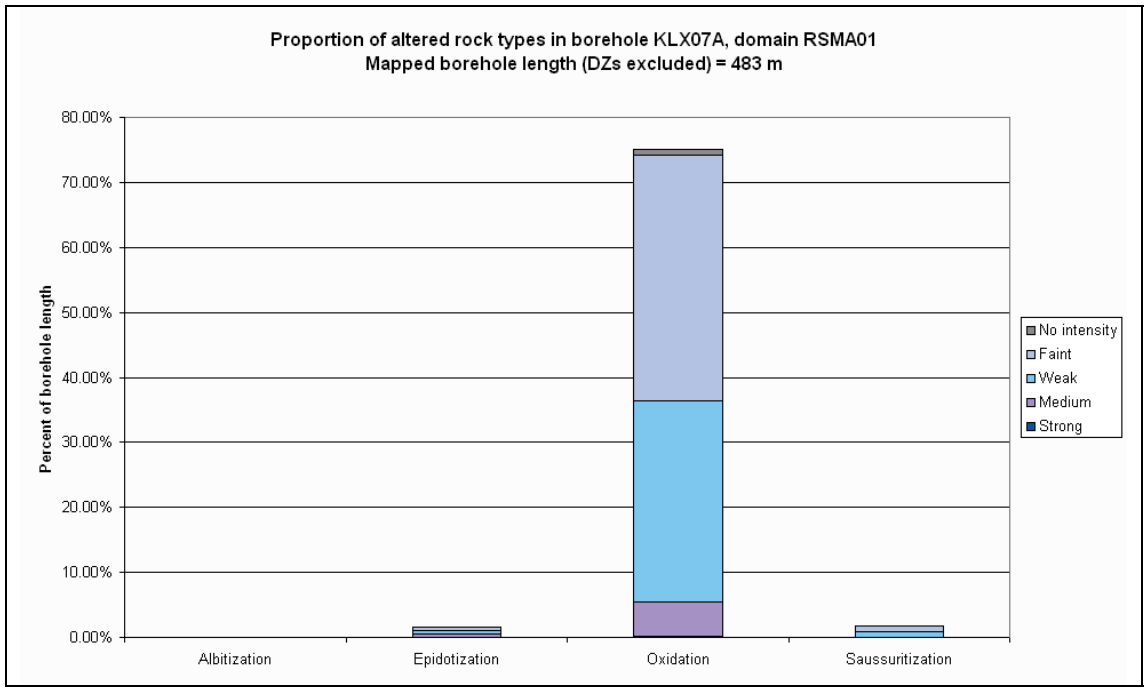
Proportion of altered rock types in borehole KLX07A, domain RSMA01
Mapped borehole length (DZs excluded) = 483 m
Percent of borehole length
80.00%
70.00%
60.00%
50.00%
40.00%
30.00%
20.00%
10.00%
0.00%
Albitization
Epidotization
Oxidation
Saussuritization
No intensity
Faint
Weak
Medium
Strong

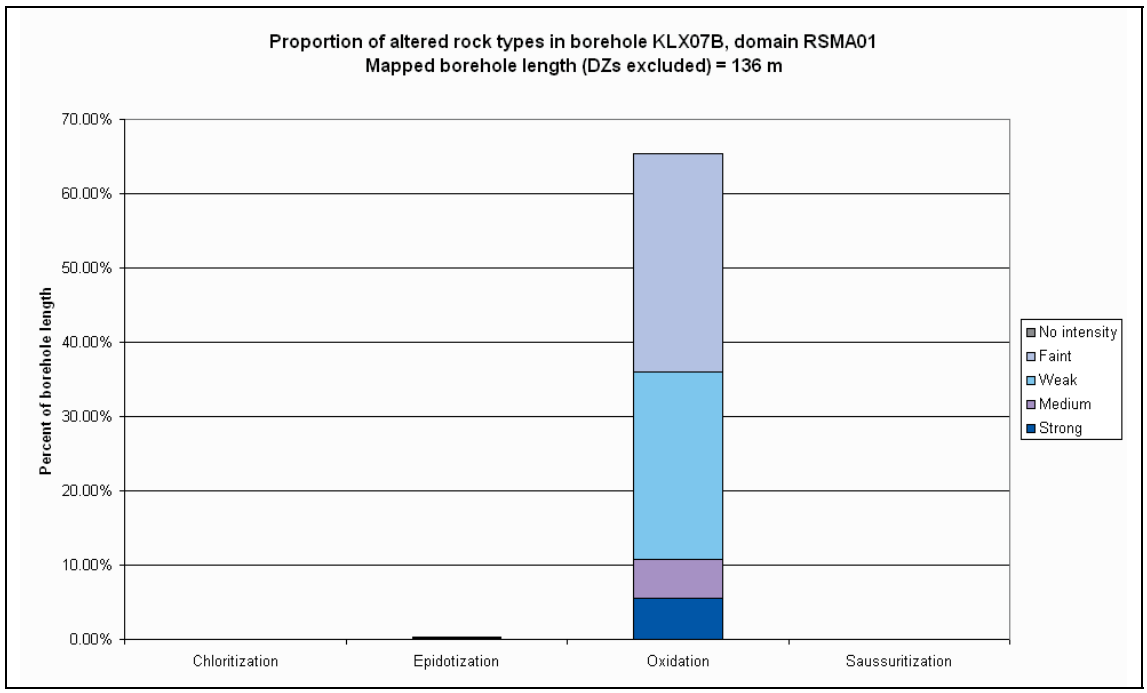
Proportion of altered rock types in borehole KLX07B, domain RSMA01
Mapped borehole length (DZs excluded) = 136 m
Percent of borehole length
70.00%
60.00%
50.00%
40.00%
30.00%
20.00%
10.00%
0.00%
Chloritization
Epidotization
Oxidation
Saussuritization
No intensity
Faint
Weak
Medium
Strong

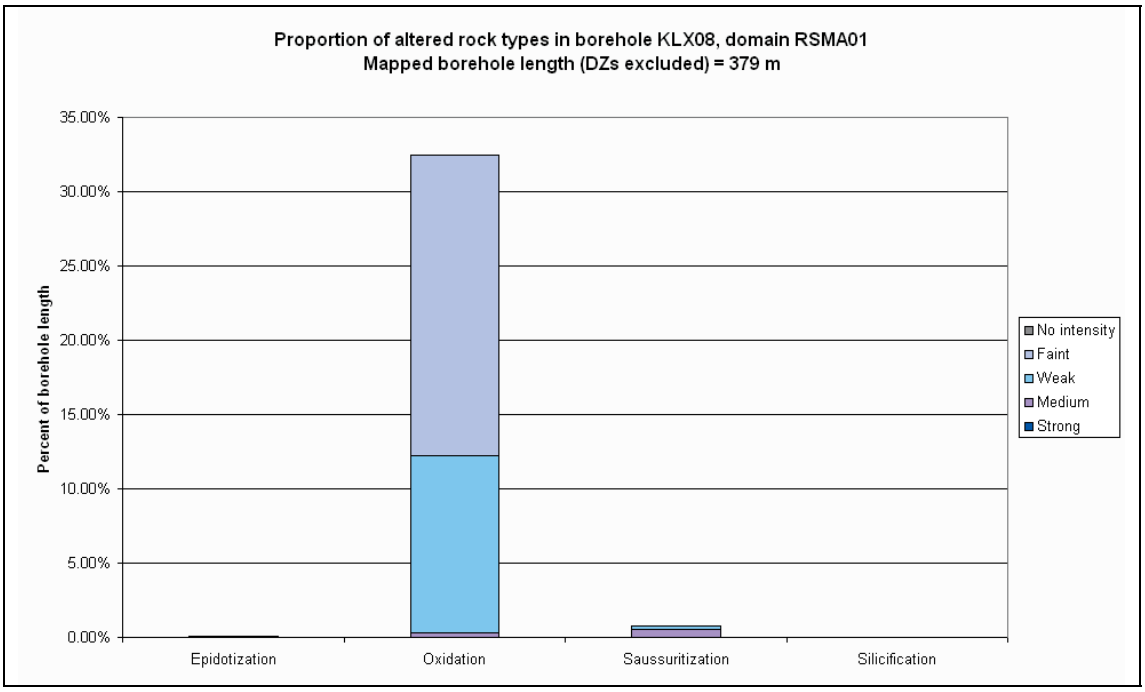
Proportion of altered rock types in borehole KLX08, domain RSMA01
Mapped borehole length (DZs excluded) = 379 m
Percent of borehole length
35.00%
30.00%
25.00%
20.00%
15.00%
10.00%
5.00%
0.00%
Epidotization
Oxidation
Saussuritization
Silicification
No intensity
Faint
Weak
Medium
Strong

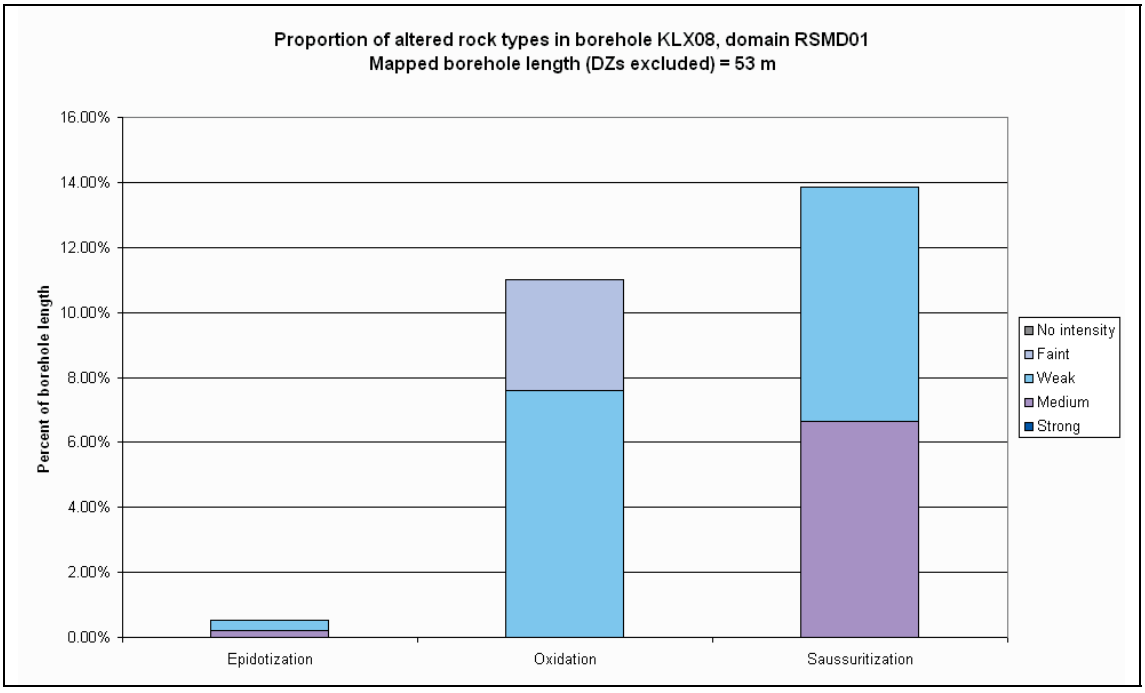
Proportion of altered rock types in borehole KLX08, domain RSMD01
Mapped borehole length (DZs excluded) = 53 m
Percent of borehole length
16.00%
14.00%
12.00%
10.00%
8.00%
6.00%
4.00%
2.00%
0.00%
Epidotization
Oxidation
Saussuritization
No intensity
Faint
Weak
Medium
Strong

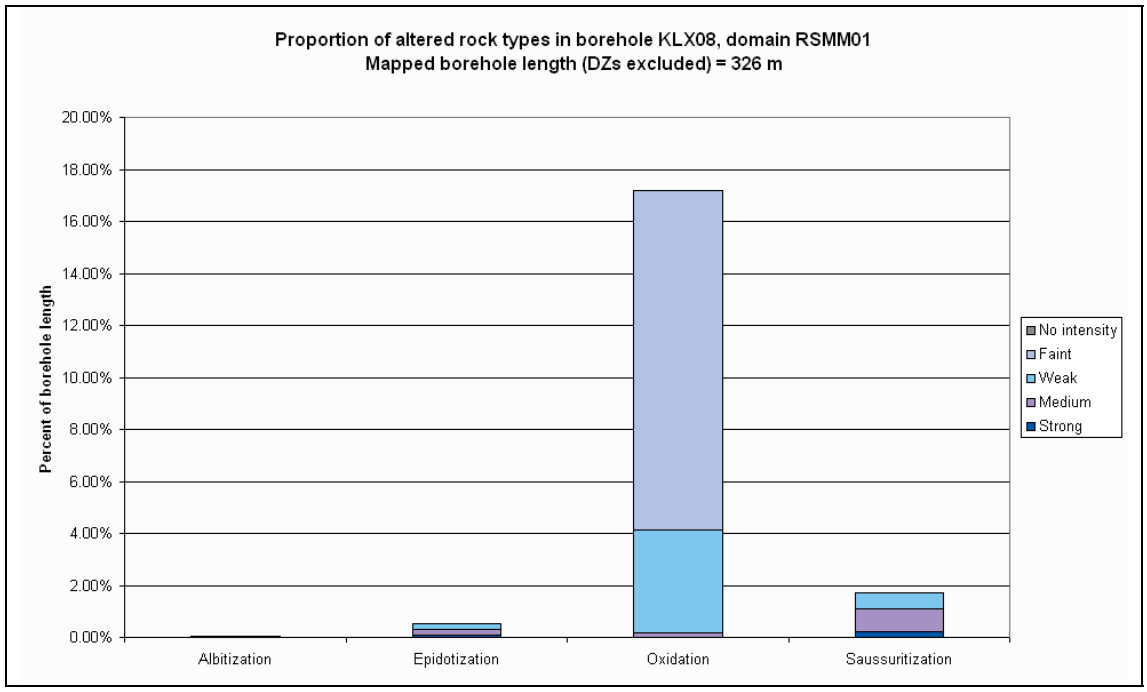
Proportion of altered rock types in borehole KLX08, domain RSMM01
Mapped borehole length (DZs excluded) = 326 m
Percent of borehole length
20.00%
18.00%
16.00%
14.00%
12.00%
10.00%
8.00%
6.00%
4.00%
2.00%
0.00%
Albitization
Epidotization
Oxidation
Saussuritization
No intensity
Faint
Weak
Medium
Strong

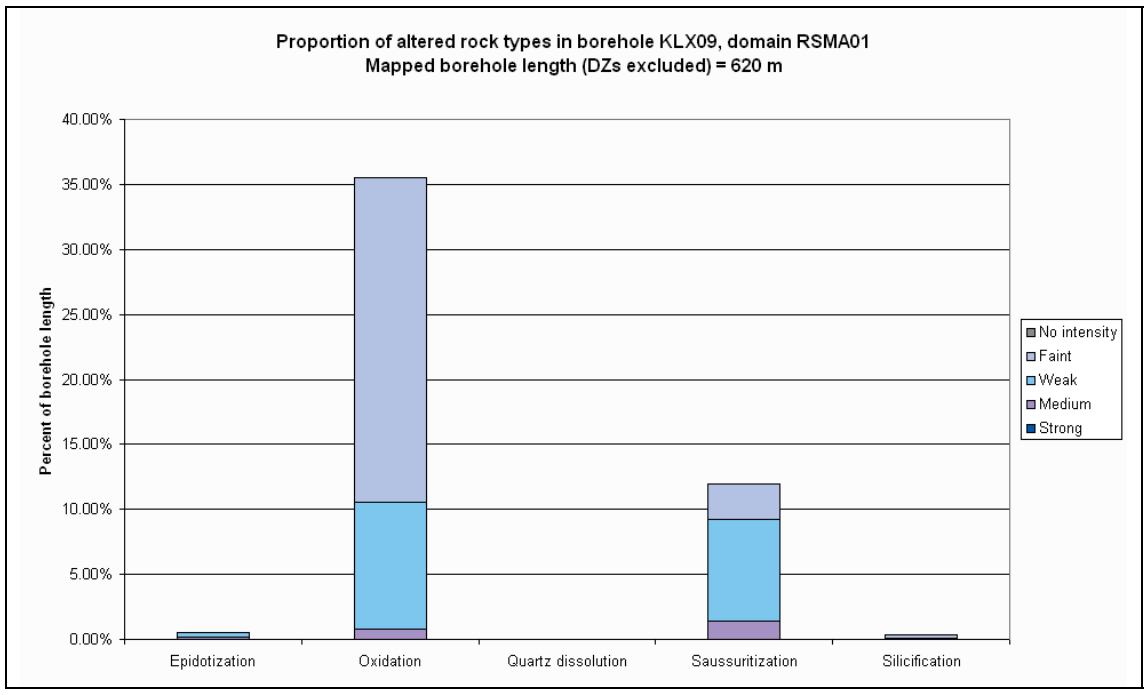
Proportion of altered rock types in borehole KLX09, domain RSMA01
Mapped borehole length (DZs excluded) = 620 m
Percent of borehole length
40.00%
35.00%
30.00%
25.00%
20.00%
15.00%
10.00%
5.00%
0.00%
Epidotization
Oxidation
Quartz dissolution
Saussuritization
Silicification
No intensity
Faint
Weak
Medium
Strong

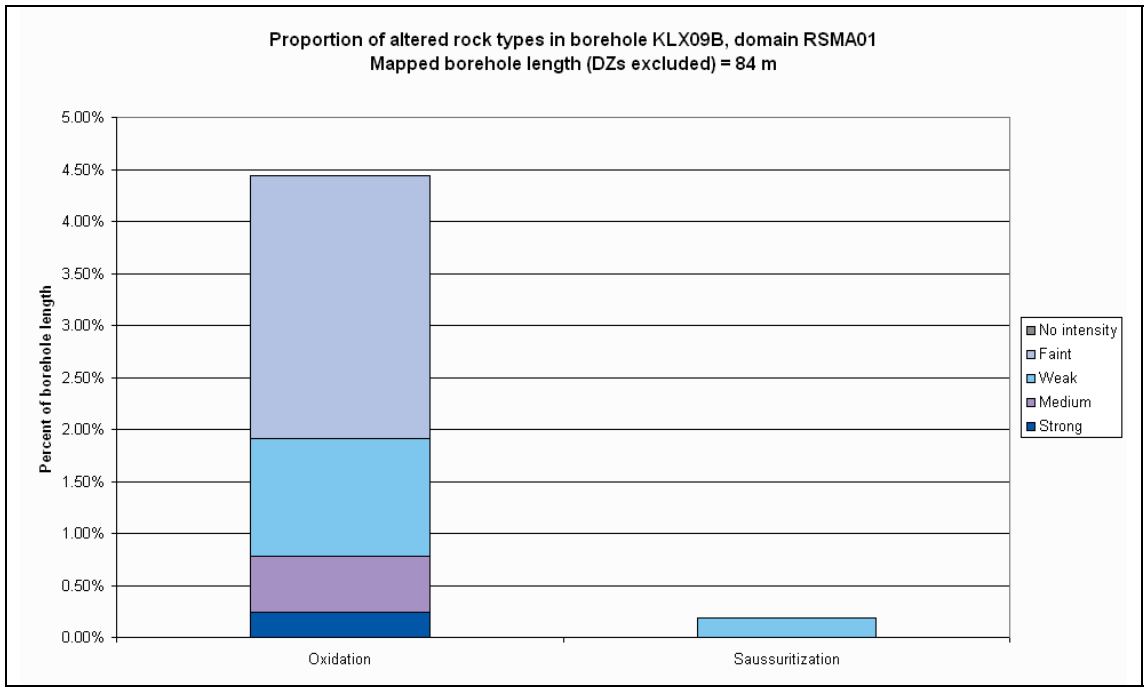
Proportion of altered rock types in borehole KLX09B, domain RSMA01
Mapped borehole length (DZs excluded) = 84 m
Percent of borehole length
5.00%
4.50%
4.00%
3.50%
3.00%
2.50%
2.00%
1.50%
1.00%
0.50%
0.00%
Oxidation
Saussuritization
No intensity
Faint
Weak
Medium
Strong

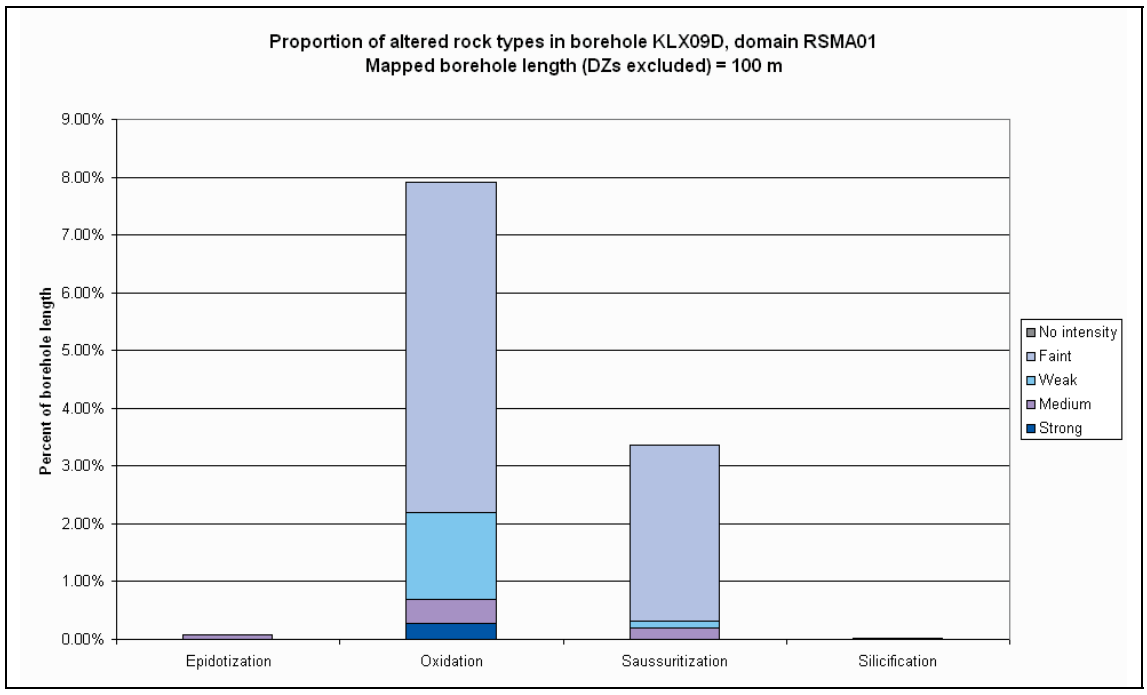
Proportion of altered rock types in borehole KLX09D, domain RSMA01
Mapped borehole length (DZs excluded) = 100 m
Percent of borehole length
9.00%
8.00%
7.00%
6.00%
5.00%
4.00%
3.00%
2.00%
1.00%
0.00%
Epidotization
Oxidation
Saussuritization
Silicification
No intensity
Faint
Weak
Medium
Strong

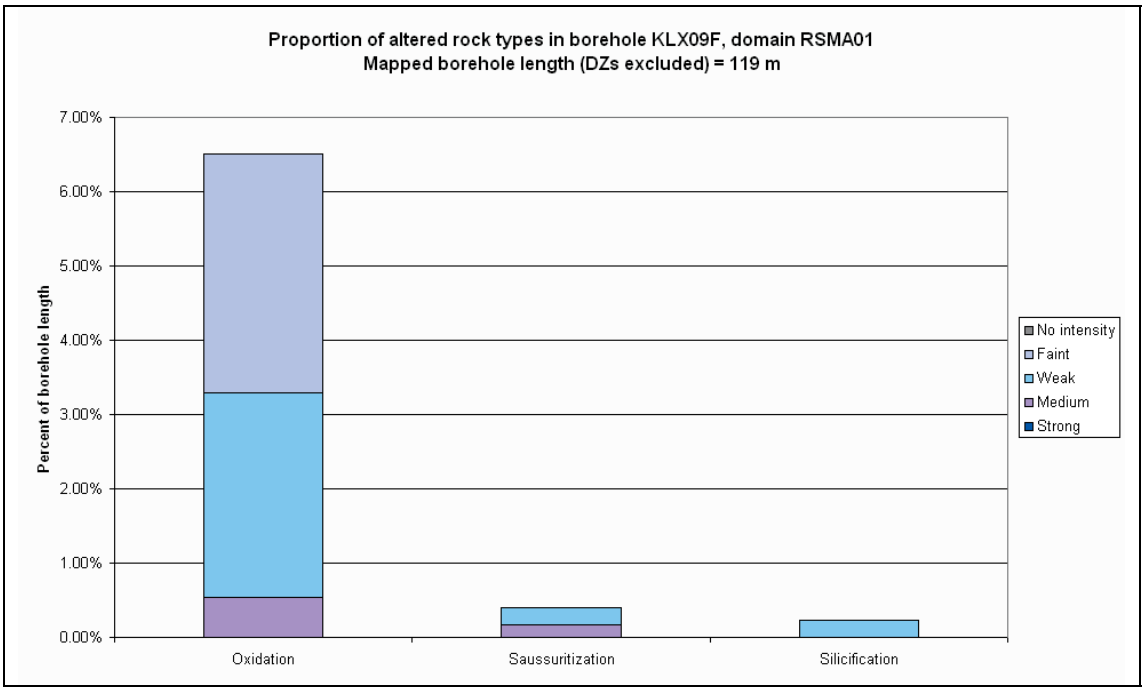
Proportion of altered rock types in borehole KLX09F, domain RSMA01
Mapped borehole length (DZs excluded) = 119 m
Percent of borehole length
7.00%
6.00%
5.00%
4.00%
3.00%
2.00%
1.00%
0.00%
Oxidation
Saussuritization
Silicification
No intensity
Faint
Weak
Medium
Strong

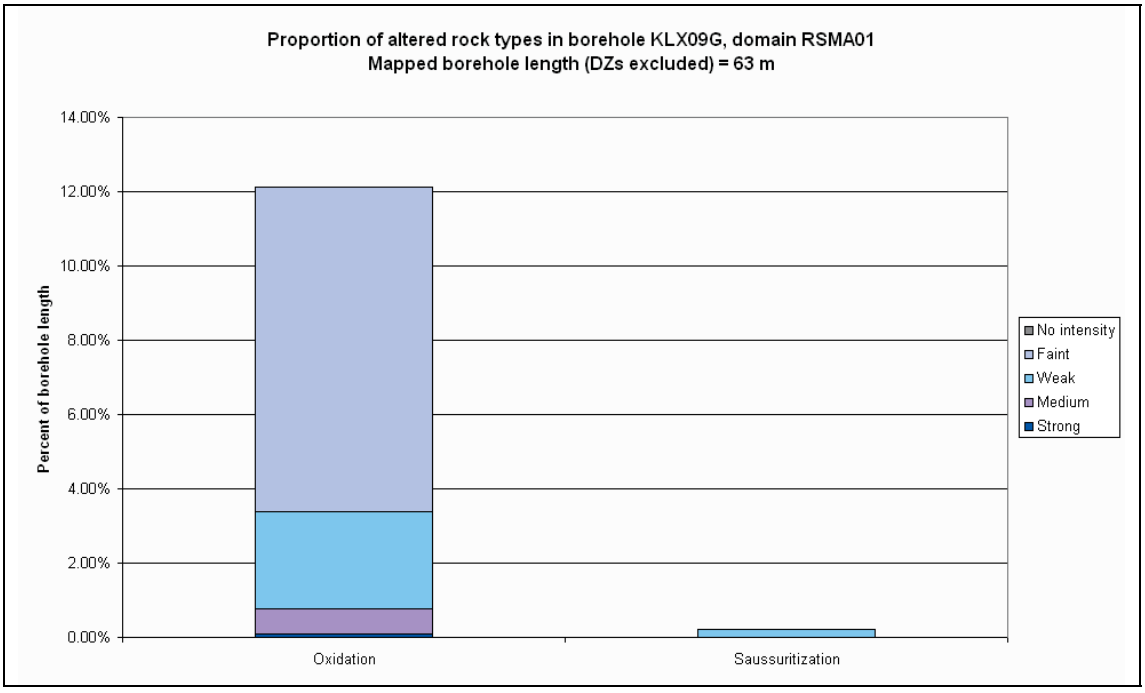
Proportion of altered rock types in borehole KLX09G, domain RSMA01
Mapped borehole length (DZs excluded) = 63 m
Percent of borehole length
14.00%
12.00%
10.00%
8.00%
6.00%
4.00%
2.00%
0.00%
Oxidation
Saussuritization
No intensity
Faint
Weak
Medium
Strong

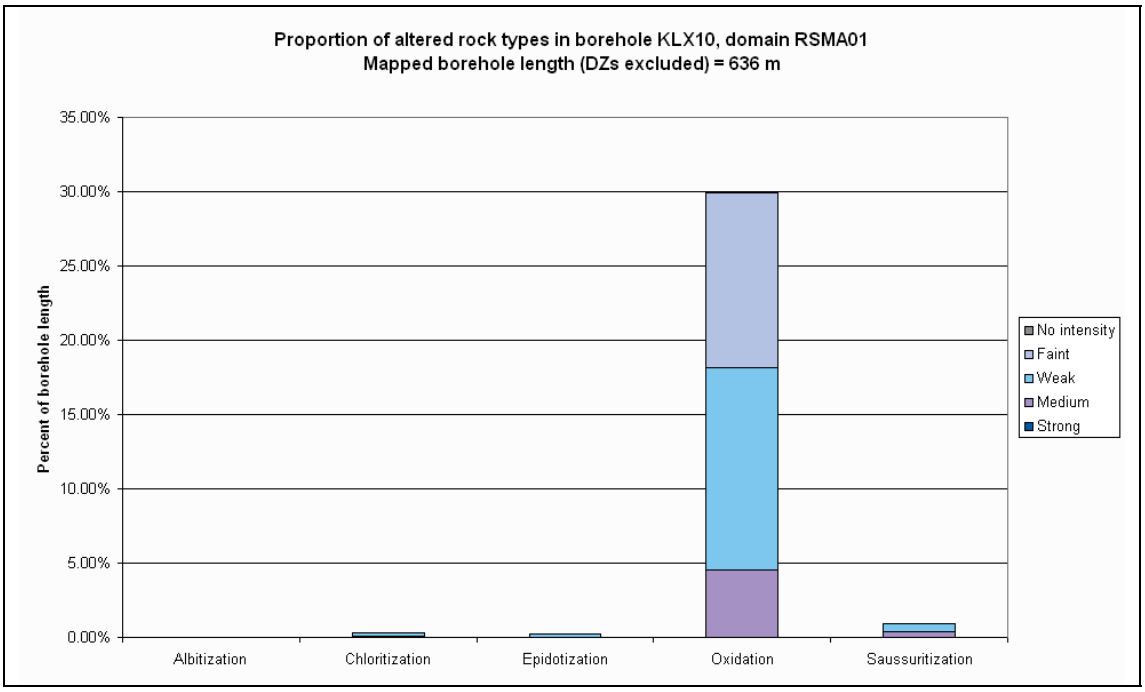
Proportion of altered rock types in borehole KLX10, domain RSMA01
Mapped borehole length (DZs excluded) = 636 m
Percent of borehole length
35.00%
30.00%
25.00%
20.00%
15.00%
10.00%
5.00%
0.00%
Albitization
Chloritization
Epidotization
Oxidation
Saussuritization
No intensity
Faint
Weak
Medium
Strong

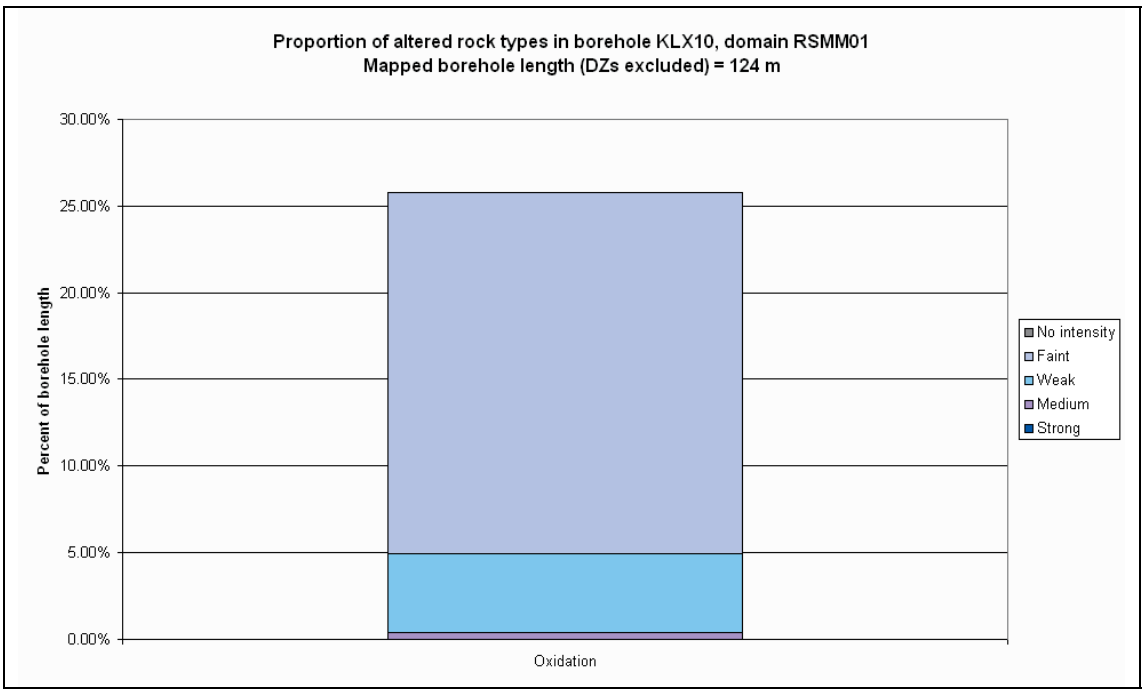
Proportion of altered rock types in borehole KLX10, domain RSMM01
Mapped borehole length (DZs excluded) = 124 m
Percent of borehole length
30.00%
25.00%
20.00%
15.00%
10.00%
5.00%
0.00%
Oxidation
No intensity
Faint
Weak
Medium
Strong

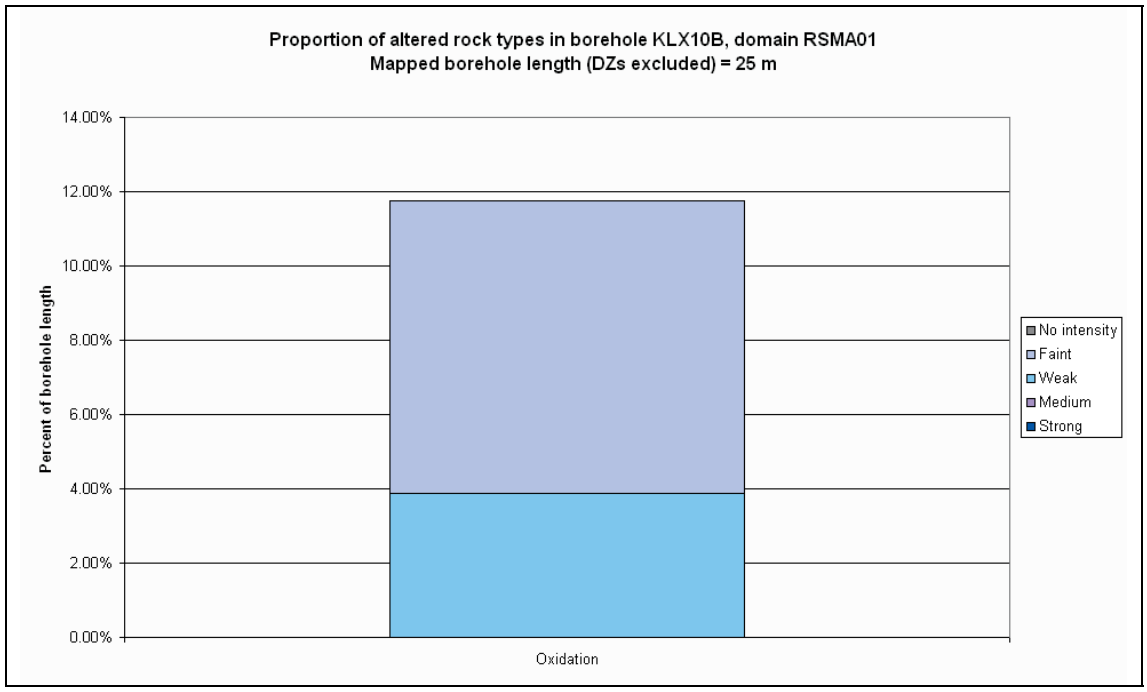
Proportion of altered rock types in borehole KLX10B, domain RSMA01
Mapped borehole length (DZs excluded) = 25 m
Percent of borehole length
14.00%
12.00%
10.00%
8.00%
6.00%
4.00%
2.00%
0.00%
Oxidation
No intensity
Faint
Weak
Medium
Strong

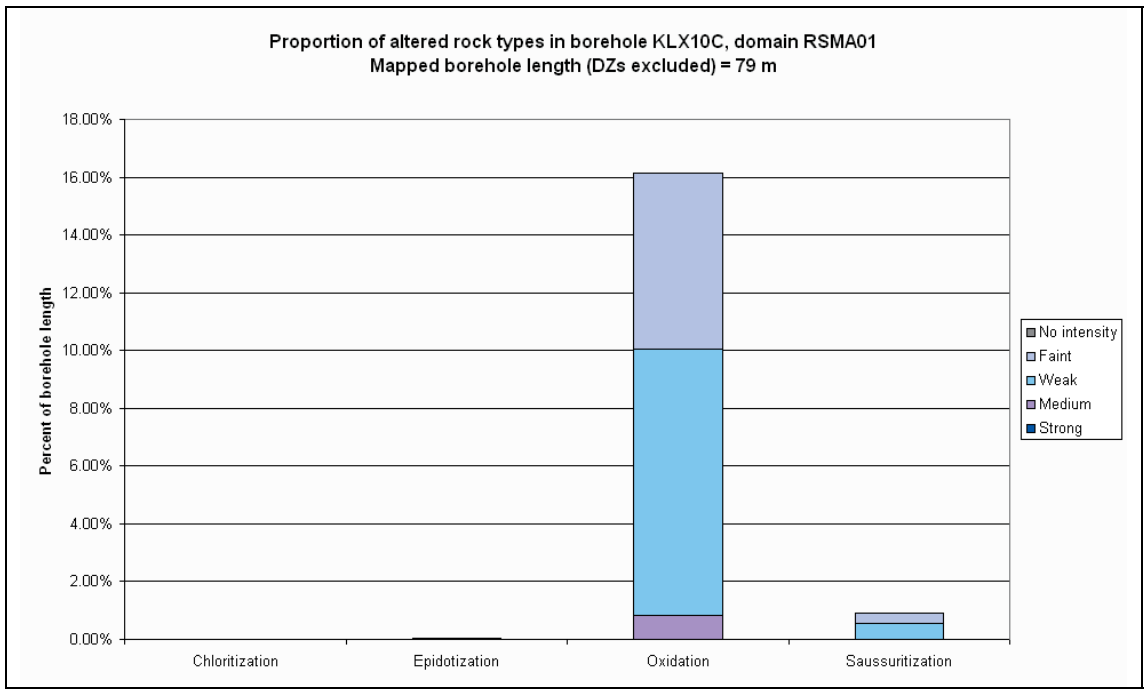
Proportion of altered rock types in borehole KLX10C, domain RSMA01
Mapped borehole length (DZs excluded) = 79 m
Percent of borehole length
18.00%
16.00%
14.00%
12.00%
10.00%
8.00%
6.00%
4.00%
2.00%
0.00%
Chloritization
Epidotization
Oxidation
Saussuritization
No intensity
Faint
Weak
Medium
Strong

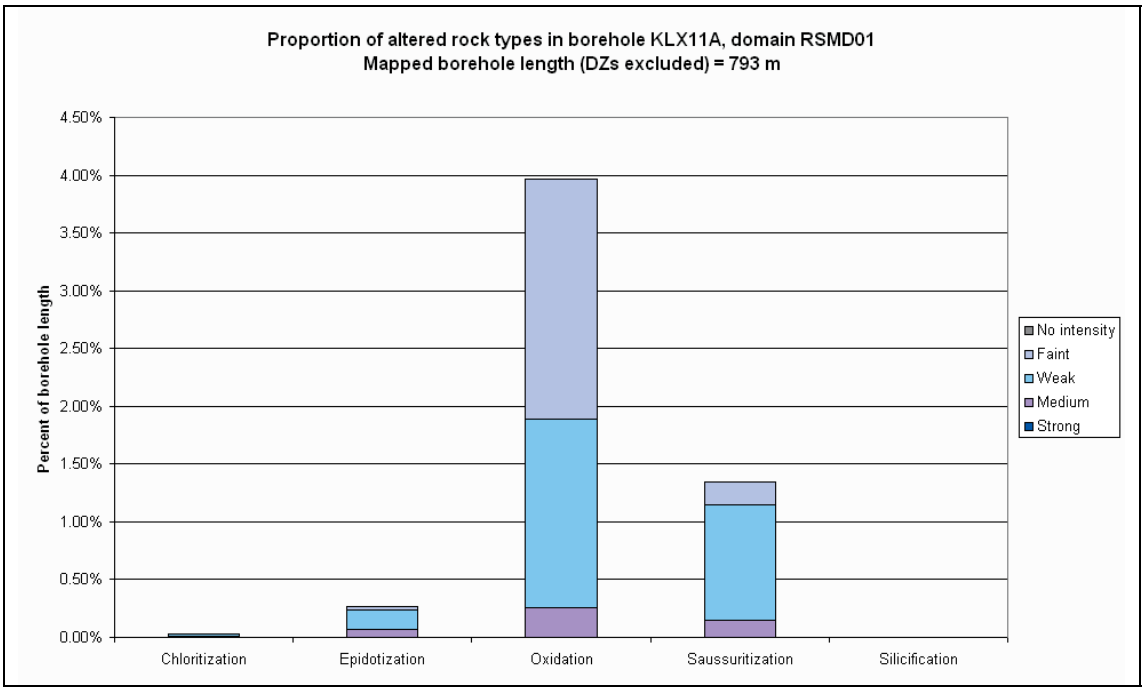
Proportion of altered rock types in borehole KLX11A, domain RSMD01
Mapped borehole length (DZs excluded) = 793 m
Percent of borehole length
4.50%
4.00%
3.50%
3.00%
2.50%
2.00%
1.50%
1.00%
0.50%
0.00%
Chloritization
Epidotization
Oxidation
Saussuritization
Silicification
No intensity
Faint
Weak
Medium
Strong

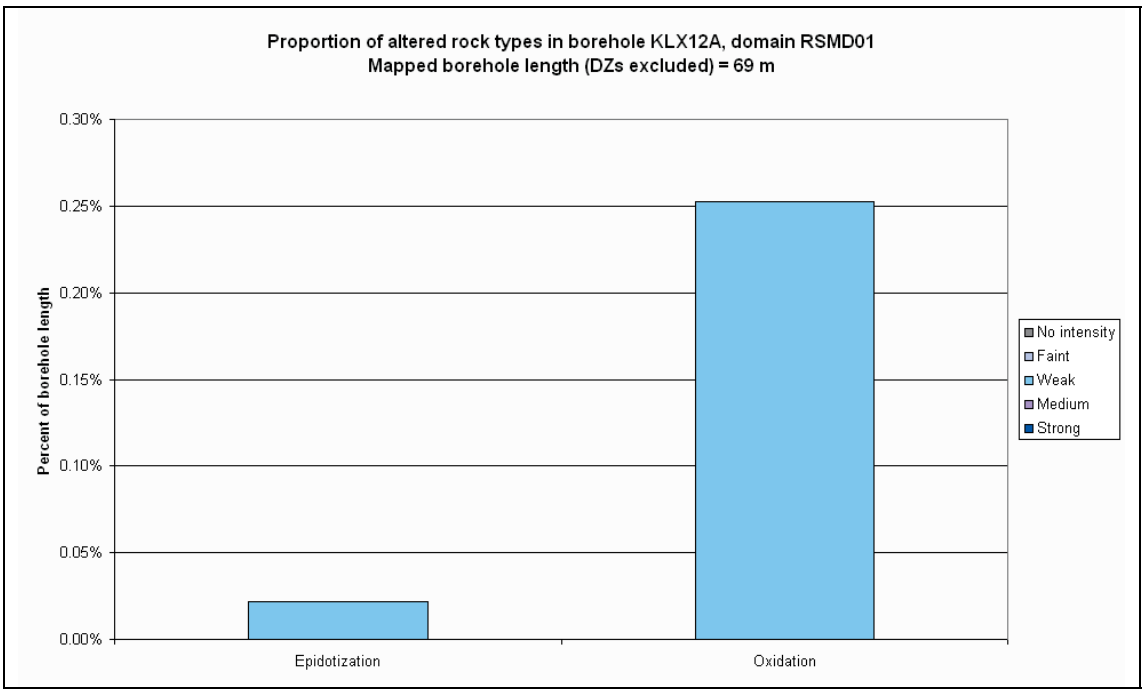
Proportion of altered rock types in borehole KLX12A, domain RSMD01
Mapped borehole length (DZs excluded) = 69 m
Percent of borehole length
0.30%
0.25%
0.20%
0.15%
0.10%
0.05%
0.00%
Epidotization
Oxidation
No intensity
Faint
Weak
Medium
Strong

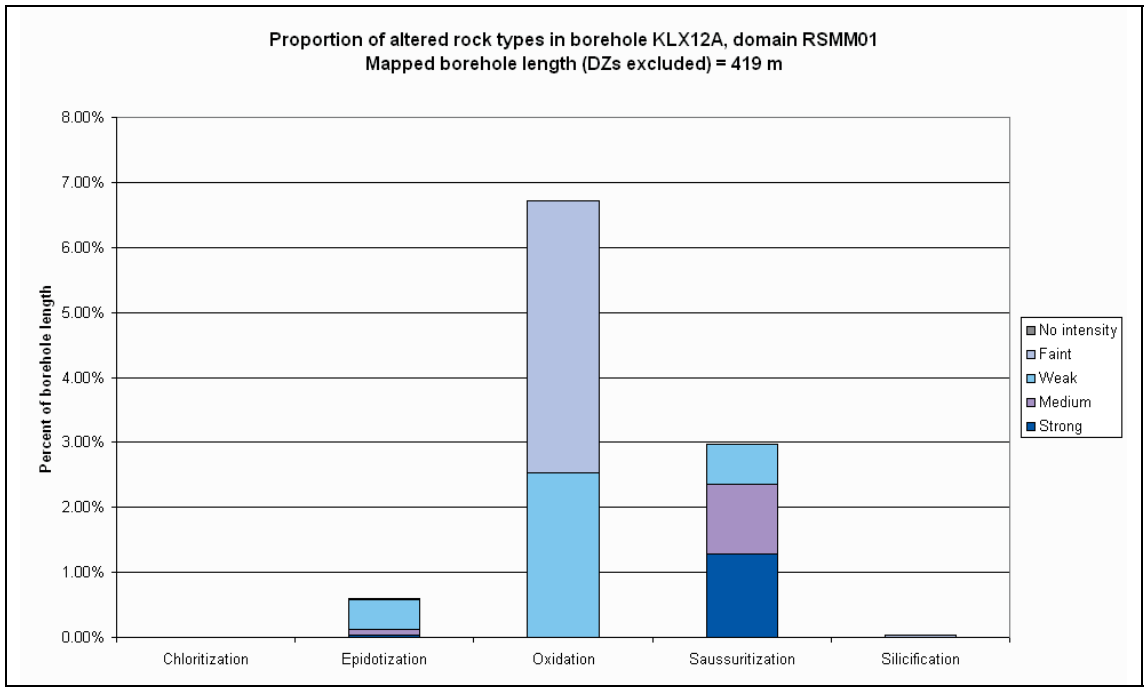
Proportion of altered rock types in borehole KLX12A, domain RSMM01
Mapped borehole length (DZs excluded) = 419 m
Percent of borehole length
8.00%
7.00%
6.00%
5.00%
4.00%
3.00%
2.00%
1.00%
0.00%
Chloritization
Epidotization
Oxidation
Saussuritization
Silicification
No intensity
Faint
Weak
Medium
Strong

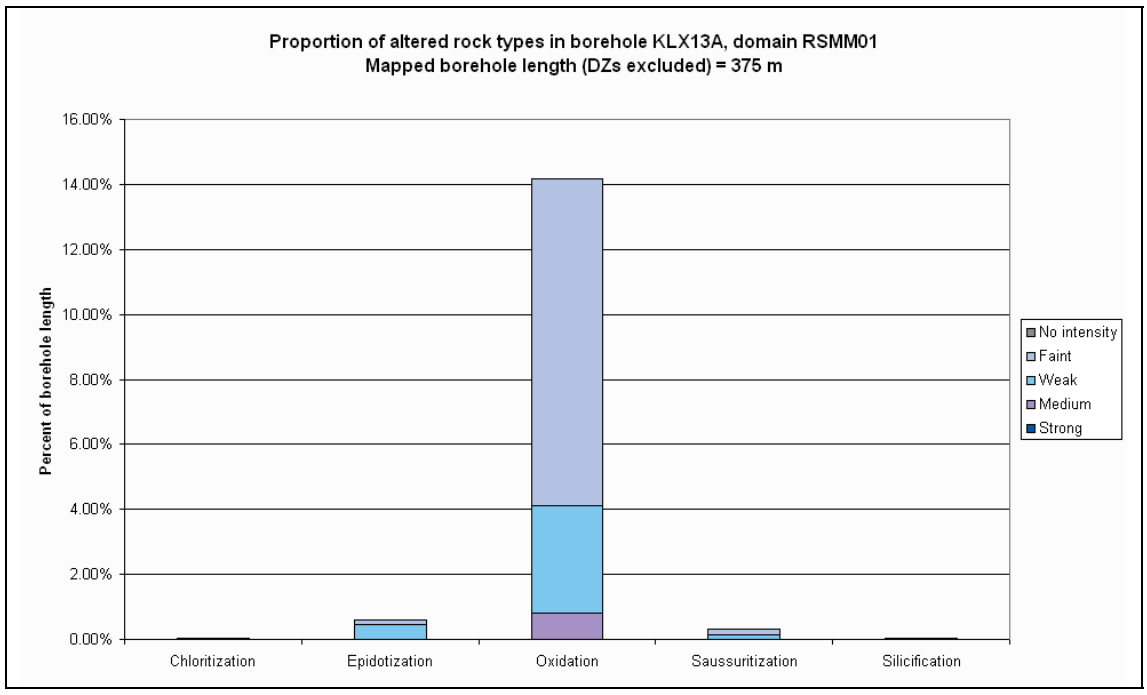
Proportion of altered rock types in borehole KLX13A, domain RSMM01
Mapped borehole length (DZs excluded) = 375 m
Percent of borehole length
16.00%
14.00%
12.00%
10.00%
8.00%
6.00%
4.00%
2.00%
0.00%
Chloritization
Epidotization
Oxidation
Saussuritization
Silicification
No intensity
Faint
Weak
Medium
Strong

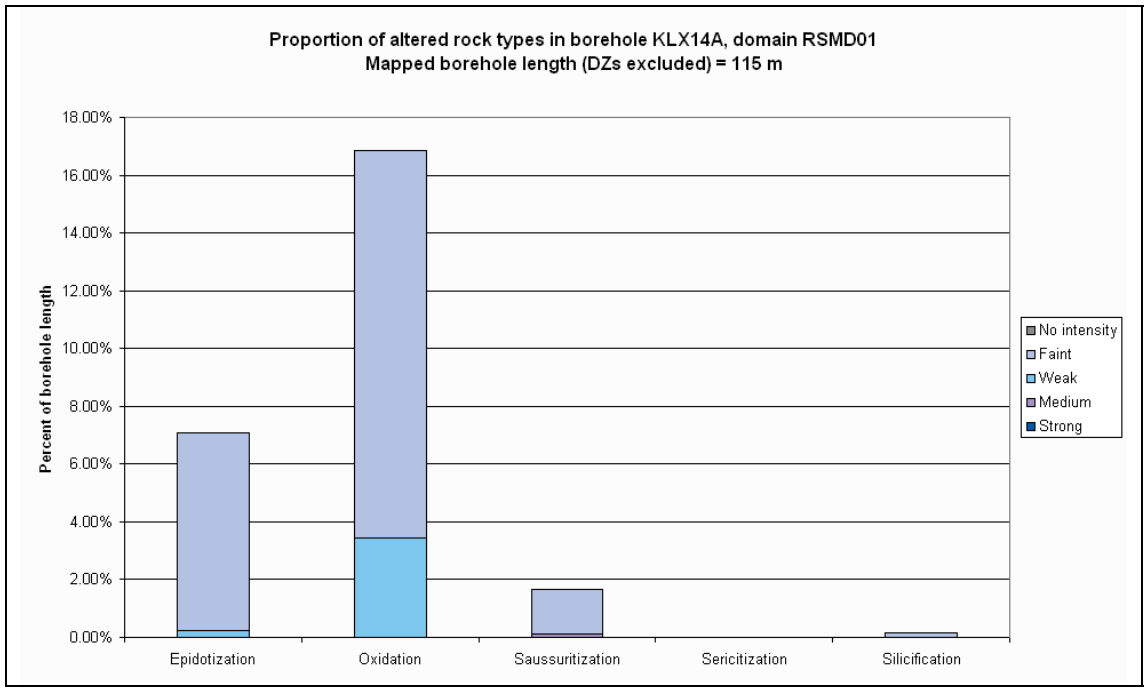
Proportion of altered rock types in borehole KLX14A, domain RSMD01
Mapped borehole length (DZs excluded) = 115 m
Percent of borehole length
18.00%
16.00%
14.00%
12.00%
10.00%
8.00%
6.00%
4.00%
2.00%
0.00%
Epidotization
Oxidation
Saussuritization
Sericitization
Silicification
No intensity
Faint
Weak
Medium
Strong

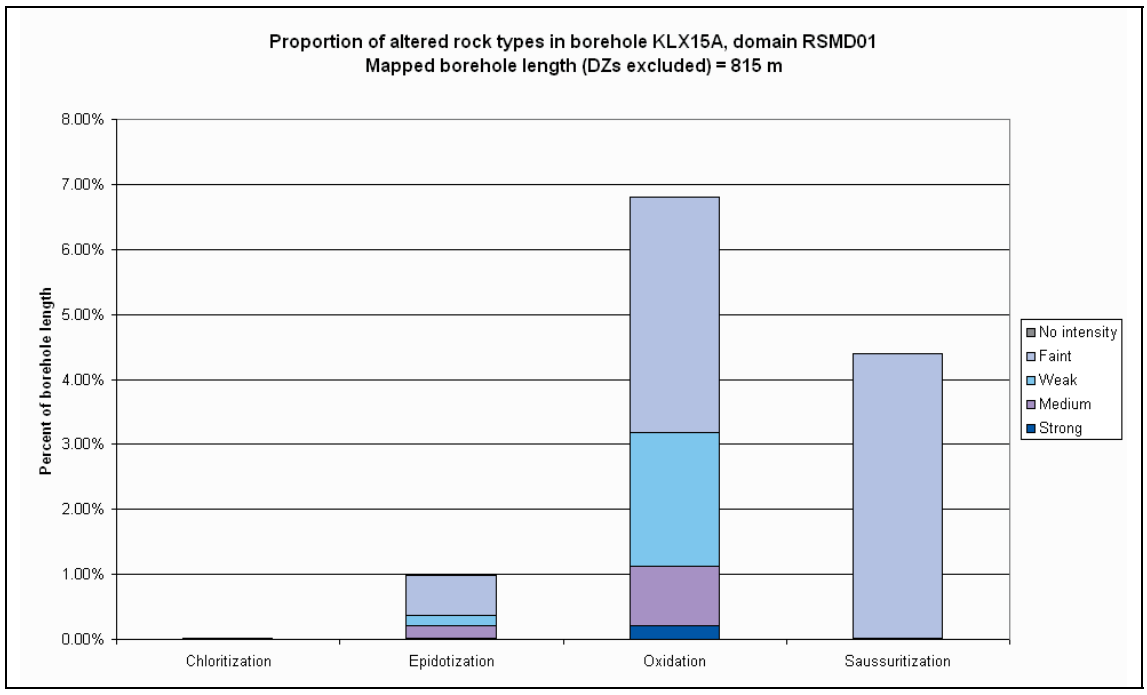
Proportion of altered rock types in borehole KLX15A, domain RSMD01
Mapped borehole length (DZs excluded) = 815 m
Percent of borehole length
8.00%
7.00%
6.00%
5.00%
4.00%
3.00%
2.00%
1.00%
0.00%
Chloritization
Epidotization
Oxidation
Saussuritization
No intensity
Faint
Weak
Medium
Strong

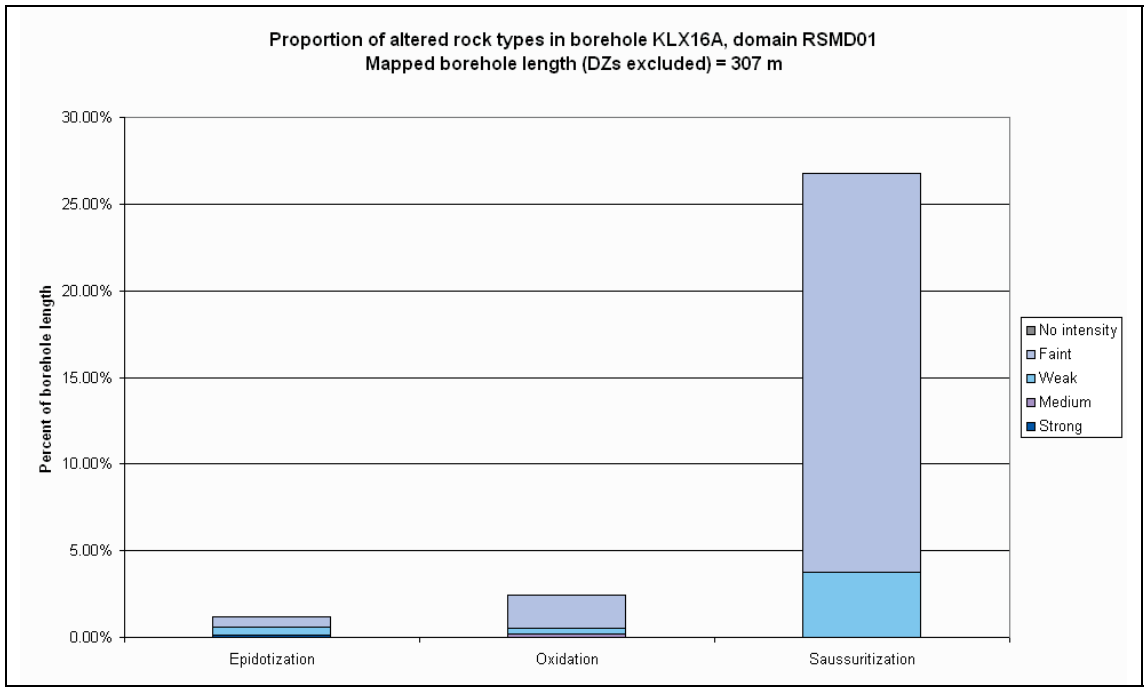
Proportion of altered rock types in borehole KLX16A, domain RSMD01
Mapped borehole length (DZs excluded) = 307 m
Percent of borehole length
30.00%
25.00%
20.00%
15.00%
10.00%
5.00%
0.00%
Epidotization
Oxidation
Saussuritization
No intensity
Faint
Weak
Medium
Strong

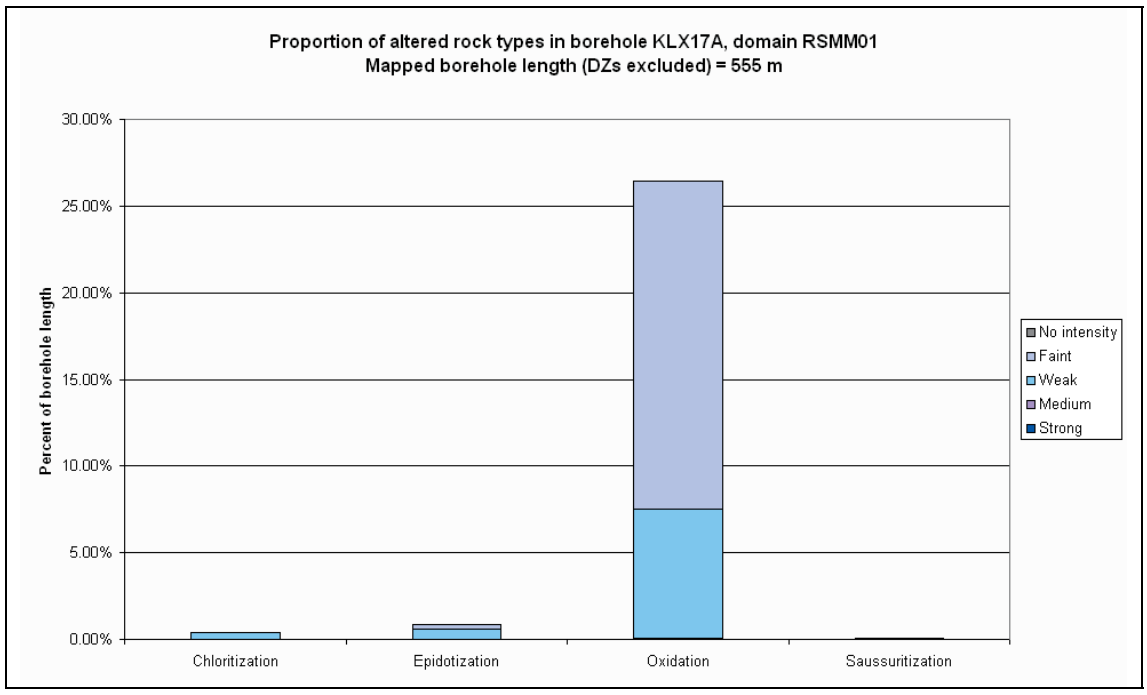
Proportion of altered rock types in borehole KLX17A, domain RSMM01
Mapped borehole length (DZs excluded) = 555 m
Percent of borehole length
30.00%
25.00%
20.00%
15.00%
10.00%
5.00%
0.00%
Chloritization
Epidotization
Oxidation
Saussuritization
No intensity
Faint
Weak
Medium
Strong

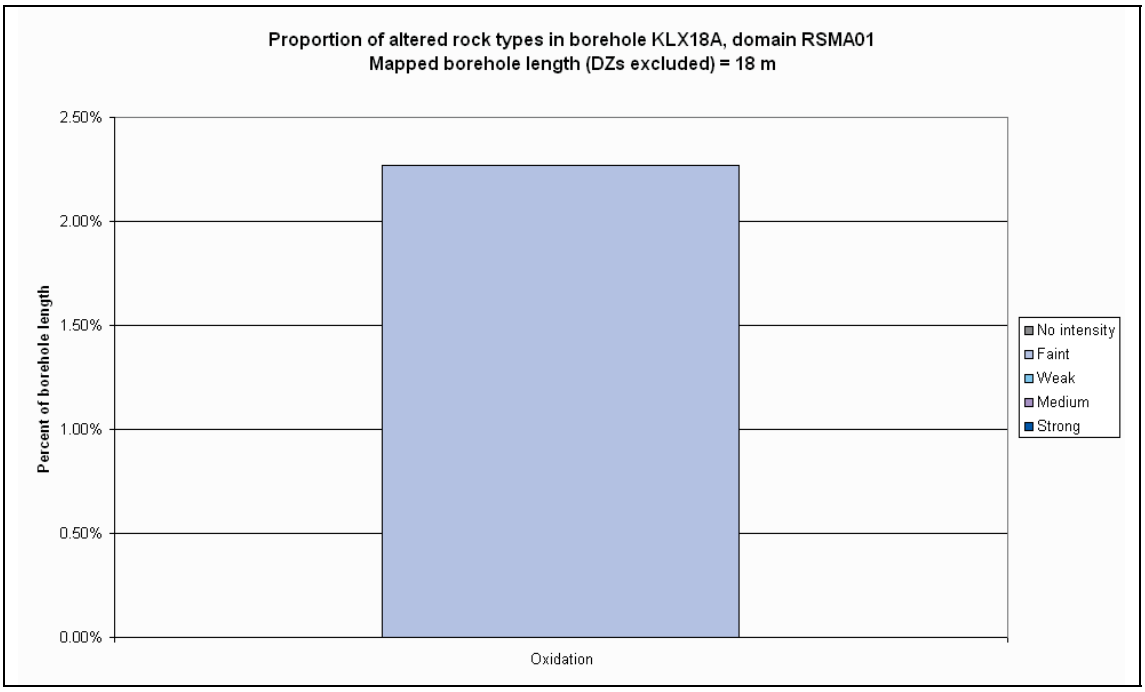
Proportion of altered rock types in borehole KLX18A, domain RSMA01
Mapped borehole length (DZs excluded) = 18 m
Percent of borehole length
2.50%
2.00%
1.50%
1.00%
0.50%
0.00%
Oxidation
No intensity
Faint
Weak
Medium
Strong

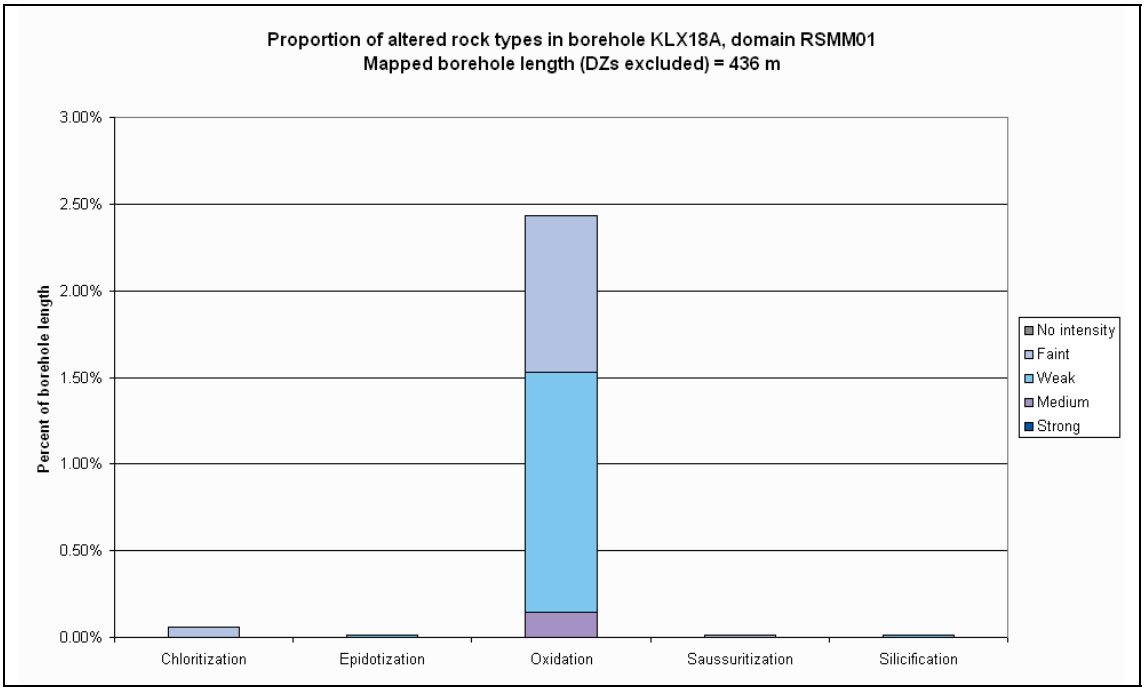
Proportion of altered rock types in borehole KLX18A, domain RSMM01
Mapped borehole length (DZs excluded) = 436 m
Percent of borehole length
3.00%
2.50%
2.00%
1.50%
1.00%
0.50%
0.00%
Chloritization
Epidotization
Oxidation
Saussuritization
Silicification
No intensity
Faint
Weak
Medium
Strong

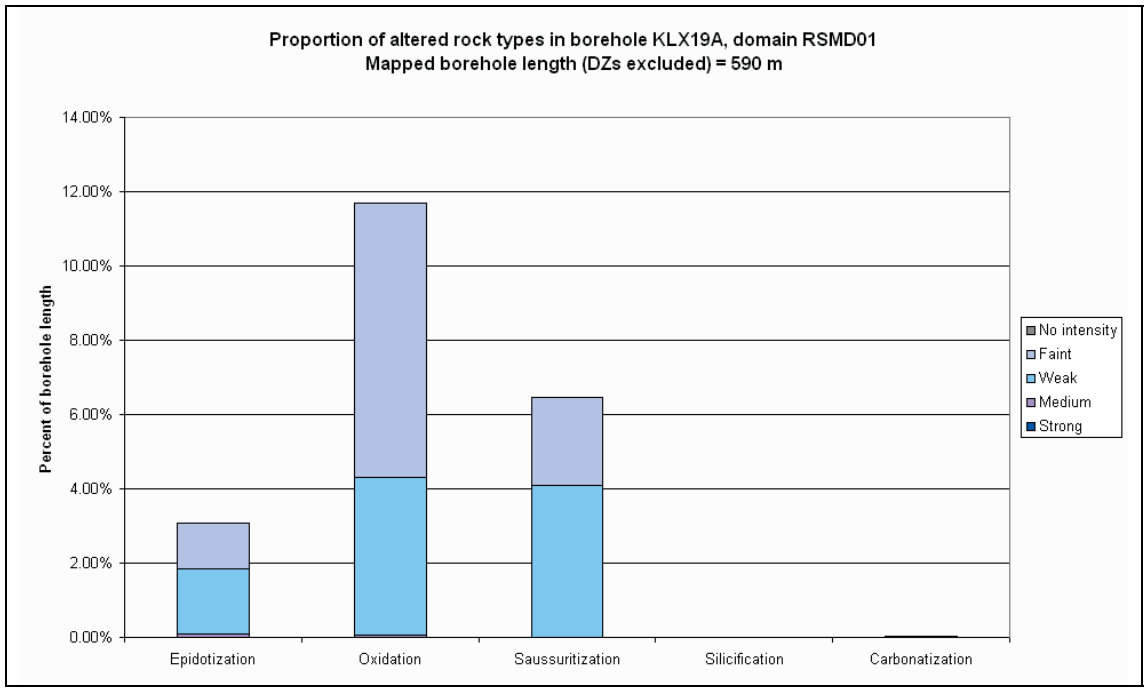
Proportion of altered rock types in borehole KLX19A, domain RSMD01
Mapped borehole length (DZs excluded) = 590 m
Percent of borehole length
14.00%
12.00%
10.00%
8.00%
6.00%
4.00%
2.00%
0.00%
Epidotization
Oxidation
Saussuritization
Silicification
Carbonatization
No intensity
Faint
Weak
Medium
Strong

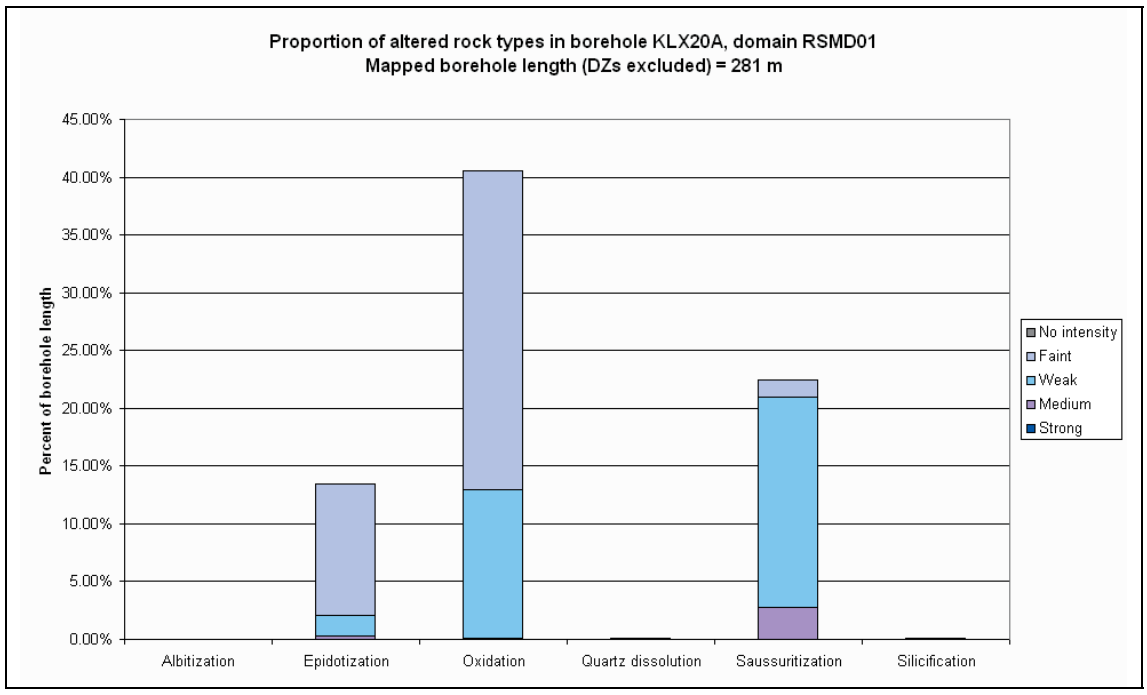
Proportion of altered rock types in borehole KLX20A, domain RSMD01
Mapped borehole length (DZs excluded) = 281 m
Percent of borehole length
45.00%
40.00%
35.00%
30.00%
25.00%
20.00%
15.00%
10.00%
5.00%
0.00%
Albitization
Epidotization
Oxidation
Quartz dissolution
Saussuritization
Silicification
No intensity
Faint
Weak
Medium
Strong

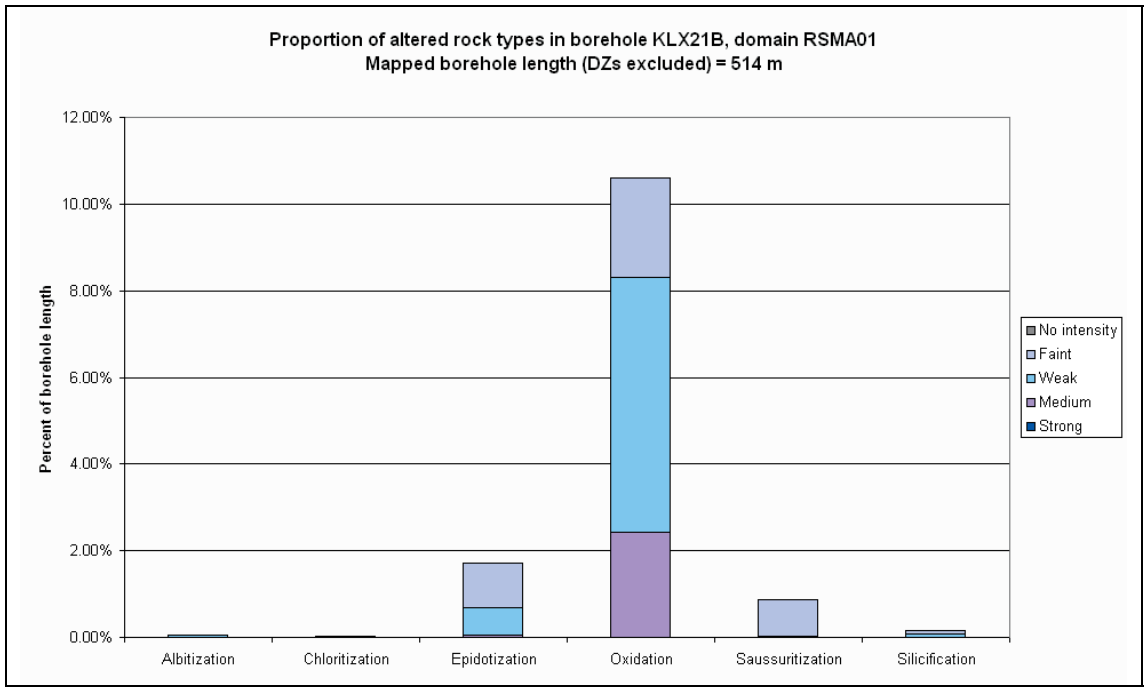
Proportion of altered rock types in borehole KLX21B, domain RSMA01
Mapped borehole length (DZs excluded) = 514 m
Percent of borehole length
12.00%
10.00%
8.00%
6.00%
4.00%
2.00%
0.00%
Albitization
Chloritization
Epidotization
Oxidation
Saussuritization
Silicification
No intensity
Faint
Weak
Medium
Strong

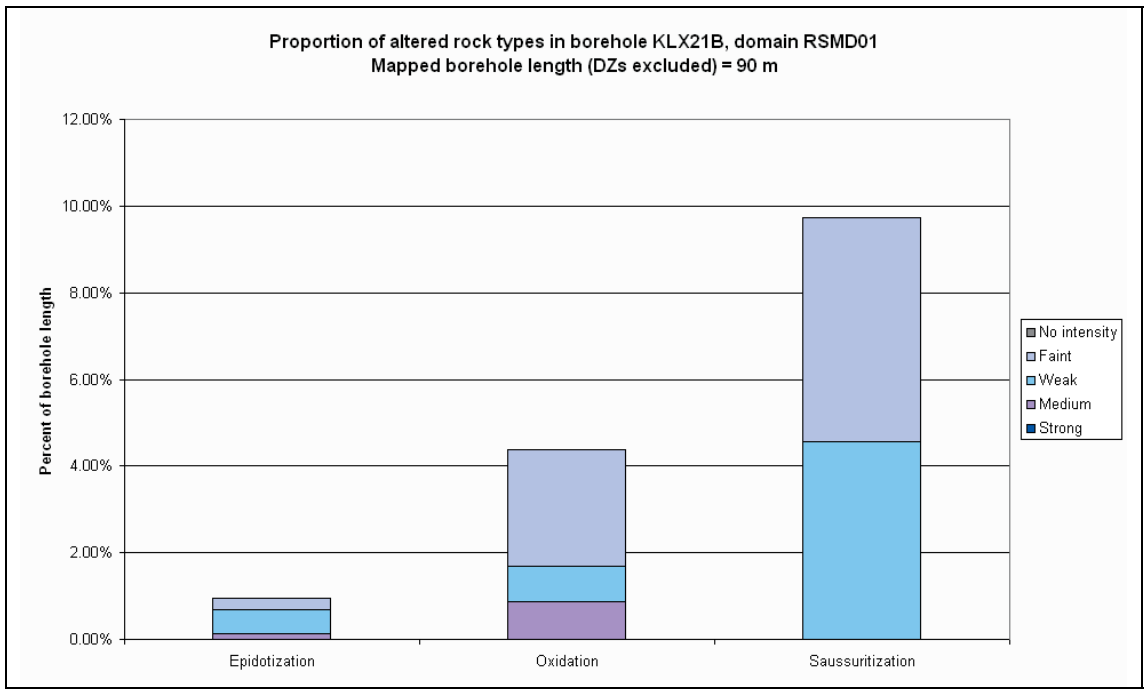
Proportion of altered rock types in borehole KLX21B, domain RSMD01
Mapped borehole length (DZs excluded) = 90 m
Percent of borehole length
12.00%
10.00%
8.00%
6.00%
4.00%
2.00%
0.00%
Epidotization
Oxidation
Saussuritization
No intensity
Faint
Weak
Medium
Strong

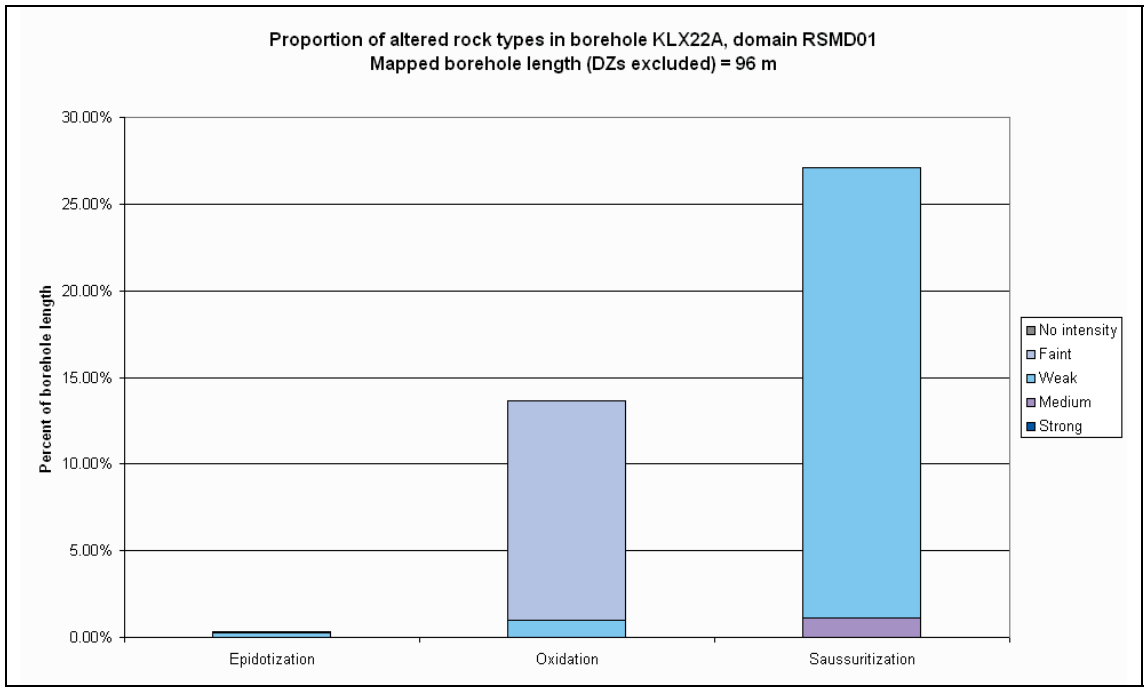
Proportion of altered rock types in borehole KLX22A, domain RSMD01
Mapped borehole length (DZs excluded) = 96 m
Percent of borehole length
30.00%
25.00%
20.00%
15.00%
10.00%
5.00%
0.00%
Epidotization
Oxidation
Saussuritization
No intensity
Faint
Weak
Medium
Strong

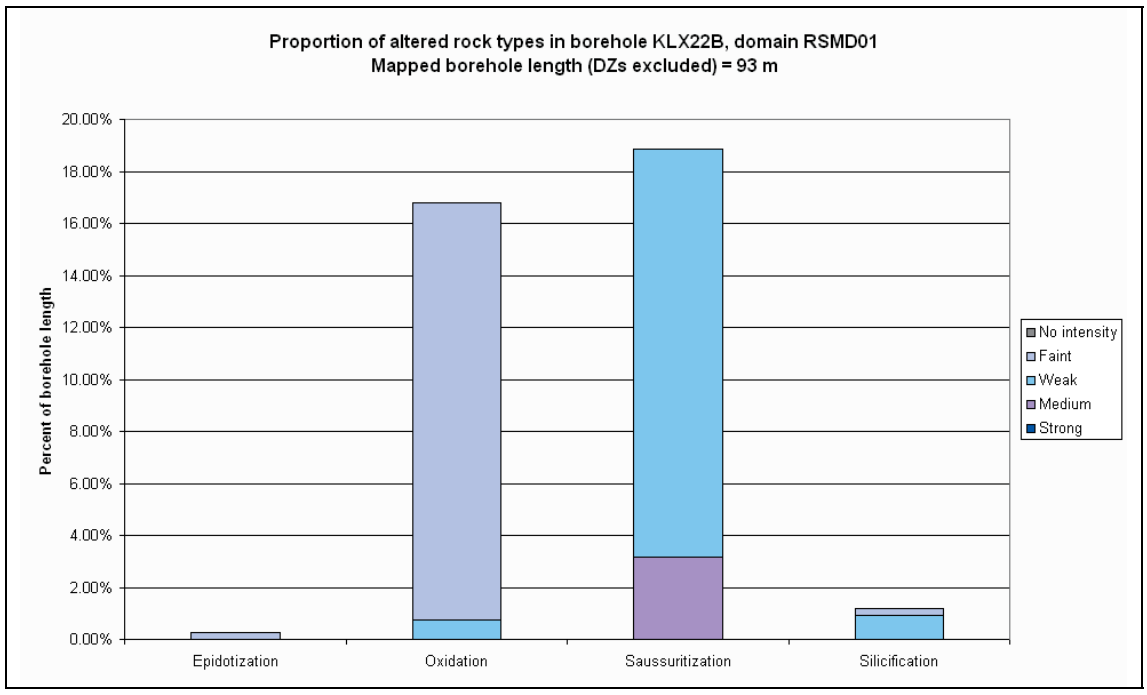
Proportion of altered rock types in borehole KLX22B, domain RSMD01
Mapped borehole length (DZs excluded) = 93 m
Percent of borehole length
20.00%
18.00%
16.00%
14.00%
12.00%
10.00%
8.00%
6.00%
4.00%
2.00%
0.00%
Epidotization
Oxidation
Saussuritization
Silicification
No intensity
Faint
Weak
Medium
Strong

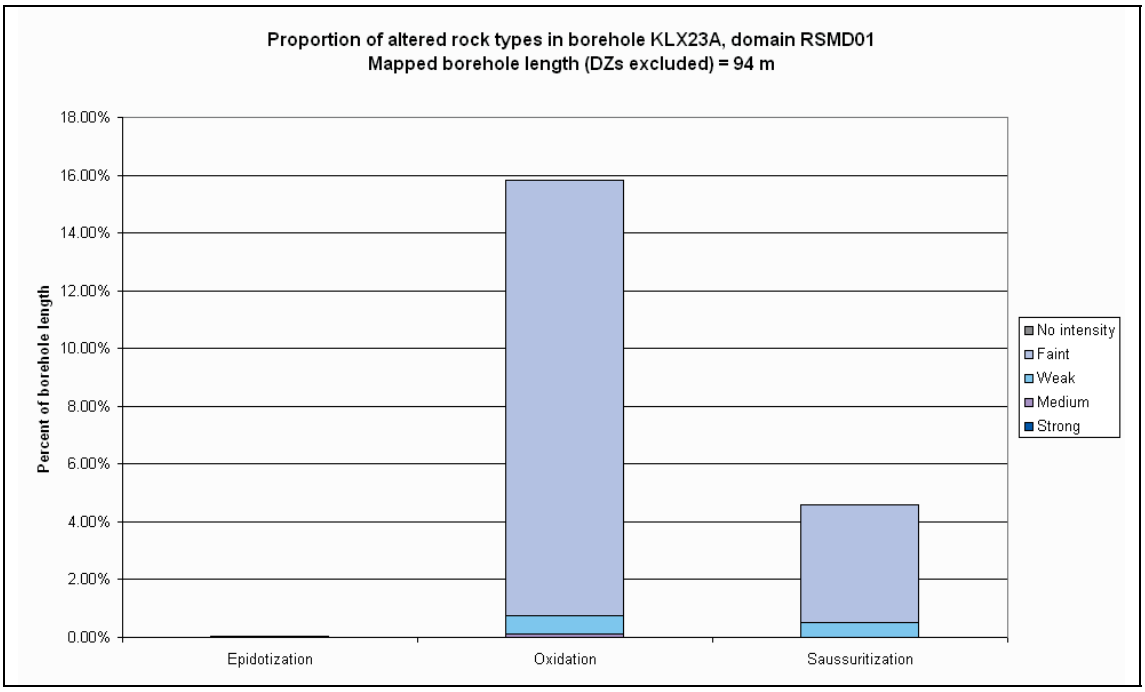
Proportion of altered rock types in borehole KLX23A, domain RSMD01
Mapped borehole length (DZs excluded) = 94 m
Percent of borehole length
18.00%
16.00%
14.00%
12.00%
10.00%
8.00%
6.00%
4.00%
2.00%
0.00%
Epidotization
Oxidation
Saussuritization
No intensity
Faint
Weak
Medium
Strong

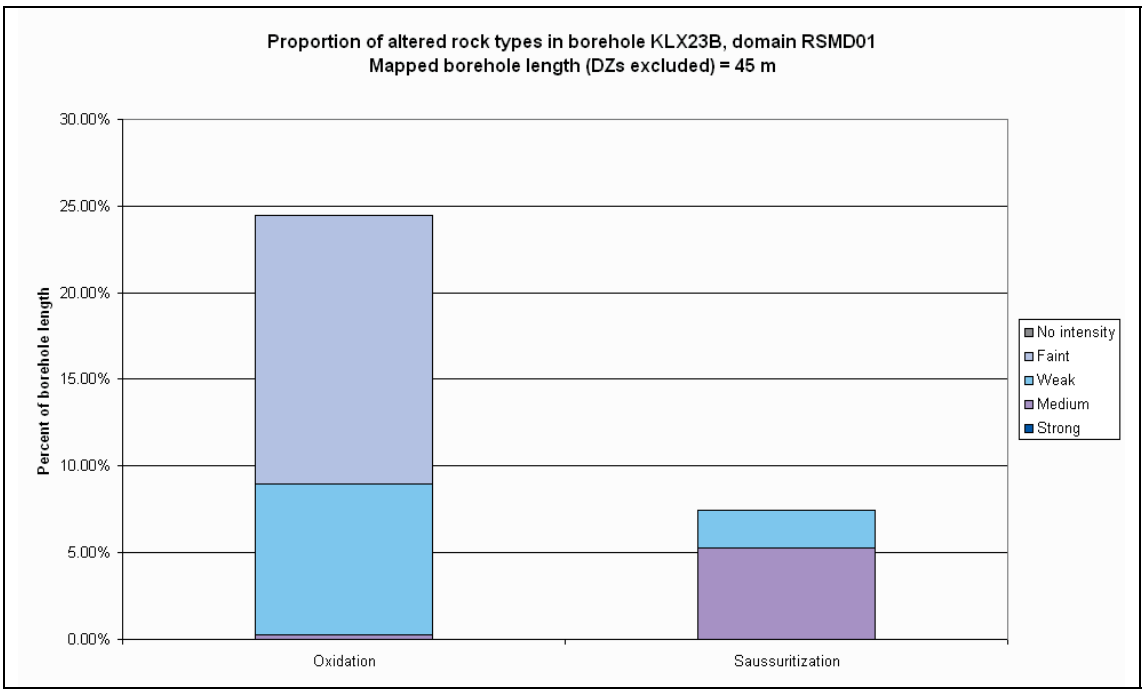
Proportion of altered rock types in borehole KLX23B, domain RSMD01
Mapped borehole length (DZs excluded) = 45 m
Percent of borehole length
30.00%
25.00%
20.00%
15.00%
10.00%
5.00%
0.00%
Oxidation
Saussuritization
No intensity
Faint
Weak
Medium
Strong

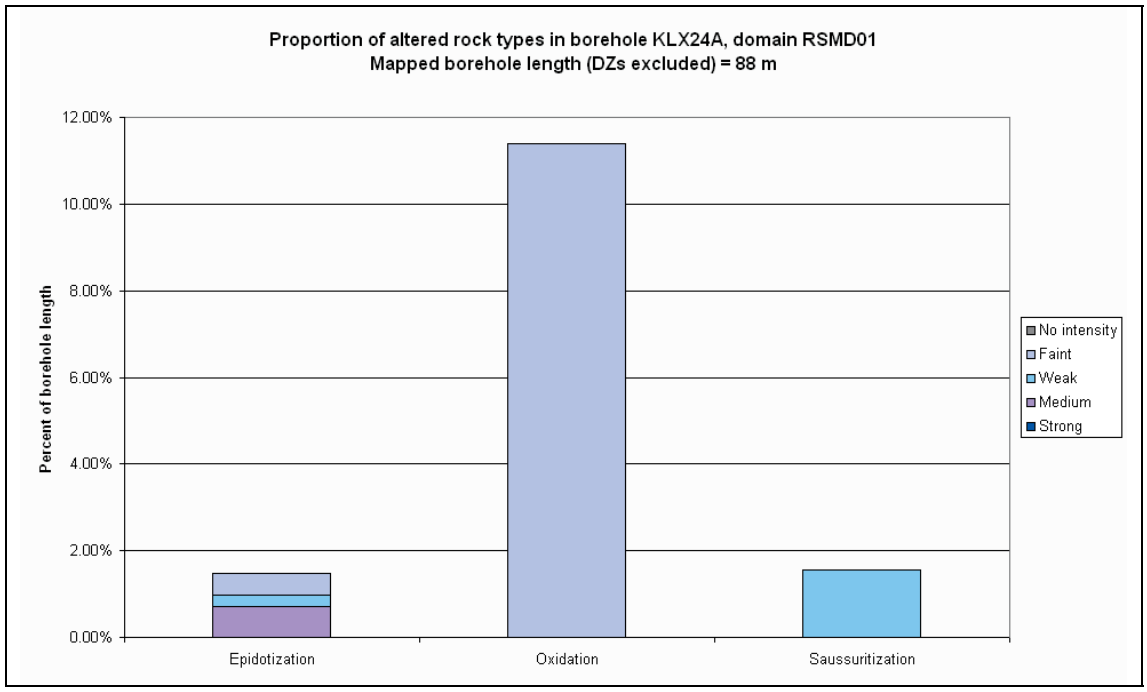
Proportion of altered rock types in borehole KLX24A, domain RSMD01
Mapped borehole length (DZs excluded) = 88 m
Percent of borehole length
12.00%
10.00%
8.00%
6.00%
4.00%
2.00%
0.00%
Epidotization
Oxidation
Saussuritization
No intensity
Faint
Weak
Medium
Strong

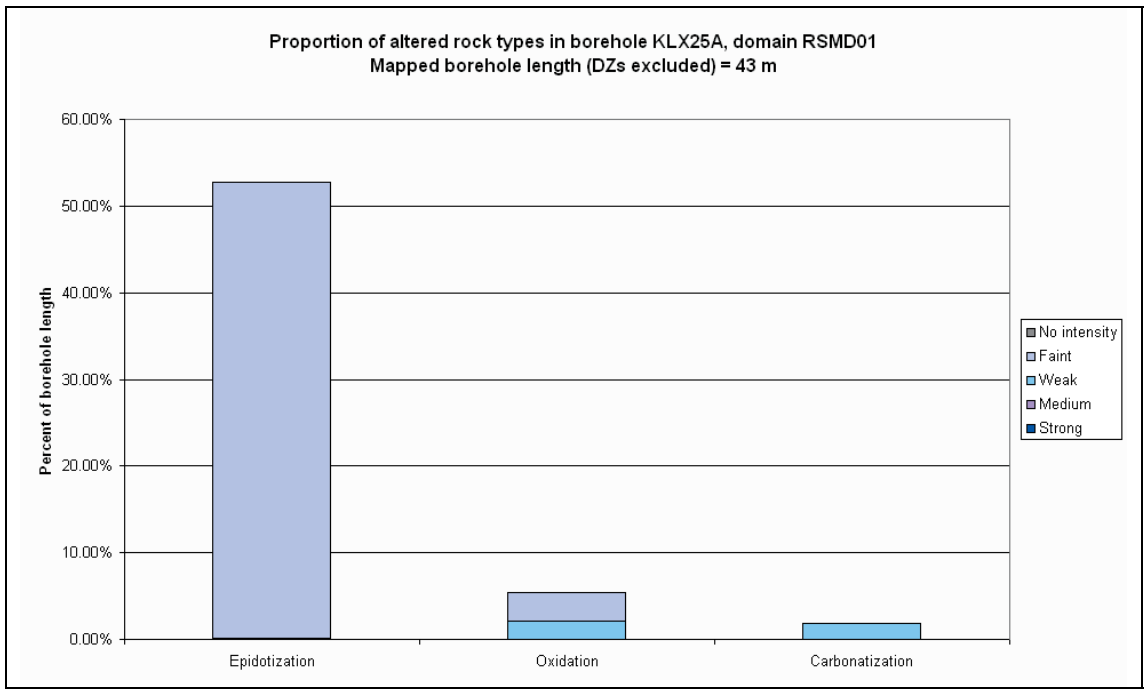
Proportion of altered rock types in borehole KLX25A, domain RSMD01
Mapped borehole length (DZs excluded) = 43 m
Percent of borehole length
60.00%
50.00%
40.00%
30.00%
20.00%
10.00%
0.00%
Epidotization
Oxidation
Carbonatization
No intensity
Faint
Weak
Medium
Strong

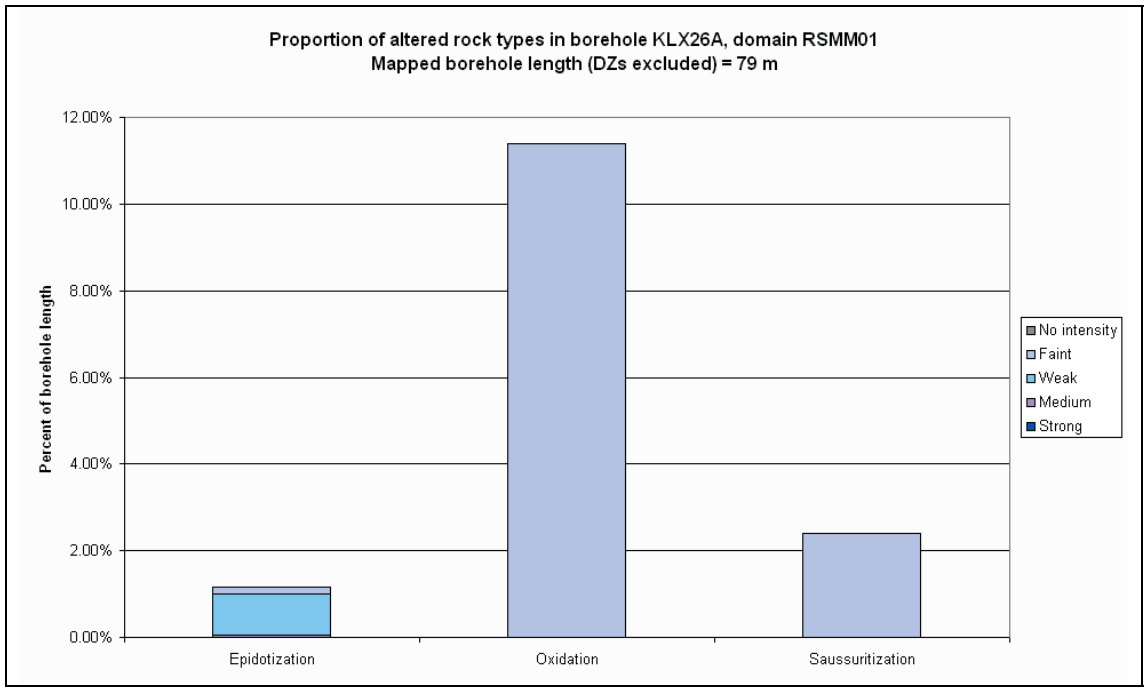
Proportion of altered rock types in borehole KLX26A, domain RSMM01
Mapped borehole length (DZs excluded) = 79 m
Percent of borehole length
12.00%
10.00%
8.00%
6.00%
4.00%
2.00%
0.00%
Epidotization
Oxidation
Saussuritization
No intensity
Faint
Weak
Medium
Strong

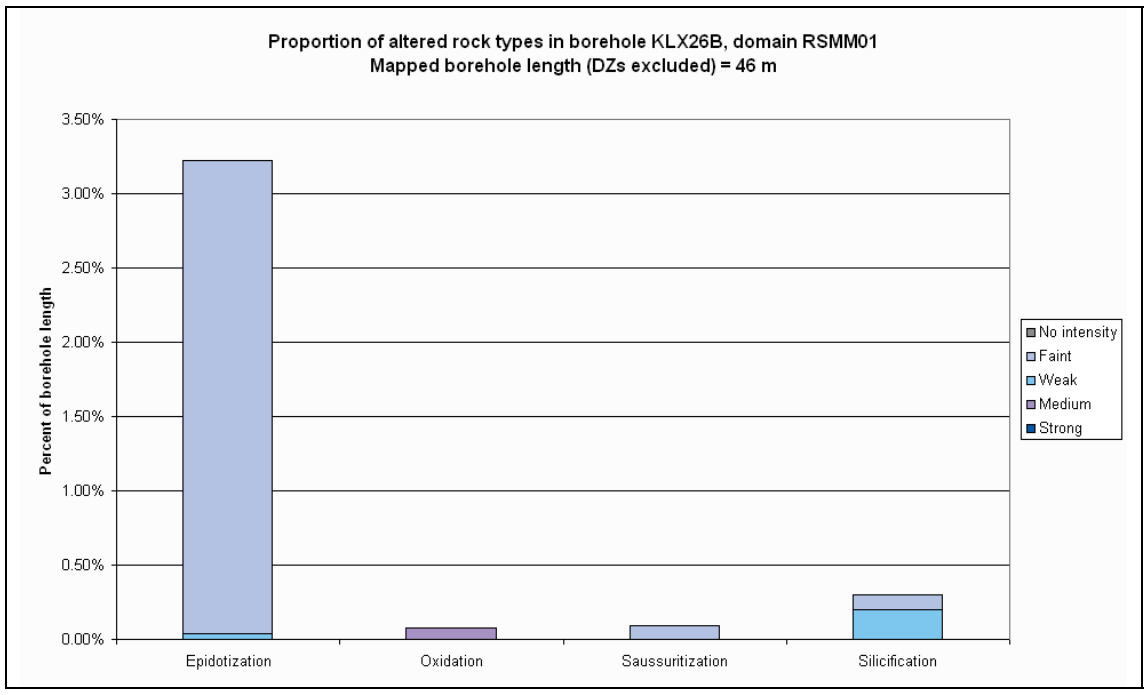
Proportion of altered rock types in borehole KLX26B, domain RSMM01
Mapped borehole length (DZs excluded) = 46 m
Percent of borehole length
3.50%
3.00%
2.50%
2.00%
1.50%
1.00%
0.50%
0.00%
Epidotization
Oxidation
Saussuritization
Silicification
No intensity
Faint
Weak
Medium
Strong

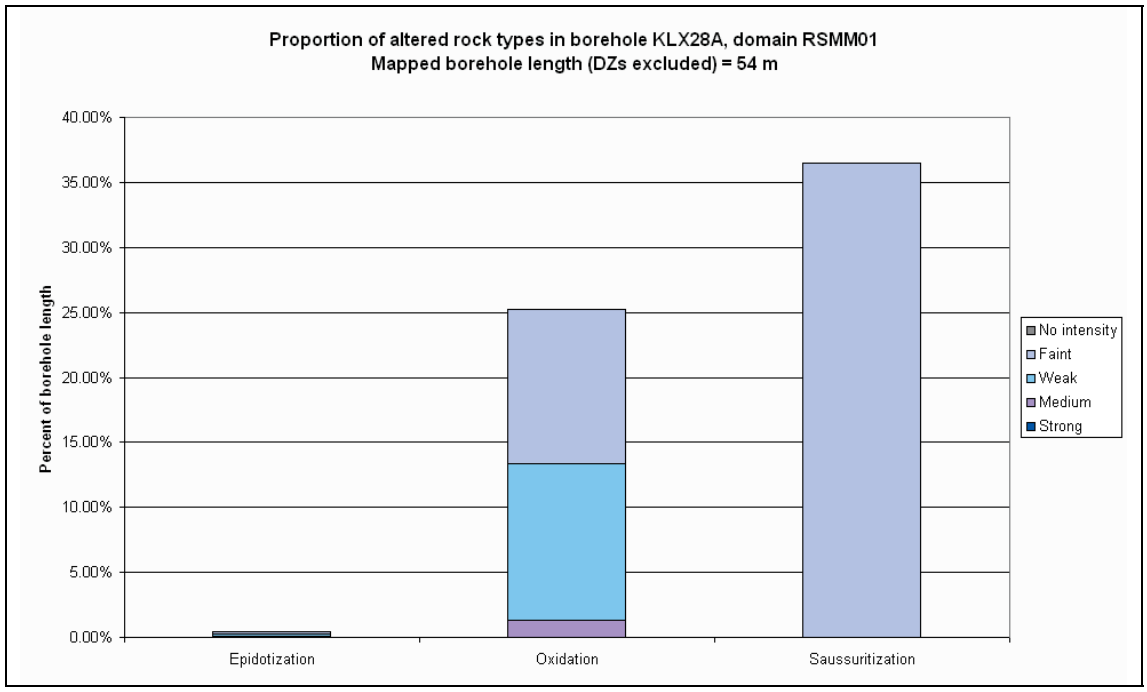
Proportion of altered rock types in borehole KLX28A, domain RSMM01
Mapped borehole length (DZs excluded) = 54 m
Percent of borehole length
40.00%
35.00%
30.00%
25.00%
20.00%
15.00%
10.00%
5.00%
0.00%
Epidotization
Oxidation
Saussuritization
No intensity
Faint
Weak
Medium
Strong

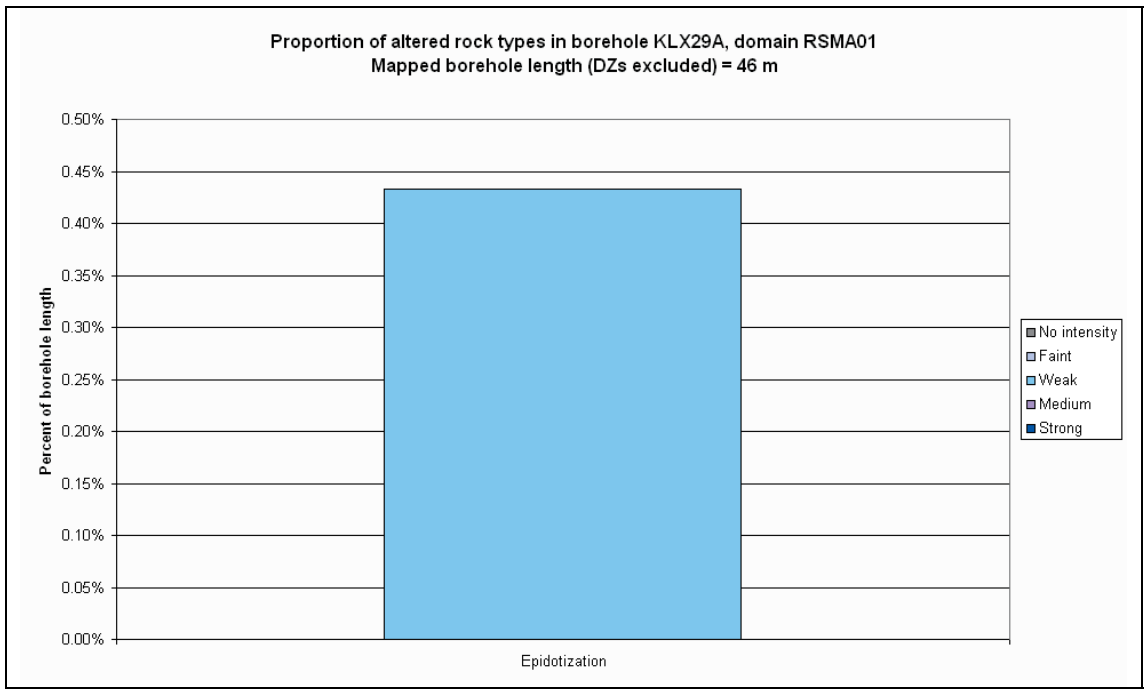
Proportion of altered rock types in borehole KLX29A, domain RSMA01
Mapped borehole length (DZs excluded) = 46 m
Percent of borehole length
0.50%
0.45%
0.40%
0.35%
0.30%
0.25%
0.20%
0.15%
0.10%
0.05%
0.00%
Epidotization
No intensity
Faint
Weak
Medium
Strong

Type and degree of alteration outside deformation zones on an overall rock domain basis

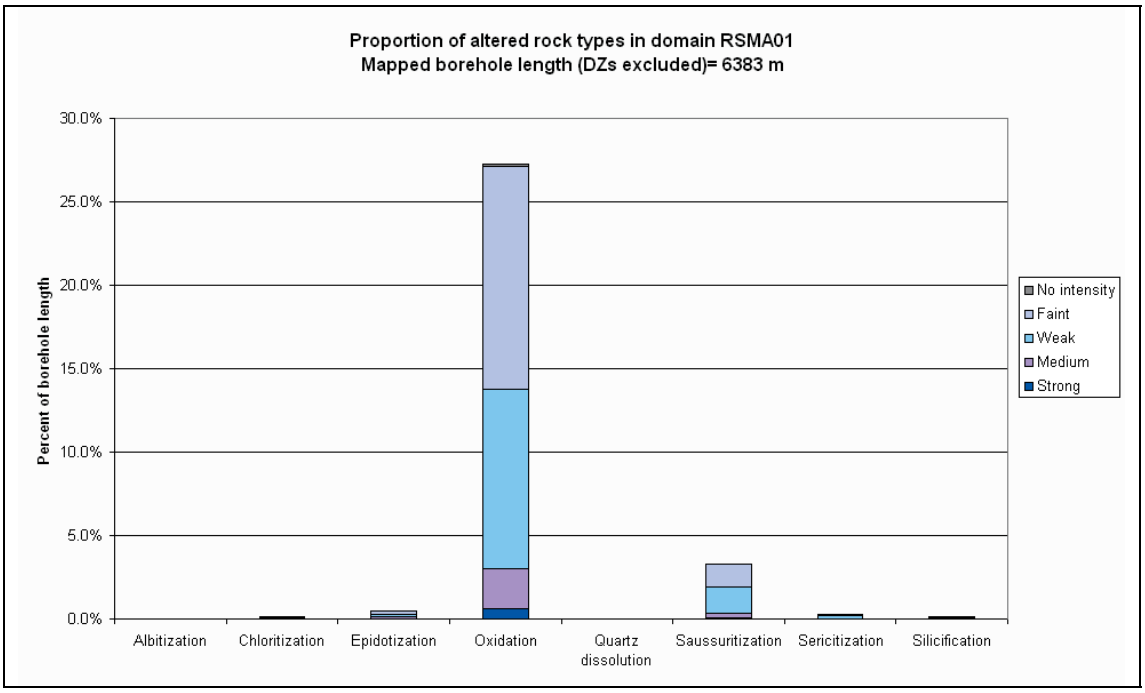

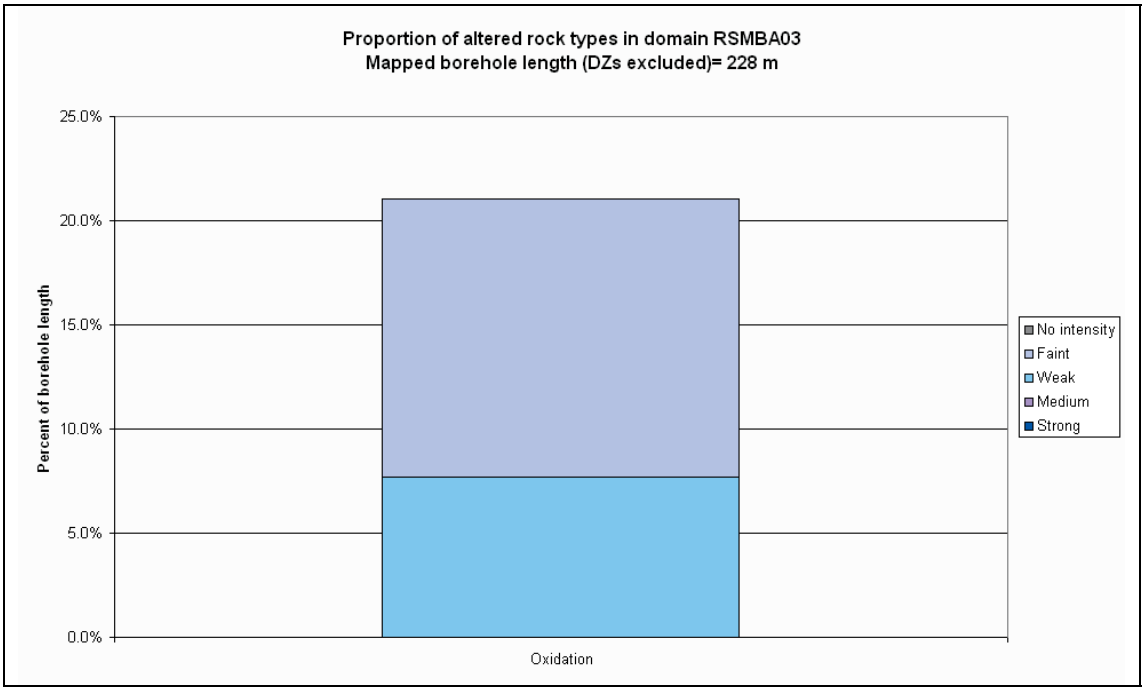

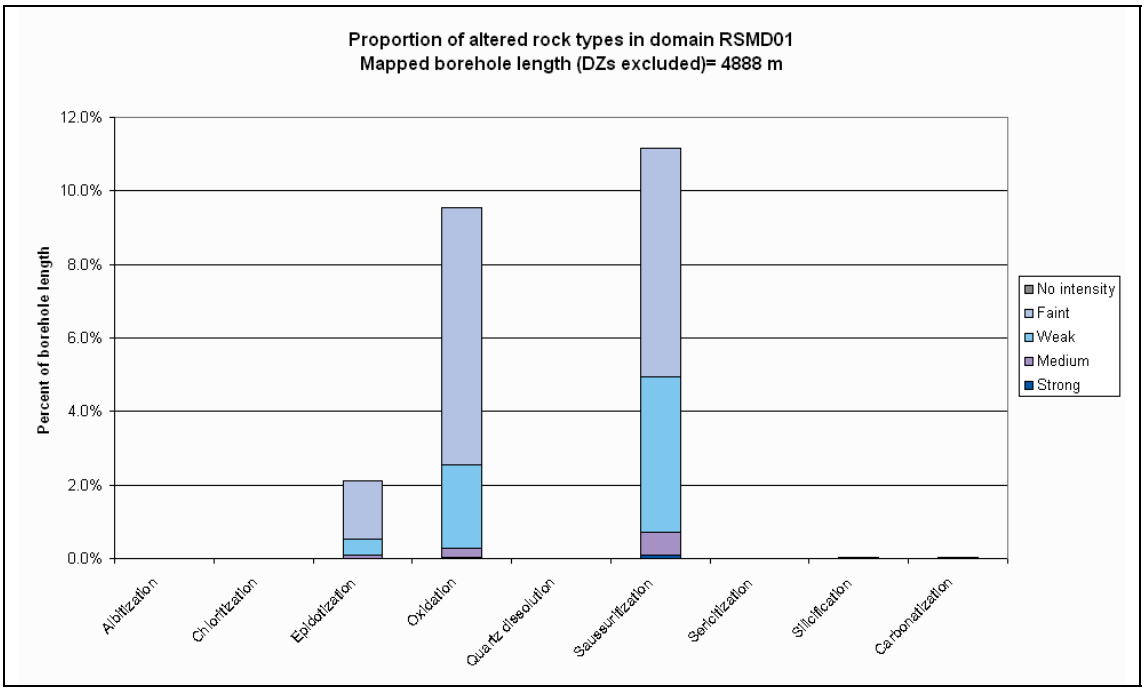
Proportion of altered rock types in domain RSMD01
Mapped borehole length (DZs excluded)= 4888 m
Percent of borehole length
12.0%
10.0%
8.0%
6.0%
4.0%
2.0%
0.0%
Albitization
Chloritization
Epidotization
Oxidation
Quartz dissolution
Saussuritization
Sericitization
Silicification
Carbonatization
No intensity
Faint
Weak
Medium
Strong

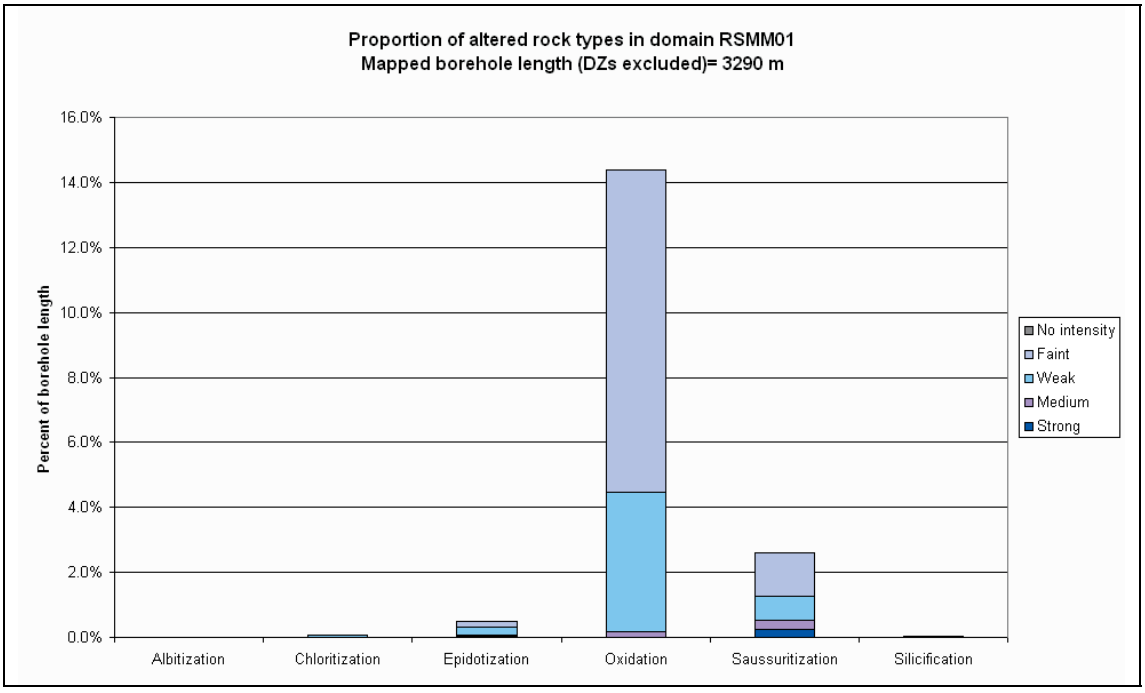
Proportion of altered rock types in domain RSMM01
Mapped borehole length (DZs excluded)= 3290 m
Percent of borehole length
16.0%
14.0%
12.0%
10.0%
8.0%
6.0%
4.0%
2.0%
0.0%
Albitization
Chloritization
Epidotization
Oxidation
Saussuritization
Silicification
No intensity
Faint
Weak
Medium
Strong

Appendix 8

Orientation of ductile structures on a borehole by borehole basis, on a rock domain basis in each borehole, on an overall rock domain basis and from combined surface and borehole data on an overall rock domain basis in the local model volume

Data from Sicada: p_rock_struct_feat.xls and outcrop data in Sicada_07_323 and Sicada_07_376.

Procedure: The orientation of the ductile structures foliation, mylonitic, ductile shear zone and brittle-ductile shear zone were extracted from Sicada and grouped in two categories: foliation is treated separately and mylonitic, ductile shear zone and brittle-ductile shear zone are grouped together. The orientation of the ductile structures is plotted as poles in an equal area stereographic projection on a borehole by borehole basis, on a rock domain basis in each borehole and on an overall rock domain basis. Contoured diagrams for the combined surface (S) and borehole (BH) data on a rock domain basis are also made. No Terzaghi correction has been applied to the data. The stereographic plots are presented both with and without inclusion of deformation zones from the extended single-hole interpretation.

The Vollmer fabric index (VFI) was calculated for the data from each borehole, in order to evaluate the nature of the distribution of orientations for studied features /Munier 2004/. VFI is based on an eigenvector analysis of poles, and the eigenvalues are used to calculate three indices: cluster (P), girdle (G) or uniform distribution (R). The VFI was used to determine whether it is suitable to represent the data set by:

• A mean pole and its dispersion (trend, plunge, and Fisher κ): $P > \max(G, R)$.

• A great circle and its pole (trend and plunge): $G > \max(P, R)$.

• Neither of the above (only visualize data as poles): $R > \max(P, G)$.

The stereographic projections can be viewed on the CD-Rom attached to this report. The results of the orientation analysis are discussed in Section 3.5.2.

Reference

Munier R, 2004. Statistical analysis of fracture data adapted for modelling Discrete Fracture Networks – Version 2. SKB R-04-66, Svensk Kärnbränslehantering AB.

Appendix 9

Comparison of orientation of ductile structures and orientation of subordinate rock types on a borehole by borehole basis and on an overall rock domain basis

In the stereoplots with Fisher contouring below a comparison between the orientation of the foliation and ductile and brittle-ductile shear zones and the orientation of subordinate rock types is presented for each of the longer cored boreholes at Laxemar, and on an overall rock domain basis for RSMA01, RSMM01 and RSMD01. KLX01, KLX02 and KLX27A are not included.

KLX03

Ductile and brittle-ductile shear zones

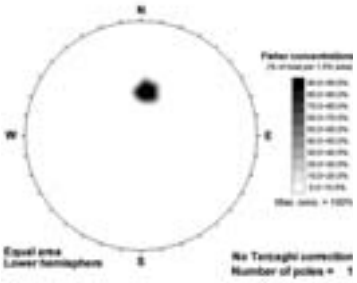

Foliation

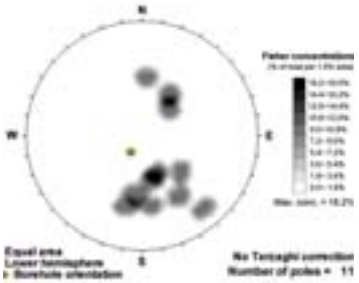

Fine-grained granite

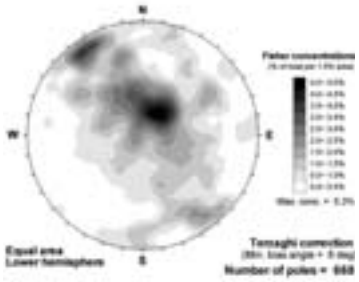

Fine-grained diorite-gabbro

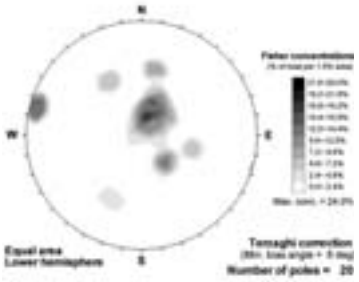

Pegmatite

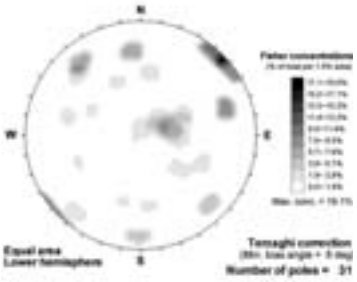

KLX04

Ductile and brittle-ductile shear zones **Foliation**

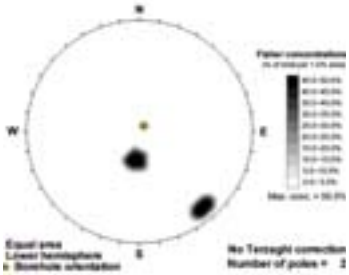
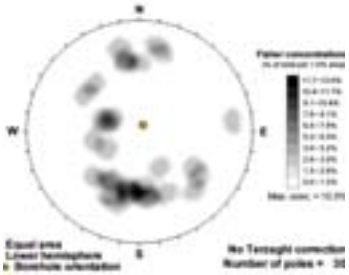

Fine-grained granite **Fine-grained diorite-gabbro** **Pegmatite**

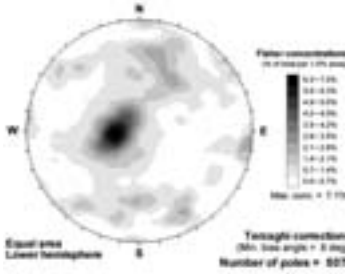
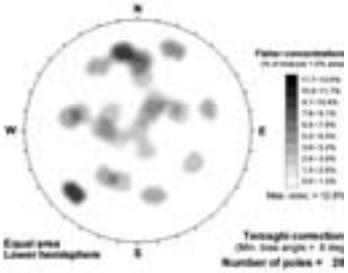
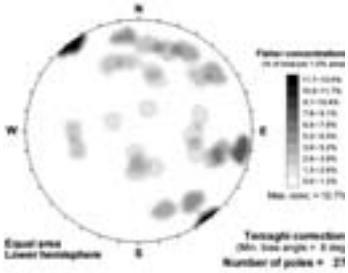

KLX05

Ductile and brittle-ductile shear zones **Foliation**

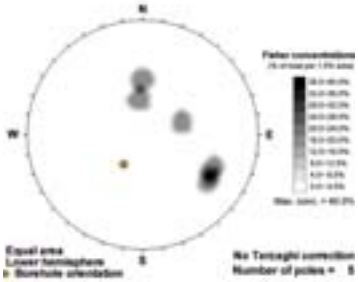
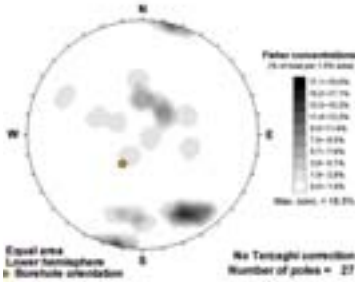

Fine-grained granite **Fine-grained diorite-gabbro** **Pegmatite**

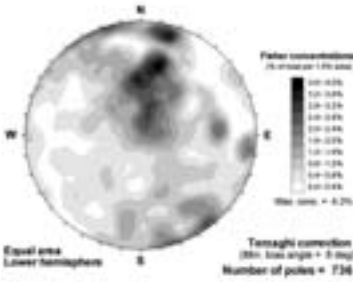
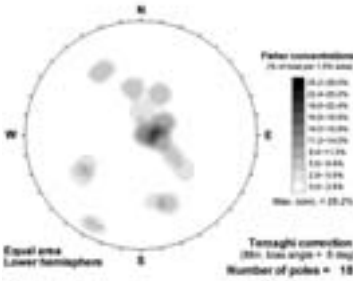
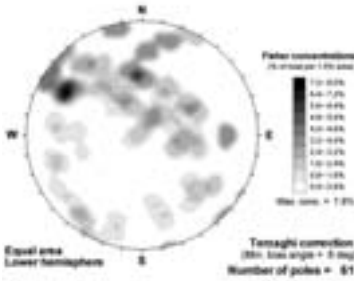

KLX06

Ductile and brittle-ductile shear zones **Foliation**

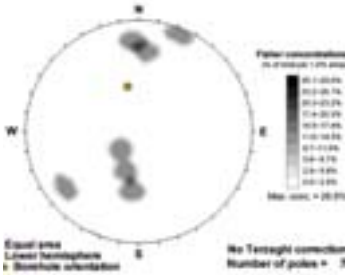
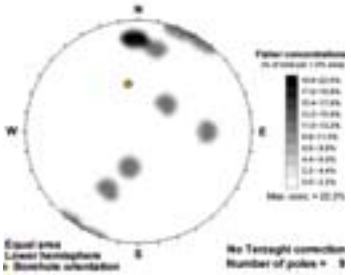

Fine-grained granite **Fine-grained diorite-gabbro** **Pegmatite**

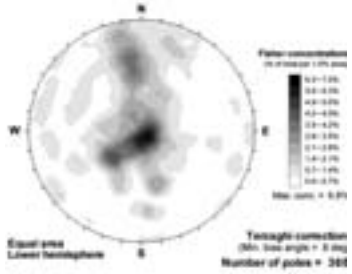
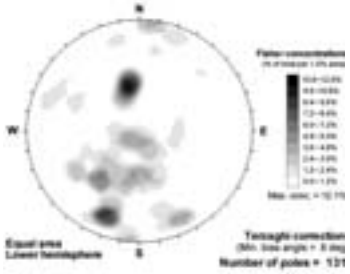
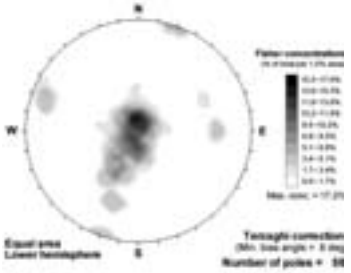

KLX07A

Ductile and brittle-ductile shear zones **Foliation**

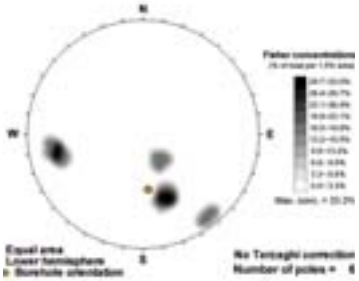
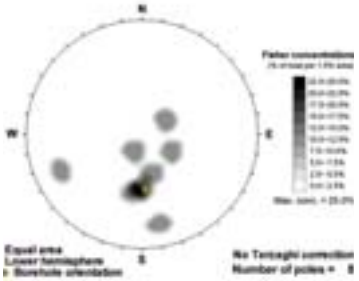

Fine-grained granite **Fine-grained diorite-gabbro** **Pegmatite**

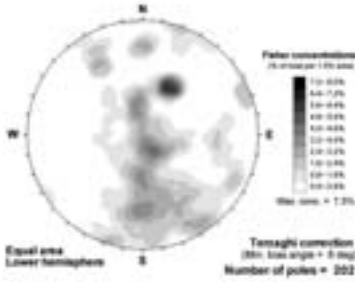
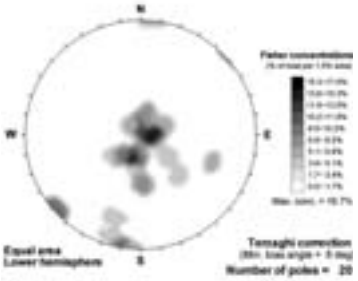
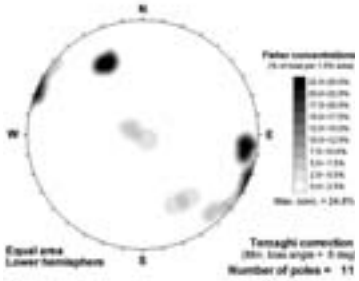

KLX07B

Ductile and brittle-ductile shear zones **Foliation**

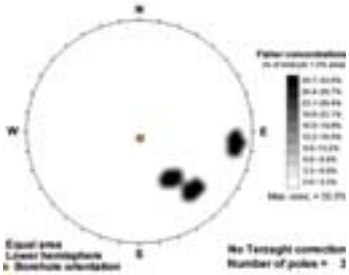
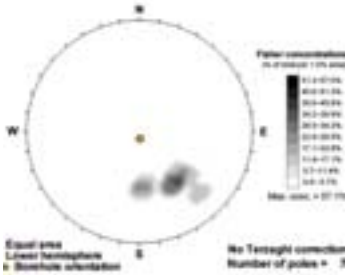

Fine-grained granite **Fine-grained diorite-gabbro** **Pegmatite**

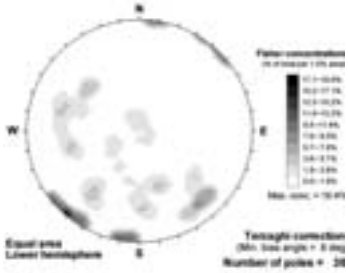
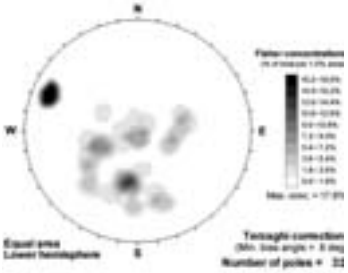
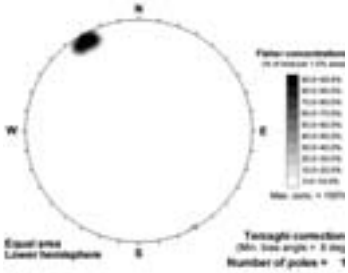

KLX08

Ductile and brittle-ductile shear zones **Foliation**

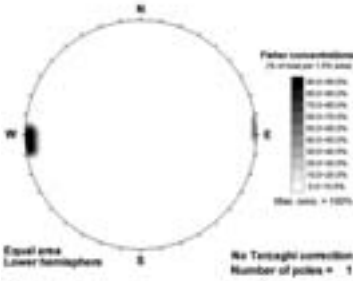
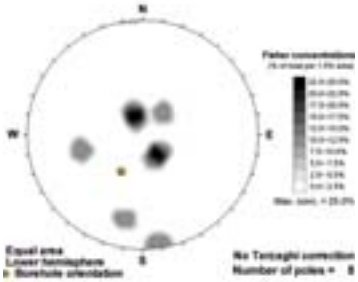

Fine-grained granite **Fine-grained diorite-gabbro** **Pegmatite**

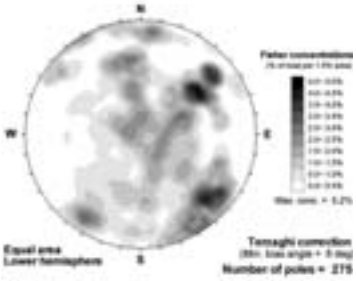
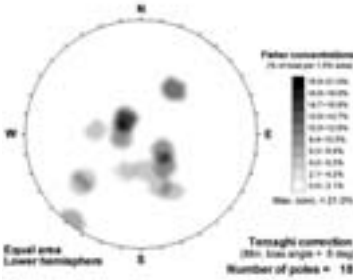
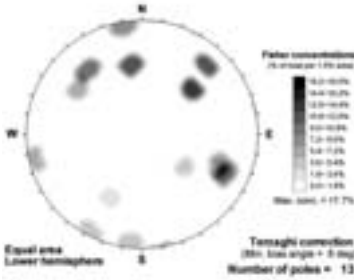

KLX09

Ductile and brittle-ductile shear zones

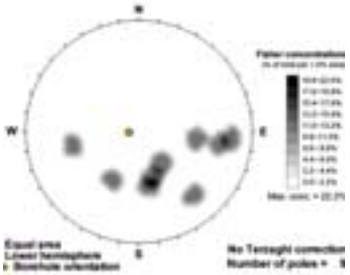

Foliation

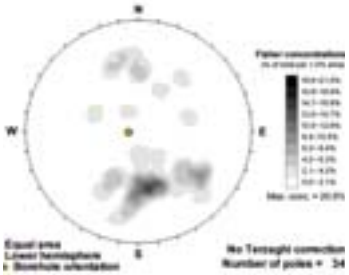

Fine-grained granite

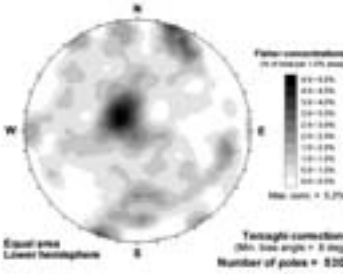

Fine-grained diorite-gabbro

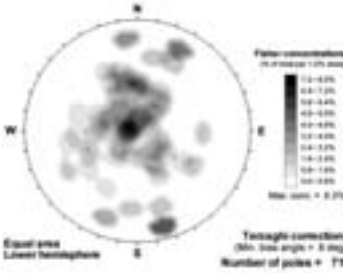

Pegmatite

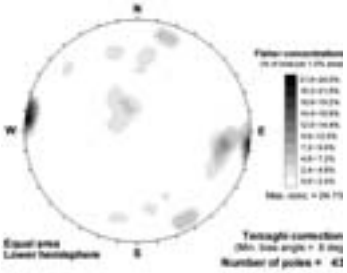

KLX10

Ductile and brittle-ductile shear zones

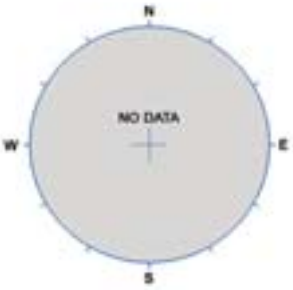

Foliation

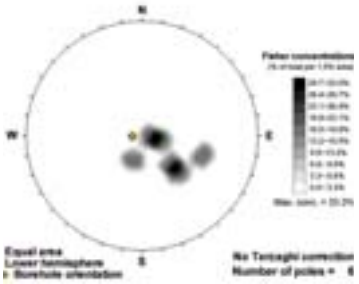

Fine-grained granite

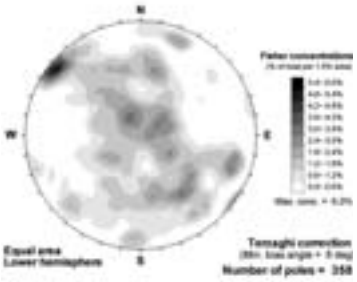

Fine-grained diorite-gabbro

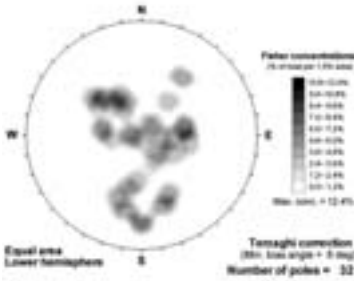

Pegmatite

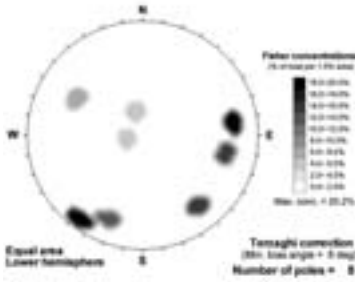

KLX11A

Ductile and brittle-ductile shear zones

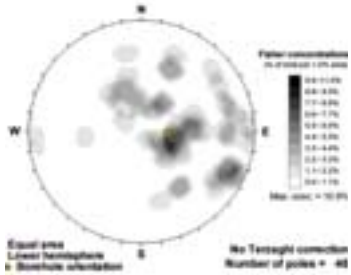

Foliation

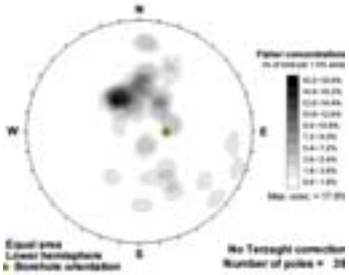

Fine-grained granite

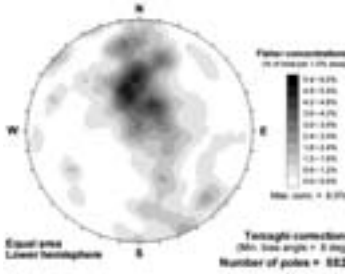

Fine-grained diorite-gabbro

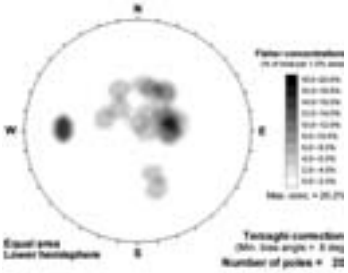

Pegmatite

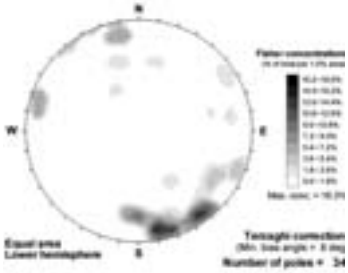

KLX12A

Ductile and brittle-ductile shear zones

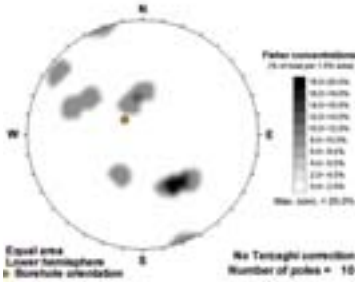

Foliation

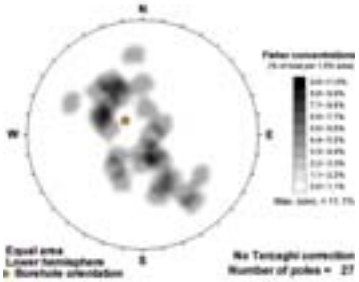

Fine-grained granite

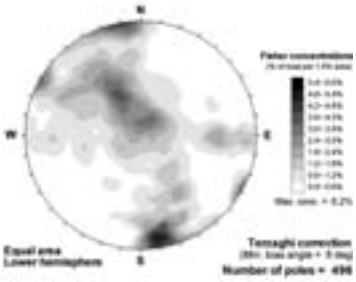

Fine-grained diorite-gabbro

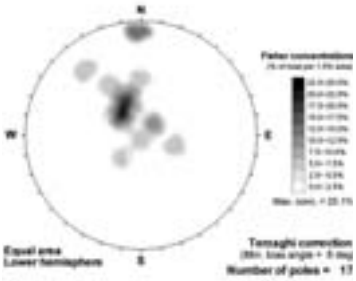

Pegmatite

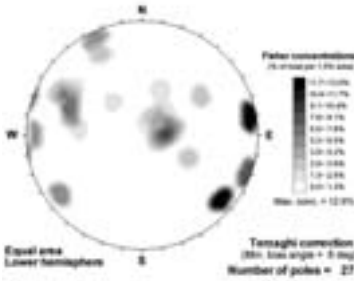

KLX13A

Ductile and brittle-ductile shear zones

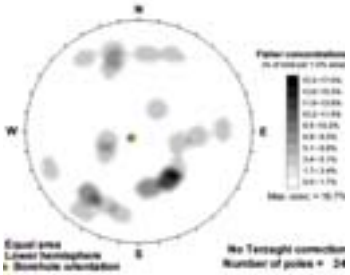

Foliation

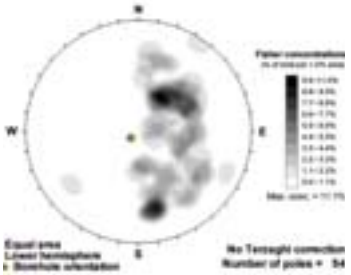

Fine-grained granite

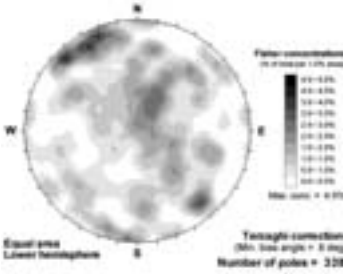

Fine-grained diorite-gabbro

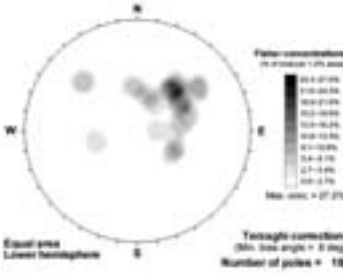

Pegmatite

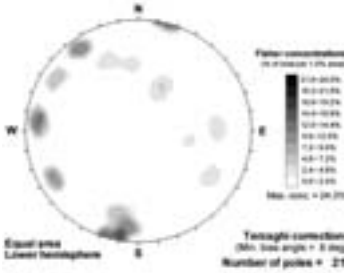

KLX14A

Ductile and brittle-ductile shear zones

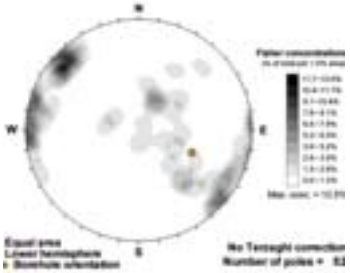

Foliation

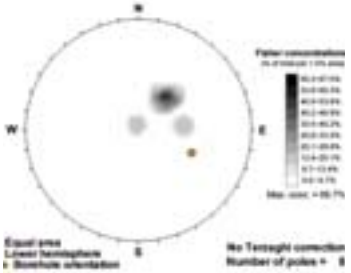

Fine-grained granite

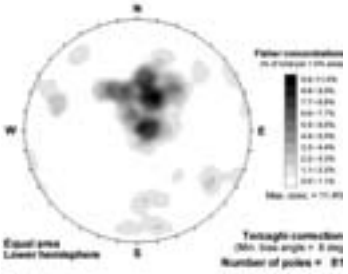

Fine-grained diorite-gabbro

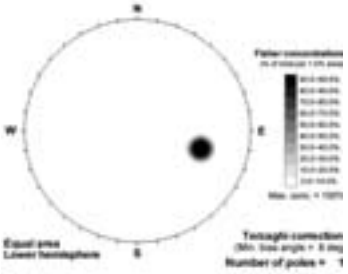

Pegmatite

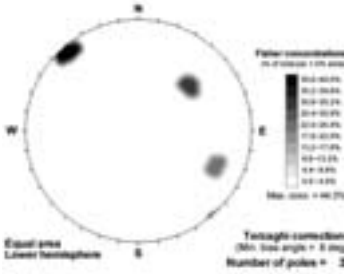

KLX15A

Ductile and brittle-ductile shear zones

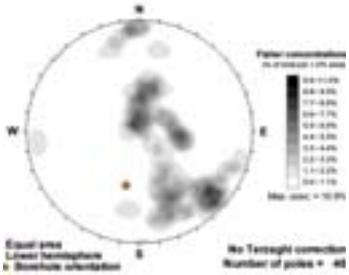

Foliation

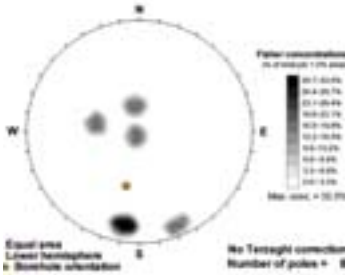

Fine-grained granite

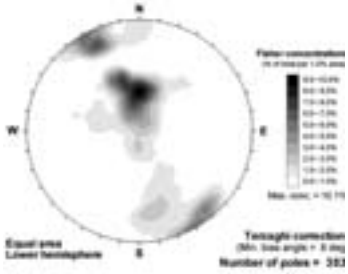

Fine-grained diorite-gabbro

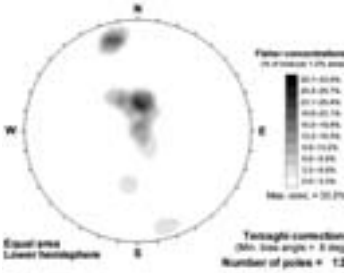

Pegmatite

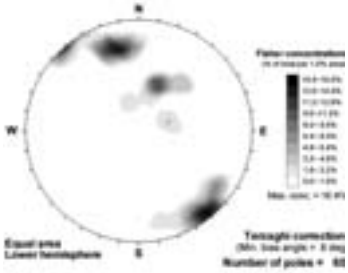

KLX16A

Ductile and brittle-ductile shear zones

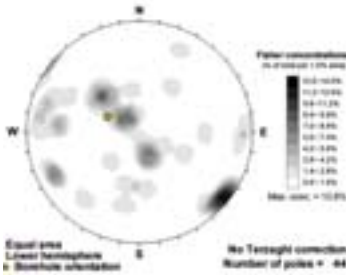

Foliation

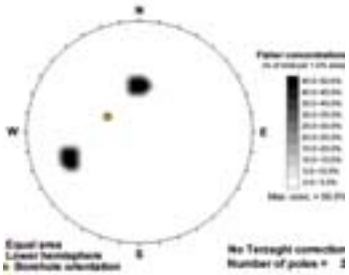

Fine-grained granite

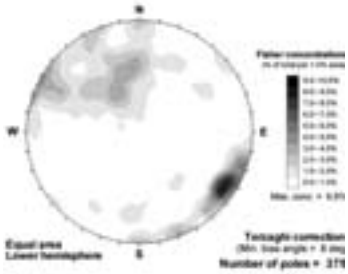

Fine-grained diorite-gabbro

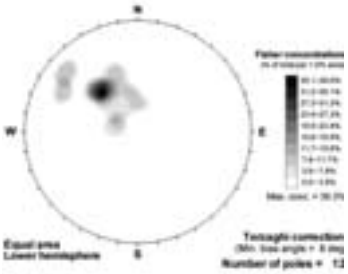

Pegmatite

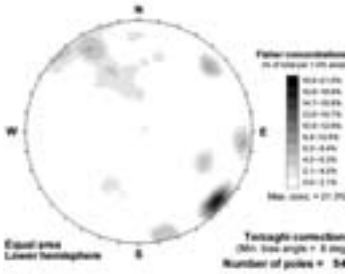

KLX17A

Ductile and brittle-ductile shear zones

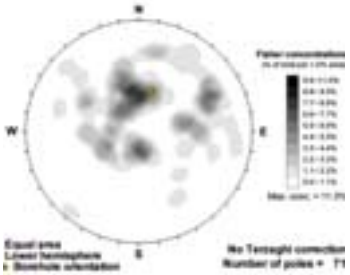

Foliation

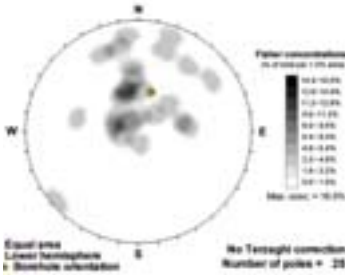

Fine-grained granite

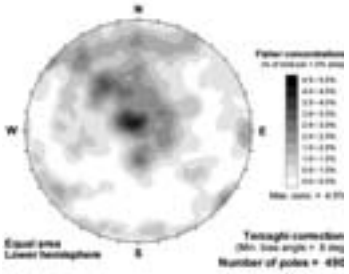

Fine-grained diorite-gabbro

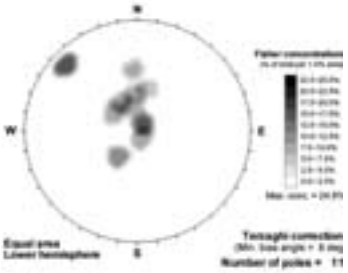

Pegmatite

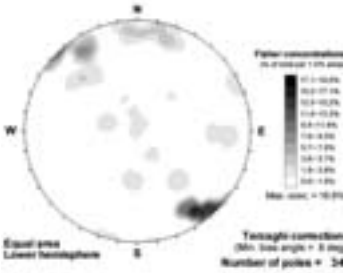

KLX18A

Ductile and brittle-ductile shear zones

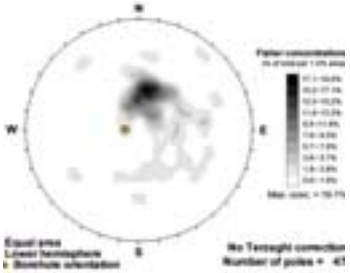

Foliation

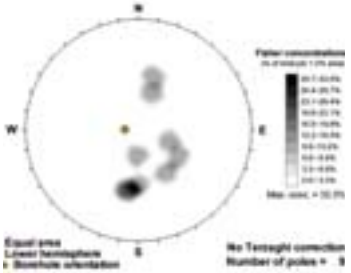

Fine-grained granite

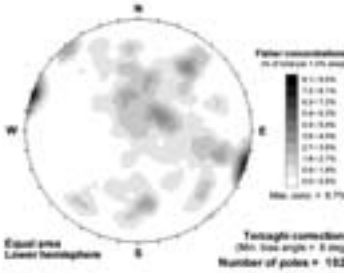

Fine-grained diorite-gabbro

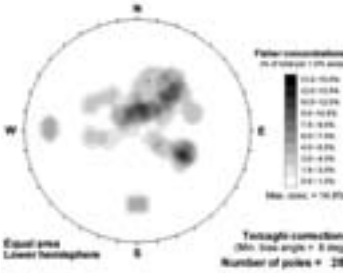

Pegmatite

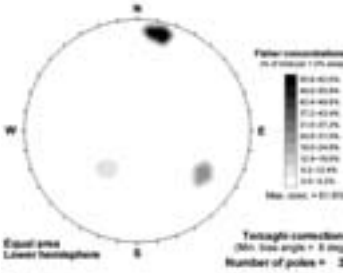

KLX19A

Ductile and brittle-ductile shear zones

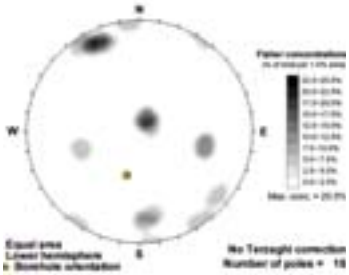

Foliation

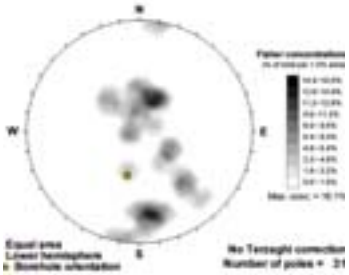

Fine-grained granite

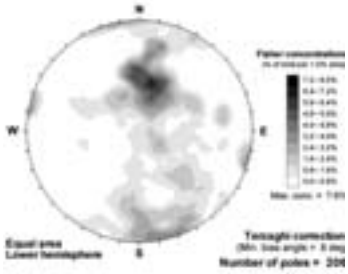

Fine-grained diorite-gabbro

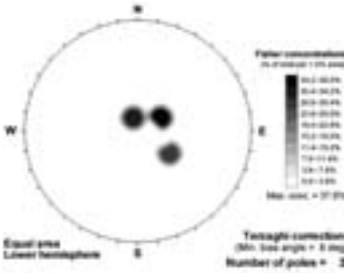

Pegmatite

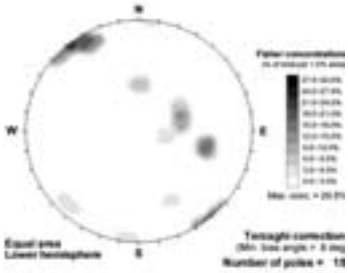

KLX20A

Ductile and brittle-ductile shear zones

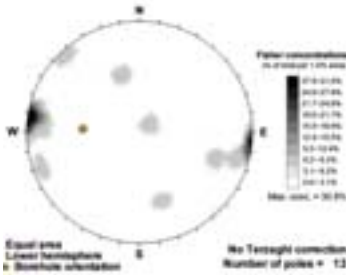

Foliation

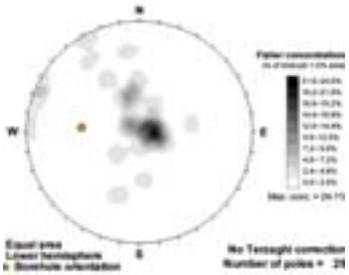

Fine-grained granite

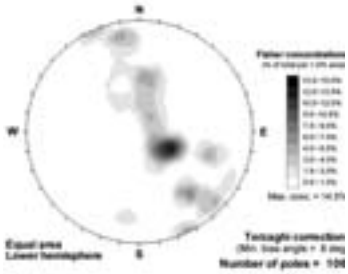

Fine-grained diorite-gabbro

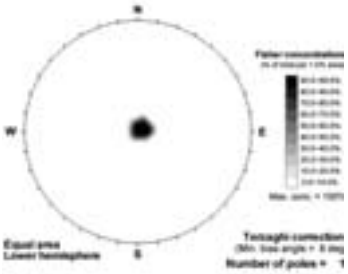

Pegmatite

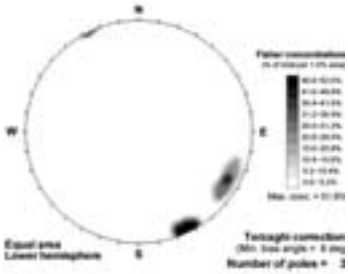

KLX21B

Ductile and brittle-ductile shear zones

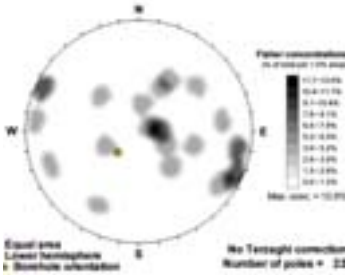

Foliation

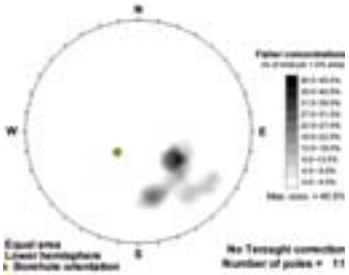

Fine-grained granite

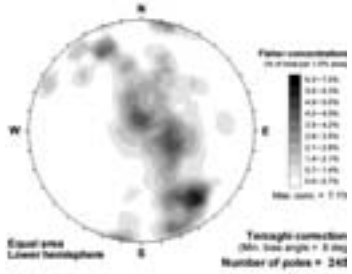

Fine-grained diorite-gabbro

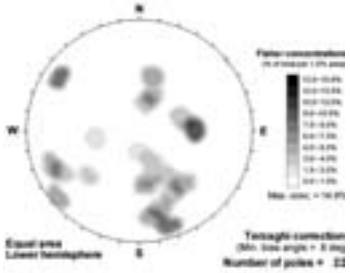

Pegmatite

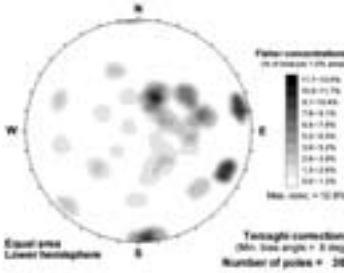

Comparison of orientation of foliation and orientation of subordinate rock types on an overall rock domain basis

RSMA01 foliation	**RSMA01 fine-grained granite**
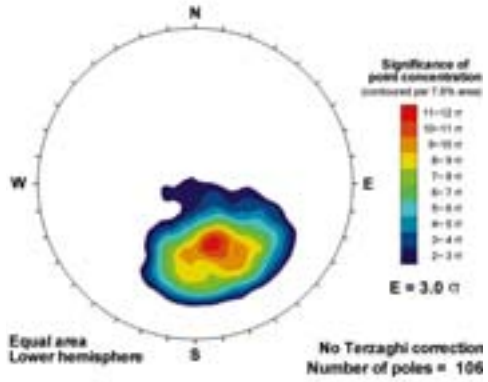	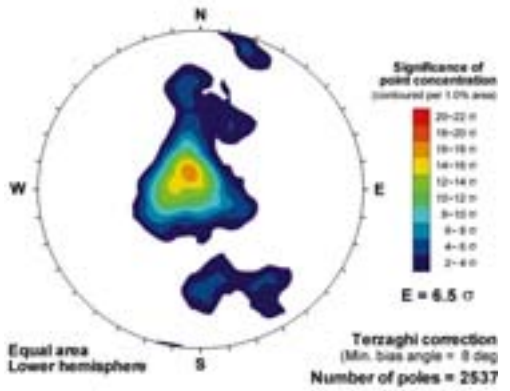
RSMM01 foliation	**RSMM01 fine-grained granite**
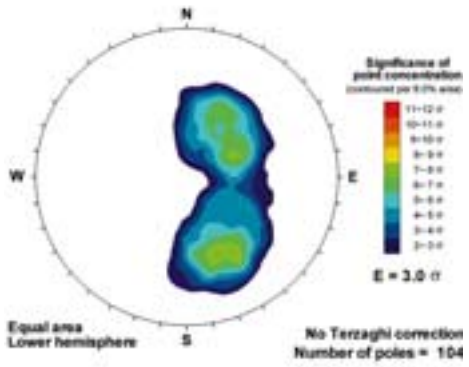	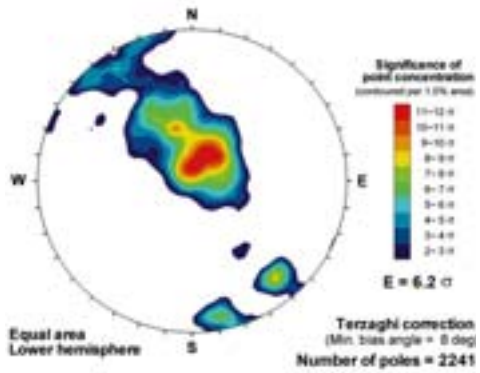
RSMD01 foliation	**RSMD01 fine-grained granite**
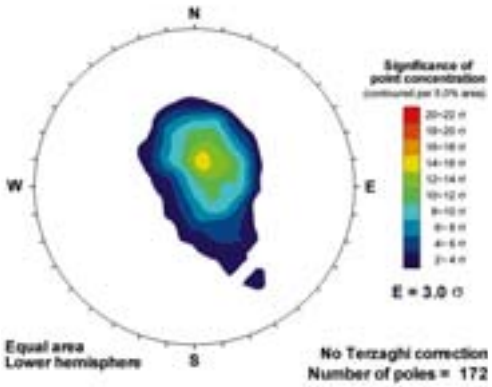	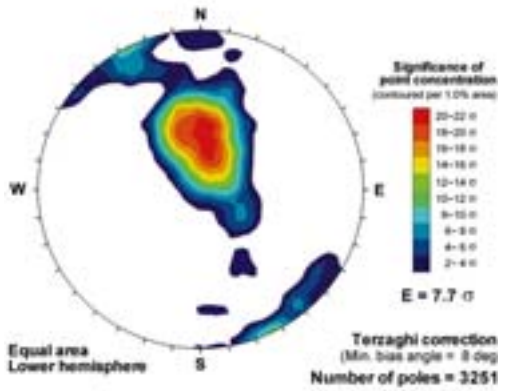

RSMA01 foliation	**RSMA01 fine-grained diorite-gabbro**
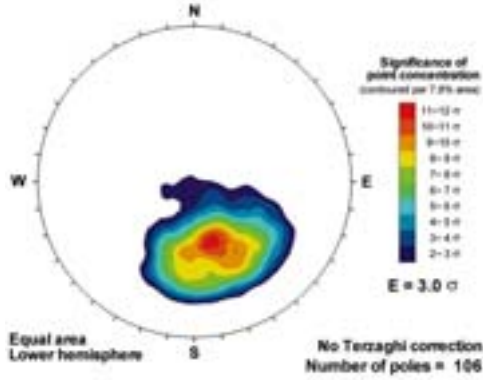	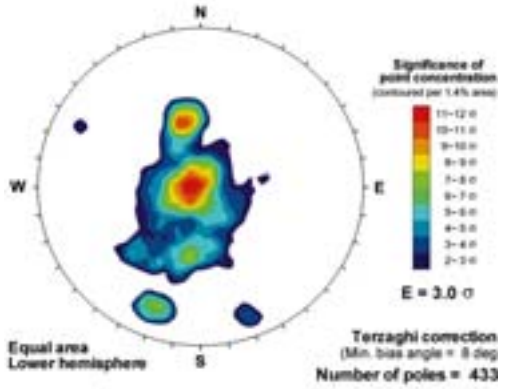
RSMM01 foliation	**RSMM01 fine-grained diorite-gabbro**
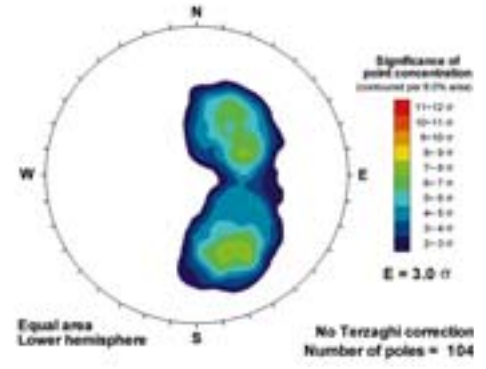	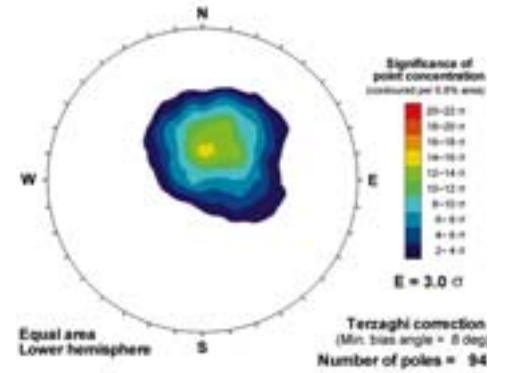
RSMD01 foliation	**RSMD01 fine-grained diorite-gabbro**
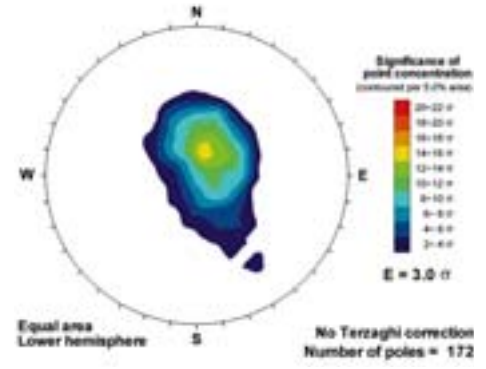	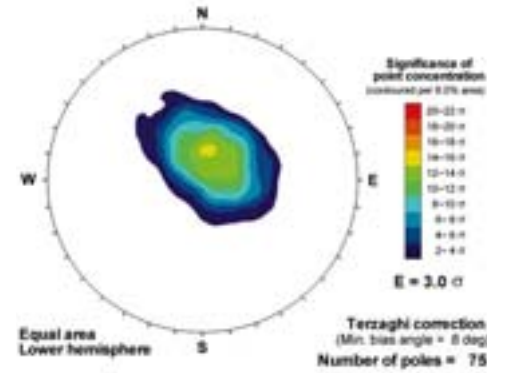

RSMA01 foliation

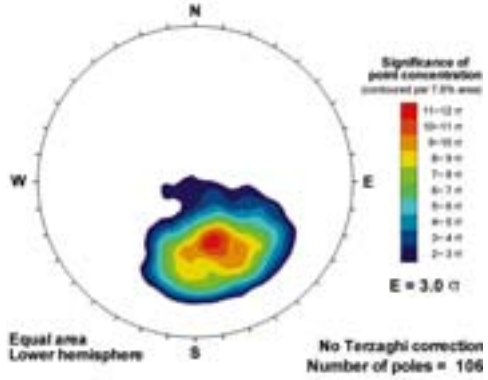

RSMA01 pegmatite

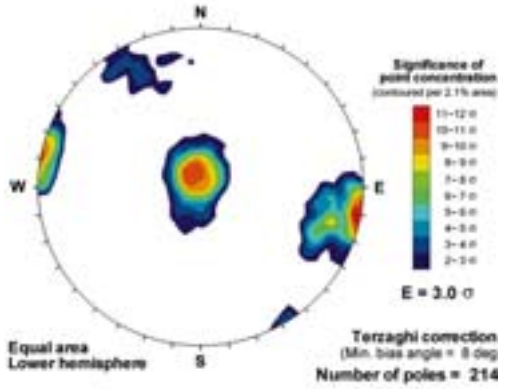

RSMM01 foliation

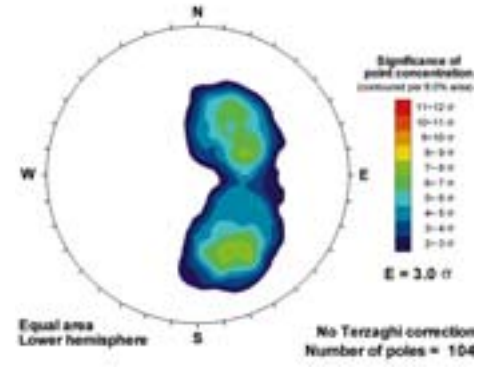

RSMM01 pegmatite

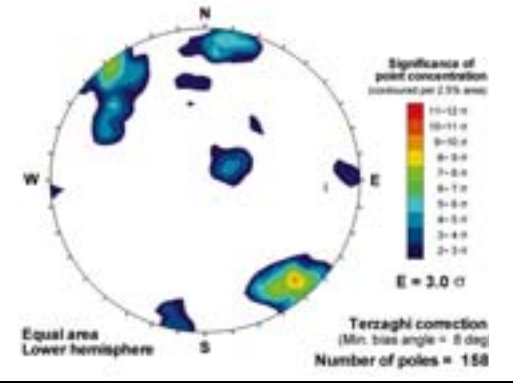

RSMD01 foliation

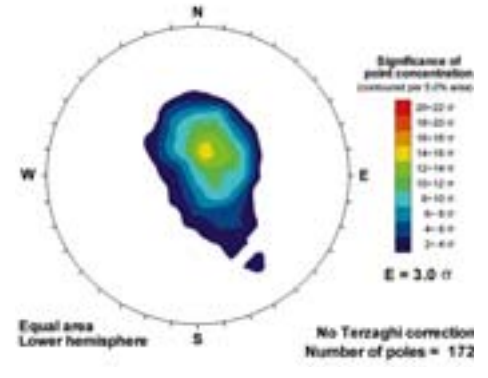

RSMD01 pegmatite

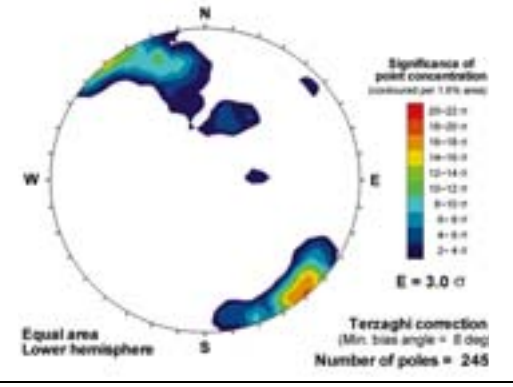

Comparison of orientation of ductile and brittle-ductile shear zones and orientation of subordinate rock types on an overall rock domain basis

RSMA01 shear zones	**RSMA01 fine-grained granite**
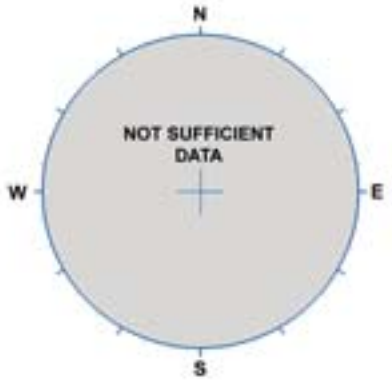	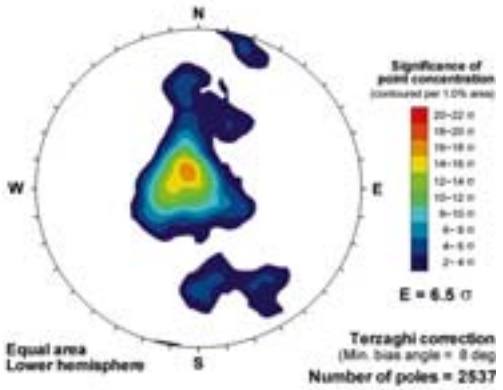
RSMM01 shear zones	**RSMM01 fine-grained granite**
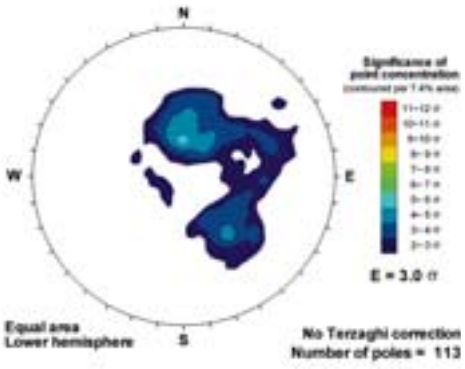	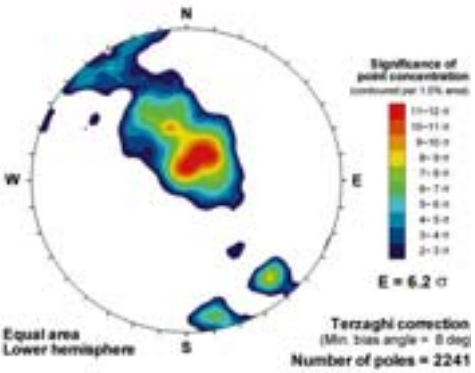
RSMD01 shear zones	**RSMD01 fine-grained granite**
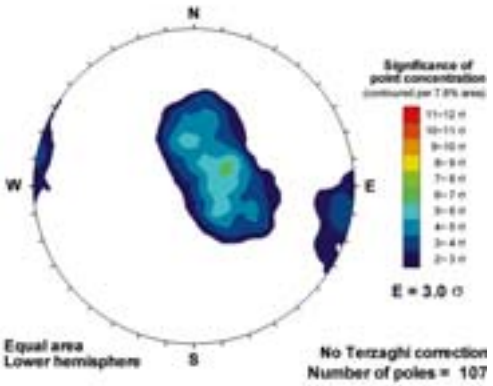	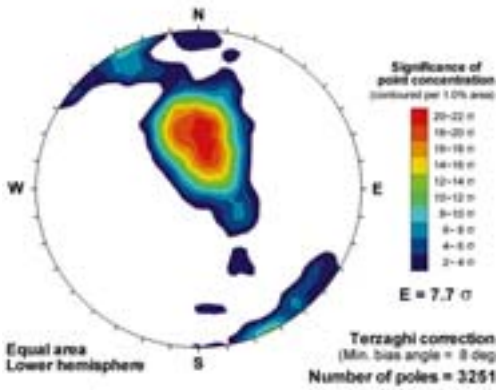

RSMA01 shear zones

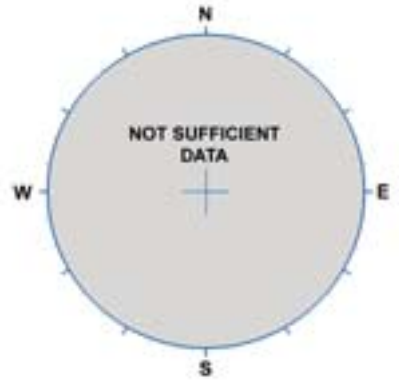

RSMA01 fine-grained diorite-gabbro

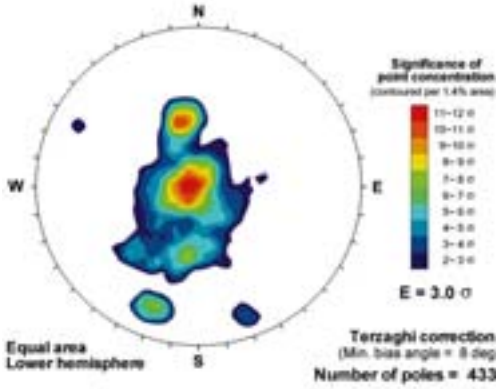

RSMM01 shear zones

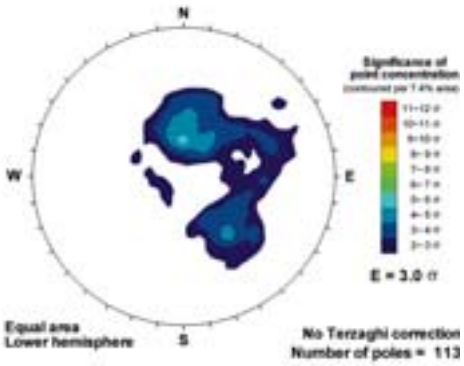

RSMM01 fine-grained diorite-gabbro

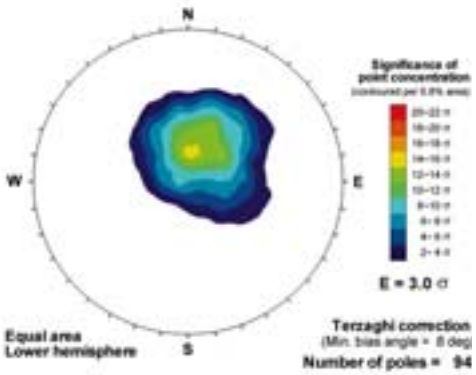

RSMD01 shear zones

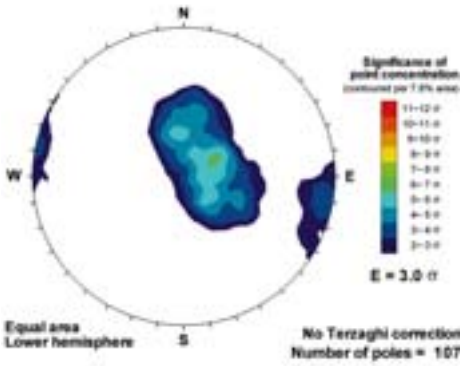

RSMD01 fine-grained diorite-gabbro

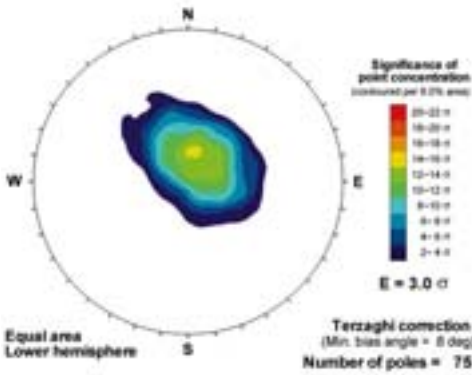

RSMA01 shear zones	**RSMA01 pegmatite**
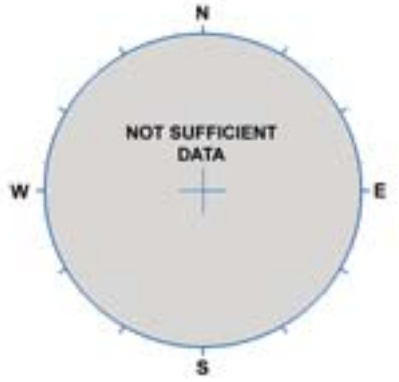	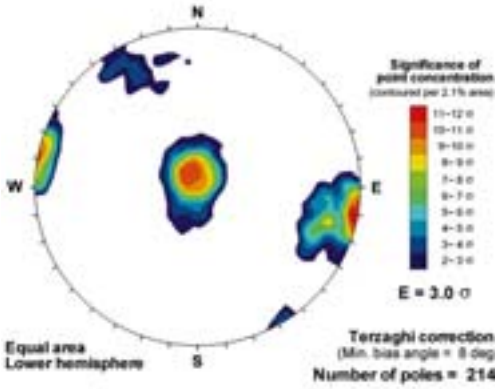
RSMM01 shear zones	**RSMM01 pegmatite**
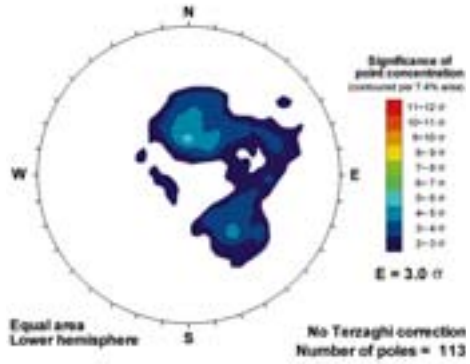	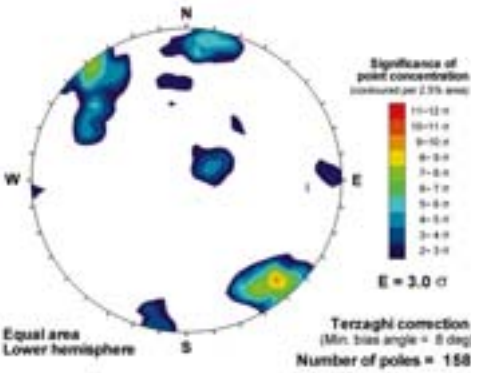
RSMD01 shear zones	**RSMD01 pegmatite**
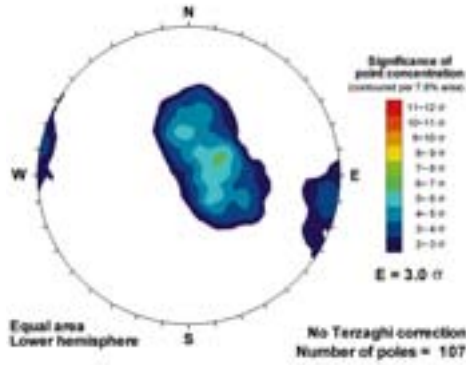	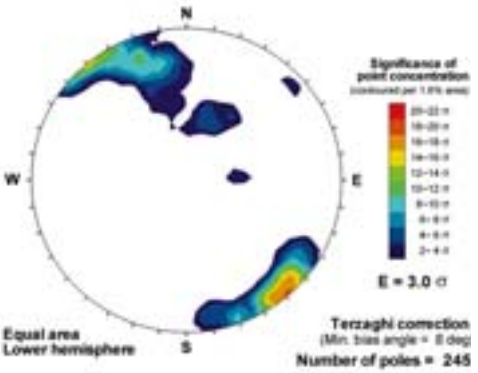

Appendix 10

Rock domains (RSM), deformation zones (ZSM) and fracture domains (FSM) presented on a borehole by borehole basis

The rock domains (RSM), deformation zones (ZSM) and fracture domains (FSM), which have been defined during the model stage SDM-Site Laxemar, are presented for the cored boreholes. The domains and zones are shown together with rock units and deformation zones from the extended single-hole interpretation, including the subdivision of the Ävrö granite by use of the density logs.

Title COMPOSITE LOG for cored borehole KLX01

Site	LAXEMAR	**Elevation [m.a.s.l.ToC]**	16.77
Borehole	KLX01	**Inclination ToC [°]**	-85.29
Diameter [mm]	56	**Drilling Start Date**	1987-12-05 00:00:00
Length [m]	1077.990	**Drilling Stop Date**	1987-12-15 00:00:00
Bearing ToC [°]	348.73	**Surveying Date**	2001-05-11 00:00:00
Coordinate System	RT90-RHB70	**Plot Date**	2008-05-05 22:04:59
Northing ToC [m]	6367485.52		
Easting ToC [m]	1549923.09		

ROCK TYPE LAXEMAR
- Fine-grained granite
- Pegmatite
- Ävrö granite
- Diorite / Gabbro
- Fine-grained diorite-gabbro

WET DENSITY
- unclassified
- dens<2710
- 2710<dens<2820
- 2820<dens<2930
- dens>2930

SUBDIVISION OF ÄVRÖ GRANITE
- Ävrö quartz monzodiorite
- Ävrö granodiorite

ROCK UNIT FROM ESHI
- Medium confidence
- High confidence

ROCK DOMAIN (RSM)
- RSMA01

DEFORMATION ZONE (ZSM)
- DZ (ZSM)

DEFORMATION ZONE FROM ESHI
- DZ

FRACTURE DOMAINS (FSM)

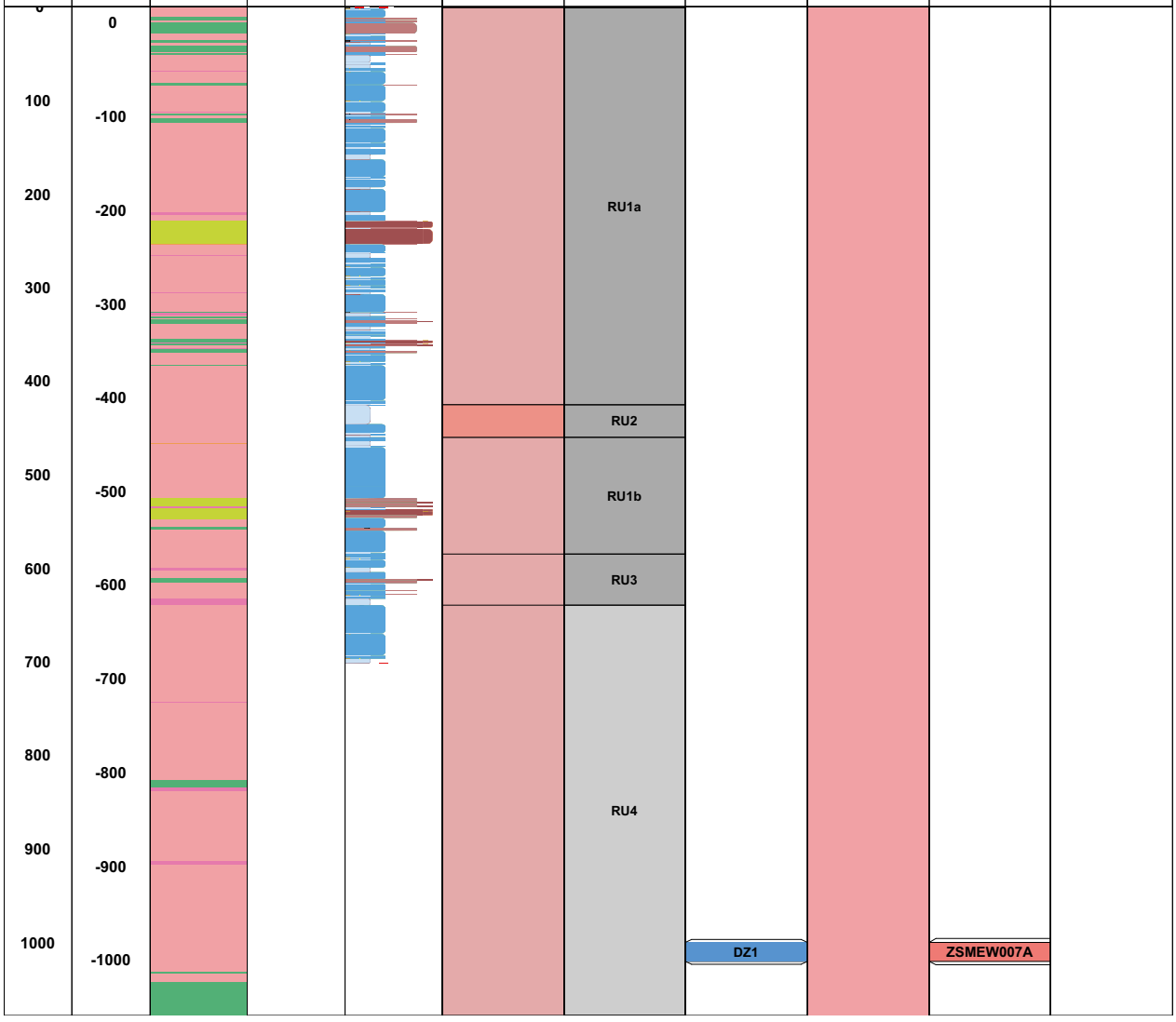

Title COMPOSITE LOG for cored borehole KLX02

Site	LAXEMAR	**Elevation [m.a.s.l.ToC]**	18.40
Borehole	KLX02	**Inclination ToC [°]**	-84.99
Diameter [mm]	76	**Drilling Start Date**	1992-08-15 00:00:00
Length [m]	1700.500	**Drilling Stop Date**	1992-09-05 00:00:00
Bearing ToC [°]	357.30	**Surveying Date**	2001-05-11 00:00:00
Coordinate System	RT90-RHB70	**Plot Date**	2008-05-04 22:04:41
Northing ToC [m]	6366768.99		
Easting ToC [m]	1549224.09		

ROCK TYPE LAXEMAR
- Fine-grained granite
- Ävrö granite
- Fine-grained dioritoid
- Fine-grained diorite-gabbro

WET DENSITY
- unclassified
- dens<2710
- 2710<dens<2820
- 2820<dens<2930
- dens>2930

SUBDIVISION OF ÄVRÖ GRANITE
- Ävrö quartz monzodiorite
- Ävrö granodiorite

ROCK UNIT FROM ESHI
- High confidence

ROCK DOMAIN (RSM)
- RSMA01
- RSMBA03

DEFORMATION ZONE (ZSM)
- DZ (ZSM)

DEFORMATION ZONE FROM ESHI
- DZ

FRACTURE DOMAINS (FSM)
- FSM EW007
- FSM NE005

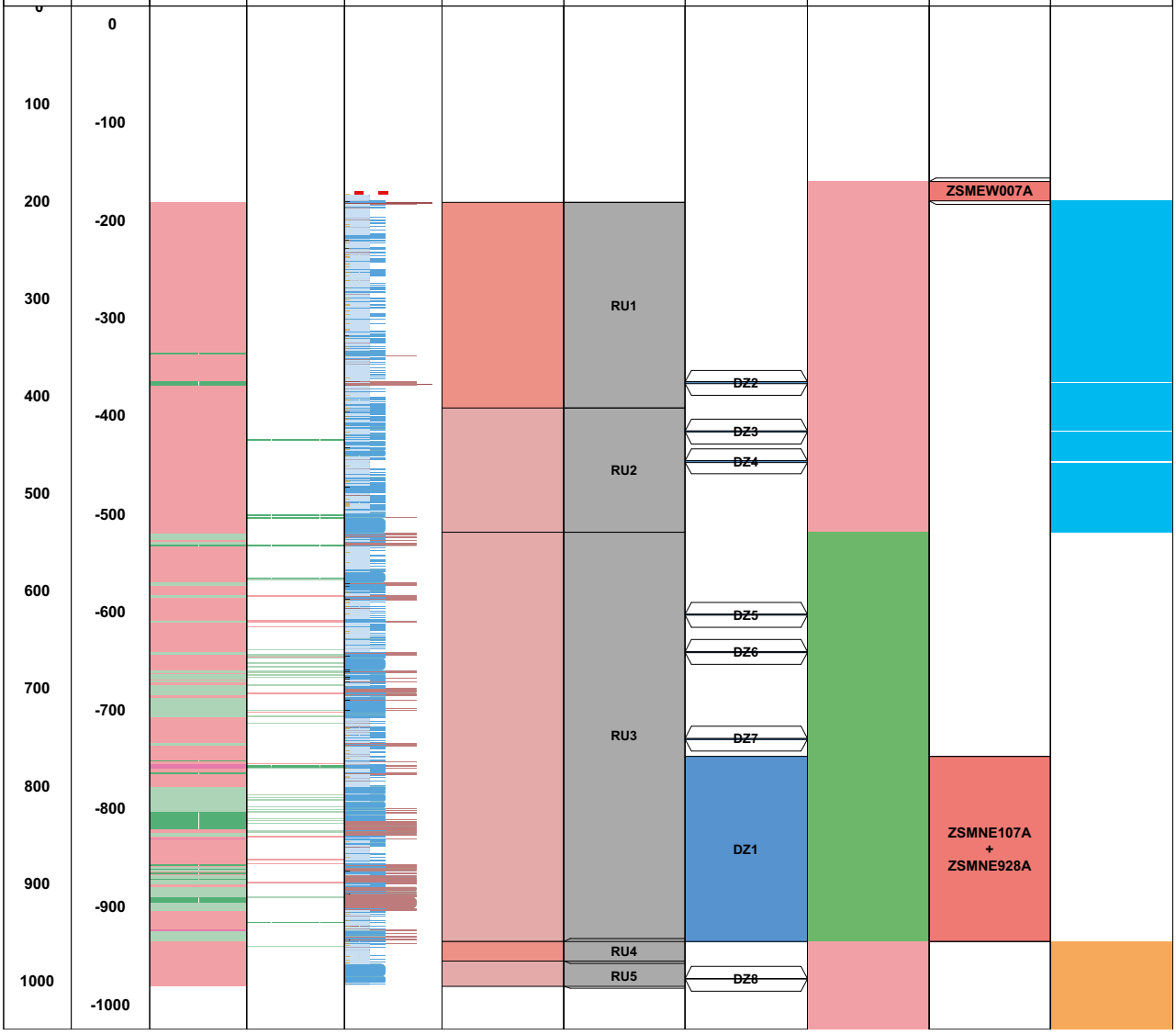

Title COMPOSITE LOG for cored borehole KLX03

Site	LAXEMAR	**Elevation [m.a.s.l.ToC]**	18.49
Borehole	KLX03	**Inclination ToC [°]**	-74.92
Diameter [mm]	76	**Drilling Start Date**	2004-05-28 18:00:00
Length [m]	1000.420	**Drilling Stop Date**	2004-09-07 09:00:00
Bearing ToC [°]	199.04	**Surveying Date**	2004-05-13 14:55:00
Coordinate System	RT90-RHB70	**Plot Date**	2008-05-04 22:04:41
Northing ToC [m]	6366112.59		
Easting ToC [m]	1547718.93		

ROCK TYPE LAXEMAR
- Fine-grained granite
- Ävrö granite
- Quartz monzodiorite
- Diorite / Gabbro
- Fine-grained dioritoid
- Fine-grained diorite-gabbro

WET DENSITY
- unclassified
- dens<2710
- 2710<dens<2820
- 2820<dens<2930
- dens>2930

SUBDIVISION OF ÄVRÖ GRANITE
- Ävrö quartz monzodiorite

ROCK UNIT FROM ESHI
- High confidence

ROCK DOMAIN (RSM)
- RSMD01
- RSMM01

DEFORMATION ZONE (ZSM)
- DZ (ZSM)
- DZ (In BH)

DEFORMATION ZONE FROM ESHI
- DZ

FRACTURE DOMAINS (FSM)
- FSM C

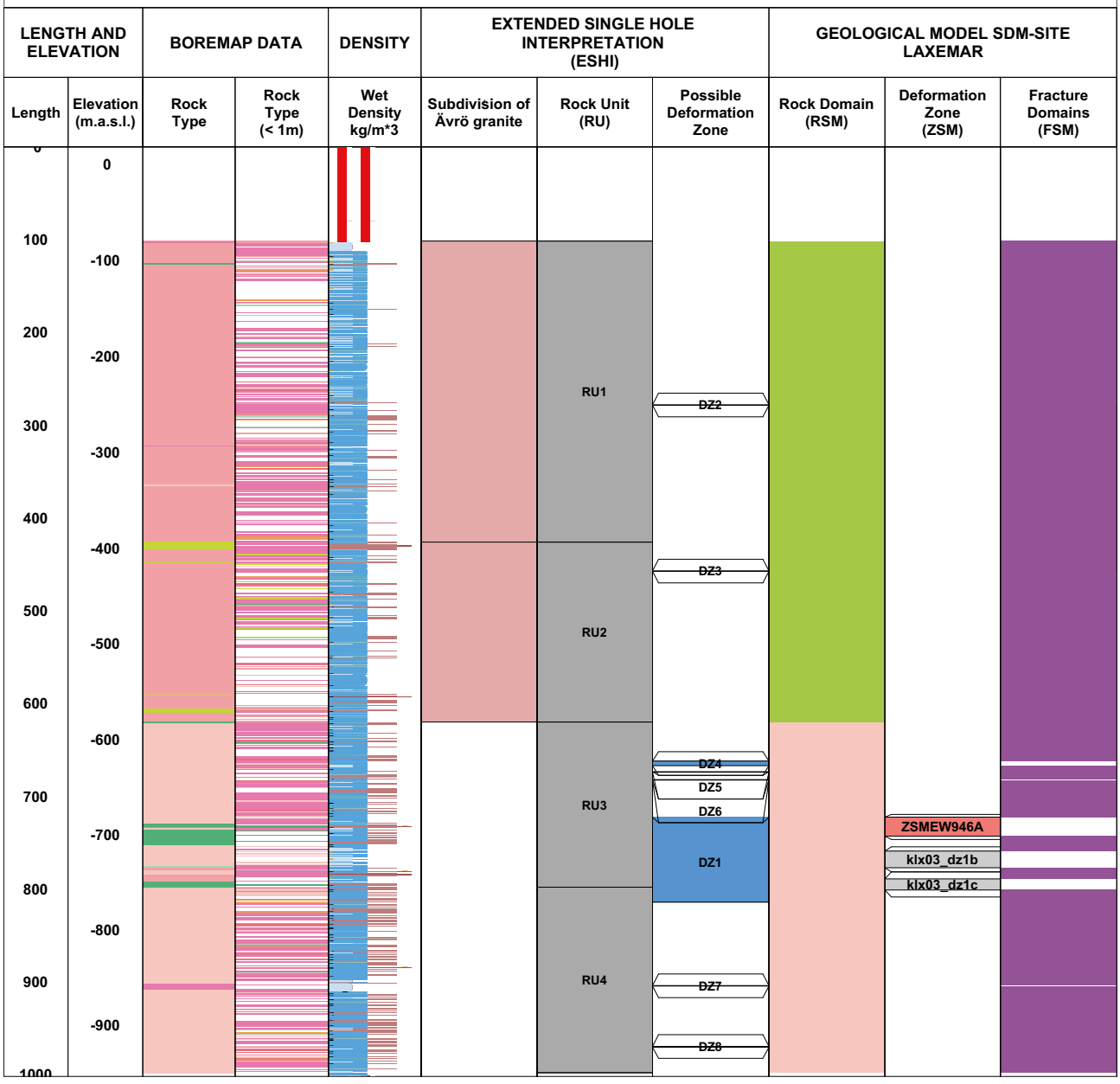

Title COMPOSITE LOG for cored borehole KLX04

Site	LAXEMAR	**Elevation [m.a.s.l.ToC]**	24.09
Borehole	KLX04	**Inclination ToC [°]**	-84.75
Diameter [mm]	76	**Drilling Start Date**	2004-03-13 11:00:00
Length [m]	993.490	**Drilling Stop Date**	2004-06-28 10:12:00
Bearing ToC [°]	0.93	**Surveying Date**	2004-02-19 13:10:00
Coordinate System	RT90-RHB70	**Plot Date**	2008-05-04 22:04:41
Northing ToC [m]	6367077.19		
Easting ToC [m]	1548171.94		

ROCK TYPE LAXEMAR
- Fine-grained granite
- Granite
- Ävrö granite
- Quartz monzodiorite
- Diorite / Gabbro
- Fine-grained dioritoid
- Fine-grained diorite-gabbro

WET DENSITY
- unclassified
- dens<2710
- 2710<dens<2820
- 2820<dens<2930
- dens>2930

SUBDIVISION OF ÄVRÖ GRANITE
- Ävrö quartz monzodiorite
- Ävrö granodiorite

ROCK UNIT FROM ESHI
- High confidence

ROCK DOMAIN (RSM)
- RSMA01

DEFORMATION ZONE (ZSM)
- DZ (ZSM)
- DZ (In BH)

DEFORMATION ZONE FROM ESHI
- DZ

FRACTURE DOMAINS (FSM)
- FSM N
- FSM C
- FSM EW007

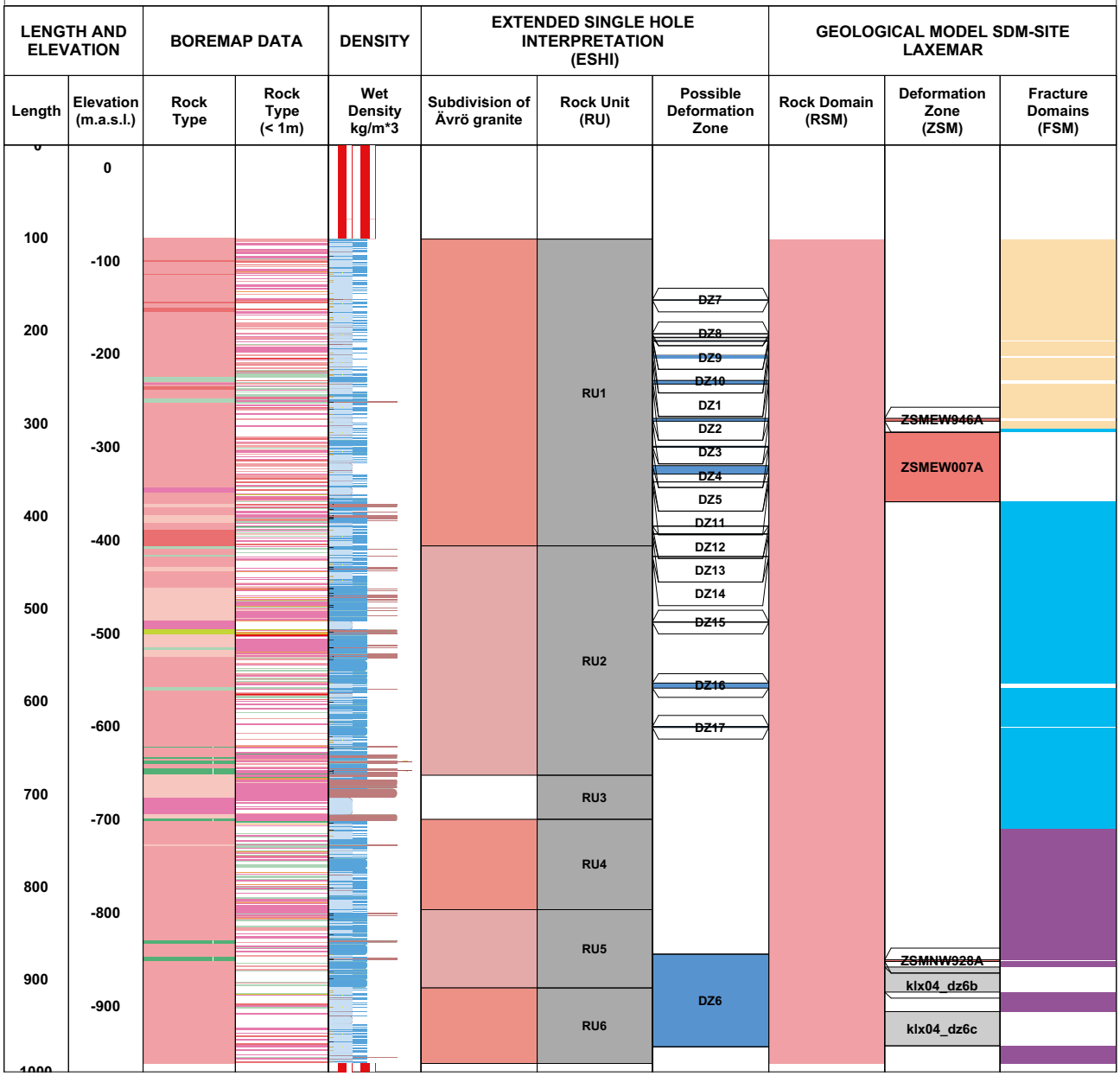

Title COMPOSITE LOG for cored borehole KLX05

Site	LAXEMAR	**Elevation [m.a.s.l.ToC]**	17.63
Borehole	KLX05	**Inclination ToC [°]**	-65.21
Diameter [mm]	76	**Drilling Start Date**	2004-10-01 14:00:00
Length [m]	1000.160	**Drilling Stop Date**	2005-01-22 13:45:00
Bearing ToC [°]	190.19	**Surveying Date**	2004-08-27 11:15:00
Coordinate System	RT90-RHB70	**Plot Date**	2008-05-04 22:04:41
Northing ToC [m]	6365633.34		
Easting ToC [m]	1548909.41		

ROCK TYPE LAXEMAR
- Fine-grained granite
- Pegmatite
- Granite
- Ävrö granite
- Quartz monzodiorite
- Diorite / Gabbro
- Fine-grained dioritoid
- Fine-grained diorite-gabbro

WET DENSITY
- unclassified
- dens<2710
- 2710<dens<2820
- 2820<dens<2930
- dens>2930

SUBDIVISION OF ÄVRÖ GRANITE
- Ävrö quartz monzodiorite
- Ävrö granodiorite

ROCK UNIT FROM ESHI
- High confidence

ROCK DOMAIN (RSM)
- RSMD01
- RSMM01

DEFORMATION ZONE (ZSM)

DEFORMATION ZONE FROM ESHI
- DZ

FRACTURE DOMAINS (FSM)
- FSM NE005

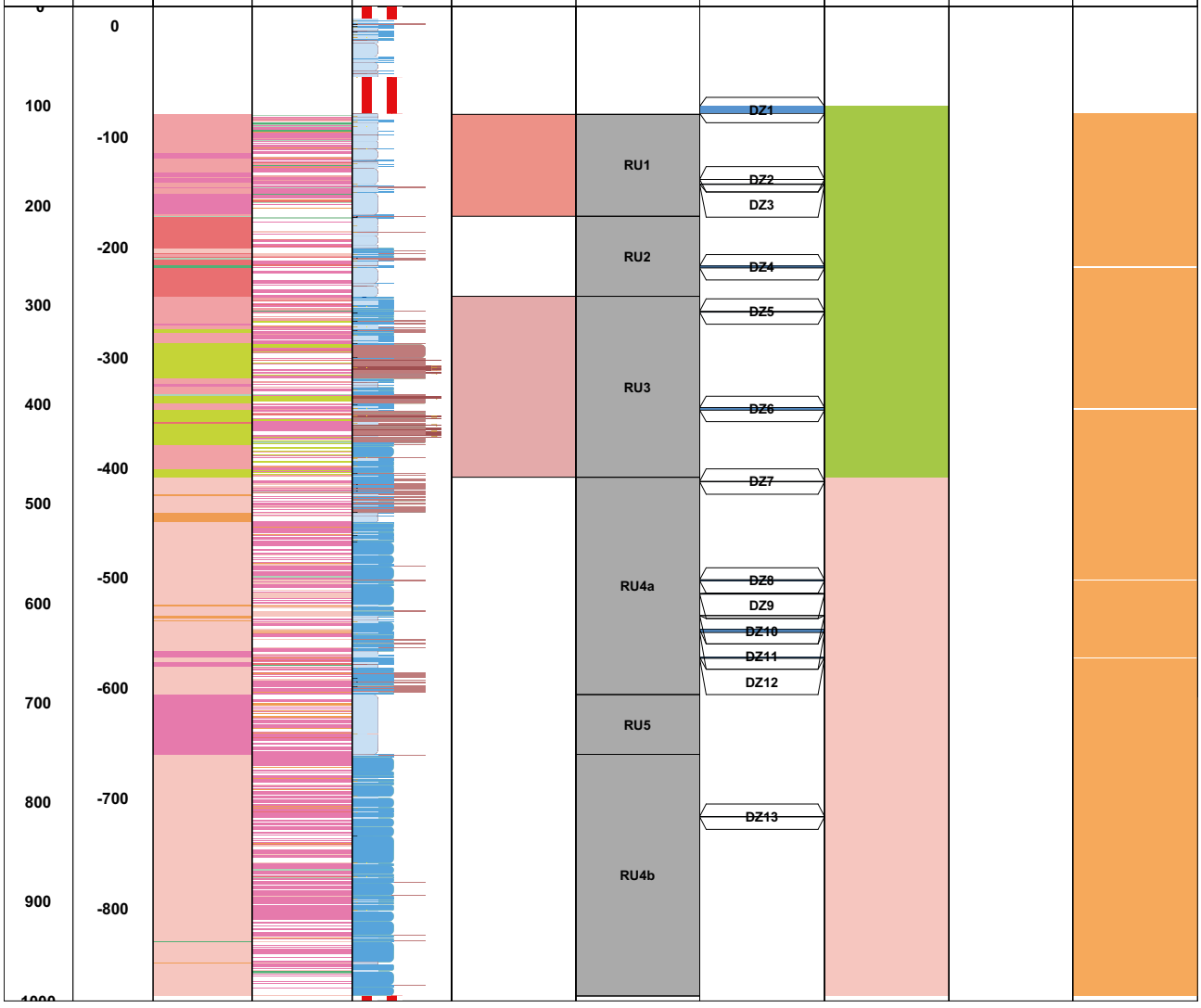

Title COMPOSITE LOG for cored borehole KLX06

Site	LAXEMAR	**Elevation [m.a.s.l.ToC]**	17.68
Borehole	KLX06	**Inclination ToC [°]**	-65.19
Diameter [mm]	76	**Drilling Start Date**	2004-08-25 17:00:00
Length [m]	994.940	**Drilling Stop Date**	2004-11-25 11:30:00
Bearing ToC [°]	329.65	**Surveying Date**	2004-08-13 10:00:00
Coordinate System	RT90-RHB70	**Plot Date**	2008-05-04 22:04:41
Northing ToC [m]	6367806.64		
Easting ToC [m]	1548566.88		

ROCK TYPE LAXEMAR
- Fine-grained granite
- Granite
- Ävrö granite
- Fine-grained dioritoid
- Fine-grained diorite-gabbro

WET DENSITY
- unclassified
- dens<2710
- 2710<dens<2820
- 2820<dens<2930
- dens>2930

SUBDIVISION OF ÄVRÖ GRANITE
- Ävrö quartz monzodiorite
- Ävrö granodiorite

ROCK UNIT FROM ESHI
- High confidence

ROCK DOMAIN (RSM)
- RSMA01

DEFORMATION ZONE (ZSM)
- DZ (ZSM)

DEFORMATION ZONE FROM ESHI
- DZ

FRACTURE DOMAINS (FSM)

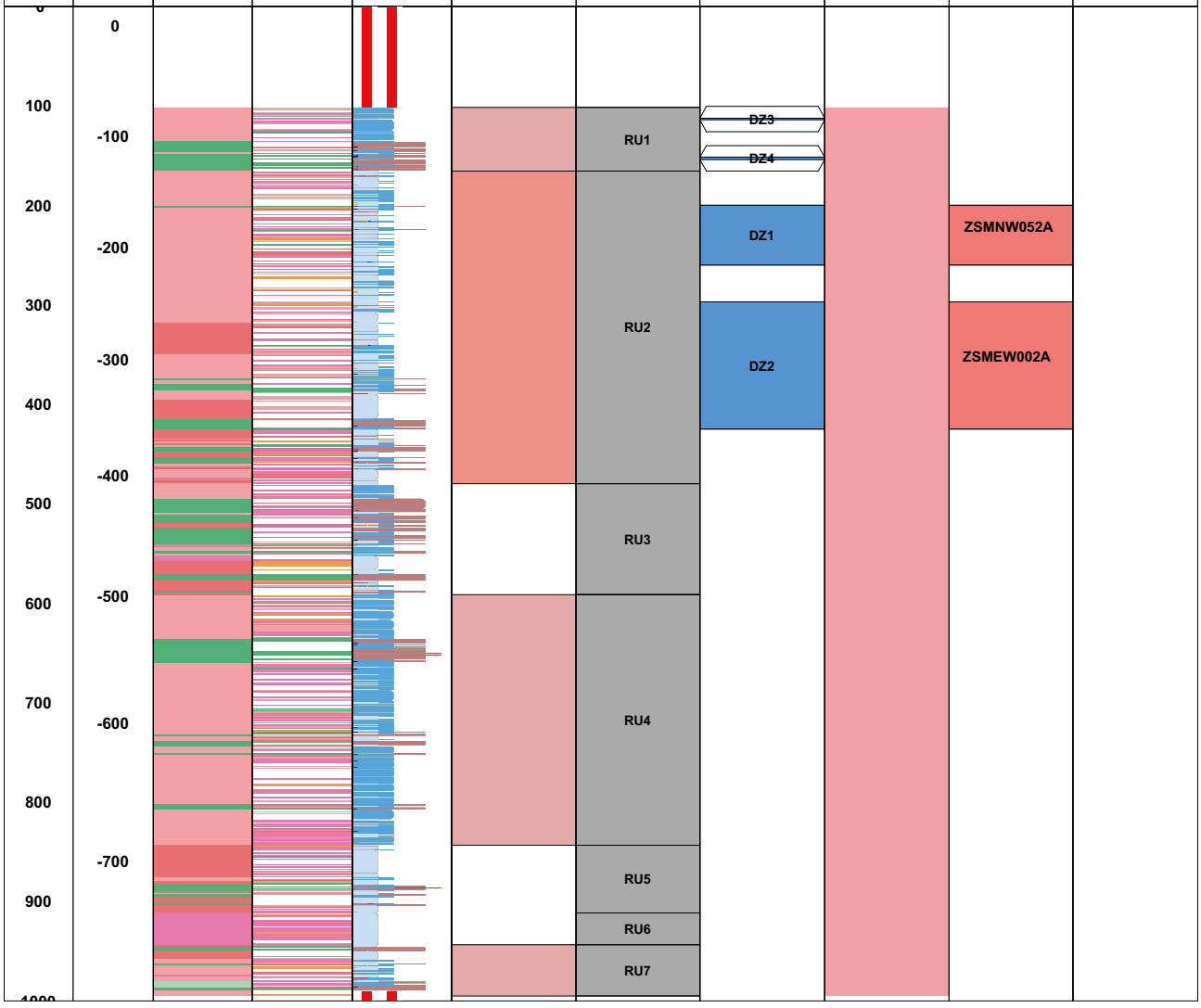

Title COMPOSITE LOG for cored borehole KLX07A

Site	LAXEMAR	**Elevation [m.a.s.l.ToC]**	18.47
Borehole	KLX07A	**Inclination ToC [°]**	-60.03
Diameter [mm]	76	**Drilling Start Date**	2005-01-06 14:00:00
Length [m]	844.730	**Drilling Stop Date**	2005-05-04 10:00:00
Bearing ToC [°]	174.18	**Surveying Date**	2005-05-23 10:20:00
Coordinate System	RT90-RHB70	**Plot Date**	2008-05-04 22:04:41
Northing ToC [m]	6366752.09		
Easting ToC [m]	1549206.86		

ROCK TYPE LAXEMAR
- Fine-grained granite
- Ävrö granite
- Fine-grained diorite-gabbro

WET DENSITY
- unclassified
- dens<2710
- 2710<dens<2820
- 2820<dens<2930

SUBDIVISION OF ÄVRÖ GRANITE
- Ävrö quartz monzodiorite
- Ävrö granodiorite

ROCK UNIT FROM ESHI
- High confidence

ROCK DOMAIN (RSM)
- RSMA01

DEFORMATION ZONE (ZSM)
- DZ (ZSM)
- DZ (In BH)

DEFORMATION ZONE FROM ESHI
- DZ

FRACTURE DOMAINS (FSM)
- FSM EW007
- FSM NE005

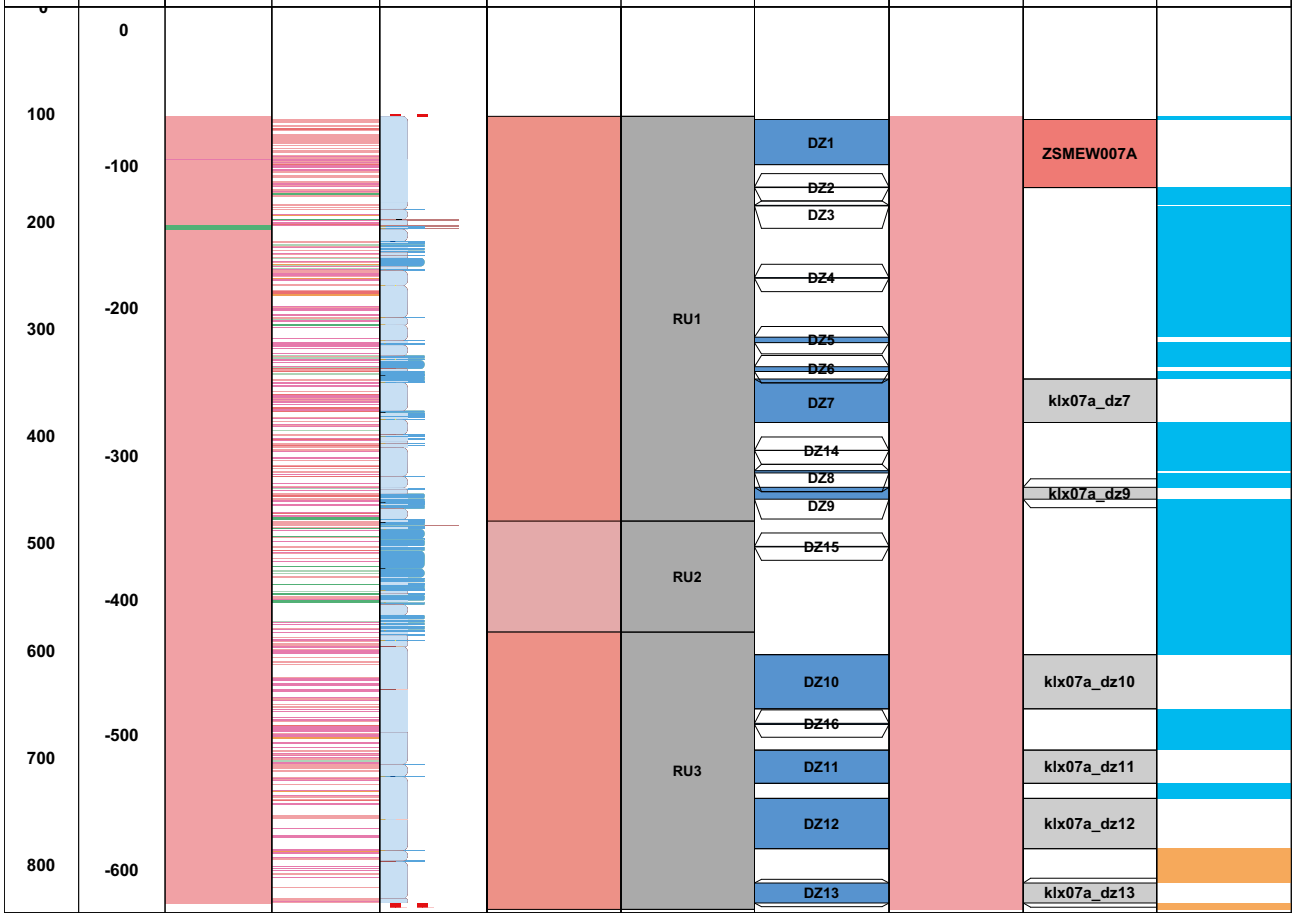

Title COMPOSITE LOG for cored borehole KLX07B

Site	LAXEMAR	**Elevation [m.a.s.l.ToC]**	18.38
Borehole	KLX07B	**Inclination ToC [°]**	-85.14
Diameter [mm]	76	**Drilling Start Date**	2005-05-23 18:00:00
Length [m]	200.130	**Drilling Stop Date**	2005-06-03 08:00:00
Bearing ToC [°]	174.33	**Surveying Date**	2005-06-07 15:55:00
Coordinate System	RT90-RHB70	**Plot Date**	2008-05-04 22:04:41
Northing ToC [m]	6366753.14		
Easting ToC [m]	1549206.76		

ROCK TYPE LAXEMAR
- Ävrö granite
- Fine-grained diorite-gabbro

WET DENSITY
- unclassified
- dens<2710
- 2710<dens<2820
- 2820<dens<2930
- dens>2930

SUBDIVISION OF ÄVRÖ GRANITE
- Ävrö quartz monzodiorite
- Ävrö granodiorite

ROCK UNIT FROM ESHI
- High confidence

ROCK DOMAIN (RSM)
- RSMA01

DEFORMATION ZONE (ZSM)
- DZ (ZSM)

DEFORMATION ZONE FROM ESHI
- DZ

FRACTURE DOMAINS (FSM)
- FSM N
- FSM EW007

LENGTH AND ELEVATION		BOREMAP DATA		DENSITY	EXTENDED SINGLE HOLE INTERPRETATION (ESHI)			GEOLOGICAL MODEL SDM-SITE LAXEMAR		
Length	Elevation (m.a.s.l.)	Rock Type	Rock Type (< 1m)	Wet Density kg/m*3	Subdivision of Ävrö granite	Rock Unit (RU)	Possible Deformation Zone	Rock Domain (RSM)	Deformation Zone (ZSM)	Fracture Domains (FSM)
0	0					RU1	DZ4			
							DZ1			
							DZ2			
100	-100					RU2				
							DZ3		ZSMEW007A	
200						RU3				

Title COMPOSITE LOG for cored borehole KLX08

Site	LAXEMAR	**Elevation [m.a.s.l.ToC]**	24.31
Borehole	KLX08	**Inclination ToC [°]**	-60.50
Diameter [mm]	76	**Drilling Start Date**	2005-04-04 13:30:00
Length [m]	1000.410	**Drilling Stop Date**	2005-06-13 14:00:00
Bearing ToC [°]	199.17	**Surveying Date**	2005-01-26 11:25:00
Coordinate System	RT90-RHB70	**Plot Date**	2008-05-04 22:04:41
Northing ToC [m]	6367079.10		
Easting ToC [m]	1548176.71		

ROCK TYPE LAXEMAR
- Fine-grained granite
- Ävrö granite
- Quartz monzodiorite
- Diorite / Gabbro
- Fine-grained dioritoid
- Fine-grained diorite-gabbro

WET DENSITY
- unclassified
- dens<2710
- 2710<dens<2820
- 2820<dens<2930
- dens>2930

SUBDIVISION OF ÄVRÖ GRANITE
- Ävrö granodiorite

ROCK UNIT FROM ESHI
- High confidence

ROCK DOMAIN (RSM)
- RSMA01
- RSMD01
- RSMM01

DEFORMATION ZONE (ZSM)
- DZ (ZSM)
- DZ (In BH)

DEFORMATION ZONE FROM ESHI
- DZ

FRACTURE DOMAINS (FSM)
- FSM N
- FSM C
- FSM EW007

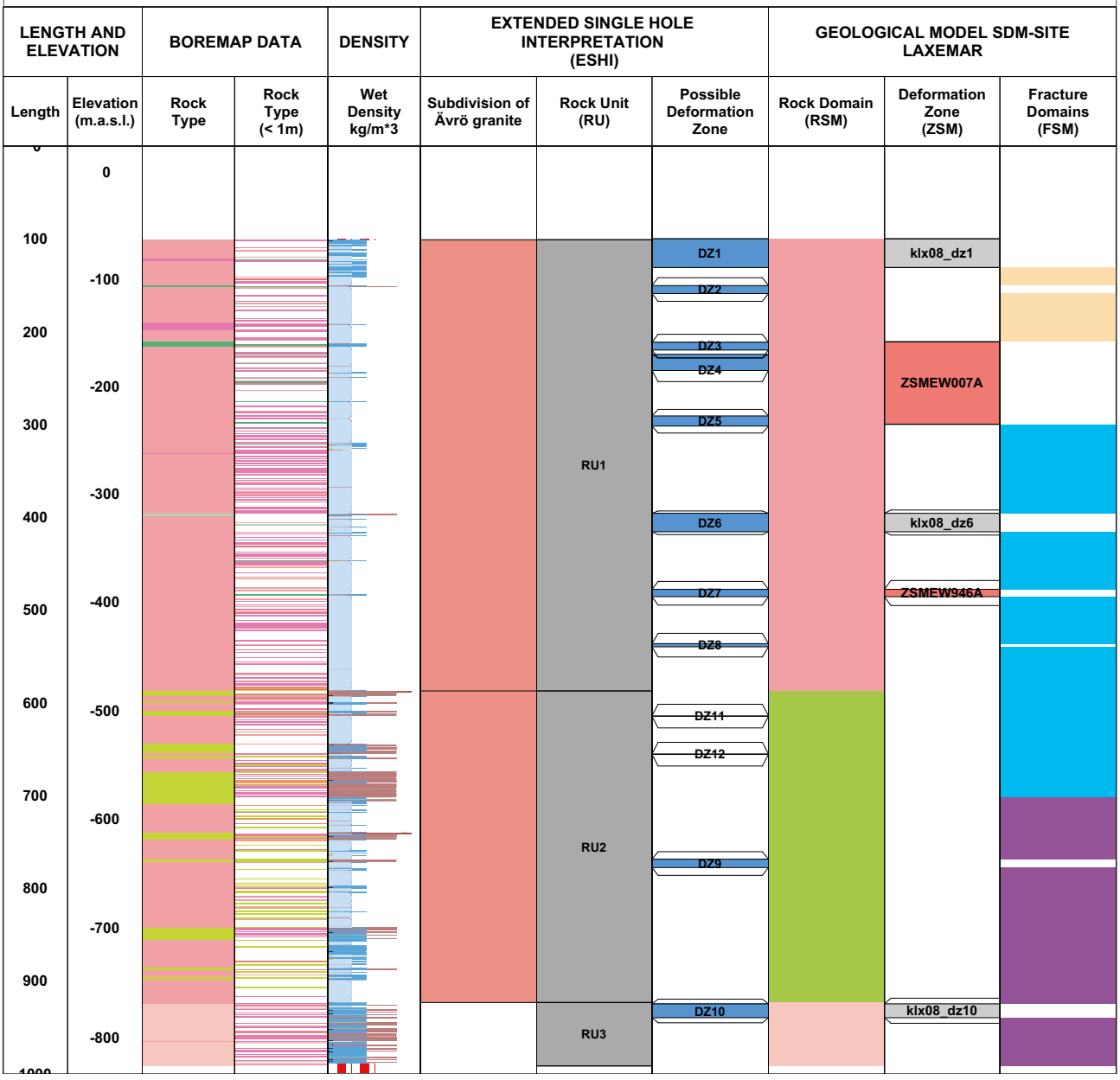

Title COMPOSITE LOG for cored borehole KLX09

Site	LAXEMAR	**Elevation [m.a.s.l.ToC]**	23.45
Borehole	KLX09	**Inclination ToC [°]**	-84.93
Diameter [mm]	76	**Drilling Start Date**	2005-08-26 09:30:00
Length [m]	880.380	**Drilling Stop Date**	2005-10-15 12:00:00
Bearing ToC [°]	267.41	**Surveying Date**	2005-06-14 13:25:00
Coordinate System	RT90-RHB70	**Plot Date**	2008-05-04 22:04:41
Northing ToC [m]	6367323.45		
Easting ToC [m]	1548863.18		

ROCK TYPE LAXEMAR
- Fine-grained granite
- Ävrö granite
- Quartz monzodiorite
- Diorite / Gabbro
- Fine-grained dioritoid
- Fine-grained diorite-gabbro

WET DENSITY
- unclassified
- dens<2710
- 2710<dens<2820
- 2820<dens<2930
- dens>2930

SUBDIVISION OF ÄVRÖ GRANITE
- Ävrö quartz monzodiorite
- Ävrö granodiorite

ROCK UNIT FROM ESHI
- High confidence

ROCK DOMAIN (RSM)
- RSMA01

DEFORMATION ZONE (ZSM)
- DZ (ZSM)
- DZ (In BH)

DEFORMATION ZONE FROM ESHI
- DZ

FRACTURE DOMAINS (FSM)
- FSM N
- FSM EW007

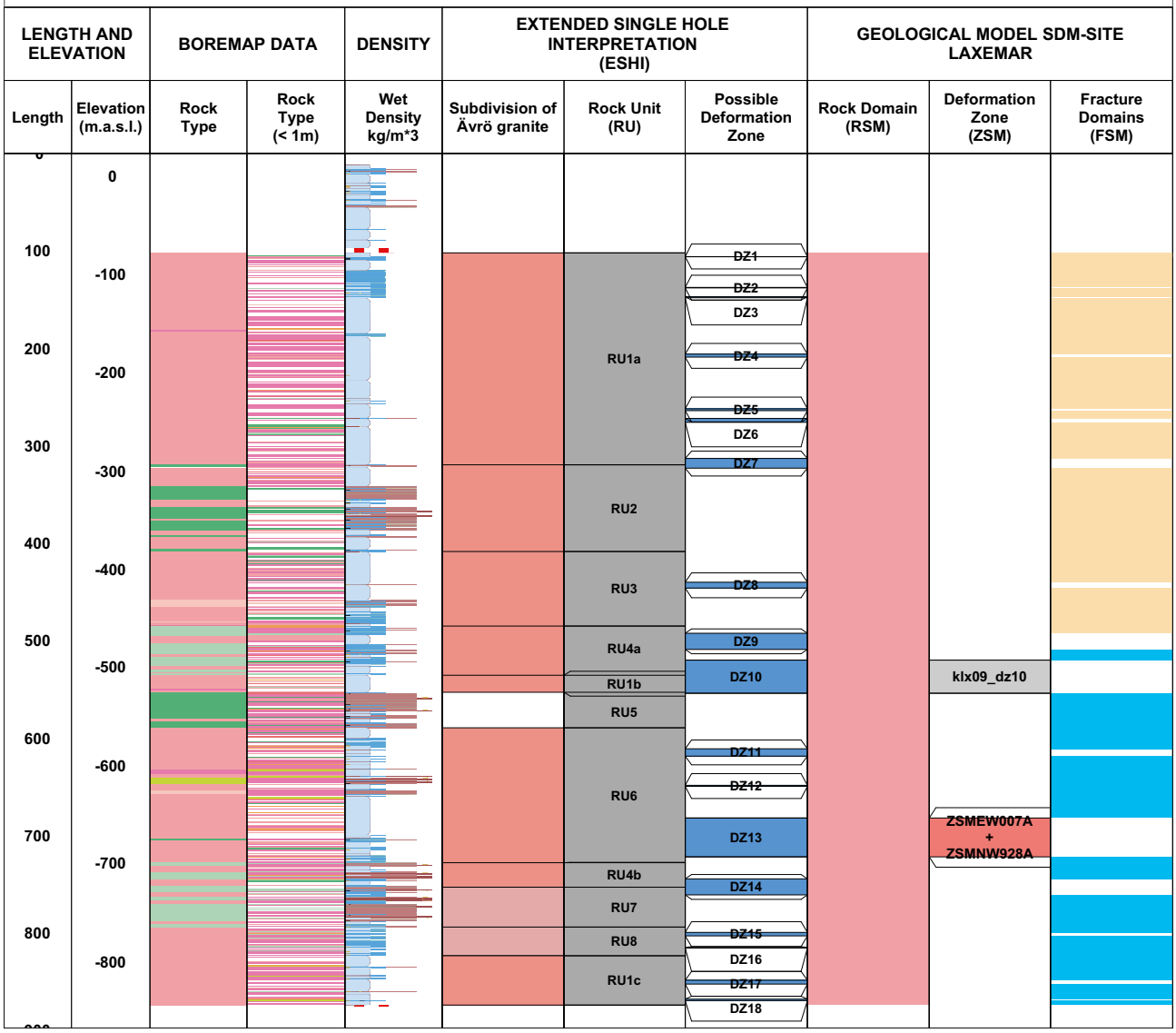

Title COMPOSITE LOG for cored borehole KLX09B

Site	LAXEMAR	**Elevation [m.a.s.l.ToC]**	23.62
Borehole	KLX09B	**Inclination ToC [°]**	-89.82
Diameter [mm]	76	**Drilling Start Date**	2006-01-16 14:00:00
Length [m]	100.220	**Drilling Stop Date**	2006-01-26 12:00:00
Bearing ToC [°]	21.25	**Surveying Date**	2006-02-01 14:42:00
Coordinate System	RT90-RHB70	**Plot Date**	2008-05-04 22:04:41
Northing ToC [m]	6367329.07		
Easting ToC [m]	1548859.01		

ROCK TYPE LAXEMAR
- Fine-grained granite
- Ävrö granite
- Fine-grained diorite-gabbro

WET DENSITY
- unclassified
- dens<2710
- 2710<dens<2820
- 2820<dens<2930
- dens>2930

SUBDIVISION OF ÄVRÖ GRANITE
- Ävrö quartz monzodiorite
- Ävrö granodiorite

ROCK UNIT FROM ESHI
- High confidence

ROCK DOMAIN (RSM)
- RSMA01

DEFORMATION ZONE (ZSM)

DEFORMATION ZONE FROM ESHI
- DZ

FRACTURE DOMAINS (FSM)
- FSM N

LENGTH AND ELEVATION		BOREMAP DATA		DENSITY	EXTENDED SINGLE HOLE INTERPRETATION (ESHI)			GEOLOGICAL MODEL SDM-SITE LAXEMAR		
Length	Elevation (m.a.s.l.)	Rock Type	Rock Type (< 1m)	Wet Density kg/m*3	Subdivision of Ävrö granite	Rock Unit (RU)	Possible Deformation Zone	Rock Domain (RSM)	Deformation Zone (ZSM)	Fracture Domains (FSM)
0	0					RU1	DZ1			
100						RU2	DZ2			

Title COMPOSITE LOG for cored borehole KLX09C

Site	LAXEMAR	**Elevation [m.a.s.l.ToC]**	23.75
Borehole	KLX09C	**Inclination ToC [°]**	-59.51
Diameter [mm]	76	**Drilling Start Date**	2006-01-07 11:00:00
Length [m]	120.050	**Drilling Stop Date**	2006-01-15 12:00:00
Bearing ToC [°]	160.39	**Surveying Date**	2006-02-01 15:12:00
Coordinate System	RT90-RHB70	**Plot Date**	2008-05-04 22:04:41
Northing ToC [m]	6367353.43		
Easting ToC [m]	1548838.82		

ROCK TYPE LAXEMAR
- Fine-grained granite
- Ävrö granite
- Fine-grained diorite-gabbro

SILICATE DENSITY

SUBDIVISION OF ÄVRÖ GRANITE
- Ävrö granite

ROCK UNIT FROM ESHI
- High confidence

ROCK DOMAIN (RSM)
- RSMA01

DEFORMATION ZONE (ZSM)

DEFORMATION ZONE FROM ESHI
- DZ

FRACTURE DOMAINS (FSM)
- FSM N

LENGTH AND ELEVATION		BOREMAP DATA		DENSITY	EXTENDED SINGLE HOLE INTERPRETATION (ESHI)			GEOLOGICAL MODEL SDM-SITE LAXEMAR		
Length	Elevation (m.a.s.l.)	Rock Type	Rock Type (< 1m)	Silicate Density kg/m*3	Subdivision of Ävrö granite	Rock Unit (RU)	Possible Deformation Zone	Rock Domain (RSM)	Deformation Zone (ZSM)	Fracture Domains (FSM)
0	0					RU1	DZ1			
100							DZ2			

Title COMPOSITE LOG for cored borehole KLX09D

Site	LAXEMAR	**Elevation [m.a.s.l.ToC]**	23.10
Borehole	KLX09D	**Inclination ToC [°]**	-60.24
Diameter [mm]	76	**Drilling Start Date**	2005-11-05 06:00:00
Length [m]	121.020	**Drilling Stop Date**	2005-11-17 14:00:00
Bearing ToC [°]	270.15	**Surveying Date**	2006-02-01 14:31:00
Coordinate System	RT90-RHB70	**Plot Date**	2008-05-04 22:04:41
Northing ToC [m]	6367336.99		
Easting ToC [m]	1548878.22		

ROCK TYPE LAXEMAR
- Fine-grained granite
- Ävrö granite
- Fine-grained diorite-gabbro

WET DENSITY
- unclassified
- dens<2710
- 2710<dens<2820
- 2820<dens<2930

SUBDIVISION OF ÄVRÖ GRANITE
- Ävrö quartz monzodiorite
- Ävrö granodiorite

ROCK UNIT FROM ESHI
- High confidence

ROCK DOMAIN (RSM)
- RSMA01

DEFORMATION ZONE (ZSM)

DEFORMATION ZONE FROM ESHI
- DZ

FRACTURE DOMAINS (FSM)
- FSM N

LENGTH AND ELEVATION		BOREMAP DATA		DENSITY	EXTENDED SINGLE HOLE INTERPRETATION (ESHI)			GEOLOGICAL MODEL SDM-SITE LAXEMAR		
Length	Elevation (m.a.s.l.)	Rock Type	Rock Type (< 1m)	Wet Density kg/m*3	Subdivision of Ävrö granite	Rock Unit (RU)	Possible Deformation Zone	Rock Domain (RSM)	Deformation Zone (ZSM)	Fracture Domains (FSM)
0	0					RU1				
100						RU2	DZ1 DZ2			

Title COMPOSITE LOG for cored borehole KLX09E

Site	LAXEMAR	**Elevation [m.a.s.l.ToC]**	22.16
Borehole	KLX09E	**Inclination ToC [°]**	-59.95
Diameter [mm]	76	**Drilling Start Date**	2005-11-23 08:25:00
Length [m]	120.000	**Drilling Stop Date**	2005-12-05 07:00:00
Bearing ToC [°]	338.90	**Surveying Date**	2006-02-01 14:38:00
Coordinate System	RT90-RHB70	**Plot Date**	2008-05-04 22:04:41
Northing ToC [m]	6367304.45		
Easting ToC [m]	1548880.37		

ROCK TYPE LAXEMAR
- Fine-grained granite
- Ävrö granite
- Fine-grained diorite-gabbro

SILICATE DENSITY

SUBDIVISION OF ÄVRÖ GRANITE
- Ävrö granite

ROCK UNIT FROM ESHI
- High confidence

ROCK DOMAIN (RSM)
- RSMA01

DEFORMATION ZONE (ZSM)
- DZ (In BH)

DEFORMATION ZONE FROM ESHI
- DZ

FRACTURE DOMAINS (FSM)
- FSM N

LENGTH AND ELEVATION		BOREMAP DATA		DENSITY	EXTENDED SINGLE HOLE INTERPRETATION (ESHI)			GEOLOGICAL MODEL SDM-SITE LAXEMAR		
Length	Elevation (m.a.s.l.)	Rock Type	Rock Type (< 1m)	Silicate Density kg/m*3	Subdivision of Ävrö granite	Rock Unit (RU)	Possible Deformation Zone	Rock Domain (RSM)	Deformation Zone (ZSM)	Fracture Domains (FSM)
0	0					RU1	DZ1			
100							DZ2		klx09E_dz2	

Title COMPOSITE LOG for cored borehole KLX09F

Site	LAXEMAR	**Elevation [m.a.s.l.ToC]**	19.57
Borehole	KLX09F	**Inclination ToC [°]**	-59.73
Diameter [mm]	76	**Drilling Start Date**	2005-12-06 09:00:00
Length [m]	152.300	**Drilling Stop Date**	2006-01-06 13:00:00
Bearing ToC [°]	90.67	**Surveying Date**	2006-02-01 14:05:00
Coordinate System	RT90-RHB70	**Plot Date**	2008-05-04 22:04:41
Northing ToC [m]	6367318.02		
Easting ToC [m]	1548817.27		

ROCK TYPE LAXEMAR
- Fine-grained granite
- Granite
- Ävrö granite
- Fine-grained diorite-gabbro

WET DENSITY
- unclassified
- dens<2710
- 2710<dens<2820
- 2820<dens<2930
- dens>2930

SUBDIVISION OF ÄVRÖ GRANITE
- Ävrö granodiorite

ROCK UNIT FROM ESHI
- High confidence

ROCK DOMAIN (RSM)
- RSMA01

DEFORMATION ZONE (ZSM)
- DZ (In BH)

DEFORMATION ZONE FROM ESHI
- DZ

FRACTURE DOMAINS (FSM)
- FSM N

LENGTH AND ELEVATION		BOREMAP DATA		DENSITY	EXTENDED SINGLE HOLE INTERPRETATION (ESHI)			GEOLOGICAL MODEL SDM-SITE LAXEMAR		
Length	Elevation (m.a.s.l.)	Rock Type	Rock Type (< 1m)	Wet Density kg/m*3	Subdivision of Ävrö granite	Rock Unit (RU)	Possible Deformation Zone	Rock Domain (RSM)	Deformation Zone (ZSM)	Fracture Domains (FSM)
0	0						DZ1		klx09F_dz1	
100	-100					RU1	DZ2 DZ3 DZ4 DZ5			

Title COMPOSITE LOG for cored borehole KLX09G

Site	LAXEMAR	**Elevation [m.a.s.l.ToC]**	19.63
Borehole	KLX09G	**Inclination ToC [°]**	-61.07
Diameter [mm]	76	**Drilling Start Date**	2006-01-27 16:00:00
Length [m]	100.100	**Drilling Stop Date**	2006-02-03 12:00:00
Bearing ToC [°]	85.41	**Surveying Date**	2006-02-07 14:50:00
Coordinate System	RT90-RHB70	**Plot Date**	2008-05-04 22:04:41
Northing ToC [m]	6367330.09		
Easting ToC [m]	1548905.77		

ROCK TYPE LAXEMAR
- Fine-grained granite
- Ävrö granite
- Fine-grained diorite-gabbro

WET DENSITY
- unclassified
- dens<2710
- 2710<dens<2820
- 2820<dens<2930

SUBDIVISION OF ÄVRÖ GRANITE
- Ävrö quartz monzodiorite

ROCK UNIT FROM ESHI
- High confidence

ROCK DOMAIN (RSM)
- RSMA01

DEFORMATION ZONE (ZSM)
- DZ (ZSM)

DEFORMATION ZONE FROM ESHI
- DZ

FRACTURE DOMAINS (FSM)
- FSM N

LENGTH AND ELEVATION		BOREMAP DATA		DENSITY	EXTENDED SINGLE HOLE INTERPRETATION (ESHI)			GEOLOGICAL MODEL SDM-SITE LAXEMAR		
Length	Elevation (m.a.s.l.)	Rock Type	Rock Type (< 1m)	Wet Density kg/m*3	Subdivision of Ävrö granite	Rock Unit (RU)	Possible Deformation Zone	Rock Domain (RSM)	Deformation Zone (ZSM)	Fracture Domains (FSM)
0	0					RU1	DZ1		ZSMNS046A	
100										

Title COMPOSITE LOG for cored borehole KLX10

Site	LAXEMAR	**Elevation [m.a.s.l.ToC]**	18.28
Borehole	KLX10	**Inclination ToC [°]**	-85.18
Diameter [mm]	76	**Drilling Start Date**	2005-06-18 08:00:00
Length [m]	1001.200	**Drilling Stop Date**	2005-10-15 07:40:00
Bearing ToC [°]	250.80	**Surveying Date**	2005-06-07 11:10:00
Coordinate System	RT90-RHB70	**Plot Date**	2008-05-04 22:04:41
Northing ToC [m]	6366319.38		
Easting ToC [m]	1548515.23		

ROCK TYPE LAXEMAR
- Fine-grained granite
- Ävrö granite
- Quartz monzodiorite
- Diorite / Gabbro
- Fine-grained dioritoid
- Fine-grained diorite-gabbro

WET DENSITY
- unclassified
- dens<2710
- 2710<dens<2820
- 2820<dens<2930
- dens>2930

SUBDIVISION OF ÄVRÖ GRANITE
- Ävrö quartz monzodiorite
- Ävrö granodiorite

ROCK UNIT FROM ESHI
- High confidence

ROCK DOMAIN (RSM)
- RSMA01
- RSMD01
- RSMM01

DEFORMATION ZONE (ZSM)
- DZ (ZSM)

DEFORMATION ZONE FROM ESHI
- DZ

FRACTURE DOMAINS (FSM)
- FSM C
- FSM EW007

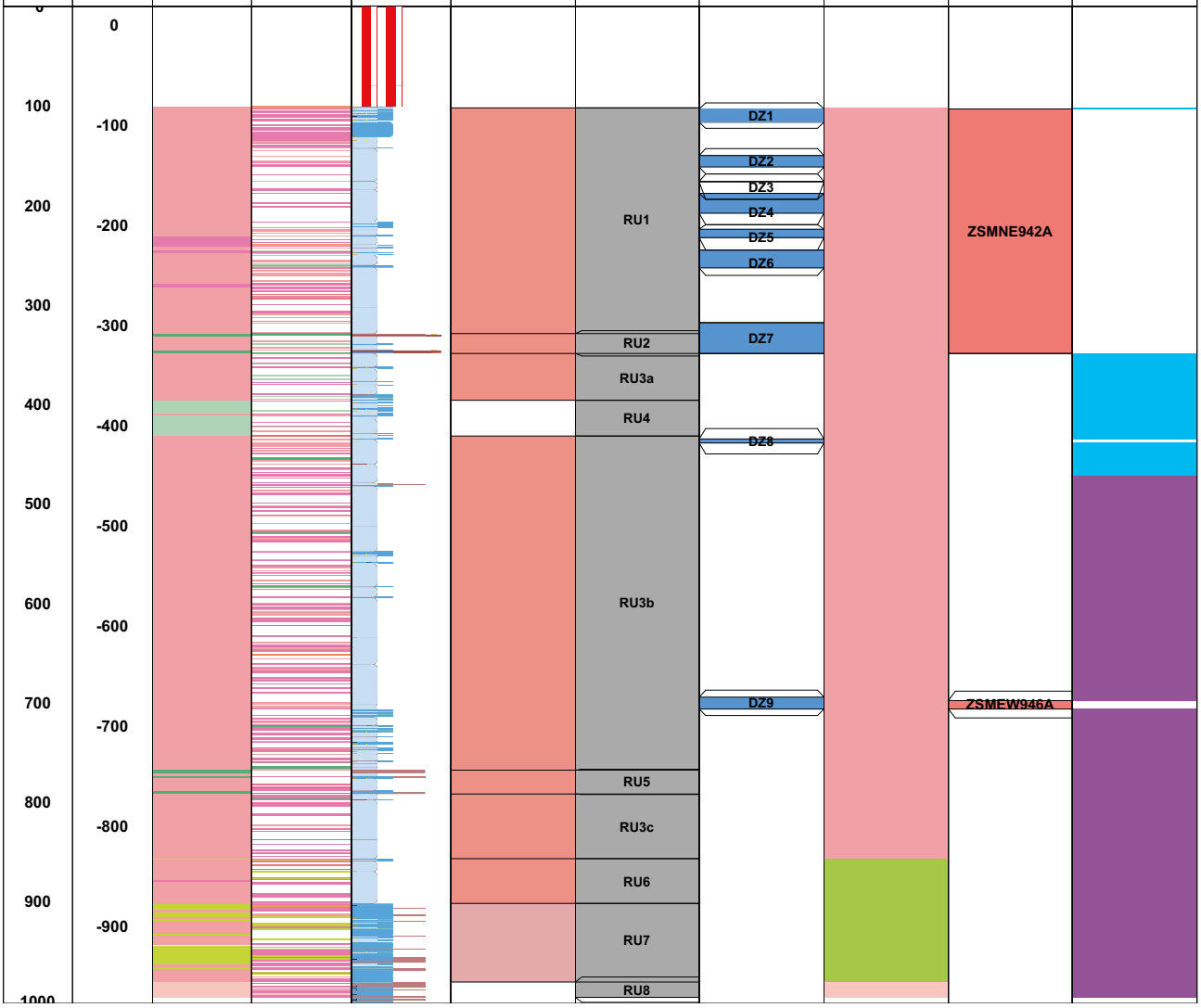

Title COMPOSITE LOG for cored borehole KLX10B

Site	LAXEMAR	**Elevation [m.a.s.l.ToC]**	18.15
Borehole	KLX10B	**Inclination ToC [°]**	-59.96
Diameter [mm]	76	**Drilling Start Date**	2006-02-08 16:35:00
Length [m]	50.250	**Drilling Stop Date**	2006-02-14 06:55:00
Bearing ToC [°]	170.33	**Surveying Date**	2006-04-03 09:25:00
Coordinate System	RT90-RHB70	**Plot Date**	2008-05-04 22:04:41
Northing ToC [m]	6366316.49		
Easting ToC [m]	1548525.15		

ROCK TYPE LAXEMAR
- Fine-grained granite
- Ävrö granite

WET DENSITY
- unclassified
- dens<2710
- 2710<dens<2820

SUBDIVISION OF ÄVRÖ GRANITE
- Ävrö quartz monzodiorite

ROCK UNIT FROM ESHI
- High confidence

ROCK DOMAIN (RSM)
- RSMA01

DEFORMATION ZONE (ZSM)
- DZ (ZSM)

DEFORMATION ZONE FROM ESHI
- DZ

FRACTURE DOMAINS (FSM)
- FSM EW007

LENGTH AND ELEVATION		BOREMAP DATA		DENSITY	EXTENDED SINGLE HOLE INTERPRETATION (ESHI)			GEOLOGICAL MODEL SDM-SITE LAXEMAR		
Length	Elevation (m.a.s.l.)	Rock Type	Rock Type (< 1m)	Wet Density kg/m*3	Subdivision of Ävrö granite	Rock Unit (RU)	Possible Deformation Zone	Rock Domain (RSM)	Deformation Zone (ZSM)	Fracture Domains (FSM)
0	0					RU1	DZ1 DZ2		ZSMNE942A	

Title COMPOSITE LOG for cored borehole KLX10C

Site	LAXEMAR	**Elevation [m.a.s.l.ToC]**	16.94
Borehole	KLX10C	**Inclination ToC [°]**	-60.02
Diameter [mm]	76	**Drilling Start Date**	2006-02-15 14:38:00
Length [m]	146.250	**Drilling Stop Date**	2006-02-28 07:22:00
Bearing ToC [°]	352.43	**Surveying Date**	2006-04-03 09:35:00
Coordinate System	RT90-RHB70	**Plot Date**	2008-05-04 22:04:41
Northing ToC [m]	6366372.07		
Easting ToC [m]	1548506.94		

ROCK TYPE LAXEMAR
- Ävrö granite
- Fine-grained dioritoid
- Fine-grained diorite-gabbro

WET DENSITY
- unclassified
- dens<2710
- 2710<dens<2820
- 2820<dens<2930

SUBDIVISION OF ÄVRÖ GRANITE
- Ävrö quartz monzodiorite
- Ävrö granodiorite

ROCK UNIT FROM ESHI
- High confidence

ROCK DOMAIN (RSM)
- RSMA01

DEFORMATION ZONE (ZSM)
- DZ (In BH)

DEFORMATION ZONE FROM ESHI
- DZ

FRACTURE DOMAINS (FSM)
- FSM EW007

LENGTH AND ELEVATION		BOREMAP DATA		DENSITY	EXTENDED SINGLE HOLE INTERPRETATION (ESHI)			GEOLOGICAL MODEL SDM-SITE LAXEMAR		
Length	Elevation (m.a.s.l.)	Rock Type	Rock Type (< 1m)	Wet Density kg/m*3	Subdivision of Ävrö granite	Rock Unit (RU)	Possible Deformation Zone	Rock Domain (RSM)	Deformation Zone (ZSM)	Fracture Domains (FSM)
0	0					RU1	DZ1			
							DZ2		klx10c_dz3	
							DZ3			
100						RU2	DZ4			
							DZ5			
	-100						DZ6		klx10c_dz7	
							DZ7			

Title COMPOSITE LOG for cored borehole KLX11A

Site	LAXEMAR	**Elevation [m.a.s.l.ToC]**	27.14
Borehole	KLX11A	**Inclination ToC [°]**	-76.76
Diameter [mm]	76	**Drilling Start Date**	2005-11-24 06:00:00
Length [m]	992.290	**Drilling Stop Date**	2006-03-02 11:00:00
Bearing ToC [°]	89.84	**Surveying Date**	2005-11-09 10:15:00
Coordinate System	RT90-RHB70	**Plot Date**	2008-05-04 22:04:41
Northing ToC [m]	6366339.72		
Easting ToC [m]	1546608.49		

ROCK TYPE LAXEMAR
- Fine-grained granite
- Pegmatite
- Quartz monzodiorite
- Fine-grained diorite-gabbro

SILICATE DENSITY
- dens<2680
- 2680<dens<2730
- 2730<dens<2800
- 2800<dens<2890
- dens>2890

SUBDIVISION OF ÄVRÖ GRANITE

ROCK UNIT FROM ESHI
- High confidence

ROCK DOMAIN (RSM)
- RSMD01

DEFORMATION ZONE (ZSM)
- DZ (In BH)

DEFORMATION ZONE FROM ESHI
- DZ

FRACTURE DOMAINS (FSM)
- FSM W

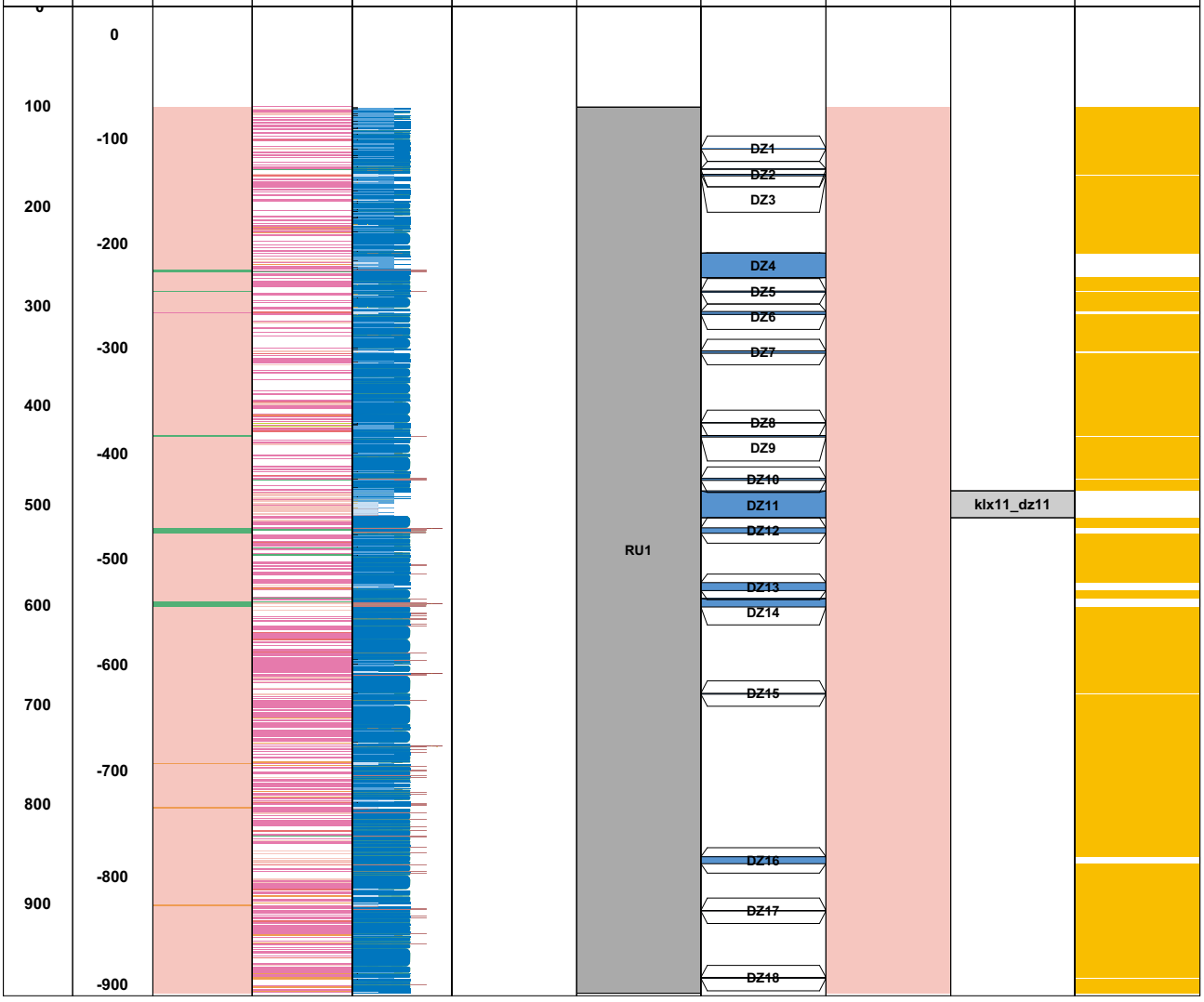

Title COMPOSITE LOG for cored borehole KLX11B

Site	LAXEMAR	**Elevation [m.a.s.l.ToC]**	27.27
Borehole	KLX11B	**Inclination ToC [°]**	-89.92
Diameter [mm]	76	**Drilling Start Date**	2006-04-22 16:00:00
Length [m]	100.200	**Drilling Stop Date**	2006-04-28 08:50:00
Bearing ToC [°]	136.16	**Surveying Date**	2006-05-09 09:25:00
Coordinate System	RT90-RHB70	**Plot Date**	2008-05-04 22:04:41
Northing ToC [m]	6366339.51		
Easting ToC [m]	1546604.89		

ROCK TYPE LAXEMAR
- Fine-grained granite
- Quartz monzodiorite

SILICATE DENSITY
- dens<2680
- 2680<dens<2730
- 2730<dens<2800
- 2800<dens<2890

SUBDIVISION OF ÄVRÖ GRANITE

ROCK UNIT FROM ESHI
- High confidence

ROCK DOMAIN (RSM)
- RSMD01

DEFORMATION ZONE (ZSM)

DEFORMATION ZONE FROM ESHI
- DZ

FRACTURE DOMAINS (FSM)
- FSM W

LENGTH AND ELEVATION		BOREMAP DATA		DENSITY	EXTENDED SINGLE HOLE INTERPRETATION (ESHI)			GEOLOGICAL MODEL SDM-SITE LAXEMAR		
Length	Elevation (m.a.s.l.)	Rock Type	Rock Type (< 1m)	Silicate Density kg/m*3	Subdivision of Ävrö granite	Rock Unit (RU)	Possible Deformation Zone	Rock Domain (RSM)	Deformation Zone (ZSM)	Fracture Domains (FSM)
0	0					RU1	DZ1			
100							DZ2			

Title COMPOSITE LOG for cored borehole KLX11C

Site	LAXEMAR	**Elevation [m.a.s.l.ToC]**	27.19
Borehole	KLX11C	**Inclination ToC [°]**	-60.72
Diameter [mm]	76	**Drilling Start Date**	2006-03-30 06:00:00
Length [m]	120.150	**Drilling Stop Date**	2006-04-05 14:30:00
Bearing ToC [°]	159.34	**Surveying Date**	2006-04-06 11:45:00
Coordinate System	RT90-RHB70	**Plot Date**	2008-05-04 22:04:41
Northing ToC [m]	6366350.26		
Easting ToC [m]	1546586.89		

ROCK TYPE LAXEMAR
Quartz monzodiorite

SILICATE DENSITY

ROCK UNIT FROM ESHI
High confidence

ROCK DOMAIN (RSM)
RSMD01

SUBDIVISION OF ÄVRÖ GRANITE

DEFORMATION ZONE FROM ESHI
DZ

FRACTURE DOMAINS (FSM)
FSM W

DEFORMATION ZONE (ZSM)

LENGTH AND ELEVATION		BOREMAP DATA		DENSITY	EXTENDED SINGLE HOLE INTERPRETATION (ESHI)			GEOLOGICAL MODEL SDM-SITE LAXEMAR		
Length	Elevation (m.a.s.l.)	Rock Type	Rock Type (< 1m)	Silicate Density kg/m*3	Subdivision of Ävrö granite	Rock Unit (RU)	Possible Deformation Zone	Rock Domain (RSM)	Deformation Zone (ZSM)	Fracture Domains (FSM)
0	0					RU1				
100										

Title COMPOSITE LOG for cored borehole KLX11D

Site	LAXEMAR	**Elevation [m.a.s.l.ToC]**	25.57
Borehole	KLX11D	**Inclination ToC [°]**	-58.99
Diameter [mm]	76	**Drilling Start Date**	2006-04-06 06:00:00
Length [m]	120.350	**Drilling Stop Date**	2006-04-13 08:00:00
Bearing ToC [°]	268.70	**Surveying Date**	2006-05-09 10:30:00
Coordinate System	RT90-RHB70	**Plot Date**	2008-05-04 22:04:41
Northing ToC [m]	6366357.37		
Easting ToC [m]	1546631.42		

ROCK TYPE LAXEMAR
- Fine-grained granite
- Quartz monzodiorite

SILICATE DENSITY

ROCK UNIT FROM ESHI
- High confidence

ROCK DOMAIN (RSM)
- RSMD01

SUBDIVISION OF ÄVRÖ GRANITE

DEFORMATION ZONE (ZSM)

DEFORMATION ZONE FROM ESHI
- DZ

FRACTURE DOMAINS (FSM)
- FSM W

LENGTH AND ELEVATION		BOREMAP DATA		DENSITY	EXTENDED SINGLE HOLE INTERPRETATION (ESHI)			GEOLOGICAL MODEL SDM-SITE LAXEMAR		
Length	Elevation (m.a.s.l.)	Rock Type	Rock Type (< 1m)	Silicate Density kg/m*3	Subdivision of Ävrö granite	Rock Unit (RU)	Possible Deformation Zone	Rock Domain (RSM)	Deformation Zone (ZSM)	Fracture Domains (FSM)
0	0					RU1	DZ1			
100							DZ2			
							DZ3			

Title COMPOSITE LOG for cored borehole KLX11E

Site	LAXEMAR	**Elevation [m.a.s.l.ToC]**	22.65
Borehole	KLX11E	**Inclination ToC [°]**	-60.91
Diameter [mm]	76	**Drilling Start Date**	2006-04-13 08:00:00
Length [m]	121.300	**Drilling Stop Date**	2006-04-21 14:08:00
Bearing ToC [°]	336.17	**Surveying Date**	2006-05-09 10:15:00
Coordinate System	RT90-RHB70	**Plot Date**	2008-05-04 22:04:41
Northing ToC [m]	6366300.39		
Easting ToC [m]	1546627.23		

ROCK TYPE LAXEMAR
Quartz monzodiorite

SILICATE DENSITY

ROCK UNIT FROM ESHI
High confidence

ROCK DOMAIN (RSM)
RSMD01

SUBDIVISION OF ÄVRÖ GRANITE

DEFORMATION ZONE (ZSM)

DEFORMATION ZONE FROM ESHI
DZ

FRACTURE DOMAINS (FSM)
FSM W

LENGTH AND ELEVATION		BOREMAP DATA		DENSITY	EXTENDED SINGLE HOLE INTERPRETATION (ESHI)			GEOLOGICAL MODEL SDM-SITE LAXEMAR		
Length	Elevation (m.a.s.l.)	Rock Type	Rock Type (< 1m)	Silicate Density kg/m*3	Subdivision of Ävrö granite	Rock Unit (RU)	Possible Deformation Zone	Rock Domain (RSM)	Deformation Zone (ZSM)	Fracture Domains (FSM)
0	0					RU1	DZ1			
100							DZ2			
							DZ3			
							DZ4			

Title COMPOSITE LOG for cored borehole KLX11F

Site	LAXEMAR	**Elevation [m.a.s.l.ToC]**	24.47
Borehole	KLX11F	**Inclination ToC [°]**	-61.13
Diameter [mm]	76	**Drilling Start Date**	2006-03-14 06:00:00
Length [m]	120.050	**Drilling Stop Date**	2006-03-17 18:00:00
Bearing ToC [°]	88.61	**Surveying Date**	2006-04-06 11:40:00
Coordinate System	RT90-RHB70	**Plot Date**	2008-05-04 22:04:41
Northing ToC [m]	6366314.09		
Easting ToC [m]	1546577.96		

ROCK TYPE LAXEMAR
- Fine-grained granite
- Quartz monzodiorite

SILICATE DENSITY

ROCK UNIT FROM ESHI
- High confidence

ROCK DOMAIN (RSM)
- RSMD01

SUBDIVISION OF ÄVRÖ GRANITE

DEFORMATION ZONE (ZSM)

DEFORMATION ZONE FROM ESHI
- DZ

FRACTURE DOMAINS (FSM)
- FSM W

LENGTH AND ELEVATION		BOREMAP DATA		DENSITY	EXTENDED SINGLE HOLE INTERPRETATION (ESHI)			GEOLOGICAL MODEL SDM-SITE LAXEMAR		
Length	Elevation (m.a.s.l.)	Rock Type	Rock Type (< 1m)	Silicate Density kg/m*3	Subdivision of Ävrö granite	Rock Unit (RU)	Possible Deformation Zone	Rock Domain (RSM)	Deformation Zone (ZSM)	Fracture Domains (FSM)
0	0					RU1	DZ1			
100										

Title COMPOSITE LOG for cored borehole KLX12A

Site	LAXEMAR	**Elevation [m.a.s.l.ToC]**	17.74
Borehole	KLX12A	**Inclination ToC [°]**	-75.30
Diameter [mm]	76	**Drilling Start Date**	2005-11-10 09:30:00
Length [m]	602.290	**Drilling Stop Date**	2006-03-04 14:48:00
Bearing ToC [°]	315.92	**Surveying Date**	2005-10-31 12:15:00
Coordinate System	RT90-RHB70	**Plot Date**	2008-05-04 22:04:41
Northing ToC [m]	6365630.78		
Easting ToC [m]	1548904.44		

ROCK TYPE LAXEMAR
- Fine-grained granite
- Ävrö granite
- Quartz monzodiorite
- Diorite / Gabbro
- Fine-grained dioritoid
- Fine-grained diorite-gabbro

WET DENSITY
- unclassified
- dens<2710
- 2710<dens<2820
- 2820<dens<2930
- dens>2930

SUBDIVISION OF ÄVRÖ GRANITE
- Ävrö quartz monzodiorite

ROCK UNIT FROM ESHI
- High confidence

ROCK DOMAIN (RSM)
- RSMD01
- RSMM01

DEFORMATION ZONE (ZSM)

DEFORMATION ZONE FROM ESHI
- DZ

FRACTURE DOMAINS (FSM)
- FSM NE005

LENGTH AND ELEVATION		BOREMAP DATA		DENSITY	EXTENDED SINGLE HOLE INTERPRETATION (ESHI)			GEOLOGICAL MODEL SDM-SITE LAXEMAR		
Length	Elevation (m.a.s.l.)	Rock Type	Rock Type (< 1m)	Wet Density kg/m*3	Subdivision of Ävrö granite	Rock Unit (RU)	Possible Deformation Zone	Rock Domain (RSM)	Deformation Zone (ZSM)	Fracture Domains (FSM)

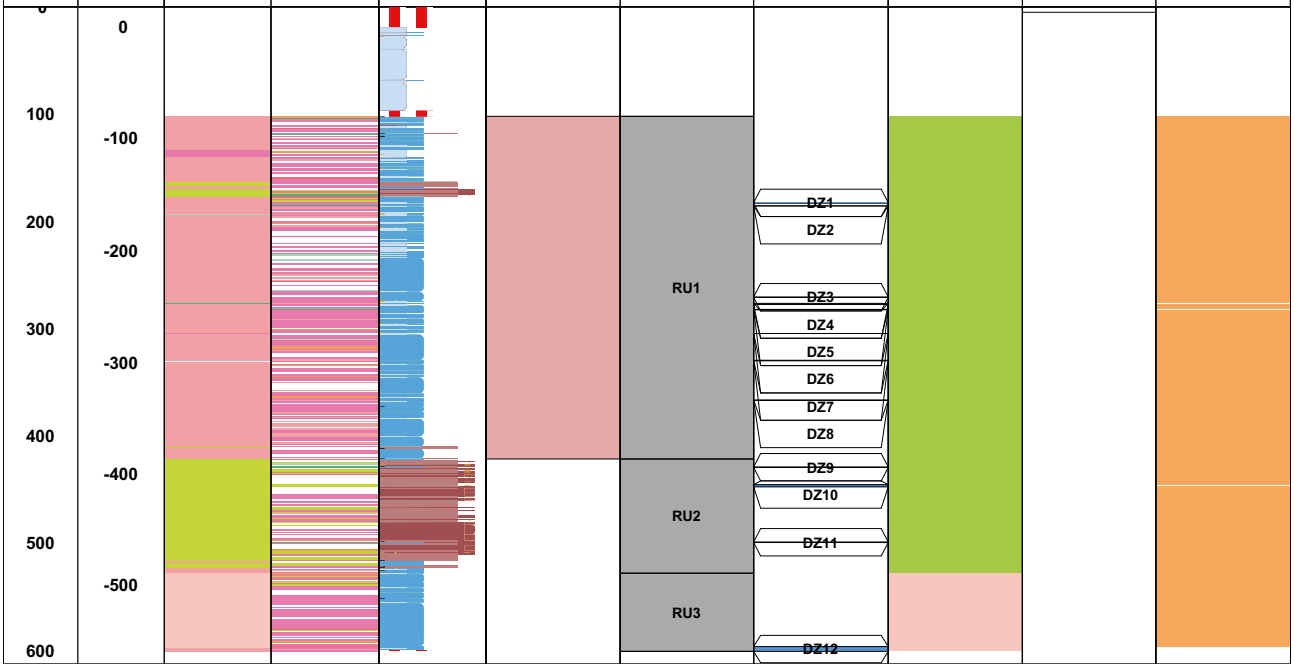

Title COMPOSITE LOG for cored borehole KLX13A

Site	LAXEMAR	**Elevation [m.a.s.l.ToC]**	24.15
Borehole	KLX13A	**Inclination ToC [°]**	-82.23
Diameter [mm]	76	**Drilling Start Date**	2006-05-19 14:02:00
Length [m]	595.850	**Drilling Stop Date**	2006-08-16 09:02:00
Bearing ToC [°]	224.48	**Surveying Date**	2006-04-03 10:15:00
Coordinate System	RT90-RHB70	**Plot Date**	2008-05-04 22:04:41
Northing ToC [m]	6367547.14		
Easting ToC [m]	1546787.36		

ROCK TYPE LAXEMAR
- Fine-grained granite
- Ävrö granite
- Diorite / Gabbro
- Fine-grained diorite-gabbro

WET DENSITY
- unclassified
- dens<2710
- 2710<dens<2820
- 2820<dens<2930
- dens>2930

SUBDIVISION OF ÄVRÖ GRANITE
- Ävrö quartz monzodiorite
- Ävrö granodiorite

ROCK UNIT FROM ESHI
- High confidence

ROCK DOMAIN (RSM)
- RSMM01

DEFORMATION ZONE (ZSM)
- DZ (ZSM)

DEFORMATION ZONE FROM ESHI
- DZ

FRACTURE DOMAINS (FSM)
- FSM W

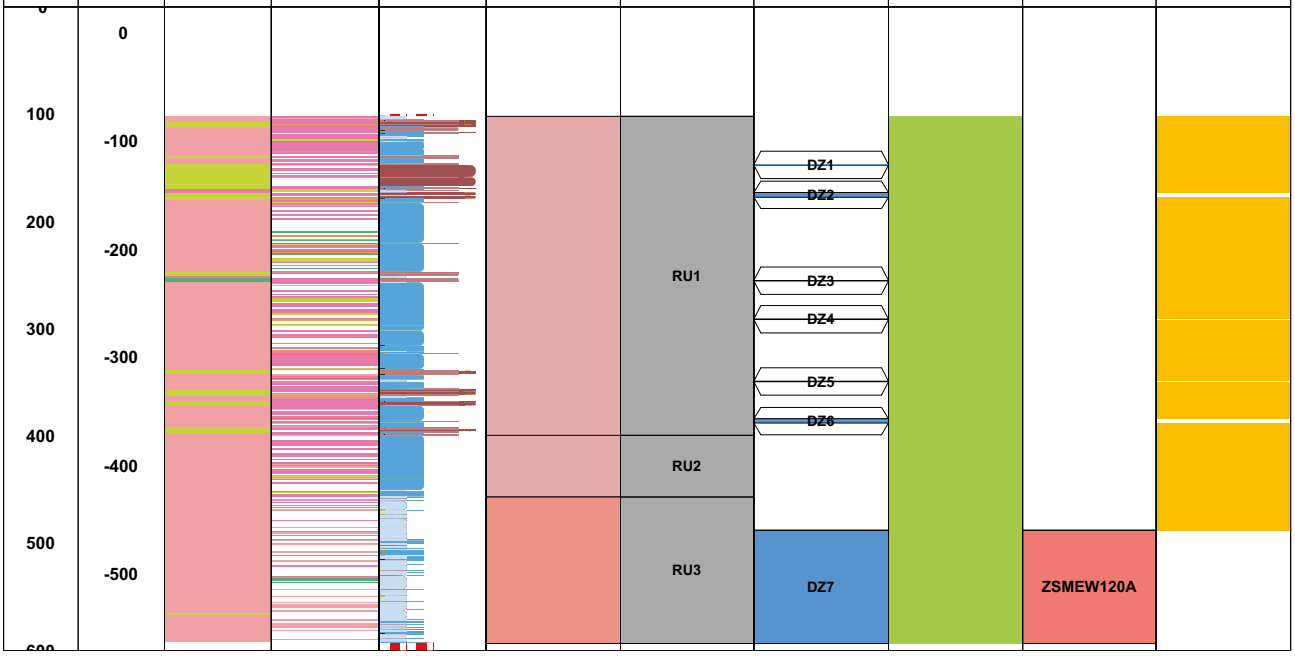

Title COMPOSITE LOG for cored borehole KLX14A

Site	LAXEMAR	**Elevation [m.a.s.l.ToC]**	16.35
Borehole	KLX14A	**Inclination ToC [°]**	-49.95
Diameter [mm]	76	**Drilling Start Date**	2006-08-19 08:00:00
Length [m]	176.270	**Drilling Stop Date**	2006-09-04 15:22:00
Bearing ToC [°]	111.95	**Surveying Date**	2006-09-11 14:55:00
Coordinate System	RT90-RHB70	**Plot Date**	2008-05-04 22:04:41
Northing ToC [m]	6365959.69		
Easting ToC [m]	1547146.87		

ROCK TYPE LAXEMAR
- Dolerite
- Fine-grained granite
- Quartz monzodiorite

SILICATE DENSITY
- dens<2680
- 2680<dens<2730
- 2730<dens<2800
- 2800<dens<2890

SUBDIVISION OF ÄVRÖ GRANITE

ROCK UNIT FROM ESHI
- High confidence

ROCK DOMAIN (RSM)
- RSMD01

DEFORMATION ZONE (ZSM)
- DZ (ZSM)

DEFORMATION ZONE FROM ESHI
- DZ

FRACTURE DOMAINS (FSM)
- FSM W

LENGTH AND ELEVATION		BOREMAP DATA		DENSITY	EXTENDED SINGLE HOLE INTERPRETATION (ESHI)			GEOLOGICAL MODEL SDM-SITE LAXEMAR		
Length	Elevation (m.a.s.l.)	Rock Type	Rock Type (< 1m)	Silicate Density kg/m*3	Subdivision of Ävrö granite	Rock Unit (RU)	Possible Deformation Zone	Rock Domain (RSM)	Deformation Zone (ZSM)	Fracture Domains (FSM)
0	0					RU1a	DZ1			
							DZ2			
							DZ3			
100						RU2	DZ4		ZSMNS059A	
	-100					RU1b	DZ5			
							DZ6			

Title COMPOSITE LOG for cored borehole KLX15A

Site	LAXEMAR	**Elevation [m.a.s.l.ToC]**	14.59
Borehole	KLX15A	**Inclination ToC [°]**	-54.41
Diameter [mm]	76	**Drilling Start Date**	2007-01-17 10:30:00
Length [m]	1000.430	**Drilling Stop Date**	2007-02-25 20:00:00
Bearing ToC [°]	198.83	**Surveying Date**	2007-01-02 12:45:00
Coordinate System	RT90-RHB70	**Plot Date**	2008-05-04 22:04:41
Northing ToC [m]	6365614.17		
Easting ToC [m]	1547987.47		

ROCK TYPE LAXEMAR
- Fine-grained granite
- Pegmatite
- Granite
- Ävrö granite
- Quartz monzodiorite
- Fine-grained diorite-gabbro

SILICATE DENSITY
- dens<2680
- 2680<dens<2730
- 2730<dens<2800
- 2800<dens<2890
- dens>2890

SUBDIVISION OF ÄVRÖ GRANITE
- Ävrö granite

ROCK UNIT FROM ESHI
- High confidence

ROCK DOMAIN (RSM)
- RSMD01

DEFORMATION ZONE (ZSM)
- DZ (ZSM)

DEFORMATION ZONE FROM ESHI
- DZ

FRACTURE DOMAINS (FSM)
- FSM C

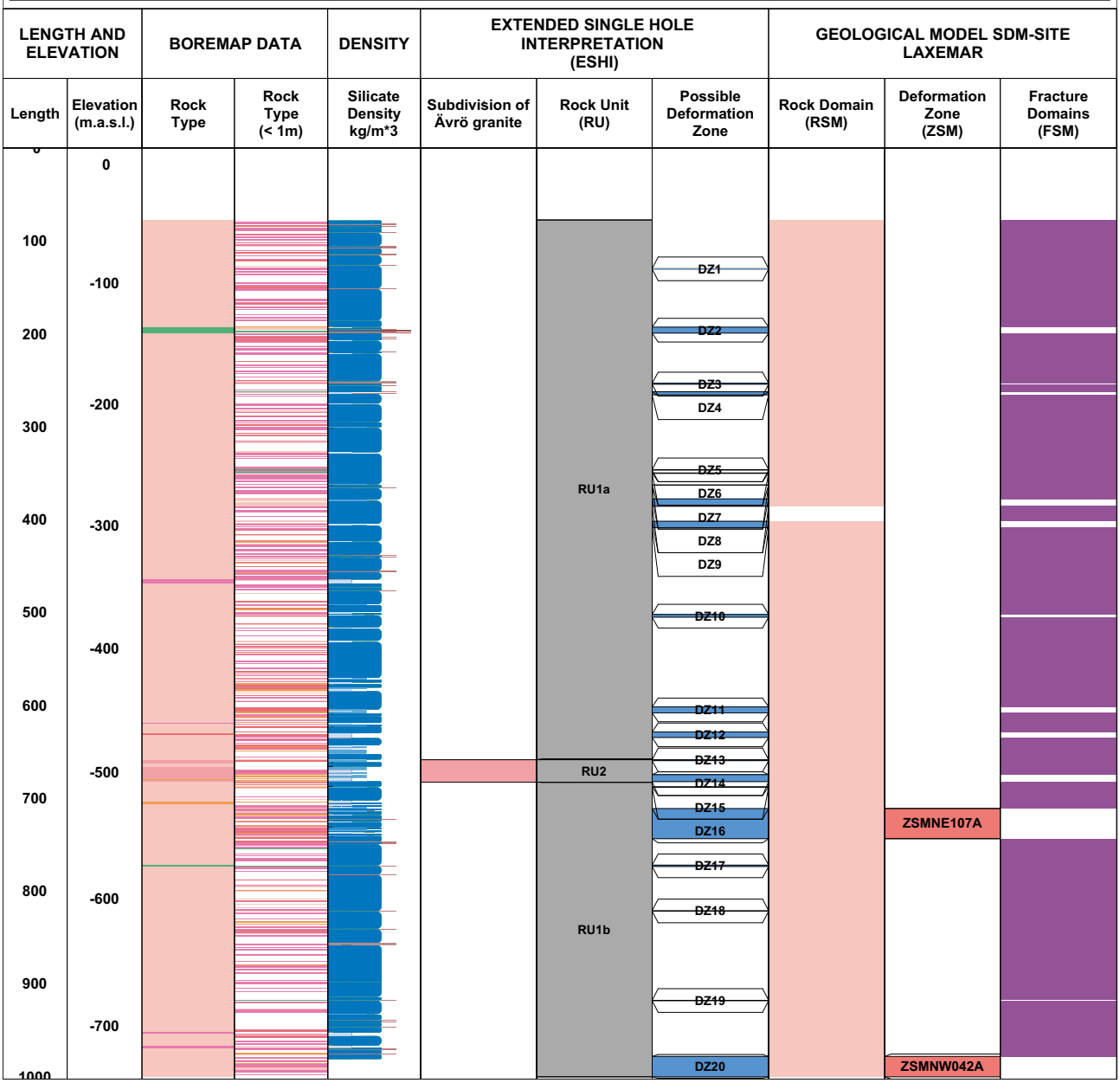

Title COMPOSITE LOG for cored borehole KLX16A

Site	LAXEMAR	**Elevation [m.a.s.l.ToC]**	18.85
Borehole	KLX16A	**Inclination ToC [°]**	-64.97
Diameter [mm]	76	**Drilling Start Date**	2006-11-28 13:00:00
Length [m]	433.550	**Drilling Stop Date**	2007-01-09 13:00:00
Bearing ToC [°]	294.37	**Surveying Date**	2007-01-17 12:30:00
Coordinate System	RT90-RHB70	**Plot Date**	2008-05-04 22:04:41
Northing ToC [m]	6364797.69		
Easting ToC [m]	1547584.06		

ROCK TYPE LAXEMAR
- Fine-grained granite
- Pegmatite
- Granite
- Quartz monzodiorite
- Fine-grained dioritoid
- Fine-grained diorite-gabbro

SILICATE DENSITY
- dens<2680
- 2680<dens<2730
- 2730<dens<2800
- 2800<dens<2890
- dens>2890

SUBDIVISION OF ÄVRÖ GRANITE

ROCK UNIT FROM ESHI
- High confidence

ROCK DOMAIN (RSM)
- RSMD01

DEFORMATION ZONE (ZSM)
- DZ (ZSM)

DEFORMATION ZONE FROM ESHI
- DZ

FRACTURE DOMAINS (FSM)
- FSM S

LENGTH AND ELEVATION		BOREMAP DATA		DENSITY	EXTENDED SINGLE HOLE INTERPRETATION (ESHI)			GEOLOGICAL MODEL SDM-SITE LAXEMAR		
Length	Elevation (m.a.s.l.)	Rock Type	Rock Type (< 1m)	Silicate Density kg/m*3	Subdivision of Ävrö granite	Rock Unit (RU)	Possible Deformation Zone	Rock Domain (RSM)	Deformation Zone (ZSM)	Fracture Domains (FSM)

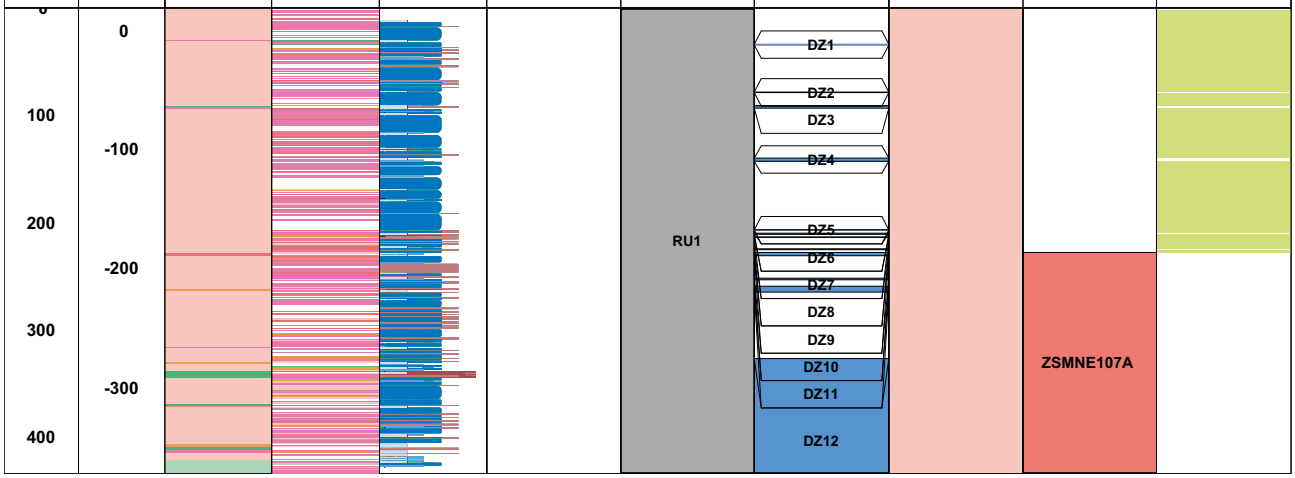

Title COMPOSITE LOG for cored borehole KLX17A

Site	LAXEMAR	**Elevation [m.a.s.l.ToC]**	27.63
Borehole	KLX17A	**Inclination ToC [°]**	-61.33
Diameter [mm]	76	**Drilling Start Date**	2006-09-13 06:00:00
Length [m]	701.080	**Drilling Stop Date**	2006-10-23 09:30:00
Bearing ToC [°]	11.21	**Surveying Date**	2006-08-16 16:03:00
Coordinate System	RT90-RHB70	**Plot Date**	2008-05-04 22:04:41
Northing ToC [m]	6366848.75		
Easting ToC [m]	1546862.09		

ROCK TYPE LAXEMAR
- Fine-grained granite
- Ävrö granite
- Diorite / Gabbro
- Fine-grained diorite-gabbro

WET DENSITY
- unclassified
- dens<2710
- 2710<dens<2820
- 2820<dens<2930
- dens>2930

SUBDIVISION OF ÄVRÖ GRANITE
- Ävrö quartz monzodiorite
- Ävrö granodiorite

ROCK UNIT FROM ESHI
- High confidence

ROCK DOMAIN (RSM)
- RSMM01

DEFORMATION ZONE (ZSM)
- DZ (ZSM)

DEFORMATION ZONE FROM ESHI
- DZ

FRACTURE DOMAINS (FSM)
- FSM W

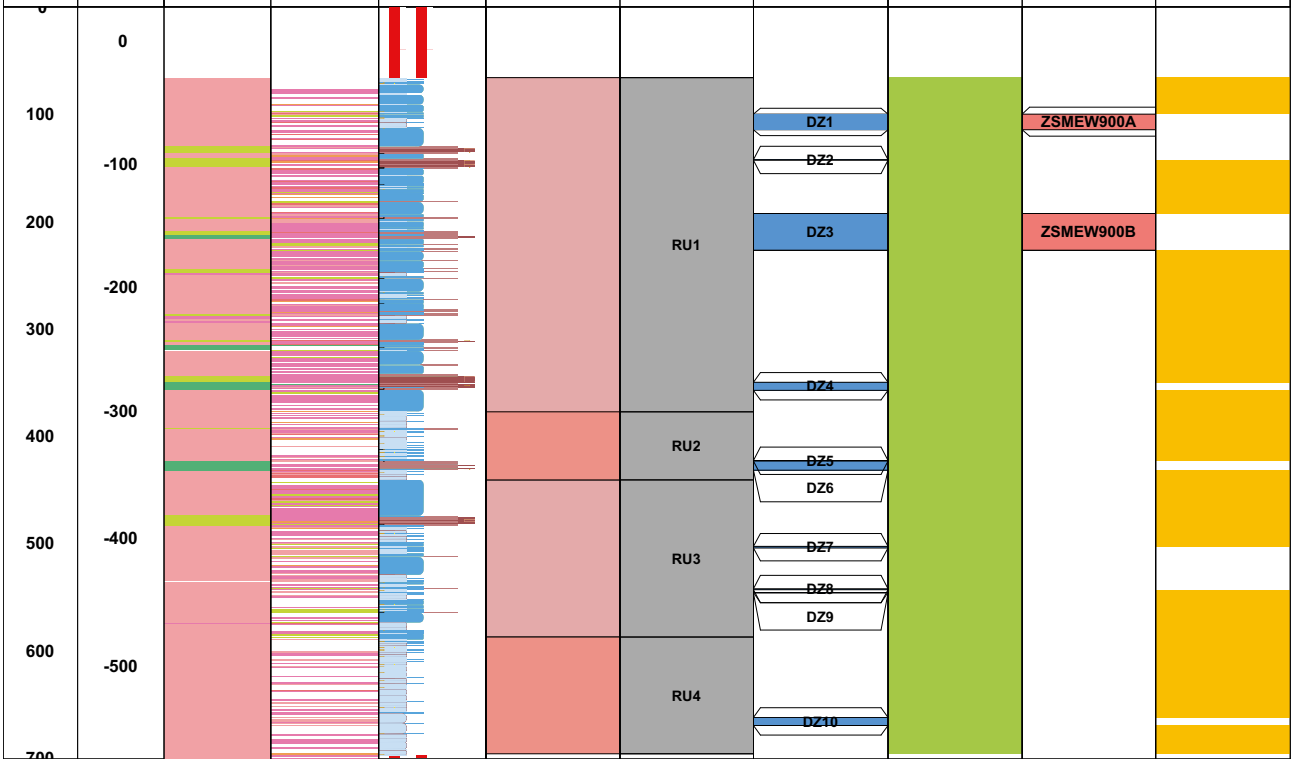

Title COMPOSITE LOG for cored borehole KLX18A

Site	LAXEMAR	**Elevation [m.a.s.l.ToC]**	21.01
Borehole	KLX18A	**Inclination ToC [°]**	-82.10
Diameter [mm]	76	**Drilling Start Date**	2006-03-29 10:00:00
Length [m]	611.280	**Drilling Stop Date**	2006-05-02 12:22:00
Bearing ToC [°]	271.40	**Surveying Date**	2006-02-22 11:15:00
Coordinate System	RT90-RHB70	**Plot Date**	2008-05-04 22:04:41
Northing ToC [m]	6366413.39		
Easting ToC [m]	1547966.35		

ROCK TYPE LAXEMAR
- Fine-grained granite
- Ävrö granite
- Diorite / Gabbro
- Fine-grained diorite-gabbro

WET DENSITY
- dens<2710
- 2710<dens<2820
- 2820<dens<2930
- dens>2930

SUBDIVISION OF ÄVRÖ GRANITE
- Ävrö quartz monzodiorite
- Ävrö granodiorite

ROCK UNIT FROM ESHI
- High confidence

ROCK DOMAIN (RSM)
- RSMA01
- RSMM01

DEFORMATION ZONE (ZSM)
- DZ (ZSM)

DEFORMATION ZONE FROM ESHI
- DZ

FRACTURE DOMAINS (FSM)
- FSM C
- FSM EW007

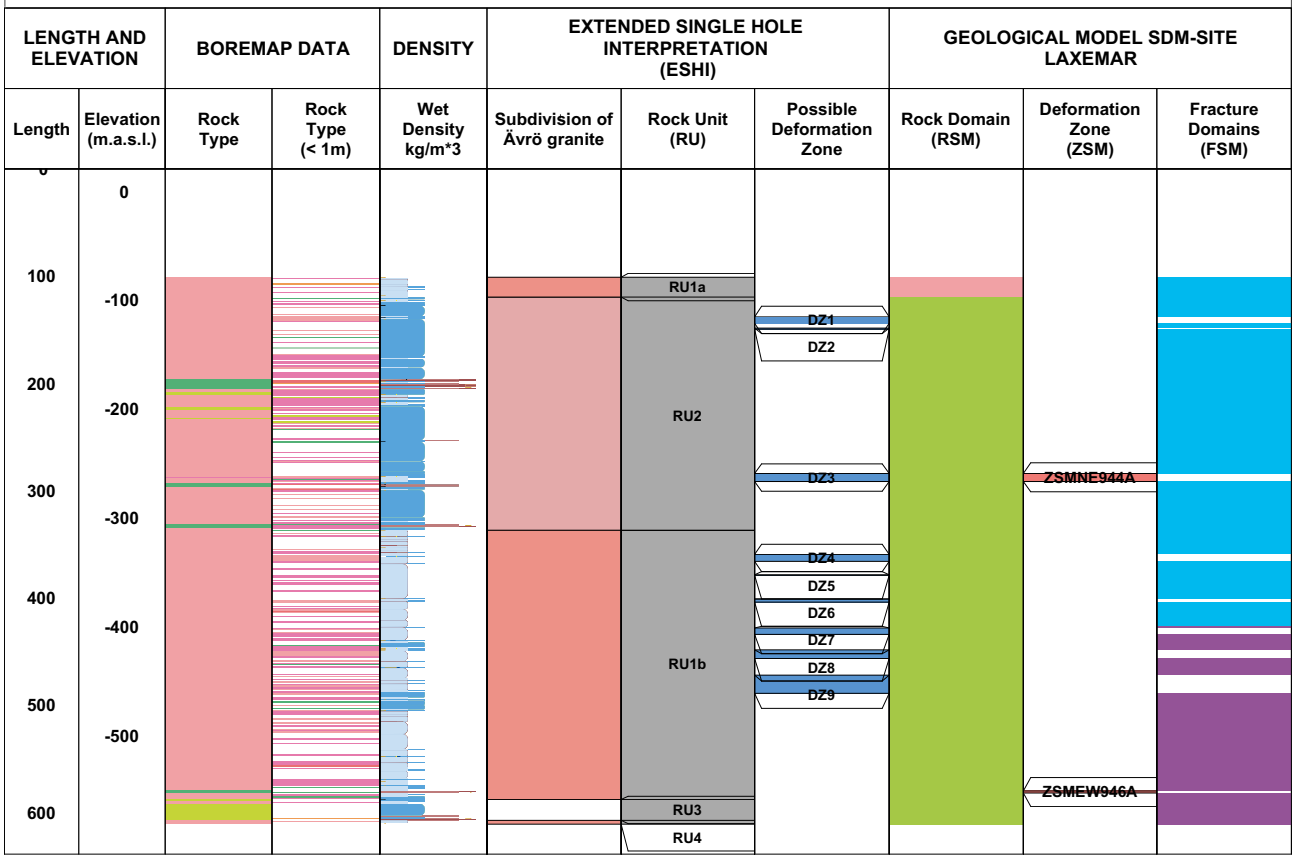

Title COMPOSITE LOG for cored borehole KLX19A

Site	LAXEMAR	**Elevation [m.a.s.l.ToC]**	16.87
Borehole	KLX19A	**Inclination ToC [°]**	-57.54
Diameter [mm]	76	**Drilling Start Date**	2006-06-03 11:00:00
Length [m]	800.070	**Drilling Stop Date**	2006-09-20 17:27:00
Bearing ToC [°]	197.13	**Surveying Date**	2006-05-22 13:39:00
Coordinate System	RT90-RHB70	**Plot Date**	2008-05-04 22:04:41
Northing ToC [m]	6365901.42		
Easting ToC [m]	1547004.62		

ROCK TYPE LAXEMAR
- Dolerite
- Fine-grained granite
- Pegmatite
- Quartz monzodiorite
- Fine-grained diorite-gabbro

SILICATE DENSITY
- dens<2710
- 2710<dens<2820
- xx<dens<yy
- 2820<dens<2930
- dens>2930

SUBDIVISION OF ÄVRÖ GRANITE

ROCK UNIT FROM ESHI
- High confidence

ROCK DOMAIN (RSM)
- RSMD01

DEFORMATION ZONE (ZSM)
- DZ (ZSM)
- DZ (In BH)

DEFORMATION ZONE FROM ESHI
- DZ

FRACTURE DOMAINS (FSM)
- FSM W

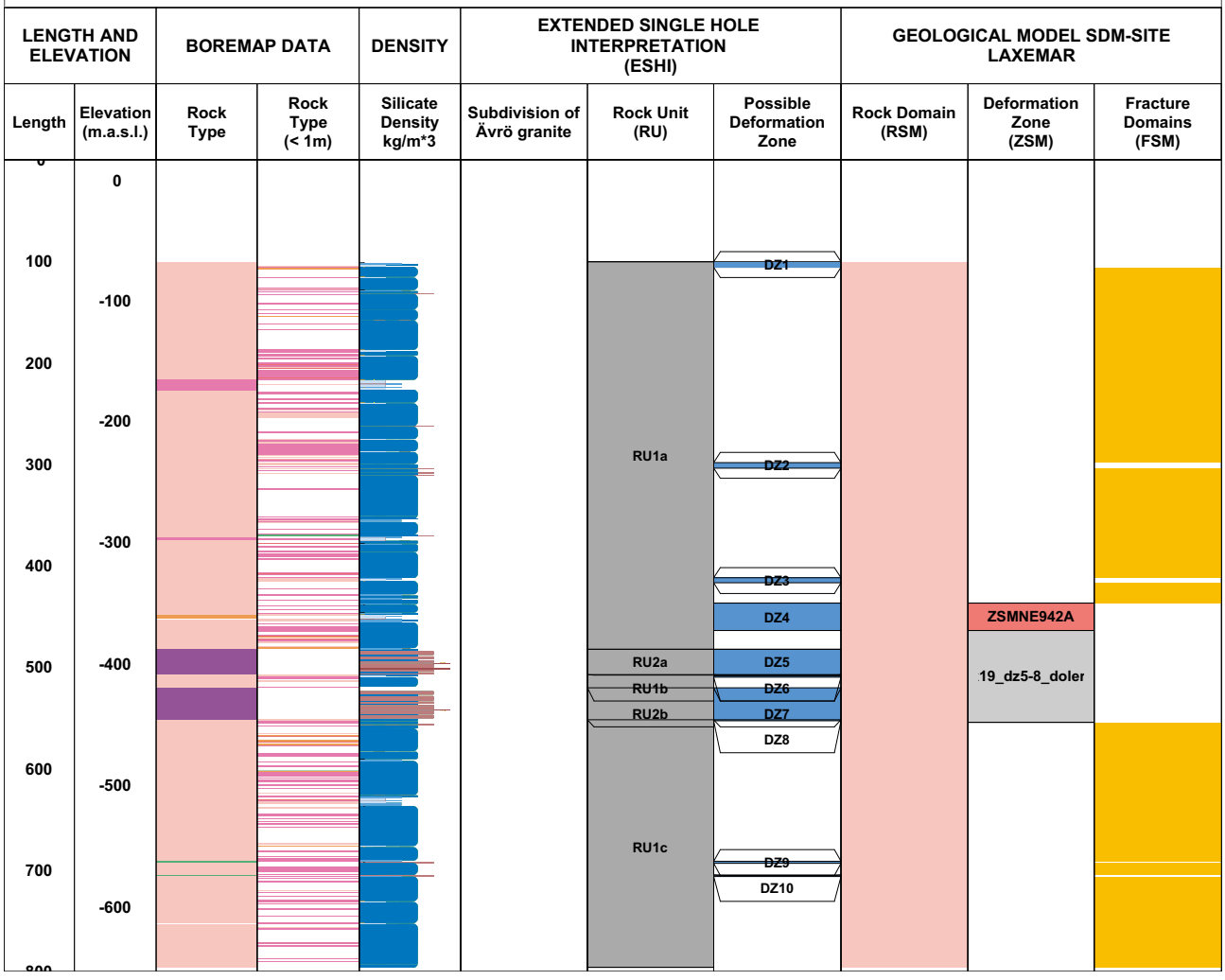

Title COMPOSITE LOG for cored borehole KLX20A

Site	LAXEMAR	**Elevation [m.a.s.l.ToC]**	27.24
Borehole	KLX20A	**Inclination ToC [°]**	-50.02
Diameter [mm]	76	**Drilling Start Date**	2006-03-25 06:00:00
Length [m]	457.920	**Drilling Stop Date**	2006-04-24 13:20:00
Bearing ToC [°]	270.60	**Surveying Date**	2006-05-09 09:15:00
Coordinate System	RT90-RHB70	**Plot Date**	2008-05-04 22:04:41
Northing ToC [m]	6366334.57		
Easting ToC [m]	1546604.89		

ROCK TYPE LAXEMAR
- Dolerite
- Fine-grained granite
- Quartz monzodiorite
- Fine-grained diorite-gabbro

SILICATE DENSITY
- dens<2680
- 2680<dens<2730
- 2730<dens<2800
- 2800<dens<2890
- dens>2890

SUBDIVISION OF ÄVRÖ GRANITE

ROCK UNIT FROM ESHI
- High confidence

ROCK DOMAIN (RSM)
- RSMD01

DEFORMATION ZONE (ZSM)
- DZ (ZSM)

DEFORMATION ZONE FROM ESHI
- DZ

FRACTURE DOMAINS (FSM)
- FSM W

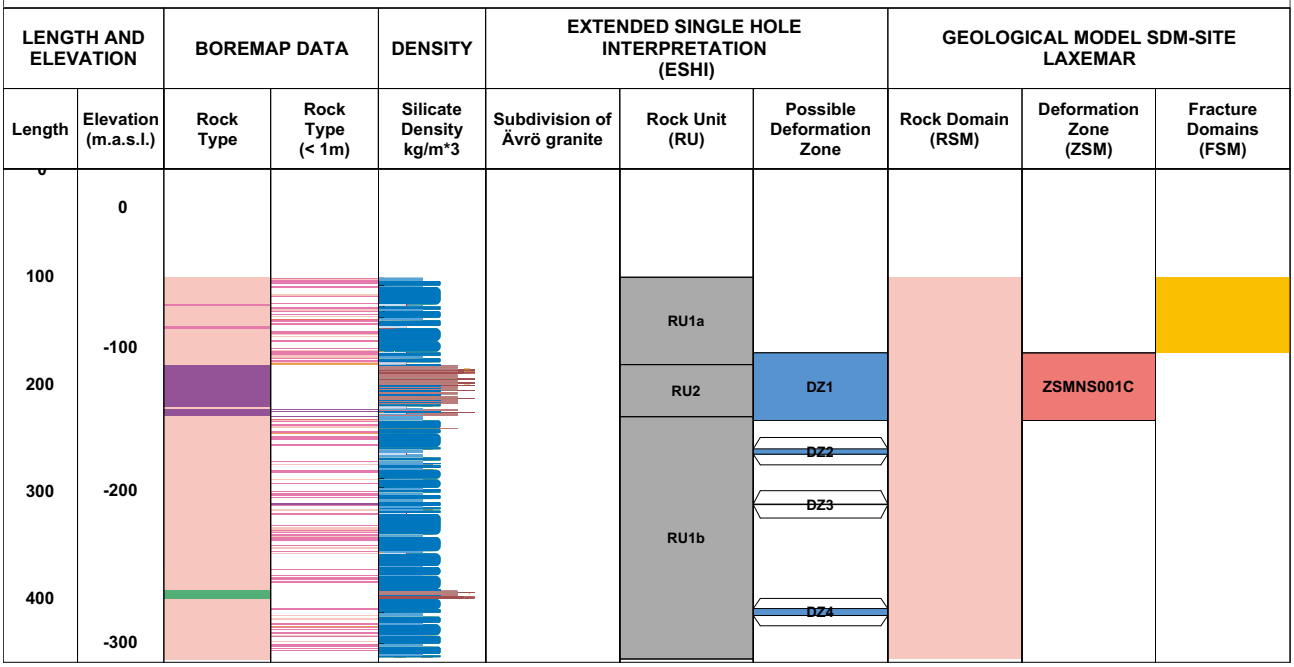

Title COMPOSITE LOG for cored borehole KLX21B

Site	LAXEMAR	**Elevation [m.a.s.l.ToC]**	10.68
Borehole	KLX21B	**Inclination ToC [°]**	-70.85
Diameter [mm]	76	**Drilling Start Date**	2006-10-12 08:00:00
Length [m]	858.780	**Drilling Stop Date**	2006-11-29 10:30:00
Bearing ToC [°]	225.05	**Surveying Date**	2006-09-27 11:15:00
Coordinate System	RT90-RHB70	**Plot Date**	2008-05-04 22:04:41
Northing ToC [m]	6366164.00		
Easting ToC [m]	1549715.10		

ROCK TYPE LAXEMAR
- Fine-grained granite
- Ävrö granite
- Quartz monzodiorite
- Diorite / Gabbro
- Fine-grained dioritoid
- Fine-grained diorite-gabbro

WET DENSITY
- unclassified
- dens<2710
- 2710<dens<2820
- 2820<dens<2930

SUBDIVISION OF ÄVRÖ GRANITE
- Ävrö quartz monzodiorite
- Ävrö granodiorite

ROCK UNIT FROM ESHI
- High confidence

ROCK DOMAIN (RSM)
- RSMA01
- RSMD01

DEFORMATION ZONE (ZSM)
- DZ (In BH)

DEFORMATION ZONE FROM ESHI
- DZ

FRACTURE DOMAINS (FSM)
- FSM NE005

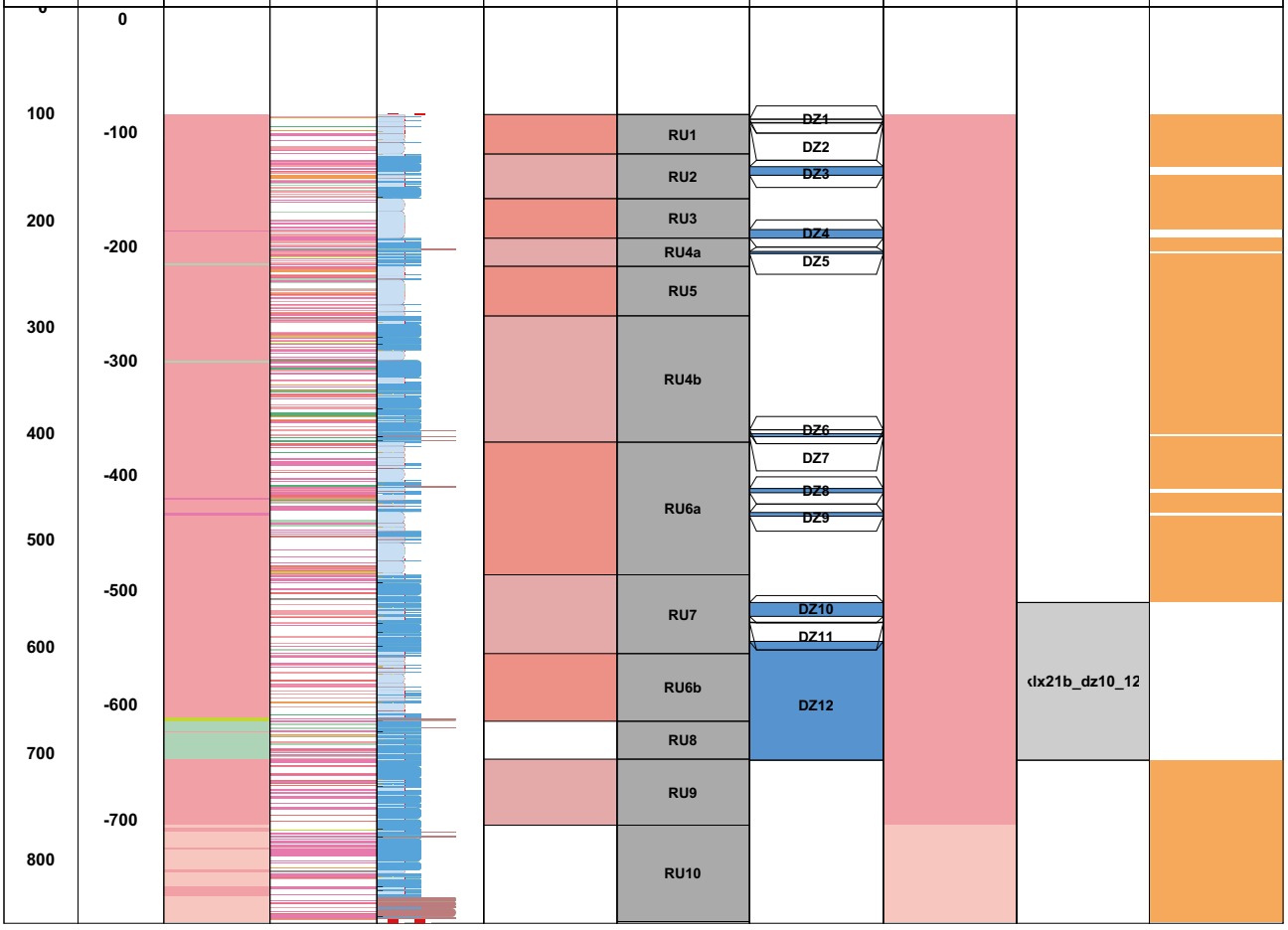

Title COMPOSITE LOG for cored borehole KLX22A

Site	LAXEMAR	**Elevation [m.a.s.l.ToC]**	21.97
Borehole	KLX22A	**Inclination ToC [°]**	-60.33
Diameter [mm]	76	**Drilling Start Date**	2006-05-05 12:00:00
Length [m]	100.450	**Drilling Stop Date**	2006-05-12 13:40:00
Bearing ToC [°]	179.19	**Surveying Date**	2006-08-03 10:51:00
Coordinate System	RT90-RHB70	**Plot Date**	2008-05-04 22:04:41
Northing ToC [m]	6366548.35		
Easting ToC [m]	1546688.60		

ROCK TYPE LAXEMAR
- Fine-grained granite
- Quartz monzodiorite
- Fine-grained diorite-gabbro

SILICATE DENSITY
- dens<2680
- 2680<dens<2730
- 2730<dens<2800
- 2800<dens<2890

SUBDIVISION OF ÄVRÖ GRANITE

ROCK UNIT FROM ESHI
- High confidence

ROCK DOMAIN (RSM)
- RSMD01

DEFORMATION ZONE (ZSM)

DEFORMATION ZONE FROM ESHI
- DZ

FRACTURE DOMAINS (FSM)
- FSM W

LENGTH AND ELEVATION		BOREMAP DATA		DENSITY	EXTENDED SINGLE HOLE INTERPRETATION (ESHI)			GEOLOGICAL MODEL SDM-SITE LAXEMAR		
Length	Elevation (m.a.s.l.)	Rock Type	Rock Type (< 1m)	Silicate Density kg/m*3	Subdivision of Ävrö granite	Rock Unit (RU)	Possible Deformation Zone	Rock Domain (RSM)	Deformation Zone (ZSM)	Fracture Domains (FSM)
0	0					RU1	DZ1			
100										

Title COMPOSITE LOG for cored borehole KLX22B

Site	LAXEMAR	**Elevation [m.a.s.l.ToC]**	21.58
Borehole	KLX22B	**Inclination ToC [°]**	-61.24
Diameter [mm]	76	**Drilling Start Date**	2006-05-13 09:13:00
Length [m]	100.250	**Drilling Stop Date**	2006-05-18 13:03:00
Bearing ToC [°]	343.97	**Surveying Date**	2006-08-03 10:46:00
Coordinate System	RT90-RHB70	**Plot Date**	2008-05-04 22:04:41
Northing ToC [m]	6366553.13		
Easting ToC [m]	1546685.41		

ROCK TYPE LAXEMAR
- Fine-grained granite
- Quartz monzodiorite
- Fine-grained diorite-gabbro

SILICATE DENSITY
- dens<2680
- 2680<dens<2730
- 2730<dens<2800
- 2800<dens<2890
- dens>2890

SUBDIVISION OF ÄVRÖ GRANITE

ROCK UNIT FROM ESHI
- High confidence

ROCK DOMAIN (RSM)
- RSMD01

DEFORMATION ZONE (ZSM)

DEFORMATION ZONE FROM ESHI
- DZ

FRACTURE DOMAINS (FSM)
- FSM W

LENGTH AND ELEVATION		BOREMAP DATA		DENSITY	EXTENDED SINGLE HOLE INTERPRETATION (ESHI)			GEOLOGICAL MODEL SDM-SITE LAXEMAR		
Length	Elevation (m.a.s.l.)	Rock Type	Rock Type (< 1m)	Silicate Density kg/m*3	Subdivision of Ävrö granite	Rock Unit (RU)	Possible Deformation Zone	Rock Domain (RSM)	Deformation Zone (ZSM)	Fracture Domains (FSM)
0	0					RU1	DZ1			
100										

Title COMPOSITE LOG for cored borehole KLX23A

Site	LAXEMAR	**Elevation [m.a.s.l.ToC]**	22.26
Borehole	KLX23A	**Inclination ToC [°]**	-61.35
Diameter [mm]	76	**Drilling Start Date**	2006-05-21 10:27:00
Length [m]	100.150	**Drilling Stop Date**	2006-05-27 07:45:00
Bearing ToC [°]	28.73	**Surveying Date**	2006-08-07 10:28:00
Coordinate System	RT90-RHB70	**Plot Date**	2008-05-04 22:04:41
Northing ToC [m]	6366106.89		
Easting ToC [m]	1546715.74		

ROCK TYPE LAXEMAR
- Quartz monzodiorite

SILICATE DENSITY
- dens<2680
- 2680<dens<2730
- 2730<dens<2800

SUBDIVISION OF ÄVRÖ GRANITE

ROCK UNIT FROM ESHI
- High confidence

ROCK DOMAIN (RSM)
- RSMD01

DEFORMATION ZONE (ZSM)

DEFORMATION ZONE FROM ESHI
- DZ

FRACTURE DOMAINS (FSM)
- FSM W

LENGTH AND ELEVATION		BOREMAP DATA		DENSITY	EXTENDED SINGLE HOLE INTERPRETATION (ESHI)			GEOLOGICAL MODEL SDM-SITE LAXEMAR		
Length	Elevation (m.a.s.l.)	Rock Type	Rock Type (< 1m)	Silicate Density kg/m*3	Subdivision of Ävrö granite	Rock Unit (RU)	Possible Deformation Zone	Rock Domain (RSM)	Deformation Zone (ZSM)	Fracture Domains (FSM)
0	0					RU1	DZ1 DZ2			
100										

Title COMPOSITE LOG for cored borehole KLX23B

Site	LAXEMAR	**Elevation [m.a.s.l.ToC]**	22.32
Borehole	KLX23B	**Inclination ToC [°]**	-60.84
Diameter [mm]	76	**Drilling Start Date**	2006-05-28 13:55:00
Length [m]	50.270	**Drilling Stop Date**	2006-05-31 11:15:00
Bearing ToC [°]	121.36	**Surveying Date**	2006-08-04 11:00:00
Coordinate System	RT90-RHB70	**Plot Date**	2008-05-04 22:04:41
Northing ToC [m]	6366101.90		
Easting ToC [m]	1546717.33		

ROCK TYPE LAXEMAR
- Quartz monzodiorite

SILICATE DENSITY
- dens<2680
- 2680<dens<2730
- 2730<dens<2800

ROCK UNIT FROM ESHI
- High confidence

ROCK DOMAIN (RSM)
- RSMD01

DEFORMATION ZONE FROM ESHI
- DZ

FRACTURE DOMAINS (FSM)
- FSM W

SUBDIVISION OF ÄVRÖ GRANITE

DEFORMATION ZONE (ZSM)

LENGTH AND ELEVATION		BOREMAP DATA		DENSITY	EXTENDED SINGLE HOLE INTERPRETATION (ESHI)			GEOLOGICAL MODEL SDM-SITE LAXEMAR		
Length	Elevation (m.a.s.l.)	Rock Type	Rock Type (< 1m)	Silicate Density kg/m*3	Subdivision of Ävrö granite	Rock Unit (RU)	Possible Deformation Zone	Rock Domain (RSM)	Deformation Zone (ZSM)	Fracture Domains (FSM)
0	0					RU1	DZ1			

Title COMPOSITE LOG for cored borehole KLX24A

Site	LAXEMAR	**Elevation [m.a.s.l.ToC]**	21.29
Borehole	KLX24A	**Inclination ToC [°]**	-59.14
Diameter [mm]	76	**Drilling Start Date**	2006-06-14 11:00:00
Length [m]	100.170	**Drilling Stop Date**	2006-06-29 08:45:00
Bearing ToC [°]	98.41	**Surveying Date**	2006-08-03 12:21:00
Coordinate System	RT90-RHB70	**Plot Date**	2008-05-04 22:04:41
Northing ToC [m]	6366423.35		
Easting ToC [m]	1546853.80		

ROCK TYPE LAXEMAR
- Fine-grained granite
- Quartz monzodiorite

SILICATE DENSITY
- dens<2680
- 2680<dens<2730
- 2730<dens<2800
- 2800<dens<2890

SUBDIVISION OF ÄVRÖ GRANITE

ROCK UNIT FROM ESHI
- High confidence

ROCK DOMAIN (RSM)
- RSMD01

DEFORMATION ZONE (ZSM)

DEFORMATION ZONE FROM ESHI
- DZ

FRACTURE DOMAINS (FSM)
- FSM W

LENGTH AND ELEVATION		BOREMAP DATA		DENSITY	EXTENDED SINGLE HOLE INTERPRETATION (ESHI)			GEOLOGICAL MODEL SDM-SITE LAXEMAR		
Length	Elevation (m.a.s.l.)	Rock Type	Rock Type (< 1m)	Silicate Density kg/m*3	Subdivision of Ävrö granite	Rock Unit (RU)	Possible Deformation Zone	Rock Domain (RSM)	Deformation Zone (ZSM)	Fracture Domains (FSM)
0	0					RU1	DZ1			
							DZ2			
100							DZ3			
							DZ4			

Title COMPOSITE LOG for cored borehole KLX25A

Site	LAXEMAR	**Elevation [m.a.s.l.ToC]**	22.84
Borehole	KLX25A	**Inclination ToC [°]**	-59.45
Diameter [mm]	76	**Drilling Start Date**	2006-07-01 14:00:00
Length [m]	50.240	**Drilling Stop Date**	2006-07-04 14:00:00
Bearing ToC [°]	145.73	**Surveying Date**	2006-08-03 11:48:00
Coordinate System	RT90-RHB70	**Plot Date**	2008-05-04 22:04:41
Northing ToC [m]	6366274.74		
Easting ToC [m]	1546769.66		

ROCK TYPE LAXEMAR
- Quartz monzodiorite

SILICATE DENSITY
- 2730<dens<2800
- 2800<dens<2890

ROCK UNIT FROM ESHI
- High confidence

ROCK DOMAIN (RSM)
- RSMD01

SUBDIVISION OF ÄVRÖ GRANITE

DEFORMATION ZONE (ZSM)

DEFORMATION ZONE FROM ESHI
- DZ

FRACTURE DOMAINS (FSM)
- FSM W

LENGTH AND ELEVATION		BOREMAP DATA		DENSITY	EXTENDED SINGLE HOLE INTERPRETATION (ESHI)			GEOLOGICAL MODEL SDM-SITE LAXEMAR		
Length	Elevation (m.a.s.l.)	Rock Type	Rock Type (< 1m)	Silicate Density kg/m*3	Subdivision of Ävrö granite	Rock Unit (RU)	Possible Deformation Zone	Rock Domain (RSM)	Deformation Zone (ZSM)	Fracture Domains (FSM)
0	0					RU1	DZ1			

Title COMPOSITE LOG for cored borehole KLX26A

Site	LAXEMAR	**Elevation [m.a.s.l.ToC]**	15.63
Borehole	KLX26A	**Inclination ToC [°]**	-60.44
Diameter [mm]	76	**Drilling Start Date**	2006-08-03 06:00:00
Length [m]	101.140	**Drilling Stop Date**	2006-08-11 11:00:00
Bearing ToC [°]	93.47	**Surveying Date**	2006-09-12 11:30:00
Coordinate System	RT90-RHB70	**Plot Date**	2008-05-04 22:04:41
Northing ToC [m]	6365546.49		
Easting ToC [m]	1549029.90		

ROCK TYPE LAXEMAR
- Fine-grained granite
- Ävrö granite
- Quartz monzodiorite
- Diorite / Gabbro
- Fine-grained diorite-gabbro

SILICATE DENSITY
- dens<2680
- 2680<dens<2730
- 2730<dens<2800
- 2800<dens<2890
- dens>2890

SUBDIVISION OF ÄVRÖ GRANITE

ROCK UNIT FROM ESHI
- High confidence

ROCK DOMAIN (RSM)
- RSMM01

DEFORMATION ZONE (ZSM)

DEFORMATION ZONE FROM ESHI
- DZ

FRACTURE DOMAINS (FSM)
- FSM NE005

LENGTH AND ELEVATION		BOREMAP DATA		DENSITY	EXTENDED SINGLE HOLE INTERPRETATION (ESHI)			GEOLOGICAL MODEL SDM-SITE LAXEMAR		
Length	Elevation (m.a.s.l.)	Rock Type	Rock Type (< 1m)	Silicate Density kg/m*3	Subdivision of Ävrö granite	Rock Unit (RU)	Possible Deformation Zone	Rock Domain (RSM)	Deformation Zone (ZSM)	Fracture Domains (FSM)
0	0					RU1a	DZ1			
						RU2	DZ2			
100						RU1b	DZ3			
							DZ4			

Title COMPOSITE LOG for cored borehole KLX26B

Site	LAXEMAR	**Elevation [m.a.s.l.ToC]**	15.82
Borehole	KLX26B	**Inclination ToC [°]**	-60.00
Diameter [mm]	76	**Drilling Start Date**	2006-08-12 09:00:00
Length [m]	50.370	**Drilling Stop Date**	2006-08-17 07:15:00
Bearing ToC [°]	137.42	**Surveying Date**	2006-09-12 11:25:00
Coordinate System	RT90-RHB70	**Plot Date**	2008-05-04 22:04:41
Northing ToC [m]	6365550.66		
Easting ToC [m]	1549025.61		

ROCK TYPE LAXEMAR
- Fine-grained granite
- Diorite / Gabbro

SILICATE DENSITY
- dens<2680
- 2730<dens<2890
- 2800<dens<2890
- dens>2890

SUBDIVISION OF ÄVRÖ GRANITE

ROCK UNIT FROM ESHI
- High confidence

ROCK DOMAIN (RSM)
- RSMM01

DEFORMATION ZONE (ZSM)

DEFORMATION ZONE FROM ESHI
- DZ

FRACTURE DOMAINS (FSM)
- FSM NE005

LENGTH AND ELEVATION		BOREMAP DATA		DENSITY	EXTENDED SINGLE HOLE INTERPRETATION (ESHI)			GEOLOGICAL MODEL SDM-SITE LAXEMAR		
Length	Elevation (m.a.s.l.)	Rock Type	Rock Type (< 1m)	Silicate Density kg/m*3	Subdivision of Ävrö granite	Rock Unit (RU)	Possible Deformation Zone	Rock Domain (RSM)	Deformation Zone (ZSM)	Fracture Domains (FSM)
0	0					RU1a RU2 RU1b				
	0									

Title COMPOSITE LOG for cored borehole KLX27A

Site	LAXEMAR	**Elevation [m.a.s.l.ToC]**	16.98
Borehole	KLX27A	**Inclination ToC [°]**	-65.36
Diameter [mm]	76	**Drilling Start Date**	2007-10-08 14:00:00
Length [m]	650.560	**Drilling Stop Date**	2007-11-21 11:30:00
Bearing ToC [°]	0.73	**Surveying Date**	2007-09-07 13:30:00
Coordinate System	RT90-RHB70	**Plot Date**	2009-02-03 23:05:00
Northing ToC [m]	6365608.29		
Easting ToC [m]	1546742.63		

ROCK TYPE LAXEMAR
- Fine-grained granite
- Quartz monzodiorite
- Fine-grained diorite-gabbro

SILICATE DENSITY
- dens<2680
- 2680<dens<2730
- 2730<dens<2800
- 2800<dens<2890

SUBDIVISION OF ÄVRÖ GRANITE

ROCK UNIT FROM ESHI
- High confidence

ROCK DOMAIN (RSM)
- RSMD01

DEFORMATION ZONE (ZSM)
- DZ (ZSM)

DEFORMATION ZONE FROM ESHI
- DZ

FRACTURE DOMAINS (FSM)
- FSM W
- FSM S

LENGTH AND ELEVATION		BOREMAP DATA		DENSITY	EXTENDED SINGLE HOLE INTERPRETATION (ESHI)			GEOLOGICAL MODEL SDM-SITE LAXEMAR		
Length	Elevation (m.a.s.l.)	Rock Type	Rock Type (< 1m)	Silicate Density kg/m*3	Subdivision of Ävrö granite	Rock Unit (RU)	Possible Deformation Zone	Rock Domain (RSM)	Deformation Zone (ZSM)	Fracture Domains (FSM)

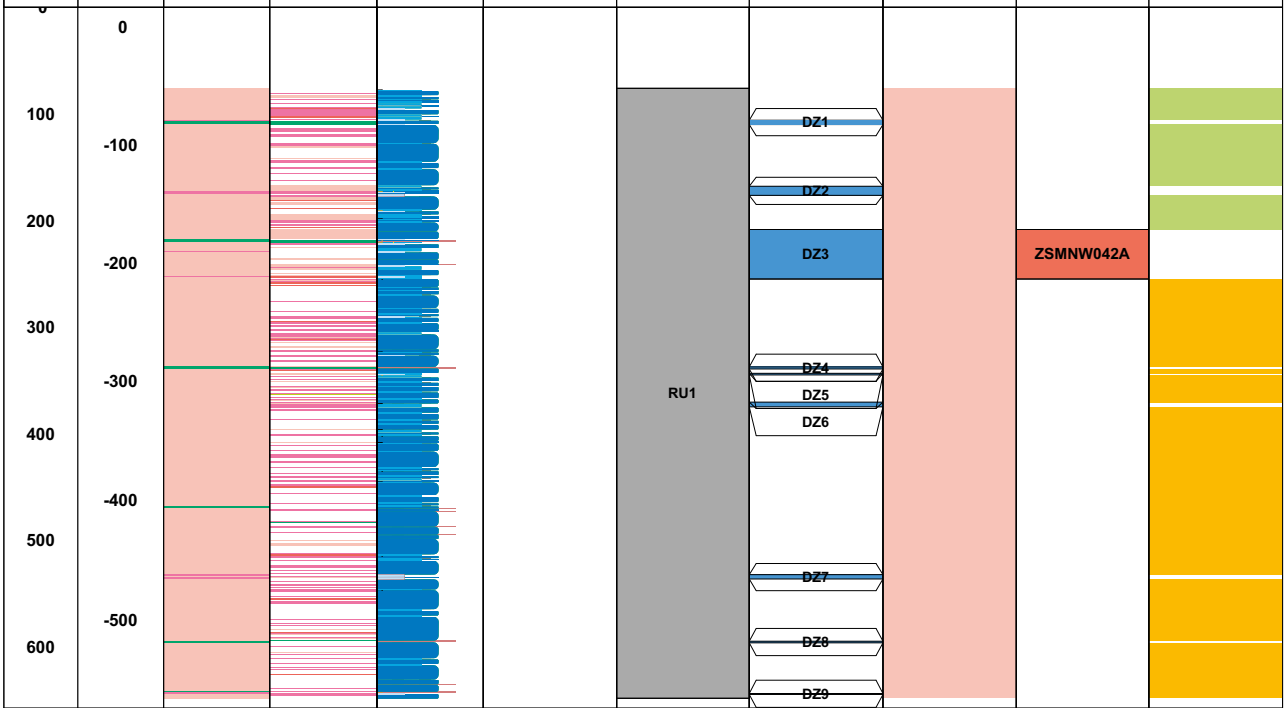

Title COMPOSITE LOG for cored borehole KLX28A

Site	LAXEMAR	**Elevation [m.a.s.l.ToC]**	10.05
Borehole	KLX28A	**Inclination ToC [°]**	-60.05
Diameter [mm]	76	**Drilling Start Date**	2006-09-14 16:00:00
Length [m]	80.230	**Drilling Stop Date**	2006-09-20 08:55:00
Bearing ToC [°]	189.70	**Surveying Date**	2006-09-27 14:45:00
Coordinate System	RT90-RHB70	**Plot Date**	2008-05-04 22:04:41
Northing ToC [m]	6365682.22		
Easting ToC [m]	1549333.71		

ROCK TYPE LAXEMAR
- Fine-grained granite
- Ävrö granite
- Fine-grained diorite-gabbro

WET DENSITY
- unclassified
- dens<2710
- 2710<dens<2820
- 2820<dens<2930

SUBDIVISION OF ÄVRÖ GRANITE
- Ävrö quartz monzodiorite

ROCK UNIT FROM ESHI
- High confidence

ROCK DOMAIN (RSM)
- RSMM01

DEFORMATION ZONE (ZSM)
- DZ (In BH)

DEFORMATION ZONE FROM ESHI
- DZ

FRACTURE DOMAINS (FSM)
- FSM NE005

LENGTH AND ELEVATION		BOREMAP DATA		DENSITY	EXTENDED SINGLE HOLE INTERPRETATION (ESHI)			GEOLOGICAL MODEL SDM-SITE LAXEMAR		
Length	Elevation (m.a.s.l.)	Rock Type	Rock Type (< 1m)	Wet Density kg/m*3	Subdivision of Ävrö granite	Rock Unit (RU)	Possible Deformation Zone	Rock Domain (RSM)	Deformation Zone (ZSM)	Fracture Domains (FSM)
0	0					RU1	DZ1 DZ2		klx28_dz1	

Title COMPOSITE LOG for cored borehole KLX29A

Site	LAXEMAR	**Elevation [m.a.s.l.ToC]**	13.63
Borehole	KLX29A	**Inclination ToC [°]**	-60.90
Diameter [mm]	76	**Drilling Start Date**	2006-09-09 10:00:00
Length [m]	60.250	**Drilling Stop Date**	2006-09-13 11:40:00
Bearing ToC [°]	321.21	**Surveying Date**	2006-09-25 10:40:00
Coordinate System	RT90-RHB70	**Plot Date**	2008-05-04 22:04:41
Northing ToC [m]	6366264.54		
Easting ToC [m]	1549443.99		

ROCK TYPE LAXEMAR
- Ävrö granite
- Fine-grained diorite-gabbro

WET DENSITY
- unclassified
- dens<2710
- 2710<dens<2820
- 2820<dens<2930
- dens>2930

SUBDIVISION OF ÄVRÖ GRANITE
- Ävrö quartz monzodiorite

ROCK UNIT FROM ESHI
- High confidence

ROCK DOMAIN (RSM)
- RSMA01

DEFORMATION ZONE (ZSM)

DEFORMATION ZONE FROM ESHI
- DZ

FRACTURE DOMAINS (FSM)
- FSM EW007

LENGTH AND ELEVATION		BOREMAP DATA		DENSITY	EXTENDED SINGLE HOLE INTERPRETATION (ESHI)			GEOLOGICAL MODEL SDM-SITE LAXEMAR		
Length	Elevation (m.a.s.l.)	Rock Type	Rock Type (< 1m)	Wet Density kg/m*3	Subdivision of Ävrö granite	Rock Unit (RU)	Possible Deformation Zone	Rock Domain (RSM)	Deformation Zone (ZSM)	Fracture Domains (FSM)
0	0					RU1	DZ1 DZ2			

Appendix 11

Confidence of existence, uncertainty in geometry and properties of rock domains in the local model volume

In the SDM-Site Laxemar model stage, the confidence of existence, uncertainty in geometry and property assignment is constrained to rock domains in the local model volume (Figure A11-1). The confidence of existence, uncertainty in geometry and properties of the rock domains outside the local model volume are identical to those presented in the Laxemar 1.2 model version /SKB 2006b, Wahlgren et al. 2006a/. The confidence of existence and uncertainty in geometry for the rock domains are presented in Table A11-1. All relevant surface and borehole data as defined in Table A11-2 have been evaluated and compiled for all rock domains in the local model volume. Since the definition of rock domains in Laxemar is primarily based on a dominant rock type, the properties compiled in the property tables refer to the dominant rock type, except for the occurrence of subordinate rock types, degree of homogeneity, metamorphism/alteration and mineral fabric.

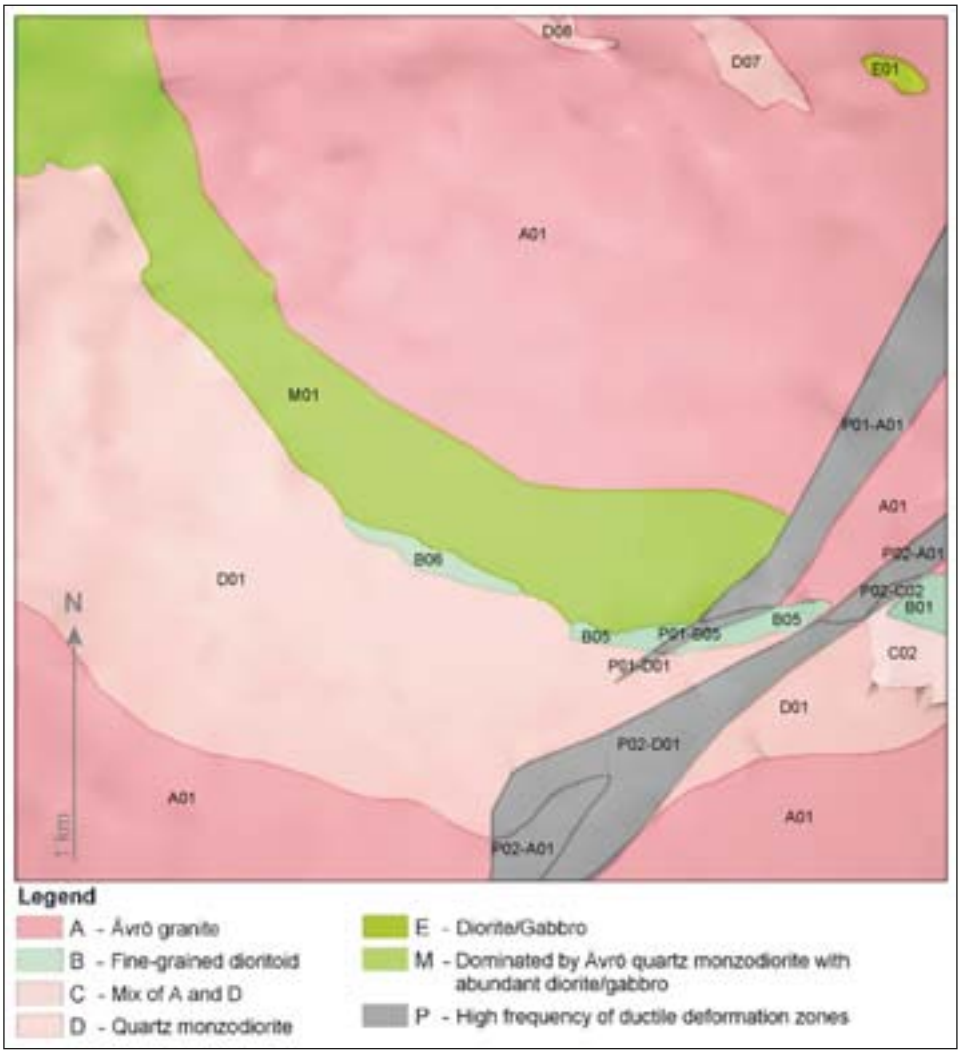

Figure A11-1. *Two dimensional model at the surface for rock domains in the local model area. The colours represent the dominant rock type in each domain, except for the P-domains which are characterised on structural basis.*

Table A11-1. Confidence of existence and uncertainty of geometry of rock domains in the Laxemar local model volume.

Domain ID	Basis for interpretation	Confidence of existence at the surface	Confidence of existence at depth	Uncertainty of geometry at the surface	Uncertainty of geometry at depth	Comment
RSMA01	Bedrock geological map of the local model area (433 outcrop observation points), KLX02, KLX04 KLX06, KLX07A, KLX07B, KLX08, KLX09, KLX09B, KLX09C, KLX09D, KLX09E, KLX09F, KLX09G, KLX10, KLX10B, KLX10C, KLX18A, KLX21B and KLX29A.	High	High	Low	Low to medium	The uncertainty of geometry at depth applies, in particular, to the boundary between RSMA01 and RSMD01 in the southern part of the model volume – possibly south-dipping.
RSMB01	Bedrock geological map of the local model area (5 outcrop observation points).	High	High	Low	Medium	
RSMB05	Bedrock geological map of the local model area (7 outcrop observation points, all of which occur in the local model area).	High	High	Medium	Medium	
RSMB06	Bedrock geological map of the local model area (6 outcrop observation points, all of which occur in the local model area).	High	High	Medium	Medium	
RSMBA03	KLX02	–	High	–	Medium	This domain only occurs at depth.
RSMC02	Bedrock geological map of the local model area (11 outcrop observation points).	High	High	Medium	Medium	
RSMD01	Bedrock geological map of the local model area, (176 outcrop observation points), KLX03, KLX05, KLX08, KLX10, KLX11A, KLX12A, KLX14A, KLX15A, KLX16A, KLX19A, KLX20A, KLX21B, KLX22A, KLX22B, KLX23A, KLX23B, KLX24A and KLX25A.	High	High	Low	Low to medium	Cf. comment for RSMA01.
RSMD07	Bedrock geological map of the local model area (10 outcrop observation points, all of which occur in the local model area).	High	High	Low	Medium	
RSMD08	Bedrock geological map of the local model area (3 outcrop observation points).	High	High	Low	Medium	
RSME01	Bedrock geological map of the local model area (5 outcrop observation points, all of which occur in the local model area).	High	High	Low	Medium	
RSMG02	Bedrock geological map version 0.	High	High	Low	Medium	
RSMM01	Bedrock geological map of the local model area (132 outcrop observation points), KLX03, KLX05, KLX08, KLX10, KLX12A, KLX13A, KLX17A, KLX18A, KLX26A, KLX26B and KLX28A.	High	High	Low	Low to medium	The uncertainty of geometry at depth applies, in particular, to the boundary between RSMA01 and RSMM01 due to diffuse transition between Ävrö granite and Ävrö quartz monzodiorite.
RSMP01	Bedrock geological map of the local model area (30 outcrop observation points).	High	High	Low	Low	
RSMP02	Bedrock geological map of the local model area (44 outcrop observation points).	High	High	Low	Low	

Table A11-2. Properties assigned to each rock domain.

Rock domain ID (RSM***, according to the nomenclature recommended by SKB)
Property
Dominant rock type
Mineralogical composition
Grain size
Age (million years)
Structure
Texture
Density
Porosity
Magnetic susceptibility (SI units)
Electric resistivity in fresh water (ohm m)
Uranium content based on gamma ray spectrometric data (ppm)
Natural exposure rate (μR/h)
Subordinate rock types
Degree of inhomogeneity
Metamorphism/alteration (%)
Mineral fabric (type/orientation)

RSMA01				
Property	**Character**	**Quantitative estimate**	**Confidence**	**Comment**
Dominant rock type	Ävrö granite (501044)	82 (88) %	High	Based on outcrop observations from the local model area, N=433, and KLX02, KLX04 KLX06, KLX07A, KLX07B, KLX08, KLX09, KLX09B, KLX09C, KLX09D, KLX09E, KLX09F, KLX09G, KLX10, KLX10B, KLX10C, KLX18A, KLX21B and KLX29A. The quantitative estimate is based on borehole data; in total 6483 m borehole length (upper diagram) The number in paranthesis is based on KLX02, KLX04, KLX07A and B, KLX08, KLX10, KLX18A and KLX21B, in total 4162 m borehole length, that are considered to be more representative for the central and southern part of the RSMA01 (lower diagram).
				
	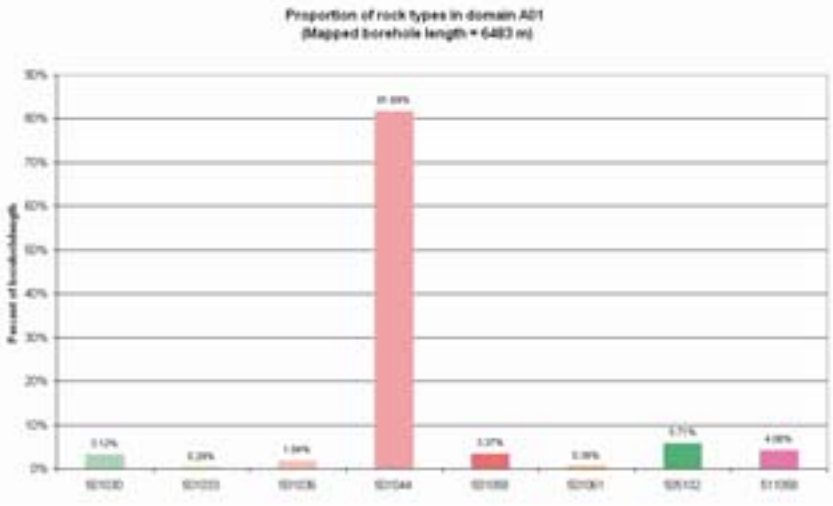			

RSMA01				
Property	**Character**	**Quantitative estimate**	**Confidence**	**Comment**
	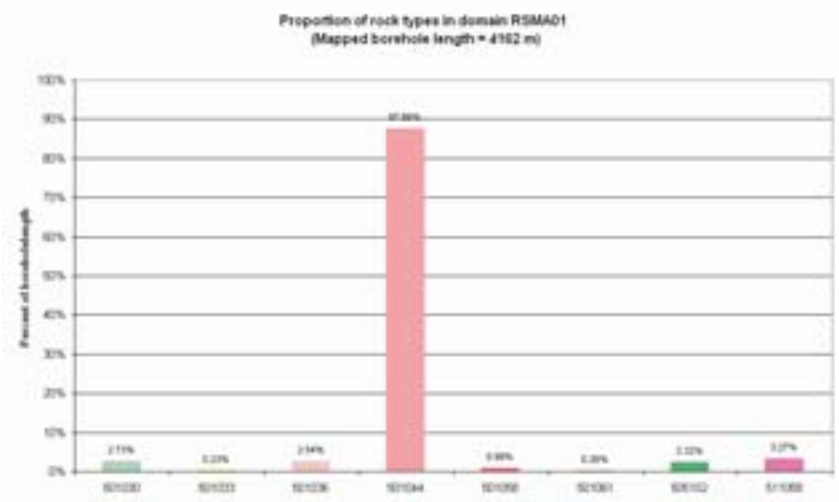			
Mineralogical composition (dominant minerals)	Quartz	21.7±6.4 %	High	N=57. The quantitative estimates are based on modal analyses of surface samples from the local model area and samples from KLX04, KLX06, KLX07A, KLX07B and KLX10.
	K-feldspar	20.1±7.2 %		
	Plagioclase	44.3±8.0 %		
	Biotite	9.3±2.8 %		
Grain size	Medium-grained		High	Based on outcrop data from the local model area, N=433, and KLX02, KLX04 KLX06, KLX07A, KLX07B, KLX08, KLX09, KLX09B, KLX09C, KLX09D, KLX09E, KLX09F, KLX09G, KLX10, KLX10B, KLX10C, KLX18A, KLX21B and KLX29A.
Age (million years)		1800±4	High	U-Pb zircon-titanite dating of Ävrö granite from the drill site for KAV01.
Structure	Massive and faintly to moderately foliated. Scattered mesoscopic, ductile shear zones		High	Cf. comment for grain size.

RSMA01				
Property	**Character**	**Quantitative estimate**	**Confidence**	**Comment**
Texture	Unequigranular to finely porphyritic		High	Cf. comment for grain size.
Density (kg/m^3)		2692±31	High	N=20. The quantitative estimate is based on surface samples from the local model area and KLX10. Mean value ± std.
Porosity (%)		0.66±0.14	High	N=15. The quantitative estimate is based on surface samples from the local model area and KLX10. Mean value ± std.
Magnetic susceptibility (SI units)		3.163±0.269	High	N=20. The quantitative estimate is based on surface samples from the local model area and KLX10. Average value in logarithmic scale ± std.
Electric resistivity in fresh water (ohm m)		3.90±0.19	High	N=15. The quantitative estimate is based on surface samples from the local model area and KLX10. Average value in logarithmic scale ± std.
Uranium content based on gamma ray spectrometric data (ppm)		4.0±1.4	High	N=39. The quantitative estimate is based on measurements on outcrops in the local model area. Mean value ± std.
Natural exposure rate (microR/h)		11.2±1.8	High	N=39. The quantitative estimate is based on measurements on outcrops in the local model area. Mean value ± std.
Subordinate rock types	Fine-grained diorite-gabbro (505102)	6 (2)%	High	The quantitative estimates are based on KLX02, KLX04 KLX06, KLX07A,

RSMA01				
Property	**Character**	**Quantitative estimate**	**Confidence**	**Comment**
	Fine-grained granite (511058)	4 (3)%		KLX07B, KLX08, KLX09, KLX09B, KLX09C, KLX09D, KLX09E, KLX09F, KLX09G, KLX10, KLX10B, KLX10C, KLX18A, KLX21B and KLX29A; in total 6483 m borehole length. The numbers in paranthesis are based on KLX02, KLX04, KLX07A and B, KLX08, KLX10, KLX18A and KLX21B, in total 4162 m borehole length, that are considered to be more representative for the central and southern part of the RSMA01
	Granite (501058)	3 (1)%		
	Fine-grained dioritoid (501030)	3 (3)%		
	Quartz monzodiorite (501036)	2 (3)%		
	Remaining rock types	<1 (1)%		
Fine-grained granite (511058)	Orientation and true thickness 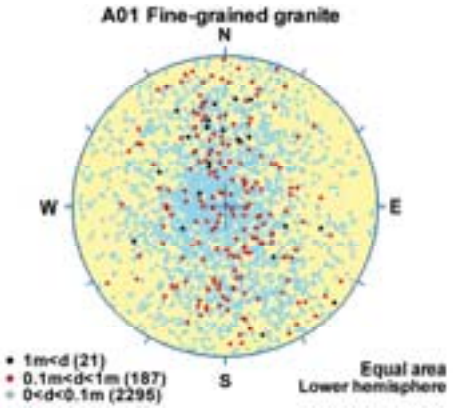		High	Based on orientation of contacts between fine-grained granite and surrounding rock type in KLX02, KLX04 KLX06, KLX07A, KLX07B, KLX08, KLX09, KLX09B, KLX09C, KLX09D, KLX09E, KLX09F, KLX09G, KLX10, KLX10B, KLX10C, KLX18A, KLX21B and KLX29A.

RSMA01				
Property	**Character**	**Quantitative estimate**	**Confidence**	**Comment**
Pegmatite (501061)	Orientation and true thickness 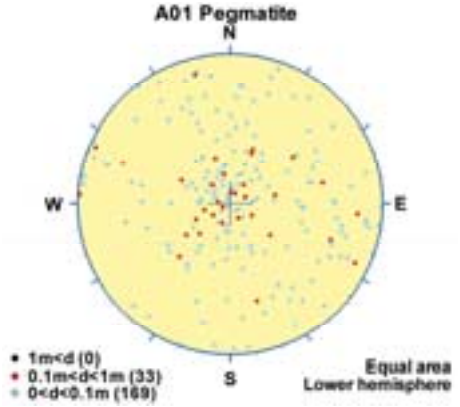		High	Based on orientation of contacts between pegmatite and surrounding rock type in KLX02, KLX04 KLX06, KLX07A, KLX07B, KLX08, KLX09, KLX09B, KLX09C, KLX09D, KLX09E, KLX09F, KLX09G, KLX10, KLX10B, KLX10C, KLX18A, KLX21B and KLX29A.
Fine-grained diorite-gabbro (505102)	Orientation and true thickness 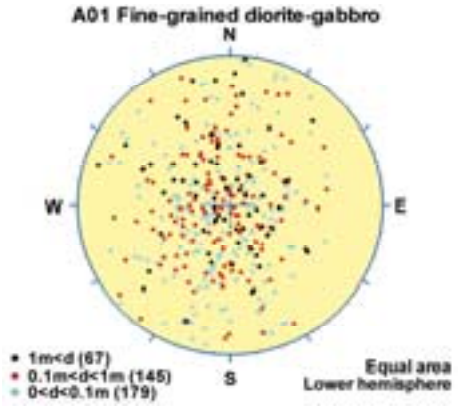		High	Based on orientation of contacts between fine-grained diorite-gabbro and surrounding rock type in KLX02, KLX04 KLX06, KLX07A, KLX07B, KLX08, KLX09, KLX09B, KLX09C, KLX09D, KLX09E, KLX09F, KLX09G, KLX10, KLX10B, KLX10C, KLX18A, KLX21B and KLX29A.
Degree of inhomogeneity	Low to medium		High	Based on outcrop observations from the local model area, N=433, and KLX02, KLX04 KLX06, KLX07A, KLX07B, KLX08, KLX09, KLX09B, KLX09C, KLX09D, KLX09E, KLX09F, KLX09G, KLX10, KLX10B, KLX10C, KLX18A, KLX21B and KLX29A. The degree of inhomogeneity is higher in the northern to northeastern part of the domain (indicated by e.g.. KLX04; KLX05 and KLX09)..

RSMA01				
Property	**Character**	**Quantitative estimate**	**Confidence**	**Comment**
Metamorphism/alteration	Fresh to inhomogeneously altered - red staining	See diagram below	High	The quantitative estimates are based on KLX02, KLX04 KLX06, KLX07A, KLX07B, KLX08, KLX09, KLX09B, KLX09C, KLX09D, KLX09E, KLX09F, KLX09G, KLX10, KLX10B, KLX10C, KLX18A, KLX21B and KLX29A, outside interpreted deformation zones in the single-hole interpretation. Epidotization, saussuritization, sericitization, chloritization and silicification also occur in subordinate amounts.
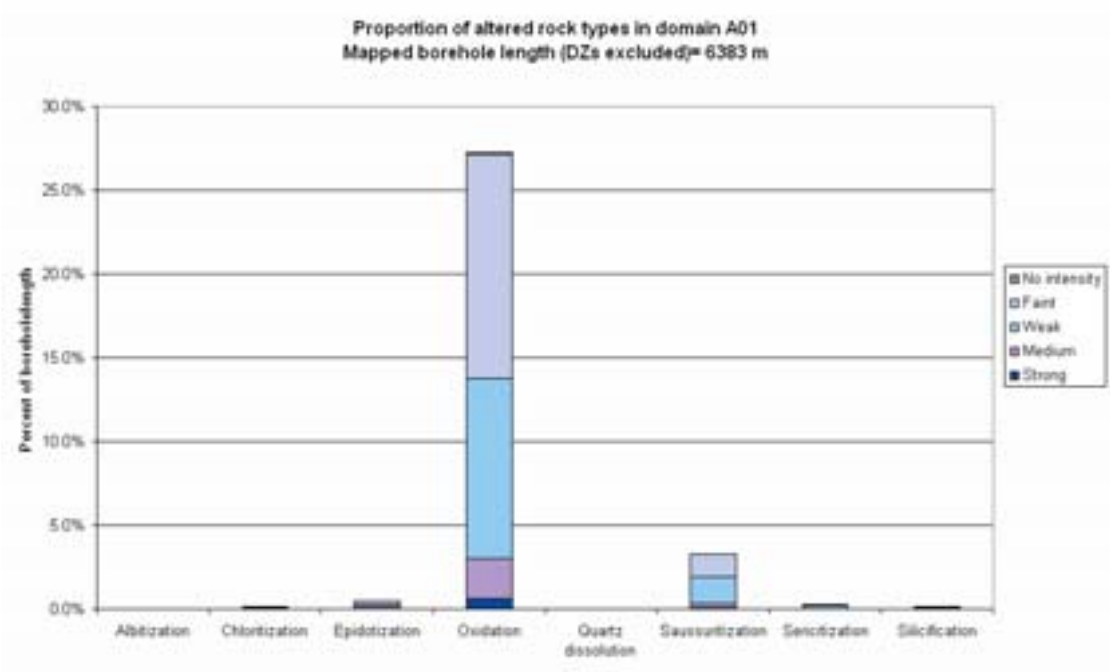				
Mineral fabric (type/orientation)	Faint to moderate magmatic to tectonic foliation		High	.

RSMA01				
Property	**Character**	**Quantitative estimate**	**Confidence**	**Comment**
	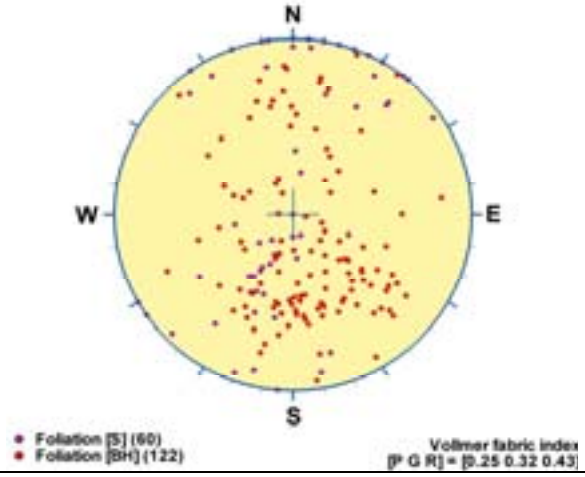			Surface (S) measurements from the local model area and borehole (BH) measurements from KLX02, KLX04 KLX06, KLX07A, KLX07B, KLX08, KLX09, KLX09B, KLX09C, KLX09D, KLX09E, KLX09F, KLX09G, KLX10, KLX10B, KLX10C, KLX18A, KLX21B and KLX29A
	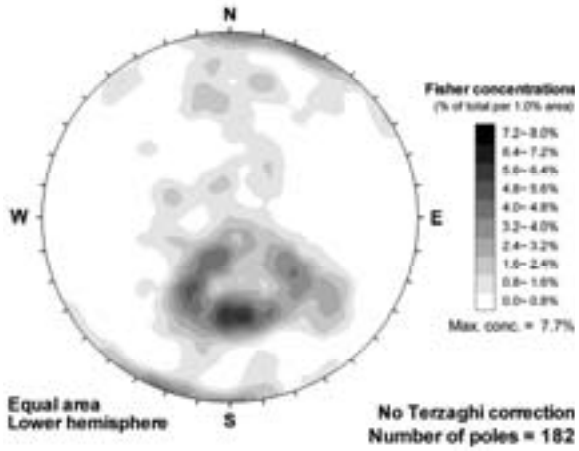			
	Ductile and brittle-ductile shear zones		High	
	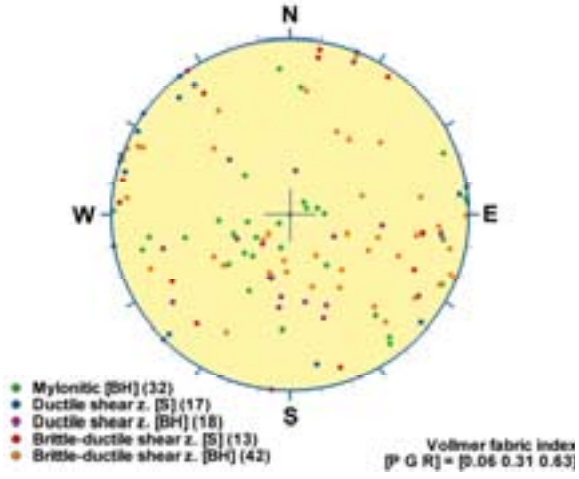			Surface (S) measurements from the local model area and borehole (BH) measurements from KLX02, KLX04 KLX06, KLX07A, KLX07B, KLX08, KLX09, KLX09B, KLX09C, KLX09D, KLX09E, KLX09F, KLX09G, KLX10, KLX10B, KLX10C, KLX18A, KLX21B and KLX29A.

RSMA01				
Property	**Character**	**Quantitative estimate**	**Confidence**	**Comment**
	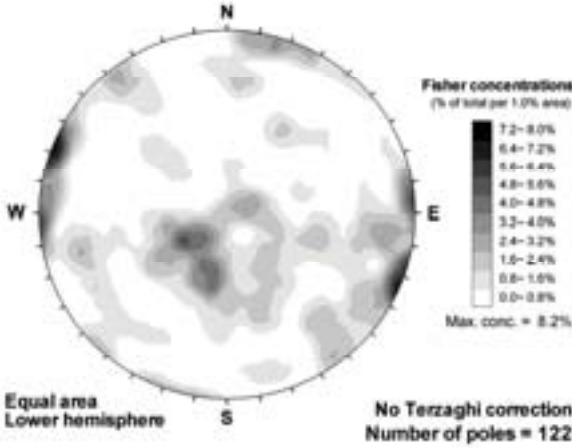		

RSMB01				
Property	**Character**	**Quantitative estimate**	**Confidence**	**Comment**
Dominant rock type	Fine-grained dioritoid (501030)	89-91 %	High	Based on outcrop observations from the local model area, N=5 and the Simpevarp subarea. The quantitative estimate is based on occurrence in KSH01A and KSH02.
Mineralogical composition (dominant minerals)	Quartz	7.4±5.0 %	High	N=21. The quantitative estimate is based on modal analyses of surface samples from the Simpevarp subarea, KSH01A and KSH02. Mean value ± std.
	K-feldspar	11.3±6.4 %		
	Plagioclase	51.4±8.7 %		
	Biotite	14.7±7.6 %		
	Amphibole	0-14 %		
	Pyroxene	0-22 %		
Grain size	Fine-grained		High	Based on outcrop observations from the local model area, N=5 and the Simpevarp subarea.
Age (million years)		c. 1800	High	Not dated. Based on U-Pb zircon age of the Ävrö granite (cf. RSMA01) and the quartz monzodiorite (cf. RSMC01). Field relationships strongly indicate that the fine-grained dioritoid is formed during the same magmatic event.
Structure	Massive to weakly foliated. Scattered mesoscopic, ductile shear zones		High	Based on outcrop observations from the local model area, N=5 and the Simpevarp subarea.
Texture	Equigranular to unequigranular		High	Based on outcrop observations from the local model area, N=5 and the Simpevarp subarea.

Density (kg/m^3)		2786±20	High	N=9. The quantitative estimate is based on surface samples from the Simpevarp subarea and KSH02. Mean value ± std.
Porosity (%)		0.33±0.08	High	N=9. The quantitative estimate is based on surface samples from the Simpevarp subarea and KSH02. Mean value ± std.
Magnetic susceptibility (SI units)		3.39±0.55	High	N=9. The quantitative estimate is based on surface samples from the Simpevarp subarea and KSH02. Mean value ± std. Average value in logarithmic scale ± std.
Electric resistivity in fresh water (ohm m)		4.54±0.37	High	N=9. The quantitative estimate is based on surface samples from the Simpevarp subarea and KSH02. Average value in logarithmic scale ± std.
Uranium content based on gamma ray spectrometric data (ppm)		4.0±1.7	High	N=9. The quantitative estimate is based on measurements on outcrops from the Simpevarp subarea. Mean value ± std.
Natural exposure rate (microR/h)		11.6±3.4	High	N=9. The quantitative estimate is based on measurements on outcrops from the Simpevarp subarea. Mean value ± std.
Subordinate rock types	Diorite/gabbro (501033)	No data	Medium	.
	Fine-grained granite (511058)	No data		
	Pegmatite (501061)	No data		

Degree of inhomogeneity	Low		Medium	Based on outcrop observations from the local model area, N=5, and the Simpevarp subarea, KSH01A and KSH02.
Metamorphism/alteration	Fresh to inhomogeneously altered (faint to weak red staining)	10-38 %	High	The quantitative estimate is based on faint to weak, including subordinate medium and strong, oxidation in KSH01A and KSH02 outside interpreted deformation zones in the single-hole interpretation.
Mineral fabric (type/orientation)				No data

RSMB05				
Property	**Character**	**Quantitative estimate**	**Confidence**	**Comment**
Dominant rock type	Fine-grained dioritoid (501030)		High	Based on outcrop observations from the local model area, N=7. Quantitative estimate, cf. RSMB01.
Mineralogical composition (dominant minerals)	Quartz	7.4±5.0 %	High	N=21. The quantitative estimate is based on modal analyses of surface samples from the Simpevarp subarea, KSH01A and KSH02. Mean value ± std
	K-feldspar	11.3±6.4 %		
	Plagioclase	51.4±8.7 %		
	Biotite	14.7±7.6 %		
	Amphibole	0-14 %		
	Pyroxene	0-22 %		
Grain size	Fine-grained		High	Based on outcrop observations from the local model area, N=7.
Age (million years)		c. 1800	High	Cf. RSMB01.
Structure	Massive to weakly foliated. Scattered mesoscopic, ductile shear zones		High	Based on outcrop observations from the local model area, N=7.
Texture	Unequigranular		High	Based on outcrop observations from the local model area, N=7.
Density (kg/m^3)		2786±20	Medium	The quantitative estimate refers to RSMB01. Mean value ± std.
Porosity (%)		0.33±0.08	Medium	The quantitative estimate refers to RSMB01. Mean value ± std.
Magnetic susceptibility (SI units)		3.39±0.55	Medium	The quantitative estimate refers to RSMB01. Average value in logarithmic scale ± std.
Electric resistivity in fresh water (ohm m)		4.54±0.37	High	The quantitative estimate refers to RSMB01. Average value in logarithmic scale ± std.
Uranium content based on gamma ray spectrometric data (ppm)		3.8±0.8	High	N=2. Mean value ± std.

RSMB05				
Property	**Character**	**Quantitative estimate**	**Confidence**	**Comment**
Natural exposure rate (microR/h)		10.3±1.0	High	N=2. Mean value ± std.
Subordinate rock types	Fine-grained granite (511058)		Medium	Based on outcrop observations from the local model area, N=7. No quantitative estimate is available.
	Fine-grained diorite-gabbro (501061)			
	Pegmatite (501061)			
Degree of inhomogeneity	Low		Medium	Based on outcrop observations from the local model area, N=7.
Metamorphism/alteration	Fresh to inhomogeneously altered (faint to weak red staining)		High	Based on outcrop observations from the local model area, N=7.
Mineral fabric (type/orientation)				No data

RSMB06				
Property	**Character**	**Quantitative estimate**	**Confidence**	**Comment**
Dominant rock type	Fine-grained dioritoid (501030)		High	Based on outcrop observations from the local model area, N=6. Quantitative estimate, cf. RSMB01.
Mineralogical composition (dominant minerals)	Quartz	7.4±5.0 %	High	N=21. The quantitative estimate is based on modal analyses of surface samples from the Simpevarp subarea, KSH01A and KSH02. Mean value ± std.
	K-feldspar	11.3±6.4 %		
	Plagioclase	51.4±8.7 %		
	Biotite	14.7±7.6 %		
	Amphibole	0-14 %		
	Pyroxene	0-22 %		
Grain size	Fine-grained		High	Based on outcrop observations from the local model area, N=6.
Age (million years)		c. 1800	High	Cf. RSMB01.
Structure	Massive to weakly foliated. Scattered mesoscopic, ductile shear zones		High	Based on outcrop observations from the local model area, N=6.
Texture	Unequigranular		High	Based on outcrop observations from the local model area, N=6.
Density (kg/m^3)		2786±20	Medium	The quantitative estimate refers to RSMB01. Mean value ± std.
Porosity (%)		0.33±0.08	Medium	The quantitative estimate refers to RSMB01. Mean value ± std.
Magnetic susceptibility (SI units)		3.39±0.55	Medium	The quantitative estimate refers to RSMB01. Average value in logarithmic scale ± std.
Electric resistivity in fresh water (ohm m)		4.54±0.37	High	The quantitative estimate refers to RSMB01. Average value in logarithmic scale ± std.
Uranium content based on gamma ray spectrometric data (ppm)		3.6	High	N=1.

RSMB06				
Property	**Character**	**Quantitative estimate**	**Confidence**	**Comment**
Natural exposure rate (microR/h)		11.1	High	N=1
Subordinate rock types	Fine-grained granite (511058) Fine-grained dioritegabbro (501061) Pegmatite (501061)		Medium	Based on outcrop observations from the local model area, N=6. No quantitative estimate is available.
Degree of inhomogeneity	Low		Medium	Based on outcrop observations from the local model area, N=6.
Metamorphism/alteration	Fresh to inhomogeneously altered (faint to weak red staining)		High	Based on outcrop observations from the local model area, N=6.
Mineral fabric (type/orientation)				No data

RSMBA03 (only occurs at depth)				
Property	**Character**	**Quantitative estimate**	**Confidence**	**Comment**
Dominant rock type	Ävrö granite (501044)	58 %	High	Mixture of fine-grained dioritoid (501030) and Ävrö granite (501044). The quantitative estimate is based on KLX02.
Mineralogical composition (dominant minerals)				Cf. data for RSMA01.
Grain size				Cf. data for RSMA01.
Age (million years)		c. 1800	High	Cf. RSMA01.
Structure	Massive		Medium	Sparse data. Cf. data for RSMA01.
Texture				Cf. data for RSMA01.
Density (kg/m^3)				Cf. data for RSMA01.
Porosity (%)				Cf. data for RSMA01.
Magnetic susceptibility (SI units)				Cf. data for RSMA01.
Electric resistivity in fresh water (ohm m)				Cf. data for RSMA01.
Uranium content based on gamma ray spectrometric data (ppm)				Cf. data for RSMA01.
Natural exposure rate (microR/h)				Cf. data for RSMA01.
Subordinate rock types	Fine-grained dioritoid (501030)	32 %	High	The quantitative estimate is based on KLX02.
	Fine-grained diorite to gabbro (505102)	8 %		
	Fine-grained granite (511058)	2 %		
	Granite (501058)	1 %		
	Pegmatite (501061)	1 %		
Degree of inhomogeneity	High		High	Based on KLX02

RSMBA03 (only occurs at depth)				
Property	**Character**	**Quantitative estimate**	**Confidence**	**Comment**
Metamorphism/alteration	Fresh to inhomogeneously altered (faint to weak red staining)	22 %	High	The quantitative estimate is based on faint to weak oxidation in KLX02 outside interpreted deformation zones in the single-hole interpretation.
Mineral fabric (type/orientation)				No data

RSMC02				
Property	**Character**	**Quantitative estimate**	**Confidence**	**Comment**
Dominant rock type	Quartz monzodiorite (501036)		High	Based on outcrop observations from the local model area, N=11. No quantitative estimate available.
	Ävrö granite (501044)			
Mineralogical composition (dominant minerals)				Cf. RSMA01 and RSMD01
Grain size				Cf. RSMA01 and RSMD01
Age (million years)		c. 1800	High	Cf. RSMA01 and RSMD01
Structure	Massive to weakly foliated. Scattered mesoscopic, ductile shear zones			Cf. RSMA01 and RSMD01
Texture				Cf. RSMA01 and RSMD01
Density (kg/m^3)	Quartz monzodiorite (501036)			Cf. RSMA01 and RSMD01
	Ävrö granite (501044)			Cf. RSMA01 and RSMD01
Porosity (%)	Quartz monzodiorite (501036)			Cf. RSMA01 and RSMD01
	Ävrö granite (501044)			Cf. RSMA01 and RSMD01
Magnetic susceptibility (SI units)	Quartz monzodiorite (501036)			Cf. RSMA01 and RSMD01
	Ävrö granite (501044)			Cf. RSMA01 and RSMD01
Electric resistivity in fresh water (ohm m)	Quartz monzodiorite (501036)			Cf. RSMA01 and RSMD01
	Ävrö granite (501044)			Cf. RSMA01 and RSMD01
Uranium content based on gamma ray spectrometric data (ppm)	Quartz monzodiorite (501036)			Cf. RSMA01 and RSMD01
	Ävrö granite (501044)			
Natural exposure rate (microR/h)	Quartz monzodiorite (501036)			Cf. RSMA01 and RSMD01
	Ävrö granite (501044)			
Subordinate rock types	Fine-grained dioritoid (501030)		Medium	Based on outcrop observations from the local model area, N=11.
	Fine-grained granite (511058)			
	Granite (501058)			

RSMC02				
Property	**Character**	**Quantitative estimate**	**Confidence**	**Comment**
	Fine-grained mafic rock (505102)			
	Pegmatite (501061)			
	Diorite to gabbro (501033)			
Degree of inhomogeneity	High		High	Based on outcrop observations from the local model area, N=11.
Metamorphism/alteration	Fresh to inhomogeneously altered (faint to weak red staining)		Medium	Based on outcrop observations from the local model area, N=11.
Mineral fabric (type/orientation)				Very sparse data

RSMD01				
Property	**Character**	**Quantitative estimate**	**Confidence**	**Comment**
Dominant rock type	Quartz monzodiorite (501036) 89 %	High		Based on outcrop observations from the local model area, N=176, and KLX03, KLX05, KLX08, KLX10, KLX11A, KLX12A, KLX14A, KLX15A, KLX16A, KLX19A, KLX20A, KLX21B, KLX22A, KLX22B, KLX23A, KLX23B, KLX24A and KLX25A. The quantitative estimate is based on borehole data; in total 5070 m borehole length.
				
	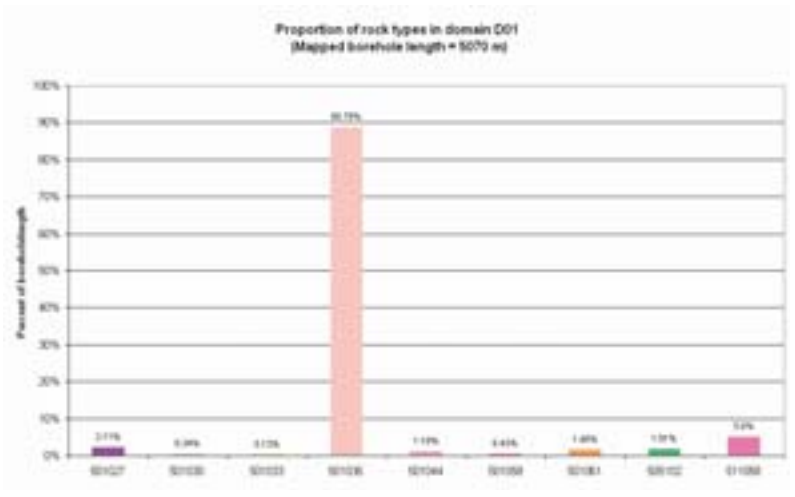			
Mineralogical composition (dominant minerals)	Quartz	13.0±3.0 %	High	N=33. The quantitative estimate is based on modal analyses of surface samples from the local model area, KLX03, KLX05, KLX08, KLX10, KLX11A, KLX12A, KLX15A, KLX16A and KLX21B.
	K-feldspar	11.4±4.8 %		
	Plagioclase	47.0±4.6 %		
	Biotite	14.0±4.2 %		
	Amphibole	9.8±6.5 %		

RSMD01				
Property	**Character**	**Quantitative estimate**	**Confidence**	**Comment**
Grain size	Medium-grained		High	Based on outcrop observations from the local model area, N=176, and KLX03, KLX05, KLX08, KLX10, KLX11A, KLX12A, KLX14A, KLX15A, KLX16A, KLX19A, KLX20A, KLX21B, KLX22A, KLX22B, KLX23A, KLX23B, KLX24A and KLX25A.
Age (million years)		1802±4	High	Based on U-Pb zircon dating of sample from the Simpevarp subarea.
Structure	Massive and faintly to moderately foliated. Scattered mesoscopic, ductile shear zones		High	Cf. comment for grain size.
Texture	Equigranular		High	Cf. comment for grain size.
Density (kg/m^3)		2782±42	High	N=18. The quantitative estimate is based on surface samples from the local model area and KLX03, KLX10 and KLX20A. Mean value ± std.
Porosity (%)		0.52±0.12	High	N=12. The quantitative estimate is based on surface samples from the Laxemar subarea and its immediate surroundings. Mean value ± std.
Magnetic susceptibility (SI units)		3.363±0.232	High	N=18. The quantitative estimate is based on surface samples from the local model area and KLX03, KLX10 and KLX20A. Average value in logarithmic scale ± std..

RSMD01				
Property	**Character**	**Quantitative estimate**	**Confidence**	**Comment**
Electric resistivity in fresh water (ohm m)		4.04±0.13	High	N=12. The quantitative estimate is based on surface samples from the local model area and KLX03, KLX10 and KLX20A. Average value in logarithmic scale ± std.
Uranium content based on gamma ray spectrometric data (ppm)		3.1±0.7	High	N=27. The quantitative estimate is based on measurements on outcrops in the local model area. Mean value ± std.
Natural exposure rate (microR/h)		9.5±1.0	High	N=27. The quantitative estimate is based on measurements on outcrops in the local model area. Mean value ± std.
Subordinate rock types	Fine-grained granite (511058)	5 %	High	The quantitative estimates are based on KLX03, KLX05, KLX08, KLX10, KLX11A, KLX12A, KLX14A, KLX15A, KLX16A, KLX19A, KLX20A, KLX21B, KLX22A, KLX22B, KLX23A, KLX23B, KLX24A and KLX25A; in total 5070 m borehole length. Note that dolerite is not judged to be evenly distributed but is only observed in the westernmost part of the domain.
	Fine-grained diorite to gabbro (505102)	1.8 %		
	Pegmatite (501061)	1.4 %		
	Ävrö granite (501044)	1.1 %		
	Granite (501058)	0.4 %		
	Fine-grained dioritoid (501030)	0.3 %		
	Diorite/gabbro (501033)	0.1 %		
	Dolerite (501027)	2.1 %		

RSMD01				
Property	**Character**	**Quantitative estimate**	**Confidence**	**Comment**
Fine-grained granite (511058)	Orientation and true thickness 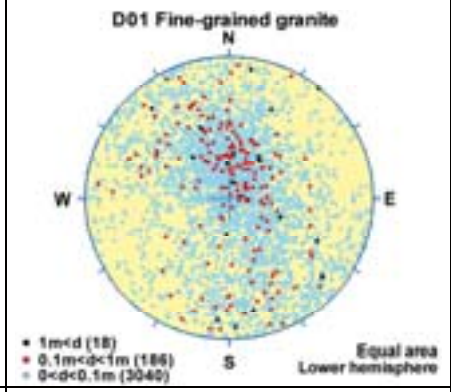		High	Based on orientation of contcts between fine-grained granite and surrounding rock type in KLX03, KLX05, KLX08, KLX10, KLX11A, KLX12A, KLX14A, KLX15A, KLX16A, KLX19A, KLX20A, KLX21B, KLX22A, KLX22B, KLX23A, KLX23B, KLX24A and KLX25A.
Fine-grained diorite-gabbro (505102)	Orientation and true thickness 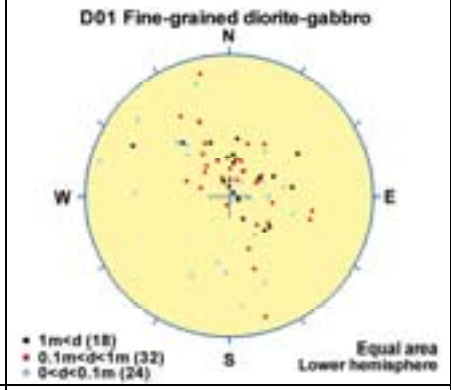		High	Based on orientation of contcts between fine-grained diorite-gabbro and surrounding rock type in KLX03, KLX05, KLX08, KLX10, KLX11A, KLX12A, KLX14A, KLX15A, KLX16A, KLX19A, KLX20A, KLX21B, KLX22A, KLX22B, KLX23A, KLX23B, KLX24A and KLX25A.
Pegmatite (501061)	Orientation and true thickness 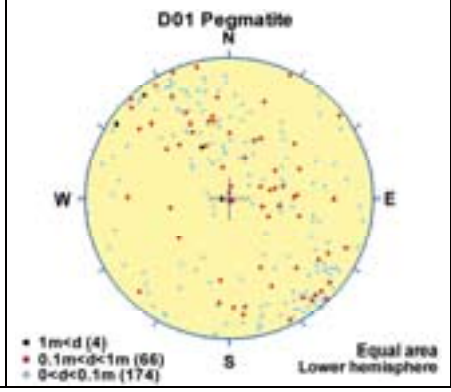		High	Based on orientation of contcts between pegmatite and surrounding rock type in KLX03, KLX05, KLX08, KLX10, KLX11A, KLX12A, KLX14A, KLX15A, KLX16A, KLX19A, KLX20A, KLX21B, KLX22A, KLX22B, KLX23A, KLX23B, KLX24A and KLX25A.

RSMD01				
Property	**Character**	**Quantitative estimate**	**Confidence**	**Comment**
Degree of inhomogeneity	Low		High	Based on outcrop observations from the local model area, N=176, and KLX03, KLX05, KLX08, KLX10, KLX11A, KLX12A, KLX14A, KLX15A, KLX16A, KLX19A, KLX20A, KLX21B, KLX22A, KLX22B, KLX23A, KLX23B, KLX24A and KLX25A.
Metamorphism/alteration	Fresh to inhomogeneously altered - saussuritization	See diagram below	High	The quantitative estimates are based on KLX03, KLX05, KLX08, KLX10, KLX11A, KLX12A, KLX14A, KLX15A, KLX16A, KLX19A, KLX20A, KLX21B, KLX22A, KLX22B, KLX23A, KLX23B, KLX24A and KLX25A; in total 4888 m borehole length, outside interpreted deformation zones in the single–hole interpretation. Epidotization, silicification, quartz dissolution occur in sparse amounts.
	Fresh to inhomogeneously altered - red staining	See diagram below		

RSMD01				
Property	**Character**	**Quantitative estimate**	**Confidence**	**Comment**
	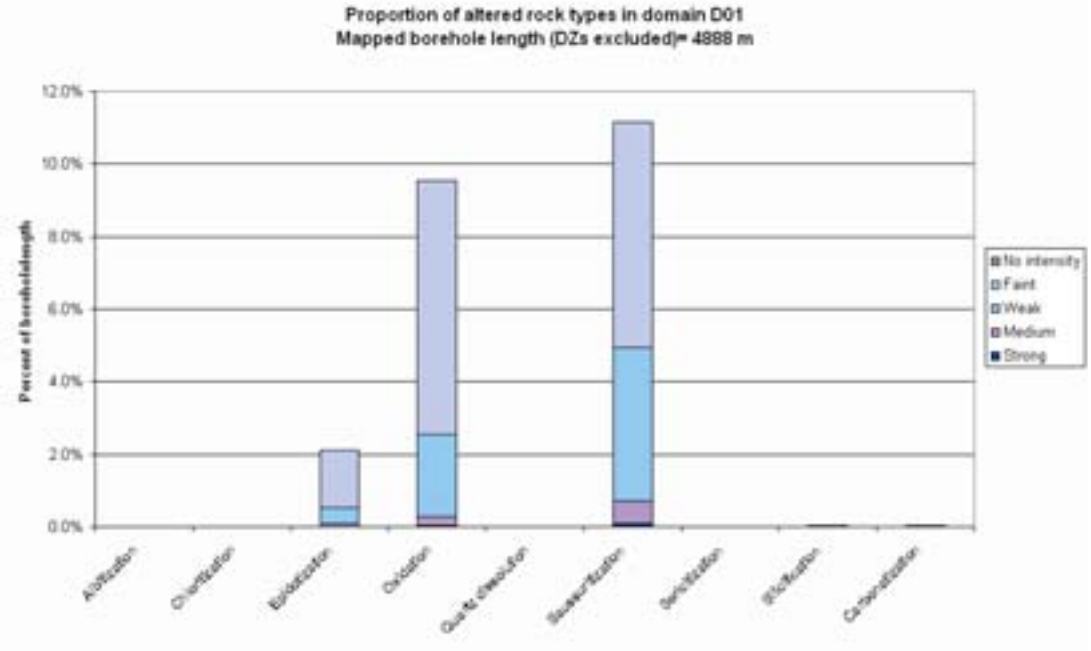			
	Faint to moderate magmatic to tectonic foliation		High	
Mineral fabric (type/orientation)	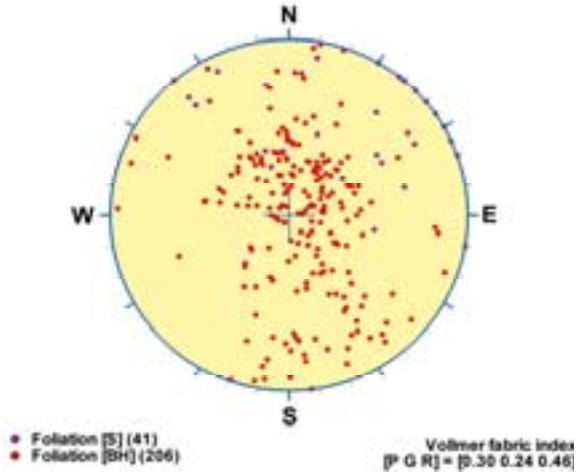			Surface (S) measurements from the local model area and borehole (BH) measurements from KLX03, KLX05, KLX08, KLX10, KLX11A, KLX12A, KLX14A, KLX15A, KLX16A, KLX19A, KLX20A, KLX21B, KLX22A, KLX22B, KLX23A, KLX23B, KLX24A and KLX25A.

RSMD01				
Property	**Character**	**Quantitative estimate**	**Confidence**	**Comment**
	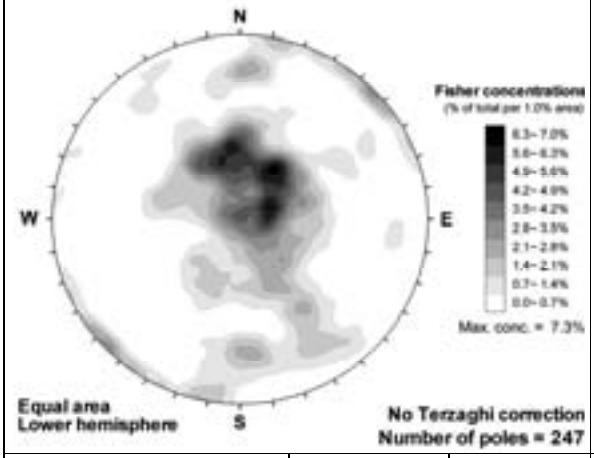			
	Ductile and brittle-ductile shear zones		High	
	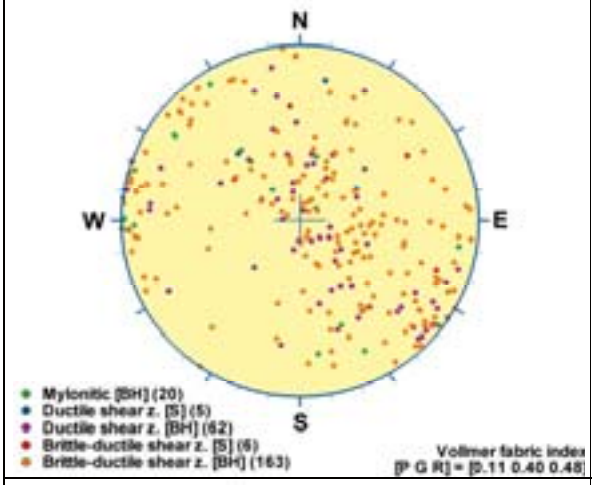			Surface (S) measurements from the local model area and borehole (BH) measurements from KLX03, KLX05, KLX08, KLX10, KLX11A, KLX12A, KLX14A, KLX15A, KLX16A, KLX19A, KLX20A, KLX21B, KLX22A, KLX22B, KLX23A, KLX23B, KLX24A and KLX25A.
	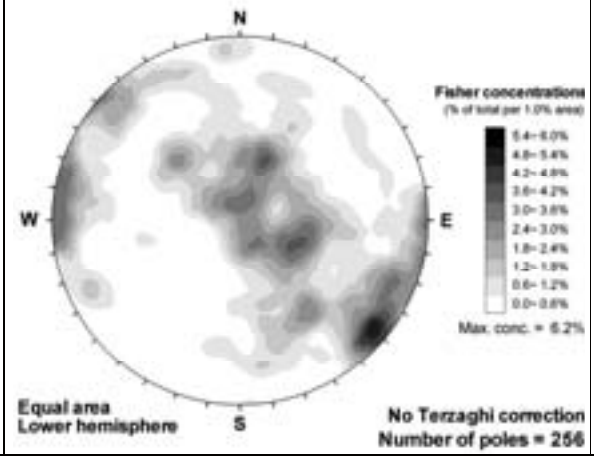			

RSMD07				
Property	**Character**	**Quantitative estimate**	**Confidence**	**Comment**
Dominant rock type	Quartz monzodiorite (501036)		High	Based on outcrop observations from the local model area, N=10.
Mineralogical composition (dominant minerals)	Quartz	6.5±1.1 %	High	N=3. The quantitative estimate is based on modal analyses of surface samples.
	K-feldspar	3.1±2.4 %		
	Plagioclase	39.8±2.0 %		
	Biotite	15.5±6.5 %		
	Amphibole	28.1±9.4 %		
Grain size	Medium-grained		High	Based on outcrop observations from the local model area, N=10.
Age (million years)		c. 1800	High	Based on U-Pb zircon dating of sample from the Simpevarp subarea.
Structure	Massive to weakly foliated		High	Based on outcrop observations from the local model area, N=10.
Texture	Equigranular		High	Based on outcrop observations from the local model area, N=10.
Density (kg/m^3)				No data
Porosity (%)				No data
Magnetic susceptibility (SI units)				No data
Electric resistivity in fresh water (ohm m)				No data
Uranium content based on gamma ray spectrometric data (ppm)				No data
Natural exposure rate (microR/h)				No data
Subordinate rock types	Fine-grained granite (511058)		Medium	Based on outcrop observations from the local model area, N=10. The confidence of occurrence is high but not the order of occurrence.
	Pegmatite (501061)			
	Ävrö granite (501044)			
	Diorite to gabbro (501033)			

RSMD07				
Property	**Character**	**Quantitative estimate**	**Confidence**	**Comment**
Degree of inhomogeneity	Medium		High	Based on outcrop observations from the local model area, N=10.
Metamorphism/alteration (%)				No data
Mineral fabric (type/orientation)				No data

RSMD08				
Property	**Character**	**Quantitative estimate**	**Confidence**	**Comment**
Dominant rock type	Quartz monzodiorite (501036)		High	Based on outcrop observations from the local model area, N=3.
Mineralogical composition (dominant minerals)	Quartz			No data from this domain.Cf. quantitative estimate in RSMD07.
	K-feldspar			
	Plagioclase			
	Biotite			
	Amphibole			
Grain size	Medium-grained		High	Based on outcrop observations from the local model area, N=3.
Age (million years)		C, 1800	High	Based on U-Pb zircon dating of sample from the Simpevarp subarea.
Structure	Massive to weakly foliated.		High	Based on outcrop observations from the local model area, N=3.
Texture	Equigranular		High	Based on outcrop observations from the local model area, N=3.
Density (kg/m^3)				No data
Porosity (%)				No data
Magnetic susceptibility (SI units)				No data
Electric resistivity in fresh water (ohm m)				No data
Uranium content based on gamma ray spectrometric data (ppm)		1.7		N=1. The quantitative estimate is based on measurement on outcrop.
Natural exposure rate (microR/h)		7.1		N=1. The quantitative estimate is based on measurement on outcrop.
Subordinate rock types	Fine-grained granite (511058)		High	Based on outcrop observations from the local model area,
	Pegmatite (501061)			

RSMD08				
Property	**Character**	**Quantitative estimate**	**Confidence**	**Comment**
	Granite (501058)			N=3. The confidence of occurrence is high but not the order of occurrence.
	Ävrö granite (501044)			
	Diorite to gabbro (501033)			
Degree of inhomogeneity	Medium		High	Based on outcrop observations from the local model area, N=3.
Metamorphism/alteration				No data
Mineral fabric (type/orientation)				No data

RSME01				
Property	**Character**	**Quantitative estimate**	**Confidence**	**Comment**
Dominant rock type	Diorite to gabbro (501033)		High	Based on outcrop observations from the local model area, N=5.
Mineralogical composition (dominant minerals)	Quartz	4±0.6 %	Medium	N=4. The quantitative estimate is based on modal analyses of surface samples from corresponding rock types in the Simpevarp subarea. No data from this domain. Mean value ± std
	Plagioclase	47.4±4.5 %		
	Biotite	10.8±3.8 %		
	Amphibole	29.4±5.3 %		
Grain size	Medium-grained		High	Based on outcrop observations from the local model area, N=5.
Age (million years)		c. 1800	High	Not dated. Based on U-Pb zircon age of the Ävrö granite and the quartz monzodiorite. Field relationships strongly indicate that the diorite to gabbro is formed during the same magmatic event.
Structure	Massive		High	Based on outcrop observations from the local model area, N=5.
Texture	Equigranular		High	Based on outcrop observations from the local model area, N=5.
Density (kg/m^3)		2960±43	Medium	N=11. The quantitative estimate is based on surface samples from corresponding rock types in the Laxemar subarea, KLX01 and KLX03. No data from this domain. Mean value ± std.

RSME01				
Property	**Character**	**Quantitative estimate**	**Confidence**	**Comment**
Porosity (%)		0.19±0.14	Medium	N=11. The quantitative estimate is based on surface samples from corresponding rock types in the Laxemar subarea, KLX01 and KLX03. No data from this domain. Mean value ± std.
Magnetic susceptibility (SI units)		2.694±0.733	Medium	N=11. The quantitative estimate is based on surface samples from corresponding rock types in the Laxemar subarea, KLX01 and KLX03. No data from this domain. Average value in logarithmic scale ± std
Electric resistivity in fresh water (ohm m)		4.38±0.24	Medium	N=11. The quantitative estimate is based on surface samples from corresponding rock types in the Laxemar subarea, KLX01 and KLX03. No data from this domain. Average value in logarithmic scale ± std
Uranium content based on gamma ray spectrometric data (ppm)		1.9±0.8	Medium	N=5. The quantitative estimate is based on surface samples from corresponding rock types in the Laxemar subarea. No data from this domain. Mean value ± std.
Natural exposure rate (microR/h)		5.7±1.2	Medium	N=5. The quantitative estimate is based on surface samples from corresponding rock types in the Laxemar subarea. No data from this domain. Mean value ± std.

RSME01				
Property	**Character**	**Quantitative estimate**	**Confidence**	**Comment**
Subordinate rock types	Fine-grained granite (511058)		High	Based on outcrop observations from the local model area, N=5.
Degree of inhomogeneity	Medium		High	Based on outcrop database for the Laxemar subarea and its immediate surroundings.
Metamorphism/alteration				No data
Mineral fabric (type/orientation)				No data

RSMM01				
Property	**Character**	**Quantitative estimate**	**Confidence**	**Comment**
Dominant rock type	Ävrö quartz monzodiorite (501046)	75 %	High	Based on outcrop observations from the local model area, N=132, and KLX03, KLX05, KLX08, KLX10, KLX12A, KLX13A, KLX17A, KLX18A, KLX26A, KLX26B and KLX28A. The quantitative estimate is based on borehole data; in total 3600 m borehole length.
				
	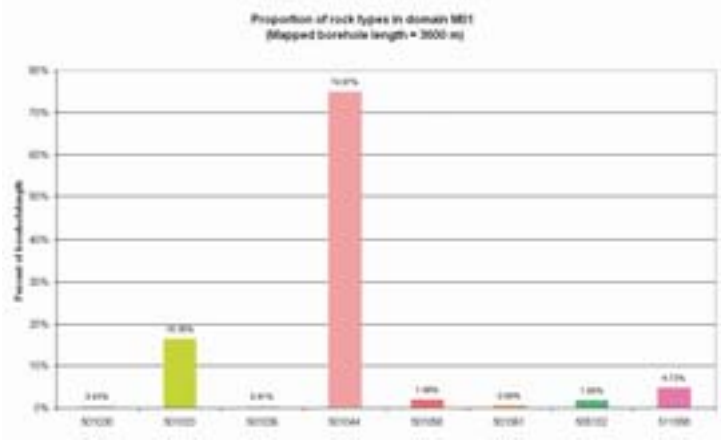			
Mineralogical composition (dominant minerals)	Quartz	13.9±6.4 %	High	N=35. The quantitative estimate is based on modal analyses of surface samples from the local model area, KLX03, KLX08, KLX10, KLX12A and KLX18A.
	K-feldspar	12.9±8.5 %		
	Plagioclase	53,4±8.8 %		
	Biotite	11.8±4.6 %		
	Amphibole	3.0±3.0 %		

RSMM01				
Property	**Character**	**Quantitative estimate**	**Confidence**	**Comment**
Grain size				Based on outcrop observations from the local model area, N=132, and KLX03, KLX05, KLX08, KLX10, KLX12A, KLX13A, KLX17A, KLX18A, KLX26A, KLX26B and KLX28A.
Age (million years)		c. 1800	High	U-Pb zircon-titanite dating of a Ävrö granite sample from the drill site for KAV01.
Structure	Massive and faintly to moderately foliated. Scattered mesoscopic, ductile shear zones			Cf. comment for grain size.
Texture	Unequigranular to finely porphyritic			Cf. comment for grain size.
Density (kg/m^3)	Ävrö quartz monzodiorite (501046)	2736±34	High	N=10 (501046), N=4 (501033). The quantitative estimate is based on surface samples from the local model area and KLX03. Mean value ± std.
	Diorite/gabbro (501033)	2959±57	High	
Porosity (%)	Ävrö quartz monzodiorite (501046)	0.57±0.18	High	N=10 (501046), N=4 (501033). The quantitative estimate is based on surface samples from the local model area and KLX03. Mean value ± std.
	Diorite/gabbro (501033)	0.30±0.10	High	
Magnetic susceptibility (SI units)	Ävrö quartz monzodiorite (501046)	3.510±0.245	High	N=10 (501046), N=3 (501033). The quantitative estimate is based on surface samples from the local model area and KLX03. Mean value ± std.
	Diorite/gabbro (501033)	3.342±0.987	High	
Electric resistivity in fresh water (ohm m)	Ävrö quartz monzodiorite (501046)	4.10±0.21	High	N=10 (501046), N=4 (501033). The quantitative estimate is based on surface

RSMM01				
Property	**Character**	**Quantitative estimate**	**Confidence**	**Comment**
	Diorite/gabbro (501033)	4.28±0.20	High	samples from the local model area and KLX03. Mean value ± std.
Uranium content based on gamma ray spectrometric data (ppm)	Ävrö quartz monzodiorite (501046)	1.8±0.5	High	N=13 (501046), N=6 (501033). The quantitative estimate is based on measurements on outcrops in the local model area. Mean value ± std.
	Diorite/gabbro (501033)	0.6±0.3	High	
Natural exposure rate (microR/h)	Ävrö quartz monzodiorite (501046)	7.5±0.8	High	N=13 (501046), N=6 (501033). The quantitative estimate is based on measurements on outcrops in the local model area. Mean value ± std.
	Diorite/gabbro (501033)	2.3±0.5	High	
Subordinate rock types			High	The quantitative estimates are based on KLX03, KLX05, KLX08, KLX10, KLX12A, KLX13A, KLX17A, KLX18A, KLX26A, KLX26B and KLX28A; in total 3600 m borehole length. The photograph shows an inclusion of diorite/gabbro in Ävrö quartz monzodiorite. .
	Diorite/gabbro (501033)	16.4 %		
	Fine-grained granite (511058)	4.7 %		
	Granite (501058)	2.0 %		
	Fine-grained diorite to gabbro (505102)	1.8 %		
	Pegmatite (501061)	0.5 %		
	Fine-grained dioritoid	0.4 %		
	Quartz monzodiorite (501036)	0.4 %		

RSMM01				
Property	**Character**	**Quantitative estimate**	**Confidence**	**Comment**
Fine-grained granite (511058)	Orientation and true thickness 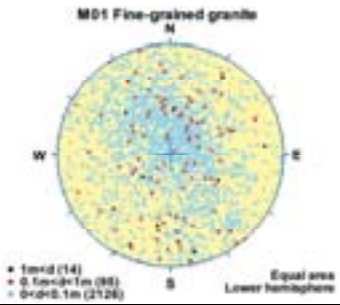		High	Based on orientation of contcts between fine-grained granite and surrounding rock type in KLX03, KLX05, KLX08, KLX10, KLX12A, KLX13A, KLX17A, KLX18A, KLX26A, KLX26B and KLX28A.
Fine-grained diorite-gabbro (505102)	Orientation and true thickness 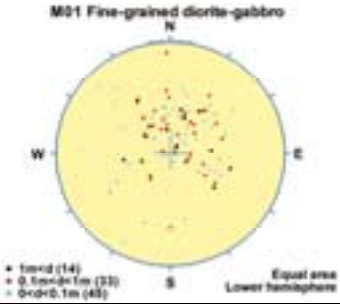		High	Based on orientation of contcts between fine-grained diorite-gabbro and surrounding rock type in KLX03, KLX05, KLX08, KLX10, KLX12A, KLX13A, KLX17A, KLX18A, KLX26A, KLX26B and KLX28A.
Pegmatite (501061)	Orientation and true thickness 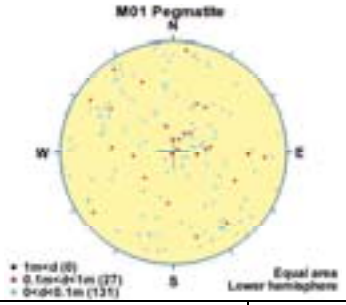		High	Based on orientation of contcts between pegmatite and surrounding rock type in KLX03, KLX05, KLX08, KLX10, KLX12A, KLX13A, KLX17A, KLX18A, KLX26A, KLX26B and KLX28A.
Degree of inhomogeneity	Medium		High	Based on outcrop observations from the local model area, N=132, and KLX03, KLX05, KLX08, KLX10, KLX12A, KLX13A, KLX17A, KLX18A, KLX26A, KLX26B and KLX28A.

RSMM01				
Property	**Character**	**Quantitative estimate**	**Confidence**	**Comment**
Metamorphism/alteration	Fresh to inhomogeneously altered – red staining	See diagram below	High	The quantitative estimates are based KLX03, KLX05, KLX08, KLX10, KLX12A, KLX13A, KLX17A, KLX18A, KLX26A, KLX26B and KLX28A; in total 3290 m borehole length, outside interpreted deformation zones in the single–hole interpretation. Epidotization, chloritization, silicification and albitizatio occur in very sparse amounts.
	Fresh to inhomogeneously altered – saussuritization	See diagram below		
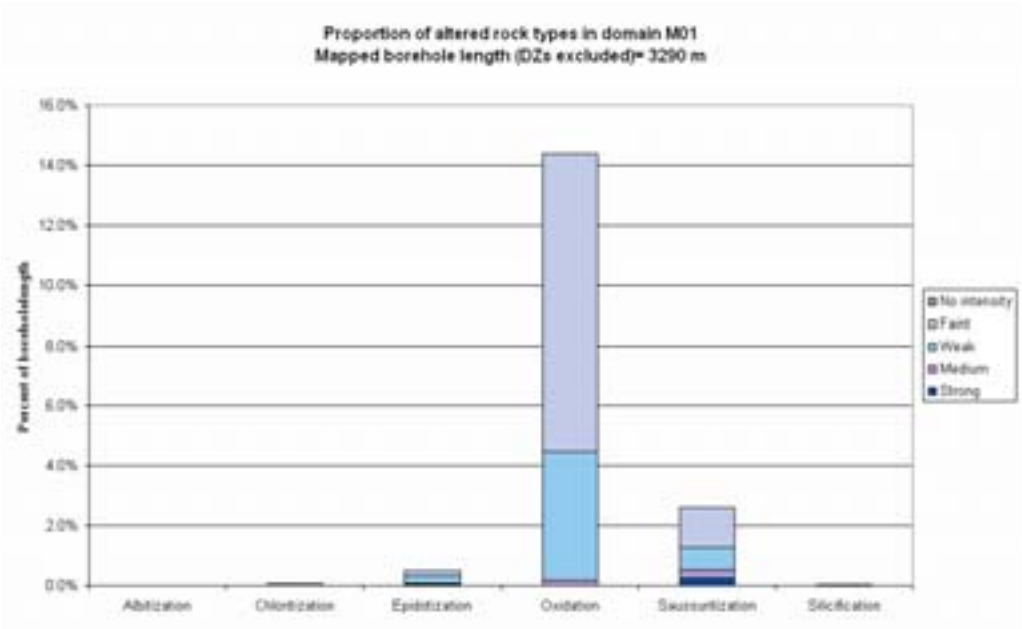				
Mineral fabric (type/orientation)	Faint to moderate magmatic to tectonic foliation		High	

RSMM01				
Property	**Character**	**Quantitative estimate**	**Confidence**	**Comment**
	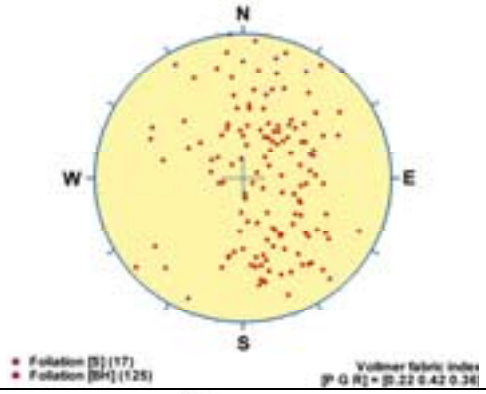			Surface (S) measurements from the local model area and borehole (BH) measurements from KLX03, KLX05, KLX08, KLX10, KLX12A, KLX13A, KLX17A, KLX18A, KLX26A, KLX26B and KLX28A.
	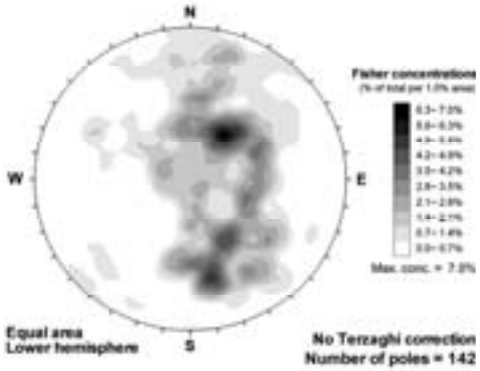			
	Ductile and brittle-ductile shear zones		High	
	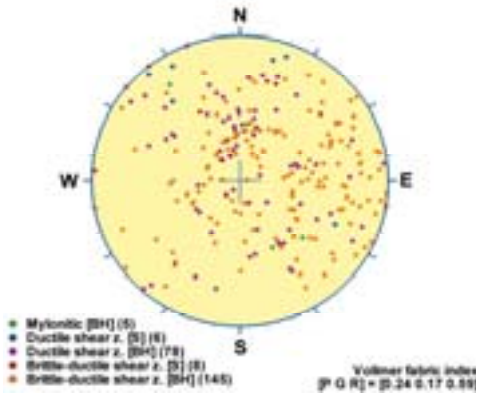			Surface (S) measurements from the local model area and borehole (BH) measurements from KLX03, KLX05, KLX08, KLX10, KLX12A, KLX13A, KLX17A, KLX18A, KLX26A, KLX26B and KLX28A.

RSMM01				
Property	**Character**	**Quantitative estimate**	**Confidence**	**Comment**
	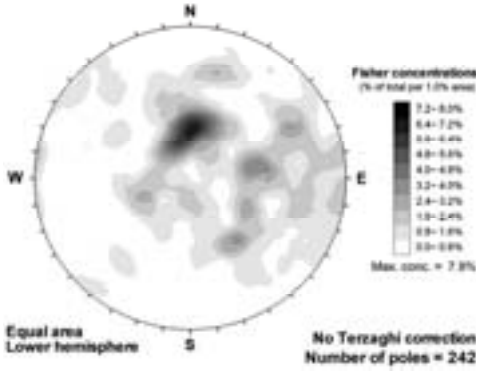			

RSMP01				
Property	**Character**	**Quantitative estimate**	**Confidence**	**Comment**
Dominant rock type	Ävrö granite (501044)		High	Based on outcrop observations from the local model area, N=30.
Mineralogical composition (dominant minerals)				Cf. RSMA01 what concerns undeformed to weakly deformed varieties of the Ävrö granite. No quantitative data for mylonitic varieties.
Grain size	Fine- to medium-grained		High	Based on outcrop observations from the local model area, N=30. Fine-grained when strongly deformed.
Age (million years)		c. 1800	High	Cf. RSMA01. Age of low-grade shear deformation is unknown, but is inferred to be close in time to the intrusion age of the rock types (i.e. c. 1800-1750 Ma).
Structure	Massive to mylonitic			Based on outcrop observations from the local model area, N=30.
Texture	Unequigranular to porphyritic to porphyroclastic		High	Based on outcrop observations from the local model area, N=30.
Density (kg/m^3)				Cf. RSMA01 for undeformed varieties. No data for mylonitic varieties.
Porosity (%)				Cf. RSMA01 for undeformed varieties. No data for mylonitic varieties.
Magnetic susceptibility (SI units)				Cf. RSMA01 for undeformed varieties. No data for mylonitic varieties.

RSMP01				
Property	**Character**	**Quantitative estimate**	**Confidence**	**Comment**
Electric resistivity in fresh water (ohm m)				Cf. RSMA01 for undeformed varieties. No data for mylonitic varieties.
Uranium content based on gamma ray spectrometric data (ppm)				Cf. RSMA01 for undeformed varieties. No data for mylonitic varieties.
Natural exposure rate (microR/h)				Cf. RSMA01 for undeformed varieties. No data for mylonitic varieties.
Subordinate rock types (%)				No quantitative estimate is available. The proportion of subordinate rock types is presumably comparable to RSMA01. In the southernmost part of the domain, fine-grained dioritoid (501030) and granite (501058) are dominating rock types.
Degree of inhomogeneity	Low		High	Based on outcrop observations from the local model area, N=30. The degree of inhomogeneity based on rock types are judged to be comparable to RSMA01. However, the degree of inhomogeneity what relates to the degree of ductile shear deformation is high
Metamorphism/alteration (%)	Inhomogeneous greenschist facies metamorphic grade and red staining		High	Based on outcrop observations from the local model area, N=30.
Mineral fabric (type/orientation)	Weak to moderate foliation		High	

RSMP01				
Property	**Character**	**Quantitative estimate**	**Confidence**	**Comment**
	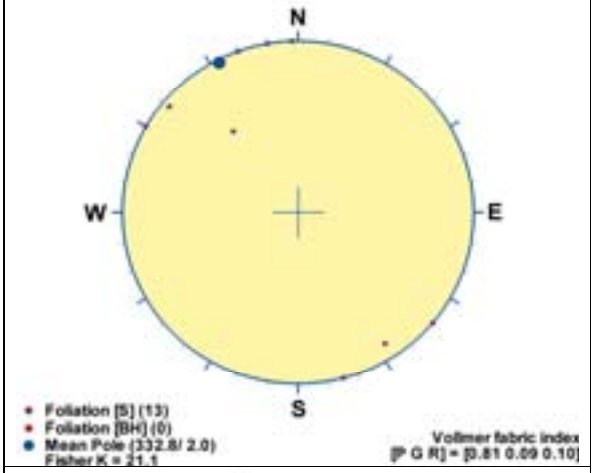 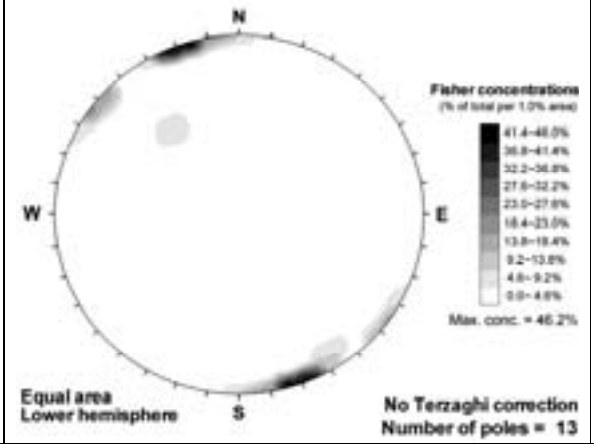			Surface (S) measurements from the local model area
	Ductile and brittle-ductile shear zones		High	
	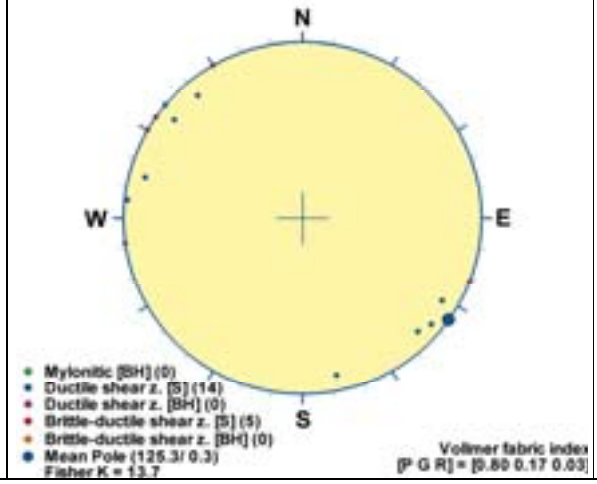			Surface (S) measurements from the local model area

Appendix 12

Prediction and outcome from drilling of cored boreholes – proportions of rock types and deformation zones

For borehole KLX11A and all subsequent boreholes, a prediction was made prior to drilling that addressed the following geological features:

- Lithological homogeneity, i.e. a prediction of the proportions of different rock types in the borehole. The prediction also included a verification of the Laxemar 1.2 rock domain model by making a prediction at what borehole length potential rock domain boundaries should be intersected. However, it must be noted that only the cored boreholes KLX01, KLX02, KLX03 and KLX04, and preliminary mapping of KLX05 and KLX06 were available in connection with the Laxemar 1.2 modelling stage.
- Borehole length for intersection of deformation zones that were included in the Laxemar 1.2 model version, including subsequent modification of the deformation zone model when new information successively became available from the ongoing site investigation work.
- An estimation of the fracture frequency in the rock volumes in between the deformation zones.

The progress of investigation has been more rapid than the progress of site descriptions which has in turn delimited the prediction capabilities of certain aspects of the geological models. Rock domain and deformation zone models have been developed sufficiently concurrent to the site investigation to serve as adequate models for prediction. The discrete fracture network models of Laxemar has not been updated at the same speed due to uncertainties in the fracture data collection as well as natural delays of up to several months for detailed fracture data to be incorporated into SICADA. The prediction of fracture frequency for all KLX boreholes was therefore performed based on the first Laxemar GeoDFN (version 1.2) which was based only on a few early drilled boreholes. The results of these predictions have been uncertain at best and are not presented in the prediction/outcome results below.

The diagrams below display a comparison between the predicted proportions of different rock types and outcome of the drilling.

As can be seen in the diagrams, there is good agreement between the prediction and outcome for the boreholes that are drilled in the quartz monzodiorite in RSMD01, i.e. KLX11A, KLX14A, KLX15A, KLX16A, KLX19A and KLX20A. The only notable difference is the documentation of dolerite in KLX14A, KLX19A and KLX20A, which was not predicted.

The boreholes with the greatest difference between prediction and outcome refer to the boreholes that were drilled through the modelled boundaries between RSMA01, RSMM01 and RSMD01 in the Laxemar 1.2 rock domain model. The latter is exemplified in KLX13A, which according to the Laxemar 1.2 model should penetrate in following order, RSMA01, RSMM01, RSMA01 and finally RSMD01 (see diagrams below). As can be seen in the diagrams, the borehole never reached the quartz monzodiorite in RSMD01at depth and the proportion of diorite/gabbro was c. 17% in what was predicted to be RSMA01 in the upper part of the borehole. A similar difference was obtained in KLX17A which never reached the quartz monzodiorite in RSMD01 either. However, in KLX21B there was a good agreement between the predicted intercept between RSMA01 and RSMD01 and the outcome.

The outcome of the drillings has generated important input for the updating of the Laxemar 1.2 model to the present SDM-Site 3D rock domain model.

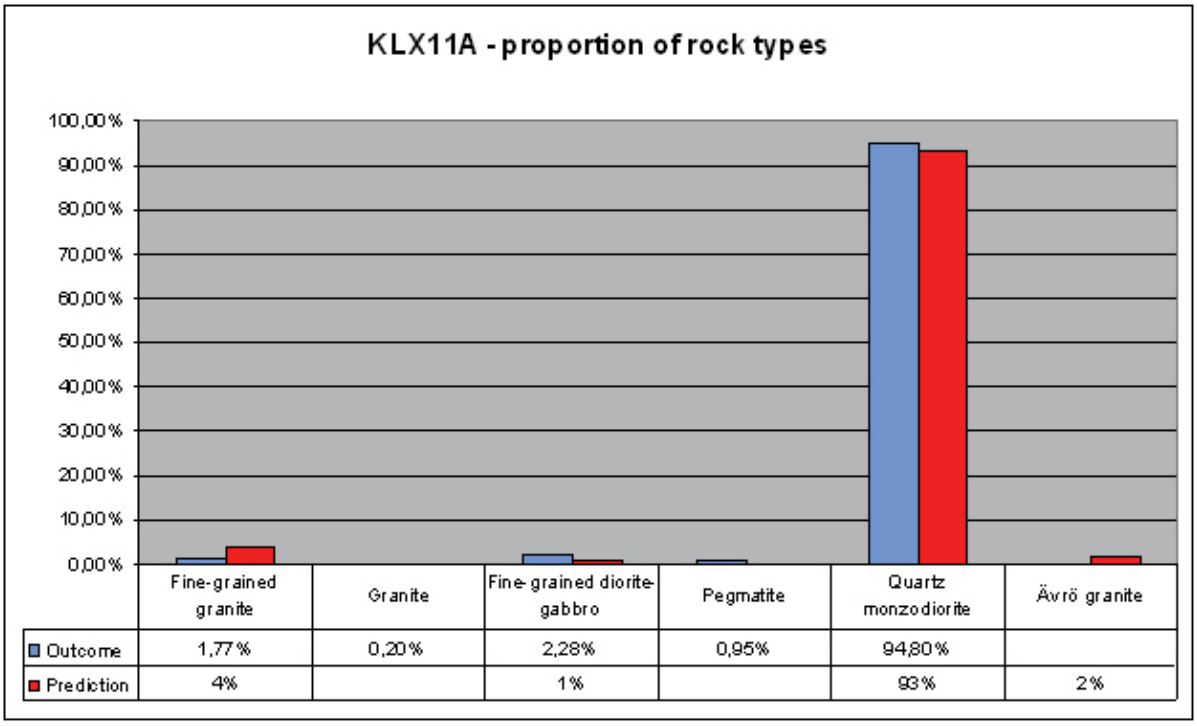

	Fine-grained granite	Granite	Fine-grained diorite-gabbro	Pegmatite	Quartz monzodiorite	Ävrö granite
Outcome	1,77%	0,20%	2,28%	0,95%	94,80%	
Prediction	4%		1%		93%	2%

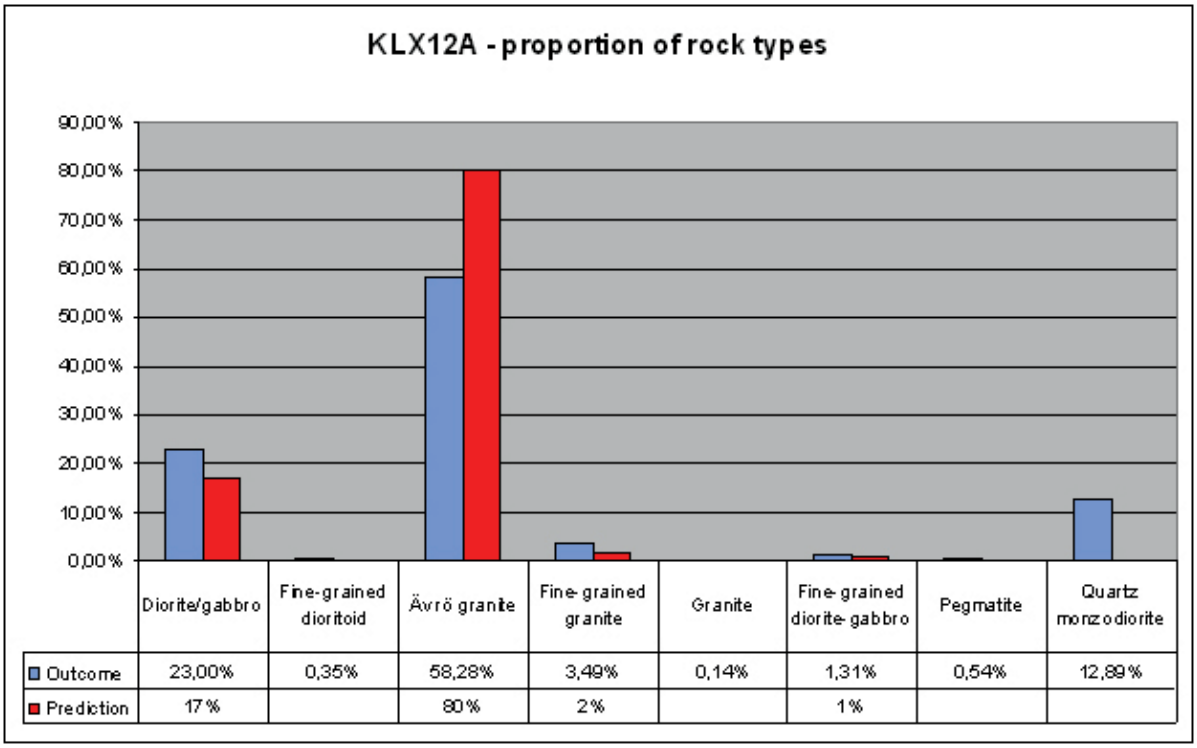

	Diorite/gabbro	Fine-grained dioritoid	Ävrö granite	Fine-grained granite	Granite	Fine-grained diorite-gabbro	Pegmatite	Quartz monzodiorite
Outcome	23,00%	0,35%	58,28%	3,49%	0,14%	1,31%	0,54%	12,89%
Prediction	17%		80%	2%		1%		

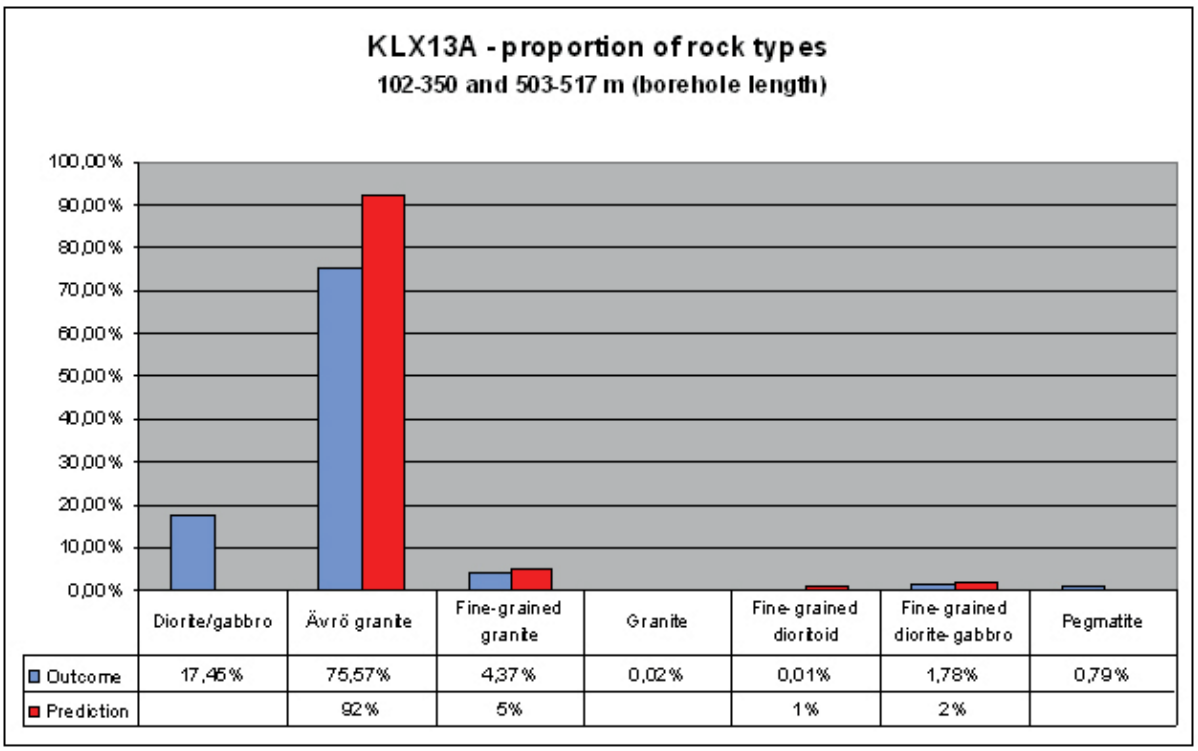
KLX13A - proportion of rock types
102-350 and 503-517 m (borehole length)
100,00%
90,00%
80,00%
70,00%
60,00%
50,00%
40,00%
30,00%
20,00%
10,00%
0,00%
Diorite/gabbro
Ävrö granite
Fine-grained granite
Granite
Fine-grained dioritoid
Fine-grained diorite-gabbro
Pegmatite
Outcome
17,45%
75,57%
4,37%
0,02%
0,01%
1,78%
0,79%
Prediction
92%
5%
1%
2%

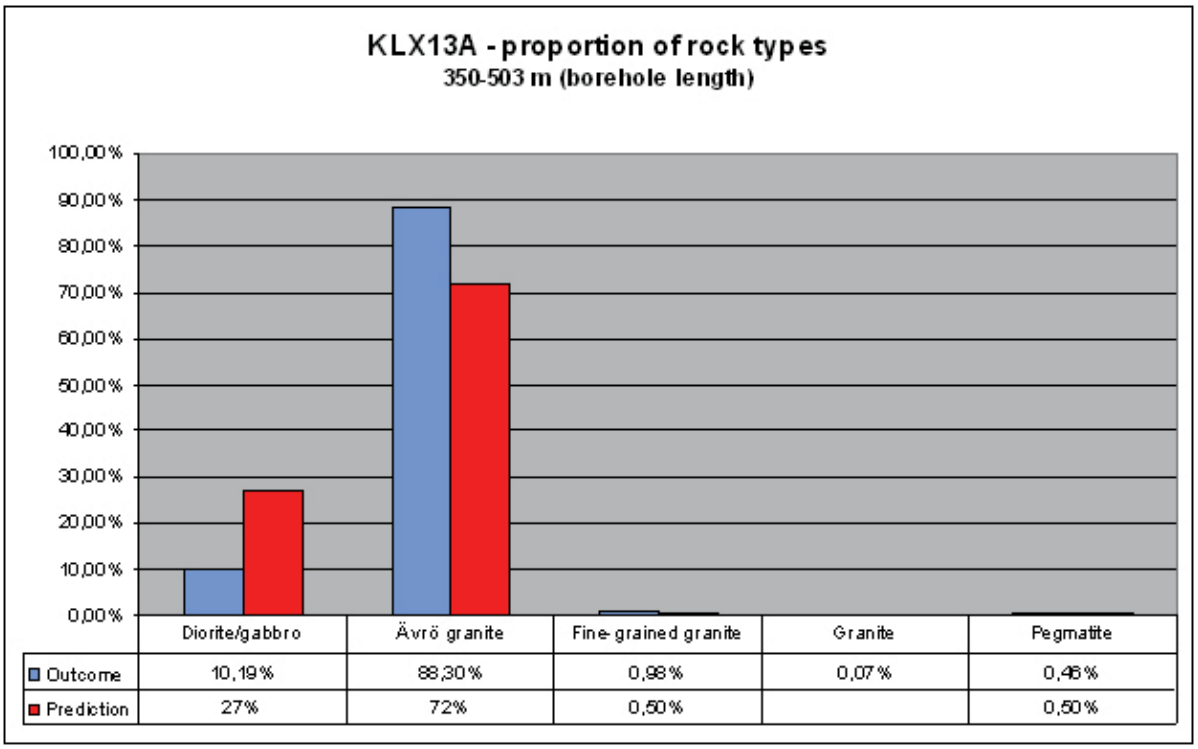
KLX13A - proportion of rock types
350-503 m (borehole length)
100,00%
90,00%
80,00%
70,00%
60,00%
50,00%
40,00%
30,00%
20,00%
10,00%
0,00%
Diorite/gabbro
Ävrö granite
Fine-grained granite
Granite
Pegmatite
Outcome
10,19%
88,30%
0,98%
0,07%
0,46%
Prediction
27%
72%
0,50%
0,50%

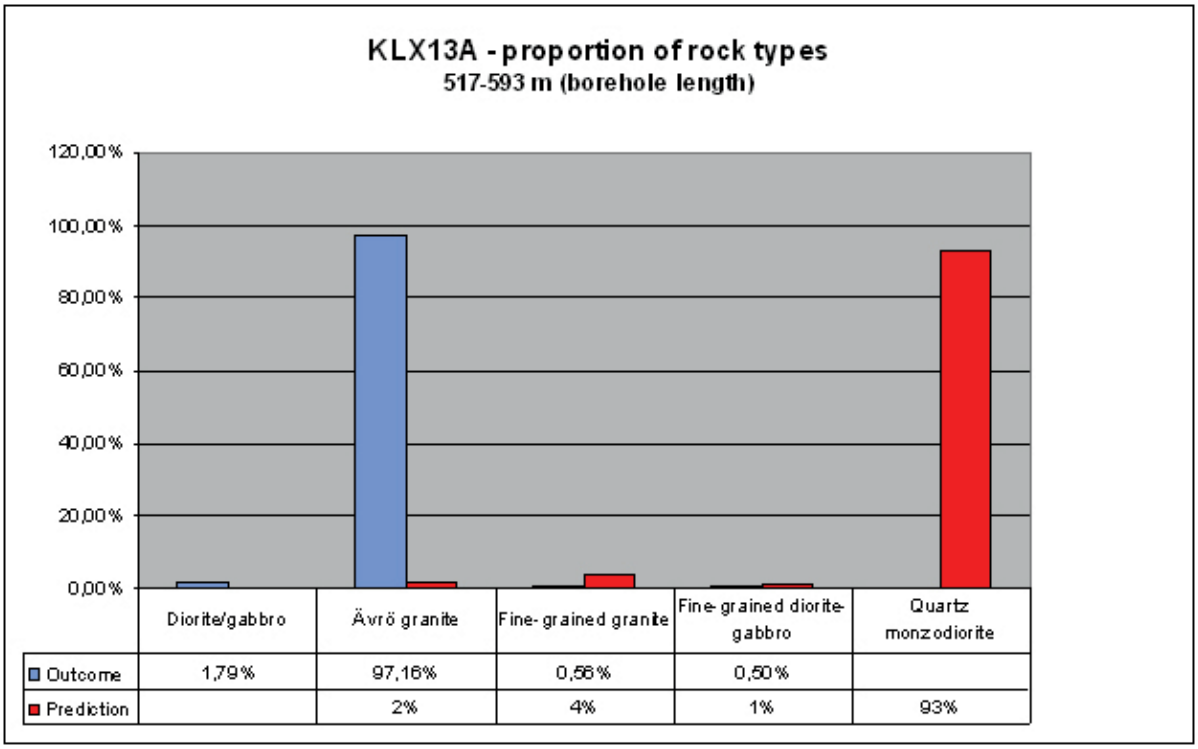

	Diorite/gabbro	Ävrö granite	Fine-grained granite	Fine-grained diorite-gabbro	Quartz monzodiorite
Outcome	1,79 %	97,16%	0,56 %	0,50 %	
Prediction		2%	4%	1%	93%

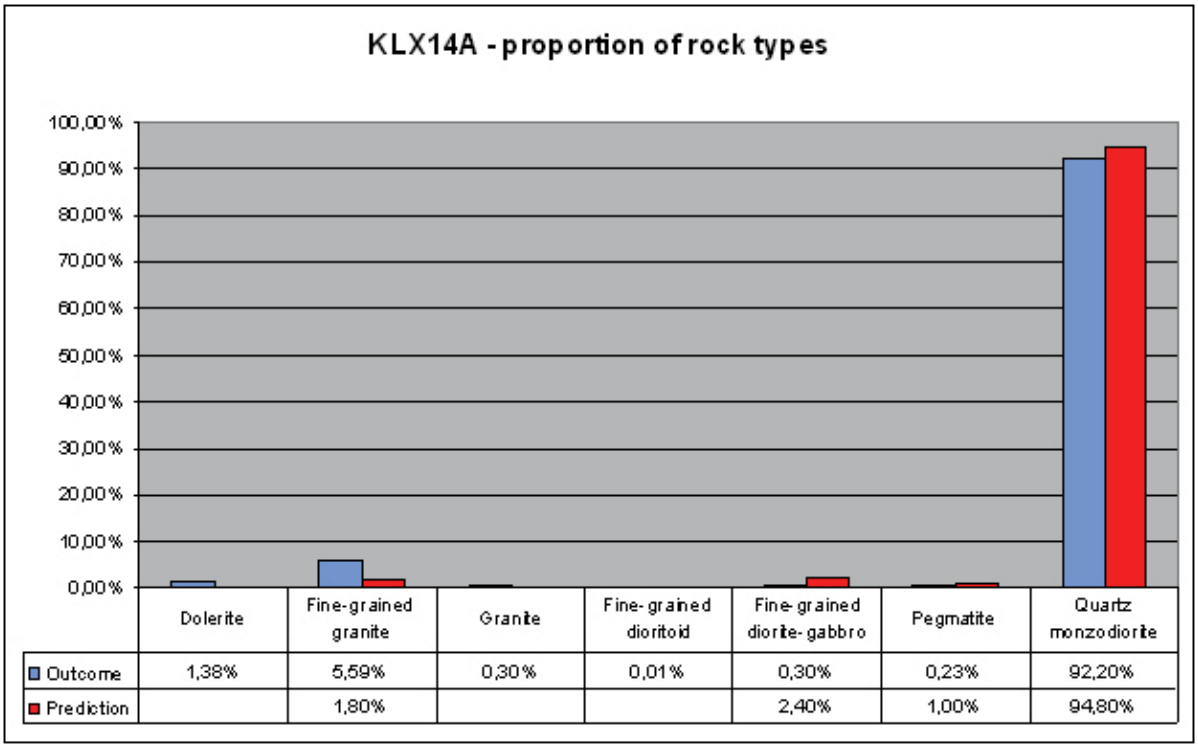

	Dolerite	Fine-grained granite	Granite	Fine-grained dioritoid	Fine-grained diorite-gabbro	Pegmatite	Quartz monzodiorite
Outcome	1,38%	5,59%	0,30 %	0,01 %	0,30%	0,23%	92,20%
Prediction		1,80%			2,40%	1,00%	94,80%

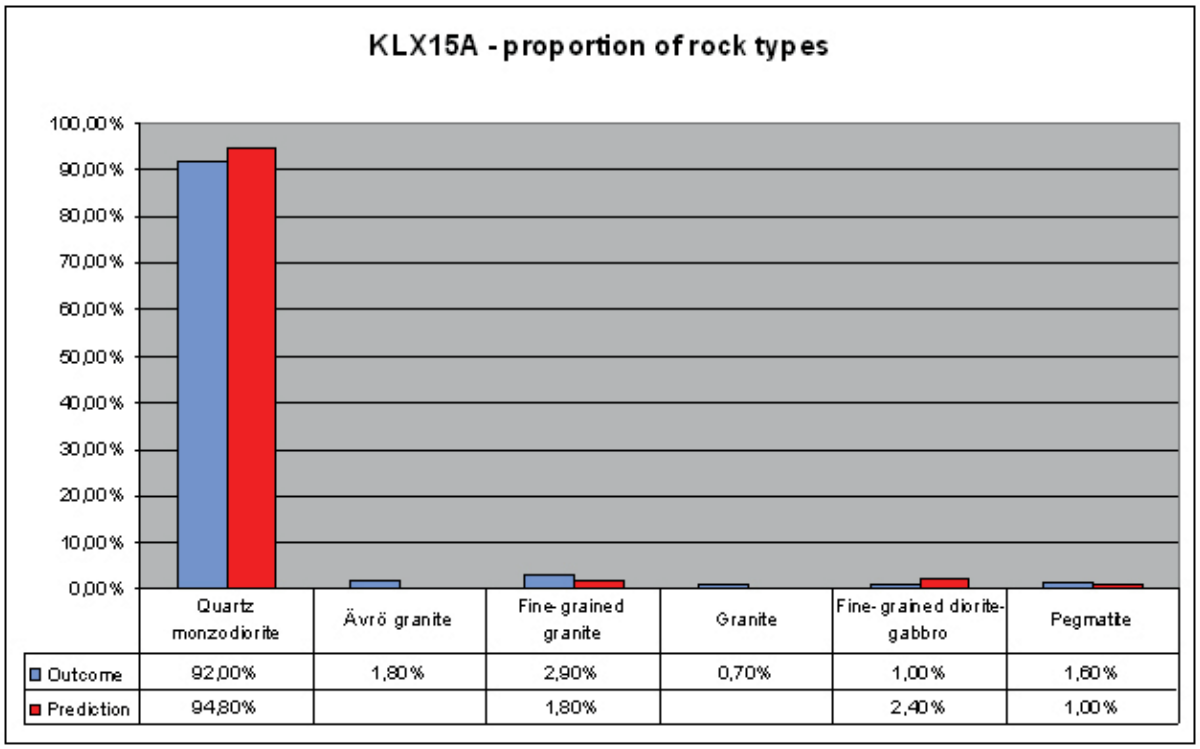

	Quartz monzodiorite	Ävrö granite	Fine-grained granite	Granite	Fine-grained diorite-gabbro	Pegmatite
Outcome	92,00%	1,80%	2,90%	0,70%	1,00%	1,60%
Prediction	94,80%		1,80%		2,40%	1,00%

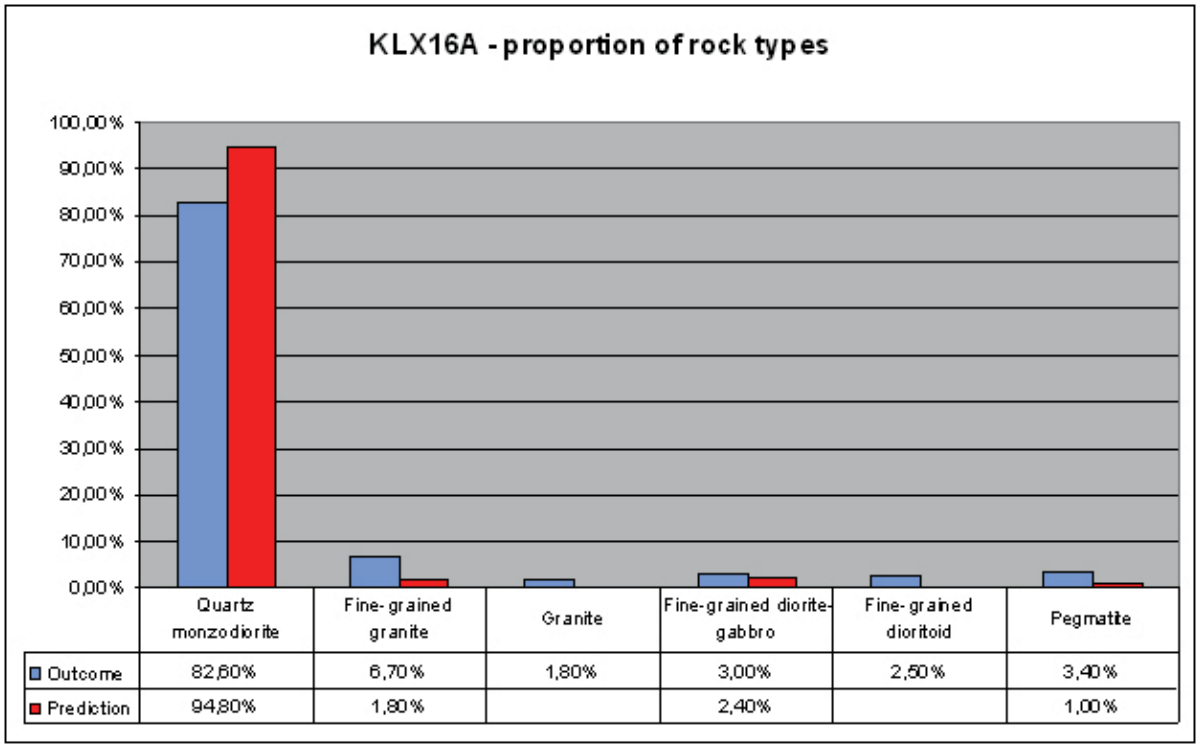

	Quartz monzodiorite	Fine-grained granite	Granite	Fine-grained diorite-gabbro	Fine-grained dioritoid	Pegmatite
Outcome	82,60%	6,70%	1,80%	3,00%	2,50%	3,40%
Prediction	94,80%	1,80%		2,40%		1,00%

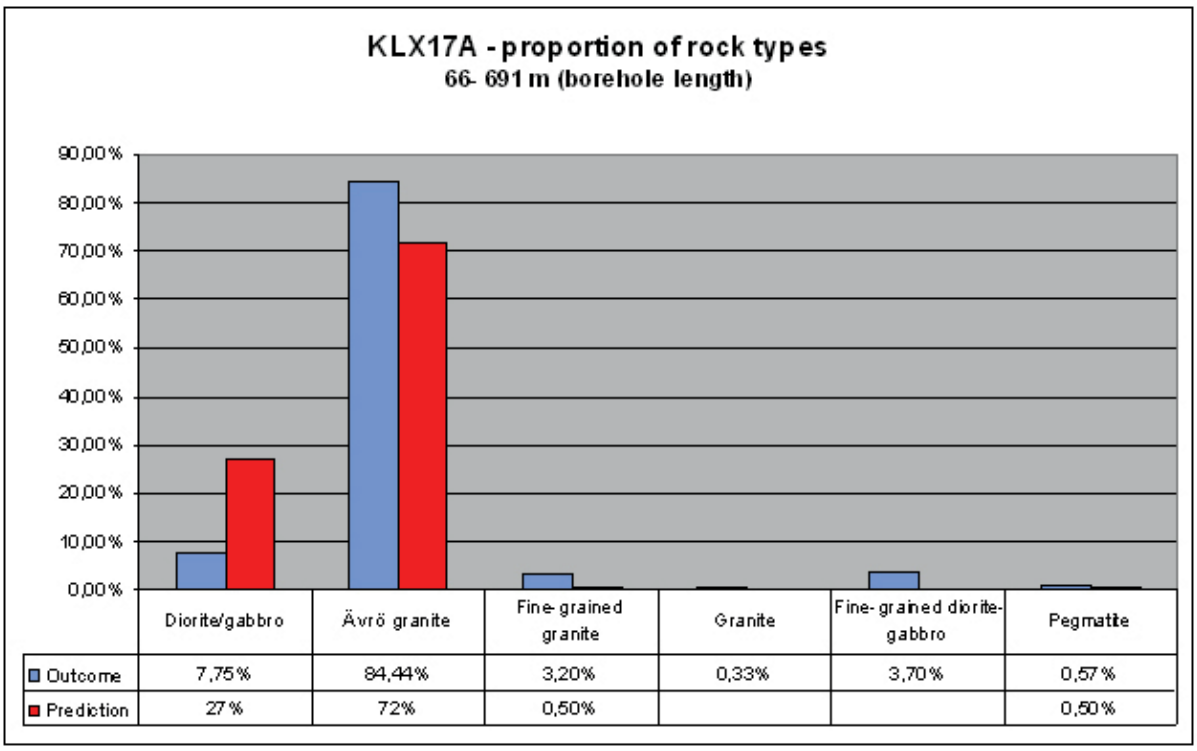
KLX17A - proportion of rock types
66- 691 m (borehole length)
90,00%
80,00%
70,00%
60,00%
50,00%
40,00%
30,00%
20,00%
10,00%
0,00%
Diorite/gabbro
Ävrö granite
Fine-grained granite
Granite
Fine-grained diorite-gabbro
Pegmatite
Outcome 7,75% 84,44% 3,20% 0,33% 3,70% 0,57%
Prediction 27% 72% 0,50% 0,50%

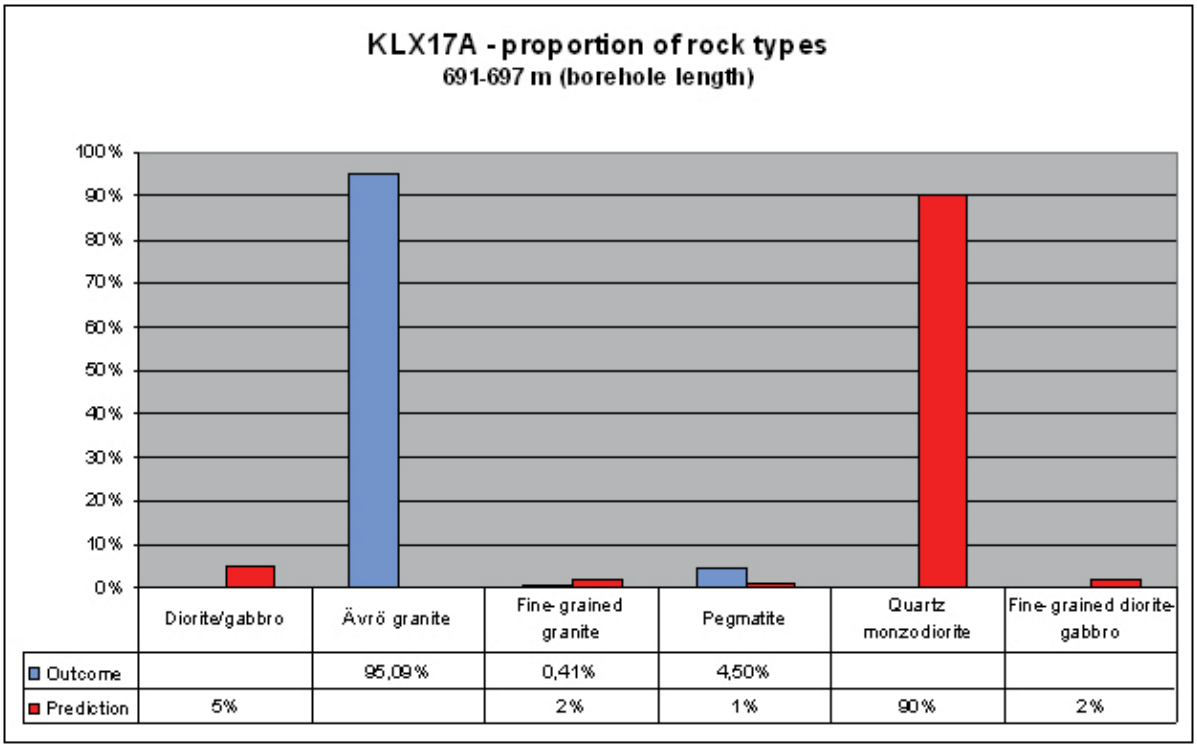
KLX17A - proportion of rock types
691-697 m (borehole length)
100%
90%
80%
70%
60%
50%
40%
30%
20%
10%
0%
Diorite/gabbro
Ävrö granite
Fine-grained granite
Pegmatite
Quartz monzodiorite
Fine-grained diorite-gabbro
Outcome 95,09% 0,41% 4,50%
Prediction 5% 2% 1% 90% 2%

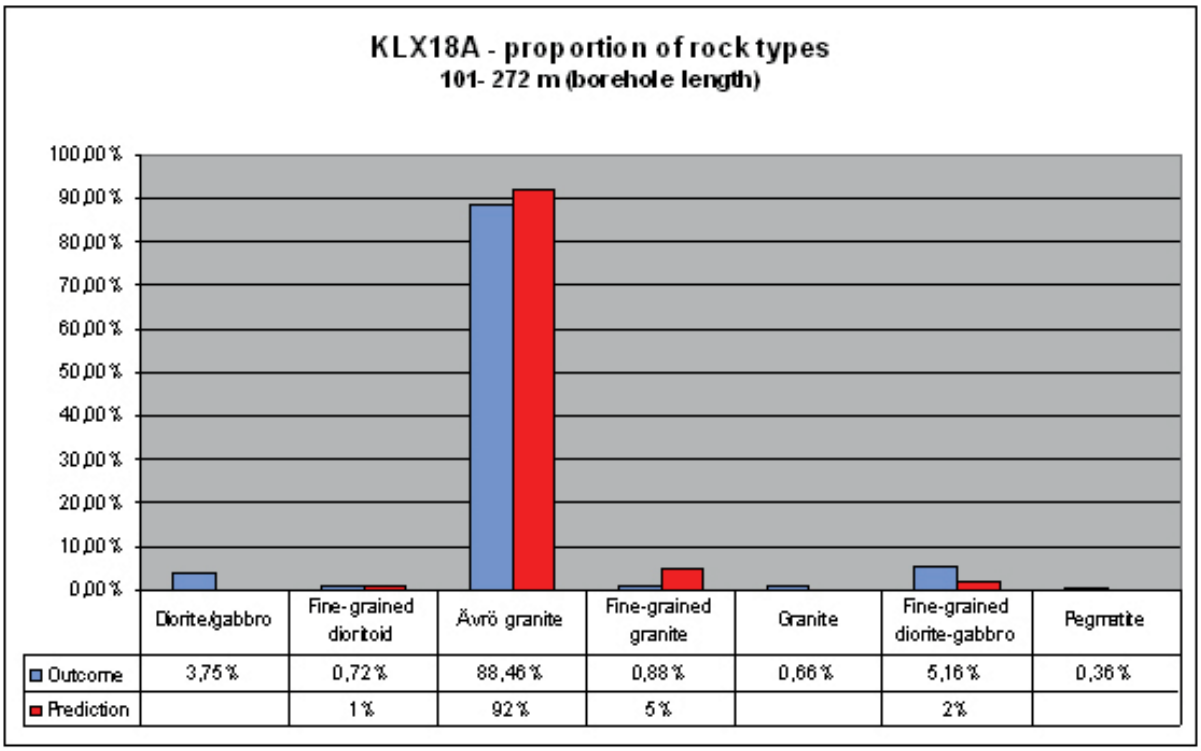
KLX18A - proportion of rock types
101- 272 m (borehole length)
100,00 %
90,00 %
80,00 %
70,00 %
60,00 %
50,00 %
40,00 %
30,00 %
20,00 %
10,00 %
0,00 %
Diorite/gabbro
Fine-grained dioritoid
Ävrö granite
Fine-grained granite
Granite
Fine-grained diorite-gabbro
Pegmatite
Outcome
3,75 %
0,72 %
88,46 %
0,88 %
0,66 %
5,16 %
0,36 %
Prediction
1 %
92 %
5 %
2 %

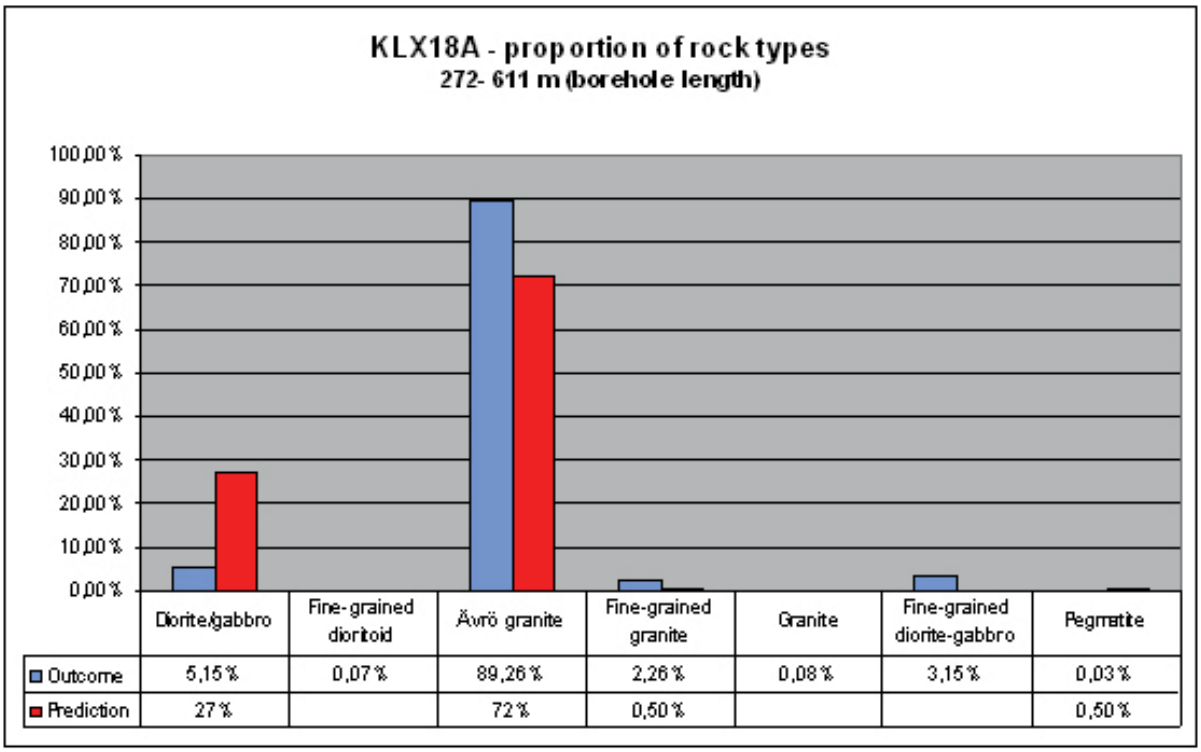
KLX18A - proportion of rock types
272- 611 m (borehole length)
100,00 %
90,00 %
80,00 %
70,00 %
60,00 %
50,00 %
40,00 %
30,00 %
20,00 %
10,00 %
0,00 %
Diorite/gabbro
Fine-grained dioritoid
Ävrö granite
Fine-grained granite
Granite
Fine-grained diorite-gabbro
Pegmatite
Outcome
5,15 %
0,07 %
89,26 %
2,26 %
0,08 %
3,15 %
0,03 %
Prediction
27 %
72 %
0,50 %
0,50 %

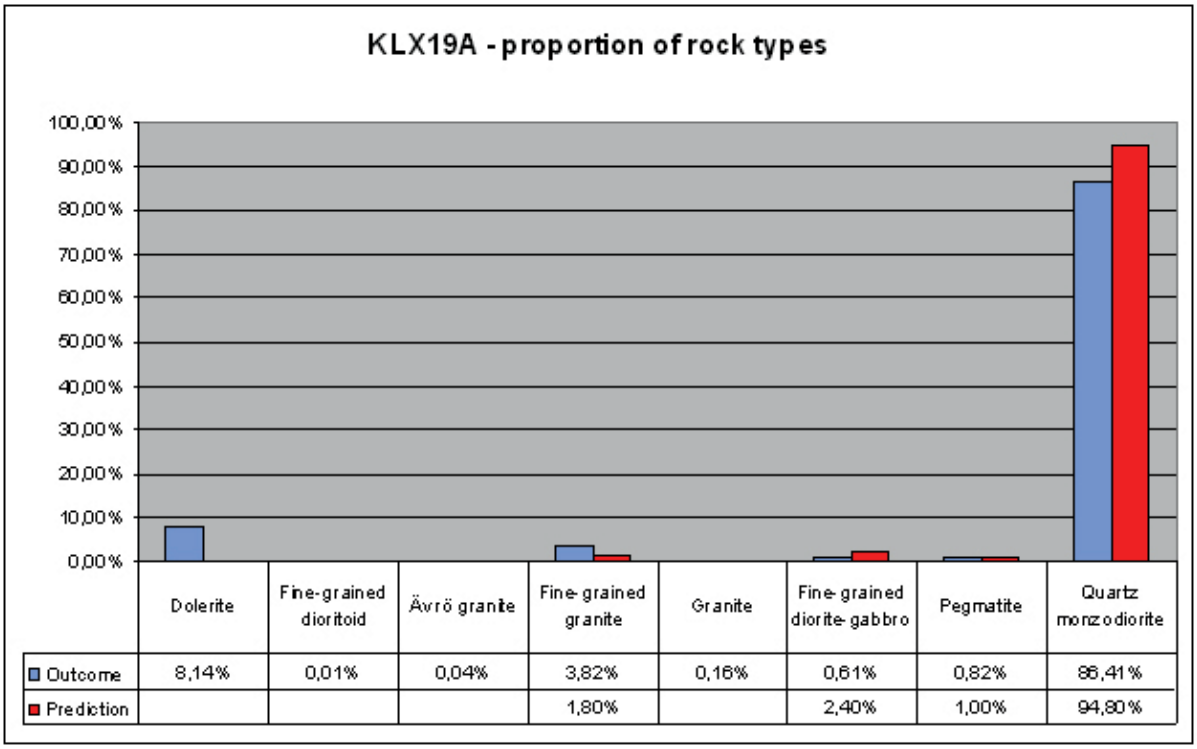

	Dolerite	Fine-grained dioritoid	Ävrö granite	Fine-grained granite	Granite	Fine-grained diorite-gabbro	Pegmatite	Quartz monzodiorite
Outcome	8,14%	0,01%	0,04%	3,82%	0,16%	0,61%	0,82%	86,41%
Prediction				1,80%		2,40%	1,00%	94,80%

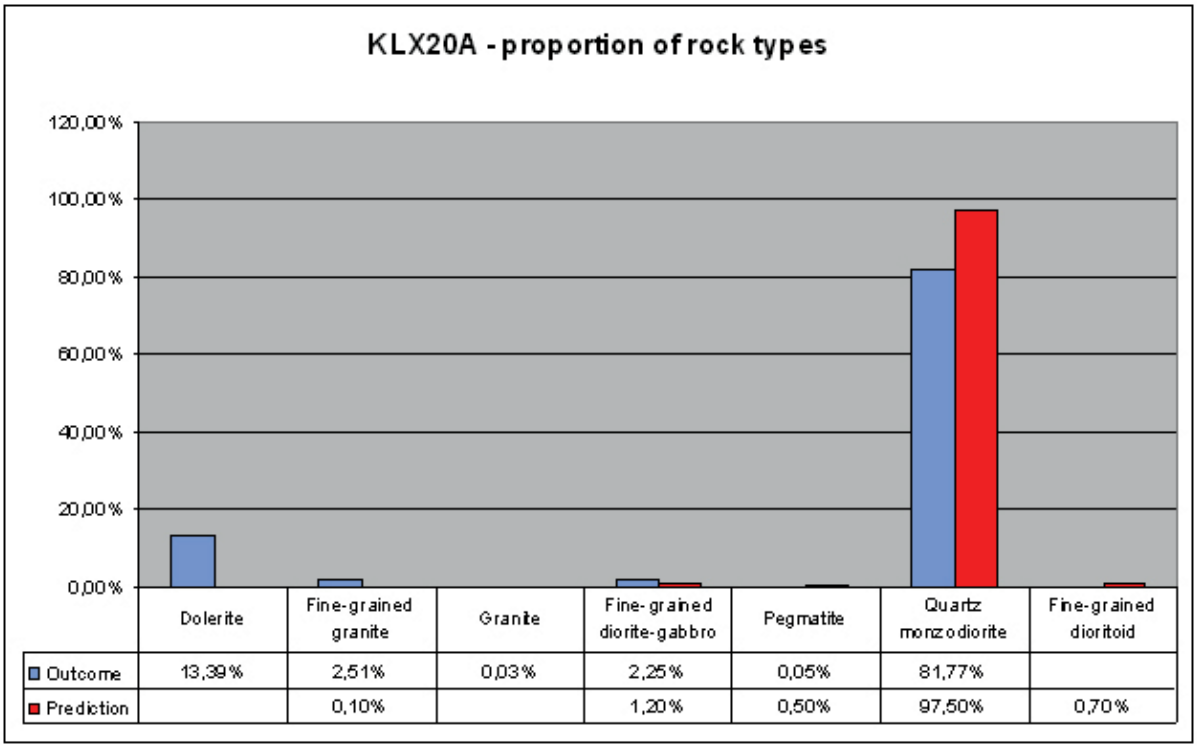

	Dolerite	Fine-grained granite	Granite	Fine-grained diorite-gabbro	Pegmatite	Quartz monzodiorite	Fine-grained dioritoid
Outcome	13,39%	2,51%	0,03%	2,25%	0,05%	81,77%	
Prediction		0,10%		1,20%	0,50%	97,50%	0,70%

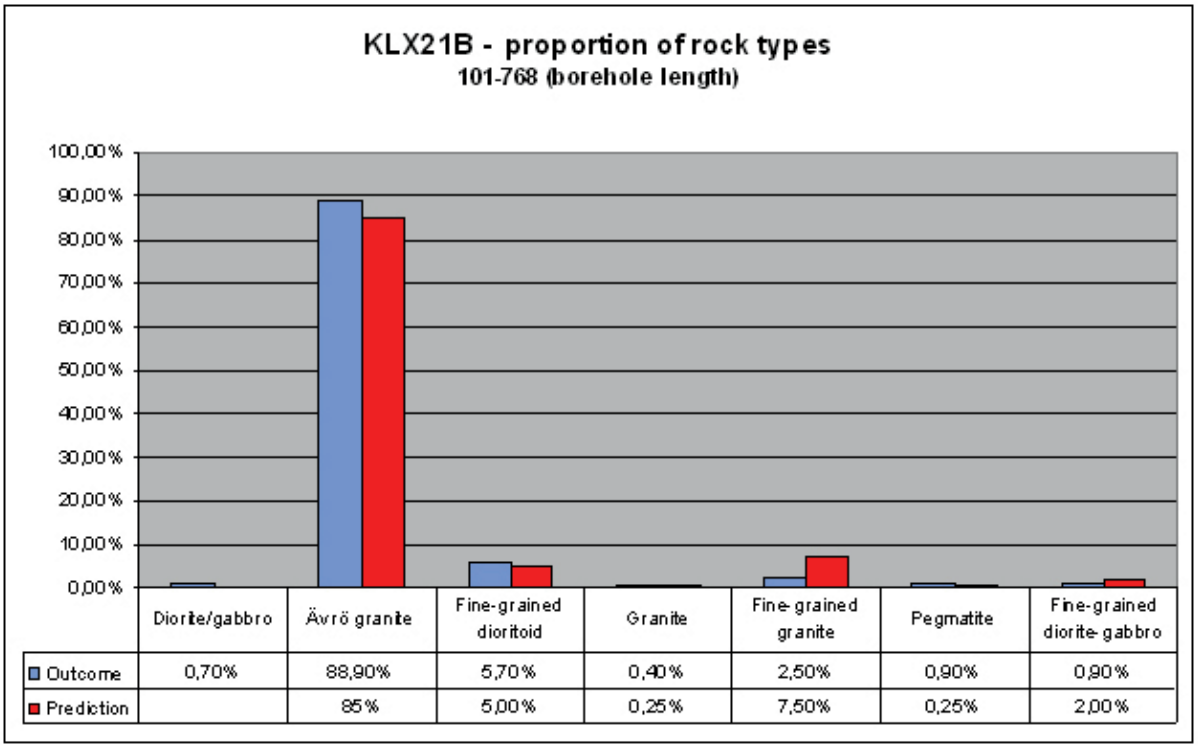

	Diorite/gabbro	Ävrö granite	Fine-grained dioritoid	Granite	Fine-grained granite	Pegmatite	Fine-grained diorite-gabbro
Outcome	0,70%	88,90%	5,70%	0,40%	2,50%	0,90%	0,90%
Prediction		85%	5,00%	0,25%	7,50%	0,25%	2,00%

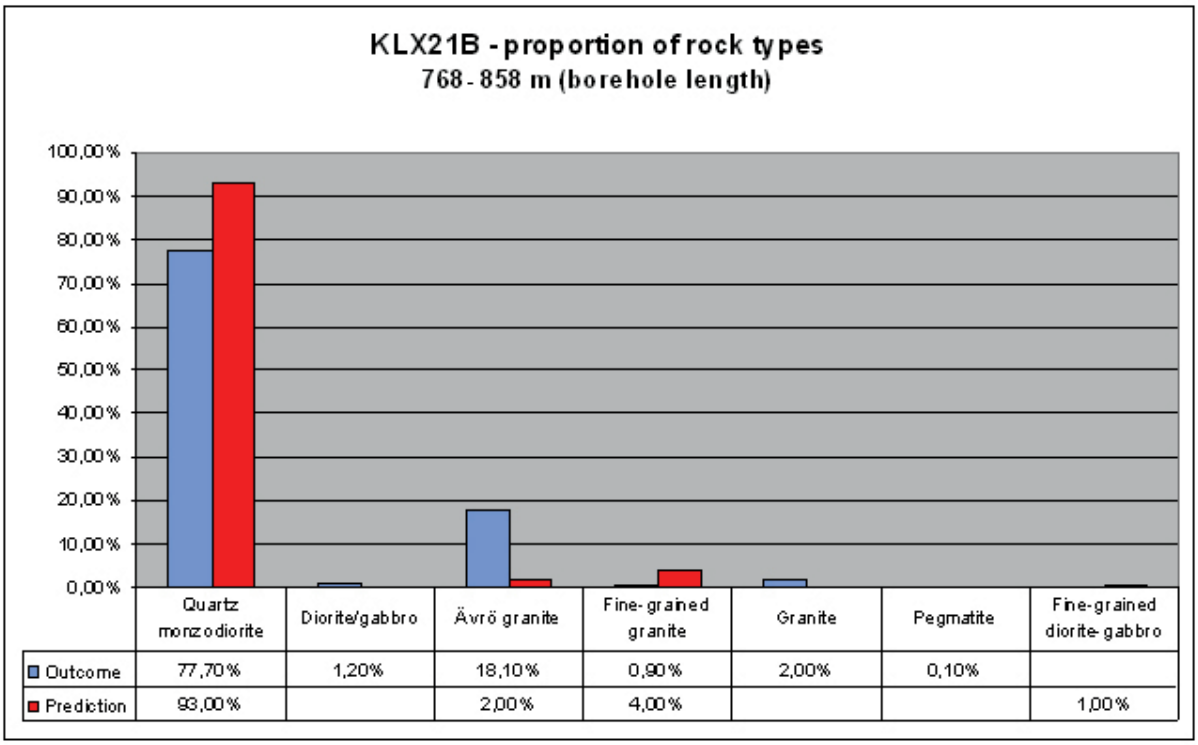

	Quartz monzodiorite	Diorite/gabbro	Ävrö granite	Fine-grained granite	Granite	Pegmatite	Fine-grained diorite-gabbro
Outcome	77,70%	1,20%	18,10%	0,90%	2,00%	0,10%	
Prediction	93,00%		2,00%	4,00%			1,00%

The diagrams below display a comparison between the predicted deformation zone intercepts and the interpreted outcome of the drilling. The diagrams and descriptions aim to give general summaries. If no other information is available then prior to drilling the target deformation zone is assumed to be vertical by default. Borehole azimuths and inclinations were optimized to intercept a maximum range of likely zone dip and dip direction alternatives.

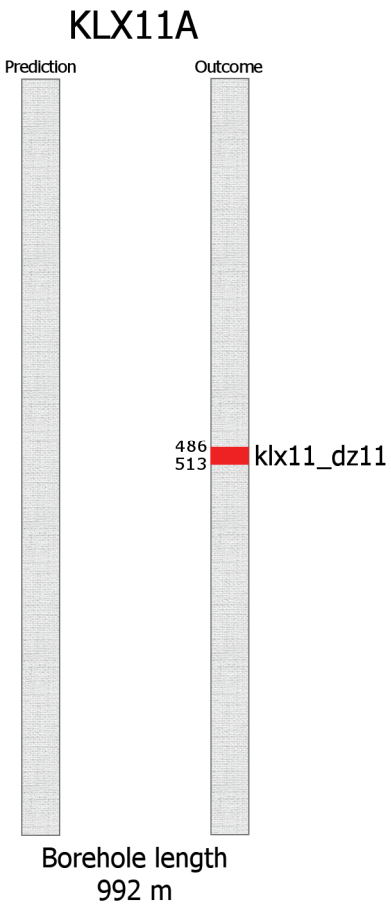	KLX11A was drilled with the aim of characterizing the rock mass block in southern Laxemar, lying between ZSMNS001C in the west and ZSMNS059A in the east. A series of possible minor structures were anticipated but no local major deformation zone. A single zone with an interpreted true thickness of >10m was encountered: a gently SE dipping brittle zone, interpreted as being possibly associated with a theoretical westerly extension of the M1 reflector (ZSMEW946A)
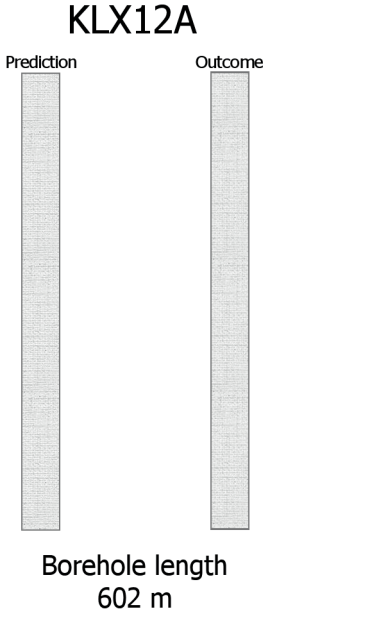	KLX12A was drilled with the aim of characterizing the rock mass in south east Laxemar. No intercepts with local major deformation zones were anticipated.

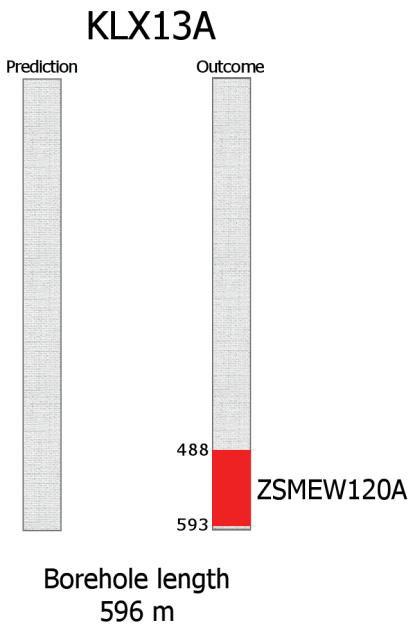	KLX13A was drilled with the aim of characterizing the rock mass block lying between ZSMNS001C and ZSMNS059A in the north of Laxemar. No regional or local major zone interception was anticipated. A major zone intercept was encountered, ZSMEW120A. This zone was earlier assumed to have a vertical dip in the model, whereas the drilling evidence suggests a steep dip to the south, more or less parallel to and merging with, ZSMEW002A.
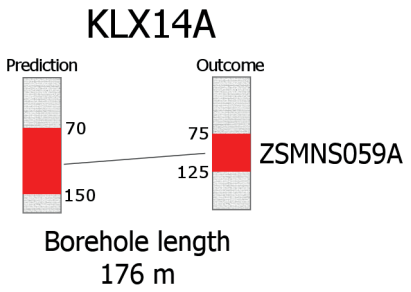	KLX14A was drilled with the aim of investigating the lineament and inferred zone ZSMNS059A.

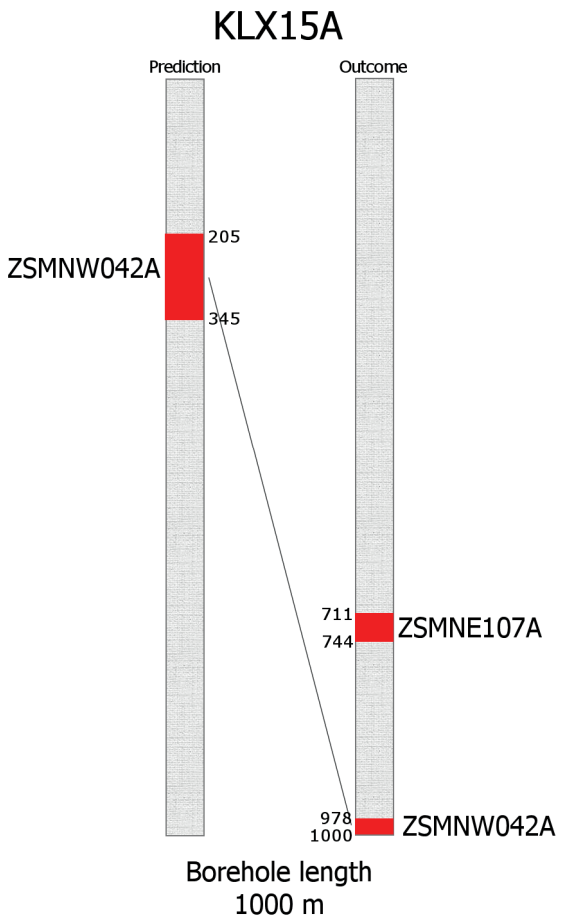	KLX15A was drilled with the aim of investigating the lineament and inferred associated zone ZSMNW042A. It was anticipated that the zone was sub vertical. The interpreted drilling results suggest the zone in fact dips moderately to the south. Another, zone ZSMNE107A is also interpreted to intercept the borehole.
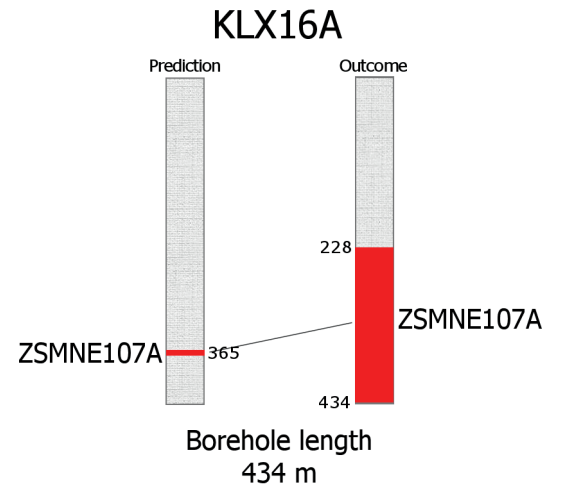	KLX16A was drilled with the aim of investigating the lineament and inferred associated zone ZSMNE107A. A central intercept position for the zone was predicted but no intercept apparent thickness. The zone is interpreted as dipping steeply and generating a long intercept section with the borehole.

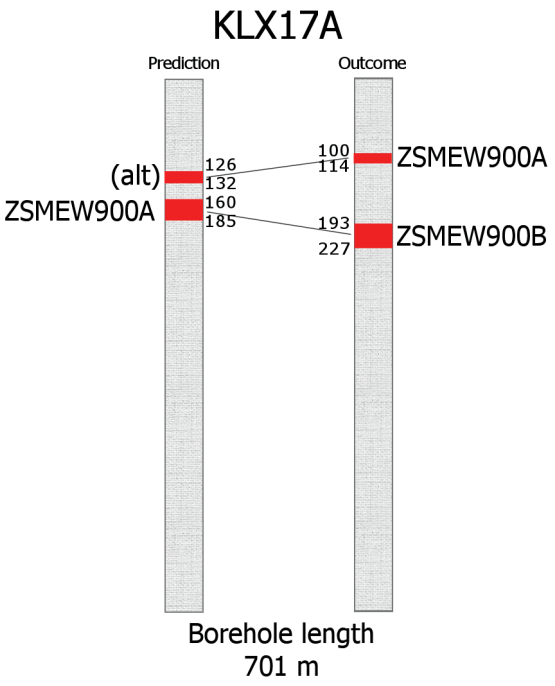	KLX17A was drilled with the aim of investigating the lineaments and inferred associated zone ZSMEW900A.
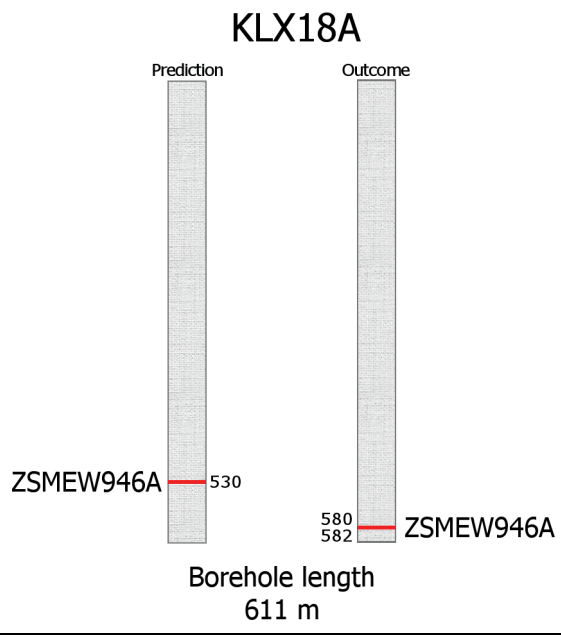	KLX18A was drilled with the aim of investigating the rock mass in central Laxemar, to the east of ZSMNS059A. No intercept with a local major deformation zone was anticipated. An intercept with an earlier interpreted version of seismic reflector M1 (ZSMEW946A, cf. Appendix 8) was predicted at approximately 530 m (borehole length).

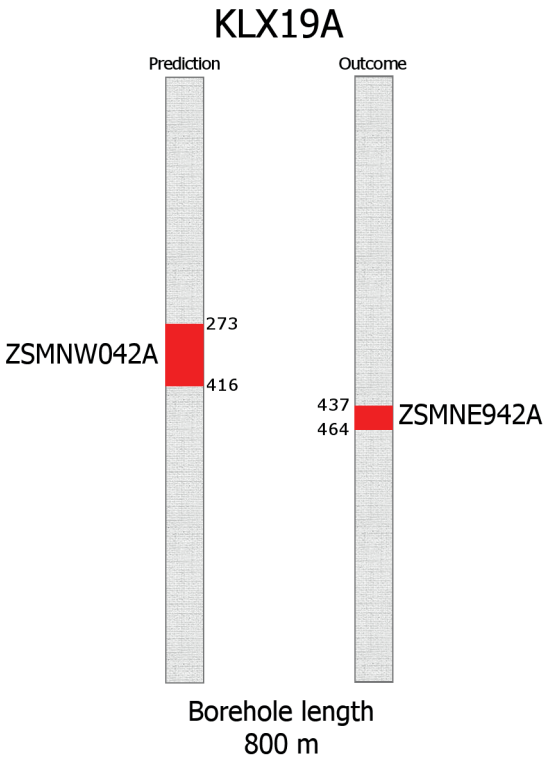	KLX19A was drilled with the aim of investigating the lineament and inferred associated deformation zone ZSMNW042A. The zone was anticipated to be sub vertical. The borehole did intercept a deformation zone at the approximately anticipated level, however, this has been taken to be associated with another zone rather than the target ZSMNW042A. ZSMNW042A subsequently was inferred to potentially dip moderately to the south and not intercept KLX19A.
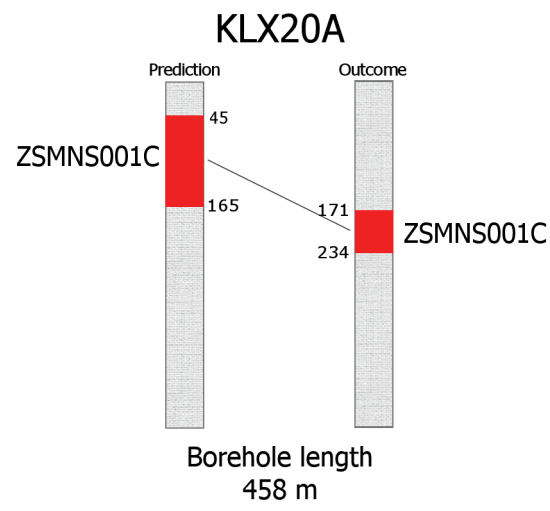	KLX20A was drilled with the aim of investigating the lineament and inferred associated deformation zone ZSMNS001C.

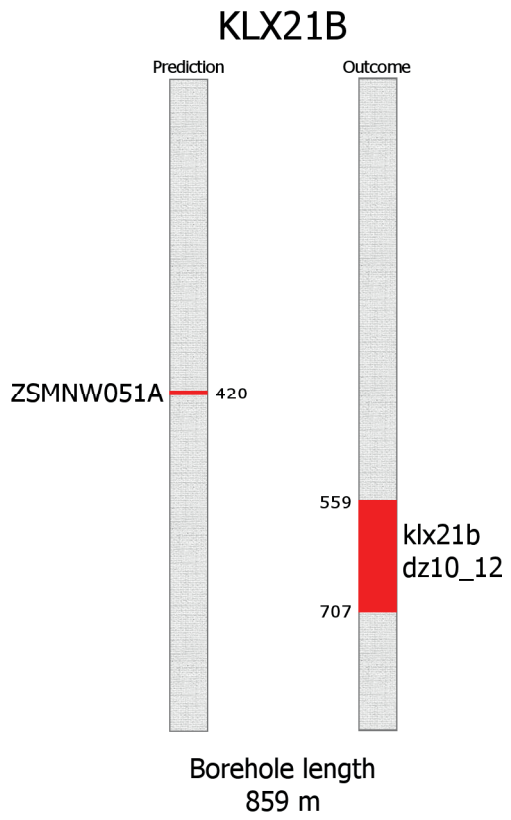	KLX21B was drilled with the aim of investigating the lineament and inferred associated deformation zone ZSMNW051A. The zone's existence was medium confidence prior to drilling. It was also anticipated, based on the magnetic map and the borehole orientation that much of the borehole may be affected by plastic deformation. The borehole was interpreted to have intercepted a series of smaller (10 m total thickness) deformation zones that together give a rather long intercept interval due to their relative orientations. ZSMNW051A is no longer in the deterministic model.
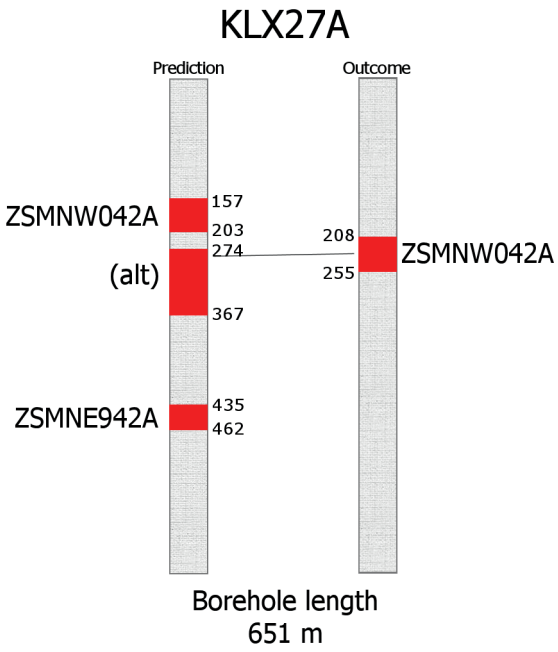	KLX27 was drilled with the aim of further investigating the lineament and inferred associated deformation zone ZSMNW042A. Two alternative interceptions were proposed based on two modelled alternatives with different dips. The interpreted drilling results confirmed the moderate dip to the south alternative. It was also anticipated that the borehole hole could intercept ZSMNE942A, although the location was near the predicted termination of this zone.

Integration of reflection seismic data from profiles 3 and 5 with borehole data at Laxemar

Christopher Juhlin
Uppsala University
Dept. of Earth Sciences
752 36 Uppsala
Sweden

October 2006

Sammanfattning

Reflektionsseismiska data från profiler 3 och 5 inom Laxemarområdet har omprocesserats i ett försök att få bättre bilder av den översta km av berg i närheten av 7 utvalda kärnborrhål. Där det har varit möjligt har ”crossdip” analys utförts för att kunna begränsa geometrin på reflektioner som härstammar utanför planen av profilerna. Baserat på denna omprocessering har geometrin (strykning och stupning) av huvudreflektionerna på profilerna uppdaterats. Ett antal av de tidigare bestämningarna har modifierats och några nya reflektionerna har identifierats. Fokus har varit på grupp M reflektionerna, som stupar flackt mot söder i de översta 1,5 km av skorpan i området. Dessa reflektioner är huvudsakligen okontinuerliga i deras natur, men är en del av det syd stupande mönstret i området.

Efter uppdateringen av geometrin har seismik sektionerna korrelerats med resultat från kärnborrhålen i ett försök att bestämma var reflektionerna härstammar ifrån. Den översta M reflektionen, M1, huvudsakligen korrelera med sprickzoner i 4 av borrhålen. Den kan inte följas på ytseismiken till de borrhål som ligger längst öster ut. M2 och M3 reflektionerna tycks kunna knytas bättre till mafiska bergarter, medan M4 reflektionen också kan korreleras bättre med sprickzoner. Utbredningen av M reflektorerna öster ut tycks begränsas av en N-S gående gräns som ligger öster om KLX04/KLX08.

Den huvudsakligen genomskinliga seismikbilden ovanför M1 reflektionen söder om KLX04/KLX08 stämmer bra överens med det homogena berget som har borrats i motsvarande borrhål. De få reflektioner som finns tolkas att ha sina ursprung från lagom till brant stupande sprickzoner i det homogena berget. Norr om KLX04/KLX08 tycks det vara nord stupande sprickzoner som ger upphov till reflektioner. Men tolkning är inte lika entydig här beroende på den stora mängden av mafiska bergarter som finns i de nordliggande borrhålen.

Rå vågforms sonic data visar huvudsakligen fördröjningar i första ankomsten där låga hastigheter indikeras på sonic loggen. Dessa låg hastighetszoner korrelera också huvudsakligen med utpekade sprickzoner i borrkärnan. En del av de densitetsloggar som gjordes tillgängliga var felkalibrerade med för höga värden på densiteten. Eftersom det är främst densitetskontrasten som påverkar reflektiviteten och inte de absoluta värden har syntetiska seismogram ändå generats baserat på densitet och sonic loggarna och jämförts med migrerade seismik sektioner i närheten av borrhålen. Även om man antar att jorden är 1D när seismogrammen genereras finns det fortfarande en bra överensstämmelse mellan de och seismik sektioner, vilket stärker tolkningen av reflektiviteten baserad på loggarna och kopplingen av vissa reflektioner till sprickzoner.

Faktum att många av reflektionerna är okontinuerliga i deras natur och att 3 av de 7 borrhålen ligger flera hundra meter bort från profilerna komplicera tolkningen. Generellt, bör inte de utpekade reflektionerna anses som diskreta zoner, men som en grupp som kan följas längst en linje. Detta är speciellt sant för grupp M reflektionerna.

Abstract

Reflection seismic data from profiles 3 and 5 in the Laxemar area have been reprocessed in an attempt to better image the uppermost km of crust in the vicinity of 7 selected cored boreholes. Where possible, crossdip analysis of the data has been done in order to constrain the orientation of reflections from out-of-the-plane of the profiles. Based on this reprocessing the orientations (strike and dip) of the main reflections observed on the profiles have been updated. A number of the orientations have been modified and new reflections identified. Focus has been on the set M reflections, which dip gently to the south in the upper 1.5 km of crust in the area. These reflections are generally discontinuous in nature, but are part of the general pattern of south dipping reflectivity seen on the profiles.

Given the updated orientation, the seismic sections have been correlated to results from the boreholes in an attempt to determine the origin of the reflections. The uppermost M reflection, M1, generally correlates with fracture zones in 4 of the boreholes. It cannot be traced on the surface seismic to the more east lying boreholes. The M2 and M3 reflections appear to be more associated with mafic rock, while M4 also correlates better with fracture zones. The lateral extent of the set M reflectors appears to be limited to the east by a N-S running boundary lying east of KLX04/KLX08.

The generally transparent seismic image above the M1 reflection south of KLX04/KLX08 corresponds well to homogeneous rock in the boreholes. The few reflections within this generally transparent zone are interpreted as originating from moderately to steeply south dipping fracture zones. North of KLX04/KLX08, north dipping reflections appear to correspond to fracture zones. However, the interpretation here is less clear here due to the presence of significant amounts of mafic rock in the more northerly lying boreholes that were studied.

Plots of the full waveform sonic data generally show delays in the first arrival where low velocities are indicated in the logs. These low velocity zones also generally correlate with deformation zones in the core that have been identified in the single hold interpretation studies. A number of density logs delivered were improperly calibrated with the densities being too high. Since it is the density contrast that determines the influence of the density log on the reflectivity it was still considered feasible to generate synthetic seismograms based on the sonic and density logs and compare these with migrated seismic data in the vicinity of the boreholes. Although the synthetic seismograms assume a 1D Earth, there is still a good correspondence between the synthetic seismograms and the observed data, supporting the interpretation of the reflectivity based on the logs and the coupling of certain reflections to fracture zones.

The fact that many of the reflections are discontinuous in nature and that 3 of the 7 boreholes are offset from the seismic profiles, on the order of 100s of meters, complicates the interpretation. In general, the picked reflections should not be viewed as discrete zones, but

as a group of reflections that line up along a relatively straight line. This is especially the case for the set M reflections.

Table of Contents

1 Introduction

Seismic data were acquired in the Oskarshamn area in southeastern Sweden (Figure 1-1) during late April to early June in the year 2004. Approximately 9.9 km of high resolution (10 m source and receiver spacing) reflection seismic data were acquired along 3 different profiles (Figure 1-2). Results from initial processing and interpretation of these profiles were presented in Juhlin et al. (2004) without taking into account any results or data from borehole investigations. There are now several well investigated deep cored boreholes located on or close to the seismic profiles (Figure 1-2). Geoscientific data from these boreholes may hold answers to important questions as to what are the lateral limits of reflectors, what is the source of the reflectivity, and why some zones in the boreholes may be transparent to seismic methods. A critical question is whether sub-horizontal reflections observed on the surface seismic are generated by fracture zones, lithological contrasts, or a combination of the two. In order to address these questions the following work has been carried out:

1. Reprocessing of profiles 3 and 5 to better focus the image on reflections M1, N, M2, M3, M4, L, K, Y1 and Y2 (Figures 1-3 and 1-4). Where the profiles are sufficiently crooked, crossdip analysis of reflections were made to determine the out-of-the-plane component. An estimate of the crossdip component allows better extrapolation of reflectors into the boreholes.
2. Calculation of synthetic (theoretical) seismograms based on sonic and density logs from KLX04, KLX08, KLX03, KLX10, KLX18, KLX12 and KLX09. These seismograms give an indication of what portions of the borehole may produce significant reflections. Results must, however, be interpreted with caution since the Earth is assumed to be 1D in this procedure.
3. Integration of surface seismic and with borehole data. Borehole data here consists of sonic and density logs, synthetic seismograms, borehole geometry, and location of interpreted deformation zones. By comparing borehole data with best estimates of seismic depth sections a visual evaluation of the source of the reflectivity has been made.

The main objective of the study has been to determine to what degree sub-horizontal reflectors need to be considered in the site studies at Laxemar.

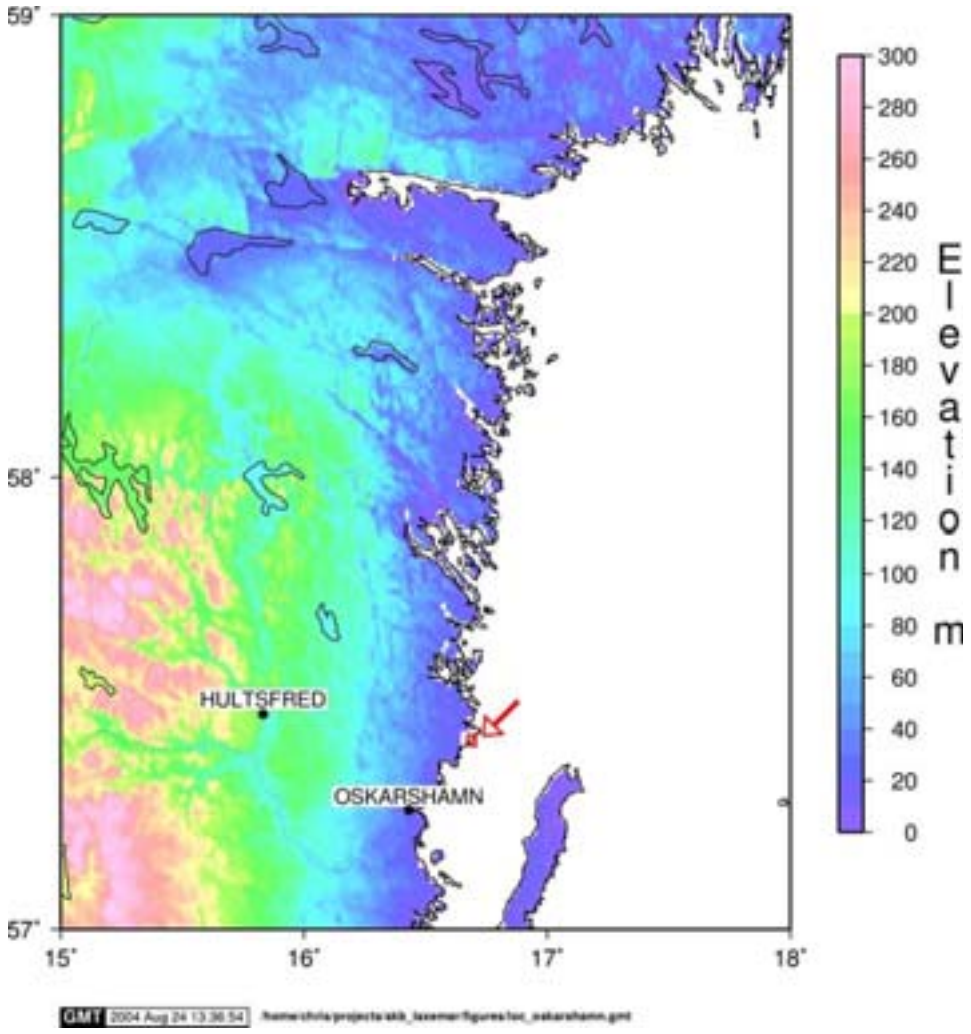

Figure 1-1. *Location of study area (red box marked by arrow).*

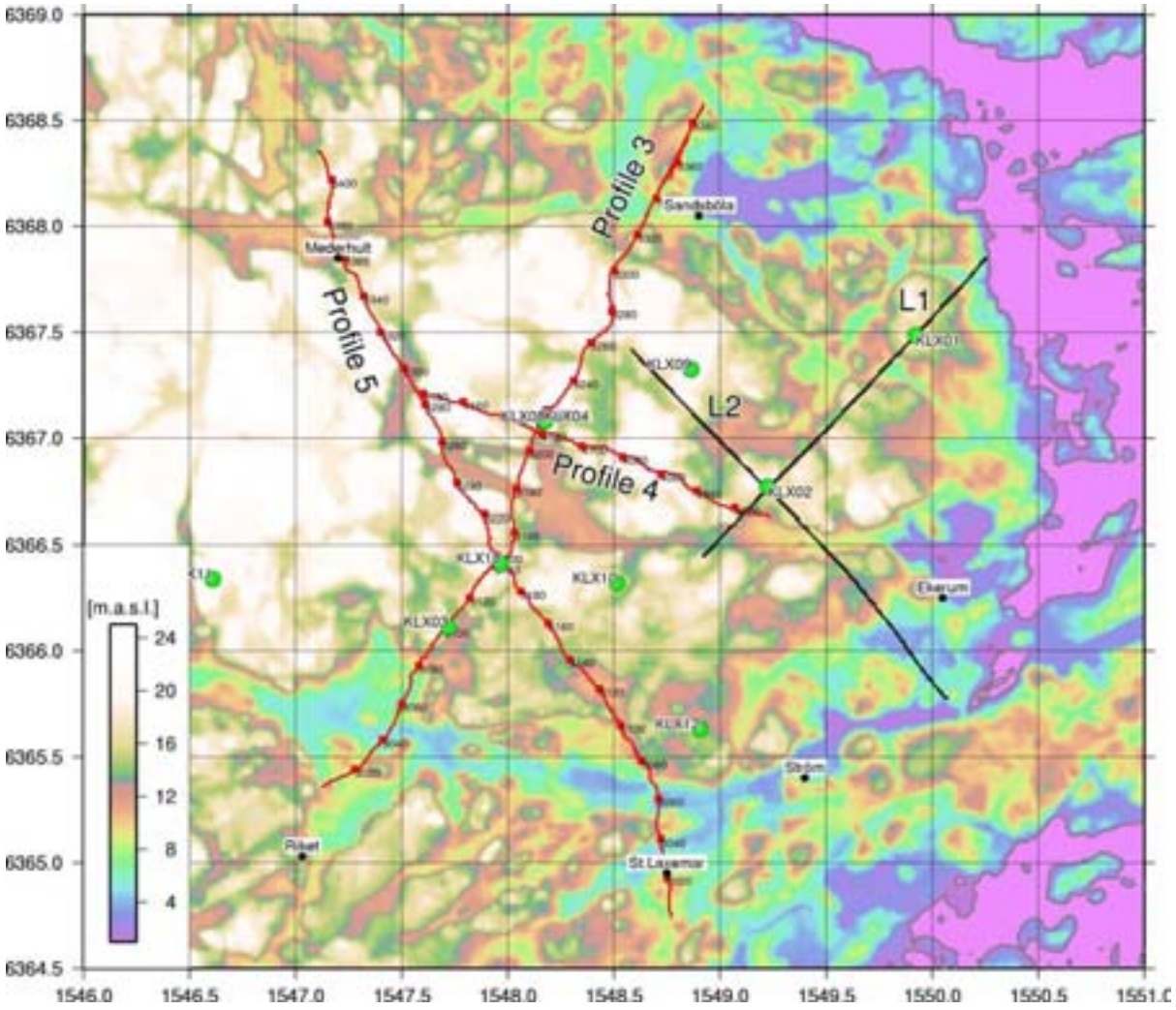

Figure 1-2. *Location of the seismic reflection profiles, profile 3, LSM000704, profile 4, LSM000705 and profile 5, LSM000706 (red lines). Reflection seismic profiles acquired in 1999 (black lines) were reported on in Bergman et al. (2002).*

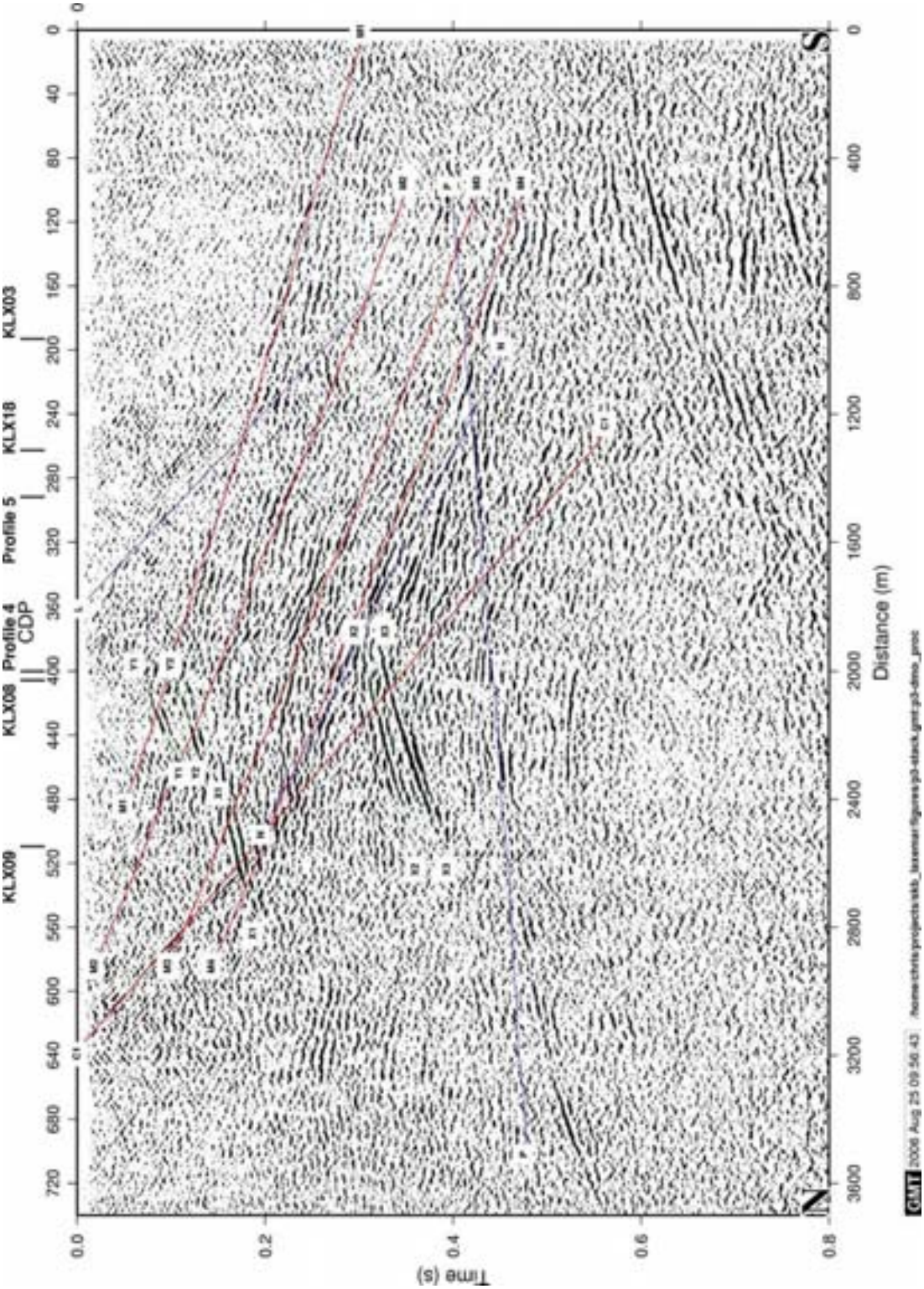

Figure 1-3. *Stacked section of profile 3 (LSM000704) down to 0.8 seconds with modelled reflections from Juhlin et al. (2004). Red-rank 1, blue-rank 2, green-rank 3. Assumed strike and dips are given in Table 1-1.*

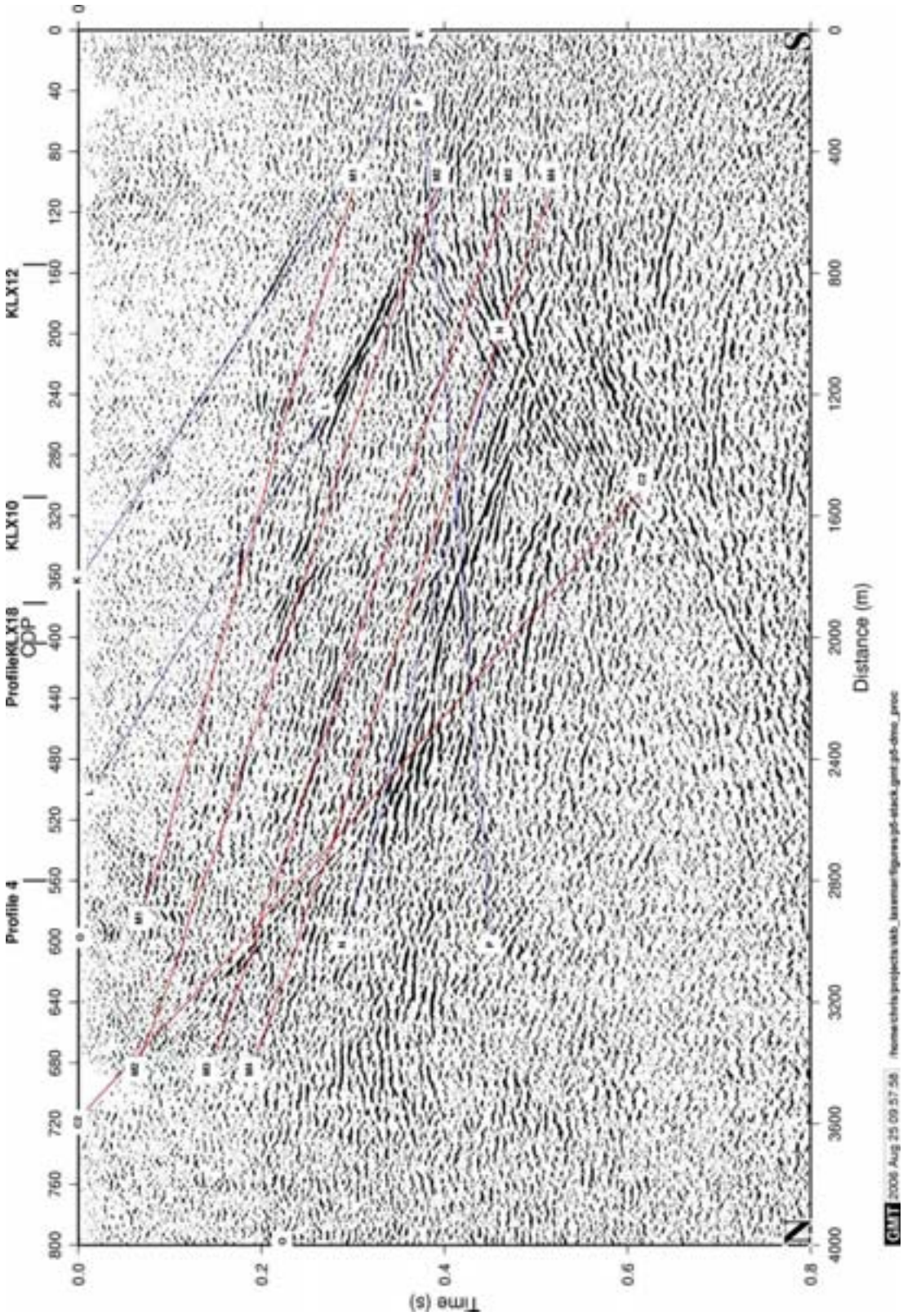

***Figure 1-4**. Stacked section of profile 5 (LSM000706) down to 0.8 seconds with modelled reflections from Juhlin et al. (2004). Red-rank 1, blue-rank 2, green-rank 3. Assumed strike and dips are given in Table 1-1.*

Table 1-1. Orientation of reflectors as determined in the initial interpretation in Juhlin et al. (2004) from the surface seismic data. Reflectors may either be defined by distance to a point on the surface (better for dipping reflectors) or by depth below this point (better for sub-horizontal reflectors). Distance refers to distance from the KLX02 borehole (6366.768 km N, 1549.224 km W) to the closest point on the surface to which the reflector projects. Depth refers to depth below the surface at this origin. Strike is measured clockwise from north. Rank indicates how sure the observation of each reflection is on the profiles that the reflection is observed on; 1 – definite, 2- probable, 3- possible.

Reflector	*Strike*	*Dip*	*Distance (m)*	*Depth (m)*	*Rank*	*Profiles observed on*
A	275	43	190		1	1, 2, 4
B	0	3		760	1	1, 2, 4
C1	90	70	1330		1	1, 2, 3, 4
C2	85	70	1330		1	4, 5
D	253	35	840		2	1, 2, 4
G	253	35	1170		2	1, 2, 4
K	30	50	800		2	4?, 5
L	110	70	-300		2	3, 5?
M1	95	20		350	1	3, 4, 5
M2	100	25		500	1	3, 4, 5
M3	100	25		750	1	3, 4, 5
M4	100	25		900	1	3, 4, 5
N	120	30		770	2	3, 4, 5
O	200	80	-1850		3	5
X1	295	15		400	3	3
X2	295	15		970	3	3
X3	295	15		1070	3	3
Y1	295	27		300	3	3, 4?
Y2	295	15		350	3	3, 4?

2 Data used

Input data for this study consisted of

1. Raw data from surface seismic seismic profiles 3 and 5.
2. Borehole geometry.
3. Processed density and P-wave sonic velocity logs. Note that there were calibration problems with some of the density logs with readings being 40-50 kg/m^3 too high. Since it was mainly density contrasts that were of interest in this study, the delivered density logs were used rather waiting for recalibrated density logs to be delivered.
4. Location of interpreted deformation zones in the boreholes.
5. Raw sonic waveform data.

3 Data processing

3.1 Reflection seismic processing

Seismic profiles 3 and 5 (Figure 3-1) were reprocessed from scratch using processing steps similar to those used earlier. Main differences were that lower frequencies were passed in the filtering and a more uniform velocity field for the DMO step prior to stacking was used. Stacked sections from the reprocessing are shown in Figures 3-2 and 3-3. As mentioned in Juhlin et al. (2004), many of the reflections in profiles 3 and 5 appear to strike close to perpendicular to the profiles. Therefore, the geometries shown in the reprocessed migrated sections (Figures 3-4 and 3-5) are are reasonably realistic. However, the reader should keep in mind that some of the reflections are from out of the plane of the profile, so that the migrated sections cannot be strictly regarded as vertical slices below the profiles. Instead the depth scale should be regarded as distance from the surface to the reflector. The approximate depth scale shown in the figures is based on the average DMO velocity and is only valid for reflections striking perpendicular to the plane of the profile.

3.2 Crossdip analysis

Where there is a significant spread in the midpoints perpendicular to the profiles it is possible to analyse the seismic data for the crossdip component of the reflections (Nedimovic and West, 2003). If the reflector dips exactly perpendicular to the strike of the profile then the crossdip component can be corrected for by

$$\Delta T = (2\Delta Y / v)\sin\phi$$

where ΔY is the signed perpendicular distance from the midpoint to the CDP stacking line, v is an appropriate constant velocity estimate of the medium, Φ is the crossdip angle and ΔT is the time delay or advance to be applied to the trace in the CDP gather. By stacking data with different crossdip corrections at a given stacking or NMO velocity, an estimate of the crossdip component can be made (Figures 3-6 to 3-8). If the strike of the reflector is not parallel to the CDP stacking line the crossdip correction also depends upon its dip. Therefore, the crossdip angle obtained should be considered with caution, but is reasonably accurate for gently dipping reflections. Crossdip analysis will be most effective on the present data set along CDPs 150-300 on profile 3 and CDPs 100-300 on profile 5 (Figure 3-1).

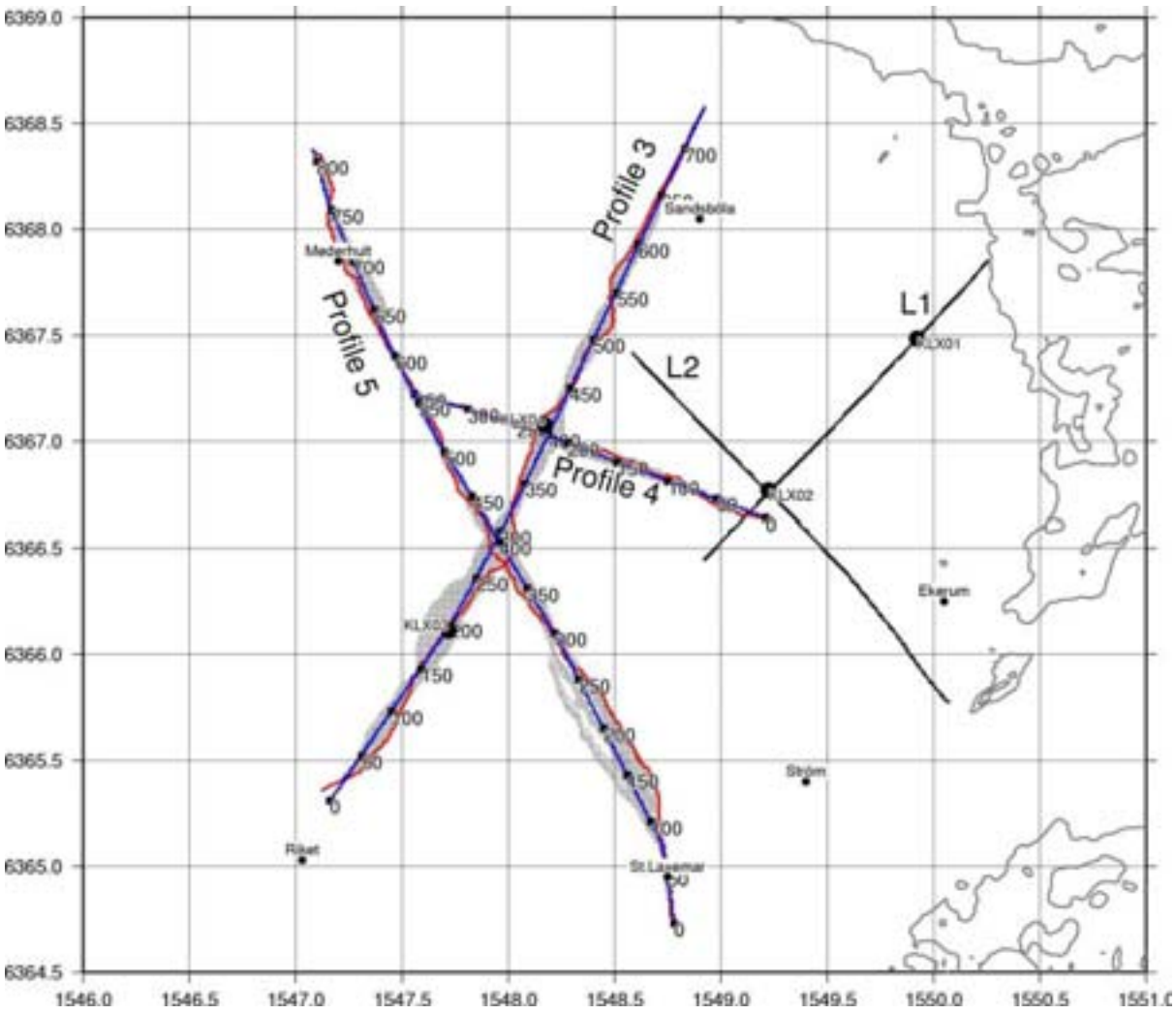

Figure 3-1*. Midpoints between shots and receivers (black dots) used in the processing and the CDP lines that the data have been projected onto and stacked along (blue). Numbering refers to CDP position along the stacking line. Actual location of the seismic profiles (red) are also shown, profile 3 (LSM000704), profile 4 (LSM000705) and profile 5 (LSM000706).*

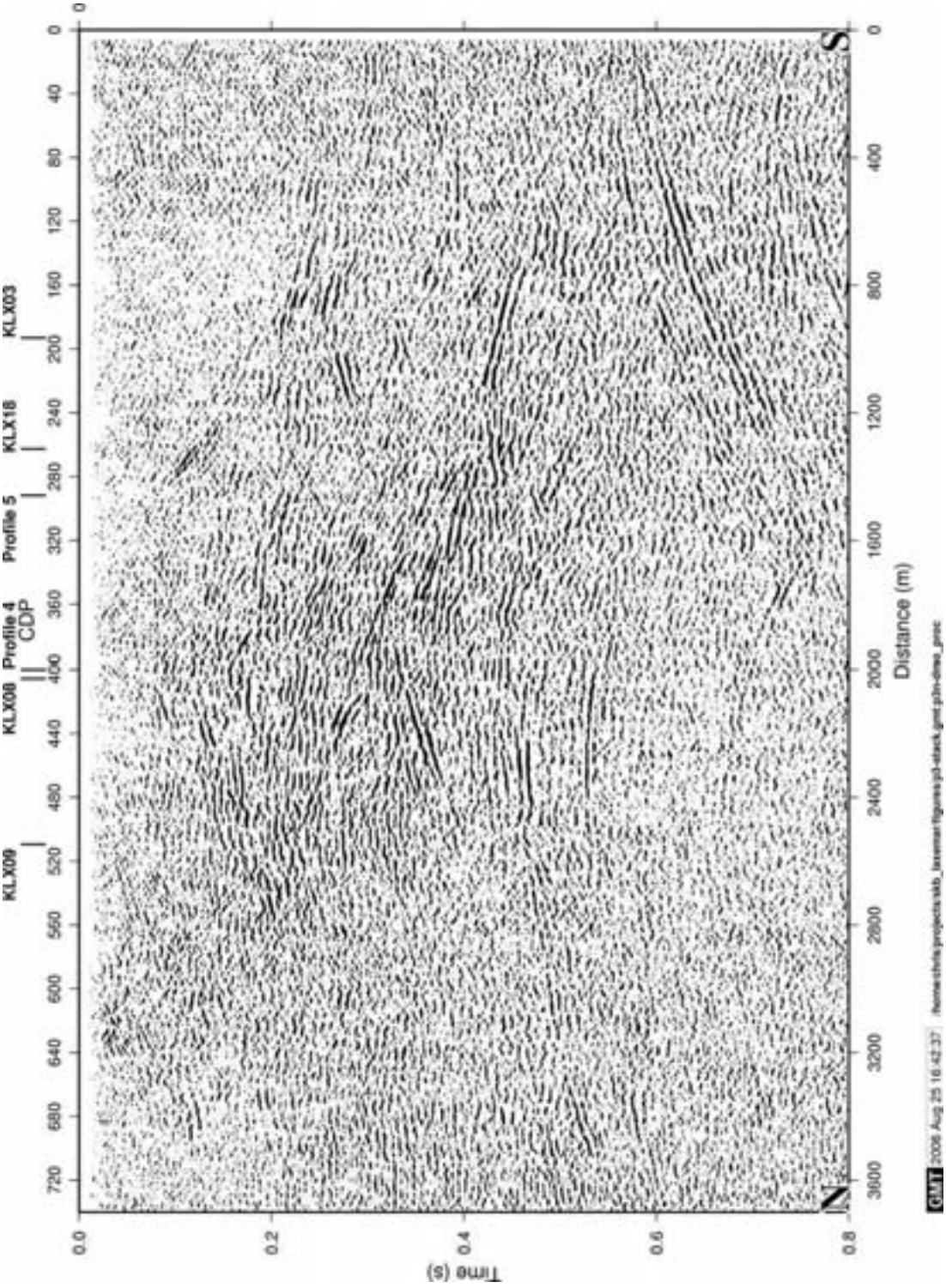

***Figure 3-2**. Reprocessed stacked section from this study of profile 3 (LSM000704) down to 0.8 seconds.*

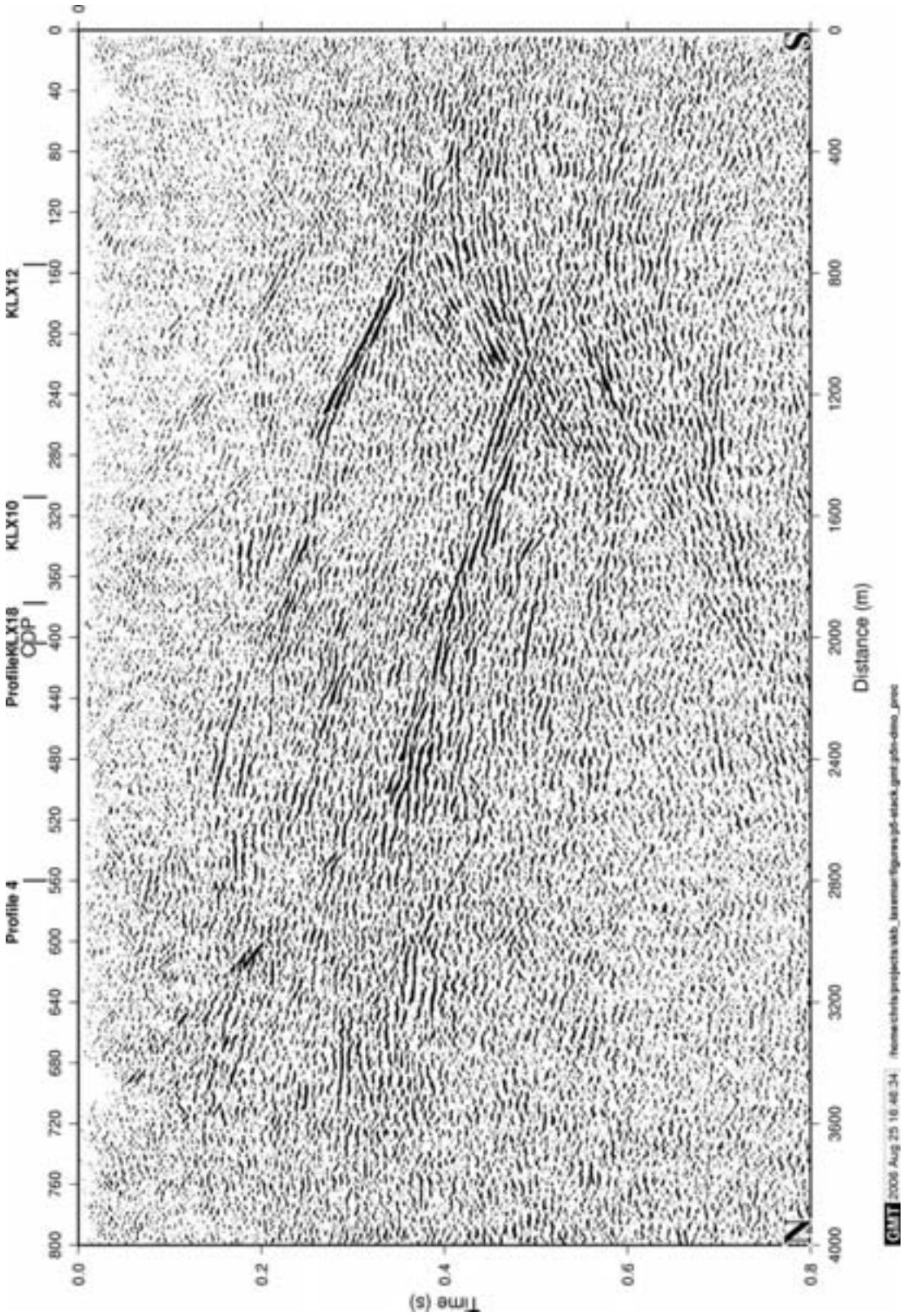

***Figure 3-3**. Reprocessed stacked section from this study of profile 5 (LSM000706) down to 0.8 seconds.*

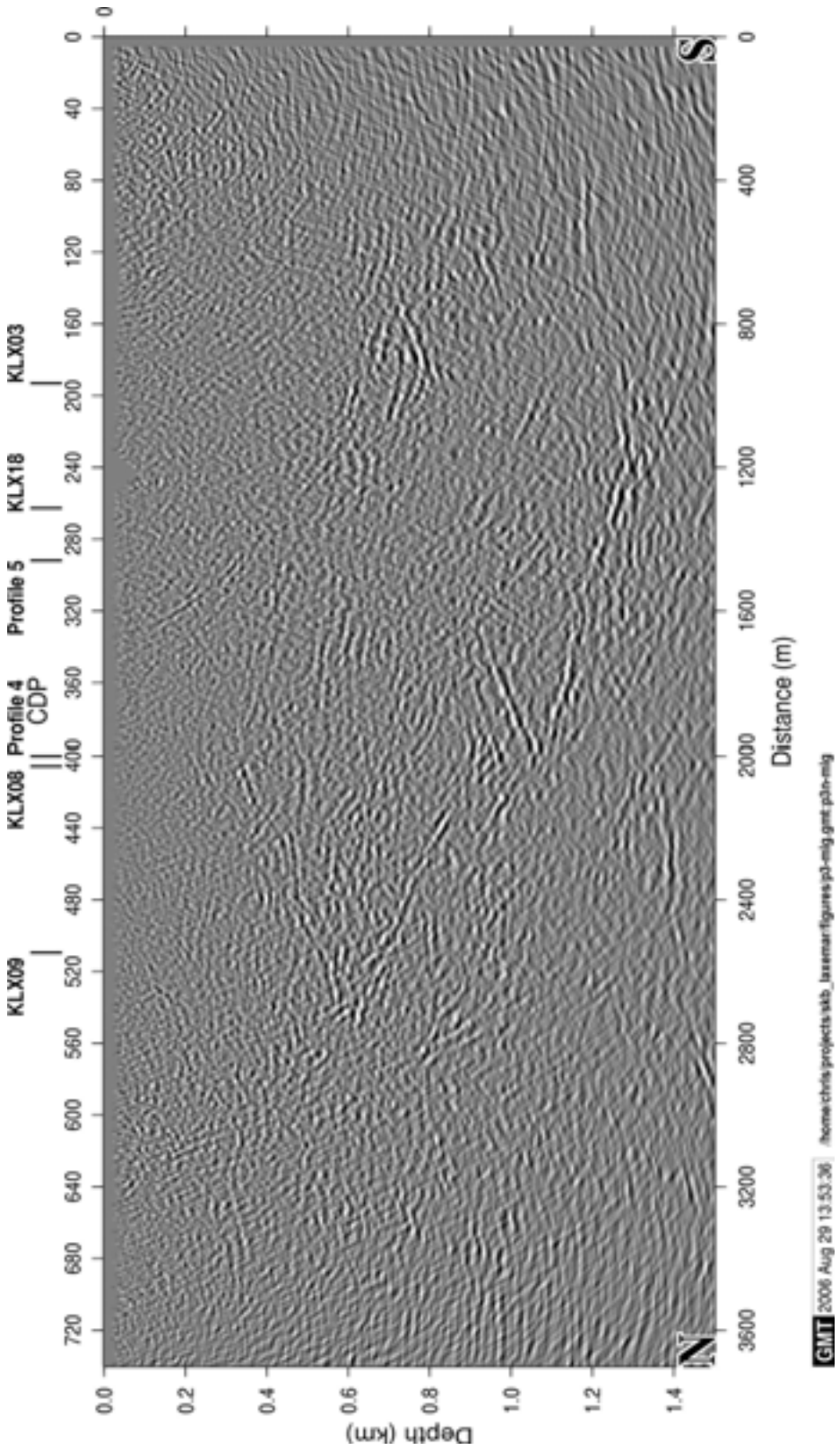

Figure 3-4*. Reprocessed migrated section from this study of profile 3 (LSM000704) down to 0.8 seconds.*

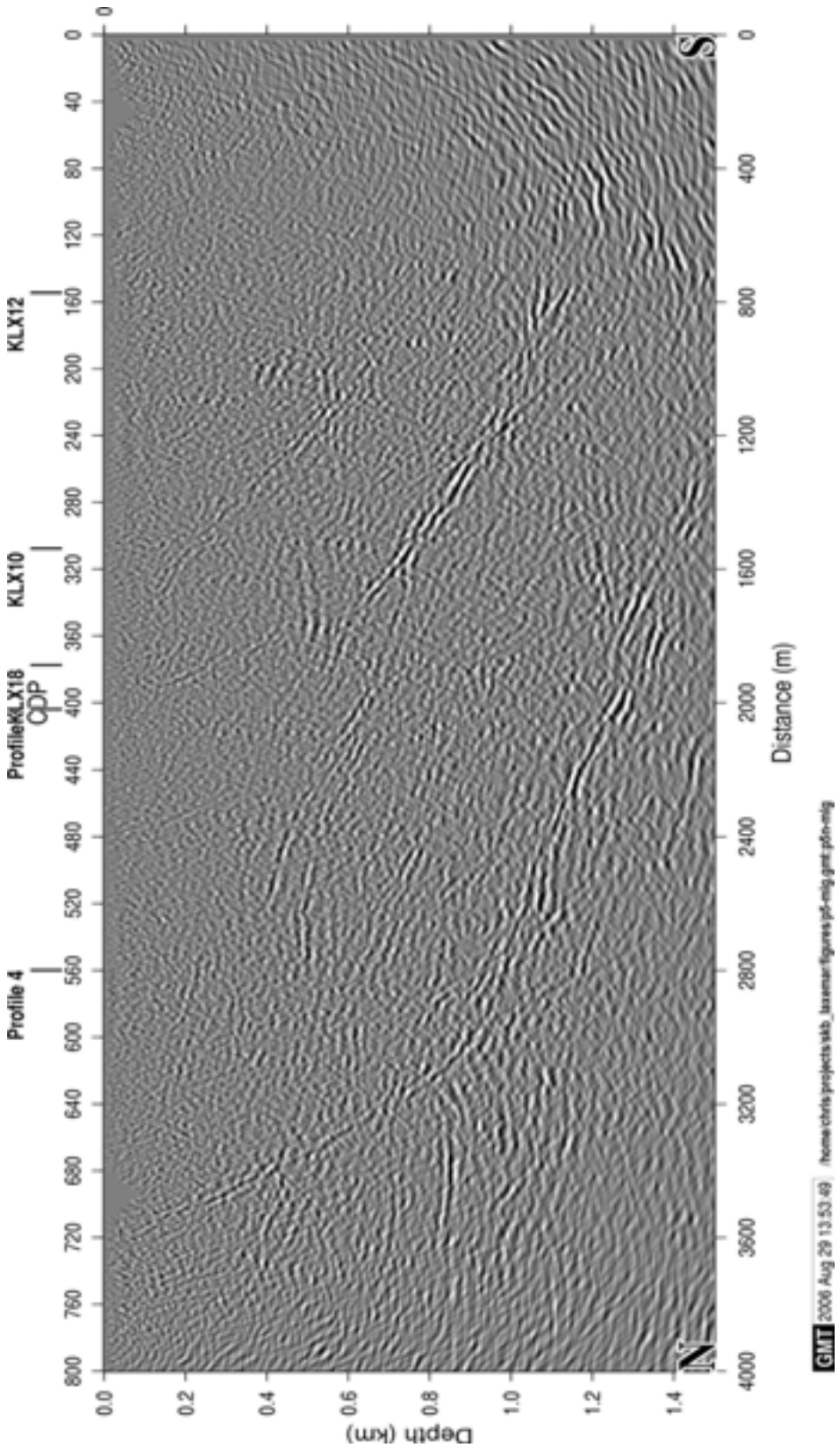

Figure 3-5*. Reprocessed migrated section from this study of profile 5 (LSM000706) down to 0.8 seconds.*

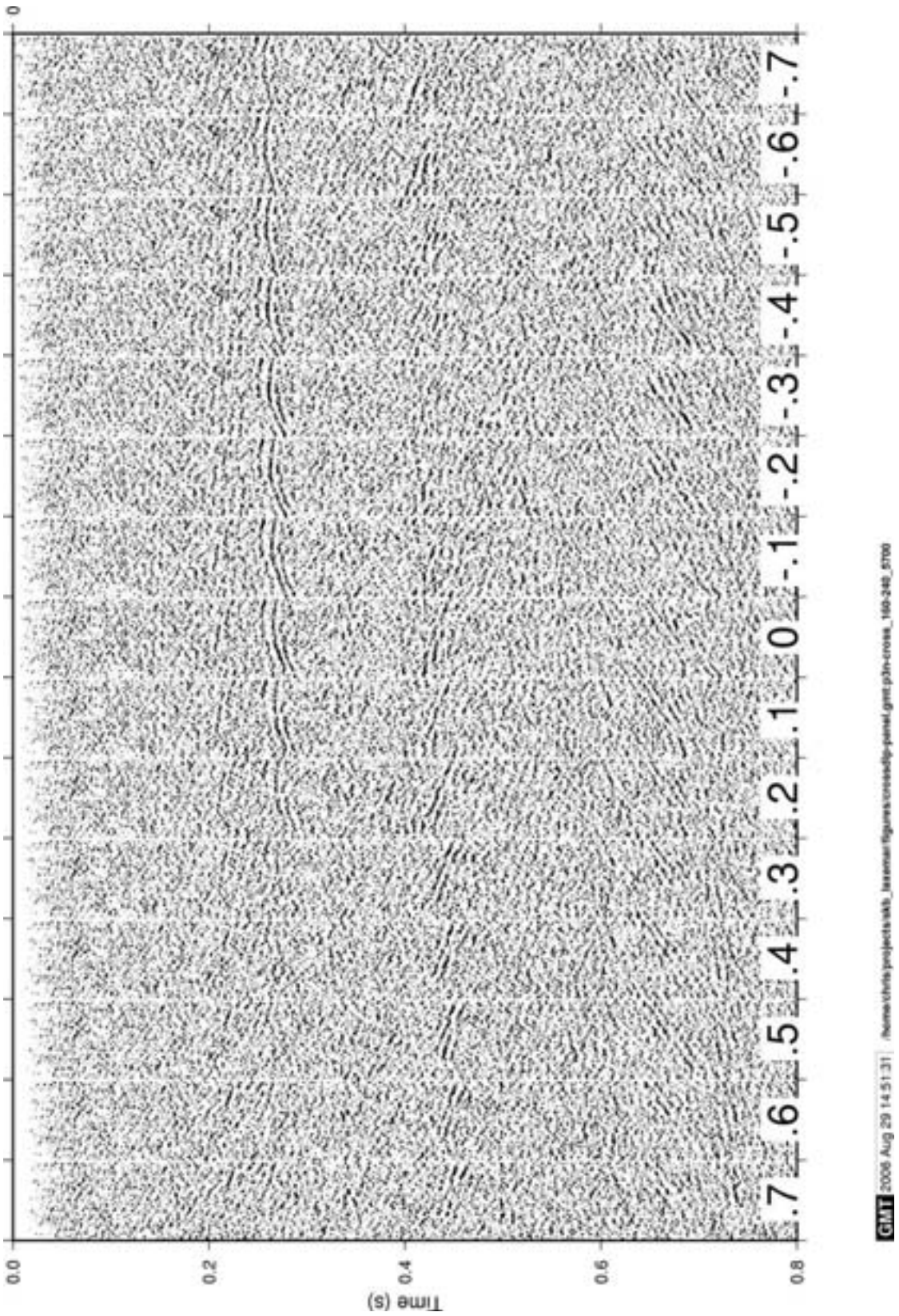

Figure 3-6*. Crossdip analysis of CDPs 160 to 240 along profile 3 (LSM000704). NMO velocity used was 5700 m/s. Numbers refer to the sine of the crossdip component.*

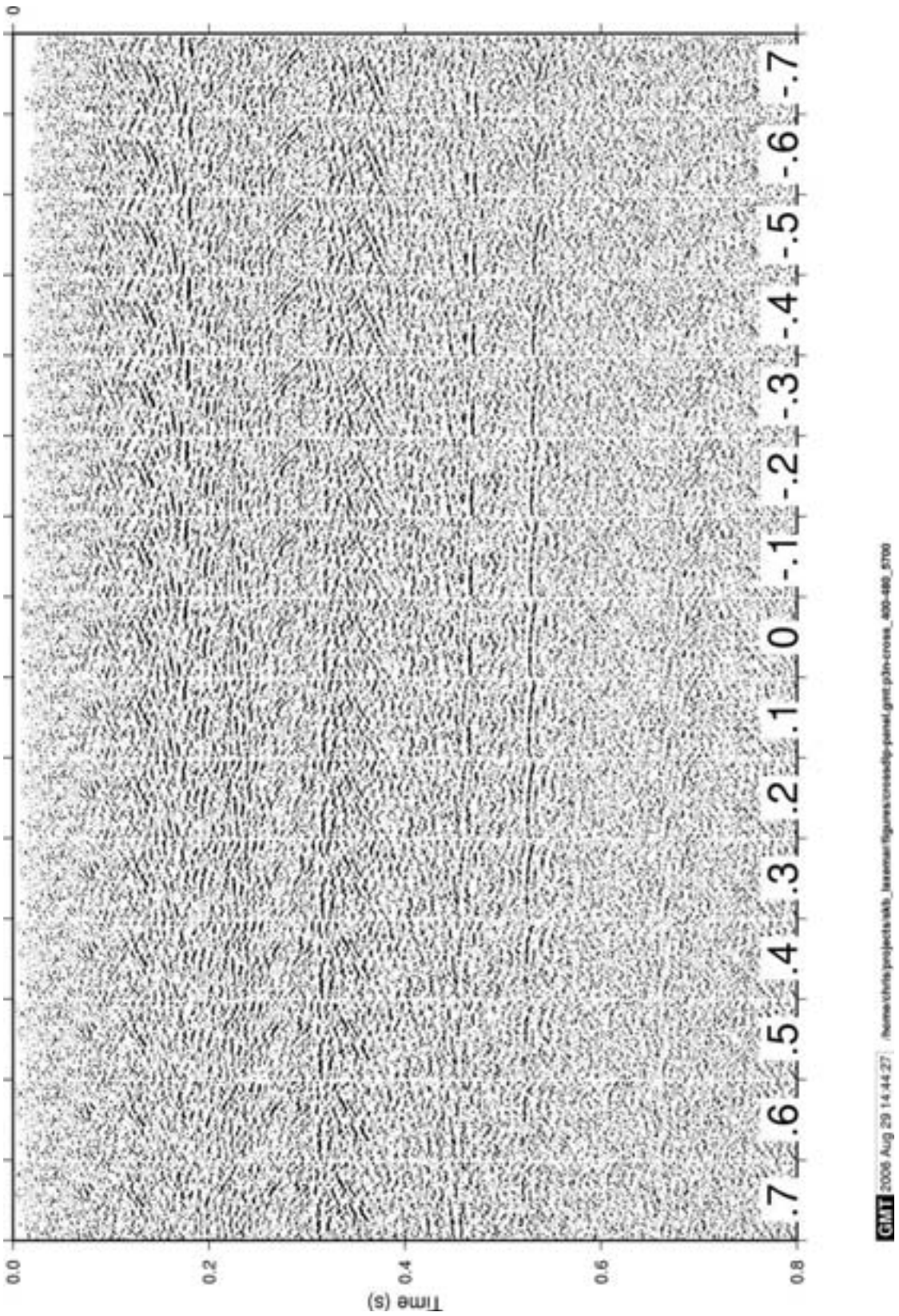

Figure 3-7*. Crossdip analysis of CDPs 400 to 480 along profile 3 (LSM000704). NMO velocity used was 5700 m/s. Numbers refer to the sine of the crossdip component.*

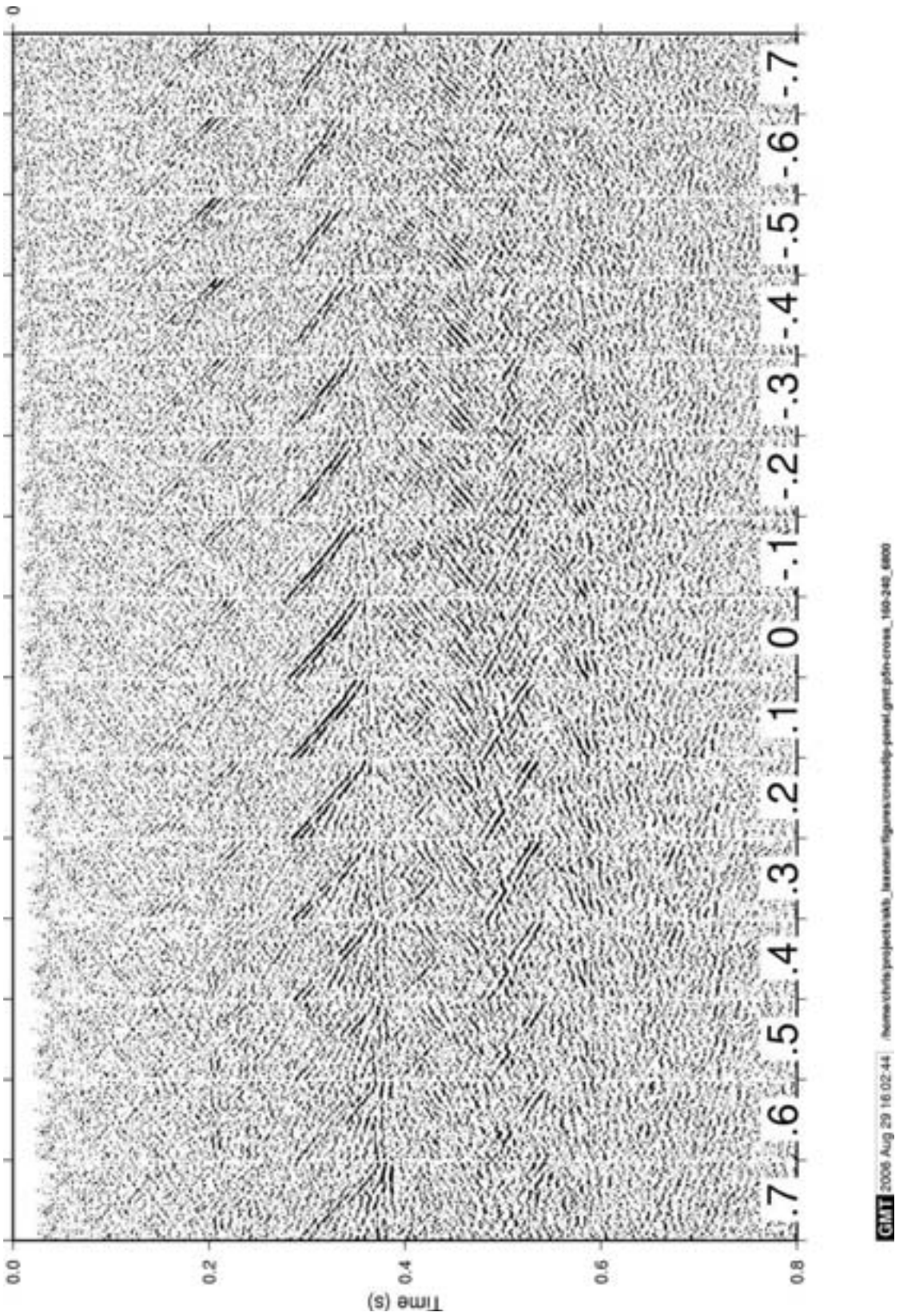

Figure 3-8*. Crossdip analysis of CDPs 160 to 240 along profile 5 (LSM000706). NMO velocity used was 6800 m/s. Numbers refer to the sine of the crossdip component.*

4 Orientation of reflections

Based on the reprocessed stacked sections and crossdip analysis (Figures 3-6 to 3-8) a new table for the orientation of reflections has been produced (Table 4-1). Where profiles 3 and 5 cross the same strategy as in Juhlin et al. (2004) was used for orienting the reflections (Ayarza et al., 2000).

Reflectors K, N, Y1 and Y2 have had their orientations modified significantly based on the new processing, while reflectors M1, M2, M4 have been slightly adjusted (Table 4-1). Comparison of the new picks with the seismic sections shows better agreement (Figures 4-1 and 4-2). Reflectors K2 and L2 are newly identified events that are now more apparent on the reprocessed sections (Figures 4-3 and 4-4). The certainty of reflector L has been reduced in rank from 2 to 3, implying that it is uncertain. Reflectors Ba and Bb are the top and bottom of the more reflective package seen on profiles 1 and 2, and in the KLX02 borehole (Juhlin et al., 2002). Reflector P was not reported on earlier, but is observed quite clearly in the stacked sections on both profiles 3 and 5. Reflector Q was considered part of the K reflector earlier, but is now treated separately. The strong reflection from it at 0.3 s appears to originate from close to within-the-plane of profile 5 (Figure 3-8).

Figures 4-5 and 4-6 show migrated sections and the locations of where the reflectors intersect the profiles. Note that only reflectors whose strike are perpendicular will have reflections falling on top of their true locations. Figure 4-7 shows where the more steeply dipping reflectors listed in Table 4-1 project to the surface. Note the different orientation of the K reflector compared to the previous report (Juhlin et al., 2004).

Table 4-1. Orientation of reflectors as determined from the surface seismic data reprocessed and interpreted in this study (values from previous report in parentheses when different, new reflectors in italics). Reflectors may either be defined by distance to a point on the surface (better for dipping reflectors) or by depth below this point (better for sub-horizontal reflectors). Distance refers to distance from the KLX02 borehole (6366.768 km N, 1549.224 km W) to the closest point on the surface to which the reflector projects. Depth refers to depth below the surface at this origin. Strike is measured clockwise from north. Rank indicates how sure the observation of each reflection is on the profiles that the reflection is observed on; 1 – definite, 2- probable, 3- possible.

Reflector	*Strike*	*Dip*	*Distance (m)*	*Depth (m)*	*Rank*	*Profiles observed on*
A	275	43	190		1	1, 2, 4
Ba	*0*	*3*		*590*	*1*	*1, 2, 4*
B	0	3		760	1	1, 2, 4
Bb	*0*	*3*		*930*	*1*	*1, 2, 4*
C1	90	70	1330		1	1, 2, 3, 4
C2	85	70	1330		1	4, 5
D	253	35	840		2	1, 2, 4
G	253	35	1170		2	1, 2, 4
K	75 (30)	40 (50)	-100 (800)		2	4?, 5
K2	*60*	*60*	*470*		*2*	*3? 5*
L	110	70	-300		3 (2)	3, 5?
L2	*110*	*38*	*-250*		*2*	*3, 5?*
M1	80 (95)	23 (20)		500 (350)	1	3, 4, 5
M2	75 (100)	22 (25)		650 (500)	1	3, 4, 5
M3	100	25		750	1	3, 4, 5
M4	100	25		950 (900)	1	3, 4, 5
N	75 (120)	23 (30)		1270 (770)	2	3, 4, 5
O	200	80	-1850		3	5
P	*270*	*5*		*1250*	*2*	*3, 4, 5*
Q	*75*	*30*		*540*	*1*	*5*
X1	295	15		400	3	3
X2	295	15		970	3	3
X3	295	15		1070	3	3
Y1	240 (295)	35 (27)		-250 (300)	3	3, 4?
Y2	240 (295)	23 (15)		50 (350)	3	3, 4?

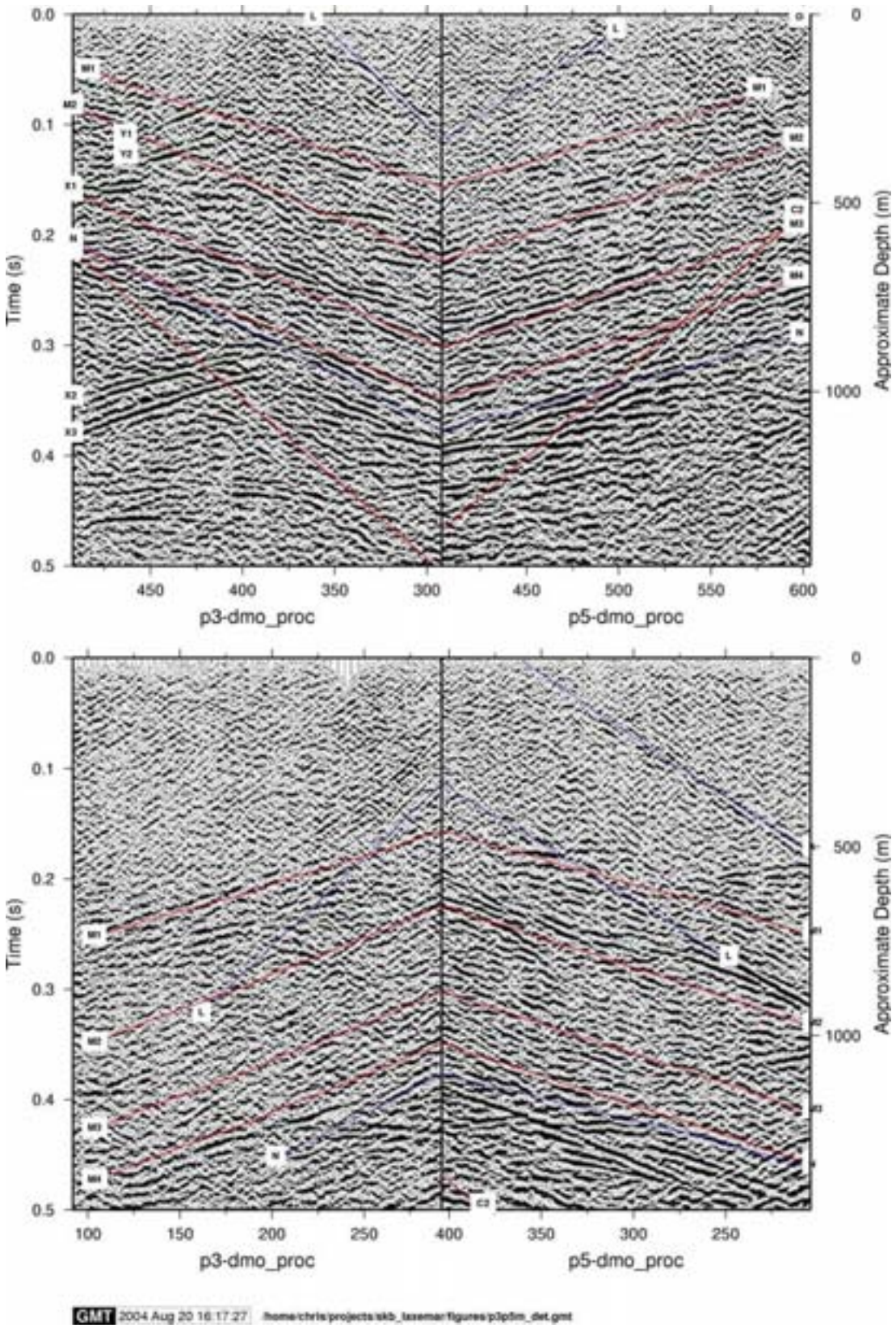

***Figure 4-1**. Correlation of original stacks from profiles 3 and 5 at their crossing point (Figure 3-1) with orientations from Table 1-1.*

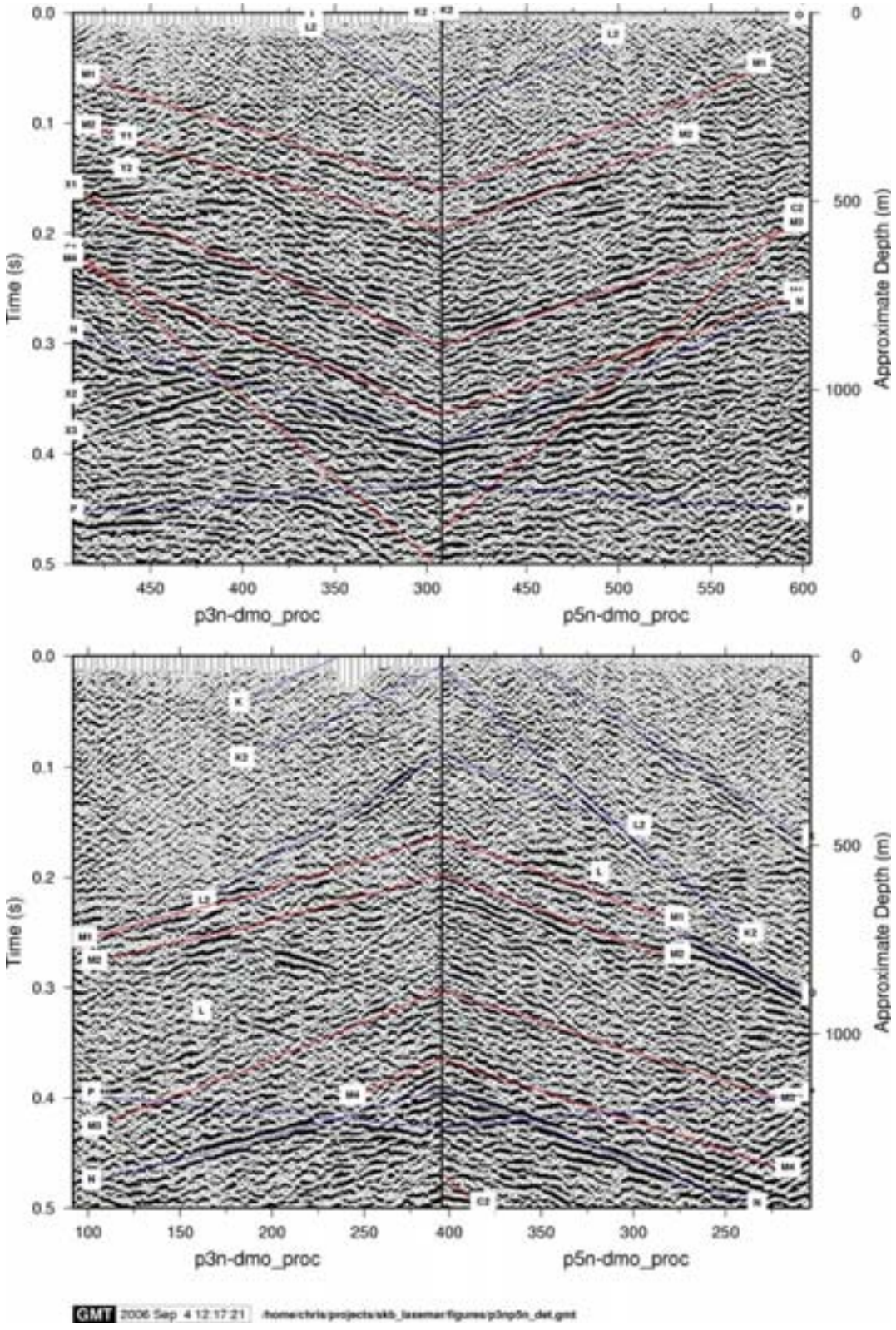

***Figure 4-2**. Correlation of reprocessed stacks from profiles 3 and 5 at their crossing point (Figure 3-1) with orientations from Table 4-1.*

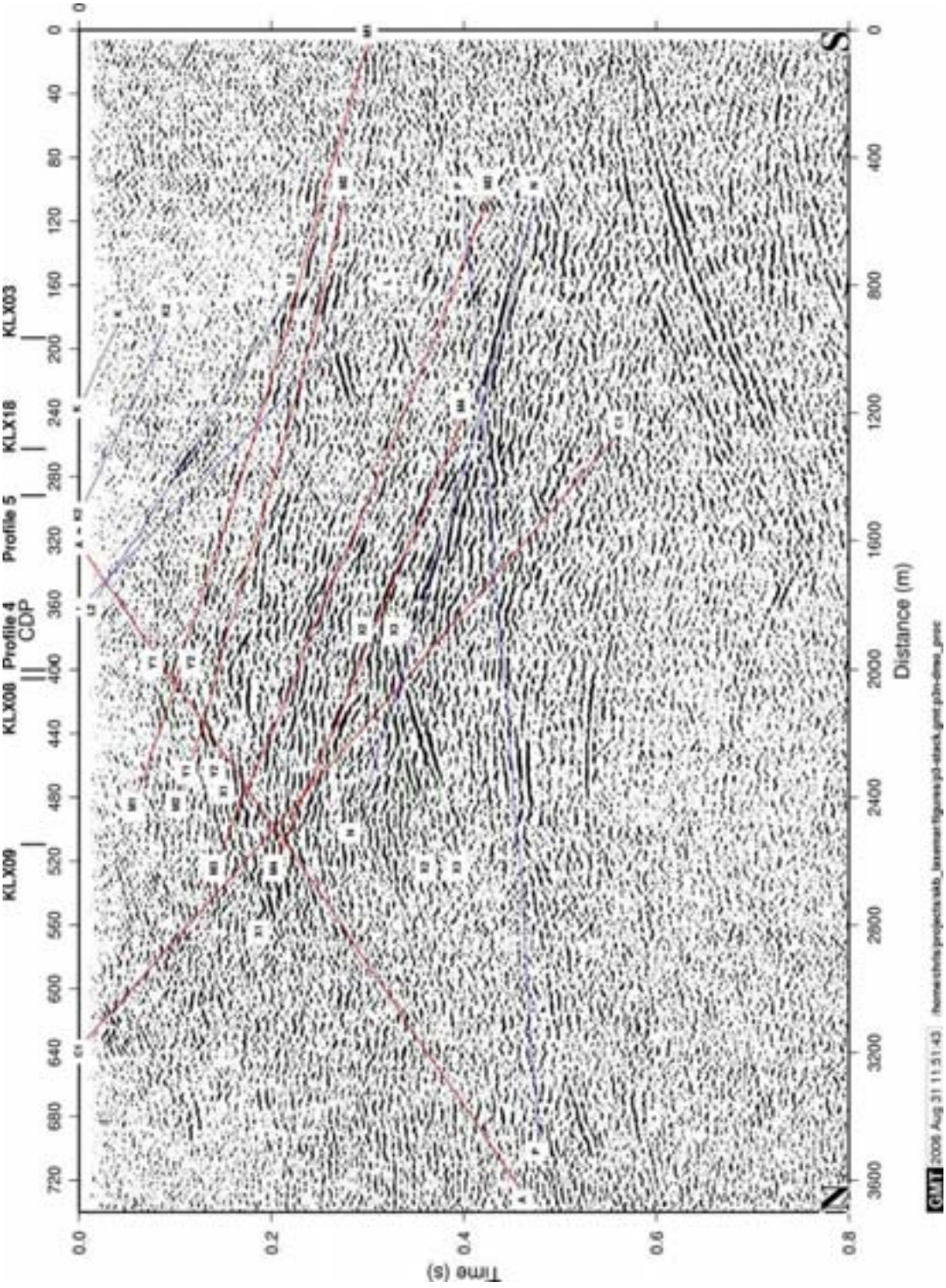

Figure 4-3. *Reprocessed stacked section from this study of profile 3 (LSM000704) down to 0.8 seconds with picked reflections. Red-rank 1, blue-rank 2, green-rank 3. Assumed strike and dips are given in Table 4-1.*

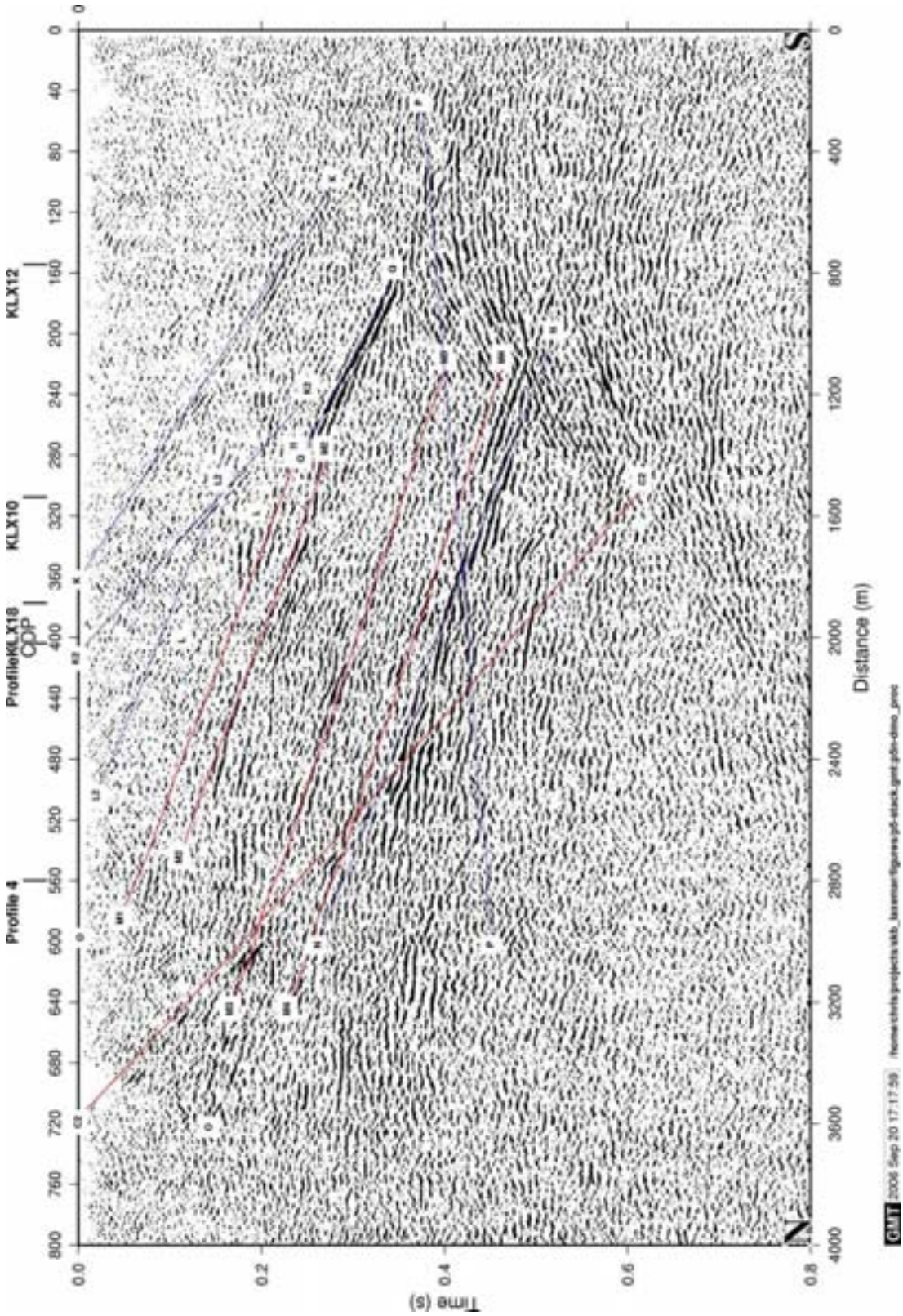

***Figure 4-4**. Reprocessed stacked section from this study of profile 5 (LSM000706) down to 0.8 seconds with picked reflections. Red-rank 1, blue-rank 2, green-rank 3. Assumed strike and dips are given in Table 4-1.*

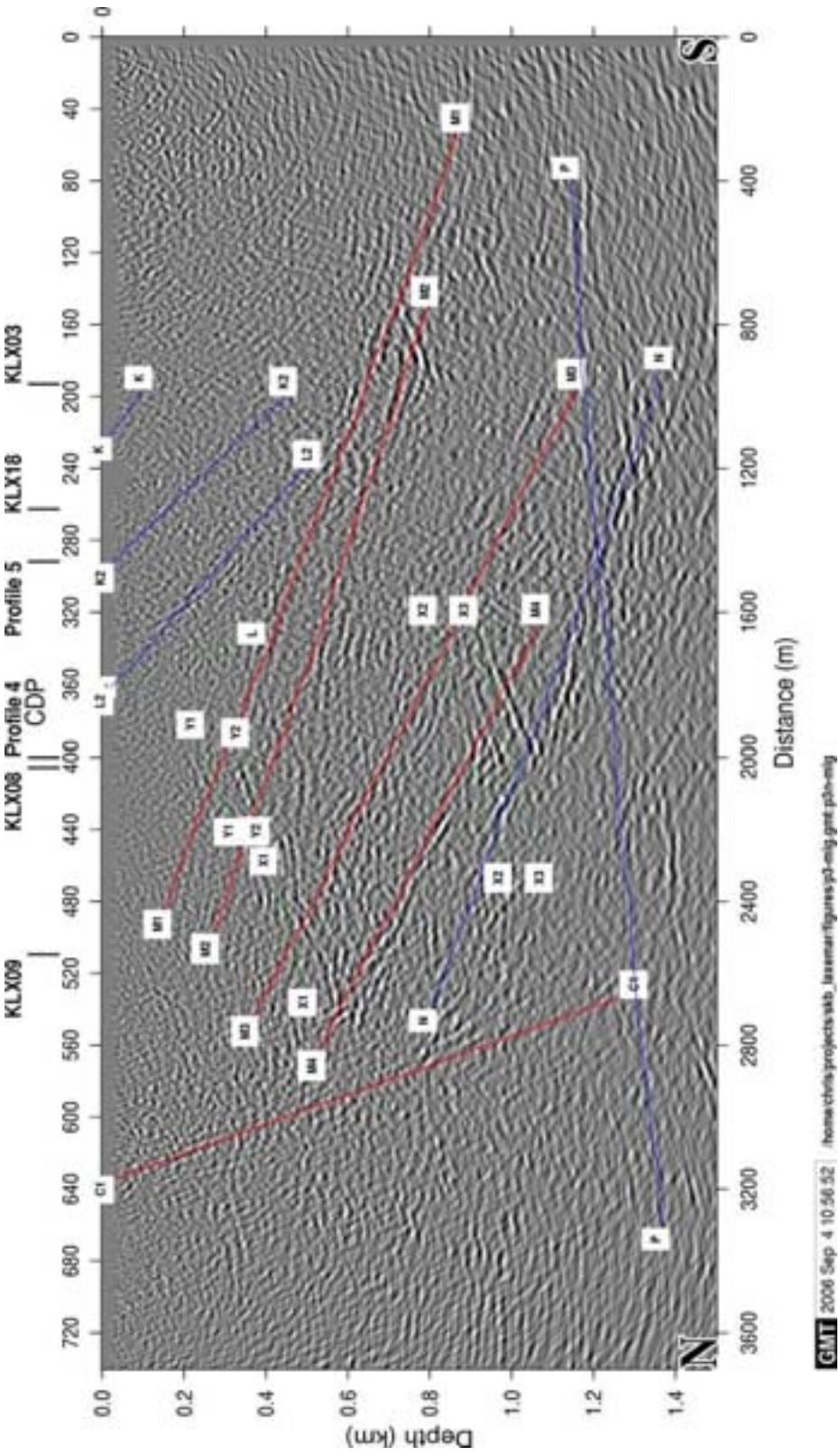

Figure 4-5. *Migrated section of profile 3 (LSM000704) down to 1500 m. Depth scale only valid for true sub-horizontal reflections.*

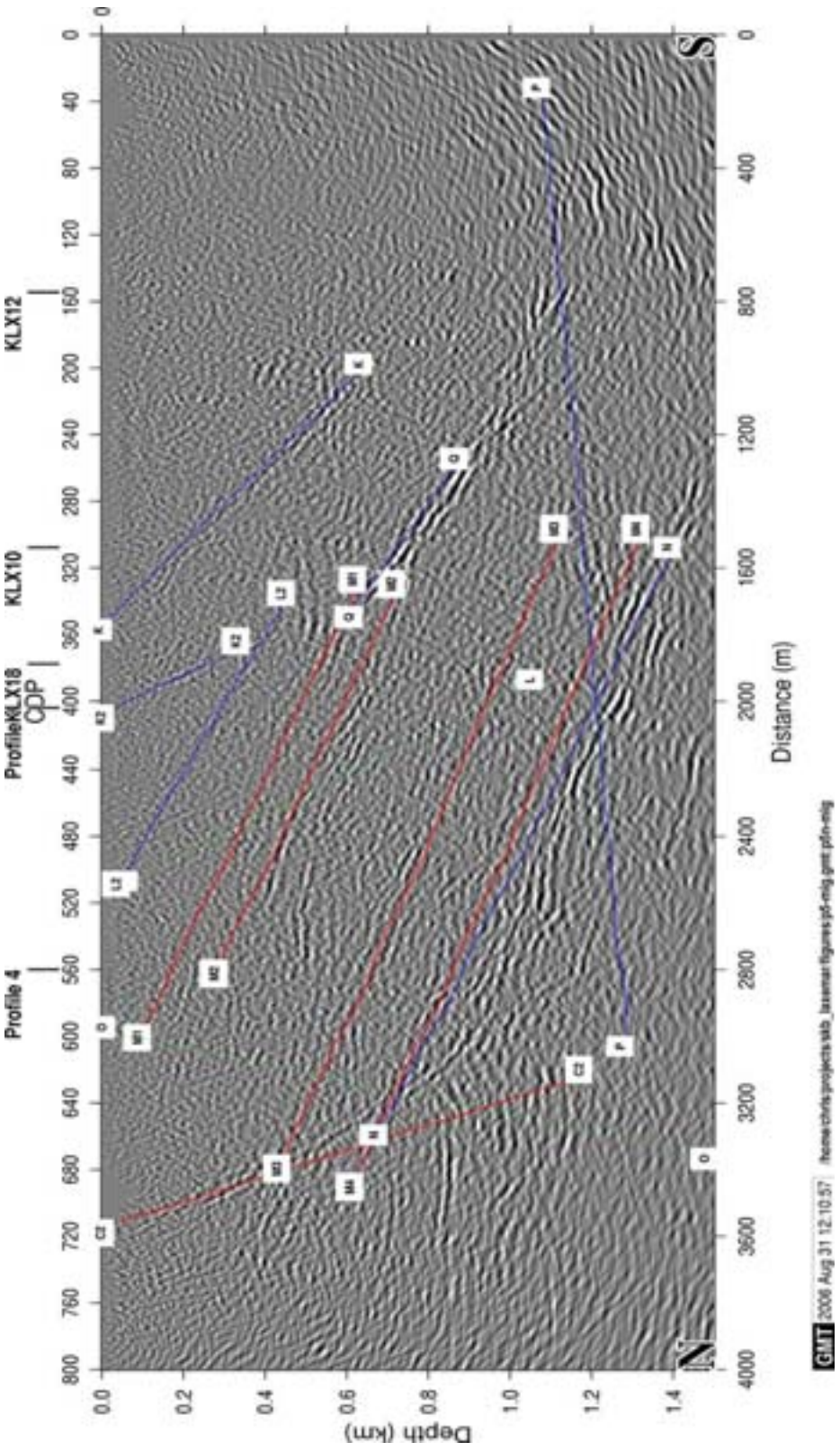

***Figure 4-6**. Migrated section of profile 5 (LSM000706) down to 1500 m. Depth scale only valid for true sub-horizontal reflections.*

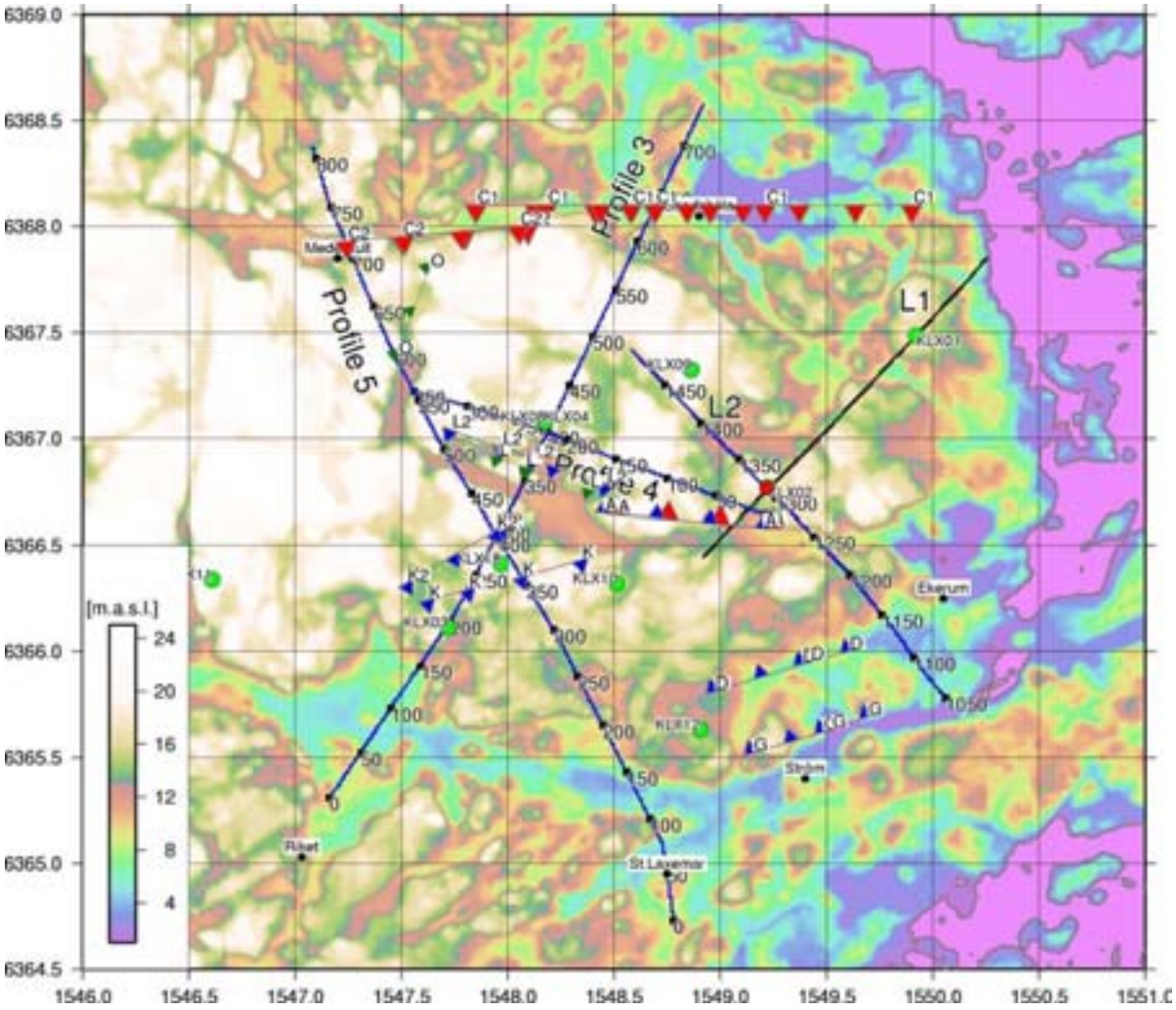

Figure 4-7*. Projected reflector intersections with the surface from this study plotted on topography for those reflectors which project up to the surface. Reflections from interfaces that clearly cannot be traced to the surface, such as N in Table 4-1, are not drawn. Picked reflectors correspond to the tops of the reflector. All indicated reflectors are interpreted to correspond to relatively thin zones (5-15 m thick). Reflectors are coded as follows: red-rank 1, blue-rank 2, green-rank 3.*

5 Correlation with borehole data

5.1 Observations

Both profiles 3 and 5 show a rather transparent crust in the upper 700-800 m at their southern ends, implying that there should be little variation in density and velocity in boreholes drilled at these locations down to these depths. Strong reflectivity becomes more shallow towards the north, at least south of the C1 and C2 reflections (Figures 4-5 and 4-6). This pattern is also observed in the boreholes. Correlations between the seismic data and the selected boreholes are summarized in Figures 5-1 to 5-7. Reflectors as identified in Table 4-1 have been plotted on the migrated seismic sections and where they intersect the boreholes in these figures. In some cases the vertical depths of theses intersections may differ significantly. This is due to the orientation of the reflectors not being within-the-plane of the profile. Intersection depths of steeply dipping reflectors are especially sensitive to small changes in strike and/or dip.

The KLX12 borehole penetrates relatively homogeneous rock, no thicker fracture zones are present (Figure 5-1). A thicker interval of mafic rock between 420 m and 520 m along the borehole may correlate with some rather diffuse reflectivity north of the borehole. The set M reflections are not observed at this borehole location on the seismic data. Note also that the borehole is offset from the seismic section by about 500 m.

The KLX03 borehole penetrates very homogeneous rock down to about 700 m. A thick low velocity zone is found at 720 m to 800 m. This is close to the expected depths of the M1 and M2 reflectors, that are clearly observed on this portion of profile 3 at these depths (Figure 5-2). The M1 reflector is projected to intersect the KLX03 borehole in the middle of the low velocity zone. Note that there is also a short N dipping reflection at this depth on the migrated section. However, this reflection appears to have a significant out-of-the-plane component (Figure 3-6) and has probably not migrated to its correct position. It is likely that the M1 and reflection originates from the fracture zone at about 750 m in KLX03 at this location along profile 3. M2 may also originate from this zone or possibly from the low density zone at 900 m (Figure 5-2). Note that the full waveform sonic shows a low velocity zone corresponding to this zone, but that these lower velocities are not indicated on the sonic log.

Profile 5 shows a relatively transparent crust down to about 700 m at the location of KLX10, except for the steeply dipping K reflection (Figure 5-3). This reflector projects into the borehole at about 150 m, where one of several fracture zones in the upper 350 m is located. The other fracture zones in the upper 350 m do not correlate with any obvious reflections on the seismic section. This may be due to that they are very steeply dipping or due to the fact that the borehole is offset from profile 5 by about 400 m. A significant low velocity anomaly is found at about 700 m in the KLX10 borehole. It is likely that this low velocity fracture zone produces the O reflection. Reflections from M1 and M2 are observed just north of the

borehole, but do not appear to extend all the way into it (Figure 5-3).

The KLX18 borehole contains relatively homogeneous rock with only a few more mafic sections (Figure 5-4). The rather strong reflectivity on profile 5 starting at a depth of about 500 m corresponds to the M1 reflector. A fairly significant fracture zone is found at about 490 m that may be related to the short high amplitude reflection above M1 or to the L2 reflection. The M2 reflection is quite clear at this location along the profile, but it was not penetrated by the borehole. The K2 reflection appears to correspond to the fracture zones at about 290 m depth along the borehole. The fracture zone at about 140 m may correspond to an unidentified south dipping reflection. It is not clear what the source to the M1 reflection is in the KLX18 borehole, there are both minor low velocity zones and a thin high density zone where the reflector projects into the borehole at 576 m.

The sonic log in the upper 300 m of the KLX08 borehole indicates the rock to be highly fractured in this interval (Figure 5-5). No clear reflections are observed from this interval, suggesting that these fracture zones are steeply dipping. However, note that the north dipping Y1 reflector projects into the KLX08 borehole at about 300 m where a distinct low velocity zone is found, suggesting that the two are related. The same is true for the Y2 reflector that projects into the borehole at about 410 m, close to a significant fracture zone. The M1 reflector projects into the borehole at about 450 m. It is possible that the fracture zone at 470 m is associated with the M1 reflector. There are no thicker mafic zones at this depth which could produce the M1 reflection. More mafic sequences are first found below 600 m and it is likely that the more sub-horizontal reflectivity seen on the seismic section between 600 m and 800 m is associated with these mafic intervals, as is the M2 reflector at this location. The fairly thick fracture zone defined from the single hole interpretations found at about 930 m does not have a low velocity anomaly associated with it. However, the low velocity zone at the bottom of the borehole may correspond to the X2 reflector.

More mafic sequences are found in the interval 400 m to 800 m in the KLX04 borehole (Figure 5-6). The M2 and M3 reflectors project into the borehole within this interval, indicating they are associated with these rocks at this location. The M1 reflector projects into the borehole the at 300 m where a distinct, but thin, fracture zone is present. The thinner ones above is have no obvious seismic signature, while the distinct one below at 350 m appears to correspond to the Y1 reflection. The Y2 reflection is quite clear on the seismic section, but there is no clear indication of it where it intersects the borehole at about 430 m. The M4 reflections corresponds well to the top of the thick fracture zone starting at about 870 m. Perhaps the N reflection corresponds to the bottom of it, but this is highly speculative. The X2 reflector also intersects the borehole at these depths.

There are number of thinner fracture zones in the rather homogeneous upper 340 m of the KLX09 borehole (Figure 5-7). The M1 and M2 reflectors project into the borehole in this interval, but it is more likely that these fracture zones are associated with the unidentified

north dipping reflections seen at these depths on this part of profile 3. The interval from 500 m to 800 m contains both mafic sequences and a number of thicker fracture zones. The fracture zones may correlate with the X1, M3 and M4 reflections, but since the borehole is offset from the profile by about 500 m all correlations are uncertain. The N reflector does not appear to have been penetrated.

5.2 Synthetic seismograms

Synthetic seismograms have been generated from the sonic and density logs using standard methods. Assumptions were that the media is 1D, the reflectivity can be represented by the convolution of a source wavelet with the reflection coefficients, and that multiple reflections are not important. The 1D assumption is obviously wrong since we know that many of the reflectors intersect the borehole at an angle and that observed variations in velocity and density may not extend laterally very far away from the borehole. However, the synthetic seismograms still provide an idea of the reflectivity that can be expected if the velocity and density contrasts observed in the borehole are relatively continuous in the lateral direction. Three cases have been considered, (i) the reflectivity is only dependent upon the velocity contrasts, (ii) the reflectivity is only dependent upon the density contrasts, and (iii) the reflectivity is dependent upon the contrast in the product of the velocity and density. Expressions for the reflection coefficient log for these three cases are then:

$$RC_v = \frac{v_2 - v_1}{v_2 + v_1}$$

$$RC_\rho = \frac{\rho_2 - \rho_1}{\rho_2 + \rho_1}$$

$$RC_{v\rho} = \frac{v_2\rho_2 - v_1\rho_1}{v_2\rho_2 + v_1\rho_1}$$

Although only the third case is strictly correct, comparison of the seismic sections with the other two cases can give some idea of how local the velocity and density contrasts observed in the borehole are. Figures 5-8 to 5-14 show synthetic seismograms generated from the three cases along with migrated surface seismic sections in the vicinity of the boreholes. In general, the synthetic seismograms confirm the interpretation discussed in the previous section.

5.3 Discussion

Table 5-1 attempts to summarize the above observations. The M1 reflection, although discontinuous, appears to correlate well with fracture zones in 4 of the boreholes. In the other 3 boreholes studied the M1 reflector is not expected to be encountered since reflections associated with it are not observed on the seismic sections. M2 and M3 appear to correlate better with mafic sequences in the boreholes, while M4 correlates better with fracture zones.

The set M reflections appear to be of a similar nature as the sub-horizontal reflections observed below KLX02 (Juhlin et al., 2002), they are associated both with fracture zones and mafic rock.

The more steeply south dipping reflections O, K2 and L2 all appear to correlate well with fracture zones, especially the O reflection. The gently north dipping set X and the more steeply north dipping set Y reflections also appear to correlate with fracture zones. However, the lateral dimensions of all these reflectors is limited and correlations can only be made with one or, at most, two boreholes.

The general large scale pattern of gently south dipping reflectivity observed on profiles 3 and 5 is probably coupled to lenses of mafic rocks. This pattern includes the set M reflections. Associated with these mafic lenses are fracture zones, some of them extensive and perhaps generating significant reflectivity. The M1 reflection zone is an example of this. Above this south dipping reflectivity pattern, generally weaker, but more continuous, moderately to steeply dipping reflections are present south of KLX08/KLX04 that correspond to fracture zones. Correlation between the surface seismic and borehole results indicates that the lateral dimensions of the M reflectors is more limited than originally suggested (Juhlin et al., 2004). The M1 and M2 reflections do not appear to extend to the KLX09, KLX10 and KLX12 boreholes, suggesting that a N-S running boundary east of KLX08/KLX04 is present. East of this boundary a system of sub-horizontal mafic lenses and fracture zones corresponding to the B reflections (Table 4-1) is present. The set X and set Y reflections were not emphasized in the previous report (Juhlin et al., 2004), mainly because their orientations were uncertain. Correlation between profile 3 and borehole results indicates that these north dipping reflections originate from fracture zones. If this interpretation is correct then their importance may have been underestimated earlier, implying that the upper crust north of KLX08/KLX04 is characterized by north dipping fracture zones.

The boreholes were not drilled deep enough to positively penetrate the structure corresponding to the most prominent sub-horizontal reflection on the seismic section, the N reflection (Figures 4-5 and 4-6). It is possible that the bottom of the thick fracture zone between 870 m and 970 m in KLX04 corresponds to the N reflector at this location, but this is speculative.

The orientation of reflections C1 and C2 (Figures 4-5 and 4-6), corresponding to reflections from the Mederhult zone have not been modified in this study and their orientation is considered reliable.

Table 5-1. Overview of which boreholes clear reflections can be correlated to and the interpreted nature of the reflector. FZ: fracture zone, M:mafic rock, D: reflection is clear, but projected intersection is below the bottom of the borehole. Number in parentheses indicates projected intersection point along the borehole.

	KLX12	***KLX03***	***KLX10***	***KLX18***	***KLX08***	***KLX04***	***KLX09***
K2				FZ (246)			
L2				FZ (447)			
M1		FZ (766)		FZ/M (576)	FZ (458)	FZ (306)	
M2		FZ? (849)		D	M (623)	M (430)	
M3		D	D	D	D	M (691)	M/FZ (558)
M4			D	D	D	FZ (884)	FZ (762)
O			FZ (700)				
X1							FZ? (513)
X2					FZ? (957)	FZ? (981)	
Y1					FZ (306)	FZ (351)	
Y2					FZ (417)	FZ?/M (426)	

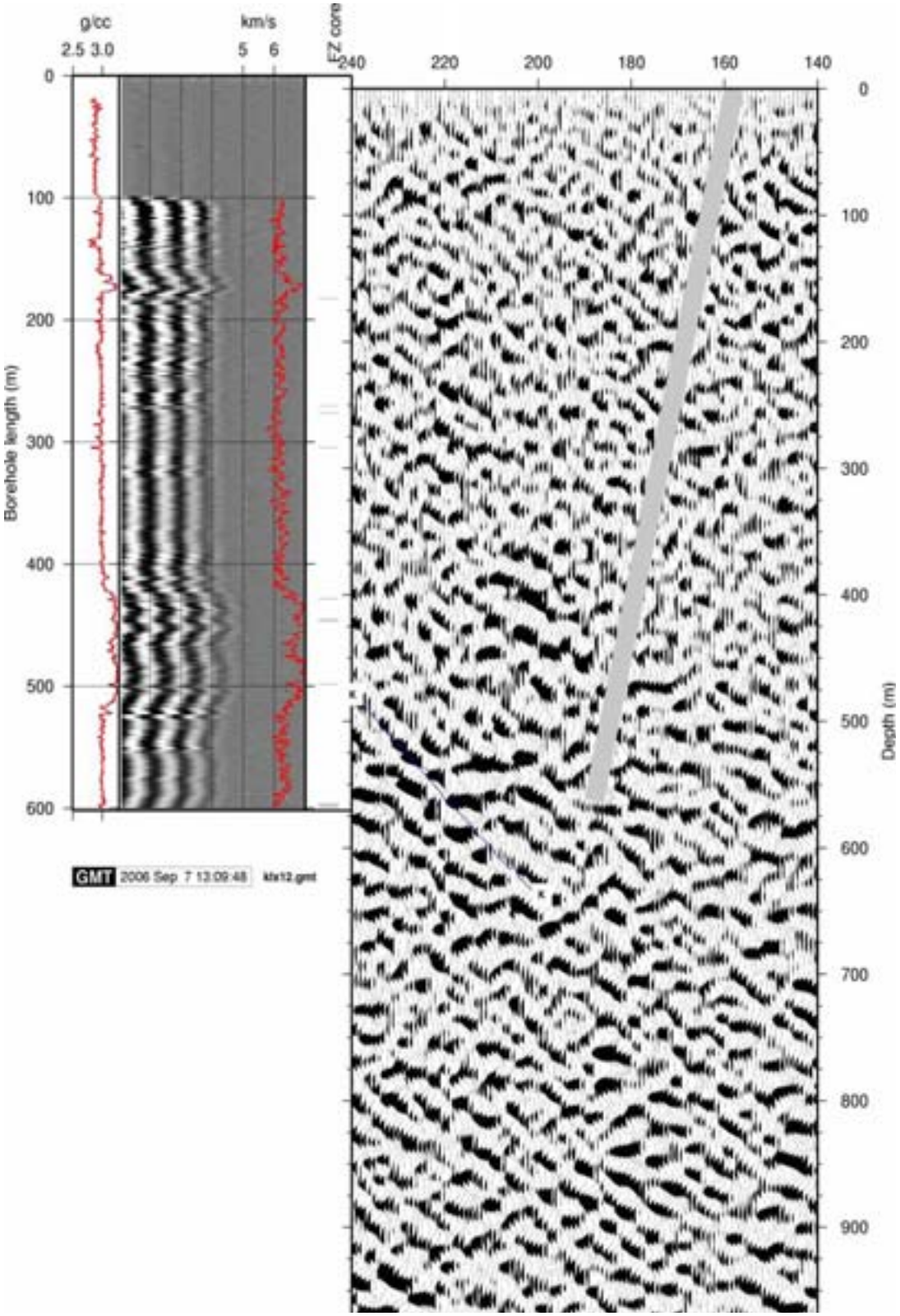

Figure 5-1*. Density log, velocity log and location of deformation zones from KLX12 plotted relative to migrated depth converted profile 5. Location of picked reflectors from Table 4-1 as they project onto the profile are also shown. Projection of borehole onto profile is approximate.*

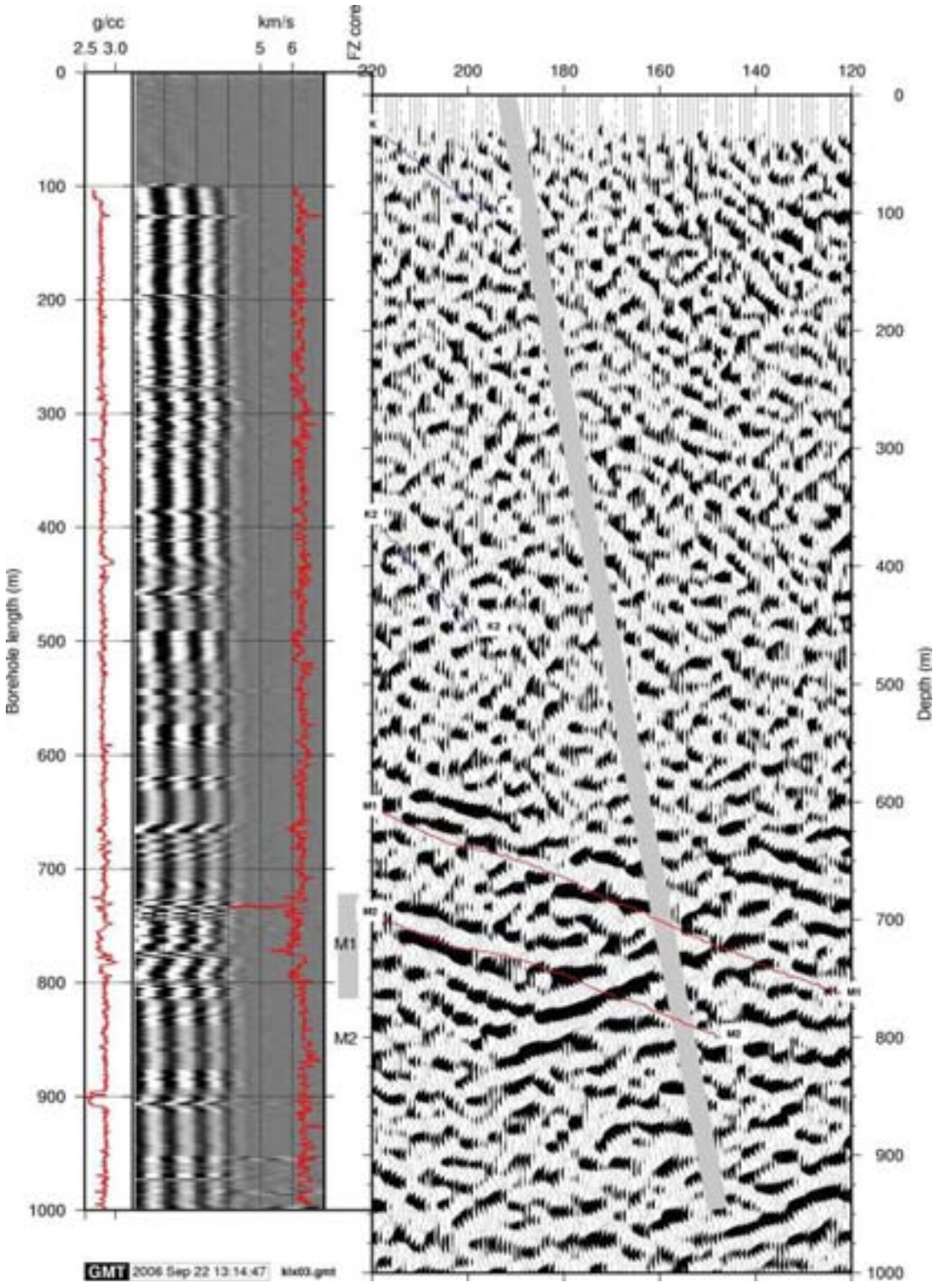

Figure 5-2*. Density log, velocity log and location of deformation zones from KLX03 plotted relative to migrated depth converted profile 3. Location of picked reflectors from Table 4-1 as they project onto the profile are also shown. Projection of borehole onto profile is approximate.*

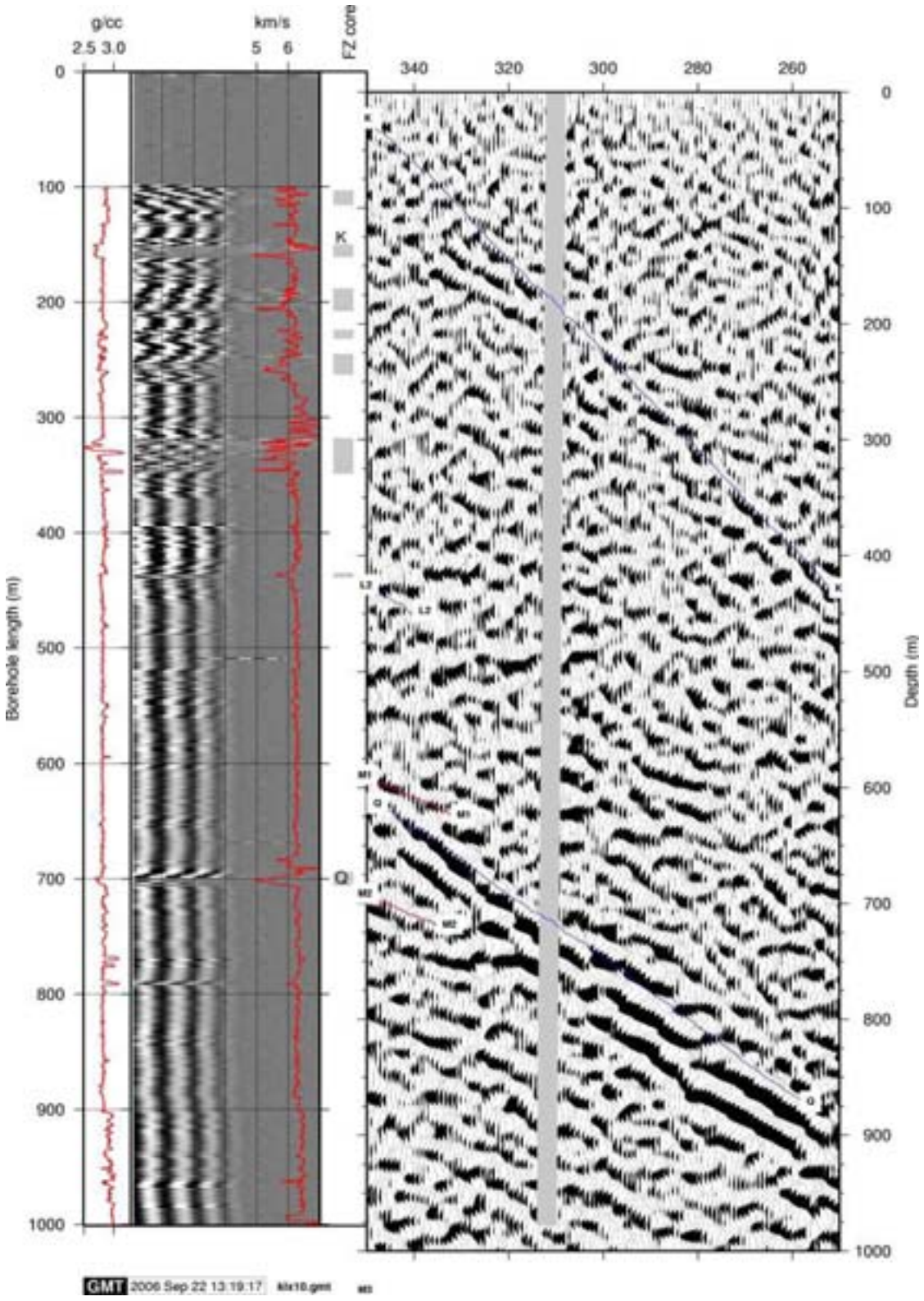

Figure 5-3*. Density log, velocity log and location of deformation zones from KLX10 plotted relative to migrated depth converted profile 5. Location of picked reflectors from Table 4-1 as they project onto the profile are also shown. Projection of borehole onto profile is approximate.*

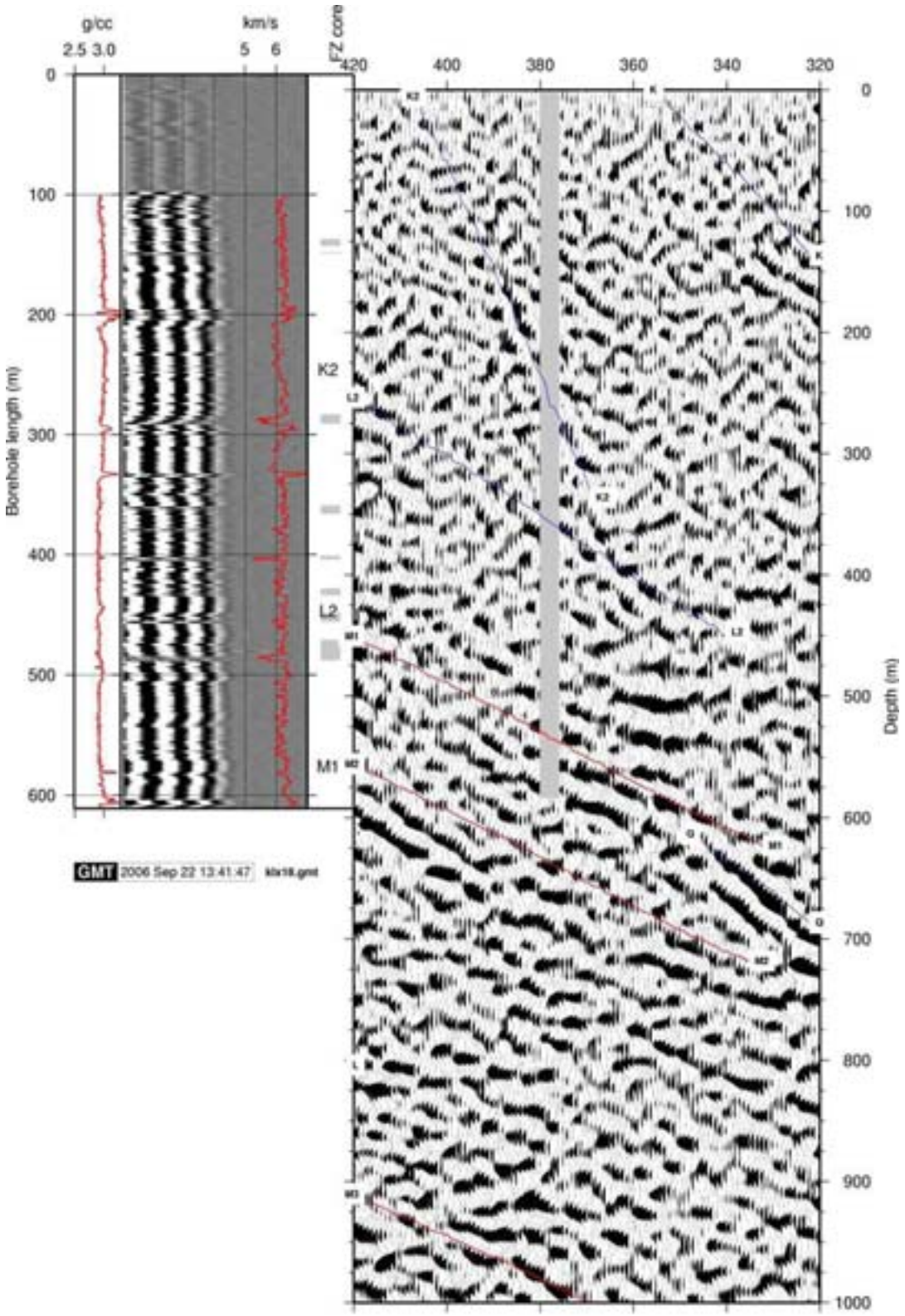

Figure 5-4*. Density log, velocity log and location of deformation zones from KLX18 plotted relative to migrated depth converted profile 5. Location of picked reflectors from Table 4-1 as they project onto the profile are also shown. Projection of borehole onto profile is approximate.*

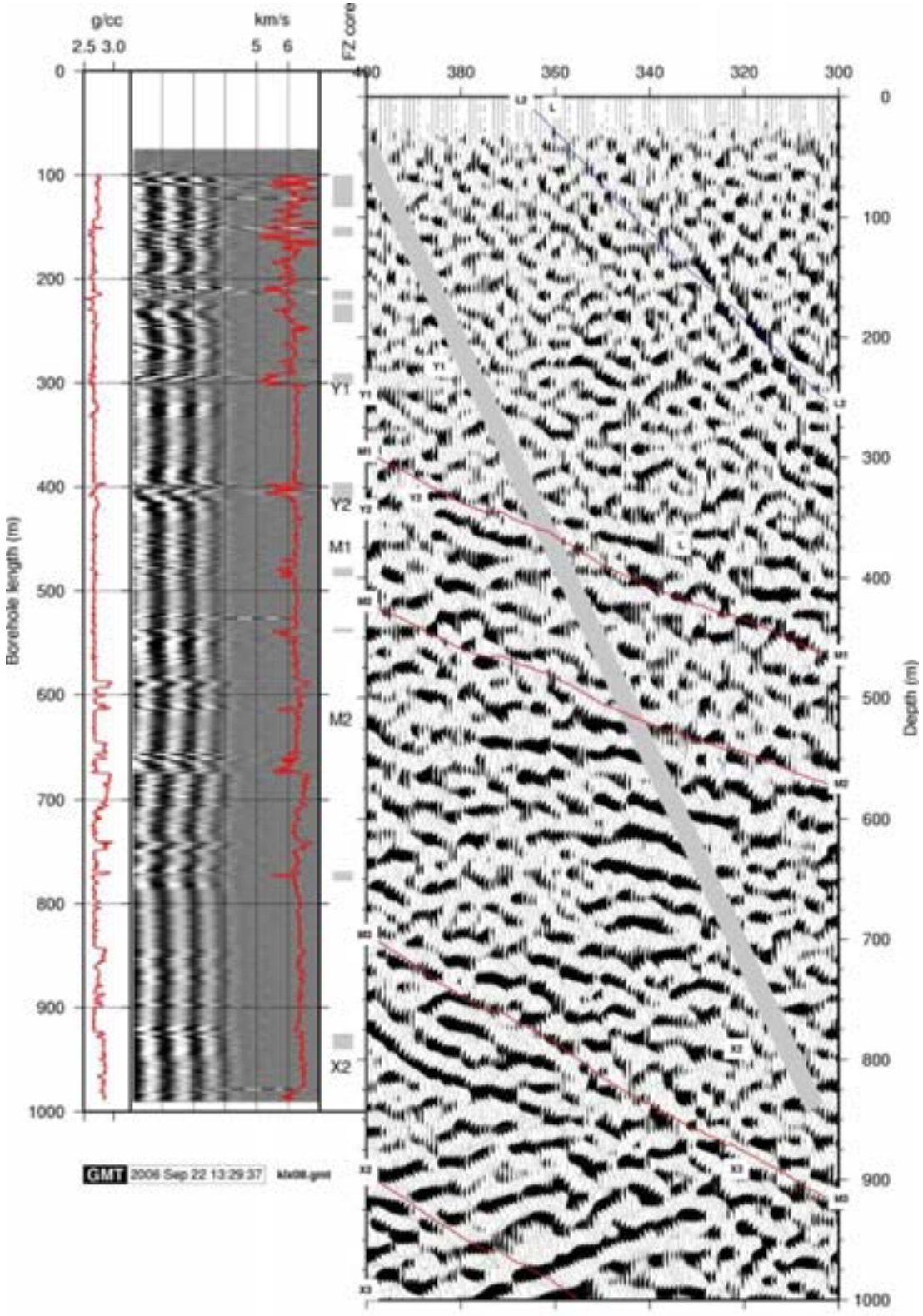

Figure 5-5*. Density log, velocity log and location of deformation zones from KLX08 plotted relative to migrated depth converted profile 3. Location of picked reflectors from Table 4-1 as they project onto the profile are also shown. Projection of borehole onto profile is approximate.*

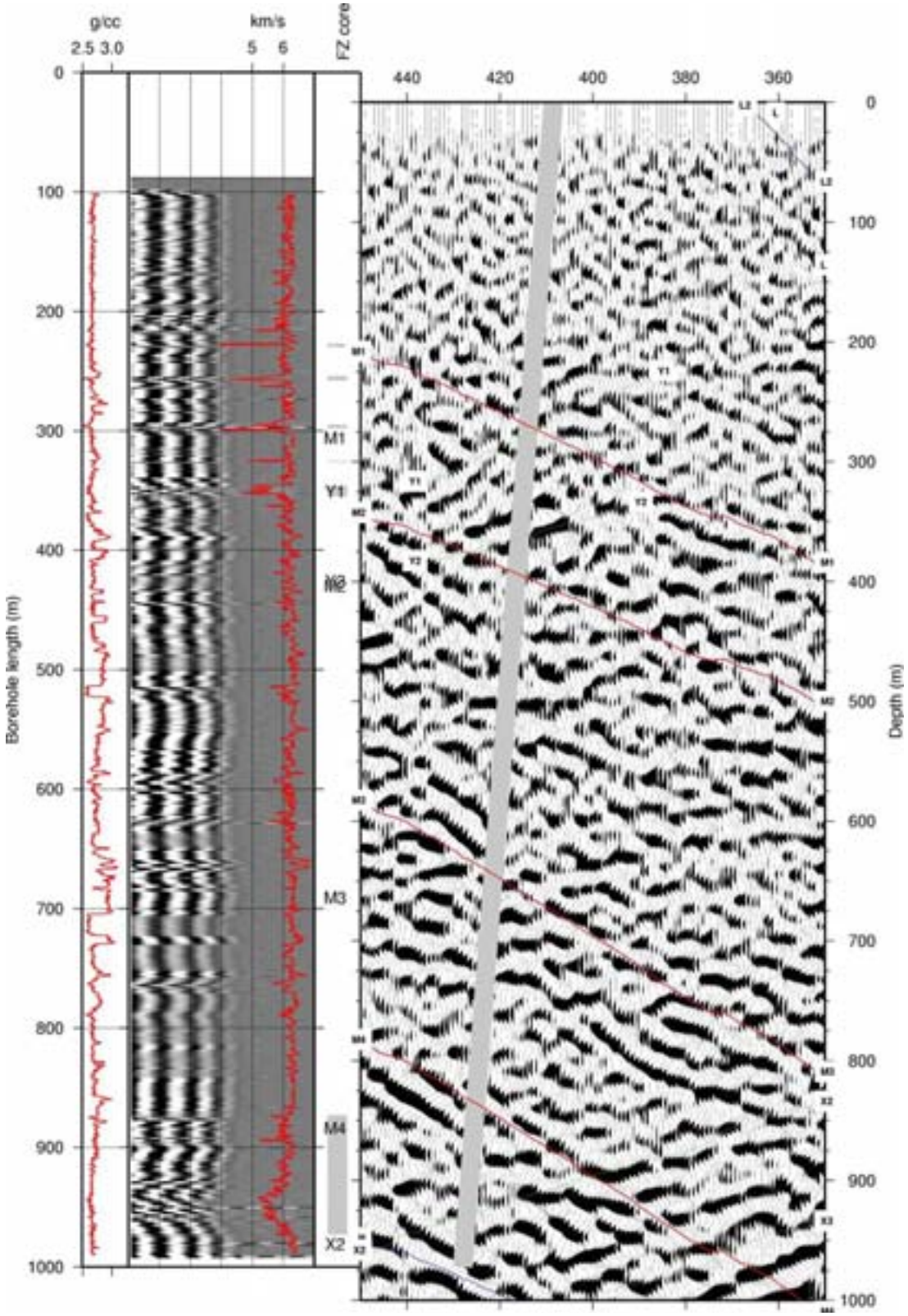

Figure 5-6*. Density log, velocity log and location of deformation zones from KLX04 plotted relative to migrated depth converted profile 3. Location of picked reflectors from Table 4-1 as they project onto the profile are also shown. Projection of borehole onto profile is approximate.*

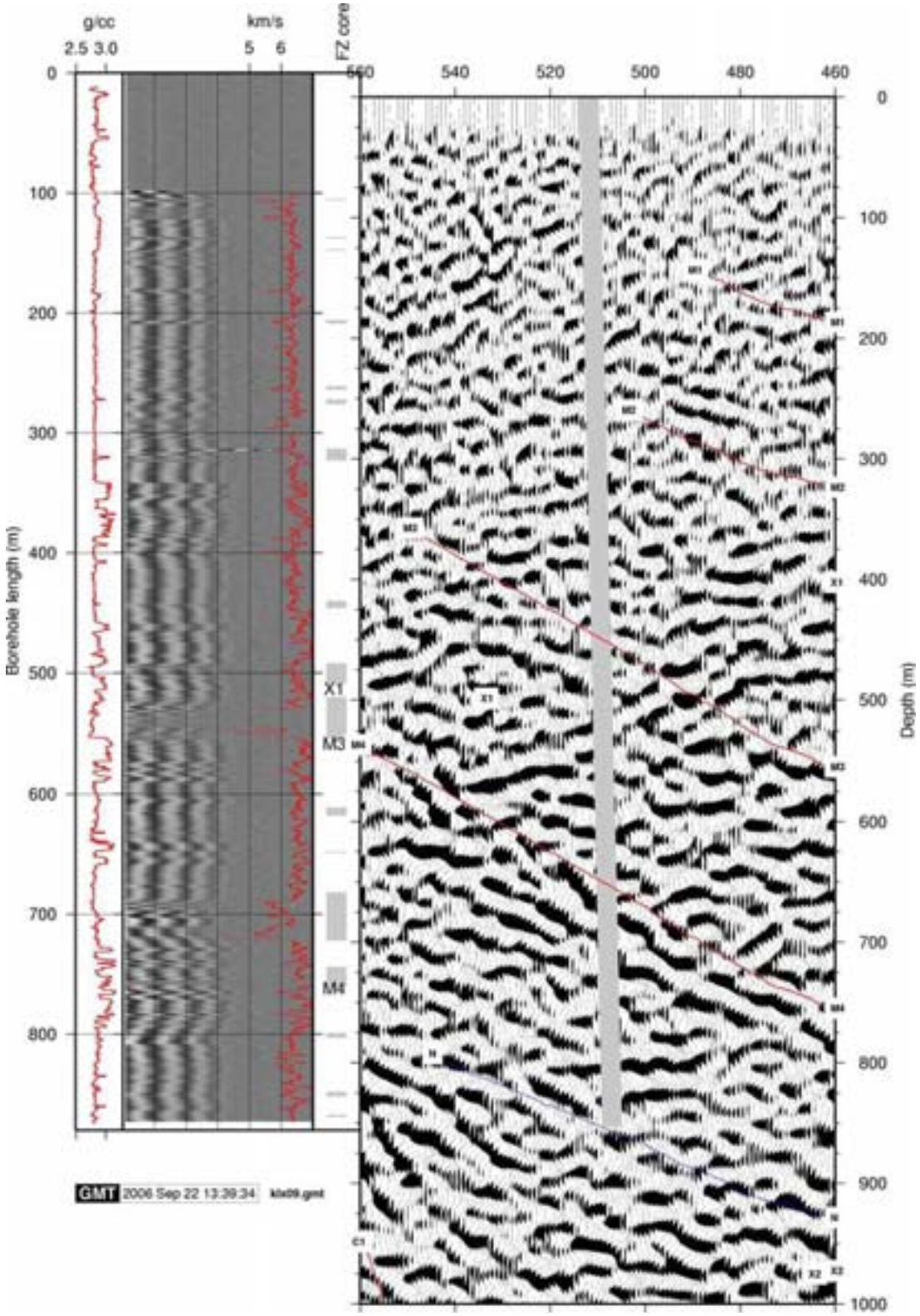

Figure 5-7*. Density log, velocity logs and location of deformation zones from KLX09 plotted relative to migrated depth converted profile 3. Location of picked reflectors from Table 4-1 as they project onto the profile are also shown. Projection of borehole onto profile is approximate.*

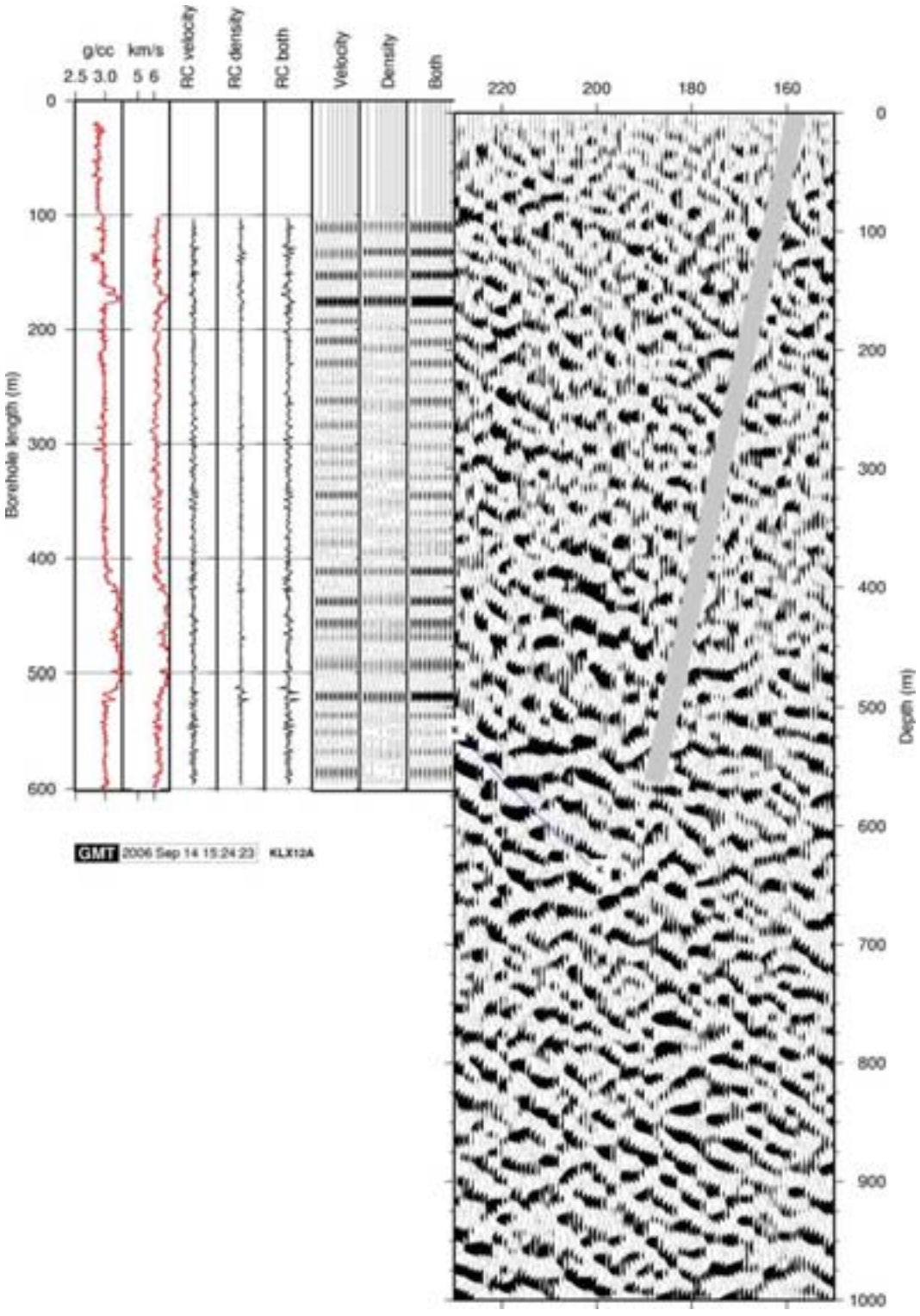

Figure 5-8*. Reflection coefficient (RC) logs and corresponding synthetic seismograms calculated from just the velocity, just the density log and both for KLX12. plotted relative to migrated depth converted profile 5. Location of picked reflectors from Table 4-1 as they project onto the profile are also shown. Projection of borehole onto profile is approximate.*

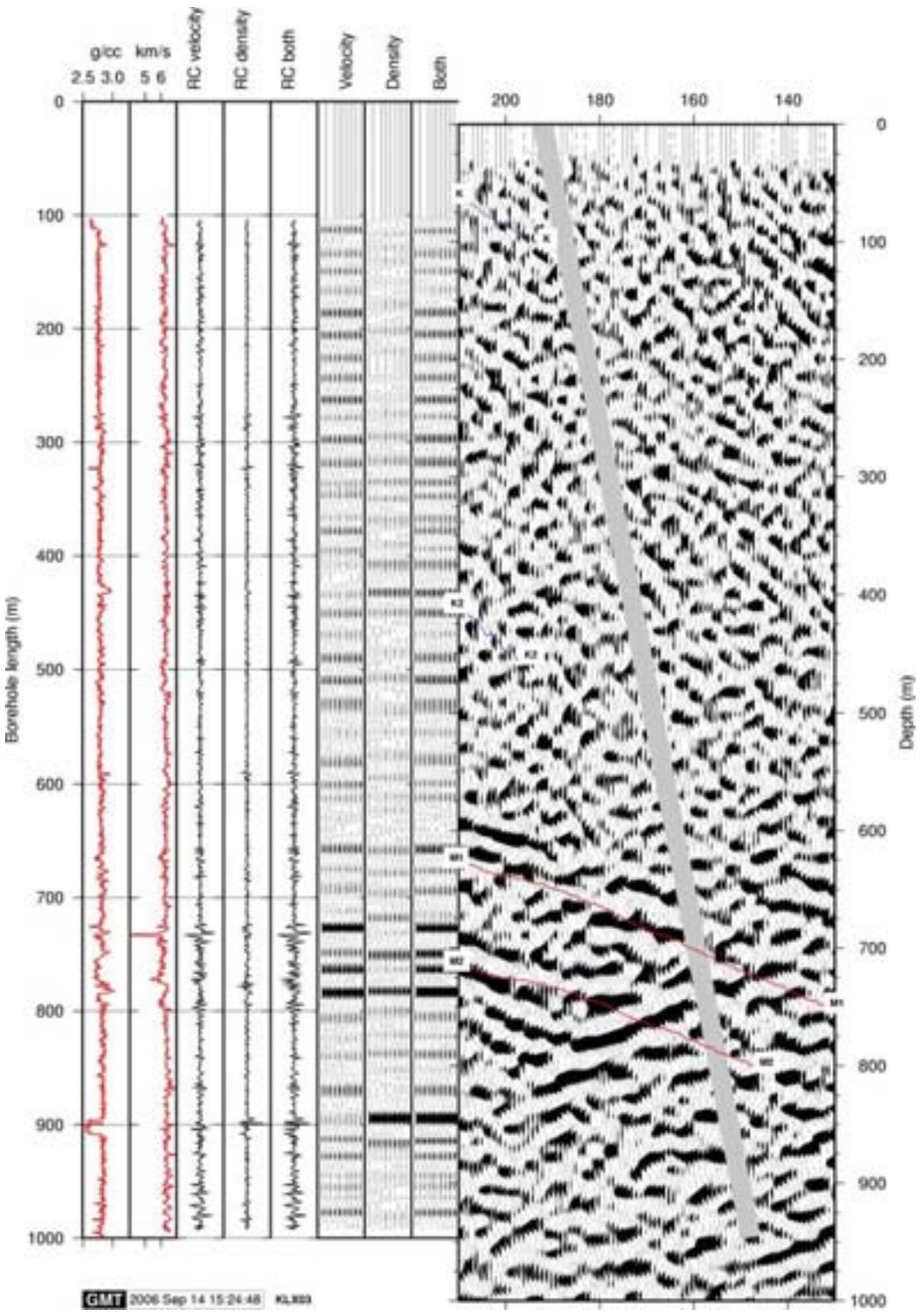

Figure 5-9. *Reflection coefficient (RC) logs and corresponding synthetic seismograms calculated from just the velocity, just the density log and both for KLX03. plotted relative to migrated depth converted profile 3. Location of picked reflectors from Table 4-1 as they project onto the profile are also shown. Projection of borehole onto profile is approximate.*

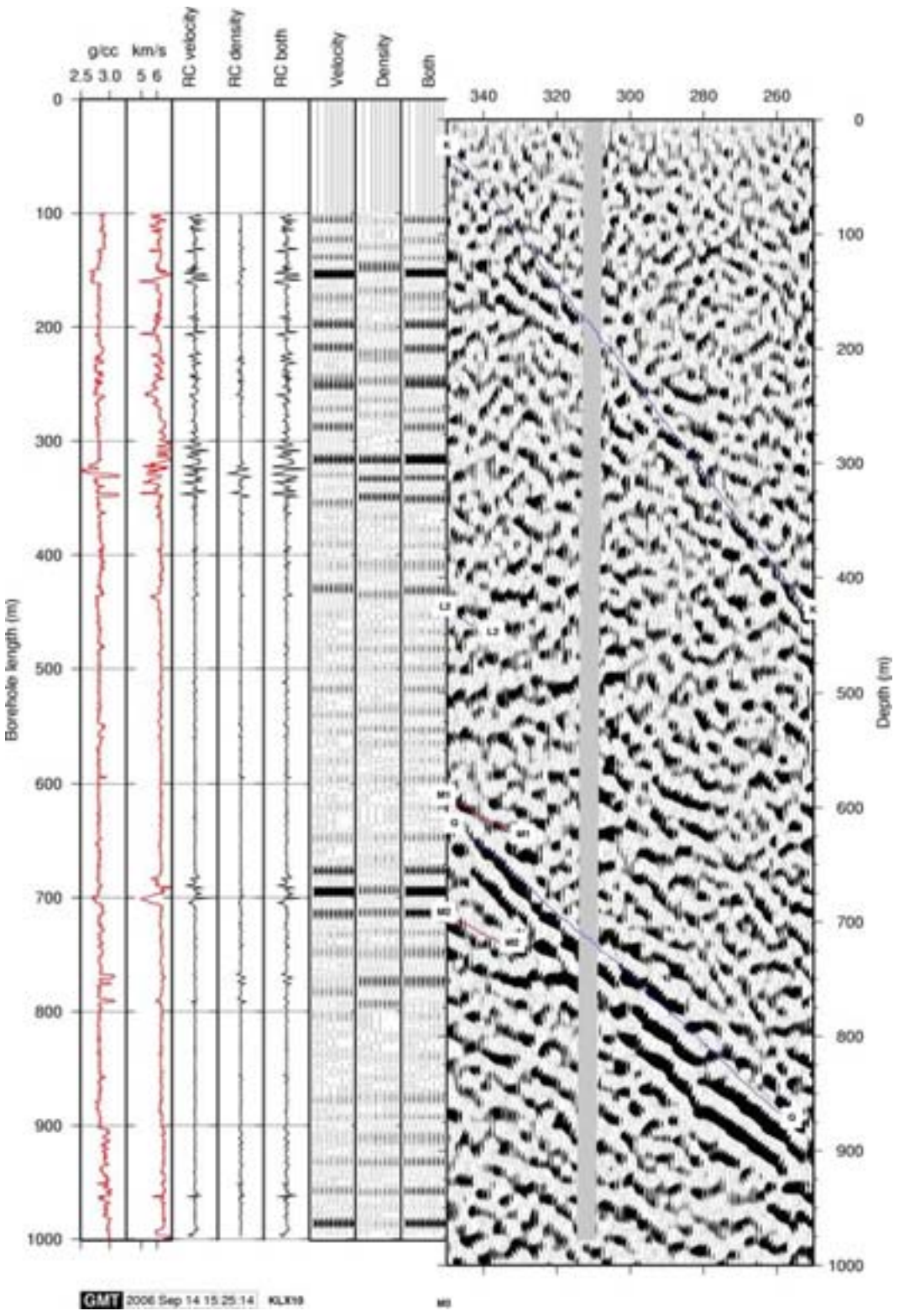

***Figure 5-10**. Reflection coefficient (RC) logs and corresponding synthetic seismograms calculated from just the velocity, just the density log and both for KLX10. plotted relative to migrated depth converted profile 5. Location of picked reflectors from Table 4-1 as they project onto the profile are also shown. Projection of borehole onto profile is approximate.*

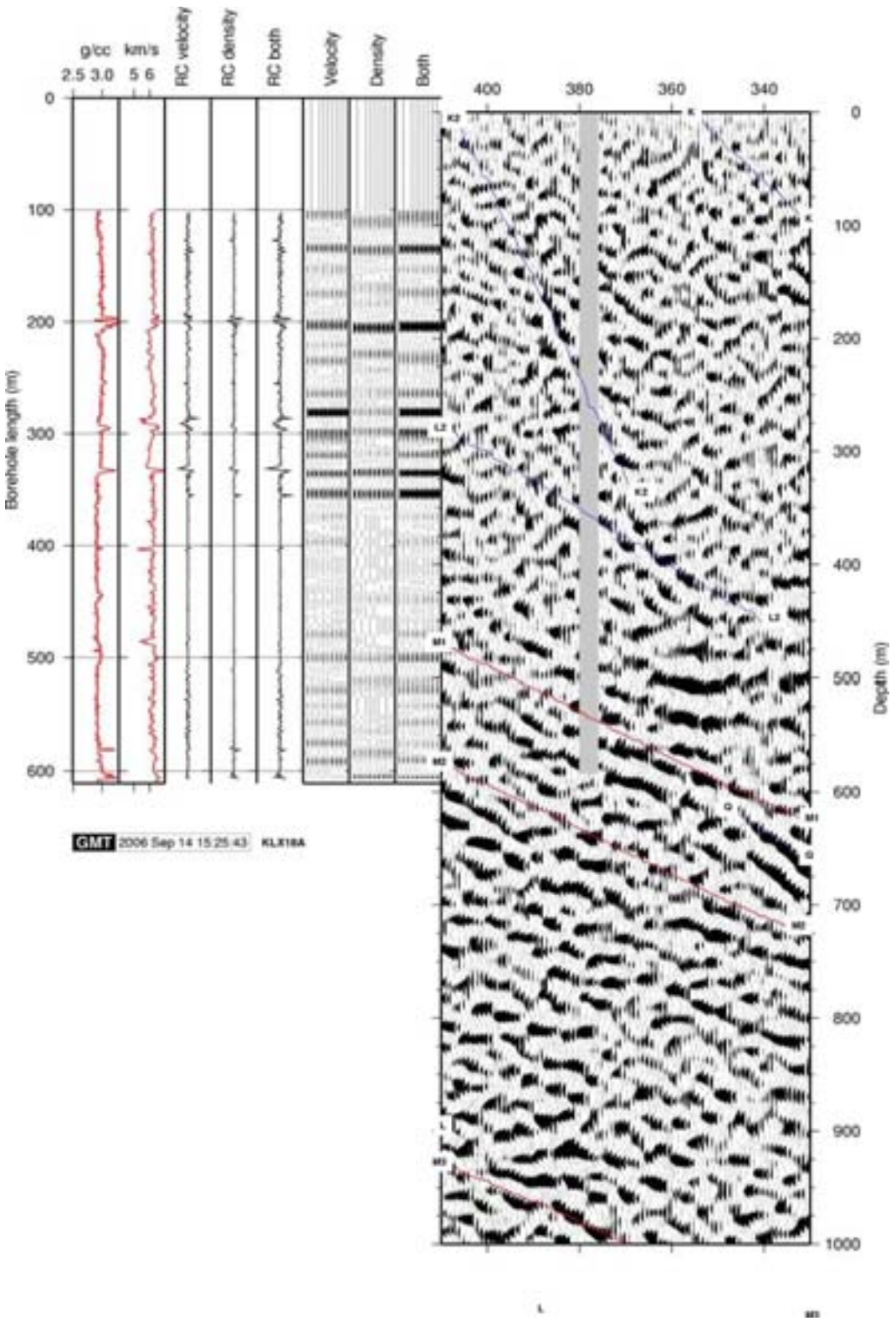

Figure 5-11*. Reflection coefficient (RC) logs and corresponding synthetic seismograms calculated from just the velocity, just the density log and both for KLX18. plotted relative to migrated depth converted profile 5. Location of picked reflectors from Table 4-1 as they project onto the profile are also shown. Projection of borehole onto profile is approximate.*

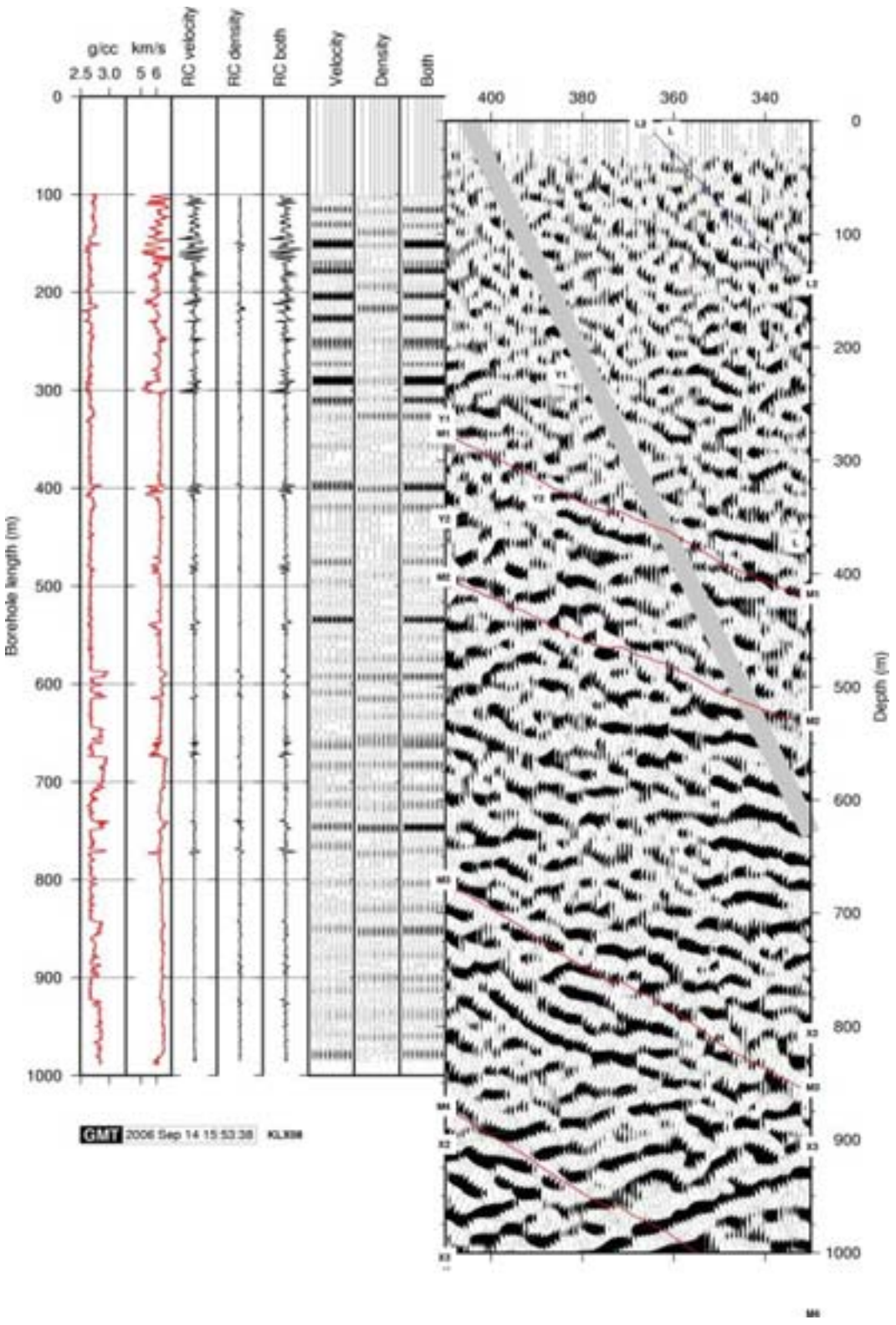

***Figure 5-12**. Reflection coefficient (RC) logs and corresponding synthetic seismograms calculated from just the velocity, just the density log and both for KLX08. plotted relative to migrated depth converted profile 3. Location of picked reflectors from Table 4-1 as they project onto the profile are also shown. Projection of borehole onto profile is approximate.*

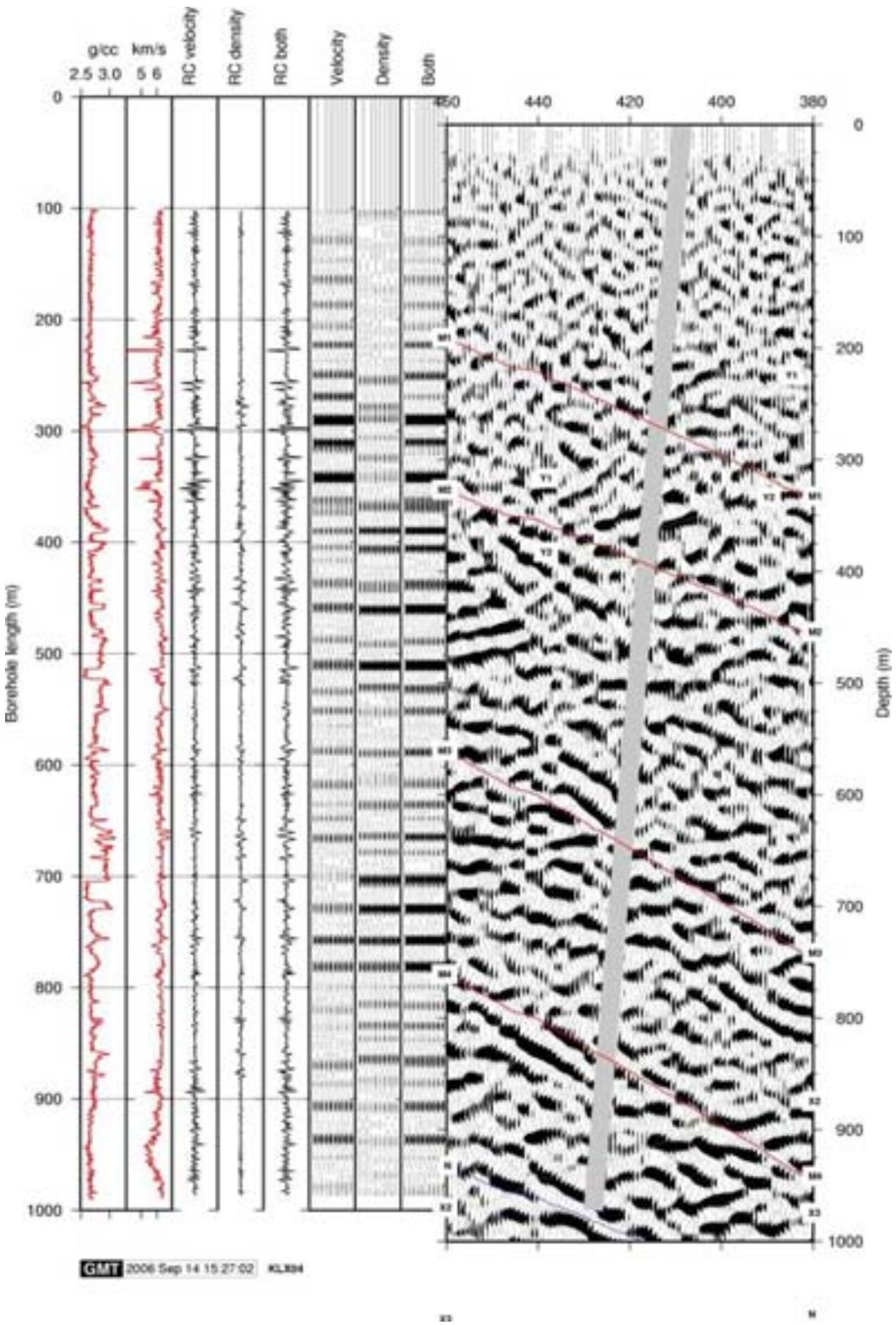

Figure 5-13*. Reflection coefficient (RC) logs and corresponding synthetic seismograms calculated from just the velocity, just the density log and both for KLX04. plotted relative to migrated depth converted profile 3. Location of picked reflectors from Table 4-1 as they project onto the profile are also shown. Projection of borehole onto profile is approximate.*

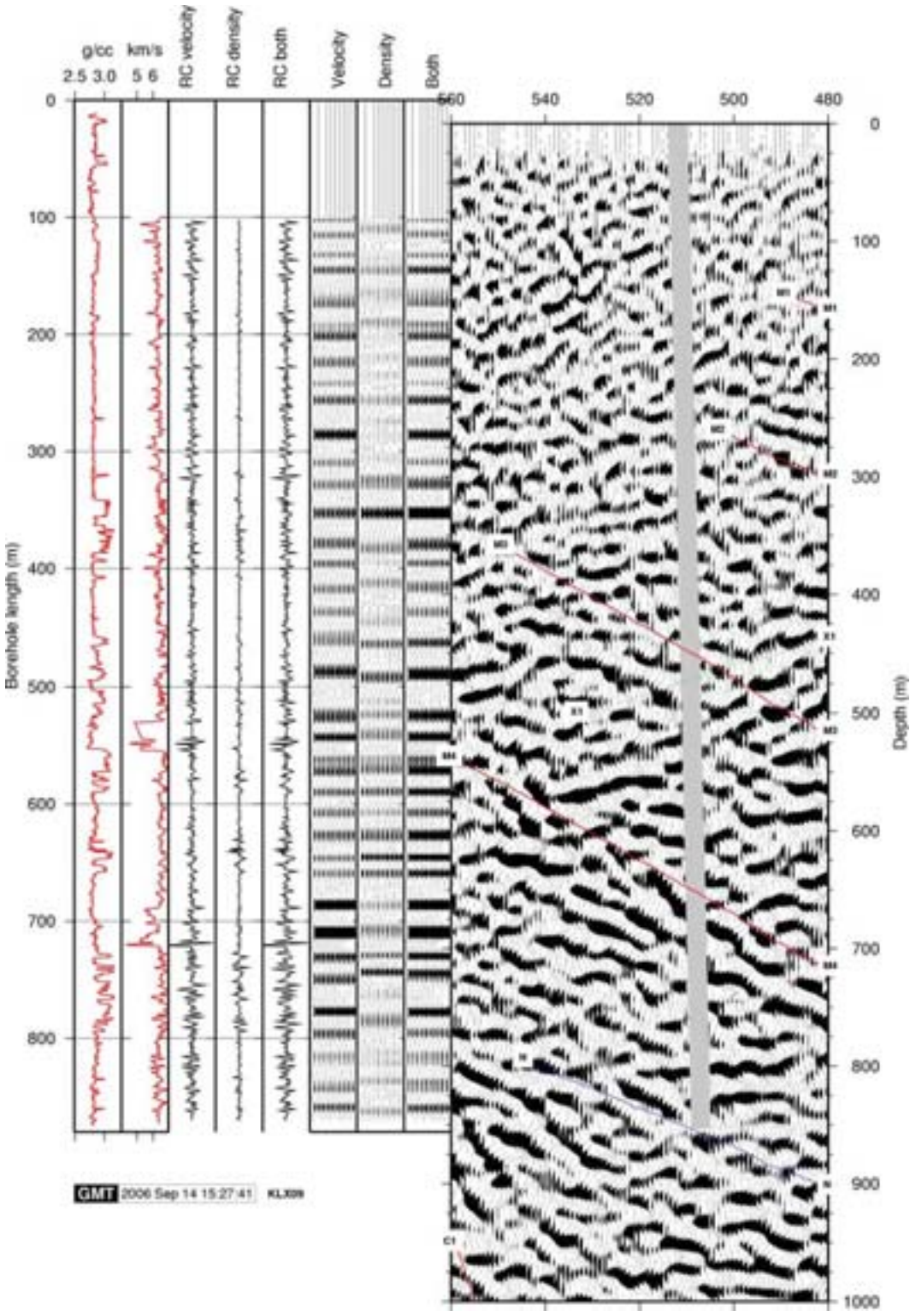

Figure 5-14*. Reflection coefficient (RC) logs and corresponding synthetic seismograms calculated from just the velocity, just the density log and both for KLX09. plotted relative to migrated depth converted profile 3. Location of picked reflectors from Table 4-1 as they project onto the profile are also shown. Projection of borehole onto profile is approximate.*

6 Final comments

Correlation of the surface seismic data with borehole results is complex due to (1) lack of 3D control of the seismic reflection data and (2) that some of the boreholes are not located directly on the seismic lines. In addition, many of the reflections are discontinuous in nature. It is not clear when adjacent reflections should be grouped together and considered as being related as opposed to being considered as separate reflections. These factors lead to a certain ambiguity in the interpretation. To properly track fracture zones, and possibly be able to distinguish between sub-horizontal mafic lenses and and sub-horizontal fracture zones, will require 3D seismic data. The interpretation presented in this report may change if such data were to become available.

References

Ayarza P., Juhlin C., Brown D., Beckholmen M., Kimbell G., Pechning, R., Pevzner, L., Pevzner, R., Ayala C., Bliznetsov, M., Glushkov A. and Rybalka A., 2000. Integrated geological and geophysical studies in the SG4 borehole area, Tagil Volcanic Arc, Middle Urals: Location of seismic reflectors and source of the reflectivity, J. Geophys. Res.: 105, 21333-21352.

Bergman, B., Juhlin, C.and Palm, H., 2002. Reflection seismic imaging of the upper 4 km of crust using small charges (15-75 grams) at Laxemar, southeastern Sweden. Tectonophysics, 355, 201-213.

Juhlin, C., Bergman, B., Cosma, C., Keskinen, J. and Enescu, N., 2002. Vertical seismic profiling and integration with reflection seismic studies at Laxemar, 2000: SKB TR-02-04.

Juhlin C., Bergman B. and Palm H., 2004. Reflection seismic studies performed in the Laxemar area during 2004. Oskarshamn site investigation. SKB P-04-215.

Nedimovic, M. R. and West, G. F., 2003. Crooked-line 2D seismic reflection imaging in crystalline terrains: Part 1, data processing. Geophysics: 68, 274-285.

Appendix 14 Deformation zone descriptions and property tables

Table of contents

FORMAT FOR ZONE DESCRIPTIONS AND PROPERTIES

(*Compass trend*) striking deformation zones Zone name					
Modelling procedure:- short description				Zone location within the local model area	
Confidence of existence: High/Medium/Low					
Property	**Quantitative estimate**	**Span**	**Confidence level**	**Basis for interpretation**	**Comments**
Position		± m or range (on ground surface)	High/ Medium /Low	Description of source	Description
Orientation (strike/dip)	XXX°/XX° Right hand rule	± span strike/±span dip	High/ Medium /Low for strike, High/ Medium /Low for dip	Description of source	Description
Thickness	True thickness estimate, from various sources	± or range m	High/ Medium /Low	Description of source	Description
Core (zone core)	True thickness estimate, from various sources m	± or range m	High/ Medium /Low	Description of source	Description
Length (regional model)	Ground surface trace length or specified alternative.	+/ - km or range	High/ Medium /Low	Description of source	Description. Includes length estimate of extent outside the regional model area, if known. Sometimes referred to as 'geological length' as opposed to the lineament trace length within the regional model area.
Ductile deformation	Yes/No (evidence of existence)	-	High/ Medium /Low	Description of source	Description

(*Compass trend*) striking deformation zones Zone name					
Brittle deformation	Yes/No (evidence of existence)	-	High/ Medium /Low	Description of source.	Description
Alteration	-	-	High/ Medium /Low	Description of source.	Description
Fracture orientation	Dominating fracture sets.	-	High/ Medium /Low	Description of source.	-most commonly estimated groupings from Terzaghi corrected fracture pole concentrations from 'best source' borehole interceptions. Rarely uncorrected ground surface /trench measurements.
Fracture frequency* Open/sealed m^{-1}	X / X	-	High/ Medium /Low	Description of source.	-Terzaghi corrected fracture frequency. Open and sealed fracture frequencies quoted separately. Includes sealed networks (the number of fractures observed = sealed section length / piece length, per definition). Does not include crush.
Crush zone Number/ total m	X / X	-	High/ Medium /Low	Description of source.	From 'best source' drill core estimate. Corrected estimate of true thickness quoted
Fracture filling	-	-	High/ Medium /Low	Description of source.	List of fracture fillings.
Kinematics	Comment if possible	-	High/ Medium /Low	Description of source.	Comment if possible.

BH	Geometrical Intercept (bh. m)	Target intercept (bh. m)	Comment
Borehole name	X-X. The BH intersection with the DZ geometry as it occurs in the RVS model.	X-X. The desired specific BH intersection with the modelled DZ.	Eshi DZ*x* (Descriptions refer to specific DZ(s) from the Extended single-hole interpretation) If the target intercepts differ from the Eshi intercepts then this is commented upon. Further description specific to a relevant particular BH intercept section.

NE-SW striking deformation zones

ZSMNE004A

In comparison with version 1.2 the interpreted geometry of the regional deformation zone, ZSMNE004A, has been modified to more closely conform to the corresponding plastic domain P02 in the rock domain model. The zone is still modelled as being vertical with a length of 15 km but the thickness now varies between 100 m and 650 m. Additional detailed field mapping /Lundberg & Sjöström, 2006/ has lead to a better characterization of the zone and the results of which are summarized later in this section.

ZSMNE004A is one of the larger regional deformation zones in the mainland area, and together with Äspö shear zone, dominates the ductile pattern in the regional model area. The deformation is complex and dominantly ductile with smaller sections of brittle deformation. It is not one single deformation zone but rather a belt with a high concentration of low-grade ductile to brittle-ductile shear zones, increased fracturing and red staining. There are clearly smaller sub parallel deformation zones and splay structures, especially in the south central part of the local model close to Äspö shear zone. However, the complexity is not well known with only a few detailed observations from field mapping and from the Äspö tunnel. The southern part of ZSMNE004A can be observed in numerous outcrops /Persson Nilsson et al. 2004/ and extends far beyond the regional model boundary. Moving northwards as the zone approaches the southern border of the local model it is interpreted to flex east and away from the southern termination of Äspö shear zone based on the airborne magnetic data and outcrop mapping. The area is characterized by a mix of different rock types, intense ductile deformation and relatively sparse surface outcrops. Two separate plastic rock domains for ZSMNE004A and Äspö shear zone (ZSMNE005A) are proposed for this area. The whole section where ZSMNE004A and the Äspö shear zone are in close proximity may be well connected, but information is not conclusive with regards to zone terminations and geological character. The northern part of ZSMNE004A turns eastwards over Ävrö and is interpreted (with lower confidence) to extend eastwards out in the Baltic Sea.

A 70° dip towards the southeast is observed in the Äspö tunnel at chainage 0/318 m. The section of ZSMNE004A across Ävrö is also indicated by seismic reflector B4 by /Juhlin et al. 2004b/ although the reflector is interpreted as being shallow dipping (28°) towards the south. Refraction seismics show a low velocity zone along one of the profiles over Ävrö. Dip measurements from field mapping vary between 75°N to 65°S /Wahlgren et al. 2004/.
ZSMNE004A is modelled with a vertical dip to accommodate the variable dips from observations in the field, tunnel and from seismics. The thickness of the plastic belt is highly variable from up to 650 m in southern Laxemar to 100 m or less over Ävrö.

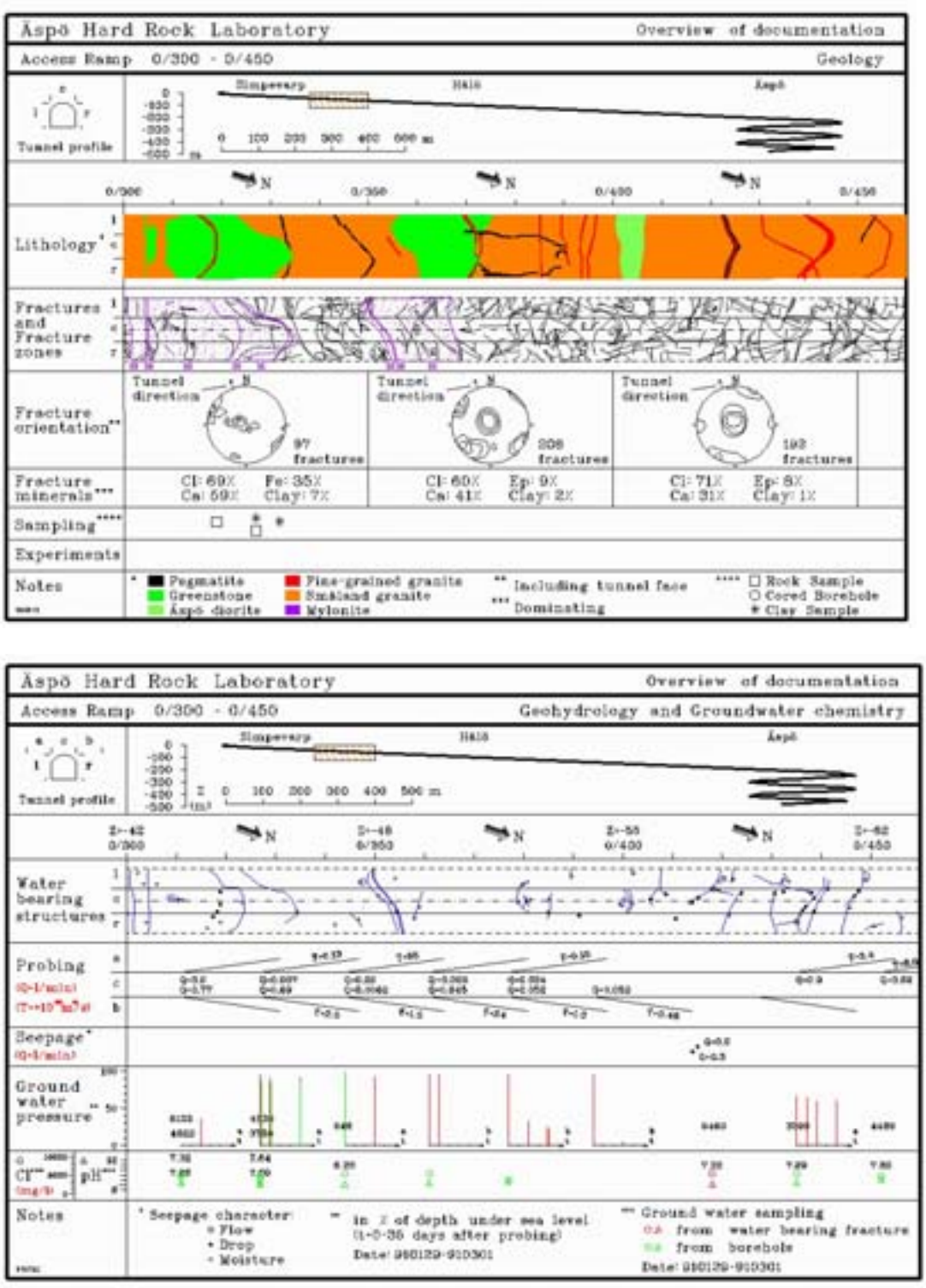

Äspö tunnel observation of ZSMNE004A at chainage 0/302–0/334 m /PR-HRL-96-19/.

Additional detailed field mapping has been performed to better characterize the zone /Lundberg & Sjöström, 2006/.

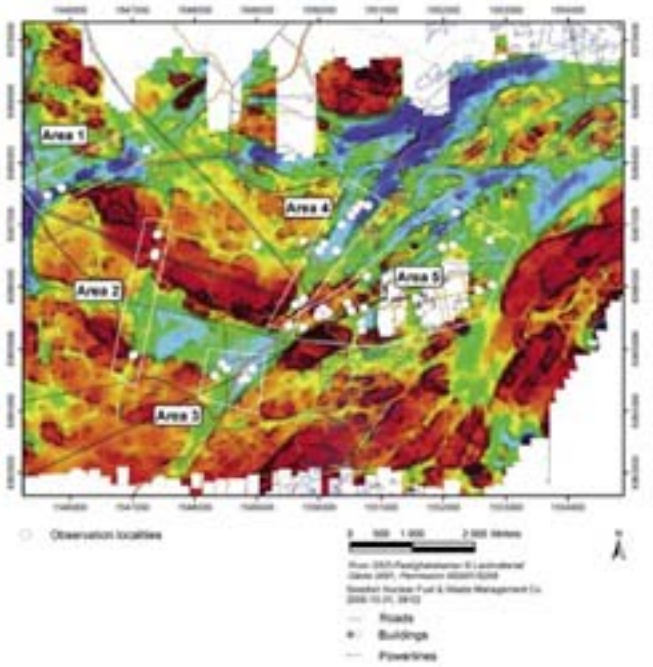

Distribution of outcrop locations examined as part of kineamatic studies. ZSMNE004A corresponds to Area 3 / Lundberg & Sjöström, 2006/.

ZSMNE004A in southern Laxemar corresponds to Area 3 in the field investigations/ Lundberg & Sjöström, 2006/. The zone is sinistral as recorded both on outcrops and in thin sections from rock samples and dominantly horizontal movements have occurred.

The shear zones here often display distinct kinematic indicators. Large parts of the surrounding quartz monzodiorite are affected by the deformation and a strong foliation that formed close to the shear zones reveal the sense of shear based on the rotation and orientation of the newly formed foliation (S) compared to the shear zone (C). Also shear bands have formed locally and were used to determine the sense of shear. Sinistral and dextral shear zones are well separated in the stereogram and the poles to all unspecified shear zones plot among the sinistral group (see below). The main zone on the magnetic anomaly map strikes approximately 35° and also plots among the poles to the sinistral shear zones in the stereogram.

Fine-grained granite dykes cut by shear zones and also boudinaged dykes exist in the area. Boudinage appears to be more frequent and more mature in a horizontal section than in a vertical section. Stretching lineations are shallow plunging and intersection lineations plunge steeply as well as intersections between sinistral and dextral shear zones and intersections between sinistral and dextral shear bands (see below). This condition indicates that mainly horizontal movement has occurred and also that the development of boudinage and stretching lineation was coeval. The axis of rotation of S (if formed due to the shear) will be perpendicular to the stretching lineation, i.e. parallel to the intersection lineation /Lundberg & Sjöström, 2006/.

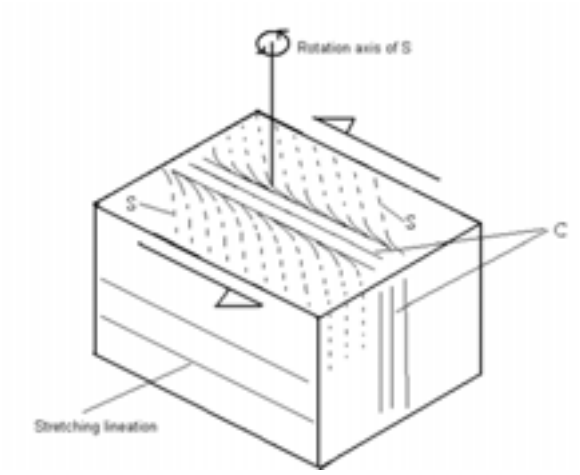

Sketch showing rotation of foliation (S) compared to a mylonite surface (C) /Lundberg & Sjöström, 2006/.

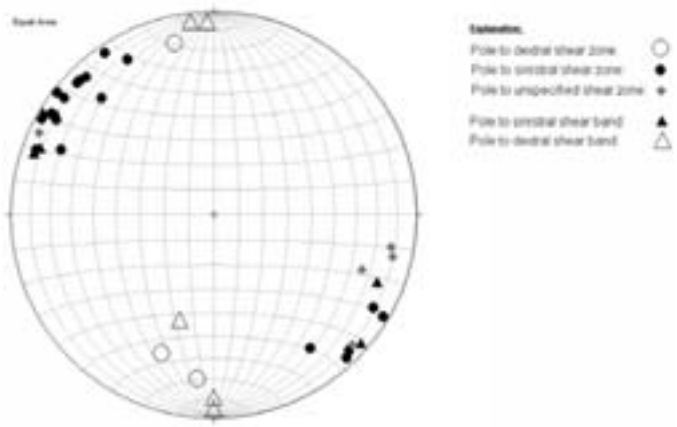

Poles to shear zones and shear bands in Area 3. Lower hemisphere of Schmidt equal area, stereographic plot /Lundberg & Sjöström, 2006/.

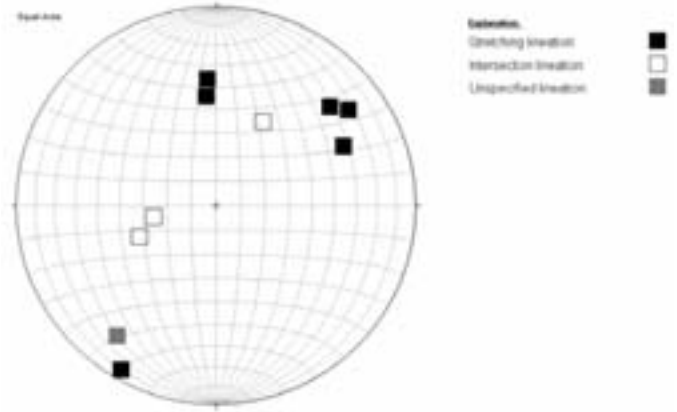

Lineations in Area 3. Lower hemisphere of Schmidt equal area, stereographic plot /Lundberg & Sjöström, 2006/.

NE-SW striking deformation zones ZSMNE004A (plastic domain)	
Modelling procedure: At the surface, corresponds to a major low magnetic belt. Modelled to base of regional model volume using dip that has been inferred from outcrop mapping. Included in regional model and also present inside local model volume.	
Confidence of existence: High	

Property	Quantitative estimate	Span	Confidence level	Basis for interpretation	Comments
Position		± 20 m (surface)	High	Lineament –low magnetic belt	
Orientation (strike/dip)	050/90	Generally 030-070/ ± 20	Medium for strike, medium for dip	Strike based on trend of lineament and outcrop mapping. Dip based on outcrop mapping	Strike 030 within the local model area, curving to 090 further north. Modelled as vertical to allow for local variations.
Thickness	150 m	20-650 m	High	Lineament –low magnetic belt and outcrop mapping	Complex zone, inferred thickness refers to total zone thickness (splays, ductile and brittle, transition zones and core)
Transition zone				low magnetic belt and outcrop mapping	Complex 'belt' – multiple minor cores and transition zones expected
core				low magnetic belt and outcrop mapping	Complex 'belt' – multiple minor cores and transition zones expected
Length (regional model)	15.6 km	8>15 km	Medium	Lineament –low magnetic belt	Possible termination at ZSMNE024A. Extension eastwards outside the regional model boundary is unknown.
Ductile deformation	Yes		High	Frequent evidence from outcrop mapping	Ductile-brittle zone. Dominantly ductile character
Brittle deformation	Yes		Medium	TASA and weak evidence from outcrops and HLX19.	Probable local reactivation.
Alteration			Medium	Evidence from bounding outcrops	Red staining.

NE-SW striking deformation zones ZSMNE004A (plastic domain)					
Fracture orientation	045/90, 300/80, 020/20		Medium	TASA	Local to Äspö
Fracture frequency Open/sealed m^{-1}	3/0		Low	HLX19	
Crush zone Number/total m	0/0		Low	HLX19	
Fracture filling			High	TASA	Chlorite, calcite, clay
Sense of displacement	Sinistral strike slip		Medium	Field mapping	*/Lundberg & Sjöström, 2006/*

BH and tunnel	**Geometrical Intercept (bh. m)**	**Target intercept (bh. m)**	**Comment**
HLX19	85,5-202,2 (base)	139-154	Scattered c.1.5 m wide sections of increased fracture frequency and related fracture zone alterations. No interpretable radar reflectors below 130 m. The section is characterized by distinct caliper anomalies, partly low resistivity and an indicated decrease in p-wave velocity.
KAV04	-	-	No geometrical intersection but the BH lies on the border of the modelled transition zone and may be responsible for the relatively high fracture frequency and degree of alteration throughout much of the BH though this is not clearly supported by fracture orientations.
TASA		302-334	Cf.

ZSMNE005A

In comparison with version 1.2 the interpreted geometry of the regional deformation zone, ZSMNE005A, has been modified to more closely conform to the corresponding plastic domain P01 in the rock domain model. In addition the southern extent has been increased by merging a previously separate zone, ZSMNE094A, with the main Äspö shear zone ZSMNE005A. This extension has been based on a general review of existing data rather than the case of new evidence coming to light and is considered to present the simplest solution to the underlying mapping and geophysical evidence. Additional detailed field mapping /Lundberg & Sjöström, 2006/ and geophysical studies /Mattsson, 2006/ have lead to a better characterization of the zone.

The Äspö shear zone forms the boundary between the more tectonically influenced rock mass in the Simpevarp subarea from Laxemar. The deformation is complex and dominantly ductile with smaller sections of brittle deformation. It is not one single deformation zone but rather a belt with a high concentration of low-grade ductile to brittle-ductile shear zones, increased fracturing and red staining.

The zone is modelled with a length of 16 km but the eastern termination out to sea is uncertain. The thickness of the zone on average is around 250m but varies from a maximum 300m down to 10m in the model. Detailed geophysical studies, discussed later in this section, suggest an even greater thickness /Mattsson, 2006/.

At Äspö, where it is best known, /Rhén et al. 1997/ describe its character as a primarily ductile shear zone with mylonites and epidotic anastomosing shear zones which are interpreted to control the orientation of later brittle deformation, evident in the form of increased fracturing and brecciation. Hydrothermal alteration and formation of different fracture filling minerals probably had an important sealing effect on the main part of the zone. The most hydraulically conductive parts appear to coincide with some narrow highly fractured sections, or single open fractures, which are probably not connected along the entire extent of the belt.

The modification to the southern termination to the zone is based on a review of the magnetic anomalies and field mapping results. The extension is of low confidence but is considered to represent the simplest solution based on the available data. Other than this narrow southern extension the overall geometry of the zone closely conforms to the ductile domain P01 in the rock domain model. The northern extension of the zone remains unchanged being based on the tectonic patterns indicated by the underlying data to the lineament map, particularly the field mapping and the magnetic map, including an estimated thickness and possible lateral continuity.

The north-eastern termination of the zone into ZSMNE024A is uncertain and similar to other zones it may terminate more to the NE. The overall dip of the zone has been modelled as vertical. However, the zone is a complex plastic ‘belt’ and local dips will vary.

A seismic refraction survey /Lindqvist 2004a/ and Äspö data suggest that while 250 m may be a reasonable thickness to use for representing the zone from a geological standpoint, such a thickness should not be taken to infer the extent of poor rock

conditions or rock mass quality /Rhen et al. 1997/. For much of this thickness the rock mass quality is likely to be ‘Fair’ (based on the RMR system).

Boreholes KA1755A, KA1754A, KA1751A, KAS04, KA3590G02, KAS02, KAS12, KAS17
have been interpreted by /Berglund et al. 2003/ to indicate the position and character of Äspö
shear zone at Äspö.

ZSMNE005A has been used as the basis for the definition of fracture domain FSM_NE005. The background to this definition and further details can be found in the main report and /Hermanson et al, 2008/. A summary of all the available fracture orientation data for this domain, which can be taken as the best source for characterizing the zone in this respect is presented in the stereoplot below.

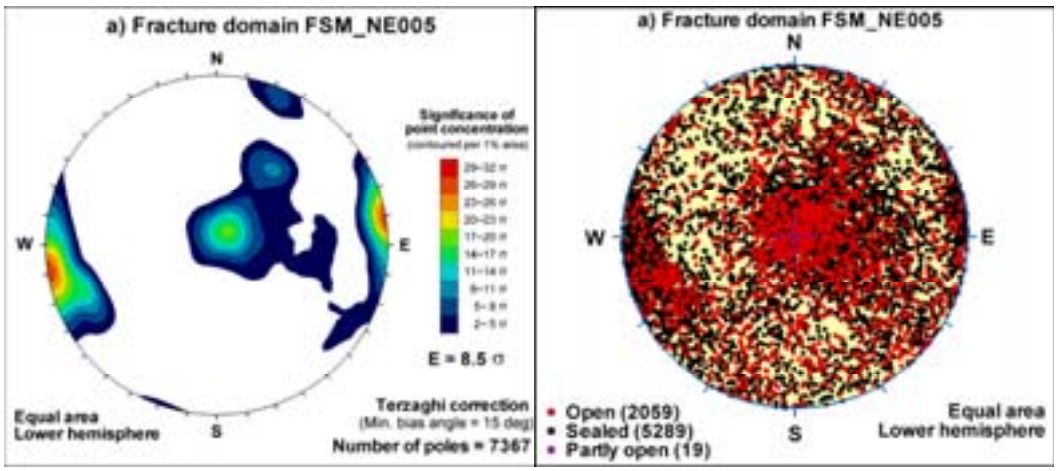

Summary fracture orientation data from fracture domain FSM_NE005

Subsequent detailed fracture mapping studies on outcrops have been performed to help characterize the zone / Lundberg & Sjöström, 2006/.

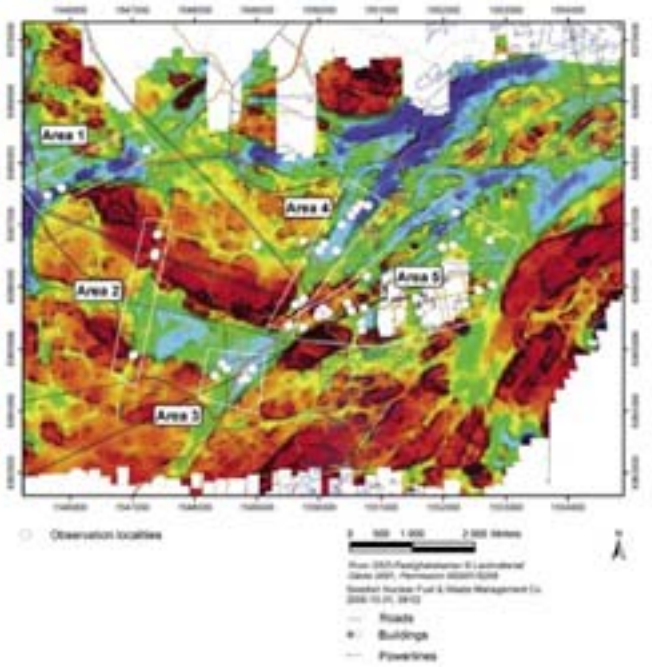

Distribution of outcrop locations examined as part of kineamatic studies. ZSMNE005A corresponds to Area 4 / Lundberg & Sjöström, 2006/.

The Äspö shear zone, corresponding to area 4, is sinistral as recorded both in field and in thin sections from rock samples. Shallow plunging stretching lineations and steep, constructed and observed, intersections as well as the shear related foliation rotating around a steep axis suggests that dominantly horizontal movements have occurred.

The shear zones in the northern part of the Äspö shear zone were found to be often thin, less than a meter wide, and considerably fractured due to reactivation. Strain is very much localized and the surrounding rock (most often Ävrö granite) is not much affected. Sheared fine-grained granite dykes are also common. It can be difficult to see with the naked eye, whether the dykes are sheared or not due to the low content of dark minerals and their originally small grain size.

Most of the measured zones are sinistral but one dextral conjugate shear zone has also been found. Sinistral and dextral shear zones are well separated and the poles to all shear zones with unknown kinematics plot among the sinistral group in the stereogram (see below). This is also the case for the main zone on the magnetic anomaly map striking approximately 040°. Lineations are poorly developed but at least two stretching lineations have been found. The stretching lineations are plunging gently towards southeast and an intersection lineation is steep indicating dominantly horizontal movement in the shear zone. This assumption is based on the general condition that shear bands (C') ideally intersect the shear surface (C) approximately perpendicular to the shear direction (stretching lineation).

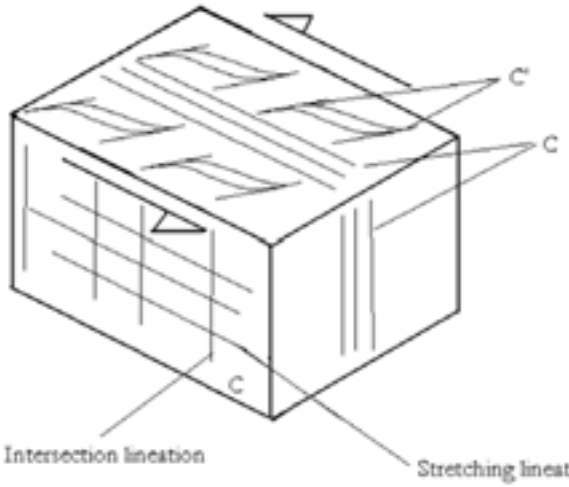

Sketch showing the principal relationship between mylonite surface C, shear bands C' and stretching and intersection lineation /Lundberg & Sjöström, 2006/.

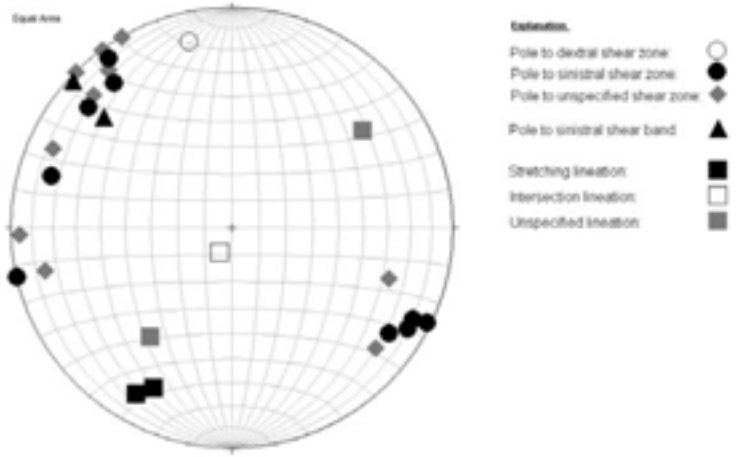

Distribution of shear zones, shear bands and lineations in Area 4. Lower hemisphere of Schmidt equal area, stereographic plot /Lundberg & Sjöström, 2006/.

In order to assess how far from the zone the rock has been affected by the ductile deformation a detailed AMS (anisotropy of magnetic susceptibility) study was performed based on rock samples collected along a profile across the zone /Mattsson, 2006/. The aim of the study was to test how far from the zone boundaries it is possible to identify variations in the magnetic properties related to the ductile deformation processes.

The oriented AMS data across the Äspö shear zone indicate a structural fabric that varies distinctly with distance from the deformation zone. Far west of the deformation zone the AMS fabric is identical with the primary fabric reported for fresh Ävrö granite in the Laxemar area. In a c. 250 m wide transition zone outside of the deformation zone centre, there is a clearly detectable counter clockwise rotation of the magnetic foliations, and there is also an increase in the dip of foliation planes. Within the zone centre there is a general increase in the counter clockwise rotation and the dip generally becomes even steeper. The magnetic foliation fabric variations fit well to the expected fabric of a ductile deformation zone with sinistral sense of movement. The fact that the magnetic lineations show little evidence of the deformation process,

apart from the mylonite at PSM007597 and the neighbouring site PSM007598, most likely indicates that the degree of deformation was low. This assumption is supported by the geological observations in outcrops within the deformation zone that indicate that the mylonite is brittle-ductile (thus mainly brittle) and that surrounding rocks mainly carry only weak foliation. It should be noted that AMS is very sensitive even to weak ductile deformation that is not visible to the naked eye.

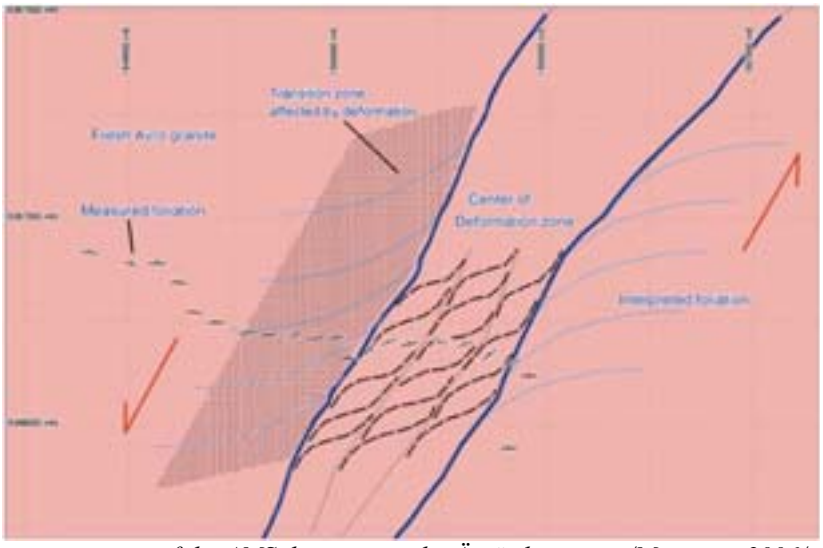

interpretation of the AMS data across the Äspö shear zone/Mattsson, 2006/

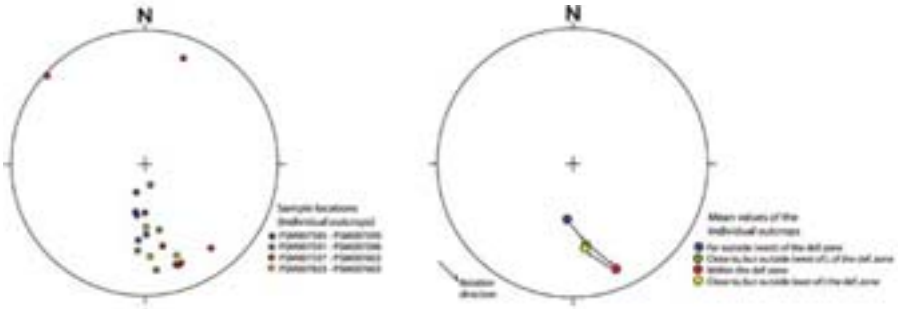

The orientation of the magnetic poles to the foliation plotted in equal area projection plots. The left plot displays individual site locations and the right plots displays mean values of the same set of sites.

NE-SW striking deformation zones ZSMNE005A (Äspö Shear Zone)	
Modelling procedure: At the surface, corresponds to a major low magnetic belt. Modelled to base of regional model volume using dip that has been inferred from outcrop mapping. Included in regional model and also present inside local model volume.	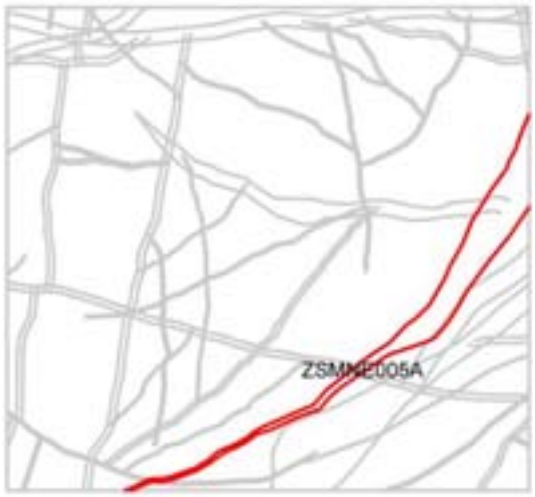
Confidence of existence: High	

Property	Quantitative estimate	Span	Confidence level	Basis for interpretation	Comments
Position		± 20 m (surface)	High	Lineament –low magnetic belt	
Orientation (strike/dip)	060/90	± 30/ 10	High for strike, medium for dip	Strike based on trend of lineament. Dip based on outcrop mapping	Strike 030 within the local model area, curving to 090 further north. Modelled as vertical to allow for local variations. However, a dip of 90 to 80 SE is considered most probable.
Thickness	250 m	10-300 m	High	Lineament –low magnetic belt	Complex zone, inferred thickness refers to total zone thickness (splays, ductile and brittle, transition zones and core)
Transition zone			High	Field mapping	Not one single deformation zone but rather a belt with a high concentration of low-grade ductile to brittle-ductile shear zones with increased fracturing.
core			High	Field mapping	
Length (regional model)	16.0 km	+/- 250 m	Medium	Lineament –low magnetic belt	Extension eastwards outside the regional model boundary is unknown.
Ductile deformation	Yes		High	Frequent evidence from outcrop mapping	Ductile-brittle zone. Dominantly ductile character but there has been clear reactivation.
Brittle deformation	Yes		Medium	Weak evidence from outcrops. Bhs show increased fracturing and brecciation	Clear local reactivation.

NE-SW striking deformation zones ZSMNE005A (Äspö Shear Zone)					
Alteration			Medium	Evidence from bounding outcrops	Red staining.
Fracture orientation	220/85, 110/80, 250/30, 025/20		Low	Parallel NE107A fracture orientations and reference to Äspö data	
Fracture frequency m^{-1}	9	20 Incl. crush	Medium		Limited data set.
Fracture filling			High	BHs	Calcite, Chlorite, Epidote, Hematite, Quartz
Sense of displacement	Sinistral stike slip		Medium	Field mapping	*/Lundberg & Sjöström, 2006/*

BH	Geometrical Intercept (bh. m)	Target intercept (bh. m)	Comment
HLX09	3,2-108,1 (base)	-	No boremap logging
HLX16	0-118,9	-	No boremap logging
HLX17	182,1-202,2 (base)	-	
KA1751A	50,1-150,1 (base)	110-114	The rock is fine grained granite, granodiorite and greenstone. No major indications of deformation in the database. However, in /Stanfors et al. 1994/ a section between core length 140 and 150 m coincides with this area and is mapped as a fracture zone and as tectonized. At approximately 110 m there is a crush zone and a tectonized area developed in fine-grained granite and “greenstone”, /Berglund et al. 2003/.
KA1754A	26,2-159,9 (base)	90-115	A crush zone and surrounding tectonization at ca 90–115 m fits geometrically with EW-1b. The area has a very high fracture frequency and the rock is finegrained granite, granodiorite and “greenstone” /Berglund et al. 2003/
KA1755A	21,6-296,1	95-140	At core length 95–140 m generally > 10 fract./m, at nine sites > 20 fract./m. This wide zone coincides geometrically with EW-1b.Most of the zone is developed in fine-grained granite and partly in granodiorite. Only a thin zone of true mylonite, with a medium tectonized area of 2–4 m around it. RQD is less than 25 at several locations in the zone. At core length 203–213 m ca 10 fract/m except for a 1–2 m wide, /Berglund et al. 2003/.
KA3590G02	20,3-30,05 (base)	19-30	Intermediate tectonization. /Berglund et al. 2003/.
KAS04	4.31-466,1	131-437	Two mylonites. Also four areas with weak to intermediate tectonization. The rock is granodiorite and fine-grained granite, /Berglund et al. 2003/.
KAS12	0-273,9	19-286	Tectonized
KAS17	84,9-352,7 (base)	-	-No final mapping completed
KA2598A	124.0-300.8 (base)	-	/Berglund et al, 2003/
KA3600F	2.4-50.1 (base)	-	/Berglund et al, 2003/
KA3510A	129.5-150.1 (base)	-	/Berglund et al, 2003/
KA2563A	347.0-363.4 (base)	-	/Berglund et al, 2003/

ZSMNE006A (NE1 on Äspö)

The zone has not been the subject of further review and the interpretation and resulting geometry remains unchanged from v1.2 /Wahlgren et al, 2005/. The zone is modelled as a 2 km long, predominantly brittle, 60-130m thick complex water bearing zone. The length of the zone is judged medium confidence and alternative, longer, interpretations of extent are possible. The zone has been the subject of a special detailed review for engineering purposes by /Chang et al, 2005/.

ZSMNE006A is directly observed through boreholes and tunnels at Äspö and indirectly in the magnetic map and is characterized mainly as a brittle deformation zone with at least three branches intermingled with minor mylonites, clay and breccia. The intercept with the Äspö tunnel occurs at chainage 1/300 m and is described by /Rhén et al. 1997/ as a highly water-bearing brittle zone approximately 15 m thick with a highly fractured, brecciated 5 m thick core. The central part of the core contains a 1 m thick sequence of crush and fault gouge. More or less tectonized granite and mylonites occur with older fracture formations found as fragments indicating that gouge formation is a reactivation of earlier deformations. The intensive core of the zone with centimeter wide open fractures and cavities is surrounded by 10–15 m wide transition zones of more or less fractured rock. The zone intersection with the tunnel extends over 30 m. A set of highly water-bearing structures gently dipping towards the north contributes to the complex character of the zone. The mylonite is quartzo-feldspatic with accessories of chlorite and corroded magnetite. The mylonite is penetrated by fractures sealed with quartz and iron hydroxides, with some fluorite and pyrite. The gouge samples consist of angular fragments of tectonized rock, which are oxidized. Late overgrowth by calcite indicates that the zone has been reactivated. Smaller fractions contain large portions of clay minerals. The clay mineralogy is dominated by mixed layer illite/smectite. No geometrical updates have been performed for this deformation zone compared to model version Simpevarp 1.2. The deformation zone is modelled with a 130 m thickness in order to envelope all borehole and tunnel indications.

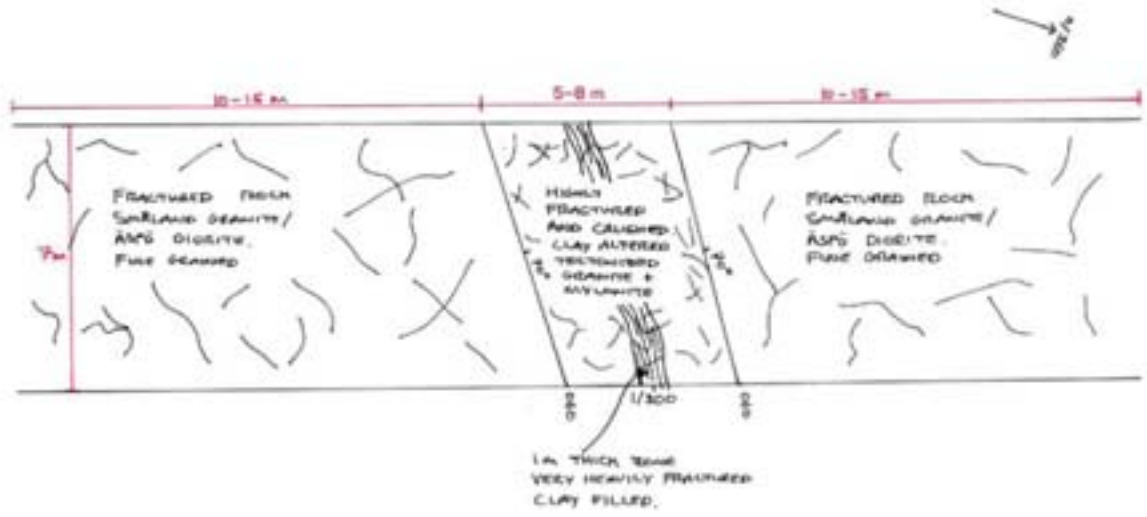

Schematic plan of the most intense branch of deformation zone NE-1 (not to scale) /Chang et al, 2005/

NE-SW striking deformation zones ZSMNE006A	
Modelling procedure: At the surface, corresponds to low magnetic and topographic lineaments. Modelled to base of regional model volume using a dip that has been inferred from BHs and tunnel mapping (Äspö). Included in the regional model and also present inside the local model volume.	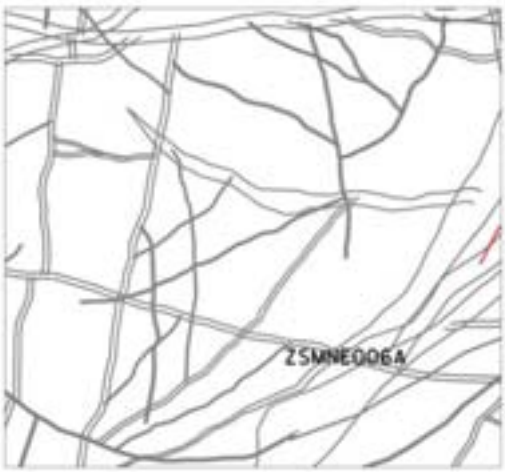

Confidence of existence: High

Property	Quantitative estimate	Span	Confidence level	Basis for interpretation	Comments
Position		± 25 m (surface)	Medium	Linked lineament	
Orientation (strike/dip)	215/65	± 10/± 20	High for strike, medium for dip	Strike based on trend of lineament. Dip based on BH and tunnel (Äspö) intercepts.	
Thickness	130 m	60-130 m	High	Linked lineaments, BH and tunnel (Äspö) intercepts.	Model thickness of 130 m represents an envelope thickness containing narrower inferred splays. At Äspö NE1 is considered to consist of 3 main branches totalling 85 m as intercepted in the tunnel.
core	1 m	10-20m	High	TASA	1m thick completely clay altered core.
Length (regional model)	2,1 km	2-4 km	Medium	Linked lineament	An alternative interpretation allows the zone to continue further north eastwards.
Ductile deformation	Yes		High	Multiple 1cm thick Mylonite bands,TASA	Dominantly brittle zone with minor plastic indicators
Brittle deformation	Yes		High	Breccia and gouge, TASA	
Alteration			High	TASA	5-8m thick partially clay altered

NE-SW striking deformation zones ZSMNE006A					
Fracture orientation	230/35, 341/45, 284/90, 045/30, 050/60, 094/60, 120/35, 310/38, 310/75		High	TASA + bhs	The first two sets are water bearing.
Fracture frequency m^{-1}	11	Frac' frq' incl' crush = 20 m^{-1}	High	KA1131B, KAS07, KAS08, KAS11, KAS14, KBH02, KAS02	Frac' frq' incl' crush = 20 m^{-1}
Fracture filling			High	KA1131B, KAS07, AS08, KAS11, KAS14, KBH02, KAS02	Calcite, Chlorite, Epidote, Hematite, Quartz

BH and tunnel indications	Geometrical Intercept (bh. m)	Target intercept (bh. m)	Comment
KA1061	94-209 (base)	198-209	/Berglund et al. 2003/
KA1131B	47-203 (base)	173-203	/Berglund et al. 2003/
KAS07	402-602 (base)	497-602	/Berglund et al. 2003/
KAS08	440-590 (base)	537-601	/Berglund et al. 2003/
KAS09	53-225	50-112	/Berglund et al. 2003/
KAS11	115-249	156-220	/Berglund et al. 2003/
KAS14	38-194	51-91	/Berglund et al. 2003/
KAS16	227.7-438.4	380-430	/Berglund et al. 2003/
KBH02	543-706 (base)	667-706	/Berglund et al. 2003/
KAS02	740-924 (base)	806-914	/Berglund et al. 2003/
TASA		1,240-1,325	/Berglund et al. 2003/
KA2048B	108.2-184.5	-	

ZSMNE011A

The background data and linking of the lineaments associated with this zone has been reviewed since version 1.2. This has lead to a modification of the northern termination of the zone. Previously the zone, based on the underlying lineament was terminated against the Mederhult zone ZSMEW002A. A review has lead to the lineament being extended to the north of ZSMEW002A, merged with a similarly oriented lineament ZSMNE058A and the removal of an earlier offset.

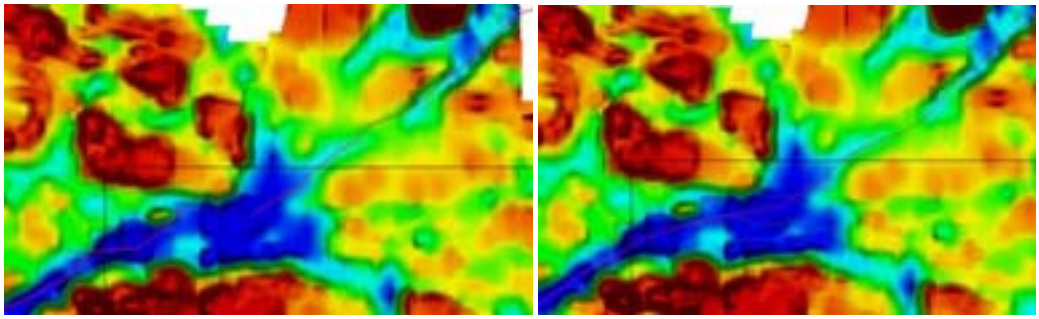

V1.2 ZSMNE011A and ZSMNE058A as they terminate and are offset across ZSMEW002A (left). V2.3 merger and removal of offset between the lineaments with the regional magnetic map as background (right).

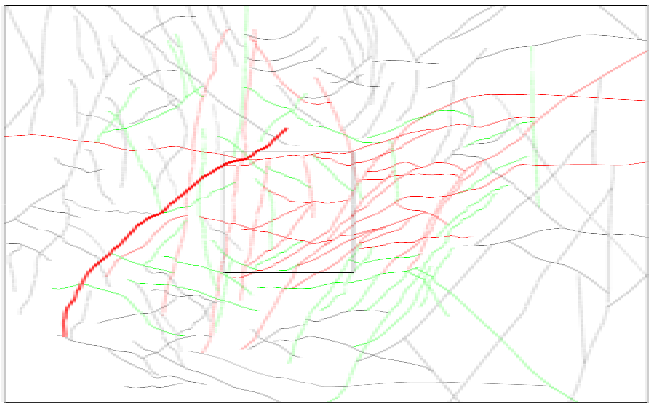

Combined v1.2 ZSMNE011A and v1.2 ZSMNE058A form v2.3 ZSMNE011A shown in bold within the regional domain.

Subsequent detailed fracture mapping studies on outcrops have been performed to help characterize the zone / Lundberg & Sjöström, 2006/.

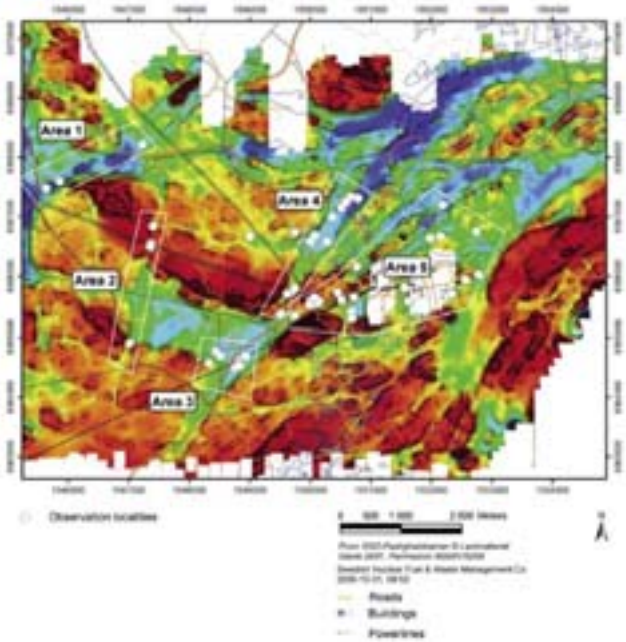

Distribution of outcrop locations examined as part of kineamatic studies. ZSMNE011A corresponds to Area 1 /Lundberg & Sjöström, 2006/.

The zone was investigated in the northwest most part of the Laxemar subarea. It included only three observation points, one of which is a likely breccia zone. The other two are from pervasive banded shear zones, one metre to a few metres wide. Around one of the zones, tens of metres of surrounding rocks are affected by deformation and a strong east-west foliation with unspecified dip occurs. All shear zones plot in the same part of the stereogram and the main shear zone strikes approximately 60°. Two shear zones display sinistral sense of shear.

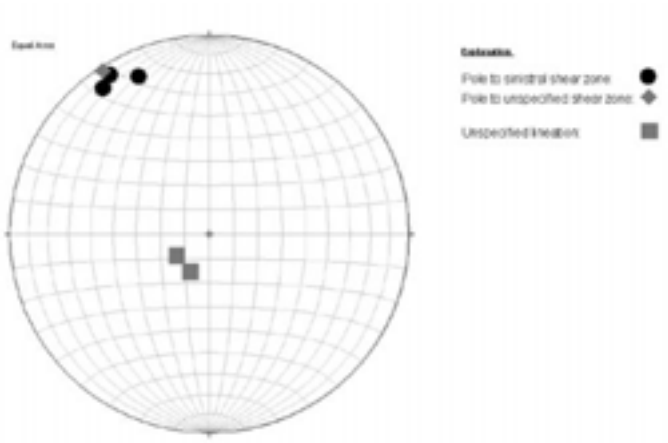

Distribution of shear zones and lineations in Area 1. Lower hemisphere of Schmidt equal
area, stereographic plot.

Outcrop PSM004118 Brittle ductile deformation ZSMNE011A

NE-SW striking deformation zones ZSMNE011A	
Modelling procedure: At the surface, corresponds to a major low magnetic belt and topographic lineament. Modelled to base of regional model volume using dip that has been inferred from outcrop mapping. Included in regional model and also present inside local model volume.	
Confidence of existence: High	

Property	Quantitative estimate	Span	Confidence level	Basis for interpretation	Comments
Position		± 25 m (surface)	High	Lineament –low magnetic belt	
Orientation (strike/dip)	0550/90	± 20/ 10	High for strike, High for dip	Strike based on trend of lineament. Dip based on outcrop mapping	
Thickness	100 m	± 50	Medium	Lineament –low magnetic belt	Ref: v0 /SKB, 2002/, 5–10 m 'cores' of highly fractured rock. 50–150 m wide transition envelope. Complex zone, inferred thickness refers to total zone thickness (splays, ductile and brittle, transition zones and core)
Transition zone			Low	Inferred from lineament – low magnetic belt	Considered not to be one single deformation zone but rather a belt with a high concentration of low-grade ductile to brittle-ductile shear zones with increased fracturing.
core			Low	Inferred from lineament – low magnetic belt	
Length (regional model)	10,5 km	10-12 km	Medium	Lineament –low magnetic belt	Possible extension to SW.
Ductile deformation	Yes		High	Evidence from outcrops. (mylonite)	Ductile-brittle zone. Dominantly ductile character but there has been clear reactivation.
Brittle deformation	Yes		High	Evidence from outcrops.	Clear local reactivation.

NE-SW striking deformation zones ZSMNE011A					
Alteration			High	Evidence from bounding outcrops	Red staining.
Fracture orientation	No information				
Fracture frequency	No data				
Fracture filling			High	Outcrop mapping	Epidote, Quartz
Sense of displacement	Sinistral strike slip		Medium	Field mapping	/Lundberg & Sjöström, 2006/

BH	Geometrical Intercept (bh. m)	Target intercept (bh. m)	Comment
None			No BH intercepts

ZSMNE012A

The zone has not been the subject of further review and the interpretation remains largely unchanged from v1.2. There has been a modification in its geometry and a significant change in its extent at depth due to a modification to the zone's termination to the south west. However, this does not alter any borehole, tunnel or geophysical intercepts but does give an improved fit with the results from in situ stress measurements in KLX12A, south east Laxemar. Previously the zone terminated against ZSMNW923A which itself was based on a lineament later judged to be associated with a major rock type boundary rather than a deformation zone and has subsequently been removed from the model. ZSMNE012A is now interpreted as extending slightly further to the south and terminates against an updated ZSMNW042A. This termination and south westerly extent of the zone is judged of low confidence. This general area is a complex meeting point of a number of major structures and the interaction between them is essentially unknown.

The zone extends from ZSMNW042A in the south to ZSMNE024A in northeast. The position and orientation of the zone is based on magnetic and topographic lineaments, seismic reflectors /Juhlin et al. 2004b/, refractions /Lindqvist 2004a/, boreholes and tunnel intercepts /Rhen et al. 1997/. The geological character is interpreted as a reactivated brittle-ductile shear zone with increased fracturing, alteration, breccias and mylonites. ZSMNE012A intersects the Äspö access tunnel at chainage 0/827 m and is locally named EW-7 and NE-4 at Äspö. The tunnel intercept, see figure below, is characterized by an 80 m thick inhomogeneous brittle-ductile deformation with cataclasites, crush, high alteration, clay filled faults and high transmissivity /Rhen et al. 1997/. Borehole intercepts at Äspö, Ävrö, Simpevarp and Laxemar indicate similar geology as well as increased transmissivity. Seismic reflector B1 and B2 /Juhlin et al. 2004b/ north of Ävrö correspond with the easterly extent of ZSMNE012A. This section of the zone was previously interpreted as ZSMNE004A, but was earlier re-assessed to be part of ZSMNE012A based on an alternative lineament interpretation. This is further indicated by refraction seismics by /Lindqvist 2004a/ which show low velocity zones in profiles LSM00192 and 193, see figure below. The strike derives from the surface lineament trend whereas the dip comes from the Äspö tunnel and from borehole intercepts at Äspö, Ävrö and Simpevarp. A modelled thickness of 120 m represents an envelope containing inferred sub-parallel splays. At Äspö this zone incorporates both EW-7 and NE-4.

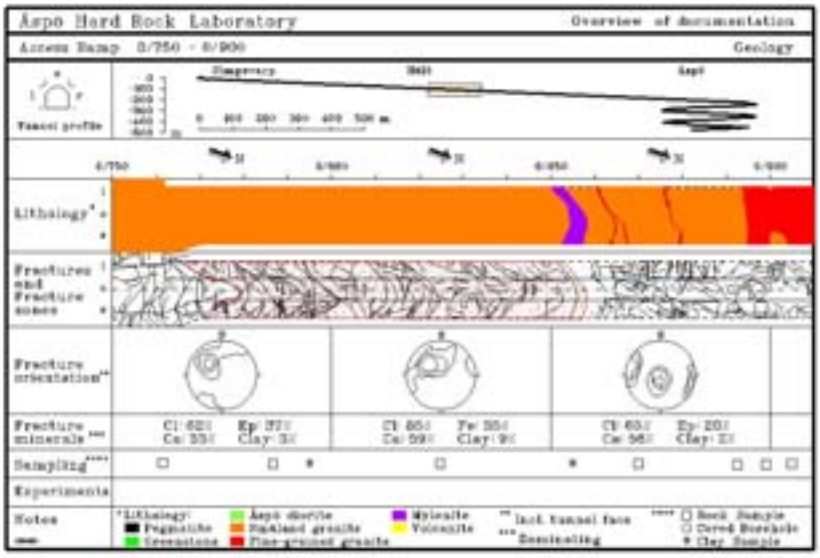

Intercept in Äspö access tunnel at chainage 0/827 m /PR-HRL-96-19/.

Seismic refraction studies on the Simpevarp peninsula and Ävrö island /Lindqvist 2004a/.

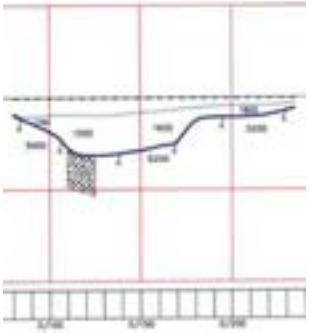

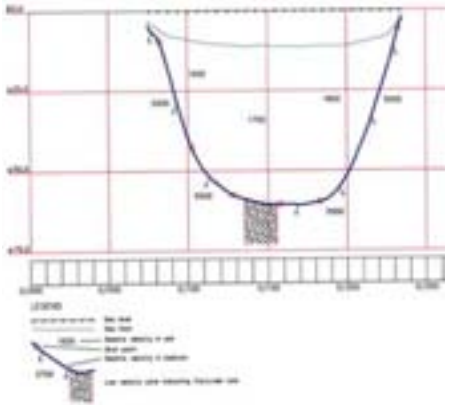

Seismic refraction profiles LSM00193 and LSM00192 /Lindqvist 2004a/. South is to the left in the figures. See Figure 4-47 for location.

NE-SW striking deformation zones ZSMNE012A	
Modelling procedure: At the surface, corresponds to low magnetic and topographic lineaments. Modelled to base of regional model volume using dip that has been inferred from outcrop mapping. Included in regional model and also present inside local model volume.	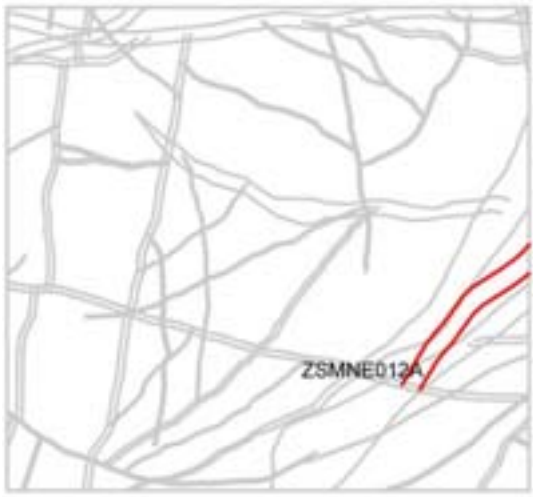
Confidence of existence: High	

Property	Quantitative estimate	Span	Confidence level	Basis for interpretation	Comments
Position		± 25 m (surface)	High	Linked lineament	
Orientation (strike/dip)	060/45	050-110/ ± 10	High for strike, medium for dip	Strike based on trend of lineament. Dip based on BH and tunnel (Äspö) intercepts.	Strike 060 within the local model area, curving to110 further north.
Thickness	120 m	60-120 m	High	Linked lineaments, BH and tunnel (Äspö) intercepts.	Model thickness of 120 m represents an envelope thickness containing narrower inferred splays. At Äspö this zone potentially incorporates both EW7 and NE4. Seismic refraction profiling indicate cores of fractured or altered rock with thicknesses of 15 to 20 m
core	15 m	10-20m	High	Seismic refraction profiling indicates cores of fractured or altered rock with thicknesses of 15 to 20 m and velocities of 2,500–3,300 m/s	
Length (regional model)	5,6 km	+/- 500 m	Low	Linked lineament	Termination of the zone both in the NE and SW are low confidence.
Ductile deformation	Yes		High	Mylonite on northern boundary (TASA)	Ductile-brittle zone.
Brittle deformation	Yes		Medium	Breccia and crushed mylonite.	

NE-SW striking deformation zones ZSMNE012A					
Alteration			High		Clay. Fracture fillings chlorite and epidote.
Fracture orientation	020/90, 110/20, 045/45, 60/90, 300/90		High	TASA	
Fracture frequency m^{-1}	9	Frac' frq' incl' crush = 20 fm^{-1}	High	KAV01, KAV04A, KBH02	
Fracture filling			High	KAV01, KAV04A, KBH02	Calcite, Chlorite, Epidote, Hematite, Quartz

BH and tunnel indications	Geometrical Intercept (bh. m)	Target intercept (bh. m)	Comment
HAV02	90-163 (base)	90-150	Penetration rate indicates fractured or weak rock from ca. 89–149 m depth.
HAV12	18-136	51-127	Penetration rate and BIPS indicate fractured or weak rock from c.51–76 m with posible extension to 93 m. Low permeability. Between c. 100–127 m is water bearing.
HAV13	0-121	-	
HLX17	1-22	-	
HLX18	1-181 (base)	16-181	Eshi DZ1 16,5-103m Scattered 2-10 m wide sections of increased fracture frequency and related fracture zone alterations. The section is characterized by minor caliper anomalies, partly low resistivity and several scattered sections of variable magnetic susceptibility. Penetration rate indicates fractured or weak rock between 16–115 m, c. 147–151 m and ca. 160–181 m. Water inflows at ca. 53 m (1.5 l/min), c.57 m (20l/min), c. 67 m (21l/min), c. 110 m (37–70 l/min) and c. 150 m (> 130 l/min).
HLX19	170-202	139-153	Eshi DZ1 139-153m Scattered c.1.5 m wide sections of increased fracture frequency and related fracture zone alterations. No interpretable radar reflectors below 130 m. The section is characterized by distinct caliper anomalies, partly low resistivity and an indicated decrease in p-wave velocity.
HMJ01	0-46 (base)	-	
KAV01	401-630	400-580	Increased fracturing; alteration; low susceptibility and resistivity; low density. Mapped minor shear zones, breccias and mylonites.
KAV03	188-248 (base)	164-232	SICADA: 183–185 m brittle-ductile shear zone.
KAV04A	756-928	840-900	Increased number of crush zones. The deformation zone is characterized by an inhomogeneous brittle-cataclastic deformation. The focused resistivity (300) is markedly low along the section ca. 860–900 m, but no other geophysical logging methods indicate significant anomalies.
KBH02	107-245	140-194	SICADA; 140.18 m–194.01 m code 42= Brittle-ductile shear zone.
KA0575A	126.4-160.1	-	Interpreted as EW7 and NE4 in /Rhen et al, 1997/. (TR 97-06)
KA0644B	68.2-119.7	-	Interpreted as EW7 and NE4 in /Rhen et al, 1997/. (TR 97-06)

ZSMNE018A

ZSMNE018A remains unchanged from version 1.2. The local major zone lies in the south east corner of the local model volume. At the surface, the zone corresponds to a low magnetic lineament and deformation indicators identified during outcrop mapping. The field mapping results and lack of a clear topographic lineament suggest the zone is predominantly low grade ductile. ZSMNE018A is considered to be a splay of the dominant plastic domain/deformation zone ZSMNE004A. Red staining, chlorite, epidote and quartz were also identified. The zone has a length of 1.3 km and a thickness of approximately 50 m with a strike varying between 070-090^{o}, the NE nomenclature has been retained for traceability from an earlier more extensive interpretation of the zone. The zone has a modelled dip of 90^{0} with an estimated span from vertical to 60^{0} to the south based on filed mapping. The zone is not included in the regional model. ZSMNE018A has not been the subject of focused investigation by either direct or indirect methods.

NE-SW striking deformation zones ZSMNE018A	
Modelling procedure: At the surface, corresponds to a low magnetic lineament and outcrop deformation indicators. Modelled to base of local model volume using dip that has been inferred from field mapping. Not included in the regional model.	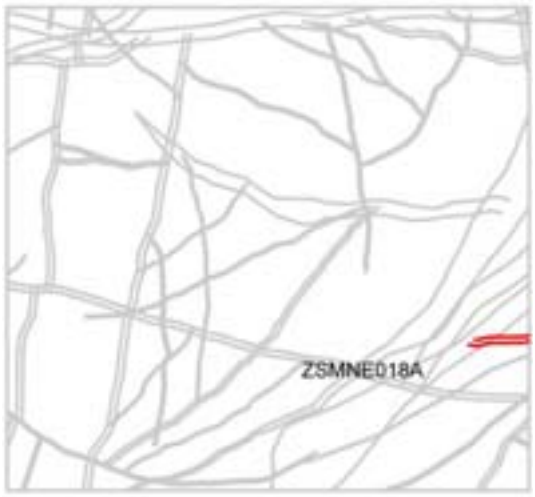
Confidence of existence: High	

Property	Quantitative estimate	Span	Confidence level	Basis for interpretation	Comments
Position		± 15 m (surface)	High	Lineament and outcrop mapping	
Orientation (strike/dip)	079/90	070-090/ 90-60S	Medium for strike and dip	Strike based on trend of lineament. Dip based on outcrop mapping.	
Thickness	50 m	30-80 m	Medium	Lineament and outcrop mapping	Thickness refers to total zone thickness (transition zone and core)
Length (regional model)	1.3 km	± 100 m	Medium	Linked lineaments	
Ductile deformation			High	Outcrop low grade ductile indicators	Ductile-brittle.
Brittle deformation			Medium	Weak outcrop indicators	Dominantly ductile.
Alteration			High	Outcrop mapping	Red staining, chloritization
Fracture orientation					No data
Fracture frequency Open/sealed m^{-1}					No data
Crush zone Number/total m					No data

NE-SW striking deformation zones ZSMNE018A					
Fracture filling			High	Outcrop mapping	Chlorite, epidote, pyrite, quartz.
Kinematics			Medium	Outcrop mapping	Sinistral

BH	Geometrical Intercept (bh. m)	Target intercept (bh. m)	Comment
None			No BH intercepts

ZSMNE019A

The zone has not been the subject of a detailed further review and the interpretation and resulting geometry remains largely unchanged from v1.2. There has been a modification to its modelled thickness from 5 m to 20 m based on updated background geophysical and later field mapping data. The zone is interpreted to be a brittle-ductile deformation zone with a length of ca. 3.7 km and a thickness of 20 m including transition zones. This interpretation is based on the topographic and magnetic lineaments, field mapping evidence and ground geophysics /Triumf et al, 2003/. There are no BH interceptions.

NE-SW striking deformation zones ZSMNE019A	
Modelling procedure: At the surface, corresponds to the low magnetic and topographic lineaments. Modelled to base of regional model volume using an assumed vertical dip. Included in regional model and also present inside local model volume.	
Confidence of existence: High	

Property	Quantitative estimate	Span	Confidence level	Basis for interpretation	Comments
Position		± 20 m (surface)	Medium	Linked lineament.	Poorly constrained by outcrops.
Orientation (strike/dip)	055/90	±10/ ±20	High for strike, low for dip	Strike based on trend of lineament. Dip assumed	Triumf et al, 2003/. Poorly constrained by outcrops.
Thickness	20 m	5-30 m	medium	Lineament and geophysical ground survey	Ground geophysical information is local to the northern end of the zone. Triumf et al, 2003/
Length (regional model)	3.7 km	± 200 m	Medium	Linked lineaments	
Ductile deformation	Yes		Medium	Outcrop mapping foliation, brittle-low grade ductile indicators	Poor spread of data.
Brittle deformation	Yes		Medium	Outcrop mapping, raised fracture frequency.	Poor spread of data.
Alteration			High	Outcrop mapping	Weak red staining.
Fracture orientation	No data				
Fracture frequency Open/sealed m^{-1}	No data				
Crush zone Number/total m	No data				
Fracture filling			High	BHs	Epidote

NE-SW striking deformation zones ZSMNE019A			
BH	**Geometrical Intercept (bh. m)**	**Target intercept (bh. m)**	**Comment**
None			No BH intercepts

ZSMNE021A

ZSMNE021A remains unchanged from version 1.2. The local major zone intercepts the south east corner of the local model volume. At the surface, the zone corresponds to a low magnetic and topographic lineament. The zone is not completely covered by airborne magnetic or topographic mapping and its southerly extent is essentially unknown. The zone has not been the focus of detailed investigation by either direct or indirect methods. The zone has a modelled length of 4.6 km with a thickness of approximately 40 m and a strike of around 030^0. The dip and dip direction of ZSMNE021A are very uncertain. The zone could be part of the ZSMNE024A major tectonic belt, in which case a westerly dip would be most likely or could be more closely associated with the plastic domains, in which case a sub vertical to easterly dip would be most likely.

NE-SW striking deformation zones ZSMNE021A	
Modelling procedure: At the surface, corresponds to a low magnetic and topographic lineament. Modelled to base of the regional model volume using an assumed vertical dip. Included in the local model volume.	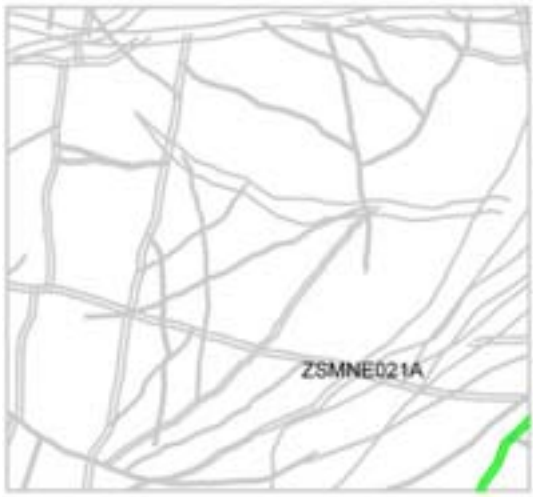
Confidence of existence: Medium	

Property	Quantitative estimate	Span	Confidence level	Basis for interpretation	Comments
Position		± 25 m (surface)	Medium	Topographic and magnetic lineament	
Orientation (strike/dip)	032/90	± 15/ ±30	Medium for strike and low for dip	Strike based on trend of lineament. Dip assumed.	Dip and dip direction are very uncertain. The zone could be part of the ZSMNE024A major tectonic belt, in which case a westerly dip would be most likely or could be more closely associated with the plastic domains, in which case a sub vertical to easterly dip would be most likely.
Thickness	40 m	20-60 m	Medium	Topographic and magnetic lineament	
Length (regional model)	4.7 km	>4.7 km	Medium	Linked lineaments	The southern extent of the zone is essentially unknown.
Ductile deformation					No data. Could be brittle if associated with the ZSMNE024A tectonic belt or could be dominantly plastic if associated with the plastic domains.
Brittle deformation					No data
Alteration					No data
Fracture orientation					No data

NE-SW striking deformation zones ZSMNE021A					
Fracture frequency Open/sealed m^{-1}					No data
Crush zone Number/total m					No data
Fracture filling					No data
Kinematics					No data

BH	Geometrical Intercept (bh. m)	Target intercept (bh. m)	Comment
None			No BH intercepts

ZSMNE024A

The interpreted geometry and characterization of the regional deformation zone, ZSMNE024A, remains unchanged from that presented in Simpevarp version 1.2 /SKB, 2005/. This zone should be viewed together with ZSMNE031A. Together they define a broad complex structural band of deformation off the coast of Ävrö. The interpretation has the zones dipping parallel at 52° NW. This dip is based on the seismic reflection results /Juhlin et al, 2004/ and taking the single hole interpretation for KSH03 as the primary constraint. The zones existence is further supported by the seismic refraction survey /Lindqvist, 2004/. The zone has been modelled with a width of 80m though this has a high uncertainty due to the potential complex nature of the zone and interaction with ZSMNE031A and other splays.

Projected reflector intersections with the surface for those reflectors which project up to the surface. Picked reflectors correspond to the tops of the reflector. Reflectors are coded as follows: red-rank 1, blue-rank 2, green-rank 3. ZSMNE024A and ZSMNE031A correspond to the A series of reflectors parallel with the coast of Ävrö.

NE-SW striking deformation zones ZSMNE024A	
Modelling procedure: At the surface, corresponds to the low magnetic and topographic lineaments. Modelled to base of regional model volume using dip that has been inferred mainly from a seismic reflector /Juhlin et al. 2004/ and KSH03A. Included in regional model and very marginally present at the base of the local model volume.	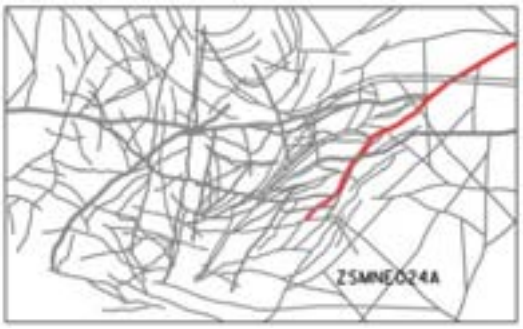
Confidence of existence: High	

Property	Quantitative estimate	Span	Confidence level	Basis for interpretation	Comments
Position		± 20 m (surface)	High	Lineament, BH and geophysical survey	This zone should be viewed together with ZSMNE031A. Together they define a broad complex structural belt of deformation off the coast of Ävrö.
Orientation (strike/dip)	225/52	± 10/ 215-235	High for strike, medium for dip	Strike based on trend of lineament. Dip based on seismic reflector, and boreholes.	
Thickness	80 m	± 20 m	Low	Lineament, BH and geophysical survey	Model thickness of 80 m represents an envelope thickness containing narrower inferred splays. OKG suggests fractured cores 2 to 10 m thick. Seismic refraction profiling indicates cores of fractured or altered rock with thicknesses of up to 30 m and velocities of 3,400–4,200 m/s. This zone should be seen as contributing to a broader tectonic belt.
Length (regional model)	11.6 km	10 to 15++ km	Medium	Linked lineaments	Lineament data for ZSMNE024A and ZSMNE031A suggests this deformationbelt extends beyond the boundaries of the regional model area.
Ductile deformation	Yes		High	BHs	
Brittle deformation	Major		High	BHs and tunnel evidence.	
Alteration			High	OKG	Noted as ‘highly weathered’ – OKG. Chloritization
Fracture orientation	-				

NE-SW striking deformation zones ZSMNE024A					
Fracture frequency m^{-1}	13		Medium	KSH01A, KSH03A, KAV01A, KAV04A	Frac' frq'incl' crush (= 20 frac/m) (m^{-1})
Fracture filling			High		Calcite, chlorite, epidote, hematite, quartz.
Kinematics	-				

BH- tunnel intercept	Geometrical Intercept (bh. m)	Target intercept (bh. m)	Comment
OKG			Moderately water bearing, highly weathered.
HAV11	95-178	124-180	Penetration rate and BIPS figs' indicate fractured or weaker rock from c. 124–180 m; water bearing measured at 145 m c. 32 l/min and judged to originate from c. 129–142 m.
KSH01A	542-669	540-631	DZ6, 540–609 m Partly increased fracturing. Partly heavy alteration. Indication: Low susceptibility, low resistivity.DZ7 609–614 m, low-grade, ductile shear-zone.DZ8, 614–631 m, Partly increased fracturing. Partly heavy alteration. Indication: Low susceptibility, low resistivity.
KSH03A	175-258	162-275	Inhomogeneous, low-grade, ductile deformation. High frequency of open and sealed fractures and crush zones. Brecciation between 220–235 m and mylonitization between 270–275 m. Marked low resistivity and, where available, lower sonic. Sonic data are missing between 203.5–255.2 m. Distinct, major caliper anomaly. Generally low magnetic susceptibility. A number of sections with increased fracturing may indicate minor deformation zones.
KAV01A	674-757 (Base)	660-757	Single hole interpretation includes no clear DZ in this location. However, examination of the log suggests that it is not unreasonable to suggest indicators are present.
KAV04A	937-1004	940-1004	Single hole interpretation gives DZ1 840–900 m with the description: Increased number of crush zones. The deformation zone is characterized by an inhomogeneous brittle-cataclastic deformation. The focused resistivity (300) is markedly low along the section c. 860–900 m, but no other geophysical logging methods indicate significant anomalies. Note that ZSMNE012A is modelled with an interception from 840–900 m. Examination of the log suggests that it is not unreasonable to suggest deformation indicators continue below 900 m of KAV04A.

ZSMNE040A

ZSMNE004A remains unchanged from version 1.2. The zone is indicated through topographic and airborne geophysical lineaments, and is also weakly supported by anomalies in geophysical profiles /Thunehed et al. 2004/. A seismic reflection survey by /Bergman et al. 2001/ suggests a reflector with a matching surface intercept to the lineament but with very weak indications for an intercept with KLX01A. The generally brittle zone has been modelled with a length of 1.6 km and a thickness of 20 m and is inferred from a seismic refraction survey to have a c. 5 m thick core of more highly fractured rock /Lindqvist, 2004/. Evidence from bordering outcrops indicates that alteration consists of epidote, chlorite and red staining.

Geophysical profiling identified a low-magnetic structure that corresponds well with the ZSMNE040A position /Thunehed et al. 2004/. The inverted resistivity and chargeability sections identifed a low-resistivity structure that also coincides approximately with the position of the interpreted zone. The results suggest a width of the structure of around 20 m. The dip appears to be steep although somewhat uncertain.

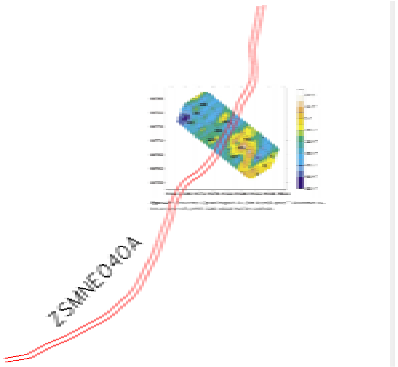

Contour map of ground magnetic data from the profile group 7crossing ZSMNE040A.

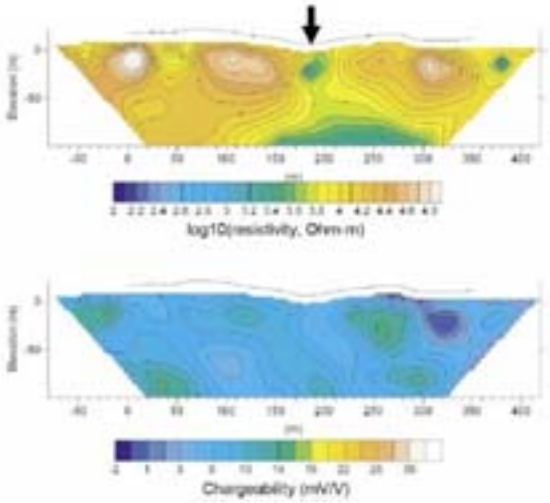

Inverted resistivity (top) and chargeability (bottom) sections for the central profile of the profile group 7 (LSM000282). The black lines show elevation data along the profile. Note that the coordinate 0 starts in south-east.

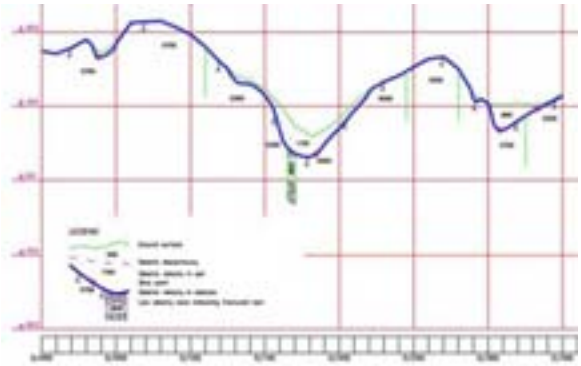

Results from interpretation of refraction seismics in Laxemar. Line LSM000282.

NE-SW striking deformation zones ZSMNE040A	
Modelling procedure: At the surface, corresponds to topographic and magnetic linked lineament. Modelled using a dip inferred from magnetic and resistivity ground profiling results. Included in the regional model and present inside local model volume.	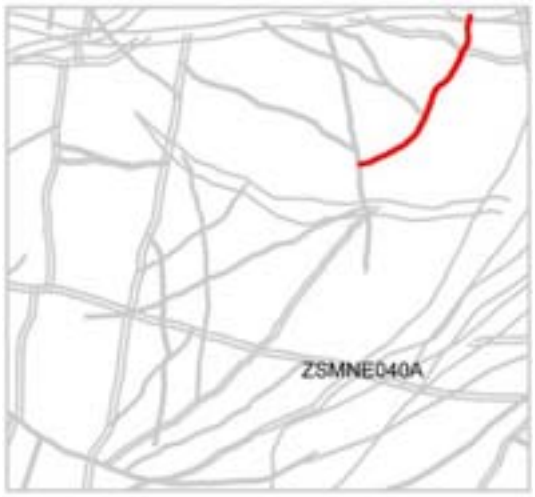
Confidence of existence: High	

Property	Quantitative estimate	Span	Confidence level	Basis for interpretation	Comments
Position		± 10 m (surface)	High	Linked lineament,	
Orientation (strike/dip)	030/90	± 10/± 10	High/medium	Strike based on trend of lineament. Dip based on outcrop mapping and geophysical profiling	Modelled as vertical to allow for local variations. However, resistivity profiling weakly indicates a steep (80) dip to SE) /Thunehed et al, 2004/
Thickness	20 m	5-20 m	Medium	Magnetic, resistivity and seismic refraction profiling.	/Thunehed et al, 2004/ /Lindqvist, 2004/
core	5m	1-7m		Seismic refraction profiling.	/Lindqvist, 2004/
Length (regional model)	1.6 km	± 50 m	Medium	Linked lineaments	
Ductile deformation	Yes		High	Outcrop mapping	
Brittle deformation	Yes		High	Outcrop mapping and seismic refraction survey	
Alteration			Medium	Outcrop mapping	Red staining.
Fracture orientation	015/78, 245/83, 040/90		Medium	Outcrop mapping	
Fracture frequency	No data				
Fracture filling			Medium	Outcrop mapping	Chlorite, epidote,

BH	Geometrical Intercept (bh. m)	Target intercept (bh. m)	Comment
HLX01	0-31.1	-	No information available
HLX04	21.0-82.0	-	No information available

ZSMNE063A

At the surface, the zone corresponds to poorly defined low magnetic and topographic lineaments. The zone is modelled with a length of 1.1 km and a thickness of 10 m. Modelling of magnetic data /Mattsson and Triumf/ 2007 suggests a dip that varies from steep to the southeast to vertical. The zone has been assigned a vertical dip in the model. The lineament has not been investigated by drilling or any other direct method. Based on similarly oriented zones ZSMNE063A is assumed to be a narrow originally low grade ductile structure that has been subject to brittle reactivation.

NE-SW striking deformation zones ZSMNE063A	
Modelling procedure: At the surface, corresponds to poorly defined low magnetic and topographic lineaments. Modelled to base of local model volume. Vertical dip is assumed. Not included in regional model.	
Confidence of existence: Medium	

Property	Quantitative estimate	Span	Confidence level	Basis for interpretation	Comments
Position		± 30 m (surface)	Medium	Lineament	Poorly constrained lineament. Local alternative variations in trace position are possible
Orientation (strike/dip)	040/90	± 10/ ±20	Medium for strike, low for dip	Strike based on trend of lineament. Dip based on magnetic modelling.	/Mattsson and Triumf/ 2007
Thickness	10 m	5-20 m	Low	Poorly restricted by outcrop mapping	Only inferred thickness. Poorly constrained lineament.
core	1 m	0-2 m	Low	Inferred association with NE-SW trending structures	
Length (regional model)	1.1 km	0.5- 1.2 km	Low	Linked lineaments	Continuity of lineament-structure is questionable
Ductile deformation			Medium	Inferred association with NE-SW trending plastic domains	No evidence from immediate bounding outcrops
Brittle deformation	yes		Low	Inferred from other NE-SW trending zones	Brittle-ductile
Alteration	yes		Low	Inferred from other NE-SW trending zones	Brittle-ductile
Fracture orientation	220/85, 100/65, 250/30, 025/20		Low	Parallel NE107A fracture orientations	
Fracture frequency	No data				
Fracture filling	Oxide, epidote, prehenite		Low	Inferred from presumed brittle-ductile character	

NE-SW striking deformation zones ZSMNE063A					
Kinematics	-				

BH	Geometrical Intercept (bh. m)	Target intercept (bh. m)	Comment
None			No BH intercepts

ZSMNE065A

At the surface, corresponds to low magnetic and topographic lineaments. The zone is modelled with a length of 1.4 km and a thickness of 10 m. The zone has a vertical dip in the model. The lineament has not been investigated by drilling or any other direct method. Based on similarly oriented zones ZSMNE065A is assumed to be a narrow originally low grade ductile structure that has been subject to brittle reactivation.

NE-SW striking deformation zones ZSMNE065A	
Modelling procedure: At the surface, corresponds to poorly defined low magnetic and topographic lineaments. Modelled to base of local model volume. Vertical dip is assumed. Not included in regional model.	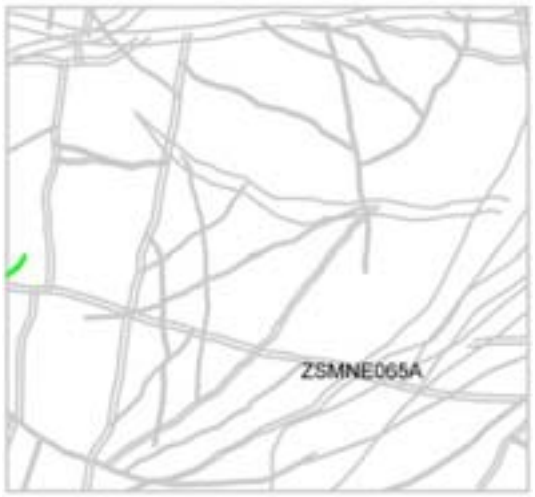
Confidence of existence: Medium	

Property	Quantitative estimate	Span	Confidence level	Basis for interpretation	Comments
Position		± 30 m (surface)	Medium	Lineament	
Orientation (strike/dip)	057/90	± 10/ ±20	Medium for strike, low for dip	Strike based on trend of lineament. Dip assumed	
Thickness	10 m	5-20 m	Low		Only inferred thickness. Poorly constrained lineament.
core	1 m	0-2 m	Low	Inferred association with NE-SW trending structures	
Length (regional model)	1.4 km	± 100	Low	Linked lineaments	
Ductile deformation			Medium	Inferred association with NE-SW trending plastic domains	
Brittle deformation	yes		Low	Inferred from other NE-SW trending zones	Brittle-ductile
Alteration	yes		Low	Inferred from other NE-SW trending zones	Brittle-ductile
Fracture orientation	220/85, 100/65, 250/30, 025/20		Low	Parallel NE107A fracture orientations	
Fracture frequency	No data				
Fracture filling	Oxide, epidote, prehenite		Low	Inferred from presumed brittle-ductile character	

BH	Geometrical Intercept (bh. m)	Target intercept (bh. m)	Comment
None			No BH intercepts

ZSMNE079A

ZSMNE079A remains unchanged from version 1.2. The local major zone intercepts the western margin of the local model volume. At the surface, the zone corresponds to low magnetic and topographic lineaments. The zone has not been the focus of detailed investigation by either direct or indirect methods. The zone has a modelled length of 2.7 km with a thickness of approximately 10 m and a strike of around 072^0. The zone is modelled with a vertical dip from an assumed ductile origin and inferred association with ZSMNE011A to the west.

NE-SW striking deformation zones ZSMNE079A	
Modelling procedure: At the surface, corresponds to a low magnetic and topographic lineament. Modelled to base of the regional model volume using an assumed vertical dip. Included in the local model volume.	
Confidence of existence: Medium	

Property	Quantitative estimate	Span	Confidence level	Basis for interpretation	Comments
Position		± 25 m (surface)	Medium	Topographic and magnetic lineament	
Orientation (strike/dip)	072/90	± 15/ ±15	Medium for strike and low for dip	Strike based on trend of lineament. Dip inferred from assumed ductile origin and inferred relationship to ZSMNE011A.	
Thickness	10 m	5-20 m	Medium	Topographic and magnetic lineament	
Length (regional model)	2.7 km	2.5-3.0 km	Medium	Linked lineaments	.
Ductile deformation	Yes		Low	Weak field indicators	Inferred ductile-brittle zone
Brittle deformation	Yes		Low	Weak field indicators	Inferred ductile-brittle zone
Alteration			High	Outcrop mapping	Red staining
Fracture orientation					No data
Fracture frequency Open/sealed m^{-1}					No data
Crush zone Number/total m					No data

NE-SW striking deformation zones ZSMNE079A					
Fracture filling			High	Outcrop mapping	Quartz,
Kinematics					No data

BH	Geometrical Intercept (bh. m)	Target intercept (bh. m)	Comment
None			No BH intercepts

ZSMNE107A

This zone's trace on the ground surface has been significantly extended and adjusted from v1.2 based on a further lineament review and a more detailed magnetic ground survey. Previously the zone had a northern termination against ZSMNW042A, whereas now the zone continues north eastwards and terminates against ZSMEW007A. In a similar fashion to many NE-SW trending structures field mapping suggests this zone is associated with both fine grained granite and composite dykes. Whilst field mapping indicates the dykes are a complex series with varying dip to the NW or SE forward modelling of magnetic data along the zone both to the north and south of ZSMNW042A show a consistently steep dip to the northwest. Field and drill core mapping show the zone to have a low grade ductile origin with subsequent brittle reactivation.

The lineament is crossed by three seismic refraction profiles all of which identify narrow, 5 to 7m wide low velocity anomalies taken to represent the thickness of a more highly fractured core zone /Lindqvist 2004, 2006/.

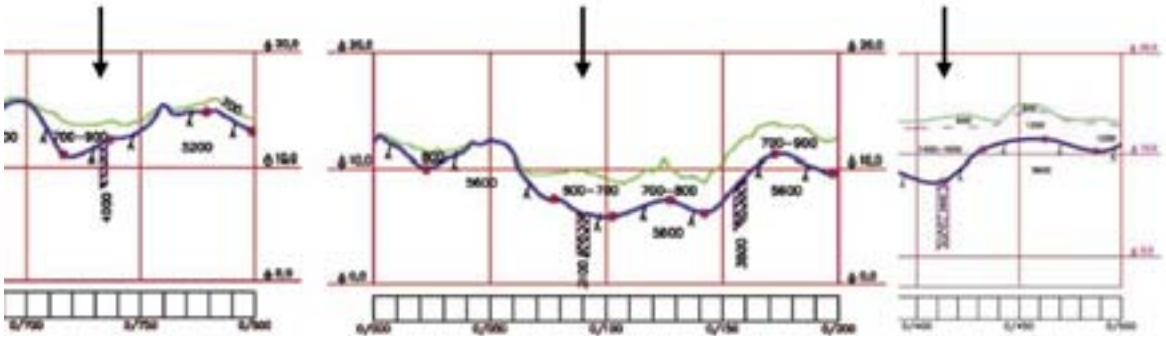

LSM000556 (North) LSM000566 (South) /Lindqvist, 2006/. LSM000506 (Central) /Lindqvist, 2004/.

NE-SW striking deformation zones ZSMNE107A	
Modelling procedure: At the surface, corresponds to the low magnetic and topographic lineaments. Modelled to base of regional model volume using dip that has been inferred from KLX16 and KLX15 along with forward modelling of magnetic data /Mattsson and Triumf 2007/. Included in regional model and also present inside local model volume.	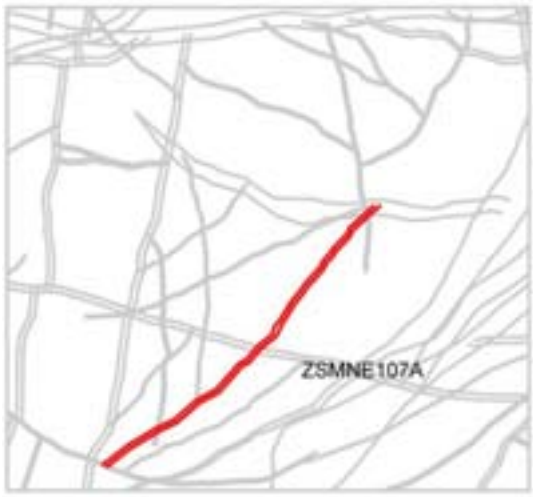
Confidence of existence: High	

Property	Quantitative estimate	Span	Confidence level	Basis for interpretation	Comments
Position		± 30 m (surface)	High	Lineament, BH and geophysical modelling	Local alternative variations in trace position are possible
Orientation (strike/dip)	225/80	± 10/ 10	High for strike, medium for dip	Strike based on trend of lineament. Dip based on boreholes and geophysical modelling.	
Thickness	35 m	10-40 m	High	Lineament, BH and geophysical ground survey	Thickness refers to total zone thickness (ductile and brittle, transition zone and core)
core	5 m	0-10 m		Bhs	Drill core shows multiple narrow ca.20 cm cores while seismic refraction anomalies indicate that the overall core of more highly fractured rock is in the order of 5m.
Length (regional model)	3.1 km	+/- 100 m	Medium	Linked lineaments	Possible break at ZSMNW042 that would give an interpretation as two separate structures would halve the length.
Ductile deformation			High	BHs brittle-low grade ductile indicators	Present
Brittle deformation			High	Cataclasites and breccia in BHs	Present
Alteration			High	KLX15, KLX16	Red staining and saussuritization.

NE-SW striking deformation zones ZSMNE107A					
Fracture orientation	220/85, 100/65, 250/30, 025/20		High	KLX15, KLX16	
Fracture frequency* Open/sealed m^{-1}	7/12		Medium	KLX15, KLX16	
Crush zone Number/total m	0/0		Medium	KLX15, KLX16	
Fracture filling			High	KLX15, KLX16	Calcite, chlorite, hematite, clay, epidote, prehnite, pyrite, geothite, laumontite, adularia
Kinematics			Ref: KLX15, Eshi DZ16, Viola et al,2007/: throughout the logged interval, but particularly below depth 730 m, several striated planes were observed, measured and constrained kinematically. The results are shown below. 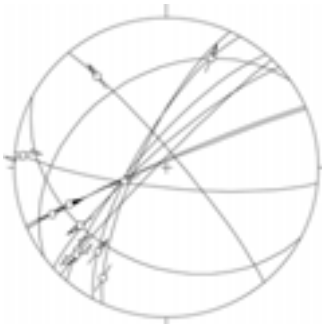 Fault-slip data for DZ 16, mostly observed below depth 730 m. Although no clear kinematic pattern emerges, it is noteworthy that most of the striated surfaces show strike-slip kinematics and there is a general lack of down-dip or highly oblique displacement vectors.4		

BH	Geometrical Intercept (bh. m)	Target intercept (bh. m)	Comment
HLX10	79.3-85.0 (Base)	-	No data
KLX02	682.31-1148.77	770-960	Eshi DZ1 770-960 m: generally increased frequency of open fractures and higher oxidation. The most intensive part of the zone is located between 845–880 m, which is indicated by distinct low p-wave velocity and partly somewhat lower resistivity. Nine radar reflectors from directional antenna have been found within the zone. The orientations of the reflectors are 29–61°/047–086. Most of them are dipping around 50°.

BH	Geometrical Intercept (bh. m)	Target intercept (bh. m)	Comment
			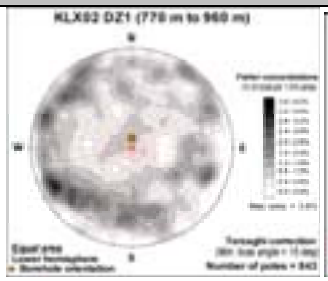 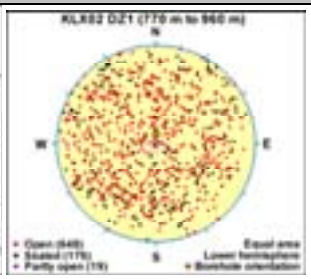
KLX15A	692.72-761.99	711-744	Eshi DZ16 711-744 m: inhomogeneous deformation zone characterized by brittle and brittle-ductile deformation. Increased frequency of sealed fractures, sealed fracture network and slight increase in open fractures, eight slickensides, partly weak to medium red staining. The most intensely deformed sections (cores) are: 711.36-711.60 m, 714.08-714.23 m, 717.85-718.60 m, 731.68-732.55 m and 743.10-743.76 m. Significant decrease in magnetic susceptibility along the major part of the section. Decreased resistivity at the section coordinates 711.7 m, 714.2 m, 716.4 m, 718.5 m, 725.5-726.5 m, 732.0 m, 734.2 m and 738.0-747.0 m. There is also decreased P-wave velocity in the section 717.5-719.0 m. Four oriented and sixteen non-oriented radar reflectors occur within DZ16. The oriented reflectors occur at 718.1 m (256/65 or 333/31), at 714.9 m (248/76 or 358/34), at 737.8 m (247/62 or 337/40) and at 743.4 m (225/75). 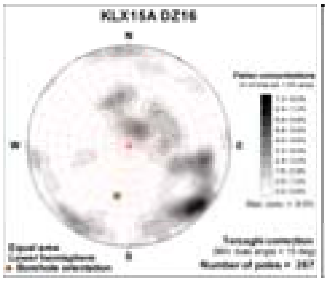 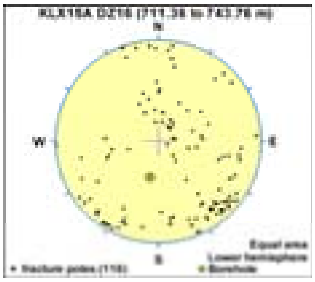 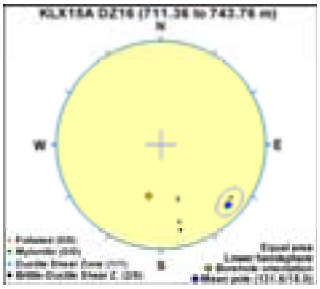 /Viola et al, 2007/ : The main rock type is a medium-grained, homogeneous quartzmonzonite, locally intruded by coarse-grained pegmatites. Red staining is diffuse and is invariably associated with localized shearing and brittle faulting. Long sections of it are made of by basically undeformed quartzmonzonites without any evidence of significant structural overprinting.

BH	Geometrical Intercept (bh. m)	Target intercept (bh. m)	Comment
			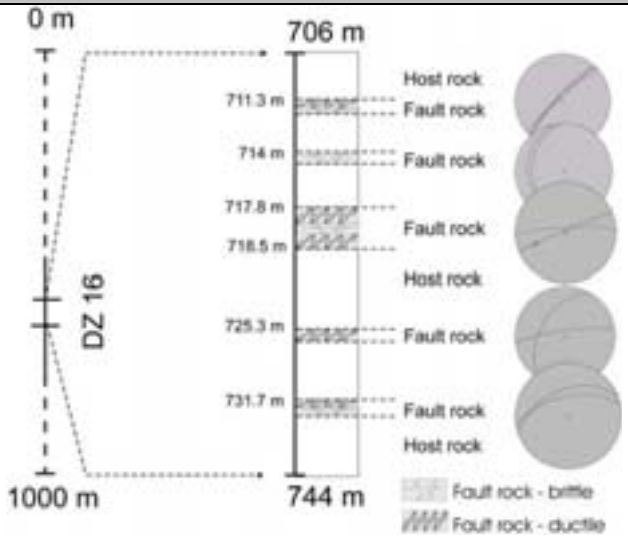 *Schematic structural log of DZ 16 in KLX15A* Four distinct fault cores at different depth within DZ 16 none exceed 50 cm in thickness. The first 25 cm thick ductile foliated sequence occurs at depth 711.379 m. Its upper limit coincides to the lower contact of a thin pegmatite that intrudes into undeformed quartzmonzonites. 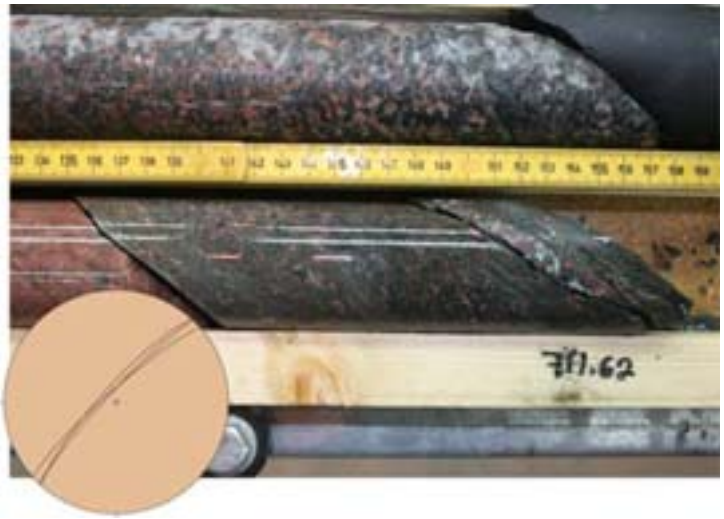 *Pervasively foliated sequence at depth 711.38 m. Foliation planes strike NE-SW and dip subvertically to the NW. A c. 4 cm thick cataclastic band marks the lower termination of the foliated sequence.* /Viola et al, 2007/ The pervasive foliation dips subvertically to the NW. At the lower end of the foliated interval there occurs a c. 4 cm thick cataclastic band. The deformation core ends at depth 711.54, and is not followed by a well-defined transition zone. A second, distinct thin core is found at depth 714.09 m, where a series of sub parallel broken fractures oriented c. NS and dipping moderately to the W define the upper limit of a c. 15 cm thick fault rock sequence containing several strands of ultracataclasite/gouge. Abundant pyrite is found coating the broken fracture surfaces.

BH	Geometrical Intercept (bh. m)	Target intercept (bh. m)	Comment
			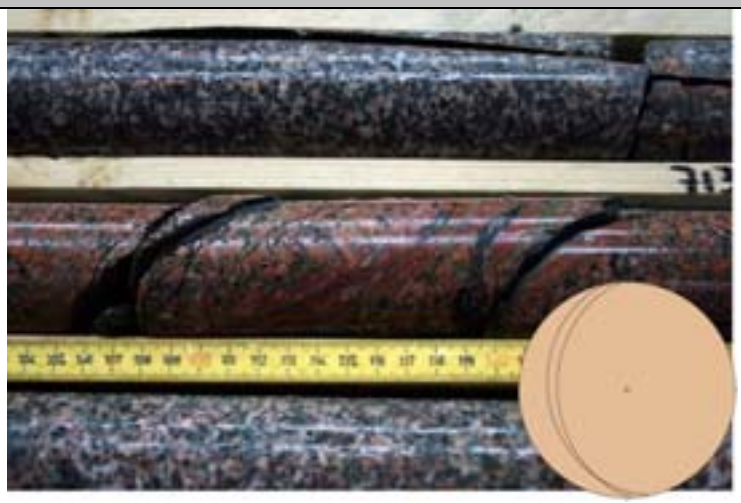 *NS striking and W dipping fractures and cataclasite/gouge bands at depth 714 m.* Another minor core starts at depth 717.86 m and is formed by pervasively foliated quartzmonzonites oriented 267/82. At the upper contact of the foliated interval, the quartzmonzonites are intruded by a pegmatite, which is in turn reworked cataclastically. Late calcite veins crosscut the contact and their associated dilation creates small pockets of coarse calcite-cemented breccias. A striated plane in the middle of the foliated interval shows dextral transpressive shearing along a subvertical ENE-WSW striking plane (black great circle in figure. No obvious transition zone is observed either above or below this narrow DZ core. /Viola et al, 2007/ 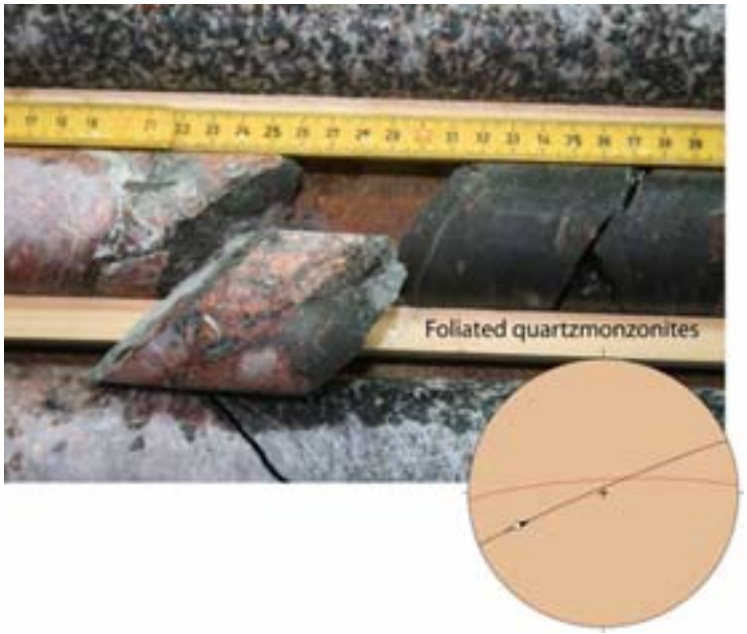 *Pervasively foliated quartzmonzonites at depth 717.8 m dip subvertically to the N (red great circle). Their upper contact to a thin pegmatitic intrusion is disrupted by cataclasis and dilatant calcite veins. The dextral transpressive kinematics shown by the black great circle and its associated striation was measured in the middle of the foliated interval.* /Viola et al, 2007/
KLX16	221-410	228-434	Eshi 228-231 m DZ9: Low-grade ductile shear zone. Increased frequency of open and sealed fractures, apertures =3 mm, minor crush and faint to weak red staining. There is significantly decreased resistivity and magnetic susceptibility. There is also partly decreased P-wave velocity and one minor

BH	Geometrical Intercept (bh. m)	Target intercept (bh. m)	Comment
			caliper anomaly. One oriented radar reflector occurs at 230.1 m with the orientation 072/85 or 268/55. The reflector is of medium strength and can be observed to a distance of 10 m outside the borehole. 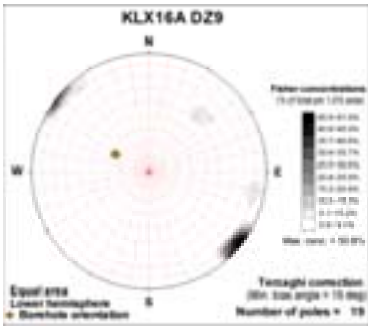 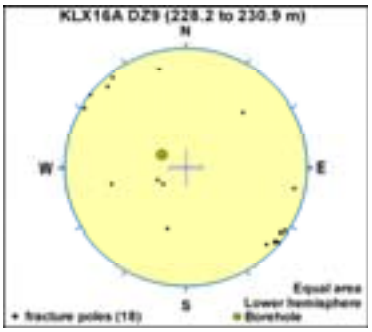 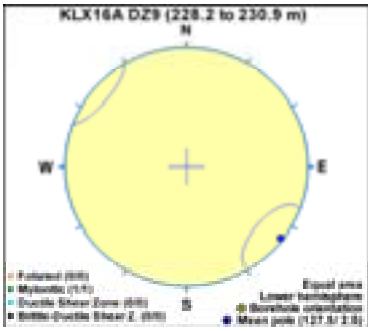 Eshi 252-254 m DZ10: Low-grade ductile shear zone. Increased frequency of sealed fractures and slight increase in open fractures. The DZ is characterized by decreased resistivity and magnetic susceptibility. 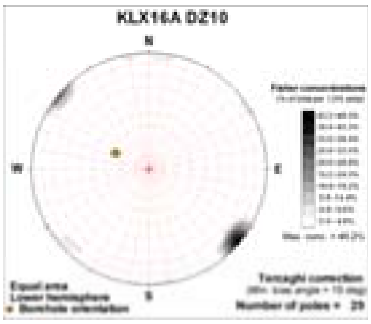 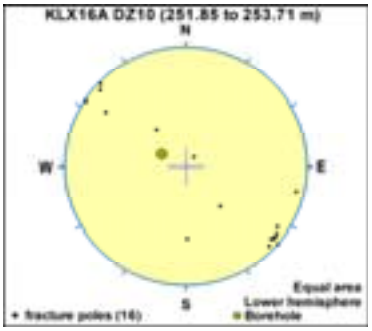 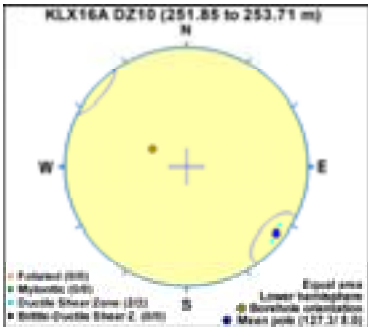 Eshi 259-266 m DZ11: Brittle deformation zone characterized by increased frequency of open and sealed fractures, apertures =5 mm, slickensides, minor crush, weak red staining and faint saussuritization. The DZ is characterized by decreased resistivity and magnetic susceptibility. There is also partly decreased P-wave velocity and one minor caliper anomaly. Two oriented and one non-oriented radar reflector occur within DZ11. The oriented reflectors occur at 260.8 m with the orientation 248/89 and at 264.6 m with the orientation 335/41. The reflectors are medium to strong and can be observed

BH	Geometrical Intercept (bh. m)	Target intercept (bh. m)	Comment
			to a distance of 15 m and 18 m outside the borehole, respectively. The non-oriented reflector occurs at 263.6 m with the angle 72° to borehole axis. 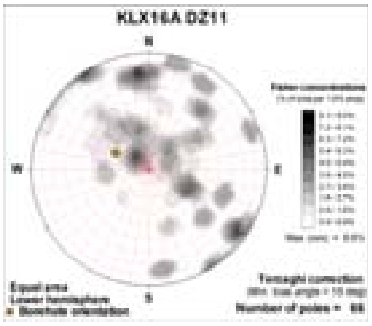 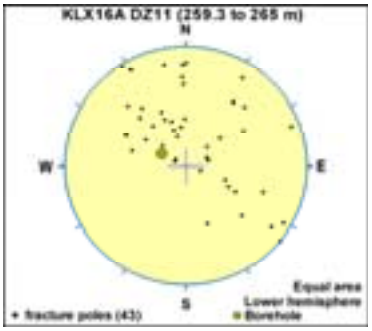 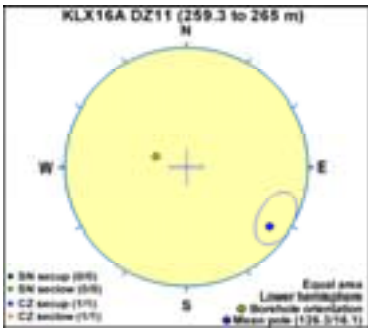 Eshi 327-434 m DZ12: Inhomogeneous brittle deformation zone including overprinting of scattered low-grade ductile shear zones. The most intensely deformed section is 327-381 m, which is characterized by marked increase in frequency of sealed fractures, increased frequency of open fractures, numerous slickensides, frequent cataclasites, inhomogeneous faint to medium red staining and saussuritization. The section 381-433.5 m (transition zone) is characterized by increased frequency of sealed fractures, slight increase in open fractures, slickensides, occasional cataclasites and faint to medium red staining and saussuritization. The entire DZ is characterized by an increased number of sections with decreased resistivity, magnetic susceptibility and P-wave velocity. The highest concentration of geophysical anomalies occurs in the core zone. In the section 338-345 m the resistivity is anomalously low, there is significantly decreased P-wave velocity and there are several caliper anomalies. Three oriented radar reflectors occur at 339.1 m with the orientation 243/62, at 344.7 m with the orientation 035/49 or 309/08 and at 370.8 m with the orientation 319/27 or 061/44. The upper radar reflector is strong and can be observed to a distance of 18 m outside the borehole 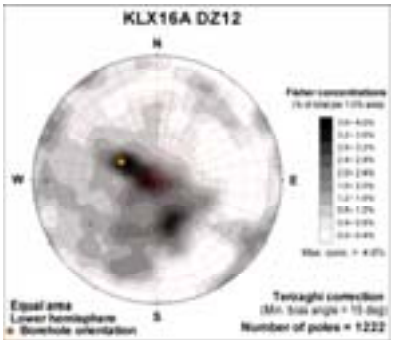

BH	Geometrical Intercept (bh. m)	Target intercept (bh. m)	Comment
			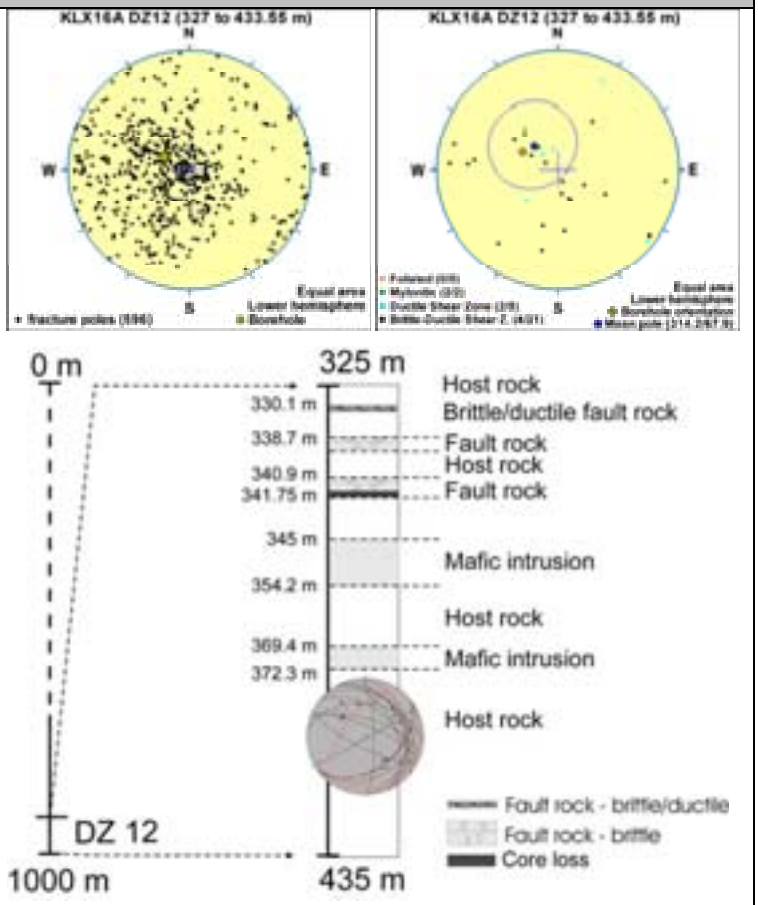 *Schematic structural log of DZ 12 in KLX16A. The stereonet shows the orientation of several thin cataclastic bands (red great circles) and slickensided fractures observed in the deepest portion of DZ 12. /Viola et al, 2007/* A first minor low-grade ductile shear zone is found at depth 330.09 m. It is characterized by a subvertical, NW-dipping foliation, defined by epidote. 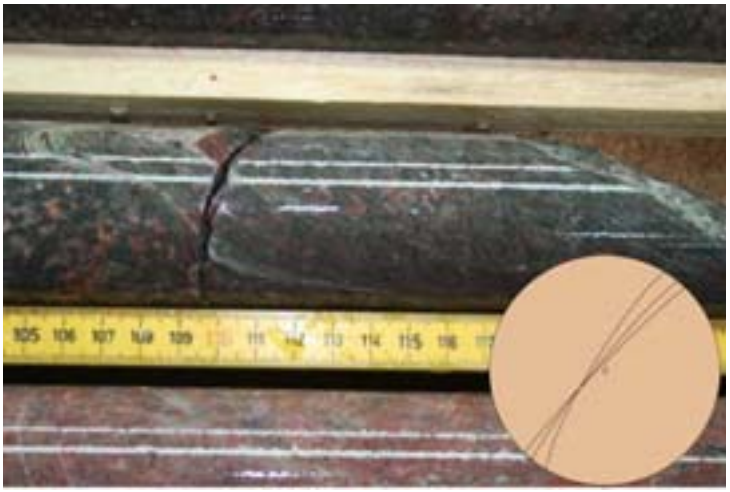 *Foliated interval at depth 330.09. Foliation planes, outlined by epidote, dip subvertically to the NW. /Viola et al, 2007/* An upper brittle core starts at depth 338.73 m, is c. 20 cm thick and is defined by a cataclastic sequence formed at the expense of the quartz monzodiorites. No clear orientation information could be obtained for the core, apart from a

BH	Geometrical Intercept (bh. m)	Target intercept (bh. m)	Comment
			single fracture in it oriented 047/45.  *Cataclastic core at depth 338.73 m in KLX16A. Note the localized high fracture frequency and the development of minor crush zones. /Viola et al, 2007/* A second cataclastic core starts at 340.908 m depth and continues down to c. 341.75 m. It is defined by a cataclasite-ultracataclasite /cemented breccia. A narrow core loss interval is also associated with this core and the core upper and lower limits were thus identified from the borehole image. No information as to the orientation of the core is available. 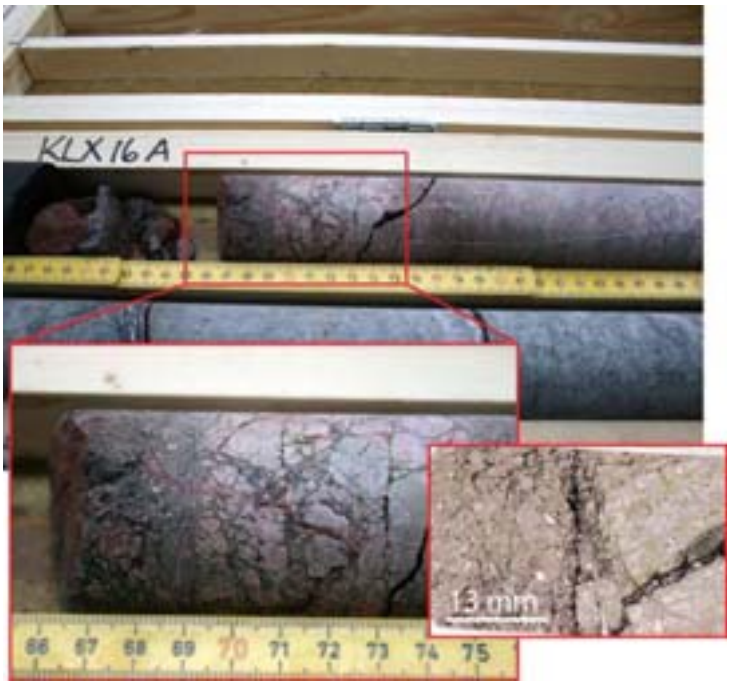 *Cataclastic core at depth 340.91. The enlargement illustrates the details of the angular nature of the poorly sorted clasts within the cataclasite. The scanned thin section of sample KLX16A1 shows several narrow brittle fault branches converging into a single broader deformation zone, which is transitional to the cataclastic component of the DZ core (to the left hand side).* The lower part of the DZ contains several striated fractures that were constrained kinematically. Shown below together with the orientation of the thin cataclastic bands. With the exception of a few highly-oblique shear fractures, most of the slickensided planes exhibit dip slip kinematics, predominantly reverse.

BH	Geometrical Intercept (bh. m)	Target intercept (bh. m)	Comment
			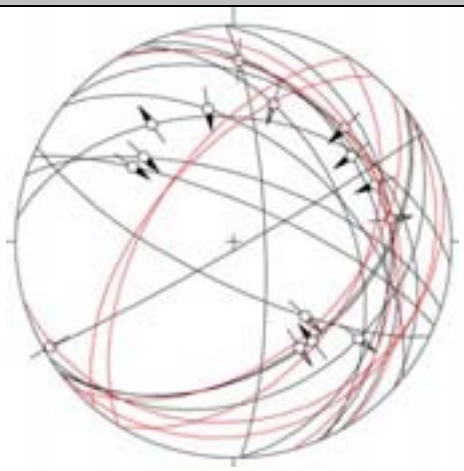 *Orientation of thin cataclastic bands (red great circles) and fault slip data for striated planes in the lower part of DZ 12.*

ZSMNE107A, KLX02A drill log extract (zone only)

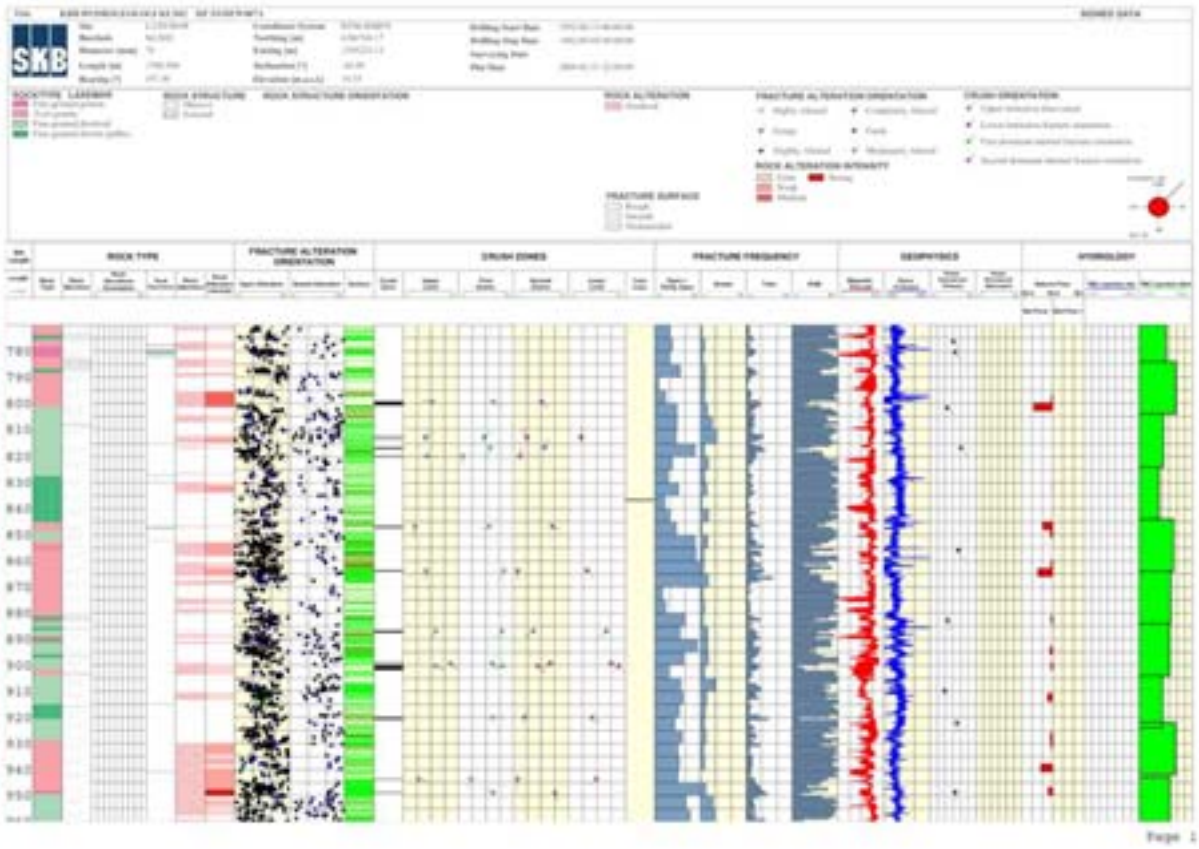

ZSMNE107A, KLX15A drill log extract (zone only)

ZSMNE107A, KLX16A drill log extract (zone only)

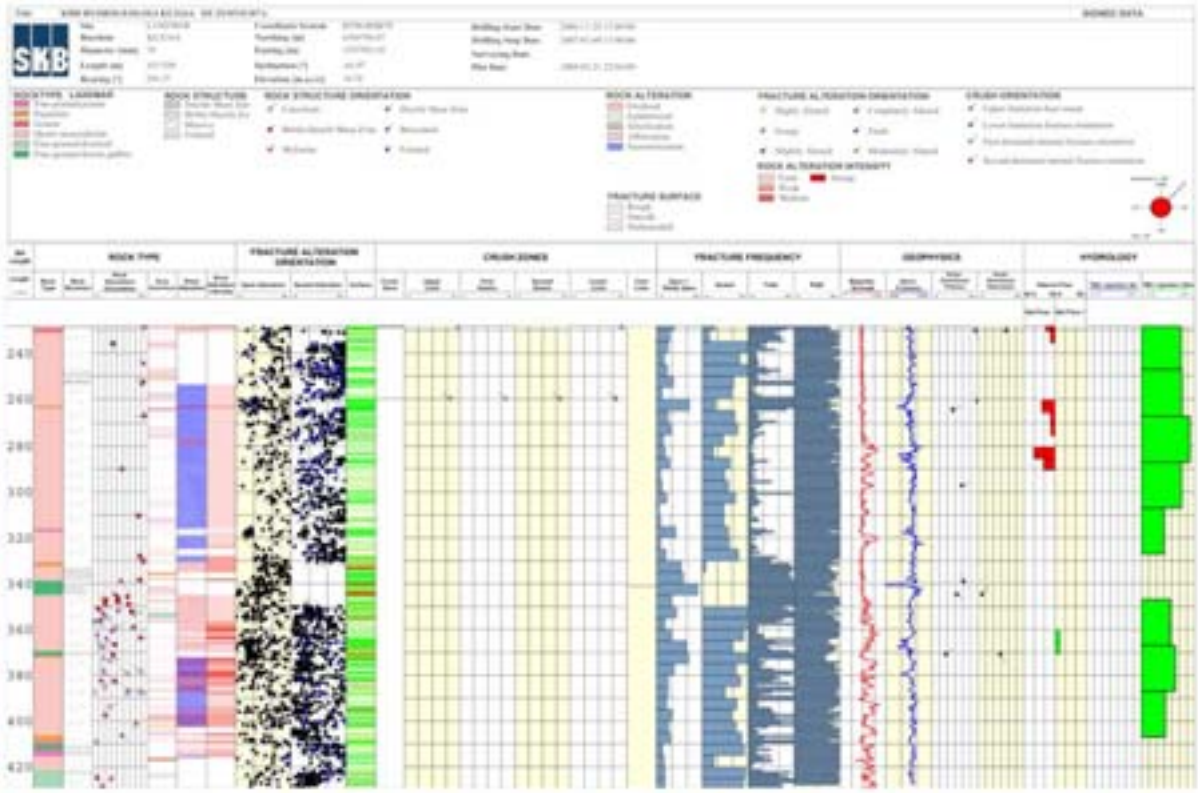

ZSMNE107A, KLX15A drill core photos (zone only)

ZSMNE108A

This zone's trace on the ground surface has been slightly adjusted from v1.2 based on a further review and a more detailed magnetic ground survey. Field mapping suggests the zone is brittle, oxidized and associated with fractured fine grained granite dykes. The inferred zone has not been investigated by borehole drilling or other direct investigations. The detailed magnetic ground survey shows a series of short lineaments that are well defined over very short distances, which may be dominated by intrusions and the inferred overall continuity is questionable. Forward modelling of the magnetic data suggests a dip that is steep but variable from being to the NW or SE. The zone has consequently been modelled as vertical.

NE-SW striking deformation zones ZSMNE108A	
Modelling procedure: At the surface, corresponds to poorly defined low magnetic and topographic lineaments. Modelled to base of regional model volume using dip that has been inferred from modelling of magnetic data /Mattsson and Triumf 2007/. Included in regional model and also present inside local model volume.	
Confidence of existence: Medium	

Property	Quantitative estimate	Span	Confidence level	Basis for interpretation	Comments
Position		± 30 m (surface)	Medium	Lineament and geophysical modelling	Local alternative variations in trace position are possible
Orientation (strike/dip)	060/90	± 10/ 15	High for strike, medium for dip	Strike based on trend of lineament. Dip based on geophysical modelling.	/Mattsson and Triumf 2007/
Thickness	10 m	5-50 m	Medium	Restricted by outcrop mapping	Only inferred thickness
Length (regional model)	1.8 km	+/- 250 m	Medium	Linked lineaments	Continuity of lineament-structure is questionable
Ductile deformation			Medium	Inferred association with NE-SW trending plastic domains	No evidence from immediate bounding outcrops
Brittle deformation			High	Evidence from bounding outcrops	
Alteration			High	Evidence from bounding outcrops	Red staining.
Fracture orientation	220/85, 100/65, 250/30, 025/20		Low	Parallel NE107A fracture orientations	
Fracture frequency	No data				
Fracture filling			Medium	Evidence from bounding outcrops	Oxide, epidote, prehenite
Kinematics					

BH	Geometrical Intercept (bh. m)	Target intercept (bh. m)	Comment
None			No BH intercepts

ZSMNE930A

ZSMNE930A remains unchanged from version 1.2. The local major zone lies in the south east corner of the local model volume to the east of ZSMNE004A (plastic domain PO2). At the surface, the zone is essentially based on deformation indicators identified during outcrop mapping. The field mapping results and lack of a clear topographic lineament suggest the zone is predominantly ductile though outcrops give clear evidence of later brittle reactivation. ZSMNE930A is considered to be a splay of the dominant plastic domain/deformation zone ZSMNE004A. Red staining and epidote fracture fillings were identified. The zone has a modelled length of 4.2 km though this is low confidence. The zone is considered to be representative of a number of thin zones with a clear plastic origin that are associated with the major plastic domains. Such zones whilst they can be traced over significant distances are thin and considered discontinuous. The zone has a modelled dip of 90^0 with an estimated span from vertical to 70^0 to the south based on field mapping. ZSMNE930A has not been the subject of focused investigation by either direct or indirect methods.

NE-SW striking deformation zones ZSMN930A	
Modelling procedure: At the surface, corresponds to outcrop deformation indicators. Modelled to base of the regional model volume using dip that has been inferred from field mapping. Included in the local model volume.	
Confidence of existence: High	

Property	Quantitative estimate	Span	Confidence level	Basis for interpretation	Comments
Position		± 25 m (surface)	Medium	Outcrop mapping	
Orientation (strike/dip)	067/90	060-075/ 90-70S	Medium for strike and dip	Strike and dip based on outcrop mapping.	
Thickness	5 m	1-20 m	Medium	Outcrop mapping	
Length (regional model)	4.2 km	± 500 m	Low	Outcrop mapping	Probably a discontinuous series of thin ductile zone 'strings'
Ductile deformation			High	Outcrop ductile indicators	Ductile-brittle.
Brittle deformation			Medium	Outcrop indicators	Dominantly ductile but with clear brittle reactivation
Alteration			High	Outcrop mapping	Red staining
Fracture orientation					No data
Fracture frequency Open/sealed m^{-1}					No data
Crush zone Number/total m					No data
Fracture filling			High	Outcrop mapping	Epidote

NE-SW striking deformation zones ZSMN930A					
Kinematics			Medium	Outcrop mapping	Sinistral

BH	Geometrical Intercept (bh. m)	Target intercept (bh. m)	Comment
None			No BH intercepts

ZSMNE942A

ZSMNE942A is a zone that has been added to the model after version 1.2. The extent and continuity of the surface lineament trace is based on the later detailed magnetic survey /Mattsson & Triumf, 2007/. The zone is located in the central part of the Laxemar model domain and has an estimated length of 2.5 km. The lineament is interpreted as representing a relatively thin (15 m) ductile-brittle, sub vertical (246°/86°) deformation zone. To a certain extent it mirrors the Äspö shear zone but on a far smaller scale. There is a general NE-SW alignment; a strong magnetic lineament that swings more W-E at the southern end; both plastic and brittle indicators and seismic refraction indicates narrow highly fractured cores.

The interpreted BH intercepts are included below. The condition of the core in the boreholes and the lengths of the intercepts mean that other structures are also almost certainly involved.

KLX10B is interpreted as starting within the zone that dips in the opposite direction to the BH inclination. Therefore the interception does not describe the full zone thickness. In KLX10B the zone is characterized as having an associated fine grained granite (mapped rock boundaries of 254°/78° and 258°/77°) with an initial ductile phase indicated by a foliation (240°/83°) that has been later reactivated as indicated by breccia (252°/89°). DZ2, 39 to 47 m is also possibly associated with this zone since the detailed magnetic map suggests an associated complex geometry at this location.

KLX10A. During the Eshi process it was evident that this hole could be divided into two based on its rock mass character. The top half of the hole down to around 430 m showed extensive evidence of deformation whilst the lower half encountered much better rock conditions. It is interpreted that the upper half is at least partly associated with a steeply dipping ZSMNE942A i.e. a steeply dipping narrow deformation zone is responsible for the rock conditions rather than a very thick more moderately dipping structure or a very large number of smaller structures.

There is no modeled intercept in KLX03 due to the lack of evidence of the existence of a sub vertical deformation zone in the lower section of this borehole.

As the lineament approaches ZSMNS059A it swings around to a more E-W alignment in a similar fashion to the Äspö shear zone (ZSMNE005A) and becomes more diffuse or masked by the influence of other structures. It is possible that the zone terminates at ZSMNS059A but is considered more likely to continue westwards beyond ZSMNS059A. The zone is interpreted still to be sub vertical generating an intercept in KLX19A corresponding to DZ4 lying just above the dolerite dyke.

Later forward modelling of more recent detailed magnetic total field data suggests the thickness of ZSMNE942A is in the order of 20 to 50 m in the two modelled profiles with a sub vertical steep dip to the west /Thunehed and Triumf, 2006/. A thickness of 15 m has been applied in the model based on the drill hole intercepts.

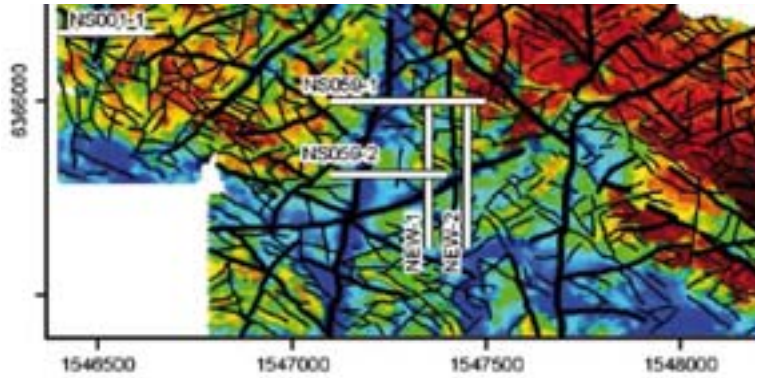

Location of profiles with forward modelling of magnetic total field data. The north-east striking lineamentis covered by two profiles (NEW-1 and NEW-2).

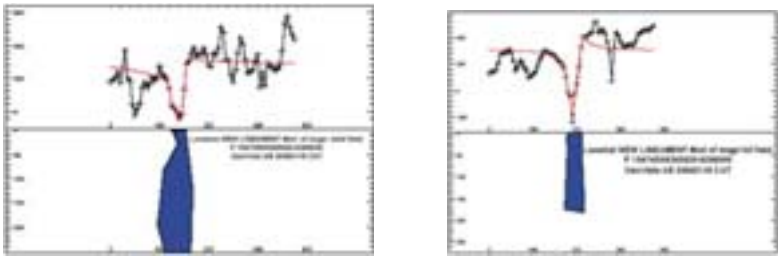

Forward modelling of magnetic total field data over north-east striking lineament (profiles NEW-1 and NEW-2). North is towards right in the figures.

The interpreted lower (eastern) transition zone intercept in KLX10A was examined in detail with the aim of better characterizing the zone /Viola & Ganerod, 2007/. The deformation is characterized by steep fractures in this section. The fractures are close to vertical and parallel to the core axis. These fractures have the character of joints, many with open apertures, and they tend to follow and exploit an older sealed network of calcite veins with a similar orientation. Examples of these joints are shown in the upper picture. In the last few meters of the section the fracture frequency decreases and there occurs a progressive transition to undisturbed rock. Joints are strongly iso-oriented and strike consistently ENE-WSW.

389-432,5 m : A strong ENE-WSW joint preferred orientation is observed in depth interval 389-432 of KLX 10A.

The lineament has been covered by seven seismic refraction profiles /Lindqvist, 2004, 2005, 2006/. Whilst there is probable interference from other structures the profiles support the brittle component of the zone and indicate the presence of a highly fractured ‘core’ with a thickness of around 5 m.

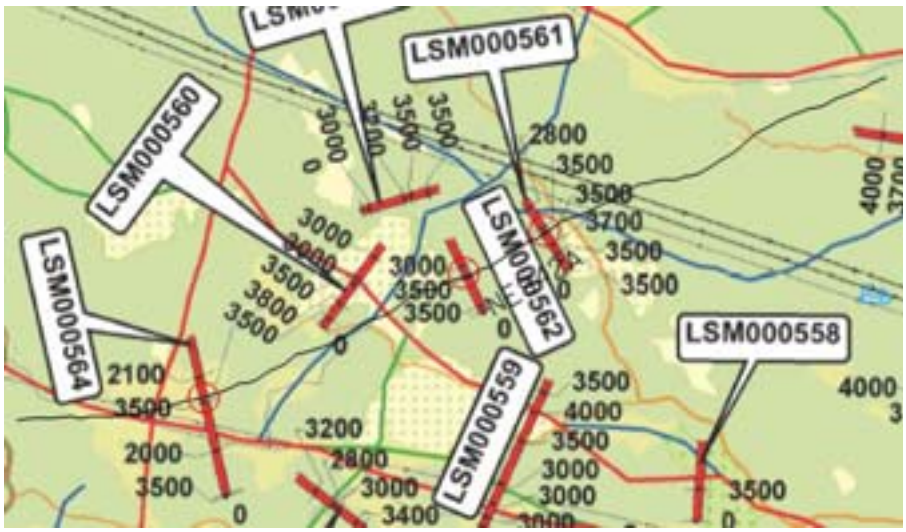

Seismic refraction profiling /Lindqvist, 2006/.

NE-SW striking deformation zones ZSMNE942A	
Modelling procedure: At the surface, corresponds to the low magnetic and topographic lineaments. Modelled to base of regional model volume using dip that has been inferred KLX10A and KLX19A along with modelling of magnetic data /Thunehed and Triumf 2006/. Included in regional model and also present inside local model volume.	
Confidence of existence: High	

Property	Quantitative estimate	Span	Confidence level	Basis for interpretation	Comments
Position		± 15 m (surface)	High	Lineament,	
Orientation (strike/dip)	246/87	245-265/ ±10	High for strike, medium for dip	Strike based on trend of lineament. Dip based on boreholes and geophysical modelling.	/Thunehed and Triumf 2006/
Thickness	15 m	10-50 m	High	Lineament, BH and geophysical ground survey	Thickness refers to total zone thickness (transition zone and core) /Thunehed and Triumf 2006/
core	5m	±2	medium		Seismic refraction profile. /Lindqvist, 2004,2005, 2006
Length (regional model)	2.5 km	2.2-2.5 km	Medium	Linked lineaments	
Ductile deformation			High	KLX10A, KLX19A brittle-low grade ductile indicators	Ductile-brittle. Weak ductile precursor but dominantly brittle.
Brittle deformation			High	Gouge and crush in KLX10A, KLX19A. Seismic refraction profile.	Seismic refraction profile. /Lindqvist, 2004/2005.
Alteration			High	KLX10A, KLX19A	Red staining, chloritization, epidotization, argillization
Fracture orientation	Sub horiz', 060/80, 000/90, 040/35, 230/40, 295/90		Medium	KLX10A, KLX19A	

NE-SW striking deformation zones ZSMNE942A					
Fracture frequency* Open/sealed m^{-1}	8/32		Medium	KLX10A, KLX19A	
Crush zone Number/total m	10/0.5	2-20/0.5-2	Low	KLX10A, KLX19A	Multiple narrow crush zones
Fracture filling			High	BHs	Calcite, clay, chlorite, epidote, hematite, pyrite, quartz, adularia, prehnite.
Kinematics					

BH	Geometrical Intercept (bh. m)	Target intercept (bh. m)	Comment
HLX23	124,3-150,0	-	
KLX10A	74,6-893,3	103-349	DZ1-DZ7 brittle deformation zone characterized by increased frequency of sealed and open fractures and weak to medium red staining. Some of the open fractures have large apertures –some with idiomorphic calcite crystals. Open fractures are parallel with the drill core and have large apertures. One open fracture with gauge. Crush zones. Local vuggy character of the Ävrö granite (dissolution of quartz). Weak to medium red staining. 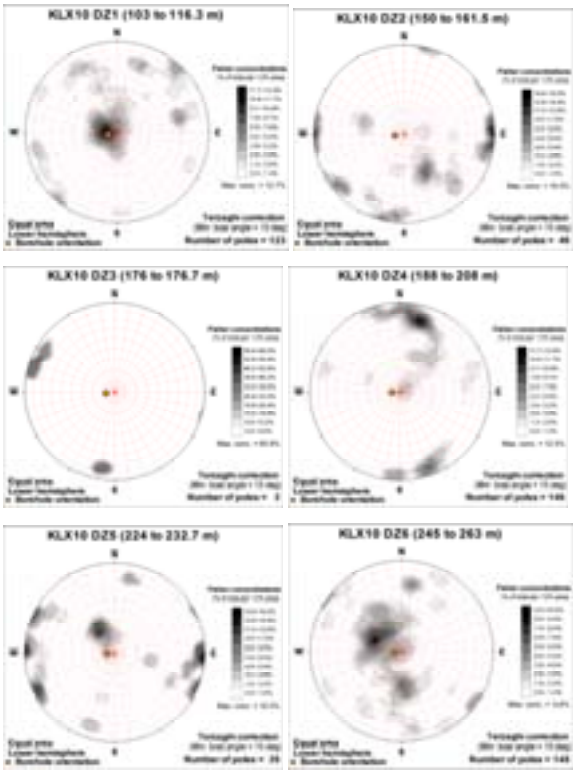

BH	Geometrical Intercept (bh. m)	Target intercept (bh. m)	Comment
			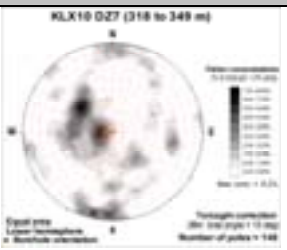
KLX10B	3.8-20,6	0-20	Increased frequency in open fractures, faint red staining. 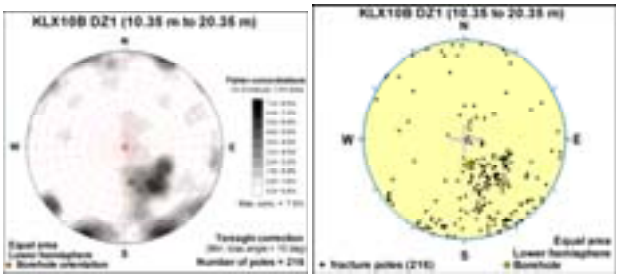
KLX19A	435,7-462,2	437-464	Brittle to brittle-ductile deformation zone characterized by increased frequency of open and sealed fractures, four crush zones, weak to medium red staining and epidotization, breccia, ductile and brittle-ductile shear zones and gouge. The most intensely deformed sections (cores) are 448.0-457.20 m and 461.40-464.0 m. The ductile to brittle-ductile deformation is concentrated to the most intensely deformed sections. 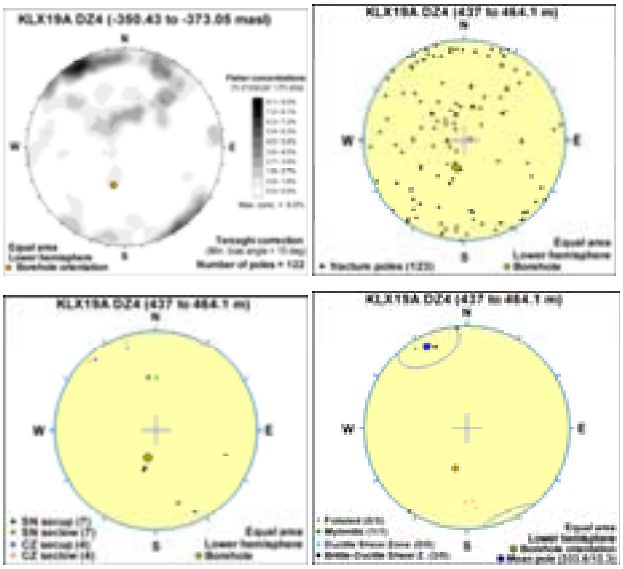 From Viola et al, 2007/. DZ 4 is located between 436 and 465 m depth and contains several thin fault cores with no or only minor transition zones.

BH	Geometrical Intercept (bh. m)	Target intercept (bh. m)	Comment
			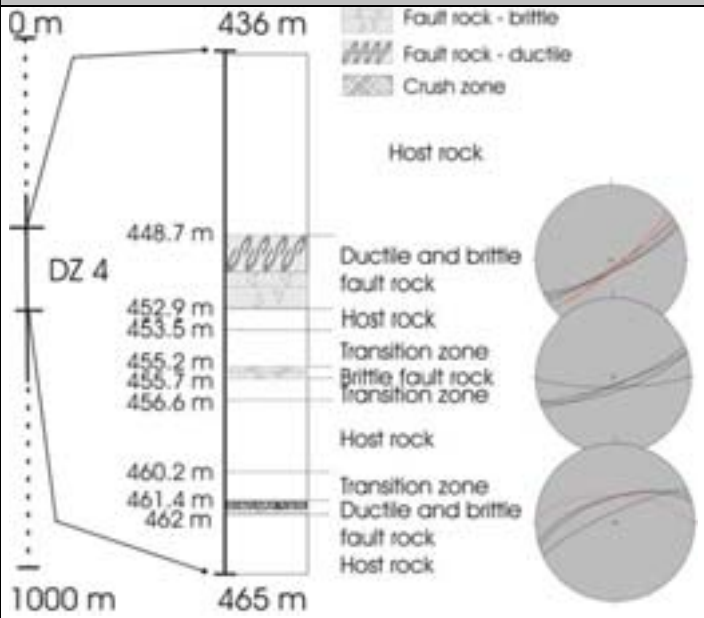 A first upper core starts at depth 448.7 m and extends down to 452.9 m. The core is formed in its upper part by foliated quartz monzonites (figure a). In its central sector, at depth 449-449.25 m, it contains a sharp cataclastic interval (figure b), which is about 25 cm thick. The stereonet of plots the orientation of the ductile fabric with black great circles and of open fractures within the cataclastic sequence with red circles. Foliation planes and open fractures dip all very steeply to the SE/SSE. 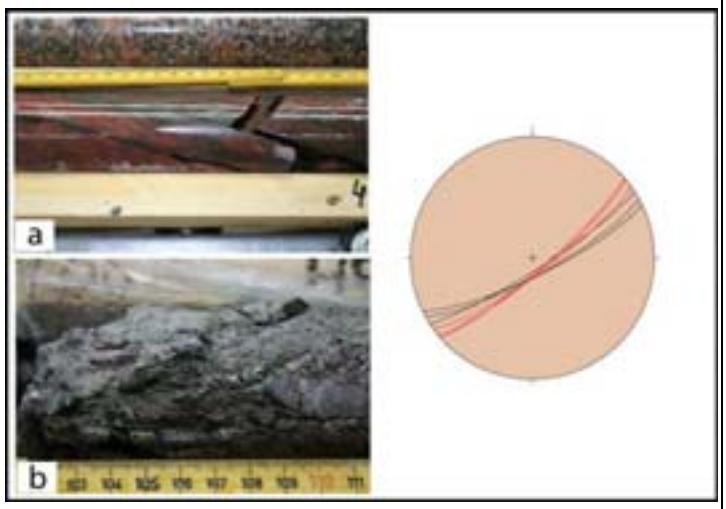 Another brittle core, preceded and followed by two minor transition zones, straddles depth interval 455.261-455.702 m (Figure XX). The core, together with its two transition zones, is a clear example of deformation zone defined on the basis of fracture frequency.

BH	Geometrical Intercept (bh. m)	Target intercept (bh. m)	Comment
			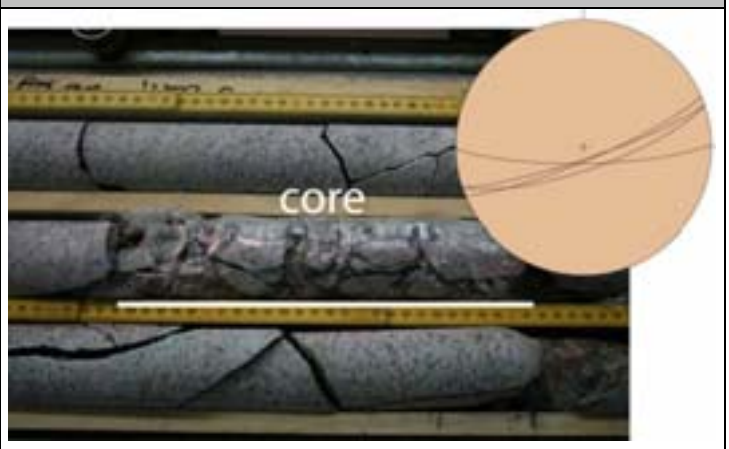 *Core, defined on a high fracture frequency, extending from 455.261 to 455.702 m depth*. As visible in the figure above, the core resembles in fact a crush zone, whereby the existence of the core is inferred on the basis of a high fracture frequency rather than on the presence of fault rock. Furthermore, fracture frequency increases progressively towards the core and away from it, thus defining an upper and lower, symmetrically-arranged transition zones. Fractures in the core dip very steeply to the SSE, similarly to the orientation of the upper core described above. A last core is located at 461.46 m and extends to c. 462 m depth. It is mainly characterised by pervasively foliated quartz monzonites, oriented 272/62. A minor crush zone is located in the middle of the ductile interval, between depths 461,585 m and 461,743 m. The ENE-WSW striking black great circles in the figure below plot the orientation of open fractures associated with the crush zone. 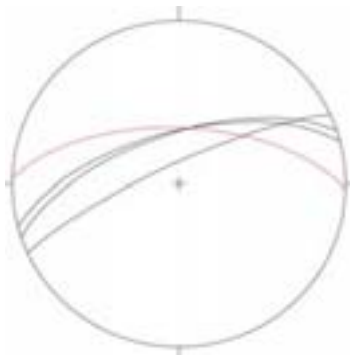 *Orientation of the quartz monzonites foliation (red great circle) and of open fractures (black great circles) in the core at depth 461.4 m.*

ZSMNE942A, KLX10A drill log extract (zone only)

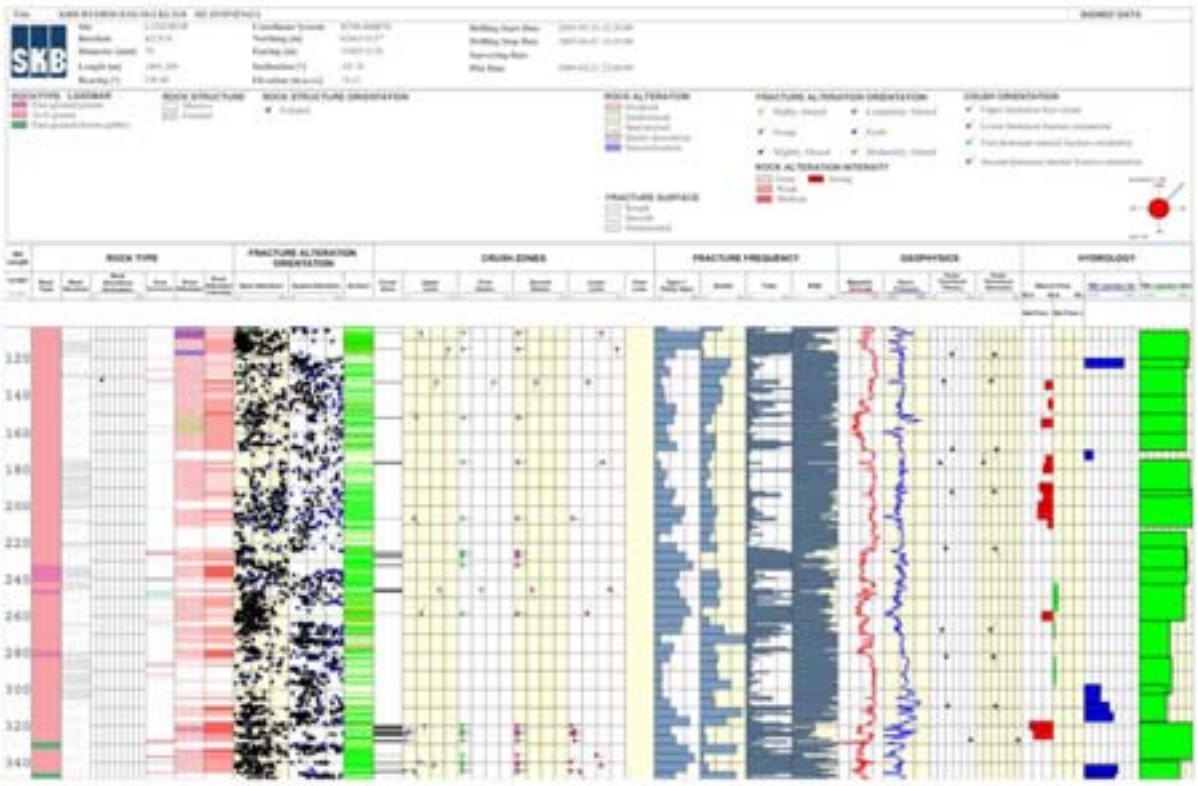

ZSMNE942A, KLX10A drill log extract (zone only)

ZSMNE944A

At the surface, the zone corresponds to poorly constrained low magnetic and topographic lineaments. Field mapping identifies intense red staining with raised fracture frequency, along with epidote and chlorite fracture fillings. The zone is interpreted as a low grade ductile zone that has been subject to brittle reactivation. The 1 to 2 m thick core is dominated by crush and cataclasites. The zone has a length of 1.2 km and a thickness of approximately 10 m with a strike of approximately 060^0 and a dip of 75^0 to the southwest. Modelled to base of local model volume using dip that has been inferred KLX18A and seismic reflector K2 /Juhlin 2006, (update of P-04-215)

NE-SW striking deformation zones ZSMNE944A	
Modelling procedure: At the surface, corresponds to poorly constrained low magnetic and topographic lineaments. Modelled to base of local model volume using dip that has been inferred KLX18 and seismic reflector K2 /Juhlin 2006, (update of P-04-215)	
Confidence of existence: High	

Property	Quantitative estimate	Span	Confidence level	Basis for interpretation	Comments
Position		± 15 m (surface)	Medium	Lineament,	Alternatives exist
Orientation (strike/dip)	058/75	030-060/ ±15	Medium for strike and dip	Strike based on trend of lineament. Dip based on borehole and seismic reflector K2.	/Juhlin 2006/
Thickness	10 m	5-20 m	Medium	Lineament and BH	Thickness refers to total zone thickness (transition zone and core)
core	1	1-3 m	High	KLX18A	
Length (regional model)	1.2 km	1.2-2.0 km	Medium	Linked lineaments	Possible alternative NW extension
Ductile deformation			High	BHs brittle-low grade ductile indicators	Ductile-brittle. Weak ductile precursor but dominantly brittle.
Brittle deformation			High	Breccia and crush in KLX18A.	
Alteration			High	KLX18A.	Red staining, chloritization
Fracture orientation	090/80, 060/70		Low	KLX18A	
Fracture frequency* Open/sealed m^{-1}	13/57		Medium	KLX18A	

NE-SW striking deformation zones ZSMNE944A					
Crush zone Number/total m	1/0.1		Medium	KLX18A	
Fracture filling			High	KLX18A	Chlorite, calcite, clay, Hematite, epidote, pyrite, quartz, prehnite
Kinematics	-	-	-	-	-

BH	Geometrical Intercept (bh. m)	Target intercept (bh. m)	Comment
HLX31	129-133 (Base)	-	Low confidence intercept. ZSMEW007A probably dominates.
KLX18A	273-299	284-292	Eshi DZ3 284-292 m: Inhomogeneous brittle to brittle-ductile deformation zone. Two small sections of breccia, 1cm and 30 cm. Faint to medium red staining. High frequency of sealed fractures and sealed network. Slightly increased frequency of open fractures and a 17 cm thick crush zone. Core loss at 285.62-285.81 and 289.07-289.98 m. Slickenside is observed. Major decrease in the bulk resistivity and magnetic susceptibility. Minor caliper anomalies and partly decreased P-wave velocity. One strong and persistent oriented reflector occurs at 287.0 m with the orientation 251/65. 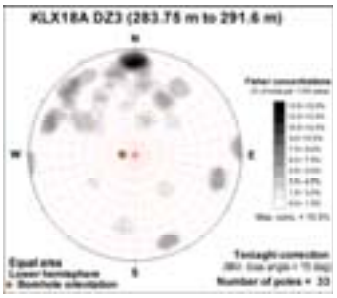 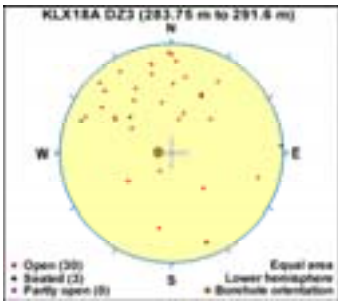 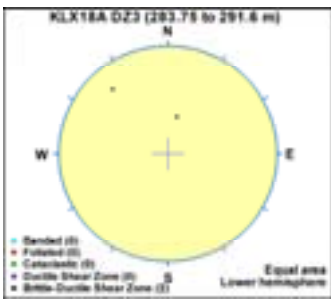 /Viola et al, 2007/: The upper transition zone extends from 284.85 to 287.288 m depth and displays a progressive increase in fracture frequency towards the fault core and includes a 20 cm thick crush zone and a zone of core loss, also 20 cm thick. Fractures, invariably coated by chlorite, calcite and clay minerals, are oriented consistently NE-SW and dip steeply to the SE

BH	Geometrical Intercept (bh. m)	Target intercept (bh. m)	Comment
			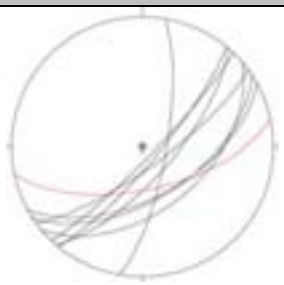 *Fracture orientation within the upper transition zone of DZ 3. The red great circle is the fracture that defines the upper contact of the crush zone extending from 285.453 down to 285.624 m depth.* The DZ fault core (287.288 – 290.701 m) has a sharp upper boundary separating the upper transition zone from its protocataclasites, which develop progressively over a 20 to 25 cm thick interval into cataclasites and ultracataclasites. The cataclastic texture of the rock is best seen in the scanned image of sample KLX 18A-1 thin section. A faint foliation, which is defined by the alternation (at the thin section scale) of protocataclastic and cataclastic bands, is also recognizable within the cataclasites. The core continues with intensively epidotized rock, intense fracturing, crush zones and an 87 cm core loss interval. Sample KLX 18A-2 shows how the texture of the rock remains throughout protocataclastic, with pervasive red staining, localized bands of more intense cataclasis and diffuse chloritization. Later dilatant calcite veins are common in this interval. The DZ lower transition zone (290.701 – 291.42 m) is shorter than the upper one, is characterized predominantly by diffuse epidotization and is transitional to undeformed granitic host rock at 291.42 m depth.  *Sample KLX 18-1 from cataclastic granites at depth 287.4 m. The scanned thin section shows a faint foliation within the sample (white dashed lines), which is defined by the alternation of protocataclastic and cataclastic domains.*

<table>
<tr><th>BH</th><th>Geometrical Intercept (bh. m)</th><th>Target intercept (bh. m)</th><th>Comment</th></tr>
<tr><td></td><td></td><td></td><td>
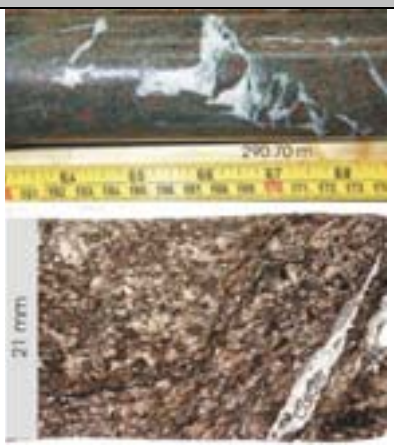

"Late" dilational calcite veins cut across altered protocataclastic granites, as shown by the scanned thin section of sample KLX 18A-2.

Summary
<table>
<tr><th>Depth (m)</th><th>Box number</th><th>Interpretation</th><th>Description</th></tr>
<tr><td>284.85 – 287.288</td><td>36</td><td>Transition zone</td><td>Increasing fracture frequency, 20 cm thick crush zone and core loss; no major fault rock (just thin bands and networks). Thickness of zone is 6.60 m.</td></tr>
<tr><td>287.288 – 290.701</td><td>36, 37</td><td>Fault core</td><td>Protocataclasites that pass laterally into cataclasites and ultracataclasites over a 20-25 cm thick interval. The core continues with heavily altered rock, with epidotization and intense fracturing, crush zones and c. 87 cm of core loss. The lower part of the core includes altered protocataclasites.</td></tr>
<tr><td>290.701 – 291.42</td><td>37</td><td>Transition zone</td><td>This transition zone is shorter and contains epidotization.</td></tr>
</table>
/Viola et al, 2007/
</td></tr>
</table>

ZSMNE944A, KLX18A drill log extract (zone only)

N-S striking deformation zones

ZSMNS001A–E

The zone borders the western boundary of the local model domain and is divided into five segments which are offset by E-W deformation zones. The segments are indicated both in topographic and airborne geophysical data and were verified through ground magnetic measurements /Stenberg and Sehlstedt 1989/. The northern segment has also been investigated in a refraction seismic survey /Rydström and Gereben 1989/. Field mapping identified increased small-scale fracturing, locally sealed by epidote, and mesoscopic brittle-ductile shear features along or close to the marked zone. Based on the geophysical data a steep to vertical dip was earlier inferred.

Within the local model area the zone has been subsequently investigated by three hammer drill holes and one rotary cored hole. The drilling results combined with additional geophysical investigations and modelling all support the steep dip to the west of the zone.

Below are shown the results from the electrical resistivity detailed ground surveys. Positive anomalies are shown as bright yellow/green and negative anomalies as light/dark blue /Thunehed och Triumf, 2006/. The modelling of ZSMNS001 indicates an almost vertical dip with only a slight inclination towards west.

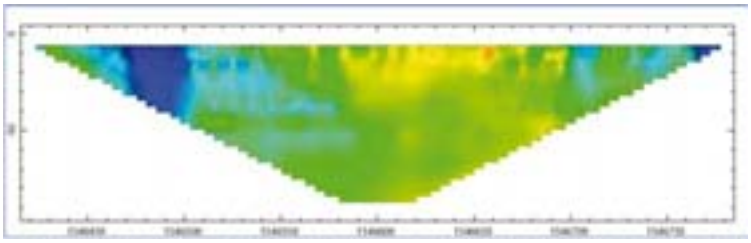

Apparent resistivity pseudo-section, 6366390N,
The low-resistive anomaly at 1546480E is at the position of NS001

Below are shown the results from magnetic total field detailed ground surveys with forward modelling of magnetic total field data over ZSMNS001. /Thunehed och Triumf, 2006/

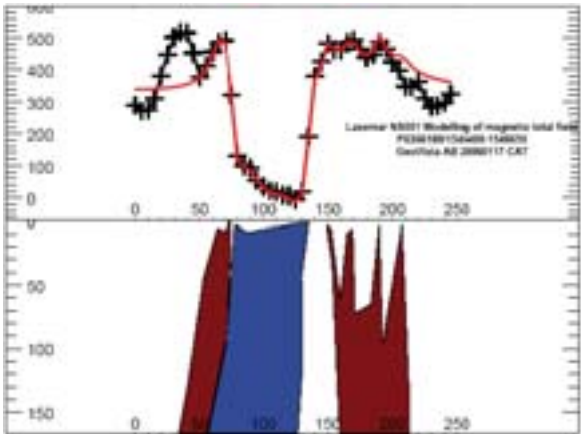

East is towards right in the figure. Blue bodies have low relative magnetic susceptibility. The low-magnetic anomaly at 100m is at the position of ZSMNS001

The zone is dominated by the presence of a large dolerite dyke and brittle deformation although ductile indicators with a similar orientaion are present outside the zone. The intercept of this zone in KLX20 has been examined in detail /Viola och Ganerod, 2006/. Brittle deformation features are widespread throughout the whole zone, with significant fracturing, crush zones and intervals of core loss. A large number striated planes are present, most of which are to be found within the mafic doleritic dyke. Most deformation features are localized within the doleritic rocks.

Striated surfaces within the doleritic dyke

Outside the upper (easterly) transition zone as seen in KLX20 the rock consists of relatively undeformed quartz monzodiorite with no significant structural features, except a few striated planes. In this section, a set of striated planes with normal kinematics dips moderately to the S, SW and coexists with two distinct sets of steep planes, which strike roughly NS and NE-SW and are transpressive sinistral. The striated planes are coated by chlorite, hematite, clay minerals and locally calcite.

At depth 182.37m in KLX20 occurs the upper contact of a major doleritic dyke. This depth is also interpreted to correspond roughly to the upper limit of the upper transition zone, defined by pervasive fracture sets, several crush zones and core loss intervals. Striated planes are very common in this transition zone and are invariably coated by chlorite and clay minerals.

The information can be resolved into two main systematic sets of fractures: i) steep, predominantly strike-slip faults striking from NNW to NNE, which can be interpreted as belonging to a set of conjugate predominantly sinistral (red great circles) and dextral fault planes (black great circles); ii) moderately S- and N-dipping normal (blue great circles in the top right stereonet) and reverse (black great circles) faults (see figure below).

Crosscutting relationships are at times visible (see figure below), where a steep fracture plane (shaded in white) truncates a flatter surface (shaded in red). This is

however not a systematic relationship and the relative time sequence is not established with confidence. Moreover, the moderately dipping surfaces are both normal and reverse fault planes and it is not clear from this section whether shortening or extension is the older tectonic regime that affected the rocks of the zone.

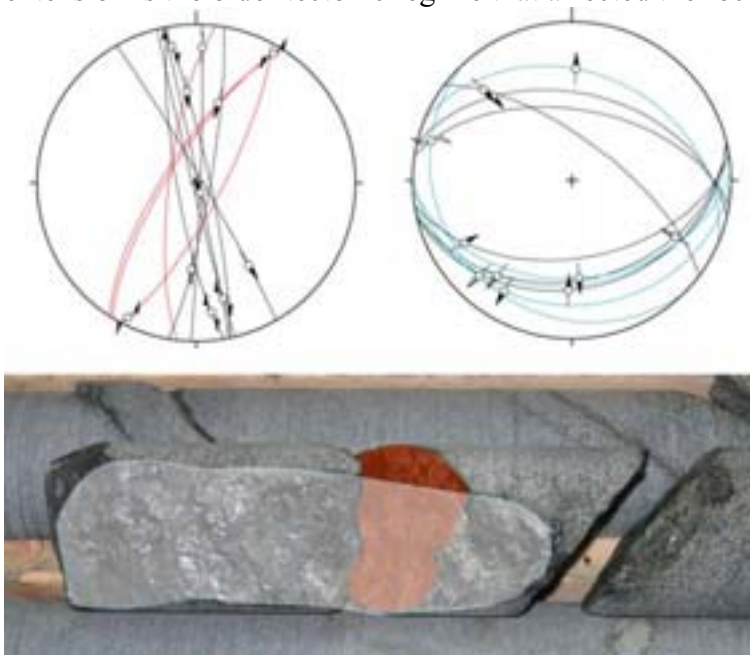

The fault slip data can be resolved in several components. Steep, NNW-_ to NNE-striking sinistral (red great circles) and dextral (black circles) striated faults (top left stereonet) are separated from moderately N and S dipping normal (blue) and reverse (black) faults. The steep surfaces locally cut across the flatter ones (shaded in white and red, respectively, in the photograph at the bottom), although it remains undetermined whether these are normal or reverse structures.

The core is characterized by the presence of numerous fracture sets and zones of crushed rock and core loss. The core consists of several thinner cores, themselves defined by zones of crushed rock or very high fracture frequency. Numerous striated planes are present, but it was not possible to identify them in the BIPS image, thus it was not possible to ascertain their orientation.

A lower transition zone starts from depth 230.89 m. The zone is highly fractured, but the fracture frequency tends to decrease away from the core. Based on the fracture distribution, the upper transition zone is the more prominent of the two.

The kinematics interpreted from the core are consistent with the detailed fracture mapping of nearby outcrops that identified planar, steep to sub-vertical, long and generally rather continuous shear fractures that strike NS to NNW-SSE. Specific structural features, such as releasing bends, en-echelon lateral stepping and Riedel shears, allowed the establishing of consistent kinematics for the set. The NS trending fracture set is interpreted as a series of predominantly sinistral fractures and faults. However, the work highlighted that many faults and fractures of the area have undergone severe reactivation during long-lived structural histories under different stress regimes /Viola and Ganerod, 2007/.

N-S striking deformation zones

ZSMNS0001A-E

Modelling procedure: At the surface, corresponds to the low magnetic and topographic lineament string. Clear brittle character. Associated with major dolerite intrusion of the same orientation. Modelled using dip that has been inferred from ground geophysical profiling and BHs. Included in the regional model and also present inside local model volume.

Confidence of existence: High

Property	Quantitative estimate	Span	Confidence level	Basis for interpretation	Comments
Position		± 20 m (surface)	High	Lineament, BH and geophysical ground survey	
Orientation (strike/dip)	187/81	± 10/± 10	High for strike, high for dip	Strike based on trend of lineament. Dip based on geophysical ground survey and boreholes	/Mattsson and Triumf, 2006/
Thickness	45 m	20-80 m	High	Lineament, BH and geophysical ground survey	Complex zone, inferred thickness refers to total zone thickness (splays, transition zones and core)
Upper transition zone (Easterly)	15 m	2-15m	Medium	KLX20	Transition from granitic bedrock to dolerite. Progressive increase in fracture frequency. Numerous striated planes. Several narrow crush zones.
Core	10m thick, includes multiple minor cores with crush and high fracture frequency.		Medium	BHs, seismic refraction profile 10m wide 2900 m/s velocity	Core closely associated with dolerite intrusion. Highly fractured, with several crush zones and core loss.
Lower transition zone (Westerly)	2 m	1-15m	Medium	KLX20	High fracture frequency.
Length (regional model)	10.9 km	+/-200 m	Medium	Linked lineaments	NS001A+B+C+D+E

N-S striking deformation zones ZSMNS0001A-E					
Ductile deformation	Minor		High	BH	Brittle deformation clearly dominates though nearby parallel ductile indicators are certainly present.
Brittle deformation	Major		High	Raised fracture frequency, crush zones, breccia, slickensides, KLX20	Present
Alteration			High	KLX20 and field mapping.	Weak red staining, saussuritization and epidotization
Fracture orientation	195/80, 085/35, 290/80, 240/90		Medium	KLX20	
Fracture frequency* Open/sealed m^{-1}	14/44		Medium	KLX20	
Crush zone Number/total m	16/5		Medium	KLX20	
Fracture filling			High	BH	Chlorite, clay, pyrite, zeolites, calcite, epidote, quartz,hematite, prehenite
Sense of displacement	Sinistral		Medium	KLX20 and nearby outcrops	Probable repeated reactivation

BH	Geometrical Intercept (bh. m)	Target intercept (bh. m)	Comment
HLX36	86,2-197,0	111-191	Eshi DZ1. High frequency of open fractures. Very low electric resistivity and low magnetic susceptibility. Caliper anomalies along the entire zone, the most prominent ones at the margins. The host rock is totally dominated by dolerite.
HLX37	102,3-156,2	122-147	Eshi DZ1. High frequency of open fractures. Very low electric resistivity, low P-wave velocity and low magnetic susceptibility. Caliper anomalies at the margins of the zone. The host rock is totally dominated by dolerite. 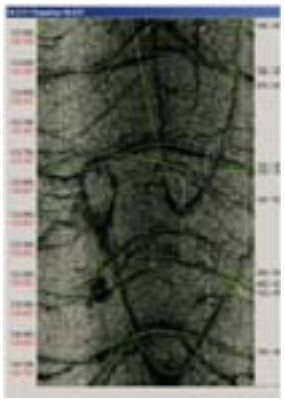 BIPS-image as seen in Boremap, showing the unaltered, fine to medium grained, homogenous and often strongly fractured dolerite. Green lines mark the probable open fractures.
HLX43	16,5-110,3	32-82	Eshi DZ1. Brittle deformation zone characterized by strong increase in frequency of open fractures. The section c. 32-74 m is characterized by a major decrease in bulk resistivity (almost two orders of magnitude), several intervals with decreased P-wave velocity and numerous caliper anomalies. The host rock is dominated by dolerite, in which the most intense deformation is concentrated. 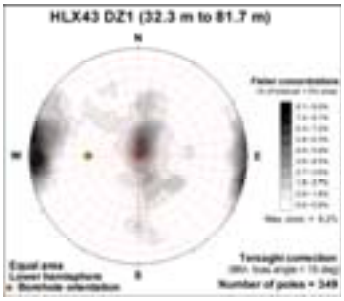

BH	Geometrical Intercept (bh. m)	Target intercept (bh. m)	Comment
KLX20	168,8-249,6	171-234	Eshi DZ1. Inhomogeneous brittle-ductile deformation zone. Large number of caliper anomalies, decreased P-wave velocity and magnetic susceptibility. Major decrease in the bulk resistivity. Upper transition zone: 171.38-182.20 m. Host rock is dominated by quartz monzodiorite. Subordinate rock types are fine- to medium-grained granite and dolerite. Three breccias (8-10 mm). Weak saussuritization and red staining. High frequency of sealed fractures. Slickensides are observed. Core zone: 182.20-231.00 m. The host rock is dominated by dolerite. 16 crush zones (highly fractured rock, total length 6.14 m). One breccia (23 mm). Weak red staining. High frequency of sealed and open fractures. One core loss (15 cm). Several slickensides are observed. Lower transition zone: 231.00-234.45 m. The host rock is dominated by quartz monzodiorite (501036). Weak saussuritization. Moderate frequency of sealed and open fractures. Slickensides are observed. 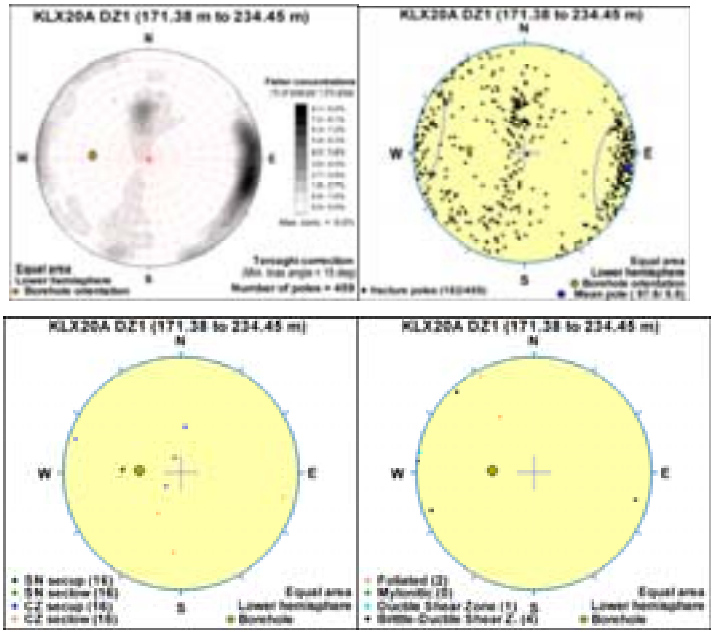

ZSMNS001C , KLX20A drill log extract (zone only)

ZSMNS001C , KLX20A drill core photos (1 of 2) (zone only)

ZSMNS001C , KLX20A drill core photos (1 of 2) (zone only)

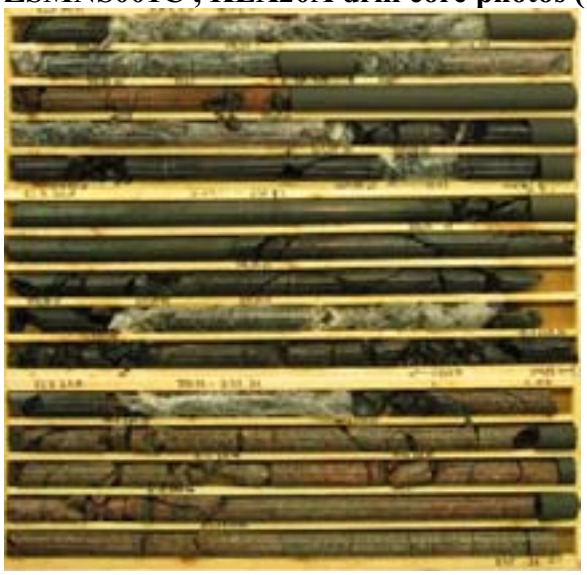

ZSMNS046A

ZSMNS046A is modelled as being vertical, with a thickness of 20m and a length of 2.1 km.
The zone is interpreted as having a clear ductile origin as evidenced by mylonites in both the field outcrops and in the drillcore but that has been subject to later brittle reactivation seen as increased fracture frequency and presence of cataclasites. Alteration is dominated by red staining and chloritization.

The southerly extent of this zone has been reduced from the previous model version based on the updated lineament analysis. There remains a possible link with a similar zone further to the south as intercepted in KLX26A. However, whilst there are reasons for the absence of the lineament in the central section: the presence of overburden and disrupting influence of the power lines; the distance involved results in this linking being considered to be too speculative. ZSMNS046A and the more southerly structure are considered to have the same character and belong to the same N-S trending set of structures but the continuity between them is very uncertain.

The thickness and subvertical nature of the zone is based the mapped orientation of the ductile and brittle ductile indicators in the core and is independently supported by the forward 3D modelling of magnetic data /Thunehed & Triumf, 2006/ along an east-west profile over the zone, to the north of KLX09A. This modelling is based on data presented in P-06-137.

The zone has also been transacted by a seismic refraction profile /Lindqvist, 2006/. The profile identified a narrow low velocity anomaly in the vicinity of the main lineament that may be related to the zone. The refraction profile, along with the drilling and magnetic evidence, suggests the zone is relatively narrow.

Siesmic refraction profile LSM000556. Low velocity zone in vicinity of ZSMNS046A marked by red ring /Lindqvist, 2006/.

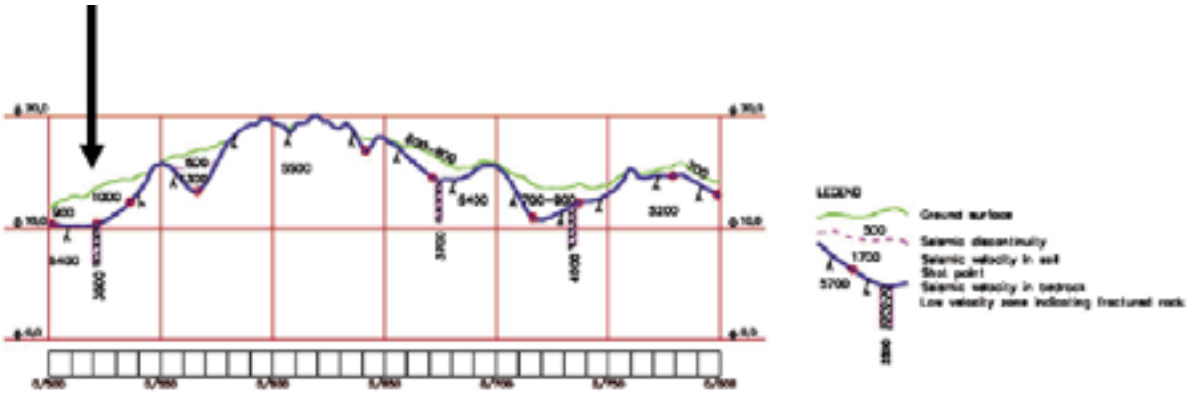

Siesmic refraction profile LSM000556. Low velocity zone in vicinity of ZSMNS046A marked by arrow /Lindqvist, 2006/.

N-S striking deformation zones ZSMNS046A	
Modelling procedure: At the surface, corresponds to the low magnetic and topographic lineament. Ductile origin but later brittle reactivation. Modelled using dip that has been inferred from modelling of magnetic data and KLX09G. Included in the regional model and also present inside local model volume.	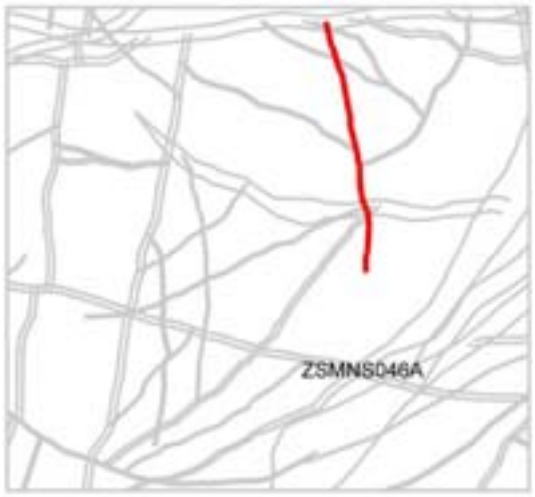
Confidence of existence: High	

Property	Quantitative estimate	Span	Confidence level	Basis for interpretation	Comments
Position		± 10 m (surface)	High	Lineament, BH and geophysical ground survey	/Thunehed et al, 2006/
Orientation (strike/dip)	170/90	± 10/± 10	High for strike, high for dip	Strike based on trend of lineament. Dip based on magnetic modelling, outcrop mapping and borehole	/Thunehed et al, 2006/
Thickness	20 m	10-30 m	High	Lineament, BH and geophysical ground survey	Complex zone, inferred thickness refers to total zone thickness (splays, ductile and brittle, transition zones and cores)
core	-		Medium	KLX09G	No clear focused core, /Lindqvist,2006/
Length (regional model)	2.1 km	2.0-2.5 km	Medium	Linked lineaments	Possible further extension to the south.
Ductile deformation	Major		High	Mylonites, outcrop mapping. and KLX09G	Present
Brittle deformation	Minor		High	Raised fracture frequency, KLX09G	Present
Alteration			High	KLX09G	Red staining and chloritization
Fracture orientation	185/90, 115/80, 070/15, 320/80		Medium	KLX09G	

N-S striking deformation zones ZSMNS046A					
Fracture frequency* Open/sealed m^{-1}	13/47		Medium	KLX09G	
Crush zone Number/total m	0/0		Medium	KLX09G	
Fracture filling			High	KLX09G	Calcite, chlorite, hematite, clay, pyrite, epidote, epidote, quartz, fluorite.
Sense of displacement	Strike slip sinistral		Low	Assumption based on ZSMNS059A and ZSMNS001C	

BH	Geometrical Intercept (bh. m)	Target intercept (bh. m)	Comment
KLX09G	33,2-73,4	40-68	Eshi DZ1. Characterized by high frequency of open and sealed fractures, with partly large aperture. Increased frequency of sealed network in the lower part. Most intense deformation between 40.38-41.50 m (low grade ductile to brittle ductile shear zone) and 53.40 – 56.15 m (low grade ductile to brittle ductile shear zone). In the section c 40-44 m there is partly decreased resistivity, decreased P-wave velocity and a caliper anomaly. The host rock is dominated by Ävrö quartz monzodiorite; subordinate rock types are fine-grained diorite-gabbro, granite, fine-grained granite and pegmatite. 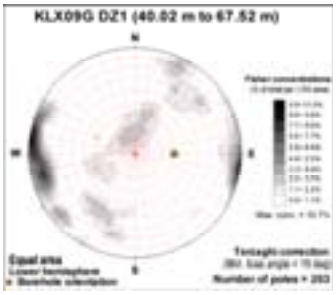

ZSMNS046A , KLX09G drill log extract (zone only)

ZSMNS057A

ZSMNS057A is marginal to the northwest corner of the local model volume with a southern termination against the Mederhult zone, ZSMEW002A. At the surface, the zone corresponds to a low magnetic and major topographic lineament. The zone has been modelled with a vertical dip based on a single field measurement though a vertical to steep dip to the west is inferred from an assumed relationship with the parallel 'paired' zone ZSMNS001. The zone has a length of at least 5 km and a thickness, inferred from topography ranging from 10 to 50 m. ZSMNS057A is assumed to be an originally ductile structure that has been subject to major brittle reactivation and may have associated narrow dolerite dykes. This character is inferred from associated geometrical similarities to nearby ZSMNS001. The zone has not been investigated by focused direct or indirect methods.

N-S striking deformation zones ZSMNS057A	
Modelling procedure: At the surface, corresponds to a low magnetic and major topographic lineament. Modelled with a vertical dip based on a single field measurement. Inferred similar dominantly brittle character to parallel zone ZSMNS001. Included in the regional model and also present inside local model volume.	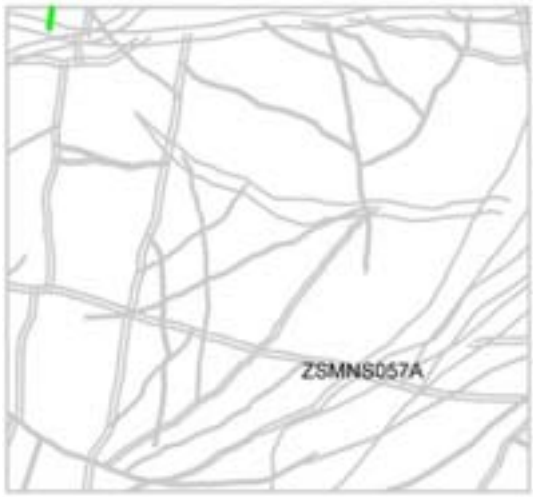
Confidence of existence: Medium	

Property	Quantitative estimate	Span	Confidence level	Basis for interpretation	Comments
Position		± 25 m (surface)	High	Lineament	Well defined topographic lineament
Orientation (strike/dip)	006/90	000-025/± 20	High for strike, low dip	Strike based on trend of lineament. Dip on single field measurement	
Thickness	20 m	10-50 m	Medium	Inferred thickness from topography	Inferred thickness refers to total zone thickness (ductile and brittle, transition zones and core)
core				No data	
Length (regional model)	5.0 km	5.0 ++ km	Medium	Linked lineaments	Possible extension beyond regional model boundary
Ductile deformation	Yes		Low	Weak mapping indicators	
Brittle deformation	Major		Low	Inferred from orientation /ZSMNS001 and topographic lineament.	Reactivation
Alteration			High	Field mapping.	Red staining.
Fracture orientation				No data	
Fracture frequency* Open/sealed m^{-1}				No data	

N-S striking deformation zones ZSMNS057A					
Crush zone Number/total m				No data	
Fracture filling				No data	
Kinematics				No data	

BH	Geometrical Intercept (bh. m)	Target intercept (bh. m)	Comment
None			No BH intercepts

ZSMNS059A

The zone lies in the western half of the local model domain and crosses both the northern and southern domain boundaries with a total length of around 5 km. The NNE-SSW trending magnetic lineament is one of the clearest lineaments in the local domain whilst the topographic lineament is clearly defined in the north but less so in the south. The zone has a clear ductile origin with frequent mylonites but has also clearly been subject to brittle reactivation as shown by the presence of crush zones, slickensides, a marked increase in apertures and the breccias seen in the drillholes. Alteration is generally weak and consists of red staining, saussuritization and epidotization. Drillhole and mapping evidence suggest that the zone is associated with the presence of minor dolerites. It maybe the presence and varying thickness of these dolerites that affect the varying clarity of the associated magnetic lineament along the strike. All evidence suggests that the zone is subvertical with a tendency to dip very steeply to the west. A thickness of 50 m has been applied in the modelling though the zone appears to be complex with a varying number of cores that are likely to have an anastomosing pattern. Detailed mapping of surface outcrops suggests strike-slip sinistral kinematics.

The updated coordinated lineaments (v2.2) indicated possible significant modifications to the associated zone concerning its continuity. This involved the northward extension of the earlier V1.2 lineament being significantly reduced. Instead of continuing north, penetrating ZSMEW002A (Mederhult zone) and terminating at ZSMNE058A, the lineament terminates approximately 420 m to the south of the Mederhult zone, whilst an isolated 400m long section, following the earlier LV1.2 lineament position, remains on the northern side of the Mederhult zone. However, the earlier V1.2 extent of the lineament has been maintained as the 'missing link' and section to the north of Mederhult are supported by field mapping data that suggest a ductile-brittle N-S deformation zone in this position. The field mapping in the location immediately to the north of Mederhult also suggests the zone may be associated with basic dykes. The rock outcrops suggest that at least locally to the north of Mederhult the apparent thickness of the zone is less than 20 m. The updated detailed lineament study (v2.2) supports the earlier removal of a significant offset to the zone as it crossed over ZSMEW900A.

Within the local model area the zone has been subsequently investigated by three hammer drill holes and one rotary cored hole. The drilling results combined with additional geophysical investigations and modelling all support the sub vertical to steep dip to the west of the zone.

Two seismic refraction profiles cross the zone corresponding to the positions of boreholes HLX34 and HLX35 at approximately 220 m and 350 m to the north of ZSMEW900A respectively /Lindqvist 2004, 2005/. The northern profile indicates possibly two cores of highly fractured rock with apparent thicknesses of 3 m to 10 m although the detailed lineament map allows for alternative interpretations. The southern profile indicates possibly three cores of highly fractured rock with apparent thicknesses of 10 m, 7 m and 7 m.

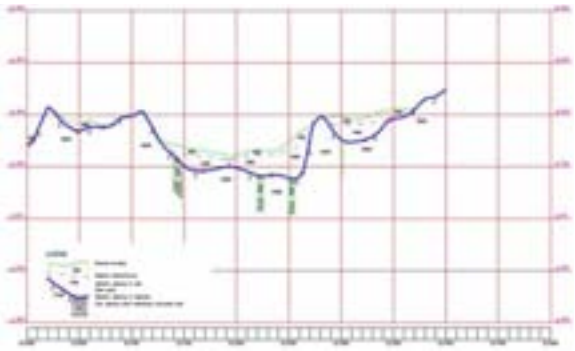

Results from interpretation of refraction seismics in Laxemar. Line LSM000278. /Lindqvist, 2004/

The geophysical resistivity profiling was also carried across the lineament in the same position as the refraction profile, approximately 220 m to the north of ZSMEW900A /Thunehed, et al, 2004/. The resistivity and chargeability profiling indicates a total apparent thickness, including transition zones, of around 50 m.

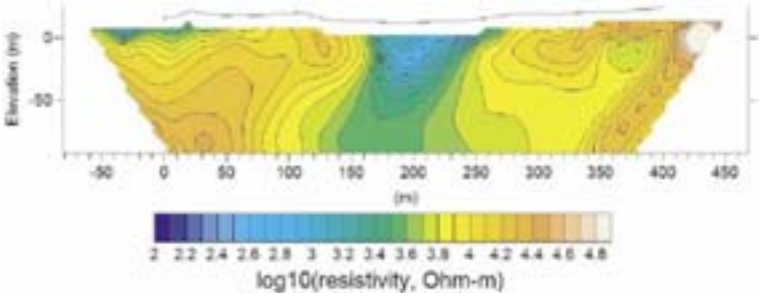

Inverted resistivity section for the central profile LSM000278. The black line shows elevation data along the profile. /Thunehed, et al, 2004/.

Five sections of core in HLX34 with interception widths of 2m to 5m were interpreted by the SHI as representing potential deformation zones. A single section of core in HLX35 with an interception width of 26m was interpreted by the SHI as representing a potential deformation zone. All of these potential deformation zones are of similar character with open fractures. The oriented fractures over the entire depth of HLX35 and from the more highly fractured section of HLX34 indicate that the associated zone is vertical to steeply dipping (80^{o}) to the west. This orientation is consistent with the results from the ground resistivity profiling and the tentative orientation assigned to a seismic reflector taken to represent a splay of ZSMNS059A /Juhlin et al., 2004/. No differentiation has been made between these deformation indicators. All have been taken as being potentially associated with ZSMNS059A and fall within the modelled 50 m thick, subvertical zone geometry.

Later forward modelling of more recent detailed magnetic total field data suggests the thickness of ZSMNS059A varies between 50–100 m in the two modelled profiles with a steep dip to the west /Thunehed and Triumf, 2006/.

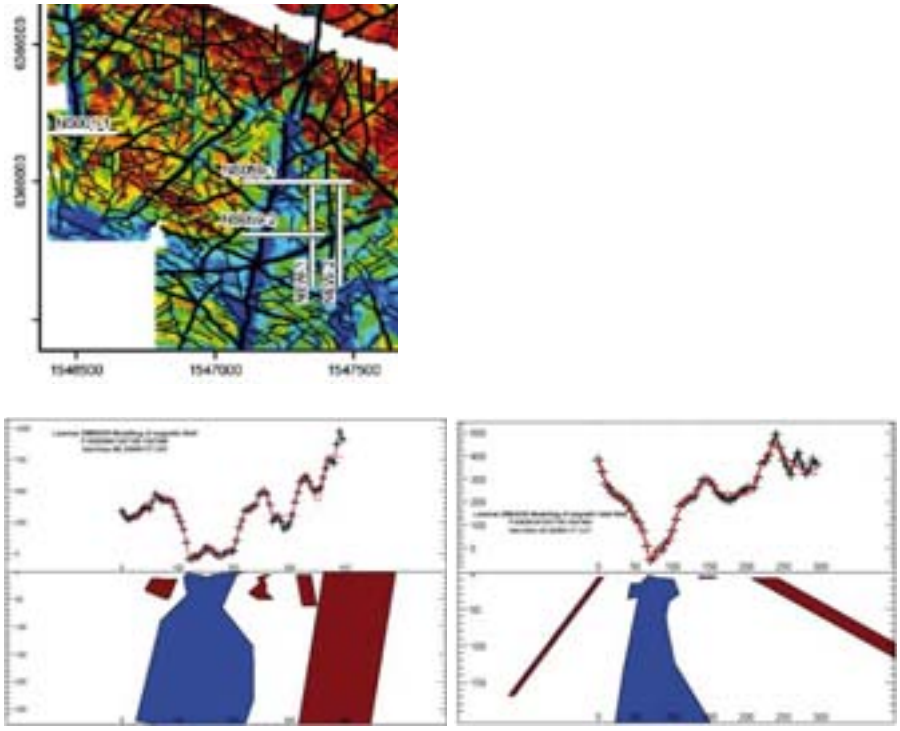

Forward modelling of magnetic total field data over ZMNS059A (profiles NS059-1 and NS059-2). East is towards right in the figure. Blue bodies have low relative magnetic susceptibility /Thunehed and Triumf, 2006/.

Modelling of apparent resistvity results also supports the subvertical, steep to the west dip interpretation

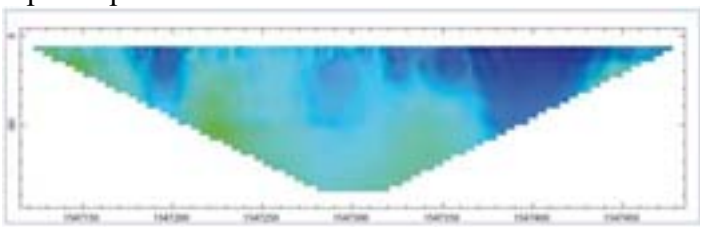

Apparent resistivity pseudo-section, 6366050N. The westernmost low-resistive area corresponds to ZSMNS059A /Thunehed and Triumf, 2006/.

Field mapping identified fairly well distributed indicators along the length of the zone in the local model area all of which support the ductile origin and brittle reactivation of the zone as well as its overall geometry.

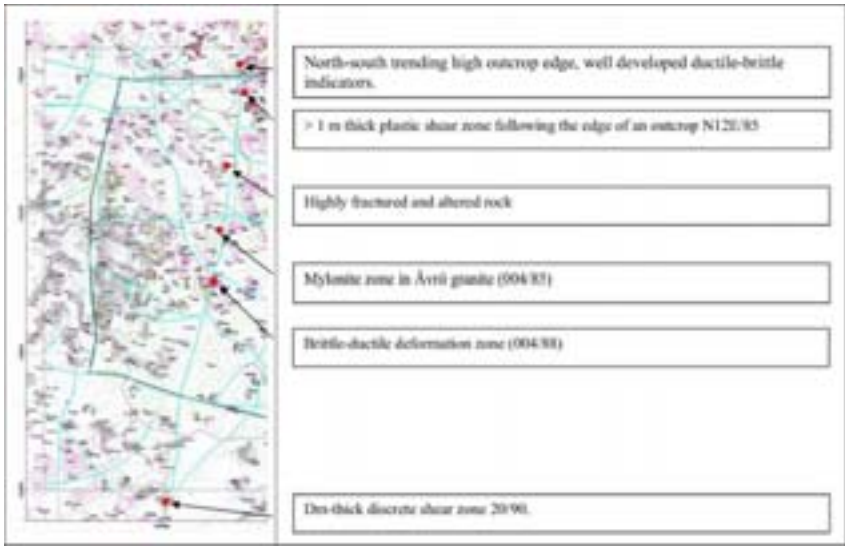

Detailed fracture mapping and kinematic analysis was subsequently performed at four outcrop locations /Lundberg and Sjöström, 2006/. Although only four observations were made the data was quite uniform. The shear zones are thin and rich in epidote or wider and fractured. The shear zones are sinistral or with unspecified sense of shear and poles to all shear zones plot in the same part of the stereogram. One observation of two uncertain lineations was made. The stretching lineation is probably gently dipping and the intersection is probably steep (see below). If so this would indicate horizontal movement.

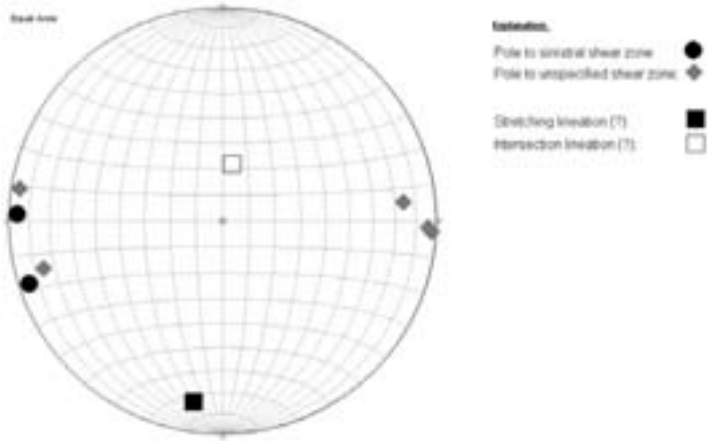

Distribution of shear zones and lineations mapped in the vicinity of ZSMNS059A. Lower hemisphere of Schmidt equalarea, stereographic plot. /Lundberg and Sjöström, 2006/

N-S striking deformation zones ZSMNS059A	
Modelling procedure: At the surface, corresponds to the low magnetic lineament. Clear ductile origin but later brittle reactivation. Associated with minor dolerite intrusions of the same orientation. Modelled using dip that has been inferred from ground geophysical profiling and BHs. Included in the regional model and also present inside local model volume.	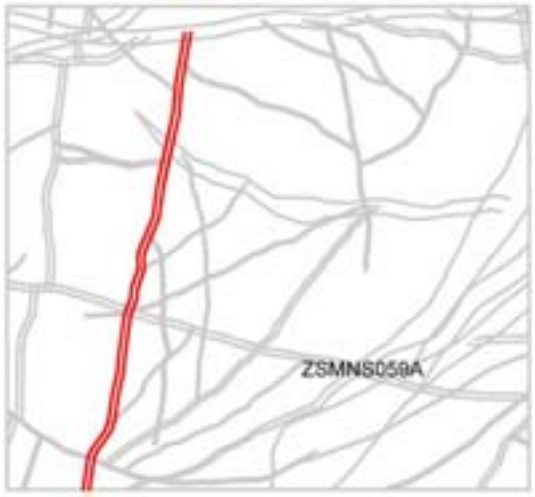
Confidence of existence: High	

Property	Quantitative estimate	Span	Confidence level	Basis for interpretation	Comments
Position		± 20 m (surface)	High	Lineament, BH and geophysical ground survey	
Orientation (strike/dip)	192/88	± 10/± 10	High for strike, high for dip	Strike based on trend of lineament. Dip based on field mapping and boreholes	
Thickness	50 m	20-80 m	High	Lineament, BH and geophysical ground survey	Complex zone, inferred thickness refers to total zone thickness (splays, ductile and brittle, transition zones and core)
core	2-10 m thick, multiple narrow cores. Crush and breccia.	2 to 6 num', 2-10 m thickness	Medium	BHs	
Length (regional model)	4.8 km	+/-200 m	Medium	Linked lineaments	
Ductile deformation	Yes		High	Mylonites, field mapping and KLX14	Present
Brittle deformation	Yes		High	Raised fracture frequency, crush zones, breccia, slickensides, overprinting ductile fabric, KLX14	Present
Alteration			High	BHs and field mapping.	Weak red staining and epidotization
Fracture orientation	195/80, 275/85, 035/35		Medium	KLX14	

N-S striking deformation zones ZSMNS059A					
Fracture frequency* Open/sealed m^{-1}	11/48		Medium	KLX14	
Crush zone Number/total m	8/0.8		Medium	KLX14	
Fracture filling			High	Trench and KLX14	Calcite, chlorite, pyrite, clay, epidote, prehnite, chalcopyrite, hematite, adularia, fluorite.
Sense of displacement	Sinistral		Medium	Nearby outcrops	Probable repeated reactivation

BH	Geometrical Intercept (bh. m)	Target intercept (bh. m)	Comment
HLX34	24,0-113,9	33-113	SHI- DZ1-DZ5, multiple narrow splays. Crush, increased frequency of open fractures, related to minor dolerites
HLX35	58,8-142,5	116-142	SHI DZ1, Major increase of open fractures in the interval 116-127 m, and a moderate increase in the interval 127-142 m. Crush zone at 141.68-141.82 m. Significant low resistivity anomalies, some caliper and p-wave velocity anomalies, and partly anomalously low magnetic susceptibility. 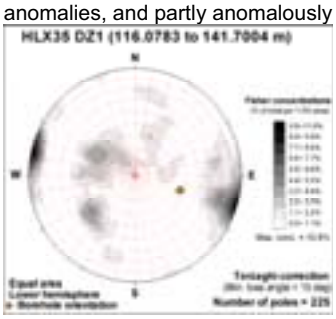
HLX38	22,5-99,1	23-67	SHI- DZ1-DZ3, multiple narrow splays. Minor crush, increased frequency of open fractures and red staining, associated minor dolerite.
KLX14	52,8-128,6	75-125	Eshi DZ4. Inhomogeneous low-grade ductile shear zone overprinted by brittle deformation, characterized by locally increased frequency of open and sealed fractures, four minor core losses, eight crush zones, slickensides, marked increase in apertures, frequent breccias and mylonites. The zone covers the majority of RU2 and is associated with minor sections of dolerite. A c. 5 m wide mylonite occurs at the base of the zone. The upper part of the zone is faintly saussuritized. Throughout the zone there are narrow sections that exhibit weak to medium red staining and weak epidotization. The most intensely deformed sections (cores) are 74.67-82.20, 89.25-93.35, 102.95-119.50 and 125.05-125.35 m. There is a large decrease in resistivity, magnetic susceptibility and P-wave velocity along a major part of the section. There are also several distinct caliper anomalies. The most significant geophysical anomalies occur in the intervals c 74.7-82.2 m, 92.0-93.5 m, 105.0-107.0 m and 112.5-115.5 m. 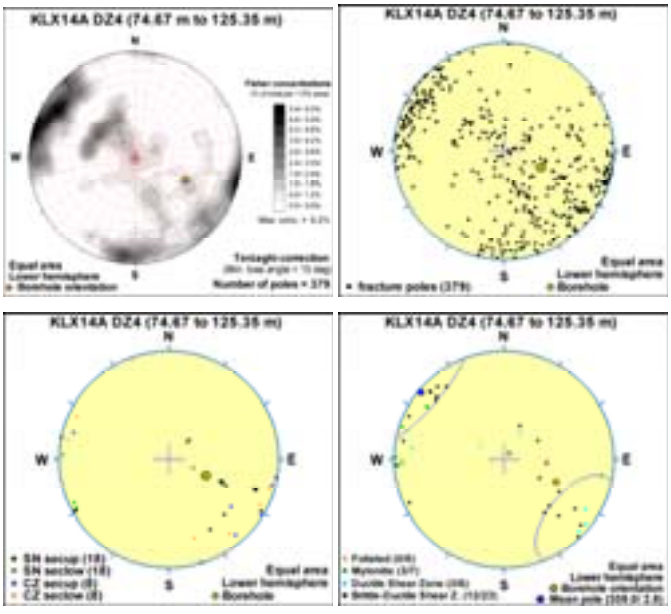

ZSMNS059A, KLX14A drill log extract (zone only)

ZSMNS059A , KLX14A drill core photos (zone only)

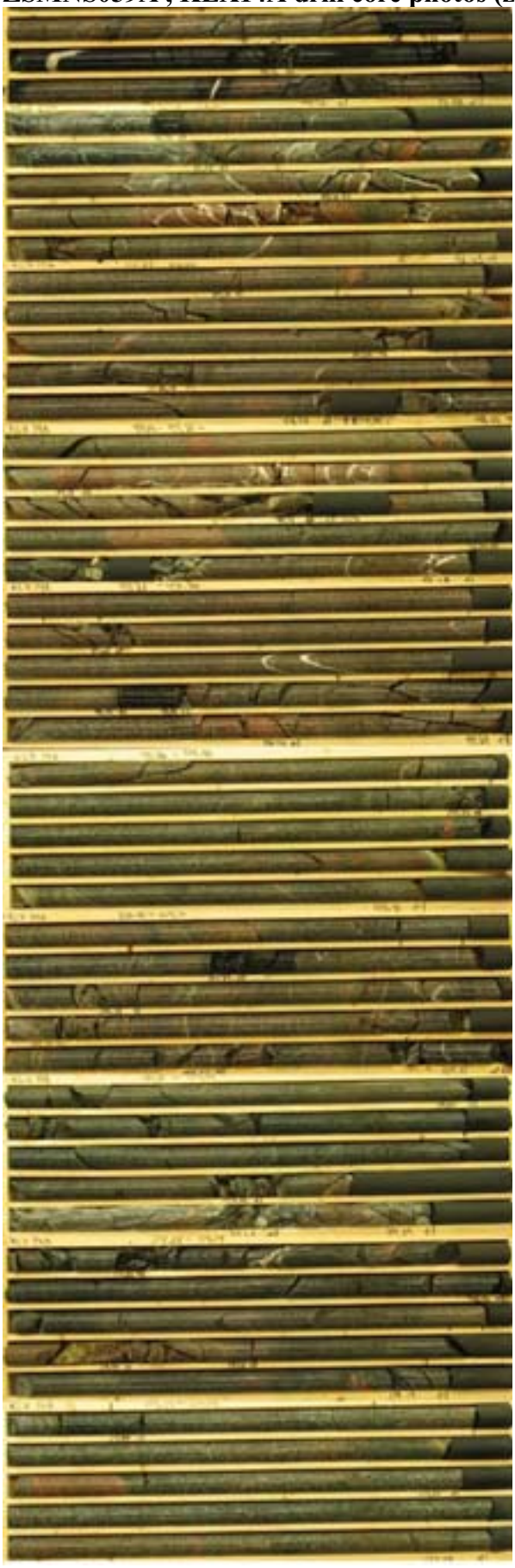

ZSMNS141A

ZSMNS057A is marginal to the southwestern corner of the local model volume with a northern termination against ZSMNW088A. At the surface, the zone corresponds to a low magnetic and clear topographic lineament. The zone has been modelled with an assumed vertical dip though field mapping identifies possibly associated fractured intrusions with steep dips to both the east and west. However, a vertical to steep dip to the west is considered most likely, inferred from an assumed relationship with the parallel zone ZSMNS001. The zone has a length of around 2.5 km and a thickness, inferred from topography ranging from 10 to 50 m. ZSMNS141A is inferred to be an originally ductile structure that has been subject to major brittle reactivation and may have associated narrow dolerite dykes. This character is inferred from associated geometrical similarities to nearby ZSMNS001. The zone has not been investigated by focused direct or indirect methods.

N-S striking deformation zones ZSMNS141A	
Modelling procedure: At the surface, corresponds to a low magnetic and topographic lineament. Modelled with an assumed vertical dip. Inferred similar dominantly brittle character to parallel zone ZSMNS001. Included in the regional model and also present inside local model volume.	
Confidence of existence: Medium	

Property	Quantitative estimate	Span	Confidence level	Basis for interpretation	Comments
Position		± 20 m (surface)	High	Lineament	Well defined topographic lineament
Orientation (strike/dip)	012/90	000-020/± 20	High for strike, low dip	Strike based on trend of lineament. Dip assumed.	A vertical to steep dip to the west is considered most likely, inferred from an assumed relationship with the parallel zone ZSMNS001
Thickness	20 m	10-50 m	Medium	Inferred thickness from topography	Inferred thickness refers to total zone thickness (ductile and brittle, transition zones and core)
core				No data	
Length (regional model)	2.5 km	2.0-2.5 km	Medium	Topographic lineament	
Ductile deformation	Yes		Low	Weak mapping indicators	
Brittle deformation	Major		Low	Inferred from orientation /ZSMNS001 and topographic lineament.	Reactivation
Alteration				No data	
Fracture orientation				No data	
Fracture frequency, m^{-1} (open/sealed)				No data	

N-S striking deformation zones ZSMNS141A					
Crush zone Number/total m				No data	
Fracture filling				No data	
Kinematics				No data	

BH	Geometrical Intercept (bh. m)	Target intercept (bh. m)	Comment
None			No BH intercepts

ZSMNS945A

At the surface, the zone corresponds to a low magnetic and poorly constrained topographic lineament. The zone has been modelled with a vertical dip based on forward modelling of magnetic data /Mattsson et al, 2007/. The zone has a length of 2 km and a thickness of approximately 10 m inferred from magnetic anomaly, topography and seismic refraction surveys. ZSMNS945A is assumed to be a narrow, originally ductile structure that has been subject to brittle reactivation and may have associated narrow dolerite dykes. This character is inferred from associated geometrical similarities to ZSMNS059A and ZSMNS046A. The zone has not been investigated by drilling or other direct methods though the lineament has been intersected by two seismic refraction profiles /Lindqvist 2005, 2006/. The profiles suggest the presence of a brittle zone with possibly multiple narrow cores. The zone is included in the regional model and also present inside the local model volume.

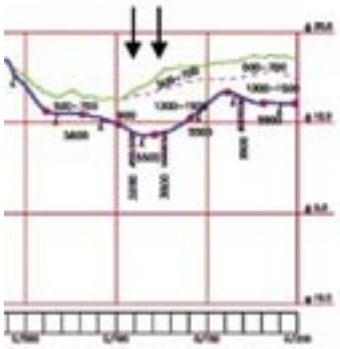

LSM000563, /Lindqvist, 2006/.

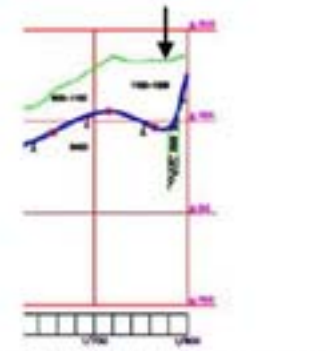

LSM000539, /Lindqvist, 2005/

N-S striking deformation zones ZSMNS945A	
Modelling procedure: At the surface, corresponds to a low magnetic and topographic lineament. Modelled with an assumed vertical dip. Inferred similar character to parallel zone ZSMNS046A. Included in the regional model and also present inside local model volume.	
Confidence of existence: Medium	

Property	Quantitative estimate	Span	Confidence level	Basis for interpretation	Comments
Position		± 20 m (surface)	High	Lineament, geophysical ground survey	
Orientation (strike/dip)	176/90	± 10/± 20	High for strike, low dip	Strike based on trend of lineament. Dip assumed	
Thickness	10 m	5-25 m	Medium	Inferred thickness from magnetic anomaly, topography and seismic refraction survey	Inferred thickness refers to total zone thickness (ductile and brittle, transition zones and core) /Lindqvist, 2005, 2006/
core	5m	+/-2 m	Medium	Seismic refraction profiles (3500m/s)	/Lindqvist, 2005, 2006/
Length (regional model)	2.0 km	2.0-2.3 km	Medium	Linked lineaments	Possible 300m Nw extension beyond ZSMEW007A
Ductile deformation	Major		Low	Inferred from orientation and development model, reference to ZSMNS046A	
Brittle deformation	Minor		Low	Inferred from orientation and development model, reference to ZSMNS046A	Reactivation
Alteration			Low	Field mapping.	Red staining. May not be exclusive to this structure
Fracture orientation	185/90, 115/80, 070/15, 320/80		Low	Inferred from orientation and development model, reference to ZSMNS046A	

N-S striking deformation zones ZSMNS945A					
Fracture frequency* Open/sealed m^{-1}	13/47		Low	Inferred from orientation and development model, reference to ZSMNS046A	
Crush zone Number/total m	0/0		Low	Inferred from orientation and development model, reference to ZSMNS046A	
Fracture filling			Low	Field mapping.	Chlorite, epidote.
Kinematics	-				

BH	Geometrical Intercept (bh. m)	Target intercept (bh. m)	Comment
None			No BH intercepts

ZSMNS947A

At the surface, corresponds to a low magnetic and poorly constrained topographic lineament. The zone has been modelled with a vertical dip based on modelling of magnetic data /Mattsson et al, 2007/. ZSMNS947A is assumed to be a narrow, originally ductile structure that has been subject to brittle reactivation and may have associated narrow dolerite dykes. This character is inferred from associated geometrical similarities to ZSMNS059A and ZSMNS046A. The zone has not been investigated by drilling or other direct methods. The zone is included in the regional model and also present inside local model volume.

N-S striking deformation zones

ZSMNS947A

Modelling procedure: At the surface, corresponds to a low magnetic and poorly constrained topographic lineament. Modelled with an assumed vertical dip. Inferred similar character to parallel zone ZSMNS046A. Included in the regional model and also present inside local model volume.

Confidence of existence: Medium

Property	Quantitative estimate	Span	Confidence level	Basis for interpretation	Comments
Position		± 20 m (surface)	High	Lineament, geophysical ground survey	
Orientation (strike/dip)	178/90	± 10/± 20	High for strike, low dip	Strike based on trend of lineament. Dip based on modelled magnetic data	/Mattsson et al., 2007/
Thickness	20 m	5-25 m	Medium	Inferred thickness from magnetic anomaly.	
core	3 m	0-5m	Low	Not identified by seismic refraction survey	/Lindqvist, 2005/
Length (regional model)	1.8 km	1.0-1.8 km	Medium	Linked lineaments	
Ductile deformation	Major		Low	Inferred from orientation and development model, reference to ZSMNS046A	
Brittle deformation	Yes		Low	Inferred from orientation and development model, reference to ZSMNS046A	Reactivation
Alteration					
Fracture orientation	185/90, 115/80, 070/15, 320/80			Inferred from orientation and development model, reference to ZSMNS046A	
Fracture frequency* Open/sealed m^{-1}	13/47			Inferred from orientation and development model, reference to ZSMNS046A	

N-S striking deformation zones ZSMNS947A					
Crush zone Number/total m	0/0			Inferred from orientation and development model, reference to ZSMNS046A	
Fracture filling			Low	Field mapping.	Chlorite, epidote
Kinematics	-				

BH	Geometrical Intercept (bh. m)	Target intercept (bh. m)	Comment
HLX42	116.1-152.6	-	No ESHI interpreted DZ. Foliation with a sub-vertical dip to the west-possible associations with the interpreted zone and possible nearby dolerite intrusions. Raised open and partly open fracture frequency in the section 130-150 m. Inconclusive.

KLX04_DZ6b

N-S striking deformation zones KLX04_DZ6b	
KLX04_DZ6b is based on a further subdivision of Eshi KLX04 DZ6 following a detailed drill core inspection by /Viola et al, 2007/. The orientation is based on this fracture mapping.	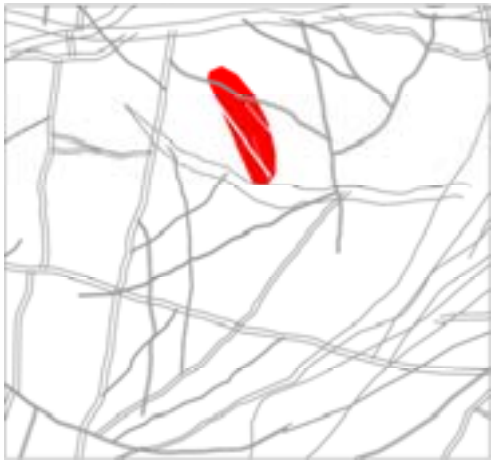
Confidence of existence: High	

Property	Quantitative estimate	Span	Confidence level	Basis for interpretation	Comments
Position			Medium	/Viola et al, 2006/ subdivision of Eshi DZ6	
Orientation (strike/dip)	156/67		Low	Core orientation /Viola et al, 2006/	
Thickness	14 m		Low		
Length (regional model)	1.0 km		Low	Assumed	
Ductile deformation	No		low		
Brittle deformation	Yes		High	Increased fracture frequency, cataclastics, crush and gouge zones,	
Alteration			High		Red staining, epidotization
Fracture frequency* Open/sealed m^{-1}	15/31		Low	Eshi KLX04 DZ6	
Crush zone Number/total m	5/0.6		Low		
Fracture filling				Eshi KLX04 DZ6	Calcite, chlorite, clay, red feldspar, quartz, hematite epidote, Laumontite, fluorite, zeolites, pyrite, kaolinite, chalcopyrite

<table>
<tr><th>BH</th><th>Geometrical Intercept (bh. m)</th><th>Target intercept (bh. m)</th><th>Comment</th></tr>
<tr><td>KLX04</td><td>886-914</td><td>887-914</td><td>Note this interval differs from Eshi DZ6, 873-973 m, based on further subdivision by NGU /Viola et al, 2007/ .
<table>
<tr><td>887-889 m</td><td>Transition zone</td><td>Increasing deformation, crush rock intervals and occurrence of fault rock.</td></tr>
<tr><td>889-897 m</td><td>Fault core</td><td>Cataclasite (c) and protocataclasite (pc) occurrences. Small zones of ultracataclasite (uc). Sample KLX04-3 and 4.</td></tr>
<tr><td>897-914 m</td><td>Transition zone</td><td>Fracture frequency: 18-30 fractures/meter (f/m)</td></tr>
</table>
The figure below shows four distinct fault rock occurrences, with complex crosscutting relationships. Epidote veins crosscut a protocataclastic zone. These are in turn brittley offset along a band of cemented breccia. The breccia contains elongated, strongly reworked fragments of cataclasite and epidote, which are cemented together by chlorite and/or epidote matrix. This is in turn crosscut by ultracataclasite/gouge (to the left end of the figure below), with abundant epidote in the matrix and only dispersed fragments of cataclasite, epidote and calcite. Calcite cemented all fragments.
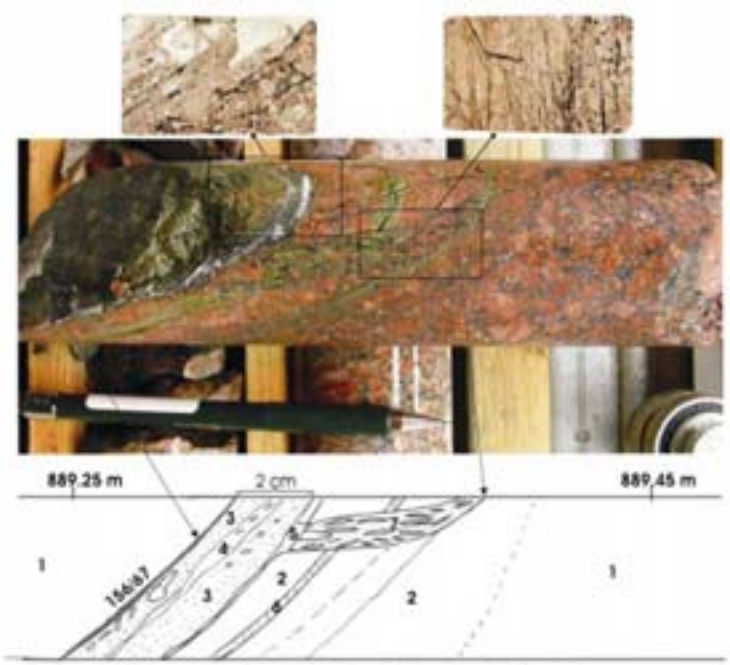

1- Protocataclasite with granite clasts and ~10% matrix.
2- Cataclasite with granite clasts and ~30% matrix.
3- Ultracataclasite with clasts of granite, cataclasite and calcite in a range of 0.1-1 mm. It consists of 80-100% matrix composed of amongst other epidote.
4- Cataclasite clasts in an epidote matrix.
5- Calcite "vein".
6- Epidote vein.
7- Brecciated clasts of cataclasite, epidote and calcite in a dark, fine fragmented matrix.</td></tr>
</table>

KLX04_DZ6c

N-S striking deformation zones KLX04_DZ6c	
KLX04_DZ6c is based on a further subdivision of Eshi KLX04 DZ6 following a detailed drill core inspection by /Viola et al, 2007/. The orientation is based on this fracture mapping.	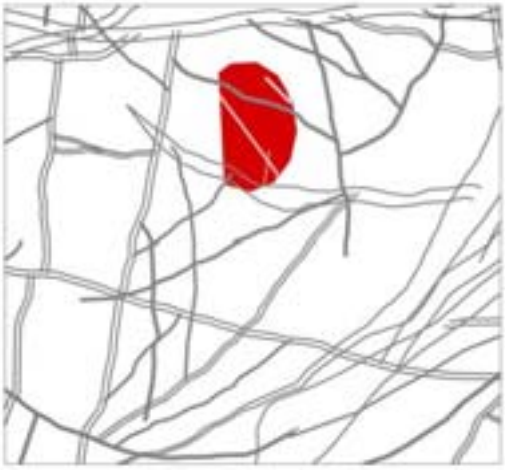
Confidence of existence: High	

Property	Quantitative estimate	Span	Confidence level	Basis for interpretation	Comments
Position			Medium	/Viola et al, 2007/ subdivision of Eshi DZ6	
Orientation (strike/dip)	177/42		Low	Orientation /Viola et al, 2007/	
Thickness	30 m		Low		
Length (regional model)	1.0 km		Low	Assumed	
Ductile deformation	No		low		
Brittle deformation	Yes		High	Increased fracture frequency, cataclastics, breccia, crush and gouge zones,	
Alteration			High		Red staining, chloritization, epidotization, saussuritization
Fracture frequency* Open/sealed m^{-1}	15/31		Low	Eshi KLX04 DZ6	
Crush zone Number/total m	14/2.3		Low		

N-S striking deformation zones KLX04_DZ6c					
Fracture filling				Eshi KLX04 DZ6	Calcite, chlorite, clay, red feldspar, quartz, hematite epidote, Laumontite, fluorite, zeolites, pyrite, kaolinite, chalcopyrite

BH	Geometrical Intercept (bh. m)	Target intercept (bh. m)	Comment
KLX04	935-972	935-972	Note this interval differs from Eshi DZ6, 873-973 m, based on further subdivision by NGU /Viola et al, 2006/.

932,5-941 m	Transition zone	Fracture frequency 30-35 f/m, and increasing occurrence of cataclastic bands.
941-956 m	Fault core	Thick fault core of ~15 m, with indurated breccia/cataclasite, and narrow gouge layers. Sample KLX04-6 and 7.
956-972 m	Transition zone	Decreasing deformation intensity and fracture frequency.

Figure B below displays a cataclasite with two distinct structural imprints, with the latest stage infilled by calcite veining. The black injection is formed by very fine-grained material, possibly gouge or a fluidized ultracataclasite, whereas the surrounding cataclasite consists of reworked granite fragments. The cataclasite is in turn crosscut by a thin band of ultracataclasites, later injected by a pervasive calcite vein network. Below in the figure C shows a chlorite rich cataclasite crosscut by a distinct red gouge.

B) 946.25 m C) 949.60 m

KLX07_DZ13

N-S striking deformation zones KLX07_DZ13	
KLX07_DZ13's orientation is based on mapped mylonite and deformation zone in the drillcore core along with a secondary fracture pole concentration and oriented crush.	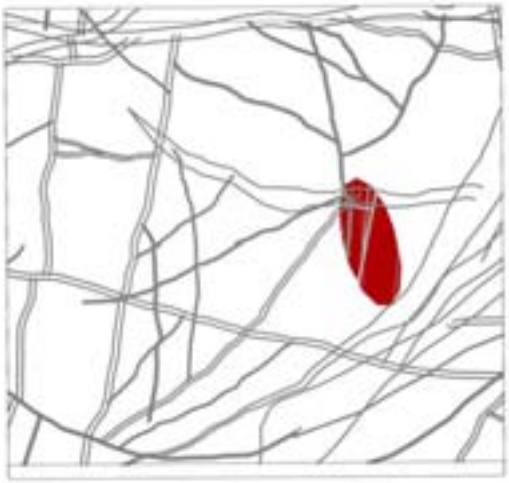
Confidence of existence: High	

Property	Quantitative estimate	Span	Confidence level	Basis for interpretation	Comments
Position			High	Eshi	
Orientation (strike/dip)	348/65		Low	Mapped mylonite and deformation zone in core; also secondary pole concentration and some oriented crush. Thickness 10m gives 812-837m.	
Thickness	10 m		Low		
Length (regional model)	1.0 km		Low	Assumed	
Ductile deformation	Yes		High	Mylonite	
Brittle deformation	Yes		High	Raised fracture frequency and crush	
Alteration			High		Red staining
Fracture frequency* Open/sealed m^{-1}	13/42		Low		
Crush zone Number/total m	2/<1		Low		
Fracture filling			High		Calcite, chlorite, hematite, quartz, epidote, clay, pyrite

BH	Geometrical Intercept (bh. m)	Target intercept (bh. m)	Comment
KLX07A	810-835	817-836	Eshi DZ13: Increased frequency of open fractures and crush at 820.83-821.04, 821.50-821.55, 825.49-825.72, 826.13-826.28, 828.60-828.65 and 831.39-832.27 m. Four radar reflectors are identified, two of them are oriented. The oriented reflectors occur at 820.9 m with orientation 85/033 and at 832.8 m with orientation 89/209. The section is characterized by several distinct anomalies in the p-wave velocity log data and only minor low resistivity and caliper anomalies. 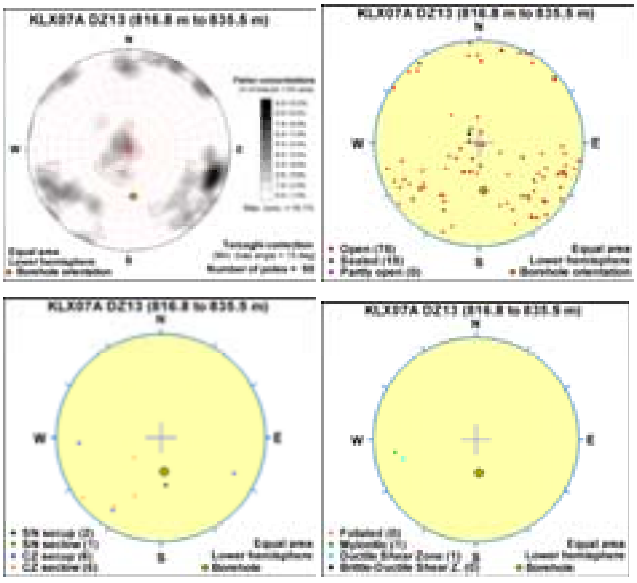 Ref: /Viola et al, 2006/: 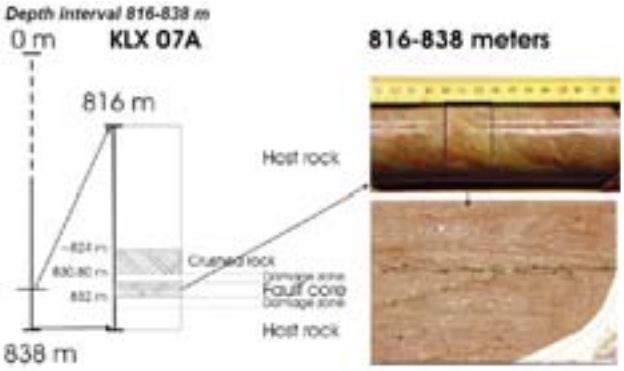 *Schematic illustration of studied section and thin section of a strongly foliated mylonitic rock locally reworked into an ultra cataclasite (brownish-red and black bands).* This relatively short interval is characterized by undisturbed rock, with only a crushed or highly fractured zone containing fault rock occurrences with abundant epidote veining. The predominant fault rocks characterising the fault zone at depth 831 m are mylonites and some volumetrically minor cataclasites. The thin section analysis shows the mylonitic fabric overprinted by thin strands of ultracataclasite (brownish red lines).

BH	Geometrical Intercept (bh. m)	Target intercept (bh. m)	Comment
			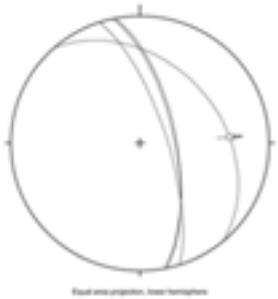 *Orientation of the mylonitic fabric in KLX 07A, depth interval 816-838 m.* The mylonitic fabric dips rather steeply to the E-ENE. One NE-dipping fault surface containing top-to-E normal kinematics is also shown.

KLX21B_DZ10-12

N-S striking deformation zones KLX21B_DZ10-12	
KLX21B_DZ12 is taken to be the main zone with DZ10 and DZ11 as associated minor structures. The orientation is based on multiple mylonite and brittle-ductile deformation zones mapped in the drillcore.	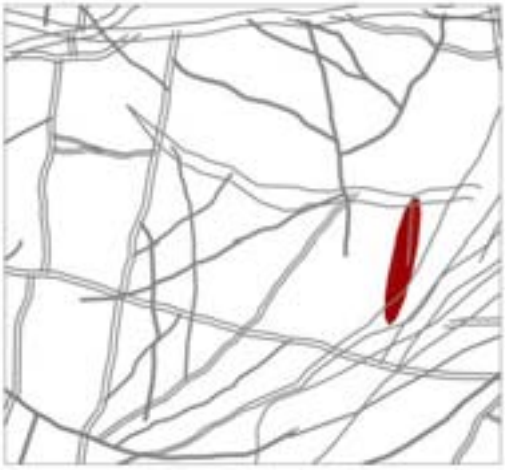
Confidence of existence: High	

Property	Quantitative estimate	Span	Confidence level	Basis for interpretation	Comments
Position			High	Eshi	
Orientation (strike/dip)	192/80		Low	Mapped ductile core orientation at 655 m.	
Thickness	10 m		Low		
Length (regional model)	1.0 km		Low	Assumed	
Ductile deformation	Yes		high	Mapped ductile core	
Brittle deformation	Yes		High	Increased frequency of sealed fractures, moderate increase in open fractures, some of which have large apertures, three crush zones,	
Alteration			High	KLX21B_DZ12	Red staining, epidotization
Fracture frequency* Open/sealed m^{-1}	10/58		Low	KLX21B_DZ12	
Crush zone Number/total m	3/0.1		Low	KLX21B_DZ12	
Fracture filling				KLX21B_DZ12	Calcite, chlorite, epidote, hematite, clay, pyrite, andularia, prehnite, quartz, laumontite, fluorite.

BH	Geometrical Intercept (bh. m)	Target intercept (bh. m)	Comment
KLX21B	455-764	559-707	Eshi DZ10 559-572 m: Inhomogeneous brittle deformation zone characterized by increased frequency of sealed fractures, slight increase in open fractures, breccias, cataclasites, weak to medium red staining and slickensides. Low resistivity, P-wave velocity and magnetic susceptibility. The oriented reflector occurs at 565.9 m with the orientation 037/16 or 289/45.The host rock is dominated by Ävrö quartz monzodiorite (501046). 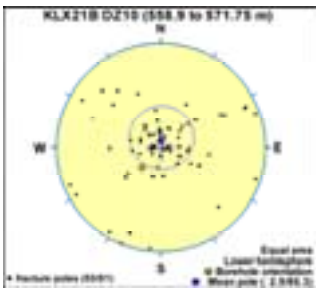 DZ11 577,7- 578 m: Brittle-ductile deformation zone characterized by increased frequency of sealed fractures, medium red staining and slickensides. Minor low-resistivity anomaly.The host rock is dominated by Ävrö quartz monzodiorite (501046). 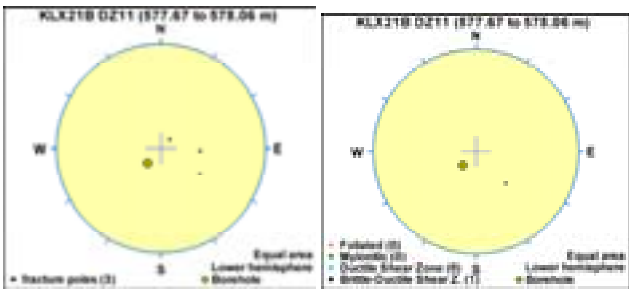 DZ12 595-707 m: Inhomogeneous low-grade, ductile deformation zone overprinted by brittle deformation. It is characterized by increased frequency of sealed fractures, moderate increase in open fractures, some of which have large apertures, three crush zones, mylonites, cataclasites, brittle-ductile shear zones, breccias, faint to strong red staining, inhomogeneous faint to weak epidotization and slickensides. The most intensely deformed sections are 605.05-609.70 m (mainly ductile), 638.78-657.88 m and 672.60-706.95 m. Low magnetic susceptibility throughout the entire section. Low resistivity and P-wave velocity in the sections 605-609 m, 624-631 m and 670-706 m. One oriented and two non-oriented radar reflectors occur within DZ4. Three oriented reflector occurs at 615.0 (orientation 318/67), 675.9 m (orientation 331/74) and at 706.9 m (orientation 054/41). The reflectors are rather strong and can be observed to a distance of 9-12 m outside the borehole.The host rock is dominated by Ävrö granodiorite (501056) in the upper part and fine-grained dioritoid 501030) in the lower part. Subordinate rock types are diorite/gabbro (501033), fine-grained granite (511058), pegmatite (501061), granite (501058) and fine-grained diorite-gabbro (505102). 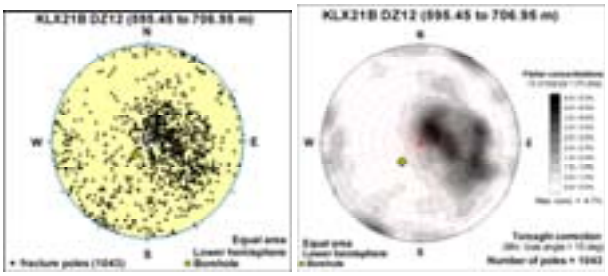

BH	Geometrical Intercept (bh. m)	Target intercept (bh. m)	Comment
			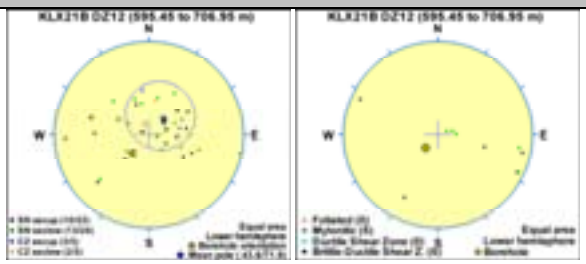 From /Viola et al, 2007/: The zone is hosted within a porphyritic, medium-grained granite to quartz monzodiorite. 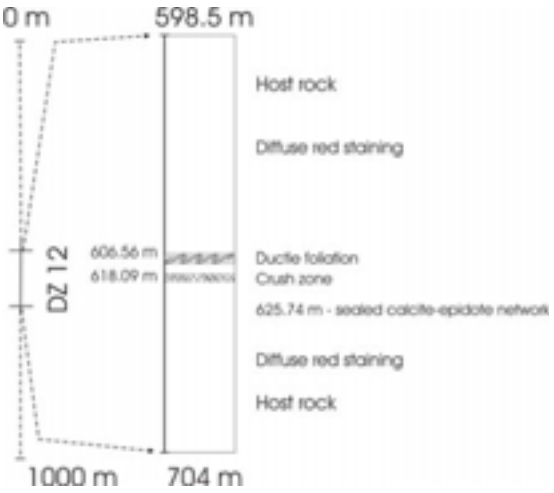 No significant structural features were observed and we do not classify DZ 12 as a proper deformation zone, because it does not fulfill the general structural criteria as it lacks core and transition zones. Nonetheless, a few minor structures are present within the logged interval. At depth 618.09 m there is a crush zone. BIPS images allowed the measurement of one of its main fractures, oriented 180/58, see figure below. The crush zone formed at the expense of a dilatant sealed network containing veins of calcite, epidote and clay minerals. Dilation led to localised, minor brecciation. 

BH	Geometrical Intercept (bh. m)	Target intercept (bh. m)	Comment
			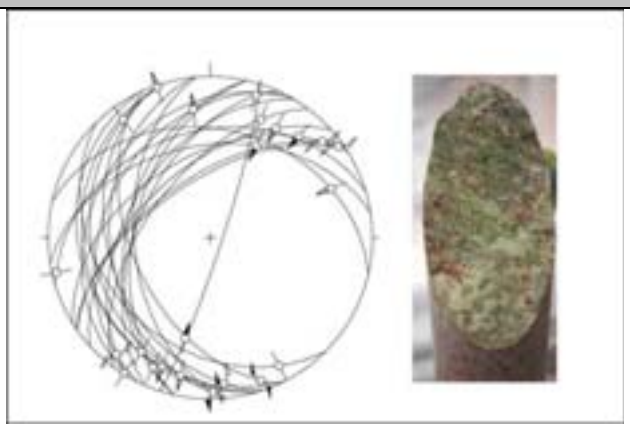 Striated surfaces in DZ 12 of KLX21B dip gently to moderately to the southwest, west and northwest. High obliquity (thus transtensional and transpressional) normal and reverse shear is observed on most of the fracture planes. These are coated predominantly by epidote, chlorite and calcite

KLX28_DZ1

N-S striking deformation zones KLX28_DZ1	
KLX28_DZ1's orientation 182/33 is based on mapped brittle ductile shear indicators in the core supported by crush and sealed network orientations. The interpreted orientation results in a true thickness of around 13 m. The modelled extent does not result in any other BH interceptions.	
Confidence of existence: High	

Property	Quantitative estimate	Span	Confidence level	Basis for interpretation	Comments
Position			High	Eshi	
Orientation (strike/dip)	182/33		Low	Mapped brittle-ductile shear indicators in the core supported by crush and sealed network orientations.	
Thickness	13 m		Low		
Length (regional model)	1.0 km		Low	Assumed.	
Ductile deformation	Yes		High	Mapped brittle-ductile shear indicators in the core.	
Brittle deformation	Yes		High	Mapped brittle-ductile shear indicators in the core supported by crush and sealed network orientations.	
Alteration			High		Red staining
Fracture frequency Open/sealed m^{-1}	6/65				
Crush zone Number/total m	3/0.2		Low		Single intercept

BH	Geometrical Intercept (bh. m)	Target intercept (bh. m)	Comment
KLX28	14-33	14-33	Eshi DZ1 14.4-33.1 Inhomogeneous brittle-ductile deformation zone characterized by slightly increased frequency of open and sealed fractures, crush zones, cataclasite, slickensides and locally faint to weak red staining. The most intensely deformed part is the section 27.70-30.35 m, which is associated with fine-grained diorite-gabbro (505102). Several distinct low resistivity and decreased P-wave velocity anomalies in the entire section. The core is also characterized by caliper anomalies and decreased magnetic susceptibility. One oriented radar reflector occurs at 27.3 m (096/76) and five non-oriented radar reflectors occur with angle in the interval 43-69° to borehole axis. The oriented reflector can be observed to a distance of 8 m outside the borehole. Low radar amplitude at 13-21 m. The host rock is dominated by Ävrö quartz monzodiorite (501046). Subordinate rock types comprise fine-grained granite (511058) and fine-grained diorite-gabbro (505102), and sparse occurrences of pegmatite (501061), granite (501058) and fine-grained dioritoid (501030). 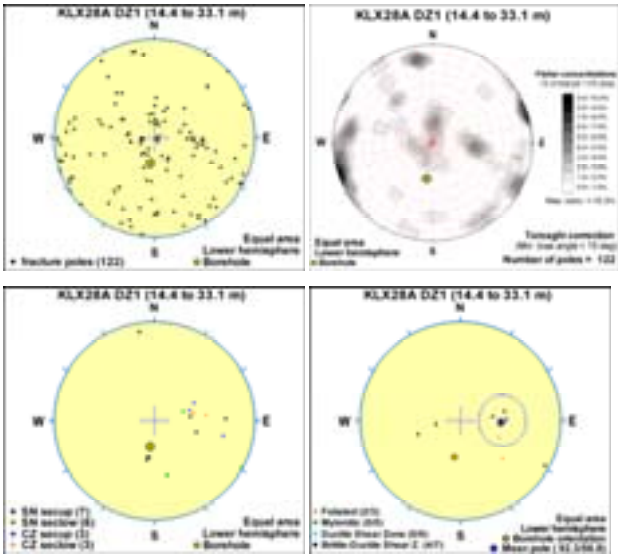

HLX28_DZ1

N-S striking deformation zones HLX28_DZ1	
HLX28_DZ1's orientation 180/20 is based on a fracture pole concentration that results in a true thickness of around 10m. The modelled extent results in interceptions in Bhs KLX11A, KLX19A, and HLX32. KLX19A was not cored at this depth but a correlation is possible. KLX11A gives correlation with two very thin DZs from the Eshi, namely DZ1 and DZ2, which are interpreted as having similar orientations to HLX28_DZ1. Fracture orientation data from the theoretical intercept DZ1 in HLX32 and DZ1 in KLX27 strongly suggests that the zone does not extend south of ZSMNW042A.	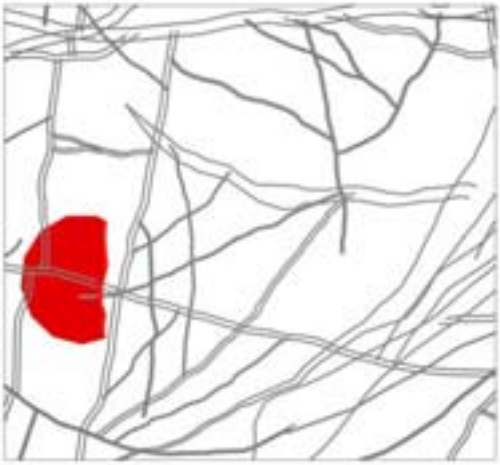
Confidence of existence: High	

Property	Quantitative estimate	Span	Confidence level	Basis for interpretation	Comments
Position			High	Eshi	
Orientation (strike/dip)	180/20		Low	Fracture pole concentration	
Thickness	10 m		Low		
Length (regional model)	1.0 km		Low	Assumed	
Ductile deformation	No		Low		
Brittle deformation	Yes		High	Raised fracture frequency	
Alteration			High		Red staining
Fracture frequency Open/sealed m^{-1}	-				
Crush zone Number/total m	0/0		Low		Single intercept

BH	Geometrical Intercept (bh. m)	Target intercept (bh. m)	Comment
HLX28	75-89	75-89	Eshi DZ1 75-89 m: Characterized by increased fracture frequency, weak to strong alteration (oxidation) and aperture up to at least 10 mm. Increased penetration rate. Several distinct anomalies in all geophysical loggings. 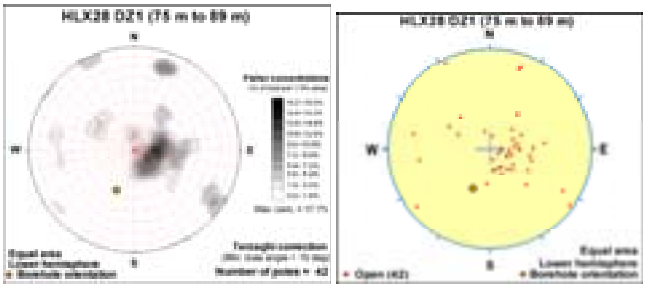
KLX11	144-154	142-143 and 162-163	Eshi DZ1 142-143 m: Minor low grade ductile shear zone. Increased frequency of open fractures and sealed fractures. Low P-wave velocity, low resistivity and low magnetic susceptibility. The host rock is dominated by quartz monzodiorite (501036). 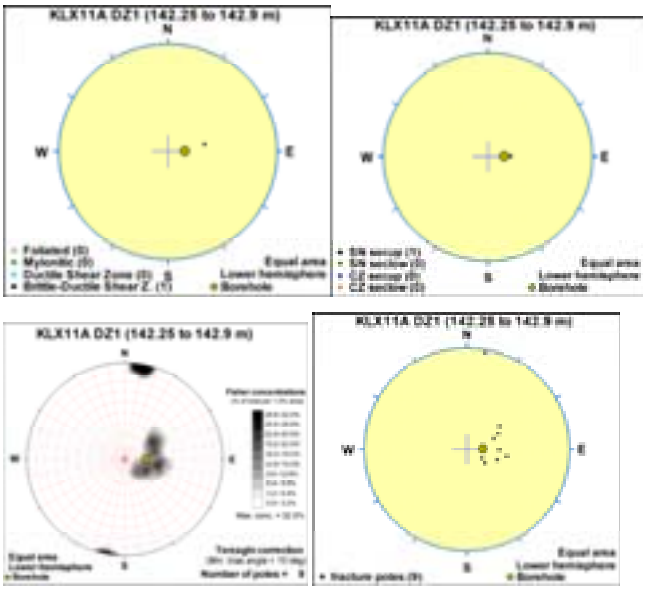 Eshi DZ2 162-163 m: Minor low grade ductile shear zone, overprinted by sealed fractures. Low P-wave velocity, low resistivity and low magnetic susceptibility. The host rock is dominated by fine-grained diorite-gabbro (505102).

BH	Geometrical Intercept (bh. m)	Target intercept (bh. m)	Comment
HLX32	98-110	104-114	-NO CORRELATION- SUGGESTS NO EXTENSION SOUTH OF ZSMNW042A Eshi DZ3 104-114 m: The deformation zone is located to a minor section of diorite/gabbro (501033). Increased fracture frequency and increased apertures in single fractures. There is a significant decrease in the resistivity logs in the section 104-125 m and there are minor caliper anomalies in the section. At c. 115 m there is a large decrease in the fluid resistivity. 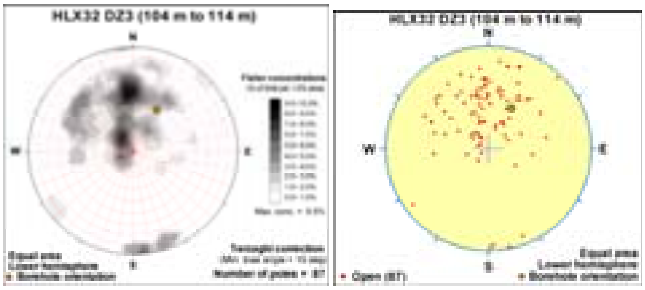
KLX27	103-115	106-110	-NO CORRELATION- SUGGESTS NO EXTENSION SOUTH OF ZSMNW042A Eshi DZ1 105.9-109.8 m: Minor brittle deformation zone in composite intrusion with increased frequency of sealed fractures, sealed network, breccia, faint to weak red staining and one slickenside. One crush and faint saussuritization. The resistivity and magnetic susceptibility are significantly decreased, whereas the P-wave velocity is partly decreased. The host rock is dominated by fine-grained diorite-gabbro (505102) and fine-grained granite (511058) in the upper part. Confidence level=3. 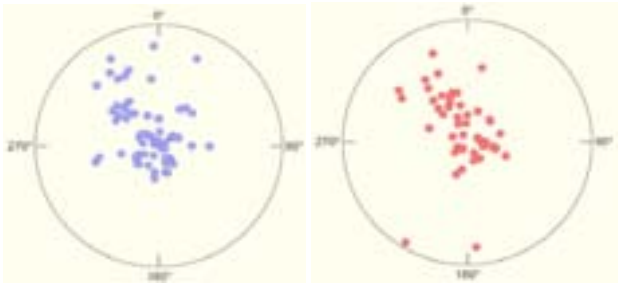 Sealed fractures Open and Partly Open fractures (Projection Wulff)

E-W and NW-SE striking, steep to moderately southward dipping deformation zones

ZSMEW002A (Mederhult zone)

The interpreted geometry of the regional Mederhult deformation zone, ZSMEW002A, remains largely unchanged from that presented in version 1.2 /Wahlgren et al, 2006/. However, subsequent drilling has confirmed the geometry and enabled a better characterization of the zone. In short it can be described as following, in the western part, the interpretation made in model version 0 and in the eastern part a topographic and magnetic lineament running along the northern coastline of Äspö. The continuation of the zone along this alignment fits well with the trends indicated by seismic reflector projections /Juhlin et al. 2002, 2004a/, the resistivity measurements from the airborne geophysical surveys, /Thunehed et al. 2004/, topographical map /Wiklund 2002/, ground geophysics /Stenberg and Sehlstedt 1989/ and the interpretation for the extension of Äspö shear zone (ZSMNE005A) /Berglund 2004/.

The zone has previously been verified by ground magnetic and VLF measurements /Stenberg and Sehlstedt 1989/, a refraction seismic survey /Rydström and Gereben 1989/, reflection seismics /Bergman et al. 2001/ and surface geology /Stanfors and Erlström 1995/. Results from the VLF measurements indicate that the zone has a steep southerly dip.

The interpreted mean geometry in terms of strike and dip of the zone within the local model volume is 90/65. The conclusion in the version 0 model regarding dextral movements during the Phanerozoic has not been verified and remains an open issue. The Mederhult deformation zone is considered to have formed under ductile conditions, but have been reactivated under brittle conditions, presumably during several events. The zone is modelled with a total thickness of 100 m (based on an attempt to provide a representative value over the entire zone length). This thickness, like others, should be interpreted as an envelope, containing the zone indicators, multiple inferred splays etc. Further, the estimated thickness is based on a combination of ‘hard’ data from field mapping, boreholes and tunnel intercepts along with ‘fuzzy’ data from the various background data sets to the original lineament interpretations-magnetic maps.

The section of drill core from KLX06, interpreted as corresponding to ZSMEW002A, was examined in detail in an attempt to characterize the zone /Braathen & Nordgulen, 2005, /Viola & Ganerod, 2006/. This section (297-425 m) corresponds to DZ 2 in the single-hole interpretation. The fault presents brittle-ductile deformation features. The section contains a narrow zone of crushed rock and a distinct fault core containing brittle fault rocks that overprint a rather pervasive foliation. The transition zone consists of foliated granites with localized brittle-ductile deformation bands. The fault core consists of protomylonites, cataclasites and red gouge. The protomylonites are affected by later brittle deformation as suggested by the presence of mylonitic fragments in the crosscutting cataclasites and are cemented by laumontite.

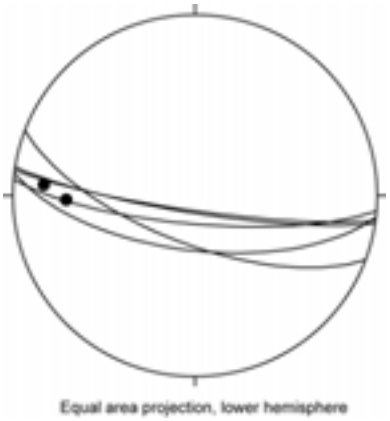

Orientation of the brittle-ductile shear zone that characterizes the 368-390 m depth interval of KLX 06. Solid dots show the azimuth of two chlorite-defined stretching lineations.

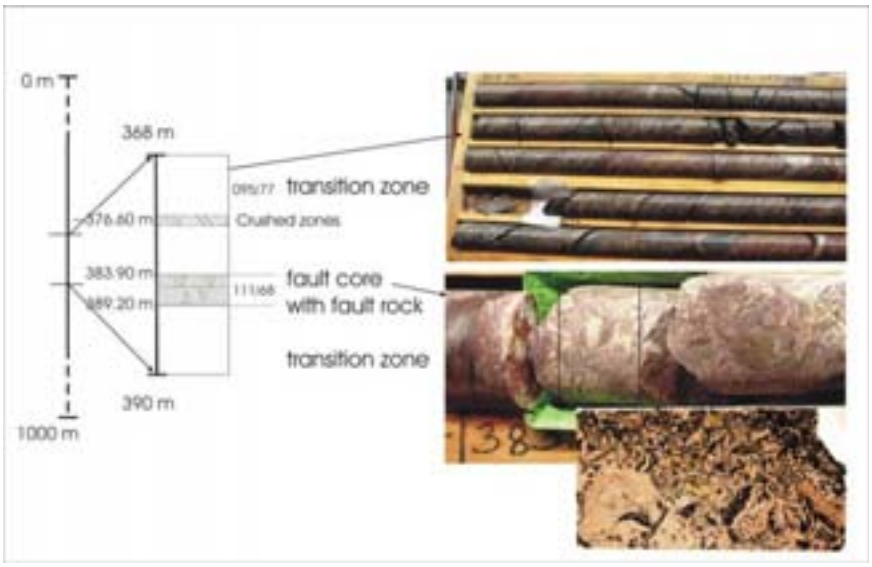

Schematic illustration of the logged section with orientation of chosen structural features. To the right, thin section of a cataclastic sample at depth ~384,7 m.

Photograph from drill core KLX06, at 395 m, showing a protobreccia to breccia that is cemented by laumontite zeolite.

E-W striking deformation zones ZSMEW002A (Mederhult zone)	
Modelling procedure: At the surface, corresponds to the low magnetic and topographic lineaments. Modelled to base of regional model volume using dip that has been inferred mainly from a seismic reflector /Juhlin et al. 2002, 2004a/ and KLX06. Included in regional model and also present inside local model volume.	
Confidence of existence: High	

Property	Quantitative estimate	Span	Confidence level	Basis for interpretation	Comments
Position		± 20 m (surface)	High	Lineament, BH and geophysical ground survey	
Orientation (strike/dip)	090/65	± 20/± 10	High for strike, medium for dip	Strike based on trend of lineament. Dip based on seismic reflector, and boreholes, primarily KLX06.	
Thickness	100 m	20-200 m	High	Lineament, BH and geophysical ground survey	Complex zone, inferred anastomosing geometry. Thickness refers to total zone thickness (ductile and brittle, transition zone and core)
Core	10 m	5-15 m	Medium	KLX06	Likely multiple cores
Length (regional model)	17.9 km	+/-5 km	Medium	Linked lineaments	30km, including extension outside the regional model area
Ductile deformation	Yes		High	Mylonites in BHs and field mapping.	Present
Brittle deformation	Yes		High	Cataclasites, breccia and crush zones in BHs	Present
Alteration			High	BHs and field mapping.	Dominated by red staining, but also sections of saussuritization, laumontite, and clay alteration
Fracture orientation	025/85, 110/80, 290/10		Medium	KLX06	

E-W striking deformation zones ZSMEW002A (Mederhult zone)					
Fracture frequency* Open/sealed m^{-1}	4/42		Medium	KLX06	
Crush zone Number/total m	23/10	±10/ 5-25	Medium	KLX06	
Fracture filling			High	KLX06	Chlorite, calcite, clay, hematite, pyrite, adularia, quartz, laumontite, epidote, fluorite
Kinematics	Dextral		low	Field mapping	

BH	Geometrical Intercept (bh. m)	Target intercept (bh. m)	Comment
HLX02	0-122,7	-	No results available.
HLX20	62,1-184,2	90-170	High frequency of open fractures, red staining. Several caliper anomalies. The most prominent geophysical anomalies are found in the interval 113 to 136 m. The host rock is dominated by Ävrö granodiorite. 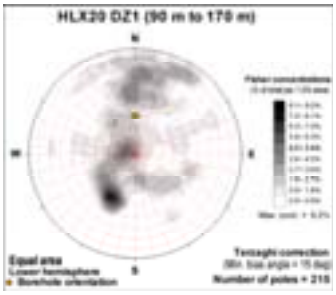
KLX06	300.3-429,8	297-425	Eshi DZ2. Increased frequency of sealed and open fractures, weak to medium alteration, dominated by oxidation, though sections of saussuritization also occur. The section ca 390-400 m is strongly altered to laumontite and the section 384-386 is clay altered. Scattered minor crush zones. The section 365-395 m is characterized by strong, protomylonitic to mylonitic foliation. Partly low resistivity, p-wave velocity, density and magnetic susceptibility. Numerous caliper anomalies. The sections 307-315 m and 380-400 m are characterized by several strong anomalies in all geophysical loggings. radar reflectors occur within the section including at 365.9 m 62/092. An interpreted seismic reflector (C1) from surface reflection seismic measurements (orientation 70/090) coincides with this section in the borehole. The host rock is dominated by a mixture of Ävrö granodiorite.

BH	Geometrical Intercept (bh. m)	Target intercept (bh. m)	Comment
			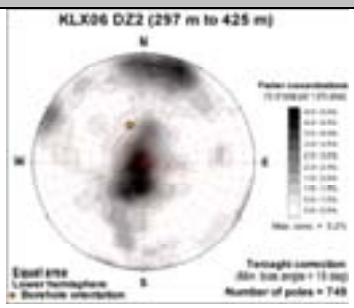
KAS03	307,1-495,6	280-480	Brittle and ductile indicators
KAS17	238,2-352,7 (base)	-	No results available.

ZSMEW002A, KLX06 drill log extract (zone only)

ZSMEW002A, KLX06 drill core (zone only) (1 of 3)

ZSMEW002A, KLX06 drill core (2 of 3)

ZSMEW002A, KLX06 drill core (3 of 3)

ZSMEW013A

ZSMEW013A remains unchanged from version 1.2. The local major zone extends E-W along a magnetic and topographic lineament across the Äspö Island and is interpreted as being a brittle-ductile zone. This zone is interpreted as EW1a at Äspö /Berglund et al. 2003, Rhén et al. 1997/, and is also supported by field mapping and borehole intersections and can be considered as a large scale splay structure between Äspö shear zone and Mederhult shear zone. The magnetic data shows weak indications of a low magnetic zone along its extent and the topography shows a well developed depression west of Äspö which is interpreted as being the extension of EW1a towards the west /Wahlgren et al, 2006/.

The zone is described as a crush zone, with enhanced fracture frequency in KA1755A /Stanfors et al. 1994/, also containing a thin breccia/mylonite and a ca 5–7 m wide zone of tectonization. KAS04 is reported to have five thin mylonites in connection with the zone. The 4.4 km long zone has been modelled with an orientation of 85/90 and a 45 m thickness based on observations at Äspö.

E-W striking deformation zones

ZSMEW013A (EW1a on Äspö)

Modelling procedure: At the surface, corresponds to the low magnetic and topographic lineaments. Modelled to base of regional model volume using a dip that has been taken from an existing interpretation made at Äspö /Berglund et al, 2003/. Included in regional model and also present inside local model volume.

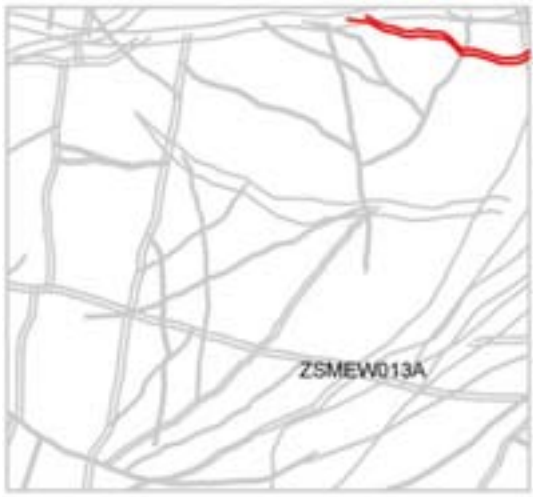

Confidence of existence: High

Property	Quantitative estimate	Span	Confidence level	Basis for interpretation	Comments
Position		± 25 m (surface)	High	Linked lineament.	
Orientation (strike/dip)	085/90	105-065/± 10	High for strike, medium for dip	Strike based on trend of lineament. Dip based on BHs	Strike 105 in west curving round to 065.
Thickness	45 m	20-50 m	High	Lineament, BH and geophysical ground survey	Thickness refers to total zone thickness.
Length (regional model)	4.4 km	2.5-4.4 km	Medium	Linked lineaments	An alternative interpretation is to terminate the zone against ZSMNE005A
Ductile deformation	Yes		High	Mylonites in BHs and field mapping.	Brittle-ductile zone
Brittle deformation	Yes		High	Breccia and crush zones in BHs	Brittle-ductile zone
Alteration			High	BHs and field mapping.	Epidotized
Fracture orientation	-			KA1755A, KAS04	
Fracture frequency	5 m^{-1}	± m^{-1}	Medium	KA1755A, KAS04	Frac' frq' incl' crush (= 20 frac/m) (m^{-1})
Fracture filling			High	KA1755A, KAS04	Calcite, chlorite, epidote, hematite, quartz,

BH	Geometrical Intercept (bh. m)	Target intercept (bh. m)	Comment
HLX03	0-17,44	-	No information
KA1755A	188,13-233,8	180-230	A crush zone, with enhanced fracture frequency. A thin breccia/mylonite and a ca 5–7 m wide zone of tectonization have been recorded. The area as interpreted as EW-1a in /Stanfors et al. 1994/.
KAS04	100,21-183,93	77-158	Five thin mylonites at depths: 87, 140, 147, 153 and 158 m. Intense tectonization around the mylonite at 147 m. as interpreted as EW-1a in /Berglund et al, 2003/.
HAS01	4-100	-	No information

ZSMEW014A

ZSMEW014A remains unchanged from version 1.2. The local major zone extends WNW along a magnetic and topographic lineament across Äspö Island, terminating against ZSMEW13A in the east and merging with the Mederhult zone belt, ZSMEW002A in the west. The zone is interpreted as being a brittle-ductile zone based on outcrop mapping that identifies red staining, raised fracture frequency with epidote fillings and a weak foliation parallel to the strike of the zone. The 1.2 km long zone has been modelled with an orientation of 100/90 and a 10 m thickness. The vertical dip is assumed and the thickness, based on magnetic and topographic lineaments is low confidence.

The zone is interpreted as having an interception with the upper part of HLX02 though no information is available for this drillhole.

E-W striking deformation zones ZSMEW014A	
Modelling procedure: At the surface, corresponds to the low magnetic and topographic lineaments. Present in the local model but not included in the regional model. The vertical dip is assumed.	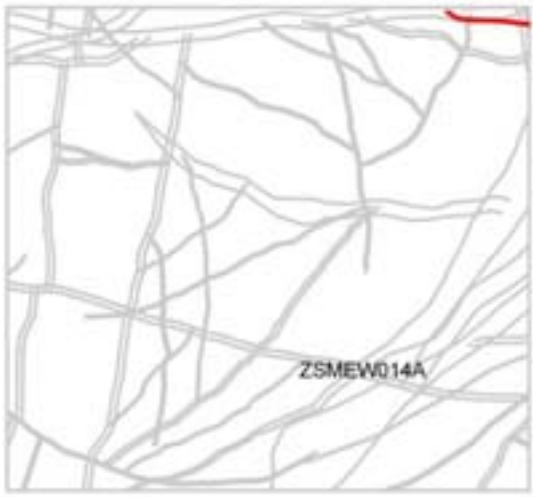
Confidence of existence: High	

Property	Quantitative estimate	Span	Confidence level	Basis for interpretation	Comments
Position		± 25 m (surface)	Medium	Linked lineament.	
Orientation (strike/dip)	100/90	± 10/± 20	Medium for strike, low for dip	Strike based on trend of lineament. Dip assumed	
Thickness	10 m	5-30 m	Low	Magnetic and topographic lineament	
Length (regional model)	1.2 km	± 100m	Medium	Linked lineaments	
Ductile deformation	Yes		Medium	Weak field mapping indicators	Inferred brittle-ductile zone. (Field evidence may not be exclusive to this zone)
Brittle deformation	Yes		Medium	Raised fracture frequency and red staining in outcrops	Inferred brittle-ductile zone. (Field evidence may not be exclusive to this zone)
Alteration			Medium	Field mapping.	Red staining and epidote fracture fillings (Field evidence may not be exclusive to this zone)
Fracture orientation	-				No data
Fracture frequency	-				No data
Fracture filling			Medium	Field mapping.	Epidote fracture fillings (Field evidence may not be exclusive to this zone)

BH	Geometrical Intercept (bh. m)	Target intercept (bh. m)	Comment
HLX02	0-16,3	-	No information

ZSMEW120A

The surface trace of the zone remains unchanged from version 1.2. However, core drilling has resulted in a change to the dip of the zone and supplied information on its character. ZSMEW120A is interpreted as being a splay of ZSMEW002A with a thickness of around 50 m and a similar dip to the south rather than being a splay of ZSMNE011A with a sub vertical dip, as per version 1.2.

The zone dip is based on the lineament and the interpreted intercept in KLX13A and the lack of an interpreted intercept in KLX17A. KLX13A does not penetrate the total thickness of the zone but rather ends within it. However, for practical purposes the northern boundary of the zone can be said to merge with ZSMEW002A.

There has been no surface evidence identified that gives any clear indication as to the dip or character of ZSMEW120A. The distribution of the magnetic, resistivity and topographic anomalies weakly suggest that the zone is a reactivated ductile brittle zone. There is not a good spread of mapping data in the vicinity of ZSMEW120A. Descriptions only cover outcrops in the central section of the zone. It should also be noted that this area is affected not only by ZSMEW120A but also ZSMNE011A and ZSMEW002A, along with other potential zones. Therefore the descriptions may not refer to ZSMEW120A in isolation.

E-W striking deformation zones ZSMEW120A	
Modelling procedure: At the surface, corresponds to a low somewhat amorphous, poorly constrained magnetic and topographic lineament. Modelled to base of local model volume using dip that has been inferred from KLX13A but not included in the regional model.	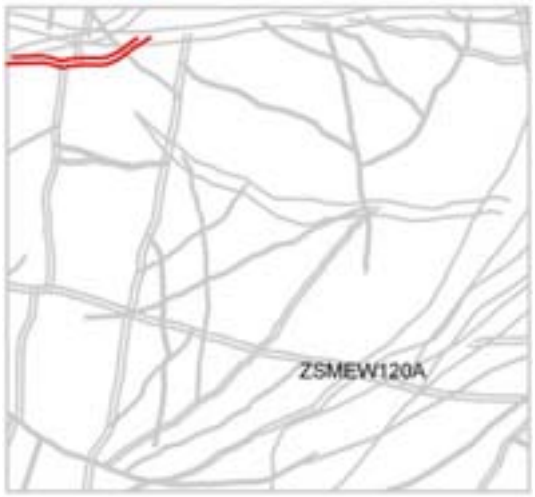
Confidence of existence: High	

Property	Quantitative estimate	Span	Confidence level	Basis for interpretation	Comments
Position		± 40 m (surface)	Low	Poorly constrained magnetic lineament,	
Orientation (strike/dip)	080/64	± 20/± 10	High for strike, medium for dip	Strike based on trend of lineament. Dip based on KLX13A.	
Thickness	50 m	30->60 m	Low	Lineament, KLX13A	50m, based on KLX13A intercept. However, the hole does not penetrate right through the zone so the true thickness remains unknown. For practical purposes it can be said to merge with ZSMEW002A to the north as indicated by the magnetic survey.
Length (regional model)	1,2 km	+/-100 m	Medium	Linked lineaments	
Ductile deformation	Yes		High	KLX13A	Present
Brittle deformation	Dominant		High	Cataclasites, breccia and crush zones in KLX13A	Present
Alteration			High	KLX13A	Dominated by red staining,
Fracture orientation	350/30, 345/75, 320/80		Medium	KLX13A	

E-W striking deformation zones ZSMEW120A					
Fracture frequency* Open/sealed m^{-1}	16/105		Medium	KLX13A	
Crush zone Number/total m	67/18,5		Medium	KLX06	
Fracture filling			High	KLX06	Chlorite, clay, calcite hematite, epidote, prehnite, adularia, chalcopyrite, laumontite, goethite, quartz, fluorite

BH	Geometrical Intercept (bh. m)	Target intercept (bh. m)	Comment
KLX13A	479,9-595,9	488-595,3 (base)	Eshi DZ7 Brittle deformation zone overprinting scattered sections of brittle-ductile shear zones in the upper part. Highly increased frequency of sealed fractures and open fractures with large apertures. 66 crush zones characterize the section. The whole deformation zone is dominated by medium alteration (red staining). Scattered sections of core loss. General decrease in the bulk resistivity and in the fluid resistivity. A large number of caliper anomalies (mainly concentrated at c 493.5-504.5 m, 520.0-525.0 m and 550.0-559.0 m), a large number of intervals with decreased P-wave velocity. The entire section is characterized by decreased magnetic susceptibility, decreased density and increased natural gamma radiation. Mapped brittle-ductile shear zones include 096/60, 072/67, 066/52, 114/65. 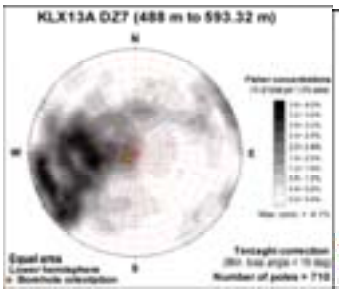 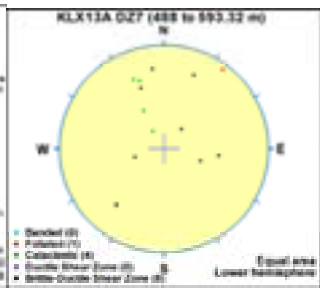 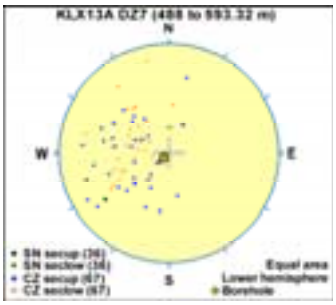 From /Viola et al, 2007/: DZ 7 of KLX13A is a long and complex deformation zone, which differs from a “typical” deformation zone due to the lack of a well-defined fault core containing fault rocks and the associated transition zones. DZ 7 is instead characterized by very pervasive sets of fractures, which lead to volumetrically significant crush zones and core loss intervals. Fault rock intervals are observed at different depths within the DZ. Given the high spatial frequency of this type of brittle features (and the impossibility to subdivide the logged interval into distinct and meaningful cores and transition zones) we assign almost the entire logged depth interval (490 to 594 m) to a single DZ core. Red staining is generally very extensive throughout DZ 7. Between the numerous crush zones and core loss intervals there are meters of intact host rock, probably reflecting the anastomosing geometry of the deformation zone, a structural feature commonly seen in fault zones.

BH	Geometrical Intercept (bh. m)	Target intercept (bh. m)	Comment
			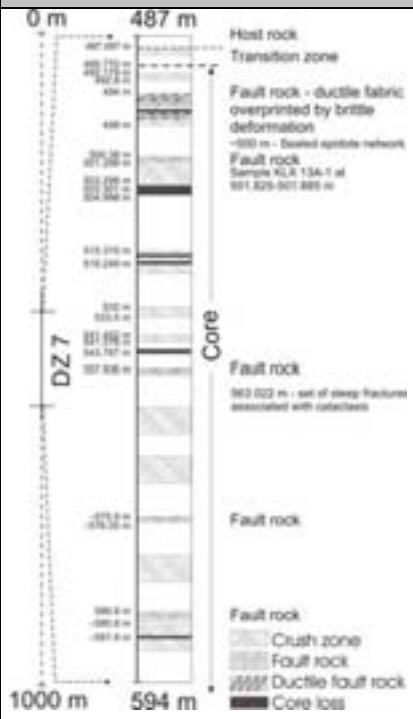  *Appearance and orientation of the uppermost crush zones within the core of DZ 7.* Between c. 494 and 498 m depth there occurs a complex structural pattern, whereby a steep brittle/ductile shear zone, characterized by a pervasive foliated interval in which foliation planes are defined by epidote layers and red stained feldspar and plagioclase (see figure **Fel! Hittar inte referenskälla.**a and b below), is overprinted by a major cataclastic core (see figure c, d and e). The latter contains cataclasites, ultracataclasites and pockets/layers of green gouge. As illustrated by the black great circles of the stereonet, foliation planes dip rather steeply to the SSE, but no kinematic indicators were observed in connection with this ductile fabric. The orientation of fractures within the cataclastic core (as derived from the BIPS images) is plotted by the red great circles. These have a very similar orientation to the ductile fabric, which in turn suggests a control of the

BH	Geometrical Intercept (bh. m)	Target intercept (bh. m)	Comment
			early ductile structures on the later brittle features. Figure **Fel! Hittar inte referenskälla.**e, an extract from the BIPS image, shows the borehole section that corresponds to the cataclastic/ultracataclastic core, within which there also occur core loss intervals due to the low cohesion of the mechanically disrupted rocks. 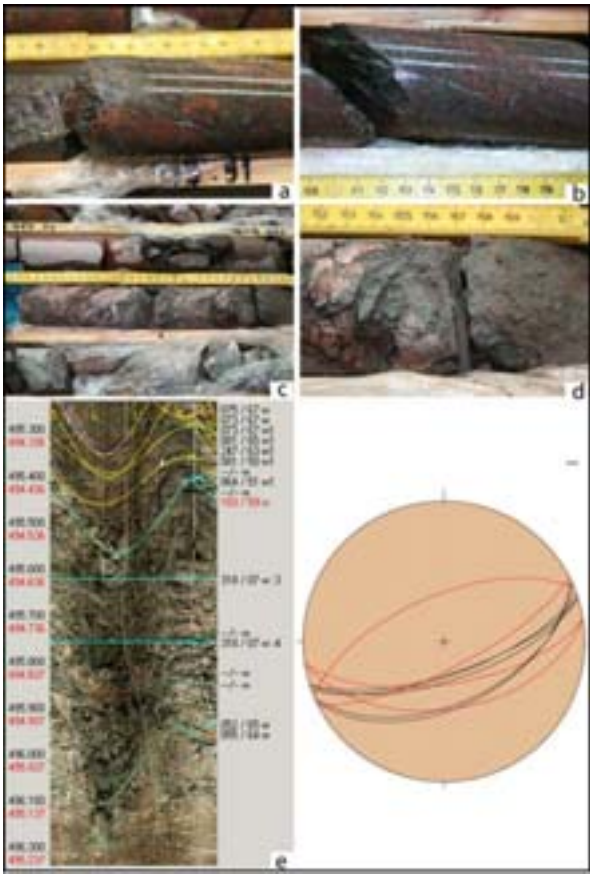

ZSMEW316A

ZSMEW316A remains unchanged from version 1.2. The local major zone is marginal to the south east corner of the local model volume extending E-W along a magnetic and topographic lineament off the coast of Laxemar and Simpevarp. The zone has an assumed brittle-ductile character based on similarly oriented zones in the study area. The 2.4 km long zone has been modelled with an orientation of 086/90 and a 30 m thickness. The vertical dip is assumed and the thickness, based on magnetic and topographic lineaments is low confidence. The zone has not been the subject of any focused indirect or direct investigation methods.

E-W striking deformation zones ZSMEW316A	
Modelling procedure: At the surface, corresponds to the low magnetic and topographic lineaments. Modelled to base of regional model volume using an assumed vertical dip. Included in regional model and also present inside local model volume.	
Confidence of existence: Medium	

Property	Quantitative estimate	Span	Confidence level	Basis for interpretation	Comments
Position		± 30 m (surface)	Medium	Linked lineament.	Zone located under the sea
Orientation (strike/dip)	086/90	± 110-70/± 30	Medium for strike, low for dip	Strike based on trend of lineament. Dip assumed	Lineament dominantly E-W swinging to NW-SE at eastern termination. Zone located under the sea.
Thickness	30 m	10-50 m	Low	Magnetic and topographic lineament	Zone located under the sea
Length (regional model)	2.4 km	± 200m	Low	Linked lineaments	Zone located under the sea
Ductile deformation	Yes		Low	Inferred from strike. No direct evidence	Inferred brittle-ductile zone.
Brittle deformation	Yes		Low	Inferred from strike. No direct evidence	Inferred brittle-ductile zone.
Alteration					No data
Fracture orientation	-				No data
Fracture* frequency	-				No data
Fracture filling					No data

BH	Geometrical Intercept (bh. m)	Target intercept (bh. m)	Comment
None			No BH intercepts

ZSMEW900A and B

For version 1.2 the zone was modelled with a strike of 100° and a dip of 70° S, based generally on field measurements and seismic reflector L /Juhlin, 2004/. The modelled width of 20m was based on inclusion of narrow transition zones. A 10m wide 'core' of more highly fractured rock was based on seismic refraction profiling /Lindqvist, 2006/. Much of the quoted supporting data involved the lineament to the east of ZSMNS059A. For v2.2 the more detailed topographic and geophysical surveys supported the partial break up of the lineament across ZSMNS059A with the western section being largely maintained but the eastern section taken to represent a number of smaller structures not directly linked to ZSMEW900A west of ZSMNS059A. This meant that the seismic reflector, along with the magnetic and resistivity profile measurements, were no longer relevant to the western segment. However, outcrop mapping evidence still indicated a southerly dip of 50-60°.

The lineament has subsequently been investigated by three percussion hammer holes and one cored drillhole. Based on the cored drillhole KLX17A and the detailed topographic LIDAR map, a splay to ZSMEW900A has been added, namely ZSMEW900B. The two arms have lengths of 890 m and 460 m respectively. Both arms have been modelled with a thickness of 25 m based on KLX17A interceptions. ZSMEW900A is modelled with a dip of 57^{o} and ZSMEW900B with a dip of 78^{o}. The dips are based on a combination of mapping results and geometrical lineament-borehole interceptions. Taken alone fracture pole concentrations suggest somewhat shallower dips.

Overall ZSMEW900A-B is interpreted as a zone with a dominantly brittle character. However, outcrop mapping bordering the zone identified ductile structures with very similar orientations to the zone that along with weaker borehole evidence suggest that the zone has a ductile origin.

The combination of a lack of clear confirmation of zone geometries in the nearby hammer holes and the multiple low velocity zones identified by the seismic refraction profiling /Lindqvist, 2006/ suggest a split and complex geometry to the zone.

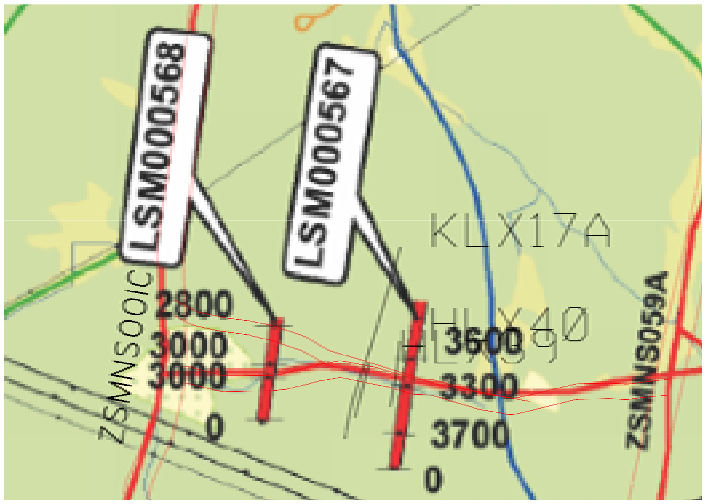

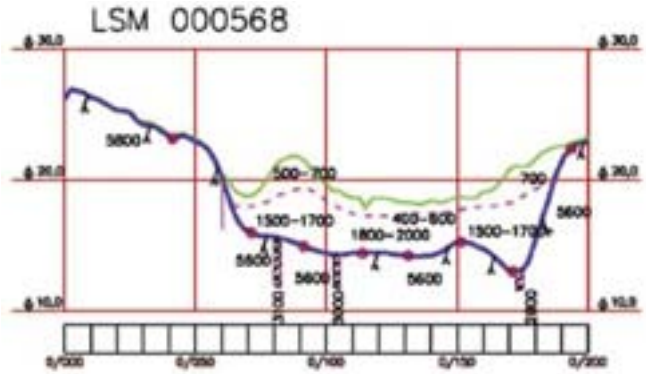

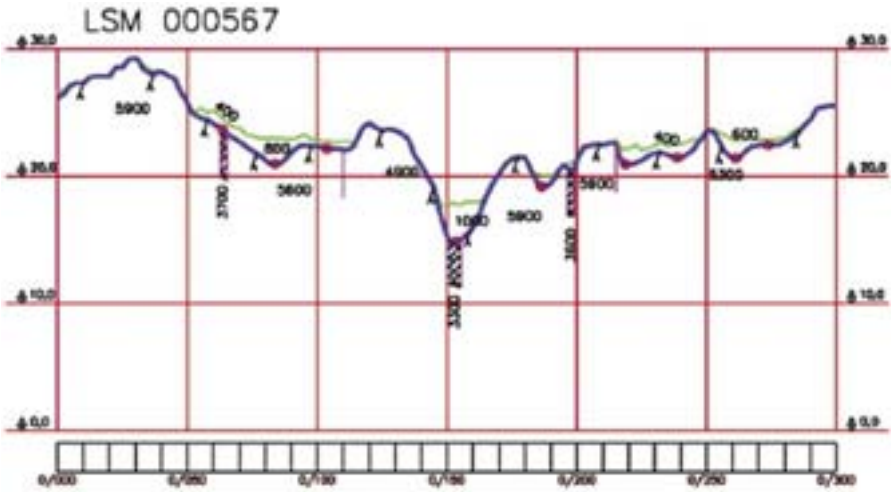

Seismic refraction profiles across ZSMEW900A and B. Seismic velocity in m/s /Lindqvist, 2006/.

E-W striking deformation zones ZSMEW900A,B	
Modelling procedure: At the surface, corresponds to the low magnetic and topographic lineaments. Modelled using dip that has been inferred from outcrop mapping BHs. Not included in the regional model but present inside local model volume. ZSMEW990B is interpreted as a splay of ZSMEW900A.	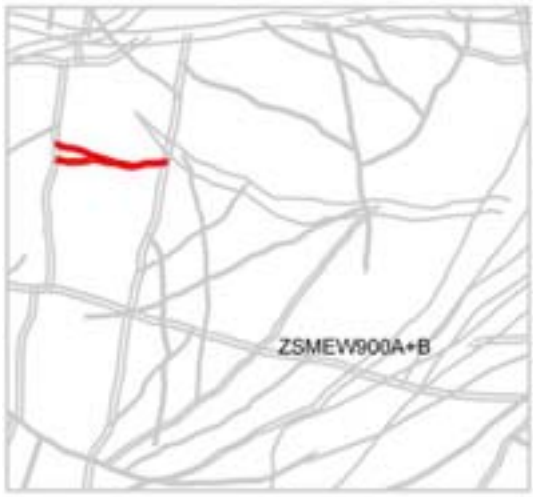
Confidence of existence: High	

Property	Quantitative estimate	Span	Confidence level	Basis for interpretation	Comments
Position		± 20 m (surface)	High	Linked lineament,	
Orientation (strike/dip)	092/57	± 10/± 10	High for strike, medium for dip	Strike based on trend of lineament. Dip based on outcrop mapping and boreholes	ZSMEW900B= 106/78
Thickness	25 m	10-30 m	High	Lineament and BH	Note: existence of EW900B, thickness 25 m
core	3m	± 2	Medium	'core' of more highly fractured rock based on general ref: geophysical profiling -refraction (P-06-49) seismic velocity 3000-3300 m/s	/Lindqvist, 2006/
Length (regional model)	0.9 km	0.9-1.2 km	Medium	Linked lineaments	
Ductile deformation	Minor		High	KLX17	Weak ductile precursor, brittle dominates
Brittle deformation	Major		High	Cataclasites, breccia, crush zones and slickensides	
Alteration			High	KLX17	Red staining, epidotization and saussuritization,
Fracture orientation	160/10, 300/75,180/90, 040/25, 110/45		High	KLX17	

E-W striking deformation zones ZSMEW900A,B					
Fracture frequency* Open/sealed m^{-1}	15/55		High	KLX17	
Crush zone Number/total m	0/0			KLX17,dz3	KLX17A DZ1 data not available
Fracture filling			High	KLX17	Calcite, chlorite, epidote, hematite, quartz, pyrite, clay,
Kinematics					

BH	Geometrical Intercept (bh. m)	Target intercept (bh. m)	Comment
HLX39	59,0-85,1	75-85	Brittle deformation zone characterized by increased frequency of open fractures and medium alteration. One crush zone at 76.86-77.11 m. General decrease in the bulk resistivity and in the magnetic susceptibility. Decreased density and a minor decrease in the P-wave velocity at c. 76.7 m. 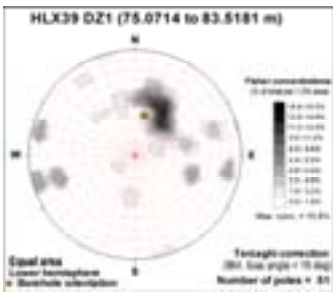 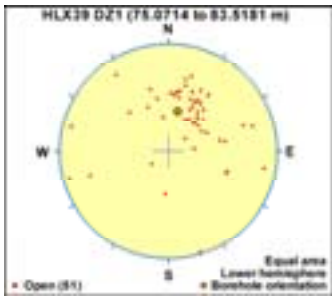
HLX40	29,7-56,4	49,8-59,6	Brittle deformation zone characterized by slight increase in open fractures, apertures, one of which is 10 mm, and medium red staining. Low resistivity, P-wave velocity and magnetic susceptibility, caliper anomalies. 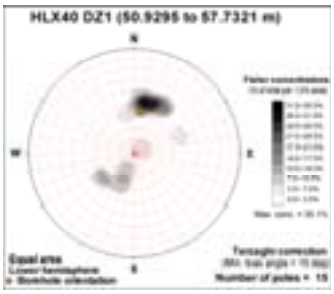 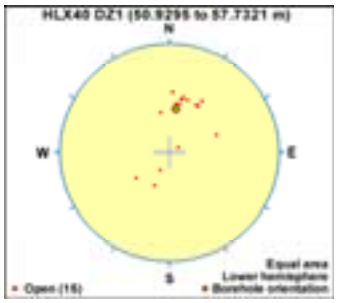
KLX17	96,0-124,1	100,1-114,3	Brittle deformation zone characterized by increased frequency of open and sealed fractures, sealed network, nine crush zones, high frequency of open fractures with large apertures, medium red staining and one slickenside. The most intensely deformed section is 104.55-114.30 m. The section 104.8-114.3 m is characterized by a major decrease in bulk resistivity and in magnetic susceptibility. There is also partly decreased P-wave velocity, density and some caliper anomalies. Foliation at 80m is 107/65. 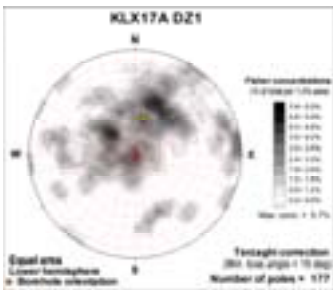 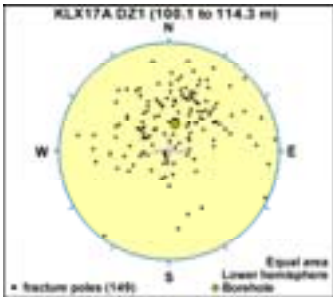 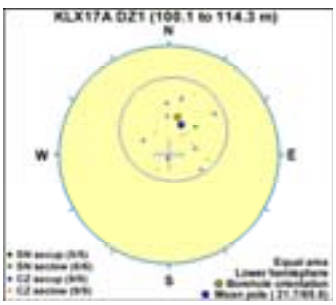 From /Viola et al, 2007/: the deformation zone is characterized primarily by

BH	Geometrical Intercept (bh. m)	Target intercept (bh. m)	Comment
			a c. 3 m thick core that extends from 108.7 m depth down to 111.4 m Large cavities in the borehole image suggest the core to be a zone of extreme mechanical weakness and did not allow the orientation of planar features in the core. 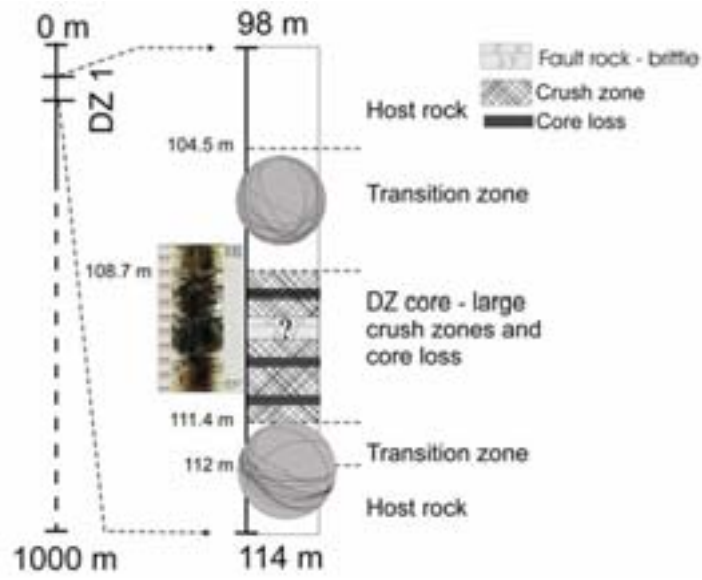 *The borehole image shows large cavities in the hole at depths corresponding to the DZ core. Stereonets show the orientation of open fractures (measured from the borehole image) from the upper and lower transition zone. Vertical scale is schematic.*
HLX39	117,0-156,0	-	ZSMEW900B
HLX40	61,0-96,0	-	ZSMEW900B
HLX41	145.2-197,6	-	ZSMEW900B

BH	Geometrical Intercept (bh. m)	Target intercept (bh. m)	Comment
KLX17	189,9-227,6	192,7-227	ZSMEW900B; Inhomogeneous brittle to brittle-ductile deformation zone which is characterized by increased frequency of sealed fractures, sealed network, moderate increase in open fractures, slickensides, weak to medium foliation, faint to strong red staining, weak to strong saussuritization, weak epidotization, breccias, cataclasites, and ductile and brittle ductile shear zones. (ductile orientation 110/65)The most intensely deformed parts are 193.45-193.80 m, 199.85-200.165 m and 221.10-224.75 m. The entire section is characterized by several short intervals of decreased resistivity, magnetic susceptibility and P-wave velocity. The most significant geophysical anomalies occur at 199.5-201.5 m and 220.5-225.5 m. Oriented reflectors occur at 195.4 m with the orientation 017/06 or 108/57 and at 222.7 m with the orientation 079/39 or 141/27. The reflectors are medium in strength and can be observed to a distance of 9-14 m outside the borehole. 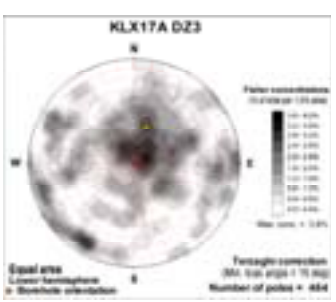 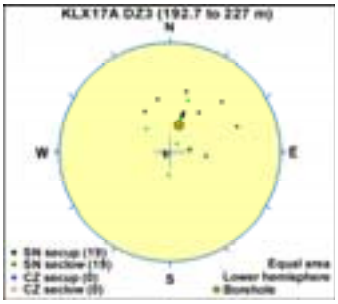 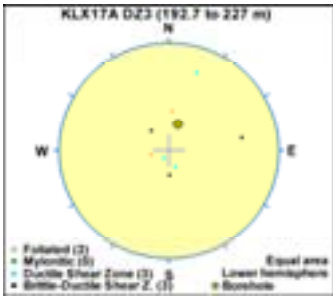

ZSMEW900A, KLX17A drill log extract (zone only)

ZSMEW900B KLX17A drill log extract (zone only)

ZSMNW042A

This zone's trace on the ground surface within the Laxemar local model remains largely unchanged from version 1.2. There has been a significant modification to the eastern termination of the zone involving an easterly extension of the zone across the plastic domains ZSMNE005A (P01) and ZSMNE004A (P02). The zone is now modelled as merging and linking with a previously separate lineament/structure, ZSMEW023A, which lies parallel with the southern coast of the Simpevarp peninsula. This has increased the zone length from 7.8 to 10.8 km. It should also be noted that an earlier termination was against ZSMNW932A, which has been reinterpreted as a lineament associated with a lithological change rather than representing a deformation zone. The modified linking and easterly extension is judged low confidence due to the lack of information and the apparent geological complexity of this area. However, the modified geometry gives a better fit with the pattern of in situ stress measurements and the conceptual geological development model of the area.

Within the local model area the surface expression of ZSMNW042A consists of clear though irregular topographic and magnetic lineaments with a very variable width that defines an irregular 'belt'. This appearance shares similarities with ZSMEW002A and ZSMEW007A. The zone is interpreted as being a 10.8 km long, 40m thick zone that dips at ca. 55^0 S. It has a dominantly brittle character though ductile precursors are present. Previously the zone's dip had been poorly constrained and during an intermediary stage the zone was modelled in the main model with a dip of 53^0 S and included in an alternative model with a dip of 81^0 S. The drilling results from KLX27A have better constrained the dip of the zone and the steeper version has now been rejected.

There are few rock exposures in the vicinity of the zone. Deformation indicators are present but no clear orientation data that can help define the overall zone geometry or character. Detailed ground geophysical profiles (Groups 1 and 2, P04-211) generally supported an interpretation of the zone being sub vertical though other interpretations are possible/Thunehed et al, 2004/. A recent additional review of earlier 2004 seismic reflection results /Juhlin, 2007/ suggested very weak evidence for the existence of a zone that dips to the south at around 50° degrees that could be correlated with the surface expression of ZSMNW042A.

A recent additional review of EM data with focus on ZSMNW042A suggests that while no clear picture can be defined the data can support the interpretation of the zone with a southerly dip of 50-75° /Thunehed, 2007/. A limited radar reflector that runs more or less parallel to KLX19 provides very weak evidence of a southerly dipping structure of around 50-55°.

Drillhole KLX27A was drilled at a late stage in the investigations with the aim of further investigating both the orientation and character of the zone. The drillhole is interpreted to make a clear intercept with the zone between BH length 210-250m. The orientation of the fractures in the core support the interpretation of an overall southerly dip to this zone but their spread means that they do not enable a quantification of the dip. Mapped brittle and brittle-ductile structures in the core also have a similar spread to the fracture orientations. However, a mapped 30cm

protomylonitic fabric has an orientation of 211/60. The ductile fabric is considered a more reliable direct indicator of the zone orientation than the brittle indicators. This orientation, if projected to the ground surface fits very well locally with the presumed ZSMNW042A lineament trend and position.

The only other cored hole that is interpreted to intercept the zone is KLX15A. The drillhole is interpreted as not penetrating the full width of the zone but ending within in it. The interpreted zone dip means that the hole is drilled at an acute angle to the zone as supported by the fractures towards the base of the hole that are sub parallel to the core. BIPS mapping data is not available for the base of this drillhole.

No dramatic or clear evidence from any of the hammer holes clearly helps define the geometry of the zone as a single major structure with a single core, transition zones and clear dip. However, the pattern of red staining within five of the hammer holes; HLX15, HLX27 and HLX28 drilled from the north and HLX26 and HLX32 from the south supports the southern dip of around 55°. With the interpreted modelled zone geometry the base of KLX15A penetrates the transition zone of ZSMNW042A and whilst not conclusive this also fits with the pattern of red staining in this hole along with interpreted core discing. The pattern of red staining conforms to the pattern seen associated with ZSMEW007A i.e. a broad belt of oxidation (red staining) that contains a number of sub parallel structures that together form a complex zone.

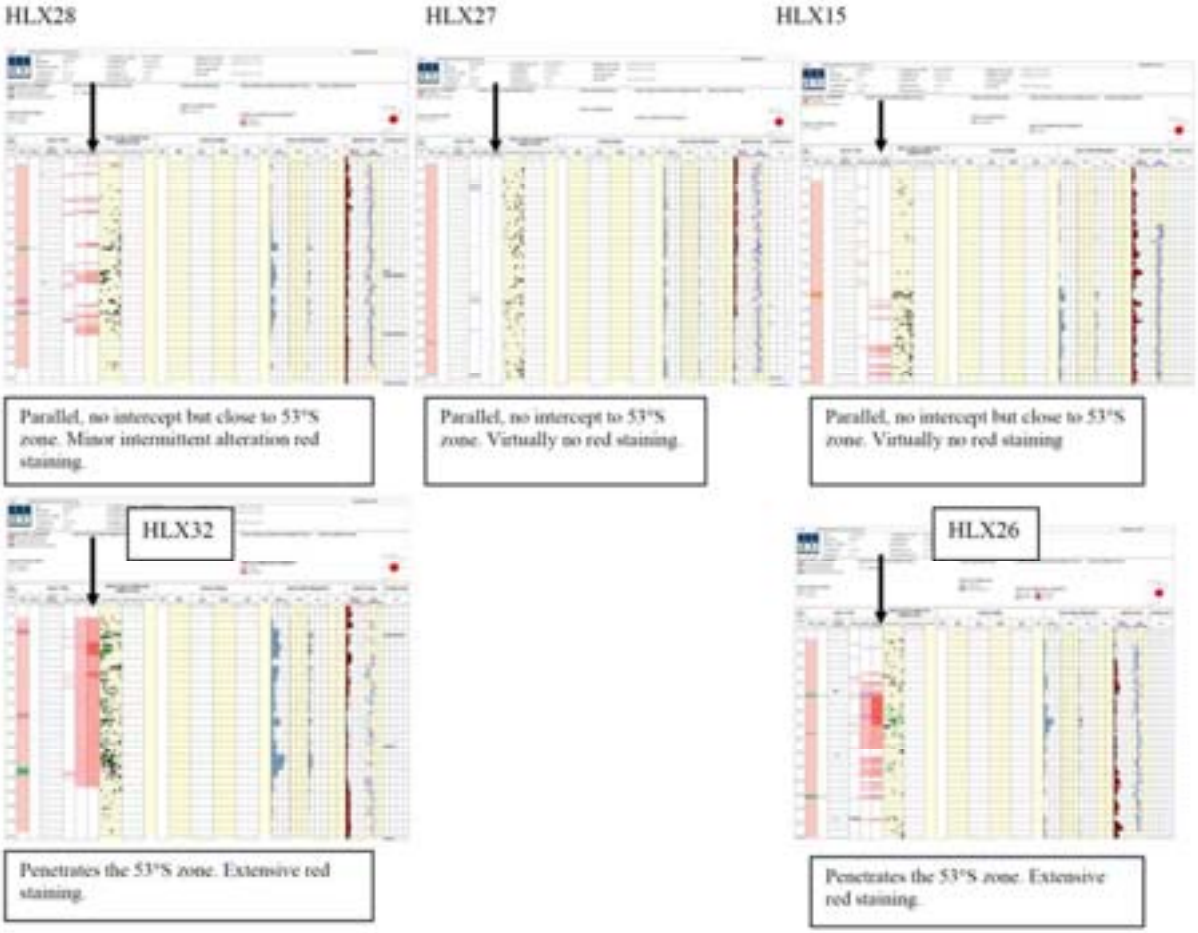

Distribution of red staining alteration in the five hammer holes associated with ZSMNW042A

The ZSMNW042A belt was investigated by two ground magnetic and resistivity profiles /Thunehed et al, 2004/

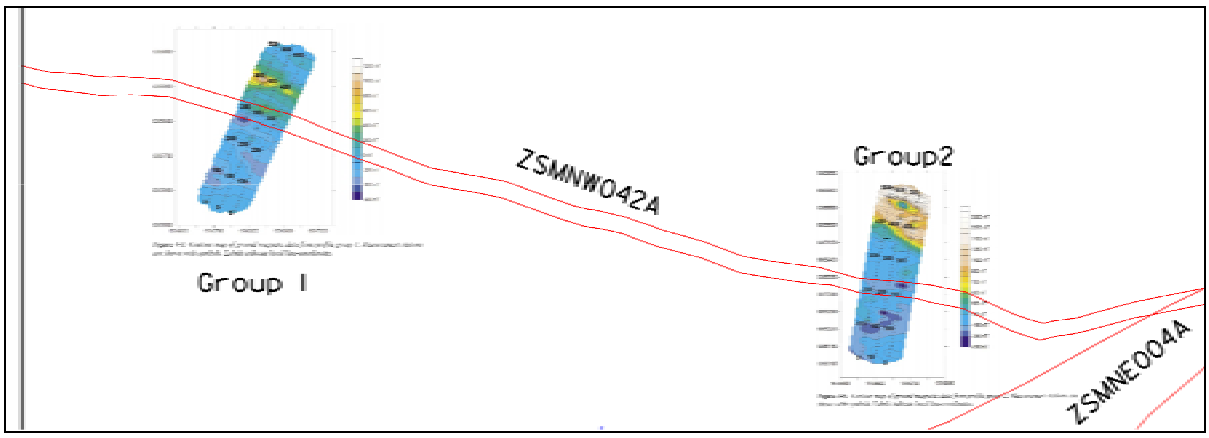

Ground magnetic data from profile groups 1 and 2 across ZSMNW042A /Thunehed et al, 2004/

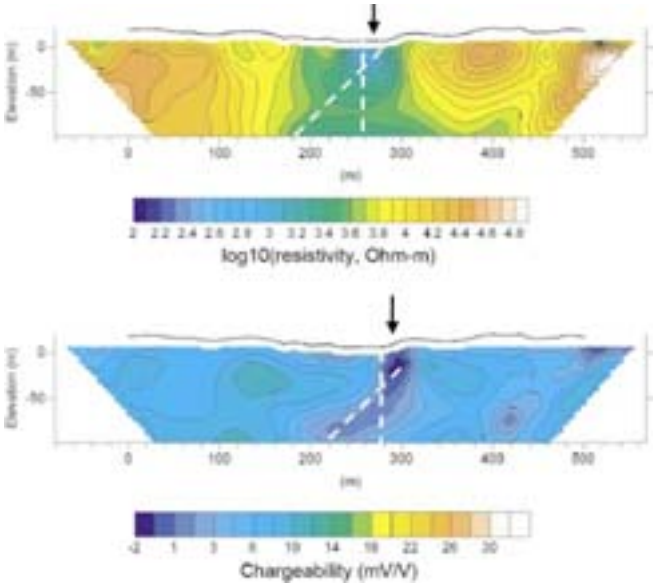

Inverted resistivity (top) and chargeability (bottom) sections for profile group 1 (LSM000276).

In the group 1 profile a magnetic low coincides with the interpreted ZSMNW042A lineament. The width of the corresponding structure is however difficult to estimate since low-magnetic rocks are present to the south. The position also corresponds to low-resistivity structure. The width of the structure is almost 100 m and the resistivity is rather low (~2,500 Ωm) in the central part. The dip seems to be subvertical though this may be due to interference from other structures. Other interpretations of dip are possible both to the north and south.

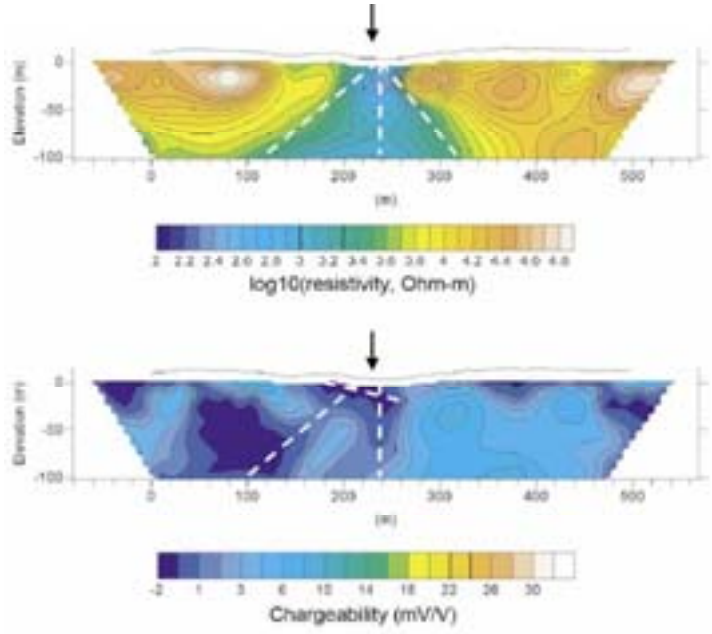

Inverted resistivity (top) and chargeability (bottom) sections for profile group 2 (LSM000277).

In the group 2 profile a magnetic low related to the lineament ZSMNW042A can be seen. The width of the corresponding structure is however difficult to estimate since low-magnetic rocks are present to the south. A low-resistivity structure coincides with the interpreted ZSMNW042A position. The width of the structure is around 50 to 60 m and the resistivity is rather low (< 2,500 Ωm) in the central part. The dip seems to be sub vertical though like for group1 other interpretations are possible.

The group 1(LSM00276) and 2 (LSM00564) profile positions were also investigated by seismic refraction /Lindqvist, 2004/. Two further profiles, LSM00564 and LSM00559 were also investigated /Lindqvist, 2006/.

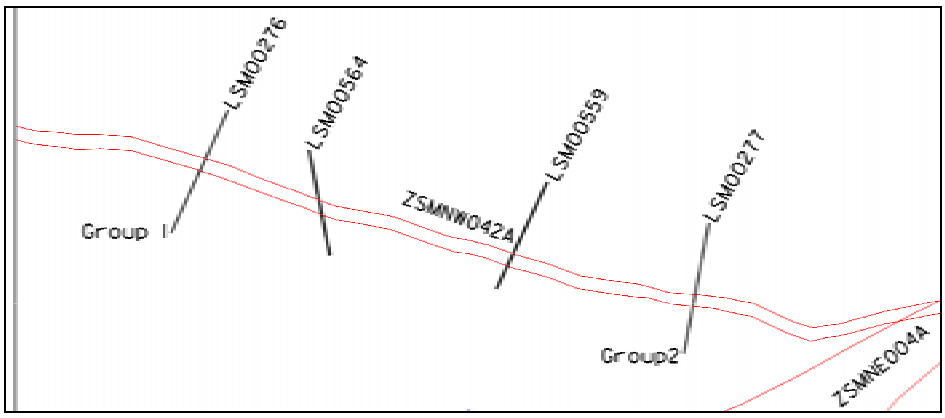

Position of seismic refraction profiles crossing ZSMNW042A

The profiles show that the broad lineament is associated with a varying number of low velocity anomalies of varying apparent thickness though it should be noted that not all the anomalies presented are likely to be exclusively associated with ZSMNW042A. Results indicate that the zone has possibly 1 to 4 cores of more highly fractured rock that give a total core thickness of around 20 m.

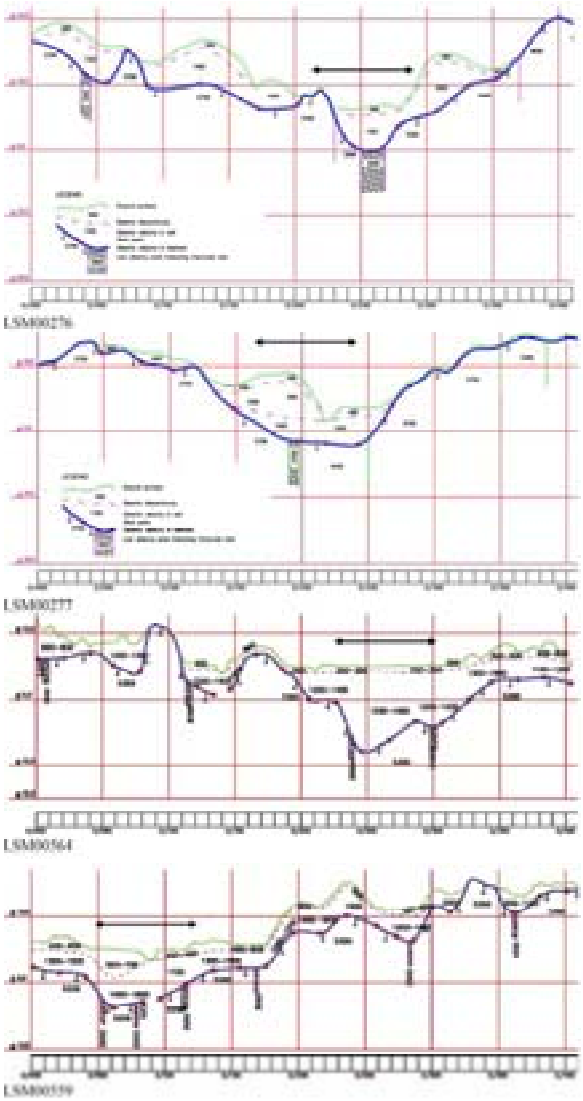

Seismic refraction profiles across ZSMNW042A

NW-SE striking deformation zones ZSMNW042A	
Modelling procedure: At the surface, corresponds to a broad irregular low magnetic and topographic 'belt'. Modelled to base of regional model volume using dip that has been inferred mainly from boreholes. Included in regional model and also present inside local model volume.	
Confidence of existence: High	

Property	Quantitative estimate	Span	Confidence level	Basis for interpretation	Comments
Position		± 25 m (surface)	High	Lineament, BH and geophysical ground survey /Thunehed et al, 2004/	Corresponds to a broad irregular low magnetic and topographic 'belt'
Orientation (strike/dip)	105/55	080-130 /± 5	High for strike, medium for dip	Strike based on trend of lineament. Dip based on boreholes, primarily KLX27.	
Thickness	40 m	20-50 m	Medium	Lineament, BH and geophysical ground survey	Model width represents an envelope width containing narrower inferred splays
Core	10 m	5-20m	Medium	Seismic refraction results indicate a narrower up to 20m wide fractured core /Lindqvist, 2004/.	Likely multiple cores
Length (regional model)	8,3 km	+/-200 m	Low	Linked lineaments	Continuity outside the local model area to the west is uncertain. The eastern termination is low confidence.
Ductile deformation	Yes		High	Mylonites in BHs	Present
Brittle deformation	Yes		High	Cataclasites, breccia and crush zones in BHs	Present. Brittle ductile zone with open fractures. Brittle character dominates.
Alteration			High	KLX27A	Oxidation, chloritization, epidotixation
Fracture orientation	090/40, 110/60, 230/90		medium	KLX27A	see KLX27A stereoplot

NW-SE striking deformation zones ZSMNW042A					
Fracture frequency Open/sealed m-1	8 / 80		Medium	KLX27A	
Crush zone Number/total m	6/1		Medium	KLX27A	
Fracture filling					Calcite, chlorite, clay, epidote, pyrite, quartz, prehnite, galena, hematite

BH	Geometrical Intercept (bh. m)	Target intercept (bh. m)	Comment
HLX26	33,8-80,8	50-80	Eshi DZ1 63-72m: Medium to strong alteration, increased fracturing and a narrow crush zone. Geophysical loggings show major caliper anomalies and low resistivity, low p-wave velocity and partly low density along the section. However, red staining alteration is more widespread. 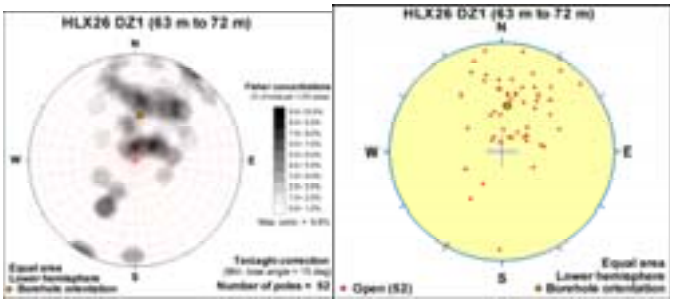
HLX32	91-135	20-130	Eshi DZ3 104-114m: The deformation zone is located to a minor section of diorite/gabbro (501033). Increased fracture frequency and increased apertures in single fractures. There is a significant decrease in the resistivity logs in the section 104-125 m and there are minor caliper anomalies in the section. At c. 115 m there is a large decrease in the fluid resistivity. However, red staining alteration and low resistivity are more widespread. 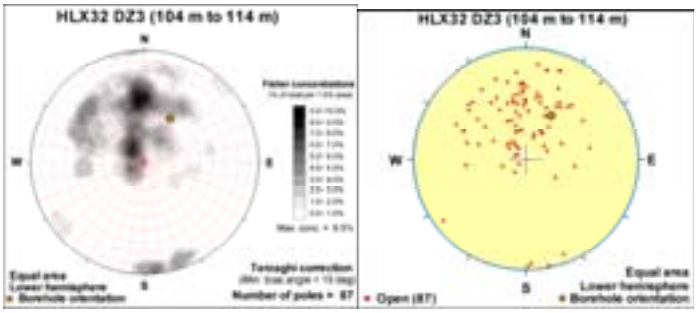

BH	Geometrical Intercept (bh. m)	Target intercept (bh. m)	Comment
KLX15A	963-1000,4 (Base)	977-1000,4+	Eshi 978-1000m: Inhomogeneous deformation zone characterized by brittle and brittle-ductile deformation. Increased frequency of sealed fractures and sealed fracture network and slight increase in open fractures, faint to strong red staining and partly faint to weak saussuritization, one core loss and ten slickensides. The most intensely deformed sections (cores) are: 994.71-997.50 m (brittle-ductile deformation) and 997.50-1000.43 m (brittle deformation; some fractures sub parallel to core). No geophysical data. The geophysical logging was interrupted at c 978 m. From /Viola et al, 2007/: 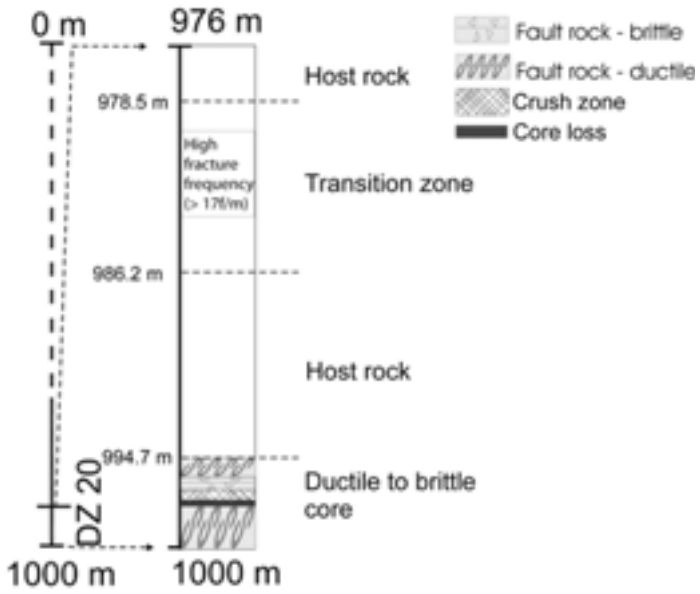 No borehole images are available for this DZ and therefore no structural features could be oriented. DZ 20 is characterized in its upper part by a transition zone extending from c. 978 to 986 m depth. This is defined by the progressive increase in fracture frequency, which in the central part of the transition zone reaches values of up to 17 f/m, thus possibly indicative of a DZ core. A proper core is, however, found starting at ~995 m depth. No information on its termination is provided here because the end of the DZ was not logged due to the termination of the KLX15A drill core. There is a sharp boundary between undeformed host rock and the core, which is defined by an early ductile fabric. This fabric is overprinted by brittle deformation that generated protocataclasites and cataclasites, with a very high fracture frequency (up to 50 f/m) forming crush zones and leading to localized core loss.

BH	Geometrical Intercept (bh. m)	Target intercept (bh. m)	Comment
KLX27A	209,8-257,1	209-255	Eshi DZ3 208.5-255.0 m: Brittle deformation zone characterized by increased frequency of sealed and, partly, also open fractures, sealed network, six crush zones, cataclasites, gouge, core loss, weak to medium red staining and two slickensides. Brittle-ductile and ductile shear zones, overprinted by the brittle deformation, also occur. The most intensely deformed sections (cores) are 221.20-221.50 m, 225.17-229.90 m and 241.40-242.50 m. There are major anomalies in all geophysical logs. The most significant geophysical anomalies occur in the sections c. 225-230 m and 240-245 m. The host rock is dominated by quartz monzodiorite (501036). Subordinate rock types comprise fine-grained diorite-gabbro (505102), fine-grained granite (511058) and very sparse occurrence of granite (501058). 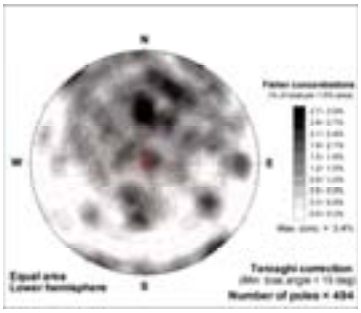 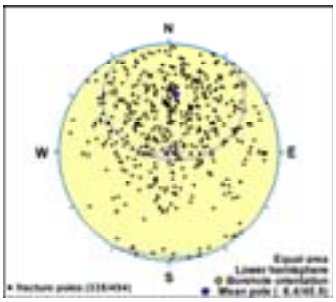 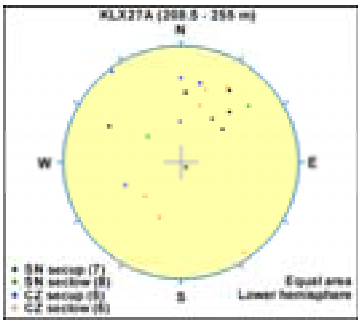 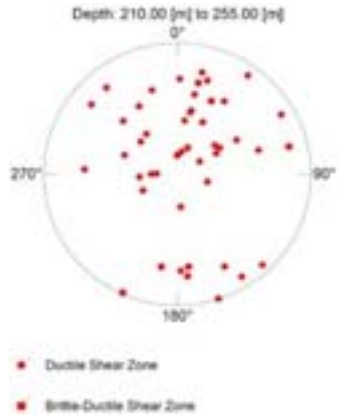

ZSMNW042A , KLX27A drill log extract (zone only)

ZSMNW042A , KLX27A drill core photos (zone only)

ZSMNW047A

ZSMNW047A remains essentially unchanged from version 1.2. No direct evidence is available concerning the presumed zone and it remains classed as medium confidence. A thickness has been added. ZSMNW047A is interpreted as being a 1.3 km long, 25 m thick brittle deformation zone. The length, thickness and character are all inferred from the detailed topographic LIDAR data.

NW-SE striking deformation zones ZSMNW047A	
Modelling procedure: At the surface, corresponds to a strong topographic lineament. Modelled using an assumed vertical dip. Not included in the regional model but present inside local model volume.	
Confidence of existence: Medium	

Property	Quantitative estimate	Span	Confidence level	Basis for interpretation	Comments
Position		± 20 m (surface)	High	Linked lineament,	
Orientation (strike/dip)	138/90	110-145 /± 10	High/low	Strike based on trend of lineament. Dip assumed	
Thickness	25 m	10-30 m	Medium	Lineament, bounding outcrops.	
Transition zone					
core	No data				
Length (regional model)	1.3 km	1.2-1.3 km	Medium	Linked lineaments	
Ductile deformation	No data				
Brittle deformation	Yes		Medium	Assumed from topographic lineament	
Alteration	No data				
Fracture orientation	No data				
Fracture frequency	No data				
Fracture filling	No data				
Sense of displacement	No data				

NW-SE striking deformation zones ZSMNW047A			
BH	**Geometrical Intercept (bh. m)**	**Target intercept (bh. m)**	**Comment**
None			No BH intercepts

ZSMNW052A

The surface trace and overall geometry of the zone remains unchanged from version 1.2. However, a previously assumed vertical dip has been confirmed as well as details concerning its thickness and character being added. ZSMNW052A is interpreted as being a c. 1.1 km long, subvertical, brittle deformation zone with an overall thickness of 15 m and a core of highly fractured rock with a thickness of around 5 m.

NW-SE striking deformation zones ZSMNW052A	
Modelling procedure: At the surface, corresponds to the low magnetic and topographic lineaments. Modelled using dip that has been inferred from KLX06A. Not included in the regional model but present inside local model volume.	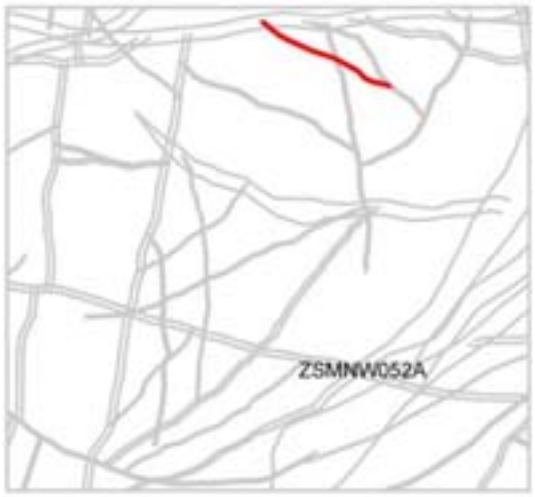
Confidence of existence: High	

Property	Quantitative estimate	Span	Confidence level	Basis for interpretation	Comments
Position		± 20 m (surface)	High	Linked lineament,	
Orientation (strike/dip)	116/90	± 10/± 10	High/high	Strike based on trend of lineament. Dip based on KLX06A	
Thickness	15 m	10-20 m	High	Lineament, bounding outcrops, KLX06A	
core	7 m	± 2	High	'core' of more highly fractured rock based on general ref: geophysical profiling -refraction (P-05-155) seismic velocity 3100 m/s	/Lindqvist, 2005/. KLX06 intercept suggests a more complex structure.
Length (regional model)	1.1 km	1.0-1.2 km	Medium	Linked lineaments	
Ductile deformation	No		High		Absent from SHI
Brittle deformation	Yes		High	KLX06A (highly fractured minor crush)	
Alteration			High	KLX06A	Red staining,
Fracture orientation	110/80, 030/85, 280/15, 330/05		Medium	KLX06A	
Fracture frequency* Open/sealed m^{-1}	5/28		Medium	KLX06A	

NW-SE striking deformation zones ZSMNW052A					
Crush zone Number/total m	16/2.5		Medium	KLX06A	
Fracture filling			High	KLX06A	Chlorite, calcite, clay, laumontite, hematite, pyrite, adularia, quartz, epidote, fluorite.
Kinematics					

BH	Geometrical Intercept (bh. m)	Target intercept (bh. m)	Comment
KLX06	203,3-260,0	200-260	Inhomogeneous deformation zone characterized by increased frequency of sealed and open fractures, weak to faint alteration (oxidation), and crush zones. Partly low resistivity, p-wave velocity, density and magnetic susceptibility. Numerous caliper anomalies. The sections 200-207m and 226-243 m are the most intensely deformed parts and are characterized by several strong anomalies in all geophysical loggings. 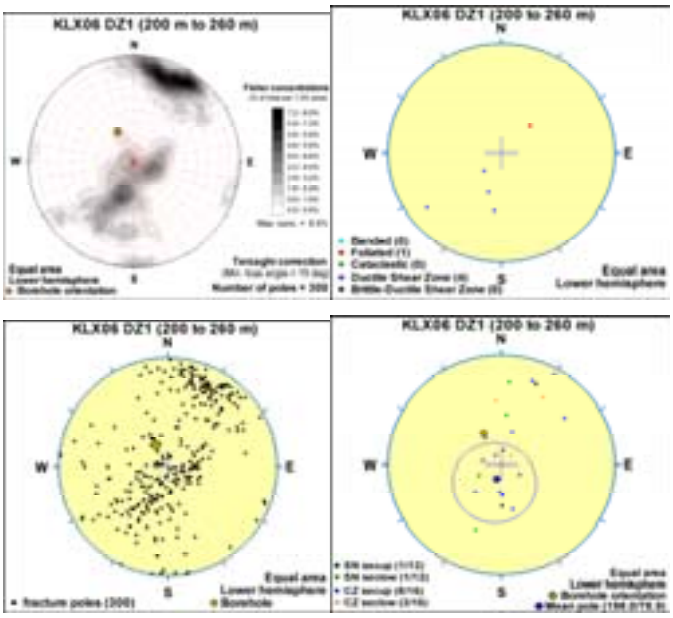

ZSMNW088A

ZSMNW088A has had its easterly extent modified and now terminates at ZSMNE004A rather than extending beyond it. The modification was based on a review of the background data to the lineament and following a ‘simplest solution’ criterion. No direct evidence is available concerning the presumed zone and it remains classed as medium confidence. A thickness has been added. ZSMNW088A is interpreted as being a 3.2 km long, 20 m thick brittle deformation zone. The length, thickness and character are all inferred from the topographic expression.

NW-SE striking deformation zones ZSMNW088A	
Modelling procedure: At the surface, corresponds to a topographic lineament. Modelled using an assumed vertical dip. Modelled to the base of the regional model and present inside local model volume.	
Confidence of existence: Medium	

Property	Quantitative estimate	Span	Confidence level	Basis for interpretation	Comments
Position		± 20 m (surface)	High	Linked lineament,	
Orientation (strike/dip)	110/90	300-090/± 20	High/low	Strike based on trend of lineament. Dip assumed	
Thickness	20 m	10-40 m	Medium	Lineament, bounding outcrops.	
core	No data				
Length (regional model)	3,2 km	3-4 km	Medium	Linked lineaments	Possible NW extension
Ductile deformation	No data				
Brittle deformation	Yes		Medium	Assumed from topographic lineament	
Alteration	No data				
Fracture orientation	No data				
Fracture frequency	No data				
Fracture filling	No data				
Sense of displacement	No data				

NW-SE striking deformation zones ZSMNW088A			
BH	**Geometrical Intercept (bh. m)**	**Target intercept (bh. m)**	**Comment**
None			No BH intercepts

ZSMNW119A

ZSMNW119A lies in the north western corner of the local model area with an easterly termination against ZSMNS059A. The zone is interpreted as a 2.0 km long sub vertical to steeply north dipping brittle-ductile deformation zone with an overall thickness varying between 5 and 20 m with an inferred 3 m thick core of more highly fractured rock. The zone has not been the subject of any focused indirect or direct investigation methods.

NW-SE striking deformation zones ZSMNW119A	
Modelling procedure: At the surface, corresponds to the low magnetic and topographic lineaments. Modelled using an assumed dip. Modelled to the base of the regional model and present inside local model volume.	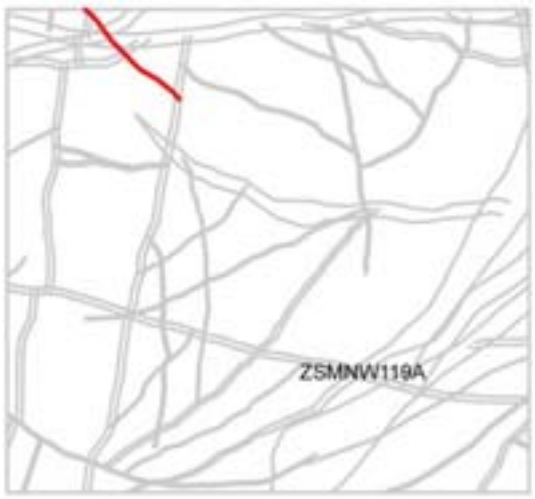
Confidence of existence: High	

Property	Quantitative estimate	Span	Confidence level	Basis for interpretation	Comments
Position		± 25 m (surface)	High	Topographic and magnetic lineament	
Orientation (strike/dip)	130/90	± 10/90-70N	High for strike, low for dip	Strike based on trend of lineament. Dip assumed	Single weak field indicator of 70N
Thickness	10 m	5-20 m	Medium	Topographic and magnetic lineament	
core	3 m	± 2	Low	Inferred from ZSMNW929A and others. 'Core' of more highly fractured rock.	
Length (regional model)	2.0 km	± 100 m	Medium	Topographic and magnetic lineament	
Ductile deformation	Yes		Medium	Evidence from bounding outcrops	Brittle-ductile. Possibly not exclusively associated with this lineament.
Brittle deformation	Yes		Medium	Evidence from bounding outcrops (raised fracture frequency)	Brittle-ductile. Possibly not exclusively associated with this lineament.
Alteration			High	Outcrop mapping	Red staining,
Fracture orientation	No data				
Fracture frequency	No data				
Fracture filling			High	Outcrop mapping	Epidote

BH	Geometrical Intercept (bh. m)	Target intercept (bh. m)	Comment
None			No BH intercepts

ZSMNW929A

The zone is interpreted as a 1.6 km long sub vertical brittle deformation zone with an overall thickness of 20 m and a 5 m thick core of more highly fracture rock.

The existing background data and v1.2 zone interpretation has been reviewed including the field observations /Wahlgren et al., 2005b/, topographic and airborne geophysical lineaments. For version V1.2 the zone was modelled with the orientation 113/79 with the dip being based on intercepts in KLX02A and KLX04A. Subsequent detailed resistivity ground surveys and modelling suggest the zone is essentially sub vertical rather than the assigned steep dip to the south west. The borehole intercepts and the shallow dipping nature of the fractures in the core are rather associated with ZSMNW928A (seismic reflector N) than a steeply dipping ZSMNW929A. The review has led the zone to be assigned a vertical dip in the model.

Outcrop mapping identified brittle indicators including breccia and red staining (E1547753, N6367597) /Wahlgren et al., 2005b/. Four seismic refraction profiles cross the lineament, all four profiles identify low velocity anomalies with widths of approximately 5-8 m and velocities between 3300 and 3500 m/s, /Lindqvist, 2005/.

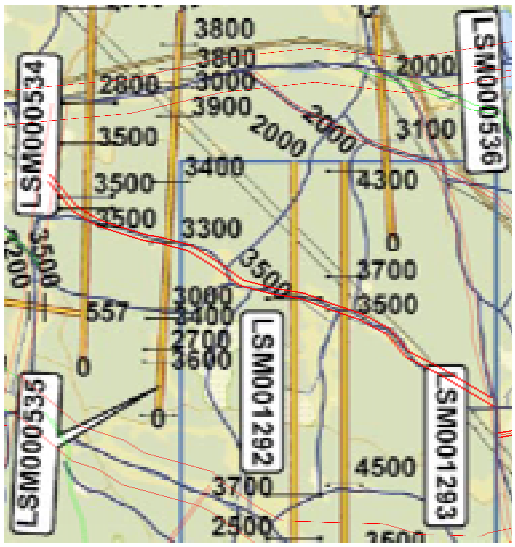

Four seismic refraction profiles cross the lineament, all four profiles identify low velocity anomalies with widths of approximately 5-8 m and velocities between 3300 and 3500 m/s, /Lindqvist, 2005/.

NW-SE striking deformation zones ZSMNW929A	
Modelling procedure: At the surface, corresponds to the low magnetic and topographic lineaments. Modelled using dip that has been inferred from detailed ground resistivity modelling. Modelled to the base of the regional model and present inside local model volume.	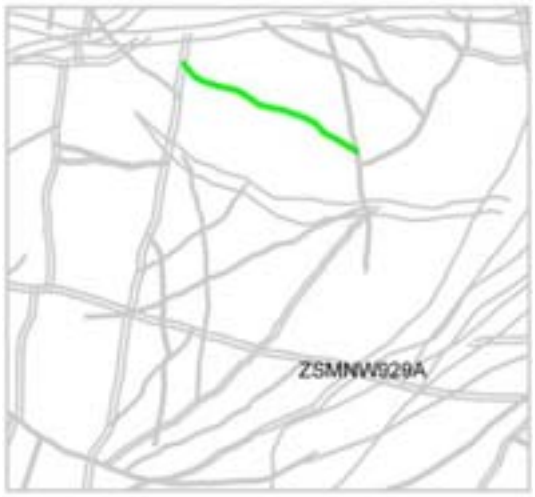
Confidence of existence: High	

Property	Quantitative estimate	Span	Confidence level	Basis for interpretation	Comments
Position		± 20 m (surface)	High	Linked lineament,	
Orientation (strike/dip)	114/90	± 10/± 10	High for strike, medium for dip	Strike based on trend of lineament. Dip based on resistivity modelling	
Thickness	20 m	10-30 m	Medium	Topographic and magnetic lineament	
core	5 m	± 2	Medium	'core' of more highly fractured rock based on general ref: geophysical profiling -refraction (P-05-155) seismic velocity 3300-3500 m/s	/Lindqvist, 2005/
Length (regional model)	1.6 km	1.6-1.8 km	Medium	Linked lineaments	
Ductile deformation	Yes		Medium	Evidence from bounding outcrops (mylonite)	Possibly not exclusively associated with this lineament.
Brittle deformation	Yes		Medium	Evidence from bounding outcrops (highly fractured with breccia)	Possibly not exclusively associated with this lineament.
Alteration			High		Red staining,
Fracture orientation	No data				
Fracture frequency	No data				

NW-SE striking deformation zones ZSMNW929A					
Fracture filling			High	Outcrop mapping	Quartz.

BH	Geometrical Intercept (bh. m)	Target intercept (bh. m)	Comment
None			No BH intercepts

ZSMNW931A

ZSMNW931A remains unchanged from version 0. Little direct evidence is available concerning the presumed zone other than ground geophysics /Stanfors and Erlström 1995/ and limited field control /SKB, 2002/. ZSMNW931A is interpreted as being a ca. 4 km long, predominantly brittle deformation zone.

NW-SE striking deformation zones ZSMNW931A	
Modelling procedure: At the surface, corresponds to strong topographic lineament. Modelled using an assumed vertical dip. Included in the regional model and present on the margin of the local model volume.	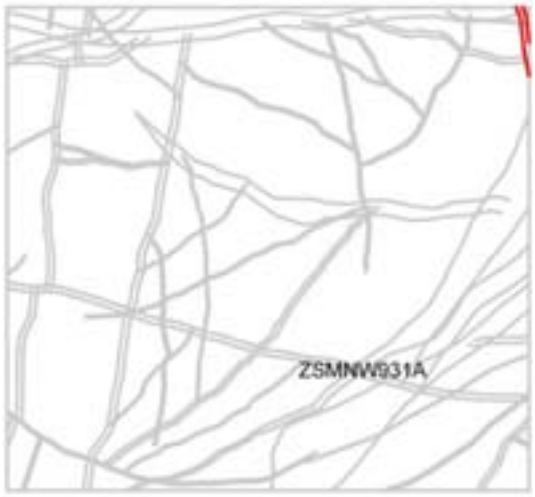
Confidence of existence: High	

Property	Quantitative estimate	Span	Confidence level	Basis for interpretation	Comments
Position		± 30 m (surface)	Medium	Linked lineaments. Ref: v.0. Verified by field control ground magnetic and VLF measurements.	Poorly contrained coastline lineament. Ground geophysics Ref: /Stanfors and Erlström 1995/
Orientation (strike/dip)	165/90	± 10/± 15	High/low	Strike based on trend of lineament. Dip assumed	
Thickness	50 m	50-100 m	Low	Lineament, bounding outcrops.	
core	No data				
Length (regional model)	3.8 km	±200m	Medium	Linked lineaments	ZSMNW931A+B= 4,4 km
Ductile deformation	No data				
Brittle deformation	Yes		Medium	Assumed from VLF and topographic lineament	
Alteration	No data				
Fracture orientation	No data				
Fracture frequency	No data				
Fracture filling	No data				
Sense of displacement	No data				

BH	Geometrical Intercept (bh. m)	Target intercept (bh. m)	Comment
None			No BH intercepts

KLX07_DZ7

E-W striking deformation zones KLX07_DZ7	
KLX07_DZ7's orientation is based on a combination of fracture orientation concentrations, radar and nearby forward modelling of magnetic data. The modelled geometry generates theoretical intercepts in HLX21, HLX22, HLX23 and HLX24. While fracture data weakly supports possible correlation with HLX21 and HLX24 no correlation with HLX22 or HLX23 exists. It should be noted that all four hammer holes lie within the complex ZSMEW007A deformation belt.	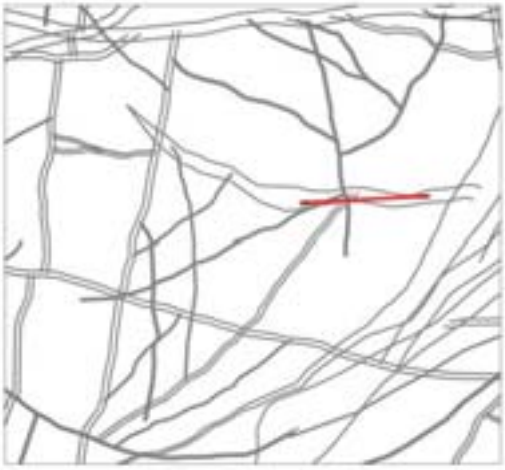

Confidence of existence: High

Property	Quantitative estimate	Span	Confidence level	Basis for interpretation	Comments
Position			High	Eshi	
Orientation (strike/dip)	267/90		Low	Radar 267/83 at 375m. Pole concentration very similar. Magnetic profile modelling just to west supports a subvertical orientation.	An alternative interpretation is a structure 250/50 based on ductile fabric and crush. However, there is no correlation in KLX02.
Thickness	30 m		Low		
Length (regional model)	1.0 km		Low	Assumed	
Ductile deformation	Yes		Low	Ductile fabric	
Brittle deformation	Yes		High	Raised fracture frequency and cataclasis	
Alteration			High		Oxidation, chloritization, epidotization
Fracture frequency* Open/sealed m^{-1}	9/22		Low		
Crush zone Number/total m	3/0.6		Low		
Fracture filling			High		Chlorite, calcite, clay, pyrite quartz, epidote.

BH	Geometrical Intercept (bh. m)	Target intercept (bh. m)	Comment
KLX07A	343-386	347-388	Eshi: DZ7 347-388 m: Slightly increased sealed fracture frequency. The section 386.30-386.70 m is characterized by a section of epidote sealed cataclasite. 14 radar reflectors have been identified, two of them are oriented. The oriented reflectors are at 348.6 m with the orientation 50/195 and at 375.3 m with the orientation 83/267. Decreased radar amplitude in the intervals 347-350 m and 375-387.5 m. Several p-wave velocity anomalies and a few low resistivity anomalies occur in the section. 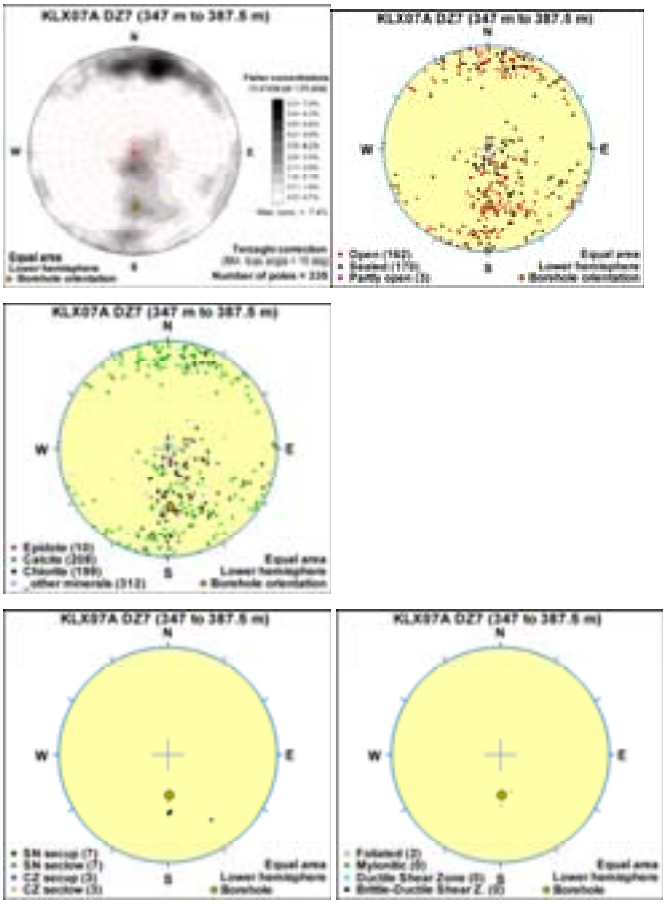
HLX21	20-71	18-24 and 83-110	Eshi DZ1 18-24m: Low resistivity, low p-wave velocity, low density, low susceptibility and caliper anomaly. Two radar reflectors with the intersection angles 67º and 59º to the borehole axis. The host rock is dominated by a mixture of Ävrö granodiorite (501056) and pegmatite (501061). Subordinate rock type is fine-grained granite (5110158) 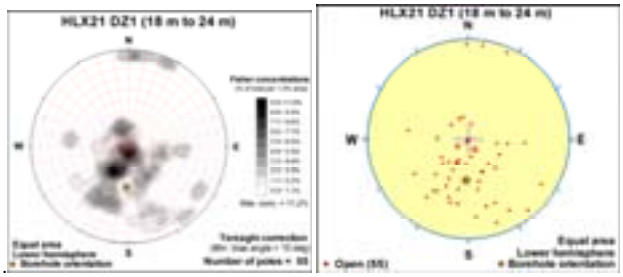 DZ2 83-110 m: Inhomogeneous brittle deformation zone characterized by certain distinctly deformed sections, with increased fracture frequency. Low resistivity, low p-wave velocity, partly low density, low susceptibility and caliper anomaly. The host rock is totally dominated by Ävrö granodiorite (501056) with subordinate fine-grained granite (511058).

BH	Geometrical Intercept (bh. m)	Target intercept (bh. m)	Comment
			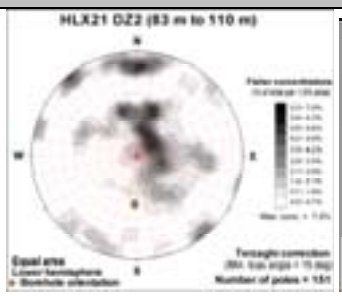 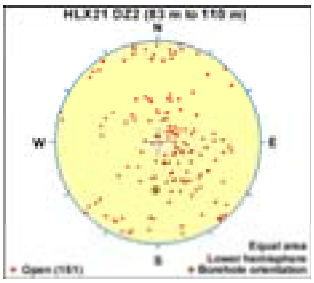
HLX22	76-125		No correlation
HLX23	105-155		No correlation
HLX24	0-26	27-40	Eshi DZ1 27-40 m: Medium alteration and increased fracturing. Distinct anomalies in all geophysical logs. The host rock is totally dominated by Ävrö granodiorite 8501056) with subordinate pegmatite (501061). 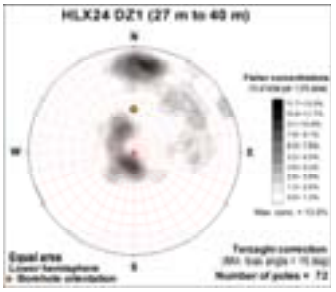 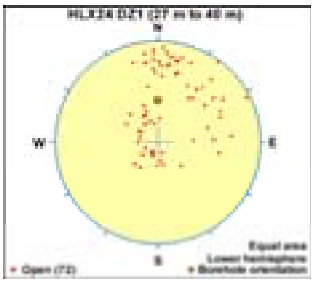

KLX18A_DZ9

E-W striking deformation zones KLX18_DZ9	
KLX18A_DZ9's orientation is based on detailed mapping of the zone core /Viola et al, 2007/. An interception at the outer edge of the modelled geometry coincides with Eshi HLX30 DZ2 though no clear correlation is established.	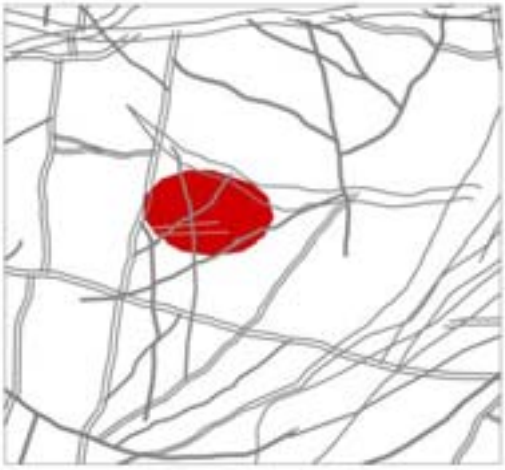
Confidence of existence: High	

Property	Quantitative estimate	Span	Confidence level	Basis for interpretation	Comments
Position			High	Eshi	
Orientation (strike/dip)	095/50		Low	Core orientation /Viola et al, 2006/	
Thickness	10 m		Low		
Length (regional model)	1.0 km		Low	Assumed	
Ductile deformation	Yes		high	Mapped ductile fabric	
Brittle deformation	Yes		High	Increased frequency of sealed fractures and open fractures, crush and gouge zones,	
Alteration			High		Red staining
Fracture frequency* Open/sealed m^{-1}	10/28		Low		
Crush zone Number/total m	3/0.3		Low		
Fracture filling			High		Chlorite, calcite, clay, pyrite, epidote, prehnite, hematite

<table>
<tr><th>BH</th><th>Geometrical Intercept (bh. m)</th><th>Target intercept (bh. m)</th><th>Comment</th></tr>
<tr><td>KLX18A</td><td>473-488</td><td>472-489</td><td>DZ9 472-489 m: Inhomogeneous brittle-ductile deformation zone. High frequency of sealed fractures and open fractures with large (2-5 mm) apertures. Gouge (15 mm) and one cataclasite (16 mm). Three crush zones (17-22 cm). Core zone at 484.00-487.90 m. Faint to medium red staining. Significantly decreased resistivity and magnetic susceptibility, and partly decreased P-wave velocity in the interval 483.5-488.9 m. Two non-oriented radar reflectors occur at 473.4 m and 476.5 m with the angle 42° and 59° to borehole axis, respectively. Two strong and persistent oriented reflectors occur at 482.3 m and 485.0 m with the orientation 018/89 and 193/37, respectively. The host rock is dominated by Ävrö granodiorite (501056). Subordinate rock type is fine-grained granite (511058).
 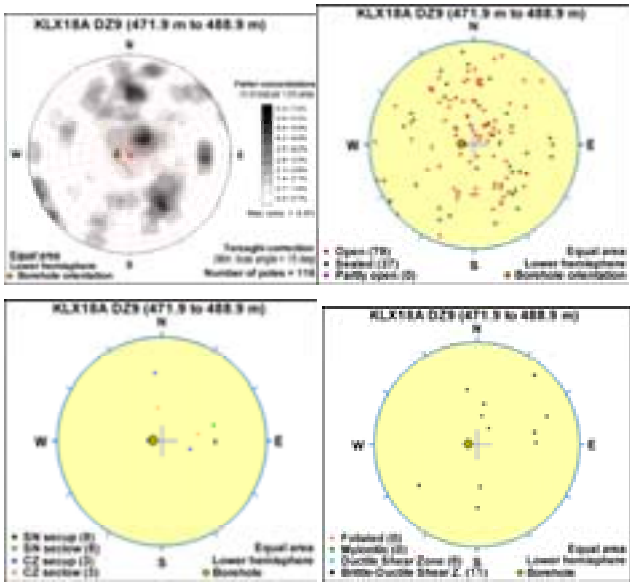
Ref: /Viola et al, 2006/
<table><tr><th>Depth (m)</th><th>Interpretation</th><th>Description</th></tr><tr><td>~483.92 – 485.491</td><td>Transition zone</td><td>Increase in fracture frequency and occurrence of epidote, sealed networks towards the core. The total thickness of the zone is 3.9 m.</td></tr><tr><td>485.491 – 485.730</td><td>Fault core</td><td>The brittle core is highly fractured and contains proto-cataclasites and a thin gouge horizon.</td></tr><tr><td>485.730 - ~487.80</td><td>Transition zone</td><td>Decrease in fracture frequency away from the core.</td></tr></table> 
Orientation of epidote bands and veins (red great circles) and open</td></tr>
</table>

BH	Geometrical Intercept (bh. m)	Target intercept (bh. m)	Comment
			fractures within the upper transition zone of DZ 9. The transition zone extends from ~483.92 to 485.491 m depth. It is defined by a progressive increase of the fracture frequency and the occurrence of cataclastic networks in the proximity of the fault core (red great circles in figure above). Fractures have a quite variable orientation, although most of them dip moderately to the S, SW and exploit similarly oriented epidote veins and bands. The fault core extends from 485.491 m to 485.730 m depth. It follows a c. 15 cm thick crush zone and is characterized by a strongly fractured interval and the occurrence of c. 5 cm of proto-, cataclasites, ultracataclasites and a c. 2 cm thick gouge horizon. Cataclasites are oriented roughly EW and dip c. 50° to the S, thus being not very dissimilar from the predominant orientation of fractures in the upper part of the DZ.  The core (details shown in the two bottom pictures) consists of cataclasites, a gouge interval and a strongly fractured rock interval. 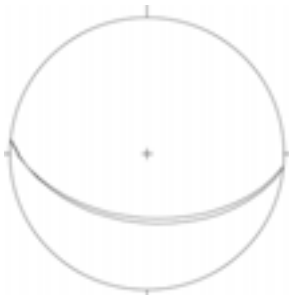 *Orientation of the DZ core cataclasites* The core is followed by a heavily fractured rock interval down to approximately 487.8 m depth. Fractures have a similar orientation to those of the upper transition zone, with an average EW/ENE-WSW strike and a c. 50° dip to the S/SSE. One SE-dipping striated plane indicates a dextral transtensional kinematics (red circle in figure, below).  *Orientation of open fractures in the lower transition zone of DZ 9. The red great circle is a striated plane at depth 487.065 m.*
HLX30	60-70	-	Eshi DZ2 60-68 m. Brittle deformation zone characterized by increased frequency of open fractures, crush at c. 62 m and medium red staining.

BH	Geometrical Intercept (bh. m)	Target intercept (bh. m)	Comment
			High frequency of negative resistivity anomalies and decreased bulk magnetic susceptibility. Host rock is totally dominated by Ävrö granite (501044) 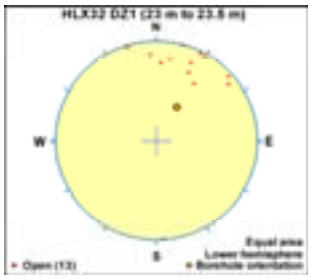

KLX08_DZ6

NW-SE striking deformation zones KLX08_DZ6	
KLX08_DZ6's orientation is based on radar that generally strikes parallel to the major structure ZSMEW007A. A sub horizontal interpretation with an undefined strike is an alternative.	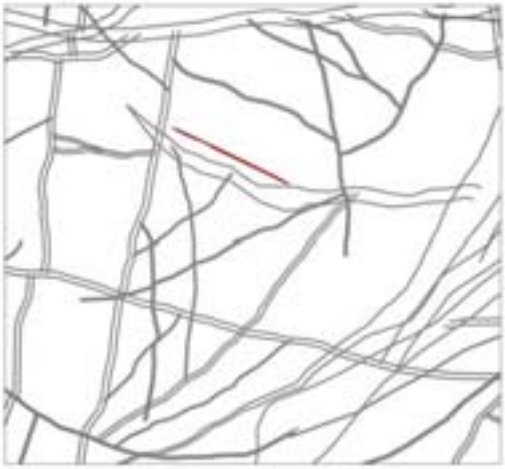

Confidence of existence: High

Property	Quantitative estimate	Span	Confidence level	Basis for interpretation	Comments
Position			High	Eshi	
Orientation (strike/dip)	296/89		Low	Radar 296/89. Strike and dip also follow pattern of other structures parallel to ZSMEW007A strike indicated by ground geophysics.	Alternatives: NGU alternative sub horizontal to E or W fractures but crush zone dips gently N. 3 cm cataclasite dips 150/41. Gentle fracture dips associated with deeper reflector M1 series?
Thickness	10 m		Low		
Length (regional model)	1.0 km		Low	Assumed	
Ductile deformation	No		Low		
Brittle deformation	Yes		High	Raised fracture frequency and cataclasis	
Alteration			High		Red staining, epidotization, saussuritzation
Fracture frequency* Open/sealed m^{-1}	11/40		Low		
Crush zone Number/total m	1/<0.2		Low		
Fracture filling			High		Calcite, chlorite, clay, hematite, pyrite, prehnite, andularia, laumontite, epidote.

BH	Geometrical Intercept (bh. m)	Target intercept (bh. m)	Comment
KLX08A	396-416	396-416	Eshi DZ6 396-416 m: Inhomogeneous brittle deformation zone characterized by red staining and increased frequency of sealed and open fractures. The section 403.9-416 m is characterized by weak to medium red staining and saussuritization. Crush zone at 408.03-408.38 m. Oriented reflector occurs at 400.2 m with the orientation 296/89. Geophysical loggings indicate general decrease in bulk resistivity, magnetic susceptibility and low p-wave velocity including several caliper anomalies along the entire section. 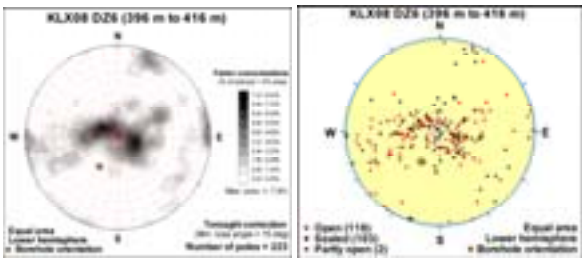 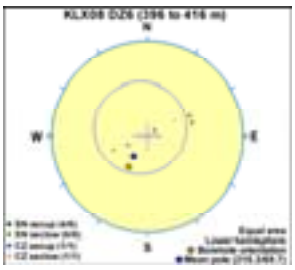 Ref /Viola. Et al, 2006/: 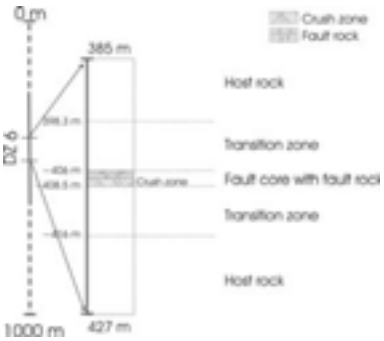 The zone is characterized by a ~1 m thick (true thickness) fault core with 2 symmetrically arranged transition zones. The upper and lower transition zones show increasing and decreasing fracture frequency towards and away from the fault core, respectively. The stereonet below shows the fault slip data observed and measured within the two transition zones; red great circles represent striated planes of the upper transition zone, whereas black great circles represent planes of the lower transition zone. The steep, roughly EW trending fractures are generally coated by epidote, whereas the shallower planes are coated by chlorite, clay minerals and calcite, which in turn may suggest the steep fractures to be older (thus formed under higher T conditions) than the gently-dipping ones. No direct crosscutting relationships were, however, observed. No straightforward kinematic framework can be obtained from the few measurements. In general, highly oblique or strike-slip kinematics is accommodated along moderately WNW or ESE dipping planes. The steep E-W epidote-coated fracture planes suggest instead strike-slip displacements along moderately plunging lineations.

BH	Geometrical Intercept (bh. m)	Target intercept (bh. m)	Comment
			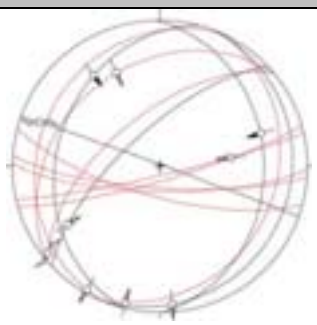 *Fault–slip data and orientation of striated planes and fractures in the transition zones above and below the core of DZ 6. Red great circles plot structures from the upper transition zone, black from the lower.* The occurrence of discrete and localized cataclasites is common throughout both transition zones. The upper boundary of DZ 6 fault core is located at approximately 405.77 m depth. The core consists of ~50 cm of cohesive cataclasites, ultracataclasites and gouge, and a ~ 2 m thick crush zone affecting the undeformed host rock. At depth 406.18 m there occurs a narrow, cataclastic zone characterized by a c. 3 cm thick green ultracataclasite and gouge. An open fracture, coated by epidote and clay minerals is oriented 150/41 and runs parallel to the ultracataclasite.  Epidote ultracataclasite at depth 406.18 m. The ultracataclasite and the open fracture are oriented 150/41. The sample above comes from this part of the DZ core and preserves complex textural characteristics indicative of multiple cataclastic episodes.

E-W and NW-SE striking, moderately northward dipping deformation zones

ZSMEW007A

This zone is the dominating structure in central Laxemar. ZSMEW007A is interpreted as being an E-W to ESE-WNW striking, 80m thick zone that dips to the north at 35º to 45º. The zone is interpreted as being wholly brittle.

In the RVS model the zone has an overall orientation of 281/44 and a thickness of 80m. The orientation remains essentially the same as version 1.2 but the thickness has been increased from 50m to 80m. This thickness follows the earlier applied 'envelope' concept and allows for splays and transition zones. For ZSMEW007A the concept is that the transition zones essentially conform to the broad belt of oxidation (red staining) that is associated with the zone and that within the envelope boundaries lie a number of sub parallel structures that together define the complex zone. It is this pattern of red staining recorded in logs of both the hammer and core holes that is taken to further support the northerly dip of the main structure. As described below, during model development the zone had been split into eastern and western sections and also modelled at various scales being represented by a number of surfaces. However, even after going through this process it is considered that the modelling of the zone as a single a coherent northerly dipping single 'slab' still gives the best fit with the data. ZSMEW007A does not appear to be continuous from a hydrological point of view. The hydrological subdivision may be due to other crosscutting deformation zone(s) or possibly N-S dolerite dyke(s). Detailed examination of the drillcore has lead to a better characterization of the zone /Viola and Ganerod, 2006/.

The surface expression of what has been termed ZSMEW007A is clearly complex and no doubt results from the interference of a number of structures with very different orientations. Smaller structures daylighting in this 'belt' have sub vertical and southerly dips as suggested by local drilling evidence and geophysical profiling and are described in the following section though the main structure (ZSMEW007A) is interpreted as dipping to the north.

The zone was modelled previously with a thickness of 50m, dipping north at an angle of 43°. The dip was based mainly on the seismic reflector. Even from looking at the surface lineament trace geometry alone it was considered likely that the zone would have to be remodelled in two or three shorter sections. Initially the most likely candidate location for a break was thought to be between HLX31 and HLX33. However, a trench excavation and the orientation of the exposed deformation zone, including a core (300/40) suggested the break point further to the east between HLX33 and HLX23. A break point in this location is supported by the currently available hydrological pumping test data that suggests the western and eastern arms of ZSMEW007A are not hydraulically connected. A comparison of the trench excavation and the magnetic and resistivity profiles available in the same position as the trench reinforces the interpretation of a northerly dip to the zone and gives more confidence to the interpretation of orientations from the other geophysical profiles crossing this zone. A re-evaluation of the lineament map and background data has lead to a significant extension of the zone geometry to the NW, crossing beyond ZSMNS059A. This extension has been modelled with a westerly narrowing thickness

and the same northerly dip but has been classed as medium confidence. The surface expression of the NW section becomes much narrower to the NW and it is likely this pattern is mirrored at depth.

During an intermediary stage (v2.1) the zone was modelled at a more local scale tying in the new, shorter, lineaments to the mapping, geophysical profiles and BH deformation indicators. These surfaces are also compatible with the 35-45° northerly dip to the zone. A third group of surfaces were also generated: a number of sub parallel lineament traces have been used to visualise other sub parallel 'splays' of the zone in an attempt to portray the assumed character of the zone. However, other than the lineament traces there is little to support these visualisations. The following figures attempt to summarise the working process behind the current interpretation.

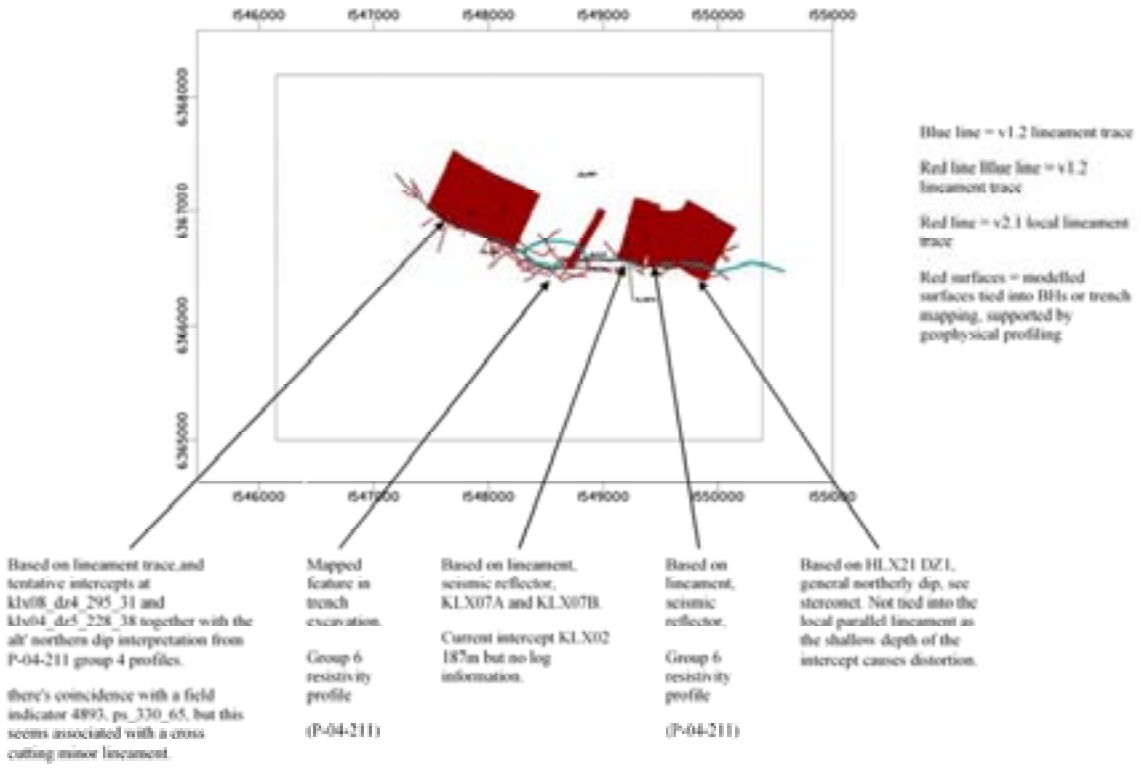

Outline of the construction of ZSMEW007A interpretation

The lineament taken to represent ZSMEW007A is also linked to other smaller, more steeply dipping to sub vertical structures, modelled as klx7_dz7 and klx08_dz6. These interpretations are not considered as alternatives for EW007 but represent other smaller structures. They are largely based on geophysics, particularly 3D modelling of magnetic susceptibility and also borehole deformation indicators.

ZSMEW007A has been investigated by three ground geophysical profiles /Thunehed, et al, 2004/

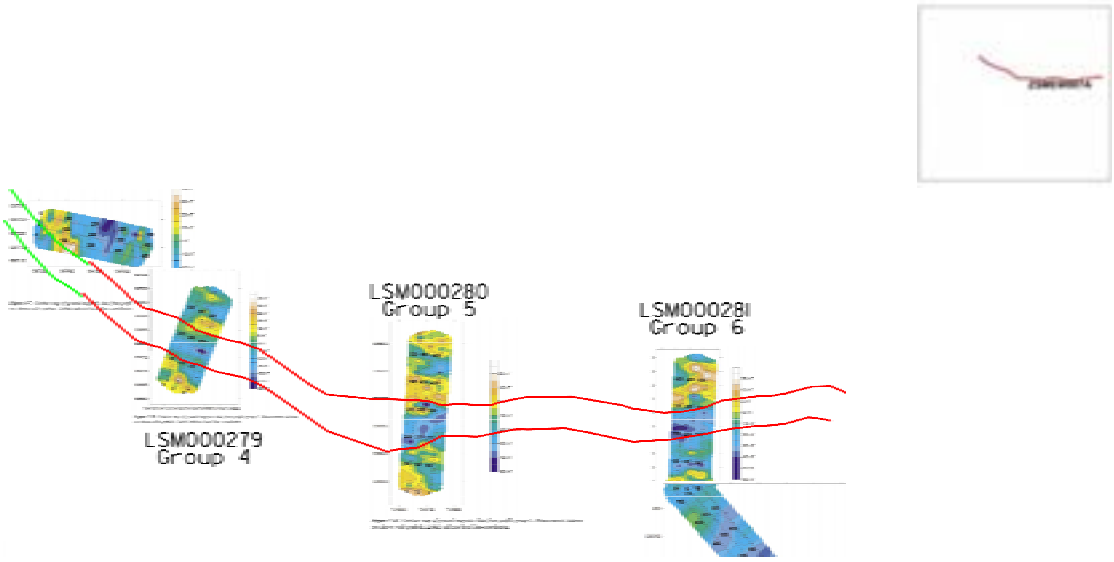

Ground magnetic and resistivity profiles across ZSMEW007A /Thunehed, et al, 2004/

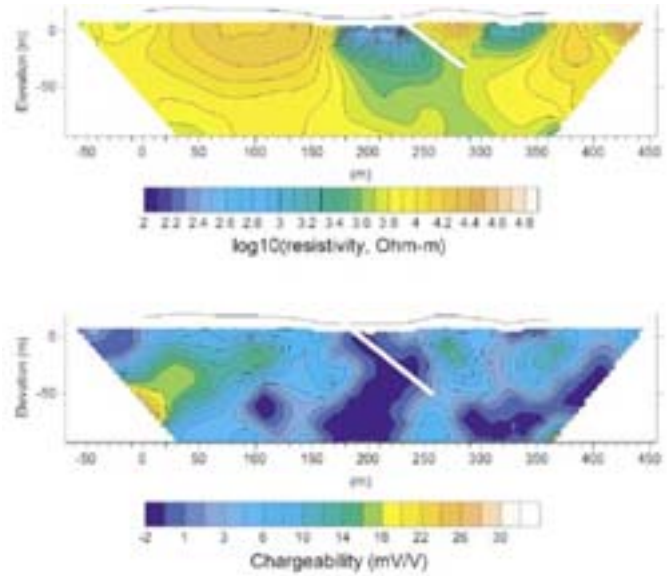

Inverted resistivity (top) and chargeability (bottom) sections for the central profile of group 4 (LSM000279) The northern leading edge of the major resistivity low, along with a similar pattern in the chargeability distribution is taken to support a northerly 35 to 45 degree dip for ZSMEW007A.

The western, WNW-ESE section of ZSMEW007A was investigated by the Group 4 profiles. The northern leading edge of the major resistivity low, along with a similar pattern in the chargeability distribution is taken to support a northerly 35 to 45 degree dip for ZSMEW007A. Along profile LSM000279 a seismic refraction survey identified a central low velocity zone with a width of approx 10m to 15m and a seismic velocity of 2800 m/s compared with 5000+ m/s in the host rock /Lindqvist, 2004/.

The western section of ZSMEW007A was further investigated by drillholes KLX04A and KLX08A. The drillcore from the interpreted zone intersection in KLX04A was inspected in detail to further characterize the zone in this location /Viola and Ganerod, 2006/. The section starts at depth 346.26 m with a c. 20 cm thick upper transition zone. The fault core, from depth 346.46 m, is characterized by c. 35 cm of cataclasites and both green and red gouge. Ultracataclasites/gouge are arranged in a complex, sinuous and anastomosing sealed network with associated grain size reduction.

Detail of the core of DZ 5, defined by a complex sealed network of ultracataclasite/gouge bands and a distinct interval of brown/green gouge at depth 346.66 m. /Viola and Ganerod, 2006/

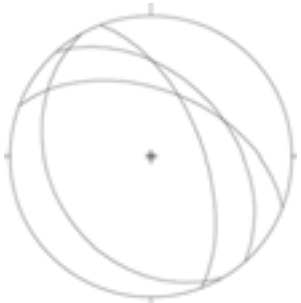

Orientation of discrete systemtic fractures within the zone core in KLX04A. /Viola and Ganerod, 2006/

Systematic fractures within the core strike roughly NW-SE. The fault core ends with a narrow zone of ultracataclasite and/or gouge. Hydrofracturing and fluidization are believed to be the mechanisms responsible for the formation of this deformation zone core, although more investigations would be necessary to fully unravel the complexities of the mechanism that generated the fault rock. A crush zone follows within the fault core. A transition zone begins at 352.81 m with abundant ultracataclasite and/or gouge strands and fractured rock. The transition zone contains numerous striated planes. No clear kinematic pattern emerges, though, with highly dispersed fracture planes (generally dipping to the west) and a predominance of very oblique shearing. Undeformed host rock is logged again at depth 357.77 m.

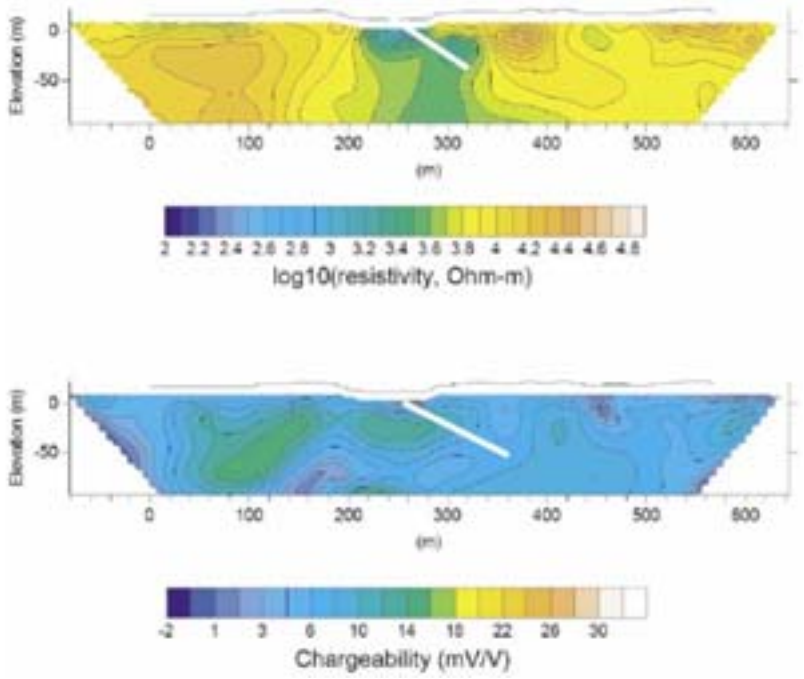

Inverted resistivity (top) and chargeability (bottom) sections for the central profile of group 5 (LSM000280). The northern leading edge of the major resistivity low is taken to support a northerly 35 to 45 degree dip for ZSMEW007A. This profile position and northern leading edge corresponds to the deformation zone identified in the trench excavation.

The central, W-E section of ZSMEW007A was investigated by the Group 5 profiles. Along profile LSM000280 a seismic refraction survey identified 2 central low velocity zones with widths of approx 5m and 10m and seismic velocities of 3800 and 3200 m/s compared with 5000+ m/s in the host rock /Lindqvist, 2004/. This position corresponds to the deformation zone exposed in a later excavated trench.

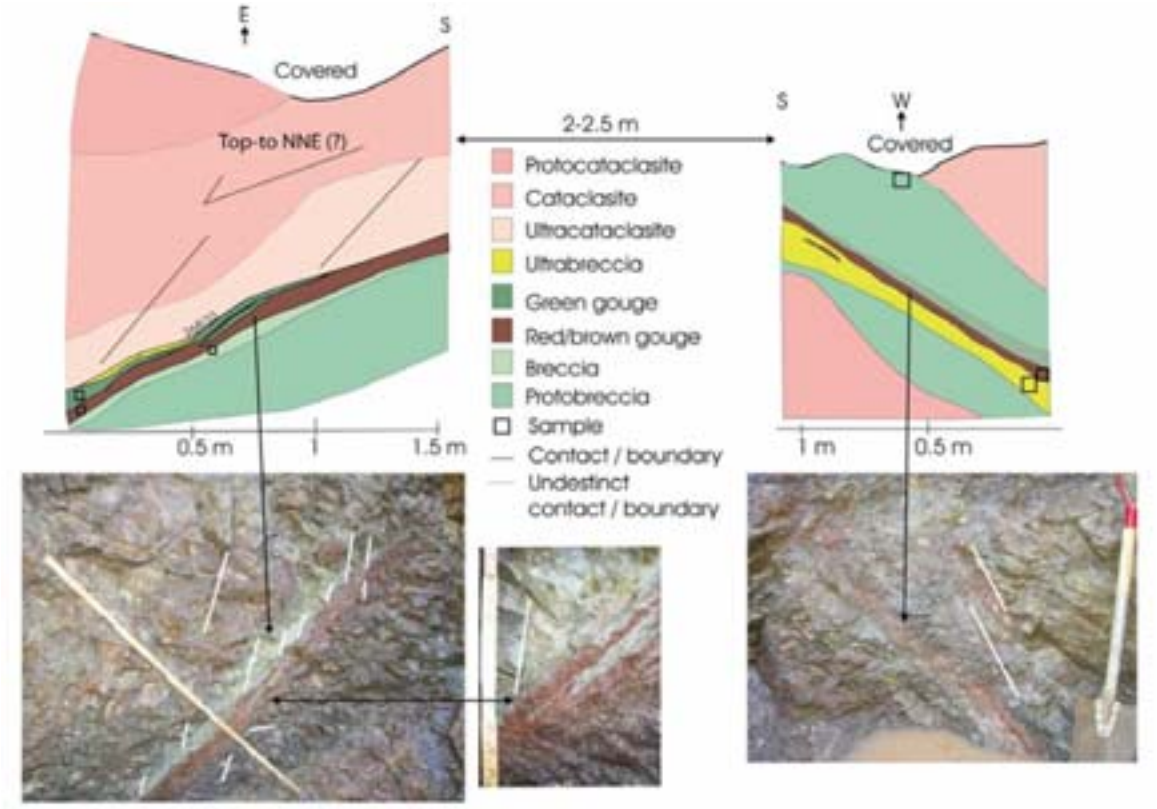

Sketch and photographs of trench walls with exposed fault rocks. As exposed in the trench located along profile LSM000280. /Viola and Ganerod, 2006/

The northern transition zone (hanging wall) as exposed in the trench consists of highly fractured Ävrö granite with red coloured alteration. Most fractures are filled with chlorite but some with epidote and calcite. Fracture fillings are typically 1-3mm thick. Dominant fracture orientations are: 314/42, 331/25, 305/58, 100/78, 198/58, 228/66, 320/30, 236/50, 276/46, 285/60, 350/64 (calcite filled), 290/54 (dm-thick zone with a number of parallel fractures). No ductile precursors were identified.

The core consists of ~3 meters of ultra- and cataclasites and a distinct ~20 cm-thick inner core composed of gouge and ultrabreccia. A certain amount of 5-10cm banding is visible consisting of alternating red and green coloration. The banding seems associated with a fracture orientation of 300-310/42-44. This orientation is dominant within the zone and defines the overall zone orientation as 300/40. A 60cm thick central section of the core is completely altered to clay. Dominant fracture orientations are: 310/42, 250/62, 220/58, 330/70, 202/70, 140/80.

The southern transition zone consists of highly fractured Ävrö granite with red coloured alteration. Epidote and chlorite filled fractures are frequent as well as occasional calcite filled fractures. Dominant fracture orientations are: 04/75, 072/60, 052/70, 070/87, 115/85, 190/80, 090/62.

The spatial arrangement of Riedel type fractures in both the hanging wall and footwall suggests normal kinematics, with the hanging wall moving down to the north. However, the absence of clear slickenlines or stretching lineations prevents the exact

extension direction to be established. Some of the Riedel shears are themselves decorated by mm-thick ultracataclastic injections.

The central section of ZSMEW007A is interpreted to be intercepted by drillhole KLX09 at around 700m BH length though this intercept is of lower confidence due to the depth and distance from the surface lineament. The drillcore from the interpreted zone intersection in KLX09A was inspected in detail to further characterize the zone the deformation in this drillhole /Viola and Ganerod, 2006/.

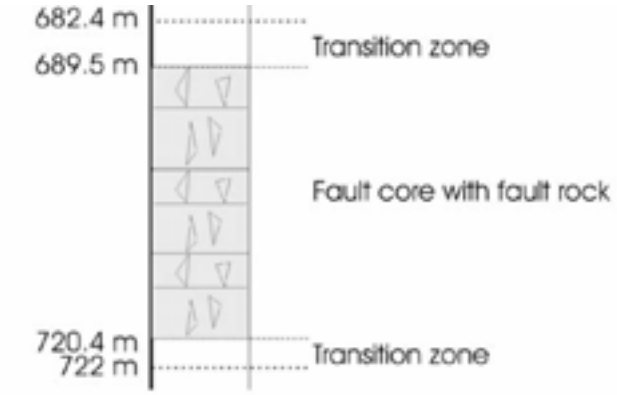

Depth (m)	Box number	Interpretation	Description
682.37	105	Transition zone	Increasing deformation and alternation in bedrock plus pervasive red staining. Fracture frequency up to 5-8 f/m. Bands of ultracataclasites/gouge arranged in networks. The total thickness of the zone is 39.6 m.
689.50	107	Fault core	Complex fault core with abundant fault rock occurrences and crush zones. 2 highly deformed zones 1) ~20 cm at ~690 m with distinct red gouge at the center. Sample KLX 09-1; 2) ~25 cm at 720.20 m with distinct red gouge (possibly non-cohesive) and green ultracataclasite. Sample KLX 09-2.
720.40	113	Transition zone	"Thin" transition zone with red staining and alternation in bedrock lithology.
721-722	113	Transition zone	Decreasing fracture frequency. Changes in lithology. Some ductile fabric. Occurrence of undeformed rock.

Interpretative log of DZ 4 in KLX 09.

The deformation zone begins with a c. 7 m thick upper transition zone defined by red staining and sporadic occurrences of bands of ultracataclasite/gouge arranged in sealed networks.

*Example of a striated plane at depth 701.676 m. Chlorite, calcite and clay minerals coat the surface. Slickensides indicate that the hanging wall to this plane moved up parallel to the striation*s. /Viola and Ganerod, 2006/

Deformation intensity increases significantly towards the core, the upper boundary of which is at 689.50 m. The core contains bands of green, brown and red ultracataclasite/gouge; indurated breccia cemented by calcite.

Cemented breccia derived from protocataclastic granites.

The core is followed by a c. 2 m thick transition zone starting at depth 720.40 m. The zone is characterized by diffuse red staining and by the progressive decrease of the fracture frequency.

A detailed kinematic analysis was performed /Viola and Ganerod, 2006/. The results are shown below. A rather complex kinematic picture emerges from the analysis of the dataset, whereby there is clear indication of sets of both compressional and extensional faults. Given the relatively large number of fault planes, a preliminary kinematic analysis was run. The analysis (strain inversion) of these meso-scale faults was carried out using so-called "paleostress analysis" techniques. The results indicate that the measured fault surfaces can be assigned to two discrete faulting events, although no indication is provided as to their relative timing. A sub horizontal compression oriented roughly NS would account for the reverse faults measured in the core that strike from W-E to N-S and display systematically top-to-S, SE reverse faulting. The extensional faults that strike from NW-SE to NS may instead have formed in response to a SW-NE-oriented extensional phase. It is the NW-SE geometry with its associated extensional tectonics that appear to mirror the western section of ZSMEW007A.

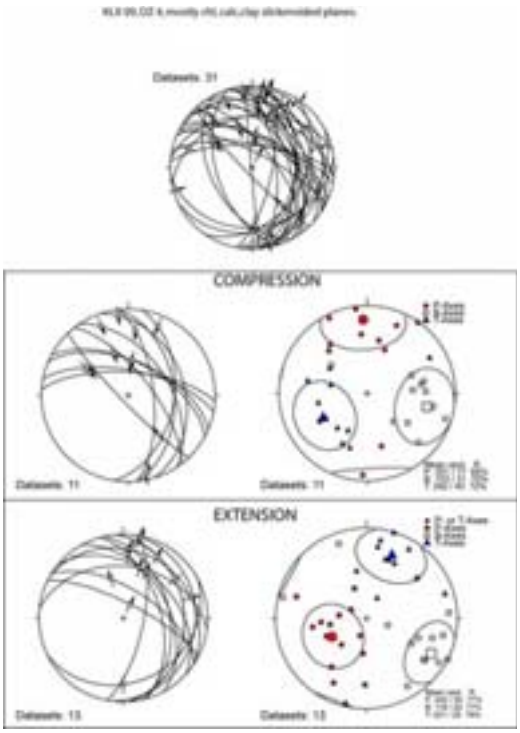

Observations and kinematic analyses for the DZ

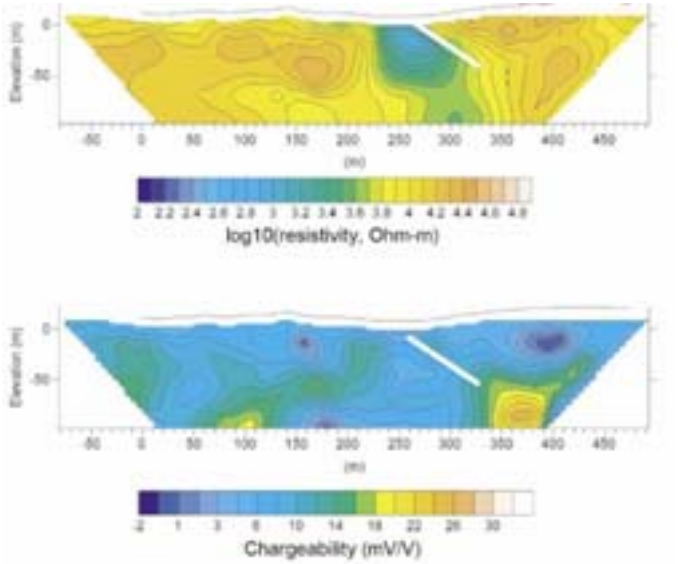

Inverted resistivity (top) and chargeability (bottom) sections for the central profile of group 6 (LSM000281). The northern leading edge of the major resistivity low is taken to support a northerly 35 to 45 degree dip for ZSMEW007A. This position and orientation corresponds to seismic reflector A /Juhlin, 2004/.

The eastern, W-E section of ZSMEW007A was further investigated by the Group 6 profiles. The northern leading edge of the major resistivity low is taken to support a northerly 35 to 45 degree dip for ZSMEW007A. This position and orientation corresponds to seismic reflector A with the orientation 275/43 /Juhlin, 2004/.

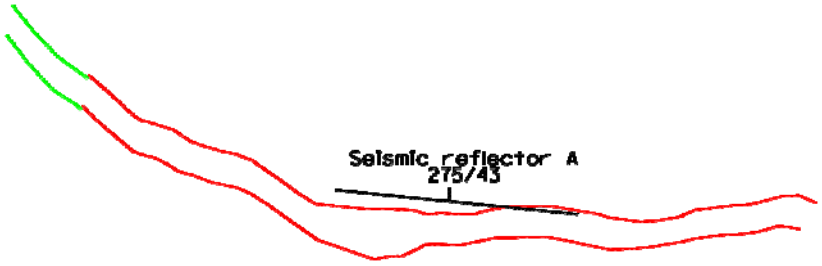

Along profile LSM000281 a seismic refraction survey identified single central low velocity zone has a width of approx 8m and seismic velocity of 2500 ms compared with 5000+ ms in the host rock /Lindqvist, 2004/.

E-W striking deformation zones ZSMEW007A	
Modelling procedure: At the surface, corresponds to the low magnetic and topographic lineament belt. Modelled using dip that has been inferred from a seismic reflector /Juhlin et al. 2002 and 2004a/ and BHs. Included in the regional model and also present inside local model volume.	
Confidence of existence: High	

Property	Quantitative estimate	Span	Confidence level	Basis for interpretation	Comments
Position		± 20 m (surface)	High	Lineament, BH and geophysical ground survey	
Orientation (strike/dip)	281/44	± 20/± 10	High for strike, medium for dip	Strike based on trend of lineament. Dip based on seismic reflector, and boreholes	
Thickness	80 m	20-80 m	High	Lineament, BH and geophysical ground survey	Complex zone, inferred thickness refers to total zone thickness (splays, ductile and brittle, transition zones and core)
core	10m	± 5	Medium	'core' of more highly fractured rock based on general ref: geophysical profiling -refraction (P-04-134) seismic velocity 2500-3200 m/s	Likely to be far more complex with multiple cores. Trench shows clay banding and 60cm thick clay core.
Length (regional model)	3.3 km	+/-200 m	Medium	Linked lineaments	
Ductile deformation	No		High	BHs	Absent
Brittle deformation	Yes		High	Characteristic red-green gouge. Cataclasites, ultracataclasites, breccia and crush zones in BHs and trench mapping.	Present
Alteration			High	BHs and field mapping.	Dominated by red staining, but also sections of epidotization and saussuritization,

E-W striking deformation zones ZSMEW007A					
Fracture orientation	Hanging wall: 314/42, 331/25, 305/58, 100/78, 198/58, 228/66, 320/30, 236/50, 276/46, 285/60, 350/64, 290/54 Core: 300-310/42-44 Core fractures: 310/42, 250/62, 220/58, 330/70, 202/70, 140/80 Footwall: 04/75, 072/60, 052/70, 070/87, 115/85, 190/80, 090/62.		Medium	Trench mapping KLX07	
Fracture frequency* Open/sealed m^{-1}	10/30		Medium	KLX07, KLX08	
Crush zone Number/total m	6/5	±3/ ±2	Medium	KLX07, KLX08	
Fracture filling			High	KLX07, KLX08	Clay, chlorite, hematite, calcite, pyrite, epidote, laumontite, adularia, quartz
Kinematics					

Summary fracture orientation data for cored drill holes penetrating ZSMEW007A.

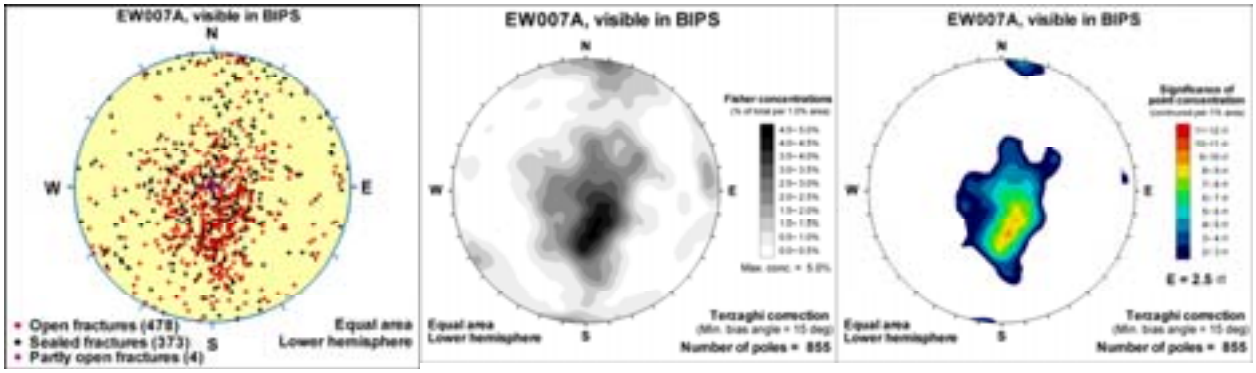

*Fractures are plotted as : stereoplot (open/sealed), Contoured fisher concentrations, and Kamb-contour of cluster significance (provided E>1.0*s, or approximately n>70)*

BH	Geometrical Intercept (bh. m)	Target intercept (bh. m)	Comment
HLX10	18,1-85 (base)	-	No data
HLX11	0-70,0 (base)	-	No data
HLX13	20,2-102,7	29-103	Eshi DZ1 75-108m: Characterized by increased fracturing in dolerite. The pattern of alteration and fractures above the intrusion conform to the general ZSMEW007A character though no dramatic indicators are identified. The hole is dominated by the presence of the dolerite. However, the entire BH is within rock with medium intense red staining.
HLX14	44,1-115,9	-	No data
HLX21	18,0-97,6	18-95	Eshi DZ1 18-24: Low resistivity, low p-wave velocity, low density, low susceptibility and caliper anomaly. 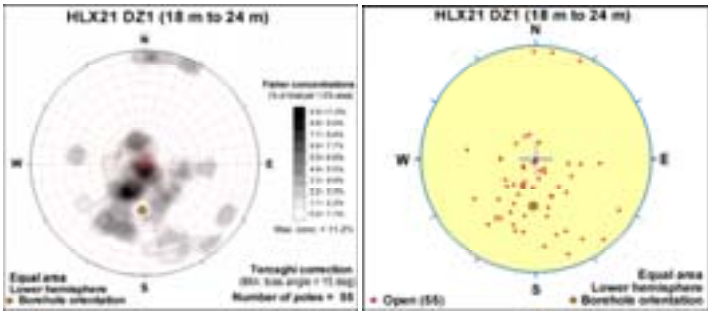 However, the majority of the hole has red staining with medium intensity between 40m and 90m. The thickness of the deformation zone is on the same scale as the borehole.
HLX22	0-163,2	0-163	Eshi DZ1 116-119m. However, the majority of the hole has red staining with medium to strong intensity from 110m to 160m (base). Geometrical intercept 0 to base (163m) The thickness of the deformation zone is on the same scale as the borehole i.e. drilling starts and ends in more or less altered and fractured rocks. However, the alteration pattern gives a general impression of drilling into a north dipping zone.
HLX23	1,1-80,5	0-80	Eshi DZ1 47-54m; DZ2 62-67m; DZ3 77-82m. However, red staining including medium to strong intensity from 0m to 85m. Geometrical intercept 0 to 80m. The thickness of the deformation zone is on the same scale as the borehole i.e. drilling starts and ends in more or less altered and fractured rocks. However, the alteration pattern gives a general impression of drilling into a north dipping zone
HLX24	0,7-119,0	0-150	Eshi DZ1 27-40m; DZ2 58-64m, DZ3 137-145m. However, red staining including medium intensity from 0m to 150m. Geometrical intercept 0-170m. The thickness of the deformation zone is on the same scale as the borehole i.e. drilling starts in more or less altered and fractured rocks. However, the alteration pattern gives a general impression of drilling sub parallel into a north dipping zone.
HLX25	7,1-57,35	0-80	Red staining including medium intensity from 0-80m. The alteration pattern gives a general impression of drilling sub parallel into a north dipping zone with the hole starting within the zone and exiting the southern boundary towards its base.

BH	Geometrical Intercept (bh. m)	Target intercept (bh. m)	Comment
HLX30	0-73,6	0-80	Eshi DZ1 10-42m Brittle deformation zone characterized by increased frequency of open fractures and weak red staining. Significantly decreased resistivity and magnetic susceptibility; DZ2 60-68m Brittle deformation zone characterized by increased frequency of open fractures, crush at c. 62 m and medium red staining. High frequency of negative resistivity anomalies and decreased bulk magnetic susceptibility; DZ3 85,5-88m Brittle deformation zone characterized by increased frequency of open fractures and weak red staining. Significantly decreased resistivity and magnetic susceptibility. Red staining including medium intensity from 0-80m. The overall pattern of alteration conforms to a hole drilled sub parallel with a northerly dipping zone.
HLX31	35,8-116,4	50-100	Eshi DZ1 60-67m Brittle deformation zone characterized by increased frequency of open fractures and medium red staining. Significantly decreased resistivity and magnetic susceptibility and several caliper anomalies; DZ2 96-98,5m Brittle deformation zone characterized by increased frequency of open fractures, crush at c. 97 m and weak red staining. Significantly decreased resistivity and magnetic susceptibility and several caliper anomalies. However, the entire hole has red staining with medium intensity between 55-68m and raised fracture frequency.
HLX33	0,5-40,1	0-70	Eshi DZ1 12-28 m Brittle deformation zone characterized by increased frequency of open fractures, crush at c. 23 m and weak to medium red staining. Significantly decreased resistivity and magnetic susceptibility. Low radar amplitude occurs in the interval 10-30 m, which is partly above and below the deformation zone. Red staining including medium intensity from 0-70m
HLX35	142,5-151,8 (base)	-	The BH has marginal geometrical intercepts with both ZSMEW007A and ZSMEW007C though evidence of deformation is judged to be dominated by ZSMNS059A.
KLX01	965,7-1078 (base)	1000-1020	Oxidation, high fracture frequency, narrow sections with crushed rock, several chlorite or calcite sealed fractures. Relatively little relevant information is available from this BH. No BIPS and no associated oriented fracture data.
KLX02	173,8-308,1	180-200	No drill core available /base of casing. No core available at this depth-casing to 200m. Hydrological testing around the level of the bottom of the casing weakly supports this interception.
KLX04	307,1-427,1	310-385	Eshi DZ5 346-355 m Brittle deformation with brecciation (sealed network). Low resistivity, variable p-wave velocity, very low susceptibility and small caliper anomaly. 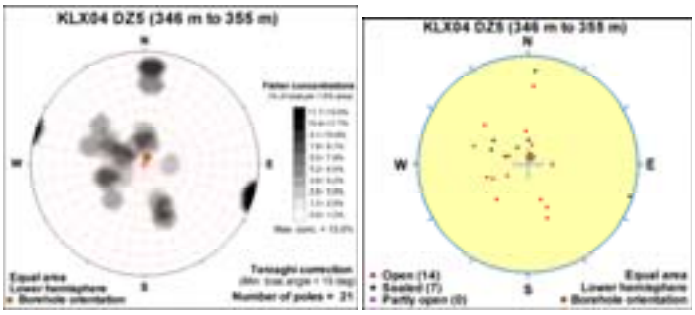

BH	Geometrical Intercept (bh. m)	Target intercept (bh. m)	Comment
KLX07A	96,1-179,3	105-147	Eshi DZ1 105-147 m Inhomogeneous deformation zone characterized by high frequency of sealed and open fractures with chlorite, epidote and iron hydroxide. Alteration mainly comprises red staining and subordinate sections of epidotization and saussuritization. The section 114.75-117.86 m is characterized by crush and core loss, and also by significant caliper anomalies and low p-wave velocity. The entire DZ1 is characterized by a general decrease in the bulk resistivity and magnetic susceptibility, and there are also numerous p-wave velocity anomalies. 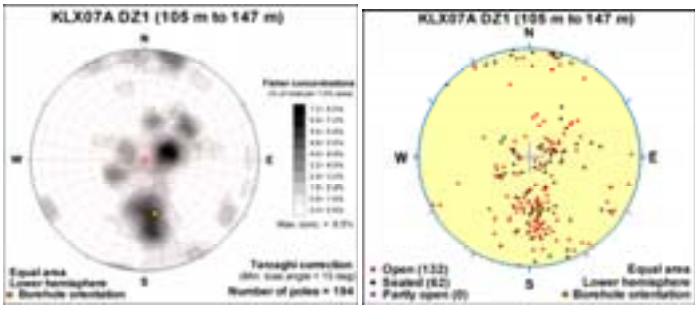 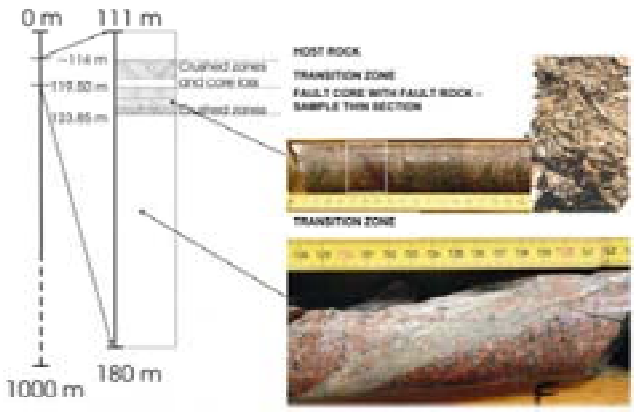 DZ2 167,9-168,3 m Minor deformation zone characterized by cataclasite with calcite, epidote and clay. Geophysical loggings indicate decreased resistivity, decreased p-wave velocity and positive caliper anomalies.
KLX07B	113,16-200,13	124-172	Eshi DZ3 124-172 m Characterized by increased frequency of sealed network and increased frequency of sealed fractures, and by increased frequency of open fractures between 128 and 155 m. Crush at 130.15-130.17 m, 130.89-131.66 m and 132.78-132.87 m. The section is characterized by a general decrease in the bulk resistivity. At ca 129-131 m there is a major decrease in the p-wave velocity and in the resistivity.

BH	Geometrical Intercept (bh. m)	Target intercept (bh. m)	Comment
			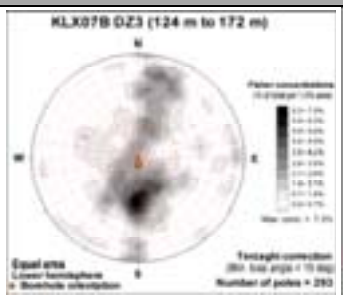 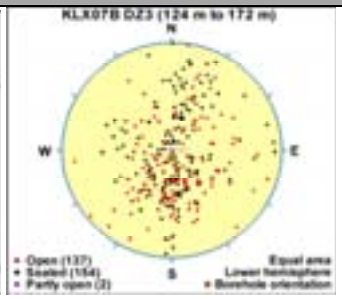 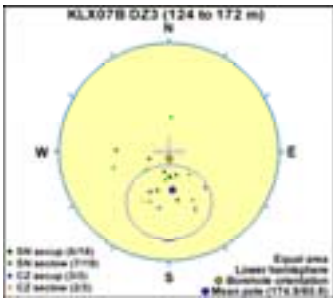 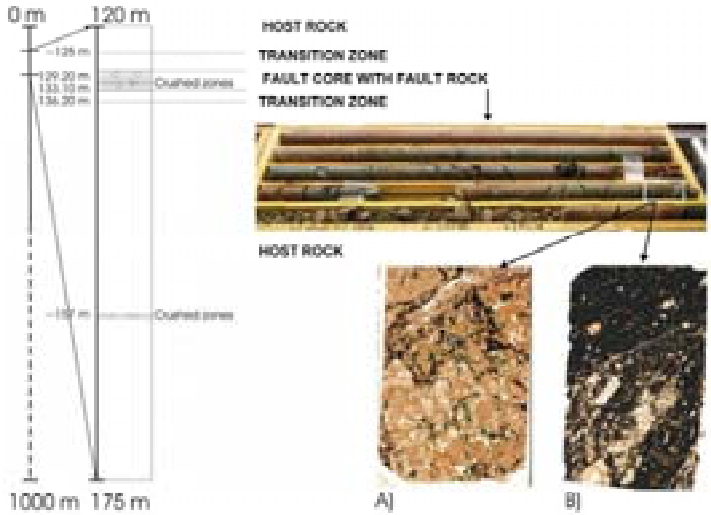 Fault rocks are protocataclasites, cataclasites and ultracataclasites. Thin sections show A) cataclasites with angular granite fragments and some fine-grained matrix (black) and abundant epidote, and B) ultracataclasites/gouge (black) with fragments of cataclasite. The gouge has very sharp contacts to the ultracataclastic bands surrounding it. Cataclastic bands dip at shallow to moderate angle to the NNE-NE, and gouge occurrences are concordant (black and red great circles. Two slickensided fault surfaces, also with moderate dip in the same direction, constrain a top-to-NNE extension episode. 
KLX08	220,1-301,4	211-300	Eshi DZ3 211,5-220 m Inhomogeneous brittle deformation zone characterized by faint to weak red staining and increased frequency of

BH	Geometrical Intercept (bh. m)	Target intercept (bh. m)	Comment
			sealed and open fractures. Crush zones at 215.79-215.91, 218.29-219.15 m. Geophysical loggings indicate general decrease in bulk resistivity and magnetic susceptibility. The section 217-220 m is characterized by distinct low resistivity and caliper anomaly. 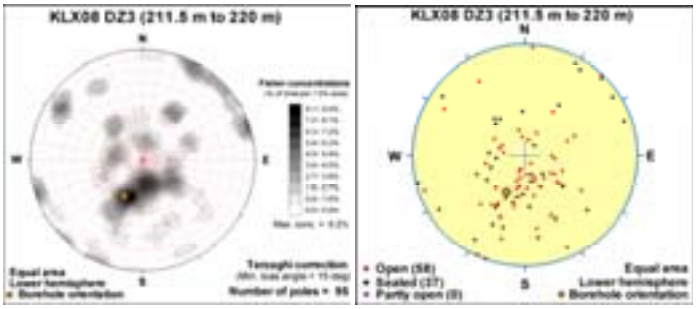 Eshi DZ4 224,5-242 m Section characterized by high frequency of sealed fractures. Scattered cm-wide cataclasites. Weak to medium red staining and weak to medium saussuritization (229.5-233 m). Geophysical loggings indicate general decrease in bulk resistivity and magnetic susceptibility. 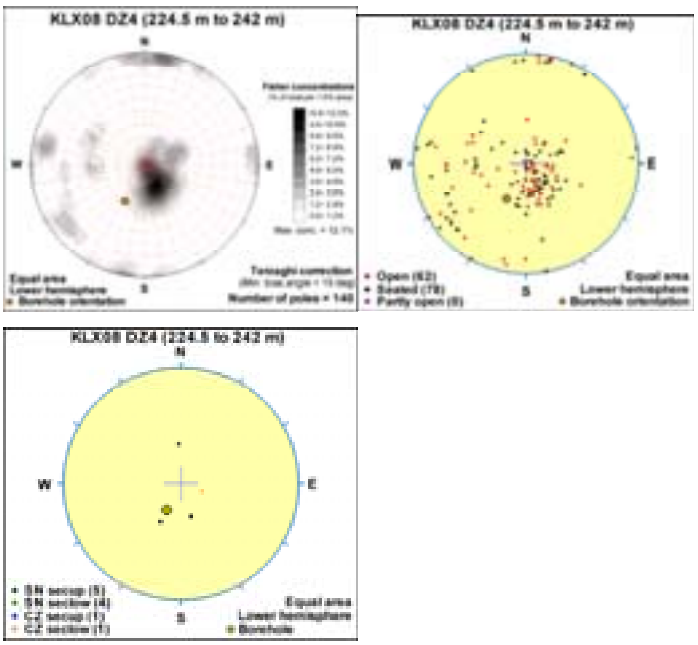 Eshi DZ5 291-302 m Section characterized by crush zones at 291.53-291.56, 291.73-292.47, 296.66-296.95, 297.36-297.45 and 300.69-301.26 m. Weak red staining. Decreased radar amplitude between 290-300 m. Geophysical loggings indicate general decrease in bulk resistivity, magnetic susceptibility and low p-wave velocity including several caliper anomalies along the entire section.

BH	Geometrical Intercept (bh. m)	Target intercept (bh. m)	Comment
KLX09	662,7-770,8	682-722	Eshi DZ13 682-722 m High frequency of sealed fractures and increased frequency of open fractures and sealed network. Crush rock in the sections 692.84-692.89 m, 700.53-700.82 m, 710.80-712.37 m and 720.20-720.30 m. Some fractures with large apertures. The section is characterized by intense red staining and increased distribution of cataclastic bands. Low P-wave velocity, low resistivity and low magnetic susceptibility. 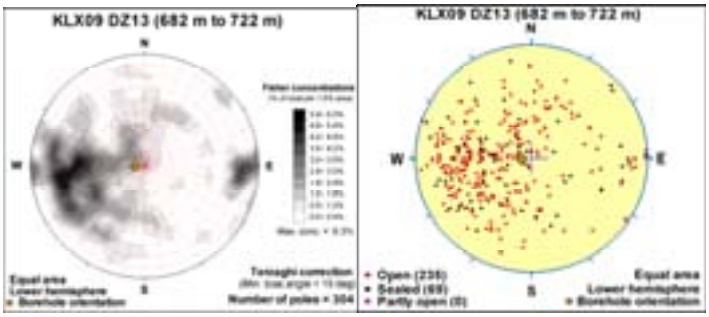 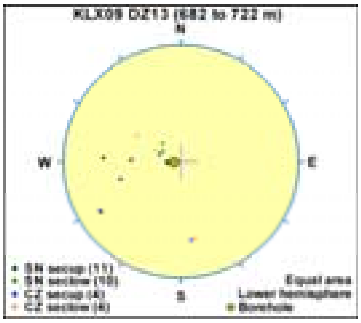 (N-S fracture set – influence from ZSMNS046A)

ZSMEW007A drill log extracts (zone only)

ZSMEW007A (zone only) KLX07A

ZSMEW007A (zone only) KLX07B

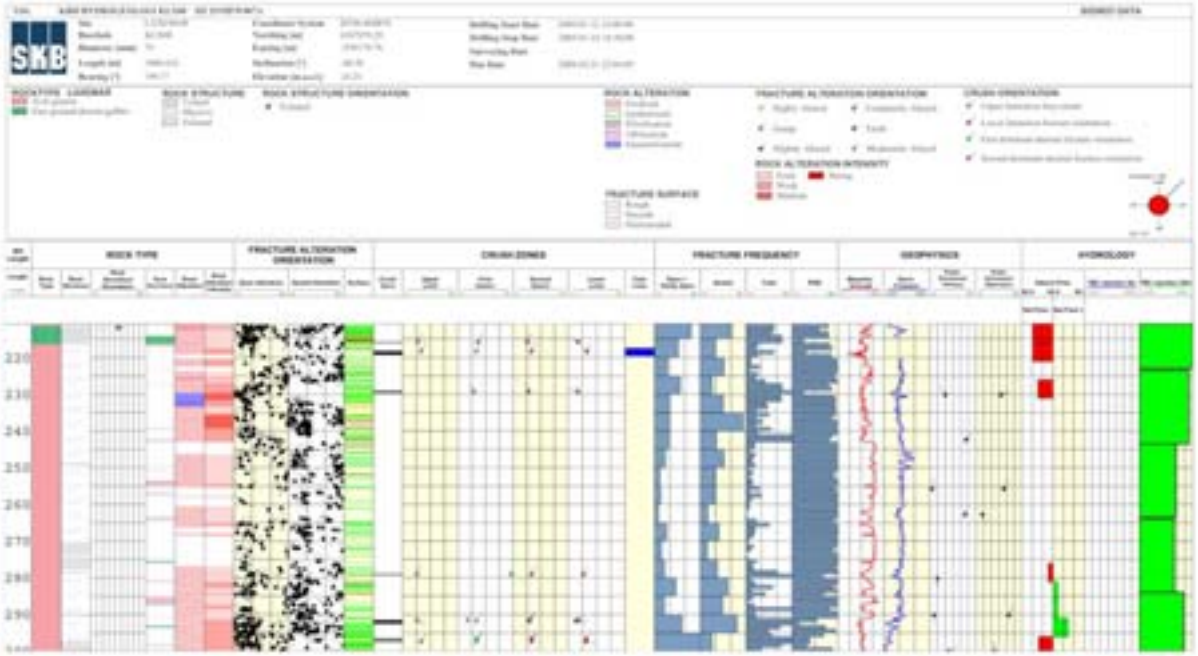

ZSMEW007A (zone only) KLX08

ZSMEW007A (zone only) KLX09A

ZSMEW007A (zone only) KLX04

ZSMEW007A (zone only) drill core photos KLX07A

Other structures associated with the ZSMEW007A lineament

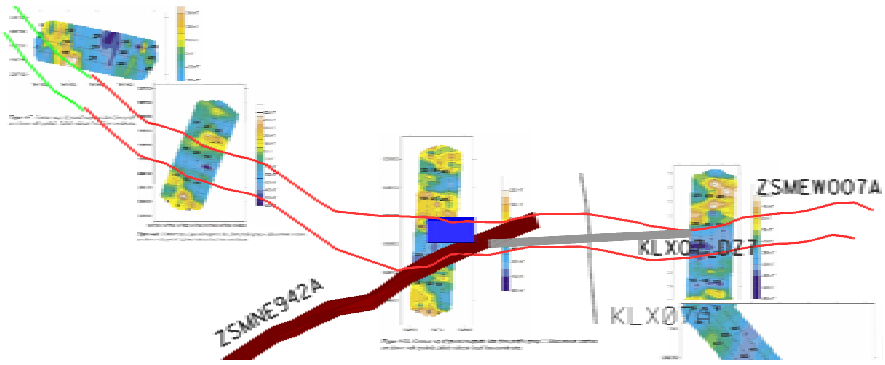

ZSMEW007A (red), KLX07_DZ7 (grey) and a sub vertical low magnetic anomaly (blue)

As previously discussed the surface expression of what has been termed ZSMEW007A is clearly complex and results from the interference of a number of structures with very different orientations. Smaller structures daylighting in this 'belt' have sub vertical and southerly dips as suggested by local drilling evidence and geophysical profiling though the main structure (ZSMEW007A) is interpreted as dipping moderately to the north. An example of this is shown above. The grey block shown in the figure represents a deformation zone identified in the Eshi of KLX07A that has been modelled with a thickness of 30m and an orientation of 267/90 based on BH radar, fracture orientations in the drill core and correlation with a sub vertical low magnetic anomaly from forward modelling /Thunehed et al, 2005/. In addition the picture is further complicated by the interception of another more NE-SW trending sub vertical deformation zone ZSMNE942A.

KLX07_DZ9

E-W striking deformation zones KLX07_DZ9	
KLX07_DZ9's orientation is based on seismic reflector 'D' /Juhlin, 2004/, generally supported by mylonite ca. 250/50; crush 270/45 and fracture orientation concentration. Towards the edge of the modelled geometry there is a theoretical intercept with KLX02 but no evidence of likely correlation.	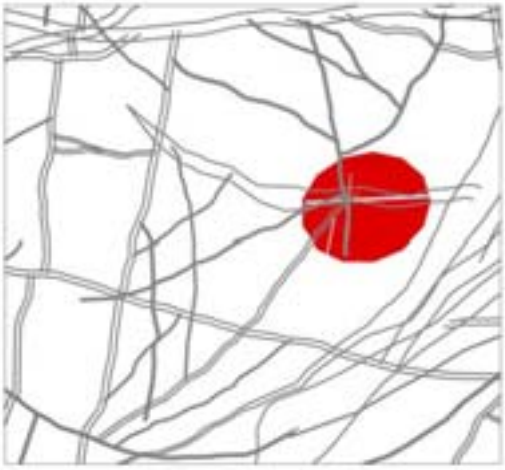
Confidence of existence: High	

Property	Quantitative estimate	Span	Confidence level	Basis for interpretation	Comments
Position			High	Eshi	
Orientation (strike/dip)	253/35		Low	Seismic reflector 'D' /Juhlin, 2004/ generally supported by mylonite ca. 250/50; crush 270/45 and fracture orientation concentration	
Thickness	10 m		Low		
Length (regional model)	1.0 km		Low	Assumed	
Ductile deformation	Yes		Low	Ductile fabric	
Brittle deformation	Yes		High	Raised fracture frequency and cataclasis	
Alteration			High		Red staining
Fracture frequency* Open/sealed m^{-1}	14/30		Low		
Crush zone Number/total m	2/2		Low		
Fracture filling			High		Calcite, chlorite, clay, epidote, pyrite, andularia, quartz

BH	Geometrical Intercept (bh. m)	Target intercept (bh. m)	Comment
KLX07A	448-459	448-459	Eshi DZ9 448-459: Increased frequency of open and sealed fractures. The section 453.8-454.40 m is intensely foliated (protomylonitic) including sections of cataclasite. Four radar reflectors, one of them oriented. The orientation is 44/210 at 455.9 m. At c. 453 m there are distinct coincident anomalies in the resistivity, p-wave velocity and caliper logs. 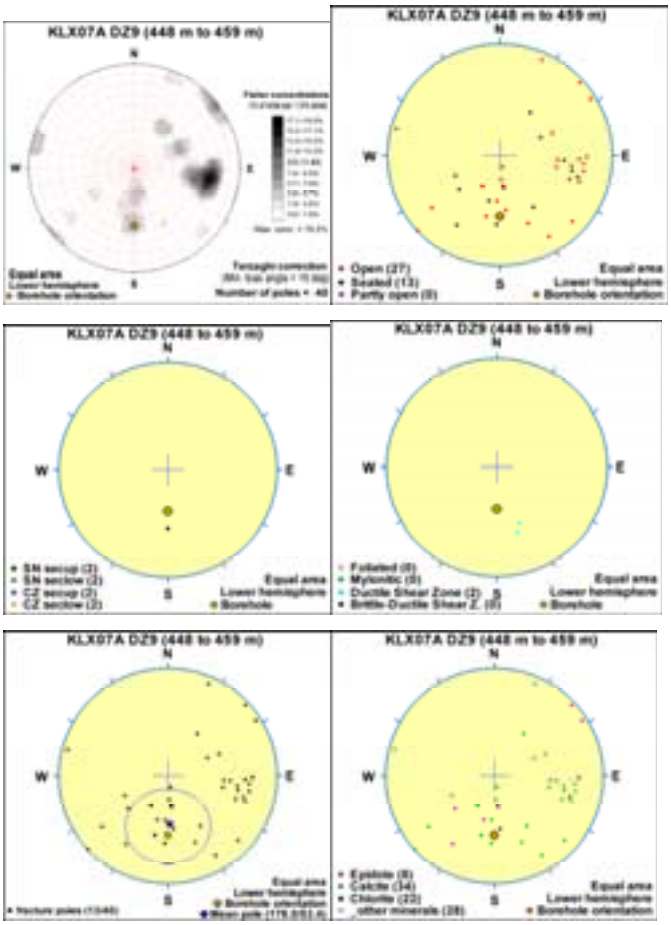

KLX07_DZ11

E-W striking deformation zones KLX07_DZ11	
KLX07_DZ11's position in the borehole coincides with the theoretical intercept with seismic reflector 'G' /Juhlin, 2004/ and has general agreement with crush orientations. At the edge of the modelled geometry a theoretical intercept occurs in KLX21B. No correlation is possible with KLX21B which superficially confirms the approximate southerly extent of the zone. The geometry of seismic reflector 'G' narrows sharply to the north. At its western edge the reflector intercepts KLX02 at a depth of 907m. While this coincides with a very complex Eshi DZ position no clear correlation with this hole is possible and the modelled northerly extent is low confidence.	

Confidence of existence: High

Property	Quantitative estimate	Span	Confidence level	Basis for interpretation	Comments
Position			High	Eshi	
Orientation (strike/dip)	253/35		Low	Seismic reflector /Juhlin, 2004/	
Thickness	30 m		Low		
Length (regional model)	1.0 km		Low	Assumed	
Ductile deformation	No		Low		
Brittle deformation	Yes		High	Raised fracture frequency and cataclasis	
Alteration			High		Red staining, epidotization
Fracture frequency* Open/sealed m^{-1}	10/66		Low		
Crush zone Number/total m	2/<0.25		Low		
Fracture filling			High		Calcite, chlorite, hematite, quartz, epidote, clay, andularia, pyrite, prehnitr

BH	Geometrical Intercept (bh. m)	Target intercept (bh. m)	Comment
KLX07A	693-723	693-724	Eshi DZ11 693-724 m: Increased red staining and frequency of open and sealed fractures. Scattered sections of chlorite and epidote sealed cataclasite. Four non-oriented and five oriented radar reflectors are identified. The oriented reflectors occur at 697.0 m with orientation 43/154, at 697.6 m with orientation 42/145, at 707.8 m with orientation 61/230, at 713.9 m with orientation 76/228, and at 717.3 m with orientation 78/269. Decreased radar amplitude in the interval 690-700 m, i.e. it starts outside DZ11. The geophysical logs indicate two subsections 694-699 m and 709-717 m with low resistivity and decreased p-wave velocity. There is a large decrease in the magnetic susceptibility along the major part of the section of DZ11. 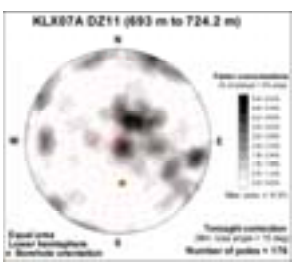 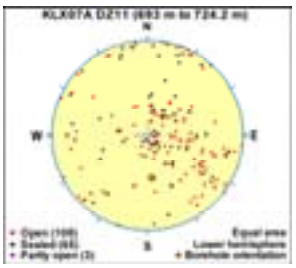

KLX07_DZ12

E-W striking deformation zones KLX07_DZ12	
KLX07_DZ12's orientation is based on a combination of crush and fracture orientation concentrations. The modelled extent generates an intercept towards the edge of modelled geometry with KLX21B. However, only two very thin MDZs occur at this level and neither supports a likely correlation.	
Confidence of existence: High	

Property	Quantitative estimate	Span	Confidence level	Basis for interpretation	Comments
Position			High	Eshi	
Orientation (strike/dip)	263/41		Low	Multiple crush orientations and pole concentration	Support- very generally follows the trends of both seismic reflectors D and G (253/35)
Thickness	47 m		Low		
Length (regional model)	1.0 km		Low	Assumed	
Ductile deformation	No		Low		
Brittle deformation	Yes		High	Raised fracture frequency and cataclasis	
Alteration			High		Red staining, epidotization
Fracture frequency* Open/sealed m^{-1}	12/28		Low		
Crush zone Number/total m	7/1		Low		
Fracture filling			High		Calcite, chlorite, hematite, quartz, epidote, clay, andularia, pyrite, prehnite

BH	Geometrical Intercept (bh. m)	Target intercept (bh. m)	Comment
KLX07A	738-785	738-785	Eshi DZ12 738-785 m: Oxidized section and increased frequency of sealed fractures. Scattered sections of chlorite and epidote sealed cataclasite. Oriented reflectors occur at 747.8 m with orientation 87/264, at 751.2 m with orientation 84/092, at 753.7 m with orientation 43/005, at 758.9 m with orientation 79/085, at 772.2 m with orientation 05/300, and at 782.9 m with orientation 14/121. Decreased radar amplitude at 745 m, at the section 755-765 m and at 785 m. There is a general decrease in the magnetic susceptibility in the section 740-760 m. The entire DZ12 is characterized by numerous low resistivity and low p-wave velocity anomalies, and a few caliper anomalies. 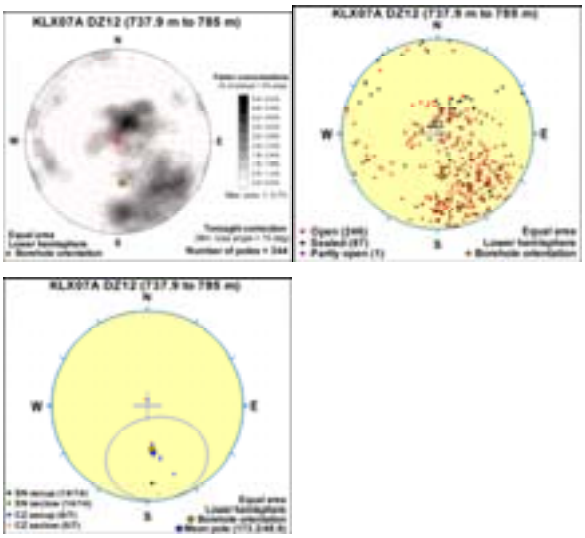

KLX09_DZ10

E-W striking deformation zones KLX09_DZ10	
KLX09_DZ10's is based on radar that is sub parallel to ZSMEW007A and partially supported by crush orientations.	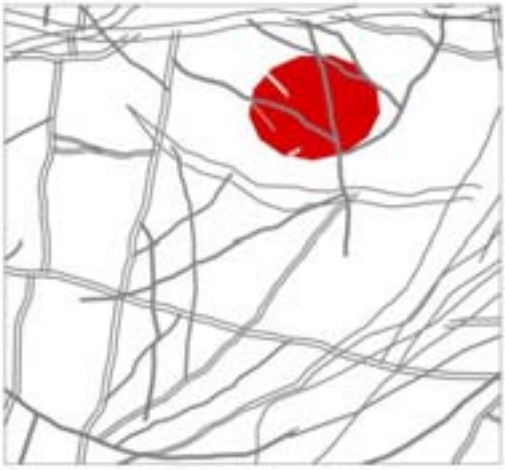
Confidence of existence: High	

Property	Quantitative estimate	Span	Confidence level	Basis for interpretation	Comments
Position			High	Eshi	
Orientation (strike/dip)	263/37		Low	Radar, some crush	Radar, sub parallel to ZSMEW007A similar character (characteristic red-green gouge)
Thickness	25 m		Low		
Length (regional model)	1.0 km		Low	Assumed	
Ductile deformation	No		Low		
Brittle deformation	Yes		High	Raised fracture frequency, cataclasis	
Alteration			High		Red staining, epidotization, saussuritzation
Fracture frequency* Open/sealed m^{-1}	16/39		Low		
Crush zone Number/total m	15/1.5		Low		
Fracture filling			High		Calcite, chlorite, clay, hematite, epidote, pyrite

BH	Geometrical Intercept (bh. m)	Target intercept (bh. m)	Comment
KLX09A	521-553	520-554	Eshi DZ10 520-554 m: High frequency of sealed and open fractures and sealed network. Several sections with crush rock in the interval. Several fractures with large apertures. Core loss in the interval 538.59-539.14 m and 540.69-540.78 m due to drill technical reason. The section is characterized by intense red staining. Low P-wave velocity, low resistivity, caliper anomaly and low magnetic susceptibility. Two relatively strong oriented radar reflectors occur at 530.3 m with the orientation 302/30 or 096/25 and at 541.6 m with the orientation 066/42 or 263/37. 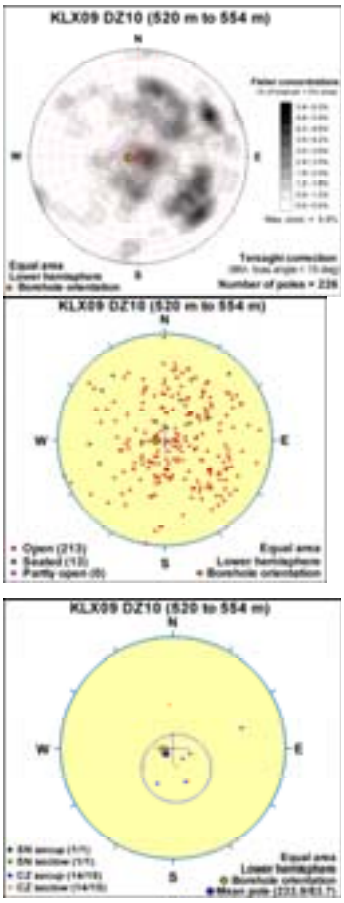 Ref /Viola et al, 2006/. There are three discrete sub-zones: (1) A sub-zone characterized by an increase in fault rock occurrence such as protocataclasite and/or cataclasite and networks of thin ultracataclasite/gouge bands. (2) A 20 cm thick sub-zone between 527.50 and 527.70 m containing a sequence of ultracataclasite, gouge, cataclasite and ultracataclasite, and in addition a crush zone in the "center of the sub-zone", and finally (3) a complex variety of fault rock occurrences and crush zones.

KLX10C_DZ3

NW-SE striking deformation zones KLX10C_DZ3	
KLX10C_DZ3's orientation is based on ductile-brittle zones mapped in the drill core. The modelled geometry generates theoretical intercepts in KLX10, KLX10B, HLX31 and HLX33. KLX10 and KLX10B were not cored at this position. HLX31 and HLX33 lack clear correlation but it should be noted both holes lie in the complex ZSMEW007A belt.	

Confidence of existence: High

Property	Quantitative estimate	Span	Confidence level	Basis for interpretation	Comments
Position			High	Eshi	
Orientation (strike/dip)	300/35		Low	Ductile-brittle zones mapped in drill core	
Thickness	10 m		Low		
Length (regional model)	1.0 km		Low	Assumed	
Ductile deformation	Yes		High	Mapped ductile-brittle indicators in drill core	
Brittle deformation	Yes		High	Raised fracture frequency mapped ductile-brittle indicators in drill core	
Alteration			High		Red staining, epidotization, saussuritization.
Fracture frequency* Open/sealed m^{-1}	5/29		Low		
Crush zone Number/total m	0/0		Low		
Fracture filling					Calcite, chlorite, hematite, epidote, andularia, laumontite, clay, pyrite, prehnite

BH	Geometrical Intercept (bh. m)	Target intercept (bh. m)	Comment
KLX10C	36-58	35-59	Eshi DZ3 35-59 m: Inhomogeneous deformation zone. Characterized by increased alteration (red staining) and increased frequency of sealed network, and partly also open fractures. Partly decreased magnetic susceptibility along the entire section. Decreased P-wave velocity and low resistivity anomalies in the section 42-47 m. 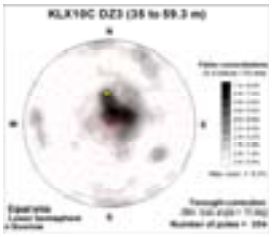 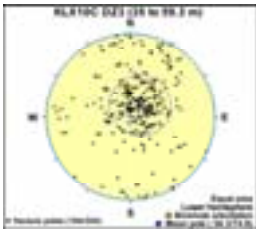 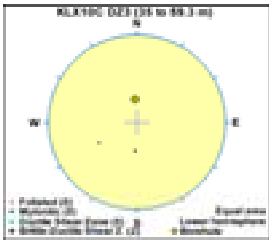

KLX10C_DZ7

NW-SE striking deformation zones KLX10C_DZ7	
KLX10C_DZ7's orientation is based on mapped brittle- ductile indicators in the drill core. The modelled geometry results in theoretical intercepts in KLX10 and HLX31. KLX10 is not cored in this position. No clear correlation with HLX31 has been identified. However, the HLX31 intercept is towards the edge of the modelled zone geometry and this hole lies within the complex ZSMEW007A zone belt.	
Confidence of existence: High	

Property	Quantitative estimate	Span	Confidence level	Basis for interpretation	Comments
Position			High	Eshi	
Orientation (strike/dip)	323/39		Low	Mapped brittle-ductile shear zone in drill core.	
Thickness	10 m		Low		
Length (regional model)	1.0 km		Low	Assumed	
Ductile deformation	Yes		High	Mapped brittle-ductile shear zone in drill core.	
Brittle deformation	Yes		High	Raised fracture frequency mapped brittle-ductile indicators in drill core	
Alteration			High		Red staining
Fracture frequency* Open/sealed m^{-1}	6/33		Low		
Crush zone Number/total m	0/0		Low		
Fracture filling			High		Chlorite, calcite, laumontite, andularia, epidote, hematite, prehnite

BH	Geometrical Intercept (bh. m)	Target intercept (bh. m)	Comment
KLX10C	119-142	121-140	Eshi DZ7 121-140 m: Increased frequency of sealed fracture and partly open fractures. Partly also medium red staining. Partly decreased magnetic susceptibility in the section 127.7-140.0 m. Only minor negative anomalies in the P-wave velocity and resistivity logging data along the section of the DZ. Two radar reflectors, one at 125.0 m with the orientation 187/32 and one at 134.52 m with the orientation 060/33 or 114/34. 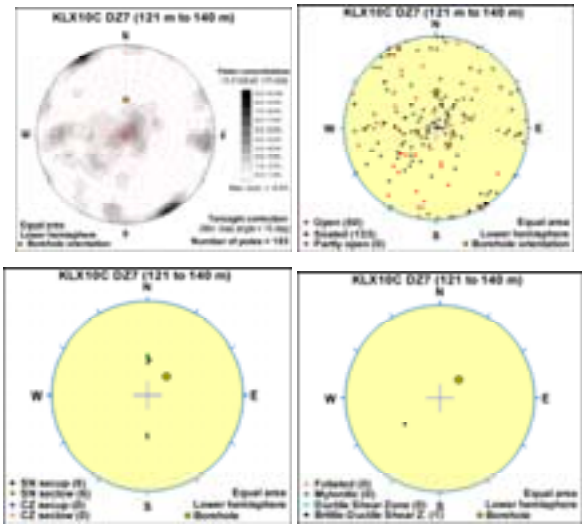

Gently dipping deformation zones

ZSMNW928A

The interpretation of this zone remains essentially unchanged from version 1.2. ZSMNW928A is based on the interpreted deep lying shallow dipping (120/28) seismic reflector N /Juhlin et al. 2004b/ and through possible intercepts with boreholes KLX02, KLX04 and KLX09A. Whilst the reflector is reasonably clear, its exact position in 3D is poorly constrained. The seismic reflector is strongly supported not to extend through the Mederhult zone in the north, which implies no surface intersection. Lateral extent in other directions has been simplistically limited to the nearest high confidence regional or local major deformation zone. A further termination to the northeast has been applied since no evidence exists for the existence of this zone under Äspö, in the vicinity of the underground laboratory. The geometry is assumed to represent a brittle deformation zone with a 'length' of around 2km though it does not intercept the ground surface. The zone's likely thickness is around 20 to 50 m though it's character is judged to be similar to ZSMEW946A (seismic reflector M1) and it is likely that the 'zone' is in fact the upper limit of a thick series (up to 100m) or packet of thin, gently dipping deformation zones that are concentrated at this general depth and generate the reflector. However, the borehole evidence also indicates that mafic intrusion(s) is (are) also involved. In addition a further review of the seismic data has been made and an alternative strike and dip of 075/23 was put forward. On further review the earlier 120/28 orientation has been maintained since it gives a better fit with borehole data though the later reinterpretation exemplifies the uncertainty in the reflector orientation. In consequence the related zone is judged medium confidence and has been modelled without thickness in the deterministic model.

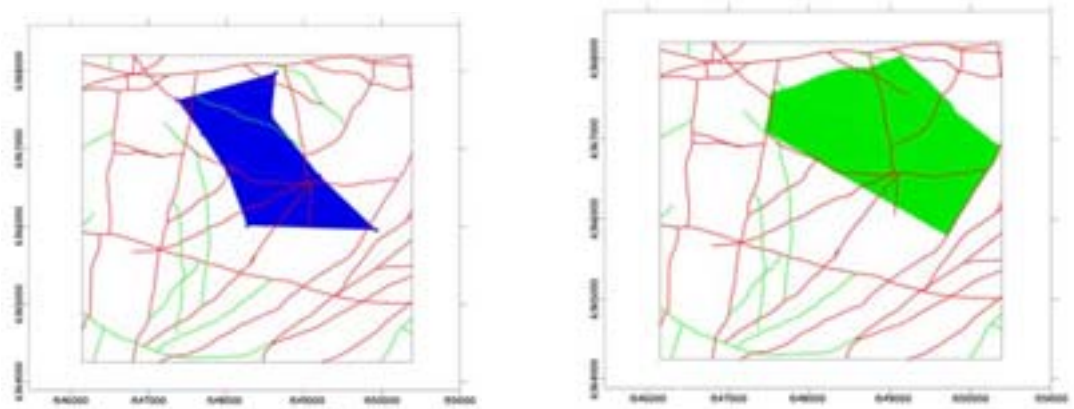

Seismic reflector geometry shown on left, modelled zone geometrywithin the local model volume on the right (both 120/28).

The borehole correlations are dominated by KLX02 and KLX04, two holes which were drilled and logged relatively early in the investigation campaign. Core mapping methodology and interpretation has developed as experience has been gained and the initial single-hole interpretation of these two holes, particularly KLX02 is somewhat simplistic. Both holes identify single potential deformation zones that have borehole intercept thicknesses of around 100-200m. It is considered very likely that such intercepts in fact represent a number of different structures with differing orientations

and origins. This fact has made exact correlation and quantification of the zone's character problematical and leads to most of the parameters being judged to be of low confidence.

The possible intersection point in KLX02 (at 770–960 m) is indicated in the single-hole interpretation as a generally increased frequency of open fractures with increased oxidation. The most intensely fractured part of the zone is located between 845–880 m, which is indicated by distinct low p-wave velocity and partly by a somewhat reduced resistivity. The interpreted possible intersection point in KLX04 (at 873 to 973 m) is indicated in the single-hole interpretation as repetitive sections of crush and sealed networks. Alteration is evident in the upper part of the section. The frequency of open fractures is relatively high, but variable throughout the section with a core zone characterised by strong inhomogeneous brittle deformation. The most intensely deformed part of the zone is found between c. 930 and 973 m. An intensely crushed part, between 936–946 m, correlates well with the seismic reflector N /Juhlin et al. 2004b/ at 940 m. Low resistivity, variable sonic, very low susceptibility and minor caliper anomalies are found in the sections 875–895 m and 935–971 m of KLX04. The interpreted intersection in KLX09 corresponds to Eshi DZ 13 between 682-722m. This section of drillhole is also interpreted as intersecting ZSMEW007A and the resulting fracture geometry and kinematics are complex (see property table below).

NW-SE striking deformation zones ZSMNW928A	
Modelling procedure: The zone position and orientation is based on a seismic reflector geometry, reflector N. Modelled to the base of the regional model and present inside local model volume.	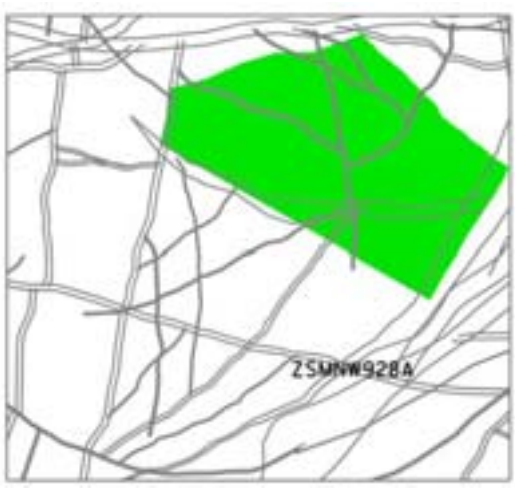
Confidence of existence: Medium	

Property	Quantitative estimate	Span	Confidence level	Basis for interpretation	Comments
Position		± 25 m (surface)	Low	The precise reflector location is poorly constrained.	
Orientation (strike/dip)	120/28	070-130/15-30	Low for strike, medium for dip	Seismic reflector N, /Juhlin, 2004/	
Thickness	10 m	5-100 m	Low	BHs	Judged most likely to consist of a series of thinner gently dipping zones concentrated at this level.
core	1.5 m	1-10	Low	BHs	Judged most likely to consist of a series of thinner gently dipping zones concentrated at this level.
Length (regional model)	1.5 km	1.5-3.0 km	Low	Extent of seismic reflector and simplistic assumptions concerning zone terminations	
Ductile deformation					
Brittle deformation	Yes		Medium	Raised fracture frequency, breccia, crush and gouge. BHs	
Alteration			Low	KLX02, KLX04, KLX09	Oxidation, chloritization, epidotization, saussuritization. Almost certainly does not refer exclusively to this zone.
Fracture orientation	Dominated by sub horizontal to gently dipping	Poorly constrained	High	KLX02, KLX04, KLX09	Zone limits have not been clearly defined. Almost certainly does not refer exclusively to a single zone.

NW-SE striking deformation zones ZSMNW928A					
Fracture frequency Open/sealed m^{-1}	15/30		Low	KLX02, KLX04, KLX09	Almost certainly does not refer exclusively to this zone.
Crush zone Number/total m	6/2		Low	KLX02, KLX04, KLX09	Almost certainly do not refer exclusively to this zone.
Fracture filling			Medium	KLX09	Chlorite, calcite, epidote, hematite, pyrite, quartz, chalcopyrite clay
Kinematics					See table below

BH	Geometrical Intercept (bh. m)	Target intercept (bh. m)	Comment
KLX02	764	Ca. 770	Eshi DZ1 770-960 m: generally increased frequency of open fractures and higher oxidation. The most intensive part of the zone is located between 845–880 m, which is indicated by distinct low p-wave velocity and partly somewhat lower resistivity. Nine radar reflectors from directional antenna have been found within the zone. The orientations of the reflectors are 29–61°/047–086. Most of them are dipping around 50°. Host rock is dominated by a mixture of Ävrö granodiorite (501056) with subordinate sections of Ävrö quartz monzodiorite (501046) and fine-grained dioritoid (501030). Subordinte rock types comprise fine-grained diorite-gabbro (505102) and fine-grained granite (511058). The upper part of this Eshi DZ contains fine grained diorite gabbro intrusions with mapped boundary orientations of 093/07 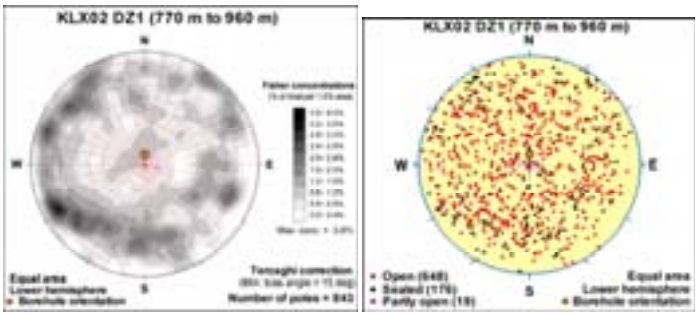
KLX04	899	Ca. 880	Eshi DZ6 873-973 m: Repeated crush and sealed network. Alteration in upper part, but missing in the central part. High frequency of open fractures. Zone core centre with strong inhomogeneous brittle deformation. The most intensely deformed part of the zone is between c. 930 and 973 m. Low resistivity, variable p-wave velocity, very low susceptibility in upper (875 – 895 m) and lower (935 – 971 m) part and minor caliper anomalies. Several radar reflectors occur within the zone. Thirteen are non-oriented and two are oriented. Oriented reflector at 877.5 m with the orientation 25/109 and at 970.7 m with the orientation 20/134. 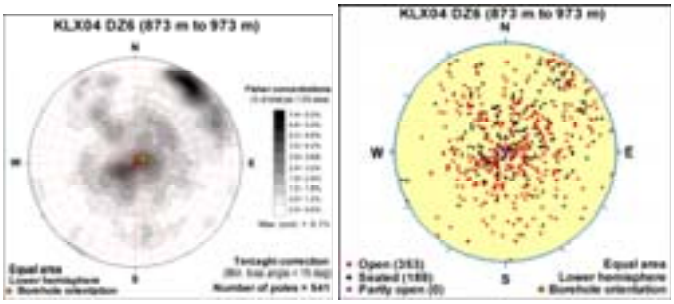 /Viola et al, 2007/ Several fault cores, commonly containing fault rocks, and their respective adjacent damage zones, characterize this section. Damage zones show increased fracture frequency towards the fault cores and occurrences of strands and thin bands of cataclasites and gouge. Red staining is common in the damage zones. Examples of fault rocks in this interval are protocataclasites, cataclasites, ultracataclasites, gouge and cemented breccias. The figure below, from around 875m BH length, shows a brecciated cataclasite, with fragments of cataclasite and ultracataclasite ripped off and cemented by late calcite to form a now cohesive fault rock. The scanned thin section reflects the same sequence, with a primary cataclasite subsequently dilated and crosscut by calcite veins.

BH	Geometrical Intercept (bh. m)	Target intercept (bh. m)	Comment
			 A) 874.70 m  B) 876.30 m *Samples from A) cemented breccia and B) red gouge/ultracataclasite. Scanned thin sections of the samples are shown to the right.* The figure below shows a complex assemblage of fault rocks, from a foliated cataclasite, to the left in the middle core, to ultracataclasites, gouge and again cataclasites containing granite fragments. The very fine-grained matrix seems to consist mainly of epidote. In addition, there are some narrow zones of a very distinct red gouge. 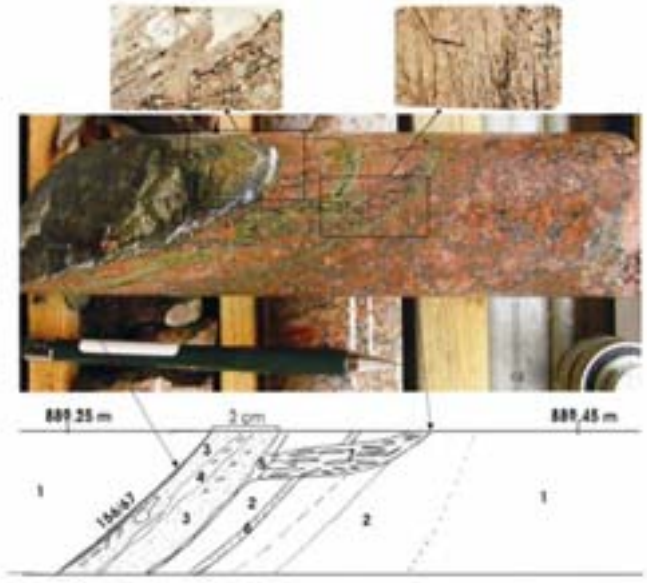 *Several generations of proto- to ultracataclasites and cemented breccias. The thin section to the left shows overall rock dilation, subsequently infilled*

BH	Geometrical Intercept (bh. m)	Target intercept (bh. m)	Comment
			by calcite. On the left-hand side of the calcite there occurs an ultra-/cataclasite, whereas protocataclasites are found on the right side. A cataclasite with abundant epidote in the matrix is visible in the thin section to the right. Strands of epidote-decorated ultracataclasites and fragments of an earlier cataclastic rock form an anastomosing network. The section is dominated by gently dipping fracture planes and slickensided surfaces. The relatively low dip angle of the measured planes generates a rather confused stereonet that indicates no strong preferred planar orientation. It is important to observe the predominance of relatively flat-lying fractures and fault planes in the whole section, with only a few steep structures observed. Kinematically constrained gently to moderately dipping planes indicate either normal or reverse kinematics, with prevalence of down- or up-dip movements and scarcity of oblique kinematics. A few steep and subvertical NW-SE and NE-SW striking fracture planes indicate mostly sinistral kinematics. 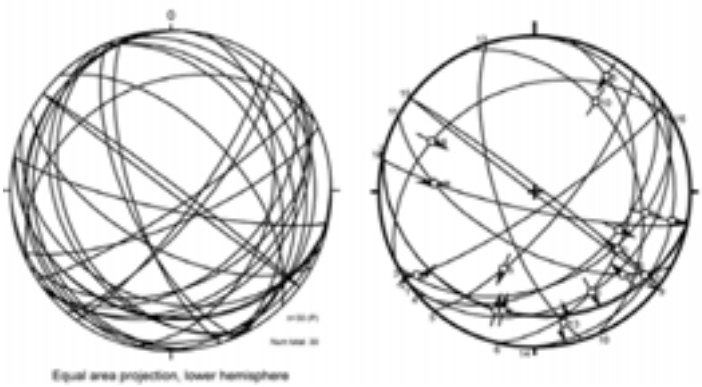 Equal area projection, lower hemisphere *Orientation of fracture planes and striated surfaces with relative kinematics measured in the drill core section.*
KLX09	670	682-722	(note: this section also correlates with ZSMEW007A) Eshi DZ13 682-722 m: High frequency of sealed fractures and increased frequency of open fractures and sealed network. Crush rock in the sections 692.84-692.89 m, 700.53-700.82 m, 710.80-712.37 m and 720.20-720.30 m. Some fractures with large apertures. The section is characterized by intense red staining and increased distribution of cataclastic bands. Low P-wave velocity, low resistivity and low magnetic susceptibility. Three relatively strong and persistent oriented radar reflectors occur at 690.7 m with the orientation 319/44, at 703.5 m with the orientation 192/70 and at 713.8 m with the orientation 160/21 or 345/34. 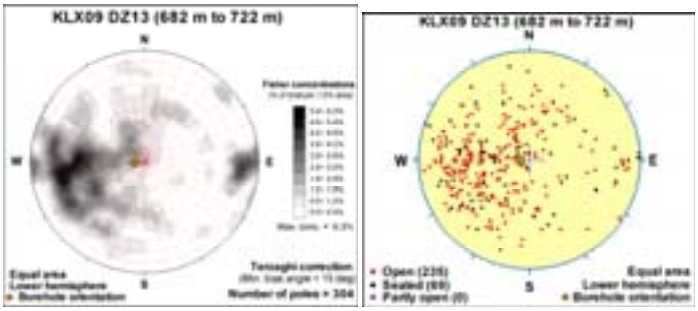

BH	Geometrical Intercept (bh. m)	Target intercept (bh. m)	Comment
			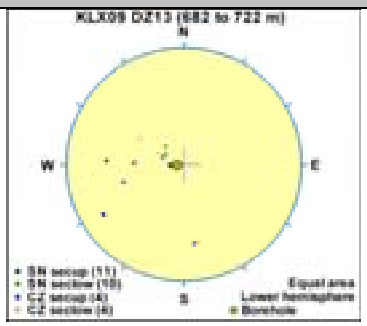 /Viola et al. 2006/ DZ 13 begins at depth 682 m and extends down to ~722 m. It is a major deformation zone that contains different types of fault rocks and is rich in kinematically unambiguous striated planes.  *Example of a striated plane at depth 701.676 m. Chlorite, calcite and clay minerals coat the surface. Slickensides indicate that the hanging wall to this plane moved up parallel to the striations.* The deformation zone begins with a c. 7 m thick upper transition zone defined by red staining and sporadic occurrences of bands of ultracataclasite/gouge arranged in sealed networks. Deformation intensity increases significantly towards the core, the upper boundary located at depth 689.50 m  *Ultracataclasites/gouge at depth 689.67 m.*

BH	Geometrical Intercept (bh. m)	Target intercept (bh. m)	Comment
			At depth 689.67 there occurs a c. 3 cm thick green/brown ultracataclastic/gougy horizon associated with a striated plane. The slickenside-bearing plane dips moderately to the S/SSE and kinematic analysis indicates an overall dextral strike-slip motion with only a very minor S-side-up component. At depth 692.80 m there occurs an indurated breccia cemented by calcite. Analysis of the individual clasts suggests that it formed at the expense of already protocataclastic granites. Immediately below there is a discrete, highly deformed sequence with ~20 cm of red gouge at its centre.  *Cemented breccia derived from protocataclastic granites* DZ 13 core is followed by a c. 2 m thick transition zone starting at depth 720.40 m. The zone is characterized by diffuse red staining and by the progressive decrease of the fracture frequency. DZ 13 is particularly rich in striated planes. The observations and kinematic analyses for the DZ are shown below. A rather complex kinematic picture emerges from the analysis of the dataset, whereby there is clear indication of sets of both compressional and extensional faults. Given the relatively large number of fault planes, a preliminary kinematic analysis for DZ 4 was run. The analysis (strain inversion) of these meso-scale faults was carried out using so-called "paleostress analysis" techniques. The analysis of fault slip data yields information concerning the orientation of the strain tensor. The aim of this procedure was 1) to determine if all fault movements are compatible with a single strain field and 2) to derive a "paleostress" tensor from the data that can be compared in future studies to regional fault patterns. The results indicate that the measured fault surfaces can be assigned to two discrete faulting events, although no indication is provided as to their relative timing. A subhorizontal compression oriented roughly NS would account for the reverse faults measured in DZ 4 that strike from W-E to N-S and display systematically top-to-S, SE reverse faulting. The extensional faults that strike from NW-SE to NS may instead have formed in response to a SW-NE-oriented extensional phase.

BH	Geometrical Intercept (bh. m)	Target intercept (bh. m)	Comment
			KLX 09, DZ 4, mostly chl, calc,clay slickensided planes. 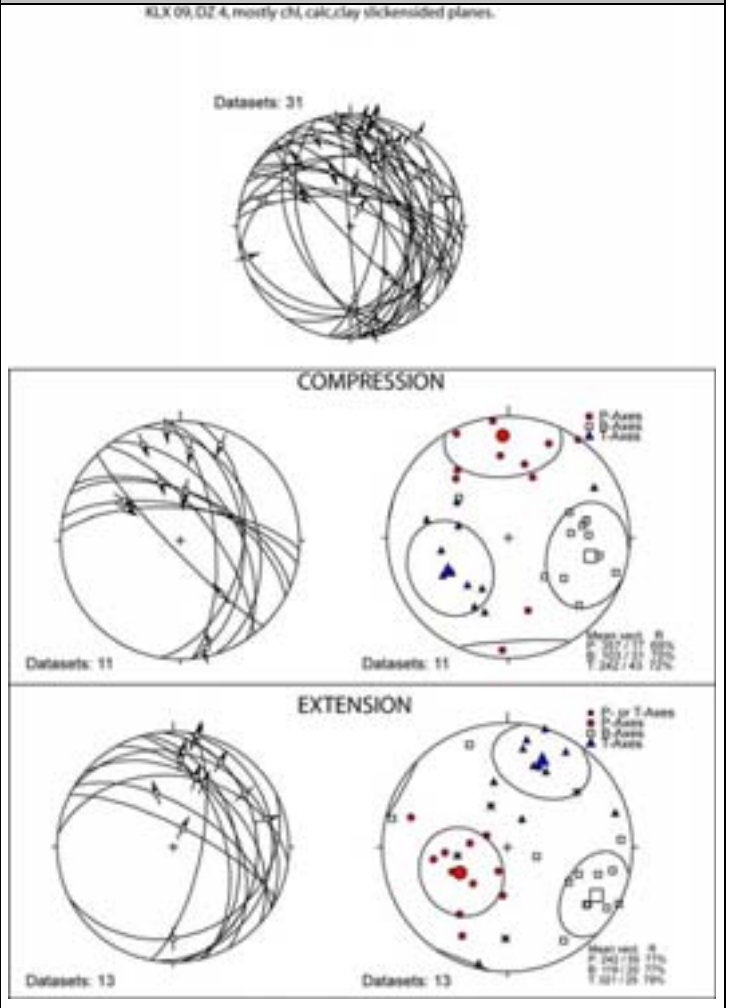

ZSMEW946A (seismic reflector M1)

This modelled geometry has been based on seismic reflector M1 /Juhlin, 2004/. After a further review and integration with new data the reflector was judged to have an orientation of 080/23, /Juhlin, 2006/. This gently dipping geometry meant that the potential zone was at least partially located at an elevation of interest to act as the main repository though with an uncertain continuity and extent. Reflector M1 is the shallowest of a series of four sub parallel reflectors, which dip gently to the south in the upper 1.5 km of crust in the area. These reflections are generally discontinuous in nature, but are part of the general pattern of south dipping reflectivity seen on the profiles. The uppermost M reflection, M1, generally correlates with relatively thin fracture zones in four of the boreholes. M2 and M3 appear to correlate better with mafic sequences, while M4 correlates better with fracture zones.

The general large scale pattern of gently south dipping reflectivity observed on profiles 3 and 5 is probably coupled to lenses of mafic rocks. This pattern includes the set of M reflections. The gently dipping nature of these rocks with a tendency to dip to the south is weakly supported by the mapped orientations of the associated rock type boundaries as measured in the drillcore, see stereonets below. Associated with these mafic lenses are fracture zones, some of them extensive and perhaps generating significant reflectivity. The M1 reflection zone is an example of this. Correlation between the surface seismic and borehole results indicates that the lateral dimensions of the M reflectors is limited. The M1 and M2 reflections do not appear to extend to the KLX09, KLX10 and KLX12 boreholes, suggesting that a NS running boundary east of KLX08/KLX04 is present. /Juhlin, 2006/

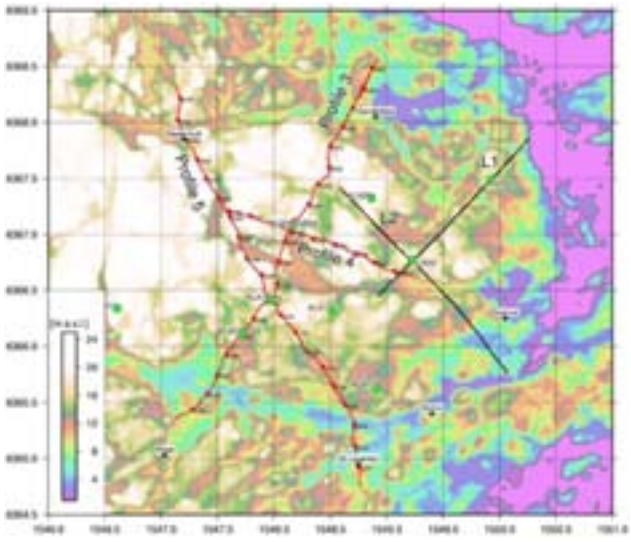

Location of the seismic reflection profiles, profile 3, LSM000704, profile 4, LSM000705 and profile 5, LSM000706 (red lines). Reflection seismic profiles acquired in 1999 (black lines) were reported on in /Bergman et al, 2002/.

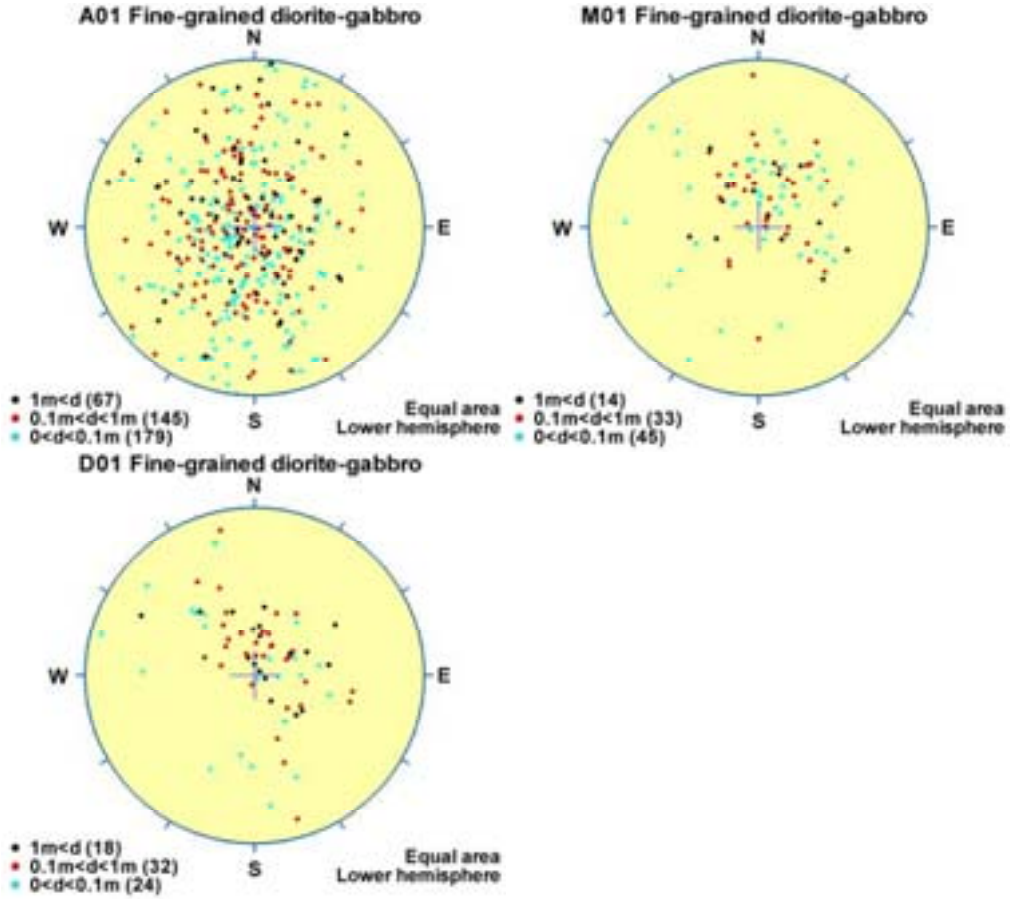

Mapped orientations of the associated rock type boundaries as measured in all drillcores arranged per rock domain.

It is considered that reflector M1 does not represent a single continuous structure, neither a major deformation zone nor a single well defined dioritoid/diorite-gabbro intrusion. It is judged that a southerly dipping discontinuous sequence of mafic intrusions and minor deformation zones spread over a considerable depth range together generate the reflector. Plastic deformation may be associated with the intrusion of the dykes and later reactivation has certainly occurred.

Even between the closely spaced boreholes KLX04 and KLX08 correlation is not clear and no candidate deformation zone in KLX18, located centrally in the reflector geometry, allows possible correlation. The theoretical M1 intercept in KLX08 (456m BH length/ -369masl) lies relatively close to Eshi DZ6 396-416m, a brittle deformation zone. The theoretical M1 intercept in KLX18 (576m BH length/-547masl) is in the vicinity of a minor fine grained diorite-gabbro intrusion (ca. 2m thick) with relatively good rock quality. It is these two intercepts that straddle the -500masl storage level. The deeper intercept in KLX03 (-730masl) that falls within the Eshi DZ1 723-814m (BH length) is considered to be partly due to a narrower section of fine grained diorite-gabbro intrusions that have associated ductile and brittle deformation as well as a subsection of the Eshi DZ1 lying between 723m and 743m (BH depth) with a narrow core located between 732m and 733m, identified by Viola /Viola et al, 2006/.

Based on a detailed inspection of the core /Viola et al, 2006/, a further potential correlation in KLX10A has been included. The correlation is not supported by the actual seismic reflector geometry, which dies out prior to intercepting KLX10A. In addition the intercept position does not coincide with a strict planar extrapolation of the reflector geometry, a warping of the zone geometry is required, though such an undulating geometry is more likely the rule rather than the exception concerning overall fault geometries. However, the brittle character and the fracture orientations do match the M1 profile. The inclusion of this correlation only marginally affects the earlier presented lateral extent of the zone.

A possible extension of the M1 geometry further west beyond the seismic survey coverage was examined. Whilst a potential correlation with Eshi DZ12 in KLX11 was identified that could generate a reflector, detailed examination of DZ12 and nearby intrusions suggested that such a reflector would not equate to a coherent deformation zone. Consequently ZSMEW946A (M1) geometry has not been extended further west beyond ZSMNS059A.

The structure is included in the RVS model as a deformation zone with the following characteristics: high confidence in existence; medium confidence in extent- limited to reflector geometry; thickness- 10m though the inferred series of minor deformation zones are spread over a much greater depth; brittle character.

Although no lineament or field mapping evidence has been associated with M1 a ground surface interception and zone ‘length’ would be in the order of 750m to 1800m depending on the westerly extension. The following discussion outlines the review that has lead to the current interpretation of the reflector.

A review of existing seismic reflection data carried out along with additional examination of core and borehole data. The resulting modified reflector M1 from /Juhlin, 2006/ was plotted in RVS and theoretical BH interceptions were identified. Although the reflector geometry may give 'exact' interception depths for M1 it should be noted that in reality these should only be taken as rough indications of likely interception depths. A spread of possible interceptions exist that generate alternative interpreted intersections based on BH evidence. The borehole geophysics, core photos, fracture orientation data and radar were all reviewed with the aim of establishing a correlation between the reflector with individual boreholes and between boreholes. The aim was to identify a signature for the potential structure and characterize any associated deformation zone. Detailed study of certain sections of drillcore by Viola and Ganerod also provided input /Viola et al, 2006/

M1 extent: the updated lateral extent of M1 is shown in below. The seismic reflection profiles and the relevant BH positions are shown in the following section. The key boreholes for correlation are KLX04, KLX08, KLX18 and KLX03. KLX11A in the west (no seismic coverage) and KLX10 (seismic coverage but no reflector signal) were also examined.

M1 orientation: previously the reflector was interpreted as having an orientation of 095/20, /Juhlin, 2004/. The current interpretation is 080/23, /Juhlin, 2006/. This has generated some significant shifts in the theoretical BH interceptions.

M1 BH geometrical interceptions:

BH	KLX04	KLX08	KLX18	KLX03	KLX11	KLX10
Theoretical M1 interception (BH length m) 2006 and interpreted correlation considered most likely. (thick=apparent thickness)	304 3m thick DZ	456 8m thick DZ	576 intrusion 'good rock'	765 Ca. 10m thick DZ +intrusion	561 6m thick DZ +intrusion	653 7m thick DZ
Target intercept (BH length m)	295-298	478-486	580	723-743	523-529	698-705

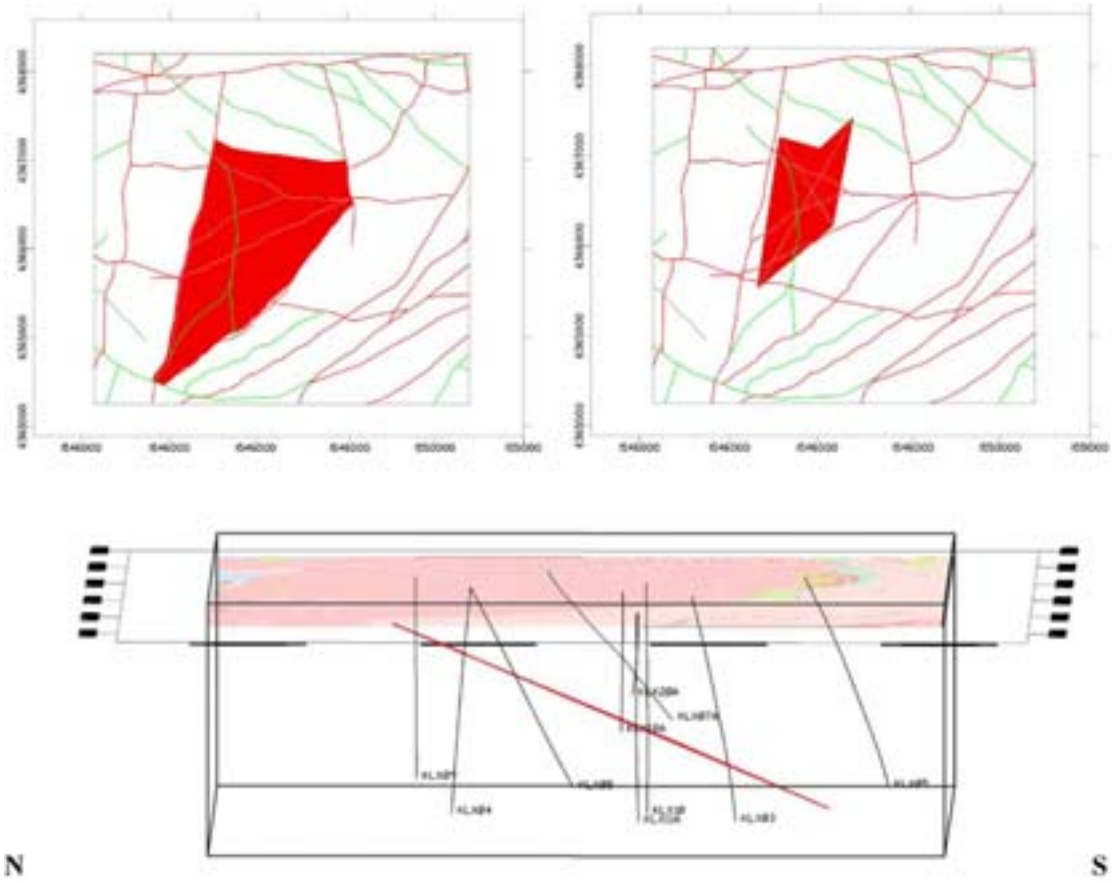

Extent of M1 reflector geometry shown on right. RVS modelled geometry shown on left. The further extent of the reflector westwards is unknown - no data coverage. All other boundaries are based on the reflector no longer being visible- 'dying out.'

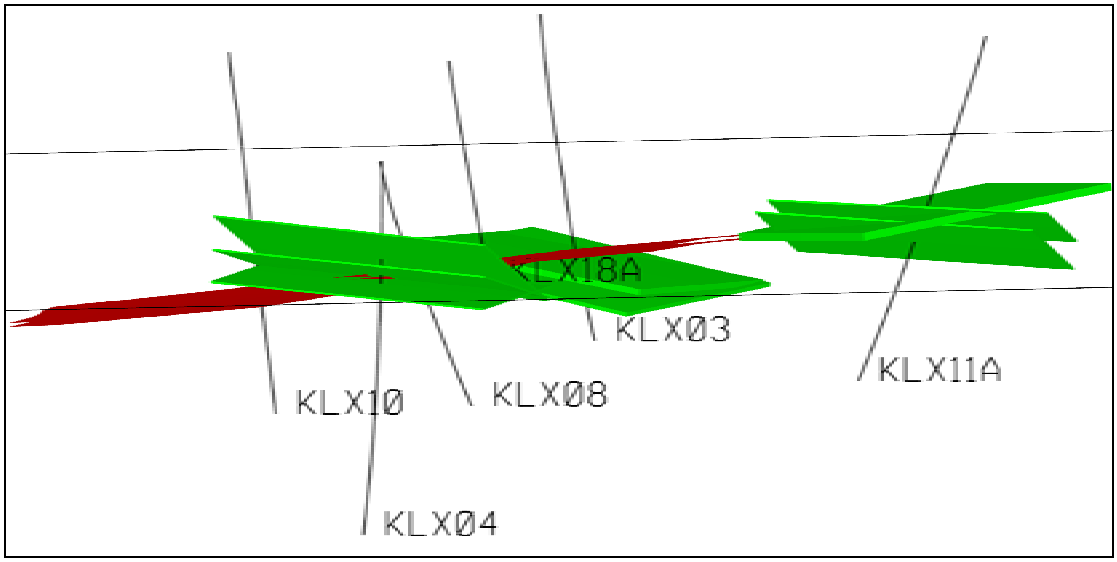

View of ZSMEW946A (red) looking south down dip. Other gently dipping zones that are considered potential members of the M1 reflector series are shown in green.

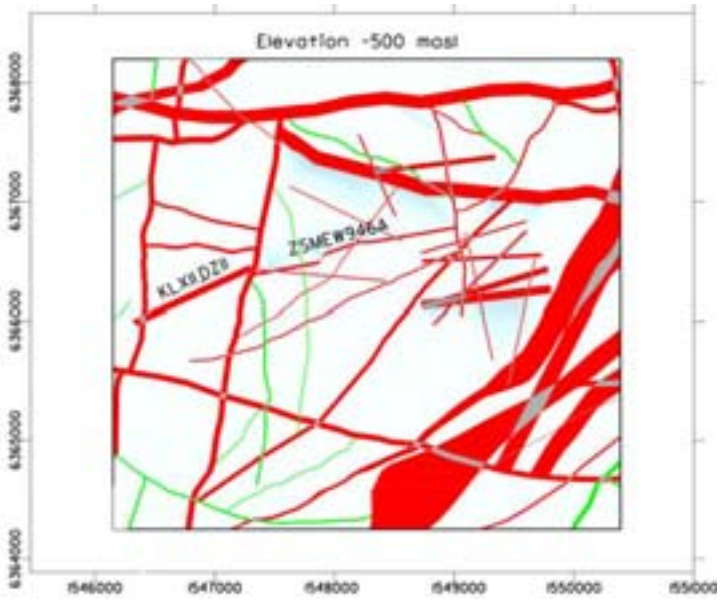

Position of modelled M1(ZSMEW946A) at level -500 masl to indicate the position at storage depth. DZ traces are also shown at their -500masl positions.

Summary of borehole interceptions and interpretations:
KLX04. Two potential intercepts are considered most likely that could generate possible sufficient reflectivity:
(theoretical intercept ca.304m)

1st option, considered most likely, ca.294-298m BH length- a distinct but thin brittle deformation zone, centred at 296-297 m. Radar reflectors at 296.8 m and 298.8 m with the angle 70º to borehole axis. Oriented crush zones: 295m, 111/32; 296m, 100/07; 299m, 125/28.

2nd option, considered slightly less likely, ca. 250-280m BH depth- upper reflector surface combination of intrusions and brittle deformation zone; logs. eshi DZ2 254-258m, One meter crush including severe alteration. Reactivated zone. Low resistivity, variable sonic, low density, low susceptibility and caliper anomaly. Radar: 258m 096/38 (or 270/26).

KLX08 Two potential intercepts are considered most likely that could generate possible sufficient reflectivity:
(theoretical intercept ca.456m)

1st option, considered most likely, ca. 478-486m BH depth, Eshi- inhomogeneous brittle deformation zone characterized by weak to medium red staining and saussuritization, and increased frequency of sealed and open fractures. Scattered cm-wide cataclasites. One dm-wide brecciated zone. Crush zones at 478.441-478.591 m and 483.670-483.756 m. Six non-oriented and one oriented radar reflector are identified in the section. The angle to borehole axis varies between 30 and 63 degrees. Geophysical loggings indicate a few distinct anomalies of low resistivity, low p-wave velocity and low magnetic susceptibility. Orientation data from the borehole is inconclusive.

2nd option, considered less likely: ca. 396-416m BH depth, SHI DZ6- Inhomogeneous brittle deformation zone and minor intrusion characterized by red staining and increased frequency of sealed and open fractures. The section 403.9-416 m is characterized by weak to medium red staining and saussuritization. Crush zone at 408.029-408.379 m. Seven non-oriented and one oriented radar reflector are identified in the section. The angle to borehole axis varies between 25 and 65º. Geophysical loggings indicate general decrease in bulk resistivity, magnetic susceptibility and low p-wave velocity including several caliper anomalies along the entire section. The orientation data is inconclusive but mapped intrusion boundaries, crush zones and oriented fracture data do not support a southerly dip to the intrusion or fracture zone. This section has a potential alternative correlation with seismic reflector Y2.

KLX18 A single potential intercepts is considered most likely
(theoretical intercept ca.576m)

ca. 580m BH depth. Alternatives are limited when the available data is inspected. The intercept coincides with the approximate position of a series of dioritoid and diorite-gabbro intrusions. Mapped rock type boundary orientations at 582m: 116/15 and 592m 087/20 correlate well with the orientation of the reflector as does a single radar reflector at 572m 102/30. The core from BH depth 500m to the base of the hole, at 611m, indicates good rock conditions and an absence of potential deformation zones.

KLX03. Two potential scenarios need to be considered that could generate possible sufficient reflectivity:
(theoretical intercept ca.765m)

The geometrical intercept around ca. 765m BH length coincides with the approximate centre of Eshi DZ1 which extends from BH depth 722m to 814m. NGU after close examination have subdivided DZ1 and identify narrower cores and transition zones. One such core located between 732m and 733m and associated transition zones ca.

723m to 743m has fracture orientations correlating with reflector M2. Thereby it can be said that the reflector correlates with the position of a deformation zone(s). However, also in the vicinity of this section between ca. 730m and 753m there is a series of fine grained diorite-gabbro intrusions whose upper surface correspond well to spikes in the density and velocity logs.

Three radar reflectors show a similar orientation. The strike and dip of these are 110/19 at 730 m, 059/29 at 734 m, and 055/29 at 768.0 m. Mapped rock boundary orientations also correlate well: 730m, 098/19; 733m, 102/09. A single oriented crush zone 083/34 within the intrusion at 730.50m also shows reasonable correlation.

KLX11 This borehole position was not covered by the seismic reflection data. *(theoretical interception ca. 561m)*

Three potential scenarios need to be considered that could generate possible sufficient reflectivity:

1st option, considered most likely: ca. 523m. BH depth: a narrow ca. 5m (apparent) thick fine grained diorite-gabbro intrusion. Mapped rock boundary orientations at 523m 090/05 and at 529m 097/19; foliation 523m 128/21; 524m 098/33; 525m 064/29; 525m 080/27. It should be noted that this intrusion coincides with Eshi DZ12: 522.85–528.66 m Low-grade ductile -brittle shear zone. Low P-wave velocity, low resistivity, caliper anomaly and low magnetic susceptibility. Two non-oriented radar reflectors occur at 523.4 m and 525.8 m with the angle 19° and 55° to borehole axis, respectively. The host rock is dominated by fine-grained diorite to gabbro.

2nd option, considered less likely: ca.578m. BH length: SHI DZ13: 577.90-586.16 m. Inhomogeneous brittle deformation zone, with scattered minor cataclasites. Two more intensely deformed sections at 579.66-579.89 m and 582.65-583.10 m, which contains crush. Low P-wave velocity, low resistivity and low magnetic susceptibility. Four non-oriented radar reflectors occur with angles between 48° and 63° to borehole axis. Also, one oriented rather strong radar reflector occurs at 578.9 m with the orientation 084/31 or 216/46. The host rock is dominated by quartz monzodiorite. Subordinate rock types are fine- to medium-grained granite (511058), medium- to coarse-grained granite and pegmatite.

3rd option, considered less likely: ca.500m. BH depth: SHI DZ11: 486.10-513.15 m. Inhomogeneous brittle deformation zone, with red staining, crush, large apertures and gouge. Scattered sections with sealed network and breccias. Low P-wave velocity, low resistivity, caliper anomaly and low magnetic susceptibility. One non-oriented radar reflector occurs at 510.1 m with the angle 66° to borehole axis. The host rock is dominated by quartz monzodiorite.

Summary of Seismic reflection results

The seismic reflection data from profiles 3 and 5 were reprocessed with particular emphasis on carrying out a review of the M1 reflector /Juhlin, 2006/. Additionally, profiles 4 (P4), L1 and L2 were referred to when estimating the limits of the reflectors. However, these lines were not reprocessed since only P3 and P5 cover the set of M reflections.

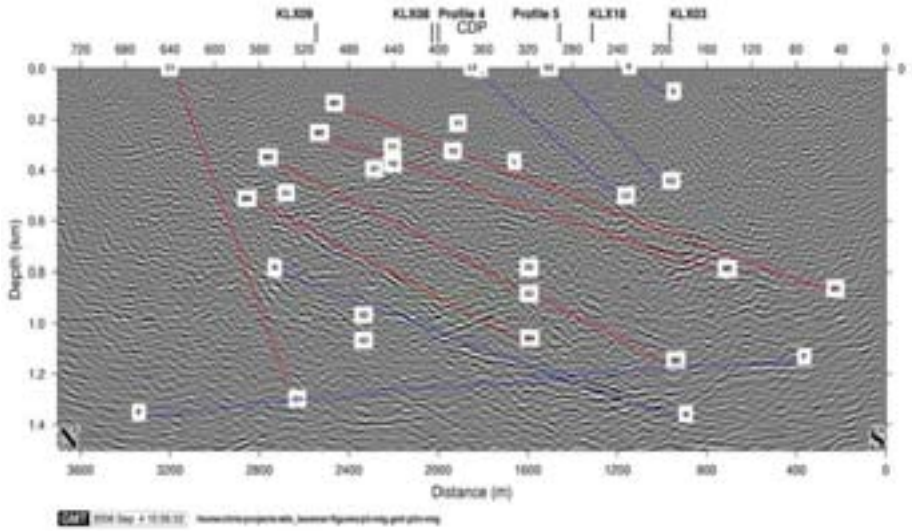

Migrated section of profile 3 (LSM000704) down to 1500 m. Depth scale only valid for true sub horizontal reflections.

E-W striking deformation zones ZSMEW946A (Seismic reflector M1)	
Modelling procedure: At the surface, the zone has no identified corresponding magnetic or topographic lineament. Modelled using dip that has been inferred mainly from a seismic reflector /Juhlin et al. 2004, 2006/. It is not Included in regional model but is present inside local model volume.	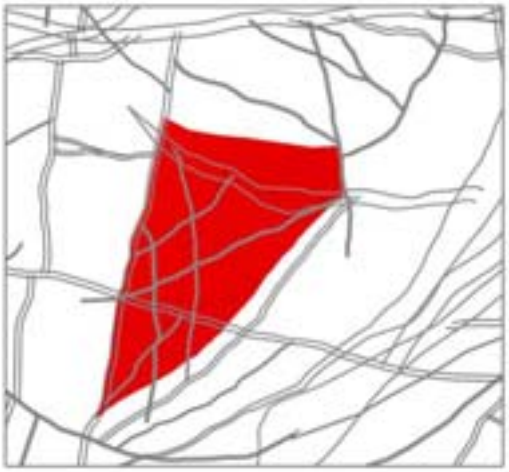
Confidence of existence: High	

Property	Quantitative estimate	Span	Confidence level	Basis for interpretation	Comments
Position					No identified ground surface intercept
Orientation (strike/dip)	080/23	± 20/± 10	Medium for strike, medium for dip	Strike and Dip based on seismic reflector.	/Juhlin, 2006/
Thickness	10 m	5-20 m	Low	BH correlations	The modelled geometry can be taken as being a general orientation for a much thicker sequence of discontinuous MDZs
Core	5 m	1-10 m	Low	BH correlations	Discontinuous
Length (regional model)	1.5 km	0,5-2,0 km	Low	Seismic reflector and BH correlations	No identified ground surface interception/lineament
Ductile deformation	Yes		Medium	BH correlations	Inferred from fabric seen in associated mafic intrusions
Brittle deformation	Yes		Medium	Cataclasites, breccia and crush zones in BHs	Present
Alteration			Medium	BH correlations	Red staining, and saussuritization.
Fracture orientation	Sub horizontal to gently dipping	Diffuse spread	Low	BH correlations	
Fracture frequency* Open/sealed m^{-1}	10/35		Medium	BH correlations	
Crush zone Number/total m	2/1	0-2/ 0-2	Medium	BH correlations	The modelled geometry can be taken as being a general orientation for a much thicker sequence of discontinuous MDZs

E-W striking deformation zones ZSMEW946A (Seismic reflector M1)					
Fracture filling			Medium		Calcite, epidote, chlorite, clay, hematite, prehnite, pyrite, quartz, laumontite

<table>
<tr><th>BH</th><th>Geometrical intercept (Bh m)</th><th>Target intercept (Bh m)</th><th>Comment</th></tr>
<tr><td>KLX04</td><td>(291,2-301,9)

Occurs at the interception between ZSMEW007A and ZSMEW946A, falling within the ZSMEW007A modelled envelope.</td><td>295-298</td><td>INTERPRETED M1: DZ3 295-298m - a distinct but thin fracture zone, core at 296-297 m. Low resistivity, low sonic, low density, very low susceptibility and caliper anomaly. Radar: 275m, 174/26 or 021/24;
 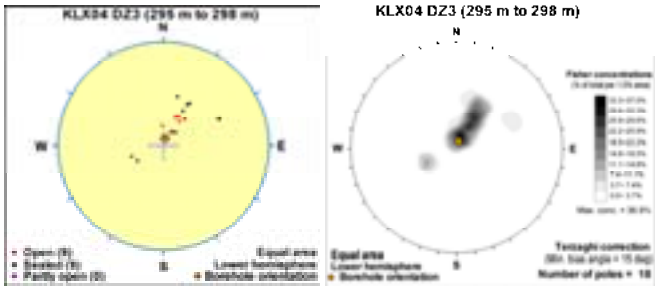

Summary of DZ 3.
<table><tr><th>Depth (m)</th><th>Interpretation</th><th>Description</th></tr><tr><td>293.60</td><td>Transition zone</td><td>Progressive increase in fracture frequency, up to 8-12 f/m.</td></tr><tr><td>295.48</td><td>Fault core

Subzone FZ 1: 295.48-295.68</td><td>Zone of crushed, non-cohesive rock. Not defined as fault rock due to the lack of structural/textural criteria.</td></tr><tr><td></td><td>Subzone FZ 2: 295.83-296.03</td><td>Cohesive fault rock with cataclasites/ultracataclasites/gouge occurrences.</td></tr><tr><td></td><td>Subzone FZ 3: 296.03-296.25</td><td>Zone of crushed, non-cohesive rock. Not defined as fault rock due to the lack of structural/textural criteria.</td></tr><tr><td>296.80</td><td>Transition zone</td><td>High fracture frequency, up to 9 f/m, and some lithological changes.</td></tr><tr><td>297.58</td><td>Host rock</td><td>Low fracture frequency, 3-5 f/m, otherwise undeformed rock.</td></tr></table>DZ3 begins at depth 293.60 m with an upper transition zone defined primarily by an increase in fracture frequency up to 8-12 f/m.
 
The red oval highlights the position of part of the cataclastic core of the deformation zone, a detail of which is shown in the inset. The core is strongly cataclastic and is rich in green ultracataclasites/gouge.

The fault core begins at 295.48 m and can be subdivided into three distinct sub zones: i) FZ1 (295.48-295.68 m), a zone of crushed, non-cohesive rock. ii) FZ2 (295.83-296.03 m), a cataclastic zone with discrete ultracataclastic/gouge occurrences (above fig). The upper contact of the cataclastic core dips moderately SE. iii) FZ3 (296.03-296.25 m), a second crush zone, probably due to</td></tr>
</table>

BH	Geometrical intercept (Bh m)	Target intercept (Bh m)	Comment
			a very high fracture frequency. The transition zone that follows from depth 296.80 m contains a high fracture frequency. The deformation zone terminates at depth 297.58 m and is transitional to undeformed granitic host rock. Overall, the DZ is asymmetric in strain distribution, with most of the observed brittle features located in the hanging wall.  Orientation of the upper contact of the cataclastic core of DZ 3. ''The M1 reflector projects into the borehole at 300 m where a distinct, but thin, fracture zone is present. The thinner ones above thiis have no obvious seismic signature, while the distinct one below at 350 m appears to correspond to the Y1 reflection'' /Juhlin, 2006/. -POTENTIAL MEMBER OF M1 SERIES: Eshi DZ2 254-258m, One meter crush including severe alteration. Reactivated zone. Low resistivity, variable sonic, low density, low susceptibility and caliper anomaly. One radar reflector with the angle 59º to borehole axis at 255.2 m and one with the orientation 096/38 or alternatively 270/26. Radar: 258m 096/38 or 270/26. Rock boundary orientation: 261m 102/18; 264m: 106/15; 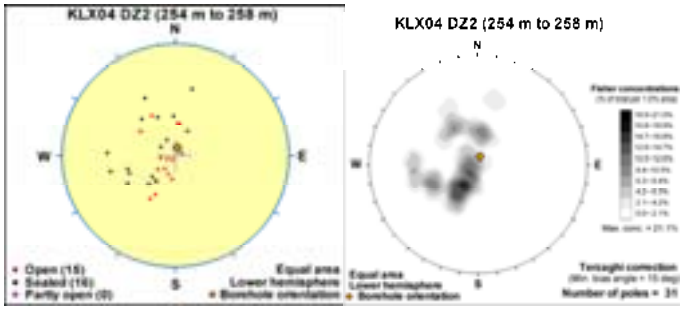 -POTENTIAL MEMBER OF M1 SERIES: DZ4 325-326m Brecciated, strongly altered rock. Low resistivity and low susceptibility. Radar: 327m, 236/12; 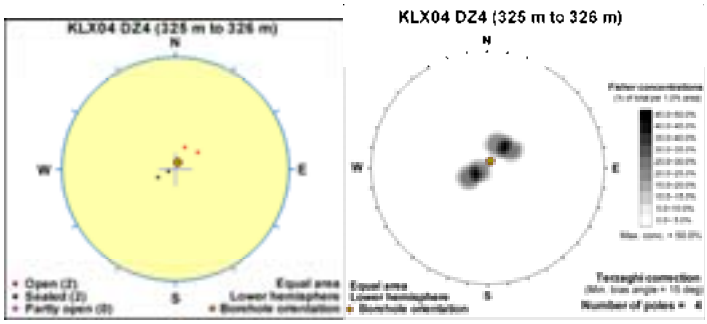

BH	Geometrical intercept (Bh m)	Target intercept (Bh m)	Comment
KLX08	471,3-489,7	478-486	INTERPRETED M1 DZ7 478-486m: inhomogeneous brittle deformation zone characterized by weak to medium red staining and saussuritization, and increased frequency of sealed and open fractures. Scattered cm-wide cataclasites. One dm-wide brecciated zone. Crush zones at 478.441-478.591 m and 483.670-483.756 m. Six non-oriented and one oriented radar reflector are identified in the section. Geophysical loggings indicate a few distinct anomalies of low resistivity, low p-wave velocity and low magnetic susceptibility. Radar: 480m, 292/59 or 012/09 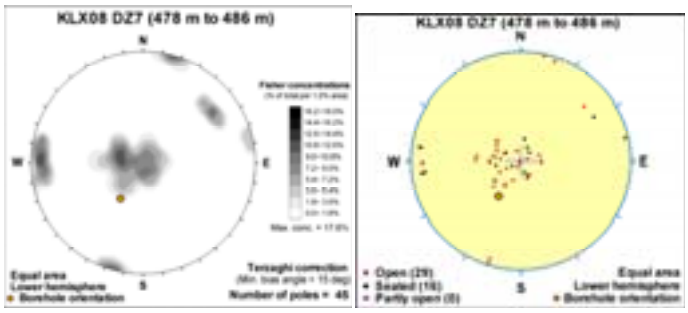 DZ 7 is a deformation zone defined by a c. 1 m thick fault core and its two upper and lower, slightly asymmetric transition zones. The upper transition zone (depth interval 477.668 – 478.31 m) is thicker than the lower counterpart and is characterized by an increase in fracture frequency towards the fault core and several discrete ultracataclasite and/or gouge bands 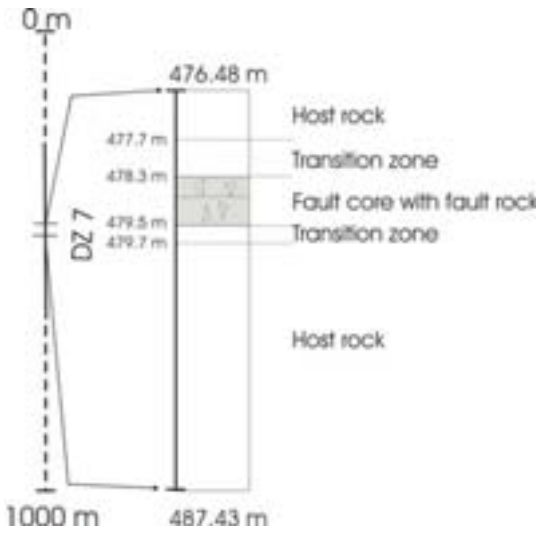 It contains very gently dipping open fractures, striking roughly NS and dipping shallowly either E or W.  Orientation of open fractures of the upper transition zone of DZ 7. The DZ fault core (depth 478.31–479.505 m) is ~1.2 m thick and is formed by a network of ultracataclasite and/or gouge bands. The most prominent

<table>
<tr><th>BH</th><th>Geometrical intercept (Bh m)</th><th>Target intercept (Bh m)</th><th>Comment</th></tr>
<tr><td></td><td></td><td></td><td>
zone in the core is located at depth 479.14 to 479.41 m. The lower transition zone extends from 479.505 m depth down to 479.696 m and consists of fractured host rock and sporadic cataclasites, including a c. 20 cm thick sealed network at depth 479. 505 m. The drill core is back into undeformed host rock at depth 479.696 m, with low fracture frequency, localized red staining and a few epidote veins.

Summary of DZ 7.

<table>
<tr><th>Depth (m)</th><th>Interpretation</th><th>Description</th></tr>
<tr><td>476.48 – 477.668</td><td>Host rock</td><td>Undeformed rock with low fracture frequency.</td></tr>
<tr><td>477.668 – 478.31</td><td>Transition zone</td><td>Progressive increase in fracture frequency towards the fault core, and increase in the occurrence of ultracataclasite/gouge bands.</td></tr>
<tr><td>478.31 – 479.05</td><td>Fault core</td><td>Occurrence of sealed ultracataclastic networks and increasing occurrence of discrete horizons of brittle fault products. The most distinct zone is from 479.14–479.41 m, while the whole fault core is ~1.2 m thick. Sample – KLX 08-2.</td></tr>
<tr><td>479.505 – 479.696</td><td>Transition zone</td><td>Cataclastic network ~20 cm thick.</td></tr>
<tr><td>479.696 -</td><td>Host rock</td><td>Undeformed rock with low fracture frequency. Some red staining and occurrence of epidote veins.</td></tr>
</table>

-POTENTIAL MEMBER OF M1 SERIES: Eshi DZ6 396-416m, Inhomogeneous brittle deformation zone characterized by red staining and increased frequency of sealed and open fractures. The section 403.9-416 m is characterized by weak to medium red staining and saussuritization. Crush zone at 408.03-408.38 m. Seven non-oriented and one oriented radar reflector are identified in the section. Oriented reflector occurs at 400.2 m with the orientation 299/89. The angle to borehole axis of non-oriented reflectors varies between 25 and 65º. Decreased radar amplitude between 395 and 415 m. Geophysical loggings indicate general decrease in bulk resistivity, magnetic susceptibility and low p-wave velocity including several caliper anomalies along the entire section. Confidence level = 3
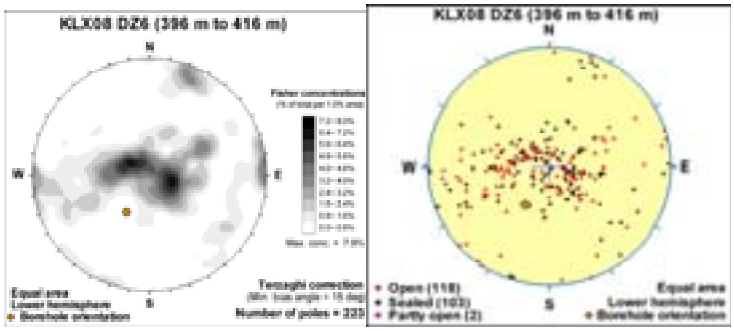

DZ 6 is characterized by a ~2.5 m thick fault core with 2 symmetrically arranged transition zones.
</td></tr>
</table>

BH	Geometrical intercept (Bh m)	Target intercept (Bh m)	Comment
			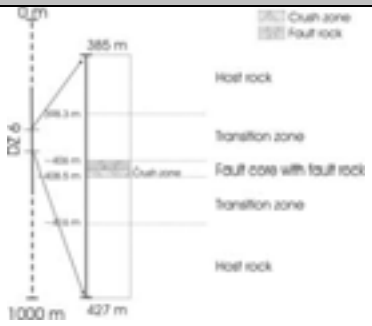 The upper and lower transition zones show increasing and decreasing fracture frequency towards and away from the fault core, respectively. The stereonet below shows the fault slip data observed and measured within the two transition zones; red great circles represent striated planes of the upper transition zone, whereas black great circles represent planes of the lower transition zone. The steep, roughly EW trending fractures are generally coated by epidote, whereas the shallower planes are coated by chlorite, clay minerals and calcite, which in turn may suggest the steep fractures to be older (thus formed under higher T conditions) than the gently-dipping ones. No direct crosscutting relationships were, however, observed. No straightforward kinematic framework can be obtained from the few measurements. In general, highly oblique or strike-slip kinematics is accommodated along moderately WNW or ESE dipping planes. The steep E-W epidote-coated fracture planes suggest instead strike-slip displacements along moderately plunging lineations. 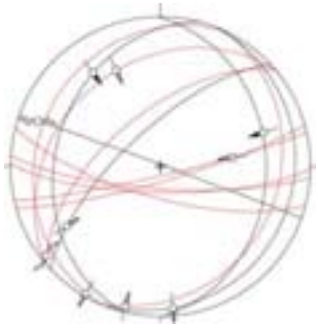 The occurrence of discrete and localized cataclasites is common throughout both transition zones. The upper boundary of DZ 6 fault core is located at approximately 405.77 m depth. The core consists of ~50 cm of cohesive cataclasites, ultracataclasites and gouge, and a ~ 2 m thick crush zone affecting the undeformed host rock. At depth 406.18 m there occurs a narrow, cataclastic zone characterized by a c. 3 cm thick green ultracataclasite and gouge. An open fracture, coated by epidote and clay minerals is oriented 150/41 and runs parallel to the ultracataclasite. Summary of DZ 6. **Depth (m) / Interpretation / Description** 385 — Host rock — Undeformed rock with low fracture frequency, 1-3 f/m. 398.30 — Transition zone — Progressive increase in fracture frequency, up to 5-15 f/m. Increase in occurrence of narrow, discrete cataclastic bands. 405.77 — Fault core — Occurrence of cohesive cataclasites, ultracataclasites and gouge and discrete crush zones. Occurrence of a pervasive cataclastic sealed network. The

<table>
<tr><th>BH</th><th>Geometrical intercept (Bh m)</th><th>Target intercept (Bh m)</th><th>Comment</th></tr>
<tr><td></td><td></td><td></td><td>
<table>
<tr><td></td><td></td><td>most distinct zone is ~45 cm thick, while the whole fault core is ~2.5 m in thickness. Sample – KLX 08-1.</td></tr>
<tr><td>408.48</td><td>Transition zone</td><td>Highly fractured transition zone. Sporadic occurrences of ultracataclastic narrow bands in relatively undeformed Ävrö granite.</td></tr>
<tr><td>416</td><td>Host rock</td><td>Undeformed rock with low fracture frequency, 1-6 f/m.</td></tr>
</table>
</td></tr>
<tr><td>KLX18</td><td>574,6-585,3</td><td>580</td><td>SHI DZ8 448.35- 456.55m: inhomogeneous brittle-ductile deformation zone. High frequency of sealed fractures. One cataclasite (2 cm). Weak red staining. Decreased resistivity and magnetic susceptibility, and partly decreased P-wave velocity.

SHI DZ9 471.9 – 488.9m: inhomogeneous brittle-ductile deformation zone. High frequency of sealed fractures and open fractures with large (2-5 mm) apertures. Gouge (15 mm) and one cataclasite (16 mm). Three crush zones (17-22 cm). Core zone at 484.00-487.90 m. Faint to medium red staining. Significantly decreased resistivity and magnetic susceptibility, and partly decreased P-wave velocity in the interval 483.5-488.9 m. Two non-oriented radar reflectors occur at 473.4 m and 476.5 m with the angle 42° and 59° to borehole axis, respectively. Two strong and persistent oriented reflectors occur at 482.3 m and 485.0 m with the orientation 018/89 and 193/37, respectively. Radar: 572m 102/30

Ductile shear zone 581m: 049/16, 071/23

Rock type boundary orientation diorite gabbro: 582m: 116/15; 592m 087/20

''It is not clear what the source to the M1 reflection is in the KLX18 borehole, there are both minor low velocity zones and a thin high density zone where the reflector projects into the borehole at 576 m'' /Juhlin, 2006/.</td></tr>
</table>

BH	Geometrical intercept (Bh m)	Target intercept (Bh m)	Comment
KLX03	727,1-738,9	723-743	Eshi DZ1, 722.5-814m. Sealed, hydrothermally altered fracture zone with relatively low frequency of open fractures. Scattered narrow sections are strongly foliated (low grade ductile shear zones) and overprinted by the hydrothermal alteration and the sealed fracture network. Several radar reflectors occur within the section. Three reflectors show a similar orientation. The strike and dip of these are 110/19 (306/44) at 729.5 m, 059/29 at 733.7 m, and 055/29 at 768.0 m. One reflector shows the orientation 193/87 at 759.5 m. The geophysical logging data show decreased resistivity, P-wave velocity and density together with fluctuating magnetic susceptibility.. Mafic intrusion 729.81-733.16 (rock boundary orientations 098/18, 102/09) (also 736.47-753.21 (rock boundary orientations 224/28, 112/13)) 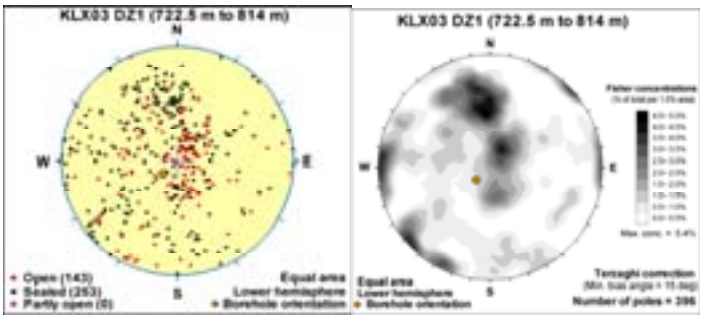 NGU. Structural data for the uppermost transition zone between 723 and 732 m are shown below. Several striated surfaces were observed and characterized kinematically, but do not provide a clear picture. Apart from a few steep strike-slip shear fractures, there are several transtensional planes dipping moderately to the SSE. These fractures are coated invariably by chlorite and epidote, with minor calcite and hematite. Red great circles plot a faint ductile tectonic planar fabric that occurs at depth c. 730 m.  Structural information for striated fracture planes (black great circles) and a zone of pervasive foliation (red great circles) in the depth interval 720 to 732 m. The first prominent fault core of DZ 1 is located at approximately 732.20 m depth. It is about 1m thick and contains foliated cataclasites and ultracataclasites. A faint foliation is visible. Later quartz and/or calcite veins crosscut the core fault rocks  Cataclasites from the uppermost fault core located at depth c. 732.5 m.

BH	Geometrical intercept (Bh m)	Target intercept (Bh m)	Comment
			The fault rock is a weakly-foliated protocataclasite formed from severely altered amphibole-bearing granites. Its faint foliation dips consistently to the SSE-SE. Chlorite is widespread throughout the section and is invariably associated with foliation and shear band planes, thus constraining shearing to the lowermost greenschist facies conditions. From microscopic observations deformation in this DZ appears to have been accommodated predominantly by processes operating at the brittle ductile transition, as demonstrated by the coexistence of ductile (pervasive foliation, shear bands, small asymmetric folds within the cataclasites) and brittle features (evidence of granular flow mechanisms and rigid-body rotation)  Orientation of the fault core at depth 732.5 m in KLX 03 The transition zone dividing this upper core from a deeper second fault core starts at approximately 733.15 m depth; it is characterized by localized red staining and abundant calcite and epidote veins and networks. Veins are generally associated with calcite- and epidote-rich millimetric bands of cataclasites and cemented microbreccias. The extent of the lower transition zone is unclear, a depth of 743m has been applied.

BH	Geometrical intercept (Bh m)	Target intercept (Bh m)	Comment
KLX11	521,0-532,7	523-529	For information a series of potential DZs from the SHI are presented below. However, DZ12 is considered the most likely candidate for correlation with an extrapolated reflector M1. However, the seismic survey does not extend this far west. DZ12 has been studied in detail by NGU. The results of NGU's work suggest that DZ12 is not a true DZ. It should also be noted that this level coincides with a fine grained diorite-gabbro intrusion. INTERPRETED M1: Eshi DZ12: 522.85–528.66m (considered most likely correlation) Low-grade ductile shear zone, except for the central brittle part (525.29-525.60 m), which is dominated by crush, gouge and large apertures. Low P-wave velocity, low resistivity, caliper anomaly and low magnetic susceptibility. Two non-oriented radar reflectors occur at 523.4 m

BH	Geometrical intercept (Bh m)	Target intercept (Bh m)	Comment
			and 525.8 m with the angle 19° and 55° to borehole axis, respectively. The host rock is dominated by fine-grained diorite to gabbro (505102). Subordinate rock types are fine- to medium-grained granite (511058) and quartz monzodiorite (501036). Confidence level: 3. 528.67m rock type boundary orientation 097/19 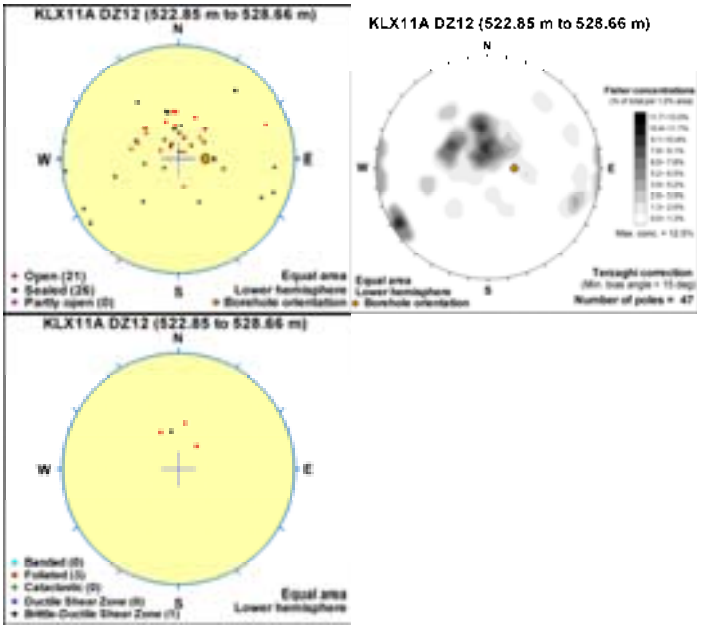 This depth interval contains a c. 6 m thick fine-grained, foliated quartz monzodiorite that intrudes otherwise undeformed granites. The quartz monzodiorite hosts a distinct deformation zone brittle-ductile core between depths 525.269 and 525.691 m. The boundaries to the deformation zone core are sharp, both above and below. The core itself is ~45 cm thick and made by intensively foliated and gently crenulated quartz monzodiorites. The core is strongly fractured; the fractures are, however, not visible in the BIPS images of the corresponding depth interval, possibly suggesting that they may have been produced by the drilling and recovery process. Foliation planes dip gently to moderately to the south. Samples KLX 11A-3 and KLX 11A-4 were collected in order to investigate further the characteristics of this deformation zone. Thin section analysis has revealed that what was initially interpreted as foliated cataclasites is actually only a package of foliated, and gently crenulated granite. There is no sign of penetrative cataclasis. They are separated from the undeformed granite by a thin ultracataclastic layer and its associated chlorite-decorated fractures. Later quartz-filled fractures crosscut the ultracataclasites. It is not obvious what actually localized the brittle core within the foliated quartz monzodiorites  Orientation of selected foliated cataclasites in the core of DZ 12.

<table>
<tr><th>BH</th><th>Geometrical intercept (Bh m)</th><th>Target intercept (Bh m)</th><th>Comment</th></tr>
<tr><td></td><td></td><td></td><td>
Summary of DZ 12.
<table>
<tr><th>Depth (m)</th><th>Interpretation</th><th>Description</th></tr>
<tr><td>517.34 – 525.269</td><td>Host rock</td><td>Undeformed rock with low fracture frequency. Lithological change from granite to quartz monzodiorite (foliated) at ~521 m.</td></tr>
<tr><td>525.269 – 525.691</td><td>Fault core</td><td>The core itself is ~45 cm and consists of S-dipping foliated quartz monzodiorite. Numerous fractures overprint the foliated rock but are not observed in the BIPS images for the same depth interval.</td></tr>
<tr><td>525.691 - 532</td><td>Host rock</td><td>Sharp contact from the DZ brittle core to foliated quartz monzodiorites. Lithological change from foliated quartz monzodiorite to undeformed granite at ~527 m.</td></tr>
</table>
-POTENTIAL MEMBER OF M1 SERIES: DZ11: 486-513m. Inhomogeneous brittle deformation zone, with red staining, crush, large apertures and gouge. Scattered sections with sealed network and breccias. Low P-wave velocity, low resistivity, caliper anomaly and low magnetic susceptibility. One non-oriented radar reflector occurs at 510.1 m with the angle 66° to borehole axis. The host rock is dominated by quartz monzodiorite (501036). Subordinate rock type is fine-grained granite (511058).
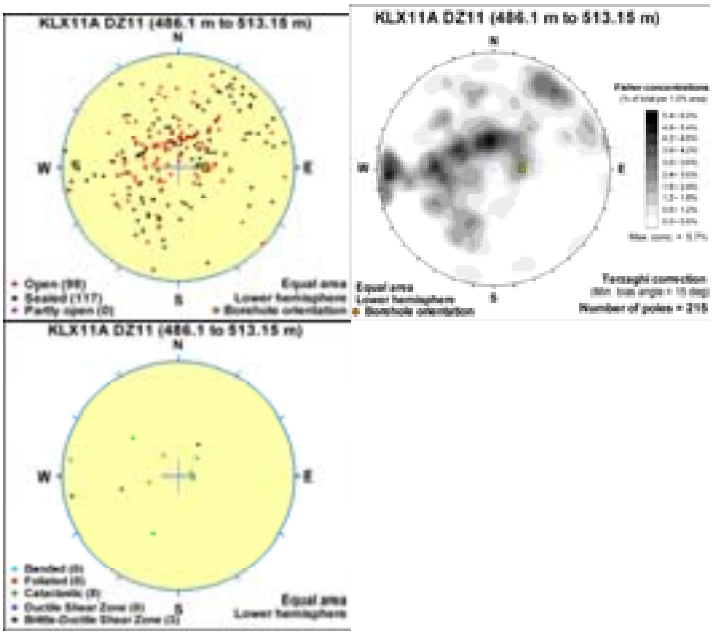

POTENTIAL MEMBER OF M1 SERIES :DZ13: 577.90-586.16 m Inhomogeneous brittle deformation zone, with scattered minor cataclasites. Two more intensely deformed sections at 579.66-579.89 m and 582.65-583.10 m, which contains crush. Low P-wave velocity, low resistivity and low magnetic susceptibility. Four non-oriented radar reflectors occur with angles between 48° and 63° to borehole axis. Also, one oriented rather strong radar reflector occurs at 578.9 m with the orientation 084/31 or
</td></tr>
</table>

BH	Geometrical intercept (Bh m)	Target intercept (Bh m)	Comment
			216/46. The host rock is dominated by quartz monzodiorite (501036). Subordinate rock types are fine- to medium-grained granite (511058), medium- to coarse-grained granite (501058) and pegmatite (501061). 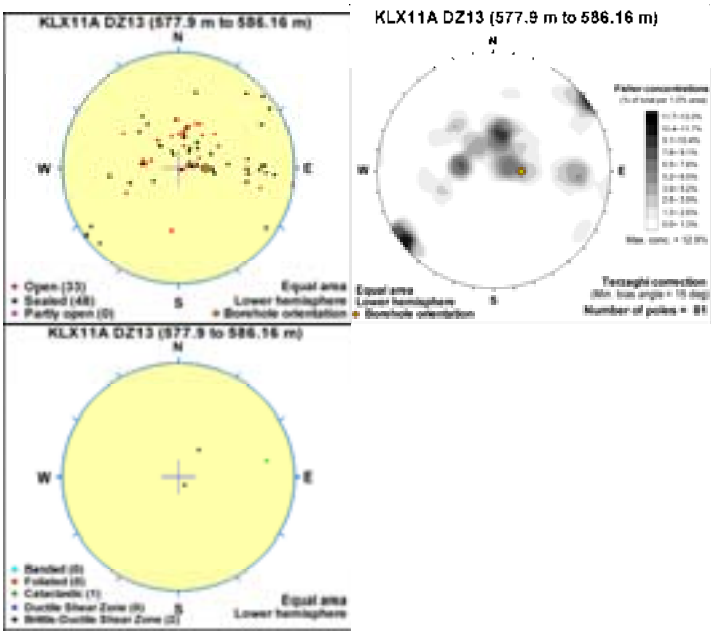

BH	Geometrical intercept (Bh m)	Target intercept (Bh m)	Comment
KLX10	695,0-706,9	698-705	No Eshi DZ at this level but DZ9 occurs at 698-705m (NGU limits including transition zones) *''Reflections from M1 and M2 are observed just north of the borehole, but do not appear to extend all the way into it'' /Juhlin, 2006/.* Eshi DZ 9 690m to 706m: Increased frequency of sealed and open fractures. A few of the latter have large apertures. Crush zone at 698.32-700.26 m. Weak to medium red staining. Very low electric resistivity, low P-wave velocity, magnetic susceptibility and density. One caliper anomaly and an anomaly in temperature gradient. One oriented radar reflector occurs at 701.1 m with the orientation 274/46. Low radar amplitude occurs in the interval 695-715 m, i.e. partly outside the deformation zone. 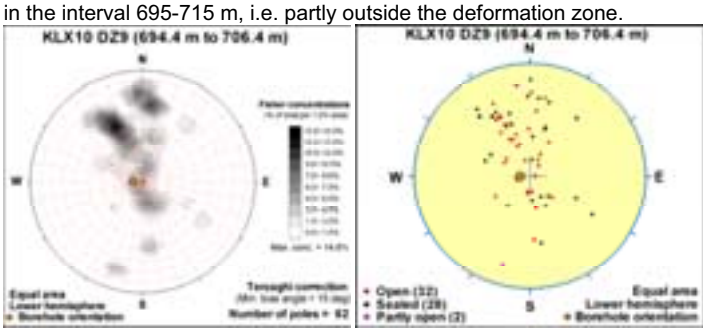 DZ 9 begins with an upper transition zone at 698.3 m characterized by a progressive increase in fracture frequency and in the number of occurrences of cataclastic networks towards the deeper fault core.

BH	Geometrical intercept (Bh m)	Target intercept (Bh m)	Comment
			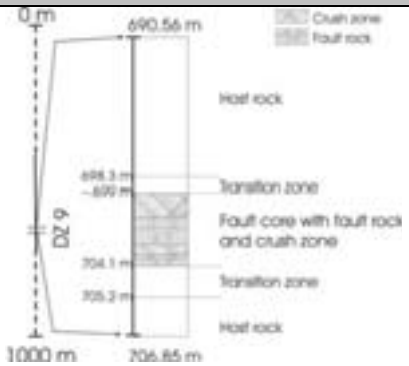 Fractures are generally open with a systematic S/SSE dip direction). Discrete crush zones also occur within the highly fractured transition zones. 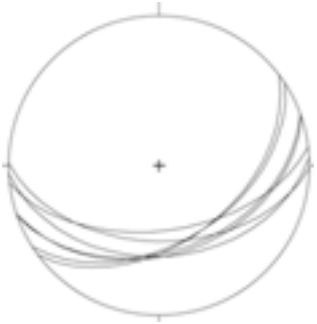 The DZ core begins at ~699 m depth a c. 5 m thick core consists of a complex sequence of fault rocks, varying from cataclasites to ultracataclasite and locally minor gouge occurrences. Intense deformation and some core loss during recovery. There is evidence of several generations of cataclasites and ultracataclasites and mutual crosscutting relationships. A second, lower transition zone follows the fault core and extends from 704.13 to 705.187 m depth. Summary of DZ 9.

Depth (m)	Interpretation	Description
690.56–698.321	Host rock	Weak red staining.
698.321 - ~699	Transition zone	Progressive increase in fracture frequency towards the fault core, and increase in the number of occurrences of cataclastic networks. The thickness of the zone is 6.85 m.
~699 – 704.13	Fault core	The core consists of a variety of fault rock products, from cataclastic networks to pc/c/uc and (minimal) gouge, plus crush zones. Sample – KLX 10-1.
704.13 – 705.187	Transition zone	High fracture frequency.
705.187	Host rock	Low fracture frequency. Some red staining and occurrence of a cataclastic network.

KLX07_DZ10

NE-SW striking deformation zones KLX07_DZ10	
KLX07_DZ10's orientation 225/28 is based on detailed mapping by NGU /Viola et al, 2007/ and generally corresponds to a fracture pole concentration and crush orientation. The modelled extent results in intersections at the very outer limits with KLX02 and KLX21B. Neither drillhole shows correlation and can superficially be taken to confirm the general limits of the zone.	

Confidence of existence: High

Property	Quantitative estimate	Span	Confidence level	Basis for interpretation	Comments
Position			High	Eshi	
Orientation (strike/dip)	225/28		Low	NGU core mapping	Alternative: minor mapped ductile shear zones: 253/52, 249/46.
Thickness	10 m		Low	NGU core mapping	Interception length and following true thickness modified from Eshi based on core mapping review by NGU.
Length (regional model)	1.0 km		Low	Assumed	
Ductile deformation	Minor		Low	Very local ductile fabric	
Brittle deformation	Yes		High	Raised fracture frequency and cataclasis, gouge	
Alteration			High		Red staining
Fracture frequency* Open/sealed m^{-1}	9/22		Low		
Crush zone Number/total m	2/<0.5		Low		
Fracture filling			High		Clay, chlorite, calcite, hematite,epidote, pyrite, andularia, quartz

BH	Geometrical Intercept (bh. m)	Target intercept (bh. m)	Comment
KLX07A	645-655	645-655	Eshi DZ10 604-655 m: Increased frequency of open and sealed fractures. The section is characterized by scattered cataclasite and clay altered fracture fillings. The oriented reflectors occur at 623.4 m with the orientation 085/82 and at 650.1 m with the orientation 143/07. Major decrease in bulk resistivity and magnetic susceptibility. Numerous low p-wave velocity anomalies and partly also caliper anomalies. Crush: 264/38, 280/35 Minor mapped ductile shear zones: 253/52, 249/46. 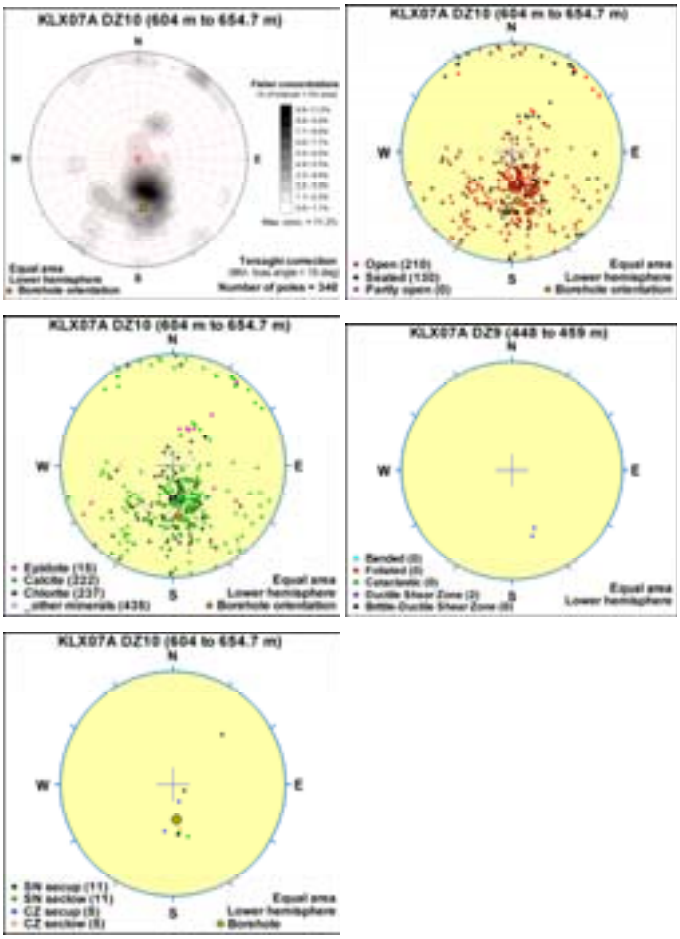 -From /Viola et al, 2006/: 604-660 m. This section is characterized by fresh granites with only sporadic occurrences of fault rock, such as networks of cataclasite strands, commonly interfingered with bands of gouge and ultracataclasite. A ca. 4-5 cm thick ultracataclasite band containing a chlorite and epidote matrix in which are dispersed angular fragments of granite occurs at depth 645 m. A calcite vein subsequently exploited this band, possibly during a later reactivation stage. Cataclasites are dark, fine-grained and contain fragments of granite. A one-meter thick zone of crushed rock occurs at the bottom of the section. Relatively flat lying cataclastic and ultracataclastic bands characterize the interval under discussion. The figure below shows them plotted as red great circles dipping 25-35º to the NW, N and NE. Only two surfaces could be constrained kinematically and provided reverse sense of shear. Epidote and quartz veins (black great circles) have very shallow planar attitudes.

KLX07A		645-655	-From /Viola et al, 2006/: 604-660 m: 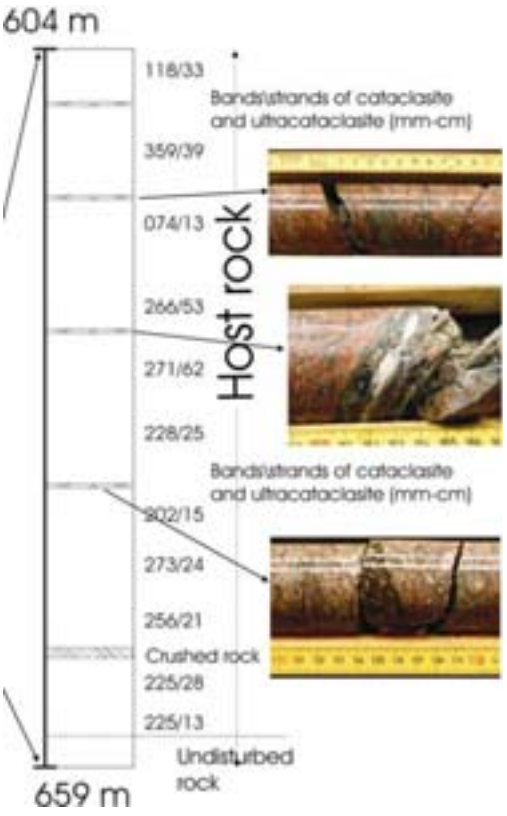 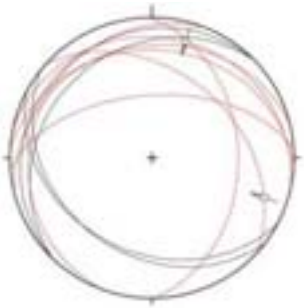 Orientation of cataclastic and ultracataclastic bands (red great circles) and quartz and epidote veins (black circles) for depth interval 604-659 m.

KLX08_DZ10

E-W striking deformation zones KLX08_DZ10	
KLX08_DZ10's orientation is based on a fracture orientation concentration. At the very edge of the modelled geometry there is a theoretical intercept with KLX04 though there is no support for a correlation.	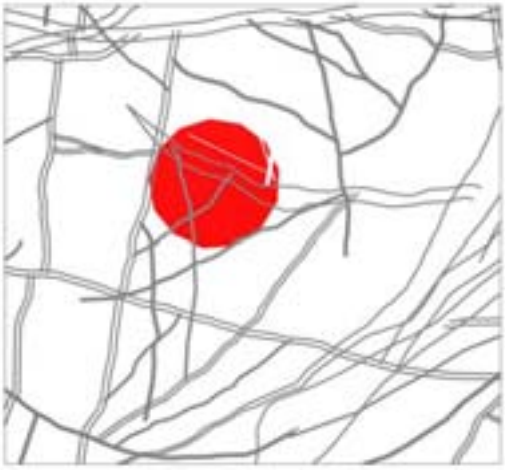

Confidence of existence: High

Property	Quantitative estimate	Span	Confidence level	Basis for interpretation	Comments
Position			High	Eshi	
Orientation (strike/dip)	079/11		Low	Pole concentration	
Thickness	11 m		Low		
Length (regional model)	1.0 km		Low	Assumed	
Ductile deformation	No		Low		
Brittle deformation	Yes		High	Raised fracture frequency	
Alteration			High		Red staining, epidotization, saussuritzation
Fracture frequency* Open/sealed m^{-1}	5/30		Low		
Crush zone Number/total m	0/0		Low		
Fracture filling			High		Calcite, chlorite, clay, pyrite, epidote, prehnite, quartz

BH	Geometrical Intercept (bh. m)	Target intercept (bh. m)	Comment
KLX08A	925-940	925-940	Eshi DZ10 925-940 m. Increased frequency of sealed fractures. Weak to medium red staining and saussuritization. Scattered sections of sealed network at 925.27-926.12, 926.78-927.23, 928.63-928.95, 933.46-933.53, 935.66-936.26, 938.66-938.73 m. No indications of significant geophysical anomalies. 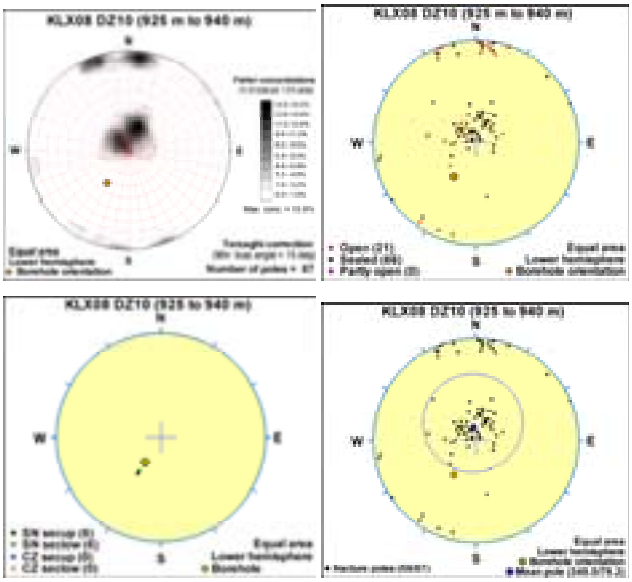

KLX08_DZ1

N-S striking deformation zones KLX08_DZ1	
KLX08_DZ1's orientation is based on crush, fracture orientations and NGU detailed core review though remains low confidence. The modelled geometry generates theoretical intercepts with KLX04 though the hole was only partly cored at this position along with HLX30 and HLX31. No clear correlation exists with either hole though it must be noted that they lie within the complex ZSMEW007A belt.	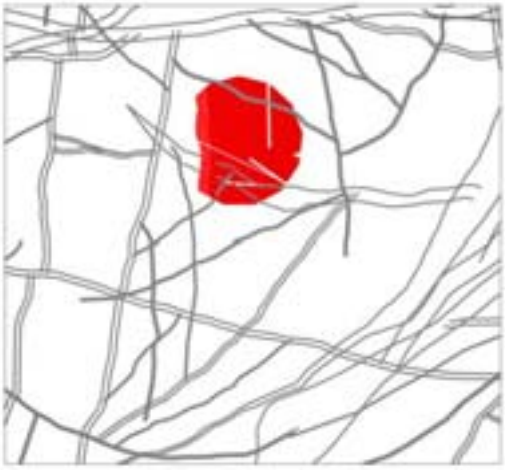

Confidence of existence: High

Property	Quantitative estimate	Span	Confidence level	Basis for interpretation	Comments
Position			High	Eshi	
Orientation (strike/dip)	000/18		Low	Crush orientations, NGU review, /Viola et al, 2007/	Alternatives: 330/60 secondary pole concentration, radar 307/67.
Thickness	27 m		Low		
Length (regional model)	1.0 km		Low	Assumed	
Ductile deformation	No		Low		
Brittle deformation	Yes		High	Raised fracture frequency and cataclasis	
Alteration			High		Red staining, chloritization, albitization
Fracture frequency* Open/sealed m^{-1}	6/30		Low		
Crush zone Number/total m	3/<0.5		Low		
Fracture filling			High		Calcite, chlorite, clay, hematite, pyrite, prehnite, quartz, epidote, chalcopyrite, andularia.

BH	Geometrical Intercept (bh. m)	Target intercept (bh. m)	Comment
KLX08A	100-131	100-131	Eshi DZ1 100-131 m: Inhomogeneous brittle deformation zone characterized by primarily faint to weak red staining and increased frequency of sealed and open fractures. Crush zones at 109.09-109.23, 118.90-118.96 and 121.57-122.06 m. Three oriented radar reflectors occur in the section. Oriented reflectors occur at 105.4 m with the orientation 307/67, at 119.9 m with the orientation 051/35, and at 122.9 m with the orientation 088/18. Anomalies in the geophysical logs generally coincide with the crush zones. They comprise narrow low resistivity and caliper anomalies, distinct low p-wave velocity anomalies and partly decreased magnetic susceptibility. 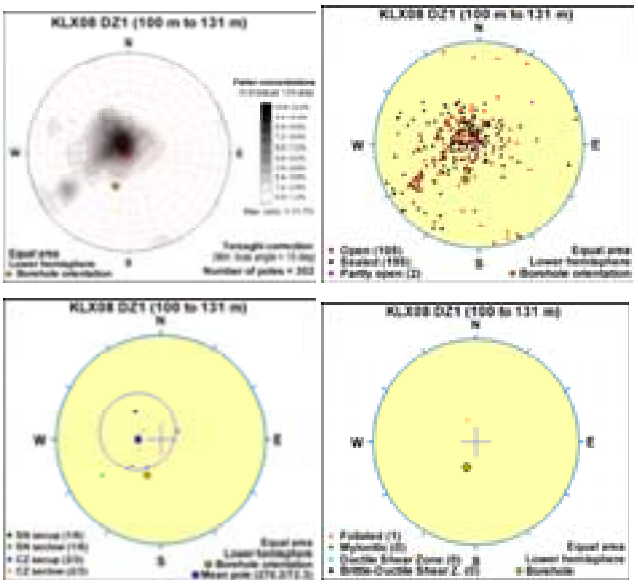 Ref: /Viola et al, 2007/: Occurrences of narrow fault rock-containing fault cores (108-109,7, 118,5-119 m). The damage zone has in general a relatively high fracture frequency and numerous strands of cataclasites, ultracataclasites and gouge. Locally there occur cemented breccias, 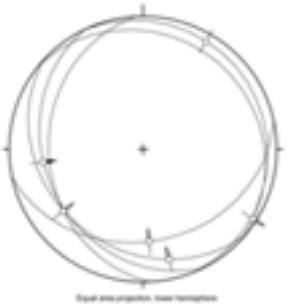 *Angelier diagram of striated planes found in the depth interval 100-165 m of drill core KLX 08.* The deformation zone displays a few striated planes that dip shallowly to the SW or NE. Slickenlines are mostly defined by chlorite and calcite. Kinematic indicators indicate mostly reverse shear along these planes.

KLX09F_DZ1

N-S striking deformation zones KLX09F_DZ1	
KLX09F_DZ1 is based on fracture and crush orientations. The modelled geometry generates theoretical intercepts with other holes but all in positions lacking core and mapping data.	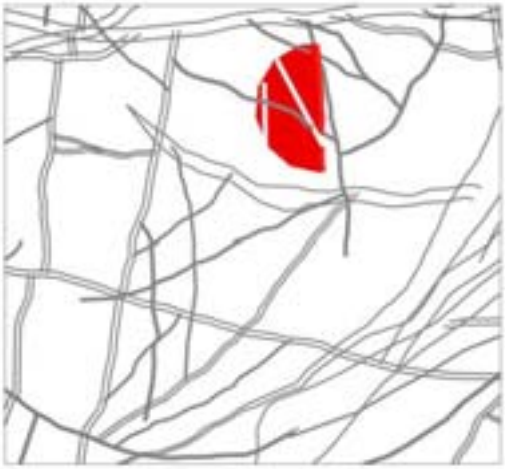
Confidence of existence: High	

Property	Quantitative estimate	Span	Confidence level	Basis for interpretation	Comments
Position			High	Eshi	
Orientation (strike/dip)	178/19		Low	Fracture pole concentration and crush orientation	
Thickness	14 m		Low		
Length (regional model)	1.0 km		Low	Assumed	
Ductile deformation	No		Low		
Brittle deformation	Yes		High	Raised fracture frequency and cataclasis	
Alteration			High		Red staining
Fracture frequency* Open/sealed m^{-1}	9/27		Low		
Crush zone Number/total m	0/0		Low		
Fracture filling	-				

BH	Geometrical Intercept (bh. m)	Target intercept (bh. m)	Comment
KLX09F	8-22	8-22	Eshi DZ1 8-22 m: Brittle deformation zone characterized by increased frequency of sealed fractures and partly by a slight increase of open fractures, scattered sections of faint to medium red staining, cataclasites, one breccia and slickensides. Decreased resistivity, magnetic susceptibility and partly decreased P-wave velocity. 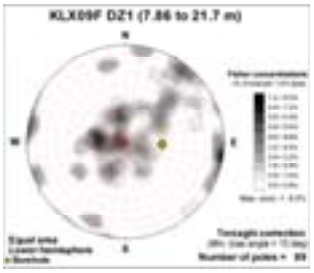 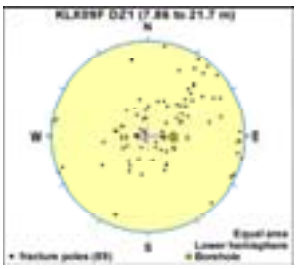 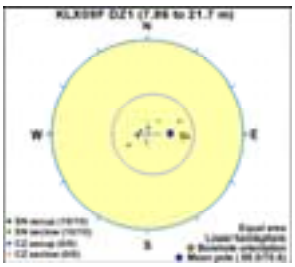

KLX03_DZ1b

NW-SE striking deformation zones KLX03_DZ1b	
KLX03_DZ1b is based on a further subdivision of Eshi KLX03 DZ1 following a detailed drill core inspection by /Viola et al, 2007/. The orientation is based on this fracture mapping.	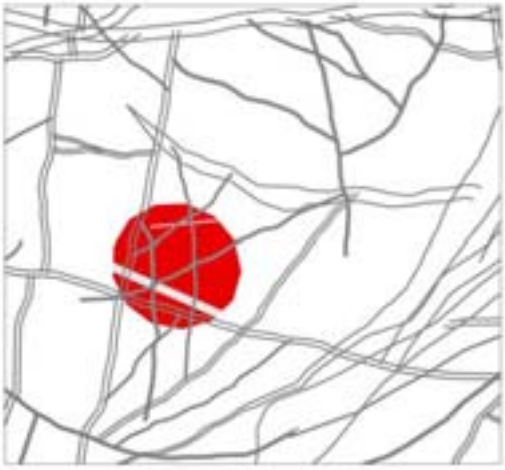

Confidence of existence: High

Property	Quantitative estimate	Span	Confidence level	Basis for interpretation	Comments
Position			High	Subdivision of Eshi based on /Viola et al, 2007/	
Orientation (strike/dip)	121/20		Low	Pole concentration based on /Viola et al, 2007/	
Thickness	10 m		Low		
Length (regional model)	1.0 km		Low	Assumed	
Ductile deformation	No		Low		
Brittle deformation	Yes		High	Raised fracture frequency, cataclasis and gouge	
Alteration			High		Epidotization
Fracture frequency Open/sealed m^{-1}	-				
Crush zone Number/total m	-				
Fracture filling					Epidote, chlorite and hematite

BH	Geometrical Intercept (bh. m)	Target intercept (bh. m)	Comment
KLX03	762-774	759-777	Note: a part of Eshi DZ1 722-814 m: /Viola et al, 2006/ NGU: contains complex structural relationships and textures defined by abundant protocataclasites “crosscut” by epidote veins and bands together with ultracataclasites and gouge levels. In contrast to the upper and lower cores, it lacks foliated intervals and evidence of brittle-ductile deformation features. The fault core dips consistently to the SW with a gentle dip and one striated plane, coated by chlorite and hematite, suggests a reverse, top-to-NE sense of shear for this brittle deformation zone. 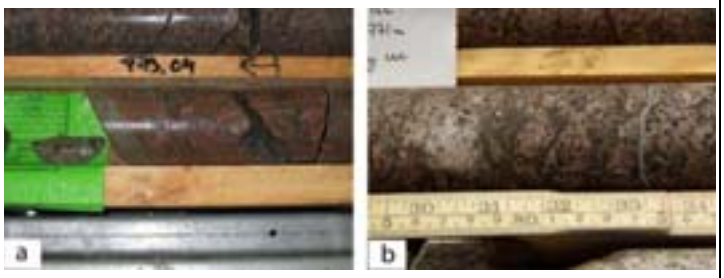 *Examples of the complex textural relationships observed in the fault core at depth 767-775 m. Coarse protocataclasites deform the Ävrö granite and are in turn crosscut by later epidote-rich bands (a) and thin dark ultracataclasites/gouge veins (b).* 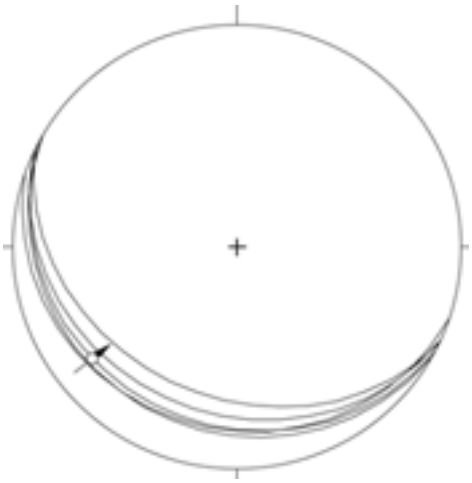 *Orientation of the fault core at depth interval 767-775 m. A striated plane at depth 773.91, coated by chlorite and hematite, indicates reverse, top-to-NE kinematics.* The lower part of this core shows very complex structural relationships, which suggest multiple episodes of cataclasis and brecciation.

KLX03_DZ1c

NW-SE striking deformation zones KLX03_DZ1c	
KLX03_DZ1c is based on a further subdivision of Eshi KLX03 DZ1 following a detailed drill core inspection by /Viola et al, 2007/. The orientation is based on this fracture mapping.	

Confidence of existence: High

Property	Quantitative estimate	Span	Confidence level	Basis for interpretation	Comments
Position			High	Eshi	
Orientation (strike/dip)	125/13		Low	Pole concentration	
Thickness	10 m		Low		
Length (regional model)	1.0 km		Low	Assumed	
Ductile deformation	Yes		High	Ductile indicators	
Brittle deformation	Yes		High	Raised fracture frequency and cataclasis.	
Alteration			High		Red staining and saussuritization
Fracture frequency Open/sealed m^{-1}	-				
Crush zone Number/total m	-				
Fracture filling					Calcite and quartz

BH	Geometrical Intercept (bh. m)	Target intercept (bh. m)	Comment
KLX03	789-801	789-801	Note: a part of Eshi DZ1 722-814 m: /Viola et al, 2006/ NGU: the fault core is located at approximately 797-798 m depth, is about ~50 cm thick and consists mainly of foliated cataclasites that deform foliated quartz monzodiorites. The core of the deformation zone dips very shallowly southwest, which is also the dip direction of the ductile foliation within the quartz monzodiorites. 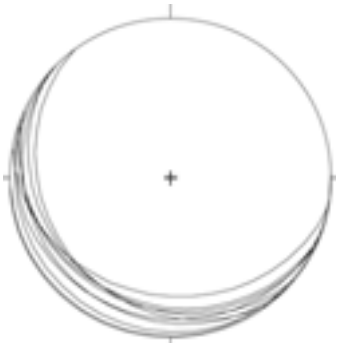 *1 Orientation of the c. 30 cm-thick deformation zone core at depth 797 m.*  *Foliated cataclastic quartz monzodiorites form the core of this very gently SW-dipping deformation zone core at depth 797-798 m.* Calcite and quartz veins are found in abundance within the core. Some of them are sub parallel to the foliation planes, others are coarse and cut across discordantly, suggesting their late formation in the deformation history of this deformation zone.

KLX09E_DZ2

NW-SE striking deformation zones KLX09E_DZ2	
KLX09E_DZ2's orientation is based on ductile fabric, fracture and crush orientation concentrations. The modelled geometry generates theoretical intercepts in KLX09B, KLX09C, KLX09D, KLX09F and KLX09G. All the named holes with the exclusion of KLX09G show reasonable correlation. KLX09G shows no correlation and the theoretical intercept lies to the east of ZSMNS046A suggesting that the zone does not extend directly beyond ZSMNS046A.	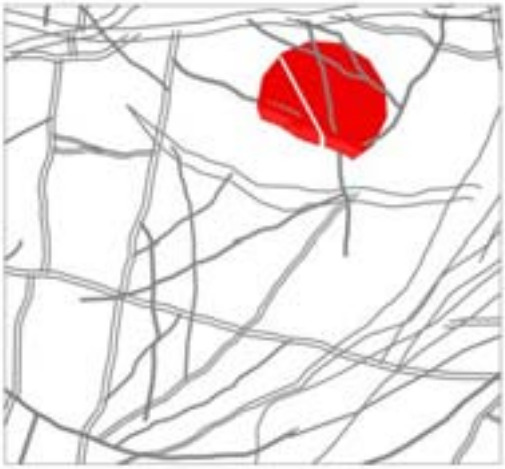
Confidence of existence: High	

Property	Quantitative estimate	Span	Confidence level	Basis for interpretation	Comments
Position			High	Eshi	
Orientation (strike/dip)	295/14		Low	Ductile fabric, fracture pole concentration and crush orientation	
Thickness	22 m		Low		
Length (regional model)	1.0 km		Low	Assumed	
Ductile deformation	Yes		High		
Brittle deformation	Yes		High	Raised fracture frequency, breccia, crush	
Alteration			High		Red staining
Fracture frequency* Open/sealed m^{-1}	6.5/37		Low		
Crush zone Number/total m	1/<1		Low		
Fracture filling	-				

BH	Geometrical Intercept (bh. m)	Target intercept (bh. m)	Comment
KLX09E	76-106	76-105	Eshi DZ2 76-105 m: brittle deformation zone overprinting ductile shear zones. Increased frequency of sealed fractures and partly also of open fractures, faint to medium red staining, one c. 0.75 m thick crush zone, one breccia and slickenside. The most intensely deformed sections (cores) are 87.40-87.80 m, 89.00-89.80 m and 96.30-99.60 m. Two oriented radar reflectors occur, one at 83.2 m with the orientation 342/61 and one at 97.6 m with the orientation 133/47 or 010/53, the latter of which is strong. 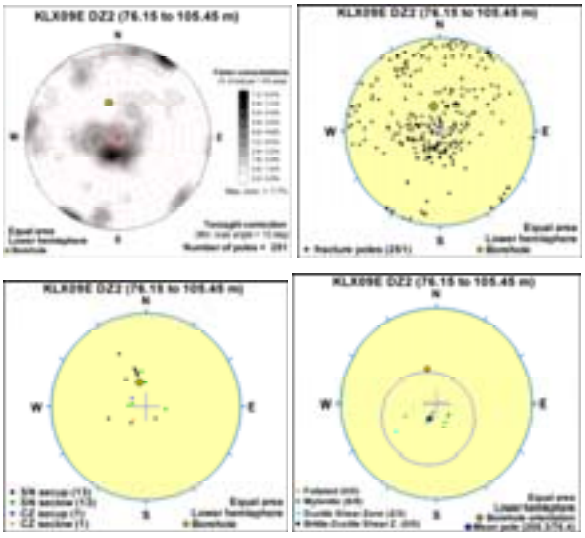
KLX09A	62-84	-	No core or information at this level
KLX09B	63-86	75-79	Eshi DZ2 75-79 m: Inhomogeneous low-grade ductile shear zone overprinted by brittle deformation. Increased frequency of particularly sealed but also open fractures, faint to strong red staining, two crush zones, large apertures, slickensides and mylonitic sections. The most intensely deformed sections (cores) are 74.75-75.06 m and 77.58-78.15 m. Significantly decreased resistivity, magnetic susceptibility and partly decreased P-wave velocity. At c. 78.0 m there is a major drop in fluid water resistivity, which is most likely related to a water bearing structure. One strong radar reflector occurs at 78.9 m with the orientation 288/18 or 108/18. Low radar amplitude at 75-80 m. The host rock is dominated by Ävrö granodiorite (501056). Subordinate rock types comprise fine-grained granite (511058) and fine-grained diorite-gabbro (505102). 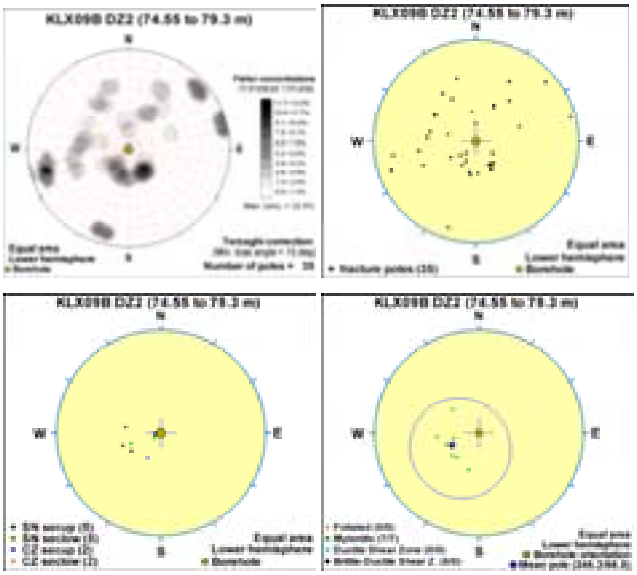

BH	Geometrical Intercept (bh. m)	Target intercept (bh. m)	Comment
KLX09C	70-94	81-86	Eshi DZ1 81-86 m: Low grade ductile shear zone overprinted by brittle deformation. Increased frequency of sealed fractures and a slight increase in open fractures, large apertures and mylonitic sections. The most intensely deformed section (core) is 82.81-85.63 m. One non-oriented radar reflector occurs at 82.9 m with the angle 72° to borehole axis and one reflector at 86.3 m with the orientation 238/11 or 253/53. Low radar amplitude at 85-90 m. The host rock is totally dominated by Ävrö granite (501044). Subordinate rock type comprises very sparse occurrence of pegmatite (501061). 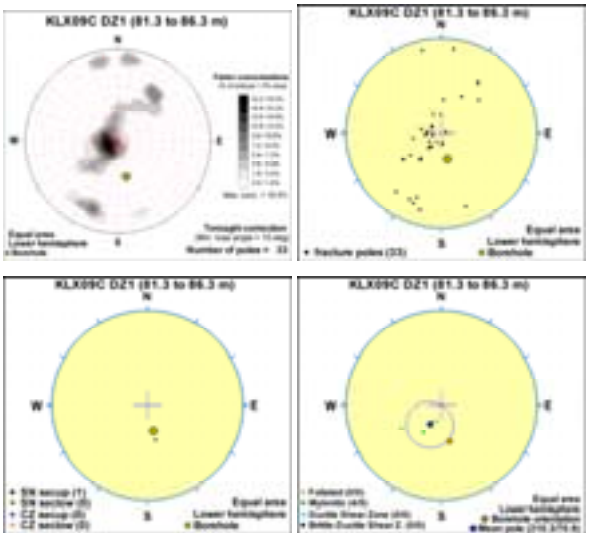
KLX09D	73-98	81-90	Eshi DZ1 81-90 m: Low grade ductile shear zone overprinted by brittle deformation. Increased frequency of sealed and open fractures, faint to medium red staining, large apertures, slickensides and mylonitic sections. Significantly decreased bulk resistivity and bulk magnetic susceptibility. Partly decreased P-wave velocity. Also, one radar reflector occurs at 88.1 m with the orientation 017/44 or 335/21. Low radar amplitude occurs at 80-90 m. The host rock is dominated by Ävrö granodiorite (501056). Subordinate rock types comprise fine-grained granite (511058) and sparse occurrences of pegmatite (501061) and granite (501058). 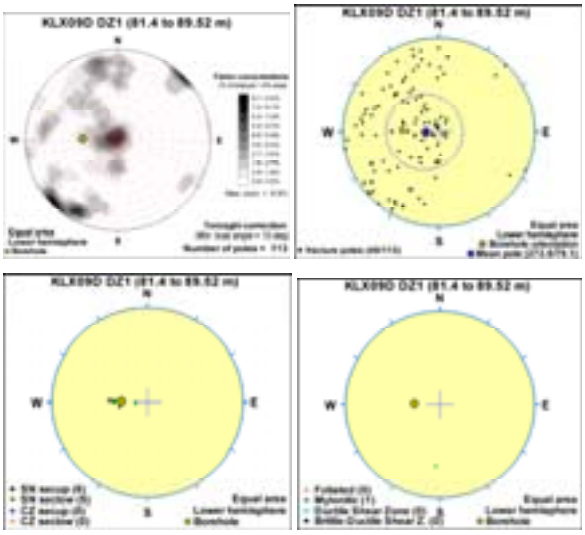
KLX09F	64-92	68-69 and 79-84	Eshi DZ2 68-69 m: Brittle deformation zone characterized by increased frequency of open fractures, faint to weak red staining and slickensides. Decreased resistivity, magnetic susceptibility and partly decreased P-wave velocity. One strong non-oriented radar reflector at 68.8 m with the anlge 34° to borehole axis. The host rock is dominated by Ävrö granodiorite

BH	Geometrical Intercept (bh. m)	Target intercept (bh. m)	Comment
			(501056). Subordinate rock types comprise fine-grained granite (511058). 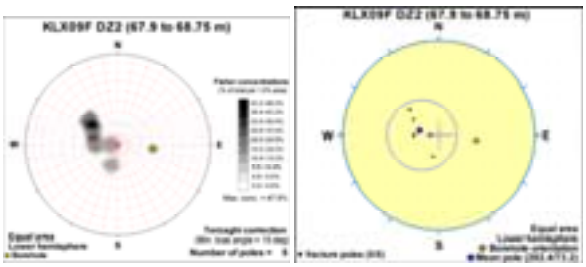 DZ3 79-84 m: Brittle deformation zone overprinting ductile structures. Increased frequency of particularly sealed fractures but also of open fractures, faint to weak red staining, slickensides, mylonitic and brittle-ductile sections. Significantly decreased resistivity and bulk magnetic susceptibility. One minor caliper anomaly but partly increased P-wave velocity. The host rock is dominated by Ävrö granodiorite (501056). Subordinate rock types comprise fine-grained granite (511058), fine-grained diorite-gabbro (505102) and very sparse occurrence of pegmatite (501061). 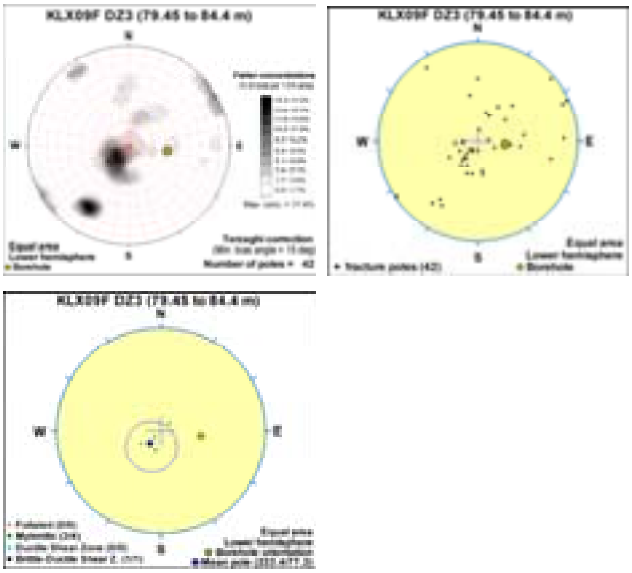
KLX09G	79-100	-	No correlation

KLX11A_DZ11

NE-SW striking deformation zones KLX11A_DZ11	
KLX11A_DZ11's orientation is based on crush and fracture concentration orientations along with kinematic mapping by /Viola et al, 2007/. Orientation and elevation makes this zone potentially a western extension of the M1 minor deformation zone series.	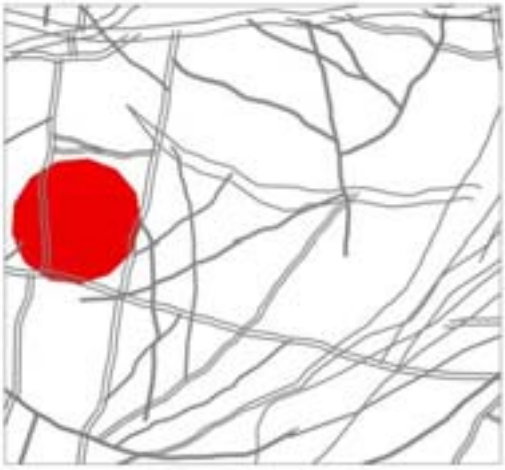

Confidence of existence: High

Property	Quantitative estimate	Span	Confidence level	Basis for interpretation	Comments
Position			High	Eshi	
Orientation (strike/dip)	065/20		Low	Crush and fracture concentrations along with /Viola et al, 2007/	
Thickness	20 m		Low		
Length (regional model)	1.0 km		Low	Assumed	
Ductile deformation	No		Low		
Brittle deformation	Yes		High	Raised fracture frequency, crush, large apertures and gouge	
Alteration			High		Red staining, epidotization
Fracture frequency* Open/sealed m^{-1}	7/30		Low		
Crush zone Number/total m	5/0.5		Low		
Fracture filling					Chlorite, calcite, clay, hematite, prehnite, epidote pyrite.

<table>
<tr><th>BH</th><th>Geometrical Intercept (bh. m)</th><th>Target intercept (bh. m)</th><th>Comment</th></tr>
<tr><td>KLX11A</td><td>488-511</td><td>486-513</td><td>Eshi DZ11 486-513 m: Inhomogeneous brittle deformation zone, with red staining, crush, large apertures and gouge. Scattered sections with sealed network and breccias. Low P-wave velocity, low resistivity, caliper anomaly and low magnetic susceptibility.
 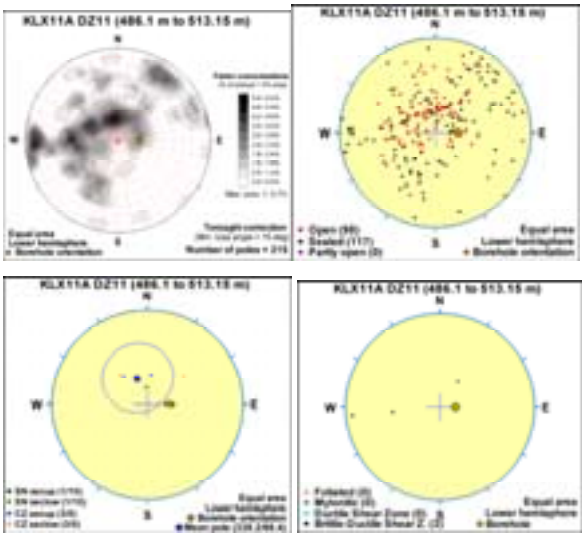
Ref /Viola et al, 2007/: drew different limits for the zone in the core namely 502-511 m.
<table><tr><th>Depth (m)</th><th>Interpretation</th><th>Description</th></tr><tr><td>479.9 – 502.1</td><td>Host rock</td><td>Undeformed rock with low fracture frequency.</td></tr><tr><td>502.1 – 509.0</td><td>Transition zone</td><td>Transition zone at 503.13 – 509.003 m defined by increasing fracture frequency and occurrence of bands/network/strands of cataclasites/ ultracataclasites and epidote veins. A thin crush zone also occurs.</td></tr><tr><td>509.0 – 510.7</td><td>Fault core</td><td>Brittle core defined by abundant fault products (protocataclasites, cataclasites and bands of gouge). The core ends at a crush zone, which caused c. 15 cm core loss during core recovery. Several slickensided planes. Set of c. NE/SW striking conjugate fractures.</td></tr><tr><td>510.7 – 517.3</td><td>Host rock</td><td>Sharp contact to host rock with some red staining and below undeformed rock.</td></tr></table>An asymmetric deformation zone (due to the lack of a well-defined transition zone below the core) with a distinct fault core defined by fault rock occurrences and a highly fractured rock interval. The deformation zone is entirely developed in granites and is accompanied by pervasive red staining. Fractures dip gently to moderately to the E, SE, S and SW. There occurs also a steep NNW trending epidote, calcite and phrenite-coated fracture.</td></tr>
</table>

BH	Geometrical Intercept (bh. m)	Target intercept (bh. m)	Comment
			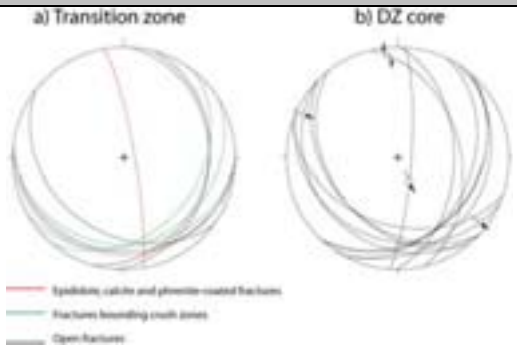 The fault core, located at depth interval 509.003 to 510.710 m, consists predominantly of fault rocks such as protocataclasites to cataclasites and bands of ultracataclasites and gouge. It contains numerous broken fractures, with millimetric apertures, and several striated planes.